



# IDENTIFICATION AND QUANTIFICATION OF DRUGS, METABOLITES, DRUG METABOLIZING ENZYMES, AND TRANSPORTERS

Concepts, Methods,  
and Translational Sciences



Edited by  
Shuguang Ma  
Swapan K. Chowdhury

IDENTIFICATION AND QUANTIFICATION  
OF DRUGS, METABOLITES,  
DRUG METABOLIZING ENZYMES,  
AND TRANSPORTERS

Concepts, Methods, and Translational Sciences

---

IDENTIFICATION AND  
QUANTIFICATION  
OF DRUGS,  
METABOLITES, DRUG  
METABOLIZING  
ENZYMES, AND  
TRANSPORTERS  
Concepts, Methods, and  
Translational Sciences

---

*Edited by*

SHUGUANG MA

SWAPAN K. CHOWDHURY



Elsevier

Radarweg 29, PO Box 211, 1000 AE Amsterdam, Netherlands  
The Boulevard, Langford Lane, Kidlington, Oxford OX5 1GB, United Kingdom  
50 Hampshire Street, 5th Floor, Cambridge, MA 02139, United States

© 2020 Elsevier B.V. All rights reserved.

No part of this publication may be reproduced or transmitted in any form or by any means, electronic or mechanical, including photocopying, recording, or any information storage and retrieval system, without permission in writing from the publisher. Details on how to seek permission, further information about the Publisher's permissions policies and our arrangements with organizations such as the Copyright Clearance Center and the Copyright Licensing Agency, can be found at our website: [www.elsevier.com/permissions](http://www.elsevier.com/permissions).

This book and the individual contributions contained in it are protected under copyright by the Publisher (other than as may be noted herein).

#### Notices

Knowledge and best practice in this field are constantly changing. As new research and experience broaden our understanding, changes in research methods, professional practices, or medical treatment may become necessary.

Practitioners and researchers must always rely on their own experience and knowledge in evaluating and using any information, methods, compounds, or experiments described herein. In using such information or methods they should be mindful of their own safety and the safety of others, including parties for whom they have a professional responsibility.

To the fullest extent of the law, neither the Publisher nor the authors, contributors, or editors, assume any liability for any injury and/or damage to persons or property as a matter of products liability, negligence or otherwise, or from any use or operation of any methods, products, instructions, or ideas contained in the material herein.

#### Library of Congress Cataloging-in-Publication Data

A catalog record for this book is available from the Library of Congress

#### British Library Cataloguing-in-Publication Data

A catalogue record for this book is available from the British Library

ISBN: 978-0-12-820018-6

For information on all Elsevier publications  
visit our website at <https://www.elsevier.com/books-and-journals>

*Publisher:* Susan Dennis

*Acquisitions Editor:* Kathryn Eryilmaz

*Editorial Project Manager:* Sara Valentino

*Production Project Manager:* Joy Christel Neumarin Honest Thangiah

*Cover Designer:* Miles Hitchen

Typeset by SPI Global, India





# Contributors

---

- Farah Al Qaraghuli** Department of Pharmaceutical Sciences, School of Pharmacy and Pharmaceutical Sciences, The State University of New York at Buffalo, Buffalo, NY, United States
- Ravindra Varma Alluri** Clinical Pharmacology and Safety Sciences, R&D BioPharmaceuticals, AstraZeneca, Cambridge, United Kingdom
- Sophie M.A. Argon** Department of Pharmaceutics, School of Pharmacy, University of Washington, Seattle, WA, United States
- Piyush Bajaj** Drug Safety Research and Evaluation, Takeda Pharmaceutical International Co., Cambridge, MA, United States
- Tashinga E. Bapiro** DMPK, Research and Early Development, Oncology R&D, AstraZeneca, Cambridge, United Kingdom
- Abdul Basit** Department of Pharmaceutics, University of Washington, Seattle; Department of Pharmaceutical Sciences, Washington State University, Spokane, WA, United States
- Andreas Brink** Roche Pharma Research and Early Development, Roche Innovation Center Basel, F. Hoffmann-La Roche Ltd, Basel, Switzerland
- Tingting Cai** Laboratory Testing Division, WuXi AppTec, Nanjing, China
- Jose Castro-Perez** Agios Pharmaceuticals, Inc., Cambridge, MA, United States
- Jae H. Chang** Preclinical Development, ORIC Pharmaceuticals, South San Francisco, CA, United States
- Eugene Chia-Te Chen** Department of Drug Metabolism and Pharmacokinetics, Genentech, South San Francisco, CA, United States
- Marie Croft** Pharmaron ABS, Germantown, MD, United States
- Liam Evans** Hypha Discovery Ltd., Oxfordshire, United Kingdom
- Raymond Evers** Department of Pharmacokinetics, Pharmacodynamics and Drug Metabolism, Merck & Co Inc., Kenilworth, NJ, United States
- Robert S. Foti** Pharmacokinetics, Pharmacodynamics and Drug Metabolism, Merck Research Laboratories, Boston, MA, United States
- Adrian J. Fretland** DMPK, Research and Early Development, Oncology R&D, AstraZeneca, Waltham, MA, United States
- Christopher Gemski** Translational Research Bioassay and Immunogenicity Group, Drug Metabolism and Pharmacokinetic Department, Takeda Pharmaceuticals International Co., Cambridge, MA, United States
- Anima Ghosal** Independent Consultant, Piscataway, NJ, United States
- Jia Hao** Drug Metabolism, Gilead Sciences Inc, Foster City, CA, United States
- Satyajeet Haridas** Translational Research Bioassay and Immunogenicity Group, Drug Metabolism and Pharmacokinetic Department, Takeda Pharmaceuticals International Co., Cambridge, MA, United States
- Simon Hauri** Roche Pharma Research and Early Development, Roche Innovation Center Basel, F. Hoffmann-La Roche Ltd, Basel, Switzerland
- Nina Isoherranen** Department of Pharmaceutics, University of Washington, Seattle, WA, United States
- Wenying Jian** DMPK, Janssen R&D, Spring House, PA, United States
- Kevin Johnson** Drug Metabolism and Pharmacokinetics, Genentech, South San Francisco, CA, United States

- Barry Jones** DMPK, Research and Early Development, Oncology R&D, AstraZeneca, Cambridge, United Kingdom
- Robert S. Jones** Drug Metabolism and Pharmacokinetics, Genentech, South San Francisco, CA, United States
- Jan Felix Joseph** Freie Universitaet Berlin, Institute of Pharmacy—Pharmaceutical Analysis; Freie Universitaet Berlin, Department of Biology, Chemistry, Pharmacy, CoreFacility BioSupraMol, Berlin, Germany
- S. Cyrus Khojasteh** Drug Metabolism and Pharmacokinetics, Genentech, South San Francisco, CA, United States
- Yurong Lai** Drug Metabolism, Gilead Sciences Inc, Foster City, CA, United States
- Hoa Le** Drug Metabolism, Gilead Sciences, Foster City, CA, United States
- Xiaomin Liang** Drug Metabolism, Gilead Sciences Inc, Foster City, CA, United States
- Liming Liu** Product Development, Curon Biopharmaceutical Ltd, Shanghai, People's Republic of China
- Filipe Lopes** Roche Pharma Research and Early Development, Roche Innovation Center Basel, F. Hoffmann-La Roche Ltd, Basel, Switzerland
- Justin Q. Ly** Drug Metabolism and Pharmacokinetics, Genentech, South San Francisco, CA, United States
- Shuguang Ma** Drug Metabolism and Pharmacokinetics, Genentech Inc., South San Francisco, CA, United States
- Roshini Markandu** DMPK, Research and Early Development, Oncology R&D, AstraZeneca, Cambridge, United Kingdom
- Rosalinde Masereeuw** Division of Pharmacology, Utrecht Institute for Pharmaceutical Sciences, Utrecht, The Netherlands
- J. Eric McDuffie** Investigative & Mechanistic Toxicology, Janssen Research & Development, San Diego, CA, United States
- Kaushik Mitra** Department of Drug Metabolism and Pharmacokinetics, Janssen Research and Development, Springhouse, PA, United States
- Diana Montgomery** Department of Pharmacokinetics, Pharmacodynamics and Drug Metabolism, Merck & Co Inc., Kenilworth, NJ, United States
- Alexandra L. Orton** DMPK, Research and Early Development, Oncology R&D, AstraZeneca, Cambridge, United Kingdom
- Katie H. Owens** Department of Pharmaceutics, School of Pharmacy, University of Washington, Seattle, WA, United States
- Axel Pähler** Roche Pharma Research and Early Development, Roche Innovation Center Basel, F. Hoffmann-La Roche Ltd, Basel, Switzerland
- Maria Kristina Parr** Freie Universitaet Berlin, Institute of Pharmacy—Pharmaceutical Analysis, Berlin, Germany
- Shefali Patel** DMPK, Janssen R&D, Spring House, PA, United States
- Ichiko D. Petrie** Department of Pharmaceutics, School of Pharmacy, University of Washington, Seattle, WA, United States
- Richard Phipps** Hypha Discovery Ltd., Oxfordshire, United Kingdom
- Chandra Prakash** Agios Pharmaceuticals, Inc., Cambridge, MA, United States
- Bhagwat Prasad** Department of Pharmaceutics, University of Washington, Seattle; Department of Pharmaceutical Sciences, Washington State University, Spokane, WA, United States
- Isabelle Ragueneau-Majlessi** Department of Pharmaceutics, School of Pharmacy, University of Washington, Seattle, WA, United States
- Venkatesh Pilla Reddy** DMPK, Research and Early Development, Oncology R&D; Departments of Modeling and Simulation, Early Oncology Drug Metabolism and Pharmacokinetics, R&D Oncology, AstraZeneca, Cambridge, United Kingdom

- Ellen Riddle** Drug Metabolism, Gilead Sciences Inc, Foster City, CA, United States
- Qian Ruan** Pharmaceutical Candidate Characterization, Bristol-Myers Squibb, Princeton, NJ, United States
- Simone Schadt** Roche Pharma Research and Early Development, Roche Innovation Center Basel, F. Hoffmann-La Roche Ltd, Basel, Switzerland
- Dhaval K. Shah** Department of Pharmaceutical Sciences, School of Pharmacy and Pharmaceutical Sciences, The State University of New York at Buffalo, Buffalo, NY, United States
- Julia Shanu-Wilson** Hypha Discovery Ltd., Oxfordshire, United Kingdom
- Kelly MacLennan Staiger** Drug Metabolism, Gilead Sciences Inc, Foster City, CA, United States
- Jonathan Steele** Hypha Discovery Ltd., Oxfordshire, United Kingdom
- Manthana V.S. Varma** Medicine Design, Worldwide R&D, Pfizer Inc., Groton, CT, United States
- Matthew P. Wagoner** Drug Safety Research and Evaluation, Takeda Pharmaceutical International Co., Cambridge, MA, United States
- Naidong Weng** DMPK, Janssen R&D, Spring House, PA, United States
- Stephen Wrigley** Hypha Discovery Ltd., Oxfordshire, United Kingdom
- Caisheng Wu** School of Pharmaceutical Sciences, Xiamen University, Xiamen, China
- Graeme C. Young** GlaxoSmithKline Research and Development Ltd., David Jack Centre, Ware, United Kingdom
- Jingjing Yu** Department of Pharmaceutics, School of Pharmacy, University of Washington, Seattle, WA, United States
- Lushan Yu** Institute of Drug Metabolism and Pharmaceutical Analysis, Zhejiang University, Hangzhou, People's Republic of China
- Su Zeng** Institute of Drug Metabolism and Pharmaceutical Analysis, Zhejiang University, Hangzhou, People's Republic of China
- Haeyoung Zhang** Department of Pharmaceutics, University of Washington, Seattle, WA, United States
- Wanying Zhang** Department of Pharmaceutical Sciences, School of Pharmacy and Pharmaceutical Sciences, The State University of New York at Buffalo, Buffalo, NY, United States
- Andy Z.X. Zhu** Department of Drug Metabolism and Pharmacokinetics, Takeda Pharmaceuticals International Co., Cambridge, MA, United States
- Mingshe Zhu** MassDefect Technologies, Princeton, NJ, United States

# Foreword

---

It is my great pleasure to write the foreword for this excellent book. The study of drug metabolism and disposition is a mature science, but still essential in drug discovery and development. Indeed, a quick search of PubMed, using “*drug metabolism*” as the search term, came up with more than 18,000 hits. One of the earlier articles is by Bernard Brodie, considered to be the founder of modern pharmacology and a major contributor to the study of drug metabolism. His article—published in the *Journal of Pharmacy and Pharmacology* in 1956—is titled “*Pathways of Drug Metabolism*” and it is based on a lecture at the University of London [1]. It describes his work over the decade and some of it is based on collaborations with other pioneers in the field such as Julius Axelrod. One sentence still resonates very much and it actually covers much of the material described in this book:

*Finally, it is thought that a detailed knowledge of enzymes involved in drug “detoxification” might help the medicinal chemist to develop compounds of either high or low stability in the body, whichever would be more desirable in gaining a desired therapeutic result.*

Drug metabolism sciences have advanced tremendously since the publication of this article and this progress was to a large extent enabled by advances in the availability of biochemical reagents and bioanalytical techniques, in particular mass spectrometry. Both academic and industrial scientists have

identified many breakthroughs that have ultimately contributed to bringing drugs to patients with an urgent need for better treatments. It is very gratifying that the number of drugs approved by the FDA is increasing steadily with 38 NMEs (new molecular entity) and 10 BLAs (biological license application) approved by the US Food and Drug Administration (FDA) in 2019 [2]. The level of innovation is best illustrated by about half of the approved drugs in 2019 having a breakthrough designation. Drug metabolism and pharmacokinetics (DMPK) scientists are fully embedded in project teams in drug discovery and work hand in hand with medicinal chemists on the identification of drugs with superior properties. These scientists have become very good at dialing out the “*known unknowns*” such as metabolism by cytochrome P450 enzymes. However, this has actually resulted in having to deal with much more complex drug disposition pathways involving less well-studied drug metabolizing enzymes and also more and more drug transporters. This trend is also fueled by a shift toward more and more drugs having beyond the “rule of five” molecular properties [3]. Indeed, the average molecular weight of drugs approved by the FDA in 2016 and 2017 was more than 500 Da and the median  $\text{clogP}$  of drugs approved from 2008 to 2017 is now 3.3, in part driven by trying, for example, to disrupt protein-protein interactions. An additional consequence of this shift in properties is that in vitro to in vivo extrapolation of ADME properties

to predict the human pharmacokinetics has become more complex and the same can be said of predicting drug-drug interaction—many of which now involve drug transporters. If anything, the involvement of DMPK scientists is now more important than ever because of the pursuit of novel molecular modalities in academia and in the pharmaceutical industry; a few that come to mind are antibody-drug conjugates, protein degraders, and macrocyclic peptides. DMPK scientists can help make drugs out of these hard-to-drug modalities. Finally, the integration of this diverse array of in vitro and in vivo data is enabled by computational modeling and simulation. Physiologically based pharmacokinetic (PBPK) modeling is a very powerful tool to predict human pharmacokinetics and study drug-drug interaction as well as the pharmacokinetics in special populations and infants. Pharmacokinetic/pharmacodynamic modeling and its extension, quantitative systems pharmacology, can help translate preclinical findings to the clinic.

This book is comprised of many excellent chapters written by experts in the field that address some of the challenges highlighted in the previous paragraph. The first section focuses on *“Techniques for identifying and quantifying drugs and metabolites.”* Chapters 1–3 introduce the readers to the latest advances in bioanalysis, in particular mass spectrometry for the analysis of drugs, their metabolites, and endogenous biomarkers. In contrast to 20 years ago, high-resolution mass spectrometry has now become routine and it has had a great impact on the study of biotransformation. Of course, mass spectrometry is frequently not sufficient to identify the definitive structure of a metabolite, and hence Chapter 4 focuses on strategies for generating metabolites and characterization via NMR. Supercritical fluid chromatography has become easier to interface and it can greatly facilitate chiral separation; the

latter topic is covered in Chapter 5. The last chapter in the first section (Chapter 6) focuses on accelerator mass spectrometry, a powerful tool to study ADME and the absolute bioavailability in humans.

The second section addresses *“Drug metabolizing enzymes, transporters and drug drug interactions.”* Cytochrome P450-mediated and non-cytochrome P450-mediated metabolism is discussed in Chapters 7 and 8. In vitro to in vivo prediction of drug-drug interaction is described in Chapter 9 while Chapter 10 specifically focuses on the role of transporters in drug disposition and drug-drug interaction, and Chapter 11 on the clinical relevance of these drug-drug interactions. Making predictions using PBPK modeling relies on accurate knowledge of physiologic constants and, most recently, mass spectrometry has been used to determine the abundance of drug metabolizing enzymes and transporters in various tissues. This is addressed in Chapter 12. Finally, Chapter 13 focuses on disease-drug interactions mediated by therapeutic proteins such as interleukins.

The third section focuses on *“Strategy related to drug metabolism and safety.”* Metabolites in safety testing continues to be a highly relevant area of research in drug discovery and development and it is addressed in Chapter 14. A close look at the (patent) literature indicates that finding drugs that balance potency and metabolic stability can still be problematic, and therefore many companies incorporate deuterium to enhance metabolite stability and lower the dose—see Chapter 15 for details. The focus on novel chemical space and more molecular diversity has introduced more chirality in molecules and the impact of that on pharmacology, toxicology, and drug metabolism is described in Chapter 16. Drug-induced liver injury and new predictive models for renal injury are described in Chapters 17 and 18, respectively.

Finally, [Chapter 19](#) focuses on immunogenicity as a key component of antibody development.

The fourth and last section is dedicated to “Translational sciences.” The use of genetically modified rodents is explored further in [Chapter 20](#), while [Chapter 21](#) speaks to the use of CRISPR to advance in vitro ADME models. In vitro to in vivo extrapolation of hepatic and renal clearance is discussed in [Chapter 22](#). The breadth of our science is nicely illustrated by [Chapter 23](#) which describes the role of mathematical modeling in translational sciences. Last, but by no means least, [Chapter 24](#) elegantly defines ways to predict the human efficacious dose using PK/PD modeling.

As is the case with many compilations, a lot of effort has gone into assembling an

excellent set of chapters that describe the state of the art in ADME sciences as it relates to drug discovery and development. The efforts by all authors, and in particular the editors Shuguang Ma and Swapan Chowdhury, are greatly appreciated. This book will be used as a resource for many years to come.

*Cornelis E.C.A. Hop*

## References

- [1] B.B. Brodie, Pathways of drug metabolism, *J. Pharm. Pharmacol.* 8 (1) (1956) 1–17.
- [2] A. Mullard, 2019 FDA drug approvals, *Nat. Rev. Drug Discov.* 19 (2) (2020) 79–84.
- [3] M.D. Shultz, Two decades under the influence of the rule of five and the changing properties of approved oral drugs, *J. Med. Chem.* 62 (4) (2019) 1701–1714.

# Preface

---

Some 15 years ago, one of us (SKC) compiled the first edition of this book that covered the most up-to-date information previously available on the strategies, methods, applications, and implications of scientific data on the role of enzymes and transporters in the disposition of pharmaceuticals. The book was a great success and was widely used as a valuable resource by scientists in both industry and academia. Since then, a lot has changed in the field of drug metabolism, including how recent scientific advances are being utilized to discover and develop safer medicines. Therefore, it has become apparent that a new edition of the book is required to fully capture these profound changes, which involves the implementation of newer technologies in the discovery and development of medicines to treat a wide range of maladies. With much enthusiasm from the publisher, we collaborated to assemble a comprehensive treatise that would capture how the latest scientific findings are having a fundamental impact on the utilization of these novel advances in drug research. This second edition is completely updated and provides an overview of the last decade's numerous improvements in analytical technologies for the detection and quantification of drugs, metabolites, and biomarkers. This new edition goes beyond conventional LC-MS and features all-new chapters, including: how to evaluate drug absorption, distribution, metabolism,

and excretion (ADME), the potential for hepatic and renal toxicity, immunogenicity of biotherapeutics, and translational tools for predicting human dosage, safety, and efficacy of small molecules and biologics.

This book is organized into four sections: (1) techniques for identifying and quantifying drugs and metabolites, (2) drug metabolism enzymes, transporters, and drug-drug interactions, (3) strategies related to drug metabolism and safety, and (4) translational sciences. The book contains 24 chapters covering the most recent, novel scientific breakthroughs and how they are utilized to develop medicines in the modern era. It is our sincere hope that this material will serve as an important tool and desk reference for pharmacologists, toxicologists, clinical scientists, and students interested in the fields of pharmacology, biochemistry, and drug metabolism.

Finally, we wish to acknowledge the contributions of the many scholars who participated in and contributed to this book from conception and passion into print. We also want to extend our gratitude to the contributions of the editorial staff and production manager at Elsevier, and last but not least, the families of the editors for their encouragement, love, and support.

*Shuguang Ma  
Swapan K. Chowdhury*





PART I

Techniques for identifying and  
quantifying drugs and  
metabolites

# Bioanalysis of small and large molecule drugs, metabolites, and biomarkers by LC-MS

*Naidong Weng, Shefali Patel, Wenying Jian*

DMPK, Janssen R&D, Spring House, PA, United States

## 1 Introduction

Bioanalysis, often shortened to BA, is a subdiscipline within pharmaceutical research and development (R&D). Contemporary bioanalysis quantitatively analyzes very low quantity but highly variable levels (pg/mL- $\mu$ g/mL) of drug candidates, their metabolites, endogenous biomarkers, etc. in extremely complicated biological matrices such as plasma, blood, urine, and tissues which are harvested from different types of animal species (rodents, dogs, nonhuman primates, etc.) and humans [1]. Bioanalysis supports discovery, nonclinical (tox), and clinical studies (Fig. 1). Fig. 1 shows typical studies an integrated bioanalytical function would support.

Bioanalytical data are used for calculating pharmacokinetic parameters such as bioavailability, bioequivalence, drug and metabolites exposure, clearance, their distribution into various body organs, correlation of pharmacokinetics (PK) effects and pharmacodynamics (PD) changes, etc. Thus, bioanalysis plays a pivotal role in moving drug candidates from early discovery all the way to regulatory filing and postmarket surveillance in the entire drug discovery and development process. In today's dynamic drug discovery and development environment, bioanalytical scientists not only provide pivotal data but also actively engage in project/program go/no-go discussions, along with colleagues from other functional areas. While the most essential element of bioanalysis is to use analytical chemistry knowledge and state-of-the-art instruments to provide reliable and accurate measurement, knowledge from relevant disciplines such as biotransformation, pharmacokinetics, biology, pharmacology, etc. is invaluable for ensuring appropriate conduct of bioanalysis.

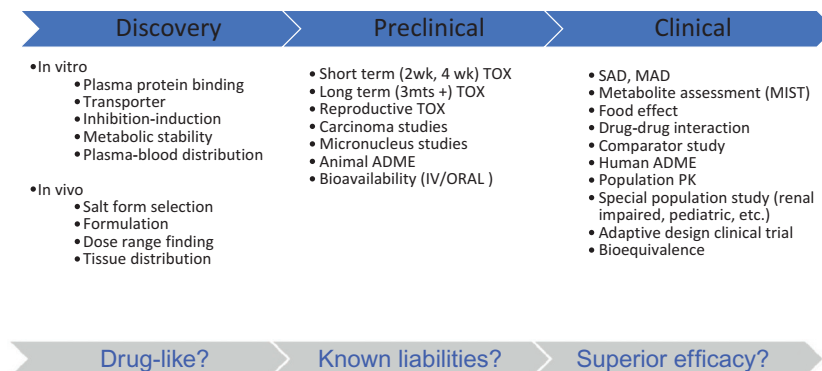


**FIG. 1** Exemplary bioanalytical support in drug discovery and development. TOX, toxicology; SAD, single ascending dose study; MAD, multiple ascending dose study; ADME, absorption, distribution, metabolism, and elimination; IV, intravenous.

In this book chapter, we try to provide a brief overview of contemporary bioanalysis using the LC-MS platform. It is an impossible task to provide a detailed and comprehensive review of LC-MS bioanalysis in a book chapter. The case studies and literature are no doubt incomplete and biased toward our own experiences and publications. Interested readers are referred to the excellent bioanalysis handbook by Li et al. for a more comprehensive overview of this discipline [1]. Nevertheless, we hope the readers can appreciate the complexity and dynamics of modern LC-MS-based bioanalysis for small and large molecule drugs, metabolites, and biomarkers.

## 2 Complexity of contemporary bioanalysis

Bioanalytical support is required for important decision-making for all types of studies, from discovery (non-GLP), to development (GLP), and to clinical (GCP) studies. Yet there are many unique and complicated attributes of cost, quality, and timely delivery at each of the abovementioned stages (or substage within each stage). For bioanalysis, the quality and integrity of the bioanalytical data are ultimately the most important attributes. The right scientific and compliance vigor must be applied to each study. The current regulatory landscape for regulated bioanalysis is highly complicated, with guidance from multiple regional health authorities [2–6]. Since guidance from different regions are not totally harmonized, and compounded by individual interpretation of different inspectors, it is still quite a challenge to fully understand and execute the right level of compliance that can be acceptable in the global filing. Efforts are currently being made to harmonize the guidelines into one single global guideline ICH-M10 [7].

While timely delivery of bioanalytical data to support project decisions is a must-do item to meet the ever-tightening drug discovery and development timelines, cost is another attribute that should not be overlooked. The cost of bioanalysis activities should be carefully managed to ensure that it stays within the predetermined budget. On the other side, the application of a

tiered approach, which typically consists of three tiers of assay qualification—screening assay, qualified assay, and validated assay with the increased levels of validation parameters—can be used with a balance of scientific vigor and cost [8]. The European Bioanalytical Forum (EBF) recommends exercising this approach for “nonregulated” nonclinical bioanalysis in drug development and using “fit-for-purpose” elements in metabolite quantitation for establishing safety coverage (MIST); urine bioanalysis; and tissue bioanalysis [9, 10]. Of course, the actual implementation of which tier to use depends on each individual study. For example, for urine bioanalysis, while a qualified assay could be used for most clinical studies for understanding the urinary excretion of a drug candidate, validated assays should be applied if renal clearance is the main route of elimination (PK end point) and/or the drug target action is at the kidney.

There is an expansion of bioanalysis scope over the past decades. In the early days, bioanalysis focused on supporting small molecule PK and bioequivalence (BE) from standard formulations such as tablets and capsules. Analysis of metabolites and biomarkers rarely occurred. Currently, PK and BE for both small and large molecules, as well as many hybrid forms of large and small molecules such as antibody drug conjugate (ADC), are supported by bioanalysis [11, 12]. Even for small molecules, advancement in formulation presents new challenges for bioanalysis. For example, liposomes are widely applied in the pharmaceutical industry due to their unique capabilities such as encapsulating and protecting the therapeutic analytes from degradation, controlling the release rate, facilitating on-target delivery, and reducing toxicity for drugs [13, 14]. For liposomal drug product development, validated bioanalytical methods to determine the concentration of the encapsulated and nonencapsulated forms (both the protein-free and protein-bound) of the active substance in biological samples should be employed. However, establishing such bioanalytical assays can be quite challenging due to the potential rapture of the liposome during sample collection, shipping, storage, and analysis, which can artificially elevate the nonencapsulated concentrations [15, 16].

Peptide and protein drugs have evolved in recent years into mainstream therapeutics, representing a significant portion of the pharmaceutical market [17]. Peptides and proteins exhibit highly diverse structures and broad biological activities as hormones, neurotransmitters, structural proteins, and metabolic modulators and therefore have a significant role as both therapeutics and biomarkers. Unspecific proteolysis is a major elimination pathway for peptides and proteins instead of the oxidative hepatic metabolism that is typical for most small molecule drugs [18]. In addition to the typical PK support, bioanalysis has been actively engaged in newly developed areas such as PKPD correlation, biomarker research in target engagement/tissue distribution, simultaneous quantitation and metabolite identification for small molecules and biologics, and antidrug antibody (ADA), etc., for many of which both science and regulatory requirements are still evolving.

Historically, bioanalysis support can be categorized into two distinct areas—liquid chromatography for small molecules, usually chemically synthesized, and ligand binding assay for large molecules, such as those which monoclonal antibodies typically produce by cell culture. With the development of modern instrumentation, especially mass spectrometers, measurement of large molecules by liquid chromatography in conjunction with a mass spectrometer (LC-MS) has become a reality. There is also a need to use LC-MS to investigate the *in vivo* fate of some of the new modalities such as a half-life extended peptide constructed by conjugating or fusing an otherwise short-lived peptide with an antibody or Fc to extensively extend its *in vivo* half-life through decreased clearance and increased stability [19].

LC-MS has also been increasingly used for discovering and measuring endogenous protein or peptide biomarkers [20, 21].

### 3 Bioanalytical requirements for supporting discovery, nonclinical, and clinical studies

---

Let us take a further look at bioanalytical requirements for supporting discovery, nonclinical development, and clinical studies using LC-MS methods. These three stages should not be viewed as three separate and consecutive ones since each can extend well into the next stage, in particular between nonclinical development and clinical phases. Many of the longer-term toxicology studies are running in parallel with the clinical studies. Discovery bioanalytical support is performed under non-GLP conditions. Generic LC-MS methods using gradient mobile phase elution and protein precipitation sample extraction are typically used to analyze the drug candidates in plasma and tissues. The results are used to rank the drug candidates as well as to obtain other important information such as tissue distribution and basic pharmacokinetic parameters, for example,  $C_{max}$ ,  $T_{max}$ , AUC,  $T_{1/2}$ , and clearance. Usually an internal bioanalysis/PK guideline is used for the conduct of this type of study. Some level of method verification such as accuracy, precision, and critical stability is performed before the sample analysis. Run acceptance criteria are usually a little bit wider than those used in GLP studies. Even though discovery bioanalysis does not follow strict GLP rules, the data generated in the discovery stage are still pivotal for compound selection, and therefore many companies institute some levels of compliance to ensure data integrity. Nonclinical bioanalytical support in development is under GLP regulations where the data generated should withstand rigorous regulatory scrutiny [2, 3]. For each method, vigorous method development and validation is performed as per regulatory guidance and internal Standard Operation Procedures (SOPs), even though method validation itself is non-GLP. Any deviation during the sample analysis, which follows the GLP principles, should be thoroughly investigated, documented, and justified. Once the candidate moves into the clinical stage, automation and other means of improving the throughput of sample analysis become more relevant. The same clinical bioanalytical method can be used by multiple bioanalytical chemists within or even among different organizations to meet the demand for analyzing a large number of samples. At the clinical stage, especially for studies in first in human (FIH), a bioanalytical method with better sensitivity than those in nonclinical studies may be required. Extensive method optimization for both sample preparation and LC-MS conditions to maximize recovery and minimize matrix effects is often pursued.

### 4 Current regulatory landscape for bioanalysis

Both nonclinical development and clinical bioanalytical support are required to follow internal SOPs and regulatory recommendations. Dozens of SOPs are usually used to address many aspects of bioanalytical activities ranging from instrument qualification, maintenance, and calibration, to bioanalytical method validation, sample storage, analysis and destruction, to data management and archiving, etc. The goal of these SOPs is to ensure the highest data

**TABLE 1** Bioanalytical full validation, partial validation and cross validation [2].

Full validation	Partial validation	Cross validation
Used for measuring analyte concentrations in biological samples. A full validation of a bioanalytical method should be performed when establishing a bioanalytical method for the quantification of an analyte in clinical and in pivotal nonclinical studies	Modifications to a fully validated analytical method may be evaluated by partial validation. Partial validation can range from as little as one accuracy and precision determination to a nearly full validation. The items in a partial validation are determined according to the extent and nature of the changes made to the method	Where data are obtained from different methods within or across studies, or when data are obtained within a study from different laboratories applying the same method, comparison of those data is needed, and a cross validation of the applied analytical methods should be carried out
Developing and validating an assay for pivotal regulatory submission (IND or NDA)	Analytical site change using same method (i.e., bioanalytical method transfers between laboratories)	Data are obtained from different fully validated methods within a study
Implementing an analytical method that is reported in the literature	A change in sample processing procedures	Data are obtained within a study from different laboratories with the same bioanalytical method

integrity which can pass the regulatory scrutiny. These SOPs are usually drafted based on specific regulations and the regulatory guidance from the Food and Drug Administration (FDA) and other international regulatory agencies, such as the European Medicines Agency (EMA), and other federal/state requirements, as well as policies at each institute. One of the most important regulatory guidelines is the US FDA guidance on bioanalytical method validation [2], which provides a general guideline on establishing important parameters, some of which are specificity/selectivity, sensitivity, linearity ranges from a lower limit of quantitation (LLOQ) to an upper limit of quantitation (ULOQ), accuracy, precision, stability, matrix effects, carryover, recovery, dilution integrity, incurred sample reanalysis (ISR), etc. The method should also demonstrate reproducibility and accuracy for incurred samples and its suitability for its intended use. However, it is up to each institute to formulate its own SOPs based on this general guidance. Typically, method validations can be categorized into full, partial, and cross validations (Table 1). Most of the validations are conducted in the form of full validation, whereas the partial or cross validation can be used when a full validation is not required, as shown in the examples in Table 1.

## 5 General considerations for bioanalysis for sample collection

During the project discussion, it is important to understand the objective of the study so that important parameters such as matrix type, sample volume, ways of sampling (regular sampling or microsampling), analytes to be measured (parent or parent plus metabolites), anticoagulant selection, condition of centrifugation for harvesting plasma, sample storage container, shipping condition and instruction, sample storage condition ( $-20^{\circ}\text{C}$  vs.  $-70^{\circ}\text{C}$ ), etc. can be provided to the project team. While during the early stage of drug

discovery/development it is not always possible to conduct the full spectrum of a stability test, it is, however, always good practice to evaluate whether there is potential instability of a metabolite that can impact the accurate quantitation of the parent analyte and/or the metabolites. Detailed PK or TK (toxicokinetic) sample collection information, including labeling, will be entered into the lab manual or study design. The following is just one typical example in a lab manual supporting a Phase 1 clinical study. It includes three parts of the instruction (material and labeling; preparation of PK samples; and shipment of PK samples). As one can see from this example, an extremely detailed instruction is needed to ensure successful conduct of bioanalysis.

*Materials and labeling:*

- Blood must be collected in a glass or plastic K<sub>2</sub>EDTA containing blood collection tubes (e.g., Vacutainer).
- No tubes with separation gel should be used. The resulting plasma samples must be stored in polypropylene storage tubes with polypropylene or polyethylene caps.
- All tubes and containers will be labeled with preprinted labels. The preprinted information will include the study number, participant identification number, treatment or treatment period, scheduled sampling day and time as stipulated in the flow chart, and the analyte name if applicable. No other information will be written on the labels. Labels should be attached to the storage tubes at least 12 h before being frozen to ensure proper adherence.
- Labels should be applied to the sample tubes as follows:
  - Apply labels to the sample tubes so that they do not overlap and obscure any information. If possible, expose an area between the two ends of the label to allow viewing of the contents of the tube.
  - Do not alter the orientation of the label on the sample tube.
  - Apply labels to all tubes in the same manner.

*Preparation of pharmacokinetic samples:*

- Collect 4 mL of blood into the appropriate K<sub>2</sub>EDTA-containing collection tube (e.g., Vacutainer) at each time point.
- Record the exact date and time of sampling.
- Before processing, gently invert the tubes 8–10 times to afford mixing; blood samples must be kept on melting ice at all times during processing.
- Centrifuge blood samples within 1 h of collection in a centrifuge at 1300g for 10 min at 4°C, to yield approximately 1.5–2 mL of plasma from each 4-mL whole blood sample. Plasma samples must be kept on melting ice at all times during processing.
- Transfer plasma immediately to a prelabeled polypropylene tube. Plasma samples must be kept on melting ice at all times until storage in a freezer.
- Store plasma samples in an upright position in a freezer, at a set temperature at –20°C until transfer to the bioanalytical facility.
- The time between blood collection and freezing the plasma will not exceed 2 h.
- Ship samples according to the instructions provided. Ship specimens to the bioanalytical facility, sorted by participant, sample collection date, and time.
- Questions regarding handling the plasma pharmacokinetic specimens should be addressed to the contact person for the sponsor.



*Shipment of pharmacokinetic samples:*

- All pharmacokinetic samples will be sent to the bioanalytical facility in a single shipment at the end of the study or in multiple shipments as agreed upon with the bioanalytical scientist.
- An inventory list must be included with each shipment. The sponsor-provided logs can be used as an inventory list. The inventory list must note each specimen drawn for each participant and note any missing specimens.
- For all international shipments, World Courier will be used. For domestic shipments, a reliable domestic courier, such as Federal Express, will be used.
- As soon as the shipment day and air bill number(s) are available, the site will send an e-mail to the principal investigator, sample management team, and site manager of the bioanalytical facility. The e-mail must specify the study number, the number of pharmacokinetic samples, the time of shipment pickup and the tracking number and include an electronic sample inventory.
- Notify the bioanalytical scientist and the courier, at least 24h in advance of the planned shipment. Provide the courier with the appropriate account number to be used, if applicable.
- Unless agreements were made with the principal investigator, samples will be shipped via overnight delivery only on Monday through Wednesday, excluding holidays.
- Preferably the frozen samples will be shipped in boxes, sorted by participant and sampling time. Boxes will be packed in bags that can withstand dry ice conditions (e.g., cryogenic bags).
- Pack the frozen samples in a sufficient quantity of dry ice in appropriate containers, to maintain a frozen state for at least 3 days.
- For all biological samples, follow the International Air Transport Association (IATA) regulations for shipment.
- Ensure that the total package weight does not exceed 27.2kg (60 pounds).
- Label the package with the sponsor name and study number.
- Include a return address (which includes the investigator's name) on the outside of each shipping container.
- Comply with all courier regulations for the shipment of biological specimens (include all paperwork).
- Retain all documents indicating the date, time, and signature(s) of person(s) making the shipment, in the study files.

## 6 Diagnosis and mitigation of nonspecific adsorption loss for urine bioanalysis

---

For urine samples, it is always advisable to conduct a nonspecific adsorption loss experiment before protocol finalization so that, if necessary, the means of preventing nonspecific adsorption can be implemented. Nonspecific adsorption happens frequently in urine assays because urine lacks proteins and lipids that can bind to the analytes or solubilize lipophilic analytes [22]. A common approach to urine method development with a focus on overcoming

adsorption issues was published [23]. A simple and quick way to identify an adsorption problem is through a series of transfers and incubations. In this test, a drug solution in control urine is prepared at a low quality control (QC) level in a test container. Dry and clean test containers that are made from the same material and are of the same size as those for future urine samples should be used. A portion of the urine solution is poured into a next container, and then the transfer process is repeated for a few more containers. Between transfers, each solution in the container should be left at room temperature for about 5–20 min to allow adsorption to take place before continuing to the next transfer step. Finally, the urine sample from each test container is assayed to determine the compound response. A sequential loss of analyte response after each transfer indicates the existence of nonspecific adsorption loss. To overcome the issue, antiadsorptive agents can be utilized, such as bovine serum albumin (BSA), zwitterionic detergents such as 3-[3-cholamidopropyl]-dimethylammonio]-1-propane sulfonate (CHAPS), sodium dodecyl benzene sulfonate (SDBS), beta-cyclodextrin, Tween 80, and Tween 20.

## 7 Tissue bioanalysis

Knowledge of distribution of drugs, metabolites, biomarkers, etc. at specific locations in the body of animal species and human subjects becomes more and more important for drug discovery and development [24]. This knowledge is often obtained through the analysis of tissue samples obtained from nonclinical and, to a lesser extent, clinical studies. Many factors can affect the tissue distribution of drugs and metabolites. Passive diffusion across the cell membrane is the primary pathway for the drug to distribute to the tissue. However, transporter proteins can also assist or minimize the uptake of the drugs and metabolites into the tissues. Other contributing factors such as drug metabolism, clearance rate, protein binding, permeability, molecular weight,  $\log P$ , and  $pK_a$  and other physicochemical properties can also have a significant impact on tissue distribution. LC-MS has become the standard toolbox for tissue sample analysis [25]. Different from plasma, which is in the liquid form, tissue samples are in a solid or semisolid format. Therefore, for typical LC-MS assays, they are homogenized prior to sample extraction. Soft tissues such as the brain, liver, lung, and kidney can be easily homogenized. Tough tissues such as the muscle, heart, stomach, intestine, and colon are more fibrous and need a more vigorous homogenization procedure. A higher shearing force and longer duration of process may be required when a rotor blade homogenizer or beads beater is used [26]. The heat generated during homogenization of tissues may cause degradation of thermolabile analyte(s), and therefore caution must be exercised. Hard tissues such as skeletal bones, skin, and hair are mostly nonvascularized tissues and need special treatment. In some extreme cases, enzymatic digestion or chemical treatment may be required for some hard tissues [27]. Once the tissue sample is homogenized, the homogenate is ready for extraction and the sample extraction approaches used for plasma samples should still apply. However, different from plasma samples, extraction recovery from solid tissue samples cannot be assumed to be 100% and fortified QC samples, prepared in tissue homogenate, cannot mimic the incurred samples [25]. Similarly, the internal standard, which was routinely used to compensate for incomplete or variable extraction recovery for the plasma samples,

does not track the analytes in the tissues. Recovery evaluation using a radiolabeled incurred sample [28] and recovery evaluation with orthogonal approaches [29] are just two examples of addressing the issue of recovery evaluation.

## 8 Managing unstable metabolites such as acyl glucuronide

When moving into the development phase, information about biotransformation of the drug candidate and its metabolites becomes more available. While the parent drug may not be subjected to glucuronidation, its phase 1 metabolism, for example, oxidation of alcohol to the carboxylic acid group, may generate metabolites that can form acyl glucuronide. If the plasma samples were collected without acidification to stabilize the acyl glucuronide, the phase 1 carboxylic acid metabolite may be overestimated due to the breakdown of acyl glucuronide during sample collection, storage, and analysis. It should also be noted that acidification of the plasma samples will affect the protein binding between the drug candidate and the endogenous proteins such as albumin [30]. If the protein-binding measurement is needed with the incurred samples, a separate pool of unbuffered plasma samples should be collected. Acidification of the samples could also lead to the instability of other metabolites. In one example of quantitation of diclofenac and metabolites in mouse plasma, acidification to stabilize diclofenac acyl glucuronide resulted in increased oxidative degradation of 5-OH diclofenac and ascorbic acid was added to the samples to prevent the degradation [31].

As we can tell from this simple acyl glucuronide example, a bioanalytical sample collection strategy may evolve, depending on the stage of the drug discovery and development. For example, at the early stage of drug development, information on parent exposure might be enough for a go-no-go decision. There, a simple stabilization of acyl glucuronide by adjusting the pH is used. With the project moving forward and gaining of information regarding acyl glucuronide migration, which may raise toxicity concern [32], the measurement of both the parent and acyl glucuronide metabolite is needed. Plasma protein binding for both the parent and acyl glucuronide metabolite may be needed to better predict the initial human dose. One would then be careful about the potential free fraction ( $F_u$ ) change with pH adjustment (nonphysiological pH).

## 9 General considerations for bioanalysis for extraction, chromatography, and MS detection

Bioanalytical methods typically consist of analyte extraction from biological samples, liquid chromatography to separate analytes of interest from endogenous components and metabolites that may cause a matrix effect or selectivity issue, and MS detection, often in the format of tandem mass spectrometers, to enhance assay selectivity and sensitivity. When developing a quantitative bioanalytical LC-MS method, one needs to holistically consider all three parts as one integrated system and sometimes trade-offs need to be carefully balanced [33]. One will always need to keep in mind the integrity of the analyte during the sample extraction, postextraction, and chromatography. It should also be noted that some labile

metabolites, even though not being measured, can convert to the analyte during sample extraction, chromatography, and MS detection and cause quantitation bias for the analytes of interest.

Biological samples are seldom amenable to direct injection onto the LC-MS system. Analytes of interest need to be extracted from the biological matrices prior to LC-MS analysis. The purpose of extraction is to eliminate or reduce interferences which can co-elute with the analytes and cause matrix effects or quantitation errors, and to concentrate the analytes and improve their detection. When optimizing the extraction, analyte rather than the matrix is the focus. This means that an extraction method with the highest recovery for the analyte may also suffer from a severe matrix effect. The commonly used sample preparation methods are direct injection, dilute and shoot, protein precipitation, liquid-liquid extraction (LLE) (solid-phase supported liquid-liquid extraction), and solid-phase extraction (SPE), the last three being the most frequently used. For example, protein precipitation is widely utilized and is also frequently the preferred extraction method during drug discovery and preclinical development. Analytes of interest are released from protein when a protein precipitation reagent such as organic solvents (e.g., acetonitrile, methanol), acids, or salt (e.g., ammonium sulfate) is added to the biological samples to denature the protein. The analyte stays in the supernatant after the centrifugation and can be analyzed directly or can go through evaporation/reconstitution steps to make the injection solution compatible with the chromatographic condition. This procedure is of low cost, easy to perform, and can be performed in the 96-well format. The extraction is also very mild and thus avoids potential analyte degradation or conversion from metabolite to parent. With the advancement of the modern mass spectrometer, assay sensitivity at low ng/mL, which in most cases is adequate for discovery and nonclinical studies, is easily achievable. However, if a simple sample extraction procedure such as protein precipitation is used, one may need to compensate for the potential ion-suppression or in-source conversion such as that from the glucuronide metabolite to the parent compound by using a more extensive chromatographic elution. The mechanism for sample extraction and chromatography ideally should be orthogonal so that a better method selectivity is provided. On the other side, SPE is very powerful for sample cleanup as it provides some level of chromatographic separation between the analytes and other matrix components. SPE is also easily automatable and provides high capacity for analyte enrichment. However, some of the SPE conditions can be harsh, especially in the case of strong cation or strong anion SPE where extreme pH conditions are used to elute the analytes. This may lead to unwanted instability of analytes or the breakdown of conjugated metabolites to the analyte of interest. Therefore, these SPE conditions should only be used when stability and biotransformation of the analyte are well established.

For large molecule bioanalysis, two approaches, namely the bottom-up and top-down, are typically used [34]. The bottom-up approach involves an enzymatic digestion and selection of a surrogate peptide that can represent the large molecule, while the top-down LC-MS measures the intact large molecule directly. Both approaches still require a good sample clean to remove the abundant endogenous proteins and other interferences. In addition to the classic sample cleanup procedures such as SPE, other novel approaches are also developed for protein bioanalysis, notably protein precipitation/pellet digestion, abundant protein depletion, and affinity enrichment. While the bottom-up approach, using a triple quadrupole mass spectrometer for the detection, typically has a superior sensitivity to the top-down approach by

the high-resolution mass spectrometer such as TOF, the latter has several advantages too [35]. For the top-down intact protein LC-MS analysis, a generic MS method is typically used, and little method development time is required. The method is independent of fragmentation efficiency, which is often not the case for surrogate peptides. The ability to acquire the complete information of posttranslational modifications (PTM) and biotransformation allows postacquisition data mining [19]. Some of the commonly observed challenges for sample preparation of large molecules include loss of protein/peptide due to nonspecific adsorption; analyte instability due to proteases; poor reproducibility of enzymatic digestion and high matrix effects due to high concentration of endogenous proteins; incomplete recovery due to binding of protein or peptides to high-abundance proteins and antibodies. Efforts have been made to overcome these challenges. Possible solutions for nonspecific adsorption include use of low-adsorption polypropylene and polyethylene containers; use of silanized glass containers; avoiding preparation of low concentration solutions in a matrix-free environment; adding a carrier such as BSA to any matrix-free solutions; and spiking high concentration stock solutions directly to plasma and preparing low concentration samples with serial dilution. Use of protease inhibitors such as diisopropylfluorophosphate (DFP), sodium fluoride/potassium oxalate/trichloroacetic acid, 4-(2-aminoethyl) benzene sulfonyl fluoride, hydrochloride (AEBSF)—Pefabloc, or phenylmethylsulfonyl fluoride (PMSF), storage of samples in an ultralow freezer ( $<-60^{\circ}\text{C}$ ), and handling the samples in an ice bath are recommended as possible solutions for protein and peptide instability. There are several possible solutions to remove abundant proteins [36]. The first step is to use urea, guanidine, or strong acid to eliminate protein binding between target peptide/protein and endogenous abundant proteins such as albumin. If the target protein/peptide is highly hydrophilic, TFA or TCA can be used to precipitate abundant proteins while keeping the analytes in the aqueous supernatant [37]. SPE (anion or cation exchange) can be used alone or in conjunction with protein precipitation—for extracting hydrophilic proteins/peptides. Immuno-affinity extraction may be used for achieving additional selectivity [38]. The largest challenge currently is still the relatively poor sensitivity (compared to ELISA), but it has been significantly improved with nano-LC-MS/MS and a better sample cleanup procedure such as immune-affinity extraction.

For LC-MS bioanalysis, chromatography plays a pivotal role to ensure assay selectivity and robustness. Phase-II conjugated metabolites such as glucuronide and glutathione conjugates need to be resolved from the analyte since they can break down back to the analyte in the ion source and cause assay bias [39]. Isomers and endogenous interference need to be resolved from the analyte. Compounds such as phospholipids and dosing vehicles like PEG need to be resolved from analytes since they can cause ion suppression [40]. Reversed-phase LC has been traditionally used for the quantitative LC-MS. With an increase of organic solvent concentration in the mobile phase, retention of the analyte decreases. However, one should be aware of the potential bimodal retention on the reversed-phase column, leading to a U-shaped retention profile where the initial retention decreases upon increasing the organic content in the mobile phase but a further increase in the organic content results in increased retention time for certain compounds, especially polar basic analytes, due to their interaction with the residual silanol groups. This bi-model retention may cause a retention shift during the run or irreproducibility of the method when a high organic content mobile phase is used on a reversed-phase column [40]. This can also lead to the mismatch of injection solvent and chromatography which may also lead to distorted chromatographic peaks [41]. In addition to

reversed-phase chromatography, separation based on other retention mechanisms can also be used complementarily such as HILIC for polar analytes [42, 43] and normal phase chromatography for chiral separations [44]. Large molecule LC-MS usually uses a shorter chain stationary phase such as C4, wider pore size (at least 300 Å), and elevated column temperature.

The principle of MS is the production of ions from analyzed compounds that are separated or filtered based on their mass to charge ratio ( $m/z$ ). Most of the applications for quantitative bioanalysis use tandem mass spectrometers (MS/MS) that employ two mass analyzers—one for the precursor ion in the first quadrupole and the other for the product ion in the third quadrupole after the collision—activated dissociation of the precursor ion in a collision cell (second quadrupole). Between the high-pressure LC and the MS operated under a high-vacuum environment, interface connections that operate at atmospheric pressure, such as electrospray ionization (ESI), atmospheric-pressure chemical ionization (APCI), and less frequently atmospheric-pressure photo ionization (APPI), have matured into highly reliable techniques necessary for quantitative LC-MS/MS bioanalysis. More recently, application high-resolution mass spectrometer (HRMS) in bioanalysis has drawn a lot of attention [45]. Due to its enhanced specificity using the high-resolution power and its capability of simultaneous quantitation and structural elucidation, HRMS could lead to a potentially rapid and reliable method development for bioanalysis as well as sample analysis, thus generating both cost and resource savings [46].

## 10 Selected applications for LC-MS bioanalysis

It is not the intention of this book chapter to cover every aspect of quantitative bioanalysis. Rather, a few relatively newly developed areas are focused on to further illustrate the impact of bioanalysis on drug discovery and development by using case studies from our own lab.

In the first example, we will discuss the status of using LC-MS, as a complementary tool to the traditional ELISA methods, to analyze large molecules, particularly some of the novel platform of biotherapeutics such as antibody-drug conjugate (ADC) and half-life extended peptides. The value of multiple LC-MS methods such as the bottom-up and top-down as well as simultaneous quantitation and catabolite identification is highlighted. The second example is the development of microsampling technology which has been widely used to support both preclinical and clinical studies. In comparison with the traditional plasma sampling technology, microsampling presents some additional challenges for method establishment, validation, and sample analysis, from both the scientific and compliance points of view. Biomarkers have become more and more important in drug discovery and development, from confirmation of target engagement to patient stratification. As biomarkers are endogenous molecules, their measurement is particularly challenging for bioanalytical scientists as there is no “true” blank matrix to prepare standards and QC samples. It is also very difficult to confirm the selectivity of a biomarker assay due its endogenous nature. Various strategies in the third example have been proposed to mitigate these challenges. Lastly, the accurate reading of important metabolites in the body has drawn a lot of attention recently since the publication of the FDA MIST guidance [47]. To establish safety coverage to ensure a safe clinical trial is pivotal. It is not always straightforward to establish the right bioanalytical strategy for metabolite measurement. In the last case study, the strategy for metabolite bioanalysis such as



measuring polar metabolites, assessment of chiral conversion, and selection of internal standard will be discussed.

## 10.1 LC-MS of large molecules

LBA is traditionally the primary platform for bioanalysis of large molecules and has the advantages of providing superior sensitivity and high throughput. However, it may also suffer from limitations such as cross-reactivity, requirement of highly specific reagents, and not being able to directly elucidate structure information. In the past decade, LC-MS has increasingly been applied for bioanalysis of large molecules as a complementary technique of LBA. LC-MS has the unique advantages of being highly specific, more resistant to matrix interference, and less stringent on reagent requirement. More importantly, LC-MS can provide valuable structure information which may be critical for understanding the ADME properties of protein drug candidates.

As discussed earlier, there are generally two approaches of analyzing proteins using LC-MS: bottom-up and top-down. In the bottom-up workflow, proteolytic (usually tryptic) peptides generated by digestion are monitored as surrogates of the protein, typically on a triple quadrupole mass spectrometer, which affords highly specific and sensitive detection. However, there could be situations when the surrogate peptide does not adequately represent the whole protein in terms of its functionality, stability, or coexistence of multiple isoforms. High-level structural information such as integrity of a multiple subunit protein or proteolytic catabolism is lost during digestion. This is when the top-down intact analysis of the protein can play an important role. The top-down intact bioanalysis of large proteins (e.g., mAb) has gained popularity in recent years thanks to applications of the advanced sample preparation technique, such as immune-affinity capture, which enables effective sample cleanup [35]. Intact mass spectra obtained from HRMS may contain the peaks of not only the unchanged intact molecule but also that of catabolites, making simultaneous quantitation and catabolite identification possible [19].

In both the bottom-up and top-down approaches, the workflow involves an up-front sample preparation. Depending on the nature of the analyte, required sensitivity, and the biological matrix, methodologies ranging from protein precipitation, solid phase extraction, abundant protein depletion, and affinity capture can be chosen or combined, with increased effectiveness in the sample cleanup. In the bottom-up approach, the surrogate (or signature) peptide is detected and analyzed in the same way as small molecules, on a triple quadrupole instrument by multiple reaction monitoring (MRM) analysis, or in some labs, on HRMS by a full scan or product ion analysis, a process also known as parallel reaction monitoring (PRM). In comparison, intact protein analysis has more diversified choices when it comes to MS detection [48]. Peptides or small proteins can be monitored in the same way as small molecules or surrogate peptides on triple quadrupole or HRMS. Large proteins such as mAb are heavily charged when analyzed under ESI, resulting in clusters of multiple charged ions which require resolution on HRMS. Peaks for a selected charged state (e.g., the three most abundant peaks) can be extracted with a certain extraction window to reconstruct an extracted ion chromatogram (EIC) which can be used for quantitation [49]. This approach is more widely adapted because it does not require additional software for data processing and thus can



be universally applied to data acquired on instruments from different vendors. Alternatively, multiple charged ions are deconvoluted to generate non- or zero-charged peaks which can be in turn quantified based on the intact molecule, a process requiring a specific software function. In the case when multiple components, such as those of catabolites or different glycosylation isoforms, are present in the sample, deconvolution is a more direct and effective way to visualize the data.

### 10.1.1 LC-MS bioanalysis of mAb

Monoclonal antibodies and related products represent one of the most promising and fast-growing classes of therapeutics. Even though the bioanalytical platform for mAb has been predominantly LBA, there have been increased numbers of applications on quantitation of mAb using LC-MS. This is particularly true for discovery study support when a specific reagent may not be readily available at an early stage before the identification of the final candidate for development. The general workflow for nonclinical LC-MS bioanalysis of mAb involved trypsin digestion and LC-MRM analysis of surrogate peptides, which are typically the conserved sequences of the human Fc region on the mAb. The choice of sample preparation depends on the required sensitivity and type of biological matrix. Protein precipitation followed by digestion of the pellet, a process known as pellet digestion, has been widely used because it is easy to operate and does not require specific reagents [50]. For better sensitivity, immune-affinity capture using antihuman Fc can provide an effective and selective cleanup of human mAb from nonclinical samples. For clinical samples, more specific capturing reagents such as the antiidiotype antibody against epitope in CDR of the mAb can be used to avoid pulling down endogenous human IgGs. Alternatively, the target protein of the mAb can also be used as an affinity capture reagent. Either way, caution has to be exercised to evaluate interference from endogenous targets on the capturing process and to understand whether the measured concentrations are those of free (not occupied by target) or total mAb. Due to the highly specific detection by LC-MS, it is possible to monitor certain modifications on the molecules. One example is deamidation, a common and spontaneous biotransformation of mAb. It has been shown that deamidation at a certain region of mAb could impact its binding affinity, potency, safety, and pharmacokinetics [51]. The surrogate peptide containing Asn, the deamidation product Asp, and the succinimide intermediate can be separated on LC and monitored by MRM to evaluate the relative levels of each species, which helps understand the dynamics of this *in vivo* biotransformation [52, 53].

The emerging technique of intact protein bioanalysis has also been exemplified on mAb in a few publications. Our lab published a workflow of quantifying large proteins in biological samples by using immune-affinity capture coupled to LC-HRMS analysis [35]. The deconvoluted intact mass spectra were processed for quantitation using a research version of the software. This deconvoluted approach was also compared with EIC and demonstrated similar bioanalytical performance in terms of sensitivity, linearity, accuracy, and precision. More importantly, the intact concentration data generated for an *in vivo* monkey PK study showed results consistent with those by the more commonly used bottom-up approach, confirming the suitability of quantifying mAb using the intact quantitation method [49]. For better sensitivity and detection resolution, mAb can be broken down into relatively smaller “intact” pieces by using reducing reagents to dissociate the light chains and heavy chains. Furthermore, mAb can be specifically cleaved around the hinge region by the IgG

protease such as IdeS to reduce the size of the heavy chain. This procedure generates three types of fragments, light chain, Fd, and Fc/2, each ~25kDa. The application of this “middle-down” approach has been demonstrated for monitoring of in vivo changes of critical quality attributes (CQA) such as glycosylation of mAb, which may play important roles in their function and PK properties [54].

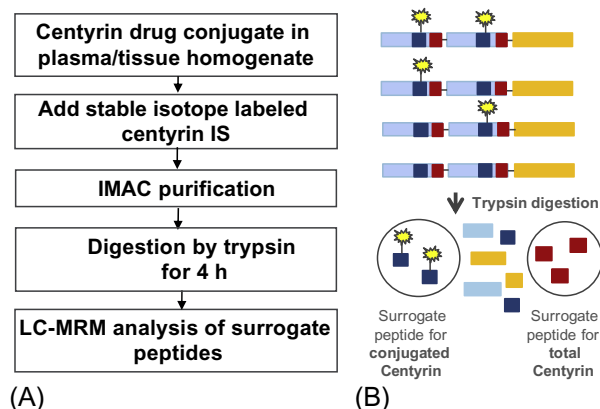
### 10.1.2 LC-MS bioanalysis of ADC

ADCs have shown great promise as novel therapeutics for treatment of cancer due to their capability to deliver potent cytotoxic agents to targeted cells, thereby reducing systemic exposure, increasing drug concentrations at the disease site, and broadening the therapeutic window. Due to their highly heterogeneous and complex structure and complicated biotransformation, multiple analytes are to be measured for an ADC to fully describe its PK in vivo: (1) total antibody for antibody related properties; (2) conjugate for activity related properties; and (3) the released small molecule payload and/or its catabolites for toxicity [55]. LC-MS has been applied in the bioanalysis of each of the analytes to different extents. The released payload/catabolites, due to their small molecule nature, are commonly analyzed using LC-MS. Total antibody is typically measured LC by LBA but can also be quantified by using immuno-affinity capture followed by enzyme digestion and LC-MS/MS analysis of the surrogate peptide. Conjugates are assessed in one of two forms, conjugated antibody or conjugated payload. A conjugated antibody is usually quantified by LBA but can also be measured by hybrid LBA LC-MS using the antipayload capture, followed by digestion and detection of the surrogate peptide from the antibody. Alternatively, for a payload conjugated by an enzymatic/chemical cleavable linker, the conjugated payload can be quantified by using the antiantibody capture, followed by release of the payload, which in turn is measured by the LC-MS method [56]. In addition to the bottom-up method, the top-down intact analysis has been applied to in vivo samples to understand the dynamic change of DAR (drug antibody ratio), metabolism of payloads on the antibody, and the fate of the dissociated payload which may bind to endogenous proteins such as albumin [57–59].

### 10.1.3 LC-MS bioanalysis of PDC

In recent years, novel nonantibody scaffold proteins have emerged as a platform to construct protein-drug conjugates to overcome challenges associated with antibodies such as complex structure and requirement for a mammalian expression system. These novel proteins possess a similar targeting binding capability but are of a much smaller size and have a simpler structure than antibodies. They are usually domain-size proteins absent of disulfide bonds or glycosylation, can be readily generated in the bacterial expression system in large quantities, and of superior thermostability making production, purification, and storage relatively easy [60]. They can be mutated to incorporate a linkage site for cytotoxic payload to construct protein-drug conjugates (PDC). Similar to ADC, it requires multiple analytes to understand the PK properties of a PDC. In our lab, an affinity-capture based LC-MS/MS method was developed to simultaneously quantify total protein and conjugated protein in plasma and tissue for a novel PDC constructed with Centyrin, an engineered scaffold protein based on the consensus sequence of fibronectin type III domains (FN3 domains) from human Tenascin C [61]. Fig. 2 depicts the workflow which utilizes immobilized ion affinity chromatography (IMAC) to extract the analytes, followed by trypsin digestion and LC-MRM analysis

**FIG. 2** (A) The workflow to quantify total and conjugated Centyryn in mouse plasma and tissue samples. (B) The scheme showing the surrogate peptides representing conjugate and total Centyryn, respectively. Overall structure of Centyryn drug conjugate is shown as two identical Centyryn motifs (light blue color), each containing one conjugation site and an albumin binding domain (orange color). Reprint with permission from C. Shi, S. Goldberg, T. Lin, V. Dudkin, W. Widdison, L. Harris, et al., *Bioanalytical workflow for novel scaffold protein-drug conjugates: quantitation of total Centyryn protein, conjugated Centyryn and free payload for Centyryn-drug conjugate in plasma and tissue samples using liquid chromatography-tandem mass spectrometry*, *Bioanalysis* 10 (20) (2018) 1651–1665.



of surrogate peptides. The peptide containing the linker and payload was monitored to quantify the conjugated Centyryn while peptide from a region that does not contain the linker was analyzed as a surrogate of the total Centyryn protein [62, 63]. This approach can be considered as a choice for PK support of other scaffold PDCs as well as next generation site-specific ADCs.

#### 10.1.4 LC-MS bioanalysis of protein biomarkers

Endogenous peptides or proteins such as cytokines, hormones, or enzymes often need to be monitored as biomarkers to elucidate the status of diseases, engagement of target, and effect of drug treatment. The challenges of analyzing biomarkers such as choice of matrix is well discussed in other sections of this chapter. Peptide/protein biomarkers present the additional challenges of being of large size, potentially unstable, heterogeneous, and less abundant. Novel LC-MS methodologies have been developed to overcome some of the limitations. The heterogeneity of a protein, such as those in posttranslation modifications, could convey biological or pharmacological meaning such as stage of a disease. LC-MS, thanks to its high specificity in detection of molecule structure, can be very effective in elucidating those heterogeneous modifications. For example, we have developed an intact LC-HRMS method to quantify the relative abundance of three different glycosylation forms of the apolipoprotein ApoC3 in human plasma and reveal that the ratio of these forms is correlated to the status of diabetes [64]. The highly abundant nature of the ApoC3 protein made a simple SPE step sufficient for the sample extraction procedure. For protein biomarkers that exist at extremely low concentrations, sequential protein and surrogate peptide immune-affinity capture has been proven to be able to effectively achieve LLOQ at low pg/mL level for protein biomarkers [65].

#### 10.1.5 LC-MS bioanalysis of drug metabolizing enzymes and transporters

Quantitation of drug metabolizing enzymes and transporters in cell lines and tissues has been considered crucial for understanding drug disposition using in vitro-in vivo extrapolation (IVIVE) and PBPK modeling. Tremendous efforts have been made in recent years to

develop reliable methods for absolute quantification of these challenging analytes using LC-MS methods [66]. However, large variability still exists among data obtained from different laboratories. In general, variables involved in analyzing metabolizing enzymes and transporters include but are not limited to incomplete and inconsistent recovery of protein from membrane fractionation and extraction, incomplete and inconsistent digestion of the protein, ion suppression, poor choice of surrogate peptides, and challenges in correlation of expression level and activity. Some of them can be overcome by using a stable isotope labeled internal standard and thorough evaluation of choice of surrogate peptides [67]. Optimization of solubilization and denaturation steps for digestion is also critical because membrane proteins may have transmembrane domains that are not directly accessible for the protease enzyme. Ideally, it is recommended to perform quantitation using a purified protein standard. However, most of the drug metabolizing enzymes and transporters are membrane proteins that are difficult to express and purify in large quantities. Therefore, the common approaches for quantifying those proteins are based on peptide standards, not being able to fully address the variability in extraction recovery and digestion efficiency. For example, a comparison of different methods showed that subcellular membrane fractionation gave incomplete enrichment of the proteins leading to underestimation of protein concentration in comparison to methods using whole tissue lysates [68]. Immuno-affinity capture at the peptide level by using antibodies against the surrogate peptide has been applied to improve sensitivity of the assays. An innovative approach using peptide group-specific antibodies that recognize the short common C-terminal tryptic peptide sequence shared by multiple drug metabolizing enzymes and transporters has been shown to effectively enrich the surrogate peptides for quantitation without the need for the membrane fractionation step [69].

### **10.1.6 LC-MS bioanalysis of half-life extended biotherapeutics**

Many peptides or proteins exhibit excellent bioactivity but are limited in their potential as biotherapeutics due to their short *in vivo* half-life caused by proteolytic degradation and/or urinary clearance. Strategies to extend half-life, such as conjugation to polymers, fusion/conjugation to Fc, mAb, or serum albumin, have been extensively investigated in recent years [70]. These novel modalities require innovative bioanalytical approaches to assess their stability and ADME properties. The bottom-up approach, by monitoring surrogate peptides, originated from different parts of the protein, for example, peptide from functional region versus that from the half-life extension scaffold, can reveal the dynamic change of the concentrations of each part of the molecule during circulation. The top-down approach, on the other hand, elucidates high-level structural alteration such as proteolytic degradation and helps pinpoint the catabolic soft spots which can be potentially modified to improve the stability. In our lab, both approaches are utilized in an integrated way for novel half-life extended molecules. This workflow is exemplified by a recent publication using dulaglutide, a GLP1-Fc fusion protein, as the model molecule [19]. In this work, dulaglutide dosed to mice, along with its *in vivo* catabolites, was purified from plasma using an anti-Fc antibody, followed by trypsin digestion and LC-MS/MS analysis on a triple quadrupole instrument, or by LC-HRMS analysis on a triple TOF mass spectrometer without digestion. In Fig. 3, the total Fc concentration (red line) was measured using a surrogate peptide on Fc by the bottom-up approach while the top-down intact assay was able to simultaneously quantify the intact concentration (green line) and reveal the proteolytic cleavage sites on the molecules. The data revealed that

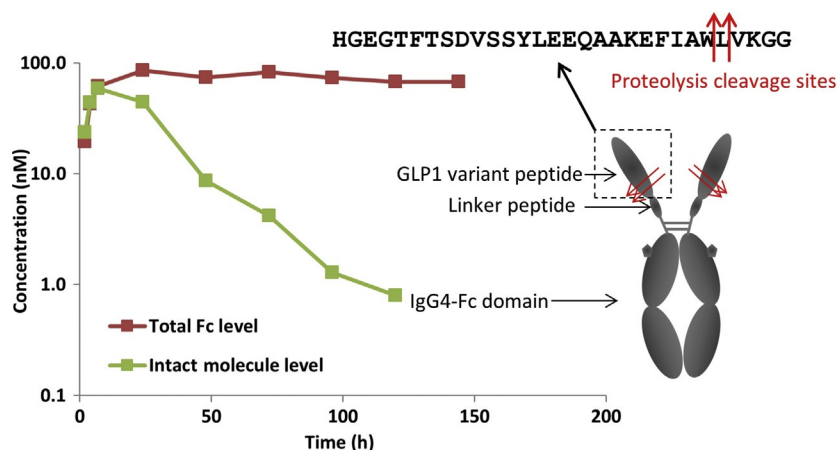


FIG. 3 Simultaneous catabolite identification and quantitation of dulaglutide at intact level by immune-affinity-LC-HRMS. Inserts show the sequence of GLP1 peptide on dulaglutide and the structure of the whole molecule. Reprint with permission from L. Kang, R.C. Camacho, W. Li, K. D'Aquino, S. You, V. Chuo, et al., *Simultaneous catabolite identification and quantitation of large therapeutic protein at the intact level by immunoaffinity capture liquid chromatography-high-resolution mass spectrometry*, *Anal. Chem.* 89 (11) (2017) 6065–6075. Copyright (2017) American Chemical Society.

while the Fc maintains stability at high concentration during circulation, GLP1 peptides fused to it are subjected to proteolytic degradation, leading to loss of intact concentration. The integrated LCMS approach provided an effective way to understand the in vivo fate of the half-life extended molecules.

## 10.2 LC-MS bioanalysis using microsampling

### 10.2.1 Microsampling sample collection in bioanalysis

Microsampling generally refers to a sample of  $\leq 50 \mu\text{L}$  and is commonly used in discovery and dose range finding studies. Recently, its application has been expanded to GLP and clinical studies. The principles of the 3Rs (Replacement, Reduction, and Refinement) were developed 50 years ago to provide a framework for performing humane animal research. Nonclinically, the use of animals can be reduced if the satellite TK and the main study groups can be consolidated. For clinical studies, the collection of lower sample volumes can be greatly beneficial, especially for pediatric studies. For small molecules pharmaceuticals and biomarkers, high sensitivity LC-MS is the technique of choice while miniaturized LBA such as Gyrolab<sup>R</sup> is the choice of instrument for supporting bioanalysis of microsampling for large biological molecules and biomarkers. Microsampling sample collection can be divided into liquid microsampling and adsorption techniques. Depending on the matrix of choice, either blood, plasma, urine, or other oral fluids can be collected and analyzed in smaller volumes.

### 10.2.2 Microsampling in blood and plasma

For blood microsampling, capillary microsampling sampling (CMS), dry blood spot (DBS) sampling as well as volumetric adsorptive microsampling (VAMS) can be utilized to collect

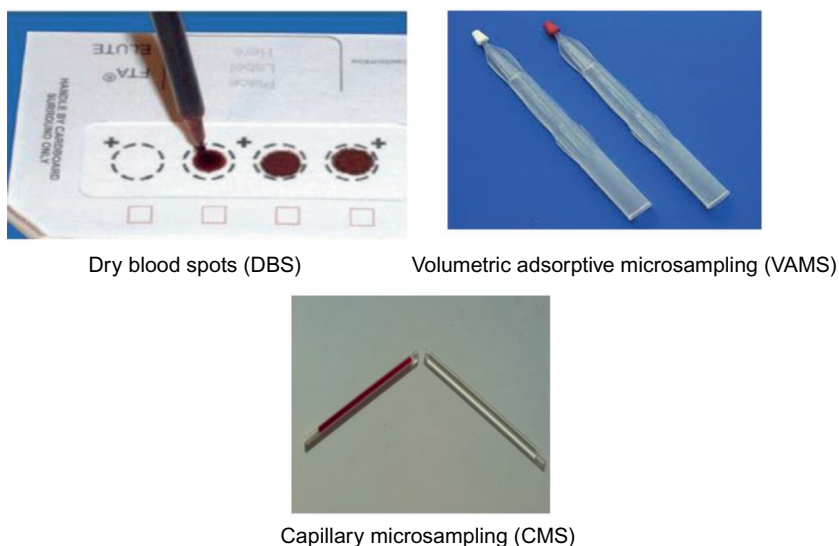


FIG. 4 Microsampling sample collection techniques.

the samples. All three sampling techniques are shown in Fig. 4. For capillary microsampling, the blood is collected in a capillary tube coated/uncoated with an anticoagulant of known volume. Prior to analysis, the blood sample is further diluted by adding aqueous or organic solvents. For DBS, a drop of blood is collected on a filter paper. Then, an accurate volume of blood from the filter paper is collected via a fixed diameter subpunch of the spot. This spot is further extracted by adding aqueous or organic solutions, analyzed by LC-MS for drug concentrations. For VAMS, the samples are collected on an adsorbent tip. The VAMS sampler can absorb a fixed volume of blood ( $\sim 10 \mu\text{L}$ ) in 2–4 s with less than 5% volume variation across the hematocrit range of 20%–70% with low tip-to-tip variability [71]. With DBS, homogeneity as well as the hematocrit of the blood sample is the main concern. Regulatory agency acceptance is still a major concern for DBS and VAMS, though regulators have been open about the utilization of new technology in sample collection. Blood to plasma partition ratio should be considered when determining exposure using blood samples. In most of the clinical studies, plasma sample collection is the method of choice. If nonclinical studies are supported with blood microsampling, data should be interpreted from blood to plasma to support clinical studies. In some instances, if the compound is unstable in whole blood, the stability experiments in whole blood should be done up front [72]. The effect of drying conditions such as the drying time of the compound in blood on the DBS card as well as VAMS should also be evaluated in the method development and validation experiments. The other advantage of using DBS cards and VAMS is the relative ease of sample collection, shipment, and storage, although temperature and humidity need to be controlled. In fact, both DBS and VAMS are suitable for other biological matrices such as urine, plasma, and oral fluids across a wide range of sampling conditions [73].

For plasma microsampling, CMS can be utilized to collect the samples. The blood sample is collected in an anticoagulant coated capillary which can collect either 64 or 32  $\mu\text{L}$  of fixed



volume. The blood-filled capillary tube is then processed to generate plasma which is further transferred into another capillary via a capillary action that can hold an exact volume of 10, 8, or 4  $\mu\text{L}$ . The exact volume plasma capillary is placed in plastic container tubes for storage and shipping. To analyze the samples, the plasma in the capillary is rinsed out using a diluent such as phosphate-saline buffer (PBS), BSA, water, or plasma to generate enough volume for sample analysis [74]. The volume of the diluent can be 5-fold or 10-fold depending on the sensitivity of the bioanalytical assay.

### **10.2.3 Bioanalytical method development for microsampling in blood and plasma**

A bioanalytical method should be developed and validated before the in-life phase of the microsampling sample collection is initiated. While developing and validating a method, sample collection, handling, and storage should be considered [75]. The sample collection capillaries as well as the container tubes used to store QC samples and QCs should be evaluated for any nonspecific adsorption loss and the containers for samples and QCs should preferably be of the same material. The other key component to consider during method development is the sensitivity of the compound on the LC-MS instrument. With recent advances in high sensitivity instrumentation, it is feasible to use a lower sample volume for sample extraction as well as quantitation without significantly affecting the assay curve range. The route of administration in a toxicological study should also be considered while developing assays for microsampling. For example, dermal and inhalation studies may have a lower systemic exposure of a compound and a smaller sample collection volume may not be enough to provide the sensitivity needed for an analytical assay. Certain classes of compounds such as peptides, oligonucleotides as well as vaccines may present analytical challenges to achieve the desired LLOQ and therefore require larger volumes. In these cases, microsampling may not be the ideal choice. During drug development, if both traditional and microsamples are used to support studies for a program, bridging the studies by validation experiments should also be considered.

During method development of DBS, sample collection microcards, extraction solvents, hematocrit, homogeneity, and stability are important factors which should be evaluated. If the DBS samples collection cards are not evaluated properly and if incorrect paper is used, it may result in poor recovery and/or reproducibility which can delay or even jeopardize the whole study. When blood is spotted on the card at ambient temperature, the humidity might have a potential impact on the size of the blood spot and the speed of drying. The conditions encountered by the sample should be evaluated and stability under those conditions should be demonstrated. Long-term stability of the analyte under the storage conditions which are likely to be encountered by the sample should be demonstrated [76].

During method development and validation of VAMS, sampling parameters such as exposure time, drying time, temperature, humidity, and light exposure should be evaluated. While filling the tips of the VAMS device, care should be taken that the tips do not immerse past the tip shoulder as it could result in excess blood being retained by the shoulder. While drying the tips, it should be ensured that the tips do not touch other tips or surroundings to prevent any cross contamination.

During method development of a compound using CMS, sample volume as well as assay sensitivity (targeted LLOQ) should be evaluated first. There should be enough volume so that the sample can be reassayed (if needed) as well as tested for ISR. The bioanalytical method

should be validated as per the bioanalytical method validation guidance [77]. The bioanalytical sample should mimic the test samples; for that reason, QC samples should be prepared in bulk and transferred into the same type of capillary in which the samples are to be collected and stored [78]. Benchtop freeze-thaw stability as well as long-term stability should be performed with and without diluent to cover the stability in both plasma as well as the plasma-diluent mix. In certain cases when samples are transferred from a centrifuged capillary to an exact volume capillary, there might not be enough sample volume or there might be an air bubble formed during the transfer. In these cases, the sample may need to be further transferred to a smaller size capillary, e.g., from a 10  $\mu$ L capillary to a 4  $\mu$ L one. To cover this scenario of collection of samples in capillaries of two different volumes, the method validation should be carried out for both sets of capillaries (10  $\mu$ L as well as 4  $\mu$ L). For labile compounds or unstable metabolites, when the samples need to be stabilized by adding a stabilizer, CMS might not be ideal because, in general, a stabilizer should be added in blood during collection or in plasma after centrifugation, which is not feasible for CMS. In the case when the stabilizer is added to the container of the capillary for storage and shipping, the homogeneity of the sample may not be achieved even after vortex, and therefore the effectiveness of the stabilizer may not be guaranteed. For that reason, labile compounds should be properly evaluated with and without addition of the stabilizer before a decision is being made about using CMS. Practical considerations such as study timelines should also be evaluated while validating the method with CMS. For example, a procedure using CMS may take longer than a traditional method due to capping and uncapping of the small tubes used for capillary storage. Use of automation for those procedures should be considered to avoid ergonomic injuries to the bioanalysts.

Finally, communication between bioanalysts and toxicologists or clinical scientists is a must when developing and validating the analytical methods using microsampling sample collection techniques. All the key factors including study design, practical aspects, in-life capabilities as well as analytical method development/validation timelines should be discussed before starting the in-life phase of the study.

### 10.3 Biomarkers quantitation

Over the last decades, endogenous bioactive small molecules, peptides, and proteins have been increasingly used as biomarkers in the drug discovery and development processes. One of the biggest challenges for biomarker quantitation originates from the endogenous nature of the target analytes. An authentic control blank matrix without the presence of the biomarker is typically unavailable, with exceptions where the biomarker level change is very significant. This also presents a significant challenge for establishing biomarker bioanalytical assays, which is how to confirm the assay selectivity [79]. Typical selectivity tests routinely used in bioanalytical LC-MS assays for PK analysis, such as evaluating interference peaks in the control blank matrix lots, are no longer adequate to deal with the endogenous nature of the biomarkers. Various approaches have been proposed to confirm the assay selectivity for biomarker LC-MS analysis. The important step toward establishing sound biomarker assay selectivity is to understand the biological/chemical origin of the analyte, and to acquire as many of the known isobaric isomers as possible and then test them to ensure that they are



chromatographically resolved from the target biomarker peak. A recently introduced ion-mobility device on a tandem mass spectrometer might be useful to enhance assay selectivity by providing another dimension of separation.

In terms of quantitation strategy, along with the straightforward authentic analyte and authentic matrix method, both “surrogate matrix” and “surrogate analyte” approaches have also been routinely and successfully applied to endogenous biomarker LC-MS analysis [80–83]. Regardless of the approaches, it is recommended that at least one level of QC samples should be prepared in an authentic matrix to better reflect the analyte stability and assay accuracy. Additionally, parallelism between the response curve obtained from serially diluted incurred samples and that of calibration standards should be investigated to reveal potential matrix effects and interference to critical reagents of the assays.

### **10.3.1 Leukotriene B<sub>4</sub> (authentic matrix and authentic analyte)**

Leukotriene B<sub>4</sub> (LTB<sub>4</sub>) is an important inflammatory biomarker in several diseases. An LC-MS/MS method for the determination of LTB<sub>4</sub> in plasma from ex vivo stimulated human blood, using LTB<sub>4</sub>-d<sub>4</sub> as the internal standard (IS), was developed and validated. An authentic matrix and authentic analyte approach was used because normal human plasma does not contain detectable LTB<sub>4</sub> without stimulation [84]. The chromatographic separation of LTB<sub>4</sub> from its three isobaric isomers (6-trans-LTB<sub>4</sub>, 6-trans-12-epi-LTB<sub>4</sub>, and 12-epi-LTB<sub>4</sub>), which share the same multiple reaction monitoring (MRM) transitions as the analyte, from human plasma was crucial to achieve the accurate determination of 0.2 ng/mL (LLOQ) of LTB<sub>4</sub>. LTB<sub>4</sub> and the IS were extracted with methyl tertiary butyl ether (MTBE) from 200- $\mu$ L human plasma. Comparison of the validated LC-MS/MS method with an ELISA method using ex vivo stimulated samples indicated that results from the two assays correlated relatively well ( $R^2 = 0.92$ ). This further confirms the specificity of the LC-MS assay.

### **10.3.2 4 $\beta$ -Hydroxylcholesterol and 7 $\alpha$ -hydroxy-4-cholesten-3-one (C<sub>4</sub>) (surrogate matrix and authentic analyte)**

Evaluation of clinically relevant drug-drug interaction (DDI) due to induction or inhibition of cytochrome P450 (CYP450) enzyme activity has been routinely assessed by using a probe CYP450 substrate (or a mixture of substrates) in DDI studies. While this is the current standard for regulatory submissions, it does require a separate protocol in a crossover design. Advantages of using an endogenous biomarker such as 4 $\beta$ -hydroxylcholesterol, which is formed through a CYP3A4/5 catalyzed metabolism of cholesterol, as an alternative probe substrate to evaluate P450 3A4/5 DDI, have been documented in the literature [85]. The advantage of this approach is its noninvasive nature, as well as resource sparing, as this can be a secondary objective in a Phase I clinical study and can be applicable to studies in patients.

Several isobaric positional isomers of 4 $\beta$ -hydroxylcholesterol generated from the biological pathways may exist in the biological matrix which share the same MRM transitions as the analyte, therefore causing selectivity problems. In particular, it is essential to achieve desirable chromatographic resolution of 4 $\beta$ -hydroxylcholesterol from 4 $\alpha$ -hydroxylcholesterol since both can be formed upon auto-oxidation during sample processing while the in vivo biotransformation only leads to the formation of 4 $\beta$ -hydroxylcholesterol [86]. Monitoring the 4 $\alpha$ -hydroxylcholesterol level in the plasma sample can be used as an indicator whether

the sample stability has been compromised [87]. In this reported study, while the calibration standards were prepared in water, quality QC samples were prepared in human plasma to mimic the incurred study samples. After being alkalized with potassium hydroxide, the human plasma sample (50  $\mu$ L) was extracted with hexane, derivatized into picolinyl esters using picolinic acid, extracted again with hexane, and then analyzed by LC-MS/MS.

7 $\alpha$ -Hydroxy-4-cholesten-3-one (C4) is a stable intermediate in the rate limiting pathway of bile acid biosynthesis [88]. It is an oxidative enzymatic product of cholesterol metabolism via cholesterol 7 $\alpha$ -hydroxylase, an enzyme also known as cholesterol 7- $\alpha$ -monooxygenase or cytochrome P450 7A1 (CYP7A1). Plasma C4 levels correlated with CYP7A1 enzymatic activity and could be used as a biomarker for bile acid synthesis [89]. An LC-MS/MS method was developed and validated to quantify C4 in rat and monkey plasma [82]. Using a surrogate matrix approach, calibration standards were prepared in 50/50: acetonitrile/water (v/v), while the QC samples were prepared in authentic plasma to mimic the incurred samples. Stable isotope labeled C4 (C4-d<sub>7</sub>) was used as the internal standard. A simple protein precipitation with acetonitrile was used to extract C4 from plasma (20  $\mu$ L). The low limit of quantitation was set up at 1 and 0.5 ng/mL for rat and monkey plasma. As in the case for LTB<sub>4</sub>, chromatographic separation of isobaric isomers from the C4 peak is also very critical to ensure the assay specificity (Fig. 5).

### 10.3.3 Fatty acid amide hydrolase biomarkers (authentic matrix and surrogate analytes)

Endogenous ethanolamides, including arachidonyl ethanolamide (anandamide, AEA), oleoyl ethanolamide (OEA), and palmitoyl ethanolamide (PEA), are substrates of fatty acid amide hydrolase (FAAH) and are potential pharmacodynamic biomarkers for the target engagement for FAAH inhibition by novel pharmaceutical agents [90]. LC-MS/MS quantitation of AEA, OEA, and PEA in human plasma simultaneously using D<sub>4</sub>-AEA, D<sub>4</sub>-OEA, and <sup>13</sup>C<sub>2</sub>-PEA as “surrogate analytes” was established [81]. This approach enabled preparation of calibration standard and QC samples in plasma devoid of interferences from the endogenous analytes with the LLOQ below the basal levels. Assay performance and stability were also demonstrated by using another set of QCs, prepared with authentic AEA, OEA, and PEA. LLE in a 96-well plate format was used to extract the analytes from 0.15 mL of human plasma. A second set of stable labeled compounds D<sub>8</sub>-AEA, D<sub>2</sub>-OEA, and D<sub>4</sub>-PEA was used as the internal standard.

A significant elevation of ethanolamide concentrations (~1.3- to 2.0-fold on ice and ~1.5- to 3.0-fold at room temperature by 2h) in fresh blood immediately following collection revealed that the de novo synthesis and release from blood cells was the predominant factor affecting ethanolamide concentrations ex vivo. Therefore, to minimize the ex vivo elevation of plasma ethanolamide concentrations, it was important to have conditions that ensured rapid separation of plasma from blood cells as well as consistency in the blood harvesting procedures. In a Phase 0 study that simulated the design of single-ascending dose and multiple-ascending dose clinical trials, the variability (intra-subject and intersubject) of plasma ethanolamide levels was evaluated. The data indicated that there was relatively large inter- and intra-subject variation in plasma ethanolamide concentrations due to the collection at different times of day and/or food effects.

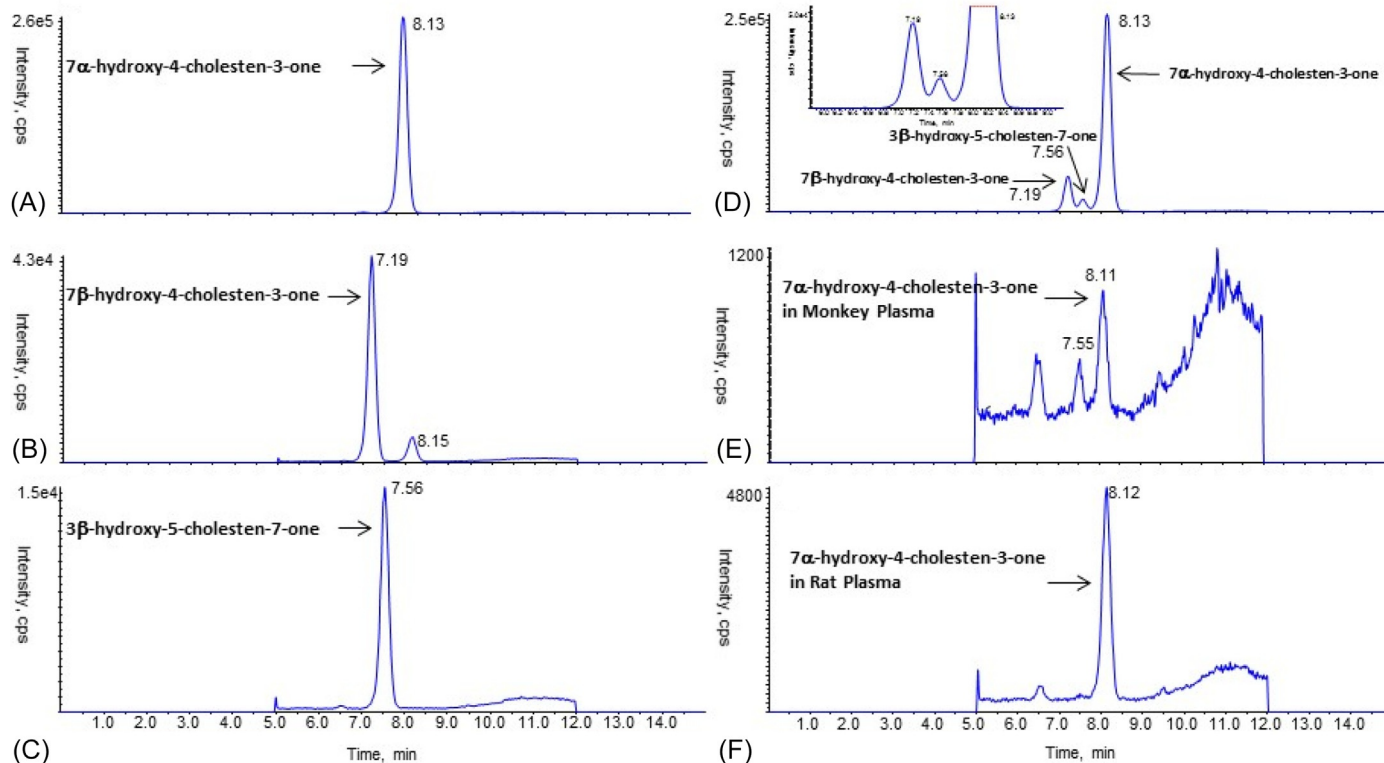


**FIG. 5** MRM chromatograms (401.4→177.2) of  $7\alpha$ -hydroxy-4-cholesten-3-one neat solution at 40 ng/mL (A),  $7\beta$ -hydroxy-4-cholesten-3-one neat solution at 40 ng/mL (B),  $3\beta$ -hydroxy-5-cholesten-7-one neat solution at 40 ng/mL (C),  $7\alpha$ -hydroxy-4-cholesten-3-one/ $7\beta$ -hydroxy-4-cholesten-3-one/ $3\beta$ -hydroxy-5-cholesten-7-one mixed neat solution at 40/40/40 ng/mL (D), control monkey plasma,  $7\alpha$ -hydroxy-4-cholesten-3-one- $d_7$  measured to be 1.88 ng/mL (E), control rat plasma,  $7\alpha$ -hydroxy-4-cholesten-3-one- $d_7$  measured to be 14.4 ng/mL (F). Reprint with permission from L. Kang, T.M. Connolly, N. Weng, W. Jian, LC-MS/MS quantification of  $7\alpha$ -hydroxy-4-cholesten-3-one (C4) in rat and monkey plasma, *J. Chromatogr. B Anal. Technol. Biomed. Life Sci.* 1064 (2017) 49–55. Copyright (2017) Elsevier.

## 10.4 LC-MS analysis of metabolites and MIST

The background of MIST is well covered in [Chapter 15](#). The Initiation of industry and FDA dialogues on MIST can be traced back to an early landmark publication titled “Drug metabolites in safety testing” in 2002 [91]. In 2008, the US FDA issued the Guidance for industry: safety testing of drug metabolites [47]. Metabolites at or above 10% of parent AUC at steady state need to be quantified. In 2009, the International Conference on Harmonization published guidance on nonclinical safety studies for the conduct of human clinical trials and marketing authorization for pharmaceuticals M3(R2). It is agreed that metabolites at or above 10% of total drug related exposure at steady state need to be quantified, which is also adopted by the current FDA guidance on MIST [92]. It should be noted that the intended safety testing generally is not required for Phase 2 metabolites except for acyl glucuronides. In a simplistic view, bioanalysis of metabolites in accordance with MIST is usually performed according to the following strategy. After identification and profiling of human metabolites from the SAD/MAD study, quantitation of major human metabolites in the MAD study as well as in GLP toxicology studies was conducted to establish metabolite exposure coverage.

Bioanalytical characteristics for MIST support can be quite different from the parent PK assay. For the parent drug candidate, usually a single analyte is measured in one assay while for metabolites, multiple molecules, usually more polar than the parent, are to be analyzed. They are either highly similar (such as Phase 1 metabolites) to or very different (such as Phase 2 metabolite) from the parent drug and therefore present analytical challenges. Chromatographic resolution of the Phase 1 metabolites from the parent or from each other, especially for the positional hydroxyl metabolites which have the identical molecular weights (isobaric) and show up in the same MRM channel, might be a challenge. On the other hand, eluting both the parent and the Phase 1 metabolites and Phase 2 conjugates under the same chromatographic condition is also difficult, even with a gradient elution. Often, the reference standards for the metabolites are not as well defined as for the parent compound and the certificate of analysis (COA) might be unavailable. A stable isotope internal standard may not also be available for metabolite quantitation. Since multiple metabolites may be measured in a single assay and their clearance may not be in parallel to the parent or to each other, a lopsided and complicated standard and QC preparation scheme might be followed. Unlike the parent drug for which the liability is usually well identified, the potential stability issue such as conversion between the metabolites could be unknown at the time of metabolite bioanalysis.

### 10.4.1 Metabolite quantitation strategy

Generally, the tiered approach for metabolite measurement is well established in the industry and is also acceptable by the regulatory authorities. Four tiers with increased qualification requirement and resource commitment are usually employed and the choice of the tier depends on the drug development stage [93, 94]. It is worth mentioning that the stability of metabolites should be evaluated since GLP samples are usually not fresh (collected in much earlier days) when metabolite exposure coverage is assessed. Catch-up stability is performed in a bioanalytical lab for most of the cases. Alternatively, MIST coverage can also be established using the samples from ongoing longer-term GLP tox studies.

First tier assays include response ratios (UV, MS) from profiling single or multiple dose human in vivo and in vitro samples. This can be used as the first indication of possible unique or disproportionate human metabolites when comparing the data from nonclinical toxicology species (rat, dog, monkey, etc.).

Second tier assays include selective and sensitive LC-MS/MS methods for targeted metabolite quantitation. A biologically isolated reference standard might be used. Crude radio-labeled compounds isolated from in vitro samples might be used to calibrate the LC-MS response. In our laboratory, we also developed a standard-free bioanalytical approach for absolute quantitation of drug metabolites utilizing biosynthesized reciprocal radio and stable isotopologues [95]. Since authentic metabolite standards are not required under this dual radio and stable isotopologue strategy using standard LC-radioactivity detection (RAD)/MS protocols, significantly fewer resources are required to support accurate metabolite quantitation, which in turn enables efficient analysis of complex profiles.

While the first and second tier assays are usually performed in the biotransformation group, the third tier assay is usually performed in the bioanalysis group and uses the LC-MS assay with qualified standards for MIST support. Typically, separate assays (not in the same assay for the parent drug measurement) were used for metabolites measurement. Qualification was conducted with 4-6-15/20 acceptance criteria with limited verification on assay performance and stability. Chemically synthesized reference standards are usually employed. Assessment of exposures in IND enabling toxicology studies and human SAD/MAD studies was used to establish the metabolite coverage. One commonly used strategy for metabolite quantitation is to adopt the stable isotope labeled parent drug (P STIL) as the internal standard in the LC-MS/MS assay. It was demonstrated that this strategy could have a potential pitfall resulting in quantitation bias if the P STIL is subject to ion suppression from the co-eluting parent drug in the incurred samples [96]. In that case, the metabolite concentration measured by using P STIL could be overestimated in comparison to that obtained using stable isotope labeled metabolite (M STIL) as demonstrated in the example (Fig. 6).

Therefore, STIL for each metabolite is preferred, and sometimes this can be achieved by generating the mixture of STILs for metabolites in vitro [97].

The final tier is a validated assay for those metabolites that need further assessment in Phase II/III studies. They include metabolites with significant activities or toxicities, and disproportional or unique human metabolites as the outcome of MIST assessment. Usually, the parent drug and metabolites are combined in a single assay. Assay validation and sample analysis follow the FDA guidance for bioanalytical assay. Reference standards with a reputable source and COA are required and investment of making stable labeled internal standards for both the parent and metabolites is essential.

#### **10.4.2 LC-MS bioanalysis of polar metabolites**

Polar metabolites are difficult to analyze using a typical reversed phase LC-MS/MS because of poor chromatographic retention that leads to significant matrix effects, low sensitivity, and inadequate separation. Co-elution of isobaric or unstable metabolites may cause errors in quantification. To overcome this challenge in our laboratory, we have been routinely using hydrophilic interaction chromatography (HILIC) in conjunction with tandem mass spectrometry (HILIC-MS/MS) for polar metabolite quantitation. HILIC is a variation of

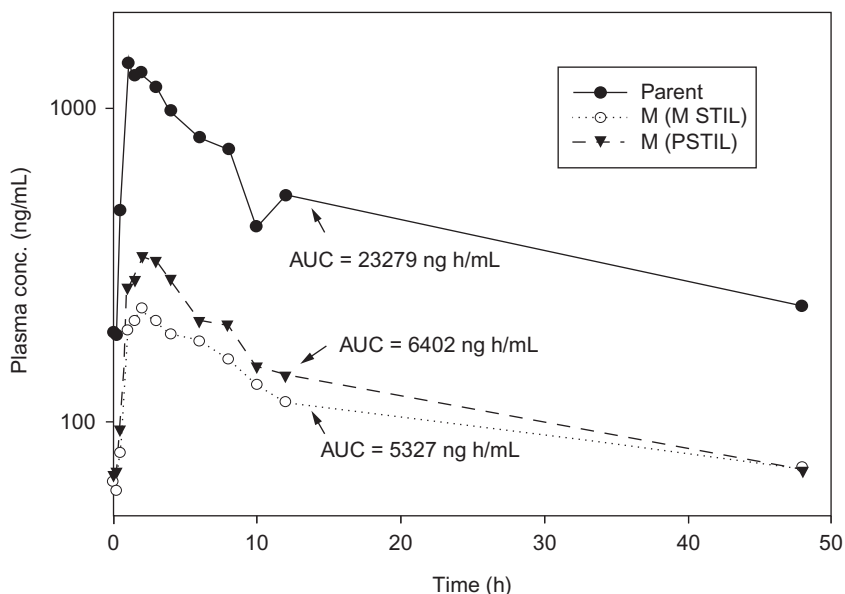


**FIG. 6** Plasma concentration—time course of compound A (Parent drug), and MA (Metabolite A), following repeated dosing of compound A for 14 days, determined using either D4-MA (M STIL) or D5-compound A (P STIL) as the internal standard, following a repeated dose of compound A for 14 days. AUC of MA was overestimated by 20.2% by using the STIL of the compound A as the internal standard. The insert shows MA concentration using a linear axis for comparison. Reprint with permission from W. Jian, R.W. Edom, Y. Xu, J. Gallagher, N. Weng, *Potential bias and mitigations when using stable isotope labeled parent drug as internal standard for LC-MS/MS quantitation of metabolites*, *J. Chromatogr. B Anal. Technol. Biomed. Life Sci.* 878 (31) (2010) 3267–3276. Copyright (2010) Elsevier.

normal-phase chromatography (NPLC) without the disadvantage of having to use solvents that are not miscible with water. HILIC has also been referred to as NPLC with an aqueous-organic mobile phase. Under the HILIC conditions, the elution strength from strong to weak is water, methanol, and acetonitrile. For very polar compounds, HILIC offers significantly more retention than reversed-phase liquid chromatography without the disadvantage of using a highly aqueous mobile phase [42]. In our lab, we have found that HILIC leads to much improved chromatographic retention and peak shape as well as much better sensitivity for polar analytes, including metabolites, as shown in Fig. 7 [43]. On the reversed-phase column, metabolite (M1) has little retention with poor peak shape and severe matrix suppression. The sensitivity is improved over at least 10-fold on the HILIC column with much better peak shape and longer retention time to avoid matrix suppression. In the application of HILIC, one should always pay attention to potential overloading of the columns, especially when protein precipitation samples are directly injected. In that case, minimizing the injection volume or dilution of the sample may improve the retention and peak shape. HILIC LC-MS is also more sensitive to the composition of injection solution. Unlike reversed-phase LC-MS, which has better toleration for the mismatch between injection solution and mobile phase and therefore allows injection of a solution with its elution strength stronger than the mobile phase, injection solution for HILIC must remain weaker than the mobile phase.



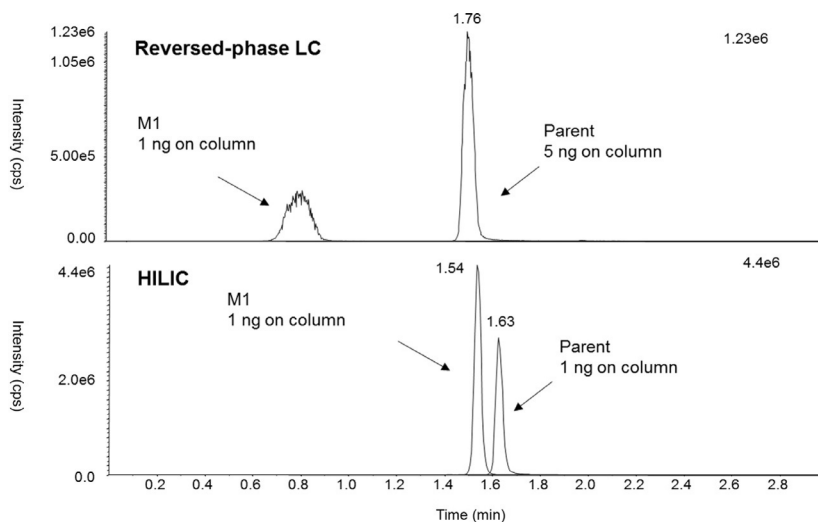


**FIG. 7** LC-MS/MS chromatograms of neat solutions of compound A and its metabolite MA on RP and HILIC columns. (top) Chromatogram of compound A and MA on an RP AquaSep column ( $50 \times 2.1$  mm,  $5 \mu\text{m}$ , ES Industries, West Berlin, NJ). Mobile phase A: 0.1% TFA in water; Mobile phase B: 0.1% TFA in acetonitrile. Gradient condition: 0–0.30 min, 10%B; 0.30–2.00 min from 10%B to 50%B; 2.00–2.50 min, 90%B; return to 10%B at 2.60 min. Flow rate 0.6 mL/min (bottom). The same sample injected onto a Luna Silica (2) column ( $50 \times 2.0$  mm,  $5 \mu\text{m}$ , Phenomenex, Torrance, CA) under HILIC conditions. Mobile phase A: 0.2% formic acid in water; Mobile phase B: 0.2% formic acid in acetonitrile. Gradient condition: 0–0.30 min, 90%B; 0.30–1.50 min from 90%B to 40%B; return to 90%B at 1.60 min. Flow rate 0.6 mL/min. Reprint with permission from W. Jian, Y. Xu, R.W. Edom, N. Weng, *Analysis of polar metabolites by hydrophilic interaction chromatography-MS/MS*, *Bioanalysis* 3 (8) (2011) 899–912.

### 10.4.3 Bioanalysis of chiral compounds

There could be a significant difference in the PK properties and PD behavior of a pair of enantiomeric molecules. In order to evaluate the activity, toxicity, ADME properties of the individual enantiomers, and any potential chiral inversion caused by the biotransformation process, chiral bioanalytical assays may be necessary. Different scenarios of chiral drug development, including development of racemate or fixed ratio (nonracemic) enantiomers, development of a single enantiomer, racemic switches, and quantitation of enantiomeric metabolites may require a different assay strategy. Based on the development strategy and molecular properties of the drug candidate, a nonchiral quantitative assay, a chiral qualitative assay, or a chiral quantitative assay should be chosen [98]. For example, for MIST assessment, if the chiral center of a metabolite was introduced by biotransformation and if the level of introduction is potentially species dependent, a qualitative chiral screening assay may be applied to selected samples to elucidate if the metabolites present in different species are identical enantiomers or in the same ratio.

In a previous published example from our lab, we demonstrated chiral inversion assessment for a drug candidate under development. In this example, JNJ-A was a single R-enantiomer and it could undergo deamination and oxidation to form a hydroxylation

metabolite JNJ-AM, which is the major metabolite of JNJ-A [98]. There is a suspected chiral inversion of JNJ-A, to generate S-enantiomer of JNJ-A, if the metabolizing process that gives rise to JNJ-AM is reversible. To address this specific chiral inversion question, a chiral LC-MS method was developed for the analysis of JNJ-A and JNJ-AM in plasma. Samples from some patients at selected time points at a PK steady state in a Phase II clinical study were analyzed using this qualified screening method where the separation of the two enantiomers was achieved and their storage stability was established. For JNJ-A, only the originally dosed R form was observed; therefore, the conclusion is that JNJ-A appears not to be undergoing chiral inversion in the human body. For JNJ-AM, a single enantiomer peak was observed, indicating that this major metabolite was generated by a stereospecific and irreversible enzyme reaction. This result guides that for further development of JNJ-A, nonchiral quantitative assays were sufficient for measurement of JNJ-A and JNJ-AM.

#### **10.4.4 Unexpected assay challenge during analysis of patient samples**

It should always be kept in mind that validation using spiked standards and QC may not fully address potential analytical issues that could unexpectedly emerge during study sample analysis. Some unusual interference may only present in incurred samples, but not in standard or QC samples as demonstrated in the two examples below.

Ibrutinib is a potent, covalently binding inhibitor of Bruton's tyrosine kinase (BTK). A bioanalytical LC-MS/MS method for measuring ibrutinib and its active major metabolite dihydrodiolibrutinib in human plasma was developed and validated. Selectivity of the assay toward isobaric metabolites and endogenous compounds was optimized and the incurred sample reproducibility and stability were assessed. However, during analysis of plasma samples from a clinical study in hepatically impaired subjects, taurocholic acid was identified as an interference to the internal standard of dihydrodiolibrutinib because of their identical MRM transitions. This interference was only significant in samples from hepatically impaired subjects who had elevated concentration of bile acids in the plasma, but not significant in samples from all the other clinical studies analyzed using the same method. The method was modified to achieve baseline separation between the dihydrodiolibrutinib internal standard and taurocholic acid, and revalidated. The original method and the new method were successfully cross-validated using incurred samples and demonstrated that both the original and revalidated assays are equivalent for the analysis of human plasma samples from nonhepatically impaired subjects [99]. Therefore, the results for nonhepatically impaired subjects that had been generated using the original method remained valid. For the study in hepatically impaired subjects, the samples were reanalyzed using the revalidated assay. Although the interference resulting from the bile acid was only observed in samples from the hepatic impairment study, to avoid any potential interference in future sample analysis, this revalidated assay was used for all the sample analyses of ongoing studies and new studies.

Recently, Yuan and Ji also reported the identification and mitigation of an unexpected isobaric sulfate metabolite interference to a phosphate prodrug [100]. During the LC-MS/MS bioanalysis of a phosphate ester prodrug in plasma samples from rat and monkey GLP toxicology studies, an unknown peak was detected in the MRM channel of the prodrug that would co-elute with the prodrug in their method, causing significant overestimation of the exposure of the prodrug. By using high-resolution mass spectrometry (HRMS), the



interfering metabolite was successfully identified to be an isobaric sulfate metabolite. The phosphate prodrug and sulfate metabolite were separated with baseline resolution in the final optimized chromatographic conditions.

## 11 Conclusion and future perspective

In this book chapter, we discussed the importance, implementation, and challenges of quantitative bioanalysis to enable successful drug discovery and development. Bioanalysis is one of the few disciplines to cover all stages of pharmaceutical research and development, from early discovery to nonclinical studies and all phases of clinical studies. Because of the diversified bioanalytical support from discovery to late phase clinical trials, the science, process, and compliance in any stage need to be balanced for both scientific and compliance rigor. Procedures for meeting today's regulatory requirements and enhancement of scientific input by using contemporary scientific advances, as well as implementation of best practices, are essential so that resources are optimized, project timelines are met, and compliances are followed. Case studies highlighted in this book chapter provide some insights on ensuring the bioanalytical quality by using sound bioanalytical strategy and scientific rigor.

In the future, bioanalysis will continue to play an even more important role in moving the drug candidates along with the discovery and development pipelines due to the better understanding of the biology and biochemistry of the targets as well as advancement in bioanalytical science. For example, the importance of measuring drug candidates and/or their target at the pharmacological sites has long been recognized but its realization was possible only recently. The measurement of free fraction of drug candidates and/or that of the target might provide a better indication of drug target engagement than the plasma concentration of the drug [101–103]. Reactive metabolites that are conjugated to protein, leading to idiosyncratic toxicity, are historically very difficult to be identified and even more challenging to quantify. With advanced instrumentation and a better understanding of protein chemistry, now they can also be quantified, for example, after protein digestion [104]. We will also see the expansion of LC-MS in the area of large molecules, not only for bioanalysis but also for catabolite identification. Multiple bioanalytical platforms including LC-MS (direct intact protein analysis and peptide analysis after enzymatic digestion), ELISA, biomarker assay, and functional bioassays may be used to reveal a more comprehensive picture of the fate of the biotherapeutic in vivo. Even for classic monoclonal antibodies where currently LC-MS bioassays have not been employed routinely, understanding the impact of biotransformation, such as deamination to their activities, has started to be recognized. We will also see the effort of expanding LC-MS-based bioanalytical technologies to other challenging areas such as analysis of oligonucleotide drugs and their metabolites in biological samples where currently sensitivity on LC-MS has not matched other traditional methods such as ELISA or LC-fluorescence assays.

In the future, we will also see bioanalysis being more integrated into quick turnaround decision-making Tox and DMPK studies. Great flexibility of adopting new technologies of reducing animal usage and reducing sample volume will be required. Appropriate resource and assay qualification strategies are important to make sure that bioanalytical organizations

are not too rigid in providing efficient study support. Bioanalysis groups will become more important partners as the demand for bioanalysis always exceeds the available resources, and therefore continuous discussions on what is “needed” versus “nice to have” with the project teams will become even more frequent. Bioanalytical scientists do not just generate data but also own the data and contribute to the data interpretation. Now and even more in the future, bioanalytical scientists will play multiple roles—not only in generating data themselves but also in managing important GLP and clinical studies at CROs. Therefore, they are in charge of budget, quality, and timelines for the bioanalysis. In that sense, good project management skill becomes ever more important.

## References

- [1] W. Li, J. Zhang, F.L.S. Tse, *Handbook of LC-MS Bioanalysis—Best Practices, Experimental Protocols, and Regulations*, John Wiley & Sons Inc., 2013.
- [2] USFDA, US Department of Health and Human Services, US FDA, Center for Drug Evaluation and Research, Center for Veterinary Medicine. <https://www.fda.gov/downloads/Drugs/Guidances/ucm070107.pdf>, 2018.
- [3] EMA—European Medicines Agency, Committee for Medicinal Products for Human Use (CHMP), Guideline on Bioanalytical Method Validation, London, [www.ema.europa.eu/docs/en\\_GB/document\\_library/Scientific\\_guideline/2011/08/WC500109686.pdf](http://www.ema.europa.eu/docs/en_GB/document_library/Scientific_guideline/2011/08/WC500109686.pdf), 2011.
- [4] H. Canada, Bureau of Pharmaceutical Sciences Therapeutic Products Directorate, Addendum to Notice: Clarification of Bioanalytical Method Validation Procedures, (2016).
- [5] C. Pharmacopeia, Section 9012, <http://wp.chp.org.cn/front/chpint/en/>, 2015.
- [6] J.M.o. Health, Japanese Ministry of Health, Labour and Welfare, Guideline on Bioanalytical Method Validation in Pharmaceutical Development, Japan, [www.nihs.go.jp/drug/BMV/250913\\_BMV-GL\\_E.pdf](http://www.nihs.go.jp/drug/BMV/250913_BMV-GL_E.pdf), 2013.
- [7] I.H. Guideline, Bioanalytical Method Validation M10 Draft Version, Endorsed on 26 February 2019, <http://www.ich.org/ichnews/newsroom/read/article/new-ich-m10-guideline-in-development-on-bioanalytical-method-validation.html>, 2019.
- [8] P. Timmerman, S. Lowes, S. McDougall, I. Colligon, J. Miksic, S. Chowdhury, et al., Scientific or regulated validation: a tiered approach? Meeting report from a joint EBF/DVDMG workshop, *Bioanalysis* 7 (14) (2015) 1703–1710.
- [9] P. Timmerman, Tiered approach revisited: introducing stage-appropriate or assay-appropriate scientific validation, *Bioanalysis* 6 (5) (2014) 599–604.
- [10] P. Timmerman, S. White, S. McDougall, M.A. Kall, J. Smeraglia, M.S. Fjording, et al., Tiered approach into practice: scientific validation for chromatography-based assays in early development—a recommendation from the European Bioanalysis Forum, *Bioanalysis* 7 (18) (2015) 2387–2398.
- [11] M. Qu, B. An, S. Shen, M. Zhang, X. Shen, X. Duan, et al., Qualitative and quantitative characterization of protein biotherapeutics with liquid chromatography mass spectrometry, *Mass Spectrom. Rev.* 36 (6) (2017) 734–754.
- [12] O.V. Friese, J.N. Smith, P.W. Brown, J.C. Rouse, Practical approaches for overcoming challenges in heightened characterization of antibody-drug conjugates with new methodologies and ultrahigh-resolution mass spectrometry, *MAbs* 10 (3) (2018) 335–345.
- [13] T.M. Allen, P.R. Cullis, Liposomal drug delivery systems: from concept to clinical applications, *Adv. Drug Deliv. Rev.* 65 (1) (2013) 36–48.
- [14] C. Zylberberg, S. Matosevic, Pharmaceutical liposomal drug delivery: a review of new delivery systems and a look at the regulatory landscape, *Drug Deliv.* 23 (9) (2016) 3319–3329.
- [15] W. Jian, N. Weng, R. Mamidi, Sample preparation for LC-MS bioanalysis of liposomal samples, in: W. Li, W. Jian, Y. Fu (Eds.), *Sample Preparation in LC-MS Bioanalysis*, John Wiley & Sons, Inc., 2019.
- [16] Y. Xie, N. Shao, Y. Jin, L. Zhang, H. Jiang, N. Xiong, et al., Determination of non-liposomal and liposomal doxorubicin in plasma by LC-MS/MS coupled with an effective solid phase extraction: In comparison with ultrafiltration technique and application to a pharmacokinetic study, *J. Chromatogr. B Anal. Technol. Biomed. Life Sci.* 1072 (2018) 149–160.

- [17] B. Leader, Q.J. Baca, D.E. Golan, Protein therapeutics: a summary and pharmacological classification, *Nat. Rev. Drug Discov.* 7 (1) (2008) 21–39.
- [18] T. Katsila, A.P. Siskos, C. Tamvakopoulos, Peptide and protein drugs: the study of their metabolism and catabolism by mass spectrometry, *Mass Spectrom. Rev.* 31 (1) (2012) 110–133.
- [19] L. Kang, R.C. Camacho, W. Li, K. D'Aquino, S. You, V. Chuo, et al., Simultaneous catabolite identification and quantitation of large therapeutic protein at the intact level by immunoaffinity capture liquid chromatography-high-resolution mass spectrometry, *Anal. Chem.* 89 (11) (2017) 6065–6075.
- [20] Q. Wang, S. Zhang, L. Guo, C.M. Busch, W. Jian, N. Weng, et al., Serum apolipoprotein A-1 quantification by LC-MS with a SILAC internal standard reveals reduced levels in smokers, *Bioanalysis* 7 (22) (2015) 2895–2911.
- [21] L. Dillen, W. Cools, L. Vereyken, P. Timmerman, A screening UHPLC-MS/MS method for the analysis of amyloid peptides in cerebrospinal fluid of preclinical species, *Bioanalysis* 3 (1) (2011) 45–55.
- [22] W. Li, S. Luo, H.T. Smith, F.L. Tse, Quantitative determination of BAF312, a S1P-R modulator, in human urine by LC-MS/MS: prevention and recovery of lost analyte due to container surface adsorption, *J. Chromatogr. B Anal. Technol. Biomed. Life Sci.* 878 (5–6) (2010) 583–589.
- [23] A.J. Ji, Z. Jiang, Y. Livson, J.A. Davis, J.X. Chu, N. Weng, Challenges in urine bioanalytical assays: overcoming nonspecific binding, *Bioanalysis* 2 (9) (2010) 1573–1586.
- [24] D. Schuster, C. Laggner, T. Langer, Why drugs fail—a study on side effects in new chemical entities, *Curr. Pharm. Des.* 11 (27) (2005) 3545–3559.
- [25] Y.J. Xue, H. Gao, Q.C. Ji, Z. Lam, X. Fang, Z.J. Lin, et al., Bioanalysis of drug in tissue: current status and challenges, *Bioanalysis* 4 (21) (2012) 2637–2653.
- [26] H.C. Bi, F.C. Law, G.P. Zhong, C.S. Xu, Y. Pan, L. Ding, et al., Study of tanshinone IIA tissue distribution in rat by liquid chromatography-tandem mass spectrometry method, *Biomed. Chromatogr.* 21 (5) (2007) 473–479.
- [27] S. Sobue, K. Sekiguchi, T. Nabeshima, Intracutaneous distributions of fluconazole, itraconazole, and griseofulvin in Guinea pigs and binding to human stratum corneum, *Antimicrob. Agents Chemother.* 48 (1) (2004) 216–223.
- [28] H. Safarpour, P. Connolly, X. Tong, M. Bielawski, E. Wilcox, Overcoming extractability hurdles of a <sup>14</sup>C labeled taxane analogue milataxel and its metabolite from xenograft mouse tumor and brain tissues, *J. Pharm. Biomed. Anal.* 49 (3) (2009) 774–779.
- [29] C. Yu, L.D. Penn, J. Hollembaek, W. Li, L.H. Cohen, Enzymatic tissue digestion as an alternative sample preparation approach for quantitative analysis using liquid chromatography-tandem mass spectrometry, *Anal. Chem.* 76 (6) (2004) 1761–1767.
- [30] C.J. Kochansky, D.R. McMasters, P. Lu, K.A. Koeplinger, H.H. Kerr, M. Shou, et al., Impact of pH on plasma protein binding in equilibrium dialysis, *Mol. Pharm.* 5 (3) (2008) 438–448.
- [31] R.W. Sparidans, J.S. Lagas, A.H. Schinkel, J.H. Schellens, J.H. Beijnen, Liquid chromatography-tandem mass spectrometric assay for diclofenac and three primary metabolites in mouse plasma, *J. Chromatogr. B Anal. Technol. Biomed. Life Sci.* 872 (1-2) (2008) 77–82.
- [32] T.R. Van Vleet, H. Liu, A. Lee, E.A.G. Blomme, Acyl glucuronide metabolites: Implications for drug safety assessment, *Toxicol. Lett.* 272 (2017) 1–7.
- [33] S. Zhou, Q. Song, Y. Tang, N. Weng, Critical review of development, validation, and transfer for high throughput bioanalytical LC-MS/MS methods, *Curr. Pharm. Anal.* 1 (2005) 3–14.
- [34] I. van den Broek, W.M. Niessen, W.D. van Dongen, Bioanalytical LC-MS/MS of protein-based biopharmaceuticals, *J. Chromatogr. B Anal. Technol. Biomed. Life Sci.* 929 (2013) 161–179.
- [35] W. Jian, L. Kang, L. Burton, N. Weng, A workflow for absolute quantitation of large therapeutic proteins in biological samples at intact level using LC-HRMS, *Bioanalysis* 8 (16) (2016) 1679–1691.
- [36] D.R. Haudenschild, A. Eldridge, P.J. Lein, B.A. Chromy, High abundant protein removal from rodent blood for biomarker discovery, *Biochem. Biophys. Res. Commun.* 455 (1-2) (2014) 84–89.
- [37] C. Santa, S.I. Anjo, B. Manadas, Protein precipitation of diluted samples in SDS-containing buffer with acetone leads to higher protein recovery and reproducibility in comparison with TCA/acetone approach, *Proteomics* 16 (13) (2016) 1847–1851.
- [38] Y. Xu, J.T. Mehl, R. Bakhtiar, E.J. Woolf, Immunoaffinity purification using anti-PEG antibody followed by two-dimensional liquid chromatography/tandem mass spectrometry for the quantification of a PEGylated therapeutic peptide in human plasma, *Anal. Chem.* 82 (16) (2010) 6877–6886.
- [39] N. Weng, J.W. Lee, X. Jiang, M. Wehling, J.D. Hulse, P.P. Lin, Simultaneous assay of morphine, morphine-3-glucuronide and morphine-6-glucuronide in human plasma using normal-phase liquid

- chromatography-tandem mass spectrometry with a silica column and an aqueous organic mobile phase, *J. Chromatogr. B Biomed. Sci. Appl.* 735 (2) (1999) 255–269.
- [40] W.Z. Shou, W. Naidong, Post-column infusion study of the ‘dosing vehicle effect’ in the liquid chromatography/tandem mass spectrometric analysis of discovery pharmacokinetic samples, *Rapid Commun. Mass Spectrom.* 17 (6) (2003) 589–597.
- [41] N. Weng, Y.L. Chen, W. Shou, X. Jiang, Importance of injection solution composition for LC-MS-MS methods, *J. Pharm. Biomed. Anal.* 26 (5-6) (2001) 753–767.
- [42] N. Weng, Bioanalytical liquid chromatography tandem mass spectrometry methods on underivatized silica columns with aqueous/organic mobile phases, *J. Chromatogr. B Anal. Technol. Biomed. Life Sci.* 796 (2) (2003) 209–224.
- [43] W. Jian, Y. Xu, R.W. Edom, N. Weng, Analysis of polar metabolites by hydrophilic interaction chromatography-MS/MS, *Bioanalysis* 3 (8) (2011) 899–912.
- [44] Y. Nie, X. Liu, X. Yang, Z. Zhao, Review: recent application of chiral liquid chromatography-tandem mass spectrometric methods for enantiomeric pharmaceutical and biomedical determinations, *J. Chromatogr. Sci.* 51 (8) (2013) 753–763.
- [45] M.Q. Huang, Z.J. Lin, N. Weng, Applications of high-resolution MS in bioanalysis, *Bioanalysis* 5 (10) (2013) 1269–1276.
- [46] R. de Vries, R.J. Vreeken, F. Cuyckens, High-throughput analysis of drugs and metabolites in biological fluids using quan-qual approaches, *LC-GC* 29 (10) (2016) 26–30.
- [47] USFDA, Guidance for Industry-Safety Testing of Drug Metabolites, (2008).
- [48] I. van den Broek, W.D. van Dongen, LC-MS-based quantification of intact proteins: perspective for clinical and bioanalytical applications, *Bioanalysis* 7 (15) (2015) 1943–1958.
- [49] X. Qiu, L. Kang, M. Case, N. Weng, W. Jian, Quantitation of intact monoclonal antibody in biological samples: comparison of different data processing strategies, *Bioanalysis* 10 (13) (2018) 1055–1067.
- [50] G. Liu, Y. Zhao, A. Angeles, L.L. Hamuro, M.E. Arnold, J.X. Shen, A novel and cost effective method of removing excess albumin from plasma/serum samples and its impacts on LC-MS/MS bioanalysis of therapeutic proteins, *Anal. Chem.* 86 (16) (2014) 8336–8343.
- [51] J. Vlasak, M.C. Bussat, S. Wang, E. Wagner-Rousset, M. Schaefer, C. Klinguer-Hamour, et al., Identification and characterization of asparagine deamidation in the light chain CDR1 of a humanized IgG1 antibody, *Anal. Biochem.* 392 (2) (2009) 145–154.
- [52] J.T. Mehl, B.G. Slecicka, E.F. Ciccimaro, A.T. Kozhich, D.G. Gilbertson, R. Vuppugalla, et al., Quantification of in vivo site-specific Asp isomerization and Asn deamidation of mAbs in animal serum using IP-LC-MS, *Bioanalysis* 8 (15) (2016) 1611–1622.
- [53] P. Bults, R. Bischoff, H. Bakker, J.A. Gietema, N.C. van de Merbel, LC-MS/MS-based monitoring of in vivo protein biotransformation: quantitative determination of trastuzumab and its deamidation products in human plasma, *Anal. Chem.* 88 (3) (2016) 1871–1877.
- [54] J.F. Kellie, J.R. Kehler, T.J. Mencken, R.J. Snell, C.S. Hottenstein, A whole-molecule immunocapture LC-MS approach for the in vivo quantitation of biotherapeutics, *Bioanalysis* 8 (20) (2016) 2103–2114.
- [55] B. Gorovits, S.C. Alley, S. Bilic, B. Booth, S. Kaur, P. Oldfield, et al., Bioanalysis of antibody-drug conjugates: American Association of Pharmaceutical Scientists Antibody-Drug Conjugate Working Group position paper, *Bioanalysis* 5 (9) (2013) 997–1006.
- [56] C. Wei, D. Su, J. Wang, W. Jian, D. Zhong, LC-MS challenges in characterizing and quantifying monoclonal antibodies (mAb) and antibody-drug conjugate (ADC) in biological samples, *Curr. Pharmacol. Rep.* 4 (1) (2018) 45–63.
- [57] K. Xu, L. Liu, R. Dere, E. Mai, R. Erickson, A. Hendricks, et al., Characterization of the drug-to-antibody ratio distribution for antibody-drug conjugates in plasma/serum, *Bioanalysis* 5 (9) (2013) 1057–1071.
- [58] D. Su, C. Ng, M. Khosraviani, S.F. Yu, E. Cosino, S. Kaur, et al., Custom-designed affinity capture LC-MSF(ab')<sub>2</sub> assay for biotransformation assessment of site-specific antibody drug conjugates, *Anal. Chem.* 88 (23) (2016) 11340–11346.
- [59] C. Wei, G. Zhang, T. Clark, F. Barletta, L.N. Tumey, B. Rago, et al., Where did the linker-payload go? A quantitative investigation on the destination of the released Linker-Payload from an antibody-drug conjugate with a maleimide linker in plasma, *Anal. Chem.* 88 (9) (2016) 4979–4986.
- [60] S.D. Goldberg, R.M. Cardoso, T. Lin, T. Spinka-Doms, D. Klein, S.A. Jacobs, et al., Engineering a targeted delivery platform using Centyrins, *Protein Eng. Des. Sel.* 29 (12) (2016) 563–572.

- [61] S.A. Jacobs, M.D. Diem, J. Luo, A. Teplyakov, G. Obmolova, T. Malia, et al., Design of novel FN3 domains with high stability by a consensus sequence approach, *Protein Eng. Des. Sel.* 25 (3) (2012) 107–117.
- [62] C. Shi, S. Goldberg, T. Lin, V. Dudkin, W. Widdison, L. Harris, et al., LC/MS/MS bioanalysis of protein-drug conjugates—the importance of incorporating succinimide hydrolysis products, *Anal. Chem.* 90 (8) (2018) 5314–5321.
- [63] C. Shi, S. Goldberg, T. Lin, V. Dudkin, W. Widdison, L. Harris, et al., Bioanalytical workflow for novel scaffold protein-drug conjugates: quantitation of total Centyrin protein, conjugated Centyrin and free payload for Centyrin-drug conjugate in plasma and tissue samples using liquid chromatography-tandem mass spectrometry, *Bioanalysis* 10 (20) (2018) 1651–1665.
- [64] W. Jian, R.W. Edom, D. Wang, N. Weng, S.W. Zhang, Relative quantitation of glycoisoforms of intact apolipoprotein C3 in human plasma by liquid chromatography-high-resolution mass spectrometry, *Anal. Chem.* 85 (5) (2013) 2867–2874.
- [65] J. Palandra, A. Finelli, M. Zhu, J. Masferrer, H. Neubert, Highly specific and sensitive measurements of human and monkey interleukin 21 using sequential protein and tryptic peptide immunoaffinity LC-MS/MS, *Anal. Chem.* 85 (11) (2013) 5522–5529.
- [66] X. Qiu, H. Zhang, Y. Lai, Quantitative targeted proteomics for membrane transporter proteins: method and application, *AAPS J.* 16 (4) (2014) 714–726.
- [67] B. Chen, L. Liu, H. Ho, Y. Chen, Z. Yang, X. Liang, et al., Strategies of drug transporter quantitation by LC-MS: importance of peptide selection and digestion efficiency, *AAPS J.* 19 (5) (2017) 1469–1478.
- [68] C. Wegler, F.Z. Gaugaz, T.B. Andersson, J.R. Wisniewski, D. Busch, C. Groer, et al., Variability in mass spectrometry-based quantification of clinically relevant drug transporters and drug metabolizing enzymes, *Mol. Pharm.* 14 (9) (2017) 3142–3151.
- [69] F. Weiss, H.S. Hammer, K. Klein, H. Planatscher, U.M. Zanger, A. Noren, et al., Direct quantification of cytochromes P450 and drug transporters—a rapid, targeted mass spectrometry-based immunoassay panel for tissues and cell culture lysates, *Drug Metab. Dispos.* 46 (4) (2018) 387–396.
- [70] R.E. Kontermann, Half-life extended biotherapeutics, *Expert. Opin. Biol. Ther.* 16 (7) (2016) 903–915.
- [71] P. Denniff, N. Spooner, Volumetric absorptive microsampling: a dried sample collection technique for quantitative bioanalysis, *Anal. Chem.* 86 (16) (2014) 8489–8495.
- [72] N.J. Patel, E. Wickremsinhe, Y.H. Hui, A. Barr, N. Masterson, K. Ruterbories, et al., Evaluation and optimization of blood micro-sampling methods: serial sampling in a cross-over design from an individual mouse, *J. Pharm. Pharm. Sci.* 19 (4) (2016) 496–510.
- [73] L. Mercolini, M. Protti, M.C. Catapano, J. Rudge, A.E. Sberna, LC-MS/MS and volumetric absorptive microsampling for quantitative bioanalysis of cathinone analogues in dried urine, plasma and oral fluid samples, *J. Pharm. Biomed. Anal.* 123 (2016) 186–194.
- [74] L. Wang, B. Wang, K.D. Chadwick, T. Su, R. Mangipudy, R.C. Pillutla, et al., A practical workflow for capillary microsampling in nonclinical studies, *Bioanalysis* (2019).
- [75] D. Coleman, G. Smith, R. Lawrence, D. McManus, S. Diaram, J. Edwards, Capillary microsampling in nonclinical safety assessment: practical sampling and bioanalysis from a CRO perspective, *Bioanalysis* 9 (10) (2017) 787–798.
- [76] P. Denniff, L. Woodford, N. Spooner, Effect of ambient humidity on the rate at which blood spots dry and the size of the spot produced, *Bioanalysis* 5 (15) (2013) 1863–1871.
- [77] *Bioanalytical Method Validation: Guidance for Industry*, U.S. Department of Health and Human Services, Food and Drug Administration, Center for Drug Evaluation and Research (CDER), Center for Veterinary Medicine, 2018.
- [78] M.J. Spreadborough, J. Day, K. Jackson-Addie, A. Wilson, Bioanalytical implementation of plasma capillary microsampling: small hurdles, large gains, *Bioanalysis* 5 (12) (2013) 1485–1489.
- [79] N. Weng, W. Jian, Selectivity for quantitation of biomarkers using liquid chromatography and mass spectrometry, *Bioanalysis* 10 (18) (2018) 1461–1465.
- [80] W. Li, L.H. Cohen, Quantitation of endogenous analytes in biofluid without a true blank matrix, *Anal. Chem.* 75 (21) (2003) 5854–5859.
- [81] W. Jian, R. Edom, N. Weng, P. Zannikos, Z. Zhang, H. Wang, Validation and application of an LC-MS/MS method for quantitation of three fatty acid ethanolamides as biomarkers for fatty acid hydrolase inhibition in human plasma, *J. Chromatogr. B Anal. Technol. Biomed. Life Sci.* 878 (20) (2010) 1687–1699.



- [82] L. Kang, T.M. Connolly, N. Weng, W. Jian, LC-MS/MS quantification of 7 $\alpha$ -hydroxy-4-cholesten-3-one (C4) in rat and monkey plasma, *J. Chromatogr. B Anal. Technol. Biomed. Life Sci.* 1064 (2017) 49–55.
- [83] J. Chen, A. Tabatabaei, D. Zook, Y. Wang, A. Danks, K. Stauber, A surrogate analyte-based liquid chromatography-tandem mass spectrometry method for the determination of endogenous cyclic nucleotides in rat brain, *J. Pharm. Biomed. Anal.* 146 (2017) 361–368.
- [84] W. Lin, M.Q. Huang, X. Xue, K. Bertelsen, G. Chen, H. Zhao, et al., A highly sensitive and selective method for the determination of leukotriene B4 (LTB4) in ex vivo stimulated human plasma by ultra fast liquid chromatography-tandem mass spectrometry, *J. Chromatogr. B Anal. Technol. Biomed. Life Sci.* 925 (2013) 54–62.
- [85] U. Diczfalussy, H. Nylen, P. Elander, L. Bertilsson, 4 $\beta$ -Hydroxycholesterol, an endogenous marker of CYP3A4/5 activity in humans, *Br. J. Clin. Pharmacol.* 71 (2) (2011) 183–189.
- [86] A.K. Goodenough, J.M. Onorato, Z. Ouyang, S. Chang, A.D. Rodrigues, S. Kasichayanula, et al., Quantification of 4 $\beta$ -hydroxycholesterol in human plasma using automated sample preparation and LC-ESI-MS/MS analysis, *Chem. Res. Toxicol.* 24 (9) (2011) 1575–1585.
- [87] Y. Xu, Y. Yuan, L. Smith, R. Edom, N. Weng, R. Mamidi, et al., LC-ESI-MS/MS quantification of 4 $\beta$ -hydroxycholesterol and cholesterol in plasma samples of limited volume, *J. Pharm. Biomed. Anal.* 85 (2013) 145–154.
- [88] D.W. Russell, K.D. Setchell, Bile acid biosynthesis, *Biochemistry* 31 (20) (1992) 4737–4749.
- [89] M. Bertolotti, M. Del Puppo, C. Gabbi, F. Corna, L. Carulli, E. Pellegrini, et al., Correlation between plasma levels of 7 $\alpha$ -hydroxy-4-cholesten-3-one and cholesterol 7 $\alpha$ -hydroxylation rates in vivo in hyperlipidemic patients, *Steroids* 73 (11) (2008) 1197–1202.
- [90] J. Lo Verme, J. Fu, G. Astarita, G. La Rana, R. Russo, A. Calignano, et al., The nuclear receptor peroxisome proliferator-activated receptor- $\alpha$  mediates the anti-inflammatory actions of palmitoylethanolamide, *Mol. Pharmacol.* 67 (1) (2005) 15–19.
- [91] T.A. Baillie, M.N. Cayen, H. Fouda, R.J. Gerson, J.D. Green, S.J. Grossman, et al., Drug metabolites in safety testing, *Toxicol. Appl. Pharmacol.* 182 (3) (2002) 188–196.
- [92] USFDA and HHS, International Conference on Harmonisation, Guidance on M3(R2) nonclinical safety studies for the conduct of human clinical trials and marketing authorization for pharmaceuticals; availability. Notice, *Fed. Regist.* 75 (13) (2010) 3471–3472.
- [93] P. Timmerman, M. Anders Kall, B. Gordon, S. Laakso, A. Freisleben, R. Hucker, Best practices in a tiered approach to metabolite quantification: views and recommendations of the European Bioanalysis Forum, *Bioanalysis* 2 (7) (2010) 1185–1194.
- [94] S. Lowes, R. Hucker, M. Jemal, J.C. Marini, V.M. Rezende, R. Shoup, et al., Tiered approaches to chromatographic bioanalytical method performance evaluation: recommendation for best practices and harmonization from the Global Bioanalysis Consortium harmonization team, *AAPS J.* 17 (1) (2015) 17–23.
- [95] Y. Gong, J. Chen, Y. Shi, H.K. Lim, N. Weng, R. Salter, Standard-free bioanalytical approach for absolute quantitation of drug metabolites utilizing biosynthesis of reciprocal radio and stable isotopologues and its application, *Anal. Chem.* 89 (16) (2017) 8399–8404.
- [96] W. Jian, R.W. Edom, Y. Xu, J. Gallagher, N. Weng, Potential bias and mitigations when using stable isotope labeled parent drug as internal standard for LC-MS/MS quantitation of metabolites, *J. Chromatogr. B Anal. Technol. Biomed. Life Sci.* 878 (31) (2010) 3267–3276.
- [97] P. Li, Y. Gong, H.K. Lim, W. Jian, R.W. Edom, R. Salter, et al., Bio-generation of stable isotope labeled internal standards for absolute and relative quantitation of drug metabolites in plasma samples by LC-MS/MS, *J. Chromatogr. B Anal. Technol. Biomed. Life Sci.* 926 (2013) 92–100.
- [98] W. Jian, R.W. Edom, M.Q. Huang, N. Weng, Bioanalysis of chiral compounds during drug development using a tiered approach, *Bioanalysis* 6 (5) (2014) 629–639.
- [99] R. de Vries, M. Huang, N. Bode, P. Jejurkar, J. Jong, J. Sukbuntherng, et al., Bioanalysis of ibuprofen and its active metabolite in human plasma: selectivity issue, impact assessment and resolution, *Bioanalysis* 7 (20) (2015) 2713–2724.
- [100] L. Yuan, Q.C. Ji, Discovery, identification and mitigation of isobaric sulfate metabolite interference to a phosphate prodrug in LC-MS/MS bioanalysis: critical role of method development in ensuring assay quality, *J. Pharm. Biomed. Anal.* 155 (2018) 141–147.
- [101] H. Sugimoto, D. Ghosh, S. Chen, M.D. Smith, A.O. Abu-Yousif, M.G. Qian, Immunocapture-LC/MS-based target engagement measurement in tumor plasma membrane, *Anal. Chem.* 90 (22) (2018) 13564–13571.

- [102] E. Ciccimaro, Y. Zhu, D. Ostanin, S. Suchard, J. MacGuire, Q. Xiao, et al., Antibody drug-target engagement measurement in tissue using quantitative affinity extraction liquid chromatography-mass spectrometry: method development and qualification, *Anal. Chem.* 89 (9) (2017) 5115–5123.
- [103] H. Zhang, H. Gu, P. Shipkova, E. Ciccimaro, H. Sun, Q. Zhao, et al., Immunoaffinity LC-MS/MS for quantitative determination of a free and total protein target as a target engagement biomarker, *Bioanalysis* 9 (20) (2017) 1573–1588.
- [104] S. Ma, R. Subramanian, Detecting and characterizing reactive metabolites by liquid chromatography/tandem mass spectrometry, *J. Mass Spectrom.* 41 (9) (2006) 1121–1139.

# Recent advances in mass spectrometric and other analytical techniques for the identification of drug metabolites

*Jose Castro-Perez, Chandra Prakash*  
Agius Pharmaceuticals, Inc., Cambridge, MA, United States

## Abbreviations

ADME	absorption distribution metabolism and excretion
APPI	atmospheric pressure photoionization
CCS	collision cross section
CID	collision-induced dissociation
CNL	constant neutral loss
CYP	cytochrome P-450
ESI	electrospray ionization
DDA	data dependent acquisition
DIA	data independent acquisition
DMS	differential mobility separation
FT-MS	Fourier transform-mass spectrometry
FTICR-MS	Fourier transform ion cyclotron resonance mass spectrometer
FWHM	full width half mass
ICP-MS	inductively coupled plasma mass spectrometry
LC	liquid chromatography
LC-MS/MS	liquid chromatography/tandem mass spectrometry
LLE	liquid-liquid extraction
MCP	microchannel plate
MRM	multiple-reaction monitoring
MS	mass spectrometry
NMR	nuclear magnetic resonance
PI	precursor ion
PPT	protein precipitation
Q-TOF	quadrupole time-of-flight



SEM	secondary emission multiplier
SFC	super fluid critical chromatography
SIR	single ion reaction
SLE	supported phase liquid extraction
SPE	solid-phase extraction
SWATH	sequential window acquisition of all theoretical
TIC	total ion chromatogram
TSQ	triple-stage quadrupole
UPLC	ultra-performance liquid chromatography
XIC	extract ion chromatogram

## 1 Introduction

When xenobiotics such as drugs enter the living systems, they undergo several events, absorption, distribution, metabolism, and excretion (ADME) and these events determine their clinical efficacy and safety. Metabolism is a biochemical process that usually converts drugs into polar and water-soluble compounds in order to eliminate them from the body and to lessen their toxicity [1]. The majority of marketed drugs are eliminated primarily by the metabolism [2]. Metabolism represents the major determinant of the drug exposure, clearance, and interactions with other compounds [3]. The rate and extent of drug metabolism determine the dose and duration of drug effect. The metabolites may possess the pharmacological activity and can modulate the efficacy of drugs in the treatment of disease [4]. The biotransformation reactions generally result in the formation of pharmacologically inactive and less toxic metabolites than their corresponding parent compound but in some cases, these reactions can also form toxic metabolites [5, 6]. In addition, the pharmaceutical industries are required by regulatory agencies to identify metabolites of new drug candidates in humans to ensure that the major human circulating metabolites ( $\geq 10\%$  of the total drug-related material) should also be present at equal or greater exposure at least in one of the toxicology species used for long-term safety assessment [7, 8]. Therefore, characterizing and understanding the pharmacological and toxicological consequences of metabolites of new drug candidates in animals and humans are very critical to pharmaceutical research and compound progression.

Drugs are metabolized by two different reactions: Phase I, or functionalization, reactions introduce or unmask a functional group (e.g.,  $-\text{OH}$ ,  $-\text{CO}_2\text{H}$ ,  $-\text{NH}_2$ ,  $\text{NH}$ , or  $-\text{SH}$ ) within a molecule to enhance its hydrophilicity [9]. It can happen by direct oxidation [e.g., aliphatic or aromatic; (N— or S—), or the modification of an existing one by dealkylation (O—, N—, or S—), reduction (nitro, keto, and aldehyde), and hydrolysis (amide and ester)]. The majority of these reactions occur in the smooth endoplasmic reticulum of the liver but also can occur in other organs (e.g., lung, intestinal epithelial, and kidney). These reactions are mediated by a battery of enzymes such as cytochrome P450 (CYPs), FAD-containing monooxygenases (FMOs), monoamine oxidases (MAOs), aldehyde oxidase/xanthine oxidase (AO/XO), alcohol dehydrogenase (ADH), aldo-keto reductase (AKR), esterases/amidases, and epoxide hydrolase (EH).

Phase II (conjugation) reactions couple a drug or a metabolite to an endogenous conjugating molecule such as sugars (glucuronic acid, glucose, and ribose), sulfuric acid, acetic acid, amino acid (glycine, glutamic acid, and taurine), and glutathione (GSH). Phase II reactions are

catalyzed by conjugative enzymes, such as UDP-glucuronosyltransferase (UGT), sulfotransferase (SULT), N-acetyl transferase (NAT), acyl-Co-A synthetase, and glutathione S-transferase (GST). Glutathione conjugates are further metabolized to cysteine and N-acetyl cysteine adducts (i.e., mercapturic acid synthesis).

In early discovery, *in vitro* systems, such as S-9, cytosol, microsomes, or hepatocytes, are used to optimize the metabolic stability and intrinsic clearance, to minimize bioactivation potential, to minimize drug-drug interactions potential, and to select the animal species used for safety evaluation studies [10]. In the development phase, ADME studies are conducted in preclinical species and humans following radiolabel administration [11].

One of the most important steps on drug metabolite identification studies is the selection of the detector to be utilized. While there are many analytical strategies from optical, radiochemical detectors, it is fair to say that mass spectrometry is one of the most widely used analytical techniques for metabolite detection and identification.

Due to high speed, enhanced resolution, and greater sensitivity and specificity of liquid chromatography-tandem mass spectrometry (LC-MS/MS), it has become a method of choice for the rapid and sensitive determination of pharmaceuticals in biological fluids [12]. With the continuous developments and improvements in LC and MS technologies, a wide range of experimental strategies and postacquisition data processing and mining modes have emerged driven by the need to identify and characterize metabolites at ever-increasing sensitivity and in ever more complex samples.

However, MS data alone do not always provide sufficient structural information for complete characterization of metabolites. In addition, other analytical techniques such as nuclear magnetic resonance (NMR) have played a very important role in the structural characterization and quantification of drug metabolites. In such cases, NMR and wet chemistry techniques (H/D exchange, derivatization, and enzymatic hydrolysis) have been proved to be very useful to enable the unambiguous structural determination of metabolites [13, 14].

## 2 Sample preparation strategies

Sample preparation is an important step in metabolite identification. There are several degrees of complexity depending on the different biological matrix used. For instance, bile samples have a high content of bile salts which can cause matrix interferences and also ion suppression, thus requires more careful attention to not just the sample preparation but also the chromatographic separation [15, 16].

In principle, the main goal in the sample preparation is to remove proteins, lipids, bile salts, and other endogenous nondrug-related components from the *in vivo* or *in vitro* samples [17–21]. This will ensure a better sample analysis outcome as some of these endogenous components can cause false positives and artifacts in the analysis which will make the metabolite identification step more challenging than it should be. So overall, spending time in understanding the biological matrix which will be utilized, the projected level of metabolites in the given biological matrix and the complexity of the sample will help in guiding the scientist in selecting the best and most suited extraction technique for drug and xenobiotics. The goals of sample preparation are to (a) remove interferences for better chromatography, (b) be more

confident in the analytical results, (c) longer chromatographic column lifetime, (d) enrich sample for better detection sensitivity, (e) make the sample more compatible for separation and detection (matching solvent strength), and (f) eliminate ion suppression in LC/MS analysis. In this section, we will describe the different approaches which can be utilized for sample preparation and cleanup steps.

## 2.1 Solid-phase extraction

Solid-phase extraction (SPE) is an old sample preparation technique which has and continues to be utilized in many applications such as pesticide analysis, food analysis, and drug metabolism [22–25]. It has many advantages over other extraction techniques such as high availability of SPE sorbents with added specificity for certain molecule types. For instance, SPE is able to accommodate reverse phase, normal phase, and ion-exchange separations.

One of the main advantages of SPE is that it combines nonlinear modes of chromatography. The sample loading or retention step involves frontal chromatography (frontal analysis or frontal separation). During this step, the SPE sorbent bed is conditioned. Then, the sample is added to the SPE bed containing the sorbent. The sample is retained in the sorbent and salts plus other endogenous components can be washed during the wash step. The final step is the elution step in which the retained compound/s can be eluted with a stronger solvent. Nonlinear chromatography is superior to linear chromatography in column load capacity, reduced mobile-phase consumption and simultaneous fractionation and concentration, and it can produce greater concentrations than the original samples. SPE is able to produce simultaneous purification, fractionation, and concentration as it is a nonequilibrium, nonlinear chromatographic procedure. When selecting the sample volume to be extracted it is important to select the correct sorbent per well as shown in Table 1.

As it can be observed, the higher the sample volume loaded the higher the sorbent bed amount required to retain the components in the sample of interest.

Another important factor to consider when selecting the chemistry of the sorbent is to have a good degree of knowledge of the expected metabolite chemical properties. For instance, are the parent drug and its metabolites basic, acidic, or neutral? This will help to select the correct stationary phase. There are also mixed-mode stationary phases which can help to provide more selectivity, including mixed-mode cation exchange for bases, and mixed-mode anion exchange for acids for a wide range of  $pK_a$  strengths.

TABLE 1 The amount of sorbent needed per typical sample volume and mass capacity.

Sorbent per well (mg)	Maximum mass capacity (mg)	Typical sample volume (predilution) ( $\mu$ L)	Typical elution volume ( $\mu$ L)
2	0.03–0.05	5–200	$\leq$ 50
5	0.15–1	10–200	$\leq$ 150
10	0.35–2	50–400	$\leq$ 250
30	1–5	100–1000	$>$ 400
60	2–10	200–2000	$>$ 800

## 2.2 Supported phase liquid extraction

This extraction technique enables the separation of drugs and metabolites based on their particular affinity for one solvent vs another immiscible solvent. It is very similar to liquid-liquid extraction (LLE) which will be described below. The main difference between supported phase liquid extraction (SLE) and LLE is that the aqueous solvent in SLE is a highly polar solid inert support. The aqueous sample is immobilized in the inert support extraction bed and is dispersed in small droplets. Then, as the organic phase flows through the support material, the analytes partition into the elution solvent and are collected.

## 2.3 Liquid-liquid extraction

LLE is another widely used sample preparation technique in drug metabolism [26–28]. In principle, the separation is based on the relative solubility of the analytes in two liquids such as water and an organic solvent. Another liquid is added which is immiscible or partially miscible with the sample of interest and two phases are formed. The measure of the amount of component in this case drug and related drug metabolites between the two liquid phases generated is called the partition coefficient. Just like SPE, the main purpose of using this solvent extraction technique is to remove interfering endogenous substances from the drug and drug-related metabolites. When selecting the solvents for the extraction it is important to consider some factors such as the solubility of the analytes in question, the  $pK_a$  and ionic strength, and whether LLE will be combined with SPE to achieve even higher sample cleanup. When compared to SPE a higher amount of solvent is utilized and it is amenable to high throughput sample extraction when using sample liquid-handling automated systems.

Sometimes LLE is assisted with salting out protein precipitation (PPT) techniques. In this case, an inorganic salt, such as zinc sulfate, magnesium sulfate, potassium bicarbonate, or calcium chloride just to name a few, is added to water and a water-immiscible solvent creating a two-layered liquid phase. This technique can also help to enhance the extraction efficiency into nonpolar water-immiscible organic solvents.

LLE has advantages over PPT extraction techniques as in general the extracts are cleaner but one of the downsides is that the selection of the right solvents for the sample partitioning can be time-consuming and quite laborious so overall it is a more labor-intensive strategy.

## 2.4 Protein precipitation

PPT is one of the most commonly used sample extraction techniques in bioanalysis. This technique is relatively simple and provides a quick sample cleanup especially in whole blood, plasma, and serum. The operating principle is based on the addition of an organic solvent, acid, or salt to the sample in question. In the case of the addition of the organic solvent to, for example, the plasma sample/s, it leads to the reduction of the dielectric constant in the sample containing the proteins, i.e., plasma, whole blood, or serum. This leads to a displacement of water from the hydrophobic region of the protein surface which in turns leads to disruption of hydrophobic interactions between the proteins in the sample, thus causing proteins to precipitate out of solution.

Another method which aids PPT is the addition of acidic reagents such as hydrogen chloride. The addition of the acidic reagent creates an insoluble salt, from the reaction with the positively charged amino groups of the proteins, this occurs at pH values below their isoelectric points (pIs). The last method of PPT is the addition of excess or high salt concentrations such as zinc sulfate which is commonly used in bioanalysis. The addition of this salt leads to the depletion of water from the hydrophobic protein surfaces and allows aggregation through hydrophobic interactions of protein molecules. Binding of metal ions reduces protein solubility by changing its pI.

### 3 Optical detectors and chromatographic separation techniques

There are a number of different analytical strategies for metabolite detection and identification ranging from ultraviolet detection (UV) [29–31], microplate scintillation counter [32–34], accurate radioisotope counting [32, 35–38], NMR [39–43], and mass spectrometry (MS) [19, 25, 44, 45]. In this section, we focus primarily on mass spectrometry and NMR and the impact that this technique in drug biotransformation detection and identification.

UV, microscintillation counter, and accurate radioisotope counting are orthogonal techniques which can be coupled to a mass spectrometer. These techniques are mainly used for quantitation of drug metabolites and especially when radioisotopes  $^{14}\text{C}$  or  $^3\text{H}$  are used since we can accurately measure the radioactivity levels given by the compounds containing the radioisotopes [8]. The radioactivity measurement makes the technique more selective than for instance UV but in drug discovery is unlikely to have the parent drug radiolabeled so UV for in vitro incubations is adequate to quantify metabolites and parent drug of interest. The optical detectors and scintillation counters can also be used to guide the user to search for mass spectral information belonging to the parent drug or xenobiotic relative to the retention times on the UV, microscintillation counter, or accurate radioisotope counting. In turn, this can help the scientist to do an additional experiment in the mass spectrometer which will help for structural elucidation purposes.

#### 3.1 Ultra-performance liquid chromatography

An integral part of mass spectrometry is the coupling to liquid chromatography (LC) as the main inlet of choice. The LC allows for separation of isomeric molecules such as hydroxylated metabolites which all share the same molecular weight. In the mass spectrometer, a single peak would be detected with the same mass-to-charge ratio. Two of the main developments of HPLC in the last decade have been the increased number of different stationary phases for different types of compounds and also the reduction in the column particle size. The reduction of the column particle size, i.e., sub- $2\mu\text{m}$  has led to the birth of the ultra-performance liquid chromatography (UPLC) system [46]. Reduction in the particle size and increase in flow rates lead to a considerably higher column back pressure  $\sim 6000\text{--}9000\text{psi}$  which is dependent on column length, diameter, and flow rate. Meaning that the current HPLC systems cannot cope with the system pressure generated with the new and novel particle sizes [47]. UPLC revolutionized the LC inlet for MS systems because it allowed for a considerable gain in

chromatographic resolution (peak capacity), speed, and sensitivity with supported back pressures up to 15,000 psi [48–52]. In addition to this, it is important to point out the fact that the improved peak capacity for the UPLC system can also help to reduce mass spectral overlap. The MS systems also needed to catch up with the speed of analysis of UPLC and new mass spectrometer systems came to the market with faster acquisition rates.

### 3.2 Supercritical fluid chromatography

There is another inlet which has also gathered more and more interest in the recent years and this is supercritical fluid chromatography (SFC). The principles of SFC are similar to those of liquid chromatography; however, SFC typically uses carbon dioxide as the main mobile phase. A supercritical fluid is any substance that is at a temperature and pressure above its critical point, where distinct liquid and gas phases do not exist. Essentially, the substance takes on properties that are intermediate to both a gas and a liquid which result in fast and efficient chromatography. SFC is essentially a normal-phase chromatographic technique with inherent high speed and efficiency due to its mobile phase.

SFC excels at separating and purifying chiral compounds because much faster separations can be attained and in the vast majority of cases exceeds LC in performance for chiral separations. There is a considerable less amount of solvent used meaning that it is a greener analytical strategy. In terms of drug metabolism and the utilization of SFC technology in metabolite identification studies [53–57] over the years, we have seen an increase in the utilization of this technique because it can offer higher throughput than the typical chemical derivatization of enantiomers or HPLC chiral separations. When supercritical CO<sub>2</sub> is paired with a number of different modifiers, a significant range of selectivity can be explored.

In metabolite identification, sometimes there is in vivo racemization happening with selective chiral metabolism [58, 59], or the drug itself has either enantiomers or diastereomers, so chiral separation is needed for the parent drug and xenobiotics. SFC is a good candidate for this. For instance, in the case of propranolol and its hydroxylated metabolites, it was possible to separate the different chiral forms by SFC in a relatively short run time [60].

## 4 Different types of Ionization techniques and mass spectrometric scan functions

### 4.1 Ionization techniques

Before the parent drug and metabolites can be detected in the mass spectrometer. The samples need to be ionized. The most common ionization techniques in drug metabolism studies are based on atmospheric pressure ionization (API) techniques such as atmospheric pressure chemical ionization (APCI), electrospray ionization (ESI), and atmospheric pressure photo-ionization techniques (APPI).

APCI technique can be used for polar and thermally stable analytes. Ionization takes place in the gas phase. The nebulizer probe is heated between 350°C and 550°C range and nitrogen gas is used as the nebulizer gas depending on a few factors such as mobile-phase composition and flow rate. For instance, a higher aqueous content requires higher nebulizer temperatures than a higher organic content of the mobile phase, and higher flow rates require higher



nebulizer temperatures. Differences may exist in the temperature optimization based on the different designs of the nebulizer probes and ion sources as the efficiency of desolvation of mobile phase could be different so ion source and other parameters in relation to the nebulization probe need to be adjusted accordingly. Typical HPLC or UPLC flow rates range from 0.3 to 2 mL/min. The utilization of nonpolar solvents in APCI has been reported and this is possible because unlike ESI ionization in APCI ionization is done in the gas phase so this ionization technique is more efficient in the desolvation step.

For the ionization of the sample to take place, there is a corona discharge needle which typically operates at 1–3 kV. Once the sample and carrying mobile phase are desolvated, the molecules are ionized by the potential at the corona discharge needle. The potential difference between the corona discharge needle and the first skimmer (ion-focusing lens or sample cone) together with the differential vacuum going from atmospheric to under vacuum makes the extraction of the ions from the source into the mass spectrometer for detection.

ESI was developed by Yamashita and Fenn [61–63] which revolutionized the utilization of mass spectrometry in biomedical research. Fenn pioneered this concept which became a reality with widespread adoption in many different industries where the analytical need of mass spectrometry was in demand. Today, ESI is the most widely used ionization technique in bioanalysis. The development of electrospray ionization for the analysis of biological macromolecules was rewarded by awarding the Nobel Prize in Chemistry to John Bennet Fenn in 2002. The ionization step occurs when a high voltage in the ESI probe (typically 2–3.5 kV) is applied to the mobile-phase liquid carrying the sample analytes which then generates an aerosol. Typical solvents in the mobile phase are water, acetonitrile, methanol, and preferably volatile modifiers. For instance, modifiers such as formic acid which increase conductivity are normally utilized in the mobile phase to enhance ionization by providing additional protons helping the overall ionization process. The ionization is also assisted by the introduction of a probe gas which is nitrogen just like in APCI where the probe and gas are heated according to mobile-phase flow rates and composition of the mobile phase following the same principles as in APCI. This process helps in the creation of the aerosol droplet.

The solvent evaporates from a charged droplet until it becomes unstable on reaching its Rayleigh limit. At this point, the droplet deforms as the electrostatic repulsion of like charges, in ever-decreasing droplet size, becomes more powerful than the surface tension holding the droplet together. At this point, the droplet undergoes Coulomb fission, whereby the original droplet ‘explodes’ creating many smaller, more stable droplets. The new droplets undergo desolvation and subsequently further Coulomb fissions. During the fission, the droplet loses a small percentage of its mass (1.0%–2.3%) along with a relatively large percentage of its charge (10%–18%).

ESI is also called a “soft ionization technique” because it is less thermally aggressive than APCI and therefore, less “in source” fragmentation is expected. Unlike APCI, it has the capability to be more amenable to a wider range of molecular weights for the analyte/s of interest, for instance, ESI is widely used in top-down or bottom-up proteomics analysis [64–67].

APPI is another very useful technique for less polar analytes [68]. In this technique, UV light photons are used to ionize drug molecules and their metabolites. The technique works well with nonpolar or low-polarity compounds that are not efficiently ionized by other ionization sources. The liquid solution is vaporized with the help of a nebulizing gas such as nitrogen and then enters an ionization chamber at atmospheric pressure. There, the mixture



of solvent and sample molecules is exposed to ultraviolet light from a krypton lamp. The photons emitted from this lamp have a specific energy level (10 eV). The energy level is high enough to ionize the target molecules.

Dopant-assisted APPI is utilized in the vast majority of cases because by doing this it is possible to increase the percentage of analyte molecules that get ionized, thus improving the results. Different compounds can be used; toluene is a commonly used dopant.

## 4.2 Mass analyzers and different acquisition modes

Mass spectrometry as a detector is a very powerful tool because it allows for rapid and sensitive detection of drugs and xenobiotics in a multitude of biological matrices. Structural elucidation is also possible with mass spectrometry and this is the final step of metabolite identification which is to identify the site of metabolism so that we can make an informative decision about the molecule soft spots which is important in the drug discovery stage or to also identify potential metabolites which could cause liabilities for the drug in question moving forward into development such as reactive metabolites with undesired idiosyncrasies. In this section, we will concentrate on three types of mass analyzers; (i) triple stage quadrupoles (TSQ), (ii) hybrid quadrupole orthogonal time of flight (QTOF), (iii) Orbitrap, and (iv) inductively coupled plasma mass spectrometry (ICP-MS).

### (i) Triple quadrupoles and different scan functions:

Triple stage quadrupole mass spectrometers are still very useful since they have specific acquisition functions such as precursor ion and neutral loss modes which are important data generating functions for structural elucidation [69]. Having said that, the vast majority of TSQ currently sold end up focusing primarily on quantitative bioanalysis.

TSQ consist of two quadrupole mass analyzers arranged in series. Each mass analyzer contains four rods usually denoted as Q1 and Q3 for first and second mass analyzer respectively. Q1 and Q3 rod operate under direct current (DC) and radio frequency (RF). In the middle of the two Q1 and Q3, there is a collision cell which operates under vacuum as well and either N<sub>2</sub> or Ar is used for collisional induced dissociation (CID). The collision cell operates under RF potential. Different collision energies can be applied to cause molecular fragmentation of the compound of interest and aid with the structural elucidation or in the case of quantitative assays to improve the limit of detection and specificity of the assay. The TSQ has six distinctive scan modes: (a) full MS scan mode, (b) daughter ion scan mode, (c) precursor ion scan mode, (d) neutral loss scan mode, (e) multiple reaction monitoring mode, and (f) single reaction monitoring mode.

#### 1. Full MS scan mode or MS:

In this mode of operation, a selected mass range of acquisition is applied and the quadrupoles in either Q1 or Q3 scans the selected mass range (Fig. 1). This mode of operation is useful when searching for known and unknown metabolites by retention time and molecular weight. But no structural elucidation can be derived from this particular mode of operation.

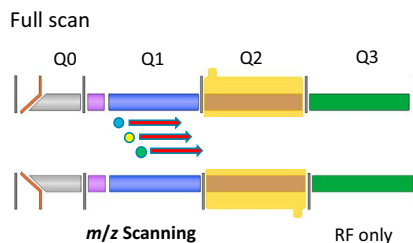


FIG. 1 Full scan MS acquisition mode using a triple quadrupole mass spectrometer.

## 2. Daughter ion scan mode or MS2:

This acquisition mode is used for obtaining fragment ion information from the parent mass for either drug or metabolite. In this mode of operation, Q1 is set to a single- or multiple-mass selection so only that single mass-to-charge ratio ( $m/z$ ) or multiple ones are allowed to enter the collision cell. Then, the selected  $m/z$  ion/s are subjected to collisional-induced dissociation so that their respective daughter or fragment ions can be generated (Fig. 2).

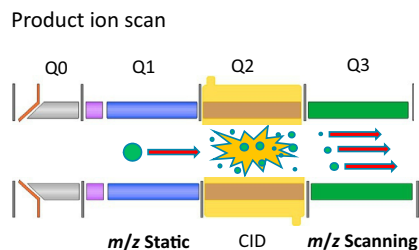


FIG. 2 Product ion scan MS acquisition mode using a triple quadrupole mass spectrometer.

## 3. Precursor ion scan mode (PI):

Q3 is fixed at a certain  $m/z$  and the precursor masses are scanned using Q1. In this acquisition mode, the molecule is also fragmented in the collision cell but the question asked in this mode of operation is which precursor can produce a certain fragment ion. This is a useful acquisition mode in metabolite identification if there are any common parent drug and xenobiotics fragment ions, which the user suspects to be present (Fig. 3). It can also be used to rule out false positives.

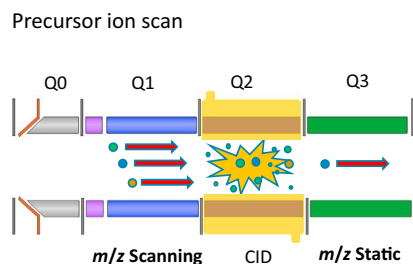


FIG. 3 Precursor ion scan MS acquisition mode using a triple quadrupole mass spectrometer.

#### 4. Neutral loss mode (NL):

In neutral loss mode, both Q1 and Q3 are in scanning mode using a constant  $m/z$  offset. Note that in this mode of operation the collision cell is utilized to generate the fragment ions which give rise to the neutral loss between the precursor and daughter ions (Fig. 4). This acquisition mode is very useful for detecting phase 2 metabolic conjugations such as glucuronides, sulfates, glutathione adducts, etc. For instance, when trying to detect glucuronide metabolites in the samples, a neutral loss scan of 176 is used which measures the loss of the sugar motif between conjugated metabolite and unconjugated precursor as the ion at 176Da is lost in the fragmentation process.

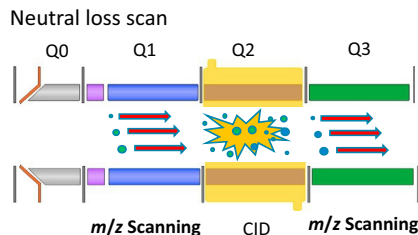


FIG. 4 Neutral loss scan MS acquisition mode using a triple quadrupole mass spectrometer.

#### 5. Multiple reaction-monitoring mode (MRM):

This acquisition mode offers a high degree of selectivity and sensitivity. Q1 selects the parent mass which is then fragmented in the collision cell. The optimized daughter ions which are normally the best one by the intensity and low background noise (by observation of chromatogram signal to noise) is selected in Q3 (Fig. 5). This mode of operation is great for detecting *known* or expected low-level metabolites which could be undetected in full-scan MS acquisitions. This mode of operation has the highest duty cycle, thus offering the best sensitivity and signal-to-noise ratio. In modern triple quadrupole mass spectrometers is possible to conduct full-scan MS and MRM acquisitions on the same run.

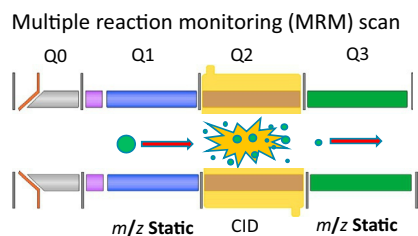


FIG. 5 Multiple reaction monitoring scan MS acquisition mode using a triple quadrupole mass spectrometer.

#### 6. Single ion reaction (SIR) monitoring:

In this acquisition mode, the parent ion is selected in Q1 but not fragmentation is utilized so no selection of daughter ions is conducted in Q3. It is also possible to use Q3 as the quadrupole for the SIR acquisition and in this case, Q1 will be used as a transmission rod. This mode of

acquisition is useful when the parent drug fragmentation is poor, which is difficult to *fragment* or low signal fragment ions and in this case, only the parent molecule is monitored. One can also use a parent-to-parent acquisition using MRM mode if the fragmentation of the parent drug and metabolite is poor. Just like in MRM mode this mode of operation is only used when the molecular weight of the metabolite is known or is an expected metabolite with a low circulating or excreted concentration but it is not as common as the other acquisition functions mentioned above.

In terms of the strategy of using the TSQ for metabolite identification, the recommendation is to first characterize the retention time of the drug of interest and conduct daughter ion scan so that we can get a picture of the fragmentation pattern of the drug of interest. Once this is done the next step will be to acquire in full-scan MS mode both control sample and metabolized sample so that we can exclude false positives. It has also been reported, specific in silico algorithm [70], which can predict the MRM transitions and therefore have an extensive list of MRM transitions to monitor 'expected' metabolites. This could be an important strategy especially for microdosing studies [71].

This should be followed by precursor ion scan which is based on the fragmentation of the data collected. This will inform us of any chromatographic peaks (putative xenobiotic) in the in vitro or in vivo sample which have common fragment ions with the parent drug. Depending on whether we expect to detect any phase 2 conjugations or not, neutral loss acquisition is generally a good approach as it will help us detect and identify common drug conjugates such as glucuronides, sulfates, and glutathione conjugates.

(ii) Hybrid quadrupole orthogonal time of flight (QTOF):

These types of mass spectrometers are ideal for metabolite identification because they allow for high-resolution spectral acquisitions and accurate mass measurements. This level of measurement is very helpful as it helps to eliminate false positives, especially when searching for unexpected metabolites in the samples of interest. The QTOF is a hybrid mass spectrometer consisting of two parts; the quadrupole and the time-of-flight region. Having a quadrupole connected in a serial fashion to the time-of-flight device offer many possibilities to the different types of acquisition experiments. Aside from the most common acquisitions such as full-scan MS and full-scan MS<sup>2</sup>, it is possible to setup data-dependent acquisition experiments and data-independent acquisition experiments. We will cover these methods of acquisition in more detail later on.

The time-of-flight mass spectrometer currently available in the market are capable of producing mass spectral resolution from 10,000 to 80,000 at full-width at half-maximum (FWHM) with routine mass accuracies of  $\sim 2\text{--}4$  ppm [72–77].

The mass-to-charge ratio detection on the mass spectrometer is achieved by measuring the time of flight of a particular ion/s. The ions are accelerated as they enter the electric field in the TOF region. The measurement in itself is relatively simple. The velocity of the ions depends on their specific  $m/z$ , meaning that heavier ions will take a longer through the flight path than the lighter ions. The time that they take to travel will be recorded for a given length of the flight tube. A longer flight tube in theory will provide higher mass spectral resolution but there could be ion losses incurred and thus a loss in sensitivity. Great strides toward improving the ion losses and better ion optics have resulted in good ion transmissions and the

possibility for very large flight paths by using folded or multiturn arrangement time-of-flight paths with exquisite mass spectral resolutions  $>350$  K FWHM [78].

The use of ion reflectrons [79–83] in the TOF is also very important because it can help to increase the ion path length of the TOF and in some instrument configurations, it is possible to make two passes in a W-mode or N-mode configuration and therefore obtaining higher spectral resolution.

The ion detection system in most cases consists of a microchannel plate (MCP) detector system or a fast secondary emission multiplier (SEM). The signal arising from the MCP or SEM is recorded using either time-to-digital converter (TDC) or now most commonly used a fast analog-to-digital converter (ADC).

One important aspect of metabolite identification is the characterization step. In terms of the QTOF technology, there are a number of strategies which can combine full-scan MS together with  $MS^2$  data acquisitions. These can be classified into two acquisition modes: (a) data-dependent acquisitions (DDA) and (b) data-independent acquisitions (DIA).

DDA acquisitions allow for obtaining MS and  $MS^2$  data in the same run, for  $MS^2$  experiments the instrument can be set up to include a list of  $m/z$  values which the user would like to include an exclusion list of  $m/z$  values which the user do not want to include in the  $MS^2$  experiments. There are a number of *in silico* bioinformatics tools [84–87] which allow for the generation of an expected metabolite list which can be used as an inclusion list in addition with other knowledge that the scientist may have about the putative metabolism of the drug in question. With this acquisition mode, there is always a risk of missing data on minor metabolites that are not predicted *in silico*. In addition, setting up DDA could be cumbersome and time consuming for the less experienced user.

Another approach is DIA. Over the years this approach has taken center stage in conducting MS and  $MS^2$  in the same run. And there are a number of reasons why it has been important in metabolite identification. One of the main reasons is the simplicity of the method set up because all ions in the experiments will be fragmented in a sequential manner and no prior *in silico* or other knowledge is required for the drug metabolism of the sample. Having said that, the software tool for the data interpretation becomes critically important to deconvolute precursor ion from corresponding daughter ion. The DIA experiments started with the  $MS^E$  concept [50, 88] in which two acquisitions in parallel were conducted in full-scan MS one at low collision energy and the other at high collision energy and a collision energy ramp was also utilized to obtain wider fragmentation coverage. Then, the experiment will alternate between both the low and high collision energy function. Acquisition speed is fast enough to keep up with UPLC chromatographic peak widths.

Fig. 6 compared the three main data acquisition approaches. The typical approach requires multiple experiments to get the answer and a lot of that relies on the experience of the bioanalyst. With regards to the DDA approach, this generates a vast amount of data for metabolites of interest but unexpected or minor metabolites may be missed in the  $MS^2$  acquisition but detected in the full-scan MS mode.

In contrast with the  $MS^E$  approach, all the information required is obtained in a single analysis and the software tool will mine and interrogate the data set. This approach may also allow the bioanalyst to make expert decisions about which other experiment/s need to be carried out to further confirm the metabolite structure of interest. It is possible by utilizing the

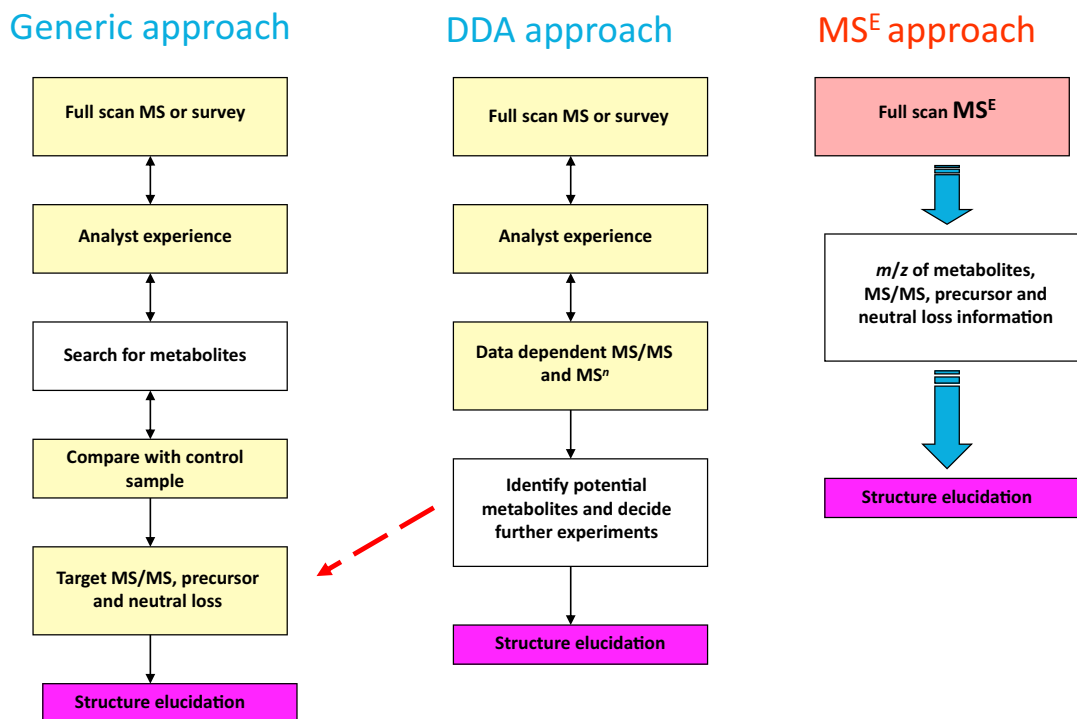


FIG. 6 Comparison between generic, data-dependent and data-independent modes of acquisition for metabolite identification experiments.

MS<sup>E</sup> acquisition function to obtain the following in the same run; (a) precursor ion spectra, (b) fragment ion spectra, and (c) neutral loss information.

Other DIA acquisitions have emerged since MS<sup>E</sup>. For instance, Sequential Window Acquisition of All Theoretical fragment-ion spectra (SWATH) has gathered popularity as another alternative DIA technique [89–91]. It first started in proteomics and quickly got adopted in metabolite identification studies [92]. The main difference between MS<sup>E</sup> and SWATH is that SWATH utilizes variable quad windows and fragment all ions in the specific windows set by the users, typically these windows are 25 Da, as shown in Fig. 7. In this mode of operation, the Q1 quadrupole is stepped at 25 Da increments across the mass range of interest for the particular metabolite identification experiment, so only the ions collected in the 25 Da window are allowed to move into the collision cell. These ions are fragmented and finally detected in the TOF MS analyzer at high resolution. This acquisition mode adds more specificity to the precursor ion selection rather than having no precursor ion selection such as in MS<sup>E</sup>. Another characteristic of SWATH is that there should not be a reduction in signal or duty cycle which could prove very valuable when measuring low-level metabolites. This technology has evolved and instead of using fixed quadrupole isolation windows now it is possible to use variable window SWATH, thus adding more selectivity and flexibility in this DIA approach.

One of the most recent DIA techniques is called SONAR acquisition [93–95]. Essentially with SONAR, the quadrupole is active meaning that is used not just to transmit the mass

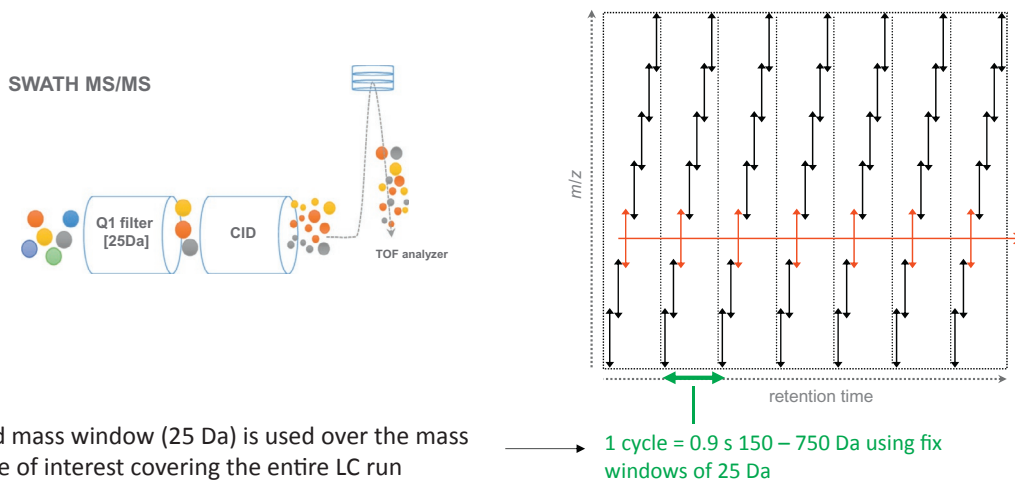


FIG. 7 Schematic of SWATH acquisition with fixed quadrupole windows over mass range desired.

range of interest as in  $MS^E$  mode but it is used in a resolving mode with narrow mass window typically over a selected mass range during each MS scan (Fig. 8). Then, just like in  $MS^E$  and in a parallel fashion, the collision cell is alternating between high and low collision energy. This data is collected in two data channels that the software aligns to associate the precursor and fragment ions. Each scan contains 200 spectra. The three-dimensional data allows the MS/MS data to be reported separately.

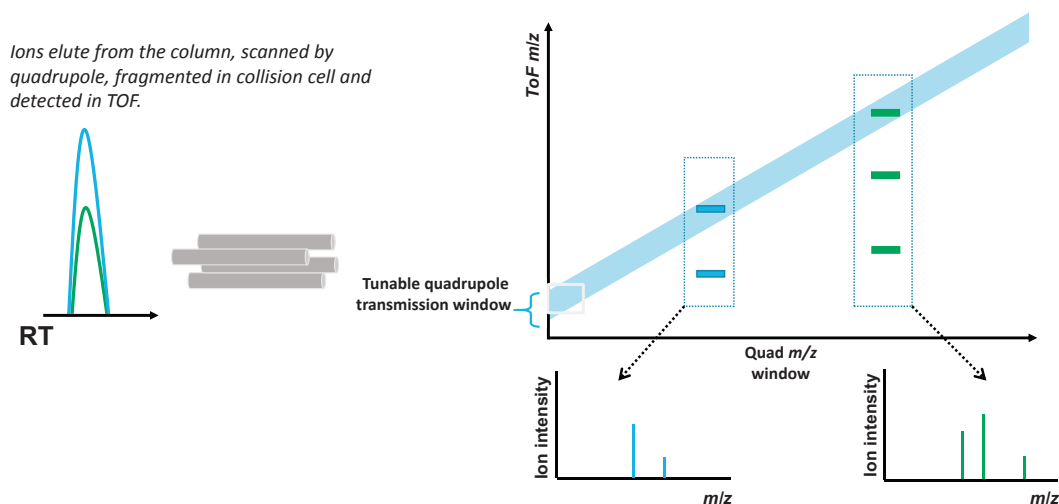
This approach has the same end result as the  $MS^2$  spectra generated from a DDA experiment as it has more selectivity over the precursor ion utilized. One limitation of SONAR because the quadrupole is being scanned very rapidly up to 10,000 Da/s and depending on the isolation window utilized, a significant loss in signal is possible and could impact the results. So caution has to be taken to understand the acquisition parameter/s such as the quad window size to be used in this acquisition mode.

### (iii) Ion mobility mass spectrometry combined with QTOF:

The QTOF has also been coupled with ion mobility separations [96–99]. Ion mobility allows for orthogonal additional metabolite information in addition to  $m/z$ , accurate mass, retention time, and fragment ion information. For instance, an important measurement that can be provided by ion mobility is collisional cross-section measurements (CCS). These are unique measurements for each molecule which depends on their molecular charge,  $m/z$  value, and their cross-sectional rotation in the gas phase. Ion mobility separate ions as they drift through a gas under the influence of an electric field. Rate of drift is dependent on the ion's mobility through the gas.

A CCS value is a precise physicochemical property of an ion which relates to its chemical structure in the gas phase, this measurement can be very complimentary in metabolite identification purposes for a number of reasons because, together with other measurements can help to remove false positives, catalogue different metabolites by their CCS values, and remove background interferences thus improving signal-to-noise for detection of low-level





- Quadrupole continuously ramps over the entire  $m/z$  range instead of transmitting all ions ( $MS^E$ ) or a narrow window of  $m/z$
- Precursor ions, not separated chromatographically, are differentiated by MS.
- Two co-eluting ions differing in precursor mass are transmitted, fragmented separately in the collision cell.

FIG. 8 SONAR data-independent acquisition schematics.

metabolites some of these examples will be further discussed in this section. It is possible to predict upon the structure of the proposed metabolite CCS values *in silico* as previously demonstrated [100–106], this means that it is possible to conduct *in silico* structure metabolite prediction and submit them for CCS value prediction. These CCS values can be used to specifically set up different acquisition modes in the ion mobility QTOF enabled the system to particularly target these predicted metabolites of interest.

Differential mobility separation (DMS) [107] is another enabling ion mobility tool which can also be utilized in conjunction with high-resolution mass spectrometers such as QTOF and triple quadrupoles. Separation of ions with this technique takes place at atmospheric pressure in between the ionization source and the entrance plate in the mass spectrometer before reaching the Q1 quadrupole region. A high-voltage radio frequency asymmetric waveform is applied which is called the separation voltage or SV. Ions oscillate between the electrodes in the DMS cell once the SV is applied, a compensation voltage is applied (CoV) which enables ion deflection and away from collisions with the electrodes which can then be detected in the MS. Chemical modifiers such as isopropanol can be used which can help with the mobility separation peak capacity.

Applications of DMS has been successfully utilized to separate diastereomeric metabolites and also reduce chemical background and thus facilitate metabolite detection [108].

#### (iv) Orbitrap mass spectrometers:

Another type of mass analyzer is the Orbitrap [108–111]. This mass analyzer due to its very high mass spectral resolution up to 1 million FWHM [109] plays a very important role in

metabolite detection and identification as it can produce elemental compositions with a high degree of mass accuracy in the 1 ppm region and it can also provide improved signal-to-noise measurement since very narrow extracted ion chromatogram windows can be used thus reducing possible interferences with chemical or endogenous matrix noise. Due to the simplicity in the design of the Orbitrap and the fact that less maintenance is needed when compared to Fourier Transform Ion Cyclotron Resonance Mass Spectrometer (FTICR-MS), the Orbitrap has taken the place of the FTICR-MS in metabolite identification.

The Orbitrap works on the principle of orbital trapping of ions and recording an image of current followed by Fourier transformation for the generation of the mass spectra. The geometry of the Orbitrap consists of two central and outer electrodes. Ions are injected and cycle around a central electrode and at the same time, they oscillate along a horizontal axis [110]. The longer the ions cycle around the central electrode the higher the mass spectral resolution. The original Orbitrap was designed based on the LTQ system from Thermo Scientific in which used a linear ion trap arrangement followed by a C-trap and then the Orbitrap mass analyzer. The C-trap works in the accumulation and cooling down of ions which are then injected in the aperture of the Orbitrap mass analyzer in short pulses. Because the linear ion trap is arranged in a sequential fashion it is also possible to conduct  $MS^n$  experiments which are very useful for structure elucidation, especially when used in combination with accurate mass as obtained by the Orbitrap mass analyzer system. Another key advantage of the hybrid ion trap-Orbitrap is the ability to conduct  $MS^n$  experiments, there are some cases in metabolite structural elucidation where  $MS^3$  can help to elucidate the structure of a putative metabolite/s [111]. One of the major disadvantages of the Orbitrap analyzer is maintaining high spectral resolution across the mass range of interest at fast acquisition rates to keep up with narrow chromatographic peak widths generated from rapid chromatography using sub 2- $\mu\text{m}$  column separations; this is not an issue with QTOF mass spectrometers since spectral resolution is not dependent on acquisition rates.

### 4.3 Inductively coupled mass spectrometry (ICP-MS)

Inductively coupled plasma mass spectrometry (ICP-MS) can detect metals and nonmetals with very good sensitivity in parts per quadrillion. This technique combines a high-temperature ICP that converts the atoms of the elements measured to ions, which can be detected by the mass spectrometer. This is done by utilizing an ICP torch in which argon gas is flowing at a constant flow. During this process the electrons are stripped off the argon atoms, thus creating argon ions. These ions collide with other argon atoms in the oscillating and magnetic fields at the end of the torch forming a plasma reaching temperatures of 6000–10,000°K. The ions formed by the ICP discharge are typically positive ions,  $M^+$  or  $M^{+2}$ . Then, these ions enter the mass spectrometer which typically is either a quadrupole mass filter or a time-of-flight mass analyzer. ICP-MS can be coupled to HPLC which makes it more amenable to current chromatographic techniques. Over the years, inorganic mass spectrometry such as ICP-MS has begun to make its way into drug metabolism because of the selectivity and sensitivity to measure certain elements such as metals in the case of oncology drugs like *cis*-platin [112]. But more recently other elements such as bromine, chlorine, and sulfur have also demonstrated the ability to measure drug and xenobiotics for molecules containing

these elements [113]. Furthermore, ICP-MS can be used in combination with other detectors such as ultraviolet detection-diode array for further confirmation of metabolites detected. The other significant advantage of ICP-MS is the extensive dynamic range up to six orders of magnitude and as mentioned the sensitivity which could be achieved with it. It has also been demonstrated that the ICP-MS can be combined with a time-of-flight mass spectrometer to achieve quantitative and qualitative metabolite detection and identification by using both systems in parallel [114].

## 5 Wet chemistry techniques combined with MS

### 5.1 Hydrogen/deuterium (H/D) exchange

Hydrogen/deuterium (H/D) exchange experiments play an important role in identification and structure elucidation of metabolites by determining the presence, numbers, and positions of exchangeable protons present in different functional groups such as  $-\text{NH}-$ ,  $-\text{NH}_2$ ,  $-\text{OH}$ ,  $-\text{COOH}$ , and  $-\text{SH}$  on the metabolite structures [115–117]. The mass shift of the deuterated molecular ion from that of the protonated molecular ion gives information about the total number of exchangeable protons present in the structures of metabolites. In addition, H/D-exchange experiments facilitate the interpretation of MS/MS fragmentation processes. Several techniques such as using  $\text{ND}_3$  as the nebulizer or curtain gas,  $\text{D}_2\text{O}$  as the LC-mobile phase and  $\text{D}_2\text{O}$  as sheath liquid have been developed for H/D exchange experiments [118]. Miao et al. [119] identified a novel metabolite intermediate of an antipsychotic drug, ziprasidone, in the cytosolic fractions of preclinical species in humans using H/D exchange technique. The MS of the metabolite formed in the incubation of ziprasidone in cytosolic fractions of rat, dog, and human showed a protonated molecular ion at 2 mass units higher ( $m/z$  415) than the parent molecule ( $m/z$  413). H/D exchange using  $\text{D}_2\text{O}$  showed a shift of the protonated molecular ion from  $m/z$  415 to  $m/z$  419 for the full exchanged species  $[\text{M}(\text{d}_3) + \text{D}]^+$ , the increase of 4 mass units compared to the deuterated molecular ion of the parent ( $m/z$  415) suggesting the presence of two exchangeable hydrogen atoms at the benzisothiazole moiety by its reductive cleavage (Fig. 9).

Imatinib is metabolized to several oxidative (hydroxy- and N-oxide) metabolites in liver microsomes and recombinant CYPs [120]. Full-scan MS of five metabolites showed the similar protonated molecular ion ( $m/z$  510), 16 mass units higher than the parent molecule ( $m/z$  494), suggesting the addition of an oxygen atom. Liquid chromatography with deuterium oxide-containing mobile phase (H/D exchange) or incorporation of  $^{18}\text{O}$  from  $\text{H}_2^{18}\text{O}$  techniques were able to elucidate the structures of two new hydroxy- and three new N-oxide metabolites (Fig. 10).

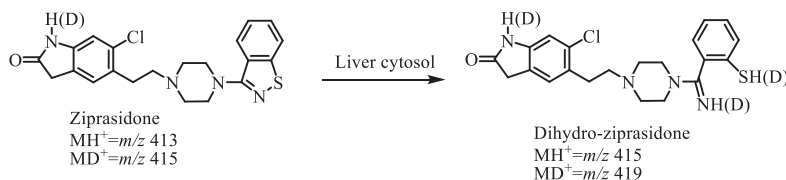


FIG. 9 H/D exchange scheme of dihydro-ziprasidone.

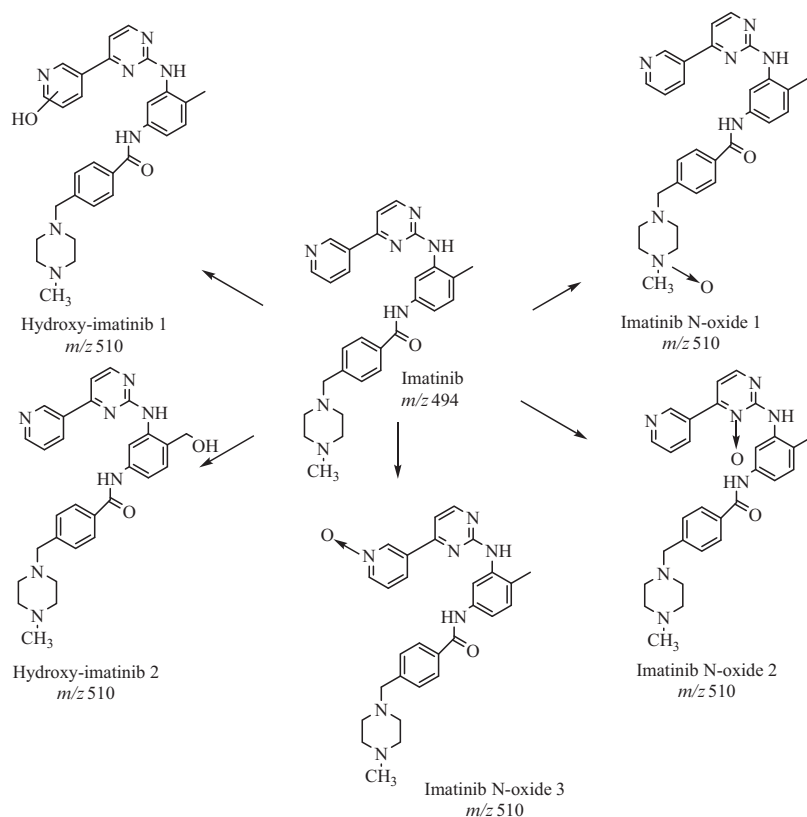


FIG. 10 The structures of isobaric metabolites of imatinib.

## 5.2 Chemical derivatization

Chemical derivatization is used to convert the non-UV absorbing and nonionizable analytes into products that are easily chromatographed or detected with high sensitivity [13]. Derivatization is useful to characterize the functional group ( $-\text{OH}$ ,  $-\text{COOH}$ ,  $-\text{NH}_2$ ,  $-\text{NH}$ , and  $-\text{SH}$ ), to identify unstable, polar, and unusual metabolites, to enhance detection of low molecular weight metabolites, to confirm MS fragmentation, and to improve sensitivity of metabolite present only in trace amounts [115, 117, 121]. Some of the common derivatization reagents for various functional groups are shown in Table 2.

In addition, several quaternary nitrogen and triphenylphosphonium compounds have been used for derivatizing low molecular weight primary and secondary amines and carboxylic acids to enhance their detection by LC-MS [122, 123]. Other reagents, such as 2-chloro-1-methylpyridinium iodide (CMPI) and 1-ethyl-3-(3-dimethylaminopropyl)-carbodiimide (EDC), have also been used for the derivatization of carboxyl acids [124].

### 5.2.1 Increased LC retention and sensitivity in LC-MS for polar metabolites

Chemical modifications by the introduction of an easily ionizable group or a permanent charge are useful for enhancing detection in LC-MS. Xu and Spink used 1,2-

**TABLE 2** Common derivatization reagents for various functional groups.

Functional group	Derivatization reagent	Product	Mass shift
Alcohol (ROH)	Acetyl chloride MTBSTFA	ROCOCH <sub>3</sub>	42
		ROSi(t-Bu)(CH <sub>3</sub> ) <sub>2</sub>	114
Phenol (PhOH)	Acetyl chloride MTBSTFA	PhOCOCH <sub>3</sub>	42
		PhOSi(t-Bu)(CH <sub>3</sub> ) <sub>2</sub>	114
	Dansyl chloride	PhO-Dansyl	233
	Diazomethane	PhOCH <sub>3</sub>	14
	1,2-Dimethylimidazole sulfonyl chloride	PhODMIS	166
Amine (RNH <sub>2</sub> )	Acetyl chloride	RNHCOCH <sub>3</sub>	42
	MBTFA	RNHCOCF <sub>3</sub>	96
	Dansyl chloride	RNH-Dansyl	233
Carboxylic acid (RCOOH)	Diazomethane	RCOOCH <sub>3</sub>	14
	Ethanol/H <sub>2</sub> SO <sub>4</sub>	RCOOCH <sub>2</sub> CH <sub>3</sub>	28
Aldehyde (RCHO)	Hydrazine	RCH=NNH <sub>2</sub>	14
N-oxide (R <sub>3</sub> NO)	Titanum(III) chloride	R <sub>3</sub> N	-16
Thiol (RSH)	Dansyl aziridine	RSCH <sub>2</sub> CH <sub>2</sub> NH-Dansyl	276
Guanidine (RC(=NH)NH <sub>2</sub> )	Hexafluoroacetyl-acetone	Cyclic product	172

dimethylimidazole-4-sulfonyl chloride (DMISC), a phenol selective reagent, to enhance sensitivity for determination of estrogens and 1-hydroxypyrene, a widely used biomarker of PAH exposure, in human urine [125].

Prakash et al. have used dansyl chloride derivatization technique to characterize the three polar metabolites (M1A, M1B, and M4) of ezlopitant in human urine [126]. These metabolites have resulted from oxidative dealkylation (Fig. 11). Derivatization of M1A and M1B with dansyl chloride formed the products, which showed MH<sup>+</sup> at *m/z* 664 and 648, respectively, 466 Da higher (addition of two dansyl moieties) than the MH<sup>+</sup> of underivatized M1A and M1B, suggesting the presence of an amine and a phenolic functionality in these metabolites. On the other hand, the derivatization of M4 with dansyl chloride gave a protonated molecule of *m/z* 429, 233 Da higher than the protonated molecule of underivatized M4, corresponding to the presence of only one amino group.

### 5.2.2 Unusual metabolite characterization

Sharma et al. used the hexafluoroacetylacetone (HFAA) as a derivatization reagent to identify an unusual metabolite of a DPP-IV inhibitor, PF-734200 in preclinical species and humans [127]. Several unusual metabolites were identified in this study. One of the metabolite M1 is derived via oxidative scission of the pyrimidine ring resulting in a net loss of three carbons and formation of a guanidino group (Fig. 12). The presence of a guanidino group was established using a highly selective reagent, HFAA. Treatment of isolated M1 with HFAA forms the cyclized bis (trifluoromethyl) pyrimidine derivative corresponding to an *m/z* value of 503.1800, 172 atomic mass units (amu) greater than the underivatized compound, indicating the addition of an HFAA moiety and subsequent loss of two molecules

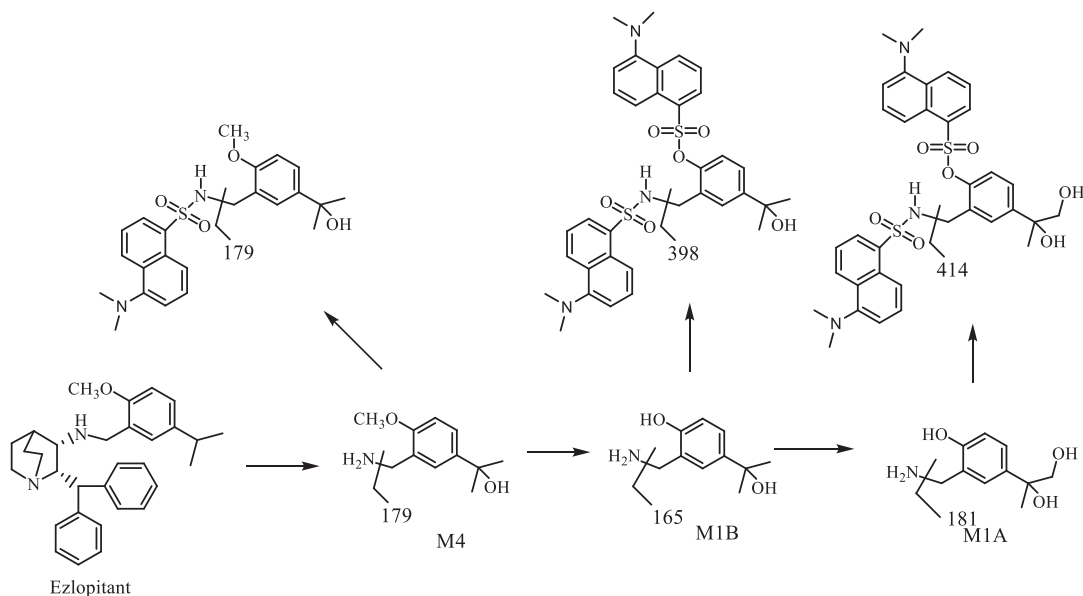


FIG. 11 Derivatization scheme of polar metabolites of ezlopitant with dansyl chloride.

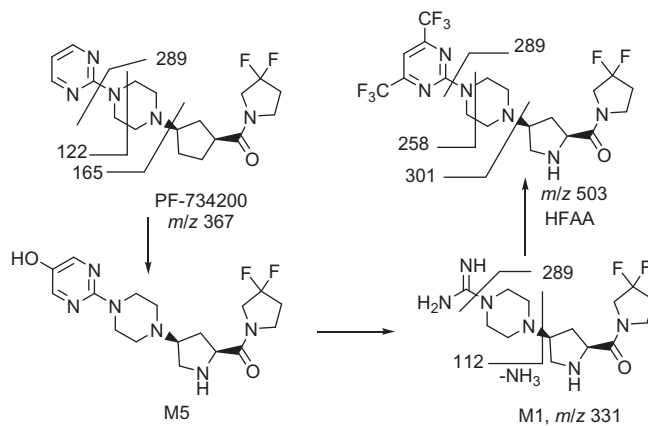


FIG. 12 Derivatization scheme for the unusual metabolite of PF-734200 with HFAA.

of water. Its MS<sup>2</sup> product ion spectrum showed diagnostic fragment ions at  $m/z$  301, 289, and 258. The presence of ions at  $m/z$  301 (189Da higher than those of parent compound), corresponding to an HFAA and ammonia, suggested the addition of HFAA to the modified pyrimidine ring. H/D exchange showed a 5Da shift of the protonated molecular ion from  $m/z$  331.2054 to 336.2370, suggesting the presence of four exchangeable hydrogen atoms on M1, one from the pyrrolidine nitrogen and the other three from the “exposed” guanidine nitrogens of the proposed ring-opened structure.

### 5.2.3 Unstable metabolites

As described above, a novel metabolite of an antipsychotic drug, ziprasidone was identified as the dihydro-ziprasidone, in the cytosolic fractions of preclinical species in humans. This metabolite was not detected *in vivo* due to either its instability or further metabolism to secondary metabolites. The proposed structure was further corroborated by its derivatization with dansyl aziridine, a specific derivatizing reagent, for the thiol group [119]. Treatment of metabolite with dansyl aziridine formed a new product which gave a protonated molecular ion at  $m/z$  691, 176Da higher than the  $(M + H)^+$  of the metabolite, suggesting the addition of a dansyl aziridine moiety (Fig. 13). The product ion spectrum of  $m/z$  691 showed fragment ions at  $m/z$  455, 412, 309, 280, 263, 194, and 170, consistent with the proposed structure.

### 5.2.4 Isomeric metabolite characterization

At the lead optimization stage, information on the exact metabolic sites of the new molecular entities can direct medicinal chemists to synthesize metabolically more stable analogs by blocking sites of metabolism with superior PK and pharmacological properties. During the course of metabolic profiling of a potential clinical candidate **1**, ((*R*)-2-(2-hydroxyphenyl)-3-(1-phenylpropan-2-yl)-5-(trifluoromethyl)pyrido[4,3-*d*]pyrimidin-4(3*H*)-one), a calcium receptor antagonist, two hydroxylated metabolites (M5 and M6) were detected in human liver microsomes in an NADPH-dependent fashion [128]. In addition to these two hydroxylated metabolites, two glutathione (GSH) conjugates of **1** were detected in human liver microsomes fortified with GSH. MS<sup>2</sup> spectra of these metabolites indicated that the hydroxylation and GSH conjugation had occurred at the 2-hydroxyphenyl moiety to form two regioisomers (Fig. 14). It was suggested that the hydroxylated metabolites underwent further oxidation to the electrophilic *ortho* quinone species. The derivatization with butyl boronic acid, a reagent used to selectively derivatize vicinal diols and catechol proved to be useful to characterize the major hydroxylated metabolite (M6).

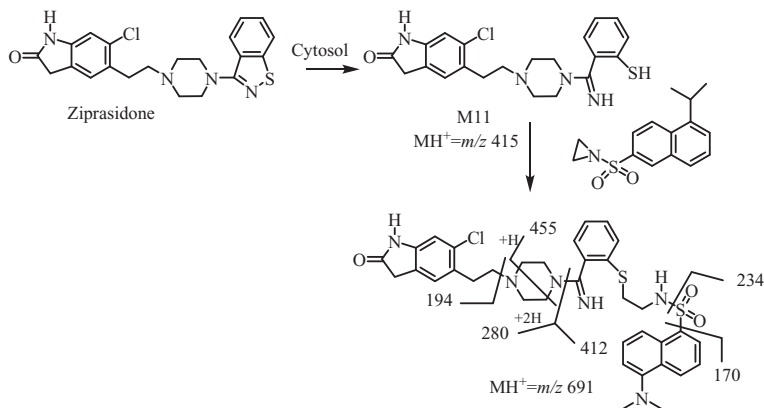


FIG. 13 Derivatization reaction of ziprasidone metabolite with dansyl aziridine.



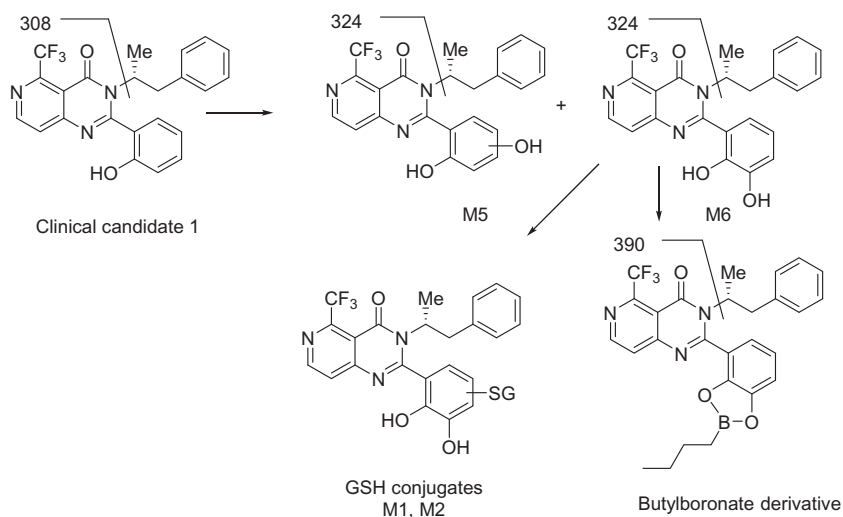


FIG. 14 The structures of isobaric metabolites of clinical candidate 1.

### 5.2.5 Determination of site of glucuronidation

In humans, approximately >20% of xenobiotics are metabolized to form glucuronides. Since the conjugation can occur with a different functional group ( $-\text{OH}$ ,  $-\text{NH}_2$ ,  $-\text{NHR}$ ,  $-\text{NR}_2$ ,  $-\text{SH}$ , and  $-\text{COOH}$ ) of a drug and therefore, isomers of the metabolites are commonly formed. It is not possible to differentiate these isomeric glucuronides from each other by MS alone since these isomeric glucuronides have the same  $\text{MH}^+$  ions and their  $\text{MS}/\text{MS}$  spectra are almost identical involving the neutral loss of 176 Da (i.e., monodehydrated glucuronic acid). It is important to determine the identity and the pharmacological activity of these glucuronides. For example, morphine forms two glucuronides, morphine-3-glucuronide (M3G) and morphine-6-glucuronide (M6G) while M6G is more pharmacologically active than morphine itself.

Chemical derivatization with DMISC has been used to differentiate an aliphatic and aromatic glucuronidation. M6G is an aliphatic hydroxylated glucuronide whereas M3G is a phenolic one [129]. Treatment of M3G and M6G with DMISC showed that only M6G formed the DMIS adduct and M3G gave no product, probably because the phenol group was blocked. Schaefer et al. used acetic anhydride for acetylation of carvedilol and carvedilol glucuronides, for structural determination [130]. Cui and Harvison used chemical modification with 3-pyridylcarbinol in combination with LC-MS/MS to determine the site of glucuronidation of an *N*-(3,5-dichlorophenyl) succinimide metabolite [131]. The structures of regioisomeric glucuronide of an angiotensin II receptor antagonist were also differentiated by preparing dimethylated glucuronides, with diazomethane [126]. Kassahun et al. [132] reported the structural characterization of two regioisomeric *N*-glucuronides of the antipsychotic olanzapine by derivatization with phenyl isothiocyanate.

Lampinen-Salomonsson et al. used chemical derivatization and LC-MS/MS to differentiate the three isomers of estriol glucuronide; estriol-16-glucuronide (E16G), estriol-17-glucuronide (E17G), and estriol-3-glucuronide (E3G) [133]. These isomers gave almost

identical product ion spectra, a neutral loss of 176 Da, which made it impossible to determine the position of conjugation by MS/MS alone. Derivatization using a combination of three reagents, 2-chloro-1-methylpyridinium iodide, 1-ethyl-3-(3 dimethylaminopropyl)-carbodiimide, and 2-picolylamine provided a selective fragmentation pattern that differentiated the isomers of E16G and E17G. E3G, which lacks a free phenolic group, was differentiated by derivatization with 2-chloro-1-methylpyridinium iodide.

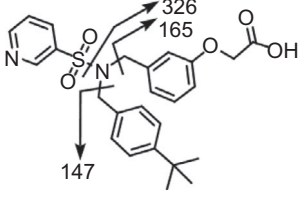
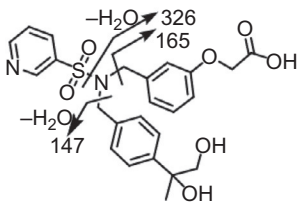
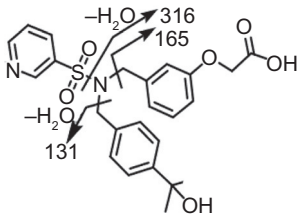
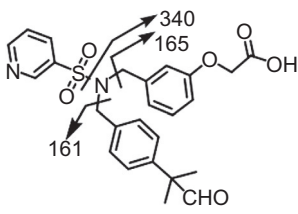
Kong et al. demonstrated that O- and N-glucuronides can be differentiated unambiguously by gas-phase ion/molecule reactions with  $\text{HSiCl}_3$  in a quadrupole ion trap mass spectrometer [134]. The glucuronides were ionized by negative mode electrospray ionization (ESI). The deprotonated glucuronides were isolated in the ion trap and allowed to react with  $\text{HSiCl}_3$  for 30 – 100 ms. Both N- and O-glucuronides generate an  $\text{HSiCl}_3$  adduct that loses one HCl molecule ( $[\text{M} - \text{H} + \text{HSiCl}_3 - \text{HCl}]^-$ ) as a primary product ion. However, the product ion spectra of deprotonated adducts for secondary and tertiary N-glucuronides yield a diagnostic dominant fragment ( $[\text{M} - \text{H} + \text{HSiCl}_3 - 2\text{HCl}]^-$ ) that loses two molecules of HCl but this product ion was not observed for deprotonated O-glucuronides.

### 5.3 Nuclear magnetic resonance spectroscopy

NMR is commonly utilized for unambiguous structural characterization of metabolites. Compared with MS, NMR spectroscopy is much less sensitive but has the key advantages of absence of quenching or enhancement phenomena, and the ability to use a huge range of the most powerful experiments for metabolite structure elucidation. NMR is a nondestructive technique and therefore it can couple with other spectroscopic methods such as mass spectrometry. The combination of HPLC with NMR and MS provides very comprehensive structural data on metabolites both from in vitro and in vivo studies. Such an approach was applied to characterize the unusual metabolites (M22, M23, M24, and M26) of a drug candidate, Compound A, (3-[[4-*tert*-butyl-benzyl)-(pyridine-3-sulfonyl)-amino]-methyl]-phenoxy)-acetic acid, an EP2 receptor-selective prostaglandin E2 agonist in human live microsomes and recombinant enzymes [135]. Full-scan MS and MS/MS spectra of all these metabolites suggested that the modification had occurred at the *tert*-butyl-benzyl moiety. LC- $^1\text{H}$  NMR was proved to be very useful to define the kind of modification on this moiety.  $^1\text{H}$  spectrum of M22 gave resonance at  $\delta$  1.36 (s, 3H,  $\text{CH}_3$ ), suggesting the presence of only one methyl group. The resonance at  $\delta$  3.50 (s, 2H,  $\text{CH}_2\text{OH}$ ) indicated the oxidation of one of the methyl group to the hydroxy methyl group. Based on these data, M22 was identified as (3-[[4-(1,2-dihydroxy-1-methyl-ethyl)-benzyl)-(pyridine-3-sulfonyl)-amino]-methyl]-phenoxy)-acetic acid (Table 3).

The product ion spectrum of M23 ( $m/z$  471) showed prominent fragment ions at  $m/z$  453, 310, 165, and 131 (Table 3). The ion at  $m/z$  453, a loss of 18 Da from the protonated molecular ion, suggested the presence of an aliphatic hydroxyl group. The ions at  $m/z$  310 and 131 (16 Da lower than those of the parent molecule) suggested that a methyl group was replaced by a hydroxyl group. It was corroborated by its  $^1\text{H}$  NMR spectrum, which gave resonance at  $\delta$  (ppm) 1.39 (s, 6H,  $2\text{CH}_3$ ), suggesting the loss of one methyl group. All the other resonances were substantially similar to the parent compound (Table 3). Based on these data, M23 was tentatively identified as (3-[[4-(1-hydroxy-1-methyl-ethyl)-benzyl)-(pyridine-3-sulfonyl)-amino]-methyl]-phenoxy)-acetic acid.

**TABLE 3** MS/MS fragment and  $^1\text{H}$  NMR data for compound A and metabolites.

Metabolite	MH <sup>+</sup>	Empirical formula	Structure	MS/MS fragment ions	$^1\text{H}$ NMR
Parent	469	C <sub>25</sub> H <sub>28</sub> N <sub>2</sub> O <sub>5</sub> S		423 (MH-HCOOH), 413, 326, 165, 147	$\delta$ 1.19 (s, 9H, 3CH <sub>3</sub> )
M22	487	C <sub>24</sub> H <sub>27</sub> N <sub>2</sub> O <sub>7</sub> S		469 (M-H <sub>2</sub> O), 335, 326, 165, 147	$\delta$ 1.36 (s, 3H, CH <sub>3</sub> ), 3.50 (s, 2H, CH <sub>2</sub> OH)
M23	471	C <sub>24</sub> H <sub>27</sub> N <sub>2</sub> O <sub>6</sub> S		453 (MH-H <sub>2</sub> O), 310, 165, 131	$\delta$ 1.39 (s, 6H, 2CH <sub>3</sub> )
M24	483	C <sub>25</sub> H <sub>27</sub> N <sub>2</sub> O <sub>6</sub> S		437 (MH-HCOOH), 340, 165, 161	1.33 (s, 6H, 2CH <sub>3</sub> ) and 9.34 (s, 1H, CHO)

M24 displayed an MH<sup>+</sup> at  $m/z$  483, 14 Da higher than the parent compound. Its product ion spectrum gave fragment ions at  $m/z$  340, 295, 266, 165, and 161 (Table 3). The ions at  $m/z$  340, and 161 were 14 Da higher than those of the parent compound, suggesting the addition of an oxygen atom with a concomitant loss of two hydrogen atoms.  $^1\text{H}$  NMR spectrum of M24 gave resonance at  $\delta$  (ppm) 1.33 (s, 6H, 2CH<sub>3</sub>) further suggesting the loss of one methyl group. The

resonance at  $\delta$  (ppm) 9.34 (s, 1H, CHO) suggested that the methyl group is oxidized to an aldehyde. M24 was identified as (3-[[[4-(1,1-dimethyl-2-oxo-ethyl)-benzyl]-(pyridine-3-sulfonyl)-amino]-methyl]-phenoxy)-acetic acid.

Full-scan of M26 displayed an  $MH^+$  at  $m/z$  453, 16Da lower than the parent compound, suggesting the loss of a methyl group and a hydrogen atom. The fragment ions at  $m/z$  310, 165, and 131 in its product ion spectrum suggested that 16 mass units were lost from the *tert*-butyl moiety (Table 3).  $^1H$  NMR spectrum of M26 gave resonances at  $\delta$  (ppm) 5.06 (s, 1H,  $-RC = CH_2$ ) and 5.34 (s, 1H,  $-RC = CH_2$ ), which are consistent with a terminal olefin group. M26 was thus identified as (3-[[[4-isopropenylbenzyl]-(pyridine-3-sulfonyl)-amino]-methyl]-phenoxy)-acetic acid.

Dowty et al. used  $^1H$  and  $^{13}C$  NMR to define the exact site of hydroxylation of one of the major metabolite of tofacitinib, 3-[(3R,4R)-4-methyl-3-(methyl(7H-pyrrolo[2,3-d]pyrimidin-4-yl)amino)-piperidin-1-yl]-3-oxopropanenitrile, a novel, oral JAK inhibitor [136]. It is extensively metabolized in human and several oxidative and conjugative metabolites were detected in excreta and plasma. Full-scan MS and MS/MS of the most abundant circulating metabolite M9 suggested that the oxidation had occurred at the pyrrole-pyrimidine moiety but the exact site of the oxidation could not be identified by MS data. The  $^1H$  NMR spectrum of M9 indicated the absence of the two aromatic hydrogen atoms from the pyrrole ring but a set of nonequivalent methylene resonances between 3.7 and 4.0 ppm. These data suggest that the oxidation had occurred at the C-5 or C-6 position of the pyrrole ring.  $^{13}C$  NMR showed three carbon chemical shifts at  $\delta$  94.7, 164.1, and 175.3 ppm, which support the oxidation at the C6 of the pyrrole moiety. Therefore, based on these data the structure of M9 was assigned as the 5,7-dihydro-6H-pyrrolo[2,3-d]pyrimidin-6-one (Fig. 15).

## 6 Conclusion and future trends

This chapter has discussed various analytical methodologies to identify and quantify metabolites of small molecule compounds while clearly highlighting mass spectrometry's invaluable contribution to the biopharmaceutical industry. In terms of sample preparation procedures, the level of sample preparation is different for drug discovery and development. In drug discovery, it is the norm to require faster sample turn around with a higher load of samples to be analyzed so PPT may be the ideal choice and most cost-effective one. This is the

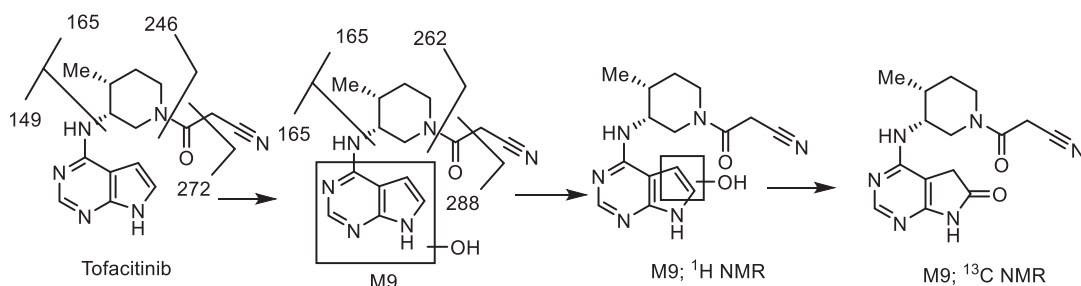


FIG. 15 MS/fragmentation of Tofacitinib and M9.

general strategy but in some cases depending on the analyte/s in question other sample preparation techniques such as SPE may be more appropriate for the problem in hand or even chemical derivatization. For drug development, higher sensitivity and better selectivity, the robustness of methods are more critical than the speed of analysis and higher sample numbers so for metabolite identification, more time can be spent in the sample preparation and also chromatographic separation.

Mass spectrometry has continued to evolve over the years. Instrument manufacturers are making the instruments more sensitive and with increased robustness to cope with the demands of drug metabolism studies. MS has been and continues to be a pivotal analytical technique in drug metabolism for quantitative and qualitative studies in both drug discovery and development. Other wet analytical techniques such as chemical derivatization, H/D exchange and LC-NMR combined with MS proved to be very useful for structural characterization and differentiation of isobaric/isomeric metabolites when this information could not be obtained by MS alone.

The advent of high-resolution mass spectrometry with accurate mass measurements has made a big impact in metabolite identification studies. In fact, this development has paved the way for a wave of new technologies introduced in the last decade such as QTOFs and Orbitraps. We have also observed a continuous fierce battle in the development of these technologies to the advantage of the end user. As far as technology goes, there is only so much more that can be done to improve sensitivity, robustness, spectral resolution, etc. The emphasis now is on the data acquisition strategies and workflows such as building more intelligent data-independent acquisition like SWATH or SONAR which will allow for a much richer data information strategy from a minimum number of acquisitions. As more data is obtained by these approaches it is very important to have the software tools available to interrogate the data and consume it with reasonable confidence. This is the real bottleneck in metabolite identification and structural elucidation. This will be a topic which will be discussed later in this book (Chapter 3) but we expect to see more and more efforts in the bioinformatics area and a rise in the implantation of machine learning and artificial intelligence to help the scientist make educated decisions about the data generated.

## References

- [1] A. Parkinson, B.W. Ogilvie, D.B. Buckley, F. Kazmi, O. Parkinson, C. Klaassen (Ed.), Casarett and Doull's Toxicology: The Basic Science of Poisons, 2018, pp. 133–224.
- [2] A. Saravanakumar, et al., Physicochemical properties, biotransformation, and transport pathways of established and newly approved medications: a systematic review of the top 200 most prescribed drugs vs. the FDA-approved drugs between 2005 and 2016, *Clin. Pharmacokinet.* (2019).
- [3] H. Yu, et al., Contribution of metabolites to P450 inhibition-based drug-drug interactions: scholarship from the drug metabolism leadership group of the innovation and quality consortium metabolite group, *Drug Metab. Dispos.* 43 (4) (2015) 620–630.
- [4] A. Fura, et al., Discovering drugs through biological transformation: role of pharmacologically active metabolites in drug discovery, *J. Med. Chem.* 47 (18) (2004) 4339–4351.
- [5] C. Prakash, et al., In vitro screening techniques for reactive metabolites for minimizing bioactivation potential in drug discovery, *Curr. Drug Metab.* 9 (9) (2008) 952–964.
- [6] R.A. Thompson, et al., In vitro approach to assess the potential for risk of idiosyncratic adverse reactions caused by candidate drugs, *Chem. Res. Toxicol.* 25 (8) (2012) 1616–1632.

- [7] S. Anderson, M.P. Knadler, D. Luffer-Atlas, Overview of metabolite safety testing from an industry perspective, *Bioanalysis* 2 (7) (2010) 1249–1261.
- [8] S. Schadt, et al., A decade in the MIST: learnings from investigations of drug metabolites in drug development under the “metabolites in safety testing” regulatory guidance, *Drug Metab. Dispos.* 46 (6) (2018) 865–878.
- [9] N. Penner, C. Woodward, C. Prakash, ADME-enabling technologies in drug design and development, in: D.Z. S. Surapaneni (Ed.), *Drug Metabolizing Enzymes and Biotransformation Reactions*, John Wiley & Sons, Inc., 2012.
- [10] D. Dalvie, et al., Assessment of three human in vitro systems in the generation of major human excretory and circulating metabolites, *Chem. Res. Toxicol.* 22 (2) (2009) 357–368.
- [11] N. Penner, L. Xu, C. Prakash, Radiolabeled absorption, distribution, metabolism, and excretion studies in drug development: why, when, and how? *Chem. Res. Toxicol.* 25 (3) (2012) 513–531.
- [12] Z.Y. Zhang, C. Prakash, L. Xu, H.A. Philip, W. Lee, L.L. Gan, C. Prakash, D. Zhong (Eds.), *Application of Triple-Quadrupole and its Hybrid Mass Spectrometers for the Identification of Drug Metabolites in Handbook of Metabolic Pathways of Xenobiotics*, John Wiley & Sons, 2013.
- [13] C. Prakash, C.L. Shaffer, A. Nedderman, Analytical strategies for identifying drug metabolites, *Mass Spectrom. Rev.* 26 (3) (2007) 340–369.
- [14] A. Kamel, S. Harriman, C. Prakash, H.A. Philip, W. Lee, L.L. Gan, C. Prakash, D. Zhong (Eds.), *Strategies for the Identification of Unusual and Novel Metabolites using Derivatization, Hydrogen-Deuterium Exchange (HDX) and Liquid Chromatography-Nuclear Magnetic Resonance (LC-NMR) Spectroscopy Techniques in Handbook of Metabolic Pathways of Xenobiotics*, John Wiley & Sons, 2013.
- [15] Y. Cheng, et al., Bile salt homeostasis in normal and bsep gene knockout rats with single and repeated doses of troglitazone, *J. Pharmacol. Exp. Ther.* 362 (3) (2017) 385–394.
- [16] Y. Cheng, et al., Biliary excretion of pravastatin and taurocholate in rats with bile salt export pump (Bsep) impairment, *Biopharm. Drug Dispos.* 37 (5) (2016) 276–286.
- [17] B.B. Chavan, et al., Identification and characterization of fluvastatin metabolites in rats by UHPLC/Q-TOF/MS/MS and in silico toxicological screening of the metabolites, *J. Mass Spectrom.* 52 (5) (2017) 296–314.
- [18] B.B. Chavan, et al., In vitro and in vivo metabolic investigation of the Palbociclib by UHPLC-Q-TOF/MS/MS and in silico toxicity studies of its metabolites, *J. Pharm. Biomed. Anal.* 157 (2018) 59–74.
- [19] S. De Baere, et al., Development and validation of a UPLC-MS/MS and UPLC-HR-MS method for the determination of fumonisin B1 and its hydrolysed metabolites and fumonisin B2 in broiler chicken plasma, *Toxins (Basel)* (2018) 10(2).
- [20] Y. Deng, et al., Rapid identification of efavirenz metabolites in rats and humans by ultra high performance liquid chromatography combined with quadrupole time-of-flight tandem mass spectrometry, *J. Sep. Sci.* 38 (9) (2015) 1529–1536.
- [21] P. Johnsi Rani, et al., Metabolite characterization of ambrisentan, in in vitro and in vivo matrices by UHPLC/QTOF/MS/MS: detection of glutathione conjugate of epoxide metabolite evidenced by in vitro GSH trapping assay, *J. Pharm. Biomed. Anal.* 155 (2018) 320–328.
- [22] D. Koller, et al., Simultaneous determination of six antipsychotics, two of their metabolites and caffeine in human plasma by LC-MS/MS using a phospholipid-removal microelution-solid phase extraction method for sample preparation, *Talanta* 198 (2019) 159–168.
- [23] A. Merou, G. Kaklamanos, G. Theodoridis, Determination of carbadox and metabolites of carbadox and olaquinox in muscle tissue using high performance liquid chromatography-tandem mass spectrometry, *J. Chromatogr. B Anal. Technol. Biomed. Life Sci.* 881-882 (2012) 90–95.
- [24] B. Raju, et al., In vivo metabolic investigation of moxifloxacin using liquid chromatography/electrospray ionization tandem mass spectrometry in combination with online hydrogen/deuterium exchange experiments, *Rapid Commun. Mass Spectrom.* 26 (16) (2012) 1817–1831.
- [25] G. Shankar, et al., Identification and structural characterization of in vivo metabolites of balofloxacin in rat plasma, urine and feces samples using Q-TOF/LC/ESI/MS/MS: in silico toxicity studies, *J. Pharm. Biomed. Anal.* 159 (2018) 200–211.
- [26] C. Cruickshank-Quinn, et al., Multi-step preparation technique to recover multiple metabolite compound classes for in-depth and informative metabolomic analysis, *J. Vis. Exp.* 89 (2014).
- [27] S.M. Friedl, et al., Comparison of liquid-liquid partition, HS-SPME and static HS GC/MS analysis for the quantification of (–)-linalool in human whole blood samples, *Nat. Prod. Commun.* 5 (9) (2010) 1447–1452.



- [28] C. Vandenbosch, et al., Determination of leucovorin and 5-fluorouracil in plasma by high-performance liquid chromatography, *J. Chromatogr.* 612 (1) (1993) 77–85.
- [29] F. Khuda, et al., Method development and validation for simultaneous determination of lumefantrine and its major metabolite, desbutyl lumefantrine in human plasma using RP-HPLC/UV detection, *J. Chromatogr. B Anal. Technol. Biomed. Life Sci.* 944 (2014) 114–122.
- [30] N. Samiei, et al., Development and validation of an HPLC method for determination of amifostine and/or its metabolite (WR-1065) in human plasma using OPA derivatization and UV detection, *Iran. J. Pharm. Res.* 14 (4) (2015) 1051–1057.
- [31] F. Sotoudegan, et al., Development of an RP-HPLC-UV method for simultaneous detection of nimodipine and its metabolite in cerebrospinal fluid of rat, *Iran. J. Pharm. Res.* 16 (2) (2017) 471–477.
- [32] A.E. Nassar, et al., Liquid chromatography-accurate radioisotope counting and microplate scintillation counter technologies in drug metabolite studies, *J. Chromatogr. Sci.* 42 (7) (2004) 348–353.
- [33] M. Zhu, et al., Analysis of low level radioactive metabolites in biological fluids using high-performance liquid chromatography with microplate scintillation counting: method validation and application, *J. Pharm. Biomed. Anal.* 39 (1-2) (2005) 233–245.
- [34] G.J. Dear, et al., TopCount coupled to ultra-performance liquid chromatography for the profiling of radio-labeled drug metabolites in complex biological samples, *J. Chromatogr. B Anal. Technol. Biomed. Life Sci.* 844 (1) (2006) 96–103.
- [35] A.E. Nassar, S.M. Bjorge, D.Y. Lee, On-line liquid chromatography-accurate radioisotope counting coupled with a radioactivity detector and mass spectrometer for metabolite identification in drug discovery and development, *Anal. Chem.* 75 (4) (2003) 785–790.
- [36] A.E. Nassar, D.Y. Lee, Novel approach to performing metabolite identification in drug metabolism, *J. Chromatogr. Sci.* 45 (3) (2007) 113–119.
- [37] Q. Li, et al., The distribution pattern of intravenous [ $^{14}\text{C}$ ] artesunate in rat tissues by quantitative whole-body autoradiography and tissue dissection techniques, *J. Pharm. Biomed. Anal.* 48 (3) (2008) 876–884.
- [38] L. Xu, et al., Identification of novel metabolites of colchicine in rat bile facilitated by enhanced online radiometric detection, *Drug Metab. Dispos.* 36 (4) (2008) 731–739.
- [39] K.E. Wade, et al.,  $^{19}\text{F}$  and  $^1\text{H}$  magnetic resonance strategies for metabolic studies on fluorinated xenobiotics: application to flurbiprofen [2-(2-fluoro-4-biphenyl)propionic acid], *J. Pharm. Biomed. Anal.* 8 (5) (1990) 401–410.
- [40] J.P. Shockcor, et al., Combined HPLC, NMR spectroscopy, and ion-trap mass spectrometry with application to the detection and characterization of xenobiotic and endogenous metabolites in human urine, *Anal. Chem.* 68 (24) (1996) 4431–4435.
- [41] O. Corcoran, et al., HPLC/ $^1\text{H}$  NMR spectroscopic studies of the reactive alpha-1-O-acyl isomer formed during acyl migration of S-naproxen beta-1-O-acyl glucuronide, *Chem. Res. Toxicol.* 14 (10) (2001) 1363–1370.
- [42] E.M. Lenz, et al., HPLC-NMR with severe column overloading: fast-track metabolite identification in urine and bile samples from rat and dog treated with [ $^{14}\text{C}$ ] ZD6126, *J. Pharm. Biomed. Anal.* 43 (3) (2007) 1065–1077.
- [43] R. Ramanathan, et al., Novel MS solutions inspired by MIST, *Bioanalysis* 2 (7) (2010) 1291–1313.
- [44] Y. Sun, et al., Metabolite identification of the antimalarial naphthoquinone using liquid chromatography-tandem high-resolution mass spectrometry in combination with multiple data-mining tools, *Biomed. Chromatogr.* 32 (6) (2018) e4207.
- [45] L. Wang, et al., Metabolism and disposition of  $^{14}\text{C}$ -labeled peliglitazar in humans, *Drug Metab. Dispos.* 39 (2) (2011) 228–238.
- [46] R. Plumb, et al., Ultra-performance liquid chromatography coupled to quadrupole-orthogonal time-of-flight mass spectrometry, *Rapid Commun. Mass Spectrom.* 18 (19) (2004) 2331–2337.
- [47] R.S. Plumb, et al., Generation of ultrahigh peak capacity LC separations via elevated temperatures and high linear mobile-phase velocities, *Anal. Chem.* 78 (20) (2006) 7278–7283.
- [48] T.J. Athersuch, et al., UPLC-MS, HPLC-radiometric, and NMR-spectroscopic studies on the metabolic fate of 3-fluoro-[ $^{14}\text{C}$ ] aniline in the bile-cannulated rat, *Xenobiotica* 40 (7) (2010) 510–523.
- [49] R.J. Mortishire-Smith, et al., Generic dealkylation: a tool for increasing the hit-rate of metabolite rationalization, and automatic customization of mass defect filters, *Rapid Commun. Mass Spectrom.* 23 (7) (2009) 939–948.
- [50] K.P. Bateman, et al., MSE with mass defect filtering for in vitro and in vivo metabolite identification, *Rapid Commun. Mass Spectrom.* 21 (9) (2007) 1485–1496.



- [51] I.D. Wilson, et al., High resolution “ultra performance” liquid chromatography coupled to oa-TOF mass spectrometry as a tool for differential metabolic pathway profiling in functional genomic studies, *J. Proteome Res.* 4 (2) (2005) 591–598.
- [52] J. Castro-Perez, et al., Increasing throughput and information content for in vitro drug metabolism experiments using ultra-performance liquid chromatography coupled to a quadrupole time-of-flight mass spectrometer, *Rapid Commun. Mass Spectrom.* 19 (6) (2005) 843–848.
- [53] M. Goel, et al., Optimization of a two-dimensional liquid chromatography-supercritical fluid chromatography-mass spectrometry (2D-LC-SFS-MS) system to assess “in vivo” inter-conversion of chiral drug molecules, *J. Chromatogr. B Anal. Technol. Biomed. Life Sci.* 1084 (2018) 89–95.
- [54] R. Hofstetter, G.M. Fassauer, A. Link, Supercritical fluid extraction (SFE) of ketamine metabolites from dried urine and on-line quantification by supercritical fluid chromatography and single mass detection (on-line SFE-SFC-MS), *J. Chromatogr. B Anal. Technol. Biomed. Life Sci.* 1076 (2018) 77–83.
- [55] G.M. Fassauer, et al., Ketamine metabolites with antidepressant effects: Fast, economical, and eco-friendly enantioselective separation based on supercritical-fluid chromatography (SFC) and single quadrupole MS detection, *J. Pharm. Biomed. Anal.* 146 (2017) 410–419.
- [56] H. Licea Perez, D. Knecht, C.A. Evans, Overcoming bioanalytical challenges associated with the separation and quantitation of GSK1278863, a HIF-prolyl hydroxylase inhibitor, and its 14 stereoisomeric metabolites, *J. Chromatogr. B Anal. Technol. Biomed. Life Sci.* 1009-1010 (2016) 7–16.
- [57] E.L. Regalado, et al., Chromatographic resolution of closely related species: drug metabolites and analogs, *J. Sep. Sci.* 37 (9-10) (2014) 1094–1102.
- [58] V. Jacques, et al., Differentiation of antiinflammatory and antitumorigenic properties of stabilized enantiomers of thalidomide analogs, *Proc. Natl. Acad. Sci. U. S. A.* 112 (12) (2015) E1471–E1479.
- [59] D. Hainzl, A. Parada, P. Soares-da-Silva, Metabolism of two new antiepileptic drugs and their principal metabolites S(+)- and R(–)-10,11-dihydro-10-hydroxy carbamazepine, *Epilepsy Res.* 44 (2-3) (2001) 197–206.
- [60] P.R. Jennifer Simeone, Enantiomeric separation of warfarin and propranolol and its hydroxylated metabolites it was possible to separate the different chiral forms by SFC, Waters Corp. (2014).
- [61] J.B. Fenn, Electrospray wings for molecular elephants (Nobel lecture), *Angew. Chem. Int. Ed. Eng.* 42 (33) (2003) 3871–3894.
- [62] J.B. Fenn, Electrospray ionization mass spectrometry: how it all began, *J. Biomol. Tech.* 13 (3) (2002) 101–118.
- [63] J.F. Mora, et al., Electrochemical processes in electrospray ionization mass spectrometry, *J. Mass Spectrom.* 35 (8) (2000) 939–952.
- [64] N.D. Doan, et al., Mass spectrometry-based proteomics to define intracellular collagen interactomes, *Methods Mol. Biol.* 1944 (2019) 95–114.
- [65] H.C. Tseng, C.N.S. Santos, Targeted mass spectrometry-based proteomics tools for strain optimization, *Methods Mol. Biol.* 1927 (2019) 191–201.
- [66] V. Mohanty, et al., Proteomics and visual health research: proteome of the human sclera using high-resolution mass spectrometry, *OMICS* 23 (2) (2019) 98–110.
- [67] T. Tucholski, et al., A top-down proteomics platform coupling serial size exclusion chromatography and Fourier transform ion cyclotron resonance mass spectrometry, *Anal. Chem.* 91 (6) (2019) 3835–3844.
- [68] I.T. Wang, Y.T. Feng, C.Y. Chen, Determination of 17 illicit drugs in oral fluid using isotope dilution ultra-high performance liquid chromatography/tandem mass spectrometry with three atmospheric pressure ionizations, *J. Chromatogr. B Anal. Technol. Biomed. Life Sci.* 878 (30) (2010) 3095–3105.
- [69] N.J. Clarke, et al., Systematic LC/MS metabolite identification in drug discovery, *Anal. Chem.* 73 (15) (2001) 430A–439A.
- [70] A. Wohlfarth, et al., Metabolic characterization of AH-7921, a synthetic opioid designer drug: in vitro metabolic stability assessment and metabolite identification, evaluation of in silico prediction, and in vivo confirmation, *Drug Test. Anal.* 8 (8) (2016) 779–791.
- [71] A.K. Majumdar, et al., Pharmacokinetics of ertapenem in healthy young volunteers, *Antimicrob. Agents Chemother.* 46 (11) (2002) 3506–3511.
- [72] S.H. Shin, et al., Analysis of vipadenant and its in vitro and in vivo metabolites via liquid chromatography-quadrupole-time-of-flight mass spectrometry, *Pharmaceutics* 10 (4) (2018).
- [73] L.P. Leonart, et al., New metabolites of coumarin detected in human urine using ultra performance liquid chromatography/quadrupole-time-of-flight tandem mass spectrometry, *Molecules* 22 (11) (2017).

- [74] P.N. Patel, et al., In vivo metabolite identification of acotiamide in rats using ultra-performance liquid chromatography-quadrupole/time-of-flight mass spectrometry, *Biomed. Chromatogr.* 31 (7) (2017).
- [75] G. Song, et al., UPLC-QTOF-MS/MS based screening and identification of the metabolites in rat bile after oral administration of imperatorin, *J. Chromatogr. B Anal. Technol. Biomed. Life Sci.* 1022 (2016) 21–29.
- [76] Y. Lecompte, et al., UPLC-ESI-Q-TOF-MS(E) identification of urinary metabolites of the emerging sport nutrition supplement methoxyisoflavone in human subjects, *J. Pharm. Biomed. Anal.* 96 (2014) 127–134.
- [77] T. Rousu, O. Pelkonen, A. Tolonen, Rapid detection and characterization of reactive drug metabolites in vitro using several isotope-labeled trapping agents and ultra-performance liquid chromatography/time-of-flight mass spectrometry, *Rapid Commun. Mass Spectrom.* 23 (6) (2009) 843–855.
- [78] S. Shimma, et al., Miniaturized high-resolution time-of-flight mass spectrometer MULTUM-S II with an infinite flight path, *Anal. Chem.* 82 (20) (2010) 8456–8463.
- [79] J. Flensburg, et al., Applications and performance of a MALDI-ToF mass spectrometer with quadratic field reflectron technology, *J. Biochem. Biophys. Methods* 60 (3) (2004) 319–334.
- [80] R.J. Cotter, et al., Tandem time-of-flight (TOF/TOF) mass spectrometry and proteomics, *J. Mass Spectrom. Soc. Jpn.* 53 (1) (2005) 7–17.
- [81] A.G. Brenton, et al., Improvement of the duty cycle of an orthogonal acceleration time-of-flight mass spectrometer using ion gates, *Rapid Commun. Mass Spectrom.* 21 (18) (2007) 3093–3102.
- [82] T. Satoh, T. Sato, J. Tamura, Development of a high-performance MALDI-TOF mass spectrometer utilizing a spiral ion trajectory, *J. Am. Soc. Mass Spectrom.* 18 (7) (2007) 1318–1323.
- [83] L. Sturiale, et al., Reflectron MALDI TOF and MALDI TOF/TOF mass spectrometry reveal novel structural details of native lipooligosaccharides, *J. Mass Spectrom.* 46 (11) (2011) 1135–1142.
- [84] M.M. Ahlstrom, M. Ridderstrom, I. Zamora, CYP2C9 structure-metabolism relationships: substrates, inhibitors, and metabolites, *J. Med. Chem.* 50 (22) (2007) 5382–5391.
- [85] B. Bonn, et al., Enhanced metabolite identification with MS(E) and a semi-automated software for structural elucidation, *Rapid Commun. Mass Spectrom.* 24 (21) (2010) 3127–3138.
- [86] A.C. Li, et al., Update on hydrocodone metabolites in rats and dogs aided with a semi-automatic software for metabolite identification *Mass-MetaSite*, *Xenobiotica* 43 (4) (2013) 390–398.
- [87] E.N. Cece-Esencan, et al., Software-aided cytochrome P450 reaction phenotyping and kinetic analysis in early drug discovery, *Rapid Commun. Mass Spectrom.* 30 (2) (2016) 301–310.
- [88] J.E. Barbara, J.M. Castro-Perez, High-resolution chromatography/time-of-flight MSE with in silico data mining is an information-rich approach to reactive metabolite screening, *Rapid Commun. Mass Spectrom.* 25 (20) (2011) 3029–3040.
- [89] X. Zhu, Y. Chen, R. Subramanian, Comparison of information-dependent acquisition, SWATH, and MS(All) techniques in metabolite identification study employing ultrahigh-performance liquid chromatography-quadrupole time-of-flight mass spectrometry, *Anal. Chem.* 86 (2) (2014) 1202–1209.
- [90] Y. Zhang, et al., The use of variable Q1 isolation windows improves selectivity in LC-SWATH-MS acquisition, *J. Proteome Res.* 14 (10) (2015) 4359–4371.
- [91] T. Bruderer, E. Varesio, G. Hopfgartner, The use of LC predicted retention times to extend metabolites identification with SWATH data acquisition, *J. Chromatogr. B Anal. Technol. Biomed. Life Sci.* 1071 (2017) 3–10.
- [92] R. Bonner, G. Hopfgartner, SWATH acquisition mode for drug metabolism and metabolomics investigations, *Bioanalysis* 8 (16) (2016) 1735–1750.
- [93] L.A. Gethings, et al., Lipid profiling of complex biological mixtures by liquid chromatography/mass spectrometry using a novel scanning quadrupole data-independent acquisition strategy, *Rapid Commun. Mass Spectrom.* 31 (19) (2017) 1599–1606.
- [94] P.R. Juvvadi, et al., Scanning quadrupole data-independent acquisition. Part B. Application to the analysis of the calcineurin-interacting proteins during treatment of *Aspergillus fumigatus* with azole and echinocandin antifungal drugs, *J. Proteome Res.* 17 (2) (2018) 780–793.
- [95] M.A. Moseley, et al., Scanning quadrupole data-independent acquisition. Part A. Qualitative and quantitative characterization, *J. Proteome Res.* 17 (2) (2018) 770–779.
- [96] A.A. Shvartsburg, R.D. Smith, Fundamentals of traveling wave ion mobility spectrometry, *Anal. Chem.* 80 (24) (2008) 9689–9699.
- [97] I. Michaelovski, N. Kirshenbaum, M. Sharon, T-wave ion mobility-mass spectrometry: basic experimental procedures for protein complex analysis, *J. Vis. Exp.* 41 (2010).

- [98] M. Fasciotti, et al., Separation of isomeric disaccharides by traveling wave ion mobility mass spectrometry using CO<sub>2</sub> as drift gas, *J. Mass Spectrom.* 47 (12) (2012) 1643–1647.
- [99] V. Shah, et al., Enhanced data-independent analysis of lipids using ion mobility-TOFMSE to unravel quantitative and qualitative information in human plasma, *Rapid Commun. Mass Spectrom.* 27 (19) (2013) 2195–2200.
- [100] Z. Zhou, et al., Large-scale prediction of collision cross-section values for metabolites in ion mobility-mass spectrometry, *Anal. Chem.* 88 (22) (2016) 11084–11091.
- [101] G.B. Gonzales, et al., Collision cross section prediction of deprotonated phenolics in a travelling-wave ion mobility spectrometer using molecular descriptors and chemometrics, *Anal. Chim. Acta* 924 (2016) 68–76.
- [102] J.R.N. Haler, et al., Comprehensive ion mobility calibration: poly(ethylene oxide) polymer calibrants and general strategies, *Anal. Chem.* 89 (22) (2017) 12076–12086.
- [103] Z. Zhou, et al., Lipid CCS: prediction of collision cross-section values for lipids with high precision to support ion mobility-mass spectrometry-based lipidomics, *Anal. Chem.* 89 (17) (2017) 9559–9566.
- [104] C.B. Mollerup, et al., Prediction of collision cross section and retention time for broad scope screening in gradient reversed-phase liquid chromatography-ion mobility-high resolution accurate mass spectrometry, *J. Chromatogr. A* 1542 (2018) 82–88.
- [105] P.L. Plante, et al., Predicting ion mobility collision cross-sections using a deep neural network: deep CCS, *Anal. Chem.* (2019).
- [106] D. Lim, et al., Application of molecular dynamics simulation to improve the theoretical prediction for collisional cross section of aromatic compounds with long alkyl chains in crude oils, *Rapid Commun. Mass Spectrom.* 33 (7) (2019) 650–656.
- [107] J.L. Campbell, J.C. Le Blanc, R.G. Kibbey, Differential mobility spectrometry: a valuable technology for analyzing challenging biological samples, *Bioanalysis* 7 (7) (2015) 853–856.
- [108] R.S. Sebastian Fabritz, F.-A. Ludwig, Separation of Diastereomeric Flubatine Metabolites using SelexION® Technology, *SCIEX Application Note*(2018).
- [109] J.O. Kafader, et al., Measurement of individual ions sharply increases the resolution of orbitrap mass spectra of proteins, *Anal. Chem.* 91 (4) (2019) 2776–2783.
- [110] S. Eliuk, A. Makarov, Evolution of orbitrap mass spectrometry instrumentation, *Annu Rev Anal Chem (Palo Alto, Calif)* 8 (2015) 61–80.
- [111] H.K. Lim, et al., Metabolite identification by data-dependent accurate mass spectrometric analysis at resolving power of 60,000 in external calibration mode using an LTQ/Orbitrap, *Rapid Commun. Mass Spectrom.* 21 (12) (2007) 1821–1832.
- [112] T. Zhang, et al., Development and validation of an inductively coupled plasma mass spectrometry (ICP-MS) method for quantitative analysis of platinum in plasma, urine, and tissues, *Appl. Spectrosc.* 70 (9) (2016) 1529–1536.
- [113] J.K. Nicholson, et al., High-performance liquid chromatography and inductively coupled plasma mass spectrometry (HPLC-ICP-MS) for the analysis of xenobiotic metabolites in rat urine: application to the metabolites of 4-bromoaniline, *Analyst* 125 (2) (2000) 235–236.
- [114] J.K. Nicholson, et al., High-performance liquid chromatography linked to inductively coupled plasma mass spectrometry and orthogonal acceleration time-of-flight mass spectrometry for the simultaneous detection and identification of metabolites of 2-bromo-4-trifluoromethyl, *Anal. Chem.* 73 (7) (2001) 1491–1494.
- [115] C. Prakash, D. Cui, Metabolism and excretion of a new antianxiety drug candidate, CP-93,393, in cynomolgus monkeys. Identification of the novel pyrimidine ring cleaved metabolites, *Drug Metab. Dispos.* 25 (1997) 1395–1406.
- [116] D. Cui, et al., In vitro and in vivo metabolism of a potent and selective integrin  $\alpha_v\beta_3$  antagonist in rats, dogs and monkeys, *Drug Metab. Dispos.* 32 (2004) 848–861.
- [117] Z. Miao, A. Kamel, C. Prakash, Characterization of a novel metabolite intermediate of ziprasidone in hepatic cytosolic fractions of rat, dog and human by ESI-MS/MS, H/D exchange and chemical derivatization, *Drug Metab. Dispos.* 33 (879–883) (2005).
- [118] W. Lam, R. Ramanathan, In electrospray ionization source hydrogen/deuterium exchange LC-MS and LC-MS/MS for characterization of metabolites, *J. Am. Soc. Mass Spectrom.* 13 (4) (2002) 345–353.
- [119] Z. Miao, A. Kamel, C. Prakash, Characterization of a novel metabolite intermediate of ziprasidone in hepatic cytosolic fractions of rat, dog, and human by ESI-MS/MS, hydrogen/deuterium exchange, and chemical derivatization, *Drug Metab. Dispos.* 33 (7) (2005) 879–883.

- [120] M. Marull, B. Rochat, Fragmentation study of imatinib and characterization of new imatinib metabolites by liquid chromatography-triple-quadrupole and linear ion trap mass spectrometers, *J. Mass Spectrom.* 41 (3) (2006) 390–404.
- [121] D.Q. Liu, C.E.C.A. Hop, Strategies for characterization of drug metabolites using liquid chromatography-tandem mass spectrometry in conjunction with chemical derivatization and on-line H/D exchange approaches, *J. Pharm. Biomed. Anal.* 37 (2005) 1–18.
- [122] W.J. Leavens, et al., Derivatization for liquid chromatography/electrospray mass spectrometry: synthesis of tris(trimethoxyphenyl)phosphonium compounds and their derivatives of amine and carboxylic acids, *Rapid Commun. Mass Spectrom.* 16 (2002) 433–441.
- [123] S.J. Barry, et al., Derivatization for liquid chromatography/electrospray mass spectrometry: synthesis of pyridinium compounds and their amine and carboxylic acid derivatives, *Rapid Commun. Mass Spectrom.* 17 (2003) 603–620.
- [124] S.J. Barry, et al., Use of *S*-pentafluorophenyl tris(2,4,6-trimethoxyphenyl)phosphonium acetate bromide and (4-hydrazino-4-oxobutyl) [tris(2,4,6-trimethoxyphenyl)phosphonium bromide] for the derivatization of alcohols, aldehydes and ketones for detection by liquid chromatography/electrospray mass spectrometry, *Rapid Commun. Mass Spectrom.* 17 (5) (2003) 484–497.
- [125] L. Xu, D.C. Spink, 1,2-Dimethylimidazole-4-sulfonyl chloride, a novel derivatization reagent for the analysis of phenolic compounds by liquid chromatography electrospray tandem mass spectrometry: application to 1-hydroxypyrene in human urine, *J. Chromatogr. B Anal. Technol. Biomed. Life Sci.* 855 (2) (2007) 159–165.
- [126] C. Prakash, et al., Metabolism, distribution and excretion of a selective N-methyl-D-aspartate receptor antagonist, traxoprodil, in rats and dogs, *Drug Metab. Dispos.* 35 (8) (2007) 1350–1364.
- [127] R. Sharma, et al., Metabolism, excretion, and pharmacokinetics of ((3,3-difluoropyrrolidin-1-yl))((2*S*,4*S*)-4-(4-(pyrimidin-2-yl)piperazin-1-yl)pyrrolidin-2-yl)methanone, a dipeptidyl peptidase inhibitor, in rat, dog and human, *Drug Metab. Dispos.* 40 (11) (2012) 2143–2161.
- [128] A.S. Kalgutkar, et al., Discovery tactics to mitigate toxicity risks due to reactive metabolite formation with 2-(2-hydroxyaryl)-5-(trifluoromethyl)pyrido[4,3-*d*]pyrimidin-4(3*h*)-one derivatives, potent calcium-sensing receptor antagonists and clinical candidate(s) for the treatment of osteoporosis, *Chem. Res. Toxicol.* 23 (6) (2010) 1115–1126.
- [129] M.L. Salomonsson, U. Bondesson, M. Hedeland, Structural evaluation of the glucuronides of morphine and formoterol using chemical derivatization with 1,2-dimethylimidazole-4-sulfonyl chloride and liquid chromatography/ion trap mass spectrometry, *Rapid Commun. Mass Spectrom.* 22 (17) (2008) 2685–2697.
- [130] W.H. Schaefer, Formation of a carbamoyl glucuronide conjugate of carvedilol in vitro using dog and rat liver microsomes, *Drug Metab. Dispos.* 20 (1) (1992) 130–133.
- [131] D. Cui, P.J. Harvison, Determination of the site of glucuronidation in an N-(3,5-dichlorophenyl)succinimide metabolite by electrospray ionization tandem mass spectrometry following derivatization to picolinyl esters, *Rapid Commun. Mass Spectrom.* 14 (21) (2000) 1985–1990.
- [132] K. Kassahun, et al., Disposition and biotransformation of the antipsychotic agent olanzapine in humans, *Drug Metab. Dispos.* 25 (1997) 81–93.
- [133] M. Lampinen-Salomonsson, et al., Differentiation of estriol glucuronide isomers by chemical derivatization and electrospray tandem mass spectrometry, *Rapid Commun. Mass Spectrom.* 20 (9) (2006) 1429–1440.
- [134] J.Y. Kong, et al., Differentiating isomeric deprotonated glucuronide drug metabolites via ion/molecule reactions in tandem mass spectrometry, *Anal. Chem.* 90 (15) (2018) 9426–9433.
- [135] C. Prakash, et al., CYP2C8- and CYP3A-mediated C-demethylation of (3-[[[4-*tert*-butylbenzyl)-(pyridine-3-sulfonyl)-amino]-methyl]-phenoxy)-acetic acid (CP-533,536), an EP2 receptor-selective prostaglandin E2 agonist: characterization of metabolites by high-resolution liquid chromatography-tandem mass spectrometry and liquid chromatography/mass spectrometry-nuclear magnetic resonance, *Drug Metab. Dispos.* 36 (10) (2008) 2093–2103.
- [136] M. Dowty, et al., The pharmacokinetics, metabolism, and clearance mechanisms of tofacitinib, a Janus kinase inhibitor, in humans, *Drug Metab. Dispos.* 42 (4) (2014) 759–773.

# High-resolution mass spectrometry-based data acquisition and data-mining technologies for detecting and characterizing drug metabolites and traditional Chinese medicine components

Tingting Cai<sup>a</sup>, Caisheng Wu<sup>b</sup>, Qian Ruan<sup>c</sup>,  
Shuguang Ma<sup>d</sup>, Mingshe Zhu<sup>e</sup>

<sup>a</sup>Laboratory Testing Division, WuXi AppTec, Nanjing, China <sup>b</sup>School of Pharmaceutical Sciences, Xiamen University, Xiamen, China <sup>c</sup>Pharmaceutical Candidate Characterization, Bristol-Myers Squibb, Princeton, NJ, United States <sup>d</sup>Drug Metabolism and Pharmacokinetics, Genentech Inc., South San Francisco, CA, United States <sup>e</sup>MassDefect Technologies, Princeton, NJ, United States

## 1 Introduction

Biotransformation reaction (also known as drug metabolism) is a biochemical process in which drugs are generally converted to more hydrophilic species (drug metabolites) to facilitate their elimination from the body. Although many of these metabolites are physiologically inactive and chemically stable, some are pharmacologically active, toxic, or chemically unstable (such as reactive metabolites [1]). Other undesirable consequences resulting from biotransformation reactions include rapid drug clearance and potential drug-drug interactions [2]. Biotransformation research that is mainly involved in drug metabolite profiling and structural characterization is an integral part of drug metabolism and pharmacokinetics (DMPK)

research. Early in the drug discovery process, biotransformation efforts are often aimed at understanding the metabolic soft-spot of a compound or a structural series, which is critical in guiding the synthetic procedures to reduce the rate of metabolism to achieve an optimum pharmacokinetic profile [3]. During late-stage drug discovery, it is important to characterize major metabolites to establish the similarity of *in vitro* metabolite profiles between human and toxicology species [4, 5], and to identify potential pharmacologically active [6], reactive, or toxic metabolites [7]. Biotransformation studies at clinical development stage focus on the determination of relative amounts of circulating metabolites in humans compared to those in the animal species used for safety assessment [8, 9] and the investigation of metabolism and disposition of radiolabeled drugs in humans. In addition, hypothesis-driven biotransformation studies are designed to address specific absorption, distribution, metabolism, excretion (ADME)-related issues, such as low bioavailability, drug's clearance mechanism, pharmacokinetic/pharmacodynamic disconnects, and disproportional metabolite in human.

Liquid chromatography coupled with mass spectrometry (LC-MS) has become the analytical tool of choice for detection, identification, and quantitation of drug metabolites in complex biological matrices [10–14]. In the past 30 years, MS technology and its applications in biotransformation research underwent rapid evolution [15]. Until the late 1980s, metabolite identification was mainly carried out by a two-step process: metabolite isolation using various separation approaches and mass spectrometric analysis of isolated metabolite samples. The tedious sample preparation process and insensitive and off-line MS analysis greatly limited the productivity and quality of biotransformation research. The emergence of commercially manufactured electrospray triple quadrupole mass spectrometry instruments at the beginning of the 1990s made it ease of analysis of drug metabolites in complex biological matrices. The way to study drug metabolism and disposition in the pharmaceutical industry has fundamentally changed since the development of robust modern high-resolution mass spectrometry (HRMS) instruments and novel data acquisition and data-mining technologies [11, 16–19] in the middle of the 2000s. Now the LC-HRMS instrument is the single dominant mass spectrometry platform used in a majority of biotransformation labs [14, 18], although linear ion trap [20, 21] and hybrid triple quadrupole linear ion trap (QTRAP) [22, 23] instruments can provide some unique and advanced scanning functions that are well suited for some drug metabolite identification tasks.

Although many HRMS-based workflows have been developed and applied for various drug metabolite profiling and identification tasks in different biotransformation labs, these workflows can be generalized in three steps [14] (Fig. 1). The first step is data acquisition of full-scan mass spectral and product ion spectral (MS/MS) datasets of a test drug and its metabolites in a test sample using various data-dependent acquisition (DDA) or data-independent acquisition (DIA) methods [16, 18]. DDA methods often used for drug metabolite profiling and identification are list-, intensity-, isotope-, mass defect-dependent acquisitions. In 2018, a novel background exclusion DDA method was introduced to targeted analysis of xenobiotics in biological matrix [24]. The second step is data mining to search for metabolite ions and retrieve their MS/MS or fragment ion data using various postacquisition data-mining tools. HRMS-based data-mining tools can be categorized to targeted data mining such as extracted ion chromatography (EIC), mass defect filter (MDF), isotope pattern filter (IPF), neutral-loss filter (NLF), and product ion filter (PIF) and untargeted data mining such as background subtraction (BS) and metabolomic analysis. The third step is data interpretation to



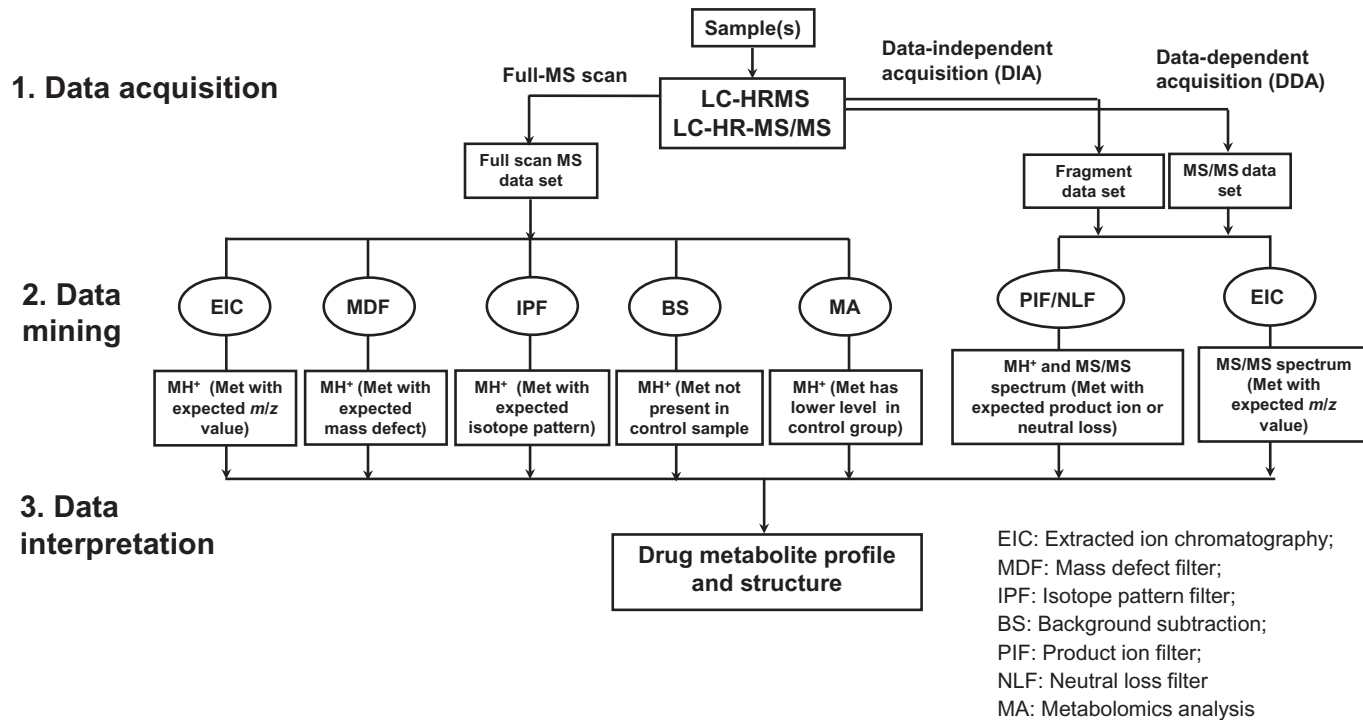


**FIG. 1** A general workflow, data acquisition technologies, and data-mining methods commonly used in drug metabolite detection and structural characterization by LC-HRMS. Adapted with permission from H. Zhang, D. Zhang, K. Ray, M. Zhu, Mass defect filter technique and its applications to drug metabolite identification by high-resolution mass spectrometry, *J. Mass Spectrom.* 44 (7) (2009) 999–1016.



determine the identity of drug metabolites and their structures based on accurate full-scan MS and MS/MS mass spectral data and biotransformation knowledge. Several reviews [10, 13, 14, 18] and book chapters [25, 26] were previously published to summarize various HRMS technologies and methods used in biotransformation research. This chapter will focus on HRMS-based data acquisition and data-mining technologies with particular emphasis on those that have not been extensively covered in the literature, such as newly introduced background exclusion DDA, untargeted data-processing tools, BS and metabolomic analysis, and software-assisted metabolite prediction and identification. In addition, applicability and advantages of these technologies in conducting biotransformation studies in drug discovery and development are elaborated and demonstrated using examples mainly come from authors' labs. Applications in the detection and structural characterization of traditional Chinese medicine (TCM) components in biological matrices are also described.

## 2 HRMS-based data acquisition technologies for metabolite identification

Acquiring high-quality MS/MS spectra of low-level metabolites is critical for structural elucidation. However, abundant and complex matrix background in biological samples poses a great challenge for mass spectrometry to select drug-related precursor ions for MS/MS fragmentation during data acquisition. Traditionally, an MS/MS experiment is carried out by targeting predicted metabolites in a specific sample. When dealing with a large number of targeted metabolites, typical MS/MS experiments comprise multiple injections with a manually setting-up precursor list for each injection. The entire metabolite identification process is knowledge-dependent, time-consuming, and labor-intensive. In the past 20 years, several HRMS-based data acquisition approaches have been developed to improve speed and efficiency on MS/MS data acquisition of both known and unknown metabolites (Fig. 1) [10, 12–15].

### 2.1 Data-dependent MS/MS acquisition

DDA [18] has been developed to simplify the data acquisition process and to increase the throughput of metabolite identification. In general, a survey scan is acquired as each analyte elutes from the LC column. The data software analyzes the mass spectra in real-time to determine the precursor ion for subsequent MS/MS experiments based on the prerequisite selection criteria. The trigger for MS/MS spectral acquisition can be based on ion intensity in the full-scan MS, fragment ions or neutral losses generated in MS/MS scan, source CID or full scan at higher collision energy. In addition, other unique properties of the analyte, such as the mass defect and isotope pattern of metabolites are utilized to selectively trigger MS/MS acquisition. Even though most DDA methods can be applied to unit resolution MS, HRMS-based DDA can significantly increase the sensitivity and selectivity to trigger MS/MS experiments of low-level analytes due to its power in differentiating drug-related ions from matrix ions.

### 2.1.1 Ion intensity-dependent acquisition

The ion intensity-dependent MS/MS acquisition is the most common DDA and is widely used for drug metabolite identification [18]. This approach uses a criterion based on predefined full-scan MS intensity threshold to trigger sequential MS/MS acquisition, i.e., the components in higher ion abundance get higher priority for MS/MS acquisition. This generic DDA method does not require the prior knowledge of the  $m/z$  values of the precursors. In each scan event, only a limited number of ions can be selected depending on LC peak width and MS scan speed. Although the intensity-dependent acquisition is not able to differentiate analytes of interest from the matrix background, it can be applied to the samples with a high abundance of analyte and low interference of background, such as drug metabolites generated by an in vitro assay. On the other hand, this approach is not well suited to analyze the samples containing low abundant analytes in high matrix background, such as in vivo metabolites of a low dose drug.

### 2.1.2 Accurate mass inclusion list-dependent acquisition

The approach that uses an inclusion list of accurate masses of expected or predicted metabolites to trigger MS/MS acquisition provides a way to maximize the usefulness of MS/MS spectral information of targeted metabolites [18]. Based on the knowledge of common biotransformation pathways and the relevant biological system, precursor ions of predicted drug metabolites of a testing compound can be generated to build an inclusion list prior to analysis. The corresponding elemental composition and  $m/z$  changes from common metabolic pathways are summarized in Table 1. Most mass spectrometry instrument vendors offer software

**TABLE 1** Common biotransformation reactions and the corresponding elemental compositions and  $m/z$  changes.

Metabolic reaction	Description	Molecular formula change	$m/z$ change
$R-CH_2C_6H_5 \rightarrow R-H$	Debenzylation	$-C_7H_6$	-90.0468
$R-^{79}Br \rightarrow R-H$	Reductive debromination	$-Br + H$	-77.9104
$R-CF_3 \rightarrow R-H$	Trifluoromethyl loss	$-CF_3 + H$	-67.9874
$2R-^{35}Cl \rightarrow 2R-H$	$2 \times$ reductive dechlorination	$-Cl_2 + H_2$	-67.9222
$R-^{79}Br \rightarrow R-OH$	Oxidative debromination	$-Br + OH$	-61.9156
$R-C(CH_3)_3 \rightarrow R-H$	<i>tert</i> -Butyl dealkylation	$-C_4H_8$	-56.0624
$R-ONO_2 \rightarrow R-OH$	Hydrolysis of nitrate ester	$-NO_2 + H$	-44.9851
$R-COOH \rightarrow R-H$	Decarboxylation	$-CO_2$	-43.9898
$R-CH(CH_3)_2 \rightarrow R-H$	Isopropyl dealkylation	$-C_3H_6$	-42.0468
$R-CH_2COCH_2CH_2CH_3 \rightarrow R-COOH$	Propyl ketone to acid	$-C_4H_8 + O$	-40.0675
$R-C(CH_3)_3 \rightarrow R-OH$	<i>tert</i> -Butyl to alcohol	$-C_4H_8 + O$	-40.0675
$2R-F \rightarrow 2R-H$	$2 \times$ reductive defluorination	$-F_2 + H_2$	-35.9811

*Continued*

**TABLE 1** Common biotransformation reactions and the corresponding elemental compositions and  $m/z$  changes—cont'd

Metabolic reaction	Description	Molecular formula change	$m/z$ change
$R-^{35}\text{Cl} \rightarrow R-H$	Reductive dechlorination	$-\text{Cl} + \text{H}$	-33.9611
$R-\text{CH}_2\text{OH} \rightarrow R-H$	Hydroxymethylene loss	$-\text{CH}_2\text{O}$	-30.0106
$R-\text{NO}_2 \rightarrow R-\text{NH}_2$	Nitro reduction	$-\text{O}_2 + \text{H}_2$	-29.9742
$R-\text{CH}_2\text{OCH}_2\text{CH}_2\text{CH}_3 \rightarrow R-\text{COOH}$	Propyl ether to acid	$-\text{C}_3\text{H}_8 + \text{O}$	-28.0675
$R-\text{C}_2\text{H}_5 \rightarrow R-H$	Deethylation	$-\text{C}_2\text{H}_4$	-28.0312
$R-\text{CO}-\text{R}' \rightarrow R-\text{R}'$	Decarboxylation	$-\text{CO}$	-27.9949
$R-\text{CH}_2\text{COCH}_2\text{CH}_3 \rightarrow R-\text{COOH}$	Ethyl ketone to acid	$-\text{C}_3\text{H}_6 + \text{O}$	-26.0519
$R-\text{CH}(\text{CH}_3)_2 \rightarrow R-\text{OH}$	Isopropyl to alcohol	$-\text{C}_3\text{H}_6 + \text{O}$	-26.0519
$R-\text{CH}_2-\text{CH}_2\text{OH} \rightarrow R-\text{CH}=\text{CH}_2$	Alcohols dehydration	$-\text{H}_2\text{O}$	-18.0105
$R-\text{CH}=\text{N}-\text{OH} \rightarrow R-\text{CN}$	Dehydration of oximes	$-\text{H}_2\text{O}$	-18.0105
$R-\text{F} \rightarrow R-H$	Reductive defluorination	$-\text{F} + \text{H}$	-17.9906
$R-^{35}\text{Cl} \rightarrow R-\text{OH}$	Oxidative dechlorination	$-\text{Cl} + \text{OH}$	-17.9662
$\text{RR}'\text{S}=\text{O} \rightarrow R-\text{S}-\text{R}'$	Sulfoxide to thioether	$-\text{O}$	-15.9949
$R-\text{NHNHR}'\text{C}=\text{S} \rightarrow R-\text{NHNHR}'\text{C}=\text{O}$	Thioureas to ureas	$-\text{S} + \text{O}$	-15.9772
$R-\text{CH}_2\text{OCH}_2\text{CH}_3 \rightarrow R-\text{COOH}$	Ethyl ether to acid	$-\text{C}_2\text{H}_6 + \text{O}$	-14.0519
$R-\text{CH}_3 \rightarrow R-H$	Demethylation	$-\text{CH}_2$	-14.0157
$R-\text{C}(\text{CH}_3)_3 \rightarrow R-\text{COOH}$	<i>tert</i> -Butyl to acid	$-\text{C}_3\text{H}_8 + \text{O}_2$	-12.0726
$R-\text{CH}_2\text{COCH}_3 \rightarrow R-\text{COOH}$	Methyl ketone to acid	$-\text{C}_2\text{H}_4 + \text{O}$	-12.0363
$R-\text{CH}_2\text{CH}_3 \rightarrow R-\text{OH}$	Ethyl to alcohol	$-\text{C}_2\text{H}_4 + \text{O}$	-12.0363
$\text{C}_4\text{H}_4\text{N}_2 \rightarrow \text{C}_3\text{H}_4\text{N}_2$	Pyrimidine ring conversion to pyrazole	$-\text{C}$	-12.0000
$\text{Ar}-\text{CH}_2\text{CN} \rightarrow \text{Ar}-\text{CH}_2\text{OH}$	Benzyl cyanide oxidation	$-\text{HCN} + \text{O} + 2\text{H}$	-9.0003
$R-\text{CH}_2-\text{CH}_2-\text{CH}_2-\text{CH}_2-\text{R}' \rightarrow R-\text{CH}=\text{CH}-\text{CH}=\text{CH}-\text{R}'$	Two sequential desaturation	$-\text{H}_4$	-4.0314
Hydroxylation + dehydration	Hydroxylation + dehydration	$-\text{H}_2$	-2.0157
$R-\text{CH}_2-\text{OH} \rightarrow R-\text{CHO}; R-\text{CHOH}-\text{R}' \rightarrow R-\text{CO}-\text{R}'$	Primary/secondary alcohols to aldehyde/ketone	$-\text{H}_2$	-2.0157
$R-\text{CH}_2-\text{CH}_2-\text{R}' \rightarrow R-\text{CH}=\text{CH}-\text{R}'$	Desaturation	$-\text{H}_2$	-2.0157
$\text{C}_5\text{H}_7\text{N} \rightarrow \text{C}_5\text{H}_5\text{N}$	1,4-Dihydropyridines to pyridines	$-\text{H}_2$	-2.0157

**TABLE 1** Common biotransformation reactions and the corresponding elemental compositions and  $m/z$  changes—cont'd

Metabolic reaction	Description	Molecular formula change	$m/z$ change
$R-F \rightarrow R-OH$	Oxidative defluorination	$-F + OH$	-1.9957
$R-CHNH_2-R' \rightarrow R-CO-R'$	Oxidative deamination to ketone	$-NH_3 + O$	-1.0316
$R-CH_2OCH_3 \rightarrow R-COOH$	Demethylation and oxidation to acid	$-CH_4 + O$	-0.0365
$R-CH(OH)CH_3 \rightarrow R-COOH$	2-Ethoxyl to acid	$-CH_4 + O$	-0.0365
$R-CH_2-NH_2 \rightarrow R-CH_2-OH$	Oxidative deamination to alcohol	$-NH + O$	0.9840
$R-CH(CH_3)_2 \rightarrow R-COOH$	Isopropyl to acid	$-C_2H_6 + O_2$	1.9430
$R-CH_3 \rightarrow R-OH$	Demethylation and hydroxylation	$-CH_2 + O$	1.9792
$R-CO-R' \rightarrow R-CHOH-R'$	Ketone to alcohol	$+H_2$	2.0157
$Ar-CH_2-CN \rightarrow Ar-COOH$	Benzyl cyanide to benzoic acid	$-HCN + O_2$	4.9789
$R-CH_2-R' \rightarrow R-C(O)-R'$	Methylene to ketone	$-H_2 + O$	13.9792
Hydroxylation and desaturation	Hydroxylation and desaturation	$-H_2 + O$	13.9792
$R-XH \rightarrow R-X-CH_3$ (X = N, O, S)	N, O, S methylation	$+CH_2$	14.0157
$R-CH_2CH_3 \rightarrow R-COOH$	Ethyl to carboxylic acid	$-CH_4 + O_2$	15.9586
$R-H \rightarrow R-OH$	Hydroxylation	$+O$	15.9949
$R-NH-R' \rightarrow R-NOH-R'$ ; $RR'R''N \rightarrow RR'R''NO$	Second/third amine to hydroxylamine/N-oxide	$+O$	15.9949
$R-S-R' \rightarrow R-SO-R'$ ; $R-SO-R' \rightarrow R-(O)S(O)-R'$	Thioether to sulfoxide, sulfoxide to sulfone	$+O$	15.9949
$R-CH=CH-R' \rightarrow R-CH(O)CH-R'$	Aromatic ring to arene oxide	$+O$	15.9949
$R-CH_2CH_3 \rightarrow R-CH-(OH)_2$	Demethylation and two hydroxylation	$-CH_2 + O_2$	17.9741
$R-CH=CH-R \rightarrow R-CH_2-CHOH-R'$	Hydration, hydrolysis (internal)	$+H_2O$	18.0106
$R-CN \rightarrow R-CONH_2$	Hydrolysis of aromatic nitriles	$+H_2O$	18.0106
$R-NH_2 \rightarrow R-NHC(O)H$	N-formylation	$+CO$	27.9949
Hydroxylation and ketone formation	Hydroxylation and ketone formation	$-H_2 + O_2$	29.9741
$C_nH_m \rightarrow C_nH_{m-2}O_2$	Quinine formation	$-H_2 + O_2$	29.9741

*Continued*

**TABLE 1** Common biotransformation reactions and the corresponding elemental compositions and  $m/z$  changes—cont'd

Metabolic reaction	Description	Molecular formula change	$m/z$ change
$R-CH_3 \rightarrow R-COOH$	Methyl to carboxylation	$-H_2 + O_2$	29.9741
$R-H \rightarrow R-O-CH_3$	Hydroxylation and methylation	$+CH_2O$	30.0105
$2 \times$ hydroxylation	$2 \times$ hydroxylation	$+O_2$	31.9898
$RR'S \rightarrow RR'SO_2$	Thioether to sulfone	$+O_2$	31.9898
$R-CH=CH-R' \rightarrow R-CH(OH)-CH(OH)-R'$	Alkenes to dihydrodiols	$+H_2O_2$	34.0054
$R-NH_2 \rightarrow R-NHCOCH_3$	Acetylation	$+C_2H_2O$	42.0106
$3 \times$ hydroxylation + dehydrogenation	$3 \times$ hydroxylation + dehydrogenation	$+3O-2H$	45.9691
$3 \times$ hydroxylation	$3 \times$ hydroxylation	$+O_3$	47.9847
$R-SH \rightarrow R-SO_3H$	Aromatic thiols to sulfonic acids	$+O_3$	47.9847
$R-COOH \rightarrow R-CONHCH_2COOH$	Glycine conjugation	$+C_2H_3NO$	57.0215
$R-OH \rightarrow R-OSO_3H$	Sulfation	$+SO_3$	79.9568
$R-H \rightarrow R-OSO_3H$	Hydroxylation and sulfation	$+SO_4$	95.9517
$R-COOH \rightarrow R-CONH-CH(CH_2SH)-COOH$	Cysteine conjugation	$+C_3H_5NOS$	103.0092
$R-COOH \rightarrow R-CONH-CH_2CH_2SO_3H$	Taurine conjugation	$+C_2H_5NO_2S$	107.0041
$R-CH_2-R' \rightarrow RR'-CH-SCH_2CH(NH_2)-COOH$	S-cysteine conjugation	$+C_3H_5NO_2S$	119.0041
$R-COOH \rightarrow R-CO-NH-CO-CH_2-CH_2-CH(NH_2)-COOH$	Acyl glutamine conjugation	$+C_5H_8N_2O_2$	128.0586
Ribose conjugate	Ribose conjugation	$+C_5H_8O_4$	132.0423
$R-COOH \rightarrow R-CO-O-CO-CH_2CH(OH)CH_2-N^+(CH_3)_3$	Acyl carnitine conjugation	$+C_7H_{13}NO_2$	143.0946
$R-COOH \rightarrow R-CO-SCH_2CH(NHCOCH_3)COOH$	S-N-acetylcysteine conjugation	$+C_5H_7NO_2S$	145.0198
$-CO + C_6H_8O_6$	Decarboxylation and glucuronidation	$+C_5H_8O_5$	148.0372
$RR'-CH_2 \rightarrow RR'-CH-SCH_2CH(NHCOCH_3)-COOH$	N-acetylcysteine conjugation	$+C_5H_7NO_3S$	161.0147
$R-OH \rightarrow R-O-C_6H_{11}O_5$	Glucosidation	$+C_6H_{10}O_5$	162.0528
+ Cys-Gly	Cysteine glycine conjugation	$+C_5H_8N_2O_3S$	176.0255

**TABLE 1** Common biotransformation reactions and the corresponding elemental compositions and  $m/z$  changes—cont'd

Metabolic reaction	Description	Molecular formula change	$m/z$ change
R—OH → R—O—C <sub>6</sub> H <sub>9</sub> O <sub>6</sub>	Glucuronide conjugation	+C <sub>6</sub> H <sub>8</sub> O <sub>6</sub>	176.0321
2 × hydroxylation + 2 × SO <sub>3</sub>	2 × hydroxylation + 2 × sulfation	+ S <sub>2</sub> O <sub>8</sub>	191.9035
R—H → R—O—C <sub>6</sub> H <sub>9</sub> O <sub>6</sub>	Hydroxylation + glucuronide	+C <sub>6</sub> H <sub>8</sub> O <sub>7</sub>	192.0270
+N-acetylglucosamine	N-Acetylglucosamine conjugation	+C <sub>8</sub> H <sub>13</sub> NO <sub>5</sub>	203.0794
5-Phosphoribose conjugate	5-Phosphoribose conjugate	+C <sub>5</sub> H <sub>9</sub> O <sub>7</sub> P	212.0086
RR'—NH <sub>2</sub> → RR'—NH—C(O)O—C <sub>6</sub> H <sub>9</sub> O <sub>6</sub>	N-carbamoyl glucuronide	+C <sub>7</sub> H <sub>8</sub> O <sub>8</sub>	220.0219
+Diphosphocholine	Diphosphocholine conjugation	+C <sub>5</sub> H <sub>13</sub> NO <sub>6</sub> P <sub>2</sub>	245.0218
R—COOH → R—CO—SG (GSH = Glutathione)	S-acyl-glutathione conjugates	+C <sub>10</sub> H <sub>15</sub> N <sub>3</sub> O <sub>3</sub> S	289.0732
+GSH — 4H	Desaturation + GSH	+C <sub>10</sub> H <sub>13</sub> N <sub>3</sub> O <sub>6</sub> S	303.0525
+GSH — 2H	GSH conjugation	+C <sub>10</sub> H <sub>15</sub> N <sub>3</sub> O <sub>6</sub> S	305.0682
+GSH	GSH conjugation	+C <sub>10</sub> H <sub>17</sub> N <sub>3</sub> O <sub>6</sub> S	307.0839
+GSH + O — 2H	Oxidation + GSH conjugation	+C <sub>10</sub> H <sub>15</sub> N <sub>3</sub> O <sub>7</sub> S	321.0631
Epoxidation + GSH	Epoxidation + GSH conjugation	+C <sub>10</sub> H <sub>17</sub> N <sub>3</sub> O <sub>7</sub> S	323.0788
+2 × C <sub>6</sub> H <sub>8</sub> O <sub>6</sub>	2 × glucuronide conjugation	+C <sub>12</sub> H <sub>16</sub> O <sub>12</sub>	352.0642
Acid to cholesterol ester	Acid to cholesterol ester	+C <sub>27</sub> H <sub>44</sub>	368.3443
Adenine dinucleotide conjugate	AD <sup>+</sup> conjugation	+C <sub>15</sub> H <sub>21</sub> N <sub>5</sub> O <sub>13</sub> P <sub>2</sub>	541.0611
Bis GSH	Bis GSH conjugation	+C <sub>20</sub> H <sub>30</sub> N <sub>6</sub> O <sub>12</sub> S <sub>2</sub>	610.1363
Adenine dinucleotide phosphate conjugate	ADP <sup>+</sup> conjugation	+C <sub>15</sub> H <sub>22</sub> N <sub>5</sub> O <sub>16</sub> P <sub>3</sub>	621.0274
R—COOH → R—C(O)—S—CoA	Acyl-S-CoA conjugation	+C <sub>21</sub> H <sub>34</sub> N <sub>7</sub> O <sub>15</sub> P <sub>3</sub> S	749.1046

Adapted with modification from M.R. Anari, R.I. Sanchez, R. Bakhtiar, R.B. Franklin, T.A. Baillie, *Integration of knowledge-based metabolic predictions with liquid chromatography data-dependent tandem mass spectrometry for drug metabolism studies: application to studies on the biotransformation of indinavir*, *Anal. Chem.* 76 (3) (2004) 823–832.

packages to build specific metabolite prediction and identification workflows. These include MetaboLynx (Waters), Compound Discoverer (Thermo Scientific), Metabolite Pilot (AB Sciex), MassHunter (Agilent), MetaboliteTools (Bruker), MetID Solution (Shimadzu), and among others, which can be used to automatically generate the inclusion list. An inclusion list-dependent acquisition approach will acquire MS/MS data whenever the ions on the list are detected by a full MS scan within a certain mass tolerance window and above defined intensity threshold. This approach substantially improves the selectivity on low abundant analytes masked by high background and reduces the number of steps used in manual or

traditional data acquisition process, therefore, increases the throughput of metabolite identification. However, this approach heavily relies on the experience and knowledge of the analyst and lacks capability in analyzing unpredictable analytes, such as drug metabolites formed via uncommon biotransformation or multiple step of metabolic reactions.

### 2.1.3 Mass defect-dependent acquisition

Mass defect is defined as the difference between the exact molecular weight and nominal molecular weight of an element [19, 27]. Besides carbon-12 with a mass of exactly 12.0000 Da, all other elements have a uniquely different mass defect. For example, the mass defects of hydrogen and oxygen are 0.007825 and  $-0.005085$  Da, respectively. Therefore, oxidation will introduce a mass defect of  $-5.1$  mDa. The mass defects are unique features of a drug and its metabolites and the differences of mass defects between a parent drug and a metabolite formed from common phase I and phase II metabolism reactions typically fall within 50 mDa. Therefore, with HRMS instruments capable of high mass accuracy ( $<5$  ppm), it is possible to filter out matrix-related interference ions whose mass defects lie outside the mass defect of a given drug. Based on this, mass defect-dependent acquisition imposes MS/MS triggering criteria on a full MS scan. Real-time mass defect filtering is applied to analyze the full-scan HRMS data and identifies precursor ions whose mass defects fall within a specific window of MDF. Only these ions are automatically followed by MS/MS acquisition. This approach is capable of performing MS/MS acquisition of both common and uncommon metabolites with little matrix interference in most cases [28, 29]. It can also use different mass defect templates for the metabolites with the big mass shift to the parent drug, such as those formed via dealkylation, hydrolysis, and conjugation. Fig. 2 depicts the application of mass

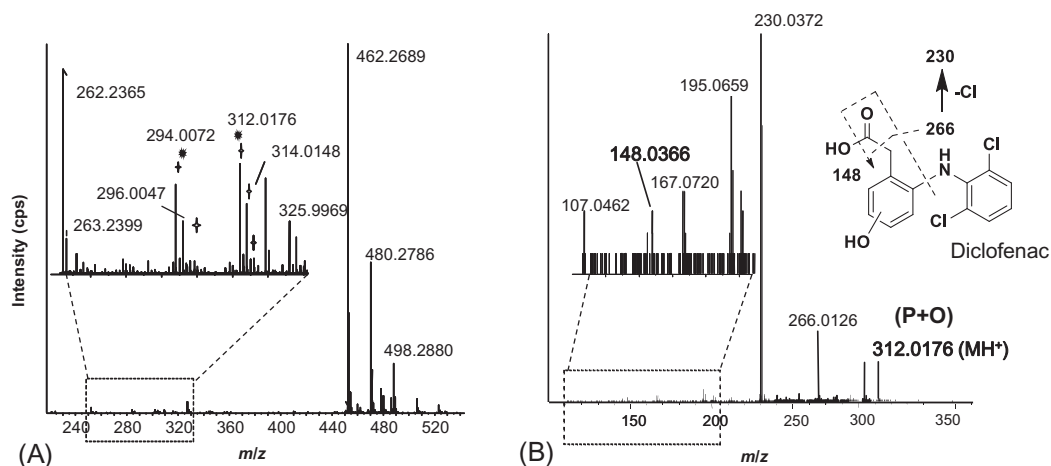


FIG. 2 Application of MDF-DDA for automatically acquiring MS/MS spectra of diclofenac metabolites in rat bile using TripleTOF 5600. (A) A full-scan MS spectrum of the rat bile sample and the insert is a zoomed range of the spectrum, where the cross sign shows the ions triggered for MS/MS acquisition by MDF-DDA and the star sign represents the ions that are metabolites. (B) MS/MS spectrum of the metabolite ion at  $m/z$  312.0176 acquired by MDF-DDA and its proposed structure. The insert is a zoomed range of the MS/MS spectrum.



defect-dependent acquisition in metabolite identification of diclofenac in rat bile, in which the MS/MS data of a low abundant hydroxylation metabolite at  $m/z$  312.0176 was automatically acquired. Mass defect-dependent acquisition keeps an optimum balance between selectivity and coverage and does not require comprehensive knowledge on analytes and has proven to be effective for rapid identification of drug metabolites in complex biological matrices.

#### **2.1.4 Isotope pattern-dependent acquisition**

Some elements, such as Cl and Br, possess unique isotopic patterns that can be easily recognized in their mass spectra. Assuming that these halogens remain intact during biotransformation, their unique isotope pattern can be used as a selective trigger in DDA for metabolite identification [20, 30]. Both ion intensity ratios and mass differences of isotopes contribute to the selection of precursor ions. Once an isotope pattern of interest is recognized in a full MS scan, MS/MS acquisition can be triggered subsequently. The majority of organic compounds are composed of C, H, O, and N that do not contain a unique isotope pattern. However, if a compound is labeled with synthetically enriched stable isotopes, such as  $^{13}\text{C}$ ,  $^{15}\text{N}$ ,  $^2\text{H}$ , the unique isotope pattern can be easily discerned by a full MS scan and thus used to trigger MS/MS analysis [20, 31–34]. The effectiveness of this DDA technology to trigger MS/MS acquisition of minor analytes of interests in the presence of a large amounts of endogenous compounds and other xenobiotics is demonstrated in MS/MS data acquisition of GSH adducts formed by incubating ticlopidine in rat liver microsomes in the presence of a mixture of natural and stable isotope-labeled GSH (Fig. 3). As shown in Fig. 3A, 19 GSH adducts of ticlopidine were generated in the incubation, which had much lower concentrations than oxidative metabolites of ticlopidine in the incubations (data not shown). The ion intensity-DDA only triggered MS/MS spectral acquisition of four GSH adducts (Fig. 3B). In contrast, the isotope pattern-DDA was able to acquire MS/MS spectral data of a majority of GSH adducts, including many minor and trace GSH adducts (Fig. 3C). Enhanced by HRMS, this approach provides outstanding selectivity and sensitivity on the compounds with characteristic isotopic patterns or isotopic labels.

#### **2.1.5 Pseudo-neutral loss-dependent acquisition**

Pseudo-neutral loss as a trigger for MS/MS acquisition was developed as a useful way for detecting metabolites which give characteristic neutral losses (NL) upon collision-induced dissociation [35]. Whenever a specific exact neutral loss within a certain mass tolerance window is detected, the instrument automatically switches to MS/MS mode to acquire the product ion spectra of those ions. This approach is particularly effective in the detection and characterization of common phase II metabolites (e.g., NL of 176.0321 for glucuronides, 129.0426 for glutathione conjugates, and 79.9568 for sulfate conjugates, etc.).

#### **2.1.6 Background-exclusion data-dependent acquisition**

The recently introduced background-exclusion data-dependent acquisition (BE-DDA) technique is designed to improve the selectivity of intensity-dependent MS/MS acquisition on drug-related ions [24]. BE-DDA consists of a series of injections as illustrated in Fig. 4A [36]. The first and second injections are full-scan MS analysis of a control sample and a test sample, respectively. An exclusion list of matrix ions that are present in both samples and an inclusion list of ions of interest that are only present or have significantly higher intensities

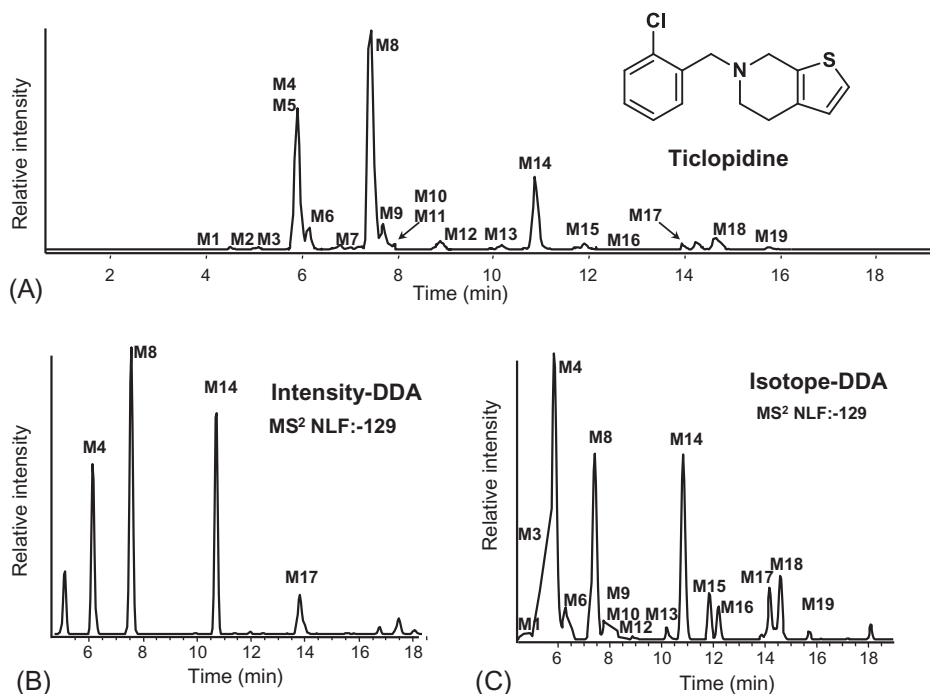
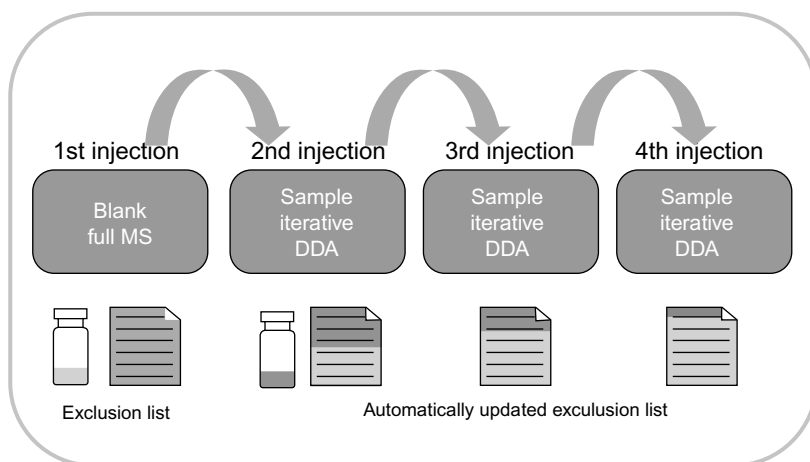


**FIG. 3** Comparison of intensity- and isotope-dependent data acquisition of GSH adducts of ticlopidine from incubation of a mixture of GSH and stable isotope-labeled GSH (1:1) in rat liver microsomes, using an LTQ-orbitrap mass spectrometer. (A) GSH adduct profile from processing full-scan MS dataset using isotope pattern filter. (B) GSH adduct profile from processing MS/MS dataset acquired by intensity-DDA using NLF of 129.0426 Da. (C) GSH adduct profile from processing MS/MS dataset acquired by isotope-DDA using NLF of 129.0426 Da.

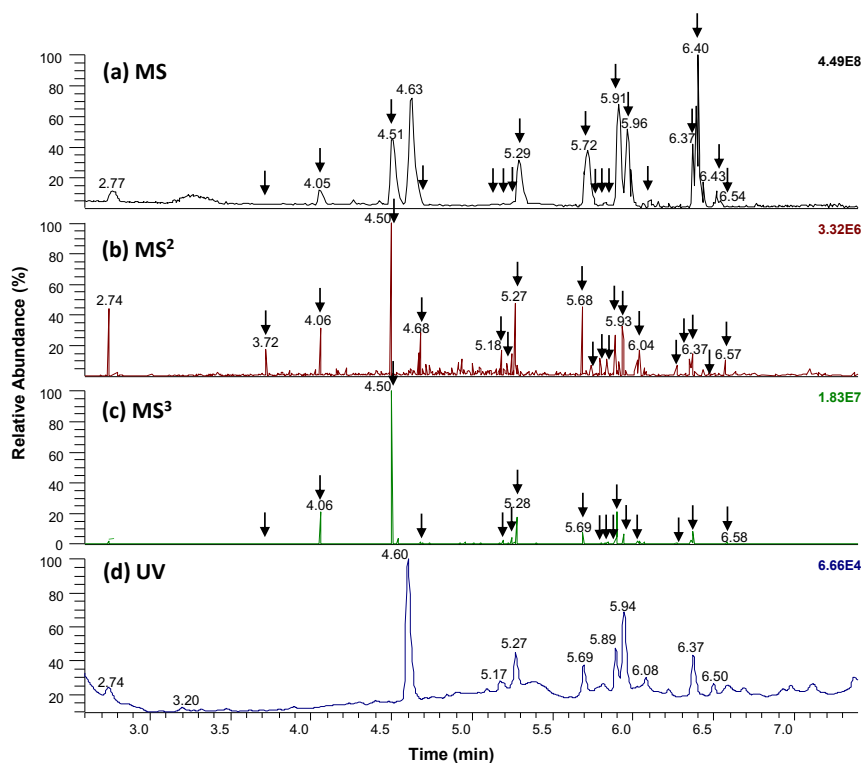
in the test sample are generated by processing the datasets from the first and second injections using a background exclusion algorithm. The third injection is MS/MS acquisition of the test sample that focuses on the ions in the inclusion list. The ions triggered in the third acquisition are then added onto the exclusion list. The fourth injection continues the same test sample with an updated exclusion list. Therefore, the fourth data acquisition targets on even lower abundant metabolites that are missed by the third injection. To maximize the MS<sup>2</sup> data coverage of drug metabolites, the BE-DDA approach can repeat injections until the ions in the inclusion list are exhausted. Fig. 4B demonstrates the high efficiency of BE-DDA in collecting MS<sup>2</sup> data of metabolites of nefazodone in rat liver microsomes. The MS<sup>2</sup> and MS<sup>3</sup> acquisitions were not triggered on the high abundant matrix ions (e.g., the base peak eluted at 4.60 min), but on the low abundant metabolite ions they were triggered (e.g., the small peak eluted at 4.68 min).

## 2.2 Data-independent acquisition

Simple and generic approaches based on nontargeted collision-induced dissociation followed by postacquisition data processing have recently emerged and rapidly gained



(A)



(B)

**FIG. 4** (A) Workflow of background exclusion DDA (BE-DDA). The first injection generates an exclusion list from a blank control analysis, followed by multiple sample analysis with the automatically updated exclusion list. (B) Selective BE-DDA in the analysis of nefazodone metabolites in rat liver microsomes: (a) base peak chromatogram of MS full scans; (b) total ion chromatogram of MS<sup>2</sup> scans; (c) total ion chromatogram of MS<sup>3</sup> scans; and (d) chromatogram of UV absorbance at 250 nm. The identified metabolite peaks are labeled by arrows.

popularity for high-throughput metabolite identification. This approach provides fragment ion information in a nonselective manner and therefore, is referred to as “data-independent acquisition.” It was first described in its application to metabolite identification using Q-TOF technology ( $MS^E$  approach) [37, 38] and was subsequently implemented in orbitraps (“All-Ion-Fragmentation” approach) and TripleTOF systems ( $MS/MS^{ALL}$  with SWATH acquisition). These nonselective approaches are analyte-independent and easy to set up, so they are readily applied to high throughput analysis of a large number and variety of samples.

### 2.2.1 $MS^E$

$MS^E$  approach involves two full-scan functions, one at low collision energy (i.e., 5 eV) and the other at a higher collision energy range (i.e., 20–40 eV). The mass spectra from low collision energy provide intact molecular ion information, while the mass spectra from the high collision energy contain fragmentation data useful for structural elucidation. The data from these two scan functions are used for postacquisition data processing to search for potential metabolites and their  $MS/MS$  spectra for structural characterization [37–39]. Since the high energy collision does not select and isolate any precursor ion, this approach does not require prior knowledge on potential analytes, isotope pattern or neutral loss. However, a large number of interfering matrix ions cause a considerable challenge in assigning low-intensity product ions with their precursor ions. High-quality chromatography and low matrices background can aid in obtaining high-quality  $MS/MS$  spectra.  $MS^E$  works well with relatively clean matrices such as microsomal and hepatocyte incubations but does not work so well with complex biological matrices (such as bile samples).

### 2.2.2 *Sequential windowed acquisition of all theoretical fragment ions (SWATH)*

In SWATH acquisition, the instrument fragments all ions across a given mass range in sequential narrow ranges as they emerge from the liquid chromatography. It has rapidly become one of the premier mass spectrometric acquisition strategies for identification and quantitation of analytes in complex samples across several research fields such as proteomics and metabolomics. There are a few reported studies that applied SWATH in drug metabolite identification [40]. This approach divides a large mass range of precursors into multiple windows, typically 20–25  $m/z$  wide. Each window of precursor ions generates its own  $MS/MS$  spectra. The relatively narrow windows strengthen the linkage between the product ions with the corresponding precursors and thus reduce the false positive and negative assignments of relevant product ions. The resulting  $MS/MS$  dataset can be processed with various postacquisition data-mining tools to identify potential metabolites. As shown in Fig. 5, the product ion spectrum of p-hydroxyatorvastatin, an oxidative metabolite of atorvastatin, in dog bile acquired by SWATH DIA (solid line) is comparable to the one with targeted fragmentation of the isolated precursor (dash line), and there are only a few small interference fragment ions observed in the fragment ion spectrum from the SWATH acquisition, indicating the improved selectivity. SWATH acquisition retains the benefits of  $MS/MS^{ALL}$  but increases the selectivity at the same time by using multiple sequential precursor ion windows at a given narrow width.

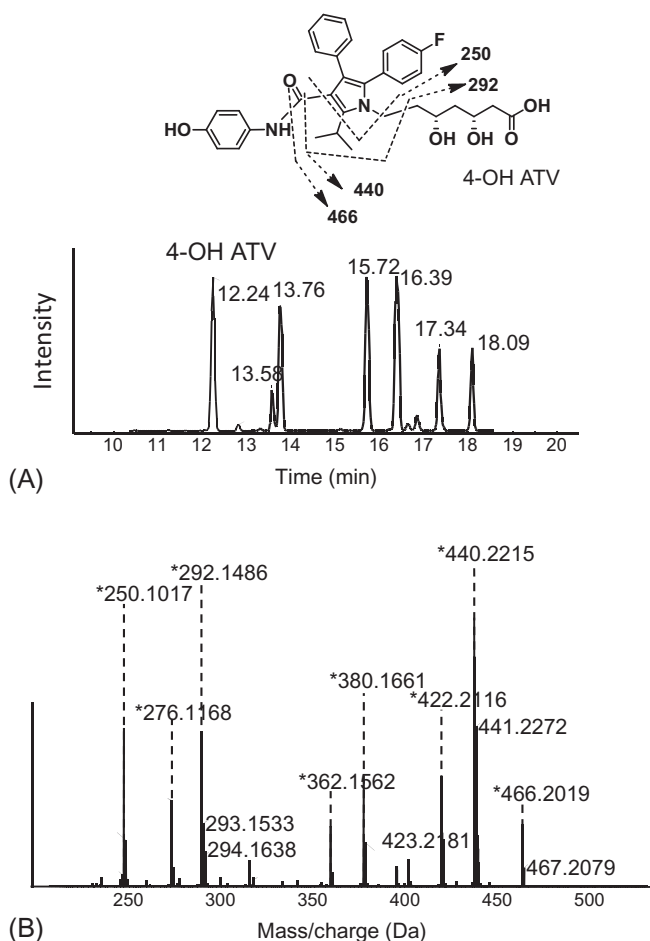


**FIG. 5** Metabolite detection of 4-hydroxyatorvastatin (4-OH-ATV) in dog bile with fragment ion filtering of MS/MS dataset acquired by SWATH. (A) EIC of a fragment ion at  $m/z$  292.1500 in a SWATH acquisition ( $m/z$  539–580 segment); (B) Comparison of fragment ion spectrum of 4-OH-ATV acquired by SWATH (solid line) with its product ion spectrum recorded by targeted MS/MS acquisition (dash line). \* annotated the fragment ions detected in both SWATH and targeted MS/MS.

### 2.2.3 All ion fragmentation

All ion fragmentation (AIF) scan in orbitraps is performed by allowing a range of precursor ions into the high-energy collision dissociation (HCD) cell where the ions are fragmented and stored. The HCD cell voltages are then ramped and all fragment ions are transferred back into the C-trap from which they are injected into the orbitrap for product ion analysis [41, 42]. Similar to SWATH acquisition in TripleTOF instruments, AIF fragments all the ions in a specific mass ranges by a given collision energy, but with more flexibility. The range of precursors can be divided into smaller windows with different sizes and applied with different collision energy. Fragment ion filtering and neutral loss filtering techniques can also be applied to the HCD product ion chromatogram for metabolite detection. This approach can be combined with inclusion list and ion intensity-dependent acquisitions on a hybrid HRMS [42].

### 3 HRMS-based data-processing techniques for metabolite identification

After data acquisition is completed, data processing is performed to identify and characterize drug metabolites. Most LC-MS acquisitions in metabolite profiling studies generate a full-scan MS dataset and an MS/MS and MS<sup>n</sup> dataset. These datasets often contain information on thousands of ions from one sample, among which only a small portion is relevant to drug metabolites. Therefore, data-processing or data-mining techniques are developed to effectively search for metabolite-related information and extract them from the original dataset (Fig. 1).

#### 3.1 Targeted data-mining technology

Targeted data mining is based on the knowledge of drug properties and the relevant metabolic pathways. The techniques use accurate mass measurements (usually <5 ppm) to differentiate drug-related ions from those of matrix background.

##### 3.1.1 *Extracted ion chromatography*

Based on the knowledge of metabolism and experience of analysts, specific known or predicted metabolites of interest can be extracted from the full-scan MS dataset and displayed in extracted ion chromatograms (EIC or XIC). HRMS allows very narrow mass tolerance (<5 ppm) and thus makes this approach highly selective. HRMS-based EIC can achieve great detection sensitivity and minimal background interference. However, it lacks the capability to detect unpredictable metabolites and to search for unknowns.

##### 3.1.2 *Mass defect filter*

MDF was developed specifically for utilization of HRMS in drug metabolite detection, which is based on the unique mass defect of the designated templates, such as the parent drug, core substructures of the drug and its conjugates [19, 21, 27, 43]. This software-assisted processing technique imposes filters on the residue mass dimension of the full-scan HRMS dataset to remove the ions derived from endogenous components. By this way, the drug-related ions can be substantially enriched in the MDF processed data for further analysis (Fig. 6A). The “metabolite-enriching” mechanism of MDF attributes to the finding that mass defects of phase I and phase II metabolites typically fall within a window related to that of the parent drug. Based on mass defects of the parent drug and core templates, multiple MDFs each with a narrow DMF filter window ~50 mDa can be applied to retain the ions of a large variety of possible drug metabolites. MDF has been widely used for both in vitro [34, 44] and in vivo metabolite profiling [30, 37, 45–48].

##### 3.1.3 *Isotope pattern filter*

An accurate-mass-based IPF algorithm has been developed to facilitate the detection of drug-derived materials that possess diagnostic isotopic patterns (e.g., chlorine- and bromine-containing compounds) or stable isotope-labeled drugs [49]. The mass difference of designated isotopic ion pairs and their relative abundance ratio are combined as criteria to filter full-scan MS dataset. HRMS can aid in accurate identification of the ions of isotopic

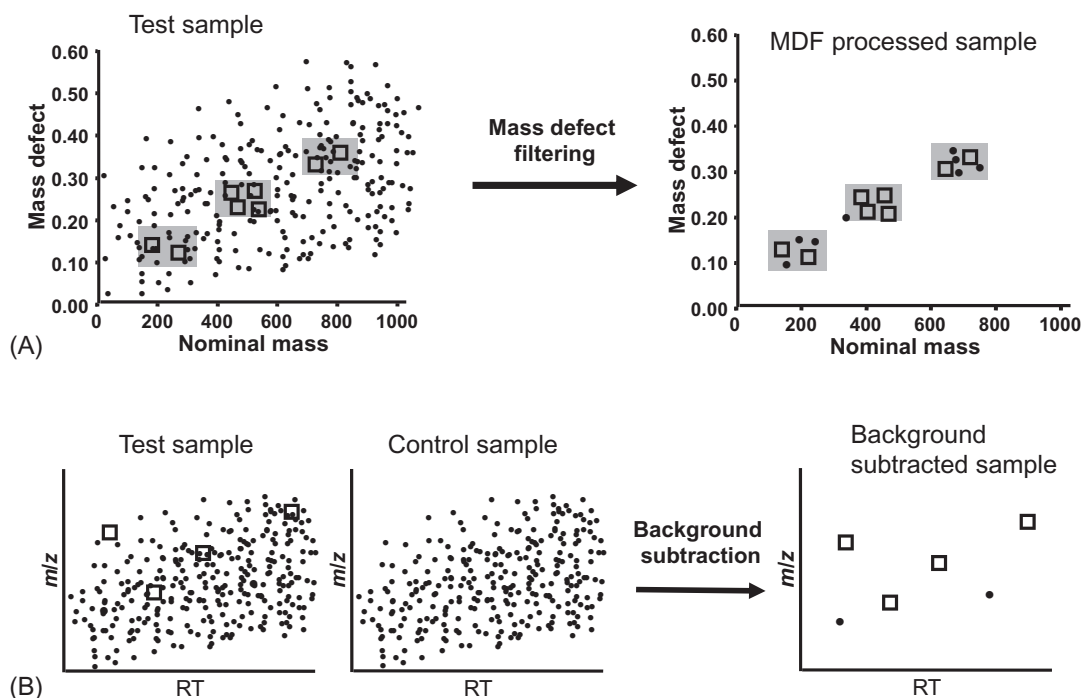


**FIG. 6** Mechanisms of detecting drug metabolites in biological samples by HRMS-based data processing using (A) mass defect filter and (B) background subtraction. Adapted with permission from H. Zhang, D. Zhang, M. Zhu, K. Ray, *High resolution LC/MS based mass defect filter approach: basic concept and application in metabolite detection*, in: R. Ramanathan (Ed.), *Mass Spectrometry in Drug Metabolism and Pharmacokinetics*, John Wiley & Sons, Hoboken, NJ, 2008, pp. 223–251.

fingerprint so that it substantially improves the sensitivity and eliminates false positives. HRMS-IPF complements the existing tool set for metabolite detection [33, 34, 49, 50]. As illustrated in Fig. 3A, IPF-processed full-scan LC-MS dataset of a rat liver microsomes incubation sample of ticlopidine with a mixture of GSH and stable isotope-GSH displays GSH adducts without any significant false-positive peaks, while high background and interference components and only two GSH adducts (M4 and M8) are present in the unprocessed LC-MS profile (data not shown). A combination of IPF-based data acquisition and data processing is the LC-MS method of choice for metabolite profiling of test compounds that have distinct isotope patterns.

### 3.1.4 Product ion filter and neutral loss filter

The metabolites carrying similar structures to the parent drug mostly undergo similar fragmentation in mass spectrometry. For example, most fragmentations of oxidative metabolites likely happen on the same sites of metabolite to the parent. Fragmentation of the metabolite likely produces either the same product ions or product ions with the same  $m/z$  shift



as the  $m/z$  difference of metabolite to parent. Fragmentation of the metabolite may also produce ions from the same neutral losses as the corresponding ones of the parent. Based on this, product ion filter (PIF) and neutral loss filter (NLF) have been developed as a pair of complementary approaches to detecting metabolites [14, 34, 51]. Extracted chromatograms of specific fragment product ions or neutral losses can be generated from the MS/MS dataset. When a positive peak is identified, the corresponding precursor ion can be retrieved from the full-scan MS dataset for identification. These approaches are commonly employed to search for conjugation metabolites. For example, the product ion at  $m/z$  272.0888 in negative ion mode is unique for GSH and GSH conjugates, so PIF of negative  $m/z$  272.0888 is applied to screening reactive metabolites trapped by GSH [51]. NLF can be utilized to detect the metabolites with easily dissociable conjugation linkage, such as neutral loss of the characteristic glucuronide moiety of glucuronide metabolites (NL of 176.0321). Additionally, HRMS can improve the sensitivity of IPF and NLF by applying narrow extraction windows. However, both approaches mainly rely on effective collection of information-rich and drug-relevant MS/MS data by proper acquisition. In this regard, nontargeted data-mining approaches with wide coverage are often more compatible with PIF and NLF.

## 3.2 Nontargeted data-processing approaches

Nontargeted data-processing methods do not require prior knowledge of the molecular weights, structures, or fragmentation pathways of drugs, thus facilitating the identification of both common and uncommon metabolites. These techniques, including BS and metabolomics approach, are independent to the subject of interest and thus can be applied as universal approaches in studies of drug metabolism, metabolomics, environmental science as well as other disciplines.

### 3.2.1 Background subtraction

Most of the ion species in LC-MS datasets are resulted from endogenous matrices of biological samples and solvents. The drug metabolites of interest are often present at very low levels and are often buried in numerous background ions. Therefore, removing the interference ions by HRMS-based BS from the original dataset can reveal drug-related information. A retention-time-shift-tolerant BS software was developed for the extraction of drug metabolites in biological matrices [52–55]. For each ion detected in the analyte file, the software algorithm searches the control file for that target ion. If such a target ion is present in the control file within the mass tolerance and retention-time-shift window, the maximal intensity of the ion is multiplied by a predefined scaling factor and subtracted from the intensity of the ion in the analyte file (Fig. 6B). This BS data-mining tool was very effective in detecting metabolites in complex matrices. The key factor contributing to the effectiveness of this program is the use of accurate mass data coupled with retention-time-shift-tolerance to determine if an ion detected in the analyte file is present in the control file.

BS is especially useful in metabolite profiling studies when the radiolabeled drug is not available. This algorithm has been applied in the detection of drug metabolites [52–54, 56] and GSH trapped reactive metabolites [53, 57]. In the past few years, BS has been widely used in multiple fields, such as detection of unknown toxic chemicals in plasma [58],

characterization of Chinese traditional medicine components *in vivo* [59], detection of toxicological biomarker in urine [60], and identification of protein adducts *in vitro* [61], etc.

### 3.2.2 Metabolomics approach

Untargeted metabolomics approach involves LC-HRMS data acquisition of samples from a test group and a control group, subsequent data processing and multivariate data analysis (MDA) to search for endogenous components, whose concentrations are significantly altered in the test group. The identity of the components can be further determined using metabolome databases or via chemical structural characterization. The same approach has been applied to detection and identification of drug metabolites and other xenobiotics that are only present or have significantly higher abundances in test samples than in the control samples [62–65]. Parallel samples from both vehicle and treatment groups are usually required for reducing acquisition bias of different injections and conducting a significant statistical analysis. Fig. 7A depicts a workflow for conducting *in vivo* metabolite profiling using a metabolomics approach. Principal components analysis (PCA) is one of the most widely used methods, which enables the comparison between control and test samples intuitively. The test samples after drug administration can be clearly separated from the control in

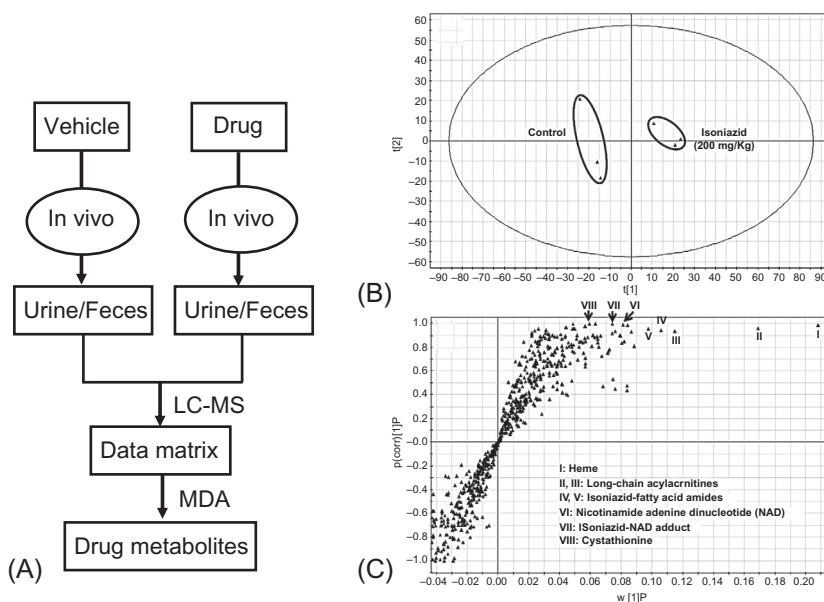


**FIG. 7** (A) A schematic representation for identification of drug metabolites *in vivo* using a metabolomics approach. Biological samples (plasma, urine, feces, bile, etc.) are analyzed using LC-MS to generate a data matrix. The data matrix is then subjected to multivariate data analysis (MDA) to screen drug metabolites. (B) Metabolomic analysis of mouse liver from the INH-treated groups. Wild-type mice were treated with vehicle or 200 mg/kg INH orally. Liver samples were collected at 30 min after treatment. All samples were analyzed by UPLC-QTOF-MS. (C) Separation of control and INH-treated groups in a PCA score plot. Adapted with permission from F. Li, P. Wang, K. Liu, M.G. Tarrago, J. Lu, E.N. Chini, et al., *A high dose of isoniazid disturbs endobiotic homeostasis in mouse liver*, *Drug Metab. Dispos.* 44 (11) (2016) 1742–1751.

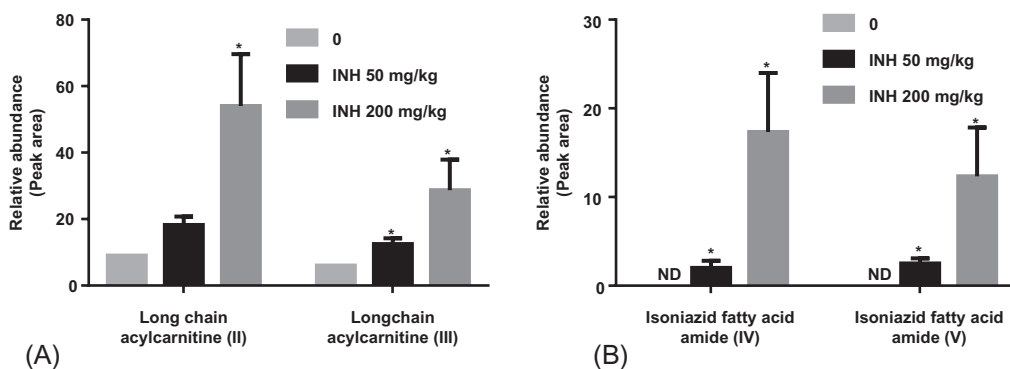


FIG. 8 (A) Accumulation of oleoyl-L-carnitine (II) and linoleoyl-L-carnitine (III) in the livers of mice treated with INH. (B) Dose-dependent formation of INH-fatty acid amides (IV and V) in the liver of mice treated with INH. The data are expressed as the mean  $\pm$  SEM ( $n=3$ ). \*\* $P < .001$  versus control group. Adapted with permission from F. Li, P. Wang, K. Liu, M.G. Tarrago, J. Lu, E.N. Chini, et al., A high dose of isoniazid disturbs endobiotic homeostasis in mouse liver, *Drug Metab. Dispos.* 44 (11) (2016) 1742–1751.

the scores plot of PCA analysis. For example, the untargeted metabolomic approach was applied to explore the acute effects of isoniazid (INH), an antituberculosis drug, on endobiotic homeostasis in mouse liver [66]. The PCA analysis revealed two clusters corresponding to the control and 200 mg/kg INH-treated groups in a score plot (Fig. 7B). The corresponding S-plot displays the ion contribution to the group separation (Fig. 7C). The top-ranking ions were identified as heme (I), oleoyl-L-carnitine (II), and linoleoyl-L-carnitine (III), INH-fatty acid amides (IV and V), NAD (VI), INH-NAD adduct (VII), and cystathionine (VIII) [66]. As shown in Fig. 8A, INH-mediated accumulation of oleoyl-L-carnitine and linoleoyl-L-carnitine was dose dependent. Overdose of INH resulted in acylcarnitine accumulation in the liver, suggesting that a high dose of INH causes mitochondrial dysfunction. The formation of INH-fatty acid amides indicated the interactions between INH and fatty acyl-CoAs (Fig. 8B) [66]. The metabolomics method has been proven for finding drug metabolites as well as discovering biomarkers for acetaminophen-induced hepatotoxicity [67]. With trapping reagents, this approach was applied to profile reactive metabolites of acetaminophen (APAP), pulegone (PLG), and clozapine (CLP) [17]. In addition, the metabolomics approach can also be combined with MDF as an integrated strategy for metabolite identification [68].

### 3.3 Software-assisted metabolite prediction and identification

#### 3.3.1 Software for site of metabolism prediction

Predictions of potential metabolites based on the chemical structure are becoming increasingly important in drug discovery to guide medicinal chemistry efforts that address metabolic stability and structural alters. The metabolic fate of a molecule depends on its intrinsic chemical reactivity and its interactions (affinity and binding orientation) with the metabolizing enzymes involved. A wide variety of software packages have been developed and are commercially available for the prediction of xenobiotic metabolism, as listed in Table 2 [69, 70].

**TABLE 2** Computer software used in predicting drug metabolites.

Software	Model Basis	Description
EAWAG-BBD Pathway Prediction System	Knowledge based	<ul style="list-style-type: none"> <li>• Uses biotransformation rules and reactions found in the EAWAG-BBD database or in the scientific literature</li> <li>• Predicts plausible pathways for microbial degradation of chemical compounds</li> </ul>
MetabolExpert	Knowledge based	<ul style="list-style-type: none"> <li>• Contains rules and lists of substructures that inhibit or activate the reactions</li> <li>• Predicts the most common metabolic pathways in animals, plants or through photodegradation</li> <li>• Metabolites are collected in compound databases</li> </ul>
Metabolizer	Knowledge based	<ul style="list-style-type: none"> <li>• Contains a built-in library of human biotransformation schemes which are collected from literature (users can also add their own library to customize the calculation)</li> </ul>
MetaDrug	Knowledge based	<ul style="list-style-type: none"> <li>• Predicts metabolites based on over 160 rules derived from a large knowledge base</li> <li>• Includes 89 rules to predict likely reactive metabolites</li> </ul>
Metaprint2D-React	Knowledge based	<ul style="list-style-type: none"> <li>• Predicts xenobiotic metabolism through data-mining and statistical analysis of known metabolic transformations reported in scientific literature</li> <li>• Predicts the types of transformation that can take place at ease site of metabolism, and the likely metabolite formed</li> </ul>
Metero Nexus	Knowledge based	<ul style="list-style-type: none"> <li>• Uses a comprehensive, expert knowledge base to predict the metabolic fate of chemicals</li> <li>• Predicts the first generation metabolites by using Absolute/Relative Reasoning, Static Scoring or Site of Metabolism (SOM) Scoring</li> </ul>
Met-PC	Knowledge based	<ul style="list-style-type: none"> <li>• Uses a set of expert rules that are coded in dictionaries to determine the part of the chemical structure of a query compound to predict the metabolic products</li> <li>• Uses optimization algorithms to fine tune relative importance of the rules</li> </ul>
MetaSite	Structure-based molecular interaction model	<ul style="list-style-type: none"> <li>• Considers both enzyme-substrate recognition and the chemical transformations induced by the enzyme</li> <li>• Predicts metabolic transformations related to cytochrome and flavin-containing monooxygenase mediated reactions</li> <li>• Does not require training set</li> </ul>

*Continued*

TABLE 2 Computer software used in predicting drug metabolites—cont'd

Software	Model Basis	Description
Systematic Generation of Potential Metabolites (SyGMa)	Knowledge-based and empirical scoring	<ul style="list-style-type: none"> <li>Covers approximately 70% of biotransformation reactions observed in humans</li> <li>Assigns an empirical probability score to each rule representing the fraction of correctly predicted metabolites in the training database. This score is used to refine the rules and to rank predicted metabolites</li> </ul>
Tissue Metabolism Simulator (TIMES)	Knowledge based	<ul style="list-style-type: none"> <li>Uses different data sources to train the metabolic simulator</li> <li>Estimates the relative probabilities for major biotransformation in a specific metabolic environment</li> </ul>

*Adapted with modification from J. Kirchmair, A.H. Goller, D. Lang, J. Kunze, B. Testa, I.D. Wilson, et al., Predicting drug metabolism: experiment and/or computation? Nat. Rev. Drug Discov. 14 (6) (2015) 387–404.*

Except for MetaSite, all other software packages listed above are ligand-based computational methods, which only consider the substrate and do not include the complex interaction and dynamics between the ligand and the protein. MetaSite, however, considers both enzyme-substrate recognition (a thermodynamic factor) and the chemical transformations induced by the enzyme (a kinetic factor) [71]. It is important to mention that these software packages have largely advanced and facilitated the metabolite detection process. However, computational approaches for the automated metabolite structural identification from LC-HRMS data are still emerging.

### 3.3.2 Software for metabolite structural identification

Structural elucidation is a time-consuming, labor-intensive process, and can be a rate-limiting process of metabolite identification in drug discovery and development. Therefore, new software-assisted approaches for structural assignment of drug metabolites are highly desired. In recent years, significant efforts have been made on developing novel fragmentation prediction algorithms for structural elucidation, leading to the advances and development of software packages, such as Mass-MetaSite, MassFragment, Mass Frontier and MetaSense, etc.

Mass-MetaSite has been rapidly gaining acceptance for automatic metabolite structure assignments since it was introduced around 2010. It combines MetaSite for in silico prediction for site of metabolism (SoM) and interrogation of high-resolution MS/MS data for structural elucidation [72–74]. The underlying principle of Mass-MetaSite is the comparison of fragmentation patterns of parent and metabolite and the subsequent in silico prediction which is used to differentiate between assignments with equivalent fragmentation patterns [74]. The software generates possible metabolites based on the parent drug structure. The MS/MS spectra of parent and metabolites are compared, and a score is assigned to the structural proposal based on the number of matching and mismatching fragments compared to the parent compound and on their intensity. Mass-MetaSite is a vendor-neutral software that is capable of handling “all-in-one” HRMS dataset from nontargeted DIA ( $MS^E$ , SWATH, All-ion-fragmentation, etc.) as well as data-dependent MS/MS dataset. Bonn et al. demonstrated this expert

system to enhance correct structure assignment to almost 80% based on 35 reference compounds. Ahlqvist and coworkers conducted *in vitro* metabolism of a diverse set of 65 compounds in human liver microsomes, rat hepatocytes, or human hepatocytes, and compared manual metabolite structural assignment workflow with Mass-MetaSite workflow. They found that the exact match or Markrush representations were in agreement for 92% of the metabolites reported between the two workflows [75].

MassFragment developed by Waters is another software tool for automatic identification of product ion fragments using a series of novel, chemically intelligent algorithms. It creates a database of all theoretically possible fragments of a compound from breaking of all theoretical bonds, which is then used to compare to the observed experimental fragment ions from metabolites for structural assignment. It is important to note that MassFragment is based on systematic bond disconnection instead of the traditional rule-based approach; therefore, it will not correctly assign structures for ions which occur via rearrangement [76]. A similar approach with an improved algorithm, called IsoScore, was introduced for automated localization of biotransformations [77]. The underline principle of IsoScore is to generate all virtual regioisomers of a given biotransformation by iterating over all plausible sites of metabolism around the parent drug, followed by the virtual fragmentation of all regioisomers and the scoring of all virtual fragments versus the experimentally observed ions. Metabolite structures are finally ranked by their cumulative scores, showing their likelihood in relation to the experimental data. IsoScore was able to correctly locate the biotransformation of a variety of metabolites from different chemical scaffold [77].

Mass Frontier software predicts comprehensive fragmentation pathways based on a set of general ionization, fragmentation, and rearrangement rules. It contains fragmentation mechanisms for small molecules collated from published literature, together with 24 general ionization, fragmentation, and rearrangement rules. The Fragments Comparator automatically identifies common and unique fragments and can be used to differentiate isomeric compounds and to determine the structures of unknowns. Fragment ion search (FISh) is a novel tool that provides fast screening of structurally similar compounds based on the fragmentation pattern of the parent compound to filter out the majority of matrix-related background ions. In addition, FISh can also automatically localize the modification site based on common fragments as well as those with mass shifts from biotransformations included in the FISh-processing parameters. Friedecký et al. presented the use of high-resolution/accurate mass spectrometry for a detailed study of imatinib metabolism in plasma samples from patients, in which Mass Frontier software was successfully used for the identification of the fragments and elucidation of the metabolite structures [78].

MetaSense, developed by ACD/Labs, is a vendor-neutral software package that utilizes a probabilistic, structure-based metabolite prediction model to determine the likelihood of a metabolic reaction taking place at each potential site of metabolism in the molecule of interest with a metabolism score that takes into account of both calculated probability and reliability of prediction confidence. Once potential metabolic hotspots are established, they are checked against a database of biotransformation rules to assess the types of metabolic reactions that are defined for the respective site of metabolism, taking into account of its chemical neighborhood. Finally, the selected biotransformation rules are applied to generate an exhaustive list of metabolite structures. Metabolite structures are assigned by comparing their MS/MS spectra to that of the parent where common fragments and  $m/z$  pairs between the parent

and metabolites are assessed. For ambiguous structures, Markush structures are notated. Watanabe et al. reported *in vitro* and *in vivo* metabolites of synthetic opioids identified using MetaSense software were in good agreement with manual processing based on predicted biotransformations [79].

## 4 Applications of HRMS technologies in metabolite identification experiments

HRMS has enabled a number of new and improved data acquisition and data-mining methods for drug metabolite identification in complex biological matrix components (Fig. 1). Each of these data-mining methods can be used independently to search for metabolites in a targeted or untargeted manner. Alternatively, these methods can be applied in a parallel or tandem manner. The selection and use of specific data acquisition methods are not only associated with the availability and distinct advantage of individual DDA and DIA technologies, but also depend on the purpose, turnaround time, and biological matrix of metabolite identification experiments. Common biotransformation and ADME studies include metabolic soft-spot analysis and reactive metabolite screening in lead optimization, *in vitro* metabolism across species and metabolism and disposition in bile duct-cannulated (BDC) animals in clinical candidate characterization, as well as metabolites-in-safety test (MIST) and radiolabeled ADME studies in human in clinical development. Additionally, investigative drug metabolism studies, which are not standard biotransformation experiments, are often conducted to address compound-specific and ADME-related issues faced in drug discovery and development. There is no longer a shortage of methods in detection and characterization of drug metabolites, but rather these methods ought to be chosen and organized in a way that is simple and efficient to accomplish the major tasks of individual experiments. In this section, we discuss how to select and apply a set of HRMS methods suited for individual biotransformation studies commonly performed in the pharmaceutical industry. Several examples are used to illustrate the specific utilities of various HRMS analytical techniques for these experiments.

### 4.1 Metabolic soft-spot analysis

Structural characterization of metabolic “soft” spots is a key task in lead optimization, which is often triggered by the fast metabolism of lead compounds observed in high-throughput metabolic stability screening. The metabolic soft-spot screening experiment is routinely carried out by incubating a test compound at 1–10  $\mu\text{M}$  in liver microsomes with NADPH followed by HRMS-based metabolite profiling [80]. The goal of the assay is to determine what are the major metabolites of a test compound by quantitative analysis and what are the sites of metabolism via structural characterization. The information is critical for medicinal chemists to design new compounds with better metabolic stability. Since the metabolic soft-spot analysis focuses on major metabolites formed in relatively clean *in vitro* incubation matrices and requires a short turnaround time, intensity-dependent acquisition [81, 82],  $\text{MS}^E$  [80, 83], and SWATH [40], which are compound-independent acquisitions, are well suited to serve the purpose of the experiment. A major challenge often faced in the soft-spot analysis is



to determine major metabolites when over 10 or 20 metabolites are detected by LC-HRMS in liver microsomal incubations. Although LC-MS peak intensity can be used as a measurement of relative abundances of metabolites, results from this approach could be misleading when ionization efficiencies of different metabolites from the same parent drug vary significantly. For this consideration, LC-HRMS coupled with UV detector is employed for metabolic soft-spot determination. As illustrated by an example present in Fig. 9A, the LC-UV profile of a human liver microsomal incubation sample of saquinavir (5  $\mu$ M, 6 min incubation) clearly displays two major metabolites (M1 and M2) along with the parent drug. Consequently, the structural characterization of saquinavir metabolites in the incubation sample focused on these two metabolites rather than several other secondary metabolites displayed in the LC-MS profiles (data not shown). In this case, the intensity-dependent acquisition by a quadrupole-orbitrap HRMS instrument was capable of recording accurate MS/MS spectra of M1 and M2 for structural identification in a single injection (Fig. 9B). In addition, preliminary information of reaction phenotyping can be obtained using various CYP-specific chemical inhibitors. As shown in Fig. 9C, ketoconazole, a potent CYP3A inhibitor, significantly inhibited the formation of M2, suggesting that CYP 3A was the main enzyme responsible for the formation of M2. This example demonstrated the use of LC-HRMS for both metabolite identification and quantification in a high-throughput manner.

## 4.2 Reactive metabolite screening

Detection of *in vitro* reactive metabolites of lead compounds followed by minimization of bioactivation via structural modification is another key task in drug discovery, which can improve the safety profile of drug candidates. HRMS-based LC-MS technology plays a key role in this area as well. A common reactive metabolite screening experiment is conducted by incubating a test compound (10  $\mu$ M) in liver microsomes in the presence of a large amount of glutathione (GSH) (1–5 mM) followed by profiling GSH-trapped reactive metabolites using HRMS instrument and various data-mining tools such as MDF [47, 84], BS [53, 57], IPF [32, 33], and NLF [35]. Unlike major metabolites characterized by metabolic soft-spot analysis, GSH-trapped reactive metabolites have much lower concentrations in liver microsome incubation samples. Therefore, high selectivity and sensitivity of data acquisition and data-mining techniques are required for the rapid reactive metabolite screening. For example, accurate neutral-loss-triggered MS/MS acquisition (NL of 129.0426) and neutral-loss filtering can be useful in reactive metabolite screening based on a common neutral-lose of the glutamate residue from GSH adducts. Mass defect-dependent MS/MS acquisition and mass defect filtering based on predicted mass defect values of potential GSH adducts are also valuable HRMS techniques for the reactive metabolite screening assay [34].

The neutral-loss and mass defect filtering-based methods are useful for high throughput reactive metabolite screening in drug discovery. However, the selectivity of the two approaches could lead to significant false negative and false positive signals as shown in the example of analyzing reactive metabolites of imipramine using MDF (Fig. 10). The unprocessed total ion chromatogram (TIC) of the incubation sample only displays the major GSH adduct (P+GSH+2H), while all of minor GSH adducts are buried under interference peaks or background noises (Fig. 10A). Although MDF revealed four additional GSH adducts

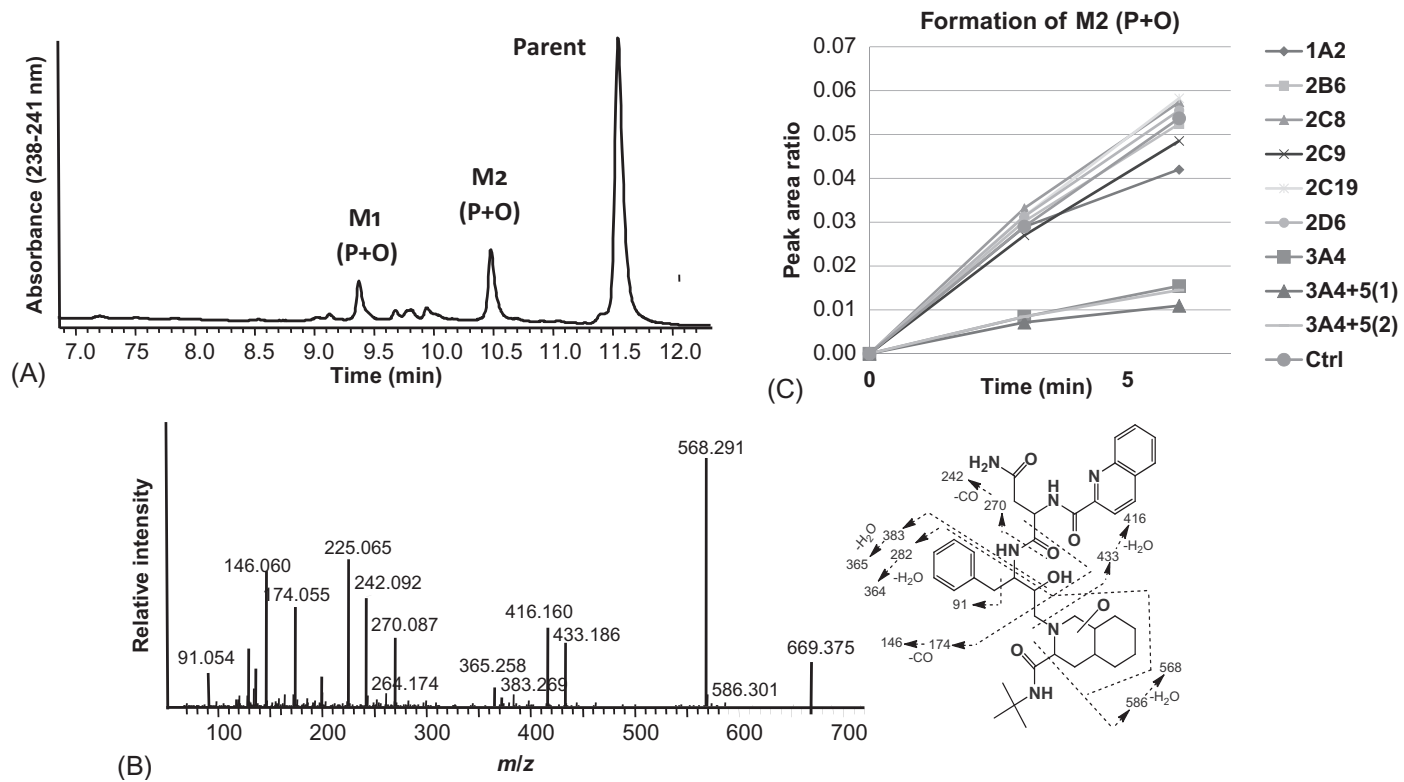


**FIG. 9** Application of HRMS in rapid metabolic “soft” spot analysis and CYP reaction phenotyping. Saquinavir (5  $\mu$ M) was incubated in human liver microsomes for 6 min, followed by LC-UV/HRMS analysis. (A) LC-UV profile of the incubation sample. (B) MS/MS spectrum and proposed structure of saquinavir metabolite M2. (C) The time-dependent inhibition of M2 formation by various chemical inhibitors of CYP enzymes.

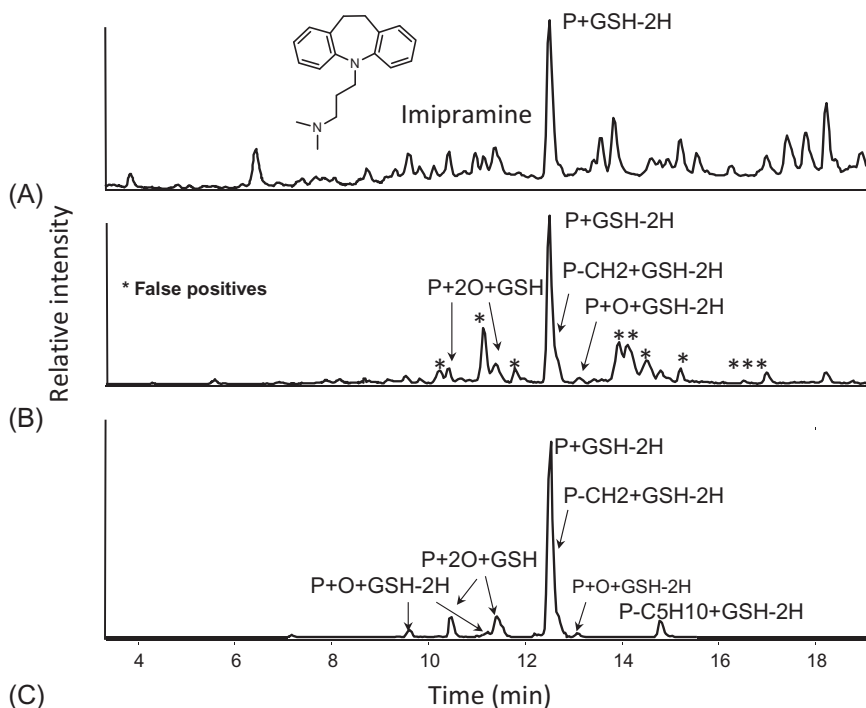


**FIG. 10** GSH adduct profiling of imipramine in rat liver microsomes in the presence of GSH by MDF and IPF. (A) Unprocessed TIC of the incubation sample. (B) MDF-processed LC-MS data, showing multiple false-positive peaks as marked with \*. (C) IPF-processed LC/MS data from imipramine incubated with rat liver microsomes in the presence of a mixture of GSH and stable isotope-labeled GSH (5 mM, 1:1 ratio).

(Fig. 10B), several false-positive peaks from unfiltered endogenous components are displayed and unremoved background noises made two minor GSH adducts (9.7 and 14.8 min) invisible. To improve the performance of LC-HRMS in reactive metabolite screening, a high throughput assay using isotope pattern-based DDA and data-processing techniques was developed. A distinct pattern of GSH adducts is introduced by using a mixture of GSH and stable isotope-labeled GSH (GSH/ $^{13}\text{C}_2$ ,  $^{15}\text{N}$ -GSH=1:1) as the trapping agent in liver microsomal incubation. HRMS coupled with these techniques significantly enhances the sensitivity and selectivity of the GSH adduct screening. As demonstrated in Fig. 10C, isotope pattern filtering in accurate mass almost completely removed interference ion species, leading to much better selectivity of detection of GSH adducts of imipramine as compared to mass defect filtering (Fig. 10B). It is worthy to mention that BS data processing is also very effective in finding *in vitro* and *in vivo* GSH adducts [52].

### 4.3 *In vivo* metabolite profiling and identification

Biotransformation studies in animals and human are important in support of drug discovery and development. Because of the extent of sample matrix complexity, unpredictable

natures of metabolism reactions catalyzed by a verity of enzymes in different organs, and low metabolite abundance in some biological samples such as plasma, in vivo metabolite profiling of nonradiolabeled drug candidates is perhaps the most challenging study among drug metabolite identification tasks. Common ADME studies of drug candidates include correlation of in vitro/in vivo metabolism, determination of major clearance pathways in animals, characterization of major circulating metabolites and investigation of active or toxic metabolites, which require excellent sensitivity, selectivity, and comprehensiveness for in vivo metabolite profiling. Thus, some HRMS-based data acquisition and processing methods that are suited for in vitro biotransformation experiments (Fig. 1) are no longer effective for the in vivo metabolite profiling. For example, extracted ion chromatogram analysis to target predicted molecular ions could potentially miss metabolites formed via unusual biotransformation or multiple common metabolic pathways and generate false-positive signals from intense interference ions. Isotope pattern filtering has excellent capability in finding unknown drug metabolites that contain chlorine or bromine atom(s) in very complex biological samples, but a very few lead compounds and drug candidates have such unique structures or their metabolites from oxidative dehalogenation have no signature isotopic patterns. In addition, searching for metabolite ions in MS/MS datasets of in vivo samples acquired via DDA or DIA often led to many false positives or negatives. Fortunately, three data-mining techniques, named mass defeat filtering [27, 37, 46], BS [52, 54], and metabolomics analysis [62–64, 68], work relatively well in finding both common and uncommon drug metabolites in complex biological samples. Their capability for comprehensive detection of in vivo metabolites is demonstrated by the similarity of the radioactivity profile of a test lead compound monkey plasma (Fig. 11A) and LC-MS profiles from data processing using MDF (Fig. 11B) and BS (Fig. 11C). Similar to BS, metabolomics analysis is capable of comprehensive and untargeted detection of in vivo metabolites in a group of test samples, which are not present in control samples (Figs. 7 and 8).

The ability to obtain comprehensive metabolite profiles without the aid of radiotracers is an area of growing interest for identifying major human circulating metabolites in phase I clinical trials to comply with MIST guidance. The first step of the MIST study is to determine profiles and structures of metabolites in human plasma after single and/or multiple dosing of a drug candidate using HRMS-based technology [5, 85–91]. Usually, a majority of metabolites in human plasma are not visible in unprocessed LC-MS profiles so that data-processing techniques capable of comprehensively detecting all metabolites regardless of their structures, molecular ions and mass defects are highly desirable. BS algorithm is especially powerful in detecting metabolites from first-in-human studies. As illustrated in Fig. 12, the BS data-process effectively detected and identified the metabolites in human plasma after oral administration of 150mg ranitidine. Intense matrix ions dominate the unprocessed TIC of human plasma, whereas the drug-related ions are almost invisible except ranitidine and ranitidine *N*-oxide (Fig. 12A). BS significantly eliminated the majority of the matrix ions, leaving for the most part only drug-related peaks (Fig. 12B). The simplicity and cleanliness of the BS-processed data allow easy detection of the molecular ion of drug-derived material. As shown in Fig. 12C, the molecular ion of a carboxylic acid metabolite (M1) at  $m/z$  300.1382 was embedded among many other predominant endogenous ions and was barely detected in the unprocessed mass spectrum. In contrast, this ion together with its in-source fragment

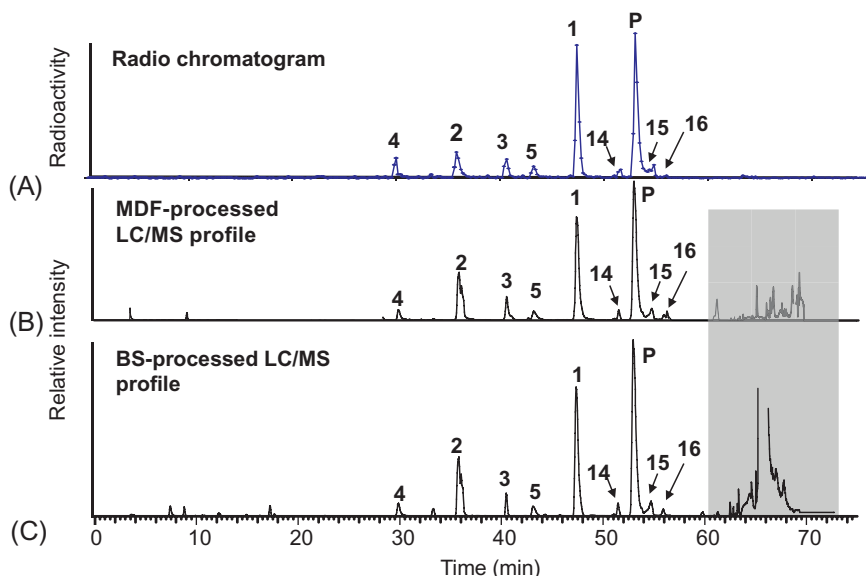


**FIG. 11** Metabolite profiles of a radiolabeled lead compound in money plasma determined by (A) LC-radioactivity analysis, (B) Ion chromatogram after mass defect filtering of LC-HRMS data, and (C) Ion chromatograms after background subtraction of LC/HRMS data. Adapted with permission from H. Zhang, D. Zhang, K. Ray, M. Zhu, *Mass defect filter technique and its applications to drug metabolite identification by high-resolution mass spectrometry*, *J. Mass Spectrom.* 44 (7) (2009) 999–1016.

ion by loss of carbon dioxide at  $m/z$  256.1476 were the only ions with no interference after applying BS (Fig. 12D).

Selectively and effectively acquiring MS/MS fragment data of *in vivo* samples “on-the-flight” by DDA and DIA remains to be very challenging due to abundant ion interference from complex biological matrices. The current common practice in the MS/MS acquisition of *in vivo* metabolites is to use the accurate mass inclusion list-dependent acquisition for the initial analysis of a sample based on predicated drug metabolites. However, the method could miss metabolites formed *in vivo* via multiple metabolic pathways or unexpected biotransformation reactions through rearrangement, ring opening and contraction [92–96], etc. Therefore, a second injection is often needed to acquire the MS/MS dataset of these metabolites that are not in the original inclusion list but are found late via postacquisition data mining. Alternatively, a complete list of drug metabolite ions can be generated through processing of a full-scan dataset (e.g., BS or metabolomics analysis), and subsequently be added in the inclusion list-dependent experiment to get all MS/MS data at once. Although DIA methods such as MS<sup>E</sup> and SWATH can be applied to metabolite profiling of *in vivo* sample, MS/MS data of minor metabolites in the presence of large amounts of endogenous components often have poor quality, which makes spectral interpretation very challenging. As exemplified in Fig. 2, mass defect-dependent MS/MS acquisition works more effective than other DDA or DIA methods for *in vivo* metabolite identification. However, this DDA function is only available in TripleTOF instruments manufactured by AB Sciex. The recently

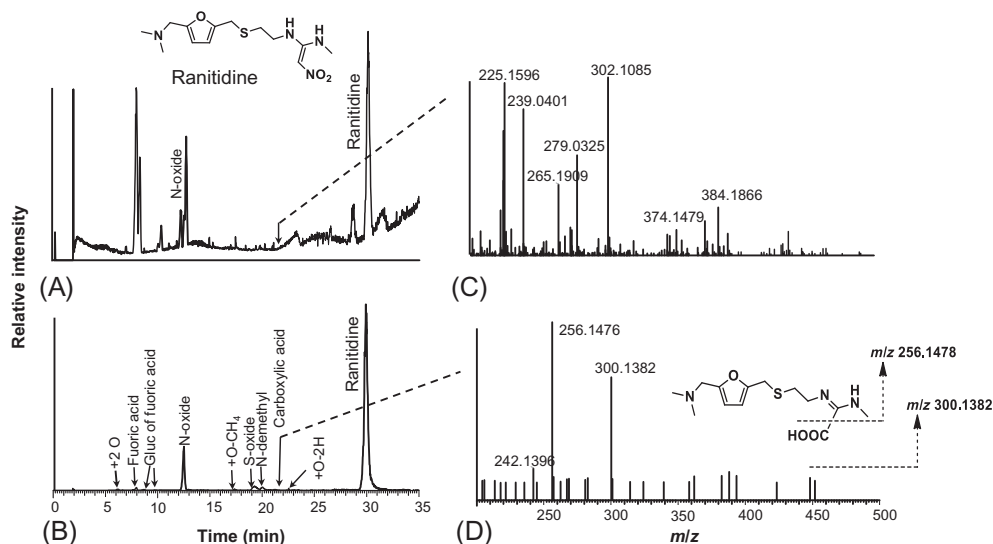


**FIG. 12** Detection and characterization of ranitidine metabolites in human plasma using LC-HRMS and data mining by background subtraction (BS). Human plasma samples were collected in predose and 6-h postdose of 150 mg ranitidine to healthy subjects. (A) Unprocessed TIC of the 6-h plasma sample. (B) BS-processed LC-MS profile of the 6-h plasma sample. (C) Full-scan MS spectrum at retention time 21.7 min in the unprocessed LC/MS data, in which metabolite ion is invisible. (D) Full-scan MS spectrum at retention time 21.7 min in the BS-processed LC/MS data, in which two ions related to a ranitidine metabolite at  $m/z$  256.1476 and 300.1382, are clearly displayed.

introduced novel BE-DDA technology (Fig. 4A) appears to be a promising approach for fast and selective MS/MS spectral acquisitions of *in vivo* samples.

## 5 Detection and structural characterization of traditional Chinese medicine components in biological systems

Traditional Chinese Medicine (TCM) has been widely used for the prevention and treatment of various diseases for more than 3500 years. The efficacy and safety of TCM are generally recognized to be associated with the chemical constituents of TCM including prototypes and their metabolites in the circulation [97, 98]. To maintain TCM therapeutic effects, it requires the maximal plasma concentrations or overall exposure of individual pharmacologically active components above certain thresholds in human, which are directly related to the whole process of absorption, distribution, metabolism, and excretion. In addition, the understanding of exposure, metabolism, and disposition of herbal medicines is very important to elucidate mechanisms of TCM-induced toxicity [99, 100]. ADME studies of a small molecule drug in human and animal are usually carried out using a radiolabeled drug. However, it is not practical or even feasible to use multiple radiolabeled TCM prototype compounds in an ADME study of a TCM product in animals or human. Thus, ADME research of TCM has heavily relied on LC-MS technology.

## 5.1 HRMS-based data acquisition techniques for profiling and characterizing TCM components in biological samples

Usually, a few dozens of TCM parent components (prototypes) and metabolite components with a verity of structures can be found in plasma, urine or feces samples after an oral administration of a TCM product to animals or humans. Therefore, targeted DDA methods based on predicted structural information, such as list-, mass defect-, isotope pattern-, and neutral loss-dependent MS/MS acquisitions [101, 102] are not well suitable for the TCM component analysis. Several research groups have tried to use untargeted DIA methods, including MS<sup>E</sup> [103, 104] and SWATH [105–107], to automatically acquire fragment ion data of TCM components in biological samples for structural confirmation of high abundant prototype components or initial structural characterization of unknown major metabolites of a TCM product. However, when concentrations of TCM components in a test sample are low or there are significant interferences from endogenous materials, these DIA methods often generate significant amount of false-positive and false-negative signals. Currently, a common practice to acquire MS/MS spectral data of TCM components in biological samples is the use of the inclusion list-DDA method to target TCM components that are found in the same samples in the first step of postacquisition data mining. In many cases, the data mining to find TCM components and sequential DDA to acquire their MS/MS spectral data are repeated for multiple times for the detection and structural characterization of TCM components in a single sample, which could take up to a few weeks. Recently a novel background exclusion DDA method (Fig. 4) was introduced. Preliminary results from our laboratory suggest that this DDA technology holds a great promise for fast and automatic acquisition of MS/MS spectral data for multiple TCM components in biological samples [101].

## 5.2 Targeted data-mining techniques applied to detection and identification of in vivo TCM components

In the past 10 years, HRMS has become the single major LC-MS instrument for detection and characterization of TCM components in the circulation and excreta of animals and humans [108–112]. The first step of such an analysis is to comprehensively detect TCM components in a biological sample. Targeted data-mining approaches have been utilized to search for metabolites of individual TCM prototypes on the basis of mass defects (MDF) [113–120], fragmentation patterns (NLF and PIF) [113, 114, 120, 121], or molecular weight (EIC) [116, 118, 120] of predicted metabolites, which are similar to the approaches used for finding drug metabolites (Fig. 1). For example, Jiang et al. found two parent compounds and 14 TCM metabolites in rat plasma and urine after an oral administration of *Scutellaria-coptis* extract [115] by using a combination of MS<sup>E</sup> acquisition and MDF. Geng and coworkers used MDF processing to find 57 prototype components and 77 metabolites in rat plasma after oral administration of *Xian-Ling-Gu-Bao* capsule [108].

Since an herbal medicine can contain up to a few hundred of prototypes, searching for their metabolites on the basis of their masses, mass defects, or product ions predicted from individual TCM prototypes is truly time-consuming and labor intensive. Many TCM metabolites are formed via multiple steps of biotransformation so that their detection by targeted data-mining tools often fail. In addition, detection of metabolites formed from a large number



of TCM parent components using EIC or MDF with multiple targeted molecular weights and mass defect ranges leads to many false positives from biological matrices. As an example shown in Fig. 13, the TIC of a rat plasma sample after an oral administration of Xiao-Ke-Wan that contains over 100 prototypes (Fig. 13A) showed a few TCM components and many large endogenous interferences. Processing the rat plasma LC/MS data using schisandrol B (a lignan) and puerarin (a flavonoid) as MDF templates revealed multiple metabolites of schisandrol B and puerarin, but many endogenous components remained (Fig. 13B and C). Much more false-positive signals would be generated when other prototype components are used as mass defect filtering templates. Differentiating true TCM metabolites from the false-positive components in the MDF-processed dataset would take very significant efforts.

### 5.3 Untargeted data-mining techniques for detection and characterization of TCM components

In order to overcome the limitations of targeted data-mining techniques, untargeted data-processing technologies have been recently applied to detection and identification of TCM components in biological samples, including metabolomics analysis [122, 123] (Fig. 7) and BS [58, 59, 110, 124] (Fig. 6B). Metabolomic approach is applicable to finding TCM components with specific  $m/z$  values at specific retention times in a group of testing samples, which are not present or have significantly lower levels in control samples. For example, Mi et al. found 170 compounds in plasma, including 51 prototype constituents and 119 metabolites after an oral administration of Dan Zhi Tablet by using cross-orthogonal partial least-squares discriminant analysis (OPLS-DA) and UNIFI platform [122].

Similar to metabolite detection of a small molecule drug, the BS data processing can eliminate the interference from endogenous components and background noises in complex biological samples and visually display TCM components in the processed LC-MS profiles regardless of their molecular weights, mass defect values, isotope patterns, or fragmentation pathways. The effectiveness of BS in finding TCM components has been demonstrated in a study of ADME of AF-XXMD, the active component of Xiao-Xu-Ming decoction [59], in rats. As shown in Fig. 14A, an unprocessed LC-HRMS profile of a rat plasma sample collected at 75 min after dosing AF-XXMD showed several intensive endogenous components and high levels of background interferences with one AF-XXME-related component H56. The BS data-processing removed a majority of endogenous peaks and significantly reduced the background noise levels. As a result, many minor AF-XXMD-related components were revealed in the processed LC/MS profiles (Fig. 14B and C). Compared to targeted data mining techniques, untargeted processing tools are much more effective in finding TCM components in complex biological samples in terms of speed, selectivity, and comprehensiveness.

### 5.4 LC-HRMS-based techniques for determining metabolic pathways of individual TCM components

Another analytical challenge faced in the study of metabolism and disposition of a TCM product in animals and human is characterization of metabolic pathways of individual TCM parent components and/or the formation pathways of individual TCM metabolites, especially when dealing with a large number of TCM components in vivo. A common practice

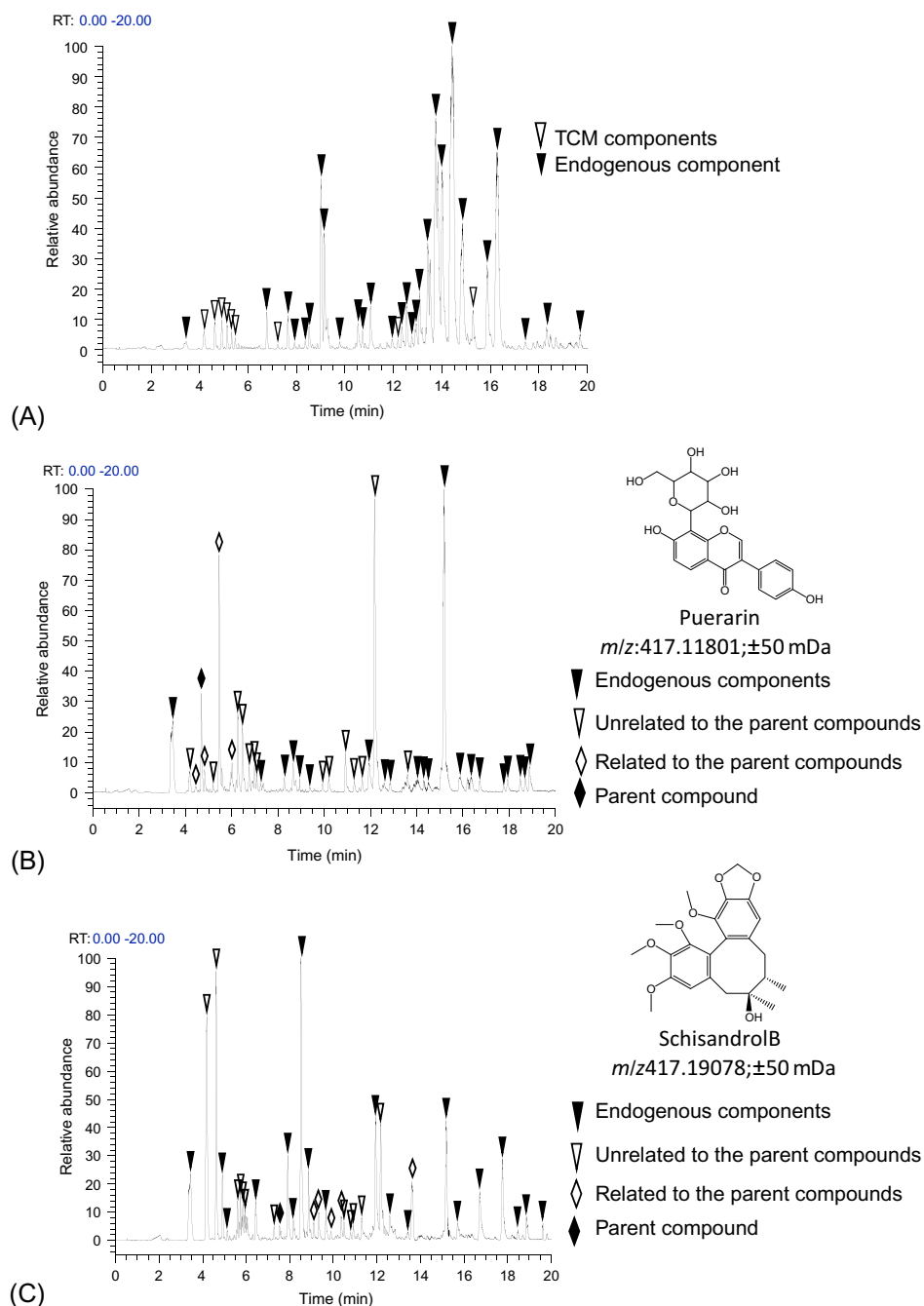


**FIG. 13** Examples of MDF-processed LC-MS profiles of rat plasma sample after oral administration of Xiao-ke Wan. (A) TIC of the rat plasma sample; (B) TIC of the same sample processed using MDF with Schisandrol B as parent compound; and (C) TIC of the same sample processed using MDF with puerarin as the parent compound.

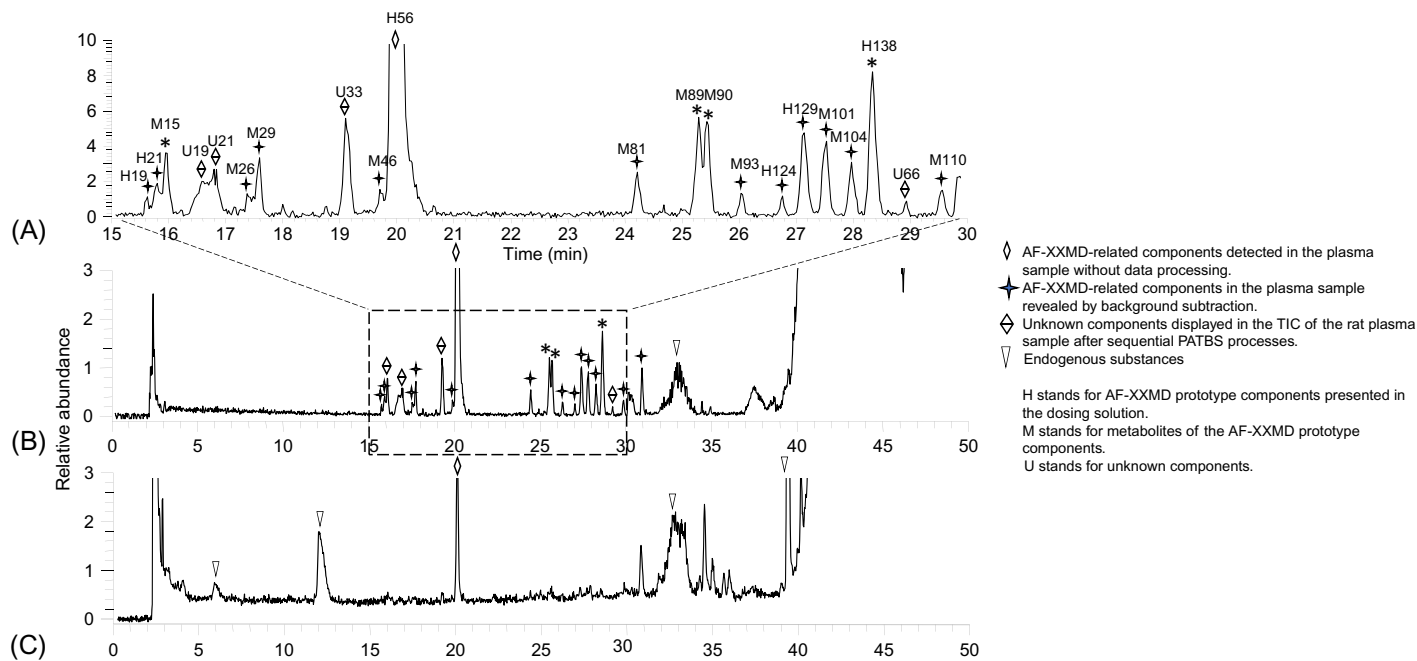


**FIG. 14** Untargeted analysis of multicomponents of AF-XXMD in a pooled rat plasma collected at 75 min postdose. (A) Zoomed in the area (15–30 min) of the TIC displayed in panel B. (B) Background subtraction processed LC-MS dataset of the rat plasma sample. (C) Unprocessed full-scan LC-MS dataset of the rat plasma sample. Adapted with permission from C. Wu, H. Zhang, C. Wang, H. Qin, M. Zhu, J. Zhang, *An integrated approach for studying exposure, metabolism, and disposition of multiple component herbal medicines using high-resolution mass spectrometry and multiple data processing tools*, *Drug Metab. Dispos.* 44 (6) (2016) 800–808.

to determine metabolic pathways of individual TCM components is dosing an isolated single TCM component to an animal species followed by profiling and identification of metabolites of the component in plasma, urine, and feces/bile. This approach can directly acquire metabolic pathway information of a single TCM component; however, it is extremely labor-intensive and time-consuming if a TCM product contains a large number of parent components. On the other hand, several research groups have explored methodologies to determine metabolic pathways of individual TCM components after administration of a TCM product to animals or humans [125, 126] using various methods or techniques. One of the data-processing techniques to link metabolites to individual prototype components is mass spectral trees similarity filter (MSTF), which can perform automatically comparisons of MS/MS spectral data of all prototype components with those of detected metabolites. As shown in Fig. 15A and B, a metabolite (M29) was detected in rats after AF-XXMD administration, and a mass spectrometric dendrogram was established based on its multistage MS/MS data [59]. By comparing the mass spectrometric dendrogram of M29 with the mass spectrometric library of AF-XXMD prototype components (constructed by collecting multilevel data of prototype components in liquid medicines), three prototype components (H35, H25, and H56) (Fig. 15C) were found to be related to M29, whose scores were higher than 650, indicating high correlation (Fig. 15D). The follow-up biotransformation matching analysis found that the molecular ion of M29 at  $m/z$  483.1493 was 176Da greater than that of H56. Therefore, M29 was identified as a glucuronide metabolite of H56. By using this data-processing approach, the correlations of all metabolites found in vivo to individual prototype components were established, which led to the assessment of the formation pathways of a majority of AF-XXMD metabolites in rats. Furthermore, connecting metabolites with their prototypes based on the spectral similarity and biotransformation knowledge greatly facilitated structural characterization of XXMD metabolites in urine, feces, and bile samples.

## 5.5 A comprehensive analytical strategy for study of exposure, metabolism, and disposition of TCM components

Recently, a generic LC-HRMS analytical strategy for detection of TCM components and characterization of structures and formation pathways of TCM metabolites in vivo has been established [118]. As illustrated in Fig. 16, the first step is to acquire accurate full MS datasets of a test sample and a control sample. The BS processing is then applied to reveal TCM components in the test sample. The TCM prototype components in the test sample are recognized by comparing the TCM component profile of the dosing solution with that of the test sample. MS/MS spectral data of the detected TCM components are acquired using a combination of intensity- and inclusion list-dependent acquisition methods with multiple injections. Identities of individual prototype components are confirmed by comparing their MS/MS spectra and retention times with those of prototype components in the dosing solution or synthetic standards. Structures and formation pathways of individual TCM metabolites are characterized based on spectral interpretation, biotransformation matching, mass defect matching and MS/MS spectral similarity analysis. In addition, the metabolism and disposition knowledge of known prototypes in the literature is utilized to facilitate TCM metabolite characterization. Results from a few pilot studies demonstrated the usefulness of this analytical strategy in investigating metabolism and disposition of TCM in animals and humans [101] although continuous improvements are needed.

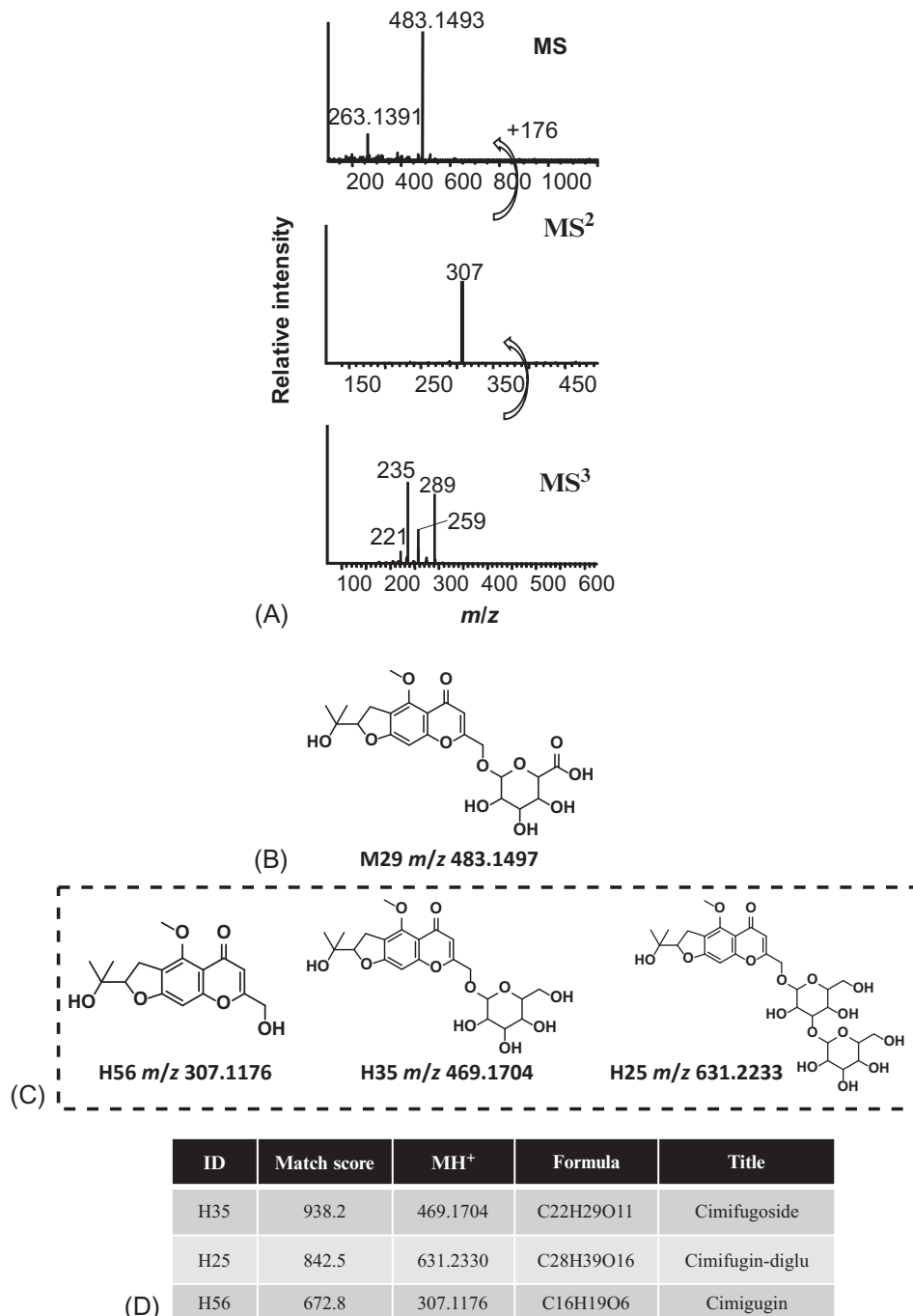


**FIG. 15** Identification of AF-XXMD components that have similar structures to M29 using MTSF. (A) Mass spectral tree of M29; (B) structure of M29 that was determined by comparing spectral trees of H56 and M29; (C) structures of H35, H25, H56; and (D) detection of H35, H25, H56 using M29 as a template and MTSF. Adapted with permission from C. Wu, H. Zhang, C. Wang, H. Qin, M. Zhu, J. Zhang. An integrated approach for studying exposure, metabolism, and disposition of multiple component herbal medicines using high-resolution mass spectrometry and multiple data processing tools, *Drug Metab. Dispos.* 44 (6) (2016) 800–808.

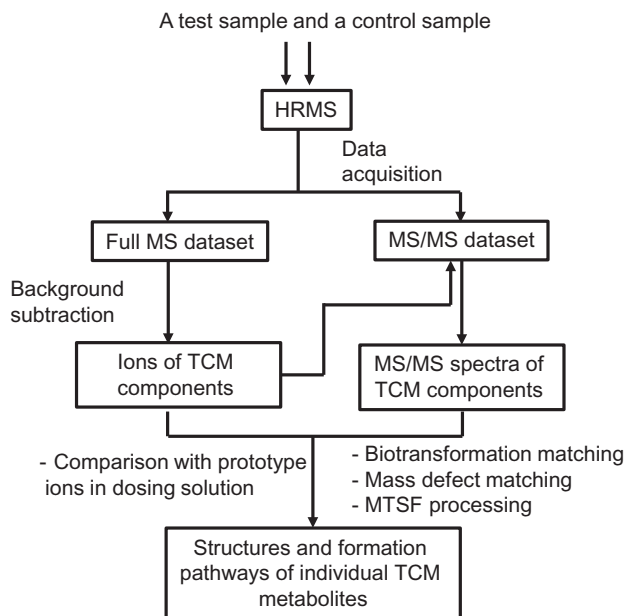


**FIG. 16** A general analytical strategy for detection, structural characterization and formation pathway identification of TCM metabolites in animals and human using HRMS.

## 6 Conclusion and future perspectives

HRMS has revolutionized the way that we tackle the task of detecting and profiling drug metabolites in complex biological samples. This chapter has described HRMS-based data acquisition and data-mining techniques for drug metabolite profiling and characterization. Applicability of the HRMS technology in common biotransformation experiments conducted in the pharmaceutical industry is discussed with respect to purpose, requirements of these experiments, and unique advantages of individual HRMS techniques. Multiple real-life examples are included to demonstrate the usefulness of HRMS techniques in performing metabolite profiling and characterization experiments to support lead optimization, selection of toxicology species, screening for bioactivation, mass balance studies for regulatory submission, and evaluation of MIST. Furthermore, current applications of HRMS-based technology in profiling and characterization of TCM components *in vivo* samples from ADME studies in animals and humans are also reviewed.

In the past 20 years, several novel or improved data-mining methods, including mass defect filtering, BS, isotope pattern filtering, and accurate mass extracted ion chromatographic processing method, have been introduced. In addition, the utility of newly developed HRMS-based DDA and DIA acquisition technologies, such as mass defect- and isotope pattern-dependent method, MS<sup>E</sup> and SWATH, in drug metabolite profiling have been fully demonstrated. Each of the HRMS instruments from different manufacturers has its own set of

unique acquisition methods and data-processing tools. For example, MDF-dependent and SWATH acquisition are only available with AB Sciex TripleTOF instruments, while MS<sup>E</sup> is equipped in Waters' Q-TOF instruments and all-ion-fragmentation and background exclusion DDA are available in Thermo orbitrap instruments, respectively. There are always multiple ways to accomplish the same biotransformation task with different HRMS instruments although their utility and limitation vary greatly when applying to different biotransformation experiments. What is remaining for biotransformation scientists is to develop an in-house analytical strategy and best practice based on the applicability of HRMS data acquisition and data-processing tools available in their labs and special needs of individual biotransformation experiment to be carried out.

HRMS technology may be approaching its maturity with respect to performing drug metabolite profiling and characterization; however, its applications in certain areas of drug metabolism research still need further improvements of technology for speed and accuracy of detection and identification of complex metabolism. One such application is in studying metabolism and disposition of herbal medicine *in vivo*. The currently available data acquisition methods are not suited for automatically recording MS/MS spectral data of unknown TCM components in complex biological samples although BS and metabolomics analysis show some promise in detecting metabolites. Improvement of the analytical throughput and productivity in conducting biotransformation studies of lead components and drug candidates is another area that requires continuous efforts. For example, mass spectral interpretation is still one of bottlenecks in drug metabolite profiling although a few software packages are commercially available. Software-assisted data acquisition, processing, and interpretation are extremely valuable and will continue to play a pivotal role.

It is expected that the scope of HRMS applications to drug metabolism research in the pharmaceutical industry will be expanded rapidly: from classical small-molecule drugs to new drug platforms or modalities, such as antibody-drug conjugates, covalent drugs, macrocyclic peptides, RNA-targeting therapeutics, and biologics. Metabolism and disposition studies of these new molecules represent great analytical challenges as well as new opportunities to develop new HRMS technology. On the other hand, the focus of small-molecule identification by HRMS will be shifted from drug metabolites to other unknown xenobiotics, such as sport enhancement drugs, pesticides, drugs of abuse, and forensic chemicals. Unlike drug metabolites, the molecular weights, mass defects, isotope patterns, and fragmentations of these totally unknown xenobiotics are not predictable. Thus, detection and identification by HRMS have to rely on untargeted data acquisition and data-mining techniques such as background exclusion DDA, BS and metabolomics analysis, since a majority of the HRMS-based data acquisition and processing methods used for drug metabolite profiling are no longer applicable. Certainly, the unknown xenobiotics identification is a new analytical frontier that requires and will lead to breakthrough HRMS technology.

## Acknowledgments

We would like to thank Dr. Hong Cai and Dr. Haiying Zhang for generating the data presented in [Figs. 5 and 12](#), respectively.



## References

- [1] J. Gan, H. Zhang, W.G. Humphreys, Drug-protein adducts: chemistry, mechanisms of toxicity, and methods of characterization, *Chem. Res. Toxicol.* 29 (12) (2016) 2040–2057.
- [2] J. Yu, Z. Zhou, K.H. Owens, T.K. Ritchie, I. Ragueneau-Majlessi, What can be learned from recent new drug applications? A systematic review of drug interaction data for drugs approved by the US FDA in 2015, *Drug Metab. Dispos.* 45 (1) (2017) 86–108.
- [3] Z. Zhang, M. Zhu, W. Tang, Metabolite identification and profiling in drug design: current practice and future directions, *Curr. Pharm. Des.* 15 (19) (2009) 2220–2235.
- [4] A.N. Nedderman, P. Wright, Looking back through the MIST: a perspective of evolving strategies and key focus areas for metabolite safety analysis, *Bioanalysis* 2 (7) (2010) 1235–1248.
- [5] P. Timmerman, M. Anders Kall, B. Gordon, S. Laakso, A. Freisleben, R. Hucker, Best practices in a tiered approach to metabolite quantification: views and recommendations of the European Bioanalysis Forum, *Bioanalysis* 2 (7) (2010) 1185–1194.
- [6] R.S. Obach, Pharmacologically active drug metabolites: impact on drug discovery and pharmacotherapy, *Pharmacol. Rev.* 65 (2) (2013) 578–640.
- [7] J. Gan, S. Ma, D. Zhang, Non-cytochrome P450-mediated bioactivation and its toxicological relevance, *Drug Metab. Rev.* 48 (4) (2016) 473–501.
- [8] M. Pellegatti, Preclinical in vivo ADME studies in drug development: a critical review, *Expert Opin. Drug Metab. Toxicol.* 8 (2) (2012) 161–172.
- [9] N. Penner, L. Xu, C. Prakash, Radiolabeled absorption, distribution, metabolism, and excretion studies in drug development: why, when, and how? *Chem. Res. Toxicol.* 25 (3) (2012) 513–531.
- [10] Y. Liang, G. Wang, L. Xie, L. Sheng, Recent development in liquid chromatography/mass spectrometry and emerging technologies for metabolite identification, *Curr. Drug Metab.* 12 (4) (2011) 329–344.
- [11] S. Ma, S.K. Chowdhury, Application of LC-high-resolution MS with ‘intelligent’ data mining tools for screening reactive drug metabolites, *Bioanalysis* 4 (5) (2012) 501–510.
- [12] S. Ma, S.K. Chowdhury, K.B. Alton, Application of mass spectrometry for metabolite identification, *Curr. Drug Metab.* 7 (5) (2006) 503–523.
- [13] C. Xie, D. Zhong, K. Yu, X. Chen, Recent advances in metabolite identification and quantitative bioanalysis by LC-Q-TOF MS, *Bioanalysis* 4 (8) (2012) 937–959.
- [14] M. Zhu, H. Zhang, W.G. Humphreys, Drug metabolite profiling and identification by high-resolution mass spectrometry, *J. Biol. Chem.* 286 (29) (2011) 25419–25425.
- [15] B. Wen, M. Zhu, Applications of mass spectrometry in drug metabolism: 50 years of progress, *Drug Metab. Rev.* 47 (1) (2015) 71–87.
- [16] P.S. Dhurjad, V.K. Marothu, R. Rathod, Post-acquisition data mining techniques for LC-MS/MS-acquired data in drug metabolite identification, *Bioanalysis* 9 (16) (2017) 1265–1278.
- [17] F. Li, J. Lu, X. Ma, Profiling the reactive metabolites of xenobiotics using metabolomic technologies, *Chem. Res. Toxicol.* 24 (5) (2011) 744–751.
- [18] S. Ma, S.K. Chowdhury, Data acquisition and data mining techniques for metabolite identification using LC coupled to high-resolution MS, *Bioanalysis* 5 (10) (2013) 1285–1297.
- [19] H. Zhang, D. Zhang, K. Ray, M. Zhu, Mass defect filter technique and its applications to drug metabolite identification by high-resolution mass spectrometry, *J. Mass Spectrom.* 44 (7) (2009) 999–1016.
- [20] L. Ma, B. Wen, Q. Ruan, M. Zhu, Rapid screening of glutathione-trapped reactive metabolites by linear ion trap mass spectrometry with isotope pattern-dependent scanning and postacquisition data mining, *Chem. Res. Toxicol.* 21 (7) (2008) 1477–1483.
- [21] Q. Ruan, S. Peterman, M.A. Szewc, L. Ma, D. Cui, W.G. Humphreys, et al., An integrated method for metabolite detection and identification using a linear ion trap/Orbitrap mass spectrometer and multiple data processing techniques: application to indinavir metabolite detection, *J. Mass Spectrom.* 43 (2) (2008) 251–261.
- [22] W. Jian, M. Yao, D. Zhang, M. Zhu, Rapid detection and characterization of in vitro and urinary N-acetyl-L-cysteine conjugates using quadrupole-linear ion trap mass spectrometry and polarity switching, *Chem. Res. Toxicol.* 22 (7) (2009) 1246–1255.
- [23] B. Wen, L. Ma, S.D. Nelson, M. Zhu, High-throughput screening and characterization of reactive metabolites using polarity switching of hybrid triple quadrupole linear ion trap mass spectrometry, *Anal. Chem.* 80 (5) (2008) 1788–1799.

- [24] K. Comstock, S. Ma, S. Sharma, Y. Chen, C. Ding, Enhanced metabolite identification using orbitrap tribrid mass spectrometer, *Drug Metab. Pharmacokinet.* 34 (1) (2019) S32–S33.
- [25] H. Zhang, D. Zhang, M. Zhu, K. Ray, High resolution LC/MS based mass defect filter approach: basic concept and application in metabolite detection, in: R. Ramanathan (Ed.), *Mass Spectrometry in Drug Metabolism and Pharmacokinetics*, John Wiley & Sons, Hoboken, NJ, 2008, pp. 223–251.
- [26] H. Zhang, M. Zhu, Drug metabolite identification with high resolution mass spectrometry, in: P.W. Lee, H. Aizawa, L.L. Gan, C. Prakash, D. Zhong (Eds.), *Handbook of Metabolic Pathways of Xenobiotics*, John Wiley & Sons, Hoboken, NJ, 2013, pp. 1–23.
- [27] M. Zhu, L. Ma, D. Zhang, K. Ray, W. Zhao, W.G. Humphreys, et al., Detection and characterization of metabolites in biological matrices using mass defect filtering of liquid chromatography/high resolution mass spectrometry data, *Drug Metab. Dispos.* 34 (10) (2006) 1722–1733.
- [28] T. Tian, Y. Jin, Y. Ma, W. Xie, H. Xu, K. Zhang, et al., Identification of metabolites of oridonin in rats with a single run on UPLC-Triple-TOF-MS/MS system based on multiple mass defect filter data acquisition and multiple data processing techniques, *J. Chromatogr. B Anal. Technol. Biomed. Life Sci.* 1006 (2015) 80–92.
- [29] X. Zhang, J. Yin, C. Liang, Y. Sun, L. Zhang, UHPLC-Q-TOF-MS/MS method based on four-step strategy for metabolism study of Fisetin in vitro and in vivo, *J. Agric. Food Chem.* 65 (50) (2017) 10959–10972.
- [30] M. Liu, S. Zhao, Z. Wang, Y. Wang, T. Liu, S. Li, et al., Identification of metabolites of deoxyschizandrin in rats by UPLC-Q-TOF-MS/MS based on multiple mass defect filter data acquisition and multiple data processing techniques, *J. Chromatogr. B Anal. Technol. Biomed. Life Sci.* 949–950 (2014) 115–126.
- [31] F. Du, Q. Ruan, M. Zhu, J. Xing, Detection and characterization of ticlopidine conjugates in rat bile using high-resolution mass spectrometry: applications of various data acquisition and processing tools, *J. Mass Spectrom.* 48 (3) (2013) 413–422.
- [32] H.K. Lim, J. Chen, K. Cook, C. Sensenhauser, J. Silva, D.C. Evans, A generic method to detect electrophilic intermediates using isotopic pattern triggered data-dependent high-resolution accurate mass spectrometry, *Rapid Commun. Mass Spectrom.* 22 (8) (2008) 1295–1311.
- [33] T. Rousu, O. Pelkonen, A. Tolonen, Rapid detection and characterization of reactive drug metabolites in vitro using several isotope-labeled trapping agents and ultra-performance liquid chromatography/time-of-flight mass spectrometry, *Rapid Commun. Mass Spectrom.* 23 (6) (2009) 843–855.
- [34] Q. Ruan, M. Zhu, Investigation of bioactivation of ticlopidine using linear ion trap/orbitrap mass spectrometry and an improved mass defect filtering technique, *Chem. Res. Toxicol.* 23 (5) (2010) 909–917.
- [35] J. Castro-Perez, R. Plumb, L. Liang, E. Yang, A high-throughput liquid chromatography/tandem mass spectrometry method for screening glutathione conjugates using exact mass neutral loss acquisition, *Rapid Commun. Mass Spectrom.* 19 (6) (2005) 798–804.
- [36] Z. Zhang, Automated precursor ion exclusion during LC-MS/MS data acquisition for optimal ion identification, *J. Am. Soc. Mass Spectrom.* 23 (8) (2012) 1400–1407.
- [37] K.P. Bateman, J. Castro-Perez, M. Wrona, J.P. Shockcor, K. Yu, R. Oballa, et al., MS<sup>F</sup> with mass defect filtering for in vitro and in vivo metabolite identification, *Rapid Commun. Mass Spectrom.* 21 (9) (2007) 1485–1496.
- [38] P.R. Tiller, S. Yu, J. Castro-Perez, K.L. Fillgrove, T.A. Baillie, High-throughput, accurate mass liquid chromatography/tandem mass spectrometry on a quadrupole time-of-flight system as a ‘first-line’ approach for metabolite identification studies, *Rapid Commun. Mass Spectrom.* 22 (7) (2008) 1053–1061.
- [39] M. Wrona, T. Mauriala, K.P. Bateman, R.J. Mortishire-Smith, D. O’Connor, ‘All-in-one’ analysis for metabolite identification using liquid chromatography/hybrid quadrupole time-of-flight mass spectrometry with collision energy switching, *Rapid Commun. Mass Spectrom.* 19 (18) (2005) 2597–2602.
- [40] G. Hopfgartner, D. Tonoli, E. Varesio, High-resolution mass spectrometry for integrated qualitative and quantitative analysis of pharmaceuticals in biological matrices, *Anal. Bioanal. Chem.* 402 (8) (2012) 2587–2596.
- [41] K.P. Bateman, M. Kellmann, H. Muenster, R. Papp, L. Taylor, Quantitative-qualitative data acquisition using a benchtop Orbitrap mass spectrometer, *J. Am. Soc. Mass Spectrom.* 20 (8) (2009) 1441–1450.
- [42] R. Cho, Y. Huang, J.C. Schwartz, Y. Chen, T.J. Carlson, J. Ma, MS(M), an efficient workflow for metabolite identification using hybrid linear ion trap Orbitrap mass spectrometer, *J. Am. Soc. Mass Spectrom.* 23 (5) (2012) 880–888.
- [43] R.J. Mortishire-Smith, J.M. Castro-Perez, K. Yu, J.P. Shockcor, J. Goshawk, M.J. Hartshorn, et al., Generic dealkylation: a tool for increasing the hit-rate of metabolite rationalization, and automatic customization of mass defect filters, *Rapid Commun. Mass Spectrom.* 23 (7) (2009) 939–948.

- [44] P. Deng, D. Zhong, F. Nan, S. Liu, D. Li, T. Yuan, et al., Evidence for the bioactivation of 4-nonylphenol to quinone methide and ortho-benzoquinone metabolites in human liver microsomes, *Chem. Res. Toxicol.* 23 (10) (2010) 1617–1628.
- [45] W. Sun, L. Tong, J. Miao, J. Huang, D. Li, Y. Li, et al., Separation and analysis of phenolic acids from *Salvia miltiorrhiza* and its related preparations by off-line two-dimensional hydrophilic interaction chromatography-reversed-phase liquid chromatography coupled with ion trap time-of-flight mass spectrometry, *J. Chromatogr. A* 1431 (2016) 79–88.
- [46] D. Zhang, P.T. Cheng, H. Zhang, Mass defect filtering on high resolution LC/MS data as a methodology for detecting metabolites with unpredictable structures: identification of oxazole-ring opened metabolites of muraglitazar, *Drug Metab. Lett.* 1 (4) (2007) 287–292.
- [47] M. Zhu, L. Ma, H. Zhang, W.G. Humphreys, Detection and structural characterization of glutathione-trapped reactive metabolites using liquid chromatography-high-resolution mass spectrometry and mass defect filtering, *Anal. Chem.* 79 (21) (2007) 8333–8341.
- [48] X. Zhu, J.G. Slatter, M.G. Emery, M.R. Deane, A. Akrami, X. Zhang, et al., Activity-based exposure comparisons among humans and nonclinical safety testing species in an extensively metabolized drug candidate, *Xenobiotica* 43 (7) (2013) 617–627.
- [49] P. Zhu, W. Tong, K. Alton, S. Chowdhury, An accurate-mass-based spectral-averaging isotope-pattern-filtering algorithm for extraction of drug metabolites possessing a distinct isotope pattern from LC-MS data, *Anal. Chem.* 81 (14) (2009) 5910–5917.
- [50] A. Yang, M. Zang, H. Liu, P. Fan, J. Xing, Metabolite identification of the antimalarial piperazine in vivo using liquid chromatography-high-resolution mass spectrometry in combination with multiple data-mining tools in tandem, *Biomed. Chromatogr.* 30 (8) (2016) 1324–1330.
- [51] X. Zhu, N. Kalyanaraman, R. Subramanian, Enhanced screening of glutathione-trapped reactive metabolites by in-source collision-induced dissociation and extraction of product ion using UHPLC-high resolution mass spectrometry, *Anal. Chem.* 83 (24) (2011) 9516–9523.
- [52] H. Zhang, L. Ma, K. He, M. Zhu, An algorithm for thorough background subtraction from high-resolution LC/MS data: application to the detection of troglitazone metabolites in rat plasma, bile, and urine, *J. Mass Spectrom.* 43 (9) (2008) 1191–1200.
- [53] H. Zhang, Y. Yang, An algorithm for thorough background subtraction from high-resolution LC/MS data: application for detection of glutathione-trapped reactive metabolites, *J. Mass Spectrom.* 43 (9) (2008) 1181–1190.
- [54] P. Zhu, W. Ding, W. Tong, A. Ghosal, K. Alton, S. Chowdhury, A retention-time-shift-tolerant background subtraction and noise reduction algorithm (BgS-NoRA) for extraction of drug metabolites in liquid chromatography/mass spectrometry data from biological matrices, *Rapid Commun. Mass Spectrom.* 23 (11) (2009) 1563–1572.
- [55] V. Shekar, A. Shah, M. Shadid, J.T. Wu, J. Bolleddula, S. Chowdhury, An accelerated background subtraction algorithm for processing high-resolution MS data and its application to metabolite identification, *Bioanalysis* 8 (16) (2016) 1693–1707.
- [56] J. Xing, M. Zang, H. Zhang, M. Zhu, The application of high-resolution mass spectrometry-based data-mining tools in tandem to metabolite profiling of a triple drug combination in humans, *Anal. Chim. Acta* 897 (2015) 34–44.
- [57] W. Chen, J. Caceres-Cortes, H. Zhang, D. Zhang, W.G. Humphreys, J. Gan, Bioactivation of substituted thiophenes including alpha-chlorothiophene-containing compounds in human liver microsomes, *Chem. Res. Toxicol.* 24 (5) (2011) 663–669.
- [58] C. Chen, A. Wohlfarth, H. Xu, D. Su, X. Wang, H. Jiang, et al., Untargeted screening of unknown xenobiotics and potential toxins in plasma of poisoned patients using high-resolution mass spectrometry: generation of xenobiotic fingerprint using background subtraction, *Anal. Chim. Acta* 944 (2016) 37–43.
- [59] C. Wu, H. Zhang, C. Wang, H. Qin, M. Zhu, J. Zhang, An integrated approach for studying exposure, metabolism, and disposition of multiple component herbal medicines using high-resolution mass spectrometry and multiple data processing tools, *Drug Metab. Dispos.* 44 (6) (2016) 800–808.
- [60] H. Zhang, L. Patrone, J. Kozlosky, L. Tomlinson, G. Cosma, J. Horvath, Pooled sample strategy in conjunction with high-resolution liquid chromatography-mass spectrometry-based background subtraction to identify toxicological markers in dogs treated with ibipinabant, *Anal. Chem.* 82 (9) (2010) 3834–3839.

- [61] H. Zhang, J. Gan, Y.Z. Shu, W.G. Humphreys, High-resolution mass spectrometry-based background subtraction for identifying protein modifications in a complex biological system: detection of acetaminophen-bound microsomal proteins including argininosuccinate synthetase, *Chem. Res. Toxicol.* 28 (4) (2015) 775–781.
- [62] C. Chen, F.J. Gonzalez, J.R. Idle, LC-MS-based metabolomics in drug metabolism, *Drug Metab. Rev.* 39 (2-3) (2007) 581–597.
- [63] S. Giri, J.R. Idle, C. Chen, T.M. Zabriskie, K.W. Krausz, F.J. Gonzalez, A metabolomic approach to the metabolism of the areca nut alkaloids arecoline and arecaidine in the mouse, *Chem. Res. Toxicol.* 19 (6) (2006) 818–827.
- [64] F. Li, Y. Miao, L. Zhang, S.A. Neuenswander, J.T. Douglas, X. Ma, Metabolomic analysis reveals novel isoniazid metabolites and hydrazones in human urine, *Drug Metab. Pharmacokinet.* 26 (6) (2011) 569–576.
- [65] J. Zhu, P. Wang, A.I. Shehu, J. Lu, H. Bi, X. Ma, Identification of novel pathways in idelalisib metabolism and bioactivation, *Chem. Res. Toxicol.* 31 (7) (2018) 548–555.
- [66] F. Li, P. Wang, K. Liu, M.G. Tarrago, J. Lu, E.N. Chini, et al., A high dose of isoniazid disturbs endobiotic homeostasis in mouse liver, *Drug Metab. Dispos.* 44 (11) (2016) 1742–1751.
- [67] F.J. Gonzalez, Z.Z. Fang, X. Ma, Transgenic mice and metabolomics for study of hepatic xenobiotic metabolism and toxicity, *Expert Opin. Drug Metab. Toxicol.* 11 (6) (2015) 869–881.
- [68] J. Guo, M. Zhang, C.S. Elmore, K. Vishwanathan, An integrated strategy for in vivo metabolite profiling using high-resolution mass spectrometry based data processing techniques, *Anal. Chim. Acta* 780 (2013) 55–64.
- [69] J. Kirchmair, A.H. Goller, D. Lang, J. Kunze, B. Testa, I.D. Wilson, et al., Predicting drug metabolism: experiment and/or computation? *Nat. Rev. Drug Discov.* 14 (6) (2015) 387–404.
- [70] L. Olsen, C. Oostenbrink, F.S. Jorgensen, Prediction of cytochrome P450 mediated metabolism, *Adv. Drug Deliv. Rev.* 86 (2015) 61–71.
- [71] G. Cruciani, E. Carosati, B. De Boeck, K. Ethirajulu, C. Mackie, T. Howe, et al., MetaSite: understanding metabolism in human cytochromes from the perspective of the chemist, *J. Med. Chem.* 48 (22) (2005) 6970–6979.
- [72] B. Bonn, C. Leanderson, F. Fontaine, I. Zamora, Enhanced metabolite identification with MS(E) and a semi-automated software for structural elucidation, *Rapid Commun. Mass Spectrom.* 24 (21) (2010) 3127–3138.
- [73] A. Pahler, A. Brink, Software aided approaches to structure-based metabolite identification in drug discovery and development, *Drug Discov. Today Technol.* 10 (1) (2013) e207–e217.
- [74] I. Zamora, F. Fontaine, B. Serra, G. Plasencia, High-throughput, computer assisted, specific MetID. A revolution for drug discovery, *Drug Discov. Today Technol.* 10 (1) (2013) e199–e205.
- [75] M. Ahlqvist, C. Leanderson, M.A. Hayes, I. Zamora, R.A. Thompson, Software-aided structural elucidation in drug discovery, *Rapid Commun. Mass Spectrom.* 29 (21) (2015) 2083–2089.
- [76] A.W. Hill, R.J. Mortishire-Smith, Automated assignment of high-resolution collisionally activated dissociation mass spectra using a systematic bond disconnection approach, *Rapid Commun. Mass Spectrom.* 19 (21) (2005) 3111–3118.
- [77] L. Leclercq, R.J. Mortishire-Smith, M. Huisman, F. Cuyckens, M.J. Hartshorn, A. Hill, IsoScore: automated localization of biotransformations by mass spectrometry using product ion scoring of virtual regioisomers, *Rapid Commun. Mass Spectrom.* 23 (1) (2009) 39–50.
- [78] D. Friedecky, K. Micova, E. Faber, M. Hrda, J. Siroka, T. Adam, Detailed study of imatinib metabolism using high-resolution mass spectrometry, *J. Chromatogr. A* 1409 (2015) 173–181.
- [79] S. Watanabe, S. Vikingsson, M. Roman, H. Green, R. Kronstrand, A. Wohlfarth, In vitro and in vivo metabolite identification studies for the new synthetic opioids acetylfentanyl, acrylfentanyl, furanylfentanyl, and 4-fluoro-isobutyrylfentanyl, *AAPS J.* 19 (4) (2017) 1102–1122.
- [80] V. Zelesky, R. Schneider, J. Janiszewski, I. Zamora, J. Ferguson, M. Troutman, Software automation tools for increased throughput metabolic soft-spot identification in early drug discovery, *Bioanalysis* 5 (10) (2013) 1165–1179.
- [81] M.F. Grubb, W.G. Humphreys, J.L. Josephs, A semi-automated method for the integrated evaluation of half-life and metabolic soft spots of discovery compounds, *Bioanalysis* 4 (14) (2012) 1747–1761.
- [82] A.A. Paiva, C. Klakouski, S. Li, B.M. Johnson, Y.Z. Shu, J. Josephs, et al., Development, optimization and implementation of a centralized metabolic soft spot assay, *Bioanalysis* 9 (7) (2017) 541–552.
- [83] M. Trunzer, B. Faller, A. Zimmerlin, Metabolic soft spot identification and compound optimization in early discovery phases using MetaSite and LC-MS/MS validation, *J. Med. Chem.* 52 (2) (2009) 329–335.
- [84] G. Yan, H. Sun, W. Sun, L. Zhao, X. Meng, X. Wang, Rapid and global detection and characterization of aconitum alkaloids in Yin Chen Si Ni Tang, a traditional Chinese medical formula, by ultra performance liquid

- chromatography-high resolution mass spectrometry and automated data analysis, *J. Pharm. Biomed. Anal.* 53 (3) (2010) 421–431.
- [85] A.F. Aubry, L.J. Christopher, J. Wang, M. Zhu, G. Tirucherai, M.E. Arnold, Reflecting on a decade of metabolite screening and monitoring, *Bioanalysis* 6 (5) (2014) 651–664.
- [86] S. Ma, S.K. Chowdhury, Analytical strategies for assessment of human metabolites in preclinical safety testing, *Anal. Chem.* 83 (13) (2011) 5028–5036.
- [87] S. Ma, Z. Li, K.J. Lee, S.K. Chowdhury, Determination of exposure multiples of human metabolites for MIST assessment in preclinical safety species without using reference standards or radiolabeled compounds, *Chem. Res. Toxicol.* 23 (12) (2010) 1871–1873.
- [88] S. Schadt, B. Bister, S.K. Chowdhury, C. Funk, C. Hop, W.G. Humphreys, et al., A decade in the MIST: learnings from investigations of drug metabolites in drug development under the “metabolites in safety testing” regulatory guidance, *Drug Metab. Dispos.* 46 (6) (2018) 865–878.
- [89] H. Xu, H. Niu, B. He, C. Cui, Q. Li, K. Bi, Comprehensive qualitative ingredient profiling of Chinese herbal formula Wu-Zhu-Yu decoction via a mass defect and fragment filtering approach using high resolution mass spectrometry, *Molecules* 21 (5) (2016) 664.
- [90] X. Yu, D. Cui, M.R. Davis, Identification of in vitro metabolites of Indinavir by “intelligent automated LC-MS/MS” (INTAMS) utilizing triple quadrupole tandem mass spectrometry, *J. Am. Soc. Mass Spectrom.* 10 (2) (1999) 175–183.
- [91] M. Zhu, D. Zhang, H. Zhang, W.C. Shyu, Integrated strategies for assessment of metabolite exposure in humans during drug development: analytical challenges and clinical development considerations, *Biopharm. Drug Dispos.* 30 (4) (2009) 163–184.
- [92] S.C. Khojasteh, Q. Yue, S. Ma, G. Castanedo, J.Z. Chen, J. Lyssikatos, et al., Investigations into the mechanisms of pyridine ring cleavage in vismodegib, *Drug Metab. Dispos.* 42 (3) (2014) 343–351.
- [93] A. Lindgren, G. Eklund, D. Turek, J. Malmquist, B.M. Swahn, J. Holenz, et al., Biotransformation of two beta-secretase inhibitors including ring opening and contraction of a pyrimidine ring, *Drug Metab. Dispos.* 41 (5) (2013) 1134–1147.
- [94] R. Takahashi, S. Ma, A. Deese, Q. Yue, H. Kim-Kang, Y. Yi, et al., Elucidating the mechanism of cytochrome P450-mediated pyrimidine ring conversion to pyrazole metabolites with the BACE1 inhibitor GNE-892 in rats, *Drug Metab. Dispos.* 42 (5) (2014) 890–898.
- [95] R.H. Takahashi, S. Ma, S.J. Robinson, Q. Yue, E.F. Choo, S.C. Khojasteh, Elucidating the mechanisms of formation for two unusual cytochrome P450-mediated fused ring metabolites of GDC-0623, a MAPK/ERK kinase inhibitor, *Drug Metab. Dispos.* 43 (12) (2015) 1929–1933.
- [96] R.H. Takahashi, X. Wang, N.L. Segraves, J. Wang, J.H. Chang, S.C. Khojasteh, et al., CYP1A1-mediated intramolecular rearrangement of aminoazepane in GDC-0339, *Drug Metab. Dispos.* 45 (10) (2017) 1084–1092.
- [97] X. Wang, H. Sun, A. Zhang, G. Jiao, W. Sun, Y. Yuan, Pharmacokinetics screening for multi-components absorbed in the rat plasma after oral administration traditional Chinese medicine formula Yin-Chen-Hao-Tang by ultra performance liquid chromatography-electrospray ionization/quadrupole-time-of-flight mass spectrometry combined with pattern recognition methods, *Analyst* 136 (23) (2011) 5068–5076.
- [98] A. Zhang, H. Sun, S. Qiu, X. Wang, Advancing drug discovery and development from active constituents of yinchenhao tang, a famous traditional chinese medicine formula, *Evid. Based Complement. Alternat. Med.* 2013 (2013) 257909.
- [99] Y.J. Ding, Y.H. Chen, Developmental nephrotoxicity of aristolochic acid in a zebrafish model, *Toxicol. Appl. Pharmacol.* 261 (1) (2012) 59–65.
- [100] A. Xiong, L. Fang, X. Yang, F. Yang, M. Qi, H. Kang, et al., An application of target profiling analyses in the hepatotoxicity assessment of herbal medicines: comparative characteristic fingerprint and bile acid profiling of *Senecio vulgaris* L. and *Senecio scandens* Buch.-Ham, *Anal. Bioanal. Chem.* 406 (29) (2014) 7715–7727.
- [101] C. Zhu, T. Cai, Y. Jin, J. Chen, G. Liu, N. Xu, et al., Artificial intelligence and network pharmacology based investigation of pharmacological mechanism and substance basis of Xiaokewan in treating diabetes, *Pharmacol. Res.* (2020) 104935. <https://doi.org/10.1016/j.phrs.2020.104935>.
- [102] X. Mu, X. Xu, X. Guo, P. Yang, J. Du, N. Mi, et al., Identification and characterization of chemical constituents in Dengzhan Shengmai Capsule and their metabolites in rat plasma by ultra-performance liquid chromatography coupled with quadrupole time-of-flight mass spectrometry, *J. Chromatogr. B Anal. Technol. Biomed. Life Sci.* 1108 (2019) 54–64.



- [103] S. Li, S. Liu, Z. Liu, Z. Pi, F. Song, Y. Jin, A target-group-change strategy based on the UPLC-Q-TOF-MS(E) method for the metabolites identification of Fufang-Xialian-Capsule in rat's plasma, *J. Chromatogr. B Anal. Technol. Biomed. Life Sci.* 1085 (2018) 42–53.
- [104] C. Yang, T. Xia, C. Wang, H. Sun, Y. Li, Z. Gong, et al., Using the UPLC-ESI-Q-TOF-MS(E) method and intestinal bacteria for metabolite identification in the nonpolysaccharide fraction from *Bletilla striata*, *Biomed. Chromatogr.* 33 (11) (2019)e4637.
- [105] M. Liao, X.P. Diao, X.Y. Cheng, Y.P. Sun, L.T. Zhang, Nontargeted SWATH acquisition mode for metabolites identification of osthole in rats using ultra-high-performance liquid chromatography coupled to quadrupole time-of-flight mass spectrometry, *RSC Adv.* 8 (27) (2018) 14925–14935.
- [106] K.B. Scheidweiler, M.J. Jarvis, M.A. Huestis, Nontargeted SWATH acquisition for identifying 47 synthetic cannabinoid metabolites in human urine by liquid chromatography-high-resolution tandem mass spectrometry, *Anal. Bioanal. Chem.* 407 (3) (2015) 883–897.
- [107] W. Xie, Y. Jin, L. Hou, Y. Ma, H. Xu, K. Zhang, et al., A practical strategy for the characterization of ponacidin metabolites in vivo and in vitro by UHPLC-Q-TOF-MS based on nontargeted SWATH data acquisition, *J. Pharm. Biomed. Anal.* 145 (2017) 865–878.
- [108] J.L. Geng, Y. Dai, Z.H. Yao, Z.F. Qin, X.L. Wang, L. Qin, et al., Metabolites profile of Xian-Ling-Gu-Bao capsule, a traditional Chinese medicine prescription, in rats by ultra performance liquid chromatography coupled with quadrupole time-of-flight tandem mass spectrometry analysis, *J. Pharm. Biomed. Anal.* 96 (2014) 90–103.
- [109] L. Wu, H. Hao, G. Wang, LC/MS based tools and strategies on qualitative and quantitative analysis of herbal components in complex matrixes, *Curr. Drug Metab.* 13 (9) (2012) 1251–1265.
- [110] G.L. Yan, A.H. Zhang, H. Sun, Y. Han, H. Shi, Y. Zhou, et al., An effective method for determining the ingredients of Shuanghuanglian formula in blood samples using high-resolution LC-MS coupled with background subtraction and a multiple data processing approach, *J. Sep. Sci.* 36 (19) (2013) 3191–3199.
- [111] M. Yang, C. Cheng, J. Yang, D.A. Guo, Metabolite profiling and characterization for medicinal herbal remedies, *Curr. Drug Metab.* 13 (5) (2012) 535–557.
- [112] R. Zuo, W. Ren, B.L. Bian, H.J. Wang, Y.N. Wang, H. Hu, et al., Metabolic fate analysis of Huang-Lian-Jie-Du Decoction in rat urine and feces by LC-IT-MS combining with LC-FT-ICR-MS: a feasible strategy for the metabolism study of Chinese medical formula, *Xenobiotica* 46 (1) (2016) 65–81.
- [113] Y. Du, B. He, Q. Li, J. He, D. Wang, K. Bi, Identification and analysis of chemical constituents and rat serum metabolites in Suan-Zao-Ren granule using ultra high performance liquid chromatography quadrupole time-of-flight mass spectrometry combined with multiple data processing approaches, *J. Sep. Sci.* 40 (14) (2017) 2914–2924.
- [114] X. Gao, J.Q. Mu, Q. Li, S.Y. Guan, R. Liu, Y.Y. Du, et al., Comprehensive identification of Guan-Xin-Shu-Tong capsule via a mass defect and fragment filtering approach by high resolution mass spectrometry: in vitro and in vivo study, *Molecules* 22 (6) (2017) 1007.
- [115] S. Jiang, J. Xu, D.W. Qian, E.X. Shang, P. Liu, S.L. Su, et al., Comparative metabolites in plasma and urine of normal and type 2 diabetic rats after oral administration of the traditional Chinese scutellaria-coptis herb couple by ultra performance liquid chromatography-tandem mass spectrometry, *J. Chromatogr. B Anal. Technol. Biomed. Life Sci.* 965 (2014) 27–32.
- [116] S.Y. Liu, Y.Y. Che, F. Wang, Z.P. Shang, J.Q. Lu, S.Y. Dai, et al., Identification of metabolites of 6'-hydroxy-3,4,5,2',4'-pentamethoxychalcone in rats by a combination of ultra-high-performance liquid chromatography with linear ion trap-Orbitrap mass spectrometry based on multiple data processing techniques, *Molecules* 21 (10) (2016) 1266.
- [117] S. Ni, D. Qian, J.A. Duan, J. Guo, E.X. Shang, Y. Shu, et al., UPLC-QTOF/MS-based screening and identification of the constituents and their metabolites in rat plasma and urine after oral administration of *Glechoma longituba* extract, *J. Chromatogr. B Anal. Technol. Biomed. Life Sci.* 878 (28) (2010) 2741–2750.
- [118] Z. Shang, F. Wang, S. Dai, J. Lu, X. Wu, J. Zhang, Profiling and identification of (–)-epicatechin metabolites in rats using ultra-high performance liquid chromatography coupled with linear trap-Orbitrap mass spectrometer, *Drug Test Anal* 9 (8) (2017) 1224–1235.
- [119] H. Sun, F. Wu, A. Zhang, W. Wei, Y. Han, X. Wang, Profiling and identification of the absorbed constituents and metabolites of schisandra lignans by ultra-performance liquid chromatography coupled to mass spectrometry, *Biomed. Chromatogr.* 27 (11) (2013) 1511–1519.

- [120] X. Zhang, M. Liao, X. Cheng, C. Liang, X. Diao, L. Zhang, Ultrahigh-performance liquid chromatography coupled with triple quadrupole and time-of-flight mass spectrometry for the screening and identification of the main flavonoids and their metabolites in rats after oral administration of *Cirsium japonicum* DC extract, *Rapid Commun. Mass Spectrom.* 32 (16) (2018) 1451–1461.
- [121] X. Wang, J. Liu, X. Yang, Q. Zhang, Y. Zhang, Q. Li, et al., Development of a systematic strategy for the global identification and classification of the chemical constituents and metabolites of Kai-Xin-San based on liquid chromatography with quadrupole time-of-flight mass spectrometry combined with multiple data-processing approaches, *J. Sep. Sci.* 41 (12) (2018) 2672–2680.
- [122] N. Mi, T. Cheng, H. Li, P. Yang, X. Mu, X. Wang, et al., Metabolite profiling of traditional Chinese medicine formula Dan Zhi Tablet: an integrated strategy based on UPLC-QTOF/MS combined with multivariate statistical analysis, *J. Pharm. Biomed. Anal.* 164 (2019) 70–85.
- [123] M.Q. Wan, Y.B. Zhang, X.Y. Liu, K.M. Li, L.Y. Jia, X.W. Yang, Systematic analysis of the metabolites of Angelol B by UPLC-Q-TOF-MS after oral administration to rats, *Chin. J. Nat. Med.* 17 (11) (2019) 822–834.
- [124] W. Feng, Q.J. Dong, M.Y. Liu, S. Li, T. Liu, X.G. Wang, et al., Screening and identification of multiple constituents and their metabolites of Zhi-zi-chi decoction in rat urine and bile by ultra-high-performance liquid chromatography quadrupole time-of-flight mass spectrometry, *Biomed. Chromatogr.* 31 (10) (2017)e3978.
- [125] J.H. Tao, M. Zhao, S. Jiang, W. Zhang, B.H. Xu, J.A. Duan, UPLC-Q-TOF/MS-based metabolic profiling comparison of four major bioactive components in normal and CKD rat plasma, urine and feces following oral administration of *Cornus officinalis* Sieb and *Rehmannia glutinosa* Libosch herb couple extract, *J. Pharm. Biomed. Anal.* 161 (2018) 254–261.
- [126] J.H. Tao, M. Zhao, D.G. Wang, C. Yang, G.T. Chen, X. Zhao, et al., UPLC-Q-TOF/MS-based screening and identification of two major bioactive components and their metabolites in normal and CKD rat plasma, urine and feces after oral administration of *Rehmannia glutinosa* Libosch extract, *J. Chromatogr. B Anal. Technol. Biomed. Life Sci.* 1001 (2015) 98–106.



# Methods for metabolite generation and characterization by NMR

*Liam Evans, Richard Phipps, Julia Shanu-Wilson,  
Jonathan Steele, Stephen Wrigley*  
Hypha Discovery Ltd., Oxfordshire, United Kingdom

## 1 Introduction

Since drug metabolites can contribute to efficacy or be involved in drug toxicity, access to major and/or disproportionate metabolites is critical to ensure adherence to regulatory guidelines issued by the European Medicines Agency (EMA) [1] and the US Food and Drug Administration (FDA) [2]. Identification and characterization ensure not only rigorous safety evaluation of significant metabolites but can also be leveraged to expand patent coverage and reveal superior potency, reduced side effects, or improved physical properties compared to the parent drug. In some cases, a metabolite will turn out to be a superior drug candidate or may supersede the original parent drug [3], recognition of which is exploited by some pharmaceutical companies, where metabolism-guided late-stage oxidation is routinely built into late-stage functionalization programs [4–6].

In the drug development process, authentic human drug metabolites are required for structure elucidation, as analytical reference standards and for pharmacology/toxicology testing. The identification of small amounts of metabolites has been facilitated by the increase in sensitivity of modern NMR instrumentation and software, notably cryoprobe technology, whereby full heteronuclear two-dimensional data sets can be generated using tens of micrograms of reasonably pure material. Such a step change in sensitivity enables scientists to submit sample amounts of metabolites that were previously considered too low for full structure elucidation. This technology, coupled with quantitative NMR (qNMR), has widened the options and changed the scale of processes that can be employed for producing metabolites for definitive MetID [7]. While it is possible to quantify metabolites using NMR techniques, validated clinical bioanalytical methods still require weighable, milligram

amounts of purified metabolites for use as reference standards, and preclinical pharmacology and toxicity testing can also require multigram quantities of metabolites for on- and off-target evaluation. Where projects require milligram to gram amounts of metabolites for biological testing and/or toxicological evaluation, production methods need to be scalable to deliver the required amounts.

There are multiple scalable options available for producing metabolites through both chemical and biological routes [8] and summarized in Fig. 1.

The preparation of metabolites can sometimes be achieved by chemical synthesis, including challenging stereospecific synthesis [9]. This can be accomplished either via direct modification of the drug candidate or via modified intermediates in the synthetic pathway, however alternative methods may be required if poor reaction yields, severe reaction conditions or unwanted by-products are encountered. Equally, constraints on organic chemistry resource can mean that investing significant time in chemical synthesis of metabolites may not always be the best route, particularly in cases where the structure of the metabolite is not known, and where multiple isomers need to be made.

Access to metabolites through direct biological methods that involve incubation of the drug with matrices such as liver fractions, recombinant enzymes, or microbial cultures, as well as direct purification of metabolites from biological matrices are also proven solutions. For difficult-to-synthesize drug metabolites with the possibility of several regio- or stereoisomers, biological approaches are generally employed to minimize costly and sometimes time-consuming speculative synthesis of all possible structures. Sometimes a suite of metabolites is accessed using a combination of both chemical and biological routes, as described in a recent paper by scientists at Janssen, Merck & Co, and Hypha Discovery [10]. Both phase I and phase II primary single-step and secondary human metabolites can be readily made via surrogate biological routes including the generation of aromatic and aliphatic hydroxylated metabolites, as well as conjugates such as glucuronides and sulfates. Additionally, metabolites made by gut microbiota can also be accessed [11].

Although the need to produce and evaluate phase I metabolites has been recognized for some years, the growing prevalence of glucuronidation-mediated clearance relies on active transport for movement across biological membranes, which increases the likelihood of transporter-mediated interactions, as recognized by three large pharma companies [12], and cited by the FDA in 2017. Innovations in medicinal chemistry and drug design, together

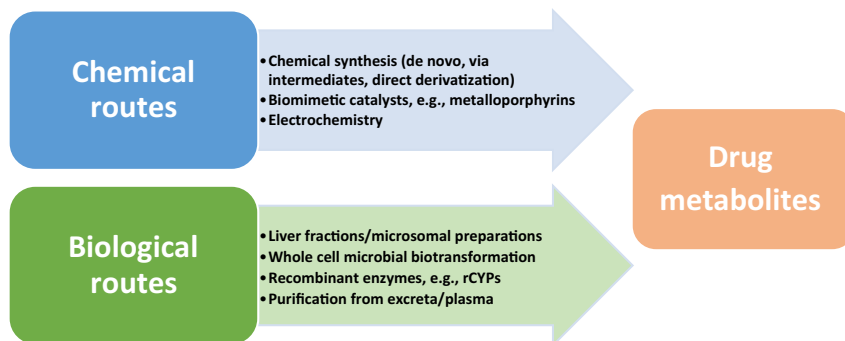


FIG. 1 Commonly used routes to access drug metabolites.

with recent strategies in pharma companies to reduce CYP mediated liabilities, are resulting in an increasing number of drug candidates eliminated via conjugative metabolism. Phase II conjugates, of which glucuronides are the most prevalent, can sometimes be the cause of drug-drug interactions (DDIs), including the inhibition of transporters and CYPs in vivo. For example, the major acyl-glucuronide of gemfibrozil is an irreversible potent inhibitor of CYP2C8 and the human organic anion transporting polypeptide 2 (OATP2) [13, 14]. Indeed, Ma et al. state that glucuronidation could be a potential liability due to glucuronides of drugs that are classified as strong CYP2C8 inhibitors by the FDA [14]. These glucuronidation-linked liabilities are a trend that has been observed for some recently registered drugs and their metabolites, e.g., the first approved sodium/glucose cotransporter 2 inhibitor canagliflozin [15]. Studies to determine the interaction of glucuronides with multiple different transporters create a need to access multimilligram quantities for understanding the impact of conjugated metabolites in the clinic and any resulting DDIs.

## 2 Methods for scaled-up production of drug metabolites

Examples of different methods employed for producing metabolites are illustrated through the following sections with representative examples.

### 2.1 Chemical synthesis

When considering options to obtain metabolite standards, classical organic synthesis is often the first option, depending on the nature and complexity of the drug candidate and structure of the target metabolite. Indeed, the synthesis of some metabolites can be facile, for example, *N*- or *S*-oxides of parent drugs, which can sometimes be made conveniently in a single step by treatment with commercially available oxidizing reagents, such as *meta*-chloroperoxybenzoic acid or hydrogen peroxide [16]. Similarly, *N*- or *O*-dealkylations can, in select cases, be achieved quickly in one step as in the example of *N*-demethylation of GSK-372475, a serotonin-, norepinephrine-, dopamine-reuptake inhibitor (SNDRI), by treatment with ethyl chloroformate [17]. Such facile chemical transformations are, however, only possible where the site of oxidation or dealkylation is reactive and the reactants are inert to other functional groups.

In other cases, metabolite generation is somewhat involved and requires lengthy and complex syntheses, to deliver even minor structural changes to the original molecule. It may be possible to leverage existing chemical synthetic routes and/or intermediates to afford less arduous access to the metabolite. If *de novo* chemistry is required, weeks to months of synthesis effort is often required for each metabolite during a period where timely confirmation of metabolite structure may be paramount to developing an underlying safety and pharmacology strategy.

#### 2.1.1 *Synthesis of phase I oxidized metabolites*

Chemical synthesis is often challenging where insertion of oxygen at unactivated carbons in complex molecules is required, or where metabolites have specific regio- or stereochemistry.

Genovino et al. investigated a wide range of C—H oxidation methods developed by several research teams for metabolite production using three drug compounds with limited success and concluded that the methods were unable to affect oxidation of complex pharmaceutical compounds [18]. They recommended that advances in this area would require the development of new catalytic reactions that tolerate common structural features of drugs such as the presence of basic nitrogen.

Particularly challenging is selective oxidation of unactivated C(sp<sup>3</sup>)—H bonds, synthetic methods for which are a future need in metabolite synthesis with the growing trend toward decreasing the number of aromatic rings in drugs and impetus for incorporating aliphatic moieties in drugs to increase molecular complexity [18].

Many chemical conditions to oxidize benzylic C—H bonds exist, however; many of these reactions are incompatible with basic functionalities which are ubiquitous in drugs [18]. Recently, new promising methods have emerged including the nondirected iridium-catalyzed borylation of primary benzylic C—H bonds and nondirected potassium *tert*-butoxide-catalyzed silylation of benzylic C—H bonds [19, 20].

Chemical oxidation of C(sp<sup>2</sup>)—H bonds is a common occurrence in the formation of metabolites, however, many reported synthetic oxidation methods use simple substrates [18]. Indirect methods using C—H borylation and C—H silylation followed by hydroxylation have high functional group tolerance and have been exploited for producing drug metabolites, such as demonstrated for the iridium-catalyzed C—H silylation of desloratadine at a known phenolic metabolic soft spot using optimized reaction conditions, resulting in a yield of 78% of the desired phenol [21]. In contrast, Borgel et al. have proposed a strategy for accessing phenol metabolites of highly functionalized arenes via the formation of aryl mesylates using bis(methanesulfonyl)peroxide as the oxidant followed by conversion to the phenols [22].

There are few reported synthetic systems for the oxidation of amine  $\alpha$ -C—H bonds to yield either amides or *N*-dealkylated metabolites [18], even though tertiary amines are commonly encountered in drugs. However, a scalable two-step sequential *N*-formamide formation/hydrolysis solution was developed for oxidation of amine motifs using a copper iodide salt and oxygen and resulting in the demethylation of drugs such as clomipramine, venlafaxine, rivastigmine, tamoxifen as well as oxidation of thenalidine and the fluoroquinolone antibiotic levofloxacin [23, 24]. Piperazine moieties in drugs can also be oxidized using this method to generate 2,3-diketopiperazine metabolites of drugs such as aripiprazole and trazodone.

#### 2.1.1.1 Example: Synthesis of multiple oxidized metabolites for bioactivity testing

Eight oxidized metabolites of AMG 221, a clinical candidate previously in trials for the treatment of type 2 diabetes, were chemically synthesized to obtain enough material for determination of bioactivity and pharmacokinetics [9]. Structures of the metabolites had previously been elucidated using material obtained from microsomal incubations or rat urine following a single dose administration of AMG 221. The metabolites were chemically synthesized via two routes using achiral norbornyl diol and thiazolone intermediates and employing chiral chromatography to separate the stereoisomers. All of the metabolites showed activity in the biochemical assay with three possessing potencies similar to the parent compound AMG221. Two of these had lower *in vivo* clearance than the parent compound resulting in one of these metabolites being taken forward for further evaluation due to its higher bioavailability. See Fig. 2A.

\*Stereochemistry was arbitrarily assigned.

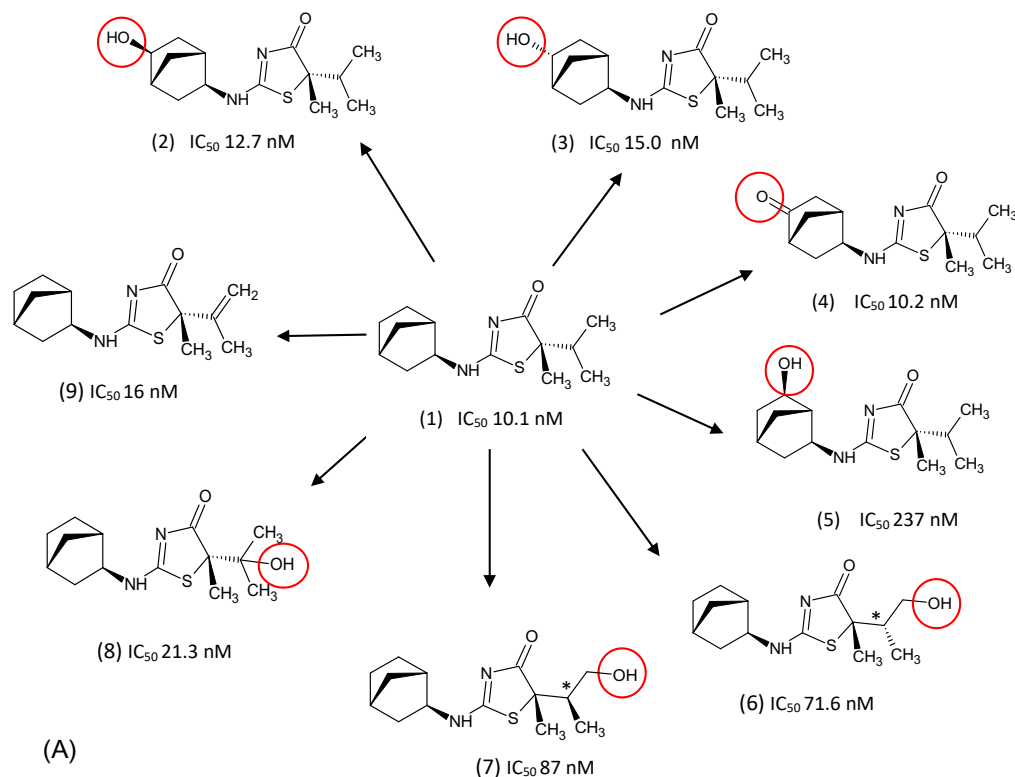


**FIG. 2** (A) Structures of metabolites of AMG 221, an inhibitor of  $11\beta$ -hydroxysteroid dehydrogenase type I ( $11\beta$ -HSD), synthesized by Li et al. [9]. Several metabolites had biochemical potency similar to the parent compound (1) with metabolites 2 and 3 having in vivo clearance less than (1).  $IC_{50}$  values were determined from a whole-cell assay using CHO cells overexpressing human  $11\beta$ -HSD. \*Stereochemistry was arbitrarily assigned. (B) Structures of active metabolites of clopidogrel, synthesized by Shaw et al. using a stereocontrolled route [25].

### 2.1.1.2 Example: Synthetic routes to active metabolites of clopidogrel

Shaw et al. explored various routes and demonstrated three orthogonal methods for the preparation of all bioactive metabolites of the prodrug anticoagulant clopidogrel [25]. Clopidogrel is bioactivated by CYPs in vivo to 4-mercapto-3-piperidinylidene acetic acid derivatives via 2-oxoclopidogrel. Synthesis of the metabolites permitted unambiguous assignment of stereochemical configuration for each metabolite, as well as providing substantial quantities of material for understanding the in vivo activities of the drug (see Fig. 2B).

### 2.1.2 Synthesis of phase II conjugated metabolites

The most common phase II (conjugate) metabolites requiring structural or quantitative analysis, or pharmacological/toxicological evaluation are glucuronides. Access to

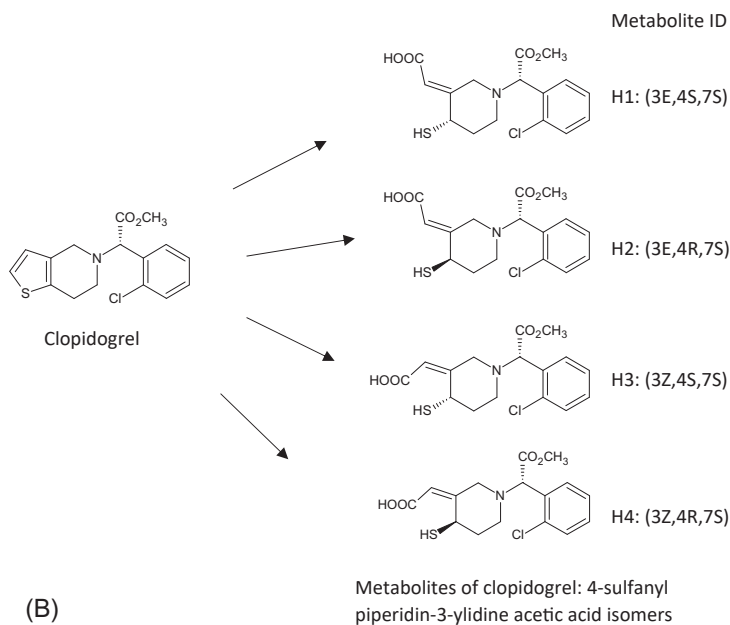


FIG. 2—Cont'd

glucuronides using chemical synthesis has generally improved over the last two decades, as documented in review publications by Stachulski in 1998 [26]. However, the author states that gram-scale synthesis of glucuronide metabolites is still challenging for all but the simplest cases, and as an example, glucuronides of hindered secondary alcohols can be particularly difficult to make. Additionally, many acyl glucuronides display low stability and are prone to both isomerization and hydrolysis during their synthesis and purification. Besides the synthetic challenges surrounding the preparation of acyl glucuronides, it is our experience that *N*-glucuronides present the greatest challenge to organic chemists, both due to the challenge of selective glucuronidation of the nitrogen atom in question and to the subsequent selective removal of any required protecting groups while keeping the glucuronide conjugate intact. As a result, incubations with liver fractions or microbes are sometimes considered the preferred strategy as a pragmatic and time-saving alternative. Stachulski's 2013 publication is a useful, comprehensive reference for the production of alkyl/phenyl *O*-glucuronides, acyl glucuronides and selected *N*-glucuronides, and should be consulted first by those looking to assemble different options for the chemical synthesis of glucuronides [27].

General methodologies for the preparation of sulfate ester compounds have been reported as recently exemplified by the development of a method utilizing tributylsulfoammonium betaine as a general agent for generating sulfate esters of compounds with diverse alcohols, including natural products [28]. This paper also provides an excellent review of different synthetic approaches for the preparation of organosulfates. Among them is a microwave-based synthetic route capable of per-sulfating multiple hydroxyl groups [29]. Literature reports

specifically describing the synthesis of sulfated metabolites are generally scarce. An example was reported by Hoshino et al. who described the stepwise and challenging synthesis of mono-, di-, and tri-sulfated metabolites of resveratrol, which necessitated selective TBDMS-protection of the three hydroxyl groups [30]. Each of the publications cited above mentions the difficulty associated with the increased aqueous solubility of the target sulfates, the consequence of which is the inability to use organic solvents to separate target compounds from aqueous-soluble reagents, instead, requiring the use of aqueous separation techniques and ion-exchange chromatography.

The last type of conjugated metabolite considered here is glutathione (GSH) conjugates. The conjugation of GSH can be reasonably simple when sufficiently reactive moieties are present in the parent molecule, as described by Pernice et al. who prepared several GSH-conjugates by the reaction of the substrate with GSH in buffer for 1 h [31]. However, the need for GSH conjugates more frequently arises due to the formation of reactive intermediates. A successful two-step strategy to synthesize such metabolites is to prepare the phase I intermediate enzymatically, or through incubation with liver fractions, and to trap the reactive intermediate *in situ* with an excess of GSH. This approach is suitable for the production of low mg amounts of GSH conjugations for definitive structural identification, which is usually the reason for the preparation of such metabolites.

## 2.2 Biomimetic chemistry

Knowledge of the mechanism of CYP oxidation of xenobiotics has led to the development of biomimetic reagents which simulate these reactions. The biomimetic system is generally composed of a reactive metal-oxo moiety (typically iron-, manganese-, or copper-based) stabilized by suitable ligands (e.g., porphyrins).

Metalloporphyrins have been utilized as biomimetic catalysts to generate cytochrome P450 mediated metabolites although it has been reported that they can lack the regio- and stereospecificity that is a key feature of biological enzymatic processes [32]. However, White and Zhao have reported that fine-tuning a Fe(PDP)-catalyst generally allows greater control of the site of oxidation in a compound, although undertaking these in drugs containing aromatic systems, nonbasic heterocycles, and olefins remains a challenge [33].

Biomimetic agents have been used successfully to generate several oxidized derivatives such as those reported by Fodi et al. who used an iron porphyrin catalyst in the production of metabolites and/or oxidation products of 43 different drug substances [34]. In the case of the biomimetic oxidation of amiodarone, the high quantity and purity of the targeted metabolites as well as new oxidation products enabled detailed NMR spectroscopic studies.

In their review of the application of transition metal-catalyzed C—H oxidation to access drug metabolites, Genovino et al. proposed the screening of susceptible substrates with different metalloporphyrin complexes, five oxidants, and two solvent systems to establish suitable conditions for metabolite production [18]. Several examples are given in which classical biomimetic catalysts were able to selectively oxidize activated C—H bonds in drugs, some of which were also *in vivo* metabolites. Three oxidized products of the antidepressant antalarmin formed using optimized porphyrin-based biomimetic oxidation is shown in Fig. 3. It is not known if these derivatives correspond to *in vivo* metabolites [18].



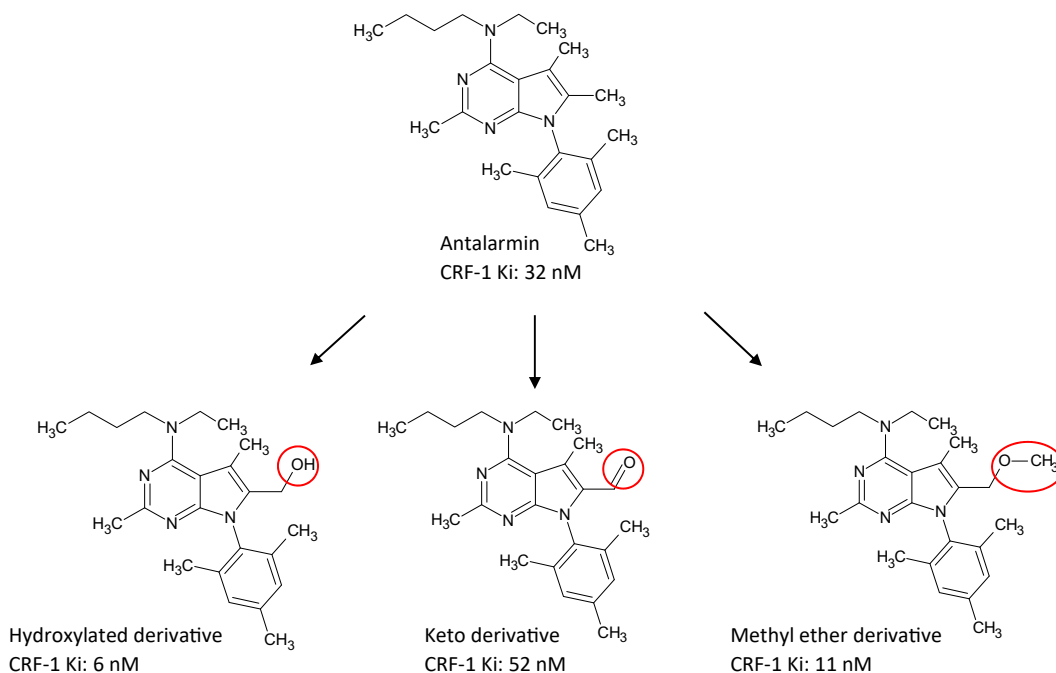


**FIG. 3** Oxidized products of the corticotropin-releasing factor (CRF-1) antagonist antalarmin, produced using optimized porphyrin-based biomimetic oxidation. Of the three products produced, the alcohol and methyl ether derivative were two to fivefold more active than the parent drug, as well as having a lowered *clogP*. Taken from *Genovino et al. T.J. Grinter, P. Moldt, F. Watjen, Hydrochloride Salt of An Azabicyclo[3.2.1]octane Derivative, PCT Int. Appl., PCT/EP2008/052417, WO/2008/104584, 2008.*

Biomimetic kits such as those supplied by HepatoChem are composed of a series of organometallic catalysts, including metalloporphyrins, mimicking cytochrome P450 enzymes to undertake aliphatic hydroxylation, *N*- and *O*-dealkylation, *N*- and *S*-oxidation, formylation as well as cleavage and rearrangement products. When a reaction condition is identified to give the desired product, it can subsequently be optimized and then scaled-up to produce mg quantities of metabolites for structure elucidation.

### 2.3 Electrochemistry

Electrochemistry (EC) has been used to mimic a variety of phase I oxidation reactions through applying a specific potential for a precise time to the drug compound in an electrochemical cell, frequently coupled to a mass spectrometer (EC-MS) and optionally also a liquid chromatography system (EC-LC-MS), the latter allowing for separation of isobaric products and characterization of stable oxidation products.

Jurva and Weidolf evaluated the technique for the generation of direct EC oxidation reactions and concluded that some, but not all, metabolic pathways can be mimicked by

EC oxidations but not all EC-oxidation products were metabolically relevant in biological systems [35]. Also, EC oxidations occurring on traditional electrode surfaces are typically not enantiospecific and often racemic oxidation products are obtained [35]. Few reports exemplify the use of the technique for generating other metabolites, but simulation of phase II reactions, including conjugation with glutathione, have been shown [36, 37].

Johansson et al. [38] reported that electrochemistry oxidation systems mimic benzylic hydroxylation, hydroxylation of aromatic rings containing electron-donating groups, *N*-dealkylation, *S*-oxidation, dehydrogenation, and less efficiently *N*-oxidation and *O*-dealkylation. Further, the electrochemically assisted Fenton reaction can mimic aliphatic hydroxylation, benzylic hydroxylation, aromatic hydroxylation, *N*-dealkylation, *N*-oxidation, *O*-dealkylation, *S*-oxidation, and dehydrogenation. The porphine system mimics all types of reactions although the yields are reportedly low for some reactions. In their evaluation, Jurva and Weidolf concluded that the EC technique is generally suitable for the synthesis of stable metabolites involving *N*-dealkylation, *S*-oxidation, *P*-oxidation, and hydroxylation of electron-rich aromatic rings. However, they recommended that other systems such as cytochrome P450 enzymes were used to generate metabolites originating from other types of hydroxylation, including aliphatic, aromatic, and benzylic hydroxylations [35].

Electrochemistry has also been applied to investigate reactive metabolites, however, Jurva and Weidolf concluded that it could not predict the risk for reactive metabolite formation and cannot currently replace biological *in vitro* experiments [38]. This was in part because epoxides are not formed by direct EC oxidation and in their experience evaluating over 2000 compounds, epoxides on various aromatic systems were the most common origin of observed glutathione adducts [36].

Scale-up of electrochemical reactions to generate milligram amounts of metabolites has been achieved although it has been reported that the absolute yield of metabolites is low, requiring careful adaptation of the EC method [39] and care must be taken not to over-oxidize the parent molecule to yield unwanted products [10]. Gul et al. conclude that for most metabolites, electrosynthesis needs to be improved by at least an order of magnitude in absolute yield to reach multimilligram amounts for follow-up studies. However, with the implementation of recent techniques such as the use of a preparative microfluidic electrosynthesis system, several drug metabolites were produced at yields of up to 100 mg [40].

### **2.3.1 Example: Production of CYP1A1 and CYP1B1-mediated amodiaquine metabolite M2 by electrochemistry**

Johansson et al. were able to mimic the metabolic oxidation of the antimalarial drug amodiaquine, withdrawn from the market as a prophylactic due to severe side effects [41]. Metabolism of amodiaquine is mediated by CYP1A1 and CYP1B1, which catalyze the formation of an aldehyde metabolite (M2) thought to be responsible for some of the toxicities of the drug through the subsequent formation of a CYP-mediated reactive metabolite. M2 was generated by a two-step EC method from amodiaquine, as shown in Fig. 4. However, three of the enzymatically generated metabolites originating from M2 were not formed in the EC system, illustrating that, in this example, prediction of metabolic fate using EC alone would have been misleading [35].

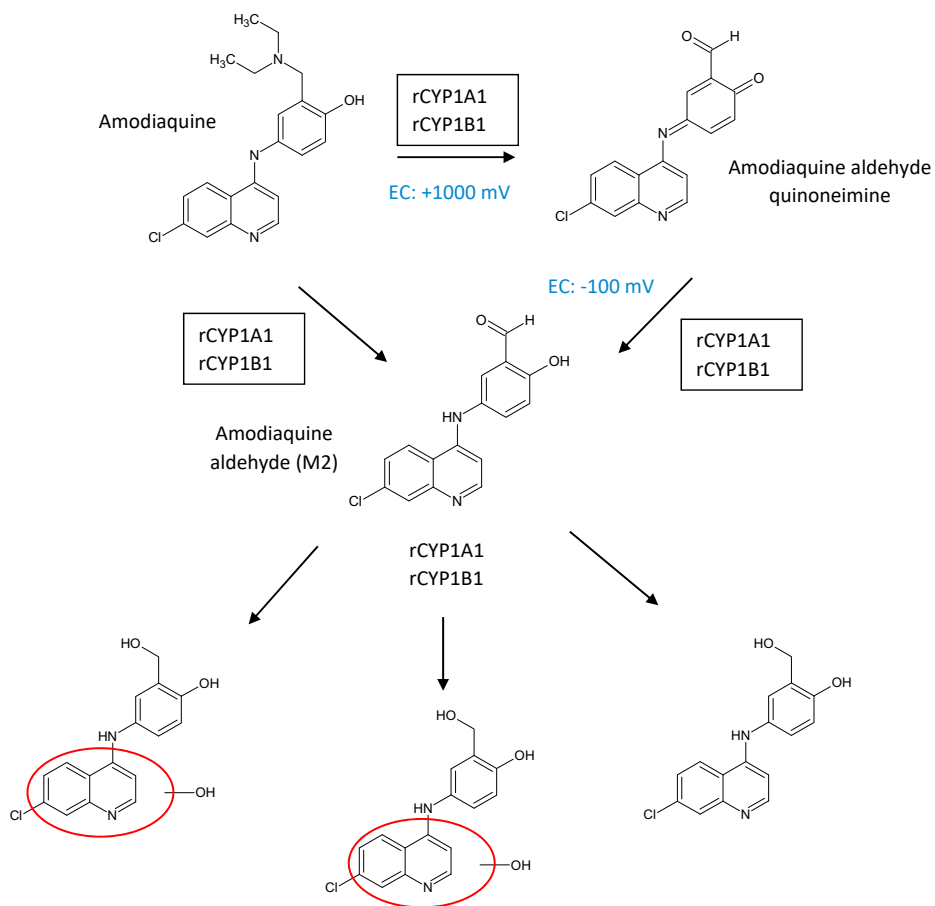


**FIG. 4** Biotransformation of amodiaquine to metabolites generated by human recombinant CYPs and EC oxidation/reduction pathway. Taken from U. Jurva, L. Weidolf, *Electrochemical generation of drug metabolites with applications in drug discovery and development*, *Trends Anal. Chem.* 70 (2015) 92–99.

## 2.4 Mammalian tissue fractions

Alternatives to chemical synthesis take advantage of the ability to generate metabolites using *in vitro* biological systems such as S9 fraction preparations or microsomes from liver, intestinal, or other tissues derived from a variety of mammalian species [42, 43]. Due to the advances in NMR spectroscopy using cryoprobe technology, even tens of microgram quantities of metabolites from scaled-up microsome incubations are sufficient to confirm structures by NMR spectroscopy. This is important for ensuring the correct metabolite has been made that matches to a clinical sample.

A current factor influencing the use of liver subcellular fractions or hepatocytes to generate sufficient quantities of metabolites for characterization is the increasing incidence of slowly

metabolized drugs. Due to the loss of activity of drug-metabolizing enzymes in these systems, a robust metabolic response for low turnover drugs cannot be obtained in the time period, particularly for secondary metabolites (metabolites more than one biotransformation step from the parent drug). Alternative longer incubation hepatocyte systems such as the HepatoPac and Hurel coculture systems provide a solution [44] although this is only useful for generating small amounts of metabolites.

While sufficient quantities of metabolites can often be isolated for structure elucidation, the drawback, where greater quantities are required for biological evaluation, can be scalability. Limitations of in vitro scaling with microsomes or hepatocytes include saturation of the enzyme system, large volumes required at relatively low drug concentrations, mixing and mass transport issues as well as large-scale specialist equipment required to handle large sample processing volumes. Cost may also be a factor where large quantities of hepatocytes or microsomes, together with their cofactors, are needed for scale-up, as well as the ethical concerns associated with the use of human and animal material.

#### **2.4.1 Example: Species-dependent regioselective hydroxylation of drugs**

In the 2019 paper by Uehara et al., metabolites of the antiarrhythmic drug propafenone were investigated [45]. Liver microsomes from humans and marmosets preferentially mediated propafenone-5-hydroxylation whereas minipig, rat, and mouse liver microsomes primarily mediated 4'-hydroxylation. They found that carbon-4' of propafenone docked favorably into the active site of rat CYP2D6, based on an in silico model, whereas the carbon-5 of propafenone docked into human CYP2D6. Regioselective biotransformations in tissue fractions from different species are thus important to consider when generating metabolites, emphasizing the need to generate a sufficient amount of material for definitive metabolite identification.

## **2.5 Whole-cell microbial biotransformation**

Microbial synthesis is often used as a contingency should chemical synthesis fail to provide a target metabolite, or as an option ahead of chemical synthesis due to the complexity and number of target metabolites [10]. The advantage of microbial biotransformation over other approaches is that prior optimization is generally not needed and scale-up is economic, affording both phase I and II metabolites from a wide range of substrates. Microbes are often employed to access difficult-to-synthesize metabolites since they are capable of generating both phase I and II metabolites at the same time, including those derived from multistep pathways, and where access to a suite of different metabolites is of interest. They are also an ethical alternative, as well as the use of cloned enzymes, to mammalian tissue for generating larger quantities of metabolites.

Since the suggestion in 1975 that microbes could be used to produce human metabolites of drugs [46], there have been many reports of the use of wild-type strains of actinomycete bacteria and fungi, and recombinant strains expressing biotransformation enzymes to produce metabolites of xenobiotics, as referenced in the paper by Salter et al. [10]. Many reviews have included a description of strategies for scaling up the production of metabolites by microbial

biotransformation [8, 47–49] although there are fewer published examples of the use of microbial biotransformation to solve metabolite issues as and when they occur in drug development programs [10, 11, 50].

The ability of wild-type microbes to mimic mammalian metabolism is linked to their expression of a wide range of drug-metabolizing enzymes, including cytochrome P450 monooxygenases and conjugating enzymes such as aryl sulfotransferases, glutathione S-transferases, and UDP-glucuronosyltransferases [51]. It is also possible to find microbial homologs of mammalian metabolic mechanisms that are becoming more prevalent due to an increasing tendency to avoid or reduce cytochrome P450 metabolism in drug design: class B flavoprotein monooxygenases from microbes have been shown to produce mammalian flavin-containing monooxygenase-derived drug metabolites [52], while aldehyde oxidases (AOs) are also known to be produced by microbes [53, 54].

A panel of microbial strains is usually screened for the ability to produce the metabolites of interest followed by scale-up to afford milligram to gram quantities. It is possible to improve the degree of conversion through manipulation of the fermentation parameters, such as oxygenation, medium composition, and harvest times. One common strategy to improve the amount of product per volume is to increase the concentration of the parent substrate. Where this can be achieved without overly compromising the percentage conversion, multigram quantities of metabolites can be accessed through a multibatch shake-flask production format of 100L or less, sufficient to service toxicology studies [10]. Conversely, inhibition of biocatalytic enzymes by the parent substrate or the products thereof may limit yields of conversion, which can be alleviated by lowering the dose of the parent substrate. Since microbial fermentation can generate multiple metabolites, as well as produce native compounds, extra purification steps may be needed when purifying metabolites from this matrix.

The ability of microbes to biotransform drugs into metabolites has also been exploited through the use of immobilized microbial systems. Quinn et al. described the production of drug metabolites using the fungus *Cunninghamella elegans*, immobilized either in alginate or as a biofilm, for semicontinuous production of hydroxylated drug metabolites through repeated addition of drug and rejuvenation of the fungus [55]. Amadio also described immobilization of a dense network of hyphae of *C. elegans* in a polysaccharide matrix to form a biofilm which rapidly transformed flurbiprofen to hydroxylated metabolites, as well as retaining transformation efficiency over time [56].

The following two examples illustrate the application of whole-cell microbial biotransformation for the production of drug metabolites.

### **2.5.1 Example: Accessing disproportionate human metabolites for toxicology studies**

In this case study, a disproportionate mono-hydroxylated metabolite (M27) of ingenol disoxate, originally under development by LEO Pharma, was formed in humans. MetID studies using LC-MS/MS failed to determine the point of hydroxylation in the metabolite. Definitive identification of the position of hydroxylation in the metabolite M27 was achieved via microbial biotransformation, and milligram quantities purified for bioanalysis requirements after structure elucidation by NMR. A subsequent request by the FDA to undertake in vitro studies to assess the DDI potential of the metabolite was facilitated by scaling up the reaction.

In total, over half a gram of this chemically intractable metabolite was made using microbial biotransformation [57].

### 2.5.2 Example: Accessing multipathway-derived metabolites

In vivo human metabolism of Incyte's investigational drug epacadostat (EPA) forms three major circulating metabolites from both primary and secondary pathways [11]. Glucuronidation of EPA forms M9, the dominant metabolic pathway, in conjunction with the formation of an amidine M11 and an *N*-dealkylated metabolite, M12, as shown in Fig. 5. EPA is metabolized by gut microbiota resulting in M11, which is absorbed and further modified by CYP enzymes to form the secondary metabolite M12. Microbial biotransformation provided a route to access all three human metabolites, where different strains and dosing regimes were found to be optimal for the production of each metabolite. M12 was straightforward to synthesize chemically and thus was not accessed via microbial biotransformation. Scale-up of the most productive biotransforming strains for M9 and M11 enabled the supply of 112mg of the glucuronide and 69mg of the gut metabolite at 95% purity. The metabolites were used for structural confirmation and as analytical standards, as well as for further characterization of metabolic pathways since M9 is deconjugated in the gut allowing for parent recirculation, and M12 is a product of M11.

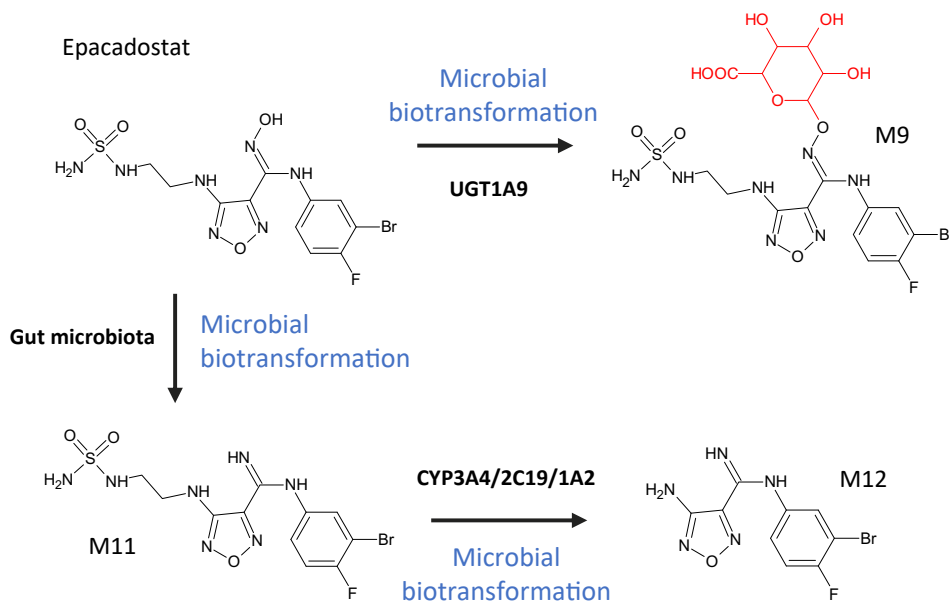


**FIG. 5** Major metabolites of epacadostat produced by microbial biotransformation via mixed metabolic pathways. Scale-up of the most productive biotransforming microbes for M9 and M11 enabled the supply of 112mg of the glucuronide (M9) and 69mg of the gut metabolite (M11) by Hypha Discovery. Although M12 was produced by the microbes, it was synthesized by Incyte in parallel and thus not targeted for scaled-up production and purification. Taken from J. Boer, R. Young-Sciame, F. Lee, K.J. Bowman, X. Yang, J.G. Shi, F.M. Nedza, W. Frietze, L. Galya, A.P. Combs, S. Yeleswaram, S. Diamond, Roles of UGT, P450, and gut microbiota in the metabolism of epacadostat in humans, *Drug Metab. Dispos.* 44 (2016) 1668–1674.

## 2.6 Recombinant enzymes

### 2.6.1 Cytochrome P450 enzymes

Recombinant cytochrome P450 enzyme systems, derived from either mammalian or microbial origins, are capable of synthesizing human metabolites on a preparative scale, catalyzing a variety of actions including hydroxylation, epoxidation, *N*- and *O*-dealkylation and Bayer-Villiger oxidation. Human enzymes relevant to drug metabolism have been cloned into a variety of different hosts including *Escherichia coli*, the yeasts *Saccharomyces cerevisiae* and *Schizosaccharomyces pombe*, and baculovirus-directed expression in insect cells. Human CYPs expressed in *E. coli* are convenient due to superior expression levels [58] and are available as single products from companies such as Cypex, who offer a range of human CYPs co-expressed with human NADPH CYP-reductase. In the work by Schroer et al., 14 isoforms of recombinant human CYPs expressed in *E. coli* were used to obtain metabolites of 60 pharmaceutical drug compounds, predominantly through the action of CYP 1A1, 2D6, 3A4, and 3A5 [58]. Examples in which milligram to gram amounts of metabolites were obtained in these systems are described by Winkler et al. [59], including an *E. coli*-based panel of the 14 major human CYP isoforms. One example illustrating the utility of this approach is the hydroxylation of the epothilone analogue sagopilone in which recombinant *E. coli* co-expressing CYP2C19 and NADPH-cytochrome P450 reductase (CPR) produced gram amounts of the main human metabolite at large scale within 23 h [60]. However, it has been reported that human purified enzymes show low catalytic activity and poor stability for industrial use [61] and thus may be less suited to larger scale preparation of metabolites.

In many cases, microbial oxygenases have high turnover and good operational stability [62] and bacterial CYPs usually have much higher specific activities [58] and thus may often be more suitable biocatalysts. Scalable systems provided by recombinant microbial-derived CYP kits are available. These include Hypha Discovery's PolyCYPs<sup>®</sup> composed of recombinant P450s cloned from various actinomycete strains and expressed in *E. coli*, and Codexis' MicroCyps, derived from a series of mutants of the P450 from *Bacillus megaterium* (BM3). Both systems enable the scalable synthesis of CYP-derived human metabolites for definitive metabolite identification and pharmacological testing. A selection of human CYP-derived metabolites produced by some of the PolyCYPs enzymes is illustrated in Fig. 6.

There have been numerous reports describing progress in optimizing the BM3 cytochrome P450 enzyme for the production of drug metabolites, such as the evolution of a P450 BM3 to stereoselectively produce a hydroxylated human metabolite of busipirone, 6'-hydroxy-busipirone (M6), at 72% yield [63]. The extensive progress made in the improvement of its catalytic performance toward drugs, the substitution of the costly NADPH cofactor and its immobilization and scale-up of the process for industrial application has been reviewed recently by Nardo and Gilani [61]. One such example is described in the paper by Beyer et al. where three variants of cytochrome P450 BM3 fused to phosphite dehydrogenase were made to enable cofactor recycling [64]. Product analysis showed that reaction types included *C*-hydroxylation, *N*-oxidation, demethylation, and aromatization of a number of the 32 commercial drugs tested.

Recently there have been efforts to covalently couple the catalytic heme domain of some cytochrome P450s to a photosensitizer to achieve selective oxidation of substrates when activated by light [65]. One approach mimics the natural pathway and utilizes photogenerated reductive species to directly deliver electrons to the heme active site. The performance of



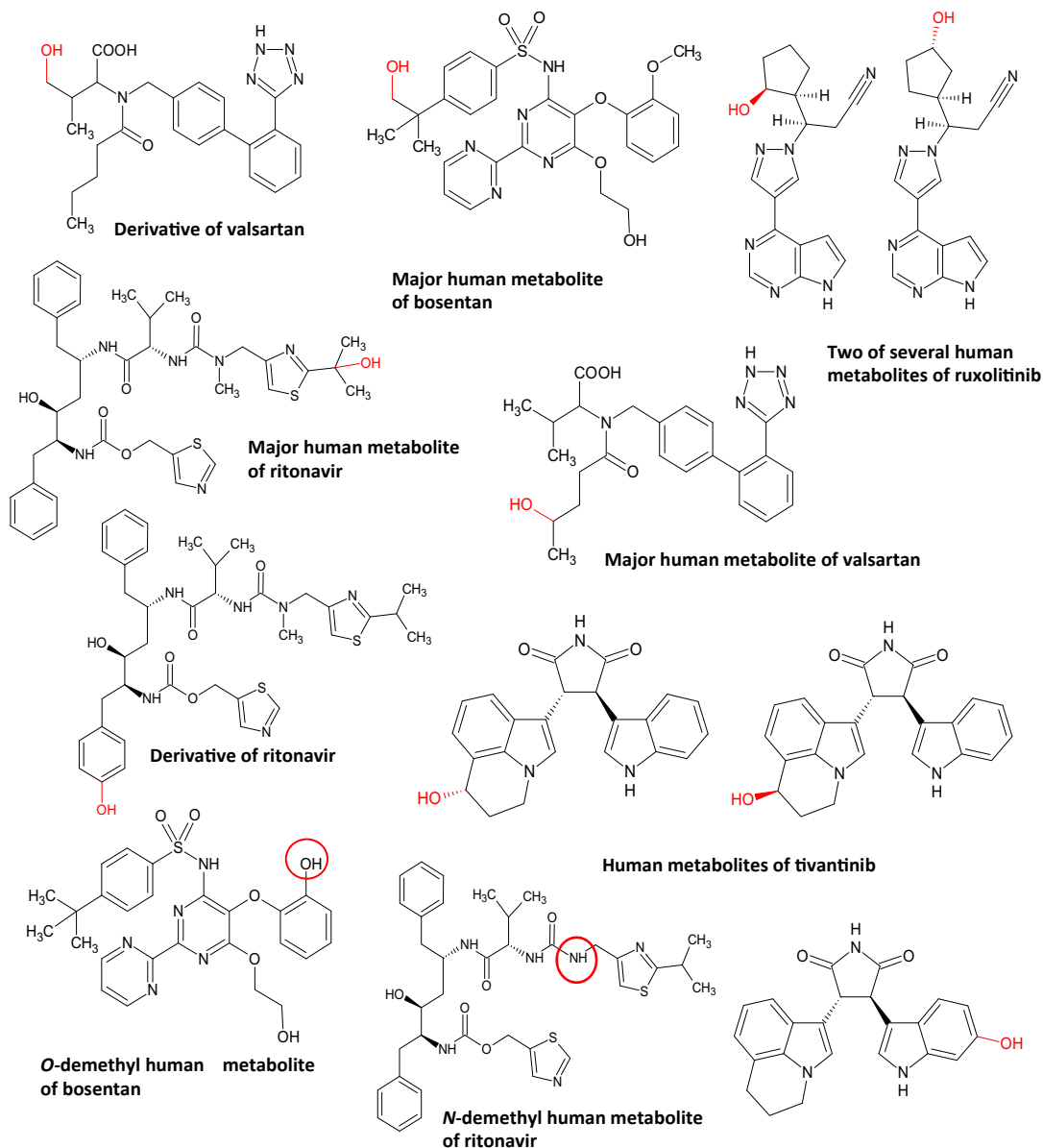


**FIG. 6** Human CYP-derived metabolites of a variety of drugs hydroxylated at different positions by recombinant microbial enzymes (PolyCYPs®).

various photosensitizers has been reviewed by Shalan et al. [65], including the use of the fluorescent dye eosin Y in a whole-cell photosensitizer approach in which P450 holoenzymes or heme domains were expressed in *E. coli*. Multiple BM3 mutants and human CYPs have been shown to produce human metabolites using this system although turnover was low and improvements are necessary for its wider use and scalability. Cheruzel's group have designed

an alternative system in which a Ru(II)-diimine photosensitizer complex is covalently attached to a heme domain, necessitating the postmodification and site-directed mutagenesis of the heme domain for assembly. Given the challenges in protein stability, activity, and coupling efficiency still to overcome in light-driven P450 enzyme systems, this technique is not yet appropriate for widespread application to scalable generation of oxidized drug metabolites.

### 2.6.2 Non-CYP phase I enzymes

Production of drug metabolites by recombinant enzymes from other non-CYP oxidative metabolic pathways has also been reported. Drug metabolism by AO, a molybdo-flavoenzyme has become more prevalent as an oxidative clearance pathway in recently designed drugs derived from nitrogen-containing heterocycles [66]. AO has profound species differences in expression and activity toward various substrates but has not always been identified prior to clinical studies [67], consequently negatively impacting on the development of several drug candidates. Rodrigues et al. reported a high-yielding recombinant human AO system expressed in *E. coli* for the conversion of famciclovir to 223 mg of its main oxidized product at 82% isolated yield in fed-batch fermentation, in which the solvent for the substrate and the buffering agent for the biotransformation were found to have a significant effect [68]. Foti et al. reported an optimized expression system for hAOX1 in *E. coli* using a codon-optimized construct which resulted in an up to 15-fold increase of protein production and a simplified purification procedure [69].

Recombinant human xanthine oxidase (XO) was successfully expressed in *E. coli* [70], where an optimized whole-cell 25-L fed-batch fermentation resulted in the production of tens of milligrams of the metabolite 4-quinazolinone. Similarly, recombinant flavin monooxygenases (FMOs) have been used as whole-cell biocatalysts, shown by Geier et al. where they demonstrated the functional expression of human FMO2 in *E. coli*. The FMO2 biocatalysts were employed for substrate screening purposes, revealing trifluoperazine and propranolol as FMO2 substrates [71]. Biomass cultivation on the 100-L scale afforded active catalyst for biotransformations on a preparative scale. The whole-cell conversion of trifluoperazine resulted in selective oxidation to 48 mg (46% yield) of the corresponding *N*-oxide with a purity >98%.

Due to the importance of non-CYP mediated oxidative mechanisms in biotransformation of drugs, recombinant phase I enzyme kits such as Hypha Discovery's PolyCYPs<sup>®</sup> kits now include cloned human AOX1 and FMO enzymes, as well as a diverse set of microbially derived CYPs.

### 2.6.3 Use of other oxidizing enzymes

In addition to phase I metabolizing enzymes, other oxidizing enzyme systems such as heme-thiolate peroxigenases (UPOs), a mechanistic analog of cytochrome P450 [72], have proved to be stable oxygen-transferring biocatalysts for H<sub>2</sub>O<sub>2</sub>-dependent transformation of drugs to create metabolites. Kiebitz et al. used a peroxigenase derived from the basidiomycete *Marasmius rotula* to selectively *N*-dealkylate the bile acid reabsorption inhibitor SAR548304 to produce both human metabolites in two separate kinetic-controlled reactions with overall yields of 66% of the *N,N*-di-desmethyl metabolite and 49% of the *N*-mono-desmethylated metabolite [73]. In contrast, chemical preparation of the *N,N*-di-desmethyl metabolite was only possible by a seven-step synthesis starting from a late precursor of SAR548304 and palladium catalysis, as well as laborious chromatographic purification with an overall yield of only 27%.

Peroxygenases have also been engineered to create highly active and stable variants to create drug metabolites. Gomez de Santos et al. used a heterologously expressed peroxygenase from the basidiomycete *Agrocybe aegerita* in different yeasts via directed evolution for the selective synthesis of 5'-hydroxypropranolol, one of the two main hydroxylated metabolites of the  $\beta$ -blocker propranolol [74]. Chemical synthesis of these metabolites is associated with poor reaction yields, an excessive number of steps, and requires high-energy input and harsh conditions. Interestingly, the peroxygenase variant reportedly outperforms any natural or engineered hydroxylating catalyst described to date.

#### 2.6.4 Recombinant UGTs

Uridine 5'-diphospho-glucuronosyltransferases (UGTs) produce glucuronidated metabolites and are expressed by many organisms from microbes to humans to facilitate the elimination of xenobiotics. There are many subtypes which catalyze the glucuronidation of different compound types, including UGTs which specifically form *O*- and *N*-glucuronides. Recombinant human UGT products currently available, e.g., Corning's Supersomes, target preclinical reaction phenotyping and inhibition studies, however, these require the addition of costly UDP-GA cofactor and are generally most suitable for small-scale production of glucuronide metabolites.

### 2.7 Combined synthetic and biosynthetic approach

Unraveling the complex metabolite maps of some drugs, especially where dominant routes of polymorphic enzyme-mediated metabolism have been eliminated, may need to harness multiple approaches to achieve the synthesis of metabolites. Where a decision is made to access only major metabolites to meet regulatory guidelines, the most suitable method for efficient generation of specific metabolites needs to be made, while taking into account the availability of in-house resources and outsourced options to achieve this.

#### 2.7.1 Example: Accessing human metabolites of drugs subject to metabolic shunting

As part of a medicinal chemistry strategy to reduce major metabolism by single polymorphic CYPs, there has been an increase in the metabolism of new drug candidates through non-CYP pathways mediated by other key drug metabolizing enzymes such as AO [66]. Further, mixed AO/CYP drug candidates may be subjected to metabolic shunting, an important consideration during toxicology and DDI assessment of these compounds [75]. Access to and evaluation of metabolites are thus important to consider for drugs subject to mixed metabolism. In work presented by Zhao et al. [54], both AO and CYP enzymes were found to be responsible for the metabolic clearance of LY3023414 with non-CYP enzymes mediating approximately half of the clearance. No metabolism was observed when tested versus human recombinant CYPs, however, a microbial biotransformation panel was able to generate several metabolites, including milligrams of an AO-mediated hydroxylated metabolite (M2) and an *N*-oxide (M4). In addition, the use of a liver S9 fraction enabled the production of a further CYP/AO metabolite (M12) from a synthetic intermediate (M5). Use of a combined biotransformation and synthesis approach, therefore, enables access to metabolites created through different pathways (see Fig. 7)

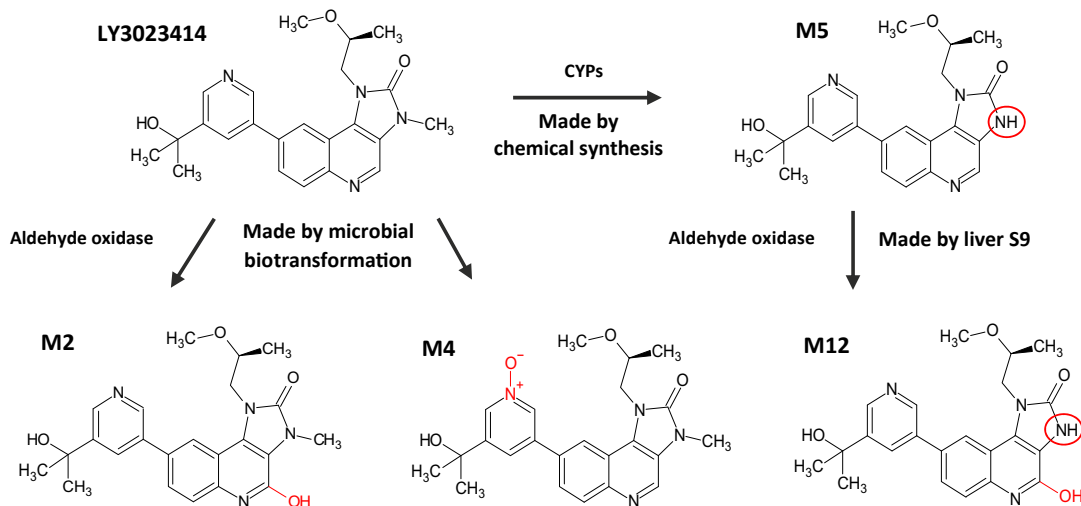


**FIG. 7** Provision of human CYP and non-CYP metabolites M2, M4, and M12 at multi mg scale utilizing a mixed approach of microbial biotransformation, chemical synthesis, and liver S9 incubations [54]. Metabolites M2 and M4 were obtained via microbial biosynthesis and metabolite M12 was obtained from incubation of M5 with liver S9. Metabolites were prepared and purified at Hypha Discovery. Parent compound and metabolites were identified by accurate mass LC-MS/MS and NMR at Eli Lilly.

These case studies described provide a snapshot of the many challenges and solutions for the provision of metabolites for drug development programs through various routes. Both chemical and biological solutions will continue to evolve to meet the challenges of ensuring that sufficient quantities of drug metabolites are accessible to meet all regulatory guidelines, enabling the provision of higher quality medicines to patients.

### 3 Purification and structure elucidation of metabolites

#### 3.1 Metabolite purification

The first step in metabolite purification from a biological matrix is extraction and different matrices present different challenges. Whole-cell microbial biotransformations will contain unused medium components such as sugars, oils, and amino acids, that can complicate extraction and endogenous metabolites that may chromatograph closely with the products of interest. Urine generally contains high levels of salts and proteins for which precipitation may be a necessary first step. Systems employing isolated enzymes are generally cleaner starting points. The extraction must be as selective as possible for the target molecule(s) to minimize downstream problems from the unused medium components and endogenous metabolites. The pH can be varied to optimize extraction into an organic solvent or trapping on a styrene-divinylbenzene resin and, in the latter case, selective elution can be used to generate an enriched fraction containing the metabolite(s). The concentration of the resulting extract or fraction and defatting using hexane to remove lipids and fatty materials may be

useful, especially in the case of fungal biotransformations. The extraction method should be appropriate to the scale of operation, with larger amounts of material better handled by resin extraction to avoid the use of large volumes of flammable solvents.

Hydroxylated or conjugated drug metabolites tend to be polar molecules and so are suited to purification by reversed-phase HPLC methods. The challenges presented by the metabolites vary on a case-by-case basis and, in addition to mixture complexity, may include solubility and stability, so a range of reversed-phase column chemistries should be available that are suitable for use in acidic (e.g., Waters Atlantis-T3 or Phenomenex Luna 2) or basic (Waters BEH C18, X-select, X-Terra, and X-Bridge C18) conditions. Generally, two or three purification stages using different column chemistries may be needed to purify a metabolite to the degree of purity required. A first stage would usually aim to further separate the metabolite fractions from unwanted materials expeditiously and efficiently rather than aiming for as much purity as possible. HPLC-MS assays are used to follow the purification and detect fractions containing the target metabolites. For later stages in the purification, automated mass-directed purification (preparative HPLC-MS) systems are ideal for metabolite purification so that once a method with a suitable resolution for the target metabolite(s) has been developed the system can be programmed only to collect column eluate in which the molecular ions for these metabolites have been detected.

Mixtures of metabolites can occasionally prove to be difficult to separate by reversed-phase HPLC as was the case for the two metabolites of imidacloprid discussed in the next section. These were hydroxylated in adjacent positions on the dihydroimidazole ring and had very similar properties. These were eventually separated from each other by normal phase chromatography using preparative silica gel TLC plates eluted with ethyl acetate saturated with water as the developing solvent. The bands containing the separated metabolites were scraped off, sonicated with methanol, concentrated and then each subjected to a final reversed-phase HPLC-based processing step to ensure removal of silica. The slower eluting band was subsequently identified as 5-hydroxyimidacloprid and the faster-eluting band as 4-hydroxyimidacloprid—their structure elucidation will be discussed later.

Depending on the intended use of the purified metabolite, a whole range of subsequent characterization methods may be deemed necessary in addition to HPLC-purity and NMR.

### **3.1.1 Example: Purification of metabolites from excreta for use as analytical standards**

If clearance mechanisms of the test drug results in sufficient quantities of the major metabolites in biological material such as faeces or urine, purification and subsequent identification of metabolites from such matrices are possible. One such project undertaken at Hypha Discovery resulted in tens of milligrams of the *R*- and *S*-*O*-glucuronides of carisbamate, a neuromodulator developed by SK Life Science, which were purified to >95% purity from 150 mL of rabbit urine using a three-step purification method. The initial step involved treating the urine with acetonitrile to precipitate proteins and salts, which were removed by centrifugation. After removal of the acetonitrile by evaporation, the supernatant was purified by preparative reversed-phase HPLC, initially by applying it directly to an Xbridge C18 OBD column, which was eluted with a shallow water-acetonitrile gradient (5%–25% acetonitrile over 11 min in the presence of 0.1% formic acid). The fractions containing the target glucuronides were concentrated and separated by further reversed-phase HPLC on a semipreparative Xbridge prep phenyl column eluted with a very shallow water-methanol

gradient (26%–28% methanol over 16 min in the presence of 0.1% formic acid). Concentration to dryness of the eluate fractions containing the two target metabolites yielded 95 and 23 mg of the *R*- and *S*-glucuronides, respectively. Confirmation of the structures was obtained by NMR spectroscopy (see later), enabling the use of the purified materials as analytical standards for bioanalysis.

### 3.2 Metabolite structure elucidation using NMR spectroscopy

NMR spectroscopy is a very valuable technique for elucidating the structures of drug metabolites and this is reviewed elsewhere [76, 77]. Modern microcryoprobe technology enables acquisition of structure elucidation datasets including heteronuclear shift correlation spectra on as little as 10–30 µg of purified material, while for simple molecules where a 1D proton NMR spectrum can be used identify the change that has occurred, single-digit µg amounts will be sufficient [77]. This is, however, a generalization and the quality of spectra obtained will vary from compound to compound. The solubility of the parent drug can be used as a guide to select the NMR solvent but metabolites are mostly more polar than the compounds they are derived from and, although DMSO-*d*<sub>6</sub> is usually a good solvent choice, it is not always suitable and conducting solubility trials is difficult with limited amounts of purified material. Other solvents useful for polar metabolites are methanol-*d*<sub>4</sub>, acetonitrile-*d*<sub>3</sub>, pyridine-*d*<sub>5</sub>, and D<sub>2</sub>O, with solvent mixtures useful occasionally. This section will address the NMR experiments that are usually used for drug metabolite structure elucidation and illustrate the steps involved in the structure elucidation process with a number of examples. It should also be noted that the use of NMR as a quantitative technique for determining purity and concentration is becoming increasingly prevalent in the field of drug metabolism. The applications of quantitative NMR (qNMR) range from the determination of the absolute purity of metabolite materials purified in milligram-gram quantities to be used as analytical reference standards, to the assessment of concentrations of metabolites in the low µg/mL range [78]. One recent example of the latter application was the use of qNMR to determine the concentrations of metabolites purified from liver microsome incubations of lead molecules using submilligram substrate amounts to enable bioactivity testing and SAR exploration [5].

#### 3.2.1 1D and 2D NMR experiments for metabolite structure elucidation

A 1D <sup>1</sup>H NMR spectrum identifies the likely local chemical environments of the protons present in a metabolite structure from their chemical shifts, their connectivity from their coupling constants and patterns, and the signal integrals indicate the number of protons represented by each signal. Interpretation of the <sup>1</sup>H NMR spectra of more complex molecules may be complicated by signal overlap. A 1D <sup>13</sup>C NMR spectrum is usually only obtained if there is plenty of material available (≥1 mg amounts) as <sup>13</sup>C NMR spectroscopy is much less sensitive than <sup>1</sup>H NMR spectroscopy. <sup>13</sup>C NMR spectra are acquired in a “decoupled” mode that eliminates one-bond <sup>1</sup>H-<sup>13</sup>C coupling to remove peak splitting so the spectrum is used to identify the likely local chemical environments of the carbons present from their chemical shifts. For metabolites where only limited material amounts are available, the carbon shifts can be detected indirectly through the 2D heteronuclear shift correlation spectra.

A range of 2D NMR experiments is available to provide extra information to help assign the 1D NMR signals and provide <sup>1</sup>H-<sup>1</sup>H and <sup>1</sup>H-<sup>13</sup>C correlations to establish the metabolite

structure. Not all of these experiments may be necessary for any given metabolite and which spectra are acquired is decided on a case-by-case basis. The COSY (correlated spectroscopy) and TOCSY (total correlated spectroscopy) experiments provide  $^1\text{H}$ - $^1\text{H}$  connectivity information with the TOCSY spectrum detecting longer through-bond connectivities. They are used to address any ambiguity in 1D  $^1\text{H}$  NMR assignments due to signal complexity or overlap. The heteronuclear shift correlation HSQC (heteronuclear single-quantum correlation) and HMBC (heteronuclear multiple bond correlation) experiments are used to establish  $^1\text{H}$ - $^{13}\text{C}$  correlations. The HSQC spectrum shows one-bond  $^1\text{H}$ - $^{13}\text{C}$  correlations and identifies all the protonated carbons in a molecule. The HMBC spectrum shows two-three bond  $^1\text{H}$ - $^{13}\text{C}$  correlations and is useful for identifying the positions of quaternary carbons in a structure and assembling fragments established through  $^1\text{H}$ - $^1\text{H}$  connectivity information.  $^1\text{H}$ - $^{15}\text{N}$  versions of these experiments are also available. The NOESY (nuclear Overhauser spectroscopy) and ROESY (rotating frame Overhauser spectroscopy) experiments can be used to detect through-space  $^1\text{H}$ - $^1\text{H}$  interactions to probe stereochemical aspects of a drug metabolite structure.

### 3.2.2 Stepwise determination of metabolite structures

Before starting to work on the structure elucidation of a metabolite, the  $^1\text{H}$  and  $^{13}\text{C}$  NMR signals of the parent molecule should be assigned, ideally in the same NMR solvent as will be used for the metabolite. The  $^1\text{H}$  NMR spectrum of the metabolite sample is then obtained to compare with that of the parent compound and also assess for sample purity and suitability for obtaining further spectra, for which qNMR can be used to quantify the amount of material present. In simple cases, the structural change that generated the metabolite may immediately be apparent. Fig. 8A shows the high field regions of the proton NMR spectra in  $\text{DMSO-}d_6$  of

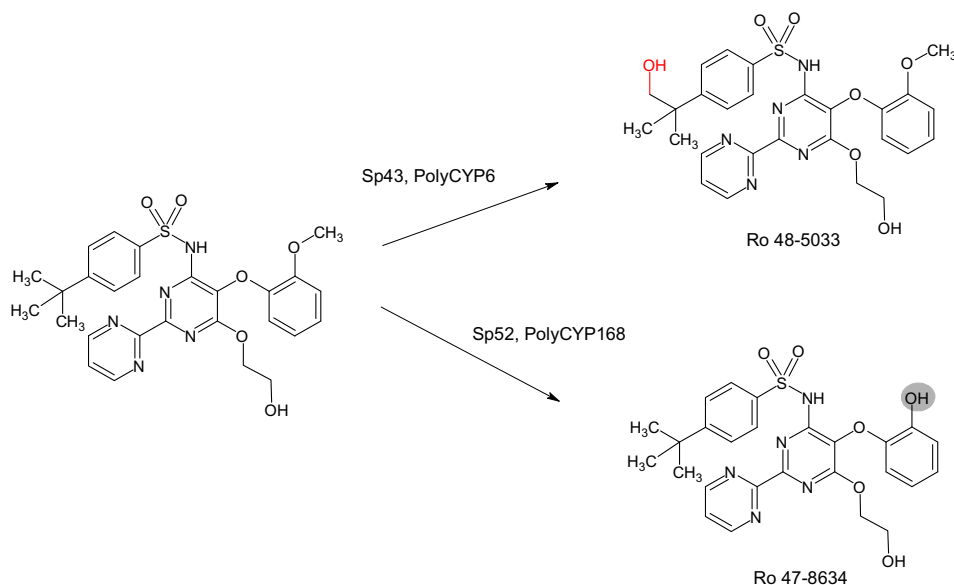


FIG. 8 (A) Comparison of high field region of 500MHz  $^1\text{H}$  NMR spectra in  $\text{DMSO-}d_6$  of bosentan (bottom), Ro 48-5033 (middle), and Ro 47-8634 (top). (B) HSQC spectrum in  $\text{DMSO-}d_6$  of 5 $\mu\text{g}$  of hydroxybosentan obtained on a 700MHz instrument.



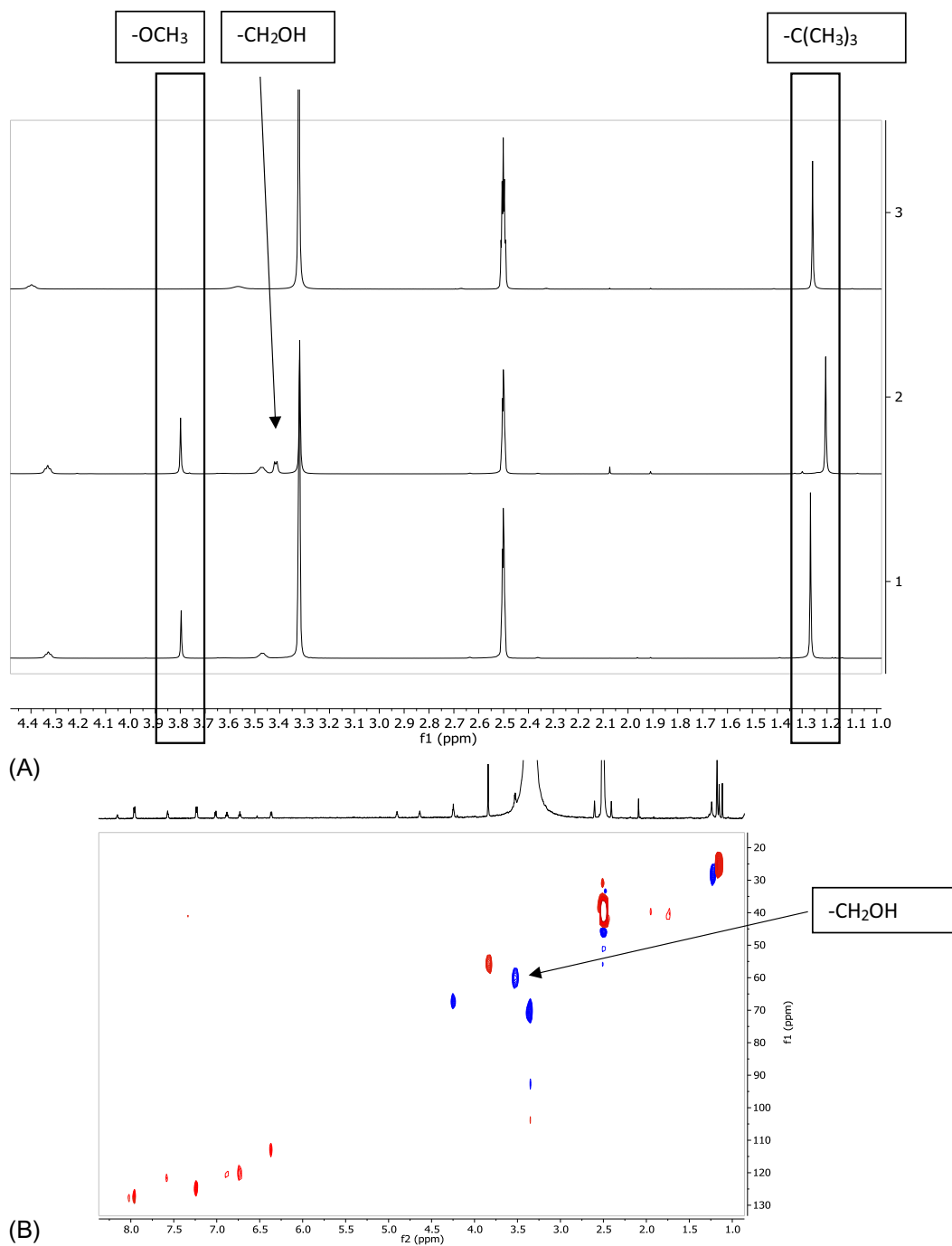


FIG. 8—Cont'd

the endothelin receptor antagonist bosentan and two of its human metabolites, Ro 48-5033 and Ro 47-8634 [79]. These were generated by biotransformation with Hypha microbial strains Sp43 and Sp52, or Hypha PolyCYPs<sup>®</sup> 6 and 168, respectively [80]. Comparison of the spectra for bosentan and Ro 48-5033 shows an upfield shift in the highest field peak from 1.27 to 1.21 ppm with a concomitant decrease in the signal integral for the peak from nine to six protons (not shown in figure) along with the appearance of a new doublet signal at 3.42 ppm integrating for two protons. These changes are consistent with hydroxylation of one of the methyl groups comprising the *t*-butyl moiety. Although no further work to confirm this assignment was undertaken at the time, this metabolite was subsequently used in an evaluation of the sensitivity of a 700 MHz NMR instrument equipped with a 1.7 mm microcryoprobe. The resulting HSQC spectrum of a 5 µg sample of Ro 48-5033 sample is shown in Fig. 8B, with the correlation representing the new hydroxymethylene moiety highlighted. Comparison of the <sup>1</sup>H NMR spectra for bosentan and Ro 47-8634 in Fig. 8A show that the *O*-methyl singlet at 3.80 ppm in the spectrum of bosentan is absent in the spectrum of the metabolite, which is consistent with the expected *O*-demethylation biotransformation.

Biotransformations of more complex drugs often require the use of 2D NMR spectroscopy to identify the location of the structural change. Fig. 9A shows the <sup>1</sup>H NMR spectrum of a metabolite of the immunosuppressive drug cyclosporin A, produced enzymatically using PolyCYP 194. Although the proton signals are well dispersed for such a complex molecule there is a lot of overlap in the high field region in particular. 2D COSY, HSQC, and HMBC spectra were obtained and a portion of the HSQC spectrum is shown in Fig. 9B. When compared with the spectrum of the parent molecule, this showed the presence of a new hydroxymethylene signal at 3.99–3.94/63.5 ppm, which is consistent with hydroxylation of the terminal methyl group of the *N*-methyl-4-(2-butenyl)-4-methylthreonine residue to generate the human metabolite AM1 [81].

2D NMR spectroscopy may also be needed for much simpler molecules as illustrated by the use of HMBC spectra to distinguish between and identify the sites of hydroxylation for two imidacloprid metabolites produced by one of Hypha Discovery's microbial

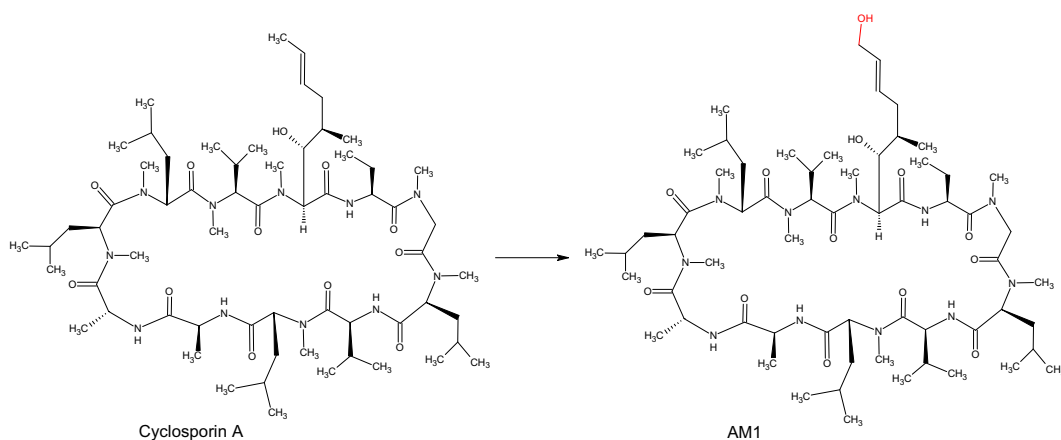


FIG. 9 (A) 500 MHz <sup>1</sup>H NMR spectrum of cyclosporin metabolite AM1 in CDCl<sub>3</sub>. (B) Expansion of the midfield region of the HSQC spectrum showing new —CH<sub>2</sub>OH signal at 3.99–3.94/63.5 ppm.

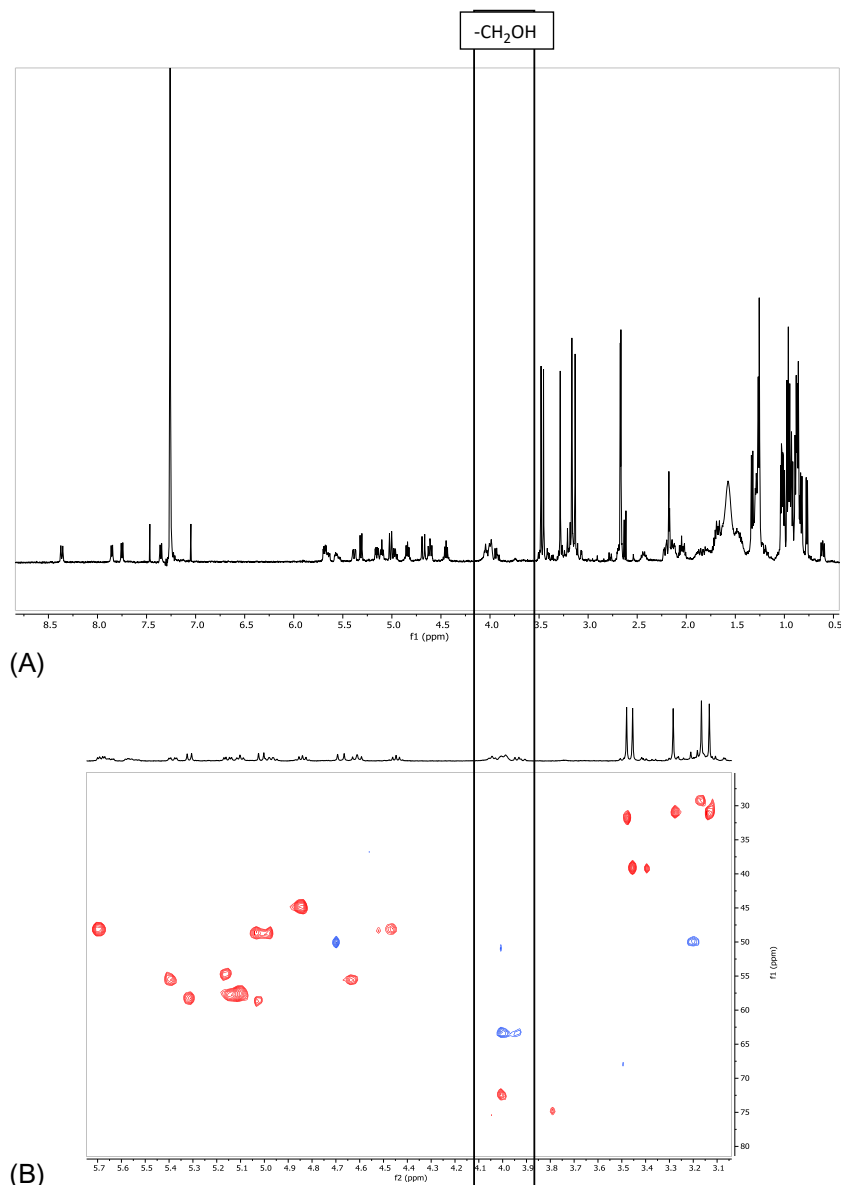
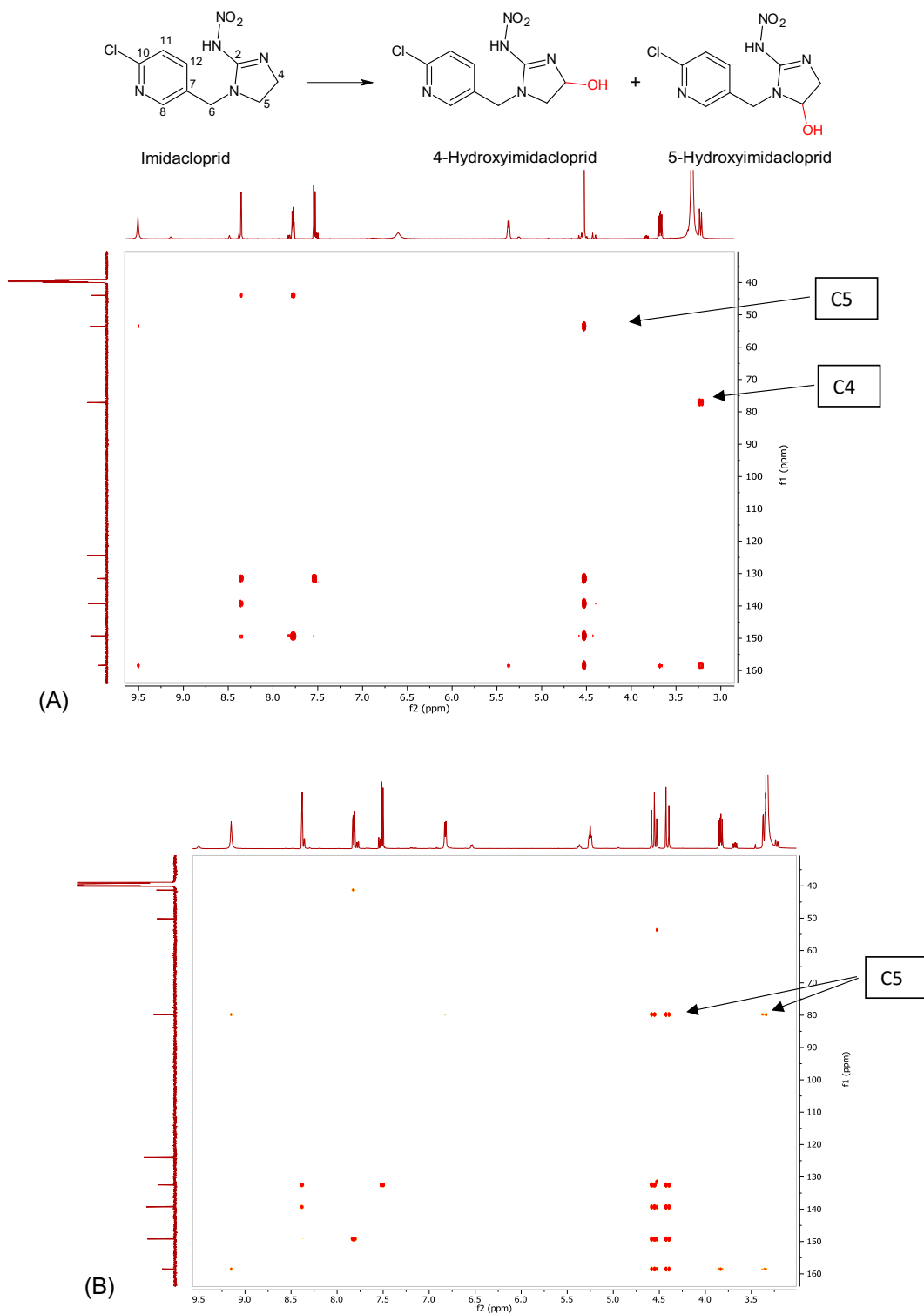


FIG. 9—Cont'd

biotransforming strains (Sp15). For both metabolites, the NMR signals for the substituted pyridine ring were almost identical and indicated no change to this portion of the molecules compared to imidacloprid. For the first metabolite, the bridging methylene protons were equivalent and evident as a singlet at 4.53 ppm sharing HMBC correlations with pyridine ring carbons. They also showed HMBC correlations with dihydroimidazole ring carbon signals at 158.4



**FIG. 10** (A) HMBC NMR spectrum of 4-hydroxyimidacloprid in  $\text{DMSO-}d_6$ . (B) HMBC NMR spectrum of 5-hydroxyimidacloprid in  $\text{DMSO-}d_6$ . A small extent of cross contamination of the two metabolite samples is evident.

and 53.3 ppm (Fig. 10A). The HSQC spectrum showed that the latter carbon corresponded to a methylene group with proton signals at 3.68 and 3.23 ppm, representing position 5. These protons were coupled to a methine proton at 5.37 ppm, corresponding to a carbon shift at 76.8 ppm and sharing an HMBC correlation with the carbon at 158.4 ppm, supporting position 4 as the site of hydroxylation.

For the second metabolite, the bridging methylene protons at position 6 were nonequivalent, identifiable as a coupled pair at 4.57 and 4.41 ppm, which, in addition to sharing HMBC correlations with pyridine ring carbons, showed HMBC correlations with carbon signals at 158.5 and 79.8 ppm in the dihydroimidazole ring (Fig. 10B). An HSQC correlation of the 79.8 ppm signal with a methine proton at 5.25 ppm confirmed position 5 as the site of hydroxylation. This carbon signal also shared HMBC correlations with one of the 4-methylene protons at 3.36 ppm.

A final example (Fig. 11) illustrates the use of 2D NOESY spectra to distinguish between two glucuronide metabolites of the anticonvulsant drug candidate carisbamate [82] purified from rabbit urine (see earlier example section). COSY, HSQC, and HMBC NMR spectra were obtained for both metabolites, with clear HMBC correlations from the 7-methine protons with the glucuronide carbons and from the glucuronide anomeric protons with the 7-methine carbons indicating glucuronidation of the 7-hydroxyl proton in both instances. The two metabolites were, therefore, epimers and there were clear differences in their NMR spectra with respect to the chemical shifts and coupling constants for some protons. In the NOESY spectra, there was one clear correlation between the 7-methine and glucuronide anomeric protons and this metabolite was proposed to be *R*-carisbamate glucuronide. There was no corresponding correlation evident in the NOESY spectrum of the second metabolite, which was therefore proposed to be *S*-carisbamate glucuronide.

This section has outlined the steps involved in establishing the structure of a drug metabolite by NMR spectroscopy with a few illustrative examples. The changes in the NMR spectra on the metabolism of drugs for a broader range of biotransformations including aromatic hydroxylation, epoxidation, *N*-oxidation, glutathione conjugation, methylation, sulfation, and amino acid conjugation are described by Huang et al. [76]. Exactly which experiments are needed for the structure elucidation of a metabolite will vary on a case-by-case basis. The advances in microcryoprobe technology mean that this can be usually achieved with low  $\mu\text{g}$  quantities of isolated metabolite although metabolites with limited solubility may prove more challenging and require the production of larger amounts.

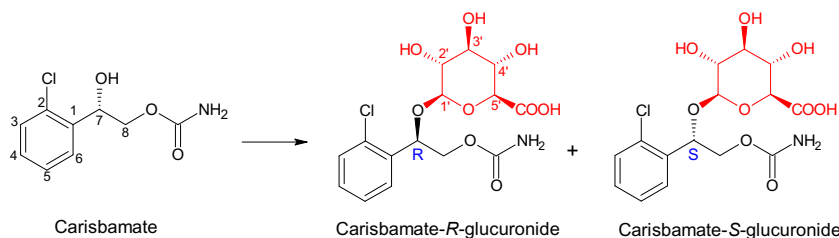


FIG. 11 Expansion of  $^1\text{H}$ - $^1\text{H}$  NOESY spectra in  $\text{DMSO-}d_6$  of (A) *R*-carisbamate glucuronide and (B) *S*-carisbamate glucuronide.

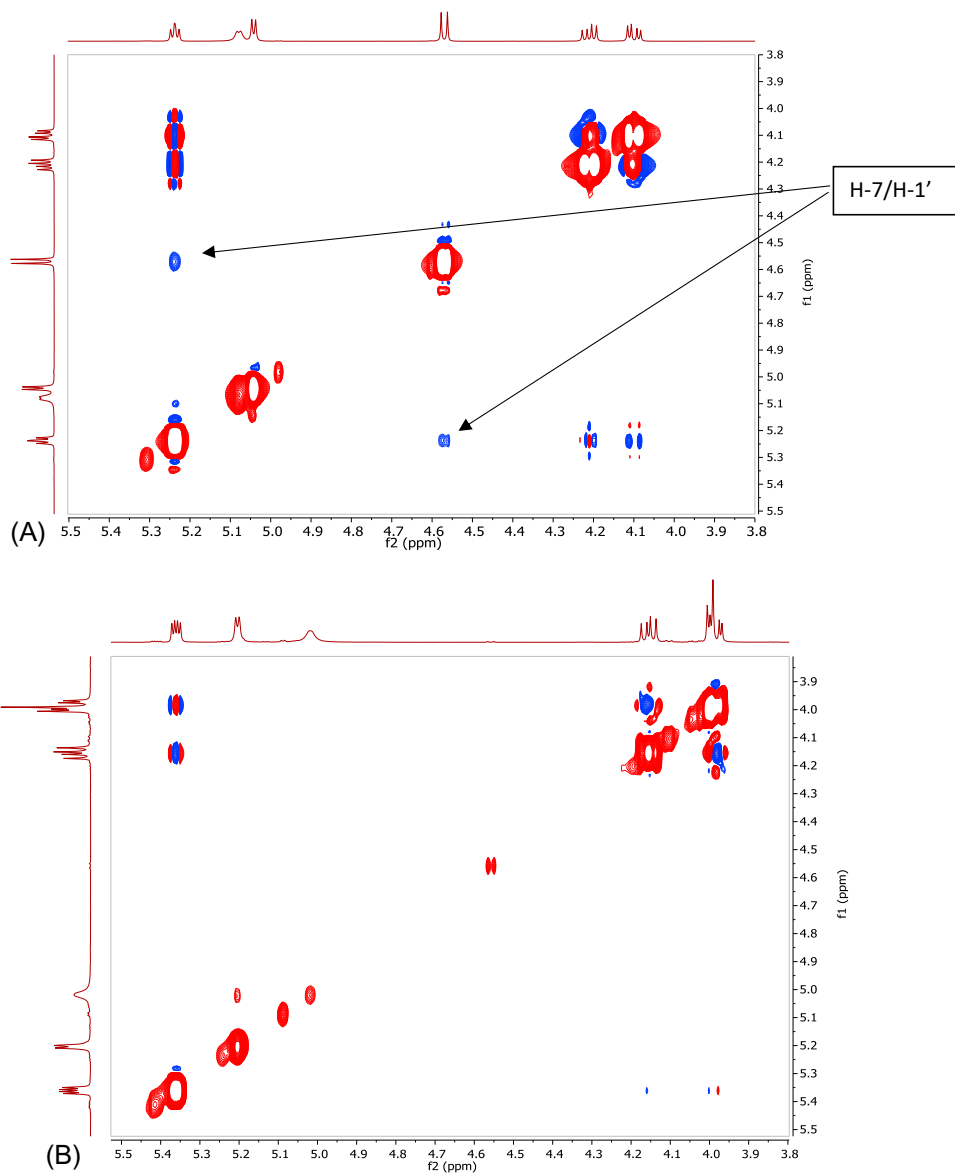


FIG. 11—Cont'd

## 4 Conclusions and future direction

A wide variety of techniques can be employed to make drug metabolites. These methods are complementary on several levels; where multiple regio- and/or stereochemical possibilities exist, biological strategies have greater relevance to the matrix where the drug is used, and hence there is a high likelihood of these strategies delivering the correct metabolite. Conversely, if a

chemical synthesis scheme is immediately available, this approach will likely be quicker and higher-yielding than the biological methods. Where chemical synthesis has not been established, biological methods can be used initially to reveal the definite structure, while providing a contingency method should chemical methods then be unsuccessfully attempted.

Establishing the identity of metabolites early can have the added benefit of flagging potential problem metabolites, such as AO metabolites, before the commencement of clinical trials. For example, oxidations of azaheterocycles by AO have been reported to contribute to high metabolic clearance and interspecies differences, resulting in the termination of several drug discovery programs in the past. In the paper by Manevski et al. [83], a recommendation is made for early consideration of AO-mediated metabolism supported by computational and *in vitro* experimental methods, but not an automatic avoidance of AO structural flags, as many of these derivatives are versatile and valuable building blocks.

The early exploration of metabolites allows ascertainment of their potential utility before the structures of the parent drugs reach the public domain, thereby strengthening protection of the intellectual property, and creating backup/second-generation development candidates. Where difficult-to-synthesize metabolites are encountered, the efforts and cost of accessing these need to be balanced against metabolite-related liabilities that may manifest as the compound advances through clinical trials. Identification, potency, and metabolic stability testing of metabolites during lead optimization could lead to the discovery of active, polar chemical space, or derivatives that possess greater metabolic stability and therefore reduce the risk of DDIs, or dosing challenges due to the action of polymorphic CYP enzymes. A consequence of the optimization of lead compounds toward metabolically stable development candidates is the potential for major and/or accumulating metabolites to manifest *in vivo* that are difficult to predict due to low *in vitro* turnover. The tools for the detection of such metabolites will evolve, while the methods described in this chapter already apply to their identification and production.

Several drugs are known to be directly metabolized by bacteria in the human gut microbiome, however, this phenomenon and the impact thereof has only just begun to be appreciated. Recent publications [84, 85] have demonstrated that human gut bacteria metabolize a significant proportion of currently used drugs. Zimmerman et al. [85] examined the ability of 76 human gut bacteria to metabolize 271 orally administered drugs and found that two-thirds were metabolized by at least one strain. Further, they showed that 30 microbiome-encoded enzymes collectively converted 20 drugs to 59 potential metabolites. Production and characterization of metabolites formed from new candidate drugs by gut microbiota and evaluation of their biological effects may become more routine as the implications of these reactions become more widely understood.

Ultimately, it is rare for even the most complicated of metabolites to be inaccessible, through the use of any one, or a combination of methods described in this chapter.

## Acknowledgments

The authors would like to thank Lisbet Kvaerno for reviewing the section on methods for chemical synthesis of metabolites and providing helpful comments. They would also like to thank Jason Boer of Incyte, Corp., for provision of information on the metabolites of epacadostat, Kazutoshi Fujioka of Albany College of Pharmacy and Health Sciences, NY, for permission to describe the work undertaken by Hypha Discovery on imidacloprid metabolites, and Lana Gabriel and Kelli Glenn of SK Life Science, Inc., for permission to describe the work on the carisbamate glucuronides.



## References

- [1] European Medicines Agency, ICH Guideline M3 (R2) on Non-Clinical Safety Studies for the Conduct of Human Clinical Trials and Marketing Authorisation for Pharmaceuticals, Available at: [http://www.ema.europa.eu/docs/en\\_GB/document\\_library/Scientific\\_guideline/2009/09/WC500002720.pdf](http://www.ema.europa.eu/docs/en_GB/document_library/Scientific_guideline/2009/09/WC500002720.pdf), 2009.
- [2] United States, Food and Drug Administration Center for Drug Evaluation and Research, Safety Testing of Drug Metabolites, Guidance for Industry, Available at: <http://www.fda.gov/downloads/Drugs/GuidanceComplianceRegulatoryInformation/Guidances/ucm079266.pdf>, 2016.
- [3] R. Scott Obach, Pharmacologically active drug metabolites: impact on drug discovery and pharmacotherapy, *Pharmacol. Rev.* 65 (2013) 578–640.
- [4] A.F. Stepan, T.P. Tran, C.J. Helal, M.S. Brown, C. Chang, R.E. O'Connor, M. De Vivo, S.D. Doran, E.L. Fisher, S. Jenkinson, D. Karanian, B.L. Kormos, R. Sharma, G.S. Walker, A.S. Wright, E.X. Yang, M.A. Brodney, T. T. Wager, P.R. Verhoest, R.S. Obach, Late-stage microsomal oxidation reduces drug-drug interaction and identifies phosphodiesterase 2A inhibitor PF-06815189, *ACS Med. Chem. Lett.* 92 (2018) 68–72.
- [5] M.A. Brodney, R. Sharma, J.T. Lazzaro, G.S. Walker, R.S. Obach, Harnessing biosynthesis and quantitative NMR for late stage functionalization of lead molecules: application to the M1 positive allosteric modulator (PAM) program, *Bioorg. Med. Chem. Lett.* 28 (2018) 2068–2073.
- [6] R.S. Obach, G.S. Walker, R. Sharma, S. Jenkinson, T.P. Tran, A.F. Stepan, Lead diversification at the nanomole scale using liver microsomes and quantitative nuclear magnetic resonance spectroscopy: application to phosphodiesterase 2 inhibitors, *J. Med. Chem.* 61 (2018) 3626–3640.
- [7] G.S. Walker, J.N. Ryder, E.B. Smith, D.K. Spracklin, R.S. Obach, Biosynthesis of drug metabolites and quantitation using NMR spectroscopy for use in pharmacologic and drug metabolism studies, *Drug Metab. Dispos.* 42 (10) (2014) 1627–1639.
- [8] K.P. Cusack, H.F. Koolman, U.E. Lange, H.M. Peltier, I. Pile, A. Vasudevan, Emerging technologies for metabolite generation and structural diversification, *Bioorg. Med. Chem. Lett.* 23 (2013) 5471–5483.
- [9] A. Li, C.C. Yuan, D. Chow, M. Chen, M.G. Emery, C. Hale, X. Zhang, R. Subramanian, D.J. St. Jean Jr., R. Komorowski, M. Veniant, M. Wang, C. Fotsch, Synthesis and evaluation of the metabolites of AMG 221, a clinical candidate for the treatment of type 2 diabetes, *ACS Med. Chem. Lett.* 2 (2011) 824–827.
- [10] R. Salter, D.C. Beshore, S.L. Colletti, L. Evans, Y. Gong, R. Helmy, Y. Liu, C.M. Maciolek, G. Martin, N. Pajkovic, R. Phipps, J. Small, J. Steele, R. de Vries, H. Williams, I.J. Martin, Microbial biotransformation—an important tool for the study of drug metabolism, *Xenobiotica* 21 (2018) 1–10.
- [11] J. Boer, R. Young-Sciame, F. Lee, K.J. Bowman, X. Yang, J.G. Shi, F.M. Nedza, W. Fietze, L. Galya, A.P. Combs, S. Yeleswaram, S. Diamond, Roles of UGT, P450, and gut microbiota in the metabolism of epacadostat in humans, *Drug Metab. Dispos.* 44 (2016) 1668–1674.
- [12] M.J. Zamek-Gliszczynski, X. Chu, J.W. Polli, M.F. Paine, A. Galetin, Understanding the transport properties of metabolites: case studies and considerations for drug development, *Drug Metab. Dispos.* 42 (2014) 650–664.
- [13] B.W. Ogilve, D. Zhang, W. Li, A.D. Rodrigues, A.E. Gipson, J. Holsapple, P. Toren, A. Parkinson, Glucuronidation converts gemfibrozil to a potent, metabolism-dependent inhibitor of CYP2C8: implications for drug-drug interactions, *Drug Metab. Dispos.* 34 (1) (2006) 191–197.
- [14] Y. Ma, Y. Fue, C. Khohasteh, D. Dalvie, D. Zhang, Glucuronides as potential anionic substrates of human cytochrome P450 2C8 (CYP 2C8), *J. Med. Chem.* 60 (21) (2017) 8691–8705.
- [15] Prescribing Information for Invokana (Canagliflozin) [https://www.accessdata.fda.gov/drugsatfda\\_docs/label/2016/204042s011lbl.pdf](https://www.accessdata.fda.gov/drugsatfda_docs/label/2016/204042s011lbl.pdf).
- [16] T.J. Jaworski, M.S. Sardessai, M. Aravagiri, G. Lin, Y.Y. Shi, E.M. Hawes, J.W. Hubbard, G. McKay, K.K. Midha, Synthesis of the N-oxides of phenothiazine antipsychotic agents, *J. Pharm. Sci.* 82 (3) (1993) 330–333.
- [17] T.J. Grinter, P. Moldt, F. Watjen, Hydrochloride Salt of An Azabicyclo[3.2.1]octane Derivative, *PCT Int. Appl., PCT/EP2008/052417, WO/2008/104584*, 2008.
- [18] J. Genovino, D. Sames, L.G. Hamann, B.B. Touré, Accessing drug metabolites via transition-metal catalyzed C–H oxidation: the liver as synthetic inspiration, *Angew. Chem.* 55 (46) (2016) 14218–14238.
- [19] A.A. Toutov, W.B. Liu, K.N. Betz, A. Fedorov, B.M. Stoltz, R.H. Grubbs, Silylation of C-H bonds in aromatic heterocycles by an Earth-abundant metal catalyst, *Nature* 518 (2015) 80–84.
- [20] A.A. Toutov, W. Liu, K.N. Betz, B.M. Stoltz, R.H. Grubbs, Catalytic C-H bond silylation of aromatic heterocycles, *Nat. Protoc.* 10 (2015) 1897–1903.
- [21] C. Cheng, J.F. Hartwig, Rhodium-catalyzed intermolecular C-H silylation of arenes with high steric regiocontrol, *Science* 343 (6173) (2014) 853–857.

- [22] J. Börgel, L. Tanwar, F. Berger, T. Ritter, Late-stage aromatic C–H oxygenation, *J. Am. Chem. Soc.* 140 (47) (2018) 16026–16031.
- [23] J. Genovino, D. Sames, B.B. Touré, Access to drug metabolites via C–H functionalization: copper-catalyzed aerobic oxidation of *N,N*-dimethylalkylamines in complex pharmaceuticals, *Tetrahedron Lett.* 56 (23) (2014) 3066–3069.
- [24] J. Genovino, S. Lütz, D. Sames, B.B. Touré, Complementation of biotransformations with chemical C–H oxidation: copper-catalyzed oxidation of tertiary amines in complex pharmaceuticals, *J. Am. Chem. Soc.* 135 (33) (2013) 12346–12352.
- [25] S.A. Shaw, B. Balasubramanian, S. Bonacorsi, J.C. Cortes, K. Cao, B.C. Chen, J. Dai, C. Decicco, A. Goswami, Z. Guo, R. Hanson, W.G. Humphreys, P.Y. Lam, W. Li, A. Mathur, B.D. Maxwell, Q. Michaudel, L. Peng, A. Pudzianowski, F. Qiu, S. Su, D. Sun, A.A. Tymiak, B.P. Vokits, B. Wang, R. Wexler, D.R. Wu, Y. Zhang, R. Zhao, P.S. Baran, Synthesis of biologically active piperidine metabolites of clopidogrel: determination of structure and analyte development, *J. Organomet. Chem.* 80 (14) (2015) 7019–7032.
- [26] A.V. Stachulski, G.N. Jenkins, The synthesis of *O*-glucuronides, *Nat. Prod. Rep.* 15 (1998) 173–186.
- [27] A.V. Stachulski, X. Meng, Glucuronides from metabolites to medicines: a survey of the *in vivo* generation, chemical synthesis and properties of metabolites, *Nat. Prod. Rep.* 30 (2013) 806–848.
- [28] D.M. Gill, L. Male, A.M. Jones, Sulfation made simple: a strategy for synthesising sulfated molecules, *Chem. Commun.* 55 (2019) 4319–4322.
- [29] A. Raghuraman, M. Riaz, M. Hindle, U.R. Desai, Rapid and efficient microwave-assisted synthesis of highly sulfated organic scaffolds, *Tetrahedron Lett.* 48 (2007) 6754–6758.
- [30] J. Hoshino, E. Park, T.P. Kondratyuk, L. Marler, J.M. Pezzuto, R.B. van Breemen, S. Mo, Y. Li, M. Cushman, Selective synthesis and biological evaluation of sulfate-conjugated resveratrol metabolites, *J. Med. Chem.* 53 (2010) 5033–5043.
- [31] R. Pernice, J. Hauder, P. Koehler, P. Vitaglione, V. Fogliano, V. Somoza, Effect of sulforaphane on glutathione-adduct formation and on glutathione *S*-transferase-dependent detoxification of acrylamide in Caco-2 cells, *Mol. Nutr. Food Res.* 53 (2009) 1540–1550.
- [32] D. Mansuy, A brief history of the contribution of metalloporphyrin models to cytochrome P450 chemistry and oxidation catalysis, *C. R. Chim.* 10 (2007) 392–413.
- [33] M.C. White, J. Zhao, Aliphatic C–h oxidations for late-stage functionalization, *J. Am. Chem. Soc.* 140 (43) (2018) 13988–14009.
- [34] T. Földi, G. Ignácz, B. Decsi, Z. Béni, G.I. Túrós, J. Kupai, D. Balogh Weiser, I. Greiner, P. Huszthy, G.T. Balogh, Biomimetic synthesis of drug metabolites in batch and continuous-flow reactors, *Chemistry* 24 (37) (2018) 9385–9392.
- [35] U. Jurva, L. Weidolf, Electrochemical generation of drug metabolites with applications in drug discovery and development, *Trends Anal. Chem.* 70 (2015) 92–99.
- [36] K.G. Madsen, J. Olsen, C. Skonberg, S.H. Hansen, U. Jurva, Development and evaluation of an electrochemical method for studying reactive Phase-I metabolites: correlation to *in vitro* drug metabolism, *Chem. Res. Toxicol.* 20 (5) (2007) 821–831.
- [37] K.G. Madsen, G. Grönberg, C. Skonberg, U. Jurva, S.H. Hansen, J. Olsen, Electrochemical oxidation of troglitazone: identification and characterization of the major reactive metabolite in liver microsomes, *Chem. Res. Toxicol.* 21 (10) (2008) 2035–2041.
- [38] T. Johansson, L. Weidolf, U. Jurva, Mimicry of phase I drug metabolism—novel methods for metabolite characterization and synthesis, *Rapid Commun. Mass Spectrom.* 21 (14) (2007) 2323–2331.
- [39] T. Gul, R. Bischoff, H.P. Permentier, Electrosynthesis methods and approaches for the preparative production of metabolites from parent drugs, *Trends Anal. Chem.* 70 (2015) 58–66.
- [40] R. Stadler, G.P. Roth, Preparative microfluidic electrosynthesis of drug metabolites, *ACS Med. Chem. Lett.* 4 (2013) 1119–1123.
- [41] T. Johansson, U. Jurva, G. Grönberg, L. Weidolf, C. Masimirembwa, Novel metabolites of amodiaquine formed by CYP1A1 and CYP1B1: structure elucidation using electrochemistry, mass spectrometry, and NMR, *Drug Metab. Dispos.* 37 (3) (2009) 571–579.
- [42] D. Dalvie, R.S. Obach, P. Kang, C. Prakash, C.M. Loi, S. Hurst, A. Nedderman, L. Goulet, E. Smith, H.Z. Bu, D. A. Smith, Assessment of three human *in vitro* systems in the generation of major human excretory and circulating metabolites, *Chem. Res. Toxicol.* 22 (2009) 357–368.

- [43] M. Clements, L. Li, Strategy of using microsome-based metabolite production to facilitate the identification of endogenous metabolites by liquid chromatography mass spectrometry, *Anal. Chim. Acta* 685 (1) (2011) 36–44.
- [44] J.M. Hutzler, B.J. Ring, S.R. Anderson, Low-turnover drug molecules—a current challenge for drug metabolism scientists, *Drug Metab. Dispos.* 43 (2015) 1917–1928.
- [45] S. Uehara, N. Murayama, H. Yamazaki, H. Suemizu, Regioselective hydroxylation of an antiarrhythmic drug, propafenone, mediated by rat liver cytochrome P450 2D2 differs from that catalyzed by human P450 2D6, *Xenobiotica* Jun 14 (2019) 1–9.
- [46] R.V. Smith, J.P. Rosazza, Microbial models of mammalian metabolism, *J. Pharm. Sci.* 64 (1975) 1737–1759.
- [47] A. Fura, Y.Z. Shu, M. Zhu, R.L. Hanson, V. Roongta, W.G. Humphreys, Discovering drugs through biological transformation: role of pharmacologically active metabolites in drug discovery, *J. Med. Chem.* 47 (2004) 4339–4351.
- [48] C.D. Murphy, Drug metabolism in microorganisms, *Biotechnol. Lett.* 37 (1) (2015) 19–28.
- [49] K. Piska, D. Zelazczyk, M. Jamrozik, P. Kubowicz-Kwasny, E. Pekala, *Cunninghamella* biotransformation—similarities to human drug metabolism and its relevance for the drug discovery process, *Curr. Drug Metab.* 17 (2016) 107–117.
- [50] R.J.P. Cannell, A.R. Knaggs, M.J. Dawson, G.R. Manchee, P.J. Eddershaw, I. Waterhouse, D.R. Sutherland, G. D. Bowers, P.J. Sidebottom, Microbial biotransformation of the angiotensin II antagonist GR117289 by *Streptomyces rimosus* to identify a mammalian metabolite, *Drug Metab. Dispos.* 23 (1995) 724–729.
- [51] D.L. Zhang, Y.F. Yand, J.E.A. Leakey, C.E. Cerniglia, Phase I and phase II enzymes produced by *Cunninghamella elegans* for the metabolism of xenobiotics, *FEMS Microbiol. Lett.* 138 (1996) 221–226.
- [52] T. Gul, M. Krzek, H.P. Permentier, M.W. Fraaije, R. Bishoff, Microbial flavoprotein monooxygenases as mimics of mammalian flavin-containing monooxygenases for the enantioselective preparation of drug metabolites, *Drug Metab. Dispos.* 44 (2016) 1270–1276.
- [53] A. Yasuhara, M. Akiba-Goto, K. Fujishiro, H. Uchida, T. Uwajima, K. Aisaka, Production of aldehyde oxidases by microorganisms and their enzymatic properties, *J. Biosci. Bioeng.* 94 (2002) 124–129.
- [54] L. Zhou, D. Satonin, J. Chappell, P. Yi, R. Moulton, S. Callies, K. Cassidy, Elimination of [14C]-LY3023414 by aldehyde oxidase and CYP enzymes in humans following oral administration, *Drug Metabol. Pharmacokinet.* 34 (1) (2019) S63.
- [55] L. Quinn, R. Dempsey, E. Casey, A. Kane, C.D. Murphy, Production of drug metabolites by immobilised *Cunninghamella elegans*: from screening to scale up, *J. Ind. Microbiol. Biotechnol.* 42 (5) (2015) 799–806.
- [56] J. Amadio, E. Casey, C.D. Murphy, Filamentous fungal biofilm for production of human drug metabolites, *Appl. Microbiol. Biotechnol.* 97 (13) (2013) 5955–5963.
- [57] M.F. Carlsen, Biosynthesis, Structural Identification and Quantification of Low pg/mL Levels of a Major Human Metabolite of a Dermal Drug Candidate—A Multidisciplinary Challenge, European Bioanalysis Forum, Barcelona, 2016. [http://www.e-b-f.eu/wp-content/uploads/2018/06/bcn2016-D2A3-2-Morten-Carlsen\\_Leo.pdf](http://www.e-b-f.eu/wp-content/uploads/2018/06/bcn2016-D2A3-2-Morten-Carlsen_Leo.pdf).
- [58] K. Schroer, M. Kittelmann, S. Lütz, Recombinant human cytochrome P450 monooxygenases for drug metabolite synthesis, *Biotechnol. Bioeng.* 106 (5) (2010) 699–706.
- [59] M. Winkler, M. Geier, S.P. Hanlon, B. Nidetzky, A. Glieder, Human enzymes for organic synthesis, *Angew. Chem. Int. Ed.* 57 (41) (2018) 13406–13423.
- [60] K. Gottfried, U. Klar, J. Platzek, L. Zorn, Biocatalysis at work: applications in the development of sagopilone, *ChemMedChem* 10 (7) (2015) 1240–1551.
- [61] G. Di Nardo, G. Gilardi, Optimization of the bacterial cytochrome P450 BM3 system for the production of human drug metabolites, *Int. J. Mol. Sci.* 13 (12) (2012) 15901–15924.
- [62] O. Ghisalba, M. Kittelmann, Preparation of drug metabolites using fungal and bacterial strains in modern biooxidation: enzymes, reactions and applications, in: R.D. Schmidt, V. Urlacher (Eds.), *Modern Biooxidation: Enzymes, Reactions and Applications*, John Wiley & Sons, 2007, p. 215. Chapter 9.
- [63] M. Landwehr, L. Hochrein, C.R. Otey, A. Kasrayan, J.E. Bäckvall, F.H. Arnold, Enantioselective alpha-hydroxylation of 2-arylacetic acid derivatives and buspirone catalyzed by engineered cytochrome P450 BM-3, *J. Am. Chem. Soc.* 128 (18) (2006) 6058–6059.
- [64] N. Beyer, J.K. Kulig, M.W. Fraaije, M.A. Hayes, D.B. Janssen, Exploring PTDH-P450BM3 variants for the synthesis of drug metabolites, *ChemBioChem* 19 (4) (2018) 326–337.
- [65] H. Shalan, M. Kato, L. Cheruzel, Keeping the spotlight on cytochrome P450, *BBA—Proteins Proteomics* 1866 (2018) 80–87.

- [66] M.R. Rashidi, S. Soltani, An overview of aldehyde oxidase: an enzyme of emerging importance in novel drug discovery, *Expert Opin. Drug Discov.* 12 (3) (2017) 305–316.
- [67] J.M. Hutzler, R.S. Obach, D. Dalvie, M.A. Zientek, Strategies for a comprehensive understanding of metabolism by aldehyde oxidase, *Expert Opin. Drug Metab. Toxicol.* 9 (2) (2013) 153–168.
- [68] D. Rodrigues, M. Kittelmann, F. Eggimann, T. Bachler, S. Abad, A. Camattari, A. Glieder, M. Winkler, S. Lütz, Production of recombinant human aldehyde oxidase in *Escherichia coli* and optimization of its application for the preparative synthesis of oxidized drug metabolites, *ChemCatChem* 6 (4) (2014) 1028–1042. Special Issue: Biocatalysis.
- [69] A. Foti, T. Hartmann, C. Coelho, T. Santos-Silva, M.J. Romão, S. Leimkühler, Optimization of the expression of human aldehyde oxidase for investigations of single-nucleotide polymorphisms, *Drug Metab. Dispos.* 44 (8) (2016) 1277–1285.
- [70] M. Ferreira Antunes, F.K. Eggimann, M. Kittelmann, S. Lütz, S.P. Hanlon, B. Wirz, T. Bachler, M. Winkler, Human xanthine oxidase recombinant in *E. coli*: a whole cell catalyst for preparative drug metabolite synthesis, *J. Biotechnol.* 235 (2016) 3–10.
- [71] M. Geier, T. Bachler, S.P. Hanlon, F.K. Eggimann, M. Kittelmann, H. Weber, S. Lütz, B. Wirz, M. Winkler, Human FMO2-based microbial whole-cell catalysts for drug metabolite synthesis, *Microb. Cell Factories* 14 (82) (2015) 1–10.
- [72] X. Wang, R. Ullrich, M. Hofrichter, J.T. Groves, Heme-thiolate ferryl of aromatic peroxygenase is basic and reactive, *PNAS* 112 (12) (2015) 3686–3691.
- [73] J. Kiebitz, W. Holla, J. Heidrich, M. Poraj-Kobielska, M. Sandvoss, R. Simonis, G. Gröbe, J. Atzrodt, M. Hofrichter, K. Scheibner, One-pot synthesis of human metabolites of SAR548304 by fungal peroxygenases, *Bioorg. Med. Chem.* 23 (15) (2015) 4324–4332.
- [74] P. Gomez de Santos, M. Cañellas, F. Tieves, S.H.H. Younes, P. Molina-Espeja, M. Hofrichter, F. Hollmann, V. Guallar, M. Alcalde, Selective synthesis of the human drug metabolite 5'-hydroxypropranolol by an evolved self-sufficient peroxygenase, *ACS Catal.* 8 (6) (2018) 4789–4799.
- [75] R.D. Crouch, M.D. Morrison, C.W. Lindsley, K.A. Emmitte, J.S. Daniels, Evaluating the disposition of a mixed aldehyde oxidase/cytochrome P450 substrate in rats with attenuated P450 activity, *Drug Metab. Dispos.* 44 (8) (2016) 1296–1303.
- [76] X. Huang, R. Powers, A. Tymiak, R. Espina, V. Roongta, Introduction to NMR and its application in metabolite structure determination, in: D. Zhang, M. Zhu, W.G. Humphreys (Eds.), *Drug Metabolism in Drug Design and Development*, John Wiley & Sons Inc., 2008, pp. 369–409.
- [77] G.S. Walker, R. Sharma, S. Wang, The role of NMR as a qualitative and quantitative analytical technique in biotransformation studies, in: P.G. Pearson, L.C. Wienkers (Eds.), *Handbook of Drug Metabolism*, third ed., CRC Press, 2019, , pp. 389–409.
- [78] G.F. Pauli, S.-N. Chen, C. Simmler, D.C. Lankin, T. Gödecke, B.U. Jaki, J.B. Friesen, J.B. McAlpine, J. G. Napolitano, Importance of purity evaluation and the potential of quantitative <sup>1</sup>H NMR as a purity assay, *J. Med. Chem.* 57 (2014) 9220–9231.
- [79] C. Weber, R. Gasser, G. Hopfgartner, Absorption, excretion and metabolism of the endothelin receptor antagonist bosentan in healthy male subjects, *Drug Metab. Dispos.* 27 (1999) 810–815.
- [80] J. Steele, A. de Riso, H. Williams, R. Phipps, S. Bardoni, C. Drake, S. Wrigley, J. Shanu-Wilson, F. Scheffler, S. Schulz, J. Ward, Human metabolites of bosentan produced by enzymes in Hypha's PolyCYPs<sup>®</sup> cytochrome P450 kit, *Drug Metabol. Pharmacokinet.* 33 (2018) S32.
- [81] K. Ohta, H. Agematu, T. Yamada, K. Kaneko, T. Tsuchida, Production of human metabolites of cyclosporin A, AM1, AM4N and AM9, by microbial conversion, *J. Biosci. Bioeng.* 99 (2005) 390–395.
- [82] G.S.J. Mannens, J. Hendrickx, C.G.M. Janssen, S. Chien, B. Van Hoof, J. Verhaeghe, M. Kao, M.F. Kelley, I. Goris, M. Bockx, B. Verreet, M. Bialer, W. Meuldermans, The absorption, metabolism and excretion of the novel neuromodulator RWJ-333369 (1,2-ethanediol, [1-2-chlorophenyl]-2-carbamate, [S-]) in humans, *Drug Metab. Dispos.* 35 (2007) 554–565.
- [83] N. Manevski, L. King, W.R. Pitt, F. Lecomte, F. Tosselli, Metabolism by aldehyde oxidase: drug design and complementary approaches to challenges in drug discovery, *J. Med. Chem.* (2019). <https://doi.org/10.1021/acs.jmedchem.9b00875>.
- [84] P. Chankhamjon, B. Javdan, J. Lopez, R. Hull, S. Chatterjee, M.S. Donia, Systematic Mapping of Drug Metabolism by the Human Gut Microbiome, *bioRxiv* 2019. <https://doi.org/10.1101/538215>.
- [85] M. Zimmermann, M. Zimmermann-Kogadeeva, R. Wegmann, A.L. Goodman, Mapping human microbiome drug metabolism by gut bacteria and their genes, *Nature* 570 (2019) 462–467.

# Application of SFC for bioanalysis

Jan Felix Joseph<sup>a,b</sup>, Maria Kristina Parr<sup>a</sup>

<sup>a</sup>Freie Universitaet Berlin, Institute of Pharmacy—Pharmaceutical Analysis, Berlin, Germany <sup>b</sup>Freie Universitaet Berlin, Department of Biology, Chemistry, Pharmacy, CoreFacility BioSupraMol, Berlin, Germany

## 1 Introduction

Supercritical fluid chromatography (SFC) represents a chromatographic separation technique, which, at present, is less well known than others like high-performance liquid chromatography (HPLC), gas chromatography (GC), or thin layer chromatography (TLC). Even if HPLC is considered as the method of choice for separation of various classes of drugs, some analytes are still challenging as HPLC shows limited resolution capabilities and highly polar analytes interact only insufficiently on the conventional analytical reversed phase columns. Especially relevant for bioanalytical methods the combination of HPLC with mass spectrometric detection, only limited possibilities for alteration in the selectivity of the stationary phase are available. SFC, which is currently valued especially in the separation of enantiomeric analytes, may help to overcome these issues.

First reports in scientific literature dated back to 1960 [1–3], when SFC was called high-pressure gas chromatography. It remained a niche technique in analytical chemistry for many years since instrumentation to achieve robust separation was not available. In these times preparative separation profited from SFC and purification of stereoisomers remained the major field for a long time [4–6]. Since the last 10 years, new generations of instruments have allowed for stable conditions suitable for analytical application and fit for purpose of SFC-based methods was also demonstrated for use in routine laboratory settings (therapeutic drug monitoring, TDM) [7–10].

In the narrow sense, SFC is characterized by the utilization of supercritical fluids as the mobile phase. In principle, any substance above its specific critical temperature and critical pressure forms a supercritical fluid. Reasonable separation may be achievable in several common solvents, out of which examples are listed in Table 1.

**TABLE 1** Solvents (examples) for potential use as supercritical fluids and their relevant properties [11].

Solvent	Tc (K)	Pc (MPa)
Carbon dioxide (CO <sub>2</sub> )	304.1	7.38
Nitrogen (N <sub>2</sub> )	126.2	3.39
Methane (CH <sub>4</sub> )	190.4	4.60
Ethylene (C <sub>2</sub> H <sub>4</sub> )	282.4	5.04
Xenon	289.7	5.84
Ethane (C <sub>2</sub> H <sub>6</sub> )	305.3	4.87
Nitrous oxide (N <sub>2</sub> O)	309.6	7.24
Sulfur hexafluoride (SF <sub>6</sub> )	318.8	3.70
Sulfur tetrafluoride (SF <sub>4</sub> )	364.0	4.63
Propylene (C <sub>3</sub> H <sub>6</sub> )	364.9	4.60
Propane (C <sub>3</sub> H <sub>8</sub> )	369.8	4.25
Ammonia (NH <sub>3</sub> )	405.5	11.4
Chloromethane (CH <sub>3</sub> Cl)	416.3	6.70
Diethylether (C <sub>2</sub> H <sub>5</sub> OC <sub>2</sub> H <sub>5</sub> )	466.7	3.64
Acetone (C <sub>3</sub> H <sub>6</sub> O)	508.1	4.70
i-PrOH (C <sub>3</sub> H <sub>7</sub> OH)	508.3	4.76
Dichloromethane (CH <sub>2</sub> Cl <sub>2</sub> )	510.0	6.30
Methanol (CH <sub>3</sub> OH)	512.6	8.09
Ethanol (C <sub>2</sub> H <sub>5</sub> OH)	513.9	6.14
Ethyl acetate (CH <sub>3</sub> COOC <sub>2</sub> H <sub>5</sub> )	523.2	3.83
Chloroform (CHCl <sub>3</sub> )	536.4	5.37
Acetonitrile (CH <sub>3</sub> CN)	545.5	4.83
Tetrachloromethane (CCl <sub>4</sub> )	556.4	4.56
Formic acid (HCOOH)	580.0	
Acetic acid (CH <sub>3</sub> COOH)	592.7	5.79
Water (H <sub>2</sub> O)	647.1	22.06

Characteristics of a supercritical fluid are seen between gases and liquids. While especially density, diffusion, and solvating power are "liquid-like," viscosity and diffusion coefficients are considered more "gas-like." Due to its relative safety, easy availability, low cost, low critical temperature and pressure, and thus convenient formation of the supercritical state, in combination with its low toxicity, carbon dioxide (CO<sub>2sc</sub>) is the most



frequently used supercritical fluid in various fields. In applied analytical SFC it is almost exclusively used, thus, SFC is also sometimes named “column chromatography using CO<sub>2sc</sub>.” CO<sub>2sc</sub> is considered as a nonpolar solvent, with a polarity similar to the polarity of hydrocarbons such as heptane. In classical SFC it is therefore used as a mobile phase in combination with polar stationary phases such as unmodified silica, offering conditions similar to normal phase HPLC. To keep the supercritical state throughout chromatography a backpressure regulator (BPR) is installed which maintains the outlet pressure above ambient conditions. Changes in temperature and/or pressure result in a strong impact in elution strength, thus early applications were performed using pressure or temperature gradients [12–14]. Although some physicochemical properties in SFC still remain unclear [15, 16], it currently returns to analytical sciences since a lot of effort has been made in optimization of instrumentation [17]. Very precise outlet pressure regulation is required to allow stable retention times, which is achieved in the latest generation of analytical SFC instrumentation.

To broaden the scope of analytes, organic modifiers may be added to the mobile phase. At present, commercial instrumentation offers two pumps, allowing for application of binary gradients or isocratic elution with variable amounts of the modifier. Named in analogy to HPLC as mobile phase A, CO<sub>2sc</sub> is generally utilized, while modifiers represent mobile phase B. For modifiers complete miscibility with CO<sub>2sc</sub> is recommended, however even small amounts of water are tolerated. To modify the elution strength of the mobile phase organic solvents are generally selected by the help of their Snyder’s *P*’ or Hildebrand values. Most commonly, primary alcohols are used, with methanol (MeOH) as dominating modifier. According to Smith et al. [18], analyte-modifier-clusters are formed, that change retention, however, alterations of the stationary phase chemistry are also discussed [19, 20]. Recently reported SFC methods for bioanalysis often utilize high amounts of modifier that may result in a loss of supercritical state of the mobile phase. However, at present, these types of separation are still subsumed under SFC by the international community.

Furthermore, the addition of further compounds to the mobile phase (so-called additives) is reported to optimize chromatographic separation especially in the case of highly polar substances such as acids or bases. Almost independent from the utilized additives slightly acidic conditions are obtained in SFC [21]. Thus, several mechanisms are discussed as relevant for factors of influences on chromatographic separation by modifier and additives. In comparison with other chromatographic techniques, SFC is especially valued for its fast and efficient separation, orthogonality and environmental friendliness (“green technique”) [22–30]. Published SFC methods report successful separations of analytes (mainly small molecules) of a very broad polarity range, i.e., log *P* or log *D* (pH 5.5) between –7 and +10 [31–36].

As reported by West et al. bioanalysis represents the second most important application domain of SFC besides natural product analysis [37] and increasing numbers of bioanalytical studies are reported by Dispas et al. [28].

To meet the analytical target profile of trace level analyses hyphenation with MS is required in lots of bioanalytical applications. General considerations and currently available instrumental designs are available from review papers of Guillarme et al. and Tarafder [38, 39].



## 2 Considerations for SFC method development

In contrast to the almost generic stationary phase such as C18 in reversed phase HPLC, there is no all-round stationary phase chemistry for SFC. Stationary phase chemistry is various and should match the chemistry of the analytes. Thus, stationary phase screening is a crucial step in method development. Initial screening of stationary phase using either isocratic or gradient elution usually precedes optimization of mobile phase (modifier and additive(s)), temperature, pressure, and flow rate. Recently, screening using a one-factor-at-a-time (OFAT) design is more often replaced by a design of experiments (DoE) approach [34, 40, 41].

In general, most columns developed for HPLC are also compatible with SFC. The first exclusive SFC phase was a 2-ethylpyridine (2-EP) bonded silica phase, which may result in better peak shapes for basic compounds without the need for an additive. SFC stationary phases are predominantly silica-based without end-capping of the residual silanol groups which may be important in terms of selectivity and retention. However, reactions between modifier and free silanol groups leading to silyl ether formation may shorten the lifetime of the column. Therefore, it may be desirable to use a small portion of water in the modifier and store the column in pure CO<sub>2</sub> [42]. Today there are various SFC phases on the market, but the 2-EP phase is still the most common in general achiral SFC applications besides bare silica, C18, and diol [37], which is also true for recent bioanalytical applications. West and Lesellier conducted comprehensive studies on the characterization of stationary phases [43–45].

Even more pronounced in chiral separations, the column selection is a key factor in method development. The most frequently used chiral selectors in SFC are cellulose and amylose polysaccharide derivative-based columns, with cellulose tris(3,5-dimethylphenylcarbamate), amylose tris(3,5-dimethylphenylcarbamate), and amylose tris(5-chloro-2-methylphenylcarbamate) being the most popular chiral stationary phases (CSPs) [46, 47]. As also for achiral SFC, CSP screening should include a wide set of orthogonal stationary phase chemistries. In recent chiral bioanalytical applications, 93% of the CSPs were polysaccharide based with amylose (54%) being employed more often than cellulose (38%). Still, the choice of appropriate columns remains challenging and more effort in CSP screening strategies is needed [48, 49].

Since 2012, the use of columns packed with particles <2 μm (sub-2-micron) started to increase [37]. In recent achiral, bioanalytical applications (since 2015), the majority used sub-2-micron columns (85%, Fig. 1). However, Berger stated that the benefits of sub-2-micron particles for ultrafast separations would need a reduction of extra column dispersion and thus, modification of the SFC system (by using capillaries with a smaller diameter) [50]. In addition, recent studies by Ismail [51] and Perrenoud [52] demonstrated the need for modification of a commercial SFC system to gain efficiency. Superficially porous particles (SPP) enable high efficiency using longer columns by producing less pressure drop which is even more important for running high modifier content at high flow rates. Several columns with SPP with different stationary phase chemistries show great potential for SPP phases in SFC [36, 53].

The second most important variable is the cosolvent or modifier, which can influence the separation in several ways [54]:

- alteration of density and solvating power of the mobile phase,
- blockage of active sites on the stationary phase and inhibition of adsorption,
- action of adsorbed modifier as a component of the stationary phase,

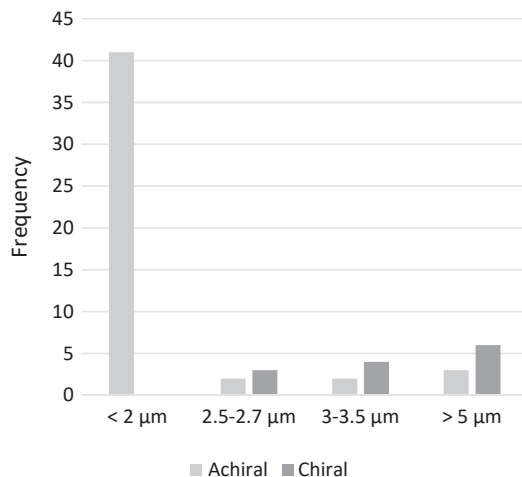


**FIG. 1** Particle size of achiral and chiral columns used in recent bioanalytical SFC methods (2015–19).

- increasing volume of the stationary phase by adsorbed modifier leading to a change in the column phase ratio, and
- selective solvation of polar compounds in the mobile phase with the formation of clusters with different distribution properties.

Methanol is usually the first choice and applied in the majority of analytical SFC applications [37, 55]. Its high eluotropic strength leading to higher separation efficiency is demonstrated by its usage (solely or in combinations) in almost 87% of recent bioanalytical methods (Fig. 2). MeOH alone as a modifier with or without additive is used in half of the

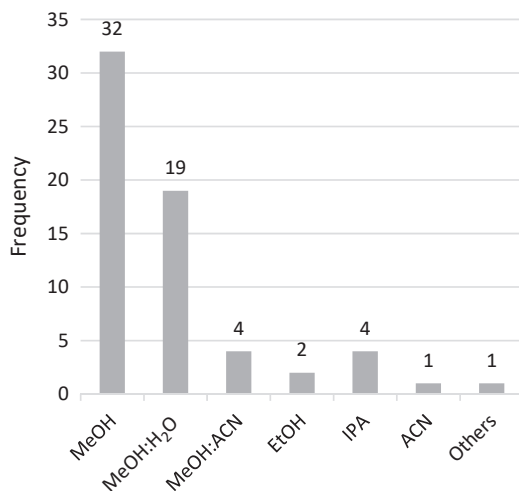


**FIG. 2** Different modifier applied in recent bioanalytical SFC methods (2015–19).

bioanalytical methods (51%, Fig. 2). However, the use of a combination of MeOH with small amounts of water is increasing (30%). Water may have various effects such as enhancing the solvating power of the mobile phase [56] as well as protecting the column (see above). Utilization of acetonitrile (ACN) as modifier might be interesting as well due to its unique selectivity. It is usually applied in mixture with alcohols (6%); pure ACN is rarely applied (2%). Ethanol may be considered as a green alternative to methanol and was used in 3% of the discussed methods. Isopropanol was applied as a modifier in 6% of the bioanalytical applications, mostly in chiral separations.

Effects of mobile phase composition on retention and selectivity in achiral SFC were recently reviewed by West et al. [57]. Mobile phase composition is a crucial parameter for optimization in chiral SFC and is usually selected early in the method development process [57]. Mobile phase gradients in super- or subcritical fluid chromatography up to modifier concentrations of 40%–50% are common. Recently, the use of very high modifier concentrations up to 100% is reported [36, 58]. It is needless to mention that the final gradient status does not represent the physicochemical conditions of a supercritical fluid. Taguchi et al. described a method starting at SFC conditions, touching the enhanced-fluidity liquid chromatography (EFCL) region, where CO<sub>2</sub> is the minor component of the mobile phase [59], and finishing at pure liquid (MeOH:water, 95:5) [58]. Those chromatographic conditions are sometimes reported as ‘unified chromatography’ and seem to be increasingly applied [36, 60, 61].

As mentioned before, many methods use pure methanol as a modifier, but often there is a need for additives to improve peak shape or selectivity. Most common additives are organic acids (formic acid, acetic acid, trifluoroacetic acid), bases (ammonia, triethylamine), or salts thereof (ammonium formate, ammonium acetate). Analysis of ionized compounds and SFC-MS hyphenation often benefits from the use of ammonium formate [62]. Generic approaches combining basic and acidic additives or buffers are being increasingly used. An important role in most bioanalytical applications is MS compatibility of the additives, thus, almost exclusively volatile buffers are used, although separation efficiency and, in case of chiral analysis, enantioselectivity may suffer [55].

Since most bioanalytical methods require low detection limits, mass spectrometric detection is clearly favored. To ensure sufficient ionization, for example, in electrospray ionization (ESI), and to avoid precipitation of the analytes after the relief of the compressed mobile phase of the SFC system in the ion source, a makeup solvent may be used. If a makeup solvent is applied, mostly MeOH with or without additive analogously to the modifier is used. An advantage over conventional HPLC-ESI-MS(/MS) instruments is the possibility to optimize makeup solvent type and flow-rate, independently from the modifier. This may result in improved ionization and thus sensitivity while having no influence on the chromatographic selectivity [31]. For instance, Fassauer and Hofstetter achieved enantioseparation of ketamine and three metabolites using isopropanol modified with 0.075% ammonia, while employing 0.1% formic acid in MeOH as makeup solvent to increase ionization [63, 64]. Akbal et al. even found that DMSO as a makeup additive up to 30% with MeOH had a positive effect in positive electrospray yielding DMSO/sodium adducts [65]. As makeup solvents mostly MeOH or mixtures with water are reported in bioanalytical methods. Only a few studies describe the use of ethanol, pure water, or isopropyl alcohol.

According to Dispas the nature of the injection solvent is another critical parameter of method optimization [62]. Since the mobile phase is largely composed of apolar CO<sub>2sc</sub>, organic solvents similar to CO<sub>2</sub> in terms of polarity were used (e.g., n-hexane) with certain

drawbacks as toxicity and volatility. Aprotic solvents with low viscosity are beneficial for large volume injections. Lower volatility in the case of ACN might be advantageous in case of quantitative analyses. Overall, as first choice, ACN or t-butyl methyl ether is highly recommended. Choice of injection solvent should be part of method development and depends on analyte and stationary phase [66]. After all, the use of organic solvents might be beneficial for bioanalytical applications since common sample preparation techniques such as solid phase extraction (SPE) or liquid-liquid extraction (LLE) use organic solvents, and a potential evaporation step required in some LC methods might be omitted.

Validation of bioanalytical methods according to guidelines of EMA and FDA is desirable but, until now, infrequently reported or methods are poorly validated [28]. However, validated analytical methods are already used (e.g., Refs. [7, 8, 67, 68]). Dispas et al. reported the first interlaboratory study including 19 laboratories in a pharmaceutical impurity testing context. Their evaluation of the detection of impurity D of salbutamol sulfate API by SFC-PDA showed similar or better reproducibility and repeatability compared to LC methods [69]. There are only a few systematic studies on matrix effects (ME) in SFC or comparison of ME in SFC and HPLC in combination with mass spectrometric detection (mainly utilizing ESI). Generally, ME seems to be lower in SFC, but further investigations with other analytes and matrices are required [28]. Desfontaine et al. evaluated matrix effects in SFC vs LC hyphenated to tandem mass spectrometry (MS/MS) using different sample preparation techniques for urine and plasma samples. They investigated two sample sets of 40 doping agents and 38 pharmaceutical compounds with three different stationary phase chemistries (2-PIC, BEH, C18) and concluded that ME for urine analysis were lower in SFC, and for plasma only after SPE clean up [70]. Also, Svan et al. reported a study on ME comparison between SFC and LC and found that the formation of metal ion clusters ( $\text{Na}^+$ ,  $\text{K}^+$ ,  $\text{Mg}^{2+}$  from different matrices) in SFC-ESI-MS may lead to unexpected ion suppression [71]. This should be considered during validation processes [72].

To sum up considerations for SFC method development, as a general starting point, a scouting gradient with a small amount of modifier (e.g., 5% MeOH) increasing to 50% modifier in 10 min is recommended to screen for a suitable stationary phase [73]. Subsequently, the same gradient is used to screen different modifiers and additives with the selected stationary phase, before adjusting column temperature which may influence selectivity. Then, gradient, flow rate (which affects pressure), and backpressure can be optimized individually [74]. A generic temperature and backpressure of 40°C and 150 bars might be a suitable first choice [75]. The makeup solvent and flow rate should be optimized accordingly. Further information on screening strategies is available from the literature [75–78]. Even if modern rational method development becomes more relevant in SFC, quality-by-design approaches are still underrepresented and structure-based predictions for method development lack of understanding of retention mechanisms.

---

### 3 Detection in SFC

---

Today mostly UV and MS detection are combined with SFC. While UV detection is more prominent in, e.g., pharmaceutical analysis, detection of trace levels or biological

matrices clearly favor mass spectrometry using common atmospheric pressure ionization sources. A detailed overview of SFC-MS hyphenation is provided by Desfontaine [79].

Exclusive UV detection is less common in bioanalytical methods. Still, the analysis of sulfonamides in serum samples [80] as well as cannabinoids in human urine [81] by SFC-UV are reported. A few studies use additional UV detection, e.g., prior to single quadrupole MS detection for tocopherols and tocotrienols in human serum [82], or MS/MS detection for various urinary metabolites [35]. The two-dimensional setup (LCxSFC) of Venkatramani and Goel used UV detection in the first dimension and single quadrupole MS detection in selected ion monitoring (SIM) mode in the second dimension [83, 84]. Goel et al. applied this setup for chiral separation of *in vitro* generated metabolites of an active pharmaceutical ingredient (API) [83].

As mentioned above, hyphenation of SFC with mass spectrometry is possible with common atmospheric pressure ionization sources [79]. The need for pressure control of the SFC system led to the development of different ways to interface SFC and MS instruments [38, 39]. In the most common interface, the (optional) UV detector is located right after the column followed by a dual splitter where an isocratic pump adds makeup solvent to the mobile phase and, subsequently, after splitting the flow again, one part of the mobile phase is directed into the MS, while the rest is directed to the BPR. Splitless hyphenation allowing the complete transfer of the sample into the MS was made available only recently [38]. Further details of SFC-MS hyphenation are available from Desfontaine et al. [85].

The vast majority of bioanalytical methods utilizes ESI (Fig. 3). Only a few methods report the use of atmospheric pressure chemical ionization (APCI), especially when very apolar compounds are analyzed. APCI was more common in earlier bioanalytical SFC methods, e.g., for the analysis of propranolol and pindolol [86], warfarin enantiomers [87], or metabolites of estrogens [88]. Still, a few recent studies used and/or compared different ionization sources in bioanalytical context. Wolrab et al. compared ESI and APCI for the analysis of amino acids

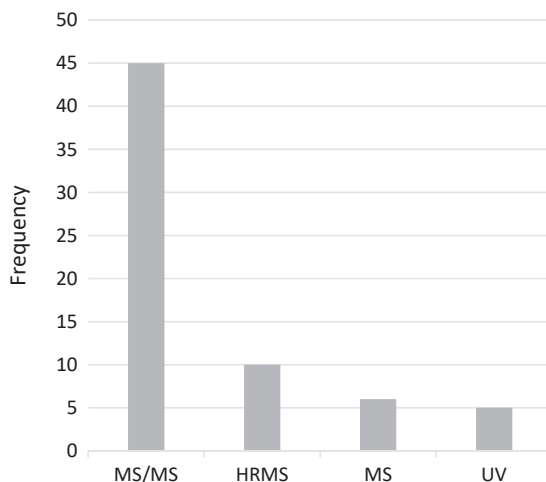


FIG. 3 Detection in recent bioanalytical SFC applications (2015–19).

and favored ESI, however, APCI was found more suitable for polar amino acids and apolar amino acids with an additional heteroatom [89]. In contrast, Jumaah et al. found ESI to be more sensitive for the analysis of vitamin D and its metabolites in human plasma [90]. Gross et al. developed a method to detect 22 hydroxylated polybrominated diphenyl ethers in human serum by SFC-MS/MS using ESI but tested APCI in early method development phase [91]. As APCI was found less sensitive in this study, they proceeded with ESI for further experiments. Similar findings were reported by Liu et al. [92] for vitamin D and its metabolites. Although no bioanalytical matrix was analyzed therein, Parr et al. tested the applicability of different atmospheric pressure ionization sources in combination with SFC for a set of 32 endogenous steroids. They compared ESI, APCI, and atmospheric pressure photoionization (APPI) and found ESI to be most suitable for the set of analytes [93]. In an experimental setup, Klink et al. developed a method for the detection of polycyclic aromatic hydrocarbons (PAHs) in human urine using another ionization technique—atmospheric pressure laser ionization (APLI) SFC-TOF-MS [94].

In summary, ESI remains the most prominent ionization source when using SFC-MS, while APCI may be beneficial in some cases due to the extended dynamic range compared to ESI as well as generally lower matrix effects [71, 72]. Some analytes (e.g., 5 $\beta$ -pregnane-3 $\alpha$ , 20 $\alpha$ -diol, basic and aromatic amino acids as well as tryptophane or tyrosin) even result in better ionization when analyzed by SFC-APCI-MS [89, 93].

Regarding the type of MS instruments coupled with SFC for bioanalysis, tandem mass spectrometers are the instrument of choice and applied in the majority of reported methods (Fig. 3). Until now, high-resolution accurate mass spectrometry (HRMS) coupled with SFC is less common than triple quadrupole or ion trap detection. Still, HRMS has been used in different fields such as food or natural product analysis [95–103]. Bioanalytical methods applying HRMS mainly focus on metabolomics, especially lipidomics, where orbitrap [104, 105] or time-of-flight (TOF) analyzers [106, 107] are reported.

## 4 Sample preparation

Sample preparation is an important part of bioanalytical method development. Common techniques include simple dilute and shoot (DS), protein precipitation (PP), LLE, and SPE, with or without evaporation. Advantageous in SFC is the possibility to inject organic solvents in the apolar mobile phase. There is no need for evaporation of organic solvent and reconstitution in the aqueous-organic mixture such as in RP-HPLC. Online coupling of sample preparation in SFC is less common than in LC. Supercritical fluid extraction (SFE) and SPE are the two major sample preparation techniques applied in SFC. Online SPE-SFC has been useful in water analysis (e.g., for analysis of pesticides, phenolic compounds, PAHs, or other common contaminants), but dates back to the 1990s [108]. More recently, online SFE-SFC has been applied in different fields of bioanalysis, directly extracting analytes from dried blood spots in case of phospholipid profiling [109] or disease biomarker profiling for colorectal cancer [110]. SFE-SFC-MS/MS analysis of carotenoids in intact human blood samples was reported by Zoccali et al. [111], whereas, Hofstetter described the potential for SFE in case of dried urine as specimen [64].

## 5 Examples

Bioanalytical applications of SFC include forensics, pharmacokinetic studies (of pharmaceuticals), TDM, metabolomics, and lipidomics. The use of SFC is increasing in all fields of bioanalysis. Several recent reviews cover bioanalytical SFC applications in general [28, 37, 47, 112], with focus on metabolite analysis [113, 114] or chiral separations [46], forensics [115], analysis of lipids [116–118], clinical analysis [119], and metabolomics [120]. A set of the most recent publications will be discussed here in more details covering publications of SFC applications in different biological matrices between 2015 and 2019 (Fig. 4).

### 5.1 Drugs of abuse, doping control, and toxicological analysis

SFC-MS/MS is being used for the analysis of drugs of abuse in forensic environments and prohibited substances according to antidoping regulations (Table 2). Recent forensic applications of SFC include the analysis of (synthetic) cannabinoids, chiral separation of amphetamine enantiomers, and analysis of different new psychoactive substances (NPS) [8, 81, 121, 122]. Geryk et al. developed a SFC-UV method using rather less conventional pure ACN as mobile phase modifier for the analysis of natural and synthetic cannabinoids and their metabolites in human urine after desalting using assisted LLE [81]. Limit of quantification (LOQ) values ranged from 0.50 to 1.73  $\mu\text{g}/\text{mL}$  in spiked urine samples. When using tandem mass spectrometric detection and positive ESI, Berg et al. reported that the sensitivity increased by 10-fold after LLE and deconjugation of potential glucuronides [121]. The authors detected two synthetic cannabinoids along with 11 metabolites in less than 7 min using 0.3% ammonia in MeOH as a modifier. To distinguish between therapeutic amphetamine administration and illegal abuse, the determination of the enantiomeric ratio might be helpful. Therefore, Hegstad et al. developed and validated a chiral high-throughput SFC-MS/MS method for R/S-amphetamine in human urine [8]. The separation was accomplished within

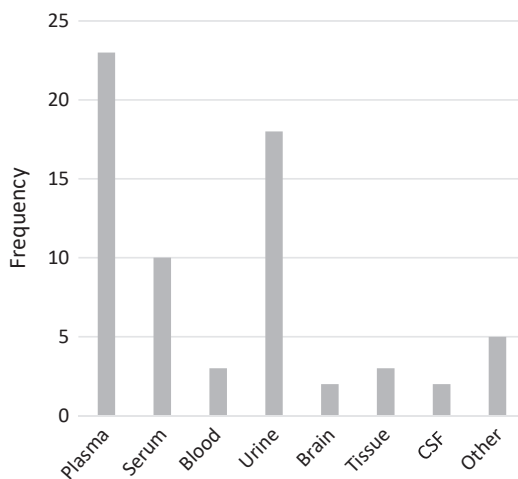


FIG. 4 Reported matrices investigated in recent bioanalytical SFC application.



**TABLE 2** Recent SFC applications in the field of drugs of abuse, doping control, and toxicological analysis.

Analyte(s)	Matrix	Column	Mobile phase	Detection	Reference
Cannabinoids	Human urine	Zorbax Rx-Sil 150 × 4.6 mm, 5 μm	ACN	UV	[81]
Synthetic cannabinoids	Human urine	BEH 100 × 3.0 mm, 1.7 μm	MeOH NH <sub>3</sub> , 0.3%	MS/MS ESI pos	[121]
R/S-amphetamine	Human urine	Chiralpak AD-3 150 × 2.1 mm, 3.0 μm	IPA cyclohexylamine, 0.2%	MS/MS ESI pos	[8]
NPS	Human urine	BEH 100 × 3.0 mm, 1.7 μm	MeOH NH <sub>4</sub> FA, 20 mM	MS/MS ESI pos	[122]
Phosphatidylethanolols	Human Whole blood	2-PIC 50 × 2.1 mm, 1.7 μm	MeOH NH <sub>3</sub> , 0.1%	MS/MS ESI neg	[124]
31 doping substances	Human urine	BEH 100 × 3.0 mm, 1.7 μm	MeOH:water, 98:2 NH <sub>4</sub> FA, 10 mM	MS/MS ESI pos/neg	[125]
110 doping substances	Human urine	BEH 100 × 3.0 mm, 1.7 μm	MeOH:water, 98:2 NH <sub>4</sub> FA, 10 mM	MS/MS ESI pos/neg	[126]
100 doping substances	Human urine	Torus Diol 100 × 3.0 mm, 1.7 μm	MeOH:water, 98:2 NH <sub>4</sub> FA, 10 mM	MS/MS ESI pos	[74]
43 doping substances	Human urine	Torus Diol 100 × 3.0 mm, 1.7 μm	MeOH:water, 98:2 NH <sub>4</sub> FA, 10 mM	MS/MS ESI pos	[29]
Polar analytes	Human urine	BEH 2-EP 100 × 3.0 mm, 1.7 μm	MeOH:water, 96.5:3.5 NH <sub>4</sub> Ac, 5 mM	MS/MS ESI pos/neg	[23]
Clenbuterol enantiomers	Human urine	Astec chirobiotic V2 150 × 4.6 mm, 5 μm	MeOH FA, 0.1%, NH <sub>3</sub> , 0.1%	MS/MS ESI pos	[127]
4 SARMs	Bovine urine	BEH 100 × 3.0 mm, 1.7 μm	MeOH FA, 0.1%, NH <sub>4</sub> HCO <sub>3</sub> , 20 mM	IM-HRMS/ MS ESI neg	[128]
Acetyl-gestagens	Bovine and porcine kidney fats	HSS C18 100 × 3.0 mm, 1.7 μm	MeOH	MS/MS ESI pos	[129]
PHDPE	Human serum	Torus Diol 100 × 2.1 mm, 1.7 μm	IPA	MS/MS ESI	[91]
PAH	Human urine	Zorbax Rx-Sil, Zorbax Eclipse PAH 150 ×, 4.6 mm, 5 μm, 250 × 4.6 mm, 5 μm	MeOH	HRMS APLI	[94]

6 min using amylose tris-(3,5-dimethylphenylcarbamate) as chiral selector. In another study, 15 different NPS from the group of cathinones and phenylethylamines were separated in less than 3 min using SFC-MS/MS (total runtime 10 min) by Pauk et al. [123]. Borovcova adapted this method and compared the SFC- with a LC-MS/MS setup for the analysis of human urine samples [122]. They applied a simple dilute-and-shoot procedure with isopropyl alcohol as sample preparation reaching a sensitivity ranging from 0.02 to 5.15 ng/mL as limit of detection (LOD) for the SFC method. Compared to the LC-MS/MS method only a few compounds were reported as less sensitive in the applied SFC-MS/MS method. The authors state that protonation may be less effective in SFC for those compounds with highest  $pK_a$  values. We assume that this may be even improved by the use of additives in the mobile phase of SFC.

To monitor alcohol consumption, the analysis of direct markers (ethyl glucuronide or ethyl sulfate) with short detection windows is considered as gold standard. To extend the detection window and detect chronic alcohol consumption indirect markers such as phosphatidylethanol, abnormal phospholipids only formed in the presence of alcohol, may be a suitable alternative. Van der Nagel et al. reported the development and validation of a SFC-MS/MS method for the analysis of three prominent phosphatidylethanol in whole blood as a marker for alcohol consumption [124]. A volume of 50  $\mu$ L blood was treated with ethyl acetate and injected into the SFC system after centrifugation. Separation of the three analytes and one internal standard was achieved on a short 2-PIC column (50  $\times$  2.1 mm, 1.7  $\mu$ m) and 0.1% ammonia in MeOH as a modifier. The same solvent was used as makeup to enhance signal intensity in negative ESI. In conclusion, the authors stated that their method provided high sensitivity (LLOQ 3.0–6.0 ng/mL), short analysis time (4.2 min), and was fit to be applied in clinical practice.

In the context of doping control analysis, SFC has already been applied for large sets of compounds. Due to its high separation efficiency, SFC enables screening of hundreds of different classes of analytes. Novakova et al. developed a screening method for more than 100 substances. In the first part of their study, the authors optimized the method based on a representative set of 31 acidic and basic analytes and compared SFC-MS/MS with LC-MS/MS. In SFC, chromatographic performance optimum was found using gradient mode on a BEH stationary phase (100  $\times$  3.0 mm, 1.7  $\mu$ m), 2% water in MeOH as mobile phase modifier and ammonium formate (10 mM) as additive. The best compromise for MS response was obtained using ethanol as makeup solvent for positive and negative ESI. For more than 50% of the tested compounds, SFC-MS/MS was found to be more sensitive than LC-MS/MS, while the remaining analytes showed no significant differences except for bumetanide, which yielded a higher MS response in LC-MS/MS [125]. The second part of the study focused on the analysis of 110 doping substances in urine samples, again, comparing SFC and LC. For SFC, optimization of injection solvent, a critical step during method development, resulted in a mixture of 25% water in ACN for dilute and shoot sample preparation. In the end, SFC was found to be more sensitive for the majority of the compounds and matrix effects were less prominent compared to LC making SFC a promising alternative for screening purposes in doping control analysis [126]. In another study, the same group aimed to develop another screening method for the detection of 100 compounds, belonging to the classes of anabolic agents, hormones and metabolic modulators, synthetic cannabinoids and glucocorticoids, in urine. For sample preparation, supported liquid extraction was beneficial to extract the 100 different analytes from the matrix. The separation was achieved on a Diol

column (100 × 3.0 mm, 1.7 μm) after testing eight different stationary phases. The same modifier and additive as in the previous two studies were used along with pure MeOH as a makeup solvent for exclusive positive ionization (ESI). Also, the same gradient was used with a slightly slower flow rate of 1.3 mL/min. The LODs obtained by this method were better than the minimum required performance levels except for three analytes [74].

Desfontaine et al. compared the performance of GC-, HPLC-, and SFC-MS/MS for the detection of 43 different anabolic agents in human urine [29]. The development of two methods (SFC- and LC-MS/MS) with regard to sample preparation, stationary phase, mobile phase, and MS conditions is reported. Both methods required SLE as sample pretreatment. For SFC, the separation was achieved using the same conditions as reported by Novakova et al. [74]. Overall, compared to GC-MS/MS analysis, which requires deconjugation of glucuronides, LLE, and derivatization, the LC- as well as the SFC-MS/MS method were advantageous in terms of analysis time, sensitivity, and matrix effects. The LC-MS/MS method showed the best sensitivity for most of the analytes whereas SFC had the weakest matrix effects.

A large set of polar analytes including metabolites was investigated by Parr et al. [23]. The authors compared the retention in RPLC, HILIC, and SFC in their study and found expected orthogonal retention for SFC which was beneficial for the analysis of the polar analytes. The optimized SFC-MS/MS method applied a BEH 2-EP column (100 × 3.0 mm, 1.7 μm) along with MeOH:water (96.5:3.5, v/v) and ammonium acetate (5 mM) as mobile phase modifier and additive as well as makeup solvent for tandem mass spectrometric detection.

In another study, the authors discriminated clenbuterol enantiomers by means of SFC-MS/MS. Clenbuterol is misused by athletes as well as in cattle breeding to increase muscle mass due to its anabolic side effects. Reports of adverse analytical findings resulting from consumption of contaminated meat complicate proper doping control analysis. Since the enantiomeric composition in the meat may be altered during body passage and tissue distribution while it persists after clenbuterol administration to humans, the enantioseparation may be helpful to distinguish intentional from unintentional administration. Chiral separation within 4 min was performed using a vancomycin-based CSP (150 × 4.6 mm, 5 μm) and MeOH with the addition of 0.1% formic acid and ammonia, respectively, as modifier [127].

Four different nonsteroidal selective androgen receptor modulators (nonsteroidal SARMs) in bovine urine were analyzed by SFC-HRMS as reported by Beucher et al. [128]. SARMs are under investigation for therapeutic use, but still exhibit anabolic effects which may be misused in sports as well as in livestock production as growth hormones. In their study, the authors present the benefit of combining SFC and ion-mobility HRMS using negative ESI for the detection of andarine, bicalutamide, hydroxyflutamide, and enobosarm. The latter was successfully analyzed after administration to a male calf.

In a toxicological context, Tao et al. analyzed growth-promoting hormones for food-producing animals in bovine and porcine kidney fats. The acetyl-gestagens were concentrated by SPE prior to analysis and separated using a C18 column and gradient elution. MeOH was used as modifier without additive, whereas MeOH with the addition of 0.1% formic acid was applied as makeup solvent. All seven analytes were separated within 5 min [129].

Although the analysis of environmental pollutants is not considered to be part of bioanalysis in here, the methods developed by Gross and Klink are briefly mentioned since

they cover bioanalytical matrices. Gross et al. separated 22 hydroxylated polybrominated diphenyl ethers (OH-BDEs) in human serum by SFC-MS/MS using ESI [91]. A gradient up to 25% isopropyl alcohol in CO<sub>2</sub> separated the analytes on a Torus Diol column (100 × 2.1 mm, 1.7 μm) within 14 min. Pure MeOH was used as makeup solvent at a rather high flow rate of 0.9 mL/min. 1-HP (1-hydroxypyrene), a hydroxylated metabolite of the polyaromatic hydrocarbon (PAH) pyrene was detected by Klink et al. in human urine. In their experimental setup using SFC-APLI-TOF-MS without derivatization a LOD of 0.5 ng/mL was possible [94].

## 5.2 Pharmaceuticals and clinical analysis

The analysis of pharmaceuticals in the biological specimen by SFC and its application for clinical analysis is another prominent area of bioanalytical SFC applications (Table 3). The fast analysis times that can be accomplished by SFC are beneficial for high-throughput methods for pharmacokinetic studies during drug development or especially TDM in a clinical context.

Zhang et al. reported the analysis of 15 sulfonamide antibiotics and their acetylated metabolites in human serum after simple protein precipitation using SFC-UV. The separation was accomplished within 7 min using ethanol as a modifier in gradient mode. Thereby, the authors provided a relatively sensitive (LOD 0.15–0.35 μg/mL) and green method [80].

In the domain of enantioseparation, where SFC was always favored, several studies proved this fact. A fast separation of racemic cetirizine in human plasma was reported by Eom et al. The authors applied a relatively low flow rate of 0.85 mL/min and isocratic elution using 95% MeOH in water as a modifier. Human plasma samples were prepared by means of SPE followed by tandem mass spectrometric detection, which resulted in slightly higher sensitivity than former methods (LOQ 0.2 ng/mL). The developed method was subsequently applied to a pharmacokinetic study comparing the administration of levocetirizine and racemic cetirizine [130]. Another chiral method was developed by Hegstad et al. where the authors separated citalopram enantiomers in human serum with the purpose of TDM. Since both enantiomers exhibit different potency and are available in different therapeutic formulations (containing racemic citalopram or S-citalopram only), knowledge about the actual serum concentration may be quite useful for clinicians. The SFC-MS/MS setup used a cellulose tris-(3-chloro-4-methylphenylcarbamate) stationary phase (150 × 2.1 mm, 2.5 μm), a mixture of MeOH and ACN as a modifier, and isopropyl alcohol containing 0.1% ammonia as makeup solvent being faster (4 min runtime) than comparable HPLC methods (12–45 min). A full validation according to FDA guidelines allowed the successful implementation in a routine laboratory [7]. The investigative drug GSK1278863 shows a complex phase I metabolism resulting in up to 14 stereoisomeric metabolites which could not be separated using UHPLC methods. Chiral analysis by SFC using a Chiralpak AD-H column [amylose tris-(3,5-dimethylphenylcarbamate)] and 0.5% formic acid in a mixture of isopropyl alcohol and ethyl acetate (80:20, v/v) as modifier was then accomplished within 17 min [131]. Ketamine is used as an anesthetic drug but was under investigation for its antidepressant effects. Both enantiomers and four metabolites, namely R- and S-norketamine, R- and S-dehydronorketamine, and (2R,6R)- and (2S,6S)-hydroxynorketamine, could be separated in one run by SFC-MS as reported by Fassauer et al. [63]. Enantioseparation was accomplished within 15 min which was 4 times faster than a comparable HPLC method. The method was validated according

**TABLE 3** Recent SFC applications in the field of Pharmaceuticals and clinical analysis.

Analyte(s)	Matrix	Column	Mobile phase	Detection	Reference
15 sulfonamide antibiotics and metabolites	Human serum	BEH 100 × 3.0 mm, 1.7 μm	EtOH	UV	[80]
Racemic cetirizine	Human plasma	Chiralpak IE 150 × 2.1 mm, 5 μm	MeOH: water, 95:5	MS/MS ESI pos	[130]
Citalopram enantiomers	Human serum	Trefoil CEL2 150 × 2.1 mm, 2.5 μm	MeOH: ACN, 70:30 NH <sub>4</sub> Ac, 10 mM	MS/MS ESI pos	[7]
GSK1278863 metabolites	Human plasma	Chiralpak AD-H 150 × 4.6 mm, 5 μm	IPA:ethyl acetate, 80:20 FA, 0.5%	MS/MS ESI	[131]
Ketamine enantiomers, 3 metabolites	Human urine	Lux Amylose-2 150 × 4.6 mm, 5 μm	IPA NH <sub>3</sub> , 0.075%	MS ESI pos	[63]
Ketamine enantiomers, 3 metabolites	Human urine	Lux Amylose-2 150 × 4.6 mm, 5 μm	IPA NH <sub>3</sub> , 0.075%	MS ESI pos	[64]
Six HIV protease inhibitors	Human dried plasma spot	Diol 150 × 3.0 mm, 2.5 μm	MeOH NH <sub>4</sub> FA, 10 mM	MS/MS ESI	[65]
API	Mouse hepatocytes	X-bridge C18, Chiralpak IB-3, Chiralpak AD-3 150 × 3.0 mm, 3.5 μm, 50 × 4.6 mm, 3.0 μm, 50 × 4.5 mm, 3.5 μm	EtOH NH <sub>3</sub> , 0.1%	MS ESI	[83]
Lobaplatine	Rat plasma	Chiralcel OZ-RH 150 × 4.6 mm, 5 μm	MeOH	MS/MS ESI pos	[68]
Three taxane drugs	Rat blood	BEH 2-EP 100 × 2.1 mm, 1.7 μm	MeOH	MS/MS ESI pos	[132]
Daidzein	Rat plasma	BEH 2-EP 100 × 3.0 mm, 1.7 μm	MeOH FA, 1.0%	MS/MS ESI pos	[133]
Risperidone and chiral metabolite	Rat plasma	Chiralpak AD-3 100 × 3.0 mm, 3.0 μm	MeOH FA, 0.1%, NH <sub>4</sub> Ac, 40 mM	MS/MS ESI pos	[134]
Lumefantrine, artemether, dihydroartemisinin	Rat plasma	BEH 2-EP 100 × 3.0 mm, 1.7 μm	MeOH NH <sub>4</sub> Ac, 2 mM	MS/MS ESI pos	[135]

*Continued*

TABLE 3 Recent SFC applications in the field of Pharmaceuticals and clinical analysis—cont'd

Analyte(s)	Matrix	Column	Mobile phase	Detection	Reference
Ginkgolides and hydrolyzed products	Rat plasma	Not reported	MeOH: water, 95:5 NH <sub>4</sub> Ac, 10 mM	MS/MS ESI pos/neg	[136]
Scholarisine, 19-episolarisine, vallesamine, picrinine	Rat plasma	BEH 2-EP 100 × 3.0 mm, 1.7 μm	MeOH NH <sub>4</sub> FA, 2 mM	MS/MS ESI pos	[137]
Coenzyme Q10	Rat plasma	BEH 2-EP 100 × 3.0 mm, 1.7 μm	MeOH	MS/MS ESI pos	[138]
25 model compounds	Rat plasma	DEA, Diol, 2PIC 50 × 2.1 mm, 1.7 μm	MeOH Different additives	MS/MS ESI pos	[139]
n-butylphthalide	Dog plasma	HSS C18 100 × 3.0 mm, 1.8 μm	MeOH	MS/MS ESI pos	[140]
Probucol	Dog plasma	BEH 2-EP 100 × 3.0 mm, 1.7 μm	MeOH	MS/MS ESI pos/neg	[141]
Piroxicam	Dog plasma	BEH 2-EP 100 × 3.0 mm, 1.7 μm	MeOH: water, 98:2 FA, 0.4%, NH <sub>4</sub> Ac, 10 mM	MS/MS ESI pos	[142]
Ezetimibe	Dog plasma	C18 100 × 3.0 mm, 1.8 μm	MeOH	MS/MS ESI neg	[143]
Rabeprazole	Dog plasma	Trefoil CEL2 100 × 3.0 mm, 2.5 μm	MeOH	MS/MS ESI pos	[144]
Oxcarbazepine and chiral licarbazepine	Dog plasma	Trefoil CEL2 150 × 3.0 mm, 2.5 μm	MeOH	MS/MS ESI pos	[67]

to EMA and FDA guidelines for bioanalytical methods and subsequently applied to a pharmacokinetic study, where the analytes were successfully quantified in human urine samples after LLE. Hofstetter et al. improved this method in terms of sample preparation with an online SFE-SFC-MS approach [64]. They used the same column (150 × 4.6 mm, 5 μm) with 5-chloro-2-methylphenylcarbamylated amylose, with modifier consisting of 0.075% ammonia in isopropyl alcohol, and makeup solvent (0.1% formic acid in MeOH) improving sensitivity in positive electrospray with single quadrupole detection. Only 20 μL of urine, instead of 1 mL of urine for LLE, were required and total runtime was reduced to around 18 min including SFE. In addition, this method was validated according to EMA guidelines.

The analysis of HIV protease inhibitors spiked in human plasma spots (dried) was reported by Akbal et al. [65]. In that study, the authors focused on the optimization of

mobile phase additives and makeup solvent additives. Separation of six protease inhibitors was accomplished by using a diol stationary phase ( $150 \times 3.0$  mm,  $2.5 \mu\text{m}$ ) and MeOH containing 10 mM ammonium formate. Postcolumn addition of different makeup solvent was investigated with regard to the type of additive and flow rates. Generally, they found ammonium to be most beneficial for positive ESI and proposed the formation of adducts with DMSO. This led to a simplification of the MS spectrum.

An advanced instrumental setup was used by Goel et al. [83]. The authors developed a two-dimensional LCxSFC-UV-MS system for the analysis of a nondisclosed API. The drug substance was metabolized by mouse hepatocytes yielding one metabolite. Both API and metabolite were successfully separated in the first dimension using a C18 column ( $150 \times 3.0$  mm,  $3.5 \mu\text{m}$ ) by HPLC. Enantioseparation in the second dimension was accomplished on two different CSP, cellulose tris-(3,5-dimethylphenylcarbamate) ( $50 \times 4.6$  mm,  $3.0 \mu\text{m}$ ) and amylose tris-(3,5-dimethylphenylcarbamate) ( $50 \times 4.5$  mm,  $3.5 \mu\text{m}$ ), respectively. Ethanol with the addition of 0.1% ammonia was used as a mobile phase additive on both columns. The enantiomers were detected by single quadrupole MS in SIM mode.

Pharmacokinetic studies involving laboratory animals are still necessary for drug development processes. Meng et al. reported the separation of lobaplatin diastereomers in rat plasma using a chiral column with cellulose tris-(3-chloro-4-methylphenylcarbamate) as CSP to investigate stereospecificity in pharmacokinetics. The SFC-MS/MS method was validated according to FDA guidelines and utilized isocratic elution with pure MeOH at 4 mL/min, and 0.1% formic acid in MeOH at 0.3 mL/min as makeup solvent. Rat plasma samples were deproteinized before analysis and the diastereomers were separated within 6 min [68]. Another example of the analysis of chemotherapeutic drugs by SFC-MS/MS was reported by Jin et al. [132]. The authors developed a fast SFC-MS/MS method for the analysis of three taxane drugs in rat whole blood. Although several LC-MS/MS methods for pharmacokinetic studies of taxanes are reported, the use of SFC may simplify sample preparation and fasten analysis. Therefore,  $50 \mu\text{L}$  blood were (spot) dried and extracted with *t*-butyl methyl ether, evaporated and reconstituted in MeOH. Paclitaxel, cabazitaxel, docetaxel, and glyburide (internal standard) were separated within 3 min on a BEH 2-EP column ( $100 \times 2.1$  mm,  $1.7 \mu\text{m}$ ) with pure MeOH as a modifier and makeup solvent in gradient mode. Lower limits of quantification (LLOQ) of 10.0–10.4 ng/mL were reached.

The isoflavone daidzein shows poor bioavailability caused by low solubility in water. Therefore, a valine carbamate prodrug of daidzein was investigated and within a pharmacokinetic study in rats. SFC-MS/MS proved to be suitable for fast analysis of daidzein and prodrug in rat plasma. After LLE with ethyl acetate, evaporation, and reconstitution in MeOH, the separation was achieved on a BEH 2-EP stationary phase ( $100 \times 3.0$  mm,  $1.7 \mu\text{m}$ ) and MeOH as a modifier (with 1% formic acid as an additive) within 3 min. Pure MeOH was deployed as makeup solvent enabling LLOQ of 2–10 ng/mL in positive ESI-MS/MS [133].

The antipsychotic drug risperidone along with its chiral metabolite 9-hydroxyrisperidone was separated by SFC within 6 min on an amylose tris-(3,5-dimethylphenylcarbamate) phase and MeOH containing 0.1% formic acid as well as 40 mM ammonium formate as mobile phase modifier. After oral and intravenous risperidone administration to rats and protein precipitation as sample pretreatment, the simultaneous quantification was possible within this validated setup of Prasad et al. [134].



Yang et al. reported the separation of lumefantrine, artemether, and its active metabolite dihydroartemisinin in rat plasma after protein precipitation. The combination of lumefantrine and artemether represents an effective oral antimalaria drug which was administered intravenously to rats in the form of a new formulation. Gradient elution on a BEH 2-EP phase ( $100 \times 3.0$  mm,  $1.7 \mu\text{m}$ ) with ammonium acetate (2 mM) in MeOH as modifier was possible within 2.5 min. Positive ESI without any reported makeup solvent yielded LLOQs of 1.0–2.0 ng/mL [135].

Separation of three ginkgolides and six hydrolyzed metabolites by SFC was favored over reversed phase LC [136]. The developed method applied 95% MeOH with ammonium acetate (10 mM) as a modifier and rather uncommon pure water with 5 mM ammonium acetate as makeup solvent. A total runtime of 6.5 min allowed for fast analysis in the course of a pharmacokinetic study after intravenous administration of a ginkgolide extract. Another phytopharmaceutical drug was investigated by Yang et al. [137]. The authors aimed for the separation of its ingredients scholarisine, 19-episolarisine, vallesamine, and picrinine, which showed the best performance on a BEH 2-EP ( $100 \times 3.0$  mm,  $1.7 \mu\text{m}$ ) stationary phase, and 2 mM ammonium formate in MeOH as modifier. Within a pharmacokinetic study in rats, the SFC-MS/MS method showed higher sensitivity and shorter run times than previous assays.

To evaluate a new formulation of the lipophilic coenzyme Q10 within a pharmacokinetic study, Yang et al. developed a fast SFC-MS/MS method for the analysis of coenzyme Q10 in rat plasma. Isocratic elution within 1.5 min using pure MeOH as mobile phase modifier and 2 mM ammonium acetate in MeOH as makeup solvent enabled a LLOQ of 2.0 ng/mL after previous protein precipitation [138].

Recently, Zhang et al. tested SFC-MS/MS for high-throughput bioanalysis in drug discovery based on 25 model compounds (log  $P$  range 0.16–6.15). For five out of those 25 test compounds, they performed an application study with rats to demonstrate the applicability of their method for bioanalytical application. SFC-MS/MS resulted in a fast (1-min total run time) analysis using sub-2-micron columns and the authors concluded that in comparison to LC-MS/MS, SFC-MS/MS showed better sensitivity and both methods resulted in similar concentration data. Furthermore, they found SFC fit for high-throughput bioanalysis of small molecule drugs [139].

Pharmacokinetic studies in advanced drug development processes are often performed with nonrodents. Several recent studies report the development of SFC-MS/MS methods for fast analysis of pharmaceuticals and their metabolites in beagle dog plasma. Li et al. developed and validated a SFC-MS/MS method for the determination of the cerebral stroke treatment drug *n*-butylphthalide. An aliquot of 200  $\mu\text{L}$  of dog plasma was deproteinized by the addition of 300  $\mu\text{L}$  MeOH. After centrifugation, 5  $\mu\text{L}$  of supernatant were injected and separation was achieved using a C18 column ( $100 \times 3.0$  mm,  $1.8 \mu\text{m}$ ), isocratic elution with pure MeOH as modifier and makeup solvent, in only 1.5 min. The authors emphasize that their method was faster than HPLC methods and, therefore, capable of high-throughput analysis for pharmacokinetic studies [140]. In another study, the same group evaluated the bioavailability of a new drug formulation of the antihyperlipidemic drug probucol. Again, a pharmacokinetic study with beagle dogs was successfully performed by SFC-MS/MS. Sample preparation by protein precipitation with MeOH and acetone was followed by fast isocratic separation (1.5 min) using a BEH 2-EP column ( $100 \times 3.0$  mm,  $1.7 \mu\text{m}$ ), pure MeOH

as a modifier, and 0.5% ammonia in MeOH as makeup solvent [141]. In another study, the authors reported the determination of the nonsteroidal antiinflammatory drug piroxicam. To evaluate the bioequivalence of two drug formulations a pharmacokinetic study with beagle dogs was conducted. Here, LLE of plasma samples with ethylacetate and subsequent injection of the organic layer enabled analysis of piroxicam within 2.5 min using a BEH 2-EP column ( $100 \times 3.0$  mm,  $1.7 \mu\text{m}$ ), 2% water in MeOH as modifier, and formic acid (0.4%) as well as ammonium acetate (10mM) as additive. MeOH containing 0.1% formic acid was used as makeup solvent and they reported sensitivity as low as LLOQ 5ng/mL [142]. Di et al. developed a method for the analysis of the antihyperlipidemic drug ezetimibe in dog plasma. After deglucuronidation and extraction with *t*-butyl methyl ether, the organic layer was dried, reconstituted in MeOH and analyzed by SFC-MS/MS. Separation using a C18 stationary phase ( $100 \times 3.0$  mm,  $1.8 \mu\text{m}$ ) and MeOH as a modifier in gradient mode was accomplished within 3.5 min. No makeup solvent was reported to assist negative ESI. Still, LLOQ of 1.0ng/mL was achieved and the method was applied to a pharmacokinetic study [143].

Examples of chiral separation by SFC in the context of pharmacokinetics are reported by Yang or Su et al. [67, 144]. The latter reported enantioseparation of rabeprazole using cellulose tris-(3-chloro-4-methylphenylcarbamate) as CSP ( $100 \times 3.0$  mm,  $2.5 \mu\text{m}$ ).  $\text{CO}_2$  modified with pure MeOH, and isocratic elution allowed for enantioseparation within 4.5 min. Yang et al. were able to separate oxcarbazepine and its active chiral metabolite licarbazepine utilizing cellulose tris-(3-chloro-4-methylphenylcarbamate) as CSP ( $150 \times 3.0$  mm,  $2.5 \mu\text{m}$ ) after LLE and isocratic elution with pure MeOH [67].

In summary, SFC-MS/MS seems to be of growing interest for fast and sensitive analysis in pharmacokinetic studies during drug discovery and development as well as for TDM in a clinical environment.

### 5.3 Endogenous metabolites, metabolomics, and lipidomics

Application of SFC in various analytical fields has been reported for parallel as well as untargeted metabolomics [120], with the latter being still less common. Nevertheless, Grand-Guillaume Perrenoud et al. showed the great potential of SFC for metabolic profiling in combination with Q-TOF in terms of plant metabolic profiling [99].

In bioanalytical applications, targeted approaches are more popular (Table 4). Recently, a few studies investigated general approaches for metabolic phenotyping utilizing SFC-MS/MS. Sen et al. investigated the potential of SFC for the analysis of polar urinary metabolites for metabolic phenotyping. A screening of 12 different column chemistries, three-column temperatures, along with nine different additives in methanol as modifier using a set of 60 polar metabolites ( $\log P$   $-7$  to  $2$ ) was performed and applied to human urine samples using a 7 min gradient [35]. The authors suggested a Torus Diol column along with methanol containing ammonium formate as modifier as a starting point for further method development. An even wider polarity range was covered by Desfontaine et al. [36]. In all, 57 hydrophilic and lipophilic substances ( $\log P$   $-6$  to  $11$ ) were analyzed by SFC-MS/MS using 'unified chromatographic' conditions. The authors applied a gradient up to 100% modifier (MeOH: water, 1:1, v:v) with 50 mM ammonium formate and 1 mM ammonium fluoride as additives.

**TABLE 4** Recent SFC applications in the field of endogenous metabolites, metabolomics, and lipidomics.

Analyte(s)	Matrix	Column	Mobile phase	Detection	Reference
60 polar metabolites	Human urine	Torus Diol 100 × 3.0 mm, 1.7 μm	Multiple	UV, MS	[35]
57 metabolites		Poroshell HILIC 100 × 3.0 mm, 2.7 μm	MeOH:water, 95:5 NH <sub>4</sub> FA, 50 mM, NH <sub>4</sub> F, 1 mM	MS/MS ESI pos/ neg	[36]
Modified nucleosides	<i>E. coli</i> tRNA digest	2-PIC 150 × 2.1 mm, 1.7 μm	MEOH:water, 98:2 NH <sub>4</sub> Ac, 10 mM	HRMS ESI pos	[145]
Melatonin, N-acetylserotonin	Human serum	BEH 150 × 4.6 mm <sup>a</sup> )	MeOH FA, 0.1%, NH <sub>4</sub> FA, 0.05%	MS/MS ESI pos	[146]
Amino acids	Human serum	Luna HILIC 150 × 3.0 mm, 3.0 μm	MeOH, EtOH, MeOH:ACN, 1:1 NH <sub>4</sub> FA, NH <sub>4</sub> Ac	MS/MS ESI/ APCI pos/neg	[89]
Steroid glucuronides (G), sulfates (S)	Urine, bovine	BEH 2-EP (S), BEH (G) 100 × 3.0 mm, 1.7 μm	MeOH:water, 95:5 NH <sub>4</sub> FA, 30 mM	MS/MS ESI neg	[149]
19 endogenous AAS	Serum, fetal bovine	BEH 2-EP 100 × 3.0 mm, 1.7 μm	MeOH	MS/MS ESI pos	[150]
Steroids	Prostate cancer cells, tissue, plasma	BEH, BEH 2-EP 100 × 3.0 mm, 1.7 μm	MeOH	MS/MS ESI pos	[151]
19 steroids	Plasma, human	BEH 100 × 3.0 mm, 1.7 μm	MeOH FA, 0.1%	MS/MS ESI pos	[152]
51 endogenous steroids, and sulfates	CSF, Human	2-EP, 100 × 3.0 mm, 1.7 μm; Silica, 200 × 3.0, 1.8 μm; Diol, 150 × 3.0 mm, 1.7 μm	MeOH:water, 97.5:2.5 NH <sub>4</sub> FA, 40 mM; Isopropyl alcohol; MeOH	MS/MS ESI pos/ neg	[153]
Vitamin D, 9 metabolites	Serum, human	Lux Cellulose-2 150 × 3.0 mm, 3.0 μm	MeOH FA, 0.1%	MS/MS ESI pos	[155]
Vitamin D, metabolites	Plasma, human	1-AA 100 × 3.0 mm, 1.7 μm	MeOH	MS ESI/ APCI	[90]
8 tocopherols, tocotrienols	Serum, human	BEH 2-EP 100 × 3.0 mm, 1.7 μm	MeOH:water, 98:2, MeOH:water, 95:5 (HT) NH <sub>4</sub> FA, 10 mM	UV, MS ESI pos	[82]
Fat-soluble vitamins, carotinoids	Plasma, human	Viridis HSS C18 SB 100 × 3.0 mm, 1.8 μm	MeOH:water, 98:2 NH <sub>4</sub> FA, 20 mM	MS/MS ESI pos	[157]

**TABLE 4** Recent SFC applications in the field of endogenous metabolites, metabolomics, and lipidomics—cont'd

Analyte(s)	Matrix	Column	Mobile phase	Detection	Reference
Carotenoids	Blood, human	C30 150 × 4.6 mm, 2.7 μm	MeOH	MS/MS APCI pos/neg	[111]
Biomarker	serum, dried spots	Inertsil Diol 150 × 2.1 mm, 3.0 μm	MeOH FA, 0.1%	MS/MS ESI pos/ neg	[110]
Arachidonic acid metabolites	Plasma, human, CSF, human	2-PIC 150 × 3.0 mm, 1.7 μm	MeOH FA, 0.1%, NH <sub>4</sub> Ac, 10 mM	MS/MS ESI neg	[158]
Lipids	Brain, porcine	BEH 100 × 3.0 mm, 1.7 μm	MeOH:water, 99:1 NH <sub>4</sub> Ac, 30 mM	HRMS ESI pos/ neg	[162]
450 lipid species within 23 lipid classes	Plasma, erythrocytes, tumor tissue	BEH 100 × 3.0 mm, 1.7 μm	MeOH:water, 99:1 NH <sub>4</sub> Ac, 30 mM	HRMS ESI pos	[163]
Oxylipins	Plasma, human	Torus 1-AA 100 × 3.0 mm, 1.7 μm	MeOH acetic acid, 0.1%	HRMS ESI neg	[164]
172 lipids	Plasma, LDL, rabbit	Inertsil ODS-4 250 × 4.6 mm, 5 μm	MeOH NH <sub>4</sub> Ac, 0.1%	HRMS ESI pos/ neg	[105]
Lipids from 22 lipid classes	Plasma, rabbit	DEA 100 × 3.0 mm, 1.7 μm	MeOH:water, 95:5 NH <sub>4</sub> Ac, 0.1%	MS/MS ESI pos/ neg	[165]
Biomarker	Tissue, mouse lung	BEH, HSS C18 SB 50 × 2.1 mm, 1.7/1.8 μm	MeOH:ACN; 1:1 NH <sub>4</sub> FA, 15 mM	HRMS ESI pos/ neg	[166]
Lipids	Brain, rat	BEH 100 × 3.0 mm, 1.7 μm	MeOH:water, 99:1 NH <sub>4</sub> Ac, 30 mM	HRMS ESI pos/ neg	[106]
18 lipid classes	Blood serum, brain tissue	Diol 100 × 3.0 mm, 1.7 μm	MeOH NH <sub>4</sub> FA, 20 mM	HRMS ESI pos/ neg	[167]
Triacylglycerols	Milk, human	BEH 2-EP 100 × 3.0 mm, 1.7 μm	MeOH:ACN, 1:1 FA, 0.1%	HRMS ESI pos	[107]

<sup>a</sup> Particle size not reported.

A superficially porous Poroshell HILIC column (100 × 3.0 mm, 2.7 μm) was found to be most suitable for analysis with regard to potential application in human metabolomics. Further studies investigated the application of SFC for polar endogenous metabolites. Laboureur et al. developed a SFC-HRMS method for the detection of canonical and modified nucleosides. The separation was achieved using a 2-PIC (150 × 2.1 mm, 1.7 μm) stationary phase

and MeOH containing 2% water and 10 mM ammonium acetate as a modifier. SFC in combination with HRMS was utilized to investigate the modification of nucleosides after digestion of tRNA by *Escherichia coli* and found SFC to be faster than comparable LC methods and an interesting alternative for epigenetic studies [145]. Wolrab et al. developed and validated two methods (LC- and SFC-MS/MS) for the analysis of the neurotransmitter melatonin and *n*-acetyl-serotonin in human serum and found SFC-MS/MS a useful alternative for the analysis of polar analytes [146]. In another study, the authors investigated the applicability of SFC-MS/MS for the analysis of polar and ionic amino acids in human serum. After simple protein precipitation analytes were separated using a Luna HILIC column (150 × 3.0 mm, 3.0 μm) using different modifiers (MeOH, ethanol, and MeOH:ACN). ESI and APCI in positive and negative mode were evaluated and resulted in compound-dependent sensitivity [89].

SFC is also a versatile tool for the analysis of more apolar substances. The analysis of endogenous steroid hormones is a challenging task caused by the vast number of isomers and isobaric substances, which cannot be discriminated in multiple reaction monitoring modes due to the same ion transitions. Thus, chromatographic separation is necessary. Routine analysis in clinical or antidoping context is typically performed using either GC-MS(/MS) after hydrolysis of conjugates and subsequent derivatization (and sometimes semipreparative HPLC-cleanup before analysis), or LC-MS/MS. The latter having no need for derivatization and hydrolysis, had less separation efficiency compared to GC. Recently, Shackleton reviewed clinically relevant steroid analysis and found SFC-MS/MS “a new player in separation” showing the capability of being an excellent option for bioanalysis [147]. Also, Storbeck sees great potential for steroid analysis by SFC in a clinical environment. SFC offered high-throughput and orthogonality compared to GC-MS and LC-MS/MS, and was well suited for applications in different matrices for steroid profiling also covering conjugated steroids [148]. One earlier bioanalytical method applying SFC-MS/MS by Xu et al. covering 15 endogenous estrogen metabolites was faster than a LC-MS analysis (10 min vs. 70 min), using two serially coupled columns (cyano-propyl silica and diol). Still, derivatization with dansyl chloride was necessary [88].

Recently, the analysis of 8 intact steroid glucuronides and 10 sulfates in bovine urine by Doue et al. was accomplished using two different methods, each separation accomplished within 8 min [149]. An even larger set of 19 endogenous androgenic steroids including 11-oxo steroids in fetal bovine serum was separated by Quanson et al. [150]. After LLE and evaporation, analysis was performed using a BEH 2-EP column (100 × 3.0 mm, 1.7 μm), additive-free methanol as a modifier, and methanol with 0.1% formic acid at 0.2 mL/min as makeup solvent within 4 min. LLOQ of 0.01–10 ng/mL were reached using tandem mass spectrometric detection with ESI in positive mode. Du Toit et al. applied the same method with a slightly different gradient for several 11-hydroxy- and 11-oxo-androgens in prostate cancer cells, tissue, and plasma [151]. The separation of 32 endogenous steroids within 21 min was reported by Parr et al. [93]. The authors did not analyze any biological matrix therein, but compared different atmospheric pressure ionization sources (ESI, APCI, APPI) and found ESI being most suitable for most of the compounds reaching LODs from 1 to 50 ng/mL. De Kock et al. reported the analysis of 19 endogenous steroids after derivatization of carbonyl groups with methoxamine hydrochloride resulting in the corresponding methoxamines. The introduction of a nitrogen moiety improved ionization efficiency due to the higher proton affinity, thus, improving the limits of detection. This derivatization procedure leads to derivatization

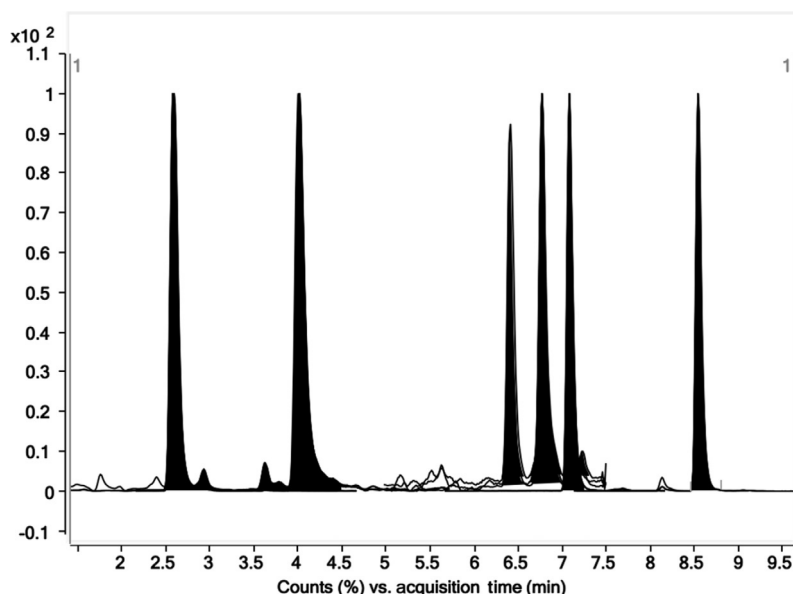


FIG. 5 MRM chromatogram showing seven corticosteroids detected in human CSF by SFC-ESI-MS/MS. Column Torus Diol ( $150 \times 3.0$  mm,  $1.7 \mu\text{m}$ ), modifier: MeOH, flow-rate 1 mL/min in gradient mode, makeup solvent: MeOH:H<sub>2</sub>O (97.5:2.5, v:v) with 1 mM NH<sub>4</sub>F at 0.150 mL/min flow rate.

isomers (for 11 out of 19 analytes), which were considered for quantification. The analytes were separated on a BEH column and MeOH with 0.1% formic acid as modifier and same makeup solvent. SFC-MS/MS and positive ESI enabled LOQs in the range of 0.05–1 ng/mL [152]. In another study, Teubel et al. compared GC-MS and SFC-MS/MS for steroid profiling. The authors found SFC-MS/MS advantageous over GC-MS since no derivatization leading to potential isomers was necessary and the high separation efficiency of SFC allowed successful separation using three different SFC-MS/MS methods for different sets of endogenous steroids (Fig. 5). In total, 51 steroids including steroid sulfates are covered. As proof of concept for bioanalysis, intact steroid sulfates were detected in human CSF [153].

Already in 2013, the analysis of 25 bile acids including glycine and taurine conjugates was accomplished in 13 min using SFC-ESI-MS/MS as reported by Taguchi et al. The quantification of 24 compounds in rat serum without the need for complex sample preparation like SPE was possible [154].

In addition, the analysis of lipophilic vitamins by SFC is well documented. Jenkinson et al. separated nine vitamin D metabolites in human serum within 6 min by SFC-MS/MS using a chiral column ( $150 \times 3.0$  mm,  $3.0 \mu\text{m}$ ) and 0.1% formic acid in MeOH as mobile phase modifier and makeup solvent. Sample pretreatment was performed by SLE with subsequent derivatization. The method resulted in similar concentrations than comparable LC-MS/MS methods. Sensitivity was similar, while the injection volume in LC was five times larger [155]. It is worth mentioning that Regaldao et al. summarized several case studies where CSPs were successfully applied for the analysis of achiral compounds [156]. Also, Jumaah et al. were able to detect vitamin D along with nine metabolites in human plasma when using



single quadrupole mass spectrometric detection [90]. For separation of the analytes, a 1-aminoanthracene column (1-AA) was applied. Further lipophilic vitamins were investigated by Pilarova et al. [82]. The authors developed a high-resolution and a high-throughput method for the analysis of tocopherols and tocotrienols in human serum samples with single quadrupole mass spectrometric detection. Sample pretreatment consisted of protein precipitation and subsequent LLE. The separation was achieved on a BEH 2-EP column (100 × 3.0 mm, 1.7 μm) using isocratic elution. Petruzzello et al. separated fat-soluble vitamins and carotinoids by UHPSFC-MS/MS applying an apolar stationary phase for lipophilic analytes. A HSS C18 column (100 × 3.0 mm, 1.8 μm) was used with a modifier consisting of MeOH:water, 98:2, and 20 mM ammonium formate as additive. MS/MS with ESI positive was used for detection and the total run time was only 8 min [157]. Zoccali et al. reported an online SFE-SFC-MS/MS method for the analysis of carotenoids in intact human blood samples. Only 10 μL blood was extracted by online SFE. Separation of analytes was achieved in 20 min on a C30 column using pure MeOH as a modifier and makeup solvent. APCI was chosen for ionization of the apolar analytes [111]. Another online SFE-SFC-MS/MS method was developed by Suzuki et al. The authors aimed for disease biomarker profiling in dried blood spots from oral, colorectal, and pancreatic cancer patients. Four hydrophilic and 17 hydrophobic metabolites were separated and detected within 15 min. The optimized method employs a diol stationary phase and tandem mass spectrometric detection. The authors stated that their method showed a similar diagnostic performance to serum analysis using LC-MS/MS [110].

Five bioactive arachidonic acid metabolites were separated within 3 min using the method reported by Kumari et al. [158]. For the matrices of interest (human plasma and CSF) after PP and evaporation a 2-PIC column (150 × 3.0 mm, 1.7 μm) and MeOH containing formic acid (0.1%) and ammonium acetate (10 mM) as mobile phase modifier was applied for analysis. ESI-MS/MS in negative mode allowed for detection up to LOQ of 0.5–2.5 ng/mL.

Further, SFC has shown to be useful in the analysis of lipids [116, 117, 159]. In different fields such as food [96], plant analysis [102], or bioanalysis [104, 109, 160, 161], lipidome analysis using SFC has already been applied. Recent bioanalytical publications include among others, a comprehensive lipidomics analysis based on the validated SFC-ESI-HRMS method of Lisa et al. which enables high-throughput (within 6 min) analysis of a large set of polar and apolar lipids. The analysis of a porcine brain extract after LLE identified 436 lipid species from 24 different lipid classes [162]. In another study, the authors compared SFC, LC, and direct infusion (DI) for lipid analysis in biological samples. The method was validated for plasma, erythrocytes, and tumor tissue from kidney cancer patients. SFC had shortest analysis time (10 min, two times faster than HPLC), identified the most lipid species (450 out of 610), while DI identified less species but more lipid classes [163].

Berkecz et al. analyzed oxylipins in human plasma and compared LC- with SFC-HRMS. Aliquots of 500 μL plasma were concentrated by SPE and for SFC analytes were separated within 15 min on a Torus 1-AA phase (100 × 3.0 mm, 1.7 μm) with 0.1% acetic acid in MeOH as modifier and pure methanol at 0.3 mL/min as makeup solvent. The authors favored LC over SFC due to better separation and higher sensitivity. Still, SFC showed lower ion suppression [164]. Another method covering a large set of lipids was reported by Takeda et al. [105]. The authors were able to quantify 172 lipids in rabbit plasma with high throughput and high mass accuracy using SFC coupled with a hybrid quadrupole-orbitrap mass spectrometer. The same group presented another method for widely targeted lipidome analysis by SFC-MS/MS. Lipids from 22 lipid classes were identified in rabbit plasma [165]. Jones et al. utilized



SFC-HRMS with data-independent tandem mass spectrometry for lipid analysis of mouse lung tissue [166] while Yang et al. developed a method for lipid profiling in rat brain tissue achieving faster separation compared to common LC-MS methods. Identification and characterization of analytes were supported by fragmentation [106]. Al Hamimi et al. reported a stationary phase screening of seven sub-2-micron phases for lipid profiling from blood, serum and brain tissue in less than 11 min. Their results showed the possibility of within lipid class and between lipid class profiling. Retention time, peak height, FWHM, asymmetry factors, and  $R_s$ , within and between lipid classes, were determined for selected lipids. A Diol column was used in the subsequent investigations due to the greater peak symmetries at a column temperature of 48°C, a backpressure at the column outlet of 131 bar, and a flow rate of 1.5 mL/min. In total, 180 lipids from 15 lipid classes were identified from a pure nonspiked serum extract [167]. Tu et al. extracted triacylglycerols from human milk and infant formula and separated the analytes on a BEH 2-EP phase using a mixture of MeOH:ACN as modifier with 0.1% formic acid as additive by SFC-QTOF-MS [107].

## 6 Conclusion

SFC is increasingly applied in all different areas of bioanalysis. Separation of analytes over a broad polarity range with high separation efficiency in a short analysis time is the major advantage of SFC. Concerning injection solvents, not only apolar solvents but small amounts of water are tolerable and enable the analysis of very polar compounds. If small amounts of water are used as mobile phase additive the altered conditions may support the analysis of those types of compounds. In that context, the use of high modifier amounts (up to 100%) may also increase elution of polar analytes and may even further broaden the polarity range suitable in future bioanalytical SFC applications. This may open the potential to run gradients from pure SFC over mixed mode to classical HPLC in future applications. Furthermore, it appears that the use of columns with sub-2-micron particles may increase separation efficiency and further shorten analysis times in SFC. The orthogonal selectivity of SFC compared to RPLC and the possibility to additionally and independently (from the mobile phase) optimize ionization by the use of makeup solvents are strong arguments for its application in bioanalysis. A better understanding of the mechanism of SFC separations will provide the basis of rational selection of stationary and mobile phase conditions. With increasing confidence in SFC and knowledge of the latest generation of instrumentation, we expect a growing interest in SFC-based applications that will also influence bioanalytical method development. However, we expect persistent limitations for the analysis of large biomolecules such as proteins or peptides even after further progress in research and development in SFC.

## References

- [1] E. Klesper, A.H. Corwin, D.A. Turner, High pressure gas chromatography above critical temperatures, *J. Organomet. Chem.* 27 (2) (1962) 700.
- [2] S.T. Sie, W. Van Beersum, G.W.A. Rijnders, High-pressure gas chromatography and chromatography with supercritical fluids. I. The effect of pressure on partition coefficients in gas-liquid chromatography with carbon dioxide as a carrier gas, *Sep. Sci.* 1 (4) (1966) 459–490.
- [3] J.C. Giddings, M.N. Myers, J.W. King, Dense gas chromatography at pressures to 2000 atmospheres, *J. Chromatogr. Sci.* 7 (5) (1969) 276.

- [4] D. Speybrouck, E. Lipka, Preparative supercritical fluid chromatography: a powerful tool for chiral separations, *J. Chromatogr. A* 1467 (2016) 33–55.
- [5] E. Lemasson, S. Bertin, C. West, Use and practice of achiral and chiral supercritical fluid chromatography in pharmaceutical analysis and purification, *J. Sep. Sci.* 39 (1) (2016) 212–233.
- [6] F. Liebetrau, M.K. Parr, Determination of enantiomeric bioactives using new analytical SFC instruments, *Chim. Oggi-Chem. Today* 33 (2) (2015) 6.
- [7] S. Hegstad, et al., Enantiomeric separation and quantification of citalopram in serum by ultra-high performance supercritical fluid chromatography-tandem mass spectrometry, *J. Chromatogr. B Anal. Technol. Biomed. Life Sci.* 1061–1062 (2017) 103–109.
- [8] S. Hegstad, et al., Enantiomeric separation and quantification of R/S-amphetamine in urine by ultra-high performance supercritical fluid chromatography tandem mass spectrometry, *J. Chromatogr. B Anal. Technol. Biomed. Life Sci.* 1077–1078 (2018) 7–12.
- [9] A. Svan, et al., Rapid chiral separation of atenolol, metoprolol, propranolol and the zwitterionic metoprolol acid using supercritical fluid chromatography-tandem mass spectrometry—application to wetland microcosms, *J. Chromatogr. A* 1409 (2015) 251–258.
- [10] U.S. Department of Health and Human Services, F.a.D.A., Bioanalytical Method Validation Guidance for Industry, (2018).
- [11] R. Reid, J. Prausnitz, T. Sherwood, *The Properties of Gases and Liquids*, third ed., McGraw-Hill, NY, 1977, pp. 149–150.
- [12] K. Anton, et al., Pressure-programming of a binary, on-line mixed mobile phase for capillary column SFC using a packed column SFC pumping system, *Chromatographia* 26 (1) (1988) 224–228.
- [13] A. Giorgetti, et al., Mixed mobile phases and pressure programming in packed and capillary column supercritical fluid chromatography—a unified approach, *J. Chromatogr. Sci.* 27 (6) (1989) 318–324.
- [14] X.W. Lou, et al., Pressure drop effects on selectivity and resolution in packed column supercritical fluid chromatography, *HRC—J. High Resolut. Chromatogr.* 19 (8) (1996) 449–456.
- [15] G. Guiochon, A. Tarafder, Fundamental challenges and opportunities for preparative supercritical fluid chromatography, *J. Chromatogr. A* 1218 (8) (2011) 1037–1114.
- [16] T.A. Berger, Characterizing pressure issues due to turbulent flow in tubing, in ultra-fast chiral supercritical fluid chromatography at up to 580 bar, *J. Chromatogr. A* 1475 (2016) 86–94.
- [17] L.T. Taylor, Supercritical fluid chromatography for the 21st century, *J. Supercrit. Fluids* 47 (3) (2009) 566–573.
- [18] S.A. Smith, V. Shenai, M.A. Matthews, Diffusion in supercritical mixtures: CO<sub>2</sub> + cosolvent + solutes, *J. Supercrit. Fluids* 3 (4) (1990) 175–179.
- [19] J.R. Strubinger, H. Song, J.F. Parcher, High-pressure phase distribution isotherms for supercritical fluid chromatographic systems. 2. Binary isotherms of carbon dioxide and methanol, *Anal. Chem.* 63 (2) (2002) 104–108.
- [20] C. West, E. Lemasson, Unravelling the effects of mobile phase additives in supercritical fluid chromatography. Part II. Adsorption on the stationary phase, *J. Chromatogr. A* 1593 (2019) 135–146.
- [21] C. West, et al., Unravelling the effects of mobile phase additives in supercritical fluid chromatography. Part I. Polarity and acidity of the mobile phase, *J. Chromatogr. A* 1492 (Supplement C) (2017) 136–143.
- [22] S. Bieber, et al., RPLC-HILIC and SFC with mass spectrometry: polarity-extended organic molecule screening in environmental (water) samples, *Anal. Chem.* 89 (15) (2017) 7907–7914.
- [23] M.K. Parr, et al., SFC-MS/MS as an orthogonal technique for improved screening of polar analytes in anti-doping control, *Anal. Bioanal. Chem.* 408 (24) (2016) 6789–6797.
- [24] Z. Wang, et al., Development of an orthogonal method for mometasone furoate impurity analysis using supercritical fluid chromatography, *J. Chromatogr. A* 1218 (16) (2011) 2311–2319.
- [25] M.D. Jones, K. Yu, W. Potts, Comparing orthogonality of convergence chromatography to reversed-phase LC, in: *Technology Brief*, W. Corporation, Editor, Milford, MA, USA, 2013, pp. 90–93.
- [26] H.N. Weller, et al., Orthogonality of SFC versus HPLC for small molecule library separation, *J. Comb. Chem.* 12 (6) (2010) 877–882.
- [27] H. Shaaban, T. Gorecki, Current trends in green liquid chromatography for the analysis of pharmaceutically active compounds in the environmental water compartments, *Talanta* 132 (2015) 739–752.
- [28] A. Dispas, et al., Supercritical fluid chromatography: a promising alternative to current bioanalytical techniques, *Bioanalysis* 10 (2) (2018) 107–124.
- [29] V. Desfontaine, et al., Liquid chromatography and supercritical fluid chromatography as alternative techniques to gas chromatography for the rapid screening of anabolic agents in urine, *J. Chromatogr. A* 1451 (2016) 145–155.

- [30] E. Lemasson, et al., Comparison of ultra-high performance methods in liquid and supercritical fluid chromatography coupled to electrospray ionization-mass spectrometry for impurity profiling of drug candidates, *J. Chromatogr. A* 1472 (2016) 117–128.
- [31] V. Desfontaine, L. Nováková, D. Guillarme, SFC-MS versus RPLC-MS for drug analysis in biological samples, *Bioanalysis* 7 (10) (2015) 1193–1195.
- [32] D.H. Kim, K.J. Lee, G.S. Heo, Analysis of cholesterol and cholesteryl esters in human serum using capillary supercritical fluid chromatography, *J. Chromatogr. B Biomed. Appl.* 655 (1) (1994) 1–8.
- [33] M.K. Parr, et al., Supercritical fluid chromatography (SFC) as orthogonal technique for improved detection of polar analytes in anti-doping control, in: W. Schänzer et al., (Eds.), *Recent Advances in Doping Analysis* (24), Sportverlag Strauß, Cologne, 2016.
- [34] C. Muscat Galea, D. Mangelings, Y. Vander Heyden, Investigation of the effect of mobile phase composition on selectivity using a solvent-triangle based approach in achiral SFC, *J. Pharm. Biomed. Anal.* 132 (2017) 247–257.
- [35] A. Sen, et al., Analysis of polar urinary metabolites for metabolic phenotyping using supercritical fluid chromatography and mass spectrometry, *J. Chromatogr. A* 1449 (2016) 141–155.
- [36] V. Desfontaine, et al., Applicability of supercritical fluid chromatography-mass spectrometry to metabolomics. I. Optimization of separation conditions for the simultaneous analysis of hydrophilic and lipophilic substances, *J. Chromatogr. A* 1562 (2018) 96–107.
- [37] C. West, Current trends in supercritical fluid chromatography, *Anal. Bioanal. Chem.* 410 (25) (2018) 6441–6457.
- [38] D. Guillarme, et al., What are the current solutions for interfacing supercritical fluid chromatography and mass spectrometry? *J. Chromatogr. B Anal. Technol. Biomed. Life Sci.* 1083 (2018) 160–170.
- [39] A. Tarafder, Designs and methods for interfacing SFC with MS, *J. Chromatogr. B Anal. Technol. Biomed. Life Sci.* 1091 (2018) 1–13.
- [40] B. Andri, et al., Combination of partial least squares regression and design of experiments to model the retention of pharmaceutical compounds in supercritical fluid chromatography, *J. Chromatogr. A* 1491 (2017) 182–194.
- [41] A. Dispas, et al., Quantitative determination of salbutamol sulfate impurities using achiral supercritical fluid chromatography, *J. Pharm. Biomed. Anal.* 134 (2017) 170–180.
- [42] L. Nováková, K. Plachká, P. Jakubec, Ultra-high performance supercritical fluid chromatography–mass spectrometry, in: M. Holčapek, W.C. Byrdwell (Eds.), *Handbook of Advanced Chromatography/Mass Spectrometry Techniques*, AOCSS Press, 2017, pp. 445–487, <https://doi.org/10.1016/B978-0-12-811732-3.00012-1>.
- [43] C. West, E. Lesellier, Characterization of stationary phases in supercritical fluid chromatography with the solvation parameter model, in: E. Grushka, N. Grinberg (Eds.), *Advances in Chromatography*, vol. 48, 2010, pp. 195–253.
- [44] C. West, et al., An improved classification of stationary phases for ultra-high performance supercritical fluid chromatography, *J. Chromatogr. A* 1440 (2016) 212–228.
- [45] C. West, Column characterization, in: C.F. Poole (Ed.), *Supercritical Fluid Chromatography*, Elsevier, 2017, pp. 103–125 (Chapter 4).
- [46] L.C. Harps, J.F. Joseph, M.K. Parr, SFC for chiral separations in bioanalysis, *J. Pharm. Biomed. Anal.* 162 (2019) 47–59.
- [47] V. Pilařová, et al., Recent developments in supercritical fluid chromatography-mass spectrometry: is it a viable option for analysis of complex samples? *TrAC—Trends Anal. Chem.* 112 (2019) 212–225.
- [48] E. Evertsson, et al., A hierarchical screening approach to enantiomeric separation, *Chirality* 29 (5) (2017) 202–212.
- [49] L. Chen, B. Dean, X. Liang, Evaluation of polysaccharide-based chiral stationary phases in modern SFC-MS/MS for enantioselective bioanalysis, *Bioanalysis* 11 (4) (2019) 251–266.
- [50] T.A. Berger, High-speed, high-efficiency achiral SFC on a  $3 \times 20$ -mm column packed with 1.8- $\mu$ m particles facilitated by a low-dispersion chromatograph, *Chromatographia* 82 (2) (2019) 537–542.
- [51] O.H. Ismail, et al., Unmatched kinetic performance in enantioselective supercritical fluid chromatography by combining latest generation whelk-o1 chiral stationary phases with a low-dispersion in-house modified equipment, *Anal. Chem.* 90 (18) (2018) 10828–10836.
- [52] A.G.G. Perrenoud, J.L. Veuthey, D. Guillarme, The use of columns packed with sub-2 gm particles in supercritical fluid chromatography, *TrAC—Trends Anal. Chem.* 63 (2014) 44–54.
- [53] A.G. Perrenoud, et al., Evaluation of stationary phases packed with superficially porous particles for the analysis of pharmaceutical compounds using supercritical fluid chromatography, *J. Chromatogr. A* 1360 (2014) 275–287.

- [54] C.F. Poole, Stationary phases for packed-column supercritical fluid chromatography, *J. Chromatogr. A* 1250 (2012) 157–171.
- [55] L. Nováková, et al., 2: Supercritical fluid chromatography in bioanalysis, *Supercrit. Fluid Chromatogr.* 2 (2018) 33.
- [56] L.T. Taylor, Packed column supercritical fluid chromatography of hydrophilic analytes via water-rich modifiers, *J. Chromatogr. A* 1250 (2012) 196–204.
- [57] C. West, E. Lesellier, Effects of mobile phase composition on retention and selectivity in achiral supercritical fluid chromatography, *J. Chromatogr. A* 1302 (2013) 152–162.
- [58] K. Taguchi, E. Fukusaki, T. Bamba, Simultaneous analysis for water- and fat-soluble vitamins by a novel single chromatography technique unifying supercritical fluid chromatography and liquid chromatography, *J. Chromatogr. A* 1362 (2014) 270–277.
- [59] R. Bennett, S.V. Olesik, Enhanced fluidity liquid chromatography of inulin fructans using ternary solvent strength and selectivity gradients, *Anal. Chim. Acta* 999 (2018) 161–168.
- [60] D. Wolrab, et al., Consequences of transition from liquid chromatography to supercritical fluid chromatography on the overall performance of a chiral zwitterionic ion-exchanger, *J. Chromatogr. A* 1517 (2017) 165–175.
- [61] A. Raimbault, M. Dorebska, C. West, A chiral unified chromatography-mass spectrometry method to analyze free amino acids, *Anal. Bioanal. Chem.* (2019).
- [62] A. Dispas, et al., Screening study of SFC critical method parameters for the determination of pharmaceutical compounds, *J. Pharm. Biomed. Anal.* 125 (2016) 339–354.
- [63] G.M. Fassauer, et al., Ketamine metabolites with antidepressant effects: Fast, economical, and eco-friendly enantioselective separation based on supercritical-fluid chromatography (SFC) and single quadrupole MS detection, *J. Pharm. Biomed. Anal.* 146 (2017) 410–419.
- [64] R. Hofstetter, G.M. Fassauer, A. Link, Supercritical fluid extraction (SFE) of ketamine metabolites from dried urine and on-line quantification by supercritical fluid chromatography and single mass detection (on-line SFE-SFC-MS), *J. Chromatogr. B Anal. Technol. Biomed. Life Sci.* 1076 (2018) 77–83.
- [65] L. Akbal, G. Hopfgartner, Effects of liquid post-column addition in electrospray ionization performance in supercritical fluid chromatography-mass spectrometry, *J. Chromatogr. A* 1517 (2017) 176–184.
- [66] V. Desfontaine, et al., A systematic investigation of sample diluents in modern supercritical fluid chromatography, *J. Chromatogr. A* 1511 (2017) 122–131.
- [67] Z. Yang, et al., Development and validation of an enantioselective SFC-MS/MS method for simultaneous separation and quantification of oxcarbazepine and its chiral metabolites in beagle dog plasma, *J. Chromatogr. B Anal. Technol. Biomed. Life Sci.* 1020 (2016) 36–42.
- [68] X. Meng, et al., Simultaneous quantitation of two diastereoisomers of lobaplatin in rat plasma by supercritical fluid chromatography with tandem mass spectrometry and its application to a pharmacokinetic study, *J. Sep. Sci.* 38 (21) (2015) 3803–3809.
- [69] A. Dispas, et al., First inter-laboratory study of a supercritical fluid chromatography method for the determination of pharmaceutical impurities, *J. Pharm. Biomed. Anal.* 161 (2018) 414–424.
- [70] V. Desfontaine, et al., Systematic evaluation of matrix effects in supercritical fluid chromatography versus liquid chromatography coupled to mass spectrometry for biological samples, *J. Chromatogr. B Anal. Technol. Biomed. Life Sci.* 1079 (2018) 51–61.
- [71] A. Svan, et al., The differences in matrix effect between supercritical fluid chromatography and reversed phase liquid chromatography coupled to ESI/MS, *Anal. Chim. Acta* 1000 (2018) 163–171.
- [72] A. Haglind, et al., Major signal suppression from metal ion clusters in SFC/ESI-MS—cause and effects, *J. Chromatogr. B Anal. Technol. Biomed. Life Sci.* 1084 (2018) 96–105.
- [73] M. Ashraf-Khorassani, M. Combs, Method development in supercritical fluid chromatography, in: C.F. Poole (Ed.), *Supercritical Fluid Chromatography*, Elsevier, 2017, pp. 127–152. Chapter 5.
- [74] L. Novakova, et al., Fast and sensitive supercritical fluid chromatography-tandem mass spectrometry multi-class screening method for the determination of doping agents in urine, *Anal. Chim. Acta* 915 (2016) 102–110.
- [75] L. Novakova, et al., Modern analytical supercritical fluid chromatography using columns packed with sub-2 μm particles: a tutorial, *Anal. Chim. Acta* 824 (2014) 18–35.
- [76] L. Novakova, M. Dousa, General screening and optimization strategy for fast chiral separations in modern supercritical fluid chromatography, *Anal. Chim. Acta* 950 (2017) 199–210.

- [77] K. De Klerck, Y. Vander Heyden, D. Mangelings, Generic chiral method development in supercritical fluid chromatography and ultra-performance supercritical fluid chromatography, *J. Chromatogr. A* 1363 (2014) 311–322.
- [78] D. Speybrouck, D. Corens, J.M. Argoullon, Screening strategy for chiral and achiral separations in supercritical fluid chromatography mode, *Curr. Top. Med. Chem.* 12 (11) (2012) 1250–1263.
- [79] V. Desfontaine, J.L. Veuthey, D. Guillarme, Hyphenated detectors: mass spectrometry, in: C.F. Poole (Ed.), *Supercritical Fluid Chromatography*, Elsevier, 2017, pp. 213–244. Chapter 8.
- [80] Y. Zhang, et al., A simple, accurate, time-saving and green method for the determination of 15 sulfonamides and metabolites in serum samples by ultra-high performance supercritical fluid chromatography, *J. Chromatogr. A* 1432 (2016) 132–139.
- [81] R. Geryk, et al., A supercritical fluid chromatography method for the systematic toxicology analysis of cannabinoids and their metabolites, *Anal. Methods* 7 (15) (2015) 6056–6059.
- [82] V. Pilarova, et al., Development and optimization of ultra-high performance supercritical fluid chromatography mass spectrometry method for high-throughput determination of tocopherols and tocotrienols in human serum, *Anal. Chim. Acta* 934 (2016) 252–265.
- [83] M. Goel, et al., Optimization of a two-dimensional liquid chromatography-supercritical fluid chromatography-mass spectrometry (2D-LC-SFS-MS) system to assess “in-vivo” inter-conversion of chiral drug molecules, *J. Chromatogr. B Anal. Technol. Biomed. Life Sci.* 1084 (2018) 89–95.
- [84] C.J. Venkatramani, et al., Simultaneous achiral-chiral analysis of pharmaceutical compounds using two-dimensional reversed phase liquid chromatography-supercritical fluid chromatography, *Talanta* 148 (2016) 548–555.
- [85] V. Desfontaine, J.L. Veuthey, D. Guillarme, Hyphenated detectors, in: C.F. Poole (Ed.), *Supercritical Fluid Chromatography*, Elsevier, 2017, pp. 213–244.
- [86] J. Chen, et al., Supercritical fluid chromatography-tandem mass spectrometry for the enantioselective determination of propranolol and pindolol in mouse blood by serial sampling, *Anal. Chem.* 78 (4) (2006) 1212–1217.
- [87] R.A. Coe, J.O. Rathe, J.W. Lee, Supercritical fluid chromatography-tandem mass spectrometry for fast bioanalysis of R/S-warfarin in human plasma, *J. Pharm. Biomed. Anal.* 42 (5) (2006) 573–580.
- [88] X. Xu, et al., Analysis of fifteen estrogen metabolites using packed column supercritical fluid chromatography-mass spectrometry, *Anal. Chem.* 78 (5) (2006) 1553–1558.
- [89] D. Wolrab, P. Fruhauf, C. Gerner, Direct coupling of supercritical fluid chromatography with tandem mass spectrometry for the analysis of amino acids and related compounds: comparing electrospray ionization and atmospheric pressure chemical ionization, *Anal. Chim. Acta* 981 (Supplement C) (2017) 106–115.
- [90] F. Jumaah, et al., A rapid method for the separation of vitamin D and its metabolites by ultra-high performance supercritical fluid chromatography-mass spectrometry, *J. Chromatogr. A* 1440 (2016) 191–200.
- [91] M.S. Gross, et al., Analysis of hydroxylated polybrominated diphenyl ethers (OH-BDEs) by supercritical fluid chromatography/mass spectrometry, *Talanta* 161 (2016) 122–129.
- [92] T.T. Liu, et al., Simultaneous profiling of vitamin D metabolites in serum by supercritical fluid chromatography-tandem mass spectrometry (SFC-MS/MS), *J. Chromatogr. B Anal. Technol. Biomed. Life Sci.* 1120 (2019) 16–23.
- [93] M.K. Parr, et al., Splitless hyphenation of SFC with MS by APCI, APPI, and ESI exemplified by steroids as model compounds, *J. Chromatogr. B Anal. Technol. Biomed. Life Sci.* 1091 (2018) 67–78.
- [94] D. Klink, O.J. Schmitz, SFC-APLI-(TOF)MS: hyphenation of supercritical fluid chromatography spectrometry, *Anal. Chem.* 88 (1) (2016) 1058–1064.
- [95] J. Duval, et al., Contribution of supercritical fluid chromatography coupled to high resolution mass spectrometry and UV detections for the analysis of a complex vegetable oil—application for characterization of a Kniphofia uvaria extract, *C. R. Chim.* 19 (9) (2016) 1113–1123.
- [96] V. Hrbek, et al., Utilization of supercritical fluid chromatography for lipidomic profilation of soya bean and cow milk: authenticity and detection of adulteration, *Chem. List.* 109 (7) (2015) 518–526.
- [97] M. Mejean, A. Brunelle, D. Touboul, Quantification of tocopherols and tocotrienols in soybean oil by supercritical-fluid chromatography coupled to high-resolution mass spectrometry, *Anal. Bioanal. Chem.* 407 (17) (2015) 5133–5142.
- [98] A.G.G. Perrenoud, et al., Combining the full potential of UHPSFC-QToF/MS and UHPLC-QToF/MS to improve the workflow efficiency of both plant metabolic profiling and natural bioactive discovery, *Planta Med.* 82 (2016).



- [99] A. Grand-Guillaume Perrenoud, et al., Ultra-high performance supercritical fluid chromatography coupled with quadrupole-time-of-flight mass spectrometry as a performing tool for bioactive analysis, *J. Chromatogr. A* 1450 (2016) 101–111.
- [100] J. Prothmann, et al., Ultra-high-performance supercritical fluid chromatography with quadrupole-time-of-flight mass spectrometry (UHPSFC/QTOF-MS) for analysis of lignin-derived monomeric compounds in processed lignin samples, *Anal. Bioanal. Chem.* 409 (30) (2017) 7049–7061.
- [101] J. Duval, et al., Hyphenation of ultra high performance supercritical fluid chromatography with atmospheric pressure chemical ionisation high resolution mass spectrometry. Part 1. Study of the coupling parameters for the analysis of natural non-polar compounds, *J. Chromatogr. A* 1509 (2017) 132–140.
- [102] X. Shi, et al., Systematic profiling and comparison of the lipidomes from *Panax ginseng*, *P. quinquefolius*, and *P. notoginseng* by ultrahigh performance supercritical fluid chromatography/high-resolution mass spectrometry and ion mobility-derived collision cross section measurement, *J. Chromatogr. A* 1548 (2018) 64–75.
- [103] J. Duval, et al., Hyphenation of ultra-high performance supercritical fluid chromatography with atmospheric pressure chemical ionisation high resolution mass spectrometry. Part 2. Study of chromatographic and mass spectrometry parameters for the analysis of natural non-polar compounds, *J. Chromatogr. A* (2019).
- [104] T. Yamada, et al., Supercritical fluid chromatography/Orbitrap mass spectrometry based lipidomics platform coupled with automated lipid identification software for accurate lipid profiling, *J. Chromatogr. A* 1301 (2013) 237–242.
- [105] H. Takeda, et al., Lipidomic analysis of plasma lipoprotein fractions in myocardial infarction-prone rabbits, *J. Biosci. Bioeng.* 120 (4) (2015) 476–482.
- [106] Y. Yang, et al., Lipidomics study of the protective effects of isosteviol sodium on stroke rats using ultra high-performance supercritical fluid chromatography coupling with ion-trap and time-of-flight tandem mass spectrometry, *J. Pharm. Biomed. Anal.* 157 (2018) 145–155.
- [107] A. Tu, et al., A comparative study of triacylglycerol composition in Chinese human milk within different lactation stages and imported infant formula by SFC coupled with Q-TOF-MS, *Food Chem.* 221 (2017) 555–567.
- [108] Y. Liang, T. Zhou, Recent advances of online coupling of sample preparation techniques with ultra high performance liquid chromatography and supercritical fluid chromatography, *J. Sep. Sci.* 42 (1) (2019) 226–242.
- [109] T. Uchikata, et al., High-throughput phospholipid profiling system based on supercritical fluid extraction-supercritical fluid chromatography/mass spectrometry for dried plasma spot analysis, *J. Chromatogr. A* 1250 (2012) 69–75.
- [110] M. Suzuki, et al., Use of on-line supercritical fluid extraction-supercritical fluid chromatography/tandem mass spectrometry to analyze disease biomarkers in dried serum spots compared with serum analysis using liquid chromatography/tandem mass spectrometry, *Rapid Commun. Mass Spectrom.* 31 (10) (2017) 886–894.
- [111] M. Zoccali, et al., Carotenoids and apocarotenoids determination in intact human blood samples by online supercritical fluid extraction-supercritical fluid chromatography-tandem mass spectrometry, *Anal. Chim. Acta* 1032 (2018) 40–47.
- [112] A. Rios, M. Zougagh, F. de Andres, Bioanalytical applications using supercritical fluid techniques, *Bioanalysis* 2 (1) (2010) 9–25.
- [113] A. Matsubara, E. Fukusaki, T. Bamba, Metabolite analysis by supercritical fluid chromatography, *Bioanalysis* 2 (1) (2010) 27–34.
- [114] K. Taguchi, E. Fukusaki, T. Bamba, Supercritical fluid chromatography/mass spectrometry in metabolite analysis, *Bioanalysis* 6 (12) (2014) 1679–1689.
- [115] V. Pauk, K. Lemr, Forensic applications of supercritical fluid chromatography—mass spectrometry, *J. Chromatogr. B Anal. Technol. Biomed. Life Sci.* 1086 (2018) 184–196.
- [116] L. Laboureur, M. Ollero, D. Touboul, Lipidomics by supercritical fluid chromatography, *Int. J. Mol. Sci.* 16 (6) (2015) 13868–13884.
- [117] S.Y. Song, H.W. Liu, Y. Bai, Supercritical fluid chromatography and its application in lipid isomer separation, *J. Anal. Test.* 1 (4) (2017) 330–334.
- [118] Y. Yang, et al., Advances of supercritical fluid chromatography in lipid profiling, *J. Pharm. Anal.* 9 (1) (2019) 1–8.
- [119] H. Kocova Vlckova, et al., Current state of bioanalytical chromatography in clinical analysis, *Analyst* 143 (6) (2018) 1305–1325.
- [120] V. Shulaev, G. Isaac, Supercritical fluid chromatography coupled to mass spectrometry—a metabolomics perspective, *J. Chromatogr. B Anal. Technol. Biomed. Life Sci.* 1092 (2018) 499–505.

- [121] T. Berg, et al., Determination of a selection of synthetic cannabinoids and metabolites in urine by UHPSFC-MS/MS and by UHPLC-MS/MS, *Drug Test. Anal.* 8 (7) (2016) 708–722.
- [122] L. Borovcova, V. Pauk, K. Lemr, Analysis of new psychoactive substances in human urine by ultra-high performance supercritical fluid and liquid chromatography: validation and comparison, *J. Sep. Sci.* 41 (10) (2018) 2288–2295.
- [123] V. Pauk, et al., Fast separation of selected cathinones and phenylethylamines by supercritical fluid chromatography, *J. Chromatogr. A* 1423 (2015) 169–176.
- [124] B.C.H. van der Nagel, et al., Quantification of phosphatidylethanol in whole blood as a proxy for chronic alcohol consumption, using ultra performance convergence chromatography tandem mass spectrometry, *Ther. Drug Monit.* 40 (2) (2018) 268–275.
- [125] L. Novakova, et al., Ultra high performance supercritical fluid chromatography coupled with tandem mass spectrometry for screening of doping agents. I. Investigation of mobile phase and MS conditions, *Anal. Chim. Acta* 853 (2015) 637–646.
- [126] V. Desfontaine, et al., Supercritical fluid chromatography in pharmaceutical analysis, *J. Pharm. Biomed. Anal.* 113 (2015) 56–71.
- [127] M.K. Parr, et al., Distinction of clenbuterol intake from drug or contaminated food of animal origin in a controlled administration trial—the potential of enantiomeric separation for doping control analysis, *Food Addit. Contam. A Chem. Anal. Control Expo. Risk Assess* 34 (4) (2017) 525–535.
- [128] L. Beucher, et al., Specific characterization of non-steroidal selective androgen receptor modulators using supercritical fluid chromatography coupled to ion-mobility mass spectrometry: application to the detection of enobosarm in bovine urine, *Drug Test. Anal.* 9 (2) (2017) 179–187.
- [129] Y. Tao, et al., Simultaneous determination of seven gestagens in kidney fats by Ultra Performance Convergence Chromatography tandem mass spectrometry, *J. Chromatogr. B Anal. Technol. Biomed. Life Sci.* 988 (2015) 143–148.
- [130] H.Y. Eom, et al., Rapid chiral separation of racemic cetirizine in human plasma using subcritical fluid chromatography-tandem mass spectrometry, *J. Pharm. Biomed. Anal.* 117 (2016) 380–389.
- [131] H. Licea Perez, D. Knecht, C.A. Evans, Overcoming bioanalytical challenges associated with the separation and quantitation of GSK1278863, a HIF-prolyl hydroxylase inhibitor, and its 14 stereoisomeric metabolites, *J. Chromatogr. B Anal. Technol. Biomed. Life Sci.* 1009-1010 (2016) 7–16.
- [132] C. Jin, et al., Supercritical fluid chromatography coupled with tandem mass spectrometry: a high-efficiency detection technique to quantify Taxane drugs in whole-blood samples, *J. Sep. Sci.* 40 (19) (2017) 3914–3921.
- [133] Y. Li, et al., A sensitive, high-throughput, and eco-friendly analysis of daidzein and its valine carbamate prodrug in rat plasma by supercritical fluid chromatography with tandem mass spectrometry, *J. Sep. Sci.* 41 (16) (2018) 3250–3257.
- [134] T.R. Prasad, et al., Enantioselective supercritical fluid chromatography-tandem mass spectrometry method for simultaneous estimation of risperidone and its 9-hydroxyl metabolites in rat plasma, *Bioanalysis* 9 (22) (2017) 1739–1750.
- [135] Y. Yang, et al., A sensitive, high-throughput, and ecofriendly method for the determination of lumefantrine, artemether, and its active metabolite dihydroartemisinin by supercritical fluid chromatography and tandem mass spectrometry, *J. Sep. Sci.* 41 (12) (2018) 2688–2696.
- [136] X.G. Liu, et al., Accurate analysis of ginkgolides and their hydrolyzed metabolites by analytical supercritical fluid chromatography hybrid tandem mass spectrometry, *J. Chromatogr. A* 1388 (2015) 251–258.
- [137] Z. Yang, et al., Simultaneous quantitation of the diastereoisomers of scholarisine and 19-epischolarisine, vallesamine, and picrinine in rat plasma by supercritical fluid chromatography with tandem mass spectrometry and its application to a pharmacokinetic study, *J. Sep. Sci.* 39 (13) (2016) 2652–2660.
- [138] R. Yang, et al., An improvement of separation and response applying post-column compensation and one-step acetone protein precipitation for the determination of coenzyme Q10 in rat plasma by SFC-MS/MS, *J. Chromatogr. B Anal. Technol. Biomed. Life Sci.* 1031 (2016) 221–226.
- [139] X. Zhang, et al., Supercritical fluid chromatography-tandem mass spectrometry for high throughput bioanalysis of small molecules in drug discovery, *J. Pharm. Biomed. Anal.* 164 (2019) 62–69.
- [140] Y. Li, et al., Quantification of 3-n-butylphthalide in beagle plasma samples by supercritical fluid chromatography with triple quadrupole mass spectrometry and its application to an oral bioavailability study, *J. Sep. Sci.* 38 (4) (2015) 697–702.



- [141] B. Guo, et al., Supercritical fluid chromatography with tandem mass spectrometry combined with postcolumn compensation and one-step acetone protein precipitation to evaluate the bioavailability of probucol solid dispersion tablet, *J. Sep. Sci.* 39 (19) (2016) 3677–3682.
- [142] X. Li, et al., A rapid analysis of piroxicam in beagle plasma applying evaporation-free liquid-liquid extraction by supercritical fluid chromatography-tandem mass spectrometry, *J. Chromatogr. B Anal. Technol. Biomed. Life Sci.* 1100–1101 (2018) 93–99.
- [143] M. Di, et al., A rapid and sensitive supercritical fluid chromatography/tandem mass spectrometry method for detection of ezetimibe in dog plasma and its application in pharmacokinetic studies, *J. Chromatogr. B Anal. Technol. Biomed. Life Sci.* 1073 (2018) 177–182.
- [144] C. Su, et al., Determination of rabeprazole enantiomers in dog plasma by supercritical fluid chromatography tandem mass spectrometry and its application to a pharmacokinetic study, *J. Sep. Sci.* 40 (4) (2017) 1010–1016.
- [145] L. Laboureur, et al., Profiling of modified nucleosides from ribonucleic acid digestion by supercritical fluid chromatography coupled to high resolution mass spectrometry, *J. Chromatogr. A* 1537 (2018) 118–127.
- [146] D. Wolrab, P. Fruhauf, C. Gerner, Quantification of the neurotransmitters melatonin and N-acetyl-serotonin in human serum by supercritical fluid chromatography coupled with tandem mass spectrometry, *Anal. Chim. Acta* 937 (2016) 168–174.
- [147] C. Shackleton, O.J. Pozo, J. Marcos, GC/MS in recent years has defined the normal and clinically disordered steroidome: will it soon be surpassed by LC/tandem MS in this role? *J. Endocr. Soc.* 2 (8) (2018) 974–996.
- [148] K.H. Storbeck, et al., The utility of ultra-high performance supercritical fluid chromatography-tandem mass spectrometry (UHPSFC-MS/MS) for clinically relevant steroid analysis, *J. Chromatogr. B Anal. Technol. Biomed. Life Sci.* 1085 (2018) 36–41.
- [149] M. Doue, et al., Analysis of glucuronide and sulfate steroids in urine by ultra-high-performance supercritical-fluid chromatography hyphenated tandem mass spectrometry, *Anal. Bioanal. Chem.* 407 (15) (2015) 4473–4484.
- [150] J.L. Quanson, et al., High-throughput analysis of 19 endogenous androgenic steroids by ultra-performance convergence chromatography tandem mass spectrometry, *J. Chromatogr. B Anal. Technol. Biomed. Life Sci.* 1031 (2016) 131–138.
- [151] T. du Toit, et al., Profiling adrenal 11 $\beta$ -hydroxyandrostenedione metabolites in prostate cancer cells, tissue and plasma: UPC(2)-MS/MS quantification of 11 $\beta$ -hydroxytestosterone, 11keto-testosterone and 11keto-dihydrotestosterone, *J. Steroid Biochem. Mol. Biol.* 166 (2017) 54–67.
- [152] N. de Kock, et al., A novel targeted analysis of peripheral steroids by ultra-performance supercritical fluid chromatography hyphenated to tandem mass spectrometry, *Sci. Rep.* 8 (1) (2018) 16993.
- [153] J. Teubel, et al., Methods in endogenous steroid profiling—a comparison of gas chromatography mass spectrometry (GC-MS) with supercritical fluid chromatography tandem mass spectrometry (SFC-MS/MS), *J. Chromatogr. A* 1554 (2018) 101–116.
- [154] K. Taguchi, E. Fukusaki, T. Bamba, Simultaneous and rapid analysis of bile acids including conjugates by supercritical fluid chromatography coupled to tandem mass spectrometry, *J. Chromatogr. A* 1299 (2013) 103–109.
- [155] C. Jenkinson, et al., Analysis of multiple vitamin D metabolites by ultra-performance supercritical fluid chromatography-tandem mass spectrometry (UPSFC-MS/MS), *J. Chromatogr. B Anal. Technol. Biomed. Life Sci.* 1087–1088 (2018) 43–48.
- [156] E.L. Regalado, C.J. Welch, Separation of achiral analytes using supercritical fluid chromatography with chiral stationary phases, *TrAC—Trends Anal. Chem.* 67 (2015) 74–81.
- [157] F. Petruzzello, et al., Quantitative profiling of endogenous fat-soluble vitamins and carotenoids in human plasma using an improved UHPSFC-ESI-MS interface, *Anal. Chem.* 89 (14) (2017) 7615–7622.
- [158] A.U.S.J. Kumari, S.R. Acharya, J. Bergquist, A novel, fast and sensitive supercritical fluid chromatography-tandem mass spectrometry (SFC-MS/MS) method for analysis of arachidonic acid metabolites, *Analyst* 143 (15) (2018) 3661–3669.
- [159] M. Lisa, M. Holcapek, M. Giera (Ed.), UHPSFC/ESI-MS analysis of lipids, in *clinical metabolomics: methods and protocols*, 2018, pp. 73–82.
- [160] J.W. Lee, et al., Development of a polar lipid profiling method by supercritical fluid chromatography/mass spectrometry, *J. Sep. Sci.* 34 (24) (2011) 3553–3560.
- [161] T. Uchikata, et al., Development of oxidized phosphatidylcholine isomer profiling method using supercritical fluid chromatography/tandem mass spectrometry, *J. Chromatogr. A* 1250 (2012) 205–211.
- [162] M. Lisa, M. Holcapek, High-throughput and comprehensive lipidomic analysis using ultrahigh-performance supercritical fluid chromatography-mass spectrometry, *Anal. Chem.* 87 (14) (2015) 7187–7195.

- [163] M. Lisa, et al., Lipidomic analysis of biological samples: comparison of liquid chromatography, supercritical fluid chromatography and direct infusion mass spectrometry methods, *J. Chromatogr. A* 1525 (2017) 96–108.
- [164] R. Berkecz, M. Lisa, M. Holcapek, Analysis of oxylipins in human plasma: comparison of ultrahigh-performance liquid chromatography and ultrahigh-performance supercritical fluid chromatography coupled to mass spectrometry, *J. Chromatogr. A* 1511 (2017) 107–121.
- [165] H. Takeda, et al., Widely-targeted quantitative lipidomics method by supercritical fluid chromatography triple quadrupole mass spectrometry, *J. Lipid Res.* 59 (7) (2018) 1283–1293.
- [166] J.W. Jones, et al., Ultrapformance convergence chromatography-high resolution tandem mass spectrometry for lipid biomarker profiling and identification, *Biomed. Chromatogr.* (2017) 31(3).
- [167] S. Al Hamimi, et al., Screening of stationary phase selectivities for global lipid profiling by ultrahigh performance supercritical fluid chromatography, *J. Chromatogr. A* 1548 (2018) 76–82.

# AMS in drug development: Exploring the current utility of AMS and future opportunities for absolute bioavailability and ADME investigations

Graeme C. Young<sup>a</sup>, Marie Croft<sup>b</sup>

<sup>a</sup>GlaxoSmithKline Research and Development Ltd., David Jack Centre, Ware, United Kingdom

<sup>b</sup>Pharmaron ABS, Germantown, MD, United States

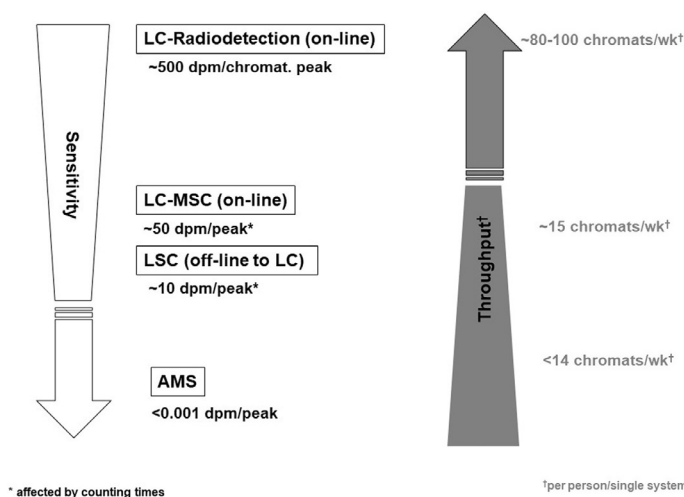
## 1 Introduction

The characterization of the rates and routes of metabolism and excretion of new drugs in humans facilitates the assessment of their safety and is an expectation for regulatory approval for new medicines [1].

Administration of radiocarbon-labeled drug (typically <sup>14</sup>C isotope) is used in studies to trace the ADME-PK of the drug during development. Until the early 2000s, the primary analytical methods used to determine blood and excreta concentrations were liquid scintillation counting (LSC) and LC with radiodetection. Although still routinely used, these techniques can lack sensitivity to deliver on study objectives in humans and nonclinical species (see Section 5).

In recent years, Accelerator Mass Spectrometry (AMS), a nuclear physics isotope ratio technique, with greater sensitivity than these primary methods, has been used as an enabling technology for novel applications in pharmaceutical drug discovery and development. The relative sensitivities and (often counterposed) sample throughput for a variety of radiodetection methods are shown in Fig. 1. A comprehensive text on Radiotracers in Drug

FIG. 1 Relative approximated sensitivities and sample throughputs for a range of analytical radiodetection techniques (as measured for chromatographic separation followed by peak detection). *Credit: Created by G. Young.*



Development [2] is available for background reading on the broad range of technologies and approaches utilized. The reader is also referred to the earlier textbook in this series [3], providing in-depth details of the sensitive technique of microplate scintillation counting (MSC) in conjunction with LC-MS, for low-level detection of radiolabeled analytes. We acknowledge that AMS is used in support of more than just clinical studies; however, the focus of this chapter is on clinical applications. Animal studies and areas of application beyond drug development such as carbon dating and environmental tracing are outside the scope of this chapter.

## 2 Introduction of the AMS technique

### 2.1 AMS vs. conventional methods

$^{14}\text{C}$  is commonly quantified by measuring the number of photons emitted over a given time during  $\beta^-$ -decay such as by LSC or MSC. A calibrated scintillation counter converts the number of photons detected to the number of decay events over a given time. Due to the long half-life of  $^{14}\text{C}$  ( $\sim 5700$  years), only  $2 \times 10^{-8}\%$  of the  $^{14}\text{C}$  in a sample decays in 1 min, making decay counting extremely inefficient [4].

Typically, the raw units of radioactive measurement from an LSC instrument are counts, which are presented as counts per minute (cpm). The background radiation in modern LSC instruments varies, by instrument, but is approximately 10 cpm. Traditionally, the lower limit of quantification (LLoQ) for LSC is defined as multiples of background, usually at least two-fold and so approximately 20 cpm [5] (with a typical counting time of 15 min). Cpm are converted to disintegrations per minute (dpm), the fundamental unit of radioactivity from which all other units are derived ( $1 \text{ Bq} = 60 \text{ dpm}$ ,  $1 \text{ Ci} = 2.22 \times 10^{12} \text{ dpm}$ ). The conversion is made via instrument calibration and assessment of counting efficiency. Although cpm does not equal dpm, these are treated as equivalent for this example and therefore an LLoQ for LSC can be approximated as 20 dpm.

To highlight the impact of this modest LLoQ by LSC, in the world of archeology, to radio-carbon date famous artifacts such as the Shroud of Turin, a large piece (probably around the size of a handkerchief) would have been required to be sampled, by destructive analysis, for adequate sensitivity to be achieved by LSC. It was largely for these reasons that a more sensitive method of  $^{14}\text{C}$  detection was sought, which culminated in the development of Accelerator Mass Spectrometry (AMS) in the mid-1970s [6,7].

The advent of AMS provided sufficient increase in sensitivity over that of LSC to allow dating through analysis of only a few milligrams of material [8]. The first experiments applying AMS to investigations in the biomedical field occurred in the 1990s [9,10] marking the transition from research-based applications to the use of AMS as an analytical technique in drug development.

## 2.2 Application of AMS to drug development

AMS is typically used instead of, or as a complementary analytical technique to, LSC for the following reasons:

- (1) To reduce radiation burden to human volunteers, for instance, where the drug under development has shown retention of either the parent drug or radioactive drug-related material (RDM) in nonclinical studies, a clinical study can be successfully conducted using a vastly reduced amount of radioactivity in the dose. This approach leads to reduced exposure of the subject to ionizing radiation [11].
- (2) Where radiolytic instability of the dose has necessitated a lower dose of radiation [12].
- (3) In studies in vulnerable populations, such as pediatric subjects [13–15], which further reinforce the need to keep radiation burden to a minimal level.
- (4) To introduce flexibility to the study design, for example, multiple radioactive doses. The possibility of reduced radiation burden to the subject allows for more than one radioactive dose to be administered if required, either as pulse doses [16] or even as multiple repeat doses of radioactivity [17]. Before the advent of AMS, such studies in human subjects were extremely rare.
- (5) To allow sample collection over an extended period. A highly sensitive method allows monitoring of the pharmacokinetics and excretion of the drug under investigation and so samples can be collected for weeks or even months after dosing [11,18] rather than just for up to 1 week which is the conventional approach for human ADME studies. When using higher doses of radioactive drug, subjects can only be discharged from the clinic once levels being excreted have reached acceptable amounts. AMS allows for very low levels of radioactivity to be administered, thereby enabling subjects to be released from the clinic at any time and they may even return for outpatient visits to provide more samples should there be a requirement to further define the excretion profile [19].
- (6) In support of the concomitant dosing approach. The design and application of the “so-called” IV microtracer study have been revolutionized using AMS (see Section 7).
- (7) To allow dosing by alternative dose routes. Administration of drug via routes such as ocular [17] and dermal [20] can be facilitated using the sensitivity of AMS.

## 2.3 Sample preparation (“graphitization”)

Unlike LSC, where radioactive samples are either added directly to liquid scintillant (or subjected to a very simple combustion/ $\text{CO}_2$  capture in scintillant), samples for analysis by AMS require conversion to a common matrix; most commonly elemental carbon (“graphite”), before isotope ratio measurement. Graphite production occurs via a two-step process of oxidation to  $\text{CO}_2$  followed by reduction to graphite [21].

Several procedures have been developed for the preparation of graphite; a typical process is outlined here and described in detail elsewhere [22].

Quartz tubes containing the sample with the addition of supplemental carbon source (so-called “carbon carrier” / “isotopic dilutor”) where required (see Fig. 2), and copper (II) oxide wire, are dried under vacuum in a centrifugal evaporator. The quartz tubes are heat-sealed inside larger evacuated quartz tubes before combustion at high temperature, for example,  $900^\circ\text{C}$  for 1–2h. The resulting  $\text{CO}_2$  is cryogenically transferred into evacuated borosilicate tubes containing zinc powder and titanium dihydride and a cobalt catalyst and the reduction tubes are heat-sealed. The sealed reduction tubes are heated for 6–10h at

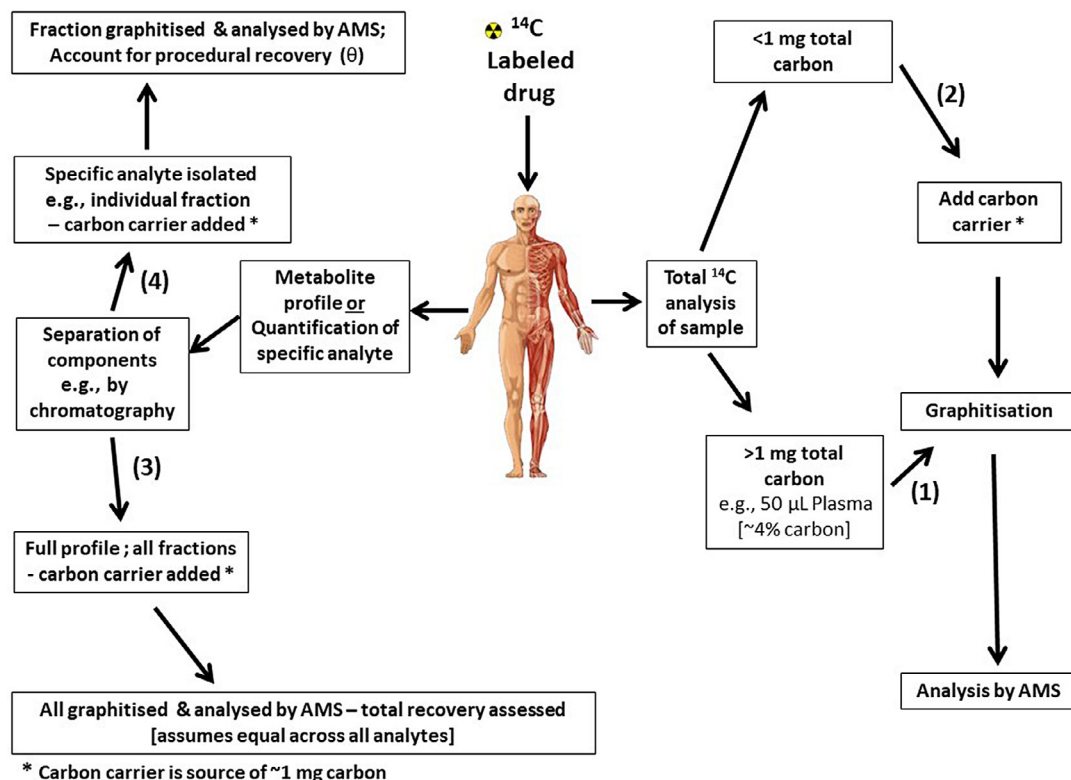


FIG. 2 Outline of the procedures for analysis by AMS depending on sample origin\*. Total  $^{14}\text{C}$  analysis by AMS [without (1) and with (2) addition of carbon carrier], metabolite profiling (3) and isolated individual analyte assay by LC+AMS (4). Credit: G. Young, PhD Thesis, University of Lincoln, UK, 2016.

approximately 500°C to complete the graphitization process. Carbon, as graphite, deposited on the cobalt, is pressed into aluminum cathodes and analyzed by AMS.

It is apparent from the above description that sample preparation is a demanding, albeit robust process. Without method optimization it can take at least 1 day (historically up to 3 days) post-preparation of the biological sample itself to complete the graphitization phase of the sample preparation. This explains the interest in finding alternative approaches to a more rapid sample preparation procedure or avoidance of it entirely [23]. In recent years, a method which allows the direct introduction of CO<sub>2</sub> has been developed [24] and is in use for the analysis of study samples in at least one facility. There are a variety of AMS instrument sizes and designs but for this chapter, we will concentrate on the single-stage AMS (SSAMS) instrument (manufactured by National Electrostatics Corporation (NEC), Wisconsin, USA).

## 2.4 Analysis by AMS

The graphite pressed into the cathode is ionized using a sputtering cesium ion beam (Cs<sup>+</sup>) which generates negative carbon ions; this is crucial as it removes interference from <sup>14</sup>N<sup>-</sup>, which is unstable and does not survive past the ion source. The <sup>12</sup>C, <sup>13</sup>C, and <sup>14</sup>C ions produced are separated based on their mass/charge ratio, sequentially accelerated to high velocities using a high potential difference (250 kV–10 MV; depending on the AMS design), and separately counted. The results are expressed as isotope ratios, which are normalized to the ratio provided by the consensus value standard (see Section 2.5), thus accounting for any variability in instrument response or sample processing. The radiocarbon content of the graphite samples is calculated from the isotope ratio, accounting for carbon content, sample volume analyzed (where relevant), extraction recovery (where applicable), and initial specific activity to provide the drug or drug-related material concentration. A detailed explanation is given in Section 2.5.

Unlike decay counting, which counts electrons emitted during β<sup>-</sup>-decay, AMS counts individual <sup>14</sup>C atoms and, typically, just 10,000 atoms are considered adequate to give a reliable result. When accounting for differences in background <sup>14</sup>C content between sample types and the larger amount of sample that can be analyzed by LSC, the inherent sensitivity of the AMS instrument translates, in practice, to a 200- to 400-fold lower limit of quantification for direct AMS (no carbon carrier added—see Section 2.3) measurements compared with total radioactivity analysis using LSC. To put this into context, if the calculated LLoQ by LSC for a plasma sample is 20 dpm/mL, then with AMS the LLoQ is around 0.07 dpm/mL. With the generation of good cathode currents (>5 μAmp high energy for <sup>12</sup>C<sup>+1</sup>; the most abundant ion at the energy generated by a 250 kV AMS), analysis times are usually around 4 min per cathode for biomedical work.

## 2.5 Data acquisition and calculations

Quantification of radiocarbon within an environment where it is present in the atmosphere and many surrounding organic molecules makes it vital that there is a thorough understanding of the carbon content for any sample under analysis [25]. Typically, a sample analyzed by



AMS requires between 0.5 and 2 mg carbon for a reliable measurement. Some samples have enough inherent carbon for direct analysis, for example, plasma has consistently 4.1% carbon and so 49  $\mu\text{L}$  will provide 2 mg carbon. The inherent carbon in urine, is much lower, typically at less than 0.5% [26]. For samples with much lower carbon content, the sample is supplemented with a known amount of additional carbon (the “carbon carrier” or “isotopic dilutor”—see Section 2.3). Carbon carrier is typically derived from petrochemical sources that are depleted of  $^{14}\text{C}$ . Addition of carbon carrier that contains a well-defined amount of  $^{14}\text{C}$ , changes the  $^{14}\text{C}:^{12}\text{C}$  isotopic ratio of the sample and therefore this must be accounted for in subsequent calculations. Fractions collected from liquid chromatography contain very low levels of carbon and so also require the addition of carbon carrier before analysis (see Section 2.6).

The  $^{14}\text{C}:^{12}\text{C}$  ratio of a sample is normalized using data generated from a known certificated standard [e.g., Australian National University (ANU) Sugar] which is graphitized alongside any samples for analysis by AMS. Further samples depleted of  $^{14}\text{C}$  are analyzed both to monitor instrument background and as further process controls to check that no introduction of unknown sources of carbon into the sample has occurred during sample preparation and that carryover during analysis is assessed. The  $^{14}\text{C}:^{12}\text{C}$  isotope ratio data generated are then used to calculate concentration values for prepared biological samples.

AMS data are provided as carbon isotope ratios, with the most important one being  $^{14}\text{C}:^{12}\text{C}$ , although  $^{13}\text{C}:^{12}\text{C}$  ratios are measured to ensure that the transmission ratio of all measured carbon isotopes is stable throughout the analysis, with no fractionation.

Due to the origin of AMS in carbon dating, the instrument output is typically expressed in units of percent Modern Carbon, which can be confusing for those involved in the development of pharmaceuticals. Modern, being 100% is defined as the atmospheric  $^{14}\text{C}:^{12}\text{C}$  isotope ratio in 1950. Because of atmospheric bomb tests after this date, background pMC had risen and ANU sugar harvested in 1969–1971 is certified at a consensus value of 150.61 pMC. 1 Modern or 100 pMC is defined as follows [27]:

$$100 \text{ pMC} = 98 \text{ attomoles}^{14}\text{C}/\text{mg C} = 0.01356 \text{ dpm}/\text{mg C} \quad (1)$$

Thus

$$\begin{aligned} \text{pMC} \times 0.0001356 &= \text{dpm}/\text{mg C} \text{ and} \\ (\text{dpm}/\text{mg}) \times \text{mg C in sample} &= \text{dpm} \text{ and} \\ \text{dpm}/\text{volume of sample } (\mu\text{L}) \times 1000 &= \text{dpm}/\text{mL}. \end{aligned}$$

The dpm/mL value and specific activity of the drug dosed are used to calculate mass per unit volume (e.g., pg drug equivalents/mL<sup>a</sup>) values.

So

$$(\text{dpm}/\text{mL})/\text{specific activity (dpm/pg)} = \text{pg drug equivalents}/\text{mL}^a$$

The fact that ANU sugar (or alternative certified standard) has been used as a single concentration standard for instrument data normalization may seem questionable considering that samples analyzed may be quite different in concentration to this standard. AMS, however, has been shown to be linear over five orders of magnitude [28,29] and of course, the

<sup>a</sup>Note that if total drug-related material is measured the final units are mass of drug equivalents per unit volume (e.g., pg drug equivalents/mL). If quantifying a specific  $^{14}\text{C}$ -analyte, then pg/mL applies.

sample analyzed in the instrument is always the same matrix (graphite) so there are no matrix variability effects to cause any analytical differences. For bioanalytical LC+AMS (Liquid Chromatography with off-line analysis by AMS) assay applications (see Section 2.7), where additional sample processing is required before AMS, additional spiked biological matrix-matched standards are prepared as further sample processing and quality control standards.

## 2.6 Calculation of analyte concentration

As stated above, to calculate the drug concentration from the isotope ratio requires knowledge of the total carbon in the sample, as described by Eq. (2) [30].

In some cases, such as when the total radioactivity ( $^{14}\text{C}$ ) of plasma is measured, there is sufficient naturally occurring carbon present within the sample to allow sufficient graphite to be prepared for analysis.

$$K = (R_m - R_n) \Psi (W/L) \quad (2)$$

where  $K$  = analyte concentration (mass equivalents per unit volume),  $R_m = ^{14}\text{C}:^{12}\text{C}$  isotope ratio of analyte (pMC),  $R_n$  = natural background  $^{14}\text{C}:^{12}\text{C}$  isotope ratio of the sample (pMC),  $\Psi$  = carbon mass fraction in the sample,  $W$  = molecular mass of the analyte,  $L$  = specific molar radioactivity (pMC/mol).

In other cases, the sample does not contain sufficient carbon to allow direct analysis as depicted in Fig. 2, therefore carrier carbon is added. Provided that a vast excess of carbon carrier is added relative to the native carbon from the sample, then  $\Psi$  in Eq. (2) is assumed to be the mass of carbon carrier added, simplifying the calculation.

In the early days of biomedical AMS, the carbon carrier was added to merely “bulk up” the mass of carbon to facilitate analysis [31]. Where samples were analyzed directly, for example, where a small volume of urine was taken for analysis, then the “carbon carrier” hypothesis was correct. In the case of LC fractions, however, it was found that another factor had to be considered when adding carbon to the sample, namely the procedural recovery. For example, where plasma samples are solvent extracted and analyzed by LC, there are potential procedural losses during this process. The addition of carbon carrier alters the isotope ratio in such a way that Eq. (2) assumes 100% of the original analyte in the matrix (e.g., plasma) is recovered in the fraction. Any loss of sample in extraction, or LC separation, results in a proportional error to the calculation of the mass of drug per volume sample from the isotope ratio. These losses are accounted for when calculating the mass of drug per volume sample, as shown in Eq. (3), derived from Eq. (2) [30] including an additional function,  $\theta$ , which represents the fraction of the analyte recovered. The value for  $\theta$  ranges from 0 to 1 [30] (also see Fig. 2).

$$K = (R_D \Phi) / (L_m \theta) \quad (3)$$

$K$  = mass concentration of drug,

$R_D = R_m - R_n$  (as defined in Eq. 2).

$\Phi$  is the equivalent of  $\Psi$  (in Eq. 3), but whereas  $\Psi$  is the intrinsic carbon in the sample,  $\Phi$  is the amount of carbon added as “carrier.” It assumes that the mass of carbon in the sample (e.g., LC fraction) is negligible as volatiles such as LC solvents are evaporated, such that only

carbon from drug-related material remains. The total carbon present is then equal to that added as the carrier. The amount of carbon carrier added is typically 1000-fold higher than that present in the sample.

$L_m$  = specific activity (expressed in terms of pMC/mass).  $\theta$  = fraction recovered, i.e., if there is a procedural loss of 20% during extraction and preparation by LC, then  $\theta = 0.8$ .

## 2.7 Validation of LC+AMS

To be able to provide reliable pharmacokinetic data in support of absolute bioavailability studies (see Section 7.1), the AMS technique [9,32] and its application as a bioanalytical approach requires validation [33,34].

For individual analyte measurement, a separation technology such as liquid chromatography is used (LC+AMS) in advance of the combustion steps detailed above. This overall approach is more akin to the conventional bioanalysis by LC-MS but uses the radiotracer present to assess the analyte content in the sample of interest, rather than the mass of the drug. There is currently no specific regulatory method validation guidance that includes AMS as an analytical technique, however, application of LC+AMS to absolute bioavailability assessment brought the need to validate this approach into sharp focus, since the reference (intravenous route) data was provided by AMS and the test (extravascular route) data was provided by validated LC-MS assay. The AMS data, therefore, had to be shown to meet acceptable criteria for a bioanalytical assay approach. Research efforts over several years and across many laboratories provided this data and indeed efforts were made to harmonize the approaches to validation of LC+AMS [35,36] and many studies have been conducted for subsequently marketed medicines [37–44].

## 2.8 Evolution of AMS

The technical evolution of AMS instrumentation has been significant over recent decades [45]. Instruments have been simplified, the size and complexity reduced while their sensitivity has been honed to be applications driven. A good example is AMS instruments which have been designed and built specifically for the analysis of carbon, whereas larger instruments can analyze a range of elemental isotopes by virtue of their higher energies. These developments have created a wide spread use of AMS in modern research fields [4]. Today, commercial high-performance instruments are in use in more than 100 AMS facilities around the world although those conducting biomedical work are only a few.

Voltages less than about 2.5 MV were thought to be inadequate for dissociating molecular background interferences until the ETH Zurich group demonstrated low background carbon AMS with 0.5 MV tandem accelerators [46]. This breakthrough led to the development of the 250 kV single-stage AMS [47]. The first carbon-dedicated AMS system was built and tested around 2003. Initial test results showed precision for  $^{14}\text{C}:^{12}\text{C}$  ratios and backgrounds for unprocessed graphite that were compatible with the requirements of  $^{14}\text{C}$  enriched biological sample measurements. From this prototype, the 250 kV SSAMS emerged as a commercially viable instrument. The most recent evolutions of the AMS instrument technology have been

a further reduction in the footprint of the instruments. Instrument size reduction was a useful practical improvement; however, the real breakthrough was around sample introduction and interfacing of the instrument with direct introduction of gas (carbon dioxide from the combusted sample, with a helium carrier). This approach removed much of the resource-intensive, low sample throughput of the graphitization process, while offering apparent further improved sensitivity [24]. Particularly for metabolite profiling, this improvement in sample throughput could bring a step change in the application of AMS to drug development by removing the time-consuming graphitization process. There are, at this time, only a very few systems capable of this in an automated fashion [24,48–50] and as inferred above there are limited data in the public domain to demonstrate the potential improvements over graphite. Sample-to-sample carryover seems to be a concern for the analysis of gas, but again there is hope that this can be managed and/or reduced with further interfacing and instrument development research. Some drug development research, such as for pediatric drug applications, is being established through these technological advances [51].

### 3 Clinical study design definitions

It is worth highlighting some commonly used definitions in the fields of application of AMS to a variety of study designs:

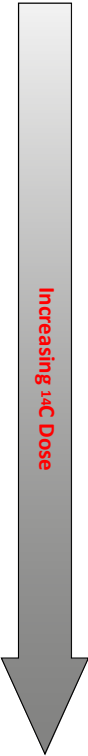
A **hybrid** (or **macrotracer**) study is one where the ionizing radiation dose is of conventional magnitude (for clinical, perhaps as high as  $\geq 100 \mu\text{Ci}$ ;  $\geq 3.7 \text{MBq}$ ) but where certain study objectives can only be achieved with AMS in addition to LSC or MSC, as mentioned above. Studies should be designed with the principle of minimizing the dose of the radioactive substance administered to humans to allow study objectives to be met in accordance with risk categories associated with ionizing radiation [52].

A **microdose** is determined to be as per the ICH guidance [53], i.e., for small molecules, it is  $\leq 100 \mu\text{g}$  and  $\leq 1/100\text{th}$  of the pharmacologically active dose; whichever is the lower dose. For detection, the drug can be either isotopically labeled or not, depending on a variety of factors (discussed later). Note that application of AMS to support of microdosing in the Phase-0 setting [54,55] is not discussed in this chapter as we have focused on Phase-1 of clinical development and beyond.

A **concomitant microtracer** is generally determined to be an isotopically labeled substance (radioactive or stable isotope) administered intravenously along with a considerably higher extravascular dose(s). In recent years, the term microtracer has been adopted to also apply to situations where merely a very low dose of ionizing radiation (typically  $\leq 1 \mu\text{Ci}$ ) is incorporated into the drug of interest (whether administered by the intravenous or extravascular alone).

As this chapter highlights, in the last two decades AMS has developed from being a little-known niche technology, only used as a last resort in drug development, to a more mainstream analytical tool that facilitates a variety of clinical study designs, providing deep insights into the pharmacokinetics and metabolic fate of new drugs (see Table 1).

TABLE 1 Summary of clinical study designs supported by AMS, typical outputs, and literature examples.

	Study category	Design features	Study outputs	Comments	Study examples (References)
	(Concomitant) microtracer	IV $^{14}\text{C}$ microdose ( $\leq 37\text{ kBq}$ ; $\leq 1\ \mu\text{Ci}$ ) and oral therapeutic dose administered concomitantly	<ul style="list-style-type: none"> <li>• Parental and therapeutic route PK incl. Abs. bioavailability</li> <li>• Metabolism insights only unless combined into human ADME study</li> <li>• Excretion routes</li> </ul>	<ul style="list-style-type: none"> <li>• AMS technology required unless <math>^{13}\text{C}</math> tracer used instead of <math>^{14}\text{C}</math></li> <li>• Metabolite standards required for retention time comparison if low chemical mass</li> </ul>	[40–43,73,74,77,78,80]
	Tracer dose	Therapeutic dose ( $\leq 111\text{ kBq}$ ; $\leq 3\ \mu\text{Ci}$ ) administered via therapeutic route	<ul style="list-style-type: none"> <li>• Mass balance incl. extended sample collections</li> <li>• Extractability</li> <li>• Metabolite profiles</li> </ul>	<ul style="list-style-type: none"> <li>• AMS technology required</li> <li>• Metabolite standards required for retention time comparison if low chemical mass</li> </ul>	[11,12,15–17,44,63,64,66,80]
	Hybrid/Macrotracer	$^{14}\text{C}$ dosed ( $\leq 3.7\text{ MBq}$ ; $\leq 100\ \mu\text{Ci}$ ) via therapeutic route; radioanalysis by both LSC/MS & AMS	<ul style="list-style-type: none"> <li>• Mass balance</li> <li>• Extractability</li> <li>• Metabolite profiles</li> <li>• Metabolite identification</li> </ul>	<ul style="list-style-type: none"> <li>• Generally prohibitive and logistically challenging for patient populations except oncology</li> </ul>	[38,56,59,60]
	Dual tracer	IV $^{13}\text{C}$ microdose and oral $^{14}\text{C}$ therapeutic dose administered concomitantly	<ul style="list-style-type: none"> <li>• Parental and therapeutic route PK incl. Abs. bioavailability</li> <li>• Mass balance</li> <li>• Extractability</li> <li>• Metabolite profiles</li> <li>• Excretion routes</li> </ul>	<ul style="list-style-type: none"> <li>• Elegant design—especially useful late in development if IV data not yet available and no need for <math>^{14}\text{C}</math> enabled outputs from IV dose</li> </ul>	[74–76]

Note that further approaches such as combining the microtracer design with the conventional human ADME leads to even richer data outputs. The table includes some generalizations for ease of reference.

Adapted from C. Beaumont, et al., *B/CP* 78 (2014) 1185–1200.

## 4 First drug development clinical study application of AMS

As stated earlier, a wide variety of clinical study designs that incorporate the use of radio-carbon as a tracer have been made possible through the application of AMS as the sensitive analytical tool.

Experiments conducted on new drugs in development using AMS across the pharmaceutical industry were first mainly focused on human ADME studies for molecules that had persistent retention, such as long pharmacokinetic elimination half-lives [39,42] or high melanin binding [56], where clinical study radioactive exposure to  $^{14}\text{C}$  to allow objectives to be met would be problematic.

The use of AMS for a pilot human ADME study was first described for work conducted around the turn of the millennium [57], with the following objectives:

- (1) To determine the rates and routes of excretion of a new chemical entity (NCE), GI181771 (a cholecystokinin-A agonist for potential use in appetite suppression), following oral administration to healthy volunteers.
- (2) To determine the biotransformation pathways for GI181771 in humans.
- (3) To investigate the utility of AMS to facilitate human ADME with reduced radiation burden to the subjects.

Before this publication, others had conducted preliminary and evaluation studies with pharmaceuticals, but these were using in vitro dilutions to scale from the range of LSC to AMS [9,32], or from studies involving human volunteers in nutritional research. Such a study was the analysis of folic acid in a single subject with the low  $^{14}\text{C}$ -folic acid dose added to dietary intake on a single occasion and subsequent assessment of extended elimination of the dose (3.7 kBq) over 1 year! [18].

In the GI181771 clinical study, six healthy male volunteers were administered 2.7 mg of  $^{14}\text{C}$ -GI181771 (121 Bq; 3.3 nCi), which equated to an exposure to ionizing radiation of only  $0.06\ \mu\text{Sv}$  (Sieverts). This very low radioactive dose was driven by a prior manufactured specific activity and unexpected pharmacology in a previous study which required the planned target dose to be lowered, thus also lowering the radioactive dose to the same extent. This radioactive dose was more than 20,000-fold lower than for most conventional radioactive dose human ADME studies and nearly 17-fold below the targeted threshold of ionizing radiation exposure of  $1\ \mu\text{Sv}$ . At the time, this was an attractive proposition, i.e., to be able to conduct a clinical study with radiocarbon- labeled drug producing exposure to ionizing radiation at such a low level. At targeted exposures of  $<1\ \mu\text{Sv}$  certain approvals and enabling work were not required, such as those to facilitate dosimetry; a series of experiments that are used to calculate the dose of ionizing radiation that will be received by the human body.

To put the level of radioactivity used in such studies (and subsequent ionizing radiation exposure) into context, a 70-kg human adult subject's natural  $^{14}\text{C}$  content is in the region of 3.7 kBq [58], so this clinical study barely raised the exposure to ionizing radiation in the study subjects to above background ( $<5\%$  increase).

As the regulatory authorities became more familiar with the concept of AMS and the consequential lowering of  $^{14}\text{C}$  doses, over the intervening years and in several parts of the world, up to 37 kBq can now be administered to human subjects without the need for dosimetry data;

the assumption is that a dose of 37kBq will produce an exposure to ionizing radiation of  $<1\mu\text{Sv}$ . These changes accelerate study implementation and reduce the enabling resource burden placed upon such clinical experiments.

## 5 Hybrid studies (macrotracer)

Many of the applications of AMS have been to studies where insufficient sensitivity has been attainable from decay counting techniques and where either by original design or indeed as a supplemental “rescue” technique, AMS has been used [38,56]. In the case of dalcetrapib (an inhibitor of the cholesteryl ester transfer plasma protein), a second human ADME study was run since the original study which used conventional radiodetection methods failed to meet the study objectives, whereas for the repeat study AMS was used and the improved sensitivity allowed all planned endpoints to be delivered [59]. This study also showed some very nice use of two-dimensional chromatography to provide the required separation of the more than 80 metabolites identified!

Another study, of the adenosine 2a receptor antagonist, tozadenant, involved oral administration of 72 kBq ( $2\mu\text{Ci}$ )  $^{14}\text{C}$ -tozadenant (the reason for this low radioactive dose is not stated in the publication), followed by an analysis of samples by LSC [60]. Where the LSC LLoQ was reached for each of the different sample matrices (plasma, urine, and feces), the sample analysis switched to AMS. At the time of the study, there were questions regarding linearity between LSC and AMS, so spiked samples were prepared and analyzed by both instruments, demonstrating linearity between the two methods. It is standard practice in some laboratories for the LSC and AMS to be cross-calibrated, ensuring linearity of data in any given study.

To determine the rates and routes of excretion of a novel boron-containing antibiotic, GSK2251052, a human ADME study was conducted with a high chemical mass dose of 1500 mg  $^{14}\text{C}$ -GSK2251052 (0.6 MBq;  $16\mu\text{Ci}$ ) by the intravenous route (driven by a high predicted therapeutic dose) [56]. The intravenous route was used as this drug was intended for the treatment of systemic infections in a critical care setting. LSC was used for the mass balance support of the study. However, the high sensitivity of AMS was required due to the anticipated low concentrations of drug-related material in plasma and the low specific activity of the dose.

In a previous ADME study with  $^{14}\text{C}$ -GSK2251052 in the rat, excretion of radioactivity was not complete with evidence of melanin binding of drug-related material through retention in the uveal tract of the eye to 840h after dosing (unpublished material). The resultant dosimetry calculations then limited the radioactive dose in humans to 0.69 MBq, so as not to exceed the  $100\mu\text{Sv}$  regulatory limit (lower end of Category IIa, ICRP 1992 [52]). AMS was used for the analysis of late timepoint blood plasma samples, where the amounts of  $^{14}\text{C}$  had reduced to below the lower limit of quantification ( $20\text{dpm/mL}$ ) for analysis by LSC. Good concordance was observed between the data provided through the use of LSC for early timepoints (plasma analysis), and of AMS for analysis of samples at later timepoints as shown in Fig. 3.

The total radioactivity data were compared to LC-MS data for parent drug and a particular individual non-active metabolite, M3 (oxidation of GSK2251052 to a carboxylic acid metabolite). Systemic concentrations of total radioactivity closely aligned to the sum of the systemic



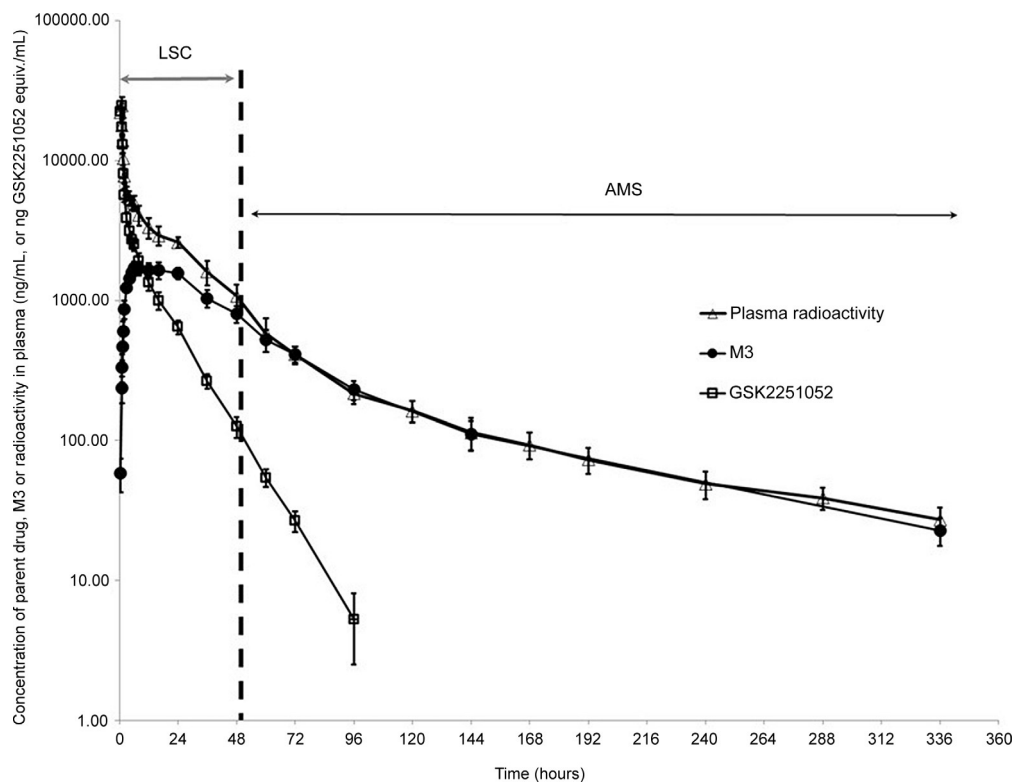


**FIG. 3** Concentration-time plot showing the transition from LSC data to AMS data for total radioactivity in plasma. Mean ( $n=6$ ) plasma concentrations of parent drug ( $\Delta$ , ng/mL), metabolite M3 ( $\bullet$ , ng/mL), and total plasma radioactivity ( $\Delta$ , ng GSK2251052 equivalents/mL). Left of the vertical dashed line, plasma radioactivity concentrations were measured using LSC (before 48 h). Right of the dashed line, the plasma radioactivity concentrations were measured using AMS (48 h and later). LLoQ for the LC-MS specific assay for M3 was 5 ng/mL; LLoQ for AMS for total radioactivity was 27.2 ng GSK2251052 equivalents/mL. Credit: Adapted from Fig. 3 in G.D. Bowers, et al., *Disposition and metabolism of GSK2251052 in humans: a novel boron-containing antibiotic*. *Drug Metab. Dispos.* 41 (5) (2013) 1070–1081 with the addition of error bars and indicators of the analytical technique applied.

concentrations of parent drug and M3, thereby indicating that no significant quantities of other metabolites were present. Further to this, parent drug elimination half-life in plasma was defined as being much shorter (11.6 h) than for total radioactivity, i.e., parent drug and metabolite(s) (96 h). This longer half-life for RDM was similar to that of the M3 metabolite ( $\sim 77$  h). As can be seen from Fig. 3, taking into account variability around the independent sample analysis conducted for the specific LC-MS assay of the M3 metabolite and the direct analysis by AMS for total radioactivity (as indicated by the error bars), the mean data from both data sets from around 72 h after dosing is close to superimposable, justifying the decision made not to conduct metabolite profiling on the plasma samples. This significantly reduced the resources/costs that were required to support the study.

In situations where the quantification of metabolites in the systemic circulation has been challenging by MSC and shown to highlight a major metabolite ( $>10\%$  of the drug-related

material present) in humans, which is disproportionate to that in nonclinical species, AMS may be used to better define the metabolite profile. In a recent example (unpublished results), the MSC could not adequately quantify the  $^{14}\text{C}$  regions of interest, due to proximity of the measurements to the LLoQ for that technology. The AMS approach was used to more adequately characterize the regions of interest, resulting in a definitive profile, absent of any disproportionate metabolites.

Another example of the utility of AMS in hybrid studies relates to addressing the MIST guidelines [61]. Using a 14-day ADME study as an example, the plasma may only be measured out to 7 days by LSC, compared to 14 days via AMS. When preparing the AUC pooled plasma (using LSC data), the sample would be pooled across  $\text{AUC}_{(0-168\text{ h})}$ , whereas via AMS, this sample would represent  $\text{AUC}_{(0-312\text{ h})}$ . If excretion was apparent to 14 days and beyond, then the presence of metabolites could be different between the two sampling periods. Using LSC data only may result in “missing” a metabolite that could represent  $>10\%$  of the AUC, or conversely, a metabolite could be  $>10\%$  of the 0–168h AUC, but  $<10\%$  of the 0–312h AUC.

## 6 Low tracer dose studies

Low tracer studies are often termed microtracer studies because of the fact that a low amount of tracer is used, with the route of administration usually being by the planned therapeutic route. As explained elsewhere, however, we will refer to them as low tracer dose studies here. The administered dose of radiocarbon-labeled drug to humans is usually in the range of  $\leq 1\ \mu\text{Ci}$  ( $\leq 37\ \text{kBq}$ ) for a variety of reasons, as stated earlier. It has been shown that the data generated from such low tracer dose studies, supported by AMS, is equally valid as that from more conventional human ADME studies with markedly higher doses, supported by LSC [62]. AMS was adopted into use for drug development because it was recognized that certain clinical studies carried an unacceptably high risk of radioactive exposure to human volunteers if supported by LSC. In retrospect, it became clear that in some cases, studies would not have attained ethical approval without the extremely sensitive analysis offered by AMS. A good example of this is the clinical study on SB-773812 summarized by Young and Ellis (2007) [11] where a dose of only  $0.5\ \mu\text{Ci}$ ;  $18.5\ \text{kBq}$  was used in the human ADME study (due to protracted elimination in the dog) and human excreta were collected intermittently out to 71 days after dosing to provide adequate mass balance recovery [63,64]. Also, a human radiolabel study was not conducted for such ethical reasons for dutasteride, a  $5\alpha$ -reductase inhibitor, due to its extremely long elimination half-life in humans (approximately 5 weeks) and excretion mass balance could only be assessed (poorly) using a  $^{19}\text{F}$ -Nuclear Magnetic Resonance spectroscopy ( $^{19}\text{F}$  NMR) approach (GSK data on file). Although there are undoubted benefits to the selectivity offered through the use of  $^{19}\text{F}$  NMR, applying this technique to mass balance studies is problematic [65] as it relies on a fluorine atom being present in the structure of the molecule of interest and it is insensitive in comparison to AMS. In countries such as Japan, there is even more heightened interest in carrying out human ADME studies using very low doses of radiation, indeed there are no clinical sites in Japan where conventional doses (e.g.,  $100\ \mu\text{Ci}$ ) can be used, whereas low tracer dosing is feasible [66].

## 7 Concomitant microtracer: Design and delivery

In the context of this chapter, a microtracer meets the following criteria:

- (1) The intravenous microtracer dose meets the regulatory guidelines for safety evaluation in terms of mass administered and solubility in the aqueous (usually saline) formulation.
- (2) The intravenous microtracer dose is sufficiently low (usually by a factor of between 100- and 1000-fold) so that it can be reasonably expected not to perturb the pharmacokinetics of the extravascular dose and does not contribute any significant pharmacological activity.
- (3) Isotopic analytical methods are available that will allow discrimination between the pharmacokinetics derived from the intravenous and extravascular doses. For example, LC-MS for the analysis of non-labeled drug and LC+AMS (liquid chromatography with off-line analysis by AMS) for the  $^{14}\text{C}$ -drug quantification.

Note that in the early studies (e.g., Ref. [67]) the extravascular and intravenous doses were given simultaneously. This design has been improved upon more recently and it has become normal practice to administer the intravenous dose as an infusion (e.g., 15 min duration) timed to end at the anticipated oral  $t_{\text{max}}$ , i.e., the intravenous dose is administered concomitantly with the oral dose (i.e., staggered dose time) rather than simultaneously (dosed at the same time), to further minimize the possibility of nonequivalent pharmacokinetics between the different dose routes (specifically during the absorption phase for the oral dose, which an infusion more closely mimics than does a bolus dose). An infusion is also usually preferred over a bolus administration for safety reasons as the infusion pump can be turned off to halt drug delivery if there are adverse safety signals in the subject.

An illustration of the principles behind microtracer dosing, through the administration of a low dose of the drug by the intravenous route, along with a much higher dose by an extravascular route, is shown in Fig. 4. The figure shows the principle of systemic mixing of the two isotopic forms ( $^{14}\text{C}$ -labeled and non-labeled, in the case illustrated) so that during the elimination phase clearance occurs at the same rate, independent of the isotopic form.

The structural position of the label, and the magnitude of the mass increase as a consequence of the label, needs to be considered to ensure that it is in a position stable to metabolism and that there is no significant Kinetic Isotope Effect (KIE; the change in the rate of a chemical reaction when one of the atoms in the reactants is substituted with one of its elemental isotopes) due to the label inclusion, leading to inappropriate use as a tracer of the unlabeled drug. KIE is more likely to have an impact when, for example, multiple  $^{13}\text{C}$  labels or deuterium labels are used as tracers but is negligible for  $^{14}\text{C}$ . Post-dose collected blood samples can be measured for isotopically labeled drug to generate intravenous pharmacokinetic data and independently analyzed for the total drug to generate extravascular route pharmacokinetic data. It is routinely possible to quantify  $^{14}\text{C}$ -parent analyte concentrations at  $\sim 0.5\text{ pg/mL}$  via LC+AMS when administering an IV dose of  $1\ \mu\text{Ci}$  per  $10\ \mu\text{g}$  of  $^{14}\text{C}$ -drug.

In summary, the concomitant microtracer design has the following advantages over the traditional two-way crossover study design:

- (1) Elimination of nonequivalent clearance effects.
- (2) No intravenous toxicology assessment is required in nonclinical species. A caveat is that if a novel formulation vehicle is employed for delivery of the intravenous dose, then local

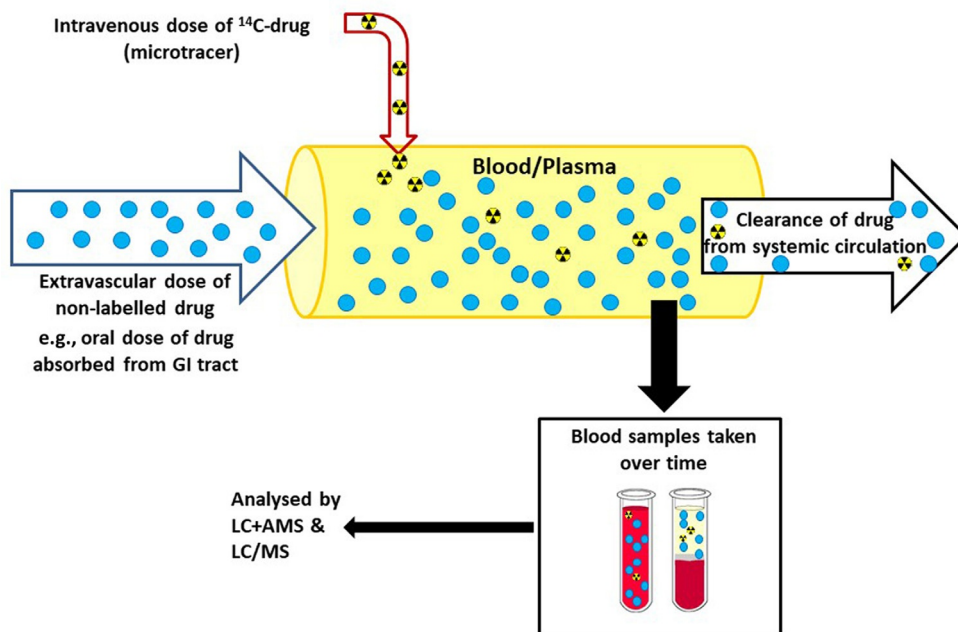


**FIG. 4** Principles of isotope mixing in systemic circulation during microtracer studies.  $^{14}\text{C}$ -labeled drug from the intravenous dose is effectively diluted into the larger mass of non-labeled drug from the extravascular route dose. Credit: G. Young, PhD Thesis, University of Lincoln, UK, 2016.

tolerance of the vehicle should be assessed (in a nonclinical hemolysis study), otherwise the safety data for the intravenous dose can be qualified by the existing oral toxicity studies [53].

- (3) Intravenous formulation development can be more straightforward due to the low dose.
- (4) No clinical dose escalation study is required to support the intravenous dose.
- (5) Removal of the temporal effect which might occur when there are two separate dosing occasions.

The concept of the microtracer approach is further summarized in Fig. 5.

## 7.1 Absolute bioavailability assessments using AMS

Absolute bioavailability ( $F$ ) is the fraction of an extravascular dose of unchanged drug that reaches the systemic circulation. To determine  $F$ , for an extravascular administration of the drug (usually by the oral route) an intravenous reference dose administration is necessary. This parameter is one of the key deliverables of the concomitant microtracer approach.

These studies are often conducted late on in development, to fulfill either mandated [69] or recommended [70,71] regulatory requirements for the provision of absolute bioavailability data [42,43,72]. Note that these studies would historically have been almost exclusively conducted as crossover studies (at least two periods) in at least 12 subjects (to provide an

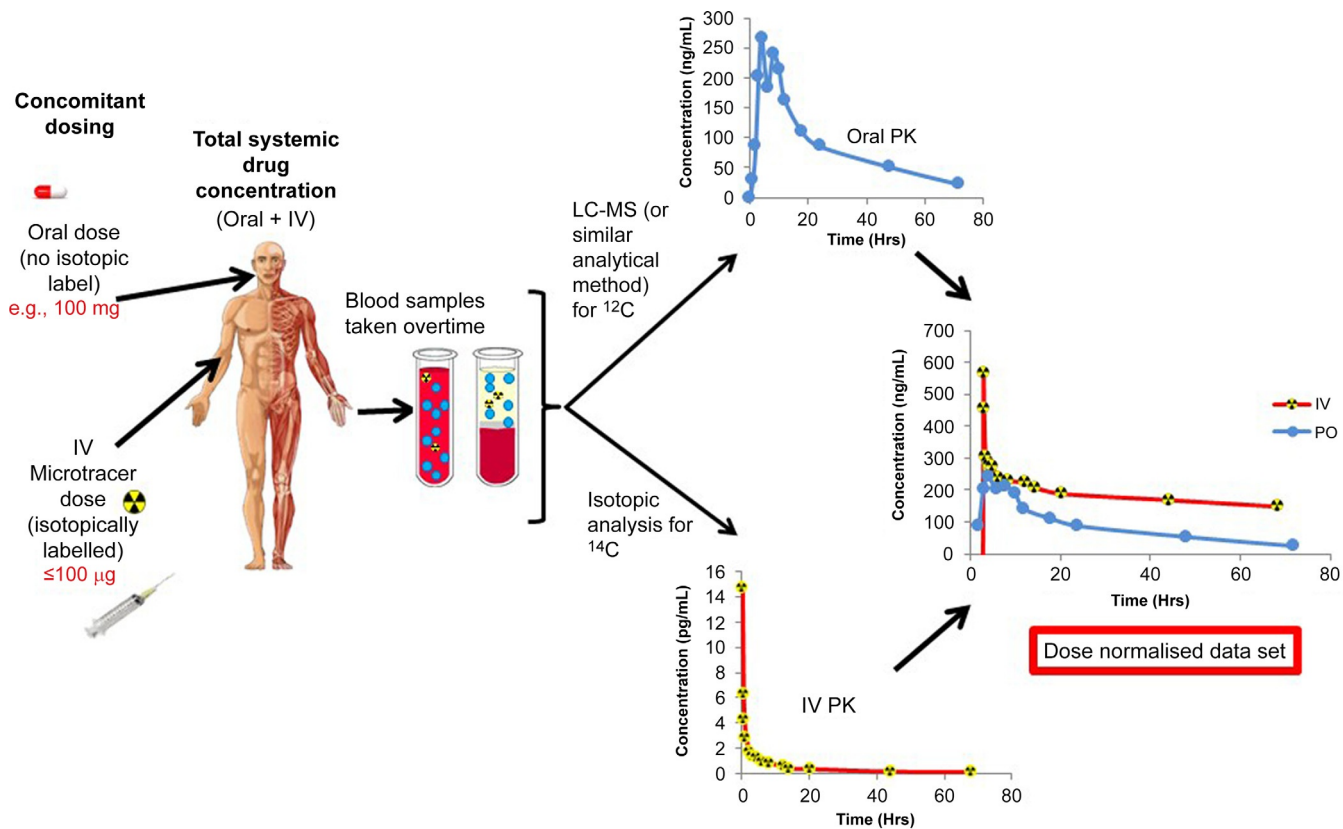


**FIG. 5** Concomitant oral and intravenous dosing microtracer concept. *Credit: Adapted from Fig. 1 of G. Lappin, Approaches to intravenous clinical pharmacokinetics: recent developments with isotopic microtracers. J. Clin. Pharmacol. 56 (1) (2016) 11–23.*

acceptable statistical power to the study, bearing in mind variabilities that will be peculiar to the fact that the reference and test dose administrations were administered on separate occasions with a washout between them). The data provided from such studies is critical to developing a thorough understanding of the pharmacokinetics of the drug in the systemic circulation and to delineating distribution and clearance characteristics of the drug but is often absent from modern oral drug development. Indeed, such assessments could be used to make decisions on the progression, or termination, of a new drug under development. Often the drug has already been progressed despite its less than ideal PK properties based on assumptions due to incomplete understanding, for example, is the poor and variable systemic availability of the drug due to poor dissolution and absorption, or due to the impact of first-pass metabolism through the gastrointestinal tract and the liver? Such questions can be answered through a greater understanding of PK and the intravenous administration can provide some of that critical data.

More recently, the intravenous microtracer approach has been included as part of the human ADME study in Phases 2 and 3 of development [73,74] to improve the efficiency of these studies in delivering all of the traditional endpoints of the human ADME study (routes and rates of elimination), as well as definitive systemic pharmacokinetics of the drug, to provide the absolute bioavailability as well as other pharmacokinetic parameters.

## 8 Improved efficiencies in drug development

Drug development companies have been experimenting with the many and varied combinations of approaches possible, resulting in some innovative designs, including double tracer studies [75,76] (combining oral administration of a  $^{14}\text{C}$ -radiolabel tracer with concomitant intravenous administration of a stable isotope ( $^{13}\text{C}$ ) tracer) and combinations of relative and absolute bioavailability designs [77].

In an elegant study design, a concomitant microtracer study was conducted with tofoglifozin (a sodium-glucose cotransporter 2 inhibitor) where a 100  $\mu\text{g}$  dose of  $^{13}\text{C}$ -labeled drug was administered intravenously along with an oral therapeutic dose of 20 mg and 3.7 MBq (100  $\mu\text{Ci}$ ) of  $^{14}\text{C}$ -labeled drug. Systemic concentrations of  $^{13}\text{C}$ -tofoglifozin were measured to define intravenous pharmacokinetics; non-labeled parent drug concentrations were measured to determine oral dose pharmacokinetics and  $^{14}\text{C}$ -drug-related material analyzed to investigate rates and routes of metabolism. All of this was from within a single cohort of subjects, in a single dose period [75].

Incorporating multiple isotopic labels into such studies is feasible as long as the different isotopes can be distinguished from each other, based on either mass discrimination, radioactive energy, or other analytical technology. Indeed at least one other study [76] has more recently been carried out using similar approaches to the tofoglifozin study.

An intravenous microtracer approach has recently been included in a first time in human (FTIH) study [78], where maximum value can be achieved from the generation of the data gained through earlier increased understanding of the asset. Other pharmaceutical companies have either embraced [79,80] or considered a similar approach [81]. If there are limitations around the clinical site that is to be used for the FTIH study, then it is possible to

bridge the study to a separate clinical site that is capable of either handling radiolabeled drug and/or preparing the intravenous dose by extemporaneous compounding with a parametric release protocol. The data that can be generated from such investigations, along with human ADME and relative bioavailability comparisons has been combined to build physiologically based pharmacokinetic (PBPK) models that were used to justify a position for not conducting a clinical formulation bioequivalence study (based around changes to particle size and dissolution rate) which was accepted by the regulatory authorities [82]. It is clear, therefore, that there are opportunities to at least consider the inclusion of this approach as part of the normal course of drug development on a more routine basis than has been the case to date.

From the perspective of the pharmaceutical industry, it is the regulatory requirements for absolute bioavailability data that drive the conduct of these studies [72]. Notwithstanding absolute bioavailability, intravenous dosing of a drug otherwise intended only for extravascular administration also provides a wealth of other information, including:

- (1) Definition of pharmacokinetic parameters such as clearance [CL; the volume of blood from which drug is irreversibly removed per unit time (e.g., L/h)] and volume of distribution [V; theoretical volume of body fluid that would be required to contain the total amount of drug at the same concentration as that measured in biological fluid (blood, plasma, or serum)] (as well as F).
- (2) Assessment of renal clearance.
- (3) First-pass metabolism vs. systemic metabolism. The intravenous and oral administrations of  $^{14}\text{C}$ -labeled drug allow estimation of fraction absorbed which can be insightful, for example, in formulation development, establishing opportunities such as for modified release products.
- (4) Assessment of biliary excretion (using an approach such as the Entero-test noninvasive string device) [83].

Additionally, there have been applications including:

- (1) Study of conversion from prodrug to the active drug [84].
- (2) Formation and elimination of active metabolites (GSK data on file).

It should be noted that since the reemergence of the microtracer approach as a favored alternative to the traditional crossover design for absolute bioavailability assessment, sparked by the use of  $^{14}\text{C}$  tracer for this purpose, several studies that used a  $^{13}\text{C}$ -labeled tracer have been conducted [75,85–87]. Advances in the sensitivity of conventional mass spectrometry (LC-MS assays) since the time of the first study of this type [67], has made the use of low dose stable isotopes feasible. There are both pros and cons to the choice of which tracer to use [88], including:

- (1) considerations around required analytical sensitivity.
- (2) inclusion of additional objectives over parent drug pharmacokinetics alone (ADME assessments are enhanced by the presence of  $^{14}\text{C}$  label).
- (3) requirement for prework to check for possible kinetic isotope effects (e.g., where multiple labels have been incorporated [85]).
- (4) availability of labeled materials.
- (5) assay development complexities including analytical capability availability.



It is likely a reflection of the sensitivity challenges for  $^{13}\text{C}$ -labeled (stable isotope) tracer measurement that studies, where this has been applied to date, have mostly used a dose toward the upper limit of the microdose definition (100  $\mu\text{g}$ ), whereas studies using  $^{14}\text{C}$ -labeled material have on some occasions utilized much lower doses, for example, 5  $\mu\text{g}$  [42]. A study was conducted for fostemsavir [89], a gp120 attachment inhibitor, which was supported by an extremely sensitive (sub-pg/mL) LC-MS assay, paving the way for such a design in the right circumstances, i.e., where study endpoints are limited to PK and a sufficiently low limit of quantification non-AMS assay exists. It is worth noting here that the intravenous PK data generated from this study was central to the development of the PBPK model for this, oral therapeutic route, asset (data on file at GSK). Arguments have been made that for PBPK model development and application, investment in the effort is required well ahead of when we may see the benefit of having a good understanding of the asset. To support this, recent draft guidance has inferred that PBPK models will be generated throughout the development lifetime of new drugs and there is an expectation that clinical intravenous route data will be available at some point [90]. It seems likely that across the pharmaceutical industry there will be an expectation that a PBPK model is developed for each asset, starting at the pre-candidate stage to improve candidate quality and efficacious clinical dose prediction. This will enable the use of PBPK modeling in clinical development for drug–drug interaction (DDI), special population assessments, and biopharmaceutics applications.

## 9 Conclusions

---

It is possible that the concomitant microtracer approach and the desire to generate intravenous data in general at an early stage of clinical development may add more value for compounds in Biopharmaceutic Classification System (BCS) [91] Classes II or IV. Equally for compounds with unclear routes of elimination or with clearance mechanisms that do not translate well between preclinical species and human (e.g., biliary clearance, metabolism via UGT (uridine diphosphate glucuronosyltransferase) enzymes, and enterohepatic recirculation) may suggest priority is given to this approach. The data generated may be a decision-making for progression/termination or provide a more informed development path as indicated throughout this chapter. As stated above, PBPK models can be developed earlier in development with the benefit of determined fundamental PK parameters (Clearance and Volume of distribution) that only comes from parenteral administration. The data provided can then be used to optimize enabling clinical studies and supporting activities to increase the overall efficiency of drug development. An interesting case arises, when a drug which was, for example, intended for administration by inhalation and for which intravenous data is available, is then repurposed for another route of administration such as dermal. In such a case, the preexisting clinical intravenous data for this asset can be very useful in developing a model to describe the systemic exposures likely from dermal administration.

From a regulatory perspective, highly soluble compounds in BCS classes I or III may be exempt from the requirements for subsequent *in vivo* bioavailability or bioequivalence studies of formulations after the initial establishment of the *in vivo* bioavailability [92].

In the case of metabolism investigations, although disproportionate or unique human metabolites are relatively uncommon, if not discovered until later in the development program their presence can have significant consequences; the inclusion of intravenous administration can be incredibly helpful as a means of describing the relative impact of first-pass metabolism and biliary elimination on the asset.

Discussions around when it may be useful to include an intravenous administration for some of the variety of reasons outlined in this chapter have led to a range of possible designs, even to the inclusion of a microdose approach as a part of the conventional Phase 1 ascending dose FTIH. These types of discussions are to be encouraged to ensure that the optimal design is settled upon based on many factors that may well be pertinent to the specific project under discussion.

## 10 Future perspectives

As indicated earlier, sample preparation for metabolite profiling and individual analyte assay is usually via liquid chromatography, performed to produce fractions that are collected into separate tubes or well plates, followed by off-line analysis by AMS. Because of the off-line nature of the analysis, the term LC+AMS is now commonly used, rather than LC-AMS which would infer a direct online interface between the LC and the AMS. Gas (CO<sub>2</sub> injection) sources have been investigated that would directly couple the LC and the AMS, but the engineering challenges have not been overcome and so the fraction collection method persists. Details of efforts to couple the LC to the AMS [93] are outside the scope of this chapter although what has been achieved to date can only be seen as a qualitative approach. Aside from the AMS approach to low-level <sup>14</sup>C analysis, a promising laser-based technique, known as cavity ring-down spectroscopy (CRDS) has been developed [94]. It is early days for this technology and it may be that it will provide sensitivity that does not reach the limits of AMS, nevertheless, it may provide additional options that span the gap between AMS and the more established and widespread less sensitive technologies (such as LSC or MSC) [95].

The sensitivity of AMS for detection of <sup>14</sup>C-labeled drugs and metabolites has enabled reduced exposure to ionizing radiation for human ADME studies, providing safety and ethical improvements that have negated the need for enabling animal studies with less complex dosing formulations and removal of the requirement for dosimetry. AMS has enabled analysis of samples to later timepoints for a more complete definition of distribution, metabolism, and elimination and concomitant microtracer designs. Microtracer studies provide important pharmacokinetic data such as plasma clearance, the volume of distribution, absolute bioavailability, definition of the extent of first-pass metabolism and in combination with bile sample collection, a more thorough understanding of routes of metabolism. A further advance is the use of repeat pulse doses of <sup>14</sup>C-labeled drug to allow assessments of ADME-PK under chronic dosing conditions.

The view of the authors of this chapter, which seem to be shared by at least some experts in the field of DMPK science [68,72,96] is that AMS is as yet underutilized and that future years may well demonstrate the increased impact of the technology as a more routine tool in drug development. That said, there are still recent examples where more significant doses of

radiation are being administered [97] to humans, it seems to avoid the need for the AMS technology and ethically that appears to be a questionable approach. Nevertheless, we hope to see the ongoing and future development of AMS (or indeed alternative technological approaches), to enable a new era of broadened applications, as well as information-rich clinical study designs earlier in drug development. It would be particularly exciting to see the scientific advance of intravenous drug administration as the normal practice, rather than the exception, to provide deep insight into the research of many new medicines.

## References

- [1] EMA, Guideline on the Investigation of Drug Interactions, Committee for Human Medicinal Products (CHMP), 2013. [www.ema.europa.eu](http://www.ema.europa.eu).
- [2] G. Lappin, S. Temple, *Radiotracers in Drug Development*, CRC Press, 2006.
- [3] M. Zhu, D. Zhang, G.L. Skiles, *Identification and Quantification of Drug, Metabolites and Metabolizing Enzymes by LC-MS*, vol. 6, Elsevier Science, 2005 (Chapter 9).
- [4] W. Kutschera, Applications of accelerator mass spectrometry, *Int. J. Mass Spectrom.* 349–350 (2013) 203–218.
- [5] G. Lappin, S. Temple, *Radiotracers in Drug Development*, CRC Press, 2006 (Chapter 7).
- [6] C.L. Bennett, et al., Radiocarbon dating using electrostatic accelerators: negative ions provide the key, *Science* 198 (4316) (1977) 508–510.
- [7] K.H. Purser, et al., An attempt to detect stable N<sup>-</sup> ions from a sputter ion source and some implications of the results for the design of tandems for ultra-sensitive carbon analysis, *Rev. Phys. Appl. (Paris)* 12 (10) (1977) 1487–1492.
- [8] P.E. Damon, et al., Radiocarbon dating of the Shroud of Turin, *Nature* 337 (6208) (1989) 611–615.
- [9] B. Kaye, et al., A preliminary evaluation of accelerator mass spectrometry in the biomedical field, *J. Pharm. Biomed. Anal.* 16 (3) (1997) 541–543.
- [10] K.W. Turteltaub, et al., Accelerator mass spectrometry in biomedical dosimetry: relationship between low-level exposure and covalent binding of heterocyclic amine carcinogens to DNA, *Proc. Natl. Acad. Sci.* 87 (14) (1990) 5288–5292.
- [11] G.C. Young, W.J. Ellis, AMS in drug development at GSK, *Nucl. Instrum. Methods Phys. Res. Sect. B* 259 (1) (2007) 752–757.
- [12] S.N. Comezoglu, et al., Biotransformation profiling of [(14)C]ixabepilone in human plasma, urine and feces samples using accelerator mass spectrometry (AMS), *Drug Metab. Pharmacokinet.* 24 (6) (2009) 511–522.
- [13] M. Gunnarsson, et al., No radiation protection reasons for restrictions on 14C urea breath tests in children, *Br. J. Radiol.* 75 (900) (2002) 982–986.
- [14] M.A. Turner, et al., Pediatric microdose and microtracer studies using 14C in Europe, *Clin. Pharmacol. Ther.* 98 (3) (2015) 234–237.
- [15] L.T. Vuong, et al., Applications of accelerator MS in pediatric drug evaluation, *Bioanalysis* 4 (15) (2012) 1871–1882.
- [16] M. Dave, et al., Disposition and metabolism of darapladib, a lipoprotein-associated phospholipase A2 inhibitor, in humans, *Drug Metab. Dispos.* 42 (3) (2014) 415–430.
- [17] G.R. Iyer, Y. Patel, N.S. Teuscher, A novel study using accelerated mass spectrometry to evaluate the pharmacokinetics of total 14C AL-8309 (Tandospirone) following topical ocular administration in healthy male subjects, *Clin. Pharmacol. Drug Dev.* 1 (1) (2012) 4–13.
- [18] A.J. Clifford, et al., The dynamics of folic acid metabolism in an adult given a small tracer dose of 14C-folic acid, *Adv. Exp. Med. Biol.* 445 (1998) 239–251.
- [19] P.A. Dickinson, et al., Metabolic disposition of osimertinib in rats, dogs, and humans: insights into a drug designed to bind covalently to a cysteine residue of epidermal growth factor receptor, *Drug Metab. Dispos.* 44 (8) (2016) 1201–1212.
- [20] T. Pene Dumitrescu, et al., A novel method for studying the pharmacokinetics of [14C]umeclidinium after application to the axilla or palm of healthy male subjects, *Clin. Transl. Sci.* 9 (4) (2016) 183–191.
- [21] J.S. Vogel, Rapid production of graphite for biomedical AMS, *Radiocarbon* 34 (3) (1992) 344–350.

- [22] G.C. Young, et al., Comparison of a 250 kV single-stage accelerator mass spectrometer with a 5 MV tandem accelerator mass spectrometer – fitness for purpose in bioanalysis, *Rapid Commun. Mass Spectrom.* 22 (24) (2008) 4035–4042.
- [23] A.T. Thomas, et al., Ultrahigh efficiency moving wire combustion interface for online coupling of high-performance liquid chromatography (HPLC), *Anal. Chem.* 83 (24) (2011) 9413–9417.
- [24] E. van Duijn, et al., Automated combustion accelerator mass spectrometry for the analysis of biomedical samples in the low attomole range, *Anal. Chem.* 86 (15) (2014) 7635–7641.
- [25] J.S. Vogel, A.H. Love, Quantitating isotopic molecular labels with accelerator mass spectrometry, *Methods Enzymol.* 402 (2005) 402–422.
- [26] S.H. Kim, et al., Carbon isotopes profiles of human whole blood, plasma, red blood cells, urine and feces for biological/biomedical <sup>14</sup>C-accelerator mass spectrometry applications, *Anal. Chem.* 83 (9) (2011) 3312–3318.
- [27] W.G. Mook, J. van der Plicht, Reporting <sup>14</sup>C activities and concentrations, *Radiocarbon* 41 (3) (1999) 227–239.
- [28] J.S. Vogel, A.H. Love, Quantitating isotopic molecular labels with accelerator mass spectrometry, in: *Methods in Enzymology*, Academic Press, 2005, , pp. 402–422.
- [29] B.D. Keck, T. Ognibene, J.S. Vogel, Analytical validation of accelerator mass spectrometry for pharmaceutical development, *Bioanalysis* 2 (3) (2010) 469–485.
- [30] G. Lappin, et al., High-performance liquid chromatography accelerator mass spectrometry: correcting for losses during analysis by internal standardization, *Anal. Biochem.* 378 (1) (2008) 93–95.
- [31] G. Lappin, R.C. Garner, Ultra-sensitive detection of radiolabelled drugs and their metabolites using accelerator mass spectrometry, in: I.D. Wilson (Ed.), *Handbook of Analytical Separations*, Elsevier Science, 2003, , pp. 331–349.
- [32] R.C. Garner, et al., A validation study comparing accelerator MS and liquid scintillation counting for analysis of <sup>14</sup>C-labelled drugs in plasma, urine and faecal extracts, *J. Pharm. Biomed. Anal.* 24 (2) (2000) 197–209.
- [33] G. Lappin, et al., AMS method validation for quantitation in pharmacokinetic studies with concomitant extravascular and intravenous administration, *Bioanalysis* 3 (4) (2011) 393–405.
- [34] X.S. Xu, et al., Overcoming bioanalytical challenges in an Onglyza(R) intravenous [(<sup>14</sup>C)]microdose absolute bioavailability study with accelerator MS, *Bioanalysis* 4 (15) (2012) 1855–1870.
- [35] D. Higton, et al., European bioanalysis forum recommendation: scientific validation of quantification by accelerator mass spectrometry, *Bioanalysis* 4 (22) (2012) 2669–2679.
- [36] G.C. Young, et al., New frontiers-accelerator mass spectrometry (AMS): recommendation for best practices and harmonization from global bioanalysis consortium harmonization team, *AAPS J.* 16 (2) (2014) 357–359.
- [37] B. Klem, et al., Determination of the bioavailability of [<sup>14</sup>C]-hexaminolevulinate using accelerator mass spectrometry after intravesical administration to human volunteers, *J. Clin. Pharmacol.* 46 (4) (2006) 456–460.
- [38] S.C. Hughes, et al., Metabolism and disposition of fluticasone furoate, an enhanced-affinity glucocorticoid, in humans, *Drug Metab. Dispos.* 36 (11) (2008) 2337–2344.
- [39] R.A. Graham, et al., Single and multiple dose intravenous and oral pharmacokinetics of the hedgehog pathway inhibitor vismodegib in healthy female subjects, *Br. J. Clin. Pharmacol.* 74 (5) (2012) 788–796.
- [40] L. van Andel, et al., Determination of the absolute oral bioavailability of niraparib by simultaneous administration of a (<sup>14</sup>C)-microtracer and therapeutic dose in cancer patients, *Cancer Chemother. Pharmacol.* 81 (1) (2018) 39–46.
- [41] D.W. Boulton, et al., Simultaneous oral therapeutic and intravenous (<sup>14</sup>C)-microdoses to determine the absolute oral bioavailability of saxagliptin and dapagliflozin, *Br. J. Clin. Pharmacol.* 75 (3) (2013) 763–768.
- [42] C. Leonowens, et al., Concomitant oral and intravenous pharmacokinetics of trametinib, a MEK inhibitor, in subjects with solid tumours, *Br. J. Clin. Pharmacol.* 78 (3) (2014) 524–532.
- [43] C.L. Denton, et al., Concomitant oral and intravenous pharmacokinetics of dabrafenib, a BRAF inhibitor, in patients with BRAF V600 mutation-positive solid tumors, *J. Clin. Pharmacol.* 53 (9) (2013) 955–961.
- [44] A.W. Harrell, et al., Metabolism and disposition of vilanterol, a long-acting beta(2)-adrenoceptor agonist for inhalation use in humans, *Drug Metab. Dispos.* 41 (1) (2013) 89–100.
- [45] H.-A. Synal, Developments in accelerator mass spectrometry, *Int. J. Mass Spectrom.* 349–350 (2013) 192–202.
- [46] H.A. Synal, S. Jacob, M. Suter, New concepts for radiocarbon detection systems, *Nucl. Instrum. Methods Phys. Res., Sect. B* 161–163 (2000) 29–36.
- [47] G.M. Klody, et al., New results for single stage low energy carbon AMS, *Nucl. Instrum. Methods Phys. Res., Sect. B* 240 (1–2) (2005) 463–467.

- [48] C.R. Bronk, P. Ditchfield, M. Humm, Using a gas ion source for radiocarbon AMS and GC-AMS, *Radiocarbon* 46 (1) (2004) 25–32.
- [49] L. Wacker, et al., A versatile gas interface for routine radiocarbon analysis with a gas ion source, *Nucl. Instrum. Methods Phys. Res., Sect. B* 294 (2013) 315–319.
- [50] E. Hoffmann, et al., Pharmacokinetics and tolerability of SRT2104, a first-in-class small molecule activator of SIRT1, after single and repeated oral administration in man, *Br. J. Clin. Pharmacol.* 75 (1) (2013) 186–196.
- [51] M.G. Mooij, et al., Pediatric microdose study of [(14)C]paracetamol to study drug metabolism using accelerated mass spectrometry: proof of concept, *Clin. Pharmacokinet.* 53 (11) (2014) 1045–1051.
- [52] ICRP, Radiological protection in biomedical research, *Ann. ICRP* 22 (3) (1992). <http://www.icrp.org/publication.asp?id=ICRP%20Publication%2062>.
- [53] ICH, I.C.o.H.o.t.r.f.r.o.p.f.h. use (Ed.), Guidance on Nonclinical Safety Studies for the Conduct of Human Clinical Trials and Marketing Authorization for Pharmaceuticals, 2009. [http://www.ich.org/fileadmin/Public\\_Web\\_Site/ICH\\_Products/Guidelines/Multidisciplinary/M3\\_R2/Step4/M3\\_R2\\_Guideline.pdf](http://www.ich.org/fileadmin/Public_Web_Site/ICH_Products/Guidelines/Multidisciplinary/M3_R2/Step4/M3_R2_Guideline.pdf).
- [54] M. Okour, et al., A human microdose study of the antimalarial drug GSK3191607 in healthy volunteers, *Br. J. Clin. Pharmacol.* (2017).
- [55] T. Burt, et al., Phase 0, including microdosing approaches: applying the three Rs and increasing the efficiency of human drug development, *Altern. Lab. Anim* 46 (6) (2018) 335–346.
- [56] G.D. Bowers, et al., Disposition and metabolism of GSK2251052 in humans: a novel boron-containing antibiotic, *Drug Metab. Dispos.* 41 (5) (2013) 1070–1081.
- [57] G. Young, et al., Accelerator mass spectrometry (AMS): recent experience of its use in a clinical study and the potential future of the technique, *Xenobiotica* 31 (8–9) (2001) 619–632.
- [58] J.S. Vogel, et al., Accelerator mass spectrometry best practices for accuracy and precision in bioanalytical (14)C measurements, *Bioanalysis* 2 (3) (2010) 455–468.
- [59] C. Husser, et al., Profiling of dalcetrapib metabolites in human plasma by accelerator mass spectrometry and investigation of the free phenothiol by derivatisation with methylacrylate, *J. Pharm. Biomed. Anal.* 152 (2018) 143–154.
- [60] V. Mancel, et al., Pharmacokinetics and metabolism of [(14)C]-tozadenant (SYN-115), a novel A2a receptor antagonist ligand, in healthy volunteers, *Xenobiotica* 47 (8) (2017) 705–718.
- [61] FDA, in: U.F.A.D. Administration (Ed.), Guidance for Industry – Safety Testing of Drug Metabolites, 2008. <http://www.fda.gov/cder/guidance/index.htm>.
- [62] A.F. Roffel, et al., An evaluation of human ADME and mass balance studies using regular or low doses of radiocarbon, *J. Label. Compd. Radiopharm.* 59 (14) (2016) 619–626.
- [63] R. Subramanian, et al., Pharmacokinetics, biotransformation, and excretion of [(14)C]etelcalcetide (AMG 416) following a single microtracer intravenous dose in patients with chronic kidney disease on hemodialysis, *Clin. Pharmacokinet.* 56 (2) (2017) 179–192.
- [64] J.J. Lee, et al., Human mass balance study of TAS-102 using (14)C analyzed by accelerator mass spectrometry, *Cancer Chemother. Pharmacol.* 77 (3) (2016) 515–526.
- [65] D. Pearson, et al., 19F-NMR-based determination of the absorption, metabolism and excretion of the oral phosphatidylinositol-3-kinase (PI3K) delta inhibitor leniolisib (CDZ173) in healthy volunteers, *Xenobiotica* (2018) 1–8.
- [66] D. Miyatake, et al., A phase I, open-label, single-dose micro tracer mass balance study of (14)C-labeled ASP7991 in healthy Japanese male subjects using accelerator mass spectrometry, *Drug Metab. Pharmacokinet.* 33 (2) (2018) 118–124.
- [67] J.M. Strong, et al., Absolute bioavailability in man of N-acetylprocainamide determined by a novel stable isotope method, *Clin. Pharmacol. Ther.* 18 (5part1) (1975) 613–622.
- [68] G. Lappin, Approaches to intravenous clinical pharmacokinetics: recent developments with isotopic microtracers, *J. Clin. Pharmacol.* 56 (1) (2016) 11–23.
- [69] TGA, in: A.G.D.o. Health (Ed.), Mandatory requirements for an effective application, 2014.
- [70] FDA, In: F.a.D.A. U.S. Department of Health and Human Services, Center for Drug Evaluation and Research (Ed.), Guidance for Industry.Waiver of In Vivo Bioavailability and Bioequivalence Studies for Immediate-Release Solid Oral Dosage Forms Based on a Biopharmaceutics Classification System, 2000.
- [71] EMA, Questions & Answers: positions on specific questions addressed to the Pharmacokinetics Working Party (PKWP), in: E.M. Agency (Ed.), EMA/618604/2008 Rev. 12, 2015. [www.ema.europa.eu](http://www.ema.europa.eu).

- [72] M.E. Arnold, F. Lacrete, When opportunity met aspirational goals: accelerator MS, microdosing and absolute bioavailability studies, *Bioanalysis* 4 (15) (2012) 1831–1834.
- [73] C. Ambery, et al., Pharmacokinetics, excretion, and mass balance of [(14) C]-batafenterol following a single microtracer intravenous dose (concomitant to an inhaled dose) or oral dose of batafenterol in healthy men, *Clin. Pharmacol. Drug Dev.* 7 (8) (2018) 901–910.
- [74] S. Raje, et al., Novel application of the two-period microtracer approach to determine absolute oral bioavailability and fraction absorbed of ertugliflozin, *Clin. Transl. Sci.* 11 (4) (2018) 405–411.
- [75] D. Schwab, et al., A novel double-tracer technique to characterize absorption, distribution, metabolism and excretion (ADME) of [14C]tofogliflozin after oral administration and concomitant intravenous microdose administration of [13C]tofogliflozin in humans, *Clin. Pharmacokinet.* 52 (6) (2013) 463–473.
- [76] E. Guerini, et al., A double-tracer technique to characterize absorption, distribution, metabolism and excretion (ADME) of [14C]-basimglurant and absolute bioavailability after oral administration and concomitant intravenous microdose administration of [13C6]-labeled basimglurant in humans, *Xenobiotica* 47 (2) (2017) 144–153.
- [77] E. Helmer, et al., A dual-administration microtracer technique to characterize the absorption, distribution, metabolism, and excretion of [14 C]seletalisib (UCB5857) in healthy subjects, *J. Clin. Pharmacol.* (2017).
- [78] M.J. Hickey, et al., The synthesis of [14C]AZD5122. Incorporation of an IV 14C-microtracer dose into a first in human study to determine the absolute oral bioavailability of AZD5122, *J. Label. Compd. Radiopharm.* 59 (6) (2016) 245–249.
- [79] K.G. Jensen, et al., Lack of exposure in a first-in-man study due to aldehyde oxidase metabolism: investigated by use of 14C-microdose, humanized mice, monkey pharmacokinetics, and in vitro methods, *Drug Metab. Dispos.* 45 (1) (2017) 68–75.
- [80] C. Muehlan, et al., Accelerated development of the dual orexin receptor antagonist ACT-541468: integration of a microtracer in a first-in-human study, *Clin. Pharmacol. Ther.* 104 (5) (2018) 1022–1029.
- [81] F. Lozac'h, et al., Evaluation of cAMS for (14)C microtracer ADME studies: opportunities to change the current drug development paradigm, *Bioanalysis* 10 (5) (2018) 321–339.
- [82] X.J. Pepin, et al., Justification of drug product dissolution rate and drug substance particle size specifications based on absorption PBPK modeling for lesinurad immediate release tablets, *Mol. Pharm.* 13 (9) (2016) 3256–3269.
- [83] W.J. Guiney, et al., Use of Entero-test, a simple approach for non-invasive clinical evaluation of the biliary disposition of drugs, *Br. J. Clin. Pharmacol.* 72 (1) (2011) 133–142.
- [84] W.F. Annes, et al., Relative contributions of presystemic and systemic peptidases to oral exposure of a novel metabotropic glutamate 2/3 receptor agonist (LY404039) after oral administration of prodrug pomaglumetad methionil (LY2140023), *J. Pharm. Sci.* 104 (1) (2015) 207–214.
- [85] H. Jiang, et al., Practical and efficient strategy for evaluating oral absolute bioavailability with an intravenous microdose of a stable isotopically-labeled drug using a selected reaction monitoring mass spectrometry assay, *Anal. Chem.* 84 (22) (2012) 10031–10037.
- [86] E.A. Cannady, et al., Absolute bioavailability of evacetrapib in healthy subjects determined by simultaneous administration of oral evacetrapib and intravenous [C]-evacetrapib as a tracer, *J. Label. Compd. Radiopharm.* 59 (6) (2015) 238–244.
- [87] R. de Vries, et al., Stable isotope-labelled intravenous microdose for absolute bioavailability and effect of grapefruit juice on ibrutinib in healthy adults, *Br. J. Clin. Pharmacol.* 81 (2) (2016) 235–245.
- [88] X.S. Xu, et al., Sensitivity-based analytical approaches to support human absolute bioavailability studies, *Bioanalysis* 6 (4) (2014) 497–504.
- [89] ClinicalTrials.gov, Absolute Bioavailability of BMS-626529 After Oral and Intravenous Dosing, Available from: <https://www.clinicaltrials.gov/ct2/show/NCT02805556?term=NCT02805556&rank=1>, 2017.
- [90] EMA, in: EMA (Ed.), Guideline on the qualification and reporting of physiologically based pharmacokinetic (PBPK) modelling and simulation, 2017.
- [91] G.L. Amidon, et al., A theoretical basis for a biopharmaceutical drug classification: the correlation of in vitro drug product dissolution and in vivo bioavailability, *Pharm. Res.* 12 (3) (1995) 413–420.
- [92] FDA, in: U.S.D.o.H.a.H.S.F.a.D. Administration (Ed.), Draft Guidance for Industry, Waiver of In Vivo Bioavailability and Bioequivalence Studies for Immediate-Release Solid Oral Dosage Forms Based on a Biopharmaceutics Classification System, 2015.



- [93] A.T. Thomas, et al., Directly coupled high-performance liquid chromatography-accelerator mass spectrometry measurement of chemically modified protein and peptides, *Anal. Chem.* 85 (7) (2013) 3644–3650.
- [94] A.D. McCartt, et al., Quantifying carbon-14 for biology using cavity ring-down spectroscopy, *Anal. Chem.* 88 (17) (2016) 8714–8719.
- [95] N.A. Kratochwil, et al., Nanotracing and cavity-ring down spectroscopy: a new ultrasensitive approach in large molecule drug disposition studies, *PLoS One* 13 (10) (2018) e0205435.
- [96] D.A. Smith, The debate is over: accelerator MS provides the route to better drug-development paradigms/protocols, *Bioanalysis* 3 (4) (2011) 391–392.
- [97] J. O'Donnell, et al., Single-dose pharmacokinetics, excretion, and metabolism of zoliflodacin, a novel spiropyrimidinetrione antibiotic, in healthy volunteers, *Antimicrob. Agents Chemother.* 63 (1) (2019).





PART II

Drug metabolism enzymes,  
transporters and drug-drug  
interaction

# Using in vitro methods to determine P450s responsible for metabolism and discrimination from other oxidative pathways

---

Adrian J. Fretland<sup>a</sup>, Tashinga E. Bapiro<sup>b</sup>, Barry Jones<sup>b,\*</sup>,  
Roshini Markandu<sup>b</sup>, Alexandra L. Orton<sup>b</sup>, Venkatesh Pilla Reddy<sup>b</sup>

<sup>a</sup>DMPK, Research and Early Development, Oncology R&D, AstraZeneca, Waltham, MA, United States <sup>b</sup>DMPK, Research and Early Development, Oncology R&D, AstraZeneca, Cambridge, United Kingdom

## 1 Introduction

---

Cytochrome P450s (CYP or P450) are expressed in the human liver and intestines are a critical family of Phase I oxidative enzymes involved in the metabolism of drugs and other xenobiotics. It has been estimated that metabolism by P450 enzymes is the main determinant of clearance for almost 50% of marketed drug molecules [1]. To this end, identification of the specific P450 enzymes which play a role in metabolizing a drug is crucial information in regard to polypharmacy when a patient is prescribed more than one medication which may result in a drug-drug interaction (DDI). In this case, the primary concern would be a so-called victim interaction where the metabolism and clearance of the subject drug is impacted by a coadministered agent. This rose to prominence with the withdrawal from the market of drugs like terfenadine and cerivastatin. In the case of terfenadine, inhibition by CYP3A inhibitors leads to an increase in circulating terfenadine concentrations producing fatal cardiotoxicity in some patients [2, 3]. With cerivastatin, the full mechanism of the

\*Current affiliation: Pharmaron.

observed DDI is complex and still under investigation but likely involves both P450 metabolism and transporters. However, it is clear that coadministration with gemfibrozil leads to a significantly increased risk of rhabdomyolysis, which again led to a market withdrawal in 2001 [4]. One of the contributing mechanisms to this DDI appears to be the inhibition of CYP2C8 by the glucuronide metabolite of gemfibrozil [5]. Both examples highlight the need to understand the victim DDI potential of new clinical agents. This understanding is gained through the conduct of in vitro reaction phenotyping studies which look to characterize a compound's metabolism in terms of the enzymes responsible.

The results of these studies are extremely beneficial in terms of being able to predict the DDI risk early on and plan any potential clinical DDI studies in the drug development phase. When the drug reaches the clinic, the knowledge of P450 isoforms involved may also then be able to provide explanations for any observations of variability in human pharmacokinetics, which could be due to gender, race, age, impaired organ function, genetic polymorphism, etc. [6].

Understanding the role of particular P450s can provide insight into the potential variability in clearance and plasma levels of a drug if an enzyme exhibits genetic polymorphism that results in the production of an enzyme with altered (either increased or reduced) metabolism capability. This is particularly important when enzymes such as CYP2D6, CYP2C19, and CYP2C9 are involved.

CYP2D6 displays a considerable amount of interindividual variability within a population, where individuals can be characterized as ultrarapid metabolizers (UMs), extensive metabolizers (EMs), intermediate metabolizers (IMs), and poor metabolizers (PMs) depending on the expression of different allelic forms of the enzyme. The presence of two nonfunctional (null) alleles of CYP2D6 means that no active enzyme is produced, resulting in the PM phenotype. In contrast, more than one extra functional gene produces the UM phenotype. Both these phenotypes experience significant clinical consequences, particularly in the selection of the dosing regimen [7], or in having to administer an alternative drug. This is the case with codeine, where CYP2D6 is responsible for the bioactivation to morphine to drive the analgesic effects. It has been well established that standard doses of codeine, together with being a certain phenotype, will dictate the potential clinical outcome of either pain relief for IMs, therapeutic failure through subtherapeutic morphine concentrations for PMs, or codeine toxicity for UMs due to higher circulating levels of morphine. In the US, the FDA has recommended that codeine should not be used to treat pain in children younger than 12 years, unless they have been genotyped to show that they are of the IM phenotype [8]. Having different recommendations for each phenotype allows the use of codeine in patients who will benefit from its therapeutic effects, whilst preventing the high-risk patients from experiencing the detrimental effects. Based on this example, drug discovery design efforts to avoid CYP2D6 as the primary route of clearance would be recommended as it would streamline the clinical development of a new molecule and simplify dosing in clinical practice.

CYP2C19 also shows the same category-based phenotypes (UMs, EMs, IMs, and PMs) with a similar degree of interindividual variability. The impact of these phenotypes is demonstrated with the treatment success of *Helicobacter pylori* infected gastric ulcers by omeprazole, a proton pump inhibitor. It has been shown that the cure rate for gastric ulcers is dependent on the individuals' CYP2C19 phenotype with 100% cure in PMs, 60% cure in

IMs, and only 29% cure in EMs. This is due to the reduced CYP2C19-mediated metabolism in PMs resulting in a markedly higher AUC of omeprazole resulting in a more favorable clinical outcome [9, 10].

Beyond the extreme null-polymorphisms of CYP2D6 and CYP2C19, other P450s also show change in function polymorphisms. For instance, CYP2C9 is a key polymorphic enzyme in the metabolism of warfarin, a widely prescribed anticoagulant leading, in part, to the need for dosage adjustments. Three major variants, \*1, \*2, and \*3, of the CYP2C9 gene have been found in Caucasian populations, resulting in great interindividual variability in warfarin dose requirements and pharmacokinetics. It is found that patients possessing the \*2 and \*3 allelic variants have reduced formation of the 7-hydroxy metabolite of the (S)-enantiomer of warfarin and are at a higher risk of major hemorrhage due to higher circulating levels of the drug. Therefore, evaluation of the CYP2C9 genotype before warfarin therapy may help physicians choose the appropriate initial dose, thus lowering the risk of bleeding complications [7].

These examples, along with the victim DDI examples, clearly demonstrate the need to understand the enzymes, particularly the P450s enzymes, responsible for a compound's metabolism using reaction phenotyping. There are several different methodologies that can be used to determine the P450-mediated metabolic clearance of drugs. The use of specific chemical inhibitors and/or inhibitory antibodies in microsomal or hepatocyte incubations, the use of recombinant P450s and correlation analysis where the rate of formation of a metabolite is compared to isoform-selective marker activities to identify P450s when multiple forms are involved in metabolism, is among the established methodologies [11]. All of these will be described in more detail below, along with the advantages and disadvantages. It is recommended by regulatory agencies such as the FDA that more than one assay type be used to define the role of a particular P450 in the metabolism of a given compound [12]. Additionally, an important aspect beyond reaction phenotyping is understanding the overall clearance mechanisms of a molecule using preclinical tools. This would include bile duct cannulated rats to understand the degree to which a molecule is excreted unchanged in bile, as well as assessing the renal clearance of a parent in preclinical species. Determining these pathways of clearance and predicting to humans along with a robust reaction phenotyping program will determine the risk of a DDI as a molecule enters human testing.

## 2 Recombinant P450 assays

One common way to identify the P450s involved in a compound's metabolism is through the use of recombinant P450 enzymes, which are often used in drug discovery due to their availability, ease of use, and ability to test a single isoform in a particular assay. Recombinant P450 (rP450) enzymes are an engineered in vitro technology, where a non-metabolizing cell line, which may be derived from bacteria, yeast, insect cells, or mammalian cells, is transfected with cDNA coding for a specific P450 isoenzyme [13, 14], thus creating a drug metabolism tool which has only a single active P450 present.

In order to perform their metabolic function, rP450s require electrons derived from NADPH. This results in the need to coexpress NADPH-cytochrome P450 reductase (POR),

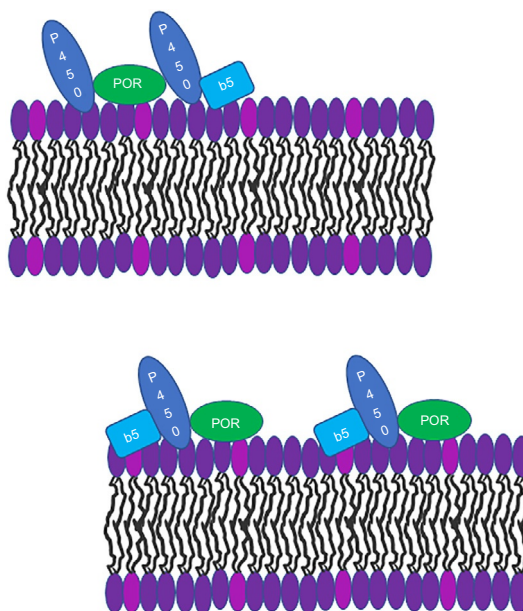


FIG. 1 Interactions of cytochrome P450s and accessory proteins.

and sometimes cytochrome  $b_5$  to carry out the electron-transfer from NADPH to the P450 to facilitate metabolism [15]. Such coexpression can be difficult to control and leads to differences in the P450/POR ratio compared to liver tissue. Fig. 1 shows how the P450 and POR proteins are arranged in the lipid membrane. In certain instances, the coexpression of cytochrome  $b_5$  increases the activity of some P450s. This is important when suboptimal activity is observed in heterologous expression systems. It, however, does create another uncertainty as the ratio of P450 to  $b_5$  in these systems may not be physiologic. This underscores the importance of well characterized systems and the utilization of correction factors for enzyme activity that will be discussed later.

In vitro rP450 experiments are a relatively quick and easy way to identify the specific isoforms involved in metabolism. These in vitro experiments can be carried out if a molecule is of interest, to help with further profiling in the early drug discovery and design phase, or to provide a definitive understanding of the P450 enzymes involved in the metabolism during the development phase. There are different permutations of experimental design when using rP450s, ranging from in vitro incubation time course experiments in each P450 with the rate of disappearance of the parent [14], to determination of the enzyme kinetic parameters ( $K_m$  and  $V_{max}$ ) for the formation of a specific metabolite.

Previously, circa 2000 and before, investigators tended to focus on the “five main” P450s [16], which covered the most abundant (CYP1A2, CYP2C9, and CYP3A4/5) and most highly polymorphic enzymes (CYP2C19 and CYP2D6). CYP3A is of particular importance because of its high expression in the human liver (~30%–50% of the total P450 content) [1], the presence of a large active site [17], and the evidence that more than 30% of chemically diverse marketed drugs are metabolized by 3A [18], leading to expectations of CYP3A to dominate

the metabolism of a majority of drugs. This is a valid assumption as, due to its large and also multi-binding site properties, CYP3A plays a major role in the metabolism of several antibiotics, antivirals, benzodiazepines, calcium channel blockers, statins, immunosuppressive drugs, opioids, and oncolytics [19], and is capable of carrying out a variety of reactions such as N- and C-oxidation, N- and O-dealkylation, nitro-reduction, dehydration, and C-hydroxylation [20].

However, more recently, the P450 panel has more than doubled to a panel of 11 P450s (CYP1A2, CYP2A6, CYP2B6, CYP2C8, CYP2C9, CYP2C19, CYP2D6, CYP2E1, CYP2J2, CYP3A4/5, and CYP4F2) being routinely investigated in accordance with the FDA guidance as to what P450s need to be taken into consideration for an investigational new drug submission [12]. One of the advantages of rP450s is the availability of this wide range of enzymes allowing the identification of a specific P450 involvement which may have been missed previously. For instance, CYP2J2 is primarily an extrahepatic P450, but is also present in the liver, constituting approximately 1%–2% of the total P450 content. The structural similarity and similar sized active sites between CYP2J2 and CYP3A4 provide an explanation as to why there is a strong overlap in substrate recognition by these two enzymes which share several substrates of diverse therapeutic areas [21, 22]. However, despite the minor presence of CYP2J2 in the liver, it can play an important part in first pass hepatic metabolism as illustrated by astemizole, an antihistamine drug. The major metabolic route for astemizole is O-demethylation which was shown to be mediated by CYP2J2 using several different P450 reaction phenotyping techniques including expression of CYP2J2 in COS-1 cells. With this expression system, the authors were able to show that CYP2J2 mediated the O-demethylation of astemizole and generate kinetic constants, in particular  $K_m$ , that were comparable to those seen for the reaction in human liver microsomes (HLM), supporting the value in the expanded panel of enzymes [22]. The value of focusing on a broader panel of enzymes is further demonstrated with AZD6738, an Ataxia Telangiectasia and Rad3-related (ATR) serine/threonine protein kinase inhibitor [23]. Jones et al. used a variety of reaction phenotyping methodologies to define the P450 enzymes involved in the metabolism of the sulfoximine moiety. This involved the use of the panel of 11 recombinant P450s to show that although CYP3A was able to carry out this metabolic conversion, there was also involvement from CYP2C8 and CYP2J2.

The above AZD6738 example also highlights one of the major drawbacks of using rP450s (or any recombinant enzyme)—the issue of differential expression which is generally realized as overexpression of the P450 and/or POR compared to the liver. If NADPH-cytochrome P450 reductase is overexpressed such that the P450/POR ratio is significantly altered, this can drive increased rates of metabolism due to greater availability of electrons from NADPH.

Human hepatocytes and HLM are two other common systems used for Phase I studies and represent a more characteristically true drug metabolizing cellular system. In terms of ranking, human hepatocytes are argued to be more physiologically relevant than HLM, and recombinant P450s signify an overexpressed and over-generated enzyme system without the same control of expression that exists in the intact tissue. It is therefore required that rP450 data are contextualized with an orthogonal system based on metabolism in hepatocytes or HLM. In the case of AZD6738, the initial rP450 data were ultimately confirmed by the use of Silensomes (to be discussed below) and were essential in demonstrating the influence of CYP2C8, therefore mitigating the CYP3A DDI risk [23].

However, whilst the expression in recombinant systems may not always reflect the original tissue, overexpression can be advantageous, particularly in the case of highly stable compounds (compounds with a low  $CL_{int}$ ). In this situation, recombinant P450s are particularly useful because of the greater metabolic activity compared to HLM [24], allowing estimates of the overall metabolic turnover as well as the enzymes responsible.

The difference in expression compared to intact tissue results in the inability to mimic the carefully balanced proportion of P450 enzymes in vivo. To correct for this, the data generated from the rP450 reaction phenotyping assays require the application of correction factors such as relative activity factors (RAF) or the intersystem extrapolation factors (ISEF). RAFs are simply the ratios of the rP450 and human liver microsomal activities for a specific marker substrate for the enzyme under consideration used to correct the rP450 activity of the target molecule rP450 data. An ISEF is similar in that it uses kinetic parameters ( $V_{max}$  or  $CL_{int}$ ) for the specific marker substrate from the rP450 and human liver microsomal enzyme in conjunction with the median P450 abundance in HLM to more effectively correct for the expression differences. ISEFs ultimately are the comparison of rP450  $CL_{int}$  to HLM activity, and to place things into cellular perspective. It is important to note that generation of ISEF values by each laboratory is recommended and preferable to ensure alignment with a specific manufacturer batch of recombinant P450s in use and to the methods used in that lab. This is because it has been shown that a combination of factors such as manufacturer batch, substrate, and assay condition in each laboratory can result in 10- to 100-fold differences in ISEF values [24, 25].

Finally, other important assay design considerations are with regard to selection of the substrate concentration and enzyme concentration. Depending on the stage of the compound, substrate concentration could be selected on either observed or expected clinical concentrations. Additionally, it may include multiple concentrations over the expected range and should include consideration of potential liver concentration after an oral dose. In the discovery setting, where these values are typically not known or reliably estimated, a standard concentration that could be expected to be below the  $K_m$  is typically used; often, 1  $\mu$ M is used. These considerations are independent of the assay system and follow a good design of enzyme kinetic experiments. The use of recombinant systems needs to carefully consider the amount of enzyme used. As described above, the activity of heterologous expressed P450s can be dependent on accessory proteins and their activity may not be physiologic. Use of the lowest amount of enzyme that results in reliable and quantifiable turnover is recommended as this minimizes the amount non-specific binding that may confound interpretation.

### 3 Human liver microsome-based methods

Human liver microsomes (HLM) are key experimental tools used in quantifying the relative contribution of individual P450 isoforms to the overall clearance of a compound. As HLM contain the full complement of constitutively expressed hepatic P450s, two approaches form the basis for current P450 reaction phenotyping methods using HLM. One approach requires the systematic inhibition of each P450 and for this to work, P450 isoform selectivity and completeness of the inhibition are key. Indeed, the search for and synthesis of specific inhibitors of P450s account for a large part of research efforts on HLM-based P450 reaction phenotyping



methods [26]. The impact of the chosen inhibitors on metabolism, with either depletion of the parent drug preferred or metabolite formation, is then used to estimate the contribution of individual P450 isoforms. The other approach relies on the availability of specific probes of P450 isoform activity with a measure of the correlation in rate of metabolism of the probe with the compound of interest providing confirmatory information on the specific P450 isoform responsible for metabolism. The detailed methods for both approaches are discussed in the following sections.

### 3.1 Antibodies

Given the need for high selectivity, it is not surprising that early studies on reaction phenotyping focused on raising antibodies against P450s. Detailed production methods of the antibodies have been previously described [27, 28] with the types falling into three categories, namely polyclonal, monoclonal, or peptide-directed. Of the three, inhibitory monoclonal antibodies which bind to specific sites on P450s that prevent substrates accessing the active sites have been the most useful and those available include CYP1A2, 2A6, 2B6, 2C8, 2C9, 2C19, 2D6, 2E1, and 3A4 (reviewed in Ref. [26]). While early work on antibody-based reaction phenotyping was carried out only by labs capable of producing the antibodies, these are now commercially available.

The experimental setup is straightforward as the antibody can be added to HLM in the ascitic fluid with a control that has no antibody-containing ascitic fluid serving as the comparator. For experiments using purified forms of antibodies, a control containing pre-immune IgG from the animal can be used [29]. As the degree of inhibition by antibodies is generally independent of substrate concentration, the concentration of the compound of interest is not a concern; however, the concentration used is typically  $<1 \mu\text{M}$ . The FDA recommends the use of antibodies that inhibit at least 80% of enzyme activity which should be demonstrated using a known probe substrate [12]. In view of the large interindividual variability in P450 activities, an HLM pool of more than 10 donors is recommended. Following preincubation of HLM and antibody, the reaction is started by adding the substrate and NADPH [30].

Results of the effect of antibodies on substrate disappearance show good agreement with data from known selective chemical inhibitors. In a study to identify the P450s responsible for metabolism of trabectedin, complete inhibition of disappearance of the parent drug was only observed with the monoclonal antibody specific for CYP3A4 [29]. This was corroborated by chemical inhibition data which showed a similar extent of inhibition by the CYP3A-specific chemical inhibitors ketoconazole and troleandomycin. When metabolite formation is considered, antibodies can reveal P450 isoforms responsible for specific metabolic routes. Using antibodies, CYP2C9 and CYP3A4 were identified as the important isoforms for (*S*)- and (*R*)-phenprocoumon hydroxylation while CYP2C8 contributed a fraction of the (*S*)-4'-hydroxylation [31].

### 3.2 Chemical inhibitors

The availability of relatively inexpensive chemical inhibitors for the majority of drug metabolizing P450s has contributed to making chemical inhibitors with HLM the most

commonly used P450 reaction phenotyping method. There are many examples in the literature of chemical inhibitor HLM-based P450 reaction phenotyping of compounds; however, when multiple P450 isoforms are involved, absolute quantitation of the fraction metabolized by each P450 can be challenging.

The chemical inhibitors used for P450 reaction phenotyping are reversible, quasi-irreversible, or mechanism-based. While reversible inhibitors generally compete for binding to the active site, quasi- and mechanism-based inhibitors (MBI) require metabolic activation to give intermediates that reversibly or irreversibly alter the enzyme [32]. While the list (Table 1) of FDA-recommended in vitro chemical inhibitors for P450 reaction phenotyping has an equal number of reversible and quasi-/irreversible inhibitors [12], the most commonly used inhibitors for each P450 are reversible. The concentration of the compound of interest is important, particularly for the reversible chemical inhibitors, as this determines the magnitude and specificity of inhibition by the chemical inhibitor. The general use of the test compound at <1  $\mu$ M, however, should work with the recommended concentrations—when used at the right concentrations, the inhibitors including furafylline, quinidine, ketoconazole, montelukast, and sulfaphenazole provide very good selectivity's [33, 34]. An additional factor to consider is the HLM protein concentration as some inhibitors such as ketoconazole show up to fivefold difference in the free fraction depending on the HLM concentration used, thus affecting the inhibition and/or specificity [35]. If higher enzyme concentrations are required for compounds with low turnover rates, as is likely for many current compounds given the designing out of structural metabolic liabilities, it is important to make the appropriate inhibitor concentration adjustments.

When certain multiple P450 isoforms are significantly involved such as CYP3A4, 3A5, and 2C8, the selectivity of the reversible inhibitors such as ketoconazole can be reduced [36]. Additionally, ketoconazole has been shown to inhibit CYP2J2 and CYP4F2 [37, 38], and in instances where these isoforms participate in the metabolism, the interpretation based on this chemical inhibitor may be confounded. With this in mind, it is not unreasonable to assume that MBI could give better selectivity, particularly if there is a wash step that removes any excess inhibitor to reduce any unwanted cross-inhibition, with the caveat of the specificity of the MBI toward a particular P450.

**TABLE 1** FDA-recommended inhibitors of P450s for use for in vitro reaction phenotyping experiments.

Enzyme	Inhibitor
CYP1A2	$\alpha$ -Naphthoflavone, Furafylline
CYP2B6	Sertraline, Phencyclidine, Thiotepa, Ticlopidine
CYP2C8	Montelukast, Quercetin, Phenelzine
CYP2C9	Sulfaphenazole, Tienilic acid
CYP2C19	S-(+)-N-3-benzyl-nirvanol, Nootkatone, Ticlopidine
CYP2D6	Quinidine, Paroxetine
CYP3A4/5	Itraconazole, Ketoconazole, Azamulin, Troleandomycin, Verapamil

### 3.3 Silensomes

Silensomes are an HLM-based P450 reaction phenotyping method in which a specific P450 isoform is inhibited by an MBI [39]. The preparation of Silensomes involves the incubation of a pool of HLM with an appropriate concentration of a chosen MBI. This is followed by a concentration step which increases the HLM protein concentration and, at the same time, washes the HLM, thus reducing the amount of MBI available to cross-react with other P450s.

The irreversible inactivation caused by an MBI can occur through modification of the heme or the P450 protein [32]. Changes to the heme invariably inactivate the enzyme, but the extent of inactivation due to P450 protein modifications will depend on the amino acid residues involved. In theory, the extent of inactivation due to P450 protein modification could be substrate-dependent, and this is supported by CYP3A4 Silensomes which show varying extents of inhibition with different substrates from 83% to 97% (certificate of analysis, BioPredic).

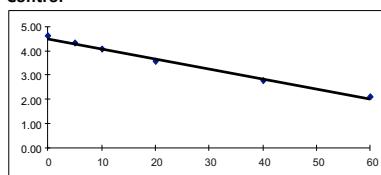
A typical experimental setup to determine the contribution of P450s to the metabolism of a compound using Silensomes is done as shown in Fig. 2. The compound (generally at a final

Typical reaction mixture for phenotyping using Silensomes

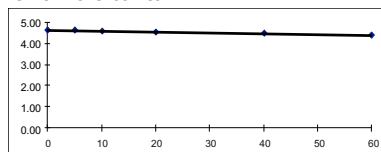
Component	Typical final concentration
Silensomes/control	1mg/mL
NADPH	1 mM
KPO <sub>4</sub> buffer pH 7.4	0.1 mM

(A)

Control



CYP3A4 Silensomes



Typical results of Silensome phenotyping experiment

Silensome	CL <sub>int</sub> (μL/min/mg)	% Contribution
CYP3A4	4.1	90
Control	42	-

(B)

$$fm_{CYP}(\%) = [1 - (CL_{int\,cyp} / CL_{int\,control})] \times 100$$

(C)

FIG. 2 P450 reaction phenotyping using CYP3A4 Silensomes—assay setup and data interpretation. (A) Assay setup. (B) Typical data output. (C) Calculation of fraction metabolized.

concentration of  $1\mu\text{M}$ ) is incubated with the panel of P450 Silensomes and control Silensomes at the same final concentration of protein. The  $\text{CL}_{\text{int}}$  or rate of metabolism is then determined by either the disappearance of the parent drug or metabolite formation. As the CYP3A inhibition of azamulin is selective for CYP3A in order to get an estimate of the contribution of CYP3A5, the CYP3A4 Silensomes are incubated with and without ketoconazole to inhibit the residual CYP3A5 activity. The contribution of each P450 to the metabolism of the compound of interest is calculated by comparing the Silensome's activity with that of the control (Fig. 2). It is therefore important to keep track of the number of freeze-thaw cycles and any other factors that might affect enzyme activities, and to keep this uniform across the control and Silensomes.

To date, only a limited number of published studies have utilized Silensomes. In one study, the contribution of P450s was assessed by monitoring the formation of a metabolite [23], while in the other study, both the disappearance of the parent and formation of metabolites were used [40]. While both studies did not report any issues with the Silensomes, the potential exists for compounds predominantly cleared by CYP3A4 and CYP2D6; the contribution by CYP2D6 was overestimated when compared with control Silensomes-containing quinidine (unpublished data).

As Silensomes are an emerging tool for drug metabolism studies, there are limited examples from the literature, and the suitability and acceptance by regulatory agencies is yet to be tested. Hence, Silensomes may be used to give or increase confidence to phenotyping data generated by the traditional approaches, and in the future they may emerge as another commonly accepted P450 phenotyping assay.

### 3.4 Correlation analysis

Correlation analysis relies on the use of activity of specific probe substrates for each of the P450s across a number (ideally more than 10) of different human liver samples and comparing it with the rate of metabolism of the compound under investigation. This approach has been used to identify other probe substrates based on the correlation with already available probes, and this is exemplified by amodiaquine N-deethylation which correlated with pacitaxel  $6\alpha$ -hydroxylation [41].

A typical experimental setup in each of at least 10 individual HLM donors comprises the HLM, probe substrate, or test compound buffered at pH7.4. The reaction is started by the addition of NADPH, and depletion of the probe substrate or metabolite formation is assessed. The list of FDA-recommended probes is listed in Table 2 [12]. For substrate depletion, a concentration of  $\leq 1\mu\text{M}$  is generally used at HLM protein concentrations sufficient to give measurable  $\text{CL}_{\text{int}}$  values. For metabolite formation, the HLM concentration and time of incubation should give linear rates of metabolite formation. Most studies are performed at concentrations around the  $K_m$  values for both the probe and compound of interest [23]. The resulting correlation coefficient should be  $\geq 0.63$  [42] with that of the selective substrate. Lower correlation coefficients ( $>0.25$ ) have been used and are suggestive/correlated with the metabolism through a specific P450 isoform. Regardless of the coefficient value used, correlation analysis should be combined with other P450 reaction phenotyping methods for a robust determination of the P450s involved in the metabolism of a compound.

**TABLE 2** FDA-recommended substrate probes of P450 activity.

<b>Enzyme</b>	<b>Marker reaction</b>
CYP1A2	Phenacetin O-deethylation, 7-Ethoxyresorufin O-deethylase
CYP2B6	Efavirenz hydroxylation, bupropion hydroxylation
CYP2C8	Paclitaxel 6 $\alpha$ -hydroxylation, amodiaquine N-deethylation
CYP2C9	S-Warfarin 7-hydroxylation, Diclofenac 4'-hydroxylation
CYP2C19	S-Mephenytoin 4'-hydroxylation
CYP2D6	Bufuralol 1'-hydroxylation, Dextromethorphan O-demethylation
CYP3A4/5	Midazolam 1'-hydroxylation, testosterone 6 $\beta$ -hydroxylation

A drawback of correlation analysis is that if more than one P450 isoform is involved in the metabolism of a test compound, it is difficult to accurately estimate the contribution of each using the correlation analysis method on its own. However, this approach can still identify the enzymes involved as in the case of voriconazole where multivariate correlation analysis was used to identify the involvement of CYP2C19 and CYP3A4 [43]. Others have proposed checking for correlation in the presence of chemical inhibitors to get better estimates of the contribution of two isoforms to the metabolism of a compound of interest [42].

#### 4 P450 vs FMO/AO metabolism

When assessing the metabolism of a compound, it is important to distinguish between the different enzymatic processes. Phase I metabolism consists of oxidative, reductive, and hydrolysis reactions, facilitated by multiple enzymes including P450s, flavin-containing monooxygenases (FMOs), aldehyde oxidase (AO), xanthine oxidase (XO), etc. While P450 mechanisms have been thoroughly investigated, the other Phase I enzymes have not yet reached a similar level of understanding. An extensive P450 structure activity relationship means new compounds are tending to move away from known P450 substrate structures. However, this does not mean that these compounds will not be subject to oxidative metabolism by other enzymes such as AO or FMO. Hence, it is key to have experimental strategies in place to assess the role of these alternative oxidases in a compound's metabolism. A quantitative understanding of the fraction metabolized via P450 (fmP450) is a critical factor in understanding the DDI risk with coadministered P450 inhibitors/inducers.

Various studies have been performed comparing *in vitro* and *in vivo* fmP450 contributions, to determine the most physiologically relevant matrix for assessment. It has been demonstrated that the best correlation is obtained through the use of hepatocytes [44]. The reasoning behind this is the presence of naturally occurring cofactors along with a full complement of enzymes in the correct orientations for activity within the intact cell membrane [45]. However, the fully intact nature of hepatocytes can sometimes be problematic when, for instance, there is overlapping specificity of enzyme inhibitors. Under these conditions, it will be more appropriate to use subcellular fractions.

**TABLE 3** Subcellular localization and cofactors of common drug metabolizing enzymes.

Metabolic enzymes	Cofactor required?	Liver S9	Liver microsomes	Liver cytosol
Aldehyde Oxidase (AO) Phase 1	No	X		X
Cytochromes P450 (CYP) Phase 1	NADPH	X	X	
Flavin monooxygenases (FMO) Phase 1	NADPH	X	X	
Glutathione transferase (GST) Phase 2	GSH in situ	X		
Monoamine oxidase (MAO) Phase 1	NADPH	X		
Xanthine oxidase (XO) Phase 1	No	X		X
Sulfotransferase (SULT) Phase 2	PAPS	X		X
Uridine glucuronide transferase (UGT) Phase 2	UDPGA	X <sup>a</sup>	X <sup>a</sup>	

<sup>a</sup> Requires the use of a pore-forming agent such as alamethicin to facilitate substrate access to enzyme.

Investigations using subcellular fractions allow the conditions to be manipulated to enable only certain enzymes to be active. This can be done by either using only subcellular fractions, where there is an enrichment of certain enzymes (e.g., P450 in the microsomal fraction), or through specific cofactors or other additives to favor one pathway over another. Table 3 lists the common enzymes, their location in the liver subcellular fractions, and their cofactor dependence.

FMOs and P450s have multiple similarities, including substrate structures, requirement for NADPH to activate their corresponding prosthetic groups, oxygen supplied via O<sub>2</sub>, and releasing water as a by-product. Whilst FMOs tend to catalyze only softer, highly polarizable nucleophiles and often produce more water-soluble and nontoxic metabolites, the main difference comes from their opposing enzymatic mechanisms of nucleophilic versus electrophilic addition (using radical intermediates) respectively [46]. In the FMO system, the flavin hydroperoxide intermediate is stabilized by the protein and waits in this form for substrate binding, before following a cascade 1-electron-2-step process, producing the oxidized product and regenerating the flavin adenine dinucleotide (FAD)-binding domain [47]. In contrast, the P450 cycle is initiated by the substrate binding, which prompts a two-step-1-electron transfer to create a radical intermediate, which goes on to produce the oxidized product. It is also important to note that, to date, FMOs—have been shown to only catalyze the oxidation of heteroatoms—predominantly nitrogen and sulfur whereas P450s can catalyze a range of different reactions at carbon and heteratomic centers. Hence, there would only be the need to consider the role of FMOs if the metabolism resulted in the production of a reasonable metabolite (N-oxide, S-oxide, etc.). Table 4 compares the different oxidative metabolic systems.

**TABLE 4** Comparison of oxidative drug metabolism enzymes.

	<b>P450s</b>	<b>FMOs</b>	<b>AO</b>
Substrates	Wide range of nucleophiles and electrophiles	Soft nucleophiles ( <i>often highly polarizable with free lone pair</i> )	Azaheterocycles ( <i>and aldehydes</i> )
Mechanism of action	C—H abstraction and heteroatom oxygenation	N- and S-oxygenation	Oxidation of C—H bond
Enzyme subfamily	Large superfamily of enzymes Predominant CYP3A4/5	5 <i>Isoforms</i> and 1 pseudogene Predominant FMO3	4 isoforms Predominant AOX1 ( <i>—only active isoform in human</i> )
Utilizes:	NADPH Molecular O <sub>2</sub>	NADPH Molecular O <sub>2</sub>	<u>No</u> cofactor Water as a source for oxygen
Produces:	Oxidized product and water	Oxidized product and water	Oxidized product and H <sub>2</sub> O <sub>2</sub>
Prosthetic group:	Heme ( <i>Fe</i> )	FAD ( <i>flavin adenine-binding domain</i> )	Molybdopterin ( <i>MoCo</i> )

The AO mechanism is distinctly different from both FMO and P450: firstly, in terms of a different substrate specificity; and secondly, in the mechanism of oxidizing the carbon-hydrogen bond on an aromatic ring. AO is a molybdoflavin dimer, with each homodimer made up of three subunits: an FAD domain, linked to two redox clusters, and finally an *in situ* molybdenum cofactor (MoCo) adjacent to the substrate-binding site. On complexing with a pyranopterin moiety containing the MoCo, the carboxy-terminal undergoes a conformational change to a MoCo pteridine tetracyclic. This biologically activates the enzyme through positioning the molybdenum atom in the correct orientation for electron transfer during catalysis [48]. It is proposed that a glutamate residue in the substrate pocket activates the MoCo, promoting nucleophilic attack on the electron-deficient carbon. Water is then utilized for oxidation, and the sulfur center of the MoCo accepts the displaced hydride and produces a peroxide by-product when reforming the activated MoCo [49]. P450 contributions to the hepatic metabolism can be measured via various methods detailed in this chapter, including hepatocytes or microsomes fortified with NADPH using chemical or antibody inhibitors, recombinant P450s, or Silensomes. There are established strategies in place to scale the results from these to predict the impact on human clearance. For FMO and AO metabolism, this is less well understood and, as a result, there are only a few models currently in place which demonstrate good IVIVE and human clearance prediction.

FMO enzymes are present in the microsomal fraction and, like P450s, are activated by the addition of NADPH, are found in similar tissues, and exhibit similar substrate specificity. They therefore require different experimental approaches to isolate the FMO metabolism component. This could be done through the use of specific chemical inhibitors, e.g., methimazole [50], although, in this case, evidence exists that it can also inhibit P450s [51]. Alternatively, FMO enzymes have a distinct heat liability such that, when incubated at 40–50°C for approximately 5min in the absence of NADPH, the FMO enzymes become inactivated. A combination of these two inhibitory methods is an effective approach for



FMO elucidation [47]. One example of this follows a series of compounds known to be metabolized predominantly by FMOs which were assessed using both of these inactivating methods and the subsequent in vitro data from both HLM and human hepatocytes scaled using point estimates, demonstrating a good IVIVE for FMO substrates [52]. Of note is that this method does not take into account variability from input parameters such as FMO expression, populations, and experimental errors, whereas a PBPK model approach reflects these uncertainties, and consequentially provides more confidence in the IVIVE predictions [53].

AO is present in the S9 and cytosolic fractions. The use of the cytosolic fraction exploits the fact that few traditional drug metabolizing enzymes are present, ensuring that the oxidative metabolism seen is likely a result of AO or XO, and so immediately distinguishing it from P450s. The S9 fraction could also be used in the absence of cofactors, again isolating the AO and XO enzymes, eliminating interference from FMOs/P450s/UGTs, etc. Similar to FMOs, a chemical inhibitor could be introduced to elucidate the metabolic route further and confirm the AO enzymatic pathway. Multiple potent AO inhibitors have been identified [11, 54]; however, some, including raloxifene, have been recognized to also inhibit P450s, and therefore have limited value in an S9 or hepatocyte system [55]. AO's unique mechanism of incorporating water into the product can also be manipulated for another method for measurement of clearance. For instance, the use of  $^{18}\text{O}$ -labeled water, where  $^{18}\text{O}$  becomes incorporated into the oxidized product, allows a shift in the  $m/z$  and a clear isotopic pattern is observed, distinguishing the AO metabolites from the other metabolites present [56].

These methods allow us to determine an in vitro fraction metabolized FMO (fmFMO) and fraction metabolized AO (fmAO), confirming the contribution to metabolism of these two enzymes versus P450 mechanisms. The difficulty comes when translating this to an in vivo situation. As mentioned earlier, there are established methods in place for compounds with a high P450 component; however, this has historically not been the case for FMO and AO enzymes. The difficulty with AO metabolism is the known tendency of in vitro systems to underpredict the in vivo situation when AO is a route of metabolism. There have been several reasons outlined for this including extrahepatic metabolism [57], large variability in AO expressions across donor lots [58], and highly variable AO activity [59], polymorphisms [60], instability of the enzyme during preparation and storage conditions [61], and significant species differences [62]. The species difference presents an opportunity to identify AO metabolism preclinically as dogs do not express AO. In situations where an oxidative metabolite is not observed or is much lower in dogs, this would be suggestive of AO metabolism and trigger additional studies to determine the contribution of AO in human systems.

With in vitro liver systems significantly underpredicting for compounds predominantly metabolized by AO, this can cause significant uncertainty when predicting human clearance. There are multiple examples of drug programs in the clinic which have been terminated due to unexpectedly high clearance, which therefore led to poor exposure: zoniporide [63], BIBX-1382 [64], carbazeran [65], and one reported example of a toxicological termination where an insoluble AO metabolite caused failure in the clinic [66]. These could all have been prevented if the extent of AO metabolism had been identified, considered, and mitigated.

One approach to take when assessing AO metabolism is described by Zientek et al. [11]. This includes a preliminary study in the liver cytosolic or S9 fraction to identify if there is significant AO contribution. A positive value here would initiate a cascade of mechanistic

studies in the presence and absence of a specific inhibitor for all active metabolizing enzymes. This helps to identify an estimation of fmAO; however, it still does not fully provide a methodology for accurate IVIVE.

## 5 Determination of fmCYP3A

As discussed in the introduction, P450s are known to be the major metabolizing enzyme family in the liver, with the CYP3A subfamily identified as most abundantly expressed and contributing at least in part to the metabolism of a large proportion of marketed drugs [67]. As the number of clearance mechanisms decreases, the risk of a clinically significant DDI increases, with the potential to decrease the therapeutic effect or increase adverse effects [68]. It is also key to note that the CYP3A isoform has demonstrated a wide range of variation in activity across individuals, which has been linked to different responses for drugs which are substrates for CYP3A [69, 70]. Due to its importance in the clearance of numerous marketed drugs, it is important to determine the proportion of CYP3A-dependent metabolic clearance for new compounds that are being dosed in man when coadministered with inhibitors or inducers of CYP3A, to limit the occurrence of DDIs. Importantly, discrimination of CYP3A contribution from other enzymes such as AO and FMO is important to fully assess the risk of a CYP3A-mediated DDI.

### 5.1 Current methods for fmCYP3A

As discussed above, there are several methods for identifying if CYP3A contributes to the *in vitro* metabolic clearance of a molecule, including recombinant enzymes [6], Silensomes [39], monoclonal antibody inhibitors [28], and human hepatocytes and HLM-based methods with selective P450 inhibitors [14]. With these methods, an estimation of the contribution of CYP3A is possible, either through direct interpretation of HLM-based data or through the scaling of recombinant P450 data. Often, these approaches can have limitations due to compound properties, such as low intrinsic clearance. Additionally, these methods only measure the CYP3A contribution to the overall P450 metabolism, thereby excluding metabolism via other Phase I pathways, e.g., AO, FMO, and Phase II metabolic pathways, e.g., UGT [71]. Another key consideration when looking to determine fmCYP3A is that current methods have shown large variability when multiple P450 enzymatic pathways are in play [72]. Based on the various limitations of these *in vitro* assays, it is often recommended to use a diverse set of approaches to confirm the CYP3A contribution to the overall metabolism of a new molecule [73].

The use of hepatocytes for metabolic clearance experiments and subsequent PK predictions has been well established [74]. In recent years, it has become increasingly popular when determining the contribution of P450s, and specifically CYP3A, to the overall metabolic clearance [72]. As previously highlighted, hepatocytes contain more intact Phase I and Phase II metabolic systems when compared with subcellular fractions and are also considered to mimic more physiologically relevant conditions. Additionally, when the assays are designed properly, the determination of the role of non-metabolic clearance

mechanisms, i.e., transporters, can also be accounted for [75]. When compounds possess moderate to high intrinsic clearance, the standard human hepatocyte-based intrinsic clearance assays can be adapted to include chemical inhibitors for calculating an fmP450 value. Specifically, the CYP3A selective inhibitor ketoconazole can be used to inhibit CYP3A and determine the contribution of this isoform not only over other P450 isoforms, but also over other metabolic routes, such as AO, FMO, UGT, etc.

The use of ketoconazole is common in these experiments, and careful experimental design needs to be considered. Ketoconazole is an antifungal reagent that is well established as a potent inhibitor of CYP3A4/5 [76] and is known to be selective at low concentrations. However, at higher concentrations, it can also exhibit an inhibitory effect on other P450 isoforms [77] and other metabolizing enzymes such as UGTs [78] and transporters [79]. If used improperly, this cross-inhibitory effect could limit the correlation of these in vitro fmCYP values with those from clinical pharmacokinetic and DDI studies [80]. Based on the lack of selectivity at higher concentrations, using a lower concentration of ketoconazole in vitro is recommended. In general, a concentration not exceeding 1  $\mu$ M would provide sufficient selectivity whilst maintaining inhibition potency so as to not confound interpretation [81, 82].

In instances where the intrinsic clearance of a molecule is too low to distinguish differences by substrate depletion, alternative approaches can be used. In these instances, the use of metabolite formation data can be especially informative in determining the contribution of CYP3A. This type of method primarily focuses on the potential reduction of a metabolite peak(s) area in the presence of ketoconazole. By focusing on changes in metabolite formation, limitations, such as sensitivity, in substrate depletion methods can be overcome. Lindmark et al. have published a method using changes in metabolite formation as a technique to discriminate fmCYP3A [83]. In addition to changes in the relative UV peak area, this method also collects accurate mass data which can be utilized to obtain structural metabolite identification data. This method is more labor intensive and would not be used as an initial first-line screen; however, for predominantly CYP3A metabolized low clearance compounds, with no available metabolite standards, this provides a mechanism to determine an accurate fmCYP3A which would otherwise not have been obtained. One key requirement for this methodology is for a test compound to have a strong chromophore, to produce a strong UV response, allowing for metabolite peaks to be identified and differentiated from endogenous material.

One key factor that should be taken into consideration is that when the CYP3A pathway is not the major enzymatic route, this method begins to show larger variability, similar to traditional substrate depletion methodologies. With this in mind, this method is often only utilized when a project knows it has a large CYP3A component and wants to gain information to quantify this contribution, rather than a first-line phenotyping assay. Where the major enzymatic route is known to be another P450 isoform, there is also the theoretical option to use another P450 specific inhibitor that has been shown to be selective in microsomal-based systems; however, this approach would require further qualification in hepatocytes.

An additional consideration that is becoming of increased interest is discrimination between CYP3A4 and CYP3A5. Polymorphisms within the CYP3A5 gene result in expresser and non-expresser populations [84]. The frequency of this polymorphism varies by ethnicity. This has been particularly important in understanding the metabolism of tacrolimus and its

implication of dosing [85]. Recent discoveries of potent and selective inhibitors of CYP3A4 that are selective against other P450 isoforms, including CYP3A5, have allowed for the in vitro discrimination of fmCYP3A4 versus CYP3A5 [86, 87]. This has become an important tool for the drug metabolism in helping define the potential variability in PK due to CYP3A5 expression and further understand CYP3A-mediated DDIs.

## 6 Regulatory guidance/risk assessment/examples

Recently, the US Food and Drug Administration (FDA) and the Japanese Pharmaceuticals and Medical Devices Agency (PMDA) issued new in vitro metabolism- and transporter mediated drug-drug interaction draft guidances [12, 88]. In addition, guidances on PBPK modeling and simulation by the US FDA and European EMA [89, 90] were also released. In this section, we share the perspective on these guidances from an experimental and a dynamic physiology-based pharmacokinetic modeling (PBPK) view.

The most recent FDA draft 2017 guidance did not suggest any new changes in terms of new chemical entities (NCEs) being a victim of DDIs. The PMDA added non-P450 enzymes such as AO, dihydropyrimidine dehydrogenase (DPD) and mentioned UGT1A1 and 2B7 enzymes to their 2017 guidance. Table 5 shows the key differences between these two regulatory agencies. Also shown in Table 5 is the current EMA guidance issued in 2013 [90]. Overall, both the 2017 FDA and PMDA guidances agree with the EMA 2013 guidance. Due to the requirements for earlier in vitro DDI data, the concentration ranges in the experiments may need to be based on the limits of solubility and/or toxicity, rather than  $C_{\max}$ , inlet hepatic concentration, or dose.

Table 6 shows an example of the DDI risk assessment for olaparib [91] using the static equations detailed in the FDA 2012 or FDA 2017 guidance and a dynamic risk assessment using PBPK modeling compared with the observed DDI ratios from a clinical study. The observed total  $C_{\max}$  and unbound  $C_{\max}$  after a 300 mg dose of olaparib is approximately 9.1 and 1.7  $\mu\text{M}$ , respectively. The total and unbound inlet concentrations are predicted to be 21 and 3.8  $\mu\text{M}$ . The free fraction in HLM ( $f_{u,inc}$ ) at 1 mg/mL protein concentration is 0.814. Both the basic static equation and dynamic PBPK modeling approaches suggest a minimal DDI risk, which concurs with the observed DDI with tamoxifen. Concomitant administration of olaparib increased the steady-state exposure of tamoxifen slightly in cancer patients ( $n = 18$ ). Since tamoxifen is mainly metabolized via CYP3A4 [92], the observed small increase in exposure of tamoxifen is consistent with the PBPK model prediction of weak CYP3A inhibition by olaparib (i.e., AUC ratio between 1.25 and 2). In vitro, olaparib has been shown to be an inhibitor of P-gp, BCRP, OATP1B1, OCT1, OCT2, OAT3, MATE1, and MATE2K, but not an inhibitor of OATP1B1/3, OAT1, or MRP2. The olaparib PBPK model was robustly defined to support the CYP3A4-mediated as well as transporter-mediated DDI predictions (specifically P-gp), suggesting a minimal DDI risk [91]. In vitro ADME studies suggested that olaparib is a substrate of CYP3A. A dedicated clinical DDI with a strong CYP3A inhibitor showed an increase of AUC ratio by 2.7-fold, which was in line with predicted AUC DDI ratios either by static equation or PBPK model (Table 6).

**TABLE 5** Summary of regulatory guidance highlighting the requirements of conducting assays toward P450 enzymes (as a victim and preparator).

Agency	Drug as a victim		Drug as an inhibitor						
	CYP	Non-CYP	CYP	Non-CYP	Intestinal CYPs		Hepatic CYPs		Induction
					Reversible Inhibition	Irreversible Inhibition	Reversible Inhibition	Irreversible inhibition	$R3 = 1/1 + d^*$ $(E_{max} * 10 * I_{max,u}) / (EC_{50} + 10 * I_{max,u})$ Cutoff for a positive result = $\leq 0.8$
US FDA 2017	CYP1A2, 2B6, 2C9, 2C8, 2C9, 2C19, 2D6, and CYP3A4/5 2nd tier: CYP2A6, 2E1, 2J2, and 4F2	MAOs, FMOs, XO, ALDHs, and UGTs	CYP1A2, 2B6, 2C9, 2C8, 2C9, 2C19, 2D6, and CYP3A4/5 with 2 substrates	None	R1, gut=1 + Igut/ Ki $\geq 11$ Unbound Ki	–	R1=1 + [Imax]u/ Ki,u $\geq 1.02$ Unbound Cmax Unbound Ki	$K_{obs} = k_{inact} \times 50 \times [I]u / KI + 50 \times [I]u$	$R = 1/1 + d^*$ $(E_{max} * 10 * [I]) / (EC_{50} + 10 * [I])$ Cutoff for a positive result = $\leq 0.8$
PMDA 2017	CYP1A2, 2B6, 2C9, 2C8, 2C9, 2C19, 2D6, 3A4, and 3A5 2nd tier: CYP2A6, 2E1, 2J2, and 4F2	MAOs, FMOs, XO, <u>AO</u> , ALDHs, and <u>DPD</u> , <u>UGT1A1</u> , and <u>2B7</u>	CYP1A2, 2B6, 2C9, 2C8, 2C9, 2C19, 2D6, and CYP3A4/5 with 2 substrates	<u>UGT1A1</u> , <u>2B7</u> , and <u>others</u>	R=1+Ig/ Ki $\geq 11$ [I]g = dose/ 250 mL Not specified for Ki	$K_{obs} = k_{inact} \times 0.1 \times [I]g / K_I + 0.1 \times [I]g$ [I]g = dose/ 250 mL Cutoff for a positive result = $\geq 1.25$	R=1+[I]/ Ki $\geq 1.02$ Unbound Cmax Not specified for Ki	$K_{obs} = k_{inact} \times 50 \times [I] / KI + 50 \times [I]$ Unbound cmax	$R3 = 1/1 + d^*$ $(E_{max} * 10 * I_{max,u}) / (EC_{50} + 10 * I_{max,u})$ Cutoff for a positive result not specified
EMA 2013	Specifies test systems, not enzymes: “CYP and UGT enzymes are present in all systems mentioned”	SULTs, GSTs, ALDHs and ADHs in S9 and hepatocytes	CYP1A2, 2B6, 2C9, 2C8, 2C9, 2C19, 2D6, and CYP3A4/5 with 2 substrates	<u>UGT1A1</u> and <u>2B7</u>	R=[I]/Ki $\geq 10$ Not specified for Ki	$K_{obs} = k_{inact} \times [I] / K_I + [I]$ Cutoff for a positive result = $\geq 1.25$	R=[I]/Ki $\geq 0.02$ Unbound Cmax Not specified for Ki	$K_{obs} = k_{inact} \times [I] / KI + \times [I]$ Unbound cmax	

Key differences between regulatory agencies highlighted with an underline.

**TABLE 6** Olaparib shows the minimal or DDIs according to FDA guidance and based on dynamic PBPK simulations.

Olaparib as a reversible inhibitor of CYP3A		FDA 2012 guidance			FDA 2017 guidance			Dynamic PBPK DDI risk	Observed DDI ratio
IC50 (μM)	Ki (Competitive = IC50/2)	$R = 1 + [I]_{total}/K_i$	DDI risk ( $R \geq 1.1$ )	Ki, u Ki × Fu, inc	$R = 1 + [I]u/K_{i,u}$	DDI risk ( $R \geq 1.1$ )	AUC ratio	AUC ratio (90% CI)	
119	59.5	1.4	Yes	48.4	1.1	Yes	1.61 (1.42–1.83)	1.16 (1.11–1.21)	
Olaparib as an irreversible inhibitor of CYP3A		FDA 2012 guidance			FDA 2017 guidance			Dynamic PBPK DDI risk including TDI	
Kinact (min <sup>-1</sup> )	KI (μM)	$K_{obs} = k_{inact} \times [I]/(K_I + [I])$	$R = (k_{obs} + k_{deg})/k_{deg}$	DDI risk ( $R \geq 1.1$ )	$K_{obs} = k_{inact} \times 50 \times [I]u / (KI + 50 \times [I]u)$	$R = K_{obs} = k_{inact} \times 50 \times [I]u / KI + 50 \times [I]u$	DDI risk ( $R \geq 1.25$ )		
0.0675 (4.05 h <sup>-1</sup> )	72.2	0.913	48	Yes	1.66 1.86 <sup>a</sup>	87 97 <sup>a</sup>	Yes Yes	1.16 (1.11–1.21)	
Olaparib as a substrate of CYP3A		FDA 2012 guidance			FDA 2017 guidance			Dynamic PBPK DDI risk	Observed DDI ratio
Ki (μM)		$R = 1 + [I]_{total}/K_i$	DDI risk ( $R \geq 1.1$ )	Ki, u Ki × Fu, inc	$R = 1 + [I]u/K_{i,u}$	DDI risk ( $R \geq 1.1$ )	AUC ratio	AUC ratio (90% CI)	
CYP3A inhibitor itraconazole	0.0013	4.22	Yes	0.0004	4.72	Yes	3.5 (3.46–3.65)	2.7 (2.44–2.97)	

<sup>a</sup> Not specified, it should use unbound  $K_i$ . Higher value uses unbound  $K_i$ .

## 7 Conclusion and future directions

Reaction phenotyping is a critical activity in drug discovery and development. Identification of the P450s responsible for the clearance of new drugs helps identify and mitigate potential DDIs early on so as to not result in drug development stage issues. The technologies used in reaction phenotyping have evolved as our understanding of P450s has developed. Early studies using microsomes have evolved to the Silensome technology. The use of recombinant P450s has incorporated learnings on expression and activity to scale data obtained from these assays. The importance of non-450 pathways has been addressed using hepatocytes as well as subcellular fractions, S9, and cytosols. Despite progress in addressing reaction phenotyping with compounds that have low metabolic turnover, challenges remain in this area. The use of long-term hepatocyte culture systems, such as Hepatopac or Hµrel, offers the opportunity for reaction phenotyping with compounds that are metabolically stable. Recent publications using humanized mice or microphysiological systems have shown promise in providing even more wholistic approaches to identifying routes of clearance and metabolism [93–95]. These tools may provide even better methods to assess the DDI risk when new compounds are administered with inhibitors or inducers of a specific clearance pathway. Regulatory agencies have long understood the importance of DDIs and issued guidance addressing their requirements. In recent years, this has expanded to the use of PBPK models in DDI assessment, which this has affected the number of clinical studies required to support DDI labeling. It is clear that a drug discovery effort should include assays for reaction phenotyping and that multiple assays should be used to get a firmer picture of the pathways of metabolism.

## References

- [1] M.F. Paine, et al., The human intestinal cytochrome P450 “pie” *Drug Metab. Dispos.* 34 (5) (2006) 880.
- [2] P.K. Honig, et al., Comparison of the effect of the macrolide antibiotics erythromycin, clarithromycin and azithromycin on Terfenadine steady-state pharmacokinetics and electrocardiographic parameters, *Drug Investig.* 7 (3) (1994) 148–156.
- [3] P.K. Honig, et al., Terfenadine-ketoconazole interaction: pharmacokinetic and electrocardiographic consequences, *JAMA* 269 (12) (1993) 1513–1518.
- [4] J.T. Backman, et al., Gemfibrozil greatly increases plasma concentrations of cerivastatin, *Clin. Pharmacol. Ther.* 72 (6) (2002) 685–691.
- [5] B.W. Ogilvie, et al., Glucuronidation converts gemfibrozil to a potent, metabolism-dependent inhibitor of CYP2C8: implications for drug-drug interactions, *Drug Metab. Dispos.* 34 (1) (2006) 191.
- [6] L. Di, Reaction phenotyping to assess victim drug-drug interaction risks, *Expert Opin. Drug Discovery* 12 (11) (2017) 1105–1115.
- [7] M.G. Scordo, et al., Influence of CYP2C9 and CYP2C19 genetic polymorphisms on warfarin maintenance dose and metabolic clearance, *Clin. Pharmacol. Ther.* 72 (6) (2002) 702–710.
- [8] R.S. Gammal, et al., The case for pharmacogenetics-guided prescribing of codeine in children, *Clin. Pharmacol. Ther.* 105 (6) (2019) 1300–1302.
- [9] J.A. Goldstein, Clinical relevance of genetic polymorphisms in the human CYP2C subfamily, *Br. J. Clin. Pharmacol.* 52 (4) (2001) 349–355.
- [10] S.-J. Lee, Clinical application of CYP2C19 pharmacogenetics toward more personalized medicine, *Front. Genet.* 3 (2013) 318.
- [11] M.A. Zientek, K. Youdim, Reaction phenotyping: advances in the experimental strategies used to characterize the contribution of drug-metabolizing enzymes, *Drug Metab. Dispos.* 43 (1) (2015) 163–181.



- [12] In vitro metabolism and transporter mediated drug-drug interaction studies guidance for industry, 2020. <https://www.fda.gov/media/134582/download>.
- [13] C.L. Crespi, V.P. Miller, The use of heterologously expressed drug metabolizing enzymes—state of the art and prospects for the future, *Pharmacol. Ther.* 84 (2) (1999) 121–131.
- [14] T.W. Harper, P.J. Brassil, Reaction phenotyping: current industry efforts to identify enzymes responsible for metabolizing drug candidates, *AAPS J.* 10 (1) (2008) 200–207.
- [15] K. Venkatakrishnan, et al., Comparison between cytochrome P450 (CYP) content and relative activity approaches to scaling from cDNA-expressed CYPs to human liver microsomes: ratios of accessory proteins as sources of discrepancies between the approaches, *Drug Metab. Dispos.* 28 (12) (2000) 1493.
- [16] C. Prakash, et al., Identification of the major human liver cytochrome P450 isoform(s) responsible for the formation of the primary metabolites of ziprasidone and prediction of possible drug interactions, *Br. J. Clin. Pharmacol.* 49 (Suppl 1) (2000) 35S–42S.
- [17] N. Plant, The human cytochrome P450 sub-family: transcriptional regulation, inter-individual variation and interaction networks, *Biochim. Biophys. Acta Gen. Subj.* 1770 (3) (2007) 478–488.
- [18] U.M. Zanger, M. Schwab, Cytochrome P450 enzymes in drug metabolism: regulation of gene expression, enzyme activities, and impact of genetic variation, *Pharmacol. Ther.* 138 (1) (2013) 103–141.
- [19] C. Loue, M. Tod, Reliability and extension of quantitative prediction of CYP3A4-mediated drug interactions based on clinical data, *AAPS J.* 16 (6) (2014) 1309–1320.
- [20] S.-F. Zhou, Drugs behave as substrates, inhibitors and inducers of human cytochrome P450 3A4, *Curr. Drug Metab.* 9 (4) (2008) 310–322.
- [21] C.A. Lee, et al., Identification of novel substrates for human cytochrome P450 2J2, *Drug Metab. Dispos.* 38 (2) (2010) 347.
- [22] S. Matsumoto, et al., Involvement of CYP2J2 on the intestinal first-pass metabolism of antihistamine drug, Astemizole, *Drug Metab. Dispos.* 30 (11) (2002) 1240.
- [23] B.C. Jones, et al., CYP-mediated sulfoximine de-amination of AZD6738, *Drug Metab. Dispos.* 45 (2017) 1133–1138.
- [24] Y. Chen, et al., Utility of intersystem extrapolation factors in early reaction phenotyping and the quantitative extrapolation of human liver microsomal intrinsic clearance using recombinant cytochromes P450, *Drug Metab. Dispos.* 39 (3) (2011) 373–382.
- [25] N.J. Proctor, G.T. Tucker, A. Rostami-Hodjegan, Predicting drug clearance from recombinantly expressed CYPs: intersystem extrapolation factors, *Xenobiotica* 34 (2) (2004) 151–178.
- [26] S. Francis, R. Delgoda, A patent review on the development of human cytochrome P450 inhibitors, *Expert Opin. Ther. Pat.* 24 (6) (2014) 699–717.
- [27] H.V. Gelboin, K. Krausz, Monoclonal antibodies and multifunctional cytochrome P450: drug metabolism as paradigm, *J. Clin. Pharmacol.* 46 (3) (2006) 353–372.
- [28] M. Shou, A.Y. Lu, Antibodies as a probe in cytochrome P450 research, *Drug Metab. Dispos.* 37 (5) (2009) 925–931.
- [29] M. Vermeir, et al., In vitro studies on the metabolism of trabectedin (YONDELIS) in monkey and man, including human CYP reaction phenotyping, *Biochem. Pharmacol.* 77 (10) (2009) 1642–1654.
- [30] Q. Mei, et al., Role of a potent inhibitory monoclonal antibody to cytochrome P-450 3A4 in assessment of human drug metabolism, *J. Pharmacol. Exp. Ther.* 291 (2) (1999) 749.
- [31] M. Ufer, et al., Identification of cytochromes P450 2C9 and 3A4 as the major catalysts of phenprocoumon hydroxylation in vitro, *Eur. J. Clin. Pharmacol.* 60 (3) (2004) 173–182.
- [32] J.H. Lin, A.Y.H. Lu, Inhibition and induction of cytochrome P450 and the clinical Implications, *Clin. Pharmacokinet.* 35 (5) (1998) 361–390.
- [33] G.C. Moody, et al., Fully automated analysis of activities catalysed by the major human liver cytochrome P450 (CYP) enzymes: assessment of human CYP inhibition potential, *Xenobiotica* 29 (1) (1999) 53–75.
- [34] R.L. Walsky, et al., Selective inhibition of human cytochrome P4502C8 by montelukast, *Drug Metab. Dispos.* 33 (3) (2005) 413–418.
- [35] T.H. Tran, Microsomal protein concentration modifies the apparent inhibitory potency of CYP3A inhibitors, *Drug Metab. Dispos.* 30 (12) (2002) 1441–1445.
- [36] C.E. Ong, et al., The xenobiotic inhibitor profile of cytochrome P4502C8, *Br. J. Clin. Pharmacol.* 50 (6) (2000) 573–580.
- [37] E.A. Evangelista, et al., Activity, inhibition, and induction of cytochrome P450 2J2 in adult human primary cardiomyocytes, *Drug Metab. Dispos.* 41 (12) (2013) 2087–2094.
- [38] J.-W. Park, K.-A. Kim, J.-Y. Park, Effects of ketoconazole, a CYP4F2 inhibitor, and CYP4F2\*3 genetic polymorphism on pharmacokinetics of vitamin K1, *J. Clin. Pharmacol.* 59 (2019) 1453–1461.

- [39] Y. Parmentier, et al., Direct and quantitative evaluation of the human CYP3A4 contribution (fm) to drug clearance using the in vitro SILENSOMES model, *Xenobiotica* 47 (7) (2017) 562–575.
- [40] V. Zabela, et al., GABAA receptor activity modulating piperine analogs: In vitro metabolic stability, metabolite identification, CYP450 reaction phenotyping, and protein binding, *J. Chromatogr. B* 1072 (2018) 379–389.
- [41] X.-Q. Li, et al., Amodiaquine clearance and its metabolism to N-desethylamodiaquine is mediated by CYP2C8: a new high affinity and turnover enzyme-specific probe substrate, *J. Pharmacol. Exp. Ther.* 300 (2) (2002) 399.
- [42] A.D. Rodrigues, Integrated cytochrome P450 reaction phenotyping: attempting to bridge the gap between cDNA-expressed cytochromes P450 and native human liver microsomes, *Biochem. Pharmacol.* 57 (5) (1999) 465–480.
- [43] R. Hyland, B.C. Jones, D.A. Smith, Identification of the cytochrome P450 enzymes involved in the N-oxidation of Voriconazole, *Drug Metab. Dispos.* 31 (5) (2003) 540–547.
- [44] K. Ito, J.B. Houston, Comparison of the use of liver models for predicting drug clearance using in vitro kinetic data from hepatic microsomes and isolated hepatocytes, *Pharm. Res.* 21 (5) (2004) 785–792.
- [45] C. Lu, et al., Comparison of intrinsic clearance in liver microsomes and hepatocytes from rats and humans: evaluation of free fraction and uptake in hepatocytes, *Drug Metab. Dispos.* 34 (9) (2006) 1600–1605.
- [46] G. Cruciani, et al., Flavin monooxygenase metabolism: why medicinal chemists should matter, *J. Med. Chem.* 57 (14) (2014) 6183–6196.
- [47] S. Eswaramoorthy, et al., Mechanism of action of a flavin-containing monooxygenase, *Proc. Natl. Acad. Sci. U. S. A.* 103 (26) (2006) 9832–9837.
- [48] C. Coelho, et al., The first mammalian aldehyde oxidase crystal structure: Insights into substrate specificity, *J. Biol. Chem.* 287 (48) (2012) 40690–40702.
- [49] J.F. Alfaro, J.P. Jones, Studies on the mechanism of aldehyde oxidase and xanthine oxidase, *J. Org. Chem.* 73 (23) (2008) 9469–9472.
- [50] G. Ubeaud, et al., Estimation of flavin-containing monooxygenase activity in intact hepatocyte monolayers of rat, hamster, rabbit, dog and human by using N-oxidation of benzydamine, *Eur. J. Pharm. Sci.* 8 (4) (1999) 255–260.
- [51] Z. Guo, et al., Orphenadrine and methimazole inhibit multiple cytochrome P450 enzymes in human liver microsomes, *Drug Metab. Dispos.* 25 (3) (1997) 390.
- [52] B.C. Jones, et al., An investigation into the prediction of in vivo clearance for a range of flavin-containing monooxygenase substrates, *Drug Metab. Dispos.* 45 (10) (2017) 1060–1067.
- [53] V.P. Reddy, et al., An investigation into the prediction of the plasma concentration-time profile and its interindividual variability for a range of flavin-containing monooxygenase substrates using a physiologically based pharmacokinetic modeling approach, *Drug Metab. Dispos.* 46 (9) (2018) 1259–1267.
- [54] R.S. Obach, et al., Human liver aldehyde oxidase: inhibition by 239 drugs, *J. Clin. Pharmacol.* 44 (1) (2004) 7–19.
- [55] R. Nirogi, et al., Chemical inhibitors of CYP450 enzymes in liver microsomes: combining selectivity and unbound fractions to guide selection of appropriate concentration in phenotyping assays, *Xenobiotica* 45 (2) (2015) 95–106.
- [56] U.A. Argikar, et al., Challenges and opportunities with non-CYP enzymes aldehyde oxidase, carboxylesterase, and UDP-glucuronosyltransferase: focus on reaction phenotyping and prediction of human clearance, *AAPS J.* 18 (6) (2016) 1391–1405.
- [57] M. Terao, et al., Structure and function of mammalian aldehyde oxidases, *Arch. Toxicol.* 90 (4) (2016) 753–780.
- [58] T. Akabane, et al., A practical and direct comparison of intrinsic metabolic clearance of several non-CYP enzyme substrates in freshly isolated and cryopreserved hepatocytes, *Drug Metab. Pharmacokinet.* 27 (2) (2012) 181–191.
- [59] C. Fu, et al., Aldehyde oxidase 1 (AOX1) in human liver cytosols: quantitative characterization of AOX1 expression level and activity relationship, *Drug Metab. Dispos.* 41 (10) (2013) 1797–1804.
- [60] T. Hartmann, et al., The impact of single nucleotide polymorphisms on human aldehyde oxidase, *Drug Metab. Dispos.* 40 (5) (2012) 856–864.
- [61] M. Chiba, Y. Ishii, Y. Sugiyama, Prediction of hepatic clearance in human from in vitro data for successful drug development, *AAPS J.* 11 (2) (2009) 262–276.
- [62] J. Sahi, K. Khan, C. Black, Aldehyde oxidase activity and inhibition in hepatocytes and cytosolic fraction from mouse, rat, monkey and human, *Drug Metab. Lett.* 2 (3) (2008) 176–183.
- [63] D. Dalvie, et al., Effect of structural variation on aldehyde oxidase-catalyzed oxidation of zoniporide, *Drug Metab. Dispos.* 40 (8) (2012) 1575.
- [64] C. Dittrich, et al., Phase I and pharmacokinetic study of BIBX 1382 BS, an epidermal growth factor receptor (EGFR) inhibitor, given in a continuous daily oral administration, *Eur. J. Cancer* 38 (8) (2002) 1072–1080.

- [65] B. Kaye, et al., A species difference in the presystemic metabolism of carbazeran in dog and man, *Xenobiotica* 14 (12) (1984) 935–945.
- [66] S. Diamond, et al., Species-specific metabolism of SGX523 by aldehyde oxidase and the toxicological implications, *Drug Metab. Dispos.* 38 (8) (2010) 1277.
- [67] P. Blower, et al., Drug–drug interactions in oncology: why are they important and can they be minimized? *Crit. Rev. Oncol. Hematol.* 55 (2) (2005) 117–142.
- [68] J.H. Beijnen, J.H.M. Schellens, Drug interactions in oncology, *Lancet Oncol.* 5 (8) (2004) 489–496.
- [69] H. Nishimuta, et al., Species differences in hepatic and intestinal metabolic activities for 43 human cytochrome P450 substrates between humans and rats or dogs, *Xenobiotica* 43 (11) (2013) 948–955.
- [70] M. Martignoni, G. Groothuis, R. De Kanter, Species differences between mouse, rat, dog, monkey and human CYP-mediated drug metabolism, inhibition and induction, *Expert Opin. Drug Metab. Toxicol.* 2 (2006) 875–894.
- [71] S.M. Huang, et al., New era in drug interaction evaluation: US Food and Drug Administration update on CYP enzymes, transporters, and the guidance process, *J. Clin. Pharmacol.* 48 (6) (2008) 662–670.
- [72] C. Desbans, C. Hilgendorf, M. Lutz, P. Bachelier, T. Zacharias, J.C. Weber, H. Dolgos, L. Richert, A.L. Ungell, Prediction of fraction metabolized via CYP3A in humans utilizing cryopreserved human hepatocytes from a set of 12 single donors, *Xenobiotica* 44 (1) (2014) 17–27.
- [73] A. Suzuki, et al., CYP isoforms involved in the metabolism of clarithromycin in vitro: comparison between the identification from disappearance rate and that from formation rate of metabolites, *Drug Metab. Pharmacokinet.* 18 (2) (2003) 104–113.
- [74] D.F. McGinnity, et al., Evaluation of fresh and cryopreserved hepatocytes as in vitro drug metabolism tools for the prediction of metabolic clearance, *Drug Metab. Dispos.* 32 (11) (2004) 1247–1253.
- [75] M. Akram, et al., Hepatocytes as a tool in drug metabolism, transport and safety evaluations in drug discovery, *Curr. Drug Discov. Technol.* 7 (3) (2010) 188–198.
- [76] O. Pelkonen, et al., Inhibition and induction of human cytochrome P450 (CYP) enzymes, *Xenobiotica* 28 (12) (1998) 1203–1253.
- [77] K. Venkatakrishnan, L.L. von Moltke, D.J. Greenblatt, Application of the relative activity factor approach in scaling from heterologously expressed cytochromes P450 to human liver microsomes: Studies on amitriptyline as a model substrate, *J. Pharmacol. Exp. Ther.* 297 (1) (2001) 326.
- [78] W.P. Yong, et al., Effects of ketoconazole on glucuronidation by UDP-glucuronosyltransferase enzymes, *Clin. Cancer Res.* 11 (18) (2005) 6699–6704.
- [79] C.Q. Xia, et al., Expression, localization, and functional characteristics of breast cancer resistance protein in Caco-2 cells, *Drug Metab. Dispos.* 33 (5) (2005) 637–643.
- [80] R.S. Obach, et al., The utility of in vitro cytochrome P450 inhibition data in the prediction of drug–drug interactions, *J. Pharmacol. Exp. Ther.* 316 (1) (2006) 336–348.
- [81] D.M. Stresser, et al., Highly selective inhibition of human CYP3Aa in vitro by azamulin and evidence that inhibition is irreversible, *Drug Metab. Dispos.* 32 (1) (2004) 105–112.
- [82] N.M. Njuguna, et al., Improvement of the chemical inhibition phenotyping assay by cross-reactivity correction, *Drug Metab. Pers. Ther.* 31 (4) (2016) 221–228.
- [83] B. Lindmark, et al., Human hepatocytes and cytochrome P450-selective inhibitors predict variability in human drug exposure more accurately than human recombinant P450s, *Br. J. Pharmacol.* 175 (11) (2018) 2116–2129.
- [84] E. Hustert, et al., The genetic determinants of the CYP3A5 polymorphism, *Pharmacogenetics* 11 (9) (2001) 773–779.
- [85] K.A. Birdwell, et al., Clinical pharmacogenetics implementation consortium (CPIC) guidelines for CYP3A5 genotype and tacrolimus dosing, *Clin. Pharmacol. Ther.* 98 (1) (2015) 19–24.
- [86] X. Li, et al., Discovery of a highly selective CYP3A4 inhibitor suitable for reaction phenotyping studies and differentiation of CYP3A4 and CYP3A5, *Drug Metab. Dispos.* 40 (9) (2012) 1803–1809.
- [87] R.L. Walsky, R. Obach, R. Hyland, P. Kang, S. Zhou, M. West, K.F. Geoghegan, C.J. Helal, G.S. Walker, T.C. Goosen, M.A. Zientek, Selective mechanism-based inactivation of CYP3A4 by CYP3Cide (PF-04981517) and its utility as an in vitro tool for delineating the relative roles of CYP3A4 versus CYP3A5 in the metabolism of drugs, *Drug Metab. Dispos.* 40 (9) (2012) 1686–1697.
- [88] PMDA, Drug Interaction Guideline for Drug Development and Labelling Recommendations, 2017.
- [89] FDA, Physiologically Based Pharmacokinetic Analyses—Format and Content Guidance for Industry, 2018.
- [90] EMA, Guideline on the Reporting of Physiologically Based Pharmacokinetic (PBPK) Modelling and Simulation, 2018.

- [91] V. Pilla Reddy, et al., Physiologically based pharmacokinetic modeling for olaparib dosing recommendations: bridging formulations, drug interactions, and patient populations, *Clin. Pharmacol. Ther.* 105 (1) (2019) 229–241.
- [92] P. Damkier, et al., CYP2C19\*2 and CYP2C19\*17 variants and effect of tamoxifen on breast cancer recurrence: analysis of the international tamoxifen pharmacogenomics consortium dataset, *Sci. Rep.* 7 (2017) 7727.
- [93] C.J. Henderson, et al., An extensively humanized mouse model to predict pathways of drug disposition and drug/drug interactions, and to facilitate design of clinical trials, *Drug Metab. Dispos.* 47 (6) (2019) 601–615.
- [94] N. Tsamandouras, et al., Integrated gut and liver microphysiological systems for quantitative in vitro pharmacokinetic studies, *AAPS J.* 19 (5) (2017) 1499–1512.
- [95] U. Sarkar, et al., Integrated assessment of diclofenac biotransformation, pharmacokinetics, and omics-based toxicity in a three-dimensional human liver-immunocompetent coculture system, *Drug Metab. Dispos.* 45 (7) (2017) 855–866.

# Evaluation of the clearance mechanism of non-CYP-mediated drug metabolism and DDI as a victim drug

*Anima Ghosal*

Independent Consultant, Piscataway, NJ, United States

## 1 Introduction

Drug metabolism is generally classified in two phases: phase I and phase II. Phase I reactions include oxidation or reduction reactions, usually through the actions of cytochrome P450 (CYP) enzymes. CYP enzymes are responsible for biotransformation of many drugs via oxidation, and are located in both hepatic and extrahepatic tissues. Phase I enzymes include CYPs, flavin monooxygenases (FMOs), carboxylesterases (CES), carbonyl reductase, ketoreductases (aldo-keto reductase, AKR), aldehyde oxidases (AOX1), xanthine oxidases (XO), and monoamine oxidase (MAO). Phase II enzymes include UDP-glucuronosyltransferases (UGT), glutathione transferases (GST), sulfotransferases, acetyl transferases, methyl transferases, etc. Although, the major pathways of xenobiotic metabolism are catalyzed by phase I enzymes (mainly CYPs) and phase II enzymes (mainly UGTs), chemical modifications to reduce the CYP-mediated drug interaction have resulted in the synthesis of compounds with structural features that favor metabolism by non-CYP pathways. Non-CYP enzymes include UGT, FMO, MAO, AOX1, XO, CES, and AKR. Non-CYP enzymes may be oxidative, hydrolytic, reductive, or conjugative. Oxidation of drugs metabolized by FMO and MAO often produce the same metabolites as those generated by CYPs, hence drug interactions may be difficult to predict without a clear knowledge of the enzymology [1]. Contributions of non-CYP enzymes to the metabolism of top 200 prescribed drugs showed that CYPs are involved in approximately 75% of all drug metabolism compared to non-CYP enzymes [2]. Therefore, characterization of non-CYP metabolic pathways may enhance the understanding of in vitro-in vivo discrepancies and may help in the better

prediction of human clearance. In this chapter, we will focus on the major non-CYP-mediated metabolism (like UGT, FMO3, MAO, AOX1, XO, CES, and AKR), their expression, mechanism of action, challenges in determination of their quantitative contribution, and clinical relevance. The methods generally used for phenotyping of each class of non-CYP enzymes are discussed in this chapter based on literature reviews and author's own experience. The methodologies can vary widely from laboratory to laboratory based on the objective of the study: screening, qualitative assessment, or quantitative assessment of the contribution of each non-CYP enzyme relative to overall clearance of a drug.

## 2 UDP-glucuronosyltransferase (UGT)

Phase II conjugation reactions are catalyzed by a group of enzymes called transferases. Most transferases are located in cytosol, except UGTs, which are located in microsomes. Glucuronidation is one of the major phase II drug-metabolizing reactions that contribute to drug biotransformation and requires a cofactor uridine 5'-diphosphate glucuronic acid (UDPGA). UGT enzymes catalyze the glucuronidation of a wide range of structurally diverse endogenous and exogenous chemicals, environmental toxicants, carcinogens, dietary toxins and participate in the homeostasis of bilirubin, steroid hormones, and biliary acids [3]. Over the years, significant progress has been made in the field of glucuronidation, especially with regard to the identification of human UGTs, study of their tissue distribution, and substrate specificities. More recently, the degree of allelic diversity has also been revealed for several human UGT genes [3, 4]. Some polymorphic UGTs have demonstrated a significant pharmacological impact in addition to being relevant to drug-induced adverse reactions and cancer susceptibility. UGT isoforms have been separated into two families as UGT1A and UGT2B based on similarities between their primary amino acid sequences.

In humans, UGTs are significantly expressed in the liver, for example, UGT1A1, UGT1A3, UGT1A4, UGT1A6, UGT1A9, UGT2B4, UGT2B7, UGT2B10, UGT2B15, and UGT2B17. In the liver, UGT2B7 is expressed to the highest level, followed by UGT1A1, UGT2B4, UGT2B15, UGT1A4, UGT2B10, UGT1A9, UGT2B17, UGT1A6, and UGT1A3. The following UGTs are also expressed in the human intestine: UGT1A1, UGT1A7, UGT1A8, UGT1A10, UGT2B7, UGT2B17, and very low levels of UGT1A3 and UGT1A4, whereas in the human kidney only four UGTs are detected at the protein level: UGT1A9, UGT2B7, UGT1A6, and UGT2B17 (Tables 1 and 2) [3, 5–7]. UGT1A1, UGT1A3, UGT1A6, and UGT1A10 are expressed in human brains. The level of UGT2B17 protein increases (~10-fold) from age 9 years to adults with ~2.6-fold higher abundance in males than in females. Its expression is very low in children below 9 years [8].

The glucuronidation reaction consists of the transfer of the glucuronosyl group from the cofactor UDPGA to drug or substrate molecules that contain oxygen, nitrogen, sulfur, or carboxyl functional groups (Fig. 1). The resulting glucuronide conjugate of a substrate is more polar (e.g., hydrophilic) and water soluble that can more easily be excreted in the urine and/or bile than the substrate molecule itself.

**TABLE 1** Substrates and tissue localization of human UGT1A isoforms.

<b>Isoforms</b>	<b>Tissue localization</b>	<b>Major substrates (endogenous)</b>	<b>Major substrates (xenobiotic)</b>
UGT1A1	Liver Intestine Colon Gallbladder Brain	Bilirubin Estriol $\beta$ -Estradiol 2-Hydroxyestrone 2-Hydroxyestradiol	Quercetin Naringenin 1-Naphthol Etoposide SN-38
UGT1A3	Liver Intestine Colon Gallbladder Brain	Estrone 2-Hydroxyestrone 2-Hydroxyestradiol 4-Hydroxy-all-trans-retinoic acid	Apigenin Naringenin Chenodeoxycholic acid
UGT1A4	Liver Intestine Colon Gallbladder	Androsterone Epiandrosterone	Benzidine Amityptiline Imipramine Trifluoperazine Clozapine Posaconazole
UGT1A6	Liver Stomach Intestine Colon Kidney Gallbladder Brain	Serotonin	Acetaminophen Methylsalicylate 4-Methylumbelliferone 1-Naphthol 4-Hydroxyindole
UGT1A7	Stomach Intestine	Not known	HFC
UGT1A8	Intestine Colon	Estrone 2-Hydroxyestrone 4-Hydroxyestrone Dihydrotestosterone	4-Methylumbelliferone Apigenin Naringenin Emodin Propafol Eugenol Propofol 9-OH-benzo[a]pyrene 1-Naphthol 7-Hydroxycoumarin Chrysin Quercetin 4-Nitrophenol
UGT1A9	Liver Colon Kidney	Thyroxine	Acetaminophen Emodin Quercetin 4-Methylumbelliferone Carvacrol

*Continued*



**TABLE 1** Substrates and tissue localization of human UGT1A isoforms—cont'd

Isoforms	Tissue localization	Major substrates (endogenous)	Major substrates (xenobiotic)
UGT1A10	Stomach	2-Hydroxyestrone	Mycophenolic acid
	Intestine	4-Hydroxyestrone	Benzo(a)pyrene
	Colon	Dihydrotestosterone	Quinoline
	Gallbladder	Dopamine	2-Acetylaminofluorene
	Brain		

Based on A. Radomska-Pandya, P.J. Czernik, J.M Little, *Structural and functional studies of UDP-glucuronosyltransferases*, *Drug Metab. Rev.* 31 (4) (1999) 817–899, M.B Fisher, M. Vandenbranden, K. Findlay, B. Burchell, K.E. Thummel, S.D. Hall, S.A. Wrighton, *Tissue distribution and interindividual variations in human UDP-glucuronosyltransferase activity: relationship between UGT1A1 promoter genotype and variability in a liver bank*, *Pharmacogenetics* 10 (2000) 727–739, A. Ghosal, R. Ramanathan, N.S. Kishmani, S. Chowdhury, K.B. Alton, *Cytochrome P450 (CYP) and UDP-glucuronosyltransferase (UGT) enzymes: role in drug metabolism, polymorphism, and identification of their involvement in drug metabolism*, In: S. Chowdhury (Ed.), *Identification and Quantification of Drugs, Metabolites and Metabolizing Enzymes by LC-MS (In Progress in Pharmaceutical and Biomedical Analysis)*, vol 6. Elsevier, 2005, pp. 295–327 (Chapter 12).

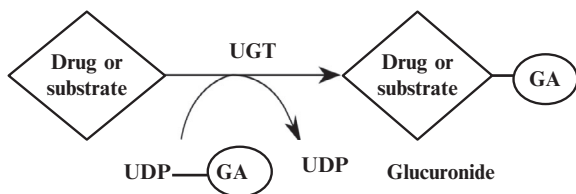
**TABLE 2** Substrates and tissue localization of human UGT2B isoforms.

Isoforms	Tissue localization	Major substrates (endogenous)	Major substrates (xenobiotic)
UGT2B4	Liver	Androsterone	Hydroxycholic acid
	Intestine		
UGT2B7	Liver	Androsterone	Morphine
	Intestine	Epitestosterone	Naloxone
	Kidney	4-Hydroxyestradiol	Codeine
		Estriol	Buprenorphine
		2-Hydroxyestrone	Nalbuphine
Linoleic acid	Naltrexone		
UGT2B10	Liver	Not known	Cotinine
			Nicotine
			Amitriptyline
			Imipramine
			Ketotifen
			Pizotifen
			Olanzapine
			Diphenhydramine
			Tamoxifen
			Ketoconazole
			Midazolam
UGT2B11	Liver	Not known	12-Hydroxyeicosatetraenoic acid
	Kidney		13-Hydroxyoctadecadienoic acid (HODE)
	Prostrate		
	Skin		
	Adrenal		
	Lung		
	Mammary gland		

**TABLE 2** Substrates and tissue localization of human UGT2B isoforms—cont'd

Isoforms	Tissue localization	Major substrates (endogenous)	Major substrates (xenobiotic)
UGT2B15	Liver Prostrate Skin Breast	Dihydrotestosterone	Eugenol 4-Methylumbelliferone Naringenin SCH 23390 Esculetin 8-Hydroxyquinoline (S)-Oxazepam
UGT2B17	Liver Intestine Kidney Testis Uterus Placenta Mammary gland Adrenal gland Skin Prostrate	Testosterone Dihydrotestosterone Androsterone 17-Beta-diol Estradiol	Eugenol 17-Dihydroexemestane, Vorinostat Lorcaserin MK-7246
UGT2B28	Breast Urinary bladder Salivary gland	Androgens	Not known

Based on A. Radominska-Pandya, P.J. Czernik, J.M Little, Structural and functional studies of UDP-glucuronosyltransferases, *Drug Metab. Rev.* 31 (4) (1999) 817–899, M.B Fisher, M. Vandenbranden, K. Findlay, B. Burchell, K.E. Thummel, S.D. Hall, S.A. Wrighton, Tissue distribution and interindividual variations in human UDP-glucuronosyltransferase activity: relationship between UGT1A1 promoter genotype and variability in a liver bank, *Pharmacogenetics* 10 (2000) 727–739, A. Ghosal, R. Ramanathan, N.S. Kishmani, S. Chowdhury, K.B. Alton, Cytochrome P450 (CYP) and UDP-glucuronosyltransferase (UGT) enzymes: role in drug metabolism, polymorphism, and identification of their involvement in drug metabolism, In: S. Chowdhury (Ed.), *Identification and Quantification of Drugs, Metabolites and Metabolizing Enzymes by LC-MS (In Progress in Pharmaceutical and Biomedical Analysis)*, vol 6. Elsevier, 2005, pp. 295–327 (Chapter 12).

**FIG. 1** Glucuronidation reaction. GA, glucuronic acid.

## 2.1 Reaction phenotyping of UGT enzyme(s)

There are several well-established approaches used for reaction phenotyping of the UGTs responsible for the metabolism of new drug/new chemical entities (NCE), which include (1) incubation with human liver microsomes (HLM) with UDPGA, (2) use of chemical inhibitors against human UGTs, and (3) incubation with recombinant human UGT enzymes [9].

UGT reaction phenotyping involves an initial assessment of Michaelis-Menten kinetics using native pooled HLM. Initial reaction rates are measured over a wide range of substrate

concentrations ( $[S]$ ) employing incubation conditions that are linear with respect to microsomal protein concentration and time of incubation. The data are analyzed by linear and nonlinear transformations [9]. In the majority of cases, the low apparent  $K_m$  component is most informative because this indicates which UGTs play a major role, at clinically relevant drug concentrations. An example of UGT phenotyping is provided in the following section using posaconazole, a triazole antifungal agent [7, 9].

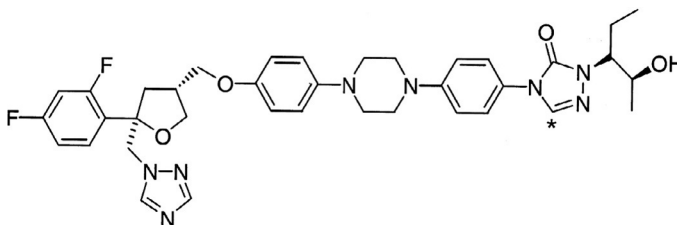
## 2.2 Incubation with pooled HLM

The enzyme assay was optimized using posaconazole (Fig. 2) concentrations of 0.5–50  $\mu\text{M}$ , microsomal protein concentrations of 0.05–2 mg/mL, and incubation time of 15–240 min. To diminish the latency of UGT activity, microsomes were pretreated with 50- $\mu\text{g}$  alamethicin/mg microsomal protein on ice for 15 min [10]. All microsomal incubations contained alamethicin-treated microsomes, 10-mM magnesium chloride, 5mM saccharolactone (an inhibitor of  $\beta$ -glucuronidase), and substrate ( $^{14}\text{C}$ -posaconazole) in 0.5mL of 0.1-M Tris buffer, pH7.4 [11]. Prior to the addition of UDPGA, the incubation mixtures were prewarmed for 3 min at 37°C. Reactions were initiated by the addition of 2mM UDPGA, allowed to proceed for various time periods at 37°C, and terminated with ice-cold methanol. The incubation mixtures were mixed, centrifuged at 4°C for 10 min, and the supernatants analyzed by HPLC coupled with a radiometric detector. Incubations without UDPGA and boiled HLM served as negative control. For LC/MS analyses, the reactions were either terminated as described above or terminated by cooling in ice water, followed by solid-phase extraction. Initially the assay was optimized where the product was formed under initial rate conditions (rate of product formation was linear with respect to enzyme concentration and incubation time). No more than 20% substrate should be utilized during incubation period to achieve initial linear rate conditions. Optimal time and optimal protein concentration were 120 min and 1 mg/mL, respectively.

## 2.3 Incubation with recombinant human UGT enzymes

Incubation of posaconazole with human UGT SUPERSOMES (UGT1A1, UGT1A3, UGT1A4, UGT1A6, UGT1A7, UGT1A8, UGT1A9, UGT1A10, UGT2B7, and UGT2B15) was performed using microsomal protein (1mg/mL) and two concentrations of substrate ( $^{14}\text{C}$ -posaconazole, 5 and 30  $\mu\text{M}$ ). All incubations were carried out as described earlier. Insect cell microsomes without cDNA for UGT served as the negative control. These samples were also

FIG. 2 Chemical structure of Posaconazole. \* Denotes  $^{14}\text{C}$ .



analyzed by LC-MS coupled in line with a flow scintillation analyzer (FSA) (LC-FSA/MS) and LC-MS to verify the formation of glucuronide conjugates. Optimal time and optimal protein concentration were determined as described earlier. Kinetic parameters ( $K_m$  and  $V_{max}$ ) for UGTs were determined using various substrate concentrations and optimal UGT protein concentration of 1 mg/mL and proceeded for optimal time as described earlier for microsomes [9].

## 2.4 Inhibition study with chemical inhibitors of UGTs

Glucuronidation of posaconazole was evaluated using known chemical inhibitors of UGTs [9]. HLM (1 mg/mL) or human UGT SUPERSOMES (1 mg/mL) were preincubated with various concentrations of bilirubin (inhibitor of UGT1A4) for 15 min at room temperature followed by the addition of buffer, alamethicin, saccharolactone, cofactor, and substrate. The final concentration of the organic solvent in the incubation system was 1%, and all control incubations contained the same volume of appropriate vehicle. All incubations were carried out as described earlier.

In vitro incubations with 10 different recombinant human UGT SUPERSOMES showed that only UGT1A4 exhibited catalytic activity for the formation of posaconazole-glucuronide [9]. The major in vitro metabolite of posaconazole formed by HLM supplemented with UDPGA was found to be a glucuronide of posaconazole by LC-MS ( $m/z$  877 Th). Since the results of inhibition studies with recombinant UGT1A4 SUPERSOMES show that bilirubin was an inhibitor of posaconazole-glucuronide formation from UGT1A4, it was used as an UGT1A4-inhibitor in this study. Bilirubin inhibited the formation of the glucuronide from HLM and UGT1A4 SUPERSOMES by 79.6% and 63.5%, respectively, with an  $IC_{50}$  of 11.1  $\mu$ M. In addition, there was a highly significant correlation between the formation of posaconazole-glucuronide and trifluoperazine glucuronidation which is known to be mediated by UGT1A4 [9]. These results confirm the involvement of UGT1A4 in the formation of posaconazole-glucuronide. Although the preceding discussion involved the characterization of enzymology of posaconazole glucuronidation, similar procedures can be applicable to other substrates as well [12–14]. Suh et al. [15] reported that the genetic polymorphism of UGT1A4\*3 is associated with low posaconazole plasma concentrations in patients receiving the oral suspension. This is the first study that revealed the association between genetic polymorphisms of UGT1A4\*3 and being a poor absorber of the posaconazole oral suspension.

## 2.5 Challenges

The determination of the contribution of each UGT isoform to the overall elimination is not as straightforward as that for CYP enzymes because of the absence of data on the abundance of the UGT isoforms, and the lack of specific inhibitors. Achour et al. [16] reported measurement of eight UGTs generated by two laboratories [using stable isotope-labeled (SIL) peptides or quantitative concatemer (QconCAT)], reflected significant disparity between proteomic methods. Several other researchers have also reported quantification of UGTs. According to Achour et al. [17], initial analysis of QconCAT data showed lack of correlation with catalytic activity for several UGTs (1A4, 1A6, 1A9, 2B15) and moderate correlations for UGTs 1A1,

1A3, and 2B7. Upon optimization, abundance-activity correlations improved significantly for six UGTs, UGT1A9 showed moderate correlation. However, methods remained suboptimal for UGT1A3 and UGT1A9 [17]. Although Achour et al. reported quantitative characterization of UGTs, the consistent correlation of UGT abundance with catalytic activity was not very promising. UGTs have overlapping substrate specificity. Lack of specific substrates and specific inhibitors are complicating factors for the calculation of relative activity factors (RAFs). In addition, Michaelis-Menten kinetics is not absolute and there are evidences for atypical kinetics, which needs to be carefully evaluated. Bhatt et al. [8] reported that association of androgen glucuronidation with UGT2B15 abundance was only observed in the low UGT2B17 expressors and these data can be used to predict variability in the metabolism of UGT2B17 substrates. High variability in UGT2B17 abundance significantly contributes to an unpredictable fate of its substrates that may lead to adverse pathophysiological consequences and drug toxicity or lack of efficacy [8]. However, UGT2B17 is a less studied enzyme and no regulatory guidance for industry currently exists for this enzyme.

There is some progress in the development of UGT1A1 probe substrates. There are a new generation of fluorescent substrate probes for UGT1A1, namely N-(3-carboxypropyl)-4-hydroxy-1,8-naphthalimide (NCHN) and N-butyl-4-(4-hydroxyphenyl)-1,8-naphthalimide (NHPN) [18]. Although the newly developed fluorescent probes for UGT1A1 (NCHN and NHPN) have been used for rapid screening of UGT1A1 inducers at the function level, the poor cell permeability of NCHN and the short emission wavelength of their glucuronides make them unsuitable probe substrates for screening UGT1A1 in hepatocytes culture. In order to make studies more meaningful, it is necessary to develop specific substrates and selective inhibitors of UGTs.

## 2.6 Clinical relevance and drug-drug interactions (DDI)

One of the clinical significances of UGT1A1 is its involvement in the conjugative detoxification of bilirubin, the by-product of heme metabolism [18]. UGT1A1 is a highly polymorphic enzyme with more than 100 variants, like UGT1A1\*28. In general, the polymorphic variants of UGT1A1 result in lower expression level, lower activity of the enzyme, or even complete activity loss [18]. The reduced expression/activity of UGT1A1 may increase the plasma concentrations of unconjugated bilirubin, leading to hyperbilirubinemia from the mild Gilbert's syndrome up to kernicterus and potentially fatal Crigler-Najjar syndrome. In addition, the liver of a newborn infant has a limited capacity to perform certain conjugation reactions when compared to older subjects. Although jaundice is common in newborns, mutations in the UGT1A1 gene increase the risk of developing a more severe condition called transient familial neonatal hyperbilirubinemia. In this condition, severe unconjugated hyperbilirubinemia and jaundice occur in newborns and usually disappear in 1–2 weeks.

There are several reports of clinical DDI with respect to UGTs. The inhibition of UGT1A1 by nilotinib could result in a significant increase in the AUC of SN-38, as well as an increased hyperbilirubinemia at high rate. The increased AUC of SN-38 due to nilotinib coadministration may serve as a good example for DDI [18]. The inhibition of UGT1A1-mediated SN-38 glucuronidation by ketoconazole is another example of DDI. Therapeutic

drugs such as UGT1A1 inhibitors are as follows: protease inhibitors (atazanavir, indinavir, and saquinavir) and tyrosine kinase inhibitors (TKIs) (lapatinib, pazopanib, regorafenib, nilotinib, and sorafenib).

UGT2B7 is involved in the conjugation of many drugs including the HIV/AIDS drugs (such as zidovudine) and the opioids (such as codeine and morphine). In a phase I clinical study, coadministration of pazopanib (an orally active, tyrosine kinase inhibitor) with irinotecan increases the area under the plasma concentration-time curve (AUC) for SN-38, an active metabolite of irinotecan. Pazopanib was found to interact with irinotecan by inhibiting UGT1A1-mediated glucuronidation [19]. Sauchinone, an herb, inhibited UGT2B7-mediated zidovudine metabolism in mice. You et al. [20] indicated that there is potential of herb-drug interaction between sauchinone and drugs that are UGT2B7 substrates. Wang et al. [21] reported that MK-7246 was a substrate of UGT2B17 and was overlooked during initial phenotyping. As a result, MK-7246 was discontinued from clinical trials due to high PK variability and, therefore, leads to clinical failure [21]. The potential for DDIs between SGLT2 inhibitor dapagliflozin (UGT1A9 substrate) and two potential UGT1A9 modulators was evaluated: rifampin, a pleiotropic drug-metabolizing enzyme inducer, and mefenamic acid, a strong UGT1A9 inhibitor. Significant changes in dapagliflozin exposure were seen with rifampin (a significant decrease of AUC: -22%) and with mefenamic acid (a significant increase of AUC ~51%) [22].

### 3 Flavin monooxygenase (FMO)

Flavin-monooxygenase (FMO) is an NADPH-dependent and oxygen-dependent microsomal FAD-containing enzyme system expressed in many tissues in various animal species including humans. FMO is thermally labile and mediates N-oxidation and S-oxidation as well as oxidation of xenobiotics containing phosphorous or selenium. There are five forms of functional human FMOs (FMO1, FMO2, FMO3, FMO4, and FMO5), out of which FMO3 is the most abundant and most catalytically important in adult liver [23]. In an adult, FMO1 is predominately expressed in the kidneys, lungs and small intestine; FMO2 is mostly expressed in the lungs, kidneys, and brain, with lower expression in the liver and small intestine. FMO3 is highly expressed in the liver, and also expressed in the lungs. FMO4 is expressed mostly in the liver and kidneys, while FMO5 is highly expressed in the liver, lungs, and small intestine. The expressions of FMOs in fetal tissues are different than in adult. The adult liver is dominated by the expression of FMO3 and FMO5, while the fetal liver is dominated by the expression of FMO1 and FMO5. In the brain, adults mostly express FMO2 and fetuses mostly express FMO1 [23]. Heterocyclic N-oxygenation can be catalyzed by both CYPs and FMOs. Therefore, the clearance estimates from *in vitro* microsomal incubations may underestimate the total clearance through N-oxidation due to the labile nature of the FMO3. Genetic polymorphism of FMO3 could also lead to unexpected catalytic efficiency for N- and S-oxygenation reactions of xenobiotics. The accuracy of human PK prediction will improve based on the understanding that the compound is likely a substrate for human liver FMO3.

### 3.1 The FMO catalytic cycle

The catalytic cycle involving the oxidation of substrates by FMO enzymes is shown in Fig. 3. NADPH binds to the oxidized state of the FAD (E-FAD) reducing it to FADH<sub>2</sub> (step 1). Molecular oxygen binds to the formed NADP<sup>+</sup>-FADH<sub>2</sub>-enzyme complex and is reduced, resulting in flavin-hydroperoxide (FAD-OOH) (step 2). The first two steps in the cycle are fast. In the presence of a substrate (S), a nucleophilic reaction occurs on the distal O-atom of the prosthetic group (step 3). The substrate is oxygenated to SO, forming the FAD-OH. The flavin product then breaks down with the release of water to reform FAD (step 4). NADP<sup>+</sup> is released by the end of the cycle and the enzyme returns to its original state (Source: Ziegler [24, 25]).

### 3.2 Determination of in vitro relative contribution of FMO vs CYP

The activity of all microsomal CYPs can be inhibited with an antibody to NADPH CYP reductase, CYP-selective chemical inhibitors (e.g., 1-aminobenzotriazole), carbon monoxide, or addition of detergent. The antibodies directed toward FMOs are typically weak inhibitors, and the only chemical inhibitor to inhibit FMO is methimazole [26, 27]. FMO activity is unaffected by nonionic detergent or carbon monoxide, however, most FMOs are readily inhibited by short incubations (2 min) at temperatures 45–50°C in the absence of NADPH. In order to estimate the relative contribution of FMO vs CYP, the standard approach is to utilize a combination of these approaches, e.g., preincubation at elevated temperature and incubation with and without FMO inhibitor methimazole. With respect to distinguishing FMO from CYP-mediated metabolism, results of inhibition with methimazole should be interpreted with caution as methimazole can be a substrate for CYPs [26, 27].

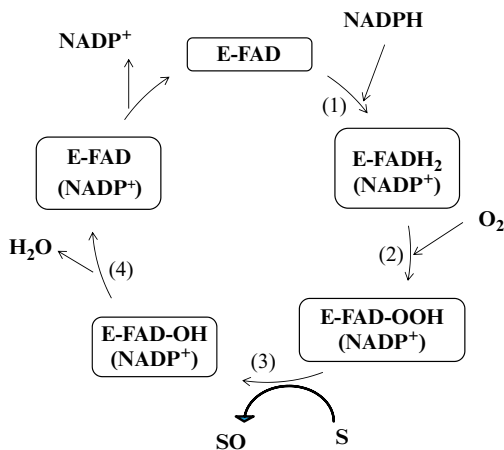


FIG. 3 FMO catalytic cycle.



### 3.3 Experimental design for FMO phenotyping

Methyl *p*-tolylsulfide (2 mM), a typical FMO substrate, is incubated for 10 min with HLM or recombinant FMO3 (0.025 mg/mL) in the presence of an NADPH or NADPH-regenerating system. Formation of methyl *p*-tolylsulfoxide (Fig. 4) is measured by LC-MS/MS. The incubation is performed in 50-mM Tris buffer, pH 8.8. Initially the assay is optimized where the product is formed under initial rate conditions (rate of product formation is linear with respect to enzyme concentration and incubation time). No more than 20% substrate should be utilized during incubation period. On a 96-well plate, liver microsomes, recombinant FMO, or insect control/blank are added separately with Tris buffer, cofactor NADPH (1 mM), and MgCl<sub>2</sub> (3 mM). The reaction mixture is preincubated for 3 min at 37°C. The reaction is initiated by adding the substrate (methyl *p*-tolylsulfide) or the test compound in a final volume of 0.2 mL. The reaction is terminated by adding 0.4 mL of acetonitrile containing internal standard (0.1 μM *p*-tolylsulfoxide), vortexed, and centrifuged. The supernatant is analyzed using LC-MS/MS. Measurement of both the formation of metabolite (if available) and disappearance of parent may provide comprehensive information on the FMO-mediated clearance. The rate of metabolite formation is calculated using a standard curve of the metabolite. Chemical inhibitor methimazole may be used for confirmation. For  $CL_{int}$ ,  $V_{max}/K_m$  values will be calculated.

### 3.4 Challenges

Recombinant FMO3 and FMO5 are commercially available. Although catalytically active FMO1 and FMO2 have been expressed in several systems (e.g., *Escherichia coli*), it is difficult to express FMO4 in heterologous systems and as a result it hampered the efforts to characterize this isoform [28]. Neither the human nor the rabbit ortholog of FMO4, each of which has been cloned and sequenced, has been expressed [28]. The relative contribution of individual FMO enzymes in the metabolism of a drug is difficult to determine due to lack of FMO-selective substrates and inhibitors. In addition, there is a lack of knowledge regarding abundance of FMO3 in human liver makes it difficult to predict the contribution of FMO in the metabolism of a drug.

### 3.5 Clinical significance and DDI

The trimethylaminuria disorder, also known as fish odor syndrome, causes abnormal FMO3-mediated metabolism or a deficiency of this enzyme in an individual. People with this disorder have a low capacity to oxidize the trimethylamine (TMA) that comes from their diet

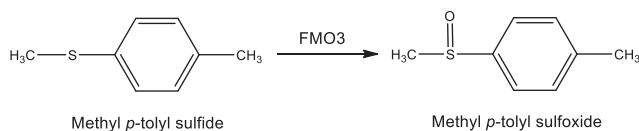


**FIG. 4** Structures of FMO3 substrate methyl *p*-tolyl sulfide and its metabolite methyl *p*-tolyl sulfoxide.

to its odorless metabolite trimethylamine oxide (TMAO). As a result, large amounts of TMA are excreted through the individual's urine, sweat, and breath, with a strong fish-like odor. As of today, there is no known cure or treatment for this disorder. There is evidence that FMOs are associated to the regulation of blood pressure. Since FMO3 is involved in the formation of TMA N-oxides (TMAO), some studies have indicated that hypertension can develop when there are no organic osmolytes (i.e., TMAO) that can counteract an increase in osmotic pressure and peripheral resistance. Individuals with deficient FMO3 activity have a higher prevalence of hypertension and other cardiovascular diseases [29]. There are reports of DDI due to the inhibition of FMO3, but the magnitude of potential DDI reported based on PBPK modeling has been very small and may not be clinically meaningful [30]. The antituberculosis drug ethionamide shows wide interindividual variability in its disposition. Nguyen et al. [30] reported the major contribution of FMO3 in the reductive elimination pathway of ethionamide as well as drug-drug interaction potential when methimazole is coadministered with ethionamide (catalyzed by FMO3). The maximum concentration ( $C_{max}$ ) and area under the curve (AUC) of ethionamide are predicted to increase by 13% and 16%, respectively, when coadministered with methimazole.

In contrast to CYPs, FMO is not easily induced nor readily inhibited, and potential adverse drug-drug interactions are minimized for drugs prominently metabolized by FMO. Therefore, recent efforts have been directed toward the development of drug candidates that incorporate functional groups that can be metabolized by FMOs. By doing this, the number of potential adverse drug-drug interactions could be minimized and the reliance on CYP-mediated metabolism is decreased [31].

## 4 Monoamine oxidase (MAO)

Monoamine oxidase (MAO) is a flavin containing enzyme catalyzes oxidative deamination of a wide variety of substrates like primary aliphatic and aromatic amines, secondary and tertiary amines, including the hormone and neurotransmitter amines epinephrine, dopamine, norepinephrine, and serotonin. Two isoforms, MAO-A and MAO-B, share 70% amino acid similarity and contain a covalently bound FAD cofactor attached to an enzyme cysteine. MAOs are composed of an FAD-binding domain, a substrate-binding domain, and a membrane-binding domain. Both MAOs bind the outer mitochondrial membrane through a C-terminal  $\alpha$ -helical region, with additional membrane interactions occurring with other hydrophobic residues [32]. The substrate-binding sites of both MAO-A and MAO-B are mainly hydrophobic, encased by predominantly aromatic and aliphatic residues. MAOs catalyze substrate oxidation via two half-reactions; in the reductive half-reaction, the flavin cofactor is reduced when it accepts a hydride equivalent from the substrate, while in the oxidative step, the reduced flavin is reoxidized by molecular oxygen (Fig. 5). Since the flavin cofactor has ability to accept one or two electrons, several mechanisms have been proposed for the transfer of electrons from the substrate to the cofactor [32, 33]. The two isoforms, MAO-A and MAO-B, differ according to substrate and inhibitor specificities. MAO-A and MAO-B are found in neurons and astroglia. Outside the central nervous system, MAO-A is also found in the liver, heart, pulmonary vascular endothelium, gastrointestinal tract, kidney, and

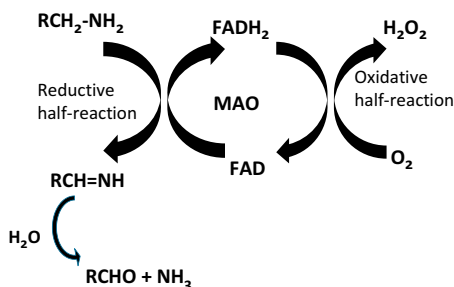


**FIG. 5** Catalytic cycle of MAO. Based on H. Gaweska, P.F. Fitzpatrick, *Structures and mechanism of the monoamine oxidase family*, *Biomol. Concepts*. 2 (5) (2011) 365–377, K. Yagyesh, S.N. Fatima, K. Kapil, *Synthesis and structure activity relationship of OPEN thiazolyl hydrazones as monoamine oxidase inhibitors: an overview*, *Curr. Trends Med. Chem.* 1 (1) (2018) 1003.

placenta. MAO-B is mostly found in blood platelets and also in liver, heart, duodenum, and kidney [34]. The liver S9 fraction represents an in vitro model containing both isoforms in their natural environment. The abnormal activities of these enzymes have been found in some psychiatric disorders where monoamine oxidase inhibitors (MAOI) drugs are prescribed as antidepressants.

#### 4.1 Experimental designs for MAO phenotyping

Kynuramine is a nonselective substrate for MAO-A and MAO-B and is transformed to the corresponding aldehyde, followed by nonenzymatic condensation to 4-hydroxyquinoline (Fig. 6). Several available assay methods are described below.

**Fluorometric assay:** MAO activity assays are conducted in 96-well plates in a final volume of 200  $\mu$ L in 0.1 M potassium phosphate (pH 7.4). The incubation consisted of assay buffer, enzymes (liver S9, mitochondrial fraction, or recombinant MAO-A/MAO-B), and substrate (160  $\mu$ M kynuramine for MAO-A and 80  $\mu$ M kynuramine for MAO-B) [35]. Other substrates of MAO-A and MAO-B are presented in Table 3. No NADPH is required. The assay is optimized where rate of product formation is linear with respect to enzyme concentration and incubation time. No more than 20% substrate should be utilized during incubation period. The 96-well plate, containing buffer and MAO substrate (150  $\mu$ L total volume), is preincubated at 37°C. The reaction is initiated with 50  $\mu$ L of enzyme/buffer mix. Reactions are stopped after 20 min by the addition of 75  $\mu$ L of 2 N NaOH. The excitation/emission wavelengths are 330/460 nm (20 nm slit width). (Note: The optimal wavelengths for detecting 4-hydroxyquinoline are approximately 310 nm excitation and 380 nm emission.) Product formation may be quantified by comparing the fluorescence emission of the samples to that of known amounts of authentic metabolite standard, 4-hydroxyquinoline. The rate of metabolite

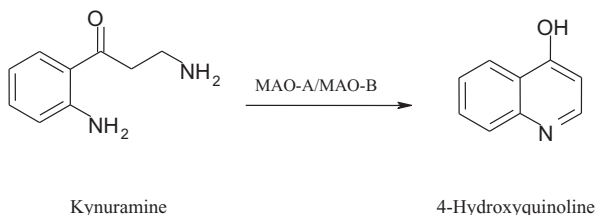


**FIG. 6** Structures of MAO substrate kynuramine and its metabolite 4-hydroxyquinoline.

**TABLE 3** Substrates of monoamine oxidases (MAO-A and MAO-B).

MAO-A	MAO-B
Almotriptan	Benzylamine
(R)-Citalopram	Bicifadine
Clomipramine	(R)-Citalopram
Dopamine	Clomipramine
Kynuramine	Decylamine
Noradrenaline	Dopamine
Octopamine	Kynuramine
Primaquine	3-Methoxy-tyramine
Rizatriptan	Milacemide
Sertraline	Methyl-histamine
Serotonin	MPTP
Sumatriptan	Octylamine
Tyramine	n-Pentylamine
Tryptamine	Sertraline
Zolmitriptan	Tyramine

*Based on M.S. Benedetti, R. Whomsley, E. Baltes, Involvement of enzymes other than CYPs in the oxidative metabolism of xenobiotics, Expert Opin. Drug Metab. Toxicol. 2 (6) (2006) 895–921.*

formation is calculated using a standard curve of the metabolite. For kinetic study, various concentrations of kynuramine may be used. The known MAO-A inhibitors like clorgyline, 5-(2-aminopropyl) indole (5-IT), harmine, harmaline, yohimbine, and MAO-B inhibitor selegiline may be used for the confirmation [36].

*Analysis by HPLC.* For HPLC analysis, the samples are acidified with 25  $\mu$ L of 70% perchloric acid after the addition of 2N NaOH prior to injection. The HPLC column is a Zorbax 5  $\mu$  SB-C18 (250  $\times$  4.6 mm). Separation may be achieved with an isocratic mobile phase of 27% methanol, 3% acetonitrile, and 0.2-mM perchloric acid. The HPLC flow rate is 1.5 mL/min. The total HPLC run time is approximately 4 min [37].

*Analysis by LC-MS.* For LC-MS analysis, reactions are stopped with equal volume of ice-cold acetonitrile, containing 10-mM amphetamine-d5 as IS. The solution is centrifuged for 2 min at 10,000 g, 50  $\mu$ L of the supernatant are transferred to an autosampler vial, and injected onto the HILIC-HR-MS/MS apparatus for analysis [36].

## 4.2 Challenges

Kynuramine is a nonselective substrate for MAO-A and MAO-B. The relative contribution of individual MAO enzymes in the metabolism of a drug is difficult to determine due to the

lack of MAO-selective substrates and inhibitors. In addition, the lack of knowledge regarding abundance of MAO in human liver makes it difficult to predict the contribution of MAO in the metabolism of a drug.

### 4.3 Clinical significance

Because MAOs play a vital role in the inactivation of neurotransmitters, MAO dysfunction (too much or too little MAO activity) is thought to be responsible for a number of psychiatric and neurological disorders. Unusually high or low levels of MAOs in the body have been associated with schizophrenia, depression, attention deficit disorder, substance abuse, and migraines. Monoamine oxidase inhibitors are one of the major classes of drug prescribed for the treatment of depression, although they are often last-line treatment due to risk of the drug's interaction with diet or other drugs. In fact, MAO-A inhibitors act as antidepressant and anti-anxiety agents, whereas MAO-B inhibitors are used alone or in combination with other drugs to treat Alzheimer's disease and Parkinson's disease. Research shows that the use of tobacco cigarettes heavily depletes MAO-B, mimicking the action of an MAO-B inhibitor. Smokers who smoke for emotional relief may therefore be unintentionally treating depression and/or anxiety that are better addressed by an MAO-B inhibitor. There are few reports of DDI with respect of MAOs. Moclobemide, an inhibitor of MAO-A, inhibits sumatriptan metabolism and leads to clinically significant drug-drug interactions [38].

---

## 5 Aldehyde oxidase

---

Aldehyde oxidases (AOXs) are molybdenum and flavin-dependent enzymes widely distributed across many tissues and involved in the oxidations, hydrolysis of amide bonds, and reductions. In general, oxidation reactions and amide hydrolysis occur at the molybdenum site and the reduction reactions occur at the flavin site [39]. AOXs are widely distributed throughout the animal kingdom in different organs, predominantly in liver and the expression varies with different animal species like rats have a range of activity, while dogs lack the activity in the liver. Due to the species differences in AOX expression, drug disposition studies for AOX substrates may not extrapolate to humans. AOX1 is the only enzyme in human and catalyzes the oxidation of various drugs and endogenous compounds, and reduction of drugs such as nitrazepam and dantrolene. Since AOX1 is present in the cytosolic fractions, standard metabolic stability studies using HLM do not capture AOX1-mediated metabolism. An increased rate of metabolism in hepatocytes compared with the microsomes or the formation of a new metabolite unique to the hepatocytes incubation (absent in microsomes) shows an early indication that the drug may be a substrate for AOX1 or xanthine oxidase (XO) [40]. Knowledge of the involvement of AOX1 in the metabolism of drugs may help to understand higher-than-expected clearance, contributing to an unfavorable half-life, the formation of a disproportionate human metabolite and may improve in vitro-in vivo correlation (IVIVC) as well as minimize the attrition of drug candidates [40]. There is limited information about the ability to scale in vitro clearance for compounds that are substrate of AOX1 for accurate human clearance predictions.

## 5.1 Experimental designs for AOX1 reaction phenotyping

Reaction phenotyping of AOX1 may be conducted using recombinant AOX1 and human liver cytosol (HLC). AOX1 does not require cofactor NADPH. The typical probe substrate for AOX1 is phthalazine which is converted to phthalazone (Fig. 7). In a typical incubation, phthalazine (0.1 mL) is incubated with HLC (0.05 mg protein/mL) or recombinant AOX1 in 50-mM phosphate buffer, pH 7.4 containing 0.1-mM ethylenediaminetetraacetic acid (EDTA). The assay is optimized where the product formation is linear with respect to enzyme concentration and incubation time. The linearity of reaction velocity with protein concentration and time is optimum up to 2.5 min [41]. Therefore, all incubations are conducted for 2–2.5 min at 37°C, and reactions are terminated by adding equal volume of acetonitrile containing 0.05% formic acid and internal standard (e.g., 4-methyl-1-phthalazinone), centrifuged, and supernatants are analyzed by LC-MS/MS. The rate of metabolite formation is calculated using a standard curve of the metabolite [41]. Other available substrates for AOX1 are zoniporide (converted to 2-oxozoniporide), O6-benzylguanine (to 8-Oxo-benzylguanine), and carbazeran (to 4-hydroxy carbazeran) (Fig. 8). Chemical inhibitors may be used to confirm the involvement of AOX1. Hydralazine is a selective inhibitor of AOX1 and can be used to determine fm (AOX1), while raloxifene is a nonspecific inhibitor [40, 42]. To estimate the contribution of AOX1 to total metabolic clearance in vitro, human

FIG. 7 Aldehyde oxidase (AOX) catalyzes phthalazine to its metabolite 1-phthalazinone.

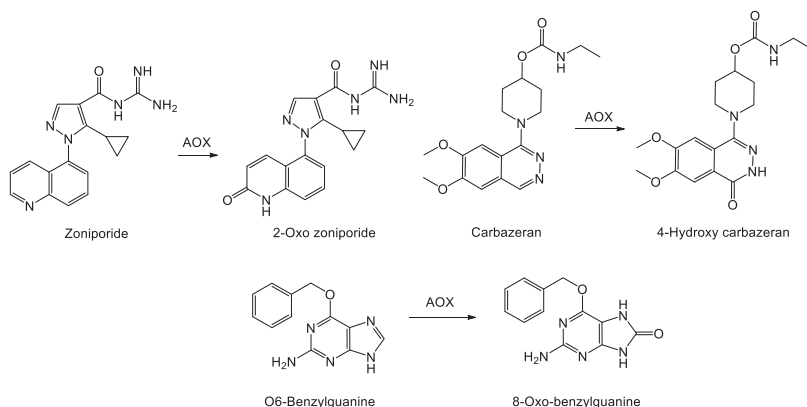
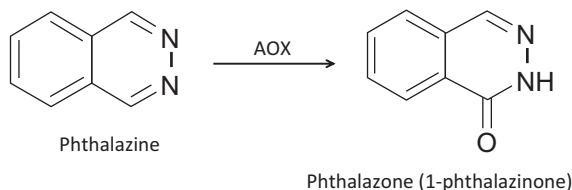


FIG. 8 Structures of aldehyde oxidase substrates and their metabolites.

hepatocytes (contain AOX1, P450 enzymes, and other drug-metabolizing enzymes) can be used as an in vitro system that offers an accurate representation of the relative activities of AOX1 involved in drug metabolism. However, Yang et al. [43] have reported that hydralazine also inhibits several CYPs (CYP1A2, 2B6, 2D6, and 3A) in human hepatocytes suspension. Therefore, precautions need to be taken when using hydralazine as an AOX inhibitor to estimate its contribution using hepatocytes because fm by AOX1 may be overestimated and the likelihood of false positives in identifying AOX1 substrates may increase [43]. Takuo et al. [44] have reported that clonazepam, flunitrazepam, flutamide, nilutamide, nimesulide, and nimetazepam are substantially reduced by recombinant AOX1 and HLC.

## 5.2 Challenges

There is a knowledge gap in the area of human tissue abundance of AOX1 as well as the intrinsic stability of AOX1 when it is isolated from the liver tissue. The lack of knowledge regarding abundance of AOX1 in human liver makes it difficult to predict quantitative contribution of AOX1 in the metabolism of a drug. Since there is no established scaling method for predicting AOX1-mediated clearance using in vitro or in vivo animal data, there is a lack of IVIVC in human [45].

## 5.3 Clinical significance and DDI

Individual differences in AOX1 activity influence drug metabolism in humans. During drug development, extensive metabolism by AOX1 has led to clinical failures due to rapid elimination, poor bioavailability or unacceptable pharmacokinetic properties in humans [38]. Since various drugs inhibit AOX1, assessments of drug-drug interactions (DDI) are critical for drug optimization. Famciclovir and O6-benzylguanine affecting AOX1 activity in humans have been reported. In human volunteers, following an 800-mg oral dose of cimetidine, the oral clearance of zaleplon is significantly decreased (to 56% of control), resulting in an increase in  $C_{\max}$  and AUC of zaleplon [40]. However, there are some caveats due to nonselectivity of cimetidine (inhibition of CYP3A) as well as CYP3A involvement in zaleplon clearance.

---

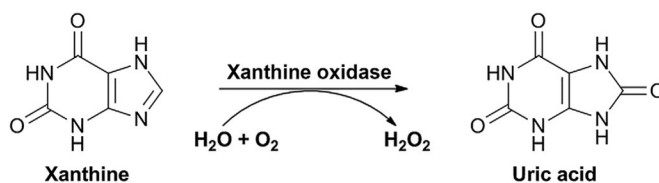
## 6 Xanthine oxidase (XO)

---

Xanthine oxidase (XO) enzyme is widely distributed in mammalian tissues (normally found in the liver and intestinal mucosa) and catalyzes the oxidation of endogenous and exogenous purines and pyrimidines. Each subunit contains one molybdopterin cofactor, two distinct [2Fe-2S] centers, and one FAD cofactor. XO catalyzes the oxidation of hypoxanthine to xanthine and xanthine to uric acid at the molybdopterin center, with concomitant reduction of  $\text{NAD}^+$  to NADH at the FAD center [46]. XO is involved in the last steps of purine catabolism and converts xanthine to uric acid with the formation of superoxide which spontaneously degrades to hydrogen peroxide ( $\text{H}_2\text{O}_2$ ) (Fig. 9). In addition to uric acid, XO products may comprise reactive oxygen and nitrogen species that have many biologic effects, including



FIG. 9 Xanthine oxidase catalyzes xanthine to uric acid.



inflammation, endothelial dysfunction, and cytotoxicity, as well as mutagenesis and induction of proliferation. The role of uric acid is characterized by both oxidant and antioxidant action; thus, it is still debatable whether control of uricemia may be helpful to improve the outcomes of tumor illness [47].

## 6.1 Experimental designs for XO phenotyping

It is a common practice to perfuse livers with UW solution (containing allopurinol) prior to liver harvest, however, the exposure to allopurinol in HLC preparations pose a problem for measuring in vitro XO activity [48]. Since allopurinol and oxypurinol (a primary metabolite of allopurinol) inhibited XO activity, commercially available pooled HLC that contained residual oxypurinol do not show any XO activity. Barr et al. [48] have recommended the screening of each HLC batch for oxypurinol and/or XO activity prior to testing for XO-mediated metabolism of a new chemical entity or using allopurinol free liver preparations for XO phenotyping studies.

The determination of XO activity is carried out in HLC and 50-mM phosphate buffer pH7.4. Several assay methods are available: (1) spectrophotometric quantitation of the final product uric acid using xanthine as a substrate, (2) fluorimetric quantitation of isoxanthopterin, XO-mediated metabolite of the substrate pterin, or (3) colorimetric. XO catalyzed xanthine to uric acid and hydrogen peroxide. In colorimetric assay, XO activity can be determined by measuring the amount of hydrogen peroxide generated which then reacts with 4-aminoantipyrine to form a red colored dye.

*Spectrophotometric assay:* XO catalyzes uric acid formation through the oxidation of the substrate xanthine and therefore its activity can be monitored by following the increase in uric acid formation by the absorbance at 295nm (UV-VIS spectrophotometer). The incubation mixture (500- $\mu\text{L}$  final volume) contains 50-mM phosphate buffer, pH7.4, 0.1mM EDTA, and 50  $\mu\text{M}$  xanthine as substrate. The reaction is started by adding 10  $\mu\text{L}$  of the enzyme stock solution (XO) or cytosolic fraction to the reaction mixture, followed by reading the absorbance up to 2 min at 20°C, thus calculating the corresponding rate in the linear range of the reaction. The quantitation may be achieved by the use of a calibration curve constructed with authentic uric acid. Because 1 unit of XO activity is defined as the velocity of the formation of 1  $\mu\text{mol}$  uric acid  $\text{min}^{-1}$ , the enzymatic activity in each sample can be calculated by using the equation:

$\text{Units/mg protein} = (\Delta A / \text{min} \times 1000) / (1.22 \times 10^4 \times \text{mg mL}^{-1} \text{ reaction mixture})$ , the molar absorption coefficient of uric acid is  $1.22 \times 10^4 \text{ M}^{-1} \text{ cm}^{-1}$  [49]. Allopurinol, a suicide inhibitor of XO, may be used to confirm the involvement of XO [46, 49].

*Fluorimetric assay:* The incubation mixture contain HLC or XO enzyme, the substrate (10  $\mu\text{M}$  pterin), and 50-mM sodium phosphate buffer (pH7.8) in a total volume of 1.0mL.

The reaction mixture is incubated for 10–60 min at 37°C and the amount of isoxanthopterin produced is measured by spectrofluorimetry. The fluorescence intensity of isoxanthopterin is measured with excitation at 345 nm and emission at 390 nm and quantitation achieved by the use of a calibration curve constructed with authentic isoxanthopterin. Inhibition by allopurinol, a specific inhibitor of XO, may be used to confirm the involvement of XO [49].

*Colorimetric assay:* The colorimetric assay using 96-well plate is based on XO-catalyzed oxidation of xanthine, in which the formed hydrogen peroxide is catalyzed by peroxidase and reacts with 4-aminoantipyrine to form the red dye. The color intensity of the reaction product at 550 nm is directly proportional to XO activity in the sample. The increase in OD<sub>550</sub> nm is measured using a plate reader over a 20 min interval, collecting data every 5 min (assay kits are commercially available).

## 6.2 Challenges

XO has been studied for many decades; however, much remains unknown regarding specific mechanistic roles for this enzyme in pathologic processes. This gap in knowledge raised several issues like the absence of tissue-specific XO-knockout models and the resistance of the endothelial-bound XO to inhibition by allopurinol, a selective XO inhibitor [50]. Although, circulating XO is elevated in hemolytic diseases including sickle cell, malaria, and sepsis, little is understood regarding its role in these pathologies. In addition, there is a lack of knowledge regarding abundance of XO in human liver and unavailability of expressed enzyme makes it difficult to predict the contribution of XO in the metabolism of a drug.

## 6.3 Clinical significance and DDI

Since XO is released into the blood during severe liver damage, a blood assay for XO is used to determine the extent of the damage. Xanthinuria is a rare genetic disorder in which the lack of XO leads to high concentration of xanthine in blood and can cause renal failure. Allopurinol is the most widely used XO inhibitor. It is effective in both lowering urate levels in the body and retarding the metabolism of chemotherapeutic agents such as 6-mercaptopurine, but serious side effects (skin rashes, allergic reactions, increased blood pressure, and increased risk of cataract) have been observed in some clinical patients [46]. Febuxostat, a new selective non-purine inhibitor, exhibits a considerably higher activity in vitro and in vivo than allopurinol [46]. It lacks most adverse effects of purine derivatives and is more effective than allopurinol in lowering serum uric acid concentration. Allopurinol is still used as first-line drug in gout, febuxostat being recommended as an option for people who are intolerant of allopurinol or for whom allopurinol is contraindicated. Recent reports have demonstrated a nitrate/nitrite ( $\text{NO}_2^-$ ) reductase function (reduction of  $\text{NO}_2^-$  to  $\cdot\text{NO}$ ) suggesting XOR to be a source of beneficial  $\cdot\text{NO}$  under these same hypoxic/inflammatory conditions [51]. The author also identified key microenvironmental factors whose interplay impacts the identity of the reactive species (oxidants vs  $\cdot\text{NO}$ ) produced [51].

## 7 Carboxylesterases (CES)

Human carboxylesterases, CES1 1 (hCE-1) and CES 2 (hCE-2) are serine esterases involved in both drug metabolism and activation. There is ~73% sequence homology between CES1 and CES2. CES are expressed in many tissues in both soluble forms exported into plasma and membrane-bound endoplasmic reticulum (ER) forms. Human CES enzymes are primarily located in ER and not in plasma, in contrast to other species such as mouse and rat which have high levels of CES present in the plasma. There are five human CES isoforms: CES1 (major liver form), CES2 (major intestinal form), CES3 (highest activity in the colon), CES4A, and CES5A, a secreted enzyme found in mammalian kidney and male reproductive fluids [52]. The highest CES2 expression occurs in small intestine mucosa, kidney proximal convoluted tubule, and adrenal cortex cells. Hybridization analyses showed that CES2 is also highly expressed in the heart, skeletal muscle, colon, spleen, kidney, and liver, but considerably less expressed in fetal tissues (fetal heart, kidney, spleen, and liver) and cancer cells. CES1 and CES2 are the main CES enzymes involved in drug metabolism. Little is known about the roles of CES3, CES4A, and CES5A [52]. Several isoforms of CES1 (CES1a, CES1b, and CES1c) have been characterized among which CES1b was found to be the predominant isoform in human liver [53]. In preclinical animal models, CES2 isozymes are also the major intestinal enzymes but they have different substrate specificities to human CES2. It is therefore difficult to predict human intestinal absorption from animal experiments. Caco-2 cells mainly express human CES1, which shows substrate specificity quite different from CES2, making Caco-2 cells unsuitable for prediction of human intestinal absorption of pro-drugs. CES enzymes are frequently involved in the activation of pro-drugs, or inactivation of molecules to reduce toxic effects. They can be considered an important enzyme to target for drug design. It is becoming increasingly common to use pro-drugs with carboxylic ester linkages, due to their ability to aid passive transport for oral absorption and only undergo hydrolysis to active drug on entering systemic circulation. CES1 hydrolyzes compounds esterified with small alcohol groups, whereas CES2 has a higher affinity for compounds with a small acyl group and large alcohol group. Due to the overlap in preferred substrate structure, using human liver or intestinal microsomes alone may not deliver the specificity required to differentiate between these two isozymes. Therefore, recombinant enzyme preparations may be preferred for investigating metabolism and inhibitory effects. The average human CES1 and CES2 expression in the subjects <1 year of age is significantly lower than that of pooled adult samples. Substrate drugs for CES1 and CES2 are presented in [Tables 4 and 5](#) [54].

### 7.1 Experimental design for CES reaction phenotyping

Reaction phenotyping of CES1 and CES2 is necessary to determine their involvement in the elimination of drugs; however, currently the tools available for this enzyme phenotyping are relatively scarce. The first approach is the use of selective inhibitors for CES1 and CES2 in the human liver or intestine subcellular fractions (S9). The second approach is based on data from recombinant CES, together with relative activity factors (if available), which relate their activities to those of the same enzymes in subcellular fractions. These two approaches will help to characterize the hydrolytic metabolism of drug candidates.

**TABLE 4** Substrates of CES1.

<b>Substrate</b>	<b>Hydrolysis product</b>	<b>Product activity</b>
<b>Antiplatelets/anticoagulants</b>		
Clopidogrel	Clopidogrel carboxylate	Inactive
Dabigatran etexilate	Dabigatran	Active
2-Oxo-clopidogrel	2-Oxo-clopidogrel carboxylate	Inactive
<b>Angiotensin-converting enzyme inhibitors</b>		
Benazepril	Benazeprilat	Active
Enalapril	Enalaprilat	Active
Imidapril	Imidaprilat	Active
Quinapril	Quinaprilat	Active
Ramipril	Ramiprilat	Active
Trandolapril	Trandolaprilat	Active
<b>Antihyperlipidemic agents</b>		
Simvastatin	Dihydroxy acid metabolite	Active
Lovastatin	Dihydroxy acid metabolite	Active
Clofibrate	Clofibric acid	Active
Fenofibrate	Fenofibric acid	Active
<b>Antiviral agents</b>		
Oseltamivir	Oseltamivir carboxylate	Active
<b>CNS agents</b>		
Cocaine	Benzoyllecgonine	Inactive
Flumazenil	Flumazenil acid	Inactive
Meperidine	Meperidinic acid	Inactive
Methylphenidate	Ritalinic acid	Inactive
Rufinamide	Rufinamide carboxylate	Inactive
<b>Immunosuppressive/oncology agents</b>		
Ciclesonide	Desisobutyryl-ciclesonide	Active
Mycophenolate mofetil	Mycophenolate	Active
Capecitabine	5'Deoxy-5-fluorocytidine	Inactive

*Based on S.C. Laizure, V. Herring, Z. Hu, K. Witbrodt, R.B. Parker, The role of human carboxylesterases in drug metabolism: have we overlooked their importance? Pharmacotherapy 33 (2) (2013) 210–222.*

TABLE 5 Substrates of CES2.

Substrate	Hydrolysis product	Product activity
<b>Antiplatelets/anticoagulants</b>		
Acetylsalicylic acid (aspirin)	Salicylate	Active
Prasugrel	Thiolactone metabolite	Inactive
<b>Angiotensin-receptor blockers</b>		
Azilsartan medoxomil	Azilsartan	Active
Candesartan cilexetil	Candesartan	Active
Olmesartan medoxomil	Olmesartan	Active
<b>Antispasmodic</b>		
Oxybutynin		Inactive
<b>Antiviral agents</b>		
Adefovir dipivoxil	Adefovir	Active
Tenofovir disoproxil	Tenofovir	Active
Valacyclovir	Acyclovir	Active
<b>CNS agents</b>		
Cocaine	Ecgonine methyl ester	Inactive
Heroin	6-Monoacetylmorphine	Active
6-Monoacetylmorphine	Morphine	Active
<b>Immunosuppressive agents</b>		
Methylprednisolone sodium succinate	Methylprednisolone	Active
<b>Oncology agents</b>		
Irinotecan	SN-38	Active

Based on S.C. Laizure, V. Herring, Z. Hu, K. Witbrodt, R.B. Parker, *The role of human carboxylesterases in drug metabolism: have we overlooked their importance?* *Pharmacotherapy* 33 (2) (2013) 210–222.

Clopidogrel is a typical probe substrate for CES1 and is converted to its carboxylic acid. Human liver S9 (HLS9) may be used for the incubation. Inhibition study with CES1-specific inhibitor nordihydroguaiaretic acid (NDGA) may be used to confirm the involvement of CES1. There are several reported CES1 substrates and their metabolites that can be used: benazepril converted to benazeprilat, oxybutynin to 2-cyclohexyl-2-phenylglycolic acid (CPGA), and trandolapril to trandolaprilat. A scheme depicting the typical hydrolysis of ester drugs is shown in Fig. 10. During hydrolysis, carboxylesterases catalyze the addition of water to an ester group producing a carboxylic acid and an alcohol (more polar than the original ester and increase renal elimination). The metabolism of clopidogrel is presented in Fig. 11.

A CES2 probe substrate is irinotecan which is metabolized to SN-38 (Fig. 12), may be used as a substrate. Irinotecan (CPT-11) is a semi-synthetic analogue of camptothecin and is

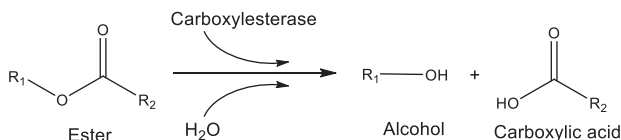


FIG. 10 Hydrolysis of ester drugs.

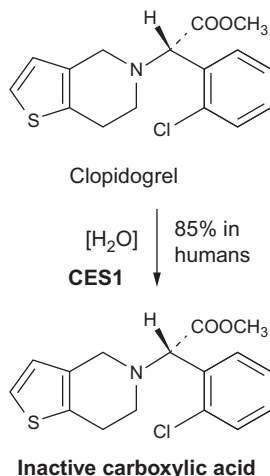


FIG. 11 CES1 hydrolyzed clopidogrel to carboxylic acid, an inactive metabolite.

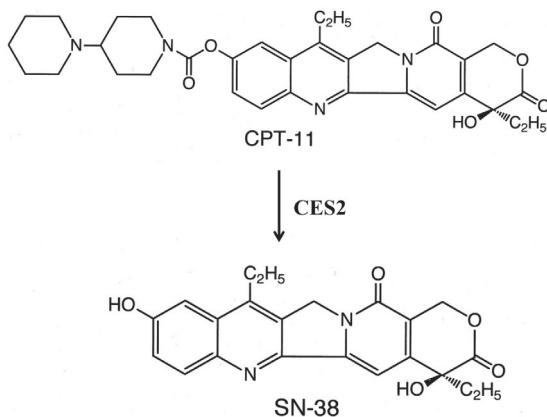


FIG. 12 Irinotecan (CPT-11) is catalyzed by CES2 to its active metabolite SN-38.

activated by CES2 to SN-38, a potent topoisomerase I inhibitor. The rate of metabolite formation is calculated using a standard curve for the metabolite formation. An inhibition study with a CES2-specific inhibitor, loperamide, may be used to confirm the involvement of CES2. The assay condition is described as reported by Umehara et al. [55]. The incubation mixture consists of the substrates (1 or 2mM), HLS9 (for CES1) or HIS9 (for CES2),

or recombinant CESs (rCES1 and rCES2) in 100-mM potassium phosphate buffer (pH7.4). Typical protein concentrations range is 0.25–1 mg/mL based on optimization. No other co-factors are needed. After preincubation of the enzymes for 3 min at 37°C in the buffer, the reactions are initiated by the addition of the substrate clopidogrel for CES1 and irinotecan for CES2 (other substrates are oseltamivir and oxybutynin). The final concentration of DMSO is 0.01% (v/v). The reactions are terminated by the addition of 50% formic acid in water (v/v) followed by the addition of the internal standard (1 or 5 mM warfarin) and the samples are mixed and saved for the LC-MS analysis. Control incubations are conducted in the absence of enzymes to determine the nonenzymatic hydrolysis. All incubations are performed in triplicate. Initially the assay is optimized where the rate of product formation is linear with respect to enzyme concentration and incubation time. The reported optimal incubation times for substrates are: 3 min for clopidogrel, 7 min for irinotecan, 10 min for oseltamivir, 30 min for oxybutynin, and protein concentrations are optimized to obtain less than 20% substrate consumption at the end of the incubation [55]. Chemical inhibitors may be used to confirm the involvement of CES1 and CES2 as described by Umehara et al. [55]. The effect of chemical inhibitors on the hydrolysis of clopidogrel (CES1 substrate) and irinotecan (CES2 substrate) by HLS9 and rCESs are evaluated using bis (p-nitrophenyl) phosphate (BNPP), diisopropylfluorophosphate (DFP), serine, tetraisopropyl pyrophosphoramidate (isoOMPA), paraoxon, tacrine, and EDTA. HLS9 and/or rCESs are preincubated with the inhibitors for 3 min at 37°C except for EDTA (preincubated for 15 min). The reactions are started by adding the substrate (final concentrations 1 or 2 mM) and terminated by the addition of 50% formic acid in water (v/v), followed by the internal standard as described above. The final concentration of DMSO in the incubation mixtures is 0.01% or 0.51%. The 0.51% of DMSO does not affect the hydrolytic reactions.

*Calculation of intrinsic clearances:* Umehara et al. [55] have reported that the intrinsic hydrolysis clearances ( $CL_{int}$ , pmol/min/mg protein) of the CES substrates are calculated by dividing the formation rates of the respective hydrolysis product (after subtraction of nonenzymatic contributions) by initial substrate concentration and protein concentration. To determine the fraction hydrolyzed by CES1 and CES2 in HLS9 using data from recombinant CES isozymes, the author applied a relative activity factor (RAF) concept (similar to CYP enzyme reaction phenotyping). The in vitro intrinsic clearance  $CL_{int}$  by HLS9 ( $CL_{int,HLS9}$  in mL/min/mg HLS9 protein) of a drug metabolized by CES1 and CES2 can be described according to Eq. (1) using RAF values calculated by Eq. (2):

$$CL_{int,HLS9} = CL_{int,rCES1} \times RAF(CES1) + CL_{int,rCES2} \times RAF(CES2) \quad (1)$$

$$RAF_{,CES} = \frac{CL_{int,HLS9}(\text{specific CES1 or CES2 substrate})}{CL_{int,rCES}(\text{same CES substrate})} \quad (2)$$

where  $CL_{int,rCES}$  represents the hydrolysis clearance measured in recombinant CES incubates (mL/min/mg microsomal protein).

The relative contribution of CES1 and CES2 to the total hydrolysis of irinotecan in HLM was determined successfully by Umehara et al. [55] using this RAF concept. Hence, for CES phenotyping, in addition to chemical inhibition, a second approach is proposed. This is based on clearance data obtained with recombinant or isolated CES, together with relative



activity factors. These approaches may help in the assessment of DDI risks of drug candidates cleared to a significant extent by CES.

## 7.2 Challenges

In recent years, there has been an increasing interest in the development of drugs that rely on CES-mediated hydrolysis to form the active therapeutic agent to take advantage of the absorption characteristics of esters. For CES-substrate drugs, several drug interactions have been identified using *in vitro* methods, but their clinical implications are unknown. Many CES substrate drugs are widely prescribed as antihypertensive drugs. As a result, the patient exposure to these drugs and the potential for alterations in hydrolytic activity might alter the therapeutic efficacy or toxicity. The scientists began to focus on CES hydrolysis whose activity may be influenced by genetic polymorphisms and drug interactions. There is growing evidence from *in vitro* and *in vivo* studies indicating that CES hydrolysis is subject to altered enzyme activity like CYPs, and represents a clinically important unrecognized reason for the individual variability of therapeutic response in patients given CES-substrate drugs [54]. Further research, especially clinical research, is needed to clarify the role of CES hydrolysis in drug metabolism, the factors that affect it, and the therapeutic implications for the safe and effective use of drugs that are CES substrates [54]. In addition, there is a lack of knowledge regarding abundance of CES in human liver which makes it difficult to predict the contribution of CES in the metabolism of a drug.

## 7.3 Clinical significance: CES and DDI

Ester prodrugs are specifically designed to enhance oral bioavailability and must be hydrolyzed to their active drug after absorption from the gastrointestinal tract. Prodrugs hydrolyzed by CES1 or CES2 have potential liabilities for DDI. Rhoades et al. [56] have reported that nelfinavir would serve as a potent CES1 inhibitor, and can cause DDI. Amprenavir, atazanavir, ritonavir, and saquinavir are shown to be CES1 inhibitors *in vitro*, although substantially less potent relative to nelfinavir. Drug interactions of prasugrel (Effient, platelet inhibitor) with other CES2 substrates and inhibitors are of potential concern. Capecitabine and irinotecan have demonstrated *in vitro* synergistic anticancer activity, and both are substrates for CES; potential drug-drug interactions observed. Aspirin (acetylsalicylic acid) and clopidogrel (Plavix) are two major antithrombotic agents that are widely used for the treatment and prevention of cerebro- and cardiovascular conditions such as stroke. Aspirin and clopidogrel both are esters, and hydrolysis leads to decreased or inactivated therapeutic activity.

## 8 Aldo-keto reductase (AKR)

The aldo-keto reductases (AKRs) are NADPH-dependent enzyme superfamilies that perform oxidoreduction on a variety of natural and foreign substrates. Previously, members of

the AKR superfamily were identified by names based on substrate specificity, e.g., the current AKR1C3 has also been named human 3 $\alpha$ -hydroxysteroid dehydrogenase (3 $\alpha$ -HSD) type II, 17 $\beta$ -HSD type V, dihydrodiol dehydrogenase (DD) type X, and prostaglandin F synthase [57–59]. The four AKR1C enzymes correspond to 3 $\alpha$ -HSD type 1 (AKR1C4), 3 $\alpha$ -HSD type II (AKR1C3), 3 $\alpha$ -HSD type III (AKR1C2), and 20 $\alpha$ -HSD (AKR1C1) share at least 86% amino acid sequence identity. AKR1C4 is virtually liver-specific, and AKR1C3 is most prominent in the liver, lung, prostate, uterus, and mammary glands (Table 6). The major isoforms in the brain are AKR1C1 and AKR1C2 [57]. AKR1C2 is also expressed in prostate, and in vitro it catalyzes the NAD<sup>+</sup>-dependent oxidation of 3 $\alpha$ -androstenediol (3 $\alpha$ -diol) to 5 $\alpha$ -dihydrotestosterone (5 $\alpha$ -DHT). Thus, in prostate cells, AKR1C2 acts as a 3-ketosteroid reductase to eliminate 5 $\alpha$ -DHT and prevents activation of the androgen receptor [60]. Tissue distribution of AKR enzymes are presented in Table 6.

### 8.1 Experimental design for AKR1C reaction phenotyping

Incubations with HLC or recombinant AKR are conducted using a constant amount of protein (1.6 mg/mL) and substrate like boceprevir (20  $\mu$ M) (Fig. 13) for 60–120 min [61]. All incubations are performed in the presence of an NADPH-generating system (0.5 mM NADP,

TABLE 6 Human aldo-keto reductases (AKRs).

AKR	Literature aliases	Location
1A1	Aldehyde reductase, ALR, ALR1	Liver, kidney, small intestine, brain
1B1	Aldose reductase, AR, ALR2	Placenta, liver, testis
1B10	Aldose reductase-like protein	Small intestine
1B11		Liver
1C1	DDH, DD1, DDH1, 20 $\alpha$ -HSD	Liver, kidney, lung, brain, testis
1C2	DD2, DDH2, BABP, 3 $\alpha$ -HSD type III	Liver, lung, brain, prostate, uterus
1C3	3 $\alpha$ -HSD type II	Liver, lung, mammary glands, prostate, uterus
1C4	DD4, CDR, CHDR, 3 $\alpha$ -HSD type I	Liver
1D1	$\Delta$ 4–3-ketosteroid-5 $\alpha$ -reductase	Liver
7A2	Aflatoxin inducible aldehyde reductase	Liver, kidney, brain, small intestine, testis
7A3	Aflatoxin inducible aldehyde reductase	Liver

Based on T.M. Penning, M.E. Burczynski, J.M. Jez, C.F. Hung, H.K. Lin, H. Ma, et al., Human 3 $\alpha$ -hydroxysteroid dehydrogenase isoforms (AKR1C1–AKR1C4) of the aldo-keto reductase superfamily: functional plasticity and tissue distribution reveals roles in the inactivation and formation of male and female sex hormones, *Biochem. J.* 351 (Pt 1) (2000) 67–77, T. O'Connor, L.S. Ireland, D.J. Harrison, J.D. Hayes, Major differences exist in the function and tissue-specific expression of human aflatoxin B1 aldehyde reductase and the principal human aldo-keto reductase AKR1 family members, *Biochem. J.* 343 (1999) 487–504.

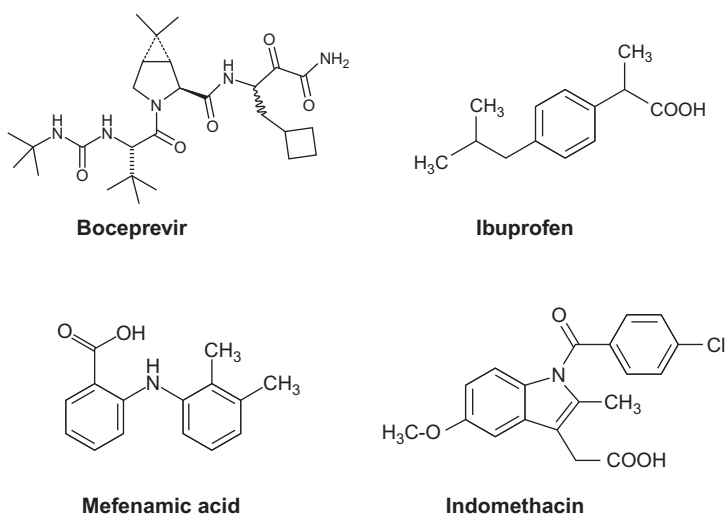


**FIG. 13** Structures of aldo-keto reductase (AKR) substrates.

5-mM glucose 6-phosphate, and 1.5 units/mL glucose-6-phosphate dehydrogenase), 3-mM magnesium chloride in 0.5 mL of 100-mM potassium phosphate buffer (pH7.4). Subcellular fractions or recombinant AKR without an NADPH-generating system are used as controls. Before the addition of drug, the reaction mixture is preincubated for 2 min at 37°C. Reactions are initiated by the addition of drug, allowed to proceed for up to 120 min at 37°C, and then terminated by the addition of 0.5 mL of ice-cold acetonitrile with 1% acetic acid. The incubation mixture is vortexed, centrifuged at 4°C for 10 min, and supernatants are saved for analysis by LC-MS/FSA [61]. The assay should be optimized so that the rate of product formation is linear with respect to enzyme concentration and incubation time. The rate of metabolite formation is calculated using a standard curve of the metabolite to determine the kinetic parameters  $K_m$  and  $V_{max}$ . Inhibition studies may be conducted using selective chemical inhibitors of AKR1C (flufenamic acid, mefenamic acid, phenolphthalein, ibuprofen, and diflunisal) to confirm the involvement of AKR1C [62]. For inhibition studies, HLC (1.6 mg protein/mL) or recombinant AKR are preincubated separately with various inhibitors for 15 min at room temperature, followed by the addition of buffer, cofactor, and substrate. All incubations are performed as described earlier [61]. The structures of some substrates of AKR are provided in Fig. 13.

## 8.2 AKR: Human-animal comparison

Experiments conducted using AKR1C3 from different species shows that the human AKR1C3 shares 95% and 78% identity with the monkey and mouse enzymes, respectively. Monkey AKR has 95% sequence homology with human [63].

### 8.3 Challenges

Although there are various drugs metabolized by AKR, there is lack of recombinant AKR enzymes available for experimental study. Despite many years of research, the physiological roles of AKRs are still unclear and the specific metabolic pathways that require these enzymes remain a mystery. It is likely that application of modern technologies such as knockout and transgenic animals, *in vivo* siRNA, fluorescent substrates and inhibitors, combined with metabolomic analysis will shed more light on the normal physiological functions of these proteins. The future developments in this area will significantly improve our basic understanding of AKRs and provide new guidance to improve human health [64]. The human AKRs have a large number of non-synonymous single nucleotide polymorphisms (nsSNPs) and splice variants; scientists are using modern genomic and informatics approaches to determine their association with human health and disease [65]. The AKRs display broad substrate specificity in *in vitro* assays and as a result *in vivo* substrates of AKRs are difficult to identify.

### 8.4 Clinical significance

Human AKRs like AKR1B1, AKR1C1-1C3, AKR1D1, and AKR1B10 have been implicated in diabetic complications, steroid hormone-dependent malignancies, bile acid deficiency, and defects in retinoic acid signaling [65]. Aldose reductase (AKR1B1), a family of AKR (Table 6), has possible role in the reduction of glucose during diabetic hyperglycemia and diabetic complications such as neuropathy [66], retinopathy [67], and cataracts [68]. Specific inhibitors of AKR1B1 that have been used clinically are sorbinil, tolrestat, epalrestat, ranirestat, and fidarestat [65]. Several drugs are metabolized by AKR enzymes. Anticancer drugs daunorubicin, doxorubicin, and oracin are substrates for several AKRs including AKR1A, 1B, and 1C as well as carbonyl reductase. The antihypertensive drug befunolol is a good substrate for AKR1C1 and AKR1C2 [64]. Opiate antagonist naloxone is reduced in the human liver stereo-specifically to 6 $\beta$ -naloxol by AKR1C4, however, AKR1C1 and 1C2 also contribute to a significant extent [69]. Boceprevir, HCV serine protease NS3 inhibitor, is metabolized primarily by AKR1C2 and AKR1C3 to ketone-reduced metabolites [61]. The first step of prostaglandins synthesis is the conversion of arachidonic acid to PGH<sub>2</sub> by cyclooxygenase. The conversion of PGH<sub>2</sub> to PGF<sub>2 $\alpha$</sub>  is catalyzed by PGF synthase which is designated as AKR1C3 in humans [70].

Specific cofactors required for the enzymatic reactions of common non-CYP-mediated enzymes, their substrates, and inhibitors are provided in Table 7 and examples of marketed drugs catalyzed by non-CYP enzymes (excluding UGT) are summarized in Table 8.

---

## 9 Future trends

The area of enzyme reaction phenotyping continues to evolve. The methodologies for CYP450 enzyme phenotyping is now a relatively mature field due to the understanding of enzyme expression levels in various tissues, liver in particular. In addition, availability of specific inhibitors both small molecules and antibodies and cDNA-expressed isozymes makes it easier for a quantitative assessment of CYP contribution to the clearance of a drug. However,

**TABLE 7** Non-CYP enzymes: Cofactors, substrate, and inhibitors for enzyme assays.

Enzymes	Tissue sources	Cofactor	Substrate	Inhibitor
CES1	Liver microsomes/S9	None	Clopidogrel	Arachidonic acid
CES2	Intestinal S9	None	Irinotecan (CPT-11)	Loperamide
FMO (FMO3)	Liver microsomes	NADPH	Methyl p-tolyl sulfide	Methimazole
MAO	Mitochondria Liver microsomes	FAD	Kynuramine	Clorgyline (MAO-A) Selegiline (MAO-B)
AOX1	Liver cytosol	Molybdenum	Phthalazine	Hydralazine Raloxifene
XAO	Liver microsomes	Molybdenum	Xanthine	Allopurinol
AKR	Liver cytosol	NADPH	Boceprevir	Diflunisal Flufenamic acid Phenolphthalein

FMO, flavin monooxygenase; AKR, aldo-keto reductases, AOX, aldehyde oxidase; XO, xanthine oxidase; MAO, monoamine oxidase; CES, carboxylesterase.

Based on C. Beedham, *The role of non-P450 enzymes in drug oxidation*, *Pharm. World Sci.* 19 (6) (1997) 255–263, R.S. Foti, D.K. Dalvie, *Cytochrome P450 and non-cytochrome P450 oxidative metabolism: contributions to the pharmacokinetics, safety, and efficacy of xenobiotics*, *Drug Metab. Dispos.* 44 (8) (2016) 1229–1245, A. Ghosal, Y. Yuan, W. Tong, A.D. Su, C. Gu, S.K. Chowdhury, et al., *Characterization of human liver enzymes involved in the biotransformation of boceprevir, a hepatitis C virus protease inhibitor*, *Drug Metab. Dispos.* 39 (2011) 510–521.

**TABLE 8** Examples of drugs catalyzed by non-CYP enzymes (excluding UGT).

Enzyme	Reaction	Typical substrate	Example
Flavin monooxygenases (FMO)	N-oxidation S-Oxidation	Secondary and tertiary amines Thiols, thioureas	Desipramine Nortriptyline Nicotine Tamoxifen Cimetidine
Monoamine oxidase (MAO-A and MAO-B)	Oxidative deamination Dehydrogenation	Primary, Secondary, Tertiary amines	Tyramine Milacemide Sumatriptan MPTP+
Aldehyde oxidase (AOX1)	Aldehyde oxidation C-oxidation	Aldehydes N-heterocycles	Tolbutamide O6-benzylguanine Zoniporide Phthalazine Famciclovir Methotrexate
Xanthine oxidase (XO)	C-oxidation	Purines	6-Mercaptopurine
Carboxylesterases (CES)	Ester, thioester, carbamates, and amide hydrolysis	Alcohol or acyl group	Irinotecan Oseltamivir Mepiridine

*Continued*

TABLE 8 Examples of drugs catalyzed by non-CYP enzymes (excluding UGT)—cont'd

Enzyme	Reaction	Typical substrate	Example
			Clopidogrel Aspirin Capcetabine Trandolapril Oxybutinin
Aldo-keto reductases (AKR)	Reduction	Aldehyde and keto groups	Befunolol Boceprevir DHT Doxorubicin Ibuprofen Indomethacin Mefenamic acid Naloxone Naltrexone Naproxen Oracin Testosterone Flufenamic acid

Based on C. Beedham, *The role of non-P450 enzymes in drug oxidation*, *Pharm. World Sci.* 19 (6) (1997) 255–263, K.-I. Umehara, M. Zollinger, E. Kigundu, M. Witschi, C. Juif, F. Huth, et al., *Esterase phenotyping in human liver in vitro: specificity of carboxylesterase inhibitors*, *Xenobiotica* 46 (10) (2016) 862–867, O.A. Barski, S.M. Tipparaju, A. Bhatnagar, *The Aldo-Keto Reductase Superfamily and its Role in Drug Metabolism and Detoxification*, *Drug Metab. Rev.* 40(4) (2008) 553–624.

the same is not true for non-CYP enzymes. Still for many non-CYP enzymes the accurate assessment of enzyme expression levels is not available. More importantly, the expression of many of these enzymes extrahepatically makes it further difficult to obtain an accurate level of contribution of these enzymes toward the clearance of a drug. Fortunately, there are new technologies in the horizon that may help to change the current state of non-CYP evaluation.

A new gene-editing technology, clustered regularly interspaced short palindromic repeats (CRISPR) associated protein 9 or CRISPRCas9 (CRISPR-Cas9), allows developing better and more predictive in vitro and in vivo ADME knockout models [71, 72]. In 2016, the first mammalian in vivo knockout ADME models (Cyp2e1 genes knocked out) were developed in Sprague Dawley or Wistar rats [73]. One in vitro CYP model established using CRISPR-Cas9 was based on the human hepatocyte cell line Huh-7 and CYP3A5 gene [74]. The gene-editing of CYP3A5 was successful and resulted in elevated CYP3A5 mRNA levels and increased metabolism of the two CYP3A5 substrates midazolam and tacrolimus [74]. CRISPR-Cas9 has a huge potential for a variety of applications in the ADME field including non-CYP enzymes. One major advantage with CRISPR-Cas9 knockout models is the complete elimination of background expression, which will facilitate investigations of clinically relevant drug metabolizing enzymes. With CRISPR-Cas9 it is possible to both completely knock out and knock in genes for CYP and non-CYP enzymes; hence this technology will help to develop better and easier-to-use models than the traditional ones.

PRINCE (Proteomics-based Research Initiative for Non-CYP Enzymes) program is a research collaboration between the University of Washington and pharmaceutical industry.

They are established to elucidate the role of non-CYP enzymes in disposition, efficacy, and toxicity of drugs. Their objectives are characterization of subcellular localization, differential tissue expression, and interindividual variability of non-CYP enzymes to develop whole body-based physiological (PBPK) models to predict drug disposition. Their goals are (1) to characterize differential tissue abundance (using quantitative proteomics) of non-CYP enzymes (UGT1A1, UGT1A3, UGT1A4, UGT1A6, UGT1A7, UGT1A8, UGT1A9, UGT1A10, UGT2B7, UGT2B15, UGT2B17, UGT2B4, AOX1, CES1, and CES2) in human intestine, kidney, heart, lung, and liver by LC-MS/MS; (2) to characterize intestinal abundance of above non-CYP enzymes in intestinal microsomes, tissue and enterocytes from the paired donors by LC-MS/MS proteomics; and (3) Preliminary LC-MS/MS method development for animal non-CYP enzymes (<https://sop.washington.edu/departments-of-pharmaceutics/research/proteomics-based-research-initiative-for-non-cyp-enzymes-prince/>).

## 10 Conclusion

The majority of oxidative metabolism of drugs is mediated by the CYP enzymes; however, non-CYP-mediated oxidative reactions can play an important role in the metabolism of xenobiotics. Non-CYP enzymes can produce active or reactive/toxic metabolites, modulate the efficacy of therapeutically active drugs, or contribute to detoxification. There is a possibility that the contribution of non-CYP oxidative enzymes to the overall metabolism of drugs is underestimated, as most investigations are conducted using optimized well-established conditions for CYP activity, which is not the same for most non-CYP enzymes [35]. Therefore, it is important to establish the contribution of CYP and non-CYP enzymes during reaction phenotyping studies of drugs which are primarily metabolized by oxidation. There are significant challenges with respect to the identification of non-CYP enzymes, their genetic polymorphism, availability of models for prediction of human clearance, and their involvement in induction and inhibition. Lack of selective probe substrates and inhibitors also poses challenge during the phenotyping of non-CYP enzymes. Although, significant progress has been made in the characterization of these non-CYP pathways, better understanding of their extra-hepatic expression and in vitro tools to measure their activity are needed. Over the years, researchers have made considerable improvement in establishing in vitro-in vivo correlation and predicting human clearance in order to avoid failure of drugs in clinical trials. However, more clinical experience is essential to translate in vitro reaction phenotyping data, enzyme contribution, and intersubject variability.

## Acknowledgment

The author acknowledges Moumita Ghosal (Consultant) for her assistance in the preparation of the chapter.

## References

- [1] C. Beedham, The role of non-P450 enzymes in drug oxidation, *Pharm. World Sci.* 19 (6) (1997) 255–263.
- [2] F.P. Guengerich, Cytochrome p450 and chemical toxicology, *Chem. Res. Toxicol.* 21 (2008) 70–83.



- [3] A. Radomska-Pandya, P.J. Czernik, J.M. Little, Structural and functional studies of UDP-glucuronosyltransferases, *Drug Metab. Rev.* 31 (4) (1999) 817–899.
- [4] M.A. Zientek, K. Youdim, Reaction phenotyping: advances in the experimental strategies used to characterize the contribution of drug-metabolizing enzymes, *Drug Metab. Dispos.* 43 (2015) 163–181.
- [5] M.B. Fisher, M. Vandenbranden, K. Findlay, B. Burchell, K.E. Thummel, S.D. Hall, S.A. Wrighton, Tissue distribution and interindividual variations in human UDP-glucuronosyltransferase activity: relationship between UGT1A1 promoter genotype and variability in a liver bank, *Pharmacogenetics* 10 (2000) 727–739.
- [6] M.B. Fisher, M.F. Paine, T.J. Strelevitz, S.A. Wrighton, The role of hepatic and extrahepatic UDP-glucuronosyltransferases in human drug metabolism, *Drug Metab. Rev.* 33 (2001) 273–297.
- [7] A. Ghosal, R. Ramanathan, N.S. Kishnani, S. Chowdhury, K.B. Alton, Cytochrome P450 (CYP) and UDP-glucuronosyltransferase (UGT) enzymes: role in drug metabolism, polymorphism, and identification of their involvement in drug metabolism, (Chapter 12). in: S. Chowdhury (Ed.), *Identification and Quantification of Drugs, Metabolites and Metabolizing Enzymes by LC-MS (In Progress in Pharmaceutical and Biomedical Analysis)*, 6, Elsevier, 2005, pp. 295–327.
- [8] D.K. Bhatt, A. Basit, H. Zhang, A. Gaedigk, S. Lee, K.G. Claw, et al., Hepatic abundance and activity of androgen and drug metabolizing enzyme, UGT2B17, are associated with genotype, age, and sex, *Drug Metab. Dispos.* (2018), <https://doi.org/10.1124/dmd.118.080952>.
- [9] A. Ghosal, N. Hapangama, Y. Yuan, J. Achanfuo-Yeboah, R. Iannucci, S. Chowdhury, et al., Identification of human UDP-glucuronosyltransferase enzyme(s) responsible for the glucuronidation of posaconazole (Noxafil), *Drug Metab. Dispos.* 32 (2) (2004) 267–271.
- [10] M.B. Fisher, K. Campanale, B.L. Ackermann, M. Vandenbranden, S.A. Wrighton, *In vitro* glucuronidation using human liver microsomes and the pore-forming peptide alamethicin, *Drug Metab. Dispos.* 28 (2000) 560–566.
- [11] D. Pless, J.N. Gouze, C. Senay, R. Herber, P. Leroy, V. Barberousse, et al., Characterization of the UDP-glucuronosyltransferases involved in the glucuronidation of an antithrombotic thioxlyoside in rat and humans, *Drug Metab. Dispos.* 27 (1999) 588–595.
- [12] A. Ghosal, N. Hapangama, Y. Yuan, J. Achanfuo-Yeboah, R. Iannucci, S. Chowdhury, et al., Identification of human UDP-glucuronosyltransferase enzyme(s) responsible for the glucuronidation of ezetimibe (Zetia), *Drug Metab. Dispos.* 32 (3) (2004) 314–320.
- [13] A. Ghosal, Y. Yuan, N. Hapangama, A.D. Su, N. Alvarez, S.K. Chowdhury, et al., Identification of human UDP-glucuronosyltransferase enzyme(s) responsible for the glucuronidation of 3-hydroxy-desloratadine, *Biopharm. Drug Dispos.* 25 (6) (2004) 243–252.
- [14] S.C. Liang, G.B. Ge, H.X. Liu, Y.Y. Zhang, L.M. Wang, J.W. Zhang, et al., Identification and characterization of human UDP-glucuronosyltransferases responsible for the *in vitro* glucuronidation of daphnetin, *Drug Metab. Dispos.* 38 (6) (2010) 973–980.
- [15] H.J. Suh, S.H. Yoon, K.-S. Yu, J.-Y. Cho, S.-I. Park, E. Lee, et al., The genetic polymorphism UGT1A4\*3 is associated with low posaconazole plasma concentrations in hematological malignancy patients receiving the oral suspension, *Antimicrob. Agents Chemother.* 62 (7) (2018), e02230–17. <https://doi.org/10.1128/AAC.02230-17>.
- [16] B. Achour, A. Dantonio, M. Niosi, J.J. Novak, J.K. Fallon, J. Barber, et al., Quantitative characterization of major hepatic UDPglucuronosyltransferase enzymes in human liver microsomes: comparison of two proteomic methods and correlation with catalytic activity, *Drug Metab. Dispos.* 45 (2017) 1102–1112.
- [17] B. Achour, A.L. Dantonio, M. Niosi, J.J. Novak, Z. Al-Majdoub, T.C. Goosen, et al., Data generated by quantitative LC-MS proteomics are only the start and not the endpoint: Optimization of QconCAT-based measurement of hepatic UDP-glucuronosyltransferase enzymes with reference to catalytic activity, *Drug Metab. Dispos.* 46 (6) (2018) 805–812.
- [18] X. Lv, Y. Xia, M. Finel, J. Wu, G. Ge, L. Yang, Recent progress and challenges in screening and characterization of UGT1A1 inhibitors, *Acta Pharm. Sin. B* 9 (2) (2019) 258–278.
- [19] M. Iwase, K. Fujita, Y. Nishimura, N. Seba, Y. Masuo, H. Ishida, et al., Pazopanib interacts with irinotecan by inhibiting UGT1A1-mediated glucuronidation, but not OATP1B1-mediated hepatic uptake, of an active metabolite SN-38, *Cancer Chemother. Pharmacol.* (2019) 1–6, <https://doi.org/10.1007/s00280-019-03784-8>.
- [20] B.H. You, E.C. Gong, Y.H. Choi, Inhibitory effect of sauchinone on UDP-glucuronosyltransferase (UGT) 2B7 activity. *Molecules* 23 (2) (2018) E366. <https://doi.org/10.3390/molecules23020366>.

- [21] Y.H. Wang, M. Trucksis, J.J. McElwee, P.H. Wong, C. Maciolek, C.D. Thompson, et al., UGT2B17 genetic polymorphisms dramatically affect the pharmacokinetics of MK-7246 in healthy subjects in a first-in-human study, *Clin. Pharmacol. Ther.* 92 (2012) 96–102.
- [22] A.J. Scheen, Drug–drug interactions with sodium-glucose cotransporters type 2 (SGLT2) inhibitors, new oral glucose-lowering agents for the management of type 2 diabetes mellitus, *Clin. Pharmacokinet.* 53 (4) (2014) 295–304.
- [23] J.R. Cashman, J. Zhang, Human flavin-containing monooxygenases, *Annu. Rev. Pharmacol. Toxicol.* 46 (2006) 65–100.
- [24] D.M. Ziegler, Microsomal flavin-containing monooxygenation of nucleophilic nitrogen and sulfur compounds, in: W.B. Jacoby (Ed.), *Enzymatic Basis of Detoxication*, 1 Academic Press, New York, 1980, pp. 201–227.
- [25] D.M. Ziegler, An overview of the mechanism, substrate specificities, and structure of FMOs, *Drug Metab. Rev.* 34 (3) (2002) 503–511.
- [26] S.K. Krueger, D.E. Williams, Mammalian flavin-containing monooxygenases: structure/function, genetic polymorphisms and role in drug metabolism, *Pharmacol. Ther.* 106 (3) (2005) 357–387.
- [27] B.C. Jones, A. Srivastava, N. Colclough, J. Wilson, V.P. Reddy, S. Amberntsson, et al., An investigation into the prediction of *in vivo* clearance for a range of flavin-containing monooxygenase substrates, *Drug Metab. Dispos.* 45 (10) (2017) 1060–1067.
- [28] K. Itagaki, G.T. Carver, R.M. Philpot, Expression and characterization of a modified flavin-containing monooxygenase 4 from humans, *J. Biol. Chem.* 27 (33) (1996) 20102–20107.
- [29] E.P. Treacy, B.R. Akerman, L.M. Chow, R. Youil, C. Bibeau, J. Lin, et al., Mutations of the flavin-containing monooxygenase gene (FMO3) cause trimethylaminuria, a defect in detoxication, *Hum. Mol. Genet.* 7 (5) (1998) 839–845.
- [30] P.T.T. Nguyen, M.M. Parvez, M.J. Kim, S.E. Yoo, S. Ahn, J.L. Ghim, et al., Physiologically based pharmacokinetic modeling approach to predict drug–drug interactions with ethionamide involving impact of genetic polymorphism on FMO3, *J. Clin. Pharmacol.* 59 (6) (2019) 880–889.
- [31] S. Castrignano, G. Gilardi, S.J. Sadeghi, Human flavin-containing monooxygenase 3 on graphene oxide for drug metabolism screening, *Anal. Chem.* 87 (5) (2015) 2974–2980.
- [32] H. Gaweska, P.F. Fitzpatrick, Structures and mechanism of the monoamine oxidase family, *Biomol. Concepts* 2 (5) (2011) 365–377.
- [33] K. Yagyesh, S.N. Fatima, K. Kapil, Synthesis and structure activity relationship of OPEN thiazolyl hydrazones as monoamine oxidase inhibitors: an overview, *Curr. Trends Med. Chem.* 1 (1) (2018) 1003.
- [34] M.J. Rodríguez, J. Saura, E.E. Billett, C.C. Finch, N. Mahy, Cellular localization of monoamine oxidase A and B in human tissues outside of the central nervous system, *Cell Tissue Res.* 304 (2011) 215–220.
- [35] M.S. Benedetti, R. Whomsley, E. Baltas, Involvement of enzymes other than CYPs in the oxidative metabolism of xenobiotics, *Expert Opin. Drug Metab. Toxicol.* 2 (6) (2006) 895–921.
- [36] L. Wagmann, S.D. Brandt, P.V. Kavanagh, H.H. Maurer, M.R. Meyer, *In vitro* monoamine oxidase inhibition potential of alpha-methyltryptamine analog new psychoactive substances for assessing possible toxic risks, *Toxicol. Lett.* 272 (2017) 84–93.
- [37] S.N. Parikh, S.R. Hanscom, P.V. Gagne, C.L. Crespi, C.J. Patten, A fluorescent based, high-throughput assay for detecting inhibitors of human monoamine oxidase A and B, *Drug Metab. Rev.* 34 (2002) 164.
- [38] R.S. Foti, D.K. Dalvie, Cytochrome P450 and non-cytochrome P450 oxidative metabolism: contributions to the pharmacokinetics, safety, and efficacy of xenobiotics, *Drug Metab. Dispos.* 44 (8) (2016) 1229–1245.
- [39] M. Cristiano, C. Catarina, S.L. Leimkühler, G. Enrico, T. Mineko, S.-S. Teresa, et al., Critical overview on the structure and metabolism of human aldehyde oxidase and its role in pharmacokinetics, *Coord. Chem. Rev.* 368 (2018) 35–59.
- [40] J.M. Hutzler, R.S. Obach, D. Dalvie, M.A. Zientek, Strategies for a comprehensive understanding of metabolism by aldehyde oxidase, *Expert Opin. Drug Metab. Toxicol.* 9 (2) (2013) 153–168.
- [41] R.S. Obach, P. Huynh, M.C. Allen, C. Beedham, Human liver aldehyde oxidase: inhibition by 239 drugs, *J. Clin. Pharmacol.* 44 (2004) 7–19.
- [42] R. Nirogi, V. Kandikere, R.C. Palacharla, G. Bhyrapuneni, V.B. Kanamarlapudi, R.K. Ponnamaneni, et al., Identification of a suitable and selective inhibitor towards aldehyde oxidase catalyzed reactions, *Xenobiotica* 44 (3) (2014) 197–204.

- [43] X. Yang, N. Johnson, L. Di, Evaluation of cytochrome P450 selectivity for hydralazine as an aldehyde oxidase inhibitor for reaction phenotyping, *J. Pharm. Sci.* 108 (4) (2019) 1627–1630.
- [44] O. Takuo, F. Tatsuki, M. Kenji, K. Keigo, P.J. Jeffrey, N. Miki, Substrate selectivity of human aldehyde oxidase 1 in reduction of nitroaromatic drugs, *Arch. Biochem. Biophys.* 659 (2018) 85–92.
- [45] M. Zientek, Y. Jiang, K. Youdin, R.S. Obach, In vitro-in vivo correlation for intrinsic clearance for drugs metabolized by human aldehyde oxidase, *Drug Metab. Dispos.* 38 (8) (2010) 1322–1327.
- [46] R.M. Vitalea, L. Antenuccib, M. Gavagnina, G. Raimob, P. Amodeoa, Structure–activity relationships of fraxamoside as an unusual xanthine oxidase inhibitor, *J. Enzyme Inhib. Med. Chem.* 32 (1) (2017) 345–354.
- [47] M.G. Battelli, L. Polito, M. Bortolotti, A. Bolognesi, Xanthine oxidoreductase-derived reactive species: physiological and pathological effects, *Oxidative Med. Cell. Longev.* (2016) 3527579. <https://doi.org/10.1155/2016/3527579>.
- [48] J. Barr, K. Choughule, S. Nepal, T. Wong, A.S. Chaudhry, C.A. Joswig-Jones, et al., Why do most human liver cytosol preparations lack xanthine oxidase activity? *Drug Metab. Dispos.* 42 (4) (2014) 695–699.
- [49] H. Shintani, Determination of xanthine oxidase. *Pharm. Anal. Acta* (2013) S7, <https://doi.org/10.4172/2153-2435.S7-004>.
- [50] H.M. Schmidt, E.E. Kelley, A.C. Straub, The impact of xanthine oxidase (XO) on hemolytic diseases, *Redox Biol.* 21 (2019) 101072, <https://doi.org/10.1016/j.redox.2018.101072>.
- [51] N. Cantu-Medellin, E.E. Kelley, Xanthine oxidoreductase-catalyzed reactive species generation: a process in critical need of reevaluation, *Redox Biol.* 1 (1) (2013) 353–358.
- [52] R.S. Holmes, M.W. Wright, S.J. Laulederkind, L.A. Cox, M. Hosokawa, T. Imai, et al., Recommended nomenclature for five mammalian carboxylesterase gene families: human, mouse, and rat genes and proteins, *Mamm. Genome* 21 (2010) 427–441.
- [53] J. Wang, E.T. Williams, J. Bourgea, Y.N. Wong, C.J. Patten, Characterization of recombinant human carboxylesterases: fluorescein diacetate as a probe substrate for human carboxylesterase 2, *Drug Metab. Dispos.* 39 (2011) 1329–1333.
- [54] S.C. Laizure, V. Herring, Z. Hu, K. Witbrodt, R.B. Parker, The role of human carboxylesterases in drug metabolism: have we overlooked their importance? *Pharmacotherapy* 33 (2) (2013) 210–222.
- [55] K.-I. Umehara, M. Zollinger, E. Kigundu, M. Witschi, C. Juif, F. Huth, et al., Esterase phenotyping in human liver *in vitro*: specificity of carboxylesterase inhibitors, *Xenobiotica* 46 (10) (2016) 862–867.
- [56] J.A. Rhoades, Y.K. Peterson, H.J. Zhu, D.I. Appel, C.A. Peloquin, J.S. Markowitz, Prediction and *in vitro* evaluation of selected protease inhibitor antiviral drugs as inhibitors of carboxylesterase 1: a potential source of drug–drug interactions, *Pharm. Res.* 29 (4) (2012) 972–982.
- [57] T.M. Penning, M.E. Burczynski, J.M. Jez, C.F. Hung, H.K. Lin, H. Ma, et al., Human 3 $\alpha$ -hydroxysteroid dehydrogenase isoforms (AKR1C1–AKR1C4) of the aldo-keto reductase superfamily: functional plasticity and tissue distribution reveals roles in the inactivation and formation of male and female sex hormones, *Biochem. J.* 351 (Pt 1) (2000) 67–77.
- [58] T.M. Penning, J.M. Jez, Enzyme redesign, *Chem. Rev.* 101 (10) (2001) 3027–3046.
- [59] T. O'Connor, L.S. Ireland, D.J. Harrison, J.D. Hayes, Major differences exist in the function and tissue-specific expression of human aflatoxin B1 aldehyde reductase and the principal human aldo-keto reductase AKR1 family members, *Biochem. J.* 343 (1999) 487–504.
- [60] T.L. Rizner, H.K. Lin, D.M. Peehl, S. Steckelbroeck, D.R. Bauman, T.M. Penning, Human type 3 3 $\alpha$ -hydroxysteroid dehydrogenase (aldo-keto reductase 1C2) and androgen metabolism in prostate cells, *Endocrinology* 144 (7) (2003) 2922–2932.
- [61] A. Ghosal, Y. Yuan, W. Tong, A.D. Su, C. Gu, S.K. Chowdhury, et al., Characterization of human liver enzymes involved in the biotransformation of boceprevir, a hepatitis C virus protease inhibitor, *Drug Metab. Dispos.* 39 (2011) 510–521.
- [62] M.J. Rosemond, L. St John-Williams, T. Yamaguchi, T. Fujishita, J.S. Walsh, Enzymology of a carbonyl reduction clearance pathway for the HIV integrase inhibitor, S-1360: role of human liver cytosolic aldo-keto reductases, *Chem. Biol. Interact.* 147 (2004) 129–139.
- [63] V. Luu-The, I. Dufort, G. Pelletier, F. Labrie, Type 5 17 $\beta$ -hydroxysteroid dehydrogenase: its role in the formation of androgens in women, *Mol. Cell. Endocrinol.* 171 (1–2) (2001) 77–82.
- [64] O.A. Barski, S.M. Tipparaju, A. Bhatnagar, The aldo-keto reductase superfamily and its role in drug metabolism and detoxification, *Drug Metab. Rev.* 40 (4) (2008) 553–624.

- [65] T.M. Penning, The aldo-keto reductases (AKRs): overview, *Chem. Biol. Interact.* 234 (2015) 236–246.
- [66] D. Greene, The pathogenesis and prevention of diabetic neuropathy and nephropathy, *Metabolism* 37 (1988) 25–29.
- [67] D. Stribling, F.M. Armstrong, M. Hardman, C.M. Perkins, J.C. Smith, Aldose reductase in the etiology of diabetic complications: 4. Retinopathy, *J. Diabet. Complicat.* 4 (1990) 102–107.
- [68] I. Bekhor, S. Shi, D. Carper, C. Nishimura, N.J. Unakar, Relative abundance of aldose reductase mRNA in rat lens undergoing development of osmotic cataracts, *Curr. Eye Res.* 8 (1989) 1299–1308.
- [69] H. Ohara, Y. Miyabe, Y. Deyashiki, K. Matsuura, A. Hara, Reduction of drug ketones by dihydrodiol dehydrogenases, carbonyl reductase and aldehyde reductase of human liver, *Biochem. Pharmacol.* 50 (1995) 221–227.
- [70] K. Matsuura, H. Shiraishi, A. Hara, K. Sato, Y. Deyashiki, M. Ninomiya, et al., Identification of a principal mRNA species for human 3 alpha-hydroxysteroid dehydrogenase isoform (AKR1C3) that exhibits high prostaglandin D-2 11-ketoreductase activity, *J. Biochem.* 124 (1998) 940–946.
- [71] M. Karlgren, I. Simoff, M. Keiser, S. Oswald, P. Artursson, CRISPR-Cas9—a new addition to the drug metabolism and disposition tool box, *Drug Metab. Dispos.* 46 (2018) 1776–1786.
- [72] X. Wang, Y. Tang, J. Lu, Y. Shao, X. Qin, Y. Li, et al., Characterization of novel cytochrome P450 2E1 knockout rat model generated by CRISPR/Cas9, *Biochem. Pharmacol.* 105 (2016) 80–90.
- [73] K. Yoshimi, Y. Kunihiro, T. Kaneko, H. Nagahora, B. Voigt, T. Mashimo, ssODN-mediated knock-in with CRISPR-Cas for large genomic regions in zygotes, *Nat. Commun.* 7 (2016) 10431, <https://doi.org/10.1038/ncomms10431>.
- [74] C.R. Dorr, R.P. Rimmel, A. Muthusamy, J. Fisher, B.S. Moriarity, K. Yasuda, et al., CRISPR/Cas9 genetic modification of CYP3A5\*3 in HuH-7 human hepatocyte cell line leads to cell lines with increased midazolam and tacrolimus metabolism, *Drug Metab. Dispos.* 45 (8) (2017) 957–965.

# In vitro characterization and in vitro to in vivo predictions of drug-drug interactions

*Nina Isoherranen<sup>a</sup>, Robert S. Foti<sup>b</sup>*

<sup>a</sup>Department of Pharmaceutics, University of Washington, Seattle, WA, United States

<sup>b</sup>Pharmacokinetics, Pharmacodynamics and Drug Metabolism, Merck Research Laboratories, Boston, MA, United States

## 1 Introduction

It has been estimated that clinically significant, potentially serious drug-drug interactions (DDIs) occur in approximately 3%–5% of patients taking multiple drugs and 26% of patients with clinically relevant DDIs require dose adjustment [1, 2]. According to the US Food and Drug Administration (FDA) “unanticipated, unrecognized or mismanaged DDIs are an important cause of morbidity and mortality associated with prescription drug use” [3]. Drug interactions become more common as patients take more drugs simultaneously. In geriatric patients, who take 4–7 concomitant medications on average, inappropriate drug combinations can lead to DDIs and consequently adverse events are common (18%–40% of elderly), with adverse drug reactions being responsible for 6.6%–41.3% of hospital admissions in this group [4, 5]. As polypharmacy becomes more common in clinical practice, a good mechanistic understanding of the potential drug-drug interactions between prescription drugs, over the counter medications, and natural products becomes increasingly important, as it is practically impossible to study and characterize every possible combination of treatments in patients or even through in vitro studies. The ability to leverage mechanistic information collected from in vitro studies and from clinical DDI assessments is the cornerstone of designing appropriate dosing strategies in patients taking multiple medications. Ultimately, the goal of any DDI assessment is to improve the safety and efficacy of the medications used. This is accomplished by determining whether the drug of interest alters the

pharmacokinetics of other drugs, and if so by what magnitude, as well as by establishing how other drugs alter the pharmacokinetics of the drug of interest [3].

The prediction and assessment of DDIs for a drug that is considered as a potential victim of a DDI starts with the characterization of its drug metabolism pathways and their quantitative importance to the overall clearance of the drug [6, 7]. In addition, the risk that the drug of interest will alter the expression or activity of drug metabolizing enzymes and/or drug transporters must be evaluated. As such, the identification of the enzymes involved in the metabolism of a new compound (reaction phenotyping), the characterization of its metabolic stability and primary biotransformation pathways, and the determination of whether the new compound inhibits or induces drug metabolizing enzymes are all major facets of the drug discovery and development continuum.

In broad terms, drug metabolizing enzymes generally convert lipophilic therapeutic agents into more water-soluble metabolites, which can be readily excreted from the body [8]. While most metabolic processes are considered to be part of a physiological detoxification process, examples of metabolic bioactivation or the formation of toxic metabolites are readily available [9–12], and the need to assess potential metabolite toxicity during drug development has been incorporated in guidance documents by the FDA and the European Medicines Agency (EMA). It has also been recognized for decades that some metabolites contribute significantly to pharmacological activity [13, 14] and more recently the potential role of circulating metabolites in inhibitory drug-drug interactions has also been highlighted [15–17]. Due to these specific roles of metabolites, DDI assessment should generally consider both drug metabolites and the parent drug itself [17].

The liver is generally considered to be the primary organ that contributes to drug metabolism, but many of the drug metabolizing enzymes are expressed in other tissues throughout the body as well [18–22]. The DDI predictions considered here focus on the inhibition of metabolic enzymes in the intestinal mucosa and in the liver as these are the major sites of drug metabolism, but the reader should be aware that DDIs can be a result of inhibition of metabolic enzymes or drug transporters in other organs and tissues as well. For example, in addition to hepatic and intestinal cytochrome P450 (CYP) expression, CYPs are also expressed in the lung, kidney, heart, nasal mucosa, brain, and testes. Similarly, UDP-glucuronosyltransferases (UGTs) are well known to be expressed in plethora of other tissues in the body in addition to the liver and intestine. The DDI predictions described here are predominantly focused on CYP-mediated DDIs as CYP inhibition accounts for the majority of clinically important drug interactions. Clinically significant inhibitory interactions involving glucuronidation are rare due to the substrate overlap between different isozymes and the high  $K_i$  values of inhibitors [23]. Still, the concepts and principles described in the following sections apply to any enzyme system that is significant in the clearance of an object drug. Tables 1 and 2 list the common phase I (oxidation, reduction, and hydrolysis) and phase II (conjugation) enzymes involved in drug clearance, their necessary cofactors, and their known marker substrates and inhibitors.

Understanding the clearance pathways and DDI potential of a given drug often relies on characterization of the in vitro clearance pathways and enzyme inhibition/induction using in vitro systems. The in vitro system used for DDI predictions depends on considerations of required assay throughput, scientific goals of the work, and the general understanding of the applicability of the system to in vitro to in vivo extrapolations (IVIVE). Commonly used

**TABLE 1** Cofactors, substrates, inhibitors and primary tissue locations for cytochrome P450 and UDP-glucuronosyltransferase drug metabolizing enzymes.

Enzyme	Cofactor	Substrate	Inhibitor	Tissue location
CYP1A2	NADPH	Phenacetin, Caffeine, Tacrine, Theophylline	$\alpha$ -naphthoflavone, Fluvoxamine, Furafylline <sup>d</sup>	Liver
CYP2A6		Coumarin, Nicotine, Cotinine, Isoglycycomarin		Liver, lung
CYP2B6		Bupropion, Efavirenz	Clotrimazole, Ticlopidine	Liver, lung
CYP2C8		Montelukast, Paclitaxel, Amodiaquine	Quercetin, Montelukast, Trimethoprim, Gemfibrozil Glucuronide <sup>d</sup>	Liver
CYP2C9		(S)-Warfarin, Diclofenac, Tolbutamide	Sulfaphenazole, Fluconazole, Fluvoxamine, Tienilic Acid <sup>d</sup>	Liver
CYP2C19		(S)-Mephenytoin, ( $\pm$ )-Omeprazole	(+)-N-3-benzylrivanol, Omeprazole, Ticlopidine	Liver
CYP2D6		Dextromethorphan, ( $\pm$ )-Bufuralol, Debrisoquine	Quinidine, Paroxetine <sup>d</sup>	Liver
CYP2E1		Chlorzoxazone, Aniline	Diethyldithiocarbamate	Liver, lung
CYP2J2		Amiodarone, Astemizole, Arachidonic Acid, Terfenadine, Ebastine,	Danazol, Ketoconazole, LKY-047	Lung
CYP3A4/5		Midazolam, Triazolam, Testosterone, Nifedipine, Terfenadine	Itraconazole, Ketoconazole, Verapamil, Mibefradil <sup>d</sup> , Mifepristone <sup>d</sup> , Troleandomycin <sup>d</sup>	Liver, small intestine (3A4), lung (3A5)
UGT1A1	UDPGA	Bilirubin, estradiol, ethynylestradiol	Atazanavir, Indinavir, Erlotinib, Ketoconazole, Flavones	Liver, intestine
UGT1A3		F <sub>6</sub> -1 $\alpha$ ,23S,25-trihydroxyvitamin-D <sub>3</sub> , Lithocholic acid, Fulvestrant, Cyproheptadine, buprenorphine	Buprenorphine, Amitriptyline, Temazepam	Liver
UGT1A4		Trifluoperazine, Imipramine	Hecogenin, Lamotrigine	Liver, stomach
UGT1A6		Serotonin	Bisphenol A, Troglitazone	Liver, brain
UGT1A7		Benzo[ $\alpha$ ]pyrene metabolites	Phenylbutazone, Quinidine, Magnolol	Esophagus, stomach
UGT1A8		Benzo[ $\alpha$ ]pyrene metabolites, Dihydrotestosterone diglucuronide	Emodin	Esophagus, intestine

*Continued*



**TABLE 1** Cofactors, substrates, inhibitors and primary tissue locations for cytochrome P450 and UDP-glucuronosyltransferase drug metabolizing enzymes—cont'd

Enzyme	Cofactor	Substrate	Inhibitor	Tissue location
UGT1A9		Propofol, Entacapone	Niflumic Acid, Diflunisal, Ketoconazole	Kidney, liver
UGT1A10		Dopamine	Tacrolimus	Kidney, intestine, Lung
UGT2B4		Hyodeoxycholic Acid	Diclofenac, Laropiprant	Liver
UGT2B7		Zidovudine, Morphine, Codeine R-Oxazepam	Diclofenac, Flurbiprofen, Mefanemic Acid, Flunitrazepam	Liver, intestine, Kidney
UGT2B10		Nicotine, Cotinine	S-Nicotine	Liver, prostate
UGT2B15		(S)-Oxazepam, Testosterone	Valproic Acid, Diclofenac	Liver, prostate
UGT2B17		Dihydrotestosterone	Diclofenac, Ibuprofen	Liver, prostate

<sup>a</sup> Mechanism-based inhibitors.

**TABLE 2** Cofactors, substrates, inhibitors and primary tissue locations for additional drug metabolizing enzymes.

Enzyme	Cofactor	Examples of substrates	Examples of inhibitors	Tissue location
Flavin monooxygenase (FMO1, FMO3, FMO5)	NADPH	Benzylamine, Clozapine, Imipramine, Tamoxifen, Nicotine, Voriconazole, Sulindac sulfide	Methimazole	Kidney, intestine, fetal liver (FMO1); liver, lung, kidney (FMO3); liver (FMO5)
Aldehyde oxidase	Molybdenum pyanopterin	Allopurinol, Carbazeran, Famciclovir, Vanillin, Phthalazine	Hydralazine, Menadione, Raloxifene, Chlorpromazine, Isovanillin	Liver, lung, kidney, small intestine
Xanthine oxidase	Molybdenum pyanopterin	1-Methylxanthine, allopurinol	FYX-051, Febuxostat	Liver, heart, lung, adipose, mammary gland
Monoamine oxidase (MAO-A, MAO-B)	FAD	5-Hydroxytryptamine and Epinephrine (MAO-A); Benzylamine and $\beta$ -phenylethylamine (MAO-B) Sertraline and clomipramine (both)	Moclobemide, Clorgyline (MAO-A) Deprenyl (MAO-B)	Liver, placenta, brain

**TABLE 2** Cofactors, substrates, inhibitors and primary tissue locations for additional drug metabolizing enzymes—cont'd

Enzyme	Cofactor	Examples of substrates	Examples of inhibitors	Tissue location
Carboxylesterase	None	Cocaine, Methylphenidate, Meperidine	Benzil, Trifluoromethyl ketones	Liver
Epoxide hydrolase (soluble and microsomal)	None	Carbamazepine and styrene oxide (mEH); Epoxyeicosatrienoic acids (sEH)	1,1,1-Trichloropropylene oxide (mEH), Valproic Acid	Liver
Aldo-ketoreductase (multiple isoforms)	NADPH	Haloperidol, Ketotifin, Oracin	NSAIDs	Liver, kidney, brain, blood
Sulfotransferase (multiple isoforms)	3'-Phosphoadenosine-5'-phosphosulfate (PAPS)	Acetaminophen and Troglitazone (1A1); Salbutamol and Dobutamine (1A3); Ethynylestradiol (1E1); Budenoside (2A1)	Pentachlorophenol	Liver, intestine, platelets, brain, kidney, endometrium, skin, prostate, placenta
Glutathione transferase (multiple isoforms)	Glutathione	1-Chloro-2,4-dinitrobenzene, Chlorambacil, Melphalan	Ethacrynic acid, piroprost, indomethacin	Liver, kidney, lung, brain, skeletal muscle, heart, small intestine, spleen
N-Acetyltransferase (NAT1, NAT2)	Acetyl Coenzyme A	<i>p</i> -Aminobenzoic acid and <i>p</i> -aminophenol (NAT1); Dapsone, Sulfmethazine, Procainamide (NAT2)	Acetaminophen, 5-Iodosalicylic acid	Liver, esophagus, small intestine, stomach, colon, bladder, lung
Acyl-CoA synthetase	ATP, Coenzyme A	Ibuprofen, Flunoxapfen, Clofibrate	Triacin C, Rosiglitazone	Liver, heart, adipose tissue
Methyltransferase (structure-dependent isoforms)	S-Adenosyl methionine	6-Mercaptopurine, 6-Thioguanine, Azathioprine, Dopamine, Captopril	Entacapone, tolcapone	Liver (adult and fetal), lung, kidney, small intestine

*in vitro* systems include whole cell preparations such as hepatocytes or mammalian cell lines, subcellular fractions such as microsomes, S9 fractions or cytosol, and recombinant enzymes expressed in *Escherichia coli* or insect cells [24–28]. Of these systems, human liver microsomes (endoplasmic reticulum vesicles that are collected by differential centrifugation [29–34]) are the most popular *in vitro* systems to assess the metabolism of a new drug candidate [35]. Still, recombinant enzymes provide some unique advantages in reaction phenotyping and

identification of specific metabolites formed by a given enzyme. For example, in a situation that multiple enzymes form a given metabolite, recombinant enzyme systems allow unequivocal identification of the metabolites formed by a given enzyme and the specific enzymes that form a given metabolite. The most commonly used recombinant enzyme system is the baculovirus-infected insect cells that are usually coinfecting with virus driving expression of the CYP of interest, cytochrome P450 reductase and cytochrome  $b_5$ . For drug metabolism studies, microsomes are usually prepared from these infected insect cells resulting in the commonly known Baculosomes and Supersomes. In addition, recombinant enzymes expressed and purified from yeast or *E. coli* [24, 36] are sometimes used for characterizing DDI potential and the specific interactions between ligands and CYP enzymes.

Complex systems such as isolated perfused livers, liver slices, and hepatocytes are generally considered to be more physiologically relevant when compared to other in vitro systems, but each of these systems also presents unique challenges to IVIVE [37]. Of the three, hepatocytes are the most commonly used system owing to recent advancements in culture, plating, and cryopreservation techniques. Hepatocytes are almost exclusively used for the assessment of induction of drug metabolizing enzymes by compounds of interest [38–41]. An evolving area of research in the use of cultured cell systems for drug metabolism purposes involves the use of human embryonic stem cells and induced pluripotent stem cell-derived hepatocytes [42, 43]. Stem cell systems have the potential to provide a virtually inexhaustible supply of hepatocytes with very limited variability. However, a number of issues such as long-term viability in culture, cellular uniformity, and the fetal-like phenotype of the derived hepatocytes, as well as ethical considerations still need to be addressed.

## 2 In vitro assessment of metabolism-based drug interaction potential

The successful prediction of clinical DDIs and DDI risk from in vitro data is one of the cornerstones of the drug development process. DDI assessments commonly occur throughout the preclinical lifetime of a drug candidate, beginning with high-throughput assays in the screening stage and followed by more rigorous experimental designs later as a drug progresses to clinical trials [44]. Good predictions of in vivo drug interactions rely on the thorough characterization of both the object drug (substrate of the inhibited or induced enzyme; victim drug) and the inhibitor/inducer (precipitant or perpetrator drug). Predicting in vivo DDIs from in vitro data is based on (1) accurate identification of the enzymes that contribute to the clearance of the substrate, (2) quantitative prediction of the fractions of total body clearance mediated by a specific enzyme(s), (3) characterization of the precipitant in terms of its inhibition potency ( $K_i$ ) or induction potential ( $EC_{50}$ ), selectivity, and mechanism of inhibition, and (4) characterization of inhibitor/inducer disposition including circulating concentrations and fluctuation of concentrations over a dosing interval. A final critical consideration regarding predictions of DDIs is to decide the target outcome of the predictions as this will affect the methods chosen. In some cases, predicting the maximal risk of any occurrence of drug interactions may be desired (risk assessment) whereas in other situations accurate prediction of substrate concentrations in the presence of an inhibitor or the magnitude of dosage change in the presence of an inhibitor needs to be predicted. Due to these different desired outcomes

either static or dynamic methods may be used for drug interaction predictions. Dynamic methods include physiologically based models of object and precipitant time courses and are described in other chapters of this book. The following discussion is focused on use of static predictions to estimate and predict drug-drug interaction risk during the development of a candidate compound.

## 2.1 Characterization of the substrate

The same inhibitor, even when administered at the same dose and for the same duration of time can cause very different magnitudes of interactions with different substrates in vivo (Table 3). The differences between the magnitude of the interaction and susceptibility of a substrate to DDIs depend primarily on the fraction of the clearances (fraction metabolized,  $f_m$ ) of the substrate by the inhibited enzyme(s) and on the fraction of the oral dose metabolized by intestinal enzymes. Therefore, careful characterization of the disposition of the object/victim drug is critically important for accurate DDI predictions. Generally, the smaller the number of enzymes that are involved in the clearance of a drug, the greater the drug's susceptibility to an interaction [55]. It is important to note that a drug that is metabolized by only a single CYP may still have a significant clearance pathway via the kidney or via biliary transport, which makes it less susceptible to inhibition DDIs in vivo. Examples of such drugs include methadone and theophylline that generally have relatively small interactions in vivo despite the small number of CYP enzymes that contribute to their clearance [56–59].

Just because an enzyme is capable of metabolizing a substrate to a particular product does not mean that the reaction is quantitatively important in substrate clearance. Other enzymes may be more efficient in making that specific metabolite, or in forming other metabolites. For example, while CYP3A and CYP2C9 are capable of metabolizing montelukast in vitro at higher substrate concentrations, the in vivo clearance of montelukast at clinically relevant concentrations has been shown to be primarily mediated by CYP2C8 [60–62]. On the other

TABLE 3 Effect of Itraconazole on various CYP3A4 substrates.

CYP3A substrate (oral dose)	Mean AUC <sub>i</sub> /AUC in vivo	$f_m$ by 3A4	F	Reference
Lovastatin (40 mg)	21.6	0.90	<0.05	[45]
Simvastatin (40 mg)	18	0.99	<0.05	[46]
Triazolam (0.25 mg)	10	0.98	0.44	[47]
Midazolam (7.5 mg)	6.4	0.99	0.36	[48]
Felodipine (5 mg)	6.3	0.99	0.20	[49]
Atorvastatin (40 mg)	3.6	0.99	0.14	[50]
Alprazolam (0.8 mg)	2.7	0.80	0.90	[51]
Quinidine (100 mg)	2.4	0.76	0.73	[52]
Cerivastatin (0.3 mg)	1.2	0.37	0.60	[53]

The  $f_m$  were obtained from Galetin et al. [54].

hand, in some cases a very inefficient metabolic pathway in vitro can be important in vivo as in the case of the CYP3A4-catalyzed clearance of carbamazepine (hepatic extraction ratio of 0.05), where the in vitro formation of 10,11-carbamazepine epoxide has been reported to have a  $K_m$  of 442  $\mu\text{M}$  and  $V_{\text{max}}$  of 1730 pmol/min/nmol in recombinantly expressed CYP3A4, but which translates into significant CYP3A drug interactions in humans [63]. The relative importance of a given enzyme or a given metabolic pathway in the overall clearance of a substrate depends of the clearance via that pathway in comparison to all other in vivo clearance pathways of the drug and is best evaluated by comparing the intrinsic clearance values for individual enzymes/metabolic pathways and assessing these as scaled up to hepatic clearance in comparison to predicted or observed renal clearance. The characterization of the substrate clearance pathways gets progressively more complex as more enzymes and metabolic pathways are involved in the clearance of the compound. In general, in vitro experiments are useful in predicting the in vivo contributions of individual enzymes and metabolites to drug clearance but alone are not sufficient to determine these values due to the potential importance of metabolic clearances in other organs, secretory or uptake clearances by transporters in liver, kidney, and gut and renal elimination. In vitro experiments are critical in determining (1) whether a single enzyme catalyzes the formation of the dominant metabolite, (2) the identity of the enzymes responsible for specific metabolite formation, and (3) whether a compound is an inhibitor or inducer of metabolic enzymes. When coupled with in vivo data, they can be used to predict in vivo relevance of specific enzyme in the elimination of a substrate.

The prediction of a particular DDI risk is largely dependent on a good quantitative understanding of the clearance pathways of the substrate (object or victim) drug, and as such on the accurate characterization of kinetic constants ( $V_{\text{max}}$  and  $K_m$ ) that establish whether a chemical entity is a good or a poor substrate of a particular enzyme. Of these kinetic constants,  $V_{\text{max}}$  is the maximum product formation velocity defined by the product of the catalytic rate constant  $k_{\text{cat}}$  and total enzyme concentration  $[E]$  (i.e.,  $V_{\text{max}} = [E] \cdot k_{\text{cat}}$ ).  $K_m$  is the concentration of substrate at which half of the total enzyme is bound as the  $[ES]$  complex and at this concentration the product formation velocity is half of  $V_{\text{max}}$ . The key for the identification of the important clearance pathways of a drug is the calculation of the intrinsic clearance ( $CL_{\text{int}}$ ) for the reaction of interest. The  $CL_{\text{int}}$  is defined as the ratio of  $V_{\text{max}}$  and  $K_m$  but it can also be calculated as the simple ratio of product formation velocity and substrate concentration ( $CL = v/[S]$ ) when substrate concentration is much below  $K_m$ . The comparison of kinetic constants between enzymes and metabolites formed provides the foundation for the understanding of the clearance pathways and potential concentration dependence of in vivo clearance. In addition, accurate kinetic constants are also a necessity for the development of predictive in silico approaches such as PBPK models for drug clearance and DDIs.

In the context of DDI predictions, the most important characteristic to define the sensitivity of a drug to DDIs is the fraction metabolized ( $f_m$ ) by a given enzyme. It is important to note that  $f_m$  can be used to generally describe the fraction of the overall clearance of the drug by metabolism in comparison to renal clearance. In such cases, the  $f_m$  is generally of interest in the context of considering how sensitive the clearance of the drug of interest is to organ impairment like renal or hepatic disease. The term "fraction metabolized" is also often used to describe the fraction of the overall clearance of a drug that results in the formation of a given metabolite regardless of the identity of the enzymes forming the metabolite. This is of particular interest if the metabolite formed is active or toxic. In such cases, it is often of additional

interest to define the  $f_m$  of a specific metabolite formation by a given enzyme. Finally, the  $f_m$  that is most commonly used in DDI risk assessment is the fraction of total metabolic clearance conducted by a given enzyme or the fraction of overall total body clearance that is accounted for by clearance by a specific enzyme. The use of these different  $f_m$ 's can be illustrated by considering the various analyses of the clearance of ramelteon (Table 4). Since ramelteon is not excreted into urine unchanged and does not appear to be a substrate for efflux transporters, its overall fraction metabolized approaches 1. The in vitro metabolism of ramelteon was characterized in human liver microsomes (HLMs), human intestinal microsomes (HIMs), and recombinant enzymes [64], and the overall metabolic pathways are shown in Fig. 1. First, the overall  $f_m$  to each of the seven metabolites was assessed in HLMs and HIMs via determining the enzyme kinetic parameters of each metabolite formation. These studies suggested that in the human liver the  $f_m$  to metabolites A, E, and F are 33%, 21%, and 31%, respectively, with the other metabolites being <10% of total metabolite formation. Selective CYP inhibitors were then used with pooled HLMs to predict the  $f_m$  by specific enzymes on each metabolite formation. In these experiments, furafylline (a CYP1A2 selective inhibitor) was found to inhibit 93% of metabolite A formation, and 52% and 53% of metabolite E and F formation suggesting that the  $f_m$  for CYP1A2 in metabolite A formation is 93%. In contrast, metabolite C and G formation was entirely inhibited by ketoconazole, suggesting that the  $f_m$  CYP3A4 was close to 100% for these metabolites. Considering the data for the three major individual metabolites (A, E, and F) in HLMs, the overall  $f_m$  by CYP1A2 in ramelteon clearance is predicted to be 0.58 (58%), or if the minor metabolites are considered, somewhat higher. In comparison, the contribution of CYP3A4 to overall ramelteon clearance is predicted to be minimal as the CYP3A4-specific metabolites are overall minor contributors to ramelteon clearance. The specific enzymes contributing to ramelteon clearance were further confirmed using recombinant enzymes that showed a role for CYP1A2, CYP3A4, and CYP2C19 in ramelteon clearance [64].

TABLE 4 Characterization of ramelteon metabolism.

Ramelteon metabolite	CL <sub>int</sub> (μL/min*mg)	% Contribution of the metabolite in HLMs	% Inhibition by selective chemical inhibitors			
			Furafylline (CYP1A2)	N-benzylnirvanol (CYP2C19)	Ketoconazole (CYP3A4)	Fluconazole (CYP3A4, CYP2C19, CYP2C9)
A	36	33	93	5	<5	<5
B	5.3	4.8	38	<5	36	37
C	5.6	5.1	<5	<5	100	89
D	4.9	4.5	78	14	14	17
E	23	21	52	<5	<5	17
F	34	31	53	25	13	33
G	1.8	1.6	<5	42	100	93
H	0.36	0.33	–	–	–	–

The metabolite labeling (A–H) corresponds to Fig. 1. The values were obtained from Obach and Ryder [64].

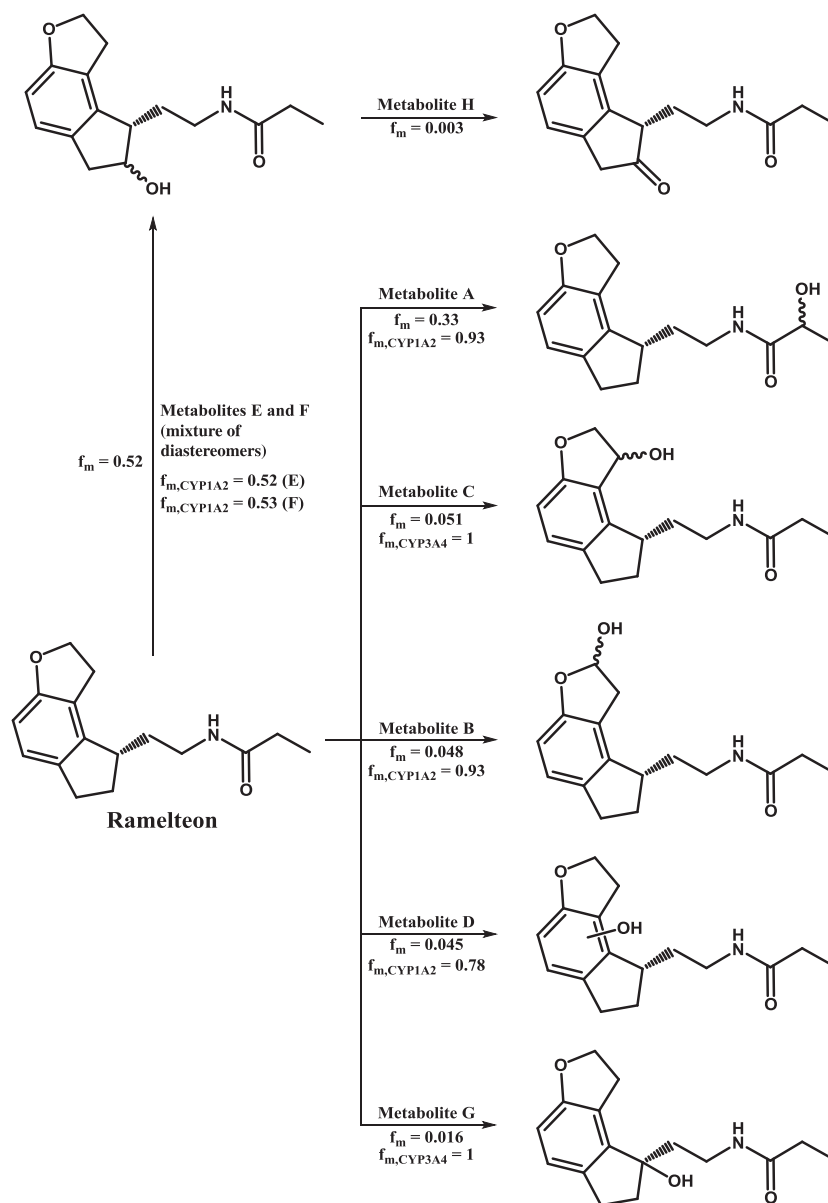


**FIG. 1** Illustration of the concept of fraction metabolized using ramelteon as an example. The percent contribution of each metabolic pathway to the overall metabolism of ramelteon is shown as the  $f_m$ . The percent contribution ( $f_{m,CYP}$ ) of the major P450 isoform for each pathway is also shown. Adapted from R.S. Obach, T.F. Ryder, *Metabolism of ramelteon in human liver microsomes and correlation with the effect of fluvoxamine on ramelteon pharmacokinetics*, *Drug Metab. Dispos.* 38 (8) (2010) 1381–1391.



Of note, while  $CL_{int}$  of ramelteon metabolism to metabolite F was higher by recombinant CYP2C19 than by CYP1A2, the much lower expression level of CYP2C19 in HLMs in comparison to CYP1A2 results in a prediction of relatively major contribution of CYP1A2 on metabolite F formation.

In the case of ramelteon, a simple comparison of intrinsic clearances is appropriate as the  $K_m$  values for all ramelteon metabolites are much above the circulating concentrations of ramelteon. However, this is not always the case and determination of accurate  $K_m$  values is critically important for the characterization and prediction of the  $f_m$ 's by specific enzymes. The determination of  $K_m$  values is important for two reasons: first to confirm that no in vivo elimination pathways are saturated, and second to support selection of appropriate substrate concentrations for in vitro inhibition experiments. If in vivo concentrations are above any one of the  $K_m$  values for individual enzymes, the contribution of that enzyme to substrate clearance is diminished in relation to the other enzymes due to the saturation of the enzyme of interest. Similarly, if relative contributions of individual enzymes are evaluated for substrate clearance, inhibition experiments should be done at clinically relevant (unbound) concentrations to avoid missing a high-affinity enzyme that is saturated at higher concentrations. High-affinity low-capacity enzymes that might not contribute significantly at the concentrations many in vitro experiments are conducted (i.e., common practice of running incubations at 1  $\mu$ M) are easily missed, but such pathways may dominate metabolism in vivo. These concepts can be illustrated by considering the metabolism of all-*trans*-retinoic acid (*atRA*) in human liver. In vitro, *atRA* is metabolized by a number of CYPs including CYP3A4, CYP2C8, and CYP26A1, the endogenous *atRA* hydroxylase (Fig. 2). In recombinant enzyme systems, the  $K_m$  value for *atRA* with CYP26A1 is 9.4 nM [65] while the  $K_m$  values with CYP3A4 and CYP2C8 are 19.4 and 13.4  $\mu$ M, respectively. While CYP26A1 is predicted to be the major enzyme clearing endogenous *atRA* (concentrations <10 nM), simulations based on in vitro  $K_m$  and  $k_{cat}$  values show that due to the saturation of CYP26A1, at concentrations often observed in circulation after administration of *atRA* therapeutically, the  $f_m$  by CYP26A1 is diminished in comparison to CYP3A4 and CYP2C8 (Fig. 2). It is important to note that if in vitro inhibition experiments are conducted with *atRA* concentrations of 1  $\mu$ M, the predicted  $f_m$  by CYP26A1 will be much smaller than that obtained at [S] of 5 nM. Further, the clearance of *atRA* can be used to illustrate the impact of enzyme expression levels to  $f_m$  as shown in Fig. 2. Due to the extensive variability in the expression of CYP26A1 in different livers, the  $f_m$  by CYP3A4 and CYP26A1 varies from nearly 0% to almost 100% between donors.

## 2.2 Characterization of the inhibitor

Evaluation of the likelihood of a drug to cause in vivo DDIs starts with determination of the inhibition potential of the drug toward specific CYPs in vitro. In general, early studies have often included only  $IC_{50}$  determinations or even single concentration inhibition studies, whereas more definitive assessments rely on the estimation of a  $K_i$  value that also allows characterization of the mechanism of inhibition. It should be noted that any substrate of an enzyme will also be a competitive inhibitor of that enzyme and according to Michaelis-Menten kinetics, the  $K_m$  of the substrate will approximate its  $K_i$  (inhibition constant). The implication of this relationship in drug development is that substrates with low  $K_m$  values (in

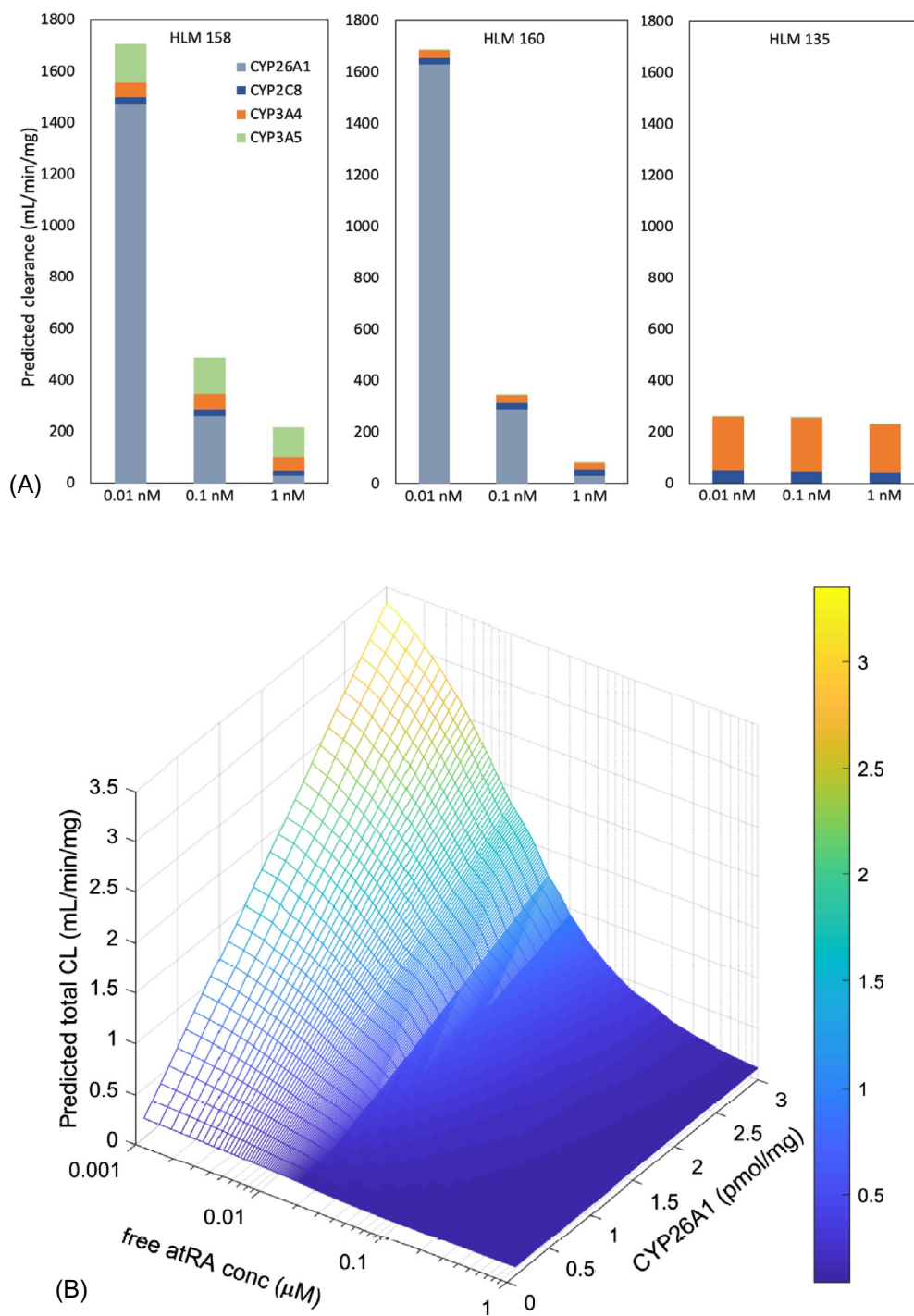


FIG. 2 See legend on opposite page.

comparison to circulating concentrations) are likely to also be inhibitors of other substrates of the same enzyme in vivo. Good examples of this relationship are fluoxetine and itraconazole, which have  $K_m$  values for CYP2D6 and CYP3A4, respectively, that are below their circulating concentrations [66, 67]. Both itraconazole and fluoxetine display nonlinear (saturation) kinetics in vivo and also inhibit these two enzymes strongly in vivo [45, 46, 68–70]. In addition, saturation of specific enzymes in in vitro experiments can have a considerable impact on the evaluation of relative importance of specific enzymatic pathways.

For inhibition assessment, selective probes are usually used with human liver microsomes or recombinant CYP enzymes to screen for inhibitory potency and an  $IC_{50}$  and/or  $K_i$  will be determined. As part of these experiments, one must assure that the new compound is not a time-dependent or irreversible inhibitor of the enzyme of interest. While it is common practice to screen for CYP inhibition using standardized protocols, it is important that the inhibition experiments are designed so that none of the basic assumptions for Michaelis-Menten kinetics are violated and microsomal protein binding and inhibitor depletion are accounted for when accurate kinetic constants are determined for quantitative IVIVE purposes. If the new compound is a tight binding inhibitor, i.e., the inhibition constant approaches the concentration of the inhibited enzyme in the incubation, the ability to quantitatively predict extent of inhibition in vivo becomes inherently more complex (since inhibition is dependent on enzyme concentration). The choice of the probe substrate used for inhibition testing also deserves some consideration. In addition to use of classic probe substrates, high throughput assays using fluorescent substrates have also been explored for inhibition screening [24]. While the utility of fluorescent probes has increased in recent years, multiple examples still exist of the disconnect between in vitro values generated from fluorescent probes and more conventional “drug-like” probes [71, 72]. The selection of probe substrates can also be a factor when choosing between two selective, nonfluorescent probe substrates [73–76]. Quite possibly the most cited example of probe substrate-dependent parameters is CYP3A4, where a large active site containing multiple binding regions can allow for multiple substrates and/or different binding modes within the same active site [54, 77–82]. The probe substrate-dependent data observed with CYP3A4 has also been shown to be an important factor when extrapolating data from in vitro to in vivo [83] and hence the US FDA also recommends testing CYP3A4 inhibition potency against multiple CYP3A substrates. More recent examples of the effects of probe substrates on the drug metabolism parameters of a test compound include the evaluation of montelukast as a probe substrate for CYP2C8 and the effect of CYP2D6 probe substrates on the observed in vitro parameters and in vivo predictions [60–62, 84–86].

There are a number of sources of variability that result in potentially discrepant results in in vitro experiments of CYP inhibition. The choice of enzyme source, relative levels of

---

**FIG. 2—cont'd** Effect of the selection of substrate concentration (as labeled on X axis) and enzyme expression levels between donors on the observed metabolic contributions of individual P450 enzymes. Panel (A) shows the predicted overall *atRA* clearance in three donors (HLM 158, 160, and 135) with the relative contributions by CYP26A1, CYP3A4, CYP3A5, and CYP2C8 shown in different colors as examples. The  $K_m$  and  $k_{cat}$  values for *atRA* are 13.4  $\mu$ M and 4.8 pmol/(min\*pmol P450) with CYP2C8, 19.4  $\mu$ M and 4.0 pmol/(min\*pmol P450) with CYP3A4, and 0.0094  $\mu$ M and 11.3 pmol/(min\*pmol P450) with CYP26A1, respectively, as described by Thatcher et al. [65]. The expression levels of the CYPs are from the reference. Panel (B) shows the impact of substrate concentration (CYP26A1 saturation) and level of CYP26A1 expression on the overall *atRA* clearance. *The authors would like to thank Weize Huang for assistance with Fig. 2B.*

accessory proteins, probe substrate, buffer concentration, and inclusion of divalent cations can all affect the results of drug interaction assays [24, 87–90]. Inhibition assays are most often conducted at substrate concentrations at or below their respective  $K_m$  values and at least one log unit higher than the concentration of the enzyme in question [79]. Probe substrate kinetic parameters and enzyme concentrations should be determined in the same enzyme preparation to be used for the inhibition assay, as significant differences in both  $K_m$  and  $V_{max}$  values as well as enzyme concentrations can be expected across different lots of in vitro reagents. The incubation time of the assay should ensure linear product formation from the probe substrate with respect to both time and protein concentration [91]. Erroneous data can also be generated if one does not account for the percent of inhibitor bound to enzyme as an  $E \cdot I$  complex for those inhibitors with very high affinities [92].

### 2.2.1 Reversible inhibitors

Reversible inhibition occurs generally via three different mechanisms: competitive, noncompetitive, and mixed type but allosteric inhibition should also be considered when in vitro parameters are determined. The overall general inhibition scheme between a substrate and an inhibitor is shown in Fig. 3 to illustrate the continuum from competitive to mixed-type and noncompetitive inhibitors. Theoretically, the inhibition constant ( $K_i$ ), the concentration at which the enzyme activity is decreased by 50%, is a characteristic constant of an enzyme-inhibitor pair. Thus,  $K_i$  should be independent of the substrate that is used in the determination of inhibitor affinity for a given enzyme. In practice, this does not seem to universally apply for CYP-mediated metabolism.

A competitive inhibitor is a substance that combines with free enzyme in a manner that prevents substrate binding (i.e., binding of the inhibitor and the substrate are mutually exclusive events). Using rapid equilibrium or steady-state assumptions, a velocity equation can be derived for the rate of product formation in the presence of a competitive inhibitor as described in Eq. (1):

$$v = \frac{V_{max} * S}{S + K_m * (1 + [I]/K_i)} \quad (1)$$

The term  $[I]/K_i$  represents the fraction of the total enzyme pool bound as the  $[EI]$  complex. Eq. (1) shows that for a competitive inhibitor  $V_{max}$  is unaffected but  $K_m$  has increased by the factor of  $1 + [I]/K_i$ . In other words, a competitive inhibitor only increases the apparent  $K_m$  for the substrate (by displacing the substrate from the active site). It does not influence  $k_{cat}$  and therefore  $V_{max}$  remains unchanged. This can be rationalized as inhibitor does not bind to the  $[ES]$  complex and hence catalysis occurs identically as without inhibitor present. Since some

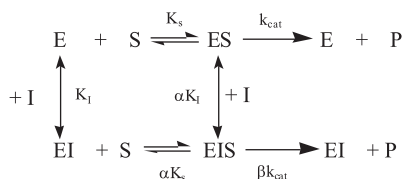


**FIG. 3** General scheme of reversible enzyme inhibition.  $K_s$  is used here instead of  $K_m$  to be specific for the affinity of substrate to the enzyme. For a more detailed description of reversible inhibition kinetics, please see *Simple Inhibition Systems* in Segel [91].

of the enzymes are occupied by the competitive inhibitor, a greater substrate concentration is needed to obtain the same fraction of  $V_{\max}$  or in other words, the same concentration of the productive [ES] complex. Since all the enzyme species are reversibly connected and  $v$  is proportional to [ES], the reaction velocity in the absence of the inhibitor can be reached in the presence of an inhibitor but higher substrate concentrations will be needed to drive the formation of [ES] complex. In the presence of an infinitely high [S], all the enzymes can be driven to form the [ES] complex. Mathematically, it can be shown that for competitive inhibition the intrinsic clearance is reduced by a factor of  $1/(1+[I]/K_i)$ . In the general scheme (Fig. 3), competitive inhibition is the situation where  $\alpha$  is an infinitely high number and  $\beta$  equals 0.

Noncompetitive inhibition is characterized by a ternary, inactive complex [ESI] formed by the simultaneous binding of inhibitor and substrate to the enzyme. The inhibitor can bind either in the active site of the enzyme or at a distal site. A classic noncompetitive inhibitor has no effect on substrate binding and substrate binding has no effect on inhibitor binding, i.e., in the general scheme in Fig. 3  $\alpha$  equals 1 and  $\beta$  equals 0. Therefore, the inhibitor binds to [E] and [ES] and [S] binds to [E] and [EI]. However, there is no catalysis from the resulting [ESI] complex. This means that the inhibitor distorts the enzyme sufficiently to prevent the proper positioning of the catalytic center and thus [ESI] is nonproductive. For noncompetitive inhibition, even infinitely high substrate concentrations cannot drive all of the enzymes to the productive [ES] form since at any inhibitor concentration a portion of the enzyme will remain as the nonproductive [ESI] complex. Consequently, since product formation velocity is dependent on [ES],  $V_{\max}$  decreases.  $K_m$  does not change with noncompetitive inhibitor and the product formation velocity is described by Eq. (2):

$$v = \frac{V_{\max}}{(1 + [I]/K_i)} * \frac{S}{(S + K_m)} \quad (2)$$

The net effect of a noncompetitive inhibitor is to reduce  $V_{\max}$  without having an effect on  $K_m$ . The degree of inhibition depends only on [I] and  $K_i$  and is independent of [S]. The ratio between the inhibited reaction velocity and uninhibited reaction velocity ( $v_i/v_0$ ) is constant at any given substrate concentration.

For a mixed-type inhibitor, a nonproductive ESI complex is formed but binding of inhibitor or substrate is changed in the presence of the alternate ligand. In the general scheme shown in Fig. 3, this refers to a situation where  $\alpha$  is a positive number different from 1 and infinity. This change in binding affinity is described by factor  $\alpha$ . The velocity equation for mixed-type inhibitor is given in the following equation:

$$v = \frac{V_{\max} * S}{S * (1 + [I]/\alpha K_i) + K_m * (1 + [I]/K_i)} \quad (3)$$

A mixed-type inhibitor affects both  $V_{\max}$  and  $K_m$ .

In DDI screening,  $IC_{50}$  values are often collected instead of  $K_i$ 's. This may be mechanistically more appropriate if the substrate displays non-Michaelis-Menten (allosteric) kinetics as the classic  $K_i$  determination assumes a simple Michaelis-Menten-type substrate. Determination of  $IC_{50}$  values may also yield more accurate estimates of inhibition potency as its determination does not require assumption of a specific inhibition mechanism (competitive, noncompetitive, mixed type, etc.). However, it is necessary to consider experimental conditions and interpretation of  $IC_{50}$  values carefully. For a competitive inhibitor, the  $IC_{50}$  value is

dependent on the concentration of substrate according to Eq. (4). This is because [S] competes with I for the occupancy of the enzyme and thus at higher concentrations of [S] more [I] will be needed to have the same fraction of enzyme bound as the [EI] complex. At low concentrations of substrate (relative to  $K_m$ ),  $IC_{50}$  is approximately equal to  $K_i$  as the  $S/K_m$  ratio approaches 0 (Eq. 4):

$$IC_{50} = K_i * \left( 1 + \frac{S}{K_m} \right) \quad (4)$$

For noncompetitive inhibitor, when  $[I]=K_i$ , 50% inhibition is always observed regardless of substrate concentration. Consequently, for noncompetitive inhibitor  $IC_{50}$  is independent of substrate concentration (Eq. 5):

$$IC_{50} = K_i \text{ for all } [S] \quad (5)$$

Eqs. (4) and (5) show that if inhibition experiments are conducted under conditions that  $[S] \ll K_m$ , one can assume that the  $IC_{50}$  value obtained is equal to the  $K_i$  value. In fact such approach has been recommended instead of the common practice of running  $IC_{50}$  values at substrate concentration that is equal to  $K_m$  [93]. The use of  $[S]=K_m$  in  $IC_{50}$  experiments not only causes the relationship between  $IC_{50}$  and  $K_i$  to be dependent on the inhibition mechanism, but also may over- or underestimate inhibition potency when substrate  $K_m$  varies from donor to donor or lot to lot of in vitro reagents.

### 2.2.2 Time-dependent inhibitors

The second aspect of drug interactions often assessed during drug development is the potential for a test compound to act as a time- or mechanism-based inhibitor. Unlike reversible drug interaction assays, which are conducted in a single incubation step, the evaluation of mechanism-based inhibition requires two incubation steps, often referred to as the primary (or preincubation) and secondary incubations, and results in the irreversible inactivation of drug metabolizing enzymes [94]. De novo synthesis is required to regain enzyme activity, meaning that enzyme inactivation can still be an issue even after the inactivator has been cleared from circulation [95]. It is important to note that not all time-dependent inhibitors are mechanism-based inhibitors and, in general, a rigid set of criteria has to be met to classify a compound as a mechanism-based inhibitor [96]. As drug metabolizing enzymes such as the cytochrome P450s do not always conform to the traditional rules of enzymology, more recent criteria state that any substrate that is metabolized to a reactive intermediate by a drug metabolizing enzyme and inactivates the enzyme prior to dissociating from the active site may be classified as a mechanism-based inhibitor [97]. The mechanisms by which a mechanism-based inhibitor may irreversibly inactivate a drug metabolizing enzyme are relatively well understood. Three irreversible mechanisms include covalent modification of the protein, alkylation or arylation of the heme prosthetic group, and heme destruction, often referred to as heme bleaching [98]. A fourth mechanism often attributed to mechanism-based inhibitors is the formation of a metabolite-intermediate complex with the heme iron, though this pathway is generally thought to be quasi-irreversible [97]. Examples of well-characterized mechanism-based inhibitors include mibefradil (heme destruction), 1-aminobenzotriazole (covalent heme adduct), raloxifene (covalent protein adduct) and troleandomycin (metabolite-intermediate



complex) [99–103]. Paroxetine, delavirdine, diltiazem, and verapamil have been shown to cause increases in the AUC of coadministered drugs due to CYP inactivation, while drugs such as mibefradil have been removed from the market due to adverse drug reactions attributed to mechanism-based inactivation [104–107].

The kinetics of mechanism-based inhibition are described by a hyperbolic kinetic model where the rate of inactivation is saturable at high inhibitor concentrations at which all the enzymes are bound with the inhibitor. Eq. (6) describes the pseudo-first-order rate of inactivation ( $k_{\text{obs}}$ ) as a function of the concentration of inhibitor  $[I]$ , the maximum theoretical rate of inactivation ( $k_{\text{inact}}$ ), and the concentration of inhibitor at half the maximum theoretical rate of inactivation ( $K_I$ ).

$$k_{\text{obs}} = \frac{k_{\text{inact}} * [I]}{K_I + [I]} \quad (6)$$

In a primary incubation, a test compound that is being evaluated for its ability to act as a mechanism-based inhibitor is incubated with human liver microsomes (or another appropriate in vitro system) and NADPH such that the test compound can be metabolized to a potential inactivating species. At set intervals, an aliquot is transferred from the primary incubation to a secondary incubation containing cofactor with a probe substrate which is usually at a saturating concentration to minimize competitive inhibition, and the formation of metabolites from the probe substrate is monitored. Discovery screening strategies generally employ either a standard dilution technique as described above or an  $IC_{50}$ -shift approach to assess test compounds for mechanism-based inhibition [108–112]. The latter method assumes that the formation of reactive metabolites in the preincubation step will result in an increase in the inhibition potency (causing a left shift in the  $IC_{50}$  curve or a decrease in the AUC under the  $IC_{50}$  curve; Fig. 4), though a number of confounding experimental factors must be taken into account [113–115]. In later development stages, it is common for compounds that have been identified as mechanism-based inhibitors to be included in more definitive experiments designed to determine the kinetic parameters of mechanism-based inhibition, namely  $K_I$  and  $k_{\text{inact}}$ . It is important to note that these experimentally derived parameters can vary depending on incubation conditions, and that care should be taken to ensure that the linear portion of the inactivation curves are captured, especially with respect to compounds such as mibefradil, which have been shown to have very rapid rates of inactivation [100].

The aforementioned assays rely heavily on two key assumptions, namely, the inactivating compound is not significantly depleted in the primary incubation and limited inactivation occurs in the secondary incubation [109]. To this end, additional methods exist to more accurately estimate the in vitro inactivation parameters for a test compound, and often involve the measurement of both formation of the probe substrate metabolite and the depletion of the inactivator. The use of a progress curve approach has been suggested to be a more mechanistic method to determine inactivation parameters in vitro [116–118]. A P450 progress curve analysis involves only a single incubation step where the probe substrate, probe metabolite, and test compound are measured from  $T_0$  to  $T_{\text{last}}$  and may work particularly well for inactivators that exhibit a high degree of metabolic instability [119]. A second approach, known as the numerical method, has also been proposed to more accurately estimate the inactivation parameters for a test compound, especially ones with nonlinear inactivation curves [120, 121]. With the numerical method, differential equations account for the metabolism of the inactivator,



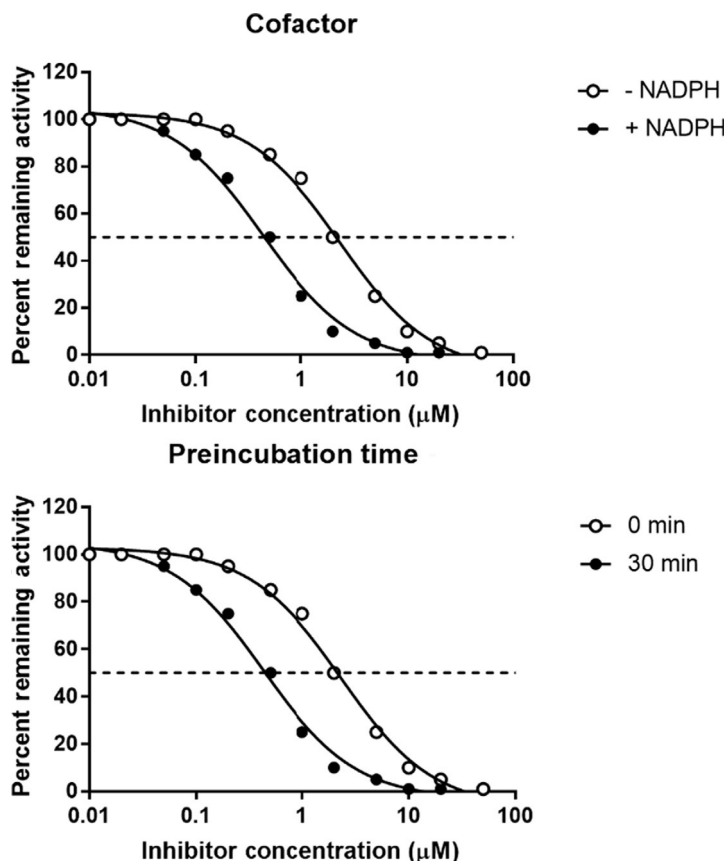


FIG. 4  $\text{IC}_{50}$ -shift approach to determine the time-dependent inhibition. Incorporation of cofactor (top panel) or preincubation time (bottom panel) results in more potent inhibition (left shift in the  $\text{IC}_{50}$  curve) for time-dependent inhibitors.

microsomal partitioning, and any lag in the onset of inactivation, in addition to the rate of inactivation of the enzyme, and there is no need to replot the percent remaining activity to determine  $k_{\text{obs}}$ . It has been suggested that the use of the numerical approach does not only aid in determining the mechanism of inactivation, but has been also shown to improve the prediction of clinical DDI parameters for a set of known CYP inactivators [122].

### 2.3 Enzyme induction

Drug interactions may also occur due to modulation of the regulation and signaling pathways of drug metabolizing enzymes or transporters. Enzyme induction, which results in an increase in the synthesis rate of the mRNA and subsequent protein corresponding to a CYP enzyme, can result in an increased rate of metabolism for drugs that are substrates for the induced enzyme, potentially causing drug concentrations to rapidly fall below efficacious

concentrations [123]. Furthermore, the additional enzyme capacity can result in a more rapid bioactivation of prodrugs or hepatotoxic drugs, again causing either decreased efficacy or undesirable toxicity [124–126].

Unlike the inhibition of drug metabolizing enzymes, which is rapid and occurs through a direct interaction between the enzyme and the inhibitor, enzyme induction is generally regulated through binding to a nuclear receptor and requires a longer timeframe with multiple doses of a perpetrator before its effects are observed *in vivo* [127]. Well-studied nuclear receptors that are involved in the induction of drug metabolizing enzymes include the pregnane X receptor (PXR), the constitutive androstane receptor (CAR), and the aryl hydrocarbon receptor (AhR) [128–134]. The pregnane X receptor is primarily located in the nucleus, while the latter two receptors are mainly expressed in the cytoplasm and as such, require translocation to the nucleus upon inducer binding to regulate enzyme expression. Upon activation by enzyme inducers, the receptors heterodimerize to other receptors such as the aryl hydrocarbon receptor nuclear translocator for AhR or the retinoid X receptor for PXR and CAR and finally bind to xenobiotic response elements found within the promoter DNA sequences of drug metabolizing enzymes [135–138]. While not as prominently studied as the aforementioned nuclear receptors with regard to enzyme induction, the estrogen receptor, retinoid X receptor, and glucocorticoid receptors have also been shown to play a role in the regulation of drug metabolizing enzymes [139–142].

Many examples of drug metabolizing enzyme inducers are available in the literature. Rifampin is probably the most widely studied CYP3A4 inducer, though other compounds such as phenobarbital (CYP2B6, CYP2C19, CYP3A4), carbamazepine (CYP2C19, CYP3A4), omeprazole (CYP1A2), and modafinil (CYP1A2) have also been studied [123, 134]. Phenobarbital, carbamazepine, and rifampin are also thought to induce expression of the UGT enzymes [19]. Often, classes of molecules such as polyaromatic hydrocarbons (CYP1A1 and CYP1A2), barbiturates (CYP1A2, CYP2C9, CYP2C19, and CYP3A), artemisinin antimalarials (CYP2B6, CYP2C19, and CYP3A) or glucocorticoids (CYP3A) can be classified as likely inducers of a drug metabolizing enzyme or enzymes [127]. Many of the drug transporter genes such as MDR1 are also regulated by PXR or other orphan nuclear receptors and as such, the aforementioned compounds may also affect the expression of these drug transporters [134]. To date, CYP2D6 is one of the few major drug metabolizing enzymes for which no xenobiotic inducer has been identified. However, its activity increases two to fivefold during pregnancy based on metoprolol clearance and dextromethorphan urinary ratio [143, 144].

A wide variety of *in vitro* systems are available to study the induction potential of new chemical entities in the drug discovery and development stage. Early in discovery where an emphasis is often placed on high-throughput generation of *in vitro* ADME data, nuclear receptor reporter gene assays are employed to rapidly evaluate the potential of a drug to bind to a nuclear receptor such as PXR [145, 146]. While the overarching hypothesis and subsequent observation is that compounds that bind to a nuclear receptors generally result in enzyme induction, disconnects between reporter gene assays and more physiologically relevant *in vitro* systems can occur and as such, the data should be used with caution [147, 148]. In general, fresh or cryopreserved human hepatocytes are considered the gold standard owing to their physiological relevance to clinical outcomes [148]. Evidence of induction in hepatocytes can be readily quantitated as a function of increases in mRNA or protein expression of the drug metabolizing enzyme of interest, as well as an increase

in the enzymatic activity of the induced enzyme [123]. While original efforts included enzyme activity or a combination of enzyme activity and mRNA expression, more recent recommendations have focused solely on increases in mRNA expression owing to the potential complexities of interpreting changes in enzyme activity for compounds which are both enzyme inducers and inhibitors [149]. The past decade has also seen the use of various immortalized cell lines evaluated for their ability to assess a compound's induction potential owing to their accessibility and constant supply relative to human hepatocytes. For example, seminal work with HepaRG or Fa2N-4 cell lines have shown these systems to be amenable to use in drug induction assays [147, 148, 150]. HepaRG cells have been shown to express the major nuclear receptors and drug metabolizing enzymes necessary to assess a drug's induction potential while Fa2N-4 cells have been shown to be acceptable to assess induction occurring through AhR or PXR pathways, though they appear to be less than optimal in regard to CAR-mediated induction mechanisms [150–153].

Induction assays in the earlier stages of a drug discovery paradigm are often designed to compare the induction activity of the test compound to that of a positive control such as rifampin, phenobarbital, or omeprazole and usually incorporate only one or two concentrations of test compound. While generation of such data in a rapid fashion can effectively be used to rank-order compounds, properly informing quantitative predictions of clinical drug interactions generally requires more complex experimental protocols designed to provide the maximum induction potential for a test compound ( $E_{\max}$ ) and the corresponding  $EC_{50}$  value obtained from plotting the fold-induction vs test article concentration on a semi-log plot, which can then be interpreted relative to the expected drug exposure in vivo [154].

### 3 Quantitative in vitro to in vivo predictions

#### 3.1 Basic principles of reversible inhibition predictions

The theory of predicting and rationally explaining DDIs was first developed in the 1970s and advances continue to be made in modeling DDIs [155]. The mathematical treatment of DDIs relies on the pharmacokinetic relationship between clearance, AUC, and intrinsic clearance. When the plasma concentration of the object drug is much below its  $K_m$  value, the effect of a competitive or noncompetitive inhibitor on intrinsic clearance by specific enzyme can be described by the following equation:

$$CL_{\text{int,u,inhibited}} = \frac{V_{\max}}{K_m * (1 + [I]/K_i)} \quad (7)$$

This equation is valid for reversible inhibitors and can be expanded to include multiple inhibitors such as combination of an inhibitor and its inhibitory metabolite [93]. This relationship shows that significant inhibition (ratio of intrinsic clearances in inhibited/control conditions  $<1$ ) is expected only when  $[I]$  approaches or exceeds  $K_i$ . Eq. (7) also shows that the magnitude of in vivo drug-drug interactions is dependent on inhibitor concentrations as well as  $K_i$ . In general, an  $[I]_u/K_i \geq 0.02$  (where  $[I]_u$  equals the maximum observed unbound concentration

in vivo) suggests the need to further evaluate the potential for drug interactions with clinical studies [156–158]. Eq. (7) is also enzyme specific, i.e., specific to the enzyme toward which  $K_i$  is determined, and thus will apply only for the metabolic clearance pathway mediated by that enzyme. Thus, assuming reversible inhibition, the decrease in clearance of the object drug will be critically dependent on the fraction of the drug clearance normally metabolized (cleared) by the pathway that is inhibited ( $f_m$ ) (Eq. 8) and the ratio of the concentration of inhibitor at the enzyme site ( $I$ ) to the inhibition constant ( $K_i$ ) (Fig. 5). This is a direct consequence of the additivity of clearances and the relationship between intrinsic clearance and metabolic clearance. It is a direct consequence of this relationship that accurate prediction and determination of the  $f_m$  is critically important in DDI predictions. The importance of accurate estimates of  $f_m$  for the “object” drug has been well illustrated in the literature [159, 160].

Most commonly, the degree of drug-drug interactions in vivo is expressed as the ratio of the area under the plasma concentration-time curve (AUC) in the presence and absence of inhibitor. Based on pharmacokinetic principles, in the absence of extrahepatic metabolism,

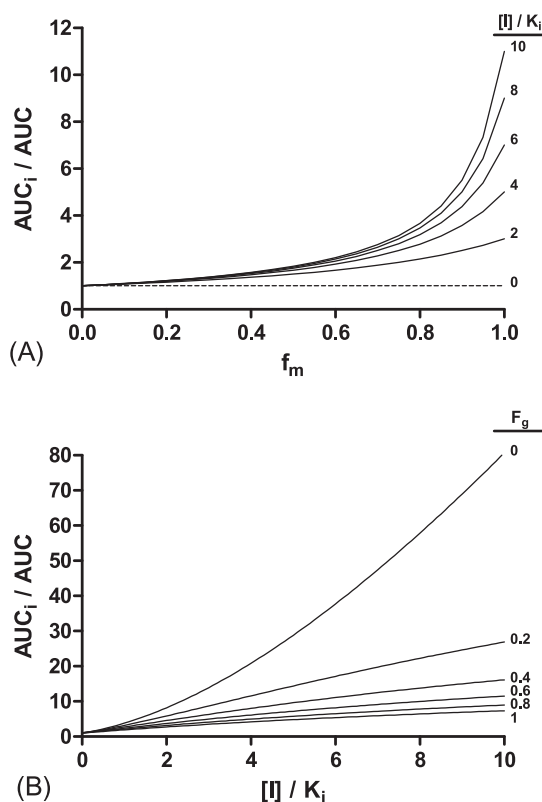


**FIG. 5** Effect of  $f_m$ ,  $[I]/K_i$ , and  $F_g$  on the change in AUC by an inhibitor of a single metabolic enzyme. Panel (A) takes into account only hepatic inhibition while panel (B) accounts for both hepatic and intestinal inhibition with an  $f_m$  of 0.95 and  $[I]/K_i$  is assumed to be identical in the liver and intestine.

the AUC is related to the ratio of intrinsic clearances and the effect of the precipitant (inhibitor) to the AUC and  $C_{ss}$  of the substrate can be described using the following equation [161]:

$$\frac{C_{ss, inhibited}}{C_{ss, control}} = \frac{AUC_{inhibited}}{AUC_{control}} = \frac{CL_{control}}{CL_{inhibited}} = \frac{1}{\sum_i^n \frac{f_m}{1 + \sum_j^m \frac{[I]}{K_i}} + \left(1 - \sum_i^n f_m\right)} \quad (8)$$

Note that when  $f_m = 1$ , Eq. (8) reduces to Eq. (9):

$$\frac{AUC_{inhibited}}{AUC_{control}} = \frac{CL_{int, control}}{CL_{int, inhibited}} = (1 + [I]/K_i) \quad (9)$$

When predicting DDIs one should consider the fundamental assumptions underlying Eqs. (8) and (9) which include: (1) metabolism occurs solely in the liver, (2) delivery of the substrate and inhibitor to the hepatic enzyme is blood flow limited (not limited by permeability, well stirred model applies), (3) substrate concentration  $\ll K_m$  (first-order kinetics, substrate does not compete with inhibitor binding), and (4) the object drug is administered orally or has a low hepatic extraction ratio. In addition, plasma and microsomal binding of the inhibitor should be incorporated into the calculations and the ratio between unbound inhibitor concentration and unbound in vitro  $K_i$  should be used. This introduces the additional assumption that  $I_{u, plasma} = I_{u, active\ site}$ .

### 3.2 Selection of inhibitor concentration, [I]

As plasma concentrations of inhibitor change as a function of time based on the kinetic characteristics of the inhibitor, there are several different options regarding the concentrations of [I] that should be used in DDI predictions. Factors that deserve attention include unbound concentrations vs total concentrations and pharmacokinetic model selection for [I]. It is obvious that inhibitor concentration is not static throughout the time-course of the elimination of the object drug. Also, depending on the residence time of the object drug in the body in relation to the half-life of the inhibitor, different models of inhibitor concentrations might be needed. Empirical analyses of the different choices of in vivo inhibitor concentrations have been conducted, though the appropriate concentration to use is still a matter of debate [162]. Ultimately, PBPK or other dynamic modeling can be used to capture time-varying changes in inhibitor concentrations, but such models invariably introduce a level of uncertainty and degrees of freedom to DDI predictions that may not be desirable or yield the best predictions. It is also worth noting that PBPK models typically assume that the hepatic concentration is equal to the concentration in the hepatic vein and therefore the effective concentration causing the inhibition may be much lower in PBPK models than that would be estimated in a conservative prediction that considers hepatic inlet concentrations. This is particularly noteworthy for inhibitors that have high extraction ratios. Similarly, due to the distribution kinetics of the inhibitor, the hepatic vein concentrations can be considerably different than those measured in a peripheral vein in clinical studies.

Static prediction models still provide the foundation for identifying DDI risk and for predicting the overall magnitude of DDIs. The inhibitor has its specific pharmacokinetic characteristics as well (i.e., absorption and elimination and the  $[I]/K_i$  changes as a function of time). However, Eq. (8) assumes that the concentration of inhibitor does not change during the period of substrate elimination, which is often unlikely in clinical practice. The ratio of intrinsic clearances of substrate would be better described as a continuous function reflecting time-dependent change in the inhibitor concentration. To overcome significant changes in  $[I]$ , in vivo studies are usually carried out at steady state of the inhibitor and using a probe that has short enough half-life to allow significant elimination prior to inhibitor elimination. Often, in studies that specifically aim to characterize in vitro-to-in vivo predictions of drug-drug interactions, the AUC of the inhibitor is measured during the administration/elimination interval of the substrate and the AUC of inhibitor is divided by the time interval in order to obtain an average concentration of  $[I]$  for the duration of the inhibition study. The interpretation of the relationship between  $[I]_{ss,ave}$  becomes complicated if the probe has a significantly longer half-life than the precipitant or if  $[I]/K_i$  varies greatly during the measurement interval (2-compartment kinetics of the inhibitor). Also, the time interval between inhibitor and substrate administration may have significant effect on the magnitude of interaction.

An alternative for the plasma average  $[I]$  has been to use portal vein  $[I]$  or maximum hepatic input concentration. The use of the “maximum unbound concentration at the inlet to liver” approach has been presented in Refs. [162, 163]. This approach takes into account both the “absorption related” contribution of inhibitor input to the liver as well as the flow of inhibitor into the liver from the systemic circulation. This approach is described in the following equation:

$$[I]_{in,max} = [I]_{max} + k_a * \frac{F_a * D}{Q_H} \quad (10)$$

The use of  $[I]_{in,max}$  gives an estimate of the worst-case scenario in terms of the maximum interaction. The terms  $k_a$  and  $F_a$  in Eq. (10) refer to the absorption rate constant and fraction of the inhibitor that is absorbed from the intestine unchanged, respectively.

All the available options for use as  $[I]$  in predicting inhibitory drug-drug interactions have been employed to some level of success in DDI predictions. Which one of these truly reflects the unbound concentration of inhibitor in the hepatocyte or the concentration driving the inhibitor-enzyme interactions might be drug and enzyme dependent. Based on free drug hypothesis, in vitro estimates of  $K_i$  should be based on unbound  $[I]$  and predictions of inhibition should be done based on both microsomal and plasma unbound fractions. The significance of correcting for unbound fraction in microsomes has been previously demonstrated for clearance predictions [164]. Measurement of unbound concentrations in medium should provide an accurate estimate of apparent unbound  $K_i$  (equivalent to unbound plasma  $K_i$ ) for scaling, irrespective of whether extensive lipid partitioning of drug occurs or not. It is assumed that unbound inhibitor ( $[I]_u$ ) equilibrates rapidly across hepatocyte plasma membrane and only unbound drug accesses the CYP active site. The general effect of nonspecific binding in vitro is to increase the apparent  $K_i$ , due to depletion of free drug in solution, leading to an underestimate of the in vivo interaction. It is difficult to determine true “unbound” concentrations of inhibitor in the liver or even more importantly in the vicinity of the enzyme active site. Active uptake transport is an obvious possibility that may cause  $[I]_{u,plasma} \ll [I]_{u,hepatocyte}$ . Other

cellular factors such as drug partitioning to lipids could also affect the true unbound concentration seen by the CYP active site [165–167].

One well-documented phenomenon that decreases  $[I]_u$  is the nonspecific binding of test compounds in microsomal incubations [168, 169]. In general, the inclusion of both plasma and microsomal-free fraction values has been shown to improve the in vitro-in vivo correlation for microsomal studies, though a dependence on the structural class of compound (i.e., basic amines vs acidic compounds) has also been noted [169]. Additional factors that may play a role in the observed results include the procedure for initiating the incubation (i.e., addition of NADPH vs substrate) and the resulting effects on enzyme stability, the choice of cofactor (i.e., direct addition of NADPH vs regenerating system), buffer characteristics, and inclusion of divalent cations such as  $Mg^{2+}$  [170, 171].

It is somewhat surprising and perhaps due to a correlation between microsomal and plasma protein binding that use of total plasma inhibitor concentrations with total in vitro  $K_i$  values for predictions often works. This is considered a conservative empirical practice and there is no obvious mechanistic basis for the approach. A risk in this approach is that  $f_{u,plasma}$  is not necessarily the same as  $f_{u,mics}$  (highly dependent on protein concentrations) and hence the microsome concentration in vitro will have a large impact on in vitro to in vivo predictions.

### 3.3 Prediction of irreversible inhibition

Upon successful determination of the in vitro parameters describing mechanism-based inhibition for a drug candidate using any of the aforementioned approaches, these values can subsequently be incorporated into various models designed to extrapolate the in vitro values to an in vivo outcome. In general, mechanistic static models are commonly used and recommended by regulatory agencies for the assessment of in vivo mechanism-based drug interactions. A comprehensive mechanistic static model that includes both hepatic and intestinal contributions to metabolism is described in Eq. (11), where  $AUC_i/AUC$  represents the fold-change in the area under the plasma concentration-time curve for a probe substrate in the presence of a mechanism-based inhibitor,  $F_g$  is the fraction of test compound that escapes gut first-pass metabolism and is absorbed under control conditions,  $k_{deg,g}$  and  $k_{deg,h}$  represent the rate of degradation for the inactivated enzyme in the gut and liver, respectively, and  $f_{mCYP}$  is the fraction of the substrate metabolized by the inactivated CYP. All other terms are identical to those described for Eq. (8) [94, 115, 172, 173].

$$\frac{AUC_i}{AUC} = \frac{1}{F_g + (1 - F_g) * \frac{1}{1 + \frac{k_{deg,g} * (K_I + [I]_g)}{k_{deg,g} * [I]_g}}} * \frac{1}{(1 - f_{mCYP}) + \frac{f_{mCYP}}{1 + \frac{k_{deg,h} * (K_I + [I])}{k_{deg,h} * [I]}}} \quad (11)$$

In general, for probe substrates not metabolized by CYP3A4, only the second term of Eq. (11) need to be considered in order to predict the fold-change in the AUC values for the compound. Similar to reversible drug interactions, confounding factors such as the choice of in vivo inhibitor concentration (i.e., total  $C_{max}$  vs unbound  $C_{max}$ ; systemic vs portal vein concentrations), the estimation of  $k_{deg,g}$ , and the accurate determination of  $F_g$  and  $f_{mCYP}$  can



all have a significant impact on the overall accuracy of the prediction of in vivo drug interactions from mechanism-based inhibitors. Of key importance in Eq. (11) is the choice of the degradation rate constant ( $k_{deg}$ ) for a given drug metabolizing enzyme, a topic which has been of considerable interest in recent years. For example, the current range of estimates of  $k_{deg}$  for CYP3A4 translate to enzymatic half-lives that range from 10 to 140 hours, with a range of 26–79 h generally being accepted as most accurate [122, 174–181].

### 3.4 Prediction of drug metabolizing enzyme induction

There are multiple prediction methods that currently exist for the extrapolation of in vitro induction data to a clinical outcome. The earliest approaches involved comparing the in vitro induction potential of a test article with a positive control such as rifampin, with compounds that increase enzyme activity by more than 40% or more relative to the positive control being classified as likely in vivo inducers [71]. In a similar simplistic fashion, compounds can also be rank ordered based on the ratio of  $E_{max}/EC_{50}$ , with the most potent inducers having the highest ratios [129, 182]. While useful in evaluating compounds at an early stage of the drug discovery process, an inherent drawback of the aforementioned approaches is that they do not incorporate clinical exposures into the prediction of drug interaction potential.

A more clinically relevant approach incorporates the hyperbolic in vitro induction parameters  $EC_{50}$  and  $E_{max}$  with the efficacious unbound plasma concentrations of the test article, resulting in the calculation of a relative induction score, as illustrated by Eq. (12) [150, 183]. It is important to note that the relative induction score does not translate linearly to an in vivo outcome but results in a sigmoidal relationship between the observed AUC differences in vivo and the calculated score.

$$\text{Relative Induction Score} = \frac{C_{eff, free} * E_{max}}{C_{eff, free} * EC_{50}} \quad (12)$$

A second, more mechanistic approach is shown in Eq. (13). As with the relative induction score, Eq. (13) not only incorporates the  $EC_{50}$  and  $E_{max}$  parameters derived from in vitro cellular assays, but also accounts for the concentration of inducer in the liver ( $[I]_h$ ) and the fraction of drug metabolized by the induced enzyme ( $f_m$ ). Note that Eq. (13) also contains a scaling parameter ( $d$ ), which generally ranges from 0.3 to 1.0, and is estimated based on a linear regression between predicted drug interactions from in vitro data and observed clinical outcomes for a specific lot of hepatocytes [184]. The scaling factor is designed to minimize the geometric mean-fold error between observed and predicted levels of induction through a linear weighted least-squares equation and is specific to the given lot. In the absence of experimental data,  $d$  is assumed to be 1 [156].

$$\frac{AUC_i}{AUC} = \left( \frac{1}{\left( 1 + \frac{d * E_{max} * [I]_h}{[I]_h + EC_{50}} \right) * f_m + (1 - f_m)} \right) \quad (13)$$

The abovementioned mechanistic models assume a static concentration of inducer and as such, generally provide a worst-case scenario with regard to the clinical outcome [182].

### 3.5 Inhibition and induction of first-pass intestinal metabolism and integration of multiple DDI mechanisms

Of the drug metabolizing enzymes, CYP3A4 is expressed to a high level in the human intestine and CYP3A4 expression in the intestine limits the bioavailability of many CYP3A4 substrates [185–188]. In general, the lower the oral bioavailability of a CYP3A substrate due to metabolism in the gut, the more profound the effect of a CYP3A inhibitor (Table 1). The overall effect of CYP3A4 inhibition of the gut availability of a CYP3A4 substrate is described by the following equation [173]:

$$\frac{AUC_{po,inhibited}}{AUC_{po,control}} = \frac{F_{g,inhibited}}{F_g} * \frac{CL}{CL_{inhibited}} \quad (14)$$

In order to predict the effects of reversible inhibition on oral AUC ( $F_g$  ratio) the following assumptions need to be made: (1) sequential gut (G) and hepatic (H) first pass, (2) systemic  $CL = CL_H$  (i.e.,  $CL_g \ll CL_H$ ), (3) elimination is first-order, and (4)  $K_i$  is the same for liver and gut CYP3A [189, 190]. Using these assumptions, reversible inhibition of sequential first-pass extraction and systemic clearance can be described according to Eq. (15). Additional evaluation with clinical studies is generally recommended when  $[I]_{gut}/K_i \geq 10$ , where  $[I]_{gut}$  is the intestinal concentration of the perpetrator drug calculated as the molar dose/250 mL [156, 157]. The influence of  $F_g$  on the  $AUC_i/AUC$  ratio is depicted in Fig. 4B.

$$\frac{AUC_i}{AUC} = \frac{1}{F_g + (1 - F_g) * \frac{1}{1 + \frac{[I]_g}{(K_i)}}} * \frac{1}{\left(1 - \sum_i^n f_{mCYP}\right) + \sum_i^n \frac{f_{mCYP}}{1 + \sum_j^m \frac{[I]}{(K_i)}}} \quad (15)$$

Similarly, irreversible inhibition of gut clearance and induction of intestinal inhibition can be incorporated using a static model. The complete effect of sequential gut metabolism and systemic clearance can be predicted by the following equations for inhibition and induction, respectively:

$$\frac{AUC_i}{AUC} = \frac{1}{F_g + (1 - F_g) * \frac{1}{1 + \frac{k_{deg,g} * [I]_g}{K_i + [I]_g}}} * \frac{1}{(1 - f_{mCYP}) + \frac{f_{mCYP}}{1 + \frac{k_{deg,h} * [I]}{K_i + [I]}}} \quad (16)$$

$$\frac{AUC_i}{AUC} = \left( \frac{1}{\left(1 + \frac{d * E_{max} * [I]_g}{[I]_g + EC_{50}}\right) * (1 - F_g) + F_g} \right) * \left( \frac{1}{\left(1 + \frac{d * E_{max} * [I]_h}{[I]_h + EC_{50}}\right) * f_m + (1 - f_m)} \right) \quad (17)$$

Special attention should be paid to the concentration of the inhibitor in the gut used in predictions [189, 190]. While circulating concentrations of the inhibitor may be most applicable for the predictions of reversible inhibition of gut CYPs, the inactivation of CYPs may be

driven by the maximum concentrations reached during the absorption phase of the precipitant. However, for many inactivators several metabolic steps are required for inactivation and the mathematical models to address this during absorption process need to be further developed.

Many drugs do alter metabolic clearance via multiple mechanisms including simultaneous induction and inactivation of CYPs and reversible inhibition. Hence static models have been developed that incorporate all the three mechanisms and gut interactions into a single prediction of complex drug-drug interactions. Fig. 6 shows the full equation that combines Eqs. (15)–(17) into a single prediction. This equation has been applied, for example, to evaluate the complex drug-drug interactions of HIV protease inhibitors [191, 192]. Given the complexity of the predictions and the fluctuation in the concentrations in the gut and the systemic circulation, dynamic predictions of the simultaneous effects have become the preferred method in the literature. However, the mathematical models used in the dynamic predictions are not well described in the literature.

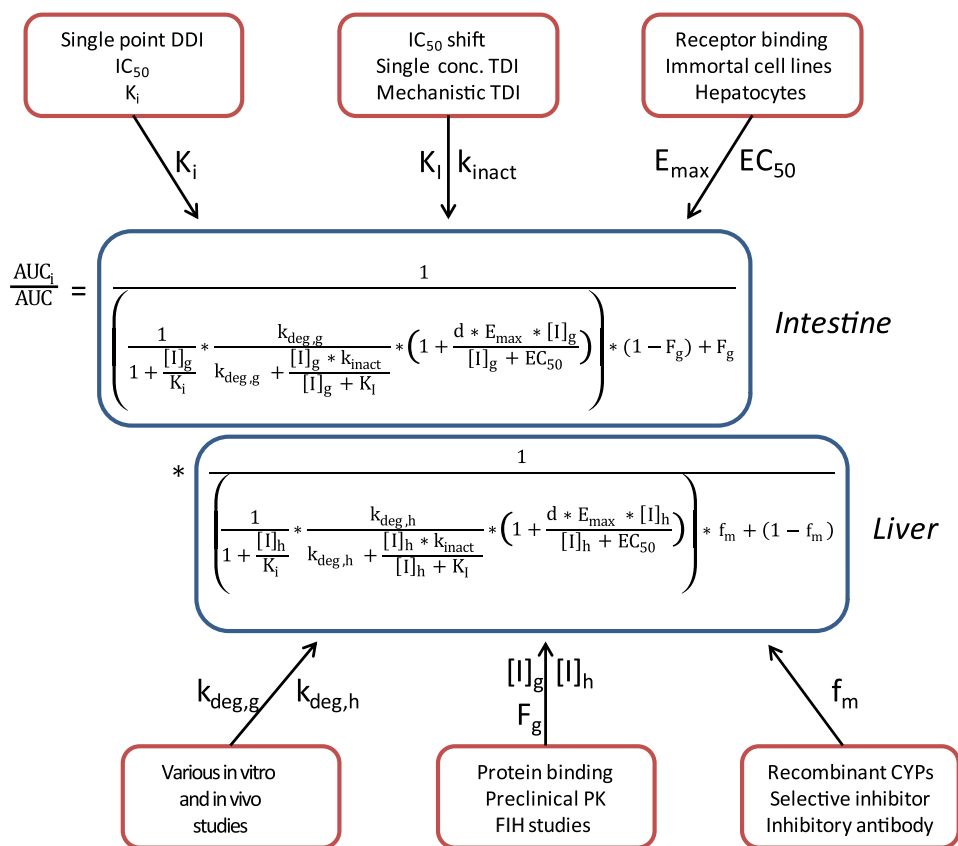


FIG. 6 Proposed flow scheme for the assessment of drug interactions and the simultaneous incorporation of in vitro reversible inhibition, mechanism-based inhibition, and enzyme induction parameters into the in vivo drug interaction prediction.

## 4 Clinical drug interaction assessment

While the aforementioned *in vitro* and mathematical approaches provide a basis from which to predict and characterize potential drug interactions, ultimately the utility of a well-designed clinical drug interaction trial cannot be overstated. Recent data suggests that even for drugs which have undergone stringent characterization and optimization in the drug discovery stage, the potential for clinically relevant drug interactions still exists [193, 194]. To that end, an updated regulatory guidance document was released by the US FDA in 2017, focusing on the timing, design, and interpretation of clinical drug interaction studies, and the subsequent management of clinical drug interactions in patient populations [3].

Prospective clinical drug interaction studies are commonly undertaken to characterize the potential for enzyme inhibition (reversible or time-dependent) either on or by the test compound in humans. Well-studied probe substrates (sometimes referred to as index substrates) are available to measure the inhibitory effect of a test compound on a given metabolic or transport pathway and characterization of a DDI can often be accomplished with only a single concomitant dose of the test compound with the probe substrate (dosed before and after administration of the test compound), unless time-dependent inhibition is suspected. Examples of probe substrates include midazolam (CYP3A), atomoxetine or dextromethorphan (CYP2D6), or omeprazole (CYP2C19), in addition to others [195]. Similarly, inhibitors or inducers such as itraconazole (CYP3A inhibitor), fluoxetine (CYP2D6/CYP2C19 inhibitor), fluvoxamine (CYP1A2/CYP2C19 inhibitor), or rifampin (nonselective P450 inducer) can be used to assess the potential of the test compound to be a victim of potential drug interactions in humans. The use of a probe substrate cocktails has also been shown to be an acceptable approach to explore the drug interaction potential of an investigational drug on multiple CYP enzymes in a single study [196, 197].

Several approaches are also available to evaluate the enzyme induction in clinical trials. Drug interaction studies with selective probe substrates (i.e., midazolam for CYP3A) provide the definitive measure of a drug's ability to increase the clearance of a coadministered drug through enzyme induction [3]. Whereas clinical trials to study the inhibitory potential of a drug candidate can generally be conducted with only a single dose of the perpetrator and victim drugs, induction DDI studies often require a prolonged dosing period with the perpetrator drug to allow drug exposure and enzyme synthesis/degradation rates to reach steady state prior to the administration of the victim drug [127]. More recent efforts have evaluated the use of endogenous biomarkers to rapidly assess a drug's induction potential in early clinical trials [198]. While yet to be adopted in the current regulatory guidance, measurement of circulating 4 $\beta$ -hydroxycholesterol concentrations or urinary 6 $\beta$ -hydroxycortisol/cortisol ratios have shown promise as indicators of *in vivo* CYP3A activity and induction [199–206]. Adding to the complexity of assessing enzyme induction in clinical trials, a review of the drug interaction potential of recently approved new drug applications reported that the majority of CYP inducers were also inhibitors of the same enzyme [207]. A more comprehensive overview of clinically relevant drug interactions can be found in Chapter 11 of this book.

## 5 Conclusions

The aim of this chapter was to illustrate many of the concepts surrounding the *in vitro* characterization of drug-drug interactions and the subsequent prediction of *in vivo* drug interactions. More specific information can be found in the numerous manuscripts, reviews, and regulatory guidances referenced within this chapter. Though many of the basic ideas have been well established and studied for years, the field continues to evolve toward more mechanistic and accurate approaches to predict and understand the potential for clinical drug interactions before they occur. A number of the advanced mathematical models and complex modeling approaches such as physiologically based pharmacokinetic modeling coupled with our constantly expanding knowledge base around *in vitro* CYP enzymology will only serve to further underwrite our ability to identify safe and efficacious therapeutics in years to come.

## References

- [1] K. Johnell, I. Klarin, The relationship between number of drugs and potential drug-drug interactions in the elderly: a study of over 600,000 elderly patients from the Swedish Prescribed Drug Register, *Drug Saf.* 30 (10) (2007) 911–918.
- [2] D.M. Qato, et al., Use of prescription and over-the-counter medications and dietary supplements among older adults in the United States, *JAMA* 300 (24) (2008) 2867–2878.
- [3] U.S. Food and Drug Administration, Clinical Drug Interaction Studies—Study Design, Data Analysis, and Clinical Implications Guidance for Industry, Available from: <https://www.fda.gov/regulatory-information/search-fda-guidance-documents/clinical-drug-interaction-studies-study-design-data-analysis-and-clinical-implications-guidance>, 2017.
- [4] I. Klarin, A. Wimo, J. Fastbom, The association of inappropriate drug use with hospitalisation and mortality: a population-based study of the very old, *Drugs Aging* 22 (1) (2005) 69–82.
- [5] H.J. Beijer, C.J. de Blaey, Hospitalisations caused by adverse drug reactions (ADR): a meta-analysis of observational studies, *Pharm. World Sci.* 24 (2) (2002) 46–54.
- [6] R.S. Foti, et al., Mechanisms of drug metabolism, in: A. Lyubimov (Ed.), *Encyclopedia of Drug Metabolism and Interactions*, Wiley, 2012.
- [7] L.C. Wienkers, T.G. Heath, Predicting *in vivo* drug interactions from *in vitro* drug discovery data, *Nat. Rev. Drug Discov.* 4 (10) (2005) 825–833.
- [8] A. Parkinson, Biotransformation of xenobiotics, in: C.D. Klaassen (Ed.), *Toxicology: The Basic Science of Poisons*, McGraw Hill, New York, 1996.
- [9] K.S. Pang, Safety testing of metabolites: Expectations and outcomes, *Chem. Biol. Interact.* 179 (1) (2009) 45–59.
- [10] W. Tang, A.Y. Lu, Metabolic bioactivation and drug-related adverse effects: current status and future directions from a pharmaceutical research perspective, *Drug Metab. Rev.* 42 (2) (2010) 225–249.
- [11] J. Uetrecht, J.S. Lee, R.S. Obach, M.B. Fisher (Eds.), *Bioactivation*, in: *Drug Metabolizing Enzymes*, FontisMedia/Marcel Dekker, Inc, New York, 2003.
- [12] J.S. Walsh, G.T. Miwa, Bioactivation of drugs: risk and drug design, *Annu. Rev. Pharmacol. Toxicol.* 51 (2011) 145–167.
- [13] J.D. Lutz, Y. Fujioka, N. Isoherranen, Rationalization and prediction of *in vivo* metabolite exposures: the role of metabolite kinetics, clearance predictions and *in vitro* parameters, *Expert Opin. Drug Metab. Toxicol.* 6 (9) (2010) 1095–1109.
- [14] M. Rowland, T.M. Tozer, *Metabolites and drug response*, in: *Clinical Pharmacokinetics and Pharmacodynamics*, Lippincott Williams & Wilkins, Baltimore, MD, 2011.
- [15] N. Isoherranen, et al., Qualitative analysis of the role of metabolites in inhibitory drug-drug interactions: literature evaluation based on the metabolism and transport drug interaction database, *Chem. Res. Toxicol.* 22 (2) (2009) 294–298.

- [16] B.M. VandenBrink, N. Isoherranen, The role of metabolites in predicting drug-drug interactions: focus on irreversible cytochrome P450 inhibition, *Curr. Opin. Drug Discov. Devel.* 13 (1) (2010) 66–77.
- [17] C.K. Yeung, et al., Are circulating metabolites important in drug-drug interactions?: quantitative analysis of risk prediction and inhibitory potency, *Clin. Pharmacol. Ther.* 89 (1) (2011) 105–113.
- [18] M.W. Coughtrie, M.B. Fisher, The role of sulfotransferases (SULTs) and UDP-glucuronosyltransferases (UGTs) in human drug clearance and bioactivation, in: J.S. Lee, R.S. Obach, M.B. Fisher (Eds.), *Drug Metabolizing Enzymes: Cytochrome P450 and Other Enzymes in Drug Discovery and Development*, Marcel Dekker/FontisMedia, New York, 2003, pp. 551–567.
- [19] R.S. Foti, M.B. Fisher, UDP-glucuronosyltransferases: pharmacogenetics, functional characterization and clinical relevance, in: A. Lyubimov (Ed.), *Encyclopedia of Drug Metabolism and Interactions*, Wiley, 2012.
- [20] A. Nakamura, et al., Expression of UGT1A and UGT2B mRNA in human normal tissues and various cell lines, *Drug Metab. Dispos.* 36 (8) (2008) 1461–1464.
- [21] R.H. Tukey, C.P. Strassburg, Human UDP-glucuronosyltransferases: metabolism, expression, and disease, *Annu. Rev. Pharmacol. Toxicol.* 40 (2000) 581–616.
- [22] X. Ding, L.S. Kaminsky, Human extrahepatic cytochromes P450: function in xenobiotic metabolism and tissue-selective chemical toxicity in the respiratory and gastrointestinal tracts, *Annu. Rev. Pharmacol. Toxicol.* 43 (2003) 149–173.
- [23] J.A. Williams, et al., Drug-drug interactions for UDP-glucuronosyltransferase substrates: a pharmacokinetic explanation for typically observed low exposure (AUC<sub>i</sub>/AUC) ratios, *Drug Metab. Dispos.* 32 (11) (2004) 1201–1208.
- [24] R.S. Foti, L.C. Wienkers, J.L. Wahlstrom, Application of cytochrome P450 drug interaction screening in drug discovery, *Comb. Chem. High Throughput Screen.* 13 (2) (2010) 145–158.
- [25] L.C. Eriksson, J.W. DePierre, G. Dallner, Preparation and properties of microsomal fractions, in: J.B. Schenkman, D. Kupfer (Eds.), *Hepatic Cytochrome P-450 Monooxygenase System*, Pergamon Press, Oxford, 1982.
- [26] F.P. Guengerich, Analysis and characterization of enzymes, in: A.W. Hayes (Ed.), *Principles and Methods of Toxicology*, Raven Press, New York, 1989, pp. 777–814.
- [27] S. Rendic, F.J. Di Carlo, Human cytochrome P450 enzymes: a status report summarizing their reactions, substrates, inducers, and inhibitors, *Drug Metab. Rev.* 29 (1-2) (1997) 413–580.
- [28] G. Somers, P. Mutch, A. Woodrooffe, In vitro techniques for investigating drug metabolism, in: G. Evans (Ed.), *A Handbook of Bioanalysis and Drug Metabolism*, CRC Press, Boca Raton, 2004.
- [29] S. Asha, M. Vidyavathi, Role of human liver microsomes in in vitro metabolism of drugs—a review, *Appl. Biochem. Biotechnol.* 160 (6) (2010) 1699–1722.
- [30] A.R. Boobis, et al., Monooxygenase activity of human liver in microsomal fractions of needle biopsy specimens, *Br. J. Clin. Pharmacol.* 9 (1) (1980) 11–19.
- [31] E.D. Kharasch, K.E. Thummel, Identification of cytochrome P450 2E1 as the predominant enzyme catalyzing human liver microsomal defluorination of sevoflurane, isoflurane, and methoxyflurane, *Anesthesiology* 79 (4) (1993) 795–807.
- [32] J.L. Raucy, J.M. Lasker, Isolation of P450 enzymes from human liver, *Methods Enzymol.* 206 (1991) 577–587.
- [33] A.D. Rodrigues, et al., Measurement of liver microsomal cytochrome p450 (CYP2D6) activity using [O-methyl-14C]dextromethorphan, *Anal. Biochem.* 219 (2) (1994) 309–320.
- [34] F.P. Guengerich, Analysis and characterization of enzymes, in: A.W. Hayes (Ed.), *Principles and Methods of Toxicology*, Raven Press, New York, 1994, pp. 1259–1313.
- [35] E.J. Buenz, A high-throughput cell-based toxicity analysis of drug metabolites using flow cytometry, *Cell Biol. Toxicol.* 23 (5) (2007) 361–365.
- [36] L. Di, et al., Comparison of cytochrome P450 inhibition assays for drug discovery using human liver microsomes with LC-MS, rhCYP450 isozymes with fluorescence, and double cocktail with LC-MS, *Int. J. Pharm.* 335 (1-2) (2007) 1–11.
- [37] P. Fasinu, P.J. Bouic, B. Rosenkranz, Liver-based in vitro technologies for drug biotransformation studies—a review, *Curr. Drug Metab.* 13 (2) (2012) 215–224.
- [38] A. Guillouzo, et al., Long-term culture of functional hepatocytes, *Toxicol. in Vitro* 4 (4-5) (1990) 415–427.
- [39] O. Luttringer, et al., Influence of isolation procedure, extracellular matrix and dexamethasone on the regulation of membrane transporters gene expression in rat hepatocytes, *Biochem. Pharmacol.* 64 (11) (2002) 1637–1650.
- [40] J. Sahi, S. Grepper, C. Smith, Hepatocytes as a tool in drug metabolism, transport and safety evaluations in drug discovery, *Curr. Drug Discov. Technol.* 7 (3) (2010) 188–198.

- [41] S. Wang, et al., Three-dimensional primary hepatocyte culture in synthetic self-assembling peptide hydrogel, *Tissue Eng. Part A* 14 (2) (2008) 227–236.
- [42] D.C. Hay, et al., Unbiased screening of polymer libraries to define novel substrates for functional hepatocytes with inducible drug metabolism, *Stem Cell Res.* 6 (2) (2011) 92–102.
- [43] H. Inoue, S. Yamanaka, The use of induced pluripotent stem cells in drug development, *Clin. Pharmacol. Ther.* 89 (5) (2011) 655–661.
- [44] R.S. Foti, J.L. Wahlstrom, Prediction of CYP-mediated drug interactions in vivo using in vitro data, *IDrugs* 11 (12) (2008) 900–905.
- [45] P.J. Neuvonen, K.M. Jalava, Itraconazole drastically increases plasma concentrations of lovastatin and lovastatin acid, *Clin. Pharmacol. Ther.* 60 (1) (1996) 54–61.
- [46] P.J. Neuvonen, T. Kantola, K.T. Kivisto, Simvastatin but not pravastatin is very susceptible to interaction with the CYP3A4 inhibitor itraconazole, *Clin. Pharmacol. Ther.* 63 (3) (1998) 332–341.
- [47] A. Varhe, K.T. Olkkola, P.J. Neuvonen, Oral triazolam is potentially hazardous to patients receiving systemic antimycotics ketoconazole or itraconazole, *Clin. Pharmacol. Ther.* 56 (6 Pt 1) (1994) 601–607.
- [48] J.T. Backman, et al., The area under the plasma concentration–time curve for oral midazolam is 400-fold larger during treatment with itraconazole than with rifampicin, *Eur. J. Clin. Pharmacol.* 54 (1) (1998) 53–58.
- [49] K.M. Jalava, K.T. Olkkola, P.J. Neuvonen, Itraconazole greatly increases plasma concentrations and effects of felodipine, *Clin. Pharmacol. Ther.* 61 (4) (1997) 410–415.
- [50] T. Kantola, K.T. Kivisto, P.J. Neuvonen, Effect of itraconazole on the pharmacokinetics of atorvastatin, *Clin. Pharmacol. Ther.* 64 (1) (1998) 58–65.
- [51] N. Yasui, et al., Effect of itraconazole on the single oral dose pharmacokinetics and pharmacodynamics of alprazolam, *Psychopharmacology* 139 (3) (1998) 269–273.
- [52] K.M. Kaukonen, K.T. Olkkola, P.J. Neuvonen, Itraconazole increases plasma concentrations of quinidine, *Clin. Pharmacol. Ther.* 62 (5) (1997) 510–517.
- [53] T. Kantola, K.T. Kivisto, P.J. Neuvonen, Effect of itraconazole on cerivastatin pharmacokinetics, *Eur. J. Clin. Pharmacol.* 54 (11) (1999) 851–855.
- [54] A. Galetin, et al., CYP3A4 substrate selection and substitution in the prediction of potential drug–drug interactions, *J. Pharmacol. Exp. Ther.* 314 (1) (2005) 180–190.
- [55] N. Isoherranen, et al., Importance of multi-p450 inhibition in drug–drug interactions: evaluation of incidence, inhibition magnitude, and prediction from in vitro data, *Chem. Res. Toxicol.* 25 (11) (2012) 2285–2300.
- [56] W.J. Lu, N. Thong, D.A. Flockhart, Reduced methadone clearance during aromatase inhibition, *J. Clin. Psychopharmacol.* 32 (4) (2012) 511–517.
- [57] M.N. Cobb, et al., The effect of fluconazole on the clinical pharmacokinetics of methadone, *Clin. Pharmacol. Ther.* 63 (6) (1998) 655–662.
- [58] S.K. Gupta, et al., The effect of multiple doses of peginterferon alfa-2b on the steady-state pharmacokinetics of methadone in patients with chronic hepatitis C undergoing methadone maintenance therapy, *J. Clin. Pharmacol.* 47 (5) (2007) 604–612.
- [59] R.L. Davis, et al., Effect of the addition of ciprofloxacin on theophylline pharmacokinetics in subjects inhibited by cimetidine, *Ann. Pharmacother.* 26 (1) (1992) 11–13.
- [60] B.M. VandenBrink, et al., Evaluation of CYP2C8 inhibition in vitro: utility of montelukast as a selective CYP2C8 probe substrate, *Drug Metab. Dispos.* 39 (9) (2011) 1546–1554.
- [61] A.M. Filppula, et al., Reevaluation of the microsomal metabolism of montelukast: major contribution by CYP2C8 at clinically relevant concentrations, *Drug Metab. Dispos.* 39 (5) (2011) 904–911.
- [62] T. Karonen, et al., Gemfibrozil markedly increases the plasma concentrations of montelukast: a previously unrecognized role for CYP2C8 in the metabolism of montelukast, *Clin. Pharmacol. Ther.* 88 (2) (2010) 223–230.
- [63] B.M. Kerr, et al., Human liver carbamazepine metabolism. Role of CYP3A4 and CYP2C8 in 10,11-epoxide formation, *Biochem. Pharmacol.* 47 (11) (1994) 1969–1979.
- [64] R.S. Obach, T.F. Ryder, Metabolism of ramelteon in human liver microsomes and correlation with the effect of fluvoxamine on ramelteon pharmacokinetics, *Drug Metab. Dispos.* 38 (8) (2010) 1381–1391.
- [65] J.E. Thatcher, A. Zelter, N. Isoherranen, The relative importance of CYP26A1 in hepatic clearance of all-trans retinoic acid, *Biochem. Pharmacol.* 80 (6) (2010) 903–912.
- [66] N. Isoherranen, et al., Role of itraconazole metabolites in CYP3A4 inhibition, *Drug Metab. Dispos.* 32 (10) (2004) 1121–1131.
- [67] J.C. Stevens, S.A. Wrighton, Interaction of the enantiomers of fluoxetine and norfluoxetine with human liver cytochromes P450, *J. Pharmacol. Exp. Ther.* 266 (2) (1993) 964–971.



- [68] A.C. Altamura, A.R. Moro, M. Percudani, Clinical pharmacokinetics of fluoxetine, *Clin. Pharmacokinet.* 26 (3) (1994) 201–214.
- [69] S.H. Preskorn, et al., Pharmacokinetics of desipramine coadministered with sertraline or fluoxetine, *J. Clin. Psychopharmacol.* 14 (2) (1994) 90–98.
- [70] I.E. Templeton, et al., Contribution of itraconazole metabolites to inhibition of CYP3A4 in vivo, *Clin. Pharmacol. Ther.* 83 (1) (2008) 77–85.
- [71] T.D. Bjornsson, et al., The conduct of in vitro and in vivo drug-drug interaction studies: a Pharmaceutical Research and Manufacturers of America (PhRMA) perspective, *Drug Metab. Dispos.* 31 (7) (2003) 815–832.
- [72] L.H. Cohen, et al., In vitro drug interactions of cytochrome p450: an evaluation of fluorogenic to conventional substrates, *Drug Metab. Dispos.* 31 (8) (2003) 1005–1015.
- [73] R.S. Foti, J.L. Wahlstrom, CYP2C19 Inhibition: the impact of substrate probe selection on in vitro inhibition profiles, *Drug Metab. Dispos.* 36 (3) (2008) 523–528.
- [74] V. Kumar, et al., CYP2C9 inhibition: impact of probe selection and pharmacogenetics on in vitro inhibition profiles, *Drug Metab. Dispos.* 34 (12) (2006) 1966–1975.
- [75] D.M. Stresser, et al., Substrate-dependent modulation of CYP3A4 catalytic activity: analysis of 27 test compounds with four fluorometric substrates, *Drug Metab. Dispos.* 28 (12) (2000) 1440–1448.
- [76] K.E. Kenworthy, et al., Multisite kinetic models for CYP3A4: simultaneous activation and inhibition of diazepam and testosterone metabolism, *Drug Metab. Dispos.* 29 (12) (2001) 1644–1651.
- [77] A. Galetin, S.E. Clarke, J.B. Houston, Multisite kinetic analysis of interactions between prototypical CYP3A4 subgroup substrates: midazolam, testosterone, and nifedipine, *Drug Metab. Dispos.* 31 (9) (2003) 1108–1116.
- [78] M.L. Schrag, L.C. Wienkers, Covalent alteration of the CYP3A4 active site: evidence for multiple substrate binding domains, *Arch. Biochem. Biophys.* 391 (1) (2001) 49–55.
- [79] G.T. Tucker, J.B. Houston, S.M. Huang, EUFEPS conference report. Optimising drug development: strategies to assess drug metabolism/transporter interaction potential—towards a consensus. European Federation of Pharmaceutical Sciences, *Eur. J. Pharm. Sci.* 13 (4) (2001) 417–428.
- [80] R.W. Wang, et al., Human cytochrome P-450 3A4: in vitro drug-drug interaction patterns are substrate-dependent, *Drug Metab. Dispos.* 28 (3) (2000) 360–366.
- [81] P.A. Williams, et al., Crystal structure of human cytochrome P450 2C9 with bound warfarin, *Nature* 424 (6947) (2003) 464–468.
- [82] J.K. Yano, et al., The structure of human microsomal cytochrome P450 3A4 determined by X-ray crystallography to 2.05-Å resolution, *J. Biol. Chem.* 279 (37) (2004) 38091–38094.
- [83] R.S. Foti, et al., Selection of alternative CYP3A4 probe substrates for clinical drug interaction studies using in vitro data and in vivo simulation, *Drug Metab. Dispos.* 38 (6) (2010) 981–987.
- [84] T. Karonen, P.J. Neuvonen, J.T. Backman, The CYP2C8 inhibitor gemfibrozil does not affect the pharmacokinetics of zafirlukast, *Eur. J. Clin. Pharmacol.* 67 (2) (2011) 151–155.
- [85] B.W. Ogilvie, et al., Glucuronidation converts gemfibrozil to a potent, metabolism-dependent inhibitor of CYP2C8: implications for drug-drug interactions, *Drug Metab. Dispos.* 34 (1) (2006) 191–197.
- [86] B.M. VandenBrink, et al., Prediction of CYP2D6 drug interactions from in vitro data: evidence for substrate-dependent inhibition, *Drug Metab. Dispos.* 40 (1) (2012) 47–53.
- [87] M. Hutzler, D.M. Messing, L.C. Wienkers, Predicting drug-drug interactions in drug discovery: where are we now and where are we going? *Curr. Opin. Drug Discov. Devel.* 8 (1) (2005) 51–58.
- [88] I. Jansson, J.B. Schenkman, Substrate influence on interaction between cytochrome P450 and cytochrome b5 in microsomes, *Arch. Biochem. Biophys.* 325 (2) (1996) 265–269.
- [89] J.B. Schenkman, I. Jansson, The many roles of cytochrome b5, *Pharmacol. Ther.* 97 (2) (2003) 139–152.
- [90] G. Vergeres, L. Waskell, Cytochrome b5, its functions, structure and membrane topology, *Biochimie* 77 (7-8) (1995) 604–620.
- [91] I.H. Segel, Simple inhibition systems, in: *Enzyme Kinetics: Behavior and Analysis of Rapid Equilibrium and Steady-State Enzyme Systems*, John Wiley & Sons, Inc, New York, 1975, p. 111.
- [92] J.F. Morrison, Kinetics of the reversible inhibition of enzyme-catalysed reactions by tight-binding inhibitors, *Biochim. Biophys. Acta* 185 (2) (1969) 269–286.
- [93] J.D. Lutz, N. Isoherranen, In vitro-to-in vivo predictions of drug-drug interactions involving multiple reversible inhibitors, *Expert Opin. Drug Metab. Toxicol.* 8 (4) (2012) 449–466.

- [94] S.W. Grimm, et al., The conduct of in vitro studies to address time-dependent inhibition of drug-metabolizing enzymes: a perspective of the pharmaceutical research and manufacturers of America, *Drug Metab. Dispos.* 37 (7) (2009) 1355–1370.
- [95] J.H. Lin, A.Y. Lu, Inhibition and induction of cytochrome P450 and the clinical implications, *Clin. Pharmacokinet.* 35 (5) (1998) 361–390.
- [96] R.B. Silverman, *Mechanism-Based Enzyme Inactivation: Chemistry and Enzymology*, CRC Press, Boca Raton, 1988, pp. 9–11.
- [97] P.F. Hollenberg, U.M. Kent, N.N. Bumpus, Mechanism-based inactivation of human cytochromes p450s: experimental characterization, reactive intermediates, and clinical implications, *Chem. Res. Toxicol.* 21 (1) (2008) 189–205.
- [98] A.L. Blobaum, Mechanism-based inactivation and reversibility: is there a new trend in the inactivation of cytochrome p450 enzymes? *Drug Metab. Dispos.* 34 (1) (2006) 1–7.
- [99] B.R. Baer, L.C. Wienkers, D.A. Rock, Time-dependent inactivation of P450 3A4 by raloxifene: identification of Cys239 as the site of apoprotein alkylation, *Chem. Res. Toxicol.* 20 (6) (2007) 954–964.
- [100] R.S. Foti, et al., Mechanism-based inactivation of cytochrome P450 3A4 by mibefradil through heme destruction, *Drug Metab. Dispos.* 39 (7) (2011) 1188–1195.
- [101] K.K. Khan, et al., Differential oxidation of mifepristone by cytochromes P450 3A4 and 3A5: selective inactivation of P450 3A4, *Drug Metab. Dispos.* 30 (9) (2002) 985–990.
- [102] T.D. Lindstrom, B.R. Hanssen, S.A. Wrighton, Cytochrome P-450 complex formation by dirithromycin and other macrolides in rat and human livers, *Antimicrob. Agents Chemother.* 37 (2) (1993) 265–269.
- [103] P.R. Ortiz de Montellano, J.M. Mathews, Autocatalytic alkylation of the cytochrome P-450 prosthetic haem group by 1-aminobenzotriazole. Isolation of an NN-bridged benzyne-protoporphyrin IX adduct, *Biochem. J.* 195 (3) (1981) 761–764.
- [104] A.S. Kalgutkar, R.S. Obach, T.S. Maurer, Mechanism-based inactivation of cytochrome P450 enzymes: chemical mechanisms, structure-activity relationships and relationship to clinical drug-drug interactions and idiosyncratic adverse drug reactions, *Curr. Drug Metab.* 8 (5) (2007) 407–447.
- [105] D.C. Liebler, F.P. Guengerich, Elucidating mechanisms of drug-induced toxicity, *Nat. Rev. Drug Discov.* 4 (5) (2005) 410–420.
- [106] K. Venkatakrishnan, R.S. Obach, Drug-drug interactions via mechanism-based cytochrome P450 inactivation: points to consider for risk assessment from in vitro data and clinical pharmacologic evaluation, *Curr. Drug Metab.* 8 (5) (2007) 449–462.
- [107] S.F. Zhou, et al., Clinically important drug interactions potentially involving mechanism-based inhibition of cytochrome P450 3A4 and the role of therapeutic drug monitoring, *Ther. Drug Monit.* 29 (6) (2007) 687–710.
- [108] F.P. Guengerich, Inhibition of drug metabolizing enzymes: molecular and biochemical aspects, in: T.F. Woolf (Ed.), *Handbook of Drug Metabolism*, Marcel Dekker, New York, 1999.
- [109] R.B. Silverman, Mechanism-based enzyme inactivators, *Methods Enzymol.* 249 (1995) 240–283.
- [110] R.B. Silverman, Mechanism-based enzyme inactivation, in: D.L. Purich (Ed.), *Contemporary Enzyme Kinetics and Mechanisms*, Academic Press, San Diego, 1996.
- [111] G.T. Tucker, J.B. Houston, S.M. Huang, Optimizing drug development: strategies to assess drug metabolism/transporter interaction potential—toward a consensus, *Pharm. Res.* 18 (8) (2001) 1071–1080.
- [112] S.G. Waley, Kinetics of suicide substrates. Practical procedures for determining parameters, *Biochem. J.* 227 (3) (1985) 843–849.
- [113] L.M. Berry, Z. Zhao, An examination of IC<sub>50</sub> and IC<sub>50</sub>-shift experiments in assessing time-dependent inhibition of CYP3A4, CYP2D6 and CYP2C9 in human liver microsomes, *Drug Metab. Lett.* 2 (1) (2008) 51–59.
- [114] P. Li, et al., A refined cytochrome P540 IC(5)(0) shift assay for reliably identifying CYP3A time-dependent inhibitors, *Drug Metab. Dispos.* 39 (6) (2011) 1054–1057.
- [115] R.S. Obach, R.L. Walsky, K. Venkatakrishnan, Mechanism-based inactivation of human cytochrome p450 enzymes and the prediction of drug-drug interactions, *Drug Metab. Dispos.* 35 (2) (2007) 246–255.
- [116] D.A. Fairman, C. Collins, S. Chapple, Progress curve analysis of CYP1A2 inhibition: a more informative approach to the assessment of mechanism-based inactivation? *Drug Metab. Dispos.* 35 (12) (2007) 2159–2165.
- [117] K.A. Salminen, et al., Simple, direct, and informative method for the assessment of CYP2C19 enzyme inactivation kinetics, *Drug Metab. Dispos.* 39 (3) (2011) 412–418.

- [118] K.A. Salminen, et al., CYP2C19 progress curve analysis and mechanism-based inactivation by three methylenedioxyphenyl compounds, *Drug Metab. Dispos.* 39 (12) (2011) 2283–2289.
- [119] H.J. Burt, et al., Progress curve mechanistic modeling approach for assessing time-dependent inhibition of CYP3A4, *Drug Metab. Dispos.* 40 (9) (2012) 1658–1667.
- [120] K. Korzekwa, et al., A numerical method for analysis of in vitro time-dependent inhibition data. Part 2. Application to experimental data, *Drug Metab. Dispos.* 42 (9) (2014) 1587–1595.
- [121] S. Nagar, J.P. Jones, K. Korzekwa, A numerical method for analysis of in vitro time-dependent inhibition data. Part 1. Theoretical considerations, *Drug Metab. Dispos.* 42 (9) (2014) 1575–1586.
- [122] J. Yadav, K. Korzekwa, S. Nagar, Improved predictions of drug-drug interactions mediated by time-dependent inhibition of CYP3A, *Mol. Pharm.* 15 (5) (2018) 1979–1995.
- [123] N.J. Hewitt, E.L. Lecluyse, S.S. Ferguson, Induction of hepatic cytochrome P450 enzymes: methods, mechanisms, recommendations, and in vitro-in vivo correlations, *Xenobiotica* 37 (10-11) (2007) 1196–1224.
- [124] F.P. Guengerich, et al., Activation of carcinogens by human liver cytochromes P-450, *Basic Life Sci.* 53 (1990) 381–396.
- [125] M.F. Hebert, et al., Bioavailability of cyclosporine with concomitant rifampin administration is markedly less than predicted by hepatic enzyme induction, *Clin. Pharmacol. Ther.* 52 (5) (1992) 453–457.
- [126] J.H. Lin, CYP induction-mediated drug interactions: in vitro assessment and clinical implications, *Pharm. Res.* 23 (6) (2006) 1089–1116.
- [127] J. Hukkanen, Induction of cytochrome P450 enzymes: a view on human in vivo findings, *Expert. Rev. Clin. Pharmacol.* 5 (5) (2012) 569–585.
- [128] L. Drocourt, et al., Calcium channel modulators of the dihydropyridine family are human pregnane X receptor activators and inducers of CYP3A, CYP2B, and CYP2C in human hepatocytes, *Drug Metab. Dispos.* 29 (10) (2001) 1325–1331.
- [129] W. El-Sankary, et al., Use of a reporter gene assay to predict and rank the potency and efficacy of CYP3A4 inducers, *Drug Metab. Dispos.* 29 (11) (2001) 1499–1504.
- [130] S.R. Faucette, et al., Relative activation of human pregnane X receptor versus constitutive androstane receptor defines distinct classes of CYP2B6 and CYP3A4 inducers, *J. Pharmacol. Exp. Ther.* 320 (1) (2007) 72–80.
- [131] P. Honkakoski, T. Sueyoshi, M. Negishi, Drug-activated nuclear receptors CAR and PXR, *Ann. Med.* 35 (3) (2003) 172–182.
- [132] M. Kato, et al., The quantitative prediction of in vivo enzyme-induction caused by drug exposure from in vitro information on human hepatocytes, *Drug Metab. Pharmacokinet.* 20 (4) (2005) 236–243.
- [133] W. Li, et al., Regulation of cytochrome P450 enzymes by aryl hydrocarbon receptor in human cells: CYP1A2 expression in the LS180 colon carcinoma cell line after treatment with 2,3,7,8-tetrachlorodibenzo-p-dioxin or 3-methylcholanthrene, *Biochem. Pharmacol.* 56 (5) (1998) 599–612.
- [134] C. Xu, C.Y. Li, A.N. Kong, Induction of phase I, II and III drug metabolism/transport by xenobiotics, *Arch. Pharm. Res.* 28 (3) (2005) 249–268.
- [135] B. Goodwin, E. Hodgson, C. Liddle, The orphan human pregnane X receptor mediates the transcriptional activation of CYP3A4 by rifampicin through a distal enhancer module, *Mol. Pharmacol.* 56 (6) (1999) 1329–1339.
- [136] J.M. Lehmann, et al., The human orphan nuclear receptor PXR is activated by compounds that regulate CYP3A4 gene expression and cause drug interactions, *J. Clin. Invest.* 102 (5) (1998) 1016–1023.
- [137] L.B. Moore, et al., Orphan nuclear receptors constitutive androstane receptor and pregnane X receptor share xenobiotic and steroid ligands, *J. Biol. Chem.* 275 (20) (2000) 15122–15127.
- [138] T. Sueyoshi, et al., The repressed nuclear receptor CAR responds to phenobarbital in activating the human CYP2B6 gene, *J. Biol. Chem.* 274 (10) (1999) 6043–6046.
- [139] S. Chen, K. Wang, Y.J. Wan, Retinoids activate RXR/CAR-mediated pathway and induce CYP3A, *Biochem. Pharmacol.* 79 (2) (2010) 270–276.
- [140] S.S. Ferguson, et al., Human CYP2C8 is transcriptionally regulated by the nuclear receptors constitutive androstane receptor, pregnane X receptor, glucocorticoid receptor, and hepatic nuclear factor 4 $\alpha$ , *Mol. Pharmacol.* 68 (3) (2005) 747–757.
- [141] S. Gerbal-Chaloin, et al., Transcriptional regulation of CYP2C9 gene. Role of glucocorticoid receptor and constitutive androstane receptor, *J. Biol. Chem.* 277 (1) (2002) 209–217.
- [142] E. Higashi, et al., Human CYP2A6 is induced by estrogen via estrogen receptor, *Drug Metab. Dispos.* 35 (10) (2007) 1935–1941.

- [143] S. Hogstedt, B. Lindberg, A. Rane, Increased oral clearance of metoprolol in pregnancy, *Eur. J. Clin. Pharmacol.* 24 (2) (1983) 217–220.
- [144] T.S. Tracy, et al., Temporal changes in drug metabolism (CYP1A2, CYP2D6 and CYP3A Activity) during pregnancy, *Am. J. Obstet. Gynecol.* 192 (2) (2005) 633–639.
- [145] G.S. Grover, et al., Development of in vitro methods to predict induction of CYP1A2 and CYP3A4 in humans, *Assay Drug Dev. Technol.* 5 (6) (2007) 793–804.
- [146] K.P. Persson, et al., Evaluation of human liver slices and reporter gene assays as systems for predicting the cytochrome p450 induction potential of drugs in vivo in humans, *Pharm. Res.* 23 (1) (2006) 56–69.
- [147] D.F. McGinnity, et al., Evaluation of multiple in vitro systems for assessment of CYP3A4 induction in drug discovery: human hepatocytes, pregnane X receptor reporter gene, and Fa2N-4 and HepaRG cells, *Drug Metab. Dispos.* 37 (6) (2009) 1259–1268.
- [148] M. Sinz, G. Wallace, J. Sahi, Current industrial practices in assessing CYP450 enzyme induction: preclinical and clinical, *AAPS J.* 10 (2) (2008) 391–400.
- [149] O.A. Fahmi, et al., Cytochrome P450 3A4 mRNA is a more reliable marker than CYP3A4 activity for detecting pregnane X receptor-activated induction of drug-metabolizing enzymes, *Drug Metab. Dispos.* 38 (9) (2010) 1605–1611.
- [150] S.L. Ripp, et al., Use of immortalized human hepatocytes to predict the magnitude of clinical drug-drug interactions caused by CYP3A4 induction, *Drug Metab. Dispos.* 34 (10) (2006) 1742–1748.
- [151] T.B. Andersson, K.P. Kanebratt, J.G. Kenna, The HepaRG cell line: a unique in vitro tool for understanding drug metabolism and toxicology in human, *Expert Opin. Drug Metab. Toxicol.* 8 (7) (2012) 909–920.
- [152] C. Aninat, et al., Expression of cytochromes P450, conjugating enzymes and nuclear receptors in human hepatoma HepaRG cells, *Drug Metab. Dispos.* 34 (1) (2006) 75–83.
- [153] K.P. Kanebratt, T.B. Andersson, Evaluation of HepaRG cells as an in vitro model for human drug metabolism studies, *Drug Metab. Dispos.* 36 (7) (2008) 1444–1452.
- [154] H.J. Einolf, et al., Evaluation of various static and dynamic modeling methods to predict clinical CYP3A induction using in vitro CYP3A4 mRNA induction data, *Clin. Pharmacol. Ther.* 95 (2) (2014) 179–188.
- [155] M. Rowland, S. Matin, Kinetics of drug-drug interactions, *J. Pharmacokinet. Biopharm.* 1 (6) (1973) 553–567.
- [156] U.S. Food and Drug Administration, In Vitro Metabolism- and Transporter- Mediated Drug-Drug Interaction Studies Guidance for Industry, Available from: <https://www.fda.gov/regulatory-information/search-fda-guidance-documents/vitro-metabolism-and-transporter-mediated-drug-drug-interaction-studies-guidance-industry>, 2017.
- [157] European Medicines Agency, Guideline on the Investigation of Drug Interactions, 2012.
- [158] M.L. Vieira, et al., Evaluation of various static in vitro-in vivo extrapolation models for risk assessment of the CYP3A inhibition potential of an investigational drug, *Clin. Pharmacol. Ther.* 95 (2) (2014) 189–198.
- [159] H.S. Brown, et al., Prediction of in vivo drug-drug interactions from in vitro data: impact of incorporating parallel pathways of drug elimination and inhibitor absorption rate constant, *Br. J. Clin. Pharmacol.* 60 (5) (2005) 508–518.
- [160] K. Ito, et al., Impact of parallel pathways of drug elimination and multiple cytochrome P450 involvement on drug-drug interactions: CYP2D6 paradigm, *Drug Metab. Dispos.* 33 (6) (2005) 837–844.
- [161] K. Ito, et al., Prediction of pharmacokinetic alterations caused by drug-drug interactions: metabolic interaction in the liver, *Pharmacol. Rev.* 50 (3) (1998) 387–412.
- [162] R.S. Obach, et al., The utility of in vitro cytochrome P450 inhibition data in the prediction of drug-drug interactions, *J. Pharmacol. Exp. Ther.* 316 (1) (2006) 336–348.
- [163] S. Kanamitsu, K. Ito, Y. Sugiyama, Quantitative prediction of in vivo drug-drug interactions from in vitro data based on physiological pharmacokinetics: use of maximum unbound concentration of inhibitor at the inlet to the liver, *Pharm. Res.* 17 (3) (2000) 336–343.
- [164] R.S. Obach, The importance of nonspecific binding in in vitro matrices, its impact on enzyme kinetic studies of drug metabolism reactions, and implications for in vitro-in vivo correlations, *Drug Metab. Dispos.* 24 (10) (1996) 1047–1049.
- [165] L.M. Berezhkovskiy, Volume of distribution at steady state for a linear pharmacokinetic system with peripheral elimination, *J. Pharm. Sci.* 93 (6) (2004) 1628–1640.
- [166] L.M. Berezhkovskiy, Determination of volume of distribution at steady state with complete consideration of the kinetics of protein and tissue binding in linear pharmacokinetics, *J. Pharm. Sci.* 93 (2) (2004) 364–374.

- [167] S. Willmann, J. Lippert, W. Schmitt, From physicochemistry to absorption and distribution: predictive mechanistic modelling and computational tools, *Expert Opin. Drug Metab. Toxicol.* 1 (1) (2005) 159–168.
- [168] R.S. Obach, Nonspecific binding to microsomes: impact on scale-up of in vitro intrinsic clearance to hepatic clearance as assessed through examination of warfarin, imipramine, and propranolol, *Drug Metab. Dispos.* 25 (12) (1997) 1359–1369.
- [169] R.S. Obach, Prediction of human clearance of twenty-nine drugs from hepatic microsomal intrinsic clearance data: an examination of in vitro half-life approach and nonspecific binding to microsomes, *Drug Metab. Dispos.* 27 (11) (1999) 1350–1359.
- [170] M. Chiba, Y. Ishii, Y. Sugiyama, Prediction of hepatic clearance in human from in vitro data for successful drug development, *AAPS J.* 11 (2) (2009) 262–276.
- [171] R.S. Foti, M.B. Fisher, Impact of incubation conditions on bufuralol human clearance predictions: enzyme lability and nonspecific binding, *Drug Metab. Dispos.* 32 (3) (2004) 295–304.
- [172] C.S. Ernest 2nd, S.D. Hall, D.R. Jones, Mechanism-based inactivation of CYP3A by HIV protease inhibitors, *J. Pharmacol. Exp. Ther.* 312 (2) (2005) 583–591.
- [173] Y.H. Wang, D.R. Jones, S.D. Hall, Prediction of cytochrome P450 3A inhibition by verapamil enantiomers and their metabolites, *Drug Metab. Dispos.* 32 (2) (2004) 259–266.
- [174] C.Y.S. Chan, et al., Derivation of CYP3A4 and CYP2B6 degradation rate constants in primary human hepatocytes: A siRNA-silencing-based approach, *Drug Metab. Pharmacokinet.* 33 (4) (2018) 179–187.
- [175] M.F. Fromm, et al., Differential induction of prehepatic and hepatic metabolism of verapamil by rifampin, *Hepatology* 24 (4) (1996) 796–801.
- [176] A. Hsu, et al., Multiple-dose pharmacokinetics of ritonavir in human immunodeficiency virus-infected subjects, *Antimicrob. Agents Chemother.* 41 (5) (1997) 898–905.
- [177] L. Pichard, et al., Effect of corticosteroids on the expression of cytochromes P450 and on cyclosporin A oxidase activity in primary cultures of human hepatocytes, *Mol. Pharmacol.* 41 (6) (1992) 1047–1055.
- [178] A.B. Renwick, et al., Differential maintenance of cytochrome P450 enzymes in cultured precision-cut human liver slices, *Drug Metab. Dispos.* 28 (10) (2000) 1202–1209.
- [179] A. Rostami-Hodjegan, et al., Population pharmacokinetics of methadone in opiate users: characterization of time-dependent changes, *Br. J. Clin. Pharmacol.* 48 (1) (1999) 43–52.
- [180] R.H. Takahashi, et al., Applying stable isotope labeled amino acids in micropatterned hepatocyte coculture to directly determine the degradation rate constant for CYP3A4, *Drug Metab. Dispos.* 45 (6) (2017) 581–585.
- [181] C. von Bahr, et al., Time course of enzyme induction in humans: effect of pentobarbital on nortriptyline metabolism, *Clin. Pharmacol. Ther.* 64 (1) (1998) 18–26.
- [182] L.M. Almond, et al., Towards a quantitative framework for the prediction of DDIs arising from cytochrome P450 induction, *Curr. Drug Metab.* 10 (4) (2009) 420–432.
- [183] O.A. Fahmi, et al., Prediction of drug-drug interactions from in vitro induction data: application of the relative induction score approach using cryopreserved human hepatocytes, *Drug Metab. Dispos.* 36 (9) (2008) 1971–1974.
- [184] O.A. Fahmi, et al., A combined model for predicting CYP3A4 clinical net drug-drug interaction based on CYP3A4 inhibition, inactivation, and induction determined in vitro, *Drug Metab. Dispos.* 36 (8) (2008) 1698–1708.
- [185] M.F. Paine, et al., First-pass metabolism of midazolam by the human intestine, *Clin. Pharmacol. Ther.* 60 (1) (1996) 14–24.
- [186] D.D. Shen, K.L. Kunze, K.E. Thummel, Enzyme-catalyzed processes of first-pass hepatic and intestinal drug extraction, *Adv. Drug Deliv. Rev.* 27 (2-3) (1997) 99–127.
- [187] K.E. Thummel, Gut instincts: CYP3A4 and intestinal drug metabolism, *J. Clin. Invest.* 117 (11) (2007) 3173–3176.
- [188] O. von Richter, et al., Cytochrome P450 3A4 and P-glycoprotein expression in human small intestinal enterocytes and hepatocytes: a comparative analysis in paired tissue specimens, *Clin. Pharmacol. Ther.* 75 (3) (2004) 172–183.
- [189] O.A. Fahmi, et al., Comparison of different algorithms for predicting clinical drug-drug interactions, based on the use of CYP3A4 in vitro data: predictions of compounds as precipitants of interaction, *Drug Metab. Dispos.* 37 (8) (2009) 1658–1666.
- [190] K.E. Thummel, D.D. Shen, N. Isoherranen, Role of the gut mucosa in metabolically based drug-drug interactions, in: A.D. Rodrigues (Ed.), *Drug-Drug Interactions*, Informa Healthcare USA, New York, 2008, pp. 471–513.



- [191] B.J. Kirby, et al., Complex drug interactions of HIV protease inhibitors 2: in vivo induction and in vitro to in vivo correlation of induction of cytochrome P450 1A2, 2B6, and 2C9 by ritonavir or nelfinavir, *Drug Metab. Dispos.* 39 (12) (2011) 2329–2337.
- [192] B.J. Kirby, et al., Complex drug interactions of HIV protease inhibitors 1: inactivation, induction, and inhibition of cytochrome P450 3A by ritonavir or nelfinavir, *Drug Metab. Dispos.* 39 (6) (2011) 1070–1078.
- [193] J. Yu, et al., Mechanisms and clinical significance of pharmacokinetic-based drug-drug interactions with drugs approved by the U.S. Food and Drug Administration in 2017, *Drug Metab. Dispos.* 47 (2) (2019) 135–144.
- [194] J. Yu, et al., Risk of clinically relevant pharmacokinetic-based drug-drug interactions with drugs approved by the U.S. Food and Drug Administration between 2013 and 2016, *Drug Metab. Dispos.* 46 (6) (2018) 835–845.
- [195] S.M. Huang, et al., Drug interaction studies: study design, data analysis, and implications for dosing and labeling, *Clin. Pharmacol. Ther.* 81 (2) (2007) 298–304.
- [196] R.F. Frye, et al., Validation of the five-drug “Pittsburgh cocktail” approach for assessment of selective regulation of drug-metabolizing enzymes, *Clin. Pharmacol. Ther.* 62 (4) (1997) 365–376.
- [197] D.S. Streetman, et al., Combined phenotypic assessment of CYP1A2, CYP2C19, CYP2D6, CYP3A, N-acetyltransferase-2, and xanthine oxidase with the “Cooperstown cocktail” *Clin. Pharmacol. Ther.* 68 (4) (2000) 375–383.
- [198] C. Dutreix, S. Lorenzo, Y. Wang, Comparison of two endogenous biomarkers of CYP3A4 activity in a drug-drug interaction study between midostaurin and rifampicin, *Eur. J. Clin. Pharmacol.* 70 (8) (2014) 915–920.
- [199] L. Bjorkhem-Bergman, et al., Comparison of endogenous 4beta-hydroxycholesterol with midazolam as markers for CYP3A4 induction by rifampicin, *Drug Metab. Dispos.* 41 (8) (2013) 1488–1493.
- [200] K. Bodin, et al., Antiepileptic drugs increase plasma levels of 4beta-hydroxycholesterol in humans: evidence for involvement of cytochrome p450 3A4, *J. Biol. Chem.* 276 (42) (2001) 38685–38689.
- [201] U. Diczfalusy, et al., 4beta-Hydroxycholesterol, an endogenous marker of CYP3A4/5 activity in humans, *Br. J. Clin. Pharmacol.* 71 (2) (2011) 183–189.
- [202] M.M. Galteau, F. Shamsa, Urinary 6beta-hydroxycortisol: a validated test for evaluating drug induction or drug inhibition mediated through CYP3A in humans and in animals, *Eur. J. Clin. Pharmacol.* 59 (10) (2003) 713–733.
- [203] X. Jiang, et al., An exposure-response modeling approach to examine the relationship between potency of CYP3A inducer and plasma 4beta-hydroxycholesterol in healthy subjects, *Clin. Pharmacol. Drug Dev.* 6 (1) (2017) 19–26.
- [204] B.C. Jones, et al., Managing the risk of CYP3A induction in drug development: a strategic approach, *Drug Metab. Dispos.* 45 (1) (2017) 35–41.
- [205] K.H. Shin, et al., Urinary 6beta-hydroxycortisol/cortisol ratio most highly correlates with midazolam clearance under hepatic CYP3A inhibition and induction in females: a pharmacometabolomics approach, *AAPS J.* 18 (5) (2016) 1254–1261.
- [206] K.H. Shin, et al., Evaluation of endogenous metabolic markers of hepatic CYP3A activity using metabolic profiling and midazolam clearance, *Clin. Pharmacol. Ther.* 94 (5) (2013) 601–609.
- [207] J. Yu, et al., Key findings from preclinical and clinical drug interaction studies presented in new drug and biological license applications approved by the Food and Drug Administration in 2014, *Drug Metab. Dispos.* 44 (1) (2016) 83–101.

# Role of transporters in drug disposition and drug-drug interactions

*Xiaomin Liang, Kelly MacLennan Staiger, Ellen Riddle,  
Jia Hao, Yurong Lai*

Drug Metabolism, Gilead Sciences Inc, Foster City, CA, United States

## 1 Introduction

Transporters are cellular membrane proteins that are broadly expressed through our bodies and function as shuttles for many endogenous and exogenous substances (i.e., amino acids, fatty acids, hormones, bile acids, xenobiotics, and toxicants) either into (influx/uptake) or out of (efflux) organ and tissue barriers. Membrane transporters facilitate the transport of endogenous substances and drugs across cellular membranes in different tissues in which absorption, distribution, metabolism, excretion (ADME), and biological/pharmacological action occur. Considering the number of drugs that share substrate specificity with metabolizing enzymes, such as cytochrome P450s (CYPs) and uridine 5'-diphospho-glucuronosyltransferase (UGTs), it is clear that transporters are important to the overall metabolism of drugs by either providing it access to intracellular enzymes or excreting the drug and its metabolites and conjugates [1,2]. Drugs can be substrates and/or modulators that inhibit or induce transporter function. Alteration of transporter functions by inhibitors or inducers can result in clinical victims or perpetrators of drug-drug interactions (DDIs). As a result, drug transporters have a great impact on drug disposition, efficacy, and interaction with other drugs [3]. Understanding clinically relevant DDIs for the concomitant use of multiple medications is an integral part of risk assessment in drug development [4,5]. Consequently, regulatory agencies provide guidelines with proposed decision trees to assess DDI potentials for drug labeling [3–13]. For the evaluation of investigational drug products, currently the United States Food and Drug Administration (US FDA) guidelines have recommended the evaluation of P-glycoprotein [P-gp or multidrug resistance 1 (MDR1) protein], breast cancer resistance protein (BCRP), organic anion transporting



polypeptide 1B1/1B3 (OATP1B1/OATP1B3), organic anion transporter 1/3 (OAT1/OAT3), organic cation transporter 2 (OCT2), and multidrug and toxin extrusion 1/2-K (MATE1/MATE2-K) proteins [14]. In addition, EMA guidance suggests evaluating organic cation transporter 1 (OCT1) and the bile salt export protein (BSEP) [15]. For the scope of this chapter, we will focus on transporters that have shown evidence of affecting drug disposition or causing clinical DDIs. The objectives are to review the current challenges and limitations of transporter DDI assessment, provide information on the state-of-the-art transporter *in vitro*/*in vivo* tools that have been developed to support clinical DDI evaluation, and discuss the regulatory landscape of evaluating transporter-mediated DDIs. Additionally, *in vitro* and *in vivo* tools to assess transporter liability and various ways of handling potential DDIs in clinical practice are described and exemplified in relation to drugs interacting with drug transporters.

## 2 Overview of membrane transporters

Over 450 human drug transporters have been identified and classified into two superfamilies—the ATP-binding cassette (ABC) proteins and solute carrier (SLC) proteins [3,16–18]. Membrane transporters are expressed ubiquitously throughout the body but can be found predominately at the barrier surface of organ tissues and cells, such as the kidney, liver, brain, placenta, and gastrointestinal tract (Fig. 1). Age, gender, ethnicity, genetic variation, protein abundance, membrane localization, disease state, and treatment with concomitant drugs each play a role in the overall functional activities of these proteins.

### 2.1 The ATP-binding cassette superfamily

The ABC superfamily of transporters, named as such because the proteins actively hydrolyze adenosine triphosphate (ATP) during the translocation process, encodes 49 protein members in the human genome, and is grouped into seven subfamilies—ABCA through ABCG [17,19,20]. The most relevant ABC transporters to the understanding of efficacy and toxicity of drugs include P-glycoprotein (P-gp/MDR1/ABCB1), breast cancer resistance protein (BCRP/ABCG2), the multidrug resistance proteins (MRPs/ABCCs), and the bile salt export protein (BSEP/ABCB11) [21]. In eukaryotes, ABC transporters are protective and responsible for the efflux of harmful substances from intracellular to extracellular spaces. These superfamily members can transport vast and diverse substrates including lipids, drugs, and metabolic products. Genomic mutations (polymorphisms), as well as drug-induced or disease-progression changes affecting transporter regulation, can occur. These alterations can make the protein less efficient (either change the binding affinity or downregulate protein expression) at clearing a toxic compound, which can lead to the accumulation of drugs and damage to tissues. Conversely, when the protein expression is induced (upregulated), an increase in transport function can be observed, thereby, decreasing the amount of drug transported through cellular barriers, making it less bioavailable.

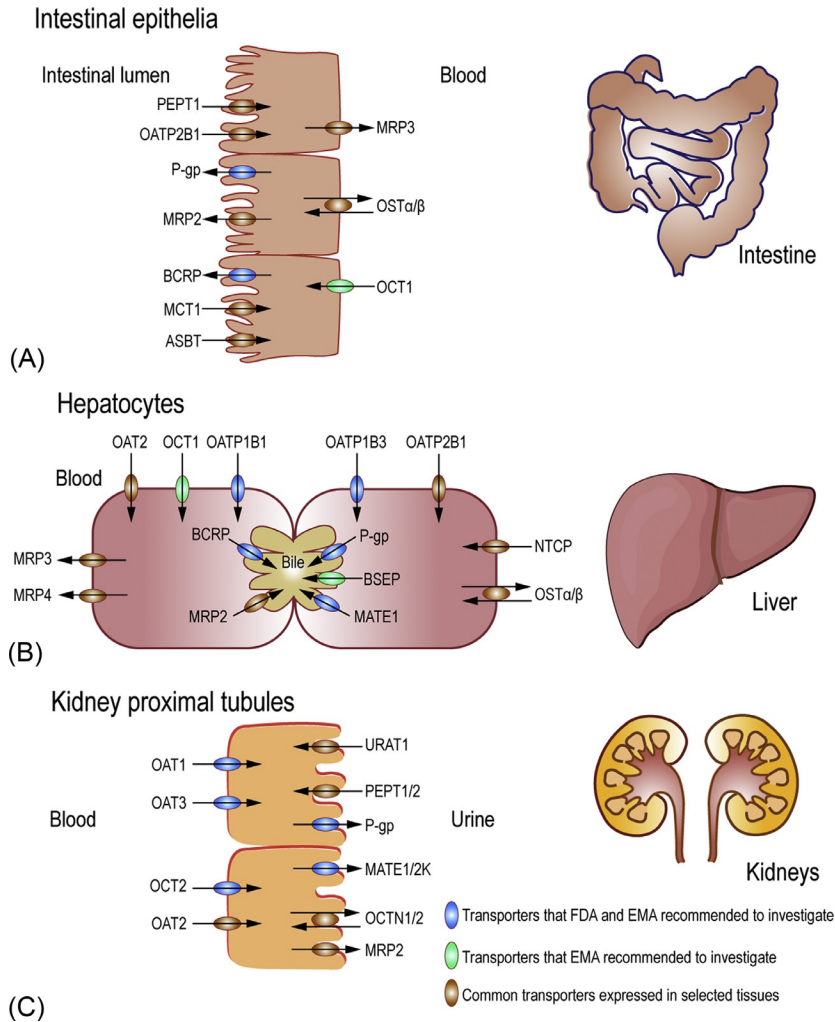


**FIG. 1** Drug transporter expressions in enterocytes (A), hepatocytes (B) and kidney proximal tubular cells (C). Transporters are highlighted based on clinical relevance to drug-drug interactions, organ toxicity or efficacy. Transporters that are recommended for evaluation in the FDA and EMA guidance on drug interactions are marked with *blue circles*. Transporters that are recommended by EMA for investigation in drug development are marked with *green circles*. Transporters that are involved in drug transport in the organ are marked with *brown circles*. *PEPT*, peptide transporter; *MCT*, monocarboxylate transporter; *ASBT*, apical sodium-dependent bile acid transporter; *OST $\alpha/\beta$* , the organ solute transporter alpha and beta; *OCTN*, organic zwitterions/cation transporters; *URAT*, urate transporter; *OAT*, organic anion transporter; *OATP*, organic anion transporting polypeptide; *OCT*, organic cation transporter; *P-gp*, p-glycoprotein; *MATE*, multidrug and toxin extrusion protein; *MRP*, multidrug resistance protein; *PEPT*, peptide transporter.

### 2.1.1 P-glycoprotein

P-gp encoded by the ABCB1 (MDR1) gene, consists of 1276–1280 amino acids and has an approximate molecular mass of 170kDa [20]. P-gp is one of the most studied and well understood ABC transporters. Members of the ABC superfamily are characterized by two nucleotide-binding domains (NBD) and two transmembrane domains (TMD) that undergo conformational changes via ATP-hydrolysis to actively pump molecules out of the intracellular space [22]. Found in most major organs in the apical/luminal membrane, P-gp has broad substrate specificity. Expressed along the intestinal tract from the duodenum to the rectum, P-gp is located on the brush-boarder (luminal) membrane [23–25]. The high protein expression of P-gp in enterocytes of the small intestine, increasing in expression from the duodenum to the ileum then decreasing in the colon, suggest that in the gastrointestinal tract these transporters are responsible for limiting the absorption of drug substrates into the bloodstream [21,23]. In elimination organs, such as the liver and kidney, P-gp functions to excrete substrate drugs, and their metabolites, into the bile or urine, respectively, allowing the drug to be detoxified within the organs and then cleared from the body. P-gp is also found at the blood-brain barrier (BBB) where it protects the brain from the entry of many harmful compounds. Substrates of P-gp cover multiple therapeutic areas such as cardiovascular drugs and anticoagulants (digoxin, ambrisentan, talinolol), anticancer and immunomodulatory agents (irinotecan, imatinib, vinblastine), infectious disease agents (clarithromycin, cobicistat, ritonavir), and metabolic diseases (statins) to name just a few [20,21]. The use of inhibitors, such as cyclosporin A (CsA), can impede P-gp efflux, allowing for improved bioavailability in the gut and higher systemic exposure, which in some cases may be deemed beneficial. In recent years, knowledge of how to harness the intrinsic capabilities of metabolizing enzymes and P-gp efflux modulation has led to intelligently designed drugs, such as cobicistat (COBI), a pharmacoenhancer, which boost the intestinal absorption of antiretroviral drugs [26]. Inhibition of efflux at the site of elimination organs, however, can cause accumulation of a drug, or its metabolites and conjugates, leading to toxicity within the cell or organ. It is important to note that, a given drug may be a substrate, an inhibitor, or an inducer of P-gp. In some complicated cases, the drug is all three, as exemplified by ritonavir and tipranavir.

### 2.1.2 BCRP

BCRP, a 655 amino acid protein, is one of five ABCG subfamily members, all of which are half-transporters, which are believed to function as homo- or heterodimers [19,27]. Noteworthy to the ABCG subfamily, is that the nucleotide-binding domain (NBD) is N-terminal to the transmembrane domain (TMD) which is the reverse of the other transporters within the ABC superfamily [19,28]. Members of the ABCG family are all considered lipid transporters, except BCRP, making it unique within its class [19]. BCRP is expressed not only in cancer cells, but along the brush border of the intestinal tract epithelium, at the bile canalicular membrane of the liver, in the kidney proximal tubule epithelium, brain capillary endothelial cell membranes at the BBB, as well as sex-based organs—at the interstitial cells of the testis, placental syncytiotrophoblasts, and lactiferous ducts of the mammary gland [19,21,29]. There is a significant overlap in substrate specificity between P-gp and BCRP transporters including statins, agents against infectious diseases (antivirals and antibiotics), as well as anticancer drugs. The magnitude of inhibition for each transporter or both is determined by the  $f_t$

(fractional contribution of a particular pathway to overall transport pathways). If the  $f_t$  is low (e.g.,  $<0.5$ ), the consequences are minor (less than two-fold). If the  $f_t$  is high (e.g.,  $>0.9$ ), the effect of inhibition is significant (at least 10-fold change) [30,31]. However, the kinetic behavior of BCRP substrates suggests that there may be multiple binding sites on the transporter [19,28]. Substrates which share a common binding site within the BCRP homodimer include doxorubicin, prazosin, and daunomycin, while methotrexate binds to a second distinct site [19,32]. BCRP is also responsible for the biliary excretion of many sulfate conjugates, fluoroquinolones, as well as the drugs rosuvastatin and nitrofurantoin [19]. Inhibitors of BCRP which have shown clinical interaction are curcumin, lapatinib, pantoprazole, elacridar, rolapitant, and febuxostat [21,28,29,33]. In addition, a few polymorphisms of ABCG2 (e.g., Q141K, F489L, and N590Y) have been identified. Clinical studies showed that Q141K polymorphism affected rosuvastatin exposure [34–36].

### 2.1.3 Multidrug resistance proteins

The multidrug resistance proteins (MRPs/ABCCs) encoded by the human genes ABCC1-ABCC6 and ABCC10-ABCC12 consist of nine MRP proteins (MRP1-MRP9) [37]. Noteworthy to drug disposition, MRP2 (ABCC2) is responsible for the excretion of many phase II metabolites of drugs and conjugated bile acids into the bile and urine. The MRP2 transporter is highly expressed on the apical membrane of hepatocytes in the liver, proximal tubular cells in the kidney, and enterocytes of the small intestine [37–39]. MRP2 substrates include methotrexate, melphalan, and pravastatin [37,40]. Genetic variants in the ABCC2 gene leading to loss of the MRP2 protein expression or function have been identified and recognized as the molecular basis of Dubin-Johnson syndrome [41–43]. The syndrome represents mild, predominantly conjugated hyperbilirubinemia. Subjects homozygous for the H2 (1249G[A]) genotype or heterozygous for H2 and H1 (wild-type) genotype of the ABCC2 gene, which results in increased MRP2 activity, have shown a significantly lower dose-normalized concentration of tacrolimus compared to the MRP2 low-activity group and reference group [44]. The mechanism underlying the observed changes in the pharmacokinetics of tacrolimus likely involves MRP2 efflux of the drug or its metabolites in the small intestine [44].

### 2.1.4 Bile salt export protein

The bile salt export protein (BSEP/ABCB11) is encoded by ABCB11 gene with 27 coding exons and belongs to the ATP-binding cassette transporter family similar to P-gp (ABCB1). The transporter is exclusively expressed in the liver on the canalicular membrane of hepatocytes and is responsible for bile salt-dependent flow. BSEP is a critical component in the elimination of monovalent bile acids, including taurine and glycine conjugates, the primary bile acids—cholic acid and chenodeoxycholic acid, as well as the secondary bile acid deoxycholic acid [45]. ABCB11 gene polymorphisms leading to reduced or even absent expression of canalicular BSEP were found to be associated with the familial intrahepatic cholestasis type 2 (PFIC-2) or benign recurrent intrahepatic cholestasis (BRIC) [46,47]. In addition to endogenous bile salts, BSEP has been shown to export pravastatin, vinblastine, and fexofenadine [48,49]. Inhibitors of BSEP include rifampin, CsA, vinblastine, troglitazone, as well as several statins and antiretrovirals [48,49]. Several other drugs such as bosentan and nefazodone are BSEP inhibitors [50]. Inhibition of BSEP can be attributed to a cholestatic form of drug-induced liver injury (DILI) [45,51].

## 2.2 The solute carrier protein superfamily

SLC membrane proteins, which make up the second superfamily of 395 identified human transporters, are primarily, but not exclusively, uptake transporters. The most relevant SLC transporters to drug disposition and DDIs include the organic anion transporting polypeptides (OATP/SLCOs), organic anion transporters and organic cation transporters (OAT and OCT/SLC22s), and multidrug and toxin extrusion transporters (MATE/SLC47s). A highly diverse superfamily, SLC transporters show structural fold differences which have been suggested to not be evolutionarily related, yet can have similar chemical substrates [52]. Members of the SLC family are antiporters, cotransporters, symporters, or ion exchangers. Facilitative or secondary-active transporters rely either on an electrochemical gradient to facilitate the movement of other substrates across membranes or the ion gradients generated by ATP-dependent pumps to transport substrates against the gradient. OAT1 is an example of a tertiary-active transporter which utilizes the energy generated and stored by secondary-active transporters to move substances against a concentration gradient [53].

### 2.2.1 Organic anion transporting polypeptides

OATP1B1/1B3 (SLCO1B1 and SLCO1B3) are reported to be exclusively expressed in the liver, localized on the basolateral/sinusoidal membranes of hepatocytes [54]. These proteins are responsible for the uptake of endogenous substrates and many structurally diversified xenobiotics from the bloodstream into the liver. OATP1B1, the more predominant of the transporters, is expressed throughout the liver, while OATP1B3 is described as focused near the central vein [54,55]. OATP1B can directly affect drug-disposition and cause DDIs. Active uptake of preferential OATP1B substrates can confer an increase of hepatic extraction and intracellular liver concentrations of drugs or their metabolites. For drugs that require access to hepatic metabolizing enzymes or additional efflux transporters to complete their route of elimination, OATP-mediated transport may be rate limiting to the clearance of the compounds. Recently, an extended clearance model in which transporter-mediated clearance is incorporated is used to predict overall hepatic clearance [56–58]. More details in the extended clearance model and its application are included in other chapters. When OATP1B transport is inhibited or reduced, increases in systemic drug exposure can often be observed, at times with deleterious effects. Similarly, it has been reported that individuals with reduced OATP gene expression have higher plasma levels of endogenous substrates—such as tetradecanedioic acid (TDA), hexadecanedioic acid (HDA), and coproporphyrin I/III [59]. Because these substrates are in vivo endogenous biomarkers for OATP functional activities, monitoring their levels during first-in-man trials could elucidate the potential of OATP inhibition DDIs [60–62]. As a result, the evaluation of selectivity and sensitivity of endogenous biomarkers in humans is underway. Since hepatic OATP1B transporters are also responsible for the influx of conjugated bilirubin, hyperbilirubinemia and jaundice have been associated with polymorphic individuals that have reduced or loss of OATP1B1 and 1B3 function [63]. Individuals with polymorphisms that exhibit reduced function variants of the SLCO1B1 gene, such as OATP1B1-Val174Ala (SLCO1B1 c.521T>C), have been shown to display increased levels of OATP1B1 drug substrates, such as statins or repaglinide, in systemic circulation [64]. The total loss of OATP1B1 and 1B3 functional uptake has resulted in the rare, yet benign, disease Rotor syndrome [63]. While OATP1B3 inhibition has shown clinical DDIs, such as

with telmisartan, there has been no consistency in reported outcomes for OATP1B3 polymorphisms to conclude a clinical impact [65,66].

In contrast to OATP1B1/1B3, OATP2B1 (SLCO2B1) has a broader tissue expression. OATP2B1 can transport many clinically used drugs including fexofenadine, atorvastatin, and rosuvastatin, which largely overlap with the substrate specificity of OATP1B1 and 1B3. OATP2B1 is the intestinal OATP transporter that was previously annotated as OATP1A2 [16,23]. In vivo evidence supports that OATP2B1 is a major intestinal transporter attributed to DDIs with fruit juice [67]. OATP2B1 is also believed to play a significant role in intestinal absorption [65,68]. In the liver, the proteomic data showed that the expression of OATP2B1 is comparable to OATP1B3 [69,70]. As such, it is thought that OATP2B1 may play a significant role in hepatic uptake for its substrates. Due to the lack of a specific inhibitor or clinically relevant OATP2B1 gene polymorphisms, OATP2B1 has not yet been proven to play a major role in hepatic drug uptake, nor does it clearly cause any OATP2B1 DDI [71]. Future studies are warranted to determine the  $f_t$  of OATP transporters.

### 2.2.2 Organic anion transporters

OAT1 and OAT3 (SLC22A6 and SLC22A8) show the highest expression at the basolateral membrane of renal proximal tubules and are responsible for the uptake of drugs from the bloodstream into the kidney for either metabolic processing or elimination into the urine [61,72]. OAT1 and OAT3, considered tertiary active transporters, are reported to transport mainly low-molecular-weight hydrophilic anionic compounds—including agents against infectious diseases (antibiotics and antivirals), diuretics, statins, anticancer agents, antihypertensives, and nonsteroidal anti-inflammatory drugs—against a negative membrane potential in exchange for  $\alpha$ -ketoglutarate [65,73]. Polymorphisms in OAT1 and/or OAT3 have been reported in association with mercury toxicity or, in Asian populations, reduced renal clearance of drugs such as cefotaxime [73,74].

### 2.2.3 Organic cation transporters

OCT1, OCT2, and OCT3 (SLC22A1, SLC22A2, and SLC22A3) mediate the facilitative diffusion of organic cations via an electrochemical gradient, and thus, can transport molecules in either direction, independent of pH [75]. Under the physiological condition of inside-negative membrane potential, OCTs can facilitate the uptake of their substrates, resulting in a higher intracellular concentration [76,77]. OCT1 is generally considered to be liver specific, located at the basolateral membrane of hepatocytes, while OCT2 is considered to be a renal transporter, mainly expressed at the basolateral surface of the kidney proximal tubule cells [78,79]. In contrast, OCT3 is the most widely distributed of the OCT transporters and is strongly expressed in the liver, kidney, placenta, and skeletal muscle tissues [78,80]. All three OCTs can transport MPP (1-methyl-4-phenylpyridinium), whereas only OCT1 and OCT2 show a good affinity for TEA (tetraethylammonium) [78]. Endogenous substrates of OCTs include choline, creatinine, and guanidine, as well as neurotransmitters and neuromodulators [79,81]. Due to a high overlapping substrate affinity with MATE transporters, OCT2 shares many common substrates and inhibitors: MPP, TEA, cimetidine, antiviral drugs (acyclovir, ganciclovir), metformin, and quinidine, as well as many tropane alkaloids and their derivatives [79,82].



### 2.2.4 Multidrug and toxin extrusion transporters

MATE (SLC47A) transporters include MATE1 (SLC47A1), expressed in the canalicular membrane of hepatocytes as well as the apical/luminal membrane of tubular epithelial cells in the kidney, and MATE2-K (SLC47A2), localized almost exclusively in the apical membrane of kidney tubular cells [79,82]. These efflux transporters often act in antipodal fashion to OCT-mediated uptake, eliminating many drug substrates and their metabolites from the liver into the bile or kidney to urine, respectively. As such, many inhibitors of OCTs can also inhibit MATEs. A careful distinction must be taken in determining if inhibition of uptake or excretion is the rate-limiting step in cases of hepatic or renal toxicity [83,84].

## 3 Clinical significance of transporter-mediated drug disposition and drug-drug interactions

Numerous clinical studies have demonstrated that drug transporters play important roles in altering pharmacokinetics (PK), pharmacodynamics (PD), and organ toxicity of drugs (Fig. 1). Altering transporter expression and activity via drugs, dietary supplements, or genetic factors can affect the PK, PD, and organ exposure of substrates. The importance of understanding transporter-based drug interactions has been discussed by regulatory agencies and introduced in recent FDA DDI guidance documents [14]. P-gp was the first transporter included in the 2006 FDA DDI guidance documents. Since then, transporter-mediated drug-drug interaction studies have increased and more transporters have been shown to have an impact on PK/PD relationships. As mentioned above, the recent FDA DDI guidance published in 2017 recommends the investigation of eight transporters for drug interactions: P-gp, BCRP, MATE1, MATE2K, OATP1B1, OATP1B3, OAT1, OAT3, and OCT2. Representative clinical DDIs are summarized in Table 1.

The P-gp transporter is expressed on the luminal surface of the small intestine and blood-brain barrier, as well as the apical membrane of hepatocytes and kidney proximal tubule epithelia (Fig. 1). P-gp plays an important role in intestinal absorption along with the biliary and urinary excretion of drugs. Therefore, inhibition of P-gp function can potentially increase bioavailability and decrease excretory pathways of P-gp substrates, resulting in an increase of systemic exposure. Generally, most P-gp substrates are organic cations or neutral molecules, and relatively hydrophobic, with molecular masses ranging from 200 Da to greater than 1000 Da [3]. Many P-gp substrates are also metabolized by cytochrome P450s (CYPs), especially CYP3A4 [3,102]. The P-gp substrate, digoxin, is one of the most well characterized drugs in interaction studies due to its narrow therapeutic window. Numerous P-gp inhibitors (e.g., quinidine, ritonavir, and ranolazine) have been shown to increase digoxin plasma exposure in clinical studies [102,103]. In addition, digoxin is devoid of CYP metabolism, therefore changes to digoxin absorption and elimination can be largely attributed to P-gp efflux activity [102]. Due to high oral bioavailability (>60%), digoxin is not sensitive enough to capture the “worse-case” victim DDI potential. Recently, other compounds, such as dabigatran etexilate (DE), have been proposed to use as a P-gp probe substrate. After orally dosing DE, it is converted to dabigatran by carboxylesterase (CES) 2 in the intestine. The oral bioavailability of dabigatran after DE administration is 3%–7%, likely because of low-intestinal absorption of DE limited by P-gp efflux. In this case, DE is a more sensitive probe



**TABLE 1** Selected transporter-mediated clinical drug-drug interactions.

Transporter	Substrate	Interacting drug	% Changes in AUC of substrate (%)	
P-gp	Digoxin	Quinidine	76	[85]
	Digoxin	Ritonavir	47	[86]
	Digoxin	Ranolazine	60	(NDA 021526)
	Fexofenadine	Verapamil	187	[87]
BCRP	Topotecan	Elacridar (GF 120918)	143	[88]
	Rosuvastatin	Osimertinib	34	[89]
	Rosuvastatin	Fostamatinib	96	[90]
OATP1B1/1B3	Pitavastatin	CsA	352	(NDA 022363)
	Pravastatin	CsA	893	[91]
	Bosentan	Lopinavir/ Ritonavir	422	[92]
	Rosuvastatin	Rifampin	367	[93]
OCT2 or MATE1/2K	Metformin	Cimetidine	54	[94]
	Metformin	Pyrimethamine	170	[95]
	Pilsicainide	Cetirizine	36	[96]
	Defetilide	Cimetidine	48	[97]
OAT1/3	Furosemide	Probenecid	223	[98]
	Cidofovir	Probenecid	78	[99]
	Cephadrine	Probenecid	139	[100]
	Adefovir	Probenecid	109	[101]

- Elacridar is used as an oral bio-enhancer but is not an approved drug.
- Inhibitors listed in the table can inhibit multiple transporters. Data interpretation should be cautious.

substrate than digoxin. However, due to its high affinity to P-gp, P-gp transport is saturated under the therapeutic dose of DE, which lowers the DDI sensitivity. Other factors (e.g., larger interindividual PK variability, CES inhibition by the perpetrator, and stability of DE in vitro) should be considered when using DE as a probe in a P-gp DDI study. DE may be a more selective probe than digoxin for the assessment of P-gp-mediated DDIs in the intestine. Clinical digoxin DDI studies with P-gp inhibitors are warranted to ensure safe comedication due to the narrow therapeutic index of digoxin. In clinical DDI studies, P-gp probes should be selected based on the specific DDI questions to be addressed [62].

In addition to P-gp, BCRP expressed in the gastrointestinal (GI) tract, liver, kidney, brain endothelium, mammary tissue, testis, and placenta, also has a role in limiting oral bioavailability and transport of its substrates across the BBB, blood-testis barrier, and the maternal-fetal barrier [3]. Individuals with the reduced function variant (Q141K) of BCRP showed altered PK of 9-aminocamptothecin [104], diflomotecan, irinotecan, rosuvastatin, sulfasalazine, and topotecan [3]. Coadministration of BCRP inhibitor elacridar was shown to increase plasma exposure of topotecan by increasing its GI absorption [88].

The OATP transporter family is responsible for the uptake of a diverse range of amphiphilic organic compounds into hepatocytes. Inhibition of OATP function has been shown to increase plasma exposure by reducing the hepatic uptake clearance of its substrates. As summarized in Table 1, inhibition of OATP-mediated hepatic uptake contributes to the significant increase in plasma concentrations of statins (i.e., rosuvastatin, pravastatin, and pitavastatin) after co-dosing with CsA [3,105]. Metabolically unstable OATP substrates, such as cerivastatin, atorvastatin, repaglinide, or bosentan, were also shown to significantly increase in plasma area under concentration-time curves (AUCs) during coadministration with OATP inhibitors [106–108] (Table 1). In addition, a series of functional polymorphisms of OATP1B1 have been characterized. Pharmacokinetic studies indicate that individuals with reduced function variants, such as SLCO1B1\*5 or \*15 haplotypes, have increased exposure of statin drugs such as pravastatin, pitavastatin, simvastatin acid, atorvastatin, and rosuvastatin [109]. Compelling clinical evidence from both DDIs and genetic polymorphisms support that OATPs play important roles in hepatic clearance and uptake-mediated drug disposition.

Transporters, such as OAT1/3, OCT2, and MATE1/2-K, expressed in the kidney play important roles in the renal elimination of drugs. Inhibition of these renal transporters can lead to increased plasma exposure by reducing renal secretion [110,111]. OAT1 and OAT3 which are expressed on the basolateral membrane of the proximal renal tubular cells facilitate the uptake of anionic drugs [112]. Probenecid, a pan inhibitor for both OAT1 and OAT3, is commonly used to assess OAT-mediated DDIs. Studies show that the plasma levels of furosemide, tenofovir, cephadrine, and ciprofloxacin were elevated by coadministration of probenecid [113]. OCT2 and MATE1/2-K are expressed on the basolateral and luminal membrane of renal proximal tubule cells, respectively. These cation transporters play important roles in the renal tubular secretion for basic drugs. Cimetidine, a common inhibitor for both OCT2 and MATEs, has been shown to decrease the renal clearance and increase the systemic exposure of metformin, dofetilide, and pindolol [114,115]. Additionally, renal clearance of metformin was reduced by coadministration with pyrimethamine, an inhibitor of MATE [116,117].

#### **4 Tools to assess transporter liabilities in drug discovery and development**

Investigation of transporter-mediated drug disposition and potential functional changes resulting from genetic polymorphism, co-medication, and/or a disease state are needed during drug discovery and development. In vitro and in vivo assessment of several major drug transporters have been recommended by regulatory agencies to identify the potential risk of

clinical DDIs. In the past decades, a variety of in vitro systems, in silico models, and genetically modified animal models have been developed to assess drug transporter activities prior to clinical testing.

#### 4.1 Recombinant transfected cell-based systems

Historically, oocytes from *Xenopus laevis* were widely used to characterize uptake transporter function. Due to the challenges associated with translating the transporter kinetics from oocytes to mammalian systems, oocytes have been less utilized in recent research [118]. Instead, human embryonic kidney (HEK 293) cells, Madin-Darby canine kidney (MDCK) cells, porcine kidney epithelial (LLC-PK1) cells, and Chinese hamster ovary (CHO) cells are frequently used to express drug transporters. Plasmids with a single cDNA encoding a transporter of interest can be introduced into the host cells chemically, mechanically, or by viral transduction. In these mammalian cells, an individual transporter can be transiently expressed or stably expressed if a chemical resistance gene is co-constructed in the plasmid.

These recombinant cell lines can be used for both substrate and inhibition assays to determine transporter kinetics. To determine whether a compound is a substrate of uptake transporters such as OATPs, OCTs, and OATs, the compound of interest is incubated with cells overexpressing an individual transporter at 37°C. In general, if the intracellular accumulation of test compounds is significantly higher (>two-fold) in the transporter transfected cells than control cells (wild-type or cells transfected with an empty vector) one can conclude that the compound is a substrate of the individual transporter. Additionally, the transporter-mediated uptake of a substrate should show  $\geq 50\%$  inhibition in the presence of known inhibitors [118]. To determine the kinetic parameters of a drug-transporter interaction, time-course uptake studies are conducted to determine the linear uptake phase. Transporter uptake rates ( $V$ ) are measured across a broad range of substrate concentrations during the early linear uptake phase. The maximal transport velocity ( $V_{\max}$ ) and affinity ( $K_m$ ) are estimated by fitting the data to the Michaelis-Menten equation. For inhibition studies, the  $IC_{50}$  (concentration needed to inhibit 50% of the transport activity) parameter can be calculated from a concentration-dependent inhibition curve. The selected probe substrate of a transporter is incubated with a range of concentrations of a test compound, and the intracellular accumulation of the probe substrate is measured. The probes used for each transporter are summarized in a recent ITC white paper [62]. The inhibition study should be conducted during the initial uptake phase determined for the probe substrate. Because some OATP1B1/3 inhibitors are known to demonstrate time-dependent inhibition (in vitro measured  $IC_{50}/K_i$  is different with or without preincubation of inhibitors), a preincubation with a test compound may be considered [14]. The inhibition constant  $K_i$  can be calculated using the Cheng-Prusoff equation.  $IC_{50}$  values will approach  $K_i$  if the probe substrate concentration is used far below the  $K_m$ .

#### 4.2 Membrane vesicle-based assay

Membrane vesicles can be prepared from *Spodoptera frugiperda* insect cells (Sf9 or Sf21) or mammalian cell lines, such as HEK-293, MDCK, HeLa, or V79 hamster cells, which are

transfected to over-express relevant ABC transporters. Vesicles can also be isolated from tissues (kidney or liver) which contain several endogenous ABC transporters. Inverted membrane vesicles are primarily used to assess efflux transporter activity, in particular for ABC transporters—BSEP, MRP2, or BCRP. Membrane vesicle inhibition assays can also be applied to the MDR1/P-gp transporter using specific probe substrates with low passive diffusion such as N-methyl-quinidine. For vesicle-based assays, ATP should be added to provide an energy source to activate the ABC transporter function. A control experiment, in which ATP is replaced by 5'-AMP, is recommended to be run in parallel for correction of background from passive diffusion and nonspecific binding. A significant difference in accumulation between the ATP and AMP treatments would suggest that the test compound is a substrate. In general, a similar experimental design and data analysis used in cell-based uptake studies to determine substrates, inhibitors, and transport kinetics parameters can be adopted in membrane vesicle-based assays. The advantages of these vesicle-based assays are a relatively high-throughput, direct measurement of drug influx to the intravesicular compartment, and reduced impact from cytotoxicity. However, for highly hydrophobic compounds or compounds with extensive passive diffusion, the high background signals can result in a relatively high rate of false negatives for substrate identification [119].

### 4.3 Polarized cell-based systems and bidirectional transporter assays

In addition to membrane vesicle-based assays, bidirectional transport assays in polarized cell monolayers (e.g., LLC-PK1, MDCK, or Caco-2) have been developed to study efflux transporters (e.g., P-gp and BCRP) or the interplay between uptake and efflux transporters in cell systems expressing multiple transporters [120]. In a bidirectional transport assay system, the integrity of the cell monolayer is monitored by transepithelial electrical resistance (TEER) values and paracellular movement of a low-permeability compound (e.g., atenolol, inulin, mannitol, or Lucifer yellow) to verify the presence of tight junctions. A high permeability compound (e.g., propranolol), as well as a positive control substrate (e.g., digoxin for P-gp, or prazosin for BCRP) are included to ensure both proper intracellular movement and efflux are observed in the cells. To initiate the assay, the test compound is added to either the apical (A) or basolateral (B) compartment. At fixed time points, samples are taken from the receiver sides. For each direction of transport, the apparent permeability ( $P_{app}$ ) is calculated and the efflux ratio ( $P_{app} B-A/A-B$ ) is reported. A corrected efflux ratio can be determined by comparing the efflux ratio observed in cells overexpressing the efflux transporter (e.g., P-gp or BCRP) to the efflux ratio derived from the non-transfected parental cells. Since efflux transporters are expressed in the canalicular membrane of hepatocytes, cell systems expressing only efflux transporters may not be an appropriate system in the absence of a relevant uptake transporter, in particular, for compounds with low-passive membrane permeability. To overcome this limitation, double-, triple-, or even quadruple-transfected cell lines, expressing both basolateral uptake transporters and apical efflux transporters (e.g., MDCK-OATPs/MRP2 or BCRP, MDCK-OCTs/MATEs, and MDCK-OATs/BCRP or MRP2), have been recently generated to study the coordinated action of uptake and efflux transport [121].

## 4.4 Primary cell-based assays

It has been well described that a compound may be a substrate for multiple uptake and/or efflux transporters in intact organs; therefore, single or even multiple transporters-expressing cell-based systems may not accurately predict what is observed *in vivo*. Primary cells, which are derived or isolated from intact tissue and express the full complement of drug transporters and metabolic enzymes presented in that given tissue may be used to study drug disposition by providing *in vitro* parameters that are more relevant to drug interactions.

Freshly isolated or cryopreserved hepatocytes have been widely accepted as a holistic model to identify substrates for hepatic uptake transporters and to predict transporter-mediated hepatic clearance. Hepatocytes can be used in suspension or cultured on plates. The oil-spin method is commonly used for hepatic uptake assays using suspended cells. In an oil-spin assay, hepatocytes are diluted with ice-cold uptake buffers [e.g., Hanks balanced salt solution (HBSS) or Krebs-Henseleit buffer (KHB)] and kept on ice until the experiment starts. Suspended hepatocytes are aliquoted into vials and pre-warmed in the water bath to reach 37°C. Active uptake is initiated by the addition of an equal volume of uptake buffer containing test compound, with and without known transporter inhibitors, to the hepatocyte suspension. At designed time points, the incubation is terminated using high-speed centrifugation of the vials to separate the cells from the incubation buffer via rapid filtration through the layer of mineral oil. The amount of drug present in the cell pellet in the bottom layer is lysed to release the drug, then quantified to calculate the uptake rate. Uptake rate, or hepatic uptake clearance, can be derived from the initial linear phase of the curve [122,123]. The passive uptake component of a test drug can be estimated from an uptake study conducted with co-incubation of a known transporter inhibitor or by conducting the uptake study at 4°C—assuming that transporter activity is halted at 4°C. Both methods have their own limitations which need to be considered. Incomplete inhibition may result in overpredicting the passive uptake clearance of a drug. Furthermore, there are many undetermined transporters present in hepatocytes, and without further understanding of them, it can be unclear as to which inhibitors can be used. Another point of consideration is that membrane fluidity is highly affected by low temperatures [124], so the passive clearance derived from uptake studies performed at 4°C may not truly reflect the physiological condition.

Although suspended hepatocytes have been shown to accurately predict hepatic uptake function, the polarity of hepatocytes found *in vivo* is rapidly lost upon isolation, leading to the inability to assess the potential for canalicular efflux. In the sandwich-cultured hepatocyte (SCH) system, hepatocytes are cultured on collagen-coated plates and overlaid with Matrigel for 4–5 days. The SCH system has successfully shown that hepatocytes can be repolarized and the canalicular networks can be reestablished. SCH is a useful tool to assess basolateral uptake and efflux, canalicular efflux, and metabolic stability simultaneously. The SCH model is commonly used to assess hepatic uptake and biliary clearance. The SCH system uses preincubation in either standard HBSS buffer or calcium and magnesium-free HBSS buffer for 15 min. The tight junctions formed in the bile canalicular network are disrupted during the incubation with calcium and magnesium-free HBSS buffer. After removing the preincubation buffers, a standard buffer containing a test compound is added to the cells.

The reaction is stopped at designed time points by removing the buffer and washing with ice-cold buffer multiple times. Cells are lysed and the amount of compound within the cell is quantitated. The amount excreted into the bile pocket is determined by the difference in concentration between the standard buffer and calcium- and magnesium-free HBSS buffer. The intrinsic biliary clearance can be estimated from the difference of the accumulation in standard buffer minus the accumulation in calcium and magnesium buffer divided by the drug concentration in the medium and incubation time. The biliary excretion index (BEI) % =  $\{[(\text{accumulation in standard buffer} - \text{accumulation in calcium and magnesium-free buffer}) / \text{accumulation in standard buffer}] * 100\%$  can be used to determine if the in vitro biliary intrinsic clearance can be reliably assessed. It is worthwhile noting that the BEI % does not necessarily correlate with in vivo biliary excretion and cannot be used as the indicator of the percentage of dose appearing in the bile. In addition, taking advantage of the long-term culture, the SCH model can be used to study gene regulation in response to compounds [118,125,126].

#### 4.5 The use of animal models to assess transporter liabilities in drug development

Animal models are commonly used to investigate the impact of transporter-mediated drug disposition in the context of whole physiological systems. Orthologues of the major human transporters which occur in preclinical species have been identified and characterized. Although limitations from species differences exist, the information derived from animal studies can be useful for prediction in humans.

Genetically modified animals, such as genetic knockout and humanized animals, have been developed and characterized, some of which are commercially available. Knockout models have illustrated the role of transporters in physiology and pharmacology by altering the exposure and clearance pathways of endogenous substrates or xenobiotics. Because of the specificity in genetic knockout animals, these models are useful in establishing the extent of contribution of the ablated pathway to overall drug clearance. For example, *Oct1* or *Oct2* knockout, and *Oct1/Oct2* double knockout rodents are used to study metformin PK and PD [127,128]. *Oat1* or *Oat3* knockout rodents showed different plasma profiles of drugs and endogenous compounds by reducing renal secretion [112,129,130]. OATP1B1/3-humanized mouse model is utilized to study OATP-mediated PK and tissue distribution for statins [131]. Recently, cynomolgus monkey was shown to be a promising preclinical model to predict OATP-mediated hepatic clearance and DDIs [132,133]. Furthermore, different doses administered to animals are used to study the potential of transporter saturation. Likewise, the co-dosing of substrates with inhibitors in wild-type animals, as a comparison to the modified animal PK, is often used to illustrate the potential for DDIs.

The direct translation of animal models to humans is challenging because of species differences in transporter expression, substrate affinity, physiological function, compensatory mechanisms, and the interplay between transporters and enzymes. For example, significant species differences in OATP/Oatp transporters make it challenging to translate PK or PD data from preclinical species to humans. In the human liver, the OATP transporters expressed are OATP1B1, 1B3, and 2B1, which are localized in the sinusoidal membrane of hepatocytes. Orthologues of human OATP1B1/1B3 are expressed in monkey as Oatp1b1/1b3, but little Oatp2b1 is expressed in monkey liver [134]. In mice and rats, Oatp2b1 is expressed similar



to humans, but direct orthologues of OATP1B1 and 1B3 are absent. Similar to rodents, *Oatp1b1* and *1b3* are absent in dogs. Instead, *Oatp1b4* is expressed in the canine liver. Additionally, the different OCT1/2 isoforms (*Oct1/2*) have species and tissue-specific distributions. OCT1/*Oct1* mRNA is highly expressed in the liver of mouse, rat, monkey, and human, and is localized on the basolateral membrane of hepatocytes. *Oct1* was also found to be highly expressed in the kidney of rodents, whereas, little expression of OCT1/*Oct1* was found in the kidneys of humans or monkeys. Human and monkey OCT2/*Oct2*, considered to be renal transporters, show similar expression in the basolateral membrane of renal proximal tubules. However, in rat and mouse kidneys, *Oct1* and *Oct2* are expressed comparably. All these variables should be considered carefully in the interpretation of data and in attempts to extrapolate findings across species.

#### 4.6 In silico modeling of transporter proteins

Although membrane transporters have been shown to play significant roles in drug discovery and development for many years, most are poorly characterized at the atomic level due to poor resolution of structures and difficulties associated with expressing and crystallizing the membrane proteins. To date, only a few structures for membrane proteins including several ABC transporters are available [135,136]. In silico modeling is a useful approach to circumvent the difficulties associated with traditional crystallization techniques and to fill in the gap between knowledge of transporter protein structure and functional properties. Recently, taking advantage of the availability of high-quality data sets and atomic resolution structures, several publications have shown successfully the ability to project transporter-substrate interactions using single and combinatorial in silico modeling [72]. In general, the modeling approaches are divided into indirect ligand-based techniques, such as pharmacophore and 3D-quantitative structure-activity relationship (3D-QSAR) modeling, and direct structure-based approaches, such as the homology or comparative modeling based on available crystallographic data.

The primary amino acid sequences of many transporters are known, while elucidation or identification of their secondary structures is facilitated by bioinformatics tools. Currently, even though only a few transporter proteins have been analyzed by X-ray crystallography and afforded high-resolution 3D information, new strategies have opened up the opportunity for generating homology or comparative models. When two proteins have adequate sequence identity, and the experimentally determined 3D structure of one of these proteins is known, comparative protein models can be constructed, even when the two proteins are not functionally related. On the other hand, when crystal structure templates are not available or cannot be utilized to complement existing homology models, ligand-based methods such as pharmacophore and 3D-QSAR can be used. As a major requirement, a high-throughput in vitro assay is used to generate a data set of transporter ligands (substrates or inhibitors) and their corresponding activity values ( $K_m/V_{max}$ ,  $K_i$ , or percentage inhibition). Data sets are divided into a training set, to construct a model, and a test set, to validate the model. In general, if the model can successfully predict the biological activity of a test set of molecules, the model is accepted. Acceptable models may be combined to generate synergistic consensus models. In recent years, the combination of 3D-QSAR models with the



comparative model has been used to increase the confidence of modeling predictions. With the aid of these modeling strategies, we can screen large compound databases to identify novel transporter ligands. The major challenges in modeling membrane transporters are low levels of sequence identity and divergent membrane topologies.

#### 4.7 Application of biomarkers for in vivo assessment of drug transporter activity

While regulatory guidance provides *in vitro* and *in vivo* assessment strategies or decision trees to guide the planning of clinical trials, limitations are applied when conducting *in vitro-in vivo* extrapolations. Static models recommended in the guidance through basic *in vitro-in vivo* extrapolations, along with the variability of substrate identification or  $IC_{50}$  determination under different testing systems or experimental settings [137,138] often produce false positive or negative outcomes [139]. This can result in conducting unnecessary confirmatory clinical DDI studies. To overcome these issues, physiologically based-pharmacokinetic (PBPK) models are increasingly applied in a mechanistic manner to refine the DDI predictions [140,141]. Unfortunately, the confidence in applying PBPK models to human PK prediction is still low for mechanisms that involve complex transporter-enzyme drug elimination processes [142,143]. Many endogenous substances are substrates of drug transporters and their disposition and elimination rely on drug transporter functional activities. These substances are potentially clinically relevant probes for *in vivo* transporter function. It is envisaged that monitoring the changes of transporter specific substances during phase I dose-escalation trials can provide an early assessment of transporter inhibition in humans. In fact, over recent years, preclinical studies and clinical evaluations were conducted to investigate endogenous biomarkers of transporter inhibition [61,93,144–148]. With appropriate validation, these endogenous substances have the potential to be biomarkers to corroborate *in vitro* inhibition data during the first-in-man dose escalation trials for drug development planning, or eventually obviate the need for dedicated clinical DDI studies [62]. Currently, endogenous molecules as potential clinical biomarkers of transporter function *in vivo* remain under investigation and the interpretation of drug (inhibitor)-endogenous substances (biomarkers) interactions can be challenging [62,149,150]. Many endogenous biomarkers have recently been reported and were reviewed in the latest International Transporter Consortium (ITC) paper [62]. The biomarkers and clinical probe drugs that show the most promising evidence for transporter inhibition in a clinical setting are summarized in Table 2. It is worthwhile noting that current clinical data for endogenous biomarkers comes mainly from clinical studies in healthy subjects following a single dose of a drug transporter inhibitor [93,98,151].

### 5 Regulatory landscape of evaluating transporter-mediated drug interactions

Despite the advancement of preclinical testing strategies that enable researchers/pharmaceutical companies to deliver favorable new molecular entities, significant attrition occurring during clinical development due to unfavorable efficacy and/or safety profiles remains a common problem in the pharmaceutical industry [152]. It is generally accepted that

**TABLE 2** ITC list of probe drugs and biomarkers that can be used to evaluate in vivo transporter inhibition [62].

Transporters	Clinical probe drugs	Endogenous biomarkers
OATP1B1/1B3	Pitavastatin; Atorvastatin; Rosuvastatin	Coproporphyrin I and III; Glycochenodeoxycholate-3-O-sulfate; Hexadecanedioate, Tetradecanedioate; Conjugated and unconjugated bilirubin
OCT1	Sumatriptan	
OCT2/ MATE1/2K	Metformin	Creatinine; N1-methylnicotinamide
OAT1	Adefovir	Taurine; Pyridoxic acid; Homovanillic acid
OAT3	Benzylpenicillin	Glycochenodeoxycholate-3-O-sulfate; 6 $\beta$ -Hydroxycortisol; Pyridoxic acid; Homovanillic acid
P-gp	Digoxin; Fexofenadine; Dabigatran etexilate	
BCRP	Sulfasalazine; Rosuvastatin,	

co-medicating other drugs, genetic polymorphisms, or a disease state which affects transporter function have each been shown to affect absorption, distribution, and elimination of drugs and have an impact on drug efficacy and toxicity by changing systemic exposure or tissue concentrations. From the in vitro-in vivo prediction perspective, to facilitate transporter studies during drug development, the International Transporter Consortium (ITC), comprised of transporter experts from the industry, academia, and regulatory agencies, was formed in 2007 and published a review article in *Nature Review Drug Discovery*, commonly known as the ITC “White Paper” [3]. The ITC white paper proposed the assessment of seven transporters and provided decision trees for assessment of new drugs as substrates or inhibitors of the seven transporters including P-gp, BCRP, OATP1B1 and 1B3, OAT1 and 3, and OCT2. Soon after the publication of the ITC white paper, both the European Medicines Agency (EMA) and the US Food and Drug Administration (FDA) expanded their sections on drug transporters and the ITC recommendations were largely adapted. The EMA guidance also recommended the assessment of OCT1 and BSEP, although they were not recommended by the ITC and were not included in the FDA guidance. The ITC organized a second workshop in March 2012, and then published six articles to summarize the key issues in assessing transporter roles in drug discovery and development, and how the regulatory guidances influence the de-risk plans for DDIs. On March 2017, the third ITC workshop was held and, in the subsequent year, 10 articles were published in *Clinical Pharmacology and Therapeutics* to summarize the current approaches in transporter research [62,71,141,153–159]. In addition to the previous 9 transporters, the ITC has recommended testing for drug interactions with OCT1 and OATP2B1, as well as drug-vitamin interactions with the thiamine transporter 2 (ThTR2) [160]. On the other hand, global regulatory agencies, including the EMA, Ministry of Health, Labor, and Welfare (MHLW) of Japan, and the US FDA, have issued guidance documents that recommend how to evaluate transporter-mediated

DDIs during development. Thus, in recent years, the evaluation of transporters has been integrated into risk assessment plans prior to entering human trials. Additionally, the number of transporter assays being tested has significantly increased in submitted applications for a new molecular entity. In 2017, the US FDA published two updated draft DDI guidance documents. One document focuses on *in vitro* DDI assessment and the other focuses on clinical DDI evaluation.

### 5.1 Determining if the investigational drug is a substrate of transporters

Investigational drugs need to be evaluated *in vitro* to determine whether they are substrates of P-gp and BCRP because these two transporters are expressed in multiple organs, including the intestine. However, P-gp and BCRP are not expected to affect the oral bioavailability of highly permeable and highly soluble drugs (e.g., biopharmaceutics classification system class 1 drugs) [161]. If the net efflux ratio (ER) is  $\geq 2$  in cells expressing P-gp for an investigational drug, and the efflux observed can be inhibited  $\geq 50\%$  by at least one known P-gp inhibitor at a concentration at least 10 times its  $K_i$ , the results suggest that this investigational drug is an *in vitro* substrate of P-gp. The same procedures can be applied to determine whether the drug is a BCRP substrate. If a drug is mainly eliminated by the liver (i.e., the drug's clearance through hepatic metabolism or biliary secretion is  $\geq 25\%$  of the total drug's clearance) or it shows significant hepatic uptake, OATP1B should be evaluated. If the investigational drug's ADME data suggest that active renal secretion is significant for a drug (i.e., active secretion of the parent drug by the kidney is  $\geq 25\%$  of the total clearance), the sponsor should evaluate the drug *in vitro* to determine whether it is a substrate of OAT1/3, OCT2, or MATE1/2-K. Similar to P-gp and BCRP transporter assessment, the investigational drug is an *in vitro* substrate for the above transporters if: (1) the ratio of the investigational drug's uptake in the cells expressing the transporter versus the drug's uptake in control cells (or cells containing an empty vector) is  $\geq 2$ ; and (2) a known inhibitor of the transporter decreases the drug's uptake to  $\leq 50\%$  at a concentration at least 10 times its  $K_i$  or  $IC_{50}$ . If *in vitro* studies indicate a new drug is a substrate of transporters, the need for clinical DDI studies should be determined based on the drug's putative site of action, route of elimination, the most likely concomitant drugs, and safety considerations.

### 5.2 Determining if the investigational drug is an inhibitor of transporters

In general, whether a drug is an inhibitor of the key drug transporters mentioned above should be evaluated. Following the determination of *in vitro*  $IC_{50}$  (or  $K_i$ ), *in vivo* DDI potential can be evaluated using a basic model. As described in Table 3, the basic model determines the ratio of a clinically relevant inhibitor concentration/*in vitro* half-maximal inhibitory concentration ( $IC_{50}$ ) or  $K_i$ . If the ratio is equal to or greater than a specified cutoff value, defined separately in each regulatory guidance document, a clinical DDI study should be considered. The clinical DDI studies should include whether the medications most likely to be used concomitantly in the indicated patient populations are known to be substrates of these transporters. In general, the choice of transporter substrates or inhibitors is typically based on the likelihood of coadministration in the patient population. The selected inhibitors recommended

**TABLE 3** Decision criteria for new drugs as inhibitors of major transporters.

Transporters	Inhibitors	FDA guidance (2017, draft)	MHLW guidance (2017)	EMA guidance (2013)
P-gp	Clarithromycin, itraconazole, quinidine, verapamil	$I_{\text{gut}}/IC_{50} \geq 10$ (for oral drugs)	$I/IC_{50} \geq 10$	$0.1 * \text{dose} / 250 \text{ mL} / K_i \geq 1$
BCRP	KO143-	$I_{\text{gut}}/IC_{50} \geq 10$ (for oral drugs)	$I/IC_{50} \geq 10$	$0.1 * \text{dose} / 250 \text{ mL} / K_i \geq 1$
OATP1B1 or OATP1B3	Cyclosporine, rifampin	$1 + f_{\text{ub}} * I_{\text{u, in, max}} / IC_{50} \geq 1.1$ ( $R_b$ used)	$1 + I_{\text{u, in, max}} / IC_{50} \geq 1.1$ ( $R_b$ not used)	$25 * I_{\text{u, in, max}} / K_i \geq 1$ (cutoff is 1.04) or $50 * C_{\text{u, max}} / K_i > 1$ , if dosed I.V. (cutoff 0.02)
OAT1 or OAT3,	Probenecid	$I_{\text{u, max}} / IC_{50} \geq 0.1$	$1 + C_{\text{u, max}} / K_i$ ( $IC_{50} \geq 1.1$ )	$50 * C_{\text{u, max}} / K_i > 1$ (cutoff 0.02)
OCT2	Cimetidine, pyrimethamine-	$I_{\text{u, max}} / IC_{50} \geq 0.1$	$1 + C_{\text{u, max}} / K_i$ ( $IC_{50} \geq 1.1$ )	$50 * C_{\text{u, max}} / K_i > 1$ (cutoff 0.02)
MATE1 or MATE2-K	Cimetidine, pyrimethamine	$I_{\text{u, max}} / IC_{50} \geq 0.02$	$1 + C_{\text{u, max}} / K_i$ ( $IC_{50} \geq 1.02$ )	$50 * C_{\text{u, max}} / K_i > 1$ (cutoff 0.02)

- P-gp, BCRP: gut concentration:  $I_2 = \text{dose} / 250 \text{ mL}$ .
- OATP1B: free hepatic inlet concentration:  $I_{\text{u, in, max}} = f_{\text{u, p}} \times (C_{\text{max}} + (F_a F_g \times k_i \times \text{Dose}) / Q_h / R_b)$ . where  $f_{\text{u, p}}$  is unbound fraction in plasma,  $F_a$  is the fraction absorbed,  $F_g$  is the intestinal availability,  $k_a$  is the absorption rate constant,  $Q_h$  is the hepatic blood flow rate, and  $R_b$  is the blood-to-plasma concentration ratio.
- OAT and OCT: free systemic concentration:  $I_{\text{u, max}} = C_{\text{max, u}}$ .
- MATE: free systemic concentration (as a "surrogate" and a different cutoff may be warranted):  $I_{\text{u, max}} = C_{\text{max, u}}$ .

by FDA are summarized in Table 3. A detailed list of transporter substrates and inhibitors is maintained on the FDA's website on Drug Development and Drug Interactions (USFDA-Guidance, 2017).

## 6 Challenges and perspectives on transporter-mediated drug interactions

During drug development, it is important to characterize which transporters mechanistically affect the ADME of an investigational drug and how that drug might affect another drugs' ADME. Lack of specific probe substrates and inhibitors can pose a challenge for interpreting DDIs studies in cases where substrates/inhibitors can interact with multiple transporters and metabolic enzymes. Practically, preclinical evaluations of DDI liabilities should initially be conducted using in vitro systems for an investigational medicinal product. Based on a basic static model with cutoff criteria established by regulatory agencies, DDI potential is assessed by comparison of in vitro transporter inhibitory potency to the predicted intestinal, liver portal, and systemic exposure concentration of drug to various transporters. Consequently, clinical development plans are prioritized to assess or confirm the extent of clinical DDIs. Lastly, model-based DDI simulation can be developed to interpret the clinical

DDI data obtained and extrapolate the results to other unstudied drugs for drug labeling recommendations. However, uncertainties exist in *in vitro* assays due to nonspecific binding, low solubility in assay buffer, the variety of assays or cell lines used, intersystem/laboratory variability, and substrate/inhibitor pairings. In many cases, a compound can be a substrate for multiple transporters and CYP enzymes; likewise, many inhibitors not only inhibit the specified transporters but also can inhibit some CYP enzymes. The limitations of *in vitro-in vivo* extrapolation-based static prediction models often result in high numbers of false-positive or -negative predictions using the different static prediction methods and cutoff criteria recommended by regulatory guidance documents. Besides concomitant medications, many factors such as disease state, genetic polymorphism, gender, ethnic group, and age can also affect the PK profiles of drugs. Furthermore, a few transporters are inducible (upregulated) and some drugs can be an inducer for a transporter, such as P-gp, that shares similarities in induction mechanisms with CYP3A. However, there has been no validated *in vitro* system developed to study P-gp regulation, leaving the assessment of transporter induction to be uncovered only after clinical data has become available. In contrast, from the industry perspective, early assessment of potential DDI risk is essential to the selection of lead compounds before entering clinical development, prior to the significant investment of late-stage clinical trials. To assess the complexity of DDIs to its full extent, significant efforts such as *in vitro* tools and model based approaches have been developed to refine the DDI prediction at the preclinical phase. Many *in vitro* tools and model-based approaches are developed to assess the risk of DDI potential. A PBPK model that integrates information from multiple parameters, such as the active uptake mediated by transporters, as well as passive diffusion, metabolism, and biliary excretion represents a useful tool to predict complex DDI. However, despite a plethora of recent publications showing that PBPK models can accurately predict complex clinical DDIs, the majority of analyses are only individual case examples that are not applicable for the development of more robust and predictable modeling principles in general [143]. Knowledge gaps remain in fully understanding transporter biology and there is a need for better tools to determine reliable transporter kinetics for *in vitro-in vivo* extrapolation.

Endogenous substances which are shown to be specifically transported by certain transporters, and have the potential to serve as biomarkers to corroborate *in vitro* assays, allowing early assessment of DDI potentials during first-in-man clinical trials, are now being sought out. While considerable published information has become increasingly available, examples of promising candidate biomarkers are limited to a few hepatic (OATP) and renal (OAT/OCT) transporters. When evaluating an investigational drug as an inhibitor, it is critical to use selective and sensitive probe substrate drugs, which can provide the mechanistic insight of an individual transporter's inhibition and can be extrapolated to other unstudied drugs. Similar criteria are applied to endogenous biomarkers that can be used for determining transporter inhibition. Notably, no transporter biomarkers are fully validated to date. Continued and more widespread investigations of endogenous biomarkers in clinical studies are critical and will ultimately enhance the confidence in using endogenous biomarkers as indicators of potential clinical transporter DDIs. With appropriate validation, the need for dedicated clinical DDI studies may be precluded in the future and robust clinical DDI assessment using specific biomarkers may ultimately drive product labeling to inform concomitant drug use.

## References

- [1] Q. Mao, Y. Lai, J. Wang, Drug transporters in xenobiotic disposition and pharmacokinetic prediction, *Drug Metab. Dispos.* 46 (5) (2018) 561–566.
- [2] M.V. Varma, A.F. El-Kattan, Transporter-enzyme interplay: deconvoluting effects of hepatic transporters and enzymes on drug disposition using static and dynamic mechanistic models, *J. Clin. Pharmacol.* 56 (Suppl 7) (2016) S99–S109.
- [3] International Transporter Consortium, et al., Membrane transporters in drug development, *Nat. Rev. Drug Discov.* 9 (3) (2010) 215–236.
- [4] D. Tweedie, et al., Transporter studies in drug development: experience to date and follow-up on decision trees from the International Transporter Consortium, *Clin. Pharmacol. Ther.* 94 (1) (2013) 113–125.
- [5] S.C. Lee, et al., Evaluation of transporters in drug development: current status and contemporary issues, *Adv. Drug Deliv. Rev.* 116 (2017) 100–118.
- [6] W.A. Alrefai, R.K. Gill, Bile acid transporters: structure, function, regulation and pathophysiological implications, *Pharm. Res.* 24 (10) (2007) 1803–1823.
- [7] M.H. Keane, et al., Bile acid treatment alters hepatic disease and bile acid transport in peroxisome-deficient PEX2 Zellweger mice, *Hepatology* 45 (4) (2007) 982–997.
- [8] M.J. Zamek-Gliszczynski, et al., ITC recommendations for transporter kinetic parameter estimation and translational modeling of transport-mediated PK and DDIs in humans, *Clin. Pharmacol. Ther.* 94 (1) (2013) 64–79.
- [9] D. Rekić, et al., Clinical drug-drug interaction evaluations to inform drug use and enable drug access, *J. Pharm. Sci.* 106 (9) (2017) 2214–2218.
- [10] K. Yoshida, et al., In vitro-in vivo extrapolation of metabolism- and transporter-mediated drug-drug interactions-overview of basic prediction methods, *J. Pharm. Sci.* 106 (9) (2017) 2209–2213.
- [11] M.J. Zamek-Gliszczynski, et al., Highlights from the international transporter consortium second workshop, *Clin. Pharmacol. Ther.* 92 (5) (2012) 553–556.
- [12] N. Fukui, et al., Dose-dependent effects of the 3435 C > T genotype of ABCB1 gene on the steady-state plasma concentration of fluvoxamine in psychiatric patients, *Ther. Drug Monit.* 29 (2) (2007) 185–189.
- [13] Japan\_MHLW\_Guidance, [https://www.mhlw.go.jp/web/t\\_doc?dataId=00tc0233&dataType=1&pageNo=1](https://www.mhlw.go.jp/web/t_doc?dataId=00tc0233&dataType=1&pageNo=1).
- [14] USFDA-Guidance, <https://www.fda.gov/downloads/Drugs/GuidanceComplianceRegulatoryInformation/Guidances/UCM581965.pdf>, 2017.
- [15] EMA-Guidance, [http://www.ema.europa.eu/docs/en\\_GB/document\\_library/Scientific\\_guideline/2012/07/WC500129606.pdf](http://www.ema.europa.eu/docs/en_GB/document_library/Scientific_guideline/2012/07/WC500129606.pdf).
- [16] J. Muller, et al., Expression, regulation and function of intestinal drug transporters: an update, *Biol. Chem.* 398 (2) (2017) 175–192.
- [17] M. Benadiba, Y. Maor, Importance of ABC transporters in drug development, *Curr. Pharm. Des.* 22 (999) (2016) 1.
- [18] C. Colas, P.M. Ung, A. Schlessinger, SLC transporters: structure, function, and drug discovery, *MedChemComm* 7 (6) (2016) 1069–1081.
- [19] M. Jani, et al., Structure and function of BCRP, a broad specificity transporter of xenobiotics and endobiotics, *Arch. Toxicol.* 88 (6) (2014) 1205–1248.
- [20] M. Lund, T.S. Petersen, K.P. Dalhoff, Clinical implications of P-glycoprotein modulation in drug-drug interactions, *Drugs* 77 (8) (2017) 859–883.
- [21] J. König, F. Müller, M.F. Fromm, Transporters and drug-drug interactions: important determinants of drug disposition and effects, *Pharmacol. Rev.* 65 (3) (2013) 944–966.
- [22] S. Wilkens, Structure and mechanism of ABC transporters, *F1000Prime. Rep.* 7 (2015) 14.
- [23] M. Drozdziak, et al., Protein abundance of clinically relevant multidrug transporters along the entire length of the human intestine, *Mol. Pharm.* 11 (10) (2014) 3547–3555.
- [24] R. Canaparo, et al., Expression of CYP3A isoforms and P-glycoprotein in human stomach, jejunum and ileum, *Clin. Exp. Pharmacol. Physiol.* 34 (11) (2007) 1138–1144.
- [25] R. Canaparo, et al., Expression of cytochromes P450 3A and P-glycoprotein in human large intestine in paired tumour and normal samples, *Basic Clin. Pharmacol. Toxicol.* 100 (4) (2007) 240–248.
- [26] E.I. Lepistö, et al., Cobicistat boosts the intestinal absorption of transport substrates, including HIV protease inhibitors and GS-7340, in vitro, *Antimicrob. Agents Chemother.* 56 (10) (2012) 5409–5413.



- [27] Y. Toyoda, T. Takada, H. Suzuki, Inhibitors of human ABCG2: from technical background to recent updates with clinical implications, *Front. Pharmacol.* 10 (2019) 208.
- [28] Z. Safar, et al., ABCG2/BCRP: variants, transporter interaction profile of substrates and inhibitors, *Expert Opin. Drug Metab. Toxicol.* 15 (4) (2019) 313–328.
- [29] Y. Toyoda, et al., Functional characterization of clinically-relevant rare variants in ABCG2 identified in a gout and hyperuricemia cohort, *Cells* 8 (4) (2019), <https://doi.org/10.3390/cells8040363>.
- [30] M.J. Zamek-Gliszczynski, et al., Relationship between drug/metabolite exposure and impairment of excretory transport function, *Drug Metab. Dispos.* 37 (2) (2009) 386–390.
- [31] P. Hsiao, J.D. Unadkat, Predicting the outer boundaries of P-glycoprotein (P-gp)-based drug interactions at the human blood-brain barrier based on rat studies, *Mol. Pharm.* (2014).
- [32] R. Clark, I.D. Kerr, R. Callaghan, Multiple drugbinding sites on the R482G isoform of the ABCG2 transporter, *Br. J. Pharmacol.* 149 (5) (2006) 506–515.
- [33] C.A. Lee, et al., Breast cancer resistance protein (ABCG2) in clinical pharmacokinetics and drug interactions: practical recommendations for clinical victim and perpetrator drug-drug interaction study design, *Drug Metab. Dispos.* 43 (4) (2015) 490–509.
- [34] W. Zhang, et al., Role of BCRP 421C>A polymorphism on rosuvastatin pharmacokinetics in healthy Chinese males, *Clin. Chim. Acta* 373 (1-2) (2006) 99–103.
- [35] J.E. Keskitalo, et al., ABCG2 polymorphism markedly affects the pharmacokinetics of atorvastatin and rosuvastatin, *Clin. Pharmacol. Ther.* 86 (2) (2009) 197–203.
- [36] D.J. Brackman, K.M. Giacomini, Reverse translational research of ABCG2 (BCRP) in human disease and drug response, *Clin. Pharmacol. Ther.* 103 (2) (2018) 233–242.
- [37] J. König, et al., Conjugate export pumps of the multidrug resistance protein (MRP) family: localization, substrate specificity, and MRP2-mediated drug resistance, *Biochim. Biophys. Acta* 1461 (2) (1999) 377–394.
- [38] C. Hilgendorf, et al., Expression of thirty-six drug transporter genes in human intestine, liver, kidney, and organotypic cell lines, *Drug Metab. Dispos.* 35 (8) (2007) 1333–1340.
- [39] C. MacLean, et al., Closing the gaps: a full scan of the intestinal expression of p-glycoprotein, breast cancer resistance protein, and multidrug resistance-associated protein 2 in male and female rats, *Drug Metab. Dispos.* 36 (7) (2008) 1249–1254.
- [40] D. Keppler, Multidrug resistance proteins (MRPs, ABCs): importance for pathophysiology and drug therapy, *Handb. Exp. Pharmacol.* 201 (2011) 299–323.
- [41] V. Keitel, et al., Impaired protein maturation of the conjugate export pump multidrug resistance protein 2 as a consequence of a deletion mutation in Dubin-Johnson syndrome, *Hepatology* 32 (6) (2000) 1317–1328.
- [42] J. Kartenbeck, et al., Absence of the canalicular isoform of the MRP gene-encoded conjugate export pump from the hepatocytes in Dubin-Johnson syndrome, *Hepatology* 23 (5) (1996) 1061–1066.
- [43] V. Keitel, et al., A common Dubin-Johnson syndrome mutation impairs protein maturation and transport activity of MRP2 (ABCC2), *Am. J. Physiol. Gastrointest. Liver Physiol.* 284 (1) (2003) G165–G174.
- [44] K. Ogasawara, et al., Multidrug resistance-associated protein 2 (MRP2/ABCC2) haplotypes significantly affect the pharmacokinetics of tacrolimus in kidney transplant recipients, *Clin. Pharmacokinet.* 52 (9) (2013) 751–762.
- [45] R. Kubitz, et al., The bile salt export pump (BSEP) in health and disease, *Clin. Res. Hepatol. Gastroenterol.* 36 (6) (2012) 536–553.
- [46] S.S. Strautnieks, et al., A gene encoding a liver-specific ABC transporter is mutated in progressive familial intrahepatic cholestasis, *Nat. Genet.* 20 (3) (1998) 233–238.
- [47] J.A. Byrne, et al., Missense mutations and single nucleotide polymorphisms in ABCB11 impair bile salt export pump processing and function or disrupt pre-messenger RNA splicing, *Hepatology* 49 (2) (2009) 553–567.
- [48] Y. Cheng, et al., Biliary excretion of pravastatin and taurocholate in rats with bile salt export pump (Bsep) impairment, *Biopharm. Drug Dispos.* 37 (5) (2016) 276–286.
- [49] M. Hirano, et al., Bile salt export pump (BSEP/ABCB11) can transport a nonbile acid substrate, pravastatin, *J. Pharmacol. Exp. Ther.* 314 (2) (2005) 876–882.
- [50] J.L. Woodhead, et al., Exploring BSEP inhibition-mediated toxicity with a mechanistic model of drug-induced liver injury, *Front. Pharmacol.* 5 (2014) 240.
- [51] A. Telbisz, L. Homolya, Recent advances in the exploration of the bile salt export pump (BSEP/ABCB11) function, *Expert Opin. Ther. Targets* 20 (4) (2016) 501–514.



- [52] C. Colas, A. Schlessinger, A.M. Pajor, Mapping functionally important residues in the Na(+)/dicarboxylate cotransporter, NaDC1, *Biochemistry* 56 (33) (2017) 4432–4441.
- [53] L. Lin, et al., SLC transporters as therapeutic targets: emerging opportunities, *Nat. Rev. Drug Discov.* 14 (8) (2015) 543–560.
- [54] M. Roth, et al., Isolation of modulators of the liver specific Organic Anion Transporting Polypeptides (OATPs) 1B1 and 1B3 from *Rollinia emarginata* Schlecht (Annonaceae), *J. Pharmacol. Exp. Ther.* (2011).
- [55] J. König, et al., A novel human organic anion transporting polypeptide localized to the basolateral hepatocyte membrane, *Am. J. Physiol. Gastrointest. Liver Physiol.* 278 (1) (2000) G156–G164.
- [56] G. Patilea-Vrana, J.D. Unadkat, Transport vs. metabolism: what determines the pharmacokinetics and pharmacodynamics of drugs? insights from the extended clearance model, *Clin. Pharmacol. Ther.* 100 (5) (2016) 413–418.
- [57] A.F. El-Kattan, M.V.S. Varma, Navigating transporter sciences in pharmacokinetics characterization using the extended clearance classification system, *Drug Metab. Dispos.* 46 (5) (2018) 729–739.
- [58] T. Watanabe, et al., Physiologically based pharmacokinetic modeling to predict transporter-mediated clearance and distribution of pravastatin in humans, *J. Pharmacol. Exp. Ther.* 328 (2) (2009) 652–662.
- [59] S.W. Yee, et al., Organic anion transporter polypeptide 1B1 polymorphism modulates the extent of drug-drug interaction and associated biomarker levels in healthy volunteers, *Clin. Transl. Sci.* 12 (4) (2019) 388–399.
- [60] D. Mori, et al., Effect of OATP1B1 genotypes on plasma concentrations of endogenous OATP1B1 substrates and drugs, and their association in healthy volunteers, *Drug. Metab. Pharmacokinet.* 34 (1) (2019) 78–86.
- [61] X. Chu, G.H. Chan, R. Evers, Identification of endogenous biomarkers to predict the propensity of drug candidates to cause hepatic or renal transporter-mediated drug-drug interactions, *J. Pharm. Sci.* 106 (9) (2017) 2357–2367.
- [62] X. Chu, et al., Clinical probes and endogenous biomarkers as substrates for transporter drug-drug interaction evaluation: perspectives from the international transporter consortium, *Clin. Pharmacol. Ther.* 104 (5) (2018) 836–864.
- [63] E. van de Steeg, et al., Complete OATP1B1 and OATP1B3 deficiency causes human Rotor syndrome by interrupting conjugated bilirubin reuptake into the liver, *J. Clin. Invest.* 122 (2) (2012) 519–528.
- [64] M. Niemi, et al., Polymorphic organic anion transporting polypeptide 1B1 is a major determinant of repaglinide pharmacokinetics, *Clin. Pharmacol. Ther.* 77 (6) (2005) 468–478.
- [65] M. Patel, K.S. Taskar, M.J. Zamek-Gliszczynski, Importance of hepatic transporters in clinical disposition of drugs and their metabolites, *J. Clin. Pharmacol.* 56 (Suppl 7) (2016) S23–S39.
- [66] Y. Lai, et al., Impact of drug transporter pharmacogenomics on pharmacokinetic and pharmacodynamic variability – considerations for drug development, *Expert Opin. Drug Metab. Toxicol.* 8 (6) (2012) 723–743.
- [67] I. Ieiri, et al., Microdosing clinical study: pharmacokinetic, pharmacogenomic (SLCO2B1), and interaction (grapefruit juice) profiles of celiprolol following the oral microdose and therapeutic dose, *J. Clin. Pharmacol.* 52 (7) (2012) 1078–1089.
- [68] M. Drozdziak, S. Oswald, Expression and regulation of drug transporters and metabolizing enzymes in the human gastrointestinal tract, *Curr. Med. Chem.* (2016).
- [69] E. Kimoto, et al., Characterization of organic anion transporting polypeptide (OATP) expression and its functional contribution to the uptake of substrates in human hepatocytes, *Mol. Pharm.* 9 (12) (2012) 3535–3542.
- [70] A. Vildhede, et al., Comparative proteomic analysis of human liver tissue and isolated hepatocytes with a focus on proteins determining drug exposure, *J. Proteome Res.* 14 (8) (2015) 3305–3314.
- [71] M.J. Zamek-Gliszczynski, et al., Transporters in drug development: 2018 ITC recommendations for transporters of emerging clinical importance, *Clin. Pharmacol. Ther.* 104 (5) (2018) 890–899.
- [72] H.C. Liu, et al., Molecular properties of drugs interacting with SLC22 transporters OAT1, OAT3, OCT1, and OCT2: a machine-learning approach, *J. Pharmacol. Exp. Ther.* 359 (1) (2016) 215–229.
- [73] S.K. Nigam, et al., The organic anion transporter (OAT) family: a systems biology perspective, *Physiol. Rev.* 95 (1) (2015) 83–123.
- [74] S.W. Yee, et al., Reduced renal clearance of cefotaxime in asians with a low-frequency polymorphism of OAT3 (SLC22A8), *J. Pharm. Sci.* 102 (9) (2013) 3451–3457.
- [75] M.J. Zamek-Gliszczynski, K.M. Giacomini, L. Zhang, Emerging clinical importance of hepatic organic cation transporter 1 (OCT1) in drug pharmacokinetics, dynamics, pharmacogenetic variability, and drug interactions, *Clin. Pharmacol. Ther.* 103 (5) (2018) 758–760.

- [76] E. Lozano, et al., Genetic heterogeneity of SLC22 family of transporters in drug disposition, *J. Pers. Med.* 8 (2) (2018).
- [77] H.C. Chien, et al., Rapid method to determine intracellular drug concentrations in cellular uptake assays: application to metformin in organic cation transporter 1-transfected human embryonic kidney 293 cells, *Drug Metab. Dispos.* 44 (3) (2016) 356–364.
- [78] M. Roth, A. Obaidat, B. Hagenbuch, OATPs, OATs and OCTs: the organic anion and cation transporters of the SLCO and SLC22A gene superfamilies, *Br. J. Pharmacol.* 165 (5) (2012) 1260–1287.
- [79] A.T. Nies, et al., Organic cation transporters (OCTs, MATEs), in vitro and in vivo evidence for the importance in drug therapy, *Handb. Exp. Pharmacol.* 201 (2011) 105–167.
- [80] X. Wu, et al., Structure, function, and regional distribution of the organic cation transporter OCT3 in the kidney, *Am. J. Physiol. Ren. Physiol.* 279 (3) (2000) F449–F458.
- [81] H. Koepsell, Role of organic cation transporters in drug-drug interaction, *Expert Opin. Drug Metab. Toxicol.* 11 (10) (2015) 1619–1633.
- [82] J. Chen, et al., Tropane alkaloids as substrates and inhibitors of human organic cation transporters of the SLC22 (OCT) and the SLC47 (MATE) families, *Biol. Chem.* (2016).
- [83] S. Zhang, et al., Organic cation transporters are determinants of oxaliplatin cytotoxicity, *Cancer Res.* 66 (17) (2006) 8847–8857.
- [84] S. Yokoo, et al., Differential contribution of organic cation transporters, OCT2 and MATE1, in platinum agent-induced nephrotoxicity, *Biochem. Pharmacol.* 74 (3) (2007) 477–487.
- [85] K.E. Pedersen, et al., Effect of quinidine on digoxin bioavailability, *Eur. J. Clin. Pharmacol.* 24 (1) (1983) 41–47.
- [86] B.J. Kirby, et al., Complex drug interactions of the HIV protease inhibitors 3: effect of simultaneous or staggered dosing of digoxin and ritonavir, nelfinavir, rifampin, or bupropion, *Drug Metab. Dispos.* 40 (3) (2012) 610–616.
- [87] T. Sakugawa, et al., Enantioselective disposition of fexofenadine with the P-glycoprotein inhibitor verapamil, *Br. J. Clin. Pharmacol.* 67 (5) (2009) 535–540.
- [88] C.M. Kruijtz, et al., Increased oral bioavailability of topotecan in combination with the breast cancer resistance protein and P-glycoprotein inhibitor GF120918, *J. Clin. Oncol.* 20 (13) (2002) 2943–2950.
- [89] R.D. Harvey, et al., Effect of multiple-dose osimertinib on the pharmacokinetics of simvastatin and rosuvastatin, *Br. J. Clin. Pharmacol.* 84 (12) (2018) 2877–2888.
- [90] P. Martin, et al., Effects of fostamatinib on the pharmacokinetics of oral contraceptive, warfarin, and the statins rosuvastatin and simvastatin: results from phase I clinical studies, *Drugs R D* 16 (1) (2016) 93–107.
- [91] M. Hedman, et al., Pharmacokinetics and pharmacodynamics of pravastatin in pediatric and adolescent cardiac transplant recipients on a regimen of triple immunosuppression, *Clin. Pharmacol. Ther.* 75 (1) (2004) 101–109.
- [92] J. Dingemans, et al., Mutual pharmacokinetic interactions between bosentan and lopinavir/ritonavir in healthy participants, *Antivir. Ther.* 15 (2) (2010) 157–163.
- [93] Y. Lai, et al., Coproporphyrins in plasma and urine can be appropriate clinical biomarkers to recapitulate drug-drug interactions mediated by organic anion transporting polypeptide inhibition, *J. Pharmacol. Exp. Ther.* 358 (3) (2016) 397–404.
- [94] Z.J. Wang, et al., OCT2 polymorphisms and in-vivo renal functional consequence: studies with metformin and cimetidine, *Pharmacogenet. Genomics* 18 (7) (2008) 637–645.
- [95] J. Oh, et al., Inhibition of the multidrug and toxin extrusion (MATE) transporter by pyrimethamine increases the plasma concentration of metformin but does not increase antihyperglycaemic activity in humans, *Diabetes Obes. Metab.* 18 (1) (2016) 104–108.
- [96] S. Tsuruoka, et al., Severe arrhythmia as a result of the interaction of cetirizine and pilsicainide in a patient with renal insufficiency: first case presentation showing competition for excretion via renal multidrug resistance protein 1 and organic cation transporter 2, *Clin. Pharmacol. Ther.* 79 (4) (2006) 389–396.
- [97] S. Abel, et al., Effect of cimetidine and ranitidine on pharmacokinetics and pharmacodynamics of a single dose of dofetilide, *Br. J. Clin. Pharmacol.* 49 (1) (2000) 64–71.
- [98] H. Shen, et al., Evidence for the validity of pyridoxic acid (PDA) as a plasma-based endogenous probe for OAT1 and OAT3 function in healthy subjects, *J. Pharmacol. Exp. Ther.* 368 (1) (2019) 136–145.
- [99] K.C. Cundy, et al., Clinical pharmacokinetics of cidofovir in human immunodeficiency virus-infected patients, *Antimicrob. Agents Chemother.* 39 (6) (1995) 1247–1252.
- [100] D.H. Roberts, et al., Pharmacokinetics of cephadrine given intravenously with and without probenecid, *Br. J. Clin. Pharmacol.* 11 (6) (1981) 561–564.
- [101] K. Maeda, et al., Inhibitory effects of p-aminohippurate and probenecid on the renal clearance of adefovir and benzylpenicillin as probe drugs for organic anion transporter (OAT) 1 and OAT3 in humans, *Eur. J. Pharm. Sci.* 59 (2014) 94–103.

- [102] K.S. Fenner, et al., Drug-drug interactions mediated through P-glycoprotein: clinical relevance and in vitro-in vivo correlation using digoxin as a probe drug, *Clin. Pharmacol. Ther.* 85 (2) (2009) 173–181.
- [103] L. Zhang, S.M. Huang, L.J. Lesko, Transporter-mediated drug-drug interactions, *Clin. Pharmacol. Ther.* 89 (4) (2011) 481–484.
- [104] N. Heyes, P. Kapoor, I.D. Kerr, Polymorphisms of the multidrug pump ABCG2: a systematic review of their effect on protein expression, function, and drug pharmacokinetics, *Drug Metab. Dispos.* 46 (12) (2018) 1886–1899.
- [105] K. Alam, et al., Regulation of organic anion transporting polypeptides (OATP) 1B1- and OATP1B3-mediated transport: an updated review in the context of OATP-mediated drug-drug interactions, *Int. J. Mol. Sci.* 19 (3) (2018), <https://doi.org/10.3390/ijms19030855>.
- [106] J.T. Backman, et al., Gemfibrozil greatly increases plasma concentrations of cerivastatin, *Clin. Pharmacol. Ther.* 72 (6) (2002) 685–691.
- [107] A. Treiber, et al., Bosentan is a substrate of human OATP1B1 and OATP1B3: inhibition of hepatic uptake as the common mechanism of its interactions with cyclosporin A, rifampicin, and sildenafil, *Drug Metab. Dispos.* 35 (8) (2007) 1400–1407.
- [108] L.I. Kajosaari, et al., Cyclosporine markedly raises the plasma concentrations of repaglinide, *Clin. Pharmacol. Ther.* 78 (4) (2005) 388–399.
- [109] L.B. Ramsey, et al., The clinical pharmacogenetics implementation consortium guideline for SLCO1B1 and simvastatin-induced myopathy: 2014 update, *Clin. Pharmacol. Ther.* 96 (4) (2014) 423–428.
- [110] A. Yonezawa, K. Inui, Importance of the multidrug and toxin extrusion MATE/SLC47A family to pharmacokinetics, pharmacodynamics/toxicodynamics and pharmacogenomics, *Br. J. Pharmacol.* 164 (7) (2011) 1817–1825.
- [111] A. Yonezawa, K. Inui, Organic cation transporter OCT/SLC22A and H(+)/organic cation antiporter MATE/SLC47A are key molecules for nephrotoxicity of platinum agents, *Biochem. Pharmacol.* 81 (5) (2011) 563–568.
- [112] W. Wu, K.T. Bush, S.K. Nigam, Key Role for the organic anion transporters, OAT1 and OAT3, in the in vivo handling of uremic toxins and solutes, *Sci. Rep.* 7 (1) (2017) 4939.
- [113] T.B. Vree, M. van den Biggelaar-Marteau, C.P. Verwey-van Wissen, Probenecid inhibits the renal clearance of frusemide and its acyl glucuronide, *Br. J. Clin. Pharmacol.* 39 (6) (1995) 692–695.
- [114] X. Liang, K.M. Giacomini, Transporters involved in metformin pharmacokinetics and treatment response, *J. Pharm. Sci.* 106 (9) (2017) 2245–2250.
- [115] E. Mutschler, H. Spahn, W. Kirch, The interaction between H2-receptor antagonists and beta-adrenoceptor blockers, *Br. J. Clin. Pharmacol.* 17 (Suppl 1) (1984) 51S–57S.
- [116] J.E. Hibma, et al., The effect of famotidine, a MATE1-selective inhibitor, on the pharmacokinetics and pharmacodynamics of metformin, *Clin. Pharmacokinet.* 55 (6) (2016) 711–721.
- [117] H. Kusuhara, et al., Effects of a MATE protein inhibitor, pyrimethamine, on the renal elimination of metformin at oral microdose and at therapeutic dose in healthy subjects, *Clin. Pharmacol. Ther.* 89 (6) (2011) 837–844.
- [118] K.L. Brouwer, et al., In vitro methods to support transporter evaluation in drug discovery and development, *Clin. Pharmacol. Ther.* 94 (1) (2013) 95–112.
- [119] G.J. Hooiveld, et al., Stereoselective transport of hydrophilic quaternary drugs by human MDR1 and rat Mdr1b P-glycoproteins, *Br. J. Pharmacol.* 135 (7) (2002) 1685–1694.
- [120] E.I. Lepist, et al., Contribution of the organic anion transporter OAT2 to the renal active tubular secretion of creatinine and mechanism for serum creatinine elevations caused by cobicistat, *Kidney Int.* 86 (2) (2014) 350–357.
- [121] M. Sasaki, et al., Transcellular transport of organic anions across a double-transfected Madin-Darby canine kidney II cell monolayer expressing both human organic anion-transporting polypeptide (OATP2/SLC21A6) and Multidrug resistance-associated protein 2 (MRP2/ABCC2), *J. Biol. Chem.* 277 (8) (2002) 6497–6503.
- [122] B.L. Morse, et al., Physiologically based pharmacokinetic modeling of transporter-mediated hepatic clearance and liver partitioning of OATP and OCT substrates in cynomolgus monkeys, *AAPS J.* 19 (6) (2017) 1878–1889.
- [123] Y.A. Bi, et al., In vitro evaluation of hepatic transporter-mediated clinical drug-drug interactions: hepatocyte model optimization and retrospective investigation, *Drug Metab. Dispos.* 40 (6) (2012) 1085–1092.
- [124] A. Poirier, et al., Design, data analysis, and simulation of in vitro drug transport kinetic experiments using a mechanistic in vitro model, *Drug Metab. Dispos.* 36 (12) (2008) 2434–2444.
- [125] X. Liu, et al., Correlation of biliary excretion in sandwich-cultured rat hepatocytes and in vivo in rats, *Drug Metab. Dispos.* 27 (6) (1999) 637–644.

- [126] N. Li, et al., Improved extrapolation of hepatobiliary clearance from in vitro sandwich cultured rat hepatocytes through absolute quantification of hepatobiliary transporters, *Mol. Pharm.* 7 (3) (2010) 630–641.
- [127] J.W. Jonker, et al., Deficiency in the organic cation transporters 1 and 2 (Oct1/Oct2 [Slc22a1/Slc22a2]) in mice abolishes renal secretion of organic cations, *Mol. Cell. Biol.* 23 (21) (2003) 7902–7908.
- [128] J.W. Higgins, D.W. Bedwell, M.J. Zamek-Gliszczynski, Ablation of both organic cation transporter (OCT)1 and OCT2 alters metformin pharmacokinetics but has no effect on tissue drug exposure and pharmacodynamics, *Drug Metab. Dispos.* 40 (6) (2012) 1170–1177.
- [129] S.A. Eraly, et al., Decreased renal organic anion secretion and plasma accumulation of endogenous organic anions in OAT1 knock-out mice, *J. Biol. Chem.* 281 (8) (2006) 5072–5083.
- [130] A.L. Vanwert, R.M. Bailey, D.H. Sweet, Organic anion transporter 3 (Oat3/Slc22a8) knockout mice exhibit altered clearance and distribution of penicillin G, *Am. J. Physiol. Ren. Physiol.* 293 (4) (2007) F1332–F1341.
- [131] J.W. Higgins, et al., Utility of Oatp1a/1b-knockout and OATP1B1/3-humanized mice in the study of OATP-mediated pharmacokinetics and tissue distribution: case studies with pravastatin, atorvastatin, simvastatin, and carboxydichlorofluorescein, *Drug Metab. Dispos.* 42 (1) (2014) 182–192.
- [132] T. De Bruyn, et al., Predicting human clearance of organic anion transporting polypeptide substrates using cynomolgus monkey: in vitro-in vivo scaling of hepatic uptake clearance, *Drug Metab. Dispos.* 46 (7) (2018) 989–1000.
- [133] H. Shen, et al., Cynomolgus monkey as a potential model to assess drug interactions involving hepatic organic anion transporting polypeptides: in vitro, in vivo, and in vitro-to-in vivo extrapolation, *J. Pharmacol. Exp. Ther.* 344 (3) (2013) 673–685.
- [134] L. Wang, et al., Interspecies variability in expression of hepatobiliary transporters across human, dog, monkey, and rat as determined by quantitative proteomics, *Drug Metab. Dispos.* 43 (3) (2015) 367–374.
- [135] C.A. Shintre, et al., Structures of ABCB10, a human ATP-binding cassette transporter in apo- and nucleotide-bound states, *Proc. Natl. Acad. Sci. U. S. A.* 110 (24) (2013) 9710–9715.
- [136] F. Montanari, G.F. Ecker, Prediction of drug-ABC-transporter interaction – recent advances and future challenges, *Adv. Drug Deliv. Rev.* 86 (2015) 17–26.
- [137] T. Prueksaritanont, et al., Drug-drug interaction studies: regulatory guidance and an industry perspective, *AAPS J.* 15 (3) (2013) 629–645.
- [138] J. Bentz, et al., Variability in P-glycoprotein inhibitory potency (IC<sub>50</sub>) using various in vitro experimental systems: implications for universal digoxin drug-drug interaction risk assessment decision criteria, *Drug Metab. Dispos.* 41 (7) (2013) 1347–1366.
- [139] J. Vaidyanathan, et al., Comparing various in vitro prediction criteria to assess the potential of a new molecular entity to inhibit organic anion transporting polypeptide 1B1, *J. Clin. Pharmacol.* 56 (Suppl 7) (2016) S59–S72.
- [140] M. Gertz, et al., Application of PBPK modeling in the assessment of the interaction potential of cyclosporine against hepatic and intestinal uptake and efflux transporters and CYP3A4, *Pharm Res.* 30 (3) (2012), <https://doi.org/10.1007/s11095-012-0918-y>.
- [141] Y. Guo, et al., Advancing predictions of tissue and intracellular drug concentrations using in vitro, imaging and physiologically based pharmacokinetic modeling approaches, *Clin. Pharmacol. Ther.* 104 (5) (2018) 865–889.
- [142] H.M. Jones, et al., Physiologically based pharmacokinetic modeling in drug discovery and development: a pharmaceutical industry perspective, *Clin. Pharmacol. Ther.* 97 (3) (2015) 247–262.
- [143] C. Wagner, et al., Application of Physiologically Based Pharmacokinetic (PBPK) modeling to support dose selection: report of an FDA public workshop on PBPK, *CPT Pharmacometrics Syst. Pharmacol.* 4 (4) (2015) 226–230.
- [144] X. Chu, et al., Evaluation of cynomolgus monkeys for the identification of endogenous biomarkers for hepatic transporter inhibition and as a translatable model to predict pharmacokinetic interactions with statins in humans, *Drug Metab. Dispos.* 43 (6) (2015) 851–863.
- [145] S.W. Yee, et al., Metabolomic and Genome-wide association studies reveal potential endogenous biomarkers for OATP1B1, *Clin. Pharmacol. Ther.* 100 (5) (2016) 524–536.
- [146] H. Shen, et al., Discovery and validation of pyridoxic acid and homovanillic acid as novel endogenous plasma biomarkers of organic anion transporter (OAT) 1 and OAT3 in cynomolgus monkeys, *Drug Metab. Dispos.* 46 (2) (2018) 178–188.
- [147] R. Thakare, et al., Leveraging of rifampicin-dosed cynomolgus monkeys to identify bile acid 3-O-sulfate conjugates as potential novel biomarkers for organic anion-transporting polypeptides, *Drug Metab. Dispos.* 45 (7) (2017) 721–733.

- [148] H. Shen, et al., Coproporphyrins I and III as functional markers of OATP1B activity: in vitro and in vivo evaluation in preclinical species, *J. Pharmacol. Exp. Ther.* 357 (2) (2016) 382–393.
- [149] D. Rodrigues, A. Rowland, From endogenous compounds as biomarkers to plasma-derived nanovesicles as liquid biopsy; has the golden age of translational pharmacokinetics-absorption, distribution, metabolism, excretion-drug-drug interaction science finally arrived? *Clin. Pharmacol. Ther.* 105 (6) (2019) 1407–1420.
- [150] F. Muller, et al., Biomarkers for in vivo assessment of transporter function, *Pharmacol. Rev.* 70 (2) (2018) 246–277.
- [151] I. Takehara, et al., Investigation of glycochenodeoxycholate sulfate and chenodeoxycholate glucuronide as surrogate endogenous probes for drug interaction studies of OATP1B1 and OATP1B3 in healthy Japanese volunteers, *Pharm. Res.* (2017).
- [152] Y. Lai, P. Hsiao, Beyond the ITC White Paper: emerging sciences in drug transporters and opportunities for drug development, *Curr. Pharm. Des.* 20 (10) (2014) 1577–1594.
- [153] L. Zhang, et al., Transporters in drug development: scientific and regulatory considerations, *Clin. Pharmacol. Ther.* 104 (5) (2018) 793–796.
- [154] M.J. Zamek-Gliszczynski, et al., ITC Commentary on metformin clinical drug-drug interaction study design that enables an efficacy- and safety-based dose adjustment decision, *Clin. Pharmacol. Ther.* 104 (5) (2018) 781–784.
- [155] S.W. Yee, et al., Influence of transporter polymorphisms on drug disposition and response: a perspective from the international transporter consortium, *Clin. Pharmacol. Ther.* 104 (5) (2018) 803–817.
- [156] A. Schlessinger, et al., Molecular modeling of drug-transporter interactions-an international transporter consortium perspective, *Clin. Pharmacol. Ther.* 104 (5) (2018) 818–835.
- [157] J.G. Kenna, et al., Can bile salt export pump inhibition testing in drug discovery and development reduce liver injury risk? an international transporter consortium perspective, *Clin. Pharmacol. Ther.* 104 (5) (2018) 916–932.
- [158] R. Evers, et al., Disease-associated changes in drug transporters may impact the pharmacokinetics and/or toxicity of drugs: a white paper from the international transporter consortium, *Clin. Pharmacol. Ther.* 104 (5) (2018) 900–915.
- [159] X. Chu, et al., Dabigatran etexilate and digoxin: comparison as clinical probe substrates for evaluation of P-gp inhibition, *Clin. Pharmacol. Ther.* 104 (5) (2018) 788–792.
- [160] K.M. Giacomini, A. Galetin, S.M. Huang, The international transporter consortium: summarizing advances in the role of transporters in drug development, *Clin. Pharmacol. Ther.* 104 (5) (2018) 766–771.
- [161] L.Z. Benet, F. Broccatelli, T.I. Oprea, BDDCS applied to over 900 drugs, *AAPS J.* 13 (4) (2011) 519–547.

# Mechanisms and clinical relevance of pharmacokinetic-based clinical drug-drug interactions for drugs recently approved by the US Food and Drug Administration

*Jingjing Yu, Ichiko D. Petrie, Sophie M.A. Argon, Katie H. Owens, Isabelle Ragueneau-Majlessi*

Department of Pharmaceutics, School of Pharmacy, University of Washington, Seattle, WA, United States

## Abbreviations

AUC	area under the time-plasma concentration curve
AUCR	AUC ratio
BCRP	breast cancer resistance protein
BCS	biopharmaceutics classification system
C <sub>max</sub>	maximum plasma concentration
DDI	drug-drug interaction
FDA	Food and Drug Administration
FDC	fixed-dose combination
H2RA	histamine receptor-2 antagonist
HCV	anti-hepatitis C virus
HIV	human immunodeficiency virus
IM	intermediate metabolizer
MRP	multidrug resistance-associated protein
NDA	new drug application
NM	normal metabolizer



NME	new molecular entity
NTR	narrow therapeutic range
OAT	organic anion transporter
OATP	organic anion transporting polypeptide
P450 or CYP	cytochrome P450
PBPK	physiologically based pharmacokinetics
P-gp	P-glycoprotein
PGx	pharmacogenetic(s)
PK	pharmacokinetic(s)
PM	poor metabolizer
PPI	proton-pump inhibitor
PXR	pregnane X receptor
UGT	UDP-glucuronosyltransferase
UM	ultrapid metabolizer

## 1 Introduction

In the last two decades, the US Food and Drug Administration (FDA) and the pharmaceutical industry have contributed to the development of a systematic, risk-based approach for evaluating pharmacokinetic (PK)-based drug-drug interactions (DDIs) and communicating the results to the scientific and medical communities. These approaches [1,2] are best expressed in New Drug Application (NDA) reviews because these documents contain pre-clinical and clinical investigational data of the new molecular entities (NMEs) and the implications of those findings in the drug labels. These NDA reviews are also useful because only a small portion of their data becomes available in the scientific literature, even at a later date. Thus, NDA reviews provide a unique perspective on the evolution of drug interaction science, acting like a snapshot of the implementation of DDI guidances and newer regulatory recommendations in the mechanistic and clinical contexts of various therapeutic classes. This chapter provides an overview of the most significant clinical DDIs associated with NDAs of drugs approved by the FDA between 2013 and 2017, discussing how to minimize the risk of large interactions and safely administer these new drugs in specific patient populations. This analysis was performed using the University of Washington Drug Interaction Database (DIDB) (<http://www.druginteractionsolutions.org>) following a methodology previously described [3]. Clinical DDI study results were obtained from dedicated DDI clinical trials, pharmacogenetics (PGx) studies, and physiologically based PK (PBPK) modeling studies that functioned as alternatives to dedicated clinical studies.

A total of 137 NDAs approved by the FDA from 2013 to 2017 (including 14 combination drugs with 2 NMEs, thus a total of 142 NMEs) were evaluated. The most represented therapeutic areas were oncology drugs (23%) and anti-infective agents (21%; including 13 antivirals, 10 antibacterials, 4 antifungals, and 2 antiparasitics), followed by central nervous system agents (12%) and metabolism disorder/endocrinology drugs (11%). Almost all NDAs (96%) had drug metabolism data and 84% had transporter data, including in vitro and/or clinical evaluations. For all DDI and PGx studies, an AUC change of 25% was used as the cutoff to define a positive study following the regulatory recommendation [1]. Given the very large amount of metabolism- and transporter-mediated DDI information provided in these documents, only the largest clinical interactions, defined as AUC ratios (AUCRs)  $\geq 5$  for strong inhibitors or sensitive substrates and  $\leq 0.2$  for strong inducers [1], are discussed in the following sections.



The numbers of PGx studies and DDI studies mediated by other mechanisms were relatively small and all positive clinical studies with AUC changes  $\geq 25\%$  were analyzed.

## 2 Enzyme-mediated DDIs

### 2.1 NMEs as substrates of enzymes

Almost all NMEs were assessed in vitro as substrates of drug-metabolizing enzymes. The numbers of NME substrates of drug-metabolizing enzymes are presented in Fig. 1A. As expected, CYP3A played a major role, metabolizing approximately 60% of the NMEs ( $N = 86$ ), followed by CYP2D6 ( $N = 30$ ), and the CYP2C family.

Clinically, 17 NMEs (12% of all NMEs) were identified to be sensitive substrates, with AUCRs  $\geq 5$  when coadministered with a strong inhibitor (Table 1). Among them, the most represented therapeutic classes were oncology drugs ( $N = 6$ ; abemaciclib, cobimetinib, ibrutinib, midostaurin, neratinib, and venetoclax) and anti-infective drugs, which included three antivirals (dasabuvir, paritaprevir, and simeprevir) and one antifungal (isavuconazole, the active moiety of the prodrug isavuconazonium sulfate).

Consistent with the in vitro findings, CYP3A was the predominant enzyme involved in these large clinical interactions, contributing to inhibition interactions with 14 NMEs, mainly as a single contributor (Table 1). Due to the large increases in drug exposure, label recommendations (contraindication, avoidance, not recommended, dose reduction, caution, monitor for increased risk of adverse reactions, and consider alternative therapies) were included in all

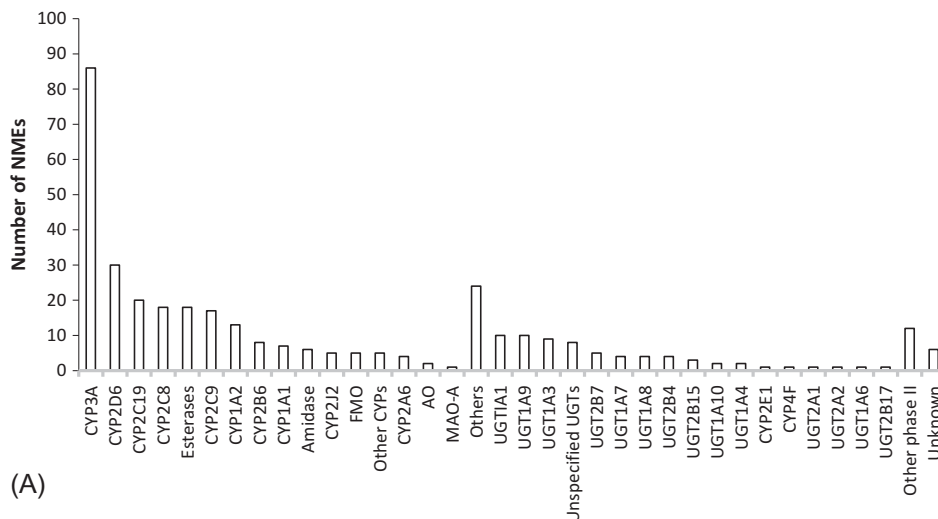


**FIG. 1A** Numbers of NMEs as enzyme substrates in vitro. Other CYPs: not specified. Other phase II: include sulfotransferases, glutathione S-transferases, acetyltransferase, cysteine conjugation enzymes, and unspecified conjugated enzymes. Others: include catecholamine pathway enzymes, epoxide hydrolase, hydrolases, phospholipidase, phosphatase, proteinase, nucleases, nucleotidase, thymidine phosphorylase, peptidase/proteases, cathepsin A, reductase, unspecified biotransformation enzymes, and unspecified enzymes for hydrolysis and oxidation. AO, aldehyde oxidase; FMO, flavin-containing monooxygenase; MAO, monoamine oxidase.

TABLE 1 Inhibition DDIs with AUCR  $\geq 5$ , NMEs as substrates.<sup>a</sup>

Victim drug	Inhibitor	Main enzymes/ transporters possibly involved	AUCR	C <sub>max</sub> R	References
Paritaprevir	Ritonavir	CYP3A, P-gp, BCRP, OATP1B1/3	47.43	28.07	[4]
Eliglustat <sup>b,c</sup>	Ketoconazole/ paroxetine	CYP3A, CYP2D6	37.85 (CYP2D6 EMs; PBPK), 24.16 (CYP2D6 EMs; PBPK), 9.81 (CYP2D6 IMs; PBPK)	18.25 (CYP2D6 EMs; PBPK), 16.68 (CYP2D6 EMs; PBPK), 7.48 (CYP2D6 IMs; PBPK)	[5]
Eliglustat	Paroxetine	CYP2D6	28.40 (CYP2D6 UMs), 10.00 (CYP2D6 EMs), 5.20 (CYP2D6 IMs)	22.00 (CYP2D6 UMs), 8.20 (CYP2D6 EMs), 4.10 (CYP2D6 IMs)	[5]
Ibrutinib <sup>d</sup>	Ketoconazole	CYP3A	23.90	28.60	[6]
Eliglustat <sup>e</sup>	Fluconazole/ terbinafine	CYP3A, CYP2D6	19.31 (CYP2D6 EMs; PBPK), 13.58 (CYP2D6 EMs; PBPK)	10.71 (CYP2D6 EMs; PBPK), 10.16 (CYP2D6 EMs; PBPK)	[5]
Abemaciclib <sup>c</sup>	Ketoconazole	CYP3A	15.73	N/P	[7]
Grazoprevir <sup>f</sup>	Cyclosporine	OATP1B1/3	15.25 <sup>g</sup>	17.03	[8]
Grazoprevir <sup>f</sup>	Lopinavir/ ritonavir	CYP3A, OATP1B1/3	12.87	7.31	[8]
Naloxegol <sup>c</sup>	Ketoconazole	CYP3A4	12.42	9.12	[9]
Grazoprevir <sup>f</sup>	Atazanavir/ ritonavir	CYP3A, OATP1B1/3	10.56	6.24	[8]
Midostaurin	Ketoconazole	CYP3A4	10.42, 3.51 (CGP62221), 1.21 (CGP52421)	1.83	[10]
Grazoprevir	Rifampin (IV)	OATP1B1/3	10.22	10.96	[8]
Dasabuvir	Gemfibrozil	CYP2C8	9.90	1.91	[4]
Voxilaprevir	Cyclosporine	OATP1B1, OATP1B3, P-gp, BCRP	9.73	14.29	[11]
Ibrutinib	Erythromycin	CYP3A	8.60 (PBPK)	N/P	[6]
Glecaprevir	Rifampin	OATP1B1, OATP1B3	8.55	6.52	[12]
Grazoprevir <sup>f</sup>	Rifampin	OATP1B1/3	8.37	6.52	[8]
Voxilaprevir	Rifampin	OATP1B1, OATP1B3	7.96	8.74	[11]
Ivabradine <sup>c</sup>	Josamycin	CYP3A4	7.70	3.60	[13]
Ivabradine <sup>c</sup>	Ketoconazole	CYP3A4	7.70	3.60	[13]
Eliglustat	Fluconazole	CYP3A	7.54 (PBPK)	3.76 (PBPK)	[5]

TABLE 1 Inhibition DDIs with AUCR  $\geq 5$ , NMEs as substrates<sup>a</sup>—cont'd

Victim drug	Inhibitor	Main enzymes/ transporters possibly involved	AUCR	C <sub>max</sub> R	References
Grazoprevir <sup>f</sup>	Darunavir/ ritonavir	CYP3A, OATP1B1/3	7.49	5.27	[8]
Simeprevir <sup>c</sup>	Ritonavir	CYP3A	7.18	4.70	[14]
Abemaciclib <sup>c</sup>	Itraconazole	CYP3A	7.15, 2.20 (abemaciclib, M2, M18, and M20)	N/P	[7]
Tasimelteon <sup>h</sup>	Fluvoxamine	CYP1A2	6.87	2.28	[15]
Pirfenidone	Fluvoxamine	CYP1A2	6.81 (smokers), 3.97 (nonsmokers)	2.24 (smokers), 1.69 (nonsmokers)	[16]
Cobimetinib <sup>c</sup>	Itraconazole	CYP3A	6.62	3.17	[17]
Simeprevir <sup>c</sup>	Erythromycin	CYP3A	6.54	4.02	[14]
Glecaprevir	Atazanavir/ ritonavir	OATP1B1, OATP1B3, P-gp, BCRP	6.53	4.51	[12]
Flibanserin	Fluconazole	CYP3A4, CYP2C19	6.41	2.11	[18]
Venetoclax	Ketoconazole	CYP3A, P-gp	6.40	2.33	[19]
Eliglustat <sup>e,i</sup>	Ketoconazole	CYP3A	6.22 (CYP2D6 PMs; PBPK), 5.54 (CYP2D6 PMs; PBPK)	4.27 (CYP2D6 PMs; PBPK), 4.55 (CYP2D6 PMs; PBPK)	[5]
Ibrutinib	Diltiazem	CYP3A	5.50 (PBPK)	N/P	[6]
Isavuconazole <sup>j</sup>	Ketoconazole	CYP3A, butyrylcholinesterase	5.22	1.09	[20]
Neratinib <sup>c</sup>	Ketoconazole	CYP3A4	5.16	3.63	[21,22]
Glecaprevir	Cyclosporine	OATP1B1, OATP1B3, P-gp, and BCRP	5.08	4.51	[12]

IV, intravenously; CGP62221, desmethylmidostaurin; CGP52421, 7-hydroxymidostaurin.

<sup>a</sup> Drugs were administered orally unless otherwise specified.

<sup>b</sup> AUCR = 37.85, eliglustat was administered at 100 mg once daily for 18 days, AUCR = 24.16 and 9.81, eliglustat was administered at 100 mg twice daily for 18 days; C<sub>max</sub>R = 18.25, eliglustat was administered at 100 mg once daily for 18 days, C<sub>max</sub>R = 16.68 and 7.48, eliglustat was administered at 100 mg twice daily for 18 days.

<sup>c</sup> Also a substrate of P-gp based on *in vitro* results. Inhibition of P-gp might contribute to the observed interaction.

<sup>d</sup> *In vitro*, ibrutinib is not a substrate of P-gp in Caco-2 cells, but its metabolite PCI-45227 is a substrate (net efflux ratio of 2).

<sup>e</sup> AUCR = 19.31, eliglustat was administered at 100 mg once daily for 18 days, AUCR = 13.58, eliglustat was administered at 100 mg twice daily for 18 days; C<sub>max</sub>R = 10.71, eliglustat was administered at 100 mg once daily for 18 days, C<sub>max</sub>R = 10.16, eliglustat was administered at 100 mg twice daily for 18 days.

<sup>f</sup> Also a substrate of P-gp and BCRP based on *in vitro* results.

<sup>g</sup> AUC<sub>24h</sub>.

<sup>h</sup> Also metabolized by CYP3A4, CYP2C9, and CYP2C19, and fluvoxamine inhibits these P450s.

<sup>i</sup> AUCR = 6.22, eliglustat was administered at 100 mg once daily for 14 days, AUCR = 5.54, eliglustat was administered at 100 mg twice daily for 14 days; C<sub>max</sub>R = 4.27, eliglustat was administered at 100 mg once daily for 14 days, C<sub>max</sub>R = 4.55, eliglustat was administered at 100 mg twice daily for 14 days;

<sup>j</sup> Active moiety of the prodrug isavuconazonium sulfate.

## II. Drug metabolism enzymes, transporters and drug-drug interaction

labels regarding concomitant use with strong CYP3A inhibitors. To illustrate, the highest CYP3A-mediated change in exposure was observed with ibrutinib, a kinase inhibitor indicated for the treatment of various B-cell malignancies. After coadministration with the strong CYP3A inhibitor ketoconazole (400 mg once daily), ibrutinib AUC and  $C_{\max}$  significantly increased 23.90- and 28.60-fold, respectively. According to ibrutinib label, coadministration with strong CYP3A inhibitors should be avoided [6]. The high sensitivity of ibrutinib to CYP3A inhibition was also predicted through PBPK modeling for concomitant administration with a moderate inhibitor, where ibrutinib AUC was predicted to increase 5.50-fold in the presence of clinical doses of diltiazem. Consequently, coadministration of ibrutinib with moderate inhibitors should also be avoided if possible, otherwise the dose of ibrutinib should be reduced [6]. Interestingly, almost all sensitive substrates of CYP3A were also substrates of P-glycoprotein (P-gp) *in vitro*, confirming the large overlap between the two systems. Given that the inhibitors used in the DDI evaluations, such as itraconazole, josamycin, ketoconazole, erythromycin, are also known inhibitors of P-gp, inhibition of P-gp is likely to have contributed to these large interactions.

Some of the observed interactions were caused by a combined effect of the perpetrator on CYP3A and other enzymes. For example, a significant change in the exposure to flibanserin was observed with the coadministration of fluconazole (400 mg loading dose followed by 200 mg once daily), a moderate CYP3A inhibitor, and a strong inhibitor of CYP2C19, with a 6.41- and 2.11-fold increase in the AUC and  $C_{\max}$  of flibanserin, respectively. In comparison, CYP3A inhibition by ketoconazole (400 mg once daily) increased the AUC and  $C_{\max}$  of flibanserin 4.61- and 1.84-fold, respectively. These results confirm the *in vitro* findings that flibanserin is mainly metabolized by CYP3A, and to a lesser extent by CYP2C19. Considering the risk of hypotension and syncope associated with increased plasma concentrations of flibanserin, its concomitant use with moderate or strong CYP3A inhibitors is contraindicated [18].

Besides CYP3A, four drugs were found to be sensitive substrates of other enzymes: CYP1A2 (pirfenidone and tasimelteon), CYP2C8 (dasabuvir), and CYP2D6 (eliglustat). Following the coadministration of multiple doses of fluvoxamine, a strong CYP1A2 inhibitor, exposure to tasimelteon increased 6.87-fold, while the increase in the exposure of pirfenidone was 6.81- and 3.97-fold in smokers and nonsmokers, respectively. The AUC of dasabuvir, a direct acting antiviral agent [component of a fixed-dose combination (FDC) drug Viekira Pak], increased 9.90-fold following coadministration with gemfibrozil (600 mg twice daily), a strong CYP2C8 inhibitor. Finally, the exposure to eliglustat, a glucosylceramide synthase inhibitor indicated for Gaucher disease type 1, significantly increased when coadministered with the strong CYP2D6 inhibitor, paroxetine (30 mg once daily). The exposure increases varied based on the CYP2D6 phenotype status of the subjects, ranging from a 5.20-fold increase in CYP2D6 intermediate metabolizers (IMs;  $N=8$ ) to a 28.40-fold increase in a CYP2D6 ultrarapid metabolizer (UM;  $N=1$ ).

Based on induction studies, 24 NMEs were found to be sensitive to induction (AUC decreases  $\geq 80\%$  [5-fold]), with some drug exposures almost completely abolished by concomitant administration with the strong inducer rifampin (Table 2). Here also, drugs for cancer treatment were predominant ( $N=10$ ), nine of them being kinase inhibitors, namely abemaciclib, acalabrutinib, brigatinib, cobimetinib, ibrutinib, midostaurin, neratinib, palbociclib, and ribociclib. All induction interactions with AUC changes  $\geq 5$ -fold ( $N=25$  DDIs) were predominantly mediated by CYP3A under coadministration with rifampin,

**TABLE 2** Induction DDIs with AUCR  $\leq 0.2$ , NMEs as substrates.

Victim drug	Inducer	Main enzymes / transporters possibly involved	AUCR	C <sub>max</sub> R	References
Isavuconazole	Rifampin	CYP3A, butyrylcholinesterase	0.03	0.25	[20]
Eliglustat	Rifampin (IV)	CYP3A	0.04 (CYP2D6 PMs), 0.09 (CYP2D6 IMs), 0.10 (CYP2D6 EMs)	0.05 (CYP2D6 PMs), 0.09 (CYP2D6 IMs), 0.11 (CYP2D6 EMs)	[5]
Flibanserin	Rifampin	CYP3A4, CYP2C19	0.04	0.10	[18]
Abemaciclib	Rifampin	CYP3A	0.05, 0.35, 1.31, 0.20 (abemaciclib, M2, M18, and M20)	0.08, 0.96, 4.26, 0.64 (abemaciclib, M2, M18, and M20)	[7]
Deflazacort	Rifampin	CYP3A4	0.06 (21-desacetyl deflazacort)	0.08	[23]
Midostaurin	Rifampin	CYP3A4	0.06 (CGP62221), 0.41 (CGP52421)	0.63 (CGP62221), 0.65 (CGP52421)	[10]
Ibrutinib	Rifampin	CYP3A	0.08 (PBPK)	0.07 (PBPK)	[6]
Naloxegol	Rifampin	CYP3A4	0.11	0.26	[9]
Olaparib	Rifampin	CYP3A	0.11	0.3	[24]
Ribociclib	Rifampin	CYP3A	0.11	0.19	[25]
Glecaprevir	Rifampin	P-gp, CYP3A	0.12	0.14	[12]
Neratinib	Rifampin	CYP3A4	0.12	0.23	[21]
Rolapitant	Rifampin	CYP3A4	0.12	0.68	[26]
Suvorexant	Rifampin	CYP3A	0.12	0.36	[27]
Pibrentasvir	Rifampin	P-gp	0.13–0.17	0.17–0.21	[12]
Tasimelteon <sup>a</sup>	Rifampin	CYP3A4	0.14	0.23	[15]
Palbociclib <sup>b</sup>	Rifampin	CYP3A	0.15	0.28	[28]
Acalabrutinib <sup>b</sup>	Rifampin	CYP3A	0.17 (acalabrutinib), 0.39 (ACP-5862)	N/P	[29]
Cobimetinib <sup>b</sup>	Rifampin	CYP3A	0.17 (PBPK)	0.37 (PBPK)	[17]
Grazoprevir <sup>c</sup>	Efavirenz	CYP3A	0.17	0.13	[8]
Naldemedine <sup>b</sup>	Rifampin	CYP3A4	0.17 (naldemedine), 2.45 (nornaldemedine)	0.61 (naldemedine), 3.17 (nornaldemedine)	[30]

*Continued*

TABLE 2 Induction DDIs with AUCR  $\leq$ 02, NMEs as substrates.—cont'd

Victim drug	Inducer	Main enzymes / transporters possibly involved	AUCR	C <sub>max</sub> R	References
Velpatasvir <sup>c</sup>	Rifampin	CYP2B6, CYP2C8, CYP3A	0.19	0.29	[31]
Abemaciclib <sup>c</sup>	Carbamazepine	CYP3A	0.20	N/P	[7]
Brigatinib <sup>c</sup>	Rifampin	CYP3A4, CYP2C8	0.20	0.40	[32]
Netupitant	Rifampin	CYP3A4	0.20	0.45	[33]

IV, intravenously; ACP-5862, *acalabrutinib hydroxylated metabolite*.

<sup>a</sup> Also metabolized by CYP1A2, CYP2C9, and CYP2C19, and rifampin is an inducer of multiple P450s.

<sup>b</sup> Also a substrate of P-gp based on *in vitro* results. Induction of P-gp may contribute to the observed interaction.

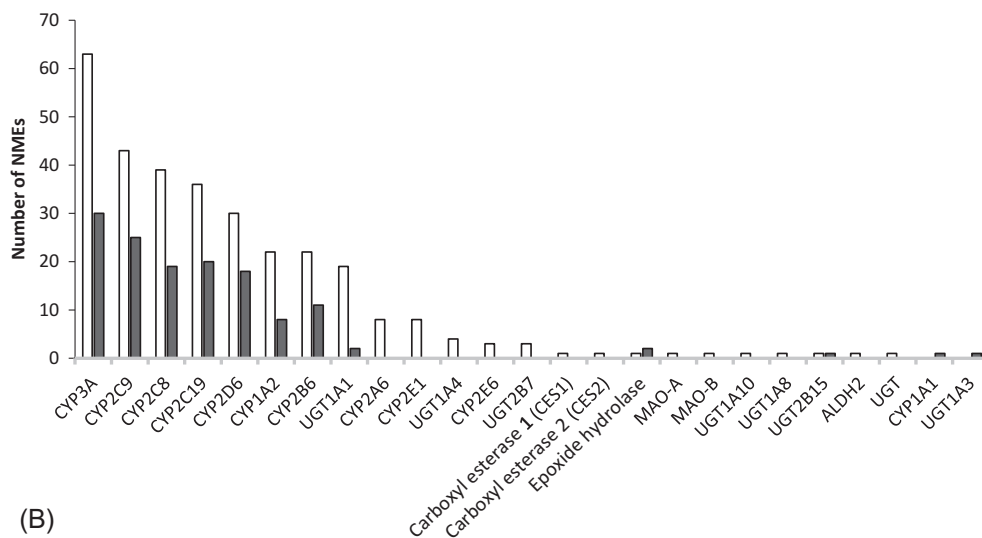
<sup>c</sup> Also a substrate of P-gp and BCRP based on *in vitro* results. Induction of P-gp and BCRP may contribute to the observed interaction.

carbamazepine, or efavirenz, some with partial contributions from other enzymes (e.g., CYP1A2, CYP2B6, CYP2C8, CYP2C19) and transporters (e.g., P-gp). Rifampin (600 mg multiple doses), a known inducer of multiple metabolic pathways and transporters, was used as a prototypical inducer in 23 (92%) DDI studies. Given the large decrease in drug exposure and associated loss of drug efficacy, concomitant use of these drugs with strong CYP3A inducers is contraindicated, avoided, or not recommended. For example, isavuconazole exhibited the greatest decrease in exposure (AUC), with only 3% of the drug remaining in plasma after coadministration of the prodrug isavuconazonium sulfate with rifampin due to the induction of both CYP3A and butyrylcholinesterase. Similarly, drug exposure of eliglustat and flibanserin has reduced by 96% when coadministered with rifampin, resulting from CYP3A and CYP3A/2C19 induction, respectively. Consequently, coadministration of isavuconazonium sulfate with strong CYP3A inducers is contraindicated, eliglustat with strong CYP3A inducers is not recommended, and flibanserin is not recommended with any CYP3A inducers [5,18,20].

Interestingly, the antiviral drug simeprevir, which was identified as a sensitive substrate of CYP3A through inhibition studies with a 7.18- and 6.54-fold increase observed when coadministered with ritonavir and erythromycin, respectively, was only modestly affected by rifampin multiple dosing (48% decrease and 30% increase in simeprevir AUC and C<sub>max</sub>, respectively). This result is likely due to the concurrent inhibition of hepatic uptake by rifampin, a known inhibitor of organic anion transporting polypeptide (OATP) transporters. In comparison, concomitant use of efavirenz, a moderate inducer of CYP3A that does not affect OATPs, decreased simeprevir AUC and C<sub>max</sub> by 71% and 51%, respectively.

## 2.2 NMEs as inhibitors of enzymes

Almost all drugs and major metabolites were tested *in vitro* for their inhibition potential on drug-metabolizing enzymes. The numbers of NMEs and metabolites with positive results are presented in Fig. 1B. The largest number of drugs were inhibitors of CYP3A ( $N = 63$ ), followed by CYP2C9 ( $N = 43$ ), CYP2C8 ( $N = 39$ ), CYP2C19 ( $N = 36$ ), CYP2D6 ( $N = 30$ ),



(B)

**FIG. 1B** Numbers of NMEs as enzyme inhibitors in vitro. Legend: open bar, parent drug; black bar, metabolite. *ALDH*, aldehyde dehydrogenase.

CYP1A2 ( $N = 22$ ), and CYP2B6 ( $N = 22$ ). A total of 19 drugs were found to be in vitro inhibitors of UGT1A1.

Clinically, only three drugs (which include a combination drug containing three NMEs) showed strong inhibition of CYP3A (Table 3). The FDC anti-hepatitis C virus (HCV) drug Viekira Pak containing ombitasvir, paritaprevir, ritonavir, and dasabuvir significantly affected the exposure to tacrolimus, a sensitive CYP3A substrate, with changes in AUC ranging from 57- to 86-fold. Mechanistically, the strong inhibition is most likely caused by ritonavir since, in vitro, only ritonavir showed strong inhibition of CYP3A [lowest reported  $IC_{50}$  values of  $0.006\ \mu\text{M}$  [36] and  $0.010\ \mu\text{M}$  [37] with the substrates midazolam and testosterone, respectively, and  $K_i$  values of  $0.06\ \mu\text{M}$  (competitive) [38] and  $0.019\ \mu\text{M}$  (mixed) [39], respectively]. Inhibition of P-gp may be involved as ritonavir also inhibits P-gp in vitro, with the lowest  $IC_{50}$  value of  $0.24\ \mu\text{M}$  [40]. Based on these results, concomitant use of Viekira Pak is contraindicated with drugs that are highly dependent on CYP3A for clearance [4]. In addition, two oncology drugs, idelalisib and ribociclib, were identified as strong inhibitors of CYP3A, increasing the AUC of midazolam (a sensitive CYP3A substrate) approximately 5-fold, when coadministered as 150 mg twice daily and 600 mg once daily, respectively. Both drugs are inhibitors of CYP3A in vitro, with an  $IC_{50}$  value of  $44\ \mu\text{M}$  for idelalisib [34], and a  $K_{i,u}$  value of  $30\ \mu\text{M}$  for ribociclib [25]. GS-563117, the major (inactive) metabolite of idelalisib, is also an inhibitor of CYP3A with even higher potency ( $IC_{50} = 5.1\ \mu\text{M}$ ) than the parent drug. Additionally, ribociclib was found to be a mechanism-based inhibitor of CYP3A ( $K_{i,u} = 4.44\ \mu\text{M}$ ,  $k_{inact} = 0.02/\text{min}$ ). According to the labels, concomitant use of idelalisib with CYP3A substrates should be avoided, while caution or dose reduction with CYP3A substrates with a narrow therapeutic range (NTR) is advised for ribociclib [25,34].



TABLE 3 Inhibition DDIs with AUCR  $\geq 5$  and induction DDIs with AUCR  $\leq 0.2$ , NMEs as perpetrators.

Victim drug	Inhibitor	Enzymes/transporters possibly involved	AUCR	C <sub>max</sub> R	References
<i>NMEs as inhibitors</i>					
Tacrolimus	Ombitasvir/paritaprevir/ritonavir	CYP3A, P-gp	85.92	24.54 <sup>a</sup>	[4]
Tacrolimus	Paritaprevir/dasabuvir/ritonavir	CYP3A, P-gp	78.68	24.88 <sup>a</sup>	[4]
Tacrolimus	Ombitasvir/paritaprevir/dasabuvir/ritonavir	CYP3A, P-gp	57.07	16.48 <sup>a</sup>	[4]
Atorvastatin	Glecaprevir/pibrentasvir	OATP1B1, OATP1B3, CYP3A	8.28	22	[12]
Rosuvastatin	Voxilaprevir	BCRP, OATP1B1, OATP1B3	7.35	17.96	[11]
Cyclosporine	Ombitasvir/paritaprevir/dasabuvir/ritonavir	CYP3A, P-gp	5.78	15.73 <sup>a</sup>	[4]
Midazolam	Ribociclib	CYP3A	5.17 (PBPK)	2.41 (PBPK)	[25]
Midazolam	Idelalisib	CYP3A	5.15	2.31	[34]
<i>NMEs as inducers</i>					
Itraconazole	Ivacaftor and lumacaftor	CYP3A	0.18	0.1	[35]
Ivacaftor	Lumacaftor	CYP3A	0.20	0.19	[35]

<sup>a</sup> C<sub>min</sub>.

### 2.3 NMEs as inducers of enzymes

The induction potential of most NMEs and some metabolites on drug-metabolizing enzymes (CYPs and phase II enzymes such as glutathione S-transferases, sulfotransferases, and UGTs) was systemically evaluated in vitro using human hepatocytes. Regulation of pregnane X receptor (PXR) was also investigated for a few drugs. The numbers of NMEs and metabolites with positive induction results are presented in Fig. 1C. The largest number of drugs were found to be inducers of CYP3A ( $N = 34$ ), followed by CYP2B6 ( $N = 25$ ) and CYP1A2 ( $N = 17$ ). However, most of the induction effects were observed at drug concentrations far greater than the clinical C<sub>max</sub> values and, based on predictions using basic or mechanistic models, these effects were not considered to be clinically relevant and therefore no clinical studies were warranted. Interestingly, some drugs exhibited both induction and inhibition toward the same P450 in vitro. For example, the antiviral drug letermovir not only induced CYP2B6 (2.70-fold and 65% of positive control at concentrations up to 20  $\mu$ M), but also weakly inhibited CYP2B6 (IC<sub>50</sub> = 54  $\mu$ M). Based on an R value for inhibition below the threshold for clinical relevance, clinical inhibition of CYP2B6 by letermovir was expected to be minimal, therefore no clinical study had to be conducted. The clinical relevance of in vitro induction of CYP2B6 is unknown [41].

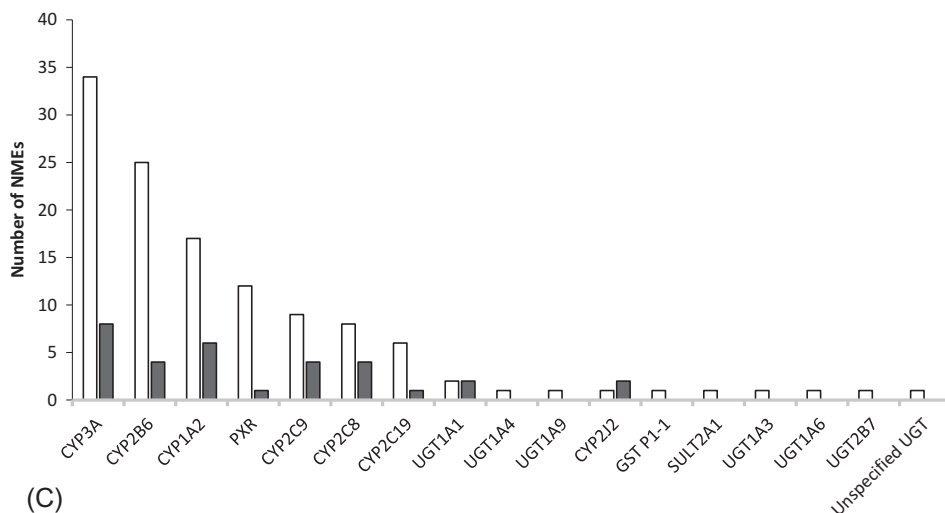


FIG. 1C Numbers of NMEs as enzyme inducers in vitro. Legend: open bar, parent drug; black bar, metabolite. GST, glutathione S-transferase.

When evaluated clinically, only one NME, lumacaftor (a component of the combination drug ivacaftor/lumacaftor), was found to be a strong inducer of CYP3A (Table 3). When ivacaftor, a sensitive substrate of CYP3A, was coadministered with lumacaftor (150 mg twice daily), ivacaftor AUC reduced by 80%. A similar decrease in the exposure of itraconazole, a likely comedication, was observed when coadministered with the combination drug due to the induction of CYP3A by lumacaftor, with AUC and  $C_{max}$  of itraconazole decreased by 82% and 90%, respectively. Consistent with these clinical observations, lumacaftor induced CYP3A activity in vitro, with an  $E_{max}$  value ranging from 2.27- to 12.9-fold in human hepatocytes. Given the expected large decrease in the exposure of coadministered CYP3A substrates, and in order to avoid therapeutic failure, coadministration of ivacaftor/lumacaftor with sensitive or NTR CYP3A substrates is not recommended [35].

### 3 Transporter-mediated DDIs

#### 3.1 NMEs as substrates of transporters

In vitro, the largest number of NMEs were found to be substrates of P-gp ( $N = 65$ ), followed by breast cancer resistance protein (BCRP;  $N = 31$ ), OATP1B1 ( $N = 10$ ), and OATP1B3 ( $N = 9$ ; Fig. 2A). Only a few metabolites were found to be substrates of the following transporters, including BCRP, P-gp, multidrug resistance-associated protein 2 (MRP2), organic anion transporter (OAT) 1, and OAT2. As discussed in the enzyme section, almost all the sensitive substrates of CYP3A were also substrates of P-gp. To avoid redundancy, these interactions are not included in this section. Regarding the other largest clinical DDIs ( $N = 13$ ; Table 1), inhibition of hepatic OATP1B1/1B3 was the predominant mechanism, with involvement of P-gp and BCRP in some of the interactions. All DDIs with

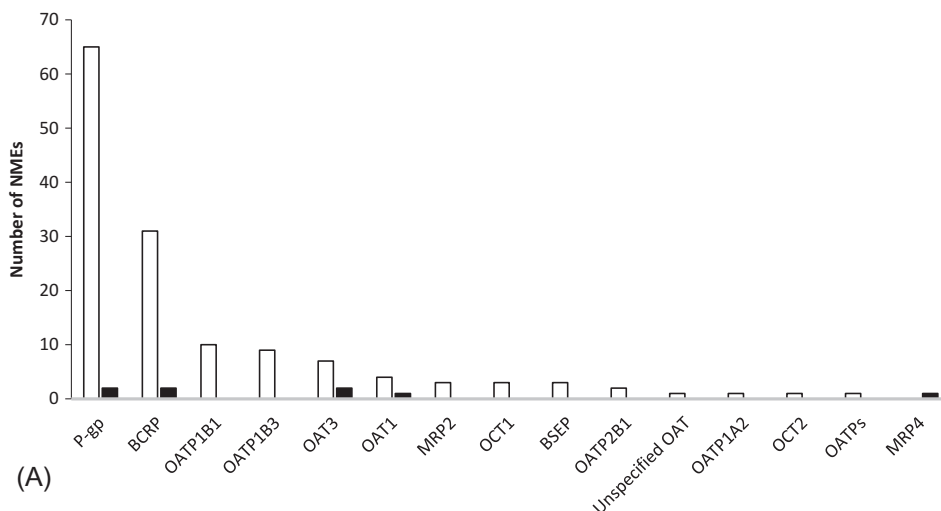


**FIG. 2A** Numbers of NMEs as transporter substrates in vitro. Legend: open bar, parent drug; black bar, metabolite. *BSEP*, bile salt export pump.

AUCR  $\geq 5$  pertained to combination drugs for the treatment of HCV infection, including glecaprevir (as glecaprevir/pibrentasvir), grazoprevir (as elbasvir/grazoprevir), paritaprevir (as ombitasvir/paritaprevir/ritonavir/dasabuvir; Viekira Pak), and voxilaprevir (as sofosbuvir/velpatasvir/voxilaprevir), consistent with the liver being the site of action of these drugs. Coadministration of a single dose of ritonavir (100 mg), administered as a booster in the combination product Viekira Pak, significantly increased paritaprevir AUC 47-fold and  $C_{\max}$  28-fold. Although CYP3A is most likely the main contributor to this drug interaction, the significant increase in paritaprevir exposure could also be attributed to the inhibition of OATP1B1/1B3, P-gp, and BCRP, since paritaprevir is a substrate and ritonavir an inhibitor of these transporters in vitro [36,40,42,43]. The label states that “coadministration of Viekira Pak with drugs that are inhibitors of CYP3A and of these transporters may increase plasma concentrations of paritaprevir” [4]. The large clinical interactions involving the other anti-HCV drugs were all primarily mediated by OATP1B1/1B3 and were observed upon their coadministration with known clinical inhibitors of these transporters. For example, cyclosporine (400 or 600 mg single dose) or rifampin (600 mg single dose orally or IV), both strong inhibitors of OATP1B1/1B3, resulted in up to a 15.25-, 8.55-, and 9.73-fold increase in the exposure of grazoprevir, glecaprevir, and voxilaprevir, respectively. Likewise, the protease inhibitors atazanavir/ritonavir, darunavir/ritonavir, and lopinavir/ritonavir increased the drug exposure to a similar extent due to the inhibition of OATP1B1/1B3. Based on these results, glecaprevir, grazoprevir, and voxilaprevir were identified as sensitive substrates of OATP1B1/1B3 and concomitant administration of these drugs with known OATP inhibitors is contraindicated or not recommended [8,11,12].

Induction data show that when glecaprevir/pibrentasvir was coadministered with multiple oral doses of rifampin (600 mg once daily), the AUC and  $C_{\max}$  values of glecaprevir and pibrentasvir significantly reduced by approximately 90%, mainly due to the induction of P-gp (with the induction of CYP3A also likely contributing based on in vitro evidence of some

glecaprevir metabolism, primarily by CYP3A). Consequently, considering the potential risk of therapeutic failure, coadministration of glecaprevir/pibrentasvir is contraindicated with rifampin [12].

### 3.2 NMEs as inhibitors of transporters

In vitro, the inhibition potential of NMEs and their metabolites was assessed toward a total of 24 transporters, showing that the in vitro evaluations went far beyond the transporters recommended by the FDA. The largest number of drugs were found to be inhibitors of P-gp ( $N = 52$ ) and BCRP ( $N = 51$ ), followed by OATP1B1 ( $N = 49$ ), and OATP1B3 ( $N = 41$ ; Fig. 2B). Clinically however, only two anti-HCV combination products, glecaprevir/pibrentasvir and sofosbuvir/velpatasvir/voxilaprevir, exhibited strong inhibition of OATP1B1/1B3 and/or BCRP, with greater than 5-fold increase in the exposure of the victim drugs atorvastatin and rosuvastatin (Table 1). Coadministration with glecaprevir/pibrentasvir (300 mg/120 mg once daily) in healthy subjects significantly increased the AUC and  $C_{max}$  of atorvastatin, a clinical substrate of OATP1B1/1B3, 8.28- and 22.00-fold, respectively. In vitro, glecaprevir inhibited OATP1B1 and OATP1B3 ( $IC_{50} = 0.017$  and  $0.064 \mu M$ , respectively), and pibrentasvir inhibited OATP1B1 ( $IC_{50} = 1.3 \mu M$  with 4% BSA), but not OATP1B3 ( $IC_{50} > 30 \mu M$ ). Of note, glecaprevir also weakly inhibited CYP3A in vitro ( $IC_{50} = 28.4 \mu M$ ) and atorvastatin is a known substrate of CYP3A, therefore inhibition of CYP3A may also contribute to the overall effect. Considering the large increase in atorvastatin exposure, coadministration of atorvastatin with glecaprevir/pibrentasvir is not recommended [12]. Similarly, sofosbuvir/velpatasvir/voxilaprevir (400mg/100mg/100 mg+100 mg voxilaprevir once daily) caused a 7.35-fold increase in AUC and an 17.96-fold increase in  $C_{max}$  of rosuvastatin, a clinical substrate of BCRP, OATP1B1, and OATP1B3 [11]. In vitro, sofosbuvir only weakly inhibited BCRP (35% inhibition at  $100 \mu M$ ) and OATP1B3 ( $IC_{50} = 203.5 \mu M$ ), while voxilaprevir showed more potent inhibition of OATP1B1 ( $IC_{50} = 0.18 \mu M$ ) and OATP1B3 ( $IC_{50} = 0.70 \mu M$ ). Velpatasvir was also an inhibitor of BCRP,

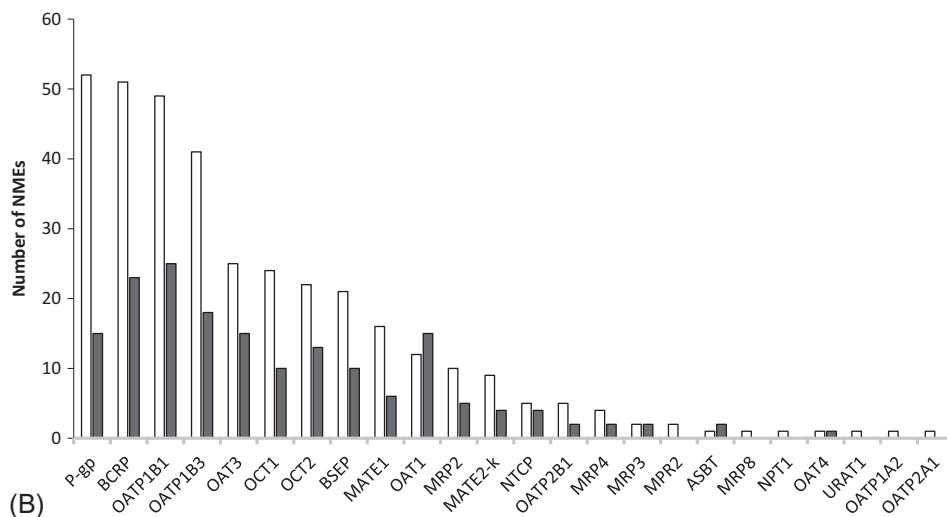


FIG. 2B Numbers of NMEs as transporter inhibitors in vitro. Legend: open bar, parent drug; black bar, metabolite.

OATP1B1, and OATP1B3 with  $IC_{50}$  values of 0.30, 1.5, and 0.26  $\mu\text{M}$ , respectively, and the clinical relevance of transporter inhibition was further confirmed by studies with pravastatin (a substrate of OATP1B1/1B3) and rosuvastatin (a substrate of BCRP and OATP1B1/1B3). The larger effect observed for rosuvastatin (2.80-fold increase in AUC) compared to pravastatin (1.40-fold increase in AUC) following coadministration of velpatasvir (100 mg once daily) is likely due to the inhibition of both OATP1B1/1B3 and BCRP [11,44]. Therefore, the significant increase in rosuvastatin during coadministration with sofosbuvir/velpatasvir/voxilaprevir may be attributable to the combined inhibition of BCRP, OATP1B1, and OATP1B3 by velpatasvir and voxilaprevir. All these results highlight the complexity of transporter-based interactions that often involve multiple mechanisms.

#### 4 PBPK modeling and simulations in DDI prediction

In recent years, PBPK models have been gaining popularity in DDI predictions in lieu of dedicated clinical DDI studies as regulatory agencies, including the FDA, incorporated this method as an acceptable means of evaluating potential drug interactions [45–48]. In a recent commentary by Grimstein et al., less than 10 NDAs per year contained PBPK analysis on DDIs in 2008–2015, while this number jumped to 15 in 2016 and to 26 in 2017, exhibiting a definite upward trend over the years [49]. Consistent with this data, our analysis found that PBPK modeling and simulations were commonly used to predict the clinical relevance of *in vitro* findings. As recommended by the most recent FDA DDI guidance issued in 2020 [1], if predictions suggest that the risk of drug interaction is unlikely, then no clinical study is warranted. For example, lenvatinib time-dependently inhibited CYP3A *in vitro* ( $K_I = 72.26 \mu\text{M}$ ;  $k_{\text{inact}} = 5.01/\text{h}$ ) and directly inhibited CYP2C8 ( $IC_{50} = 10.1 \mu\text{M}$ ). A PBPK model of lenvatinib that takes into account both CYP inhibition mechanisms predicted no significant PK changes on midazolam (a sensitive CYP3A substrate) or repaglinide (a sensitive CYP2C8 substrate) with lenvatinib at therapeutic doses, therefore no clinical study had to be conducted [50].

PBPK models are also increasingly used to guide drug label dosing recommendations, with a total of 13 drugs having labels based on prediction results. Interestingly, all of these drugs were substrates of CYP3A and one drug (ribociclib) was also an inhibitor of CYP3A. In the current NDA dataset, predictions were often made to evaluate NMEs as victim drugs, where the drug interaction potential with strong inhibitors and inducers were assessed using clinical studies, while the DDI potential with less potent inhibitors and inducers were predicted using PBPK models. For example, coadministration of acalabrutinib (predominantly metabolized by CYP3A) with itraconazole, a strong CYP3A inhibitor, increased the AUC of acalabrutinib 4.96-fold. Consistently, a PBPK model predicted a 3.34-fold increase after coadministration with clarithromycin, also a strong CYP3A inhibitor. Furthermore, moderate CYP3A inhibitors such as erythromycin, diltiazem, and fluconazole were predicted to increase acalabrutinib AUC 2.28- to 2.76-fold, while the weak CYP3A inhibitor fluvoxamine was predicted to increase its exposure only 1.37-fold. Based on these clinical and predicted results, it is recommended to avoid coadministration of acalabrutinib with strong CYP3A inhibitors and reduce its dose with moderate CYP3A inhibitors, while no dose

adjustment is necessary for concomitant administration with weak CYP3A inhibitors [29]. Likewise, for NMEs acalabrutinib, deflazacort, naldemedine, and ribociclib, the effect of strong CYP3A inducers (e.g., rifampin and carbamazepine) was investigated clinically, while the effect of moderate inducers (e.g., efavirenz) was predicted using PBPK models. As expected, changes in drug exposure were consistent with the inducer potency and label recommendations were given accordingly. On the other hand, the antineoplastic ribociclib provides a good example of evaluating an NME as a perpetrator using PBPK models to predict its clinical DDI potential. In vitro, ribociclib showed both reversible ( $K_{i,u} = 30.0 \mu\text{M}$ ) and mechanism-based ( $K_{L,u} = 4.44 \mu\text{M}$ ,  $k_{\text{inact}} = 0.02/\text{min}$ ) inhibition of CYP3A. The effect of subtherapeutic doses of ribociclib (400 mg once daily) on a sensitive CYP3A substrate was evaluated in a clinical study, where the AUC and  $C_{\text{max}}$  of midazolam increased 3.89-fold and 2.11-fold, respectively. PBPK simulations were further performed to assess the effect of ribociclib at its therapeutic dose of 600 mg once daily. As expected, a higher increase of 5.17-fold in AUC and 2.41-fold in  $C_{\text{max}}$  of midazolam was predicted. Consequently, caution is recommended when ribociclib is coadministered with NTR CYP3A substrates. Also, the dose of a sensitive CYP3A substrate with an NTR may need to be reduced as ribociclib may increase its exposure [25].

Finally, PBPK modeling and simulations have also been proven useful in DDI studies that incorporate pharmacogenetic information. For example, for eliglustat, which is extensively metabolized mainly by CYP2D6 and to a lesser extent by CYP3A4, the impact of strong CYP2D6 or CYP3A4 inhibitors in CYP2D6 normal metabolizers (NMs) were evaluated using clinical trials, where a 10- and 4.40-fold increase in eliglustat AUC was observed with paroxetine (30 mg once daily) and ketoconazole (400 mg once daily) coadministration, respectively. Considering the increased risk associated with even higher drug exposures expected in patients with impaired CYP2D6 function, the DDI risks of strong and moderate CYP2D6 and CYP3A inhibitors in such subjects were all predicted using PBPK models. Based on the PBPK predicted results, dose modifications based on patient CYP2D6 metabolizer status are recommended for concomitant use of CYP2D6 or CYP3A inhibitors. For example, coadministration with strong CYP3A4 inhibitors is contraindicated in CYP2D6 IMs, whereas coadministration with moderate CYP3A inhibitors is not recommended in CYP2D6 IMs and poor metabolizers (PMs). To illustrate the potential gravity of the interaction, it is contraindicated to coadminister eliglustat with a strong or moderate CYP2D6 inhibitor together with a strong or moderate CYP3A4 inhibitor in any CYP2D6 metabolizer status [5].

---

## 5 PGx studies

---

In all, 30 NMEs (21% of total) were investigated for the potential impact of genetic variants of polymorphic enzymes and transporters on the drugs' pharmacokinetics. Among them, two-thirds were evaluated using population PK analysis, PBPK modeling, or meta-analysis, and 10 NMEs were evaluated through dedicated clinical studies. A positive clinical impact of genetic variations on drug exposure (defined as an AUCR  $\geq 1.25$  compared to the reference group, following the FDA recommendation) was found for seven NMEs, with six drugs metabolized by CYP enzymes and one metabolized by UGT. CYP2D6 was the main enzyme

responsible for the metabolism of four of the drugs (aripiprazole lauroxil, brexpiprazole, deutetrabenazine, and eliglustat), while CYP2C9, CYP2C19, and UGT1A9 variants affected the exposure of lesinurad, flibanserin, and canagliflozin, respectively. All of these PGx results were in line with inhibition or induction DDI findings and triggered dose recommendations for five of the drugs, namely aripiprazole lauroxil, brexpiprazole, deutetrabenazine, eliglustat, and lesinurad.

The largest change in exposure due to PGx was observed for eliglustat, which, as discussed in the previous section, is mainly metabolized by CYP2D6 (and to a lesser extent by CYP3A4). The drug displayed a >5-fold increase in exposure when administered in subjects with genetic polymorphisms of CYP2D6 compared to CYP2D6 NMs (*CYP2D6*\*1/\*1, \*2/\*2). Specifically, there was a 5.52-fold increase in eliglustat AUC and 4.28-fold increase in  $C_{\max}$  in CYP2D6 IMs (genotypes not provided;  $N=2$ ) after an 84 mg single dose, and a 7.29-fold increase in AUC and 5.35-fold increase in  $C_{\max}$  in CYP2D6 PMs (*CYP2D6*\*4/\*4, \*4/\*5, \*4/\*6;  $N=3$ ) after multiple doses of 168 mg twice daily. In CYP2D6 UMs (*CYP2D6*\*1/\*2  $\times$  2;  $N=2$ ), eliglustat AUC and  $C_{\max}$  decreased by 80%–91% after either a single 84 mg dose or multiple 168 mg doses twice daily, compared to NM subjects ( $N=24$  to 32). Consistent with these findings, eliglustat (84 mg twice daily for 17 days) AUC increased 10-fold in CYP2D6 NMs ( $N=24$ ), 28.4-fold in UMs ( $N=1$ ), and 5.20-fold in IMs ( $N=8$ ), when coadministered with the strong CYP2D6 inhibitor paroxetine (30 mg once daily). Both DDI and PGx studies demonstrated the primary role of CYP2D6 in eliglustat clearance. Based on these results and considering the safety concerns at higher plasma concentrations when a treatment with eliglustat is initiated, an appropriate dose needs to be selected based on the patient CYP2D6 genotype status, detected by an FDA-cleared test [5]. The use of eliglustat in CYP2D6 UMs should be limited because these patients may not achieve adequate concentrations to achieve a therapeutic effect. In patients with CYP2D6 NMs or IMs, eliglustat 84 mg twice daily is the recommended dose, while in CYP2D6 PMs, decreasing the dosing interval to once daily is recommended. Eliglustat is the first drug marketed that requires CYP2D6 genotyping prior to administration in patients.

## 6 Other mechanisms: Absorption-based DDIs

In addition to first-pass metabolism and intestinal transporter-mediated interactions, other absorption-based interactions can also have a significant impact on drug disposition. Although the current FDA DDI guidance does not include specific recommendations for absorption-based DDI evaluations during clinical development, a framework for the evaluation of pH-dependent DDIs has been proposed. An integrated approach is recommended in order to better understand the interplay between the multiple physicochemical, material, formulation, and physiological factors ([www.iqconsortium.com](http://www.iqconsortium.com)). The number of NDAs including absorption-based DDI studies has doubled from 5 in 2013 to 10 in 2017. Drugs were evaluated as both victims and perpetrators, with the majority being investigated as victim drugs. The most commonly reported absorption-based DDIs were with NMEs that had pH-dependent solubility. It is now recognized that concomitant administration with drugs that alter gastric pH, such as proton-pump inhibitors (PPIs), histamine receptor-2 antagonists



(H<sub>2</sub>RAs), and antacids, can affect the solubility and subsequent intestinal absorption of these NMEs. Previous studies have shown that the absorption of Biopharmaceutics Classification System (BCS) Class II (low solubility, high permeability) and Class IV (low solubility, low permeability) compounds are moderately to highly impacted by acid-reducing therapy [51]. This was also well observed in NMEs. Regarding the clinical relevance of such findings, although none of the drugs had contraindications relating to absorption-based DDIs, it is recommended to avoid concomitant acid-reducing agents and dose staggering to mitigate the effect on drug absorption.

Through clinical studies and modeling, 18 NDAs had at least one positive absorption-based DDI study (defined as a  $\geq 25\%$  change in victim AUC) and 22 NDAs (containing 28 NMEs) had label recommendations. Binding/chelation mechanisms accounted for the majority of the absorption-based interactions mentioned in drug labels ( $N=8$ ). For pH-dependent absorption-based interactions, perpetrators investigated were PPIs (including omeprazole, rabeprazole, lansoprazole, and esomeprazole), H<sub>2</sub>RAs (famotidine, ranitidine), and antacids (mostly aluminum hydroxide, calcium carbonate, and simethicone). Dolutegravir, an human immunodeficiency virus (HIV)-1 integrase strand transfer inhibitor indicated in combination with other antiretroviral agents for the treatment of HIV-1 infection, is presented here as an example. Dolutegravir is a BCS Class II compound and is practically insoluble at normal gastric pH range. To investigate the effect of pH dependency on dolutegravir absorption, a dedicated DDI study was conducted with omeprazole. Coadministration with omeprazole (40 mg once daily) had no impact on the PK profile of dolutegravir (50 mg single dose), therefore dolutegravir can be coadministered with PPIs and H<sub>2</sub>RAs without dose adjustment. To investigate the effects of binding/chelation on dolutegravir absorption, dedicated DDI studies were conducted with antacid and multivitamins. In the antacid study, healthy male volunteers received dolutegravir (50 mg single dose) alone, simultaneously with, or 2h prior to antacid (Maalox) administration. Simultaneous coadministration with antacid resulted in a 74% decrease in dolutegravir AUC, whereas delaying antacid administration by 2h mitigated the decrease in dolutegravir AUC to 26%. In the multivitamin study, coadministration with multivitamins (One A Day Maximum; containing 200 mg elemental calcium, 100 mg magnesium, 18 mg iron, 15 mg zinc, and trace elements) resulted in a 33% and 36% decrease in dolutegravir (50 mg single dose) AUC and  $C_{\max}$ , respectively. Based on these observations, it is recommended to administer dolutegravir 2h before or 6h after taking cation containing antacids or laxatives, sucralfate, oral iron supplements, oral calcium supplements, or buffered medications [52].

Regarding gastrointestinal motility-based interactions, the diabetes treatments lixisenatide, semaglutide, dulaglutide, and albiglutide included label recommendations based on their potential for delayed gastric emptying. Semaglutide delays gastric emptying and has the potential to impact the absorption of concomitantly administered oral medication. An absorption-based study was conducted to evaluate the effect of delayed gastric emptying caused by semaglutide (1 mg once a week subcutaneously for 4 weeks) on the PK of acetaminophen (1500 mg single dose with a standard meal) in obese, nondiabetic subjects. A 23% and 27% decrease in  $C_{\max}$  and  $AUC_{0-1h}$  of acetaminophen was observed, while the  $AUC_{0-5h}$  of acetaminophen was not affected, suggesting a delay only in the early postprandial phase, but no delay over the total postprandial period. Further DDI studies were conducted to evaluate the effect of delayed gastric emptying by semaglutide on the PK of the following drugs from

different BCS classes, drugs with an NTR, and those commonly co-prescribed in patients with type 2 diabetes: atorvastatin, digoxin, metformin, warfarin, and oral contraceptives. Results indicate that delayed gastric emptying due to semaglutide has no clinically relevant effect on the PK of these drugs; therefore, no label recommendations are required when these drugs are coadministered with semaglutide. However, caution should still be exercised when concomitant oral drugs are administered. According to the drug label, semaglutide causes a delay in gastric emptying and therefore may impact the absorption of concomitantly orally administered drugs [53].

In all, 24 drugs had absorption-based DDI studies with no effect (defined as a <20% decrease or 25% increase in victim AUC), which were mostly investigated for pH dependency with PPIs, H<sub>2</sub>RAs, or antacids. In addition to clinical trials, population PK modeling (with concomitant acid-reducing agents included in covariate analyses) was used as a tool to rule out absorption-based DDIs for six NMEs (eliglustat, lenvatinib, venetoclax, rucaparib, safinamide, and ribociclib), and PBPK modeling of gastric pH and its impact on drug absorption was used in the evaluation of two NMEs (panobinostat and ribociclib).

## 7 Conclusion

The mechanistic analysis of PK-based DDI data contained in the 2013–2017 NDA reviews found that, not surprisingly, CYP3A was the major contributor to large clinical DDIs involving new drugs as substrates and/or perpetrators. Regarding transporter-mediated DDIs, OATP1B1/1B3 played a significant role in drug interactions with AUC changes  $\geq 5$ -fold, which were observed mainly with anti-HCV drugs. Overall, the prevalence of oncology and antiviral drugs (often as FDC products) in these large interactions highlights the continuous challenge of managing DDIs in these patient populations. In addition to metabolism- and transporter-mediated drug interactions, the evaluation found that absorption-based DDIs are now investigated more systematically and 14 drugs had label recommendations based on alterations of drug absorption, with binding/chelation mechanisms accounting for the majority of these interactions. Finally, PBPK modeling continues to establish itself as a critical tool in drug interaction evaluation, allowing the assessment of multiple and/or complex clinical scenarios, including the effects of genetic variations.

## References

- [1] FDA, Guidance for Industry: In Vitro Drug Interaction Studies—Cytochrome P450 Enzyme- and Transporter-Mediated Drug Interactions, 2020, Center for Drug Evaluation and Research, FDA, Silver Spring, MD.
- [2] FDA, Guidance for industry Physiologically Based Pharmacokinetic Analyses—Format and Content, Center for Drug Evaluation and Research, FDA, Silver Spring, MD, 2018.
- [3] J. Yu, Z. Zhou, J. Tay-Sontheimer, R.H. Levy, I. Ragueneau-Majlessi, Risk of clinically relevant pharmacokinetic-based drug-drug interactions with drugs approved by the U.S. Food and Drug Administration between 2013 and 2016, *Drug Metab. Dispos.* 46 (6) (2018) 835–845.
- [4] FDA, Drug Approval Package: VIEKIRA PAK (ombitasvir, paritaprevir, and ritonavir co-packaged with dasabuvir), FDA Application NDA 206619, FDA, Silver Spring, MD, 2014.
- [5] FDA, Drug Approval Package: CERDELGA (eliglustat), FDA Application NDA 205494, FDA, Silver Spring, MD, 2014.
- [6] FDA, Drug Approval Package: IMBRUVICA (ibrutinib), FDA Application NDA 205552, FDA, Silver Spring, MD, 2013.

- [7] FDA, Drug Approval Package: VERZENIO (abemaciclib), FDA Application NDA 208716, FDA, Silver Spring, MD, 2017.
- [8] FDA, Drug Approval Package: ZEPATIER (elbasvir and grazoprevir), FDA application NDA 208261, FDA, Silver Spring, MD, 2016.
- [9] FDA, Drug Approval Package: MOVANTIK (naloxegol), FDA Application NDA 204760, FDA, Silver Spring, MD, 2014.
- [10] FDA, Drug Approval Package: RYDAPT (midostaurin), FDA Application NDA 207997, FDA, Silver Spring, MD, 2017.
- [11] FDA, Drug Approval Package: VOSEVI (sofosbuvir, velpatasvir, and voxilaprevir), FDA Application NDA 209195, FDA, Silver Spring, MD, 2017.
- [12] FDA, Drug Approval Package: MAVYRET (glecaprevir and pibrentasvir), FDA Application NDA 209394, FDA, Silver Spring, MD, 2017.
- [13] FDA, Drug Approval Package: CORLANOR (ivabradine), FDA Application NDA 206143, FDA, Silver Spring, MD, 2015.
- [14] FDA, Drug Approval Package: OLYSIO (simeprevir), FDA Application NDA 205123, FDA, Silver Spring, MD, 2013.
- [15] FDA, Drug Approval Package: HETLIOZ (tasimelteon), FDA Application NDA 205677, FDA, Silver Spring, MD, 2014.
- [16] FDA, Drug Approval Package: ESBRIET (pirfenidone), FDA Application NDA 022535, FDA, Silver Spring, MD, 2014.
- [17] FDA, Drug Approval Package: COTELLIC (cobimetinib), FDA Application NDA 206192, FDA, Silver Spring, MD, 2015.
- [18] FDA, Drug Approval Package: ADDYI (flibanserin), FDA Application NDA 022526, FDA, Silver Spring, MD, 2015.
- [19] FDA, Drug Approval Package: VENCLEXTA (venetoclax), FDA Application NDA 208573, FDA, Silver Spring, MD, 2016.
- [20] FDA, Drug Approval Package: CRESEMBA (isavuconazonium sulfate), FDA Application NDA 207500, FDA, Silver Spring, MD, 2015.
- [21] FDA, Drug Approval Package: NERLYNX (neratinib), FDA Application NDA 208051, FDA, Silver Spring, MD, 2017.
- [22] R. Abbas, B.A. Hug, C. Leister, J. Burns, D. Sonnichsen, Pharmacokinetics of oral neratinib during co-administration of ketoconazole in healthy subjects, *Br. J. Clin. Pharmacol.* 71 (4) (2011) 522–527.
- [23] FDA, Drug Approval Package: EMFLAZA (deflazacort), FDA Application NDA 208684, FDA, Silver Spring, MD, 2017.
- [24] FDA, Drug Approval Package: LYNPARZA (olaparib), FDA Application NDA 206162, FDA, Silver Spring, MD, 2014.
- [25] FDA, Drug Approval Package: KISQALI (ribociclib succinate), FDA Application NDA 209092, FDA, Silver Spring, MD, 2017.
- [26] FDA, Drug Approval Package: VARUBI (rolapitant), FDA Application NDA 206500, FDA, Silver Spring, MD, 2015.
- [27] FDA, Drug Approval Package: BELSOMRA (suvorexant), FDA Application NDA 204569, FDA, Silver Spring, MD, 2014.
- [28] FDA, Drug Approval Package: IBRANCE (palbociclib), FDA Application NDA 207103, FDA, Silver Spring, MD, 2015.
- [29] FDA, Drug Approval Package: CALQUENCE (acalabrutinib), FDA Application NDA 210259, FDA, Silver Spring, MD, 2017.
- [30] FDA, Drug Approval Package: SYMPROIC (naldemedine), FDA Application NDA 208854, FDA, Silver Spring, MD, 2017.
- [31] FDA, Drug Approval Package: EPCLUSA (sofosbuvir and velpatasvir), FDA Application NDA 208341, FDA, Silver Spring, MD, 2016.
- [32] FDA, Drug Approval Package: ALUNBRIG (brigatinib), FDA Application NDA 208772, FDA, Silver Spring, MD, 2017.
- [33] FDA, Drug Approval Package: AKYNZEO (netupitant and palonosetron), FDA Application NDA 205718, FDA, Silver Spring, MD, 2014.

- [34] FDA, Drug Approval Package: ZYDELIG (idelalisib), FDA Application NDA 206545, FDA, Silver Spring, MD, 2014.
- [35] FDA, Drug Approval Package: ORKAMBI (lumacaftor and ivacaftor), FDA Application NDA 206038, FDA, Silver Spring, MD, 2015.
- [36] M. Shebley, J. Liu, O. Kavetskaia, J. Sydor, S.M. de Morais, V. Fischer, et al., Mechanisms and predictions of drug-drug interactions of the hepatitis C virus three direct-acting antiviral regimen: paritaprevir/ritonavir, ombitasvir, and dasabuvir, *Drug Metab. Dispos.* 45 (7) (2017) 755–764.
- [37] G. Luo, J. Lin, W.D. Fiske, R. Dai, T.J. Yang, S. Kim, et al., Concurrent induction and mechanism-based inactivation of CYP3A4 by an L-valinamide derivative, *Drug Metab. Dispos.* 31 (9) (2003) 1170–1175.
- [38] J. Mao, M.A. Mohutsky, J.P. Harrelson, S.A. Wrighton, S.D. Hall, Prediction of CYP3A-mediated drug-drug interactions using human hepatocytes suspended in human plasma, *Drug Metab. Dispos.* 39 (4) (2011) 591–602.
- [39] V.A. Eagling, D.J. Back, M.G. Barry, Differential inhibition of cytochrome P450 isoforms by the protease inhibitors, ritonavir, saquinavir and indinavir, *Br. J. Clin. Pharmacol.* 44 (2) (1997) 190–194.
- [40] L.M. Vermeer, C.D. Isringhausen, B.W. Ogilvie, D.B. Buckley, Evaluation of ketoconazole and its alternative clinical CYP3A4/5 inhibitors as inhibitors of drug transporters: the in vitro effects of ketoconazole, ritonavir, clarithromycin, and itraconazole on 13 clinically-relevant drug transporters, *Drug Metab. Dispos.* 44 (3) (2016) 453–459.
- [41] FDA, Drug Approval Package: PREVYMIS (letermovir), FDA Application NDA 209939, FDA, Silver Spring, MD, 2017.
- [42] FDA, FDA Website: Drug Development and Drug Interactions: Table of Substrates, Inhibitors and Inducers, 27 March 2019. Available from: <https://www.fda.gov/Drugs/DevelopmentApprovalProcess/DevelopmentResources/DrugInteractionsLabeling/ucm093664.htm>, 2019.
- [43] R.M. Menon, C.E. Klein, T.J. Podsadecki, Y.L. Chiu, S. Dutta, W.M. Awni, Pharmacokinetics and tolerability of paritaprevir, a direct acting antiviral agent for hepatitis C virus treatment, with and without ritonavir in healthy volunteers, *Br. J. Clin. Pharmacol.* 81 (5) (2016) 929–940.
- [44] E. Mogalian, P. German, B.P. Kearney, C.Y. Yang, D. Brainard, J. McNally, et al., Use of multiple probes to assess transporter- and cytochrome P450-mediated drug-drug interaction potential of the pangenotypic HCV NS5A inhibitor velpatasvir, *Clin. Pharmacokinet.* 55 (5) (2016) 605–613.
- [45] R. Leong, M.L. Vieira, P. Zhao, Y. Mulugeta, C.S. Lee, S.M. Huang, et al., Regulatory experience with physiologically based pharmacokinetic modeling for pediatric drug trials, *Clin. Pharmacol. Ther.* 91 (5) (2012) 926–931.
- [46] S.M. Huang, D.R. Abernethy, Y. Wang, P. Zhao, I. Zineh, The utility of modeling and simulation in drug development and regulatory review, *J. Pharm. Sci.* 102 (9) (2013) 2912–2923.
- [47] V. Sinha, P. Zhao, S.M. Huang, I. Zineh, Physiologically based pharmacokinetic modeling: from regulatory science to regulatory policy, *Clin. Pharmacol. Ther.* 95 (5) (2014) 478–480.
- [48] P. Zhao, M. Rowland, S.M. Huang, Best practice in the use of physiologically based pharmacokinetic modeling and simulation to address clinical pharmacology regulatory questions, *Clin. Pharmacol. Ther.* 92 (1) (2012) 17–20.
- [49] M. Grimstein, Y. Yang, X. Zhang, J. Grillo, S.M. Huang, I. Zineh, et al., Physiologically based pharmacokinetic modeling in regulatory science: an update from the U.S. Food and Drug Administration's Office of Clinical Pharmacology, *J. Pharm. Sci.* 108 (1) (2019) 21–25.
- [50] FDA, Drug Approval Package: LENVIMA (lenvatinib), FDA Application NDA 207103, FDA, Silver Spring, MD, 2015.
- [51] N.R. Budha, A. Frymoyer, G.S. Smelick, J.Y. Jin, M.R. Yago, M.J. Dresser, et al., Drug absorption interactions between oral targeted anticancer agents and PPIs: is pH-dependent solubility the Achilles heel of targeted therapy? *Clin. Pharmacol. Ther.* 92 (2) (2012) 203–213.
- [52] FDA, Drug Approval Package: TIVICAY (dolutegravir), FDA Application NDA 204790, FDA, Silver Spring, MD, 2013.
- [53] FDA, Drug Approval Package: OZEMPIC (semaglutide), FDA Application NDA 209637, FDA, Silver Spring, MD, 2017.

# Quantifying drug metabolizing enzymes and transporters by LC-MS/MS proteomics

Haeyoung Zhang<sup>a</sup>, Abdul Basit<sup>a,b</sup>, Bhagwat Prasad<sup>a,b</sup>

<sup>a</sup>Department of Pharmaceutics, University of Washington, Seattle, WA, United States

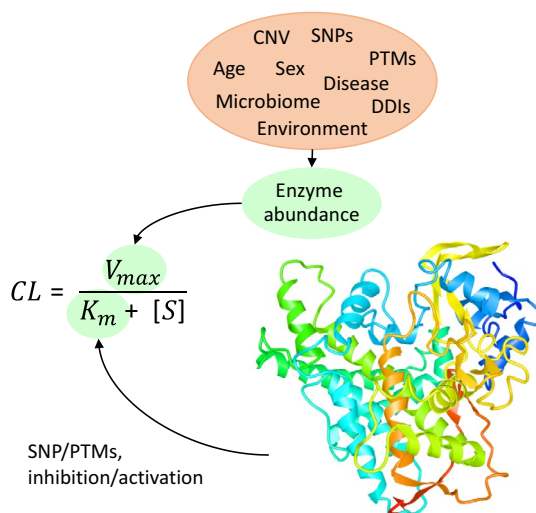
<sup>b</sup>Department of Pharmaceutical Sciences, Washington State University, Spokane, WA, United States

## 1 Introduction

Prediction and characterization of drug absorption, distribution, metabolism, excretion, and toxicity (ADMET) in humans are important for safe and effective drug development. Traditionally, allometric scaling has been used to predict human drug disposition using *in vivo* preclinical pharmacokinetic (PK) data [1]. Although allometric scaling is simple and successful for drugs which are primarily eliminated unchanged, its application is limited for drugs that are extensively metabolized and actively transported across cell membranes, due to interspecies differences in drug metabolizing enzymes and transporters (DMET) proteins [2]. To overcome these limitations, *in vitro* to *in vivo* extrapolation (IVIVE) [3, 4], which can also employ physiologically based pharmacokinetic (PBPK) modeling [5, 6], is considered a better alternate to predict drug disposition in humans. However, there can be marked differences in DMET protein expression in tissues compared to *in vitro* models (e.g., cell lines), making quantification of DMET proteins a prerequisite for accurate scaling of *in vitro* data.

In the last decade, quantitative proteomics has emerged as a promising tool to fill the knowledge gap in protein expression and aid in better translation and *in vivo* prediction of drug disposition. One of the major kinetic model used to describe drug metabolism and transport is Michaelis-Menten kinetics ( $v = V_{\max} * [S] / (K_m + [S])$  and  $V_{\max} = k_{\text{cat}} * [E]$ ). Major assumptions in IVIVE is that substrate-binding characteristics ( $K_m$ ) and catalytic efficiency ( $k_{\text{cat}}$ ) remain unchanged between systems (e.g., *in vitro* to *in vivo*) but changes in expression influence  $V_{\max}$  (Fig. 1). While shifts in  $K_m$  are commonly seen in drug-drug interactions (DDI) with a different

**FIG. 1** Mechanisms of change in activity for DMET proteins. Protein abundance alters  $V_{max}$ , whereas substrate affinity ( $K_m$ ) is affected by changes in the protein structure (active site). Cytochrome P450 2C19 is shown as an example (<https://www.ncbi.nlm.nih.gov/protein/P33261.3>).



substrate, changes in  $K_m$  of a substrate resulting from inherent protein structural changes due to polymorphisms or posttranslational modifications (PTMs) are less commonly observed (Fig. 1). Conversely, many different factors affect enzyme levels ( $[E]$ ) that lead to changes in  $V_{max}$ , ranging from genetic to epigenetic aspects such as polymorphisms to environmental exposure (Fig. 1). Changes in  $k_{cat}$  are also infrequently observed, and  $k_{cat}$  can only be determined with the knowledge of protein expression. Thus,  $[E]$  is used as an intersystems scaling factor (e.g., in vitro to in vivo), and accurate measurement of  $[E]$  is crucial in obtaining reliable scaling and predictions [7]. Similarly for transporters, it is important to quantify active transporters that are localized on the membrane (vs internalized transporters which are inactive) for accurate IVIVE and scaling factors. Methods such as immunohistochemistry, surface biotinylation, and confocal microscopy have been applied to determine membrane localization [8–10].

Historically, mRNA levels have been used as surrogate measurements for proteins, but have limitations such as lower stability as well as posttranscriptional regulations and downstream events, which may inaccurately reflect true protein expression and activity. Indeed, poorer correlation between mRNA levels and activity has been shown [11], and remains a major limitation of using mRNA in IVIVE [12]. Traditionally, direct protein measurements are commonly performed using immunoassay-based techniques, such as Western blotting or enzyme-linked immunosorbent assay (ELISA). While these techniques offer semiquantitative sensitivity and selectivity, they require specific antibodies, retain possibility of cross-reactivity, have low throughput, and show poor reproducibility, leading to inadequate quality assurance [13]. Mass spectrometry (MS)-based quantitative proteomics addresses these hurdles with high selectivity, reproducibility, and throughput [12]. Hence, MS-based quantitative proteomics allows for extrapolation between different systems, such as scaling from recombinant enzymes or transporter overexpressing cells or vesicles to the human liver, thus connecting in vitro protein abundance scaled to in vivo expression and enabling IVIVE.



In addition, MS-based quantitative proteomics is applicable in high-throughput analysis of proteins in big sample cohorts, thus can be used in determining interindividual variability [14]. It has been well established that interindividual variability arising from genetic differences such as single nucleotide polymorphisms (SNP) and copy number variation (CNV) have significant clinical impacts on drug disposition [15]. Furthermore, epigenetic regulation such as DNA or histone modification has also been shown to affect drug response [16]. While such modifications does not always result in changes in protein expression, quantitative proteomics facilitates better characterization of interindividual variability, as it measures the end product of the central dogma (i.e., functional enzyme or transporter), yielding good correlation between protein expression and activity [17, 18].

Quantitative proteomics is an emerging field, and many groups are applying this approach in the ADMET field. However, employed techniques require appropriate training and expertise to address multiple technical challenges, which are often unavailable in conventional ADMET laboratories. In particular, significant interlaboratory variabilities have been reported [19–22], which are attributed to differences in sample preparation, protein digestion protocols, standardization tools, and analysis [23]. The aim of this chapter is to provide an overview of the basic principles, methodology, and applications of quantitative proteomics, with a focus on targeted LC-MS/MS-based multiple reaction monitoring (MRM) analysis, including discussion on technical challenges and recommended best practices.

## 2 Basic workflow of DMET quantitative proteomics

Quantitative proteomics relies on selective quantification of a unique (proteotypic or surrogate) peptide of a protein in a biological sample by LC-MS/MS. Two main quantification approaches in proteomics are targeted and untargeted proteomics. Targeted proteomics measures prespecified protein or peptide targets of interest using stable isotope-labeled (SIL) or tagged standards, while untargeted or global proteomics is a label-free approach in measuring the sample proteome with no labeled standards, and rely on computational strategies for quantification [24]. Targeted proteomics is more commonly used in the field of ADMET than untargeted or global proteomics, due to limited number of target proteins and simpler operation of the technique, and requires proteotypic peptides which are prospectively selected. The basic targeted proteomics workflow (Fig. 2) includes the following steps: (i) selection of proteotypic peptide, (ii) biological sample preparation, (iii) protein digestion using proteases such as trypsin, (iv) desalting and peptide enrichment before LC-MS analysis, (v) LC separation of peptides, (vi) MS quantification, and (vii) quantitative data analysis. The following section provides discussion of these individual steps.

### 2.1 Selection of proteotypic peptides

Proteotypic peptide refers to a unique peptide fragment that is not present in any other proteins in the biological sample and is used as a surrogate for the protein of interest. Selection of proteotypic peptides utilizes several *in silico* or experimental methods and applies optimized criteria to ensure that selected peptides are representative of target proteins and remain unaffected by technical variability (Fig. 3).



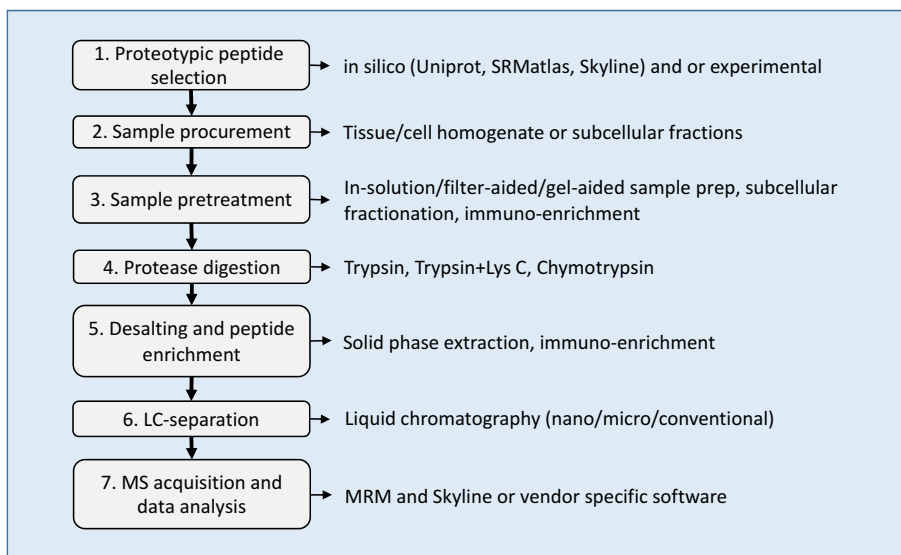
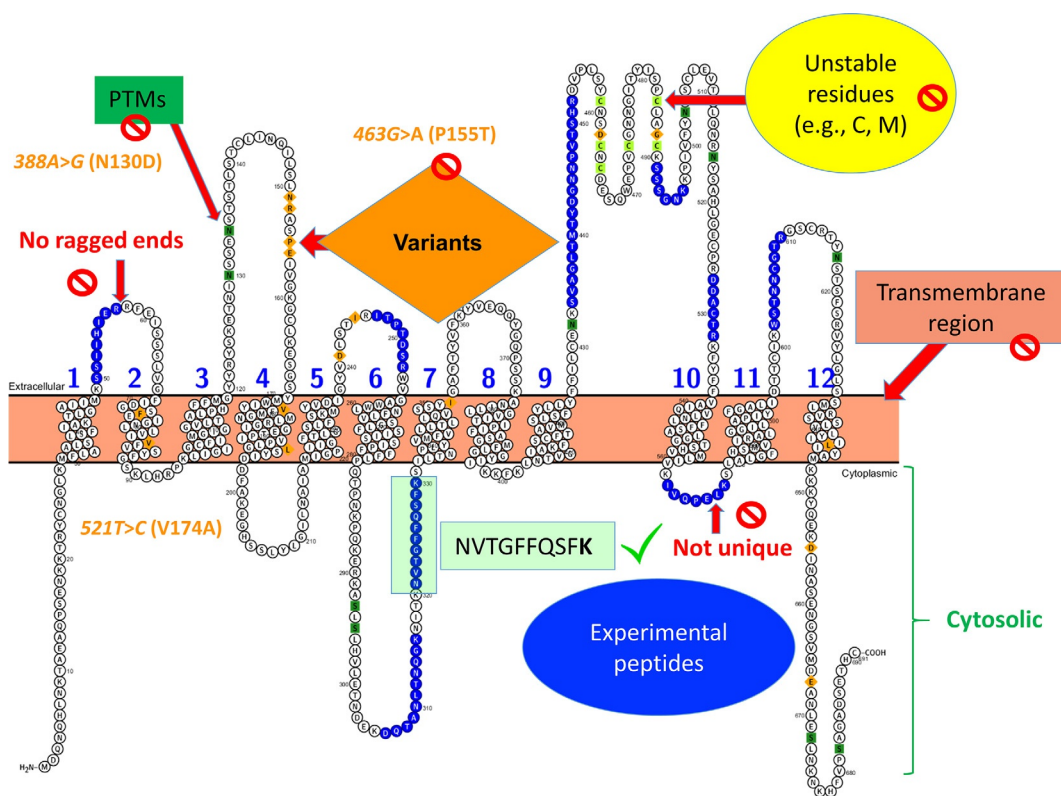


FIG. 2 Typical targeted LC-MS/MS quantitative analysis workflow. Multiple variations and approaches exist for each workflow step.

Peptide uniqueness is the most important criteria to allow selective quantitative measurement of the protein without any contamination or crosstalk with other proteins. In addition, other factors such as localization, stability (unstable residues), solubility, MS response, LC-retention, and digestion efficiency of the peptide need to be considered. A peptide with potential change in sequence due to posttranslational modification (PTM) and nonsynonymous (or missense) SNPs is usually excluded, unless intentionally included to assess the impact of SNP or PTM on protein expression. An example of a transmembrane protein, organic anion transporting polypeptide 1B1 (OATP1B1) is shown in Fig. 3. Potential experimental peptide candidates selected in silico are highlighted in blue. These peptides are then screened for localization, as transmembrane regions have lower peptide extraction and digestion efficiency, while extracellular regions are more prone to glycosylation. Peptide candidates are further examined to eliminate those with known or predicted PTMs, unstable peptides containing methionine that are prone to oxidation, ragged ends (i.e., the presence of RR, KK, RK, or KR) that are susceptible to missed cleavages, and nonsynonymous SNP variants with amino acid changes. Uniqueness is confirmed with an online database tool such as MS-Homology, and more than one unique peptide is selected whenever possible, as it allows for examining peptide correlation to solidify confidence in quantitation. However, in case of transporters (e.g., OATP1B1), large transmembrane localization and high degree of PTMs often limit the number of available proteotypic peptides.

## 2.2 Sample procurement, homogenization, and protein extraction

Collection of high-quality cell or tissue samples is important. Sample quality can be influenced by pathology (scarred, fatty, or healthy), time (from surgery to storage), and long-term storage conditions. Sample preparation differs depending on the type of stored



**FIG. 3** A representative example of proteotypic peptide selection for OATP1B1. Identified experimental peptides (filled in blue) are screened for uniqueness, stability (unstable residues, e.g., C and M), posttranslational modifications (PTM), genetic variants, cellular localization (i.e., extracellular, intracellular, transmembrane), and ragged ends (e.g., RR) to identify ideal unique proteotypic peptides.

tissue, i.e., fresh, frozen, formalin-fixed paraffin-embedded (FFPE), or optimal cutting temperature (OCT) compound-embedded tissue. Anatomical localization of the tissue sample and tissue-specific characteristics can also influence protein quantification. Some tissues are fairly homogeneous (e.g., liver), while others exhibit regional expression of DMET proteins. In the kidney, drug transporters are primarily expressed in proximal tubules in the cortex. Region-specific expression of DMEs (e.g., CYP3A4) and transporters (e.g., P-glycoprotein) in the intestine is also widely recognized [25–27]. In order to control for technical variability while addressing regional variability, the use of tissue cell-specific markers is suggested (e.g., aquaporin 1 for renal proximal tubular cells and villin for mature enterocytes).

The choice of tissue homogenization or cell lysis technique depends on the sample type (e.g., fixed or freshly frozen) and available sample volume. Completeness and consistency in homogenization and maximum recovery of proteins should be optimized. Typical homogenization methods include manual cryogenic grinding, mechanical bead or rotary homogenization, sonication, and reagent-based methods (e.g., Mem-PER Kit) [28–30]. In DMET proteomics, membrane protein recovery in microsomes or membrane fractions is highly

dependent on homogenization method [29]. DMET proteins are localized in specific cell compartments, mostly the endoplasmic reticulum (ER), thus homogenization or cell lysis should be complete to ensure good recovery.

In general, the simplest approach in sample preparation should be used to avoid technical variability, but fractional/protein enrichment is oftentimes necessary to achieve better sensitivity. Proteomic quantifications of subcellular fractions are commonly required due to the widespread use of enriched subcellular fractions for *in vitro* assays. If subcellular fraction enrichment occurs during sample processing such as microsomal isolation, fractional recovery (e.g., milligram of protein recovered per gram of liver, MPPGL) should be established. Total protein quantification should first be performed in enriched fractions or tissue homogenate, and is commonly measured using bicinchoninic acid (BCA), Lowry, or Bradford assays [31]. However, protein loss can occur during protein enrichment, which requires estimation in the form of loss or recovery factors [32]. For example, scaling factors are used for IVIVE, which describe membrane protein per gram tissue [e.g., microsomal protein per gram liver/kidney (MPPGL/MPPGK)]. As these scaling factors are estimated based on total protein yield relative to tissue mass (mg total protein per gram liver/kidney), large technical variability is observed in these scalars [33]. Enrichment of transporters can be performed using sucrose-gradient ultracentrifugation or reagent-based membrane extraction methods. For example, transporter data are generated using commercially available membrane extraction kits to produce consistent data. Microsomal and cytosolic proteins can also be extracted and enriched from cell systems using commercial kits [27]. For transporter quantification, purified plasma membrane fractions can be generated using gradient ultracentrifugation or biotinylation methods [9, 34].

### 2.3 Protein extraction and digestion methods

Protein solubilization and denaturation is performed prior to proteolytic digestion, and utilizes detergents [e.g., sodium dodecyl sulfate (SDS) or deoxycholate], MS-compatible products (e.g., Rapigest or ProteaseMax), or chaotropic agents (e.g., urea). Denatured proteins are subsequently reduced using dithiothreitol (DTT) and alkylated with iodoacetamide (IAA). Denatured, reduced, and alkylated proteins are precipitated or extracted using chloroform-methanol or acetone to remove detergents/salts that might interfere with the protein digestion [35, 36]. The extracted protein is then digested using protease enzymes, typically trypsin. Protease: protein ratios and incubation times are optimized for maximum digestion efficiency. Trypsin: protein ratio generally ranges from 1:10 to 1:100, with typical digestion times of 4–18h. Protein digestions are generally performed using *in-solution* methods, but gel-aided (GASP) and filter-aided (FASP) sample preparation methods are also utilized as an effort toward digestion optimization [37, 38].

### 2.4 Post-digestion processing

Digestion is generally stopped using an acidic buffer. Desalting is usually necessary to remove buffers before chromatography to minimize ion suppression and interference in the mass spectrometer to yield better detection. Desalting can also be accomplished by using

desalting resins or solid-phase extraction [39]. Spiking of stable isotope-labeled (SIL) peptide is done at this stage, which can serve as internal standards [14] or calibrators [24]. In targeted MRM proteomics, SIL peptides are generally added after digestion to address other post-digestion processing variables, matrix effect, and variable MS sensitivity. Immuno-enrichment using anti-peptide antibodies is utilized to further increase sensitivity, and is performed post-digestion for peptides (SISCAPA, iMALDI, and immune-SILAC) and pre- or post-digestion for proteins [40].

## 2.5 Peptide separation using liquid chromatography (LC)

Due to the limited number of target proteins in DMET proteomics, peptide separation is achievable on a conventional-LC system. However, nano- and micro-LC with or without ion mobility are used for more efficient separation, particularly when protein identification is desired. LC separation is predicted using peptide hydrophathy [14]. Exogenous peptide standards, such as iRT peptides (Biognosys, Beverly, MA), can be used to calibrate retention time. Peptide separation is necessary to avoid matrix effect or interference due to an isobaric peptide. For instance, two peptides differing only leucine and isoleucine cannot be distinguished based on the MRM method but can be chromatographically resolved. Carboxylesterase (CES) 1 has a tryptic peptide differing only in the leucine position from CES4's isoleucine, which can lead to false positive results (Fig. 4A).

Labile PTMs (e.g., gamma-glutamyl carboxylation) can undergo in-source fragmentation leading to both modified and unmodified peptides, which exhibit similar parent ion and MS fragmentation pattern and should be separated by LC. This is illustrated with peptide NISVPETVK in Fig. 4B, which harbors a glutamic acid (E) and show three peaks with matching fragmentation patterns. Typically, a reverse-phase column is used for tryptic peptide (6–25 amino acids) separation.

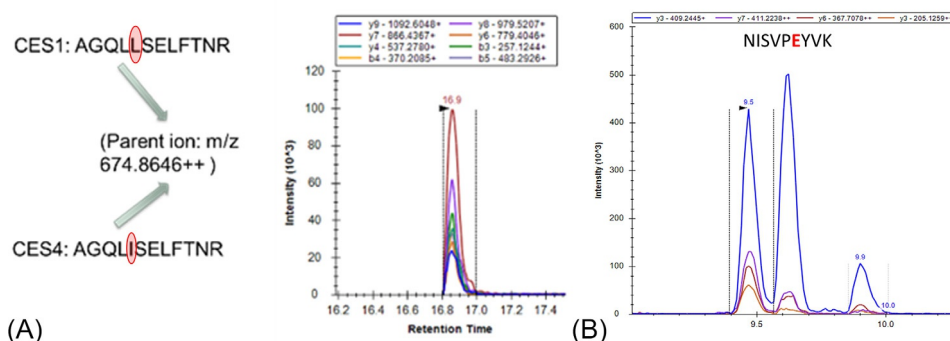


**FIG. 4** Examples of confounding factors in proteotypic peptide selection. (A) Peptides differing only by leucine (L) and isoleucine (I) (e.g., CES1 and CES4) cannot be distinguished based on MRM and requires LC separation. (B) Labile peptides with PTM-prone residues such as gamma-carboxylated glutamate (E) are susceptible to in-source ionization. Retention time shift indicates different carboxylation states and multiple common fragments confirm peptide identity, NISVPEYVK.

## 2.6 Mass spectrometry (MS) analysis of peptide signal

Different MS acquisition approaches are utilized depending on the type of protein quantification approaches (targeted or untargeted). Targeted proteomics uses triple-quadrupole MS instruments, which requires selection of surrogate peptides prior to data acquisition. Targeted proteomics using multiple reaction monitoring (MRM) is the most common approach used in drug development because of its simple operation; however, only a limited number of proteins (10–100) can be simultaneously quantified by this approach. Fragmentation pattern of a peptide generally results in y and b ions as shown in Fig. 5A. The b ions extend from the amino (N)-terminus and y ions from the carboxyl (C)-terminus. In MRM proteomics, preselected precursor ions are filtered in the first quadrupole (Q1) after ionization, and fragmented to their corresponding product ions in Q2. The product ions are subsequently filtered in Q3 and measured. This results in a quantitative detection overtime that produces a signal in the chromatogram (Fig. 5B). Targeted proteomics can also utilize a high-resolution mass spectrometry (HR-MS) platform, e.g., parallel-reaction monitoring (PRM) or high-resolution MRM (MRM-HR), where all product ions are measured for specified precursor ions or ion ranges. In general, MRM acquisition is more sensitive, while PRM acquisition offers more precision and selectivity [23].

### 2.6.1 Untargeted MS acquisition approaches

Common MS acquisition approaches employed for untargeted proteomics are data-independent (DIA) and data-dependent acquisition (DDA) approaches. MS acquisition for untargeted proteomics requires HR-MS instruments, such as Orbitrap or time-of-flight (TOF). Although HR-MS platforms are less sensitive for low-abundant proteins compared to MRM, these methods can be used for simultaneous quantification of 100–1000s of proteins in a biological sample [41].

## 2.7 Protein quantification approaches

Protein quantification can be achieved by label-free or label-based methods. Label-free method is a simpler approach, where ion intensities in a test and control samples are compared assuming that matrix effect remains minimal or consistent across samples. However, successful protein quantification is difficult with label-free methods, as it demands high-resolution and high-accuracy data as well as optimal use of software tools. Key limitations of label-free method arise from both sample and instrumentation, such as matrix effect, run-to-run variability, and retention time shift. These can be addressed with isotope dilution methods using external standards, by adding synthetic stable isotope-labeled (SIL) peptides or labeled proteins. Fig. 6 shows an example of peptide quantification using spike-in method with SIL. Signal of these fragment ions of a nonlabeled (native) proteotypic peptide, corresponding SIL peptide, and an overlay of nonlabeled and SIL are shown in Fig. 6A–C, respectively. The SIL peptide signal can be used in two ways. First, as a calibrator to calculate absolute peptide abundance if concentration of SIL peptide is known, and second, as an internal standard to generate a more accurate quantitation across a dynamic range, if nonlabeled peptides are used as external single or multipoint calibrators [42].

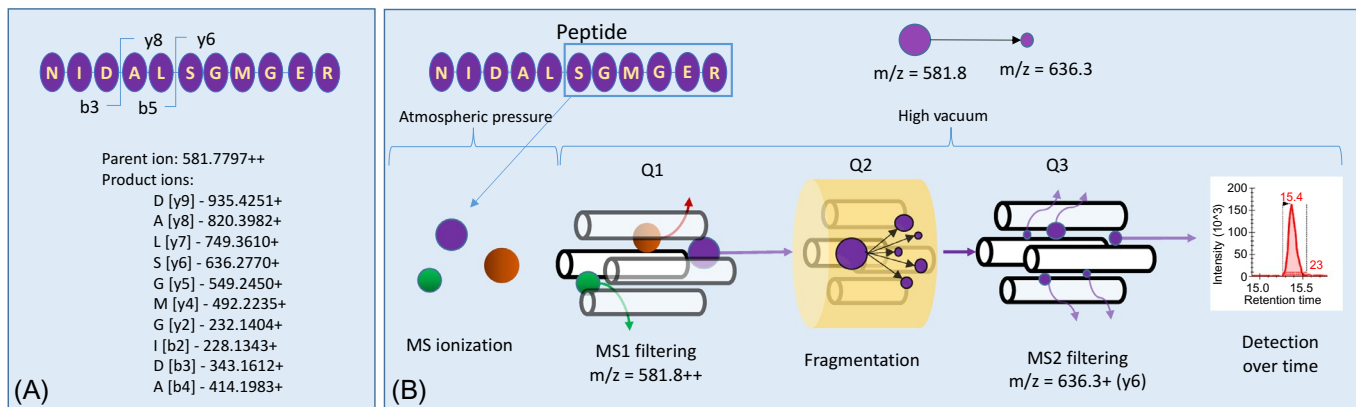


**FIG. 5** A representative MS/MS fragmentation pattern of a proteotypic peptide and LC-MS/MS analysis. (A) Peptide fragmentation pattern commonly extends from the amino (N)-terminus, producing b ions, or carboxyl (C)-terminus, resulting in y ions. (B) Proteotypic peptide is ionized as parent ion, filtered in Q1, then undergoes further fragmentation into product ions in Q2, which are then filtered and detected in Q3.

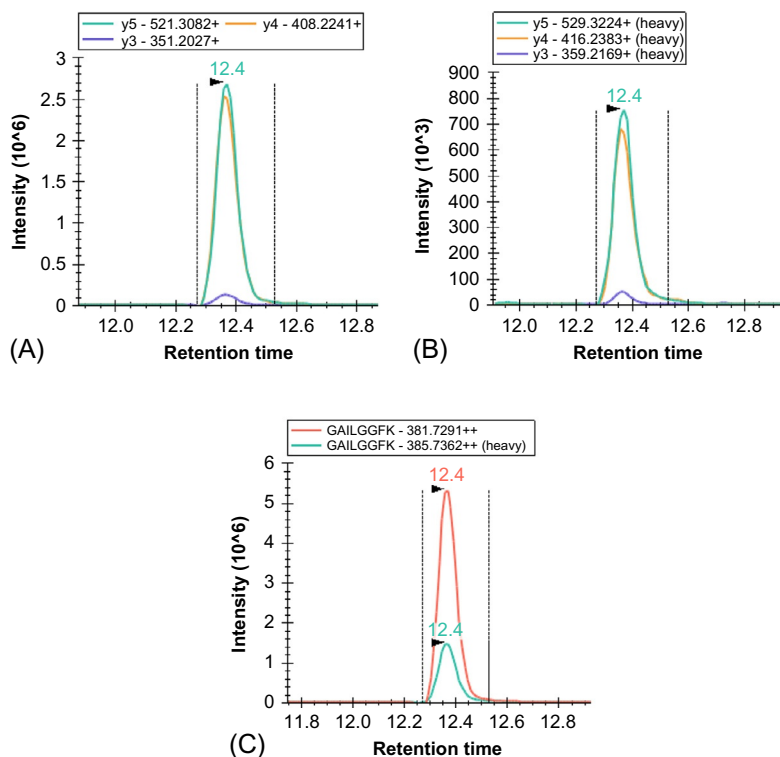


**FIG. 6** A representative example of quantification of a proteotypic peptide using spike-in method. (A) Signal of three fragment ions of nonlabeled peptide, GAILGGFK. (B) Signal of three corresponding fragment ions of SIL peptide. (C) Overlaid signals from nonlabeled and SIL peptides. If the SIL peptide concentration is known, the ratio of nonlabeled to SIL peptide signals can be used to calculate absolute peptide abundance. Alternatively an external calibration method can be employed, where nonlabeled peptides can be used as calibrators (multiple concentrations) and SIL peptide is used as an internal standard.

Various protein quantification methods utilize isotope dilution with external spiked-in SIL peptides or proteins, such as absolute quantification (AQUA) peptides, quantitative concatemers (QconCAT), and protein standards for absolute quantification (PSAQ). In AQUA, a known quantity of a purified SIL peptide standard is added to the sample, allowing quantitation of proteins. QconCAT is a modification of the AQUA method that employs concatenated peptide sequences taken from target proteins to generate artificial proteins as spiked-in calibrators or internal standards. Multiple proteotypic peptides are assembled in a single artificial protein for multiplexed quantification, which addresses inter-sample variability in protease digestion. Absolute quantification generated from AQUA or QconCAT assumes complete and uniform protein digestion. Thus, if the digestion efficiency is incomplete or different between target proteins and concatemer, the measured values will underestimate true abundance. This drawback is perhaps the key reason for the observed interlaboratory variability in protein abundance [19–22]. Thus, PSAQ, in which purified labeled proteins are used as spiked-in calibrators, is considered the best approach for accurate measurements. However, purified labeled proteins are not readily available for most DMET proteins.



In biological multiplexed proteomics, metabolic or chemical isotope labeling is routinely used to address variability in protease digestion and MS ionization. For example, in stable isotope labeling with amino acids in cell culture (SILAC), cells are cultured in both nonlabeled and SIL culture media to metabolically incorporate SIL amino acids [43, 44]. The nonlabeled and SIL samples are extorted and pooled before digestion and MS analysis. SILAC method is highly precise and can be used to assess protein induction [45]. Other multiplexing approaches such as isobaric tags for relative and absolute quantitation (iTRAQ) or tandem mass tag (TMT) utilize commercially available kits for covalently tagging primary amine groups of peptides [46]. Table 1 summarizes commonly employed isotopic or tagging methods, and Fig. 7 shows the points of labeling addition in a general workflow timeline.

**TABLE 1** Common approaches for peptide labeling and quantification/calibration.

Abbreviation	Definition	Description	References
SILAC	Stable isotope labeling by amino acids in cell culture	Stable isotope labels are introduced in cell culture to be incorporated metabolically into proteins	[47–49]
SILAM	Stable isotope labeling in mammals	Complete metabolic labeling of all proteins in live mammals (rodents) with SIL nitrogen ( $^{15}\text{N}$ ) as an internal standard	[50, 51]
TAQSI	Targeted absolute quantitative proteomics with SILAC internal standards	Uses full-length native proteins that are labeled and unlabeled. Unlabeled full-length proteins are used as calibrators	[52]
TMT	Tandem mass tags	Multiple peptides are chemically labeled post-digestion with isobaric chemical tag variants with the same molecular structure and mass (2-plex, 6-plex, 10-plex, 11-plex). Fragmentation yields unique reporter ions. (Vendor Thermo Fisher)	[53–55]
iTRAQ	Isobaric tags for relative and absolute quantification	Multiple peptides are chemically labeled post-digestion with isobaric chemical tag variants with the same molecular structure and mass (2-plex, 3-plex, 4-plex, 8-plex). Fragmentation yields unique reporter ions. (Vendor AB Sciex)	[55–57]
mTRAQ	Mass differential tags for relative and absolute quantification	Non-isobaric tags that target primary amines are used for quantification by comparing unlabeled and SIL peptide signals from tagged peptides	[58, 59]
SIL/AQUA	Stable isotope labeled/absolute quantification	Stable isotope labeled peptides unique to the target protein used as internal standards for LC-MS proteomics	[60]
QconCAT	Quantitative concatemers	Stable isotope labeled set of peptides unique to target proteins concatenated in a single protein used as internal standards for digestion and LC-MS proteomics	[61, 62]
PSAQ	Protein standards for absolute quantification	Stable isotope labeled version of the target protein used as internal standard for sample preparation and LC-MS proteomics	[63, 64]

Refer to Refs. [13, 65] for an in-depth comprehensive review on comparison of different approaches

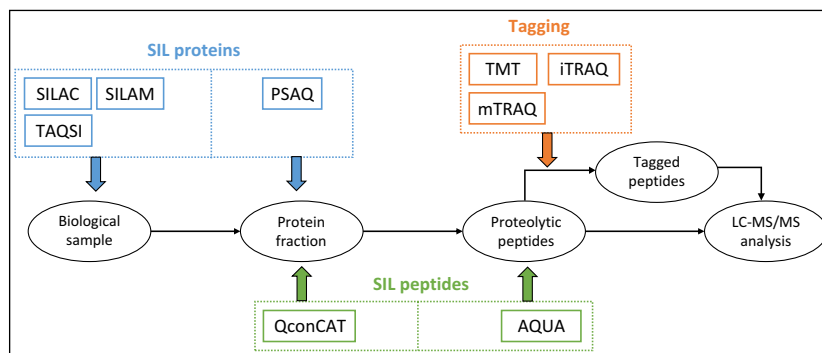


**FIG. 7** Protein labeling approaches and typical timeline for modification during workflow. Refer to [Table 1](#) for method descriptions. Adapted from F. Calderón-Celis, J.R. Encinar, A. Sanz-Medel, *Standardization approaches in absolute quantitative proteomics with mass spectrometry*, *Mass Spectrom. Rev.* 37 (2018) 715–737, doi:10.1002/mas.21542; O. Chahrour, D. Cobice, J. Malone, *Stable isotope labelling methods in mass spectrometry-based quantitative proteomics*, *J. Pharm. Biomed. Anal.* 113 (2015) 2–20, doi:10.1016/j.jpba.2015.04.013.

### 3 Factors affecting DMET protein quantification

Multiple factors affect protein quantification, such as sample loss during preparation, digestion efficiency, protein or peptide stability, calibrator purity, matrix effect, sample quality, and biological variables like SNPs or PTMs. Subcellular fractions (e.g., microsomes or membrane fractions) are commonly used matrices in DMET proteomics. However, as previously discussed, sample loss during subcellular fractionation or protein extraction introduces sample-to-sample variability. We recently reported that microsomal preparation is affected by both the homogenization method as well as sample type, e.g., fatty vs normal liver tissue [29]. In particular, luminal proteins of ER (e.g., calreticulin) and mitochondria (e.g., hsp60) were significantly enriched in cytosolic fractions as they were released during homogenization, while they were retained with the membrane fraction during protein extraction [29]. Also, relative recovery of the membrane fraction differed between cells and tissue samples. Similarly, membrane extraction can result in a significant loss of proteins in centrifugation, and as high as 47% loss of microsomal proteins have been reported [32]. Differential loss of microsomal proteins from sample-to-sample would retain technical variability that is unrelated to biological or interindividual variability, unless corrected. Accounting for these procedural losses while retaining enrichment using recovery factors is necessary for accurate scaling of *in vitro* data. In addition, an underlying assumption in quantitative proteomics is that 100% of peptide is released and digested. However, this cannot be confirmed without a purified protein standard, which is not routinely available [14]. While digestion efficiency can be optimized, it cannot be guaranteed. Sample enrichment can also affect quantification, which can be addressed by using marker proteins for different cell compartments, e.g., calnexin, calreticulin, and Na<sup>+</sup>/K<sup>+</sup> ATPase as markers for ER membrane, ER lumen, and plasma membrane, respectively [29]. Protein or peptide stability is another concern that should be controlled in proteomics analysis. Long-term stability, benchtop stability, and autosampler stability should be assessed for individual peptides used for standardization

and calibration during method validation. Absolute quantity of calibrators is generally measured by amino acid analysis. Matrix effect also influences peptide MS signal; however, this can be controlled using SIL labeled standards. If a proteotypic peptide contains cysteine residue, complete or consistent alkylation is warranted. Effects of SNPs and PTMs should be considered prospectively during proteotypic peptide selection. For example, a high-frequency nonsynonymous SNP in UGT2B15 (rs1902023 or \*2) results in change in the 85th amino acid (Y85D) from tyrosine to aspartate, which could lead to erratic data [35]. A peptide distinct from this region SVINDPVYK allows quantification of UGT2B15 irrespective of the SNP. The use of fixed (e.g., FFPE or OCT-compound embedded) tissue generally affects peptide ionization in mass spectrometry [66–68]. Other characteristics of tissue such as fatty, scarred, or fibrous can also influence protein quantification due to unrepresentative sampling, unless documented [69].

## 4 Optimized quantitative analysis approaches

### 4.1 Use of multiple peptides

Ideally, two or more proteotypic peptides should be used to gain confidence in proteomics results. Particularly, a single peptide can be affected by a rare or unknown SNP, PTM, or peptide stability, as discussed above. If more than one peptide is used, correlation between peptides will confirm quantitative differences in the protein levels across samples (Fig. 8A). If a single peptide is chosen for quantification and is affected by SNP, PTM, or stability, one can expect misleading results as shown in Fig. 8B for SNP-containing peptide in UGT2B15.

### 4.2 Use of multiple product ions

Multiple fragments of a peptide are measured for optimized quantification, as illustrated with fragment correlations for ADH1C proteotypic peptide GAIFGGFK (Fig. 8A inset). Consistency in fragmentation pattern between labeled and SIL peptides confirm any interference, and if any interference is noted, the fragment can be removed from analysis (Fig. 8C).

### 4.3 Inclusion of a positive control sample

Inclusion of a positive control sample (e.g., a pool of individual control samples) in each batch of experiment is advantageous. All the data can be normalized by individual day positive control sample, which increases the robustness by controlling for interday variability. Interday variability arises from many small shifts in sample processing and instrument platform, such as slight changes in buffer, protease lot, LC column performance, and electrospray tips [14]. Quality control (QC) normalization where the same pooled QCs samples are included with each batch processing is especially useful in a large number of samples, where processing and analysis is carried out overtime. It is also a useful tool to relatively gauge results across different laboratories, partly accounting for technical interlaboratory variabilities.

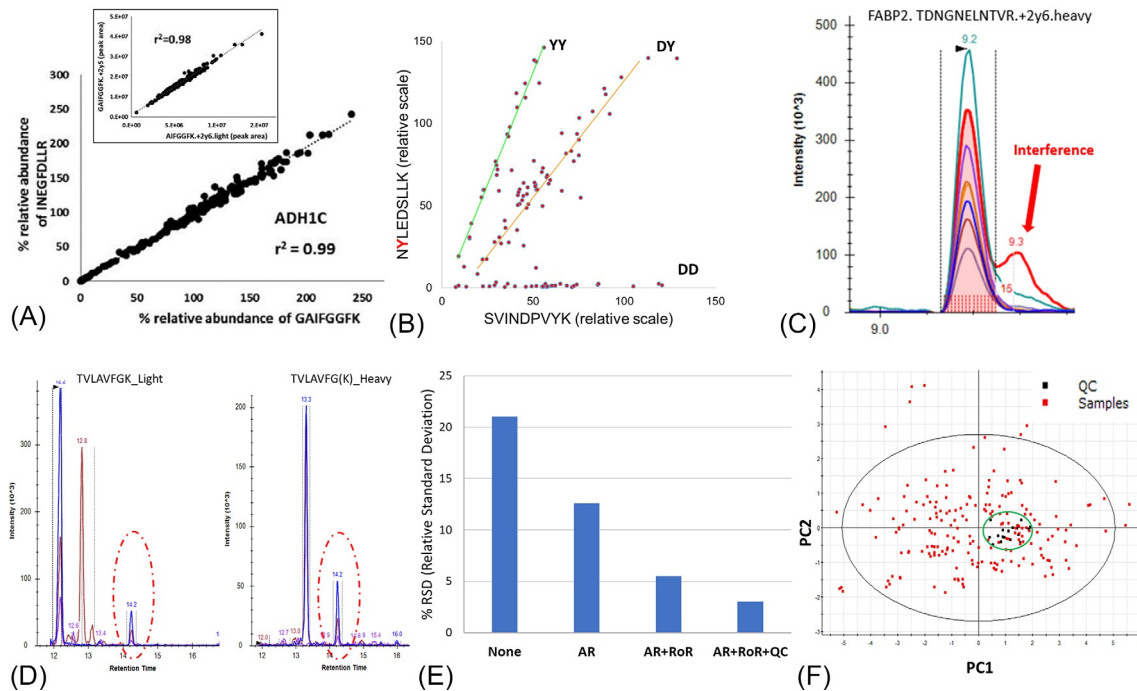


**FIG. 8** Considerations in optimization of DMET protein quantification. (A) Correlation between different proteotypic peptides and multiple product ions (inset) provides visual confirmation for specificity. (B) Peptides with nonsynonymous SNP can confound quantification. (C) Product ions should be assessed for interference and removed. (D) Retention time and fragmentation pattern from SIL peptide helps to identify the correct peak. (E) Percent relative standard deviation (% RSD) decreases with additional normalization, indicating better control for technical and instrumental variabilities. (F) Principal component analysis (PCA) from samples analyzed on three different days. Black dots show technical variability from multiday processing of quality controls (QC), while red dots indicate biological variability.

#### 4.4 Calibration curve, surrogate matrix, and LLOQ

Establishing analytical sensitivity, accuracy, and precision are important in constructing an acceptable assay range for measurement within the linear range of response [24]. However, unpredictable matrix effects exist between the peptide and complex biological matrices, and are highly dependent on the type of matrices. A surrogate matrix, such as albumin can be used to generate a calibration curve of nonlabeled peptide standards, or SIL peptides can be spiked into samples to produce a calibration curve that is sample-matrix matched [70]. Incorporation of matrix effect in quantification is especially important in determining lower limit of quantification (LLOQ) [23].

Most DMET proteins are of low abundance; therefore, the LLOQ should be established. This parameter is determined using multiple measurements (typically six to eight) of serial dilutions of the analyte in an appropriate matrix, until measured amounts are too low to yield consistent quantification (e.g.,  $CV \leq 20\%$ ). Selectivity, or lack of interference, should be carefully examined in the diluent matrix before use. Signal-to-noise (S/N) ratio of  $>5$  is a minimal consideration for method validation [23].

#### 4.5 SIL peptide and exogenous protein internal standards

SIL peptides address sample-to-sample instrumental variability, i.e., matrix effect, MS sensitivity, retention time shift (Fig. 8D), as well as post-digestion technical variability. Addition of exogenous protein internal standards such as bovine serum albumin provides additional control over technical variability, including predigestion variability, sample processing, and instrumentation. Three-step normalization process, which combines SIL peptides [area ratios (AR)], exogenous proteins [ratio of ratios (RoR)], and pooled QC (%), adds confidence and robustness in data quantification. This is shown by subsequent decrease in relative standard deviation (% RSD) with additional normalization (Fig. 8E).

#### 4.6 Optimized practices in targeted quantitative proteomics

Optimized experimental protocols and controls are required to address different methodological variables [14]. Processing and analysis of triplicates on separate days incorporates interday assay variability. Addition of exogenous proteins such as BSA during processing addresses experimental (e.g., protease digestion) reproducibility. Inclusion of pooled QCs in each batch helps account for interday reproducibility. SIL peptide as internal standard controls for instrumental measurement reproducibility. Examining correlation among multiple fragments and peptides increases confidence in quantification. Generation of calibration curve considering matrix effects allows for accurate and precise measurements. Data quality can be further assessed using principal component analysis (PCA) to assess biological and technical variability and confirm QC standards. For example, QCs processed on different days should form a close cluster, with degree of deviation indicating technical variability (Fig. 8F).

## 5 Applications of quantitative DMET proteomics

Applications of quantitative proteomics are broad and promising in multiple areas of drug metabolism and pharmacokinetics (DMPK) and are widely utilized in DMET protein quantification (Table 2).

**TABLE 2** Application of LC-MS/MS proteomics in quantification of DMET proteins.

Tissue	Protein family	Proteins quantified	Ref.
Liver	Phase I enzymes	CYP1A2, CYP2A6, CYP2B6, CYP2C8, CYP2C9, CYP2C18, CYP2C19, CYP2D6, CYP2E1, CYP2J2, CYP3A4, CYP3A5, CYP3A7, CYP3A43, CYP4A11, CYP4F2	[69, 71–78]
	Phase II enzymes	UGT1A1, UGT1A3, UGT1A4, UGT1A6, UGT1A9, UGT2B4, UGT2B7, UGT2B10, UGT2B15, UGT2B17	[18, 69, 75, 77–85]
	Transporters	ABCA8, ABCB1, ABCB3, ABCB4, ABCB11, MATE1, ABCC1, ABCC2, ABCC3, ABCC4, ABCC5, ABCC6, ABCA6, ABCA8, ABCG2, ABCG11, SLC22A18, OAT2, OAT7, OATP1B1, OATP1B3, OATP2B1, OCT1, NTCP, MCT1, ENT1, CNT1	[20, 42, 70, 75, 86–95]
Intestine	Phase I enzymes	CYP1A1, CYP1A2, CYP1B1, CYP3A4, CYP3A5, CYP3A7, CYP2B6, CYP2C8, CYP2C18, CYP2C9, CYP2C19, CYP2D6, CYP2E1, CYP2J2, CYP2S1, CYP4A11, CYP5A1	[96–99]
	Phase II enzymes	UGT1A1, UGT1A3, UGT1A4, UGT1A6, UGT1A7, UGT1A8, UGT1A9, UGT1A10, UGT2B4, UGT2B7, UGT2B15, UGT2B17	[78, 80, 96–99]
	Transporters	ABCB1, ABCC2, ABCC3, ABCC4, ABCC5, ABCC6, ABCG2, ABCG8, OATP1A2, OATP2A1, OATP2B1, OATP1B3, OATP3A1, OATP4A1, OCT1, OCT3, OCTN1, SLC6A6, CNT2, SLC22A18, GLUT4, GLUT5, PEPT1, PEPT2, ASBT, SGLT1	[25, 26, 97–101]
Kidney	Phase I enzymes	CYP4A11, CYP5A1	[77]
	Phase II enzymes	UGT1A1, UGT1A4, UGT1A6, UGT1A7, UGT1A8, UGT1A9, UGT1A10, UGT2B7	[77, 78, 80, 81, 102]
	Transporters	ABCB1, ABCC2, ABCC4, OAT1, OAT2, OAT3, OAT4, OCT2, OCTN2, SLC22A13, SLC22A18, MCT1, LSC7A8, SLC27A2, MATE1, SGLT2	[77, 103]
Brain	Phase I enzymes	CYP1B1, CYP2U1	[104]
	Transporters	SLC1A2, SLC1A3, SLC1A4, SLC2A1, SLC2A3, SLC2A14, SLC3A2, SLC6A12, SLC7A1, SLC7A5, SLC15A2, SLC16A1, SLC16A2, SLC19A1, SLC21A9, SLC21A11, SLC27A1, SLC29A1, SLC29A4, SLC47A1, ABCA2, ABCA8, ABCB1, ABCC4, ABCG2	[104–107]
Lung	Transporters	ABCB1, ABCC2, ABCG2, OCT2, OCT3, OATP2B1, OATP1A2, OATP2A1, OATP4C1, OCTN1, OCTN2, PEPT2	[108]

## 5.1 Characterization of *in vitro* and *in vivo* models

*In vivo* translation of clearance data that is generated using recombinant proteins or overexpression systems (transporter expressing cell lines or vesicles) requires protein abundance information. Moreover, it is commonly noticed that endogenous transporter expression in cell lines (e.g., MDCKII or HEK293 cells) can confound data analysis [109, 110]. Proteomic characterization in these systems can screen for other DMET proteins that may confound assay results and provides confidence in model systems and data extrapolation [111].

## 5.2 *In vitro* to *in vivo* extrapolation (IVIVE) of drug clearance

Assuming  $V_{max}$  is directly proportional to protein abundance and  $K_m$  remains constant between *in vitro* models and *in vivo* (Fig. 1), the ratio of protein expression in tissues and *in vitro* models can be utilized as a scaling factor for IVIVE. Reliability of UGT proteomic quantification in liver microsomes was demonstrated by high correlation between protein expression and activity [79]. Similarly, significant correlation between UGT protein abundance and activity in human kidney microsomes has been shown, which was used to predict renal glucuronidation [112]. Successful IVIVE was reported for OCT2 transporter in predicting metformin renal clearance by incorporating plasma membrane abundance [113]. Mechanistic *in vitro* transporter data can be scaled up to predict *in vivo* disposition, as illustrated with testosterone glucuronide and efflux transporters MRP2 and MRP3 [114]. Although proteomics-informed IVIVE is promising, it is important to address sample preparation differences and the nature of the *in vitro* model. For example, for IVIVE efflux transport from vesicles, the %inside out should be measured experimentally to account for inactive transporters [114]. In overexpressing cells, a significant fraction of transporter could be present intracellularly (i.e., in trafficking process), which should be characterized to avoid overprediction of drug clearance [8, 9, 113]. These examples illustrate that proteomics-informed absolute scaling factor (ASF) approach can be used for accurate IVIVE, when consistency in sample extraction, recovery, and digestion are experimentally confirmed [14].

## 5.3 Interspecies differences in protein expression

Allometric scaling of clearance data is often unsuccessful when metabolism or transport processes are involved. For example, unexpected lower bioavailability of raloxifene in humans (2%) compared to rats (39%) was attributed to expression of UGT1A10 in the human intestine [115]. Tenofovir-associated nephrotoxicity is mediated in concert by OAT1 uptake and MRP4 efflux [116], and interspecies differences in transporters are associated with significant differences in the kidney toxicity. Therefore, to obtain accurate and representative allometric scaling, it is important to characterize interspecies differences in homologous as well as nonhomologous proteins. Interspecies differences in  $K_m$  can be examined using *in vitro* models (recombinant enzymes or transporter overexpressing vesicles and cells), as reported with OAT1 and antiviral drugs [117].  $V_{max}$  scaling from animal to human requires estimation of protein abundance data, as reported for hepatobiliary transporters in human, dog, monkey, and rat [86].



## 5.4 Differential tissue and regional protein distribution

Accurate PBPK modeling requires quantitative knowledge of DME abundance across different tissues. For instance, if a drug is a substrate of UGT2B17, which is highly variable and primarily expressed in human intestine, high intestinal first pass metabolism is expected [27]. MK7246, an oral drug candidate for asthma treatment, was discontinued during clinical development due to poorly predicted variability in PK, which was retrospectively attributed to UGT2B17 variability [118]. Similarly, fraction metabolized by individual enzymes in different tissues varies depending on the regional expression. Quantitative proteomics can be used to characterize differential tissue abundances of DMET proteins. For instance, UGT1A composition and abundance are significantly different between human liver, kidney, and intestine [80], which would lead to differential fraction metabolized by individual UGT1As (fm) and tissue-specific drug-drug interaction potential. Differential regional expression within tissue can also be addressed with proteomics. UGT1A1 intestinal expression shows an increasing trend from duodenum to jejunum, while decreasing in ileum to below limit of quantification in colon [119]. These are important factors to incorporate into modeling, especially in delayed or modified absorption or with substantial enterohepatic recycling.

## 5.5 Subcellular localization of proteins

Although immunolocalization using imaging methods is ideal for subcellular localization of DMET proteins (particularly transporters), it requires selective and sensitive antibodies. Quantitative proteomics does not rely on antibodies and thus provides a better alternative for characterization of subcellular localization of DMET proteins. The localization of DMET proteins is essential for selecting an optimum in vitro model and for IVIVE. This application requires the use of subcellular marker proteins. As an example, in quantifying transporter expression, Na<sup>+</sup>/K<sup>+</sup> ATPase can be used as a plasma membrane marker along with biotinylation to discern cellular transporter localization [9]. Differential recovery and enrichment for calreticulin as an ER luminal marker can aid in determining the proper system to use in investigating CES, an ER lumen-residing protein [29].

## 5.6 Interindividual variability and precision medicine

Precision medicine strives to address interindividual variability in drug response to attain maximum effectiveness and safety in patients, thus improving health-care quality [120]. Interindividual variability arises from numerous factors from genetic differences to epigenetic changes that impacts protein abundance levels, as mentioned above. Nongenetic factors affecting DMET protein abundance include age, sex, disease, ethnicity, environment (e.g., diet, smoking), and pregnancy. Progress is being made toward predicting interindividual variability using physiologically based pharmacokinetic and pharmacodynamic (PBPK/PD) modeling. However, a knowledge gap still exists in quantifying population protein abundance levels and effects of different contributing factors, especially in complex physiological states such as organ dysfunctions and orphan populations such as pregnant women or children. DMET proteomics can fill in the knowledge gap by characterizing abundance levels across different populations. For example, UGT2B17 showed a

162-fold variability in liver protein abundance, with correlating highly variable activities [121], which can be used to predict variable PK. Ontogeny proteomics data can also be utilized in modeling to better predict accurate doses for children [35]. Exosomes are an emerging area of interest. Coined as liquid biopsies, exosomes are promising noninvasive tools for individual “fingerprinting” to assess interindividual variability, and proteomic quantification plays an essential role [122, 123]. It should be noted that protein quantification by mass spectrometry cannot be confirmed as absolute quantification, due to possibility of incomplete extraction, recovery, and digestion. Nevertheless, as long as there is confidence in consistency across samples in extraction, recovery, and protein digestion, the data acquired by quantitative proteomics can be used to generate absolute scaling factor (ASF) for accurate translation [14].

### 5.7 Drug-drug interaction (DDI) potential (induction/suppression)

Quantitative proteomics can be used to predict CYP/UGT/transporter induction. The main advantage of this approach is that the induction potential of drug for all proteins can be determined simultaneously, with the potential for better understanding of complex DDIs. Williamson et al. were able to quantify robust proteomic increases upon induction in CYP isoforms 1A2, 2B6, 3A4, and 3A5, which correlated well with mRNA changes [124]. Particularly, SILAC approach is useful for predicting induction of several DMEs and transporters simultaneously.

### 5.8 Drug/metabolite-protein interactions

Electrophilic functional groups in a drug or its reactive metabolite can covalently bind to endogenous proteins and nucleic acids, leading to idiosyncratic interactions and toxicity. Such interactions can be characterized using quantitative proteomics. Nitrotryptophan, which results from interaction with reactive nitrogen species (RNS) has been quantified using proteomics [125], which may further serve as a biomarker of RNS-mediated damage. Proteomics has been utilized to identify modified drug-protein adducts *in vivo*, formed by various xenobiotics including acetaminophen, penicillin, diclofenac, and carbamazepine [126]. Investigation into these phenomena can provide better insight into mechanisms of idiosyncratic adverse drug reactions and drug toxicity. LC-MS/MS proteomics is sensitive for targeted analysis of protein-drug adducts, whereas HR-MS allows structural identification of site of protein modification. Furthermore, HR-MS data can be analyzed using software tools (e.g., Kojak) for high-throughput *de novo* identification of modified residues by drugs or metabolites [127].

---

## 6 Conclusion

Quantitative DMET proteomics is an emerging and expanding field that supports drug discovery and development research. It allows accurate measurements of DMET protein levels, which is important for improved application of *in vitro* data and prediction of

interindividual variability. Here, we outline a general quantitative proteomics workflow, with a focus on targeted MRM-based proteomics. A typical workflow starts with proteolytic peptide selection, followed by sample treatment and processing, protease digestion, peptide enrichment, and ending in LC-separation with MS acquisition. Each step requires careful consideration of different factors that can affect the quality of proteomics data. These factors can be addressed with different optimization approaches, such as examination of multiple unique peptides and product ions, careful validation of calibration curve in surrogate matrix, use of tissue and subcellular marker proteins, and adoption of multiple quality control layers for normalization, i.e., pooled QCs, SIL peptides, and exogenous standards. DMET proteomics application is presently increasing in IVIVE, DDIs, and characterization of experimental models, and shows potential in precision medicine, particularly in characterizing interindividual variability. Although mentioned only in brief here, untargeted proteomics and DIA approaches yield comprehensive data, and further hold promising applications in investigating systems-based biology and pharmacology [128, 129].

## References

- [1] R.S. Obach, J.G. Baxter, T.E. Liston, B.M. Silber, B.C. Jones, F. MacIntyre, D.J. Rance, P. Wastall, The prediction of human pharmacokinetic parameters from preclinical and in vitro metabolism data, *J. Pharmacol. Exp. Ther.* 283 (1997) 46–58. <http://www.ncbi.nlm.nih.gov/pubmed/9336307>. (Accessed 5 March 2019).
- [2] J.E. Sager, J. Yu, I. Ragueneau-Majlessi, N. Isoherranen, Physiologically based pharmacokinetic (PBPK) modeling and simulation approaches: a systematic review of published models, applications, and model verification, *Drug Metab. Dispos.* 43 (2015) 1823–1837, <https://doi.org/10.1124/dmd.115.065920>.
- [3] H.-J. Cho, J.-E. Kim, D.-D. Kim, I.-S. Yoon, *In vitro*–*in vivo* extrapolation (IVIVE) for predicting human intestinal absorption and first-pass elimination of drugs: principles and applications, *Drug Dev. Ind. Pharm.* 40 (2014) 989–998, <https://doi.org/10.3109/03639045.2013.831439>.
- [4] Y. Naritomi, F. Nakamori, T. Furukawa, K. Tabata, Prediction of hepatic and intestinal glucuronidation using *in vitro*–*in vivo* extrapolation, *Drug Metab. Pharmacokinet.* 30 (2015) 21–29, <https://doi.org/10.1016/j.dmpk.2014.10.001>.
- [5] A. Rostami-Hodjegan, Physiologically based pharmacokinetics joined with *in vitro*–*in vivo* extrapolation of ADME: a marriage under the arch of systems pharmacology, *Clin. Pharmacol. Ther.* 92 (2012) 50–61, <https://doi.org/10.1038/clpt.2012.65>.
- [6] K.R. Yeo, M. Jamei, A. Rostami-Hodjegan, Predicting drug–drug interactions: application of physiologically based pharmacokinetic models under a systems biology approach, *Expert. Rev. Clin. Pharmacol.* 6 (2013) 143–157, <https://doi.org/10.1586/ecp.13.4>.
- [7] A.T. Heikkinen, F. Lignet, P. Cutler, N. Parrott, The role of quantitative ADME proteomics to support construction of physiologically based pharmacokinetic models for use in small molecule drug development, *Proteomics Clin. Appl.* 9 (2015) 732–744, <https://doi.org/10.1002/prca.201400147>.
- [8] V. Kumar, T.B. Nguyen, B. Tóth, V. Juhasz, J.D. Unadkat, Optimization and application of a biotinylation method for quantification of plasma membrane expression of transporters in cells, *AAPS J.* 19 (2017) 1377–1386, <https://doi.org/10.1208/s12248-017-0121-5>.
- [9] V. Kumar, L. Salphati, C.E.C.A. Hop, G. Xiao, Y. Lai, A. Mathias, X. Chu, W.G. Humphreys, M. Liao, S. Heyward, J.D. Unadkat, A comparison of total and plasma membrane abundance of transporters in suspended, plated, sandwich-cultured human hepatocytes versus human liver tissue using quantitative targeted proteomics and cell surface biotinylation, *Drug Metab. Dispos.* 47 (2019) 350–357, <https://doi.org/10.1124/dmd.118.084988>.
- [10] A. Crowe, W. Zheng, J. Miller, S. Pahwa, K. Alam, K.-M. Fung, E. Rubin, F. Yin, K. Ding, W. Yue, Characterization of plasma membrane localization and phosphorylation status of organic anion transporting polypeptide

- (OATP) 1B1 c.521 T>C nonsynonymous single-nucleotide polymorphism, *Pharm. Res.* 36 (2019) 101, <https://doi.org/10.1007/s11095-019-2634-3>.
- [11] R. Jamwal, B.J. Barlock, S. Adusumalli, K. Ogasawara, B.L. Simons, F. Akhlaghi, Multiplex and label-free relative quantification approach for studying protein abundance of drug metabolizing enzymes in human liver microsomes using SWATH-MS, *J. Proteome Res.* 16 (2017) 4134–4143, <https://doi.org/10.1021/acs.jproteome.7b00505>.
- [12] B. Prasad, J.D. Unadkat, Optimized approaches for quantification of drug transporters in tissues and cells by MRM proteomics, *AAPS J.* 16 (2014) 634–648, <https://doi.org/10.1208/s12248-014-9602-y>.
- [13] F. Calderón-Celis, J.R. Encinar, A. Sanz-Medel, Standardization approaches in absolute quantitative proteomics with mass spectrometry, *Mass Spectrom. Rev.* 37 (2018) 715–737, <https://doi.org/10.1002/mas.21542>.
- [14] D.K. Bhatt, B. Prasad, Critical issues and optimized practices in quantification of protein abundance level to determine interindividual variability in DMET proteins by LC-MS/MS proteomics, *Clin. Pharmacol. Ther.* (2017), <https://doi.org/10.1002/cpt.819>.
- [15] S.-F. Zhou, J.-P. Liu, B. Chowbay, Polymorphism of human cytochrome P450 enzymes and its clinical impact, *Drug Metab. Rev.* 41 (2009) 89–295, <https://doi.org/10.1080/03602530902843483>.
- [16] V.M. Lauschke, L. Milani, M. Ingelman-Sundberg, Pharmacogenomic biomarkers for improved drug therapy—recent progress and future developments, *AAPS J.* 20 (2018) 4, <https://doi.org/10.1208/s12248-017-0161-x>.
- [17] A. Cieślak, I. Kelly, J. Trottier, M. Verreault, E. Wunsch, P. Milkiewicz, G. Poirier, A. Droit, O. Barbier, Selective and sensitive quantification of the cytochrome P450 3A4 protein in human liver homogenates through multiple reaction monitoring mass spectrometry, *Proteomics* 16 (2016) 2827–2837, <https://doi.org/10.1002/pmic.201500386>.
- [18] B. Achour, A. Dantonio, M. Niosi, J.J. Novak, J.K. Fallon, J. Barber, P.C. Smith, A. Rostami-Hodjegan, T. C. Goosen, Quantitative characterization of major hepatic UDP-glucuronosyltransferase enzymes in human liver microsomes: comparison of two proteomic methods and correlation with catalytic activity, *Drug Metab. Dispos.* 45 (2017) 1102–1112, <https://doi.org/10.1124/dmd.117.076703>.
- [19] M.D. Harwood, B. Achour, S. Neuhoff, M.R. Russell, G. Carlson, G. Warhurst, A. Rostami-Hodjegan, In vitro-in vivo extrapolation scaling factors for intestinal P-glycoprotein and breast cancer resistance protein: part I: a cross-laboratory comparison of transporter-protein abundances and relative expression factors in human intestine and Caco-2 cells, *Drug Metab. Dispos.* 44 (2016) 297–307, <https://doi.org/10.1124/dmd.115.067371>.
- [20] C. Wegler, F.Z. Gaugaz, T.B. Andersson, J.R. Wiśniewski, D. Busch, C. Gröer, S. Oswald, A. Norén, F. Weiss, H. S. Hammer, T.O. Joos, O. Poetz, B. Achour, A. Rostami-Hodjegan, E. van de Steeg, H.M. Wortelboer, P. Artursson, Variability in mass spectrometry-based quantification of clinically relevant drug transporters and drug metabolizing enzymes, *Mol. Pharm.* 14 (2017) 3142–3151, <https://doi.org/10.1021/acs.molpharmaceut.7b00364>.
- [21] J. Badée, B. Achour, A. Rostami-Hodjegan, A. Galetin, Meta-analysis of expression of hepatic organic anion-transporting polypeptide (OATP) transporters in cellular systems relative to human liver tissue, *Drug Metab. Dispos.* 43 (2015) 424–432, <https://doi.org/10.1124/dmd.114.062034>.
- [22] B. Achour, J. Barber, A. Rostami-Hodjegan, Expression of hepatic drug-metabolizing cytochrome p450 enzymes and their intercorrelations: a meta-analysis, *Drug Metab. Dispos.* 42 (2014) 1349–1356, <https://doi.org/10.1124/dmd.114.058834>.
- [23] B. Prasad, B. Achour, P. Artursson, C.E.C.A. Hop, Y. Lai, P.C. Smith, J. Barber, J.R. Wisniewski, D. Spellman, Y. Uchida, M.A. Zientek, J.D. Unadkat, A. Rostami-Hodjegan, Toward a consensus on applying quantitative liquid chromatography-tandem mass spectrometry proteomics in translational pharmacology research: a white paper, *Clin. Pharmacol. Ther.* 106 (2019), <https://doi.org/10.1002/cpt.1537>.
- [24] V. Vidova, Z. Spacil, A review on mass spectrometry-based quantitative proteomics: targeted and data independent acquisition, *Anal. Chim. Acta* 964 (2017) 7–23, <https://doi.org/10.1016/j.aca.2017.01.059>.
- [25] M. Drozdziak, D. Busch, J. Lapczuk, J. Müller, M. Ostrowski, M. Kurzawski, S. Oswald, Protein abundance of clinically relevant drug transporters in the human liver and intestine: a comparative analysis in paired tissue specimens, *Clin. Pharmacol. Ther.* (2019), <https://doi.org/10.1002/cpt.1301>.
- [26] M. Drozdziak, C. Gröer, J. Pensi, J. Lapczuk, M. Ostrowski, Y. Lai, B. Prasad, J.D. Unadkat, W. Siegmund, S. Oswald, Protein abundance of clinically relevant multidrug transporters along the entire length of the human intestine, *Mol. Pharm.* 11 (2014) 3547–3555, <https://doi.org/10.1021/mp500330y>.

- [27] H. Zhang, A. Basit, D. Busch, K. Yabut, D.K. Bhatt, M. Drozdziak, M. Ostrowski, A. Li, C. Collins, S. Oswald, B. Prasad, Quantitative characterization of UDP-glucuronosyltransferase 2B17 in human liver and intestine and its role in testosterone first-pass metabolism, *Biochem. Pharmacol.* 156 (2018) 32–42, <https://doi.org/10.1016/j.bcp.2018.08.003>.
- [28] S. Goldberg, Mechanical/physical methods of cell distribution and tissue homogenization, *Methods Mol. Biol.* 1295 (2015) 1–20, [https://doi.org/10.1007/978-1-4939-2550-6\\_1](https://doi.org/10.1007/978-1-4939-2550-6_1).
- [29] M. Xu, N. Saxena, M. Vrana, H. Zhang, V. Kumar, S. Billington, C. Khojasteh, S. Heyward, J.D. Unadkat, B. Prasad, Targeted LC-MS/MS proteomics-based strategy to characterize in vitro models used in drug metabolism and transport studies, *Anal. Chem.* (2018), <https://doi.org/10.1021/acs.analchem.8b01913>.
- [30] V. Kumar, B. Prasad, G. Patilea, A. Gupta, L. Salphati, R. Evers, C.E.C.A. Hop, J.D. Unadkat, Quantitative transporter proteomics by liquid chromatography with tandem mass spectrometry: addressing methodologic issues of plasma membrane isolation and expression-activity relationship, *Drug Metab. Dispos.* 43 (2015) 284–288, <https://doi.org/10.1124/dmd.114.061614>.
- [31] C.V. Sapan, R.L. Lundblad, N.C. Price, Colorimetric protein assay techniques, *Biotechnol. Appl. Biochem.* 29 (Pt 2) (1999) 99–108. <http://www.ncbi.nlm.nih.gov/pubmed/10075906>. (accessed May 3, 2019).
- [32] M.D. Harwood, M.R. Russell, S. Neuhoff, G. Warhurst, A. Rostami-Hodjegan, Lost in centrifugation: accounting for transporter protein losses in quantitative targeted absolute proteomics, *Drug Metab. Dispos.* 42 (2014) 1766–1772, <https://doi.org/10.1124/dmd.114.058446>.
- [33] Z.E. Barter, M.K. Bayliss, P.H. Beaune, A.R. Boobis, D.J. Carlile, R.J. Edwards, J.B. Houston, B.G. Lake, J. C. Lipscomb, O.R. Pelkonen, G.T. Tucker, A. Rostami-Hodjegan, Scaling factors for the extrapolation of in vivo metabolic drug clearance from in vitro data: reaching a consensus on values of human microsomal protein and hepatocellularity per gram of liver, *Curr. Drug Metab.* 8 (2007) 33–45. <http://www.ncbi.nlm.nih.gov/pubmed/17266522>. (accessed August 14, 2019).
- [34] G.E. Schaller, *Isolation of Endoplasmic Reticulum and Its Membrane*, Humana Press, New York, NY, 2017, pp. 119–129, [https://doi.org/10.1007/978-1-4939-6533-5\\_10](https://doi.org/10.1007/978-1-4939-6533-5_10).
- [35] D.K. Bhatt, A. Mehrotra, A. Gaedigk, R. Chapa, A. Basit, H. Zhang, P. Choudhari, M. Boberg, R.E. Pearce, R. Gaedigk, U. Broeckel, J.S. Leeder, B. Prasad, Age- and genotype-dependent variability in the protein abundance and activity of six major uridine diphosphate-glucuronosyltransferases in human liver, *Clin. Pharmacol. Ther.* (2018), <https://doi.org/10.1002/cpt.1109>.
- [36] E.Y. Dotsey, K.-M. Jung, A. Basit, D. Wei, J. Daglian, F. Vaccondio, A. Armirotti, M. Mor, D. Piomelli, Peroxide-dependent MGL sulfenylation regulates 2-AG-mediated endocannabinoid signaling in brain neurons, *Chem. Biol.* 22 (2015) 619–628, <https://doi.org/10.1016/j.chembiol.2015.04.013>.
- [37] R. Fischer, B.M. Kessler, Gel-aided sample preparation (GASP)-a simplified method for gel-assisted proteomic sample generation from protein extracts and intact cells, *Proteomics* 15 (2015) 1224–1229, <https://doi.org/10.1002/pmic.201400436>.
- [38] J.R. Wiśniewski, Quantitative evaluation of filter aided sample preparation (FASP) and multienzyme digestion FASP protocols, *Anal. Chem.* 88 (2016) 5438–5443, <https://doi.org/10.1021/acs.analchem.6b00859>.
- [39] A. Eshghi, C.H. Borchers, Multiple reaction monitoring using double isotopologue peptide standards for protein quantification, *Methods Mol. Biol.* 1788 (2018) 193–214, <https://doi.org/10.1007/978-1-4939-7651-112>.
- [40] T. Boström, J.O. Takanen, S. Hober, Antibodies as means for selective mass spectrometry, *J. Chromatogr. B* 1021 (2016) 3–13, <https://doi.org/10.1016/j.jchromb.2015.10.042>.
- [41] G. Rosenberger, C.C. Koh, T. Guo, H.L. Röst, P. Kouvonen, B.C. Collins, M. Heusel, Y. Liu, E. Caron, A. Vichalkovski, M. Faini, O.T. Schubert, P. Faridi, H.A. Ehardt, M. Matondo, H. Lam, S.L. Bader, D. S. Campbell, E.W. Deutsch, R.L. Moritz, S. Tate, R. Aebersold, A repository of assays to quantify 10,000 human proteins by SWATH-MS, *Sci. Data* 1 (2014) 140031, <https://doi.org/10.1038/sdata.2014.31>.
- [42] B. Prasad, R. Evers, A. Gupta, C.E.C.A. Hop, L. Salphati, S. Shukla, S.V. Ambudkar, J.D. Unadkat, Interindividual variability in hepatic organic anion-transporting polypeptides and P-glycoprotein (ABCB1) protein expression: quantification by liquid chromatography tandem mass spectroscopy and influence of genotype, age, and sex, *Drug Metab. Dispos.* 42 (2013) 78–88, <https://doi.org/10.1124/dmd.113.053819>.
- [43] S.-E. Ong, B. Blagoev, I. Kratchmarova, D.B. Kristensen, H. Steen, A. Pandey, M. Mann, Stable isotope labeling by amino acids in cell culture, SILAC, as a simple and accurate approach to expression proteomics, *Mol. Cell. Proteomics* 1 (2002) 376–386. <http://www.ncbi.nlm.nih.gov/pubmed/12118079>. (accessed May 4, 2019).



- [44] S.-E. Ong, M. Mann, A practical recipe for stable isotope labeling by amino acids in cell culture (SILAC), *Nat. Protoc.* 1 (2006) 2650–2660, <https://doi.org/10.1038/nprot.2006.427>.
- [45] A.K. Macleod, T. Zang, Z. Riches, C.J. Henderson, C.R. Wolf, J.T.-J. Huang, A targeted in vivo SILAC approach for quantification of drug metabolism enzymes: regulation by the constitutive androstane receptor, *J. Proteome Res.* 13 (2014) 866–874, <https://doi.org/10.1021/pr400897t>.
- [46] P.L. Ross, Y.N. Huang, J.N. Marchese, B. Williamson, K. Parker, S. Hattan, N. Khainovski, S. Pillai, S. Dey, S. Daniels, S. Purkayastha, P. Juhasz, S. Martin, M. Bartlett-Jones, F. He, A. Jacobson, D.J. Pappin, Multiplexed protein quantitation in *Saccharomyces cerevisiae* using amine-reactive isobaric tagging reagents, *Mol. Cell. Proteomics* 3 (2004) 1154–1169, <https://doi.org/10.1074/mcp.M400129-MCP200>.
- [47] M. Mann, Functional and quantitative proteomics using SILAC, *Nat. Rev. Mol. Cell Biol.* 7 (2006) 952–958, <https://doi.org/10.1038/nrm2067>.
- [48] X. Chen, S. Wei, Y. Ji, X. Guo, F. Yang, Quantitative proteomics using SILAC: principles, applications, and developments, *Proteomics* 15 (2015) 3175–3192, <https://doi.org/10.1002/pmic.201500108>.
- [49] Y. Reinders, D. Völler, A.-K. Bosserhoff, P.J. Oefner, J. Reinders, Testing suitability of cell cultures for SILAC-experiments using SWATH-mass spectrometry, *Methods Mol. Biol.* (2016) 101–108, [https://doi.org/10.1007/978-1-4939-3341-9\\_8](https://doi.org/10.1007/978-1-4939-3341-9_8).
- [50] N. Rauniyar, D.B. McClatchy, J.R. Yates, Stable isotope labeling of mammals (SILAM) for in vivo quantitative proteomic analysis, *Methods* 61 (2013) 260–268, <https://doi.org/10.1016/j.ymeth.2013.03.008>.
- [51] D.B. McClatchy, J.R. Yates, Stable isotope labeling in mammals (SILAM), *Methods Mol. Biol.* (2014) 133–146, [https://doi.org/10.1007/978-1-4939-0685-7\\_8](https://doi.org/10.1007/978-1-4939-0685-7_8).
- [52] X. Wang, Y. Liang, L. Liu, J. Shi, H.-J. Zhu, Targeted absolute quantitative proteomics with SILAC internal standards and unlabeled full-length protein calibrators (TAQSI), *Rapid Commun. Mass Spectrom.* 30 (2016) 553–561, <https://doi.org/10.1002/rcm.7482>.
- [53] H. Erdjument-Bromage, F.-K. Huang, T.A. Neubert, Sample preparation for relative quantitation of proteins using tandem mass tags (TMT) and mass spectrometry (MS), *Methods Mol. Biol.* (2018) 135–149, [https://doi.org/10.1007/978-1-4939-7659-1\\_11](https://doi.org/10.1007/978-1-4939-7659-1_11).
- [54] L. Zhang, J.E. Elias, Relative protein quantification using tandem mass tag mass spectrometry, *Methods Mol. Biol.* (2017) 185–198, [https://doi.org/10.1007/978-1-4939-6747-6\\_14](https://doi.org/10.1007/978-1-4939-6747-6_14).
- [55] R. Moulder, S.D. Bhosale, D.R. Goodlett, R. Lahesmaa, Analysis of the plasma proteome using iTRAQ and TMT-based isobaric labeling, *Mass Spectrom. Rev.* 37 (2018) 583–606, <https://doi.org/10.1002/mas.21550>.
- [56] S. Aggarwal, A.K. Yadav, Dissecting the iTRAQ data analysis, *Methods Mol. Biol.* (2016) 277–291, [https://doi.org/10.1007/978-1-4939-3106-4\\_18](https://doi.org/10.1007/978-1-4939-3106-4_18).
- [57] C. Evans, J. Noirel, S.Y. Ow, M. Salim, A.G. Pereira-Medrano, N. Couto, J. Pandhal, D. Smith, T.K. Pham, E. Karunakaran, X. Zou, C.A. Biggs, P.C. Wright, An insight into iTRAQ: where do we stand now? *Anal. Bioanal. Chem.* 404 (2012) 1011–1027, <https://doi.org/10.1007/s00216-012-5918-6>.
- [58] U.-B. Kang, J. Yeom, H. Kim, C. Lee, Quantitative analysis of mTRAQ-labeled proteome using full MS scans, *J. Proteome Res.* 9 (2010) 3750–3758, <https://doi.org/10.1021/pr9011014>.
- [59] J. Yeom, M.J. Kang, D. Shin, H.K. Song, C. Lee, J.E. Lee, mTRAQ-based quantitative analysis combined with peptide fractionation based on cysteinyl peptide enrichment, *Anal. Biochem.* 477 (2015) 41–49, <https://doi.org/10.1016/j.ab.2015.03.005>.
- [60] A.N. Kettenbach, J. Rush, S.A. Gerber, Absolute quantification of protein and post-translational modification abundance with stable isotope-labeled synthetic peptides, *Nat. Protoc.* 6 (2011) 175–186, <https://doi.org/10.1038/nprot.2010.196>.
- [61] D.M. Simpson, R.J. Beynon, QconCATs: design and expression of concatenated protein standards for multiplexed protein quantification, *Anal. Bioanal. Chem.* 404 (2012) 977–989, <https://doi.org/10.1007/s00216-012-6230-1>.
- [62] K.B. Scott, I.V. Turko, K.W. Phinney, QconCAT, *Methods Enzymol.* (2016) 289–303, <https://doi.org/10.1016/bs.mie.2015.09.022>.
- [63] V. Brun, A. Dupuis, A. Adrait, M. Marcellin, D. Thomas, M. Court, F. Vandenesch, J. Garin, Isotope-labeled protein standards: Toward absolute quantitative proteomics, *Mol. Cell. Proteomics* 6 (2007) 2139–2149, <https://doi.org/10.1074/mcp.M700163-MCP200>.

- [64] G. Picard, D. Lebert, M. Louwagie, A. Adrait, C. Huillet, F. Vandenesch, C. Bruley, J. Garin, M. Jaquinod, V. Brun, PSAQ™ standards for accurate MS-based quantification of proteins: from the concept to biomedical applications, *J. Mass Spectrom.* 47 (2012) 1353–1363, <https://doi.org/10.1002/jms.3106>.
- [65] O. Chahrour, D. Cobice, J. Malone, Stable isotope labelling methods in mass spectrometry-based quantitative proteomics, *J. Pharm. Biomed. Anal.* 113 (2015) 2–20, <https://doi.org/10.1016/j.jpba.2015.04.013>.
- [66] P.P. Olszowy, A. Burns, P.S. Ciborowski, Pressure-assisted sample preparation for proteomic analysis, *Anal. Biochem.* 438 (2013) 67–72, <https://doi.org/10.1016/j.ab.2013.03.023>.
- [67] R.W. Sprung, J.W.C. Brock, J.P. Tanksley, M. Li, M.K. Washington, R.J.C. Slebos, D.C. Liebler, Equivalence of protein inventories obtained from formalin-fixed paraffin-embedded and frozen tissue in multidimensional liquid chromatography-tandem mass spectrometry shotgun proteomic analysis, *Mol. Cell. Proteomics* 8 (2009) 1988–1998, <https://doi.org/10.1074/mcp.M800518-MCP200>.
- [68] P. Ostasiewicz, D.F. Zielinska, M. Mann, J.R. Wiśniewski, Proteome, phosphoproteome, and N-glycoproteome are quantitatively preserved in formalin-fixed paraffin-embedded tissue and analyzable by high-resolution mass spectrometry, *J. Proteome Res.* 9 (2010) 3688–3700, <https://doi.org/10.1021/pr100234w>.
- [69] B. Prasad, D.K. Bhatt, K. Johnson, R. Chapa, X. Chu, L. Salphati, G. Xiao, C. Lee, C.E.C.A. Hop, A. Mathias, Y. Lai, M. Liao, W.G. Humphreys, S.C. Kumer, J.D. Unadkat, Abundance of phase 1 and 2 drug-metabolizing enzymes in alcoholic and hepatitis C cirrhotic livers: a quantitative targeted proteomics study, *Drug Metab. Dispos.* 46 (2018) 943–952, <https://doi.org/10.1124/dmd.118.080523>.
- [70] A.K. Deo, B. Prasad, L. Balogh, Y. Lai, J.D. Unadkat, Interindividual variability in hepatic expression of the multidrug resistance-associated protein 2 (MRP2/ABCC2): quantification by liquid chromatography/tandem mass spectrometry, *Drug Metab. Dispos.* 40 (2012) 852–855, <https://doi.org/10.1124/dmd.111.043810>.
- [71] M.Z. Wang, J.Q. Wu, J.B. Dennison, A.S. Bridges, S.D. Hall, S. Kornbluth, R.R. Tidwell, P.C. Smith, R. D. Voyksner, M.F. Paine, J.E. Hall, A gel-free MS-based quantitative proteomic approach accurately measures cytochrome P450 protein concentrations in human liver microsomes, *Proteomics* 8 (2008) 4186–4196, <https://doi.org/10.1002/pmic.200800144>.
- [72] C. Seibert, B.R. Davidson, B.J. Fuller, L.H. Patterson, W.J. Griffiths, Y. Wang, Multiple-approaches to the identification and quantification of cytochromes P450 in human liver tissue by mass spectrometry, *J. Proteome Res.* 8 (2009) 1672–1681, <https://doi.org/10.1021/pr800795r>.
- [73] E. Langenfeld, U.M. Zanger, K. Jung, H.E. Meyer, K. Marcus, Mass spectrometry-based absolute quantification of microsomal cytochrome P450 2D6 in human liver, *Proteomics* 9 (2009) 2313–2323, <https://doi.org/10.1002/pmic.200800680>.
- [74] H. Kawakami, S. Ohtsuki, J. Kamiie, T. Suzuki, T. Abe, T. Terasaki, Simultaneous absolute quantification of 11 cytochrome P450 isoforms in human liver microsomes by liquid chromatography tandem mass spectrometry with in Silico target peptide selection, *J. Pharm. Sci.* 100 (2011) 341–352, <https://doi.org/10.1002/jps.22255>.
- [75] S. Ohtsuki, O. Schaefer, H. Kawakami, T. Inoue, S. Liehner, A. Saito, N. Ishiguro, W. Kishimoto, E. Ludwig-Schwellinger, T. Ebner, T. Terasaki, Simultaneous absolute protein quantification of transporters, cytochromes P450, and UDP-glucuronosyltransferases as a novel approach for the characterization of individual human liver: comparison with mRNA levels and activities, *Drug Metab. Dispos.* 40 (2012) 83–92, <https://doi.org/10.1124/dmd.111.042259>.
- [76] X. Liu, L. Hu, G. Ge, B. Yang, J. Ning, S. Sun, L. Yang, K. Pors, J. Gu, Quantitative analysis of cytochrome P450 isoforms in human liver microsomes by the combination of proteomics and chemical probe-based assay, *Proteomics* 14 (2014) 1943–1951, <https://doi.org/10.1002/pmic.201400025>.
- [77] K. Nakamura, M. Hirayama-Kurogi, S. Ito, T. Kuno, T. Yoneyama, W. Obuchi, T. Terasaki, S. Ohtsuki, Large-scale multiplex absolute protein quantification of drug-metabolizing enzymes and transporters in human intestine, liver, and kidney microsomes by SWATH-MS: comparison with MRM/SRM and HR-MRM/PRM, *Proteomics* 16 (2016) 2106–2117, <https://doi.org/10.1002/pmic.201500433>.
- [78] M. Drozdziak, D. Busch, J. Lapczuk, J. Müller, M. Ostrowski, M. Kurzawski, S. Oswald, Protein abundance of clinically relevant drug-metabolizing enzymes in the human liver and intestine: a comparative analysis in paired tissue specimens, *Clin. Pharmacol. Ther.* 104 (2018) 515–524, <https://doi.org/10.1002/cpt.967>.
- [79] G. Margailan, M. Rouleau, K. Klein, J.K. Fallon, P. Caron, L. Villeneuve, P.C. Smith, U.M. Zanger, C. Guillemette, Multiplexed targeted quantitative proteomics predicts hepatic glucuronidation potential, *Drug Metab. Dispos.* 43 (2015) 1331–1335, <https://doi.org/10.1124/dmd.115.065391>.
- [80] D.E. Harbourt, J.K. Fallon, S. Ito, T. Baba, J.K. Ritter, G.L. Glish, P.C. Smith, Quantification of human uridine-diphosphate glucuronosyl transferase 1A isoforms in liver, intestine, and kidney using nanobore liquid chromatography-tandem mass spectrometry, *Anal. Chem.* 84 (2012) 98–105, <https://doi.org/10.1021/ac201704a>.



- [81] J.K. Fallon, D.E. Harbourt, S.H. Maleki, F.K. Kessler, J.K. Ritter, P.C. Smith, Absolute quantification of human uridine-diphosphate glucuronosyl transferase (UGT) enzyme isoforms 1A1 and 1A6 by tandem LC-MS, *Drug Metab. Lett.* 2 (2008) 210–222. <http://www.ncbi.nlm.nih.gov/pubmed/19356096>. (accessed May 16, 2019).
- [82] C. Sridar, I. Hanna, P.F. Hollenberg, Quantitation of UGT1A1 in human liver microsomes using stable isotope-labelled peptides and mass spectrometry based proteomic approaches, *Xenobiotica* 43 (2013) 336–345, <https://doi.org/10.3109/00498254.2012.719089>.
- [83] Y. Sato, M. Nagata, A. Kawamura, A. Miyashita, T. Usui, Protein quantification of UDP-glucuronosyltransferases 1A1 and 2B7 in human liver microsomes by LC-MS/MS and correlation with glucuronidation activities, *Xenobiotica* 42 (2012) 823–829, <https://doi.org/10.3109/00498254.2012.665950>.
- [84] Y. Sato, M. Nagata, K. Tetsuka, K. Tamura, A. Miyashita, A. Kawamura, T. Usui, Optimized methods for targeted peptide-based quantification of human uridine 5'-diphosphate-glucuronosyltransferases in biological specimens using liquid chromatography-tandem mass spectrometry, *Drug Metab. Dispos.* 42 (2014) 885–889, <https://doi.org/10.1124/dmd.113.056291>.
- [85] J.K. Fallon, H. Neubert, T.C. Goosen, P.C. Smith, Targeted precise quantification of 12 human recombinant uridine-diphosphate glucuronosyl transferase 1A and 2B isoforms using nano-ultra-high-performance liquid chromatography/tandem mass spectrometry with selected reaction monitoring, *Drug Metab. Dispos.* 41 (2013) 2076–2080, <https://doi.org/10.1124/dmd.113.053801>.
- [86] L. Wang, B. Prasad, L. Salphati, X. Chu, A. Gupta, C.E.C.A. Hop, R. Evers, J.D. Unadkat, Interspecies variability in expression of hepatobiliary transporters across human, dog, monkey, and rat as determined by quantitative proteomics, *Drug Metab. Dispos.* 43 (2015) 367–374, <https://doi.org/10.1124/dmd.114.061580>.
- [87] C. Ji, W.R. Tschantz, N.D. Pfeifer, M. Ullah, N. Sadagopan, Development of a multiplex UPLC-MRM MS method for quantification of human membrane transport proteins OATP1B1, OATP1B3 and OATP2B1 in in vitro systems and tissues, *Anal. Chim. Acta* 717 (2012) 67–76, <https://doi.org/10.1016/j.aca.2011.12.005>.
- [88] L.M. Balogh, E. Kimoto, J. Chupka, H. Zhang, Y. Lai, Membrane protein quantification by peptide-based mass spectrometry approaches: studies on the organic anion-transporting polypeptide family, *J. Proteomics Bioinform.* 06 (2013) 1–8, <https://doi.org/10.4172/jpb.1000285>.
- [89] N. Li, Y. Zhang, F. Hua, Y. Lai, Absolute difference of hepatobiliary transporter multidrug resistance-associated protein (MRP2/Mrp2) in liver tissues and isolated hepatocytes from rat, dog, monkey, and human, *Drug Metab. Dispos.* 37 (2009) 66–73, <https://doi.org/10.1124/dmd.108.023234>.
- [90] N. Li, J. Palandra, O.V. Nemirovskiy, Y. Lai, LC – MS/MS mediated absolute quantification and comparison of bile salt export pump and breast cancer resistance protein in livers and hepatocytes across species, *Anal. Chem.* 81 (2009) 2251–2259, <https://doi.org/10.1021/ac8024009>.
- [91] J.K. Fallon, P.C. Smith, C.Q. Xia, M.-S. Kim, Quantification of four efflux drug transporters in liver and kidney across species using targeted quantitative proteomics by isotope dilution NanoLC-MS/MS, *Pharm. Res.* 33 (2016) 2280–2288, <https://doi.org/10.1007/s11095-016-1966-5>.
- [92] K.-W. Peng, J. Bacon, M. Zheng, Y. Guo, M.Z. Wang, Ethnic variability in the expression of hepatic drug transporters: absolute quantification by an optimized targeted quantitative proteomic approach, *Drug Metab. Dispos.* 43 (2015) 1045–1055, <https://doi.org/10.1124/dmd.115.063362>.
- [93] L. Wang, C. Collins, E.J. Kelly, X. Chu, A.S. Ray, L. Salphati, G. Xiao, C. Lee, Y. Lai, M. Liao, A. Mathias, R. Evers, W. Humphreys, C.E.C.A. Hop, S.C. Kumer, J.D. Unadkat, Transporter expression in liver tissue from subjects with alcoholic or hepatitis C cirrhosis quantified by targeted quantitative proteomics, *Drug Metab. Dispos.* 44 (2016) 1752–1758, <https://doi.org/10.1124/dmd.116.071050>.
- [94] A. Vildhede, E. Kimoto, A.D. Rodrigues, M.V.S. Varma, Quantification of hepatic organic anion transport proteins OAT2 and OAT7 in human liver tissue and primary hepatocytes, *Mol. Pharm.* 15 (2018) 3227–3235, <https://doi.org/10.1021/acs.molpharmaceut.8b00320>.
- [95] A. Vildhede, C. Nguyen, B.K. Erickson, R.C. Kunz, R. Jones, E. Kimoto, F. Bourbonais, A.D. Rodrigues, M.V.S. Varma, Comparison of proteomic quantification approaches for hepatic drug transporters: multiplexed global quantitation correlates with targeted proteomic quantitation, *Drug Metab. Dispos.* 46 (2018) 692–696, <https://doi.org/10.1124/dmd.117.079285>.
- [96] C. Gröer, D. Busch, M. Patrzyk, K. Beyer, A. Busemann, C.D. Heidecke, M. Drozdziak, W. Siegmund, S. Oswald, Absolute protein quantification of clinically relevant cytochrome P450 enzymes and UDP-glucuronosyltransferases by mass spectrometry-based targeted proteomics, *J. Pharm. Biomed. Anal.* 100 (2014) 393–401, <https://doi.org/10.1016/j.jpba.2014.08.016>.
- [97] E. Miyauchi, M. Tachikawa, X. Declèves, Y. Uchida, J.-L.L. Bouillot, C. Poitou, J.-M.M. Oppert, S. Mouly, J.-F. Bergmann, T. Terasaki, J.-M.M. Scherrmann, C. Lloret-Linares, Quantitative atlas of cytochrome P450, UDP-

- glucuronosyltransferase, and transporter proteins in jejunum of morbidly obese subjects, *Mol. Pharm.* 13 (2016) 2631–2640, <https://doi.org/10.1021/acs.molpharmaceut.6b00085>.
- [98] T. Akazawa, Y. Uchida, E. Miyauchi, M. Tachikawa, S. Ohtsuki, T. Terasaki, High expression of UGT1A1/1A6 in monkey small intestine: comparison of protein expression levels of cytochromes P450, UDP-glucuronosyltransferases, and transporters in small intestine of *Cynomolgus* monkey and human, *Mol. Pharm.* 15 (2018) 127–140, <https://doi.org/10.1021/acs.molpharmaceut.7b00772>.
- [99] P. Erdmann, H. Bruckmueller, P. Martin, D. Busch, S. Haenisch, J. Müller, A. Wiechowska-Kozłowska, L. I. Partecke, C.-D. Heidecke, I. Cascorbi, M. Drozdziak, S. Oswald, Dysregulation of mucosal membrane transporters and drug-metabolizing enzymes in ulcerative colitis, *J. Pharm. Sci.* 108 (2019) 1035–1046, <https://doi.org/10.1016/j.xphs.2018.09.024>.
- [100] C. Gröer, S. Brück, Y. Lai, A. Paulick, A. Busemann, C.D. Heidecke, W. Siegmund, S. Oswald, LC–MS/MS-based quantification of clinically relevant intestinal uptake and efflux transporter proteins, *J. Pharm. Biomed. Anal.* 85 (2013) 253–261, <https://doi.org/10.1016/j.jpba.2013.07.031>.
- [101] H. Bruckmueller, P. Martin, M. Kähler, S. Haenisch, M. Ostrowski, M. Drozdziak, W. Siegmund, I. Cascorbi, S. Oswald, Clinically relevant multidrug transporters are regulated by microRNAs along the human intestine, *Mol. Pharm.* 14 (2017) 2245–2253, <https://doi.org/10.1021/acs.molpharmaceut.7b00076>.
- [102] G. Margailan, M. Rouleau, J.K. Fallon, P. Caron, L. Villeneuve, V. Turcotte, P.C. Smith, M.S. Joy, C. Guillemette, Quantitative profiling of human renal UDP-glucuronosyltransferases and glucuronidation activity: a comparison of normal and tumoral kidney tissues, *Drug Metab. Dispos.* 43 (2015) 611–619, <https://doi.org/10.1124/dmd.114.062877>.
- [103] B. Prasad, K. Johnson, S. Billington, C. Lee, G.W. Chung, C.D.A. Brown, E.J. Kelly, J. Himmelfarb, J.D. Unadkat, Abundance of drug transporters in the human kidney cortex as quantified by quantitative targeted proteomics, *Drug Metab. Dispos.* 44 (2016) 1920–1924, <https://doi.org/10.1124/dmd.116.072066>.
- [104] R. Shawahna, Y. Uchida, X. Declèves, S. Ohtsuki, S. Yousif, S. Dauchy, A. Jacob, F. Chassoux, C. Dumas-Duport, P.-O. Couraud, T. Terasaki, J.-M. Scherrmann, Transcriptomic and quantitative proteomic analysis of transporters and drug metabolizing enzymes in freshly isolated human brain microvessels, *Mol. Pharm.* 8 (2011) 1332–1341, <https://doi.org/10.1021/mp200129p>.
- [105] Y. Uchida, S. Ohtsuki, Y. Katsukura, C. Ikeda, T. Suzuki, J. Kamiie, T. Terasaki, Quantitative targeted absolute proteomics of human blood-brain barrier transporters and receptors, *J. Neurochem.* 117 (2011) 333–345, <https://doi.org/10.1111/j.1471-4159.2011.07208.x>.
- [106] S. Billington, L. Salphati, C.E.C.A. Hop, X. Chu, R. Evers, D. Burdette, C. Rowbottom, Y. Lai, G. Xiao, W. G. Humphreys, T.B. Nguyen, B. Prasad, J.D. Unadkat, Interindividual and regional variability in drug transporter abundance at the human blood–brain barrier measured by quantitative targeted proteomics, *Clin. Pharmacol. Ther.* (2019) <https://doi.org/10.1002/cpt.1373>.
- [107] Y. Uchida, Z. Zhang, M. Tachikawa, T. Terasaki, Quantitative targeted absolute proteomics of rat blood-cerebrospinal fluid barrier transporters: comparison with a human specimen, *J. Neurochem.* 134 (2015) 1104–1115, <https://doi.org/10.1111/jnc.13147>.
- [108] J.K. Fallon, N. Houvig, C.L. Booth-Genthe, P.C. Smith, Quantification of membrane transporter proteins in human lung and immortalized cell lines using targeted quantitative proteomic analysis by isotope dilution nanoLC–MS/MS, *J. Pharm. Biomed. Anal.* 154 (2018) 150–157, <https://doi.org/10.1016/j.jpba.2018.02.044>.
- [109] R. Miyamoto, T. Nozawa, K. Shiozuka, K. Tabata, The impact of endogenous breast cancer resistance protein on human P-glycoprotein-mediated transport assays using LLC-PK1 cells transfected with human P-glycoprotein, *J. Pharm. Sci.* 108 (2019) 1085–1089, <https://doi.org/10.1016/j.xphs.2018.10.012>.
- [110] K.R. Brimacombe, M.D. Hall, D.S. Auld, J. Inglese, C.P. Austin, M.M. Gottesman, K.-L. Fung, A dual-fluorescence high-throughput cell line system for probing multidrug resistance, *Assay Drug Dev. Technol.* 7 (2009) 233–249, <https://doi.org/10.1089/adt.2008.165>.
- [111] M. Karlgren, I. Simoff, M. Backlund, C. Wegler, M. Keiser, N. Handin, J. Müller, P. Lundquist, A.-C. Jareborg, S. Oswald, P. Artursson, A CRISPR-Cas9 generated MDCK cell line expressing human MDR1 without endogenous canine MDR1 (cABCB1): an improved tool for drug efflux studies, *J. Pharm. Sci.* 106 (2017) 2909–2913, <https://doi.org/10.1016/j.xphs.2017.04.018>.
- [112] K.M. Knights, S.M. Spencer, J.K. Fallon, N. Chau, P.C. Smith, J.O. Miners, Scaling factors for the in vitro-in vivo extrapolation (IV-IVE) of renal drug and xenobiotic glucuronidation clearance, *Br. J. Clin. Pharmacol.* 81 (2016) 1153–1164, <https://doi.org/10.1111/bcp.12889>.

- [113] V. Kumar, J. Yin, S. Billington, B. Prasad, C.D.A. Brown, J. Wang, J.D. Unadkat, The importance of incorporating OCT2 plasma membrane expression and membrane potential in IVIVE of metformin renal secretory clearance, *Drug Metab. Dispos.* 46 (2018) 1441–1445, <https://doi.org/10.1124/dmd.118.082313>.
- [114] C.Y. Li, A. Basit, A. Gupta, Z. Gáborik, E. Kis, B. Prasad, Major glucuronide metabolites of testosterone are primarily transported by MRP2 and MRP3 in human liver, intestine and kidney, *J. Steroid Biochem. Mol. Biol.* (2019)<https://doi.org/10.1016/j.jsbmb.2019.03.027>.
- [115] E.J. Jeong, Y. Liu, H. Lin, M. Hu, Species- and disposition model-dependent metabolism of raloxifene in gut and liver: role of UGT1A10, *Drug Metab. Dispos.* 33 (2005) 785–794, <https://doi.org/10.1124/dmd.104.001883>.
- [116] J.J. Kohler, S.H. Hosseini, E. Green, A. Abuin, T. Ludaway, R. Russ, R. Santoianni, W. Lewis, Tenofovir renal proximal tubular toxicity is regulated by OAT1 and MRP4 transporters, *Lab. Investig.* 91 (2011) 852–858, <https://doi.org/10.1038/labinvest.2011.48>.
- [117] L. Zou, A. Stecula, A. Gupta, B. Prasad, H.-C. Chien, S.W. Yee, L. Wang, J.D. Unadkat, S.H. Stahl, K.S. Fenner, K. M. Giacomini, Molecular mechanisms for species differences in organic anion transporter 1, OAT1: implications for renal drug toxicity, *Mol. Pharmacol.* 94 (2018) 689–699, <https://doi.org/10.1124/mol.117.111153>.
- [118] Y.H. Wang, M. Trucksis, J.J. McElwee, P.H. Wong, C. Maciolek, C.D. Thompson, T. Prueksaritanont, G. C. Garrett, R. Declercq, E. Vets, K.J. Willson, R.C. Smith, J.A. Klappenbach, G.J. Opitck, J.A. Tsou, C. Gibson, T. Laethem, P. Panorchan, M. Iwamoto, P.M. Shaw, J.A. Wagner, J.C. Harrelson, UGT2B17 genetic polymorphisms dramatically affect the pharmacokinetics of MK-7246 in healthy subjects in a first-in-human study, *Clin. Pharmacol. Ther.* 92 (2012) 96–102, <https://doi.org/10.1038/clpt.2012.20>.
- [119] M. Drozdzik, D. Busch, J. Lapczuk, J. Müller, M. Ostrowski, M. Kurzawski, S. Oswald, Protein abundance of clinically relevant drug-metabolizing enzymes in the human liver and intestine: a comparative analysis in paired tissue specimens, *Clin. Pharmacol. Ther.* (2017)<https://doi.org/10.1002/cpt.967>.
- [120] B. Prasad, M. Vrana, A. Mehrotra, K. Johnson, D.K. Bhatt, The promises of quantitative proteomics in precision medicine, *J. Pharm. Sci.* 106 (2017) 738–744, <https://doi.org/10.1016/j.xphs.2016.11.017>.
- [121] D.K. Bhatt, A. Basit, H. Zhang, A. Gaedigk, S. Lee, K.G. Claw, A. Mehrotra, A.S. Chaudhry, R.E. Pearce, R. Gaedigk, U. Broeckel, T.A. Thornton, D.A. Nickerson, E.G. Schuetz, J. Amory, J.S. Leeder, B. Prasad, Hepatic abundance and activity of androgen and drug metabolizing enzyme, UGT2B17, are associated with genotype, age, and sex, *Drug Metab. Dispos.* (2018), <https://doi.org/10.1124/dmd.118.080952>.
- [122] D. Rodrigues, A. Rowland, From endogenous compounds as biomarkers to plasma-derived nanovesicles as liquid biopsy; has the golden age of translational pharmacokinetics-absorption, distribution, metabolism, excretion-drug-drug interaction science finally arrived? *Clin. Pharmacol. Ther.* (2018), <https://doi.org/10.1002/cpt.1328>.
- [123] A. Rowland, W. Ruanglertboon, M. van Dyk, D. Wijayakumara, L.S. Wood, R. Meech, P.I. Mackenzie, A. D. Rodrigues, J.-C. Marshall, M.J. Sorich, Plasma extracellular nanovesicle (exosome)-derived biomarkers for drug metabolism pathways: a novel approach to characterize variability in drug exposure, *Br. J. Clin. Pharmacol.* 85 (2019) 216–226, <https://doi.org/10.1111/bcp.13793>.
- [124] B.L. Williamson, S. Purkayastha, C.L. Hunter, L. Nuwaysir, J. Hill, L. Easterwood, J. Hill, Quantitative protein determination for CYP induction via LC-MS/MS, *Proteomics* 11 (2011) 33–41, <https://doi.org/10.1002/pmic.201000456>.
- [125] Y. Ishii, A. Ogara, T. Katsumata, T. Umemura, A. Nishikawa, Y. Iwasaki, R. Ito, K. Saito, M. Hirose, H. Nakazawa, Quantification of nitrated tryptophan in proteins and tissues by high-performance liquid chromatography with electrospray ionization tandem mass spectrometry, *J. Pharm. Biomed. Anal.* 44 (2007) 150–159, <https://doi.org/10.1016/j.jpba.2007.01.012>.
- [126] A. Tailor, J.C. Waddington, X. Meng, B.K. Park, Mass spectrometric and functional aspects of drug-protein conjugation, *Chem. Res. Toxicol.* 29 (2016) 1912–1935, <https://doi.org/10.1021/acs.chemrestox.6b00147>.
- [127] M.R. Hoopmann, A. Zelter, R.S. Johnson, M. Riffle, M.J. MacCoss, T.N. Davis, R.L. Moritz, Kojak: efficient analysis of chemically cross-linked protein complexes, *J. Proteome Res.* 14 (2015) 2190–2198, <https://doi.org/10.1021/pr501321h>.
- [128] M.G. Degan, L. Ryadinskiy, G.M. Fujimoto, C.S. Wilkins, C.F. Lichti, S.H. Payne, A skyline plugin for pathway-centric data browsing, *J. Am. Soc. Mass Spectrom.* 27 (2016) 1752–1757, <https://doi.org/10.1007/s13361-016-1448-3>.
- [129] J.G. Meyer, B. Schilling, Clinical applications of quantitative proteomics using targeted and untargeted data-independent acquisition techniques, *Expert Rev. Proteomics* 14 (2017) 419–429, <https://doi.org/10.1080/14789450.2017.1322904>.

# Protein drug-drug interactions for therapeutic modalities

*Liming Liu<sup>a</sup>, Raymond Evers<sup>b</sup>, Diana Montgomery<sup>b</sup>*

<sup>a</sup>Product Development, Curon Biopharmaceutical Ltd, Shanghai, People's Republic of China

<sup>b</sup>Department of Pharmacokinetics, Pharmacodynamics and Drug Metabolism, Merck & Co Inc., Kenilworth, NJ, United States

## 1 Introduction

In the past several years, the number of therapeutic modalities has increased dramatically and now includes small molecules, antibodies, peptides, RNA therapeutics, gene therapies, nanobodies, oncolytic viruses, and cell therapies. Although small molecule drugs (SMDs) are still the most commonly used modality to treat human disease, alternative therapeutic modalities are fast growing due to the rapid advances in molecular biology, genetics, protein engineering, cell biology, and major investments in applied sciences by the biotechnology and pharmaceutical industry. In fact, among the top 10 best-selling therapeutics in 2018, seven are monoclonal antibodies (mAbs): adalimumab, pembrolizumab, trastuzumab, bevacizumab, rituximab, nivolumab, and ustekinumab [1]. Moreover, the unprecedented efficacy of chimeric antigen T cells (CAR-T) cell therapies in advanced liquid tumors attracts more and more pharmaceutical companies to enter the cell therapy field. Two CAR-T therapies have been approved by the FDA, axicabtagene ciloleucel for diffuse large B-cell lymphoma in 2017 and tisagenlecleucel for B-cell precursor acute lymphoblastic leukemia in 2017 (Table 1). After more than two decades, gene therapies are emerging as a promising modality to treat genetic diseases with the approval of voretigene neparvovec-rzyl in 2017 for correction of an inherited abnormal gene expressed in the eye that leads to blindness [11]. The FDA approved nusinersen, an anti-sense oligonucleotide in 2016. It was the first drug approved to treat children and adults with spinal muscular atrophy, a rare and often fatal genetic disease affecting muscle strength and movement. More recently, the FDA approved onasemnogene abeparvovec-xioi, a single-dose gene therapy for spinal muscular atrophy

**TABLE 1** New modalities approved or in clinical development in recent years.

Modality	INN	Trade name	Indication	Approved year
CAR-T therapy	Axicabtagene ciloleucel	Yescarta	Diffuse large B-cell lymphoma	2017 <sup>1</sup>
CAR-T therapy	Tisagenlecleucel	Kymriah	B-cell acute lymphoblastic leukemia	2017 <sup>2</sup>
Gene therapy	Voretigene neparvovec-rzyl	Luxturna	Blindness caused by abnormal eye gene	2017 <sup>3</sup>
Anti-sense oligonucleotide	Nusinersen	Spinraza	Spinal muscular atrophy	2016 <sup>4</sup>
Gene therapy	Onasemnogene abeparvovec-xioi	Zolgensma	Spinal muscular atrophy	2019 <sup>5</sup>
SiRNA	Patisiran	Onpattro	Transthyretin-mediated amyloidosis	2018 <sup>6</sup>
Hepatitis B surface antigen and CpG oligonucleotide	Hepatitis B vaccine (recombinant), adjuvanted	HEPLISAV-B	Two dose Hep B vaccine	2017 <sup>7</sup>
Oncolytic virus	Talimogene laherparepvec (T-VEC)	Imlygic	Recurrent melanoma	2015 <sup>8</sup>
mRNA encoded mAb	Not applicable	mRNA-1944	Multiple indications anti-Chikungunya virus	In early clinical trials <sup>9</sup>

1. [2], 2. [3], 3 [4], 4. [5], 5. [6], 6. [7], 7. [8], 8. [9], 9. [10].

(Table 1). SiRNA therapeutics, after overcoming some major hurdles during development, finally have a proof of efficacy in certain areas, for example, with the approval of patisiran in 2018, a therapy for the rare hereditary disease transthyretin-mediated amyloidosis in adults (Table 1). A toll-like receptor-9 (TLR-9) agonist oligonucleotide CpG (cytosine and guanine separated by only one phosphate group) was approved as an adjuvant for the hepatitis B vaccine HEPLISAV-B (Table 1). In addition, mRNA therapeutics as vaccines and replacement of protein therapeutics are entering clinical trials by Moderna. An oncolytic virus as therapeutic has been realized by the approval of talimogene laherparepvec (T-VEC) for the treatment of recurrent melanoma (Table 1). Each of these novel approaches have their unique advantages for the treatment of disease and, therefore, leading pharmaceutical companies are adopting modality agnostic approaches as a strategy to increase the success of drug discovery and development to meet unmet medical needs.

An important trend occurring in the treatment of human disease is the increasing use of combination therapies or polypharmacy, especially in oncology and in diseases of the elderly. The combinations of SMDs targeting tumor mutations, chemotherapies, and checkpoint blockade antibodies are becoming a norm in the management of cancer. Addition of oncolytic viruses or other modalities in oncology settings may become more common. The ever-evolving treatment options for human diseases make it critical to increase the understanding

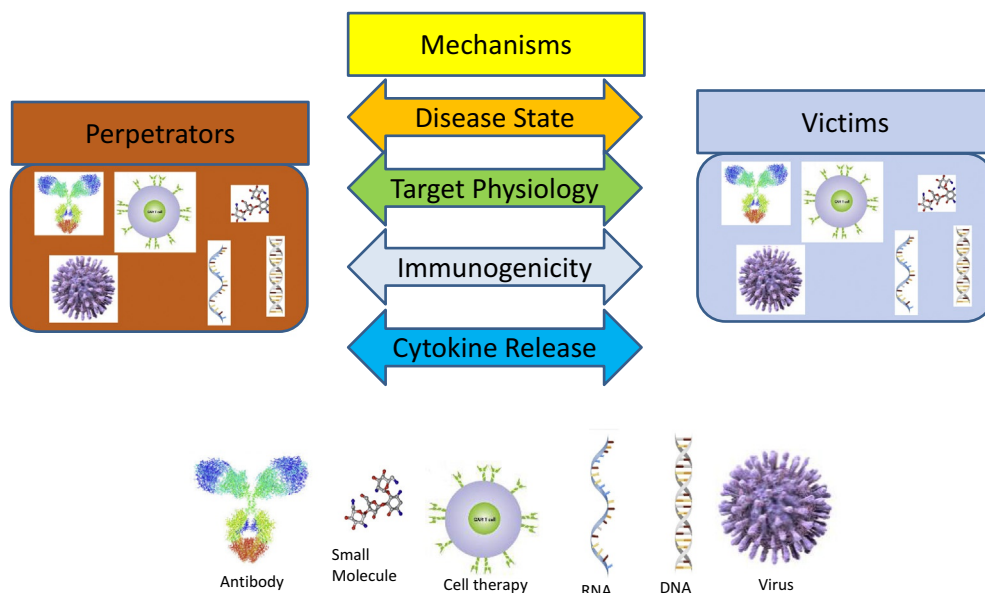


**FIG. 1** TP-DDI risk among different modalities. Different modalities could potentially be either a perpetrator or victim through several different mechanisms.

of mechanisms causing potential drug-drug interactions (DDI) beyond the classical pharmacokinetic SMD-SMD interactions. The potential DDI that could be caused by the various modalities currently being explored and how they might interact with one another is depicted in Fig. 1.

In this chapter, we focus on the major mechanisms of therapeutic protein-drug-drug interactions (TP-DDI). We discuss the potential DDI between small molecules and protein drugs, between two different TPs and potential interactions between known and emerging therapeutic modalities. Based on TP-DDI risk, clinical design considerations are also discussed.

## 2 DDI mechanisms

### 2.1 Major mechanisms of TP-DDI

The primary mechanisms behind clinically observed TP and SMD interactions involve disease state changes in cytokines, target physiology, immunogenicity, and cytokines as therapeutic interventions (Fig. 1).

Pro-inflammatory cytokines such as IL-6, IL-1 $\beta$ , TNF- $\alpha$ , IFN- $\gamma$ , INF- $\alpha$ , and IFN- $\beta$  can be elevated in autoimmune diseases, certain infections, or as a result of therapeutic interventions. Some examples of disease states in which cytokines are increased include rheumatoid arthritis (RA), psoriasis, Crohn's disease, and some viral infections such as those caused by the influenza virus. In other cases, the goal of a therapeutic intervention is to increase the levels of cytokines in the tumor environment, such as in immuno-oncology.



It is known that elevated pro-inflammatory cytokines suppress cytochrome P450 (CYP) enzymes and thus can potentially increase the exposure of SMD co-medications that are substrates of CYP enzymes. Therapeutic interventions to correct these disease states can decrease pro-inflammatory cytokine levels, thus increasing or normalizing CYP enzyme and/or drug transporter activity, resulting in normalization of the exposure of a SMD. It has been known for some time that infections can affect SMD metabolism: for example, influenza virus infection impairs clearance of theophylline, a CYP1A2 substrate [12, 13]. This phenomenon is attributed to the IFNs released after the virus infection, which cause suppression of CYP enzymes and, therefore, a reduction in the clearance of the CYP1A2 substrate theophylline [14]. In patients undergoing allogeneic bone marrow transplantation, pro-inflammatory cytokine production (i.e., IL-6) correlated with a significant increase in cyclosporine systemic exposure [15]. Therefore, disease states such as inflammation or infection can impact metabolism of SMDs through cytokine release. Treatment of pro-inflammatory disease states can reduce cytokine levels and normalize (increase) the metabolism of SMDs. The hypothetical scenario where SMD metabolism is impacted by the disease state and how treatment of the disease can alleviate this effect is depicted in Fig. 2.

Therapeutic targets can also play an important role in TP-DDIs. SMDs or TPs that modulate the target levels can have an impact on the exposure of drugs that bind to the same target. Many mAbs display target-mediated drug disposition in which changes in the amount of available target can affect the observed systemic levels of a mAb (or a targeting fusion TP). Therefore, if a second drug modulates the available target of a mAb, there can be an effect on the mAb PK. There have been several reports illustrating such mechanisms, as discussed in Section 3.3.

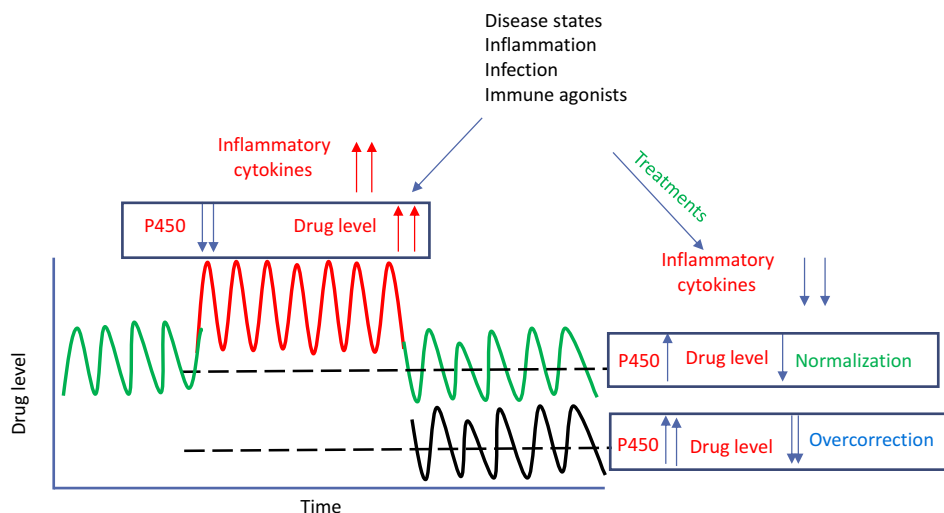


**FIG. 2** Effect of inflammation and anti-inflammatory therapeutic proteins on CYP enzyme expression, activity, and substrate concentrations. Disease states such as inflammation or infection can impact metabolism of SMDs through cytokine release. Treatment of inflammatory disease states can reduce cytokine levels and normalize (increase) the metabolism SMDs.



Another well-known mechanism by which TP-DDI can occur is through immunogenicity. If one drug either stimulates or suppresses the immune system, it is conceivable that the immunogenicity toward the TP could be altered relative to monotherapy. Stimulating the immune system can lead to an increased antidrug antibody (ADA) response, which can lead to reduced exposure of the TP and vice versa. For example, a mAb coadministered with an immunosuppressant such as methotrexate may show a higher exposure due to a reduced ADA response, as discussed in [Section 3.2](#).

Therapeutic cytokines have been used in the treatment of a variety of human diseases. For example, IL-2 and interferons are being used in the treatment of cancer and autoimmune diseases. These exogenously administered cytokines can also affect CYP enzyme levels [16].

In general, SMDs as a perpetrator of TP-DDIs act through modulating immunogenicity or target biology to change the PK of TPs. TPs as perpetrators typically change CYP enzymes and drug transporters through the modulation of cytokine levels. TPs can also be a perpetrator by changing the target levels of a second TP.

## 2.2 In vitro effects on CYP enzymes and transporters

Historically, the emphasis in the field of TP-DDIs has been on cytokines and cytokine modulators. In vitro studies in cultured human hepatocytes have shown that pro-inflammatory cytokines in general do reduce the expression of cytochrome P450 enzymes and drug transporters in hepatocytes isolated from humans and preclinical species, although the extent of effects is not the same for all enzymes and transporters [17–21], suggesting that multiple mechanisms could be at play.

Various mechanisms have been described that may be involved in the inflammation-mediated effects on drug-metabolizing enzymes and transporters. These have been described in numerous reviews previously [22–27] and are summarized briefly below:

- (i) Nuclear factor (NF)  $\kappa$ B-mediated cross talk with the pregnane X receptor (PXR) has been implicated in CYP gene expression regulation, and a direct interaction with NF  $\kappa$ B (p65 subunit) with the DNA-binding domain of retinoic X receptor (RXR) and constitutive androstane receptor (CAR) has been demonstrated [28, 29]. An inflammation-induced effect has been postulated on the subcellular localization of RXR [30], which could be important because RXR is a partner in the heterodimeric transcription factors PXR, CAR, farnesoid X receptor (FXR), liver X receptor (LXR), and the peroxisome proliferator-activated receptor (PPAR).
- (ii) A change in nitric oxide (NO)-dependent ubiquitination and subsequent proteasomal degradation has been implicated in cytokine-dependent degradation of CYP enzymes such as rat CYP2B1, although non-ubiquitin-dependent degradation has been observed as well for CYP2C22 [31]. The latter suggests the involvement of another proteolytic pathway. The effect of NO on CYP levels has mostly been studied in rodents [32], but recent work has shown that cellular NO—as is produced during infection and inflammation—can cause CYP2B6 enzyme degradation in human hepatocytes [33]. It is interesting that the NO-dependent mechanism is specific for CYP2B6 protein, because, although CYP3A4 mRNA was affected more strongly by a pro-inflammatory stimulus than CYP2B6, CYP3A4 protein was affected less [34].

Further work is needed to determine which other mechanisms are involved in the regulation of individual human drug-metabolizing enzymes and transporters and which of these are clinically relevant.

Unexpected effects of non-small molecule therapeutics other than cytokine modulators have been described. For instance, it was shown that several nontherapeutic oligonucleotides (ON) with a phosphorothioate linkage caused inhibition of almost all CYP and uridine-glucuronosyltransferase (UGT) enzymes when tested in human liver microsomes, whereas no such inhibition was observed for oligonucleotides containing phosphodiester linkages. Most potent inhibition was observed for CYP1A2 with  $IC_{50}$  values between 0.8 and 4.2  $\mu$ M [35]. In several cases, time-dependent inhibition of CYP enzymes was observed as well. However, no inhibition of the same enzymes was observed in cultured human hepatocytes, except for weak inhibition of CYP2C19. Overall, these data indicate that the inhibition measured in microsomes has no clinical significance [35, 36]. In another example, four 20-ribose-modified phosphorothioates antisense oligonucleotides (PS-ASOs), including one GalNAc conjugate, were reported neither to inhibit nor induce any of the investigated CYP enzymes *in vitro* [37]. The lack of *in vitro* metabolism by human liver microsomes as well as inhibition of the major CYP enzymes has been shown for mipomersen [38], and for eteplirsen which also lacks *in vitro* induction potential of CYP enzymes [39]. Inhibition of drug transporters was also studied in recombinant cell lines expressing transporters, and although inhibition was observed,  $IC_{50}$  values were high and not deemed of clinical significance [40]. In the subsequent work by the same group, the 13 base oligonucleotide imetelstat, a telomerase inhibitor with a N3'-P5' thio-phosphoramidate backbone to increase stability and a palmitoyl tail at the 5'-position to enhance cellular permeability [41], was studied in cultured human hepatocytes. Assessment of the inhibition of both CYP and UGT enzymes by imetelstat demonstrated that inhibition was weak and not of clinical significance [40]. In another study, transporter interactions were evaluated using a panel of nine uptake and efflux transporters (P-gp, OAT1, OAT3, OCT1, OCT2, OATP1B1, OATP1B3, BCRP, and BSEP) and the results showed that 20-ribose-modified PS-ASO was not a substrate nor an inhibitor of the transporter panel, indicating that interactions between ASOs and SMDs on the transporter level in the clinical setting are unlikely [42].

*In vitro* studies to assess the effects of cytokines and cytokine modulators on absorption, distribution, metabolism, and excretion (ADME) genes have been mainly conducted in primary cultured human hepatocytes (for reviews see Refs. [22, 43]). Although studies in hepatocytes have been instrumental in identifying the effect of these agents on CYP enzymes and transporters [18, 21, 44, 45], it has not been possible to extrapolate findings from *in vitro* to the clinic. Factors contributing to the difficulty to extrapolate data obtained in hepatocytes to *in vivo* are [16]: (i) the mechanisms contributing to downregulation of ADME genes are incompletely understood. Therefore, inclusion of positive controls representative for each pathway is not feasible; (ii) isolated hepatocytes are not representative for the disease state. This may be a reason why cytokine concentrations used *in vitro* typically are supraphysiological; and (iii) although studies in plated hepatocytes are employed routinely across the pharmaceutical industry and academia, there remains a substantial inter-lab variability [22]. This makes comparisons of data between labs difficult; (iv) in inflammatory disease states, the levels of more than one cytokine are increased. Currently, there is no experience in studying the interplay of multiple cytokines *in vitro*; and (v) the effect of cytokines can be indirect by the activation of

immune cells resident in the liver such as Stellate and Kupffer cells. Some progress regarding the latter point has been made by the establishment of a micropatterned hepatocyte-Kupffer cell coculture model supported by mouse fibroblasts [46]. Hepatocytes in this model are viable for multiple weeks and it could be demonstrated that more physiologically relevant cytokine concentrations could be used to elicit an effect on CYP and transporter expression. Overall, it was concluded that hepatocyte:Kupffer cell cocultures were a more robust *in vitro* system than hepatocytes alone. Coculture systems are a first step toward a more predictive *in vitro* model, but in their current form are still not representative for the complexity of the immune system and disease states.

### 3 TP-DDI observed in clinical studies

#### 3.1 Cytokine-dependent interactions

##### **3.1.1 Cytokines and therapeutic proteins targeting cytokines**

The dosing of cytokines in the clinic such as IFN $\alpha$ , INF $\alpha$ 2b, IL-2, IL-10, and IL-6 has been shown to decrease clearance of SMDs, as has been reviewed by Lee et al. [20]. Effects were typically in the range of 12%–81%. A specific example is a study in healthy subjects, which found that following dosing with PEG-IFN  $\alpha$ 2a, theophylline (CYP1A2 substrate) clearance was reduced by 20% with no effect on substrates of CYP2C9, CYP2C19, CYP2D6, or CYP3A4 [47].

Patients with diseases characterized by inflammation tend to show elevated pro-inflammatory cytokines such as TNF- $\alpha$ , IL1 $\beta$ , and IL-6, which can lead to reduced CYP and transporter expression and activity. Upon dosing with a mAb which targets a pro-inflammatory cytokine, the CYP expression is expected to be normalized and return to levels observed in healthy subjects as shown in Fig. 2 [43].

In rheumatoid arthritis (RA), where inflammation is characterized by elevated serum C-reactive protein (CRP) levels, the area under the curve (AUC) of simvastatin decreased by 43% and 54.7%, following treatment with the anti-IL-6R mAbs tocilizumab and sarilumab, respectively [48, 49]. Following treatment with an anti-IL-6 mAb (sirukumab) for 3 weeks, the probe substrates of midazolam (CYP3A4), omeprazole (CYP2C19), and S-warfarin (CYP2C9) showed AUC reductions of ~35%, ~41%, and ~18%, respectively [50] (Table 2). The decreased exposure of SMDs correlated with reduced CRP levels, following treatment to reduce inflammation. In the tocilizumab study, the mean CRP levels changed from 40 to 50 mg/L at baseline to 3 mg/L (close to upper limit of normal) from week 1 through week 4 following tocilizumab treatment. In the sarilumab study, the mean serum CRP levels were elevated at baseline (22.1 mg/L) and decreased to 5.9 mg/L on day 15. In the sirukumab study, mean CRP levels were 25.3 mg/L and decreased to 0.7 mg/L through 6 weeks after sirukumab administration.

The effects of cytokine modulation leading to changes in CYP enzyme levels were thought to potentially be a concern in other inflammatory diseases such as psoriasis [59]. Data are now available from dedicated TP-DDI studies in autoimmune diseases like psoriasis, atopic dermatitis, and multiple sclerosis. TP-DDI has been assessed between anti-cytokine mAbs (anti-IL-23: tildrakizumab, risankizumab, guselkumab) and anti-cytokine receptor mAbs (anti-IL4R: dupilumab; anti-IL-2R: daclizumab) and SM probe cocktails monitoring CYP1A1,

**TABLE 2** Clinical studies in which a therapeutic protein (TP) was tested for effects on small molecule drugs (SMDs).

TP	TP modality	Target	Population	SM	AUC <sub>inf</sub> geometric mean ratio <sup>a</sup> (90% CI)	Timepoint post-TP treatment	Reference
PEG-IFN $\alpha$ 2a	Small protein		Healthy subjects	Theophylline	1.24 (1.05–1.47)	22 days following 4 doses every 7 days	[47]
				Tolbutamide	No change <sup>1</sup>		
				Mephenytoin	No change <sup>1</sup>		
				Debrisoquine	No change <sup>1</sup>		
				Dapsone	No change <sup>1</sup>		
Tocilizumab	mAb	IL-6R	Rheumatoid arthritis	Simvastatin	0.43 (0.34–0.55) <sup>2</sup>	1 weeks	[48]
					0.61 (0.47–0.78) <sup>2</sup>	5 weeks	
Sarilumab	mAb	IL-6R	Rheumatoid arthritis	Simvastatin	0.547 (0.472–0.633)	7 days	[49]
Sirukumab	mAb	IL-6	Rheumatoid arthritis	Caffeine	1.34 (0.84–2.15)	3 weeks	[50]
				S-warfarin	0.82 (0.73–0.92)		
				Omeprazole	0.59 (0.34–1.02)		
				Midazolam	0.65 (0.47–0.89)		
Denosumab	mAb	RANKL	Osteoporosis	Midazolam	1.02 (0.96–1.09)	16 days	[51]
Dupilumab	mAb	IL-4 receptor $\alpha$	Atopic dermatitis	Caffeine	1.12 (0.87–1.45) <sup>2</sup>	36 days	[52]
				S-warfarin	0.90 (0.83–0.98) <sup>2</sup>		
				Omeprazole	1.00 (0.83–1.12) <sup>2</sup>		
				Metoprolol	1.29 (1.10–1.51) <sup>2</sup>		
				Midazolam	0.98 (0.87–1.09) <sup>2</sup>		
Daclizumab	mAb	IL-2R	Multiple sclerosis	Caffeine	1.03 (0.93–1.14) <sup>2</sup>	7 days after 3rd dose of TP Q4 weeks	[53]
				S-warfarin	1.00 (0.95–1.06)		
				Omeprazole	1.00 (0.88–1.13)		
				Dextromethorphan	1.01 (0.76–1.34) <sup>3</sup>		
				Midazolam	1.01 (0.89–1.15)		

Tildrakizumab	mAb	IL-23p19	Psoriasis	Caffeine	1.14 (1.01–1.28)	57 days	[54]
				S-warfarin	1.07 (0.98–1.17)		
				Omeprazole	0.96 (0.77–1.19)		
				Dextromethorphan	1.20 (1.00–1.45)		
				Midazolam	1.11 (0.94–1.32)		
Risankizumab	mAb	IL-23p19	Psoriasis	Caffeine	1.03 (0.90–1.19)	7 days after 4th dose of TP Q4 weeks	[55]
				S-warfarin	0.93 (0.90–0.97)		
				Omeprazole	0.94 (0.82–1.07)		
				Metoprolol	1.01 (0.92–1.10)		
				Midazolam	1.01 (0.94–1.09)		
Secukinumab	mAb	IL-17A	Psoriasis	Midazolam	0.97 (0.85–1.09)	7 days after 5th dose of TP Q1 weeks	[56]
Belatacept	CTLA-4-IgG1 Fc fusion	CD80 and CD86 on antigen-presenting cells	Prevention of transplant rejection	Caffeine	1.002 (0.914–1.098)	7 days	[57]
				Losartan	1.016 (0.938–1.101)		
				Omeprazole	1.227 (1.093–1.379)		
				Dextromethorphan	1.031 (0.885–1.200)		
				Midazolam	0.968 (0.892–1.049)		
Exenatide	GLP-1 peptide	GLP1-R	Healthy subjects	Acetaminophen	AUC (0–12 h) 0.77 Tmax sevenfold later	1 h	[58]

*Caffeine and theophylline are substrates of CYP1A2; losartan, tolbutamide, and S-warfarin are substrates of CYP2C9; omeprazole and mephenytoin are substrates of CYP2C19; dextromethorphan, metoprolol, and debrisoquine are substrates of CYP2D6; midazolam and dapson are substrates of CYP3A4, simvastatin and its active metabolite simvastatin acid are a substrate of CYP3A4 and OATP1B1.*

*1: mean effect ratio not calculated; 2: AUClast; 3: 12-h urine dextromethorphan to dextrophan ratio.*

CYP2C9, CYP2C19, CYP2D6, and CYP3A4; in summary, no reductions in SMD exposures were observed [52–55, 60] (Table 2). In addition, three programs looked at the effects on midazolam. The exposure of midazolam was unaffected by treatment with an anti-RANKL mAb, denosumab [51] or with an anti-IL-17A mAb [56], but was shown to increase by 24% in the presence of the anti-IL-17R mAb brodalumab for unexplained reasons [61].

These studies showing no effect on SMDs suggest that it is important to consider if treatment with a given TP induces notable changes in cytokine levels and if those changes affect the tissues, which express CYPs. If the cytokine effects are limited to the local tissues such as the skin, CNS, or intestine, there may be minimal to no effect on hepatic CYP expression. A study in ulcerative colitis patients which evaluated changes in intestinal CYP mRNA expression rather than CYP enzyme activity observed minimal change in expression following treatment with an anti- $\alpha_4\beta_7$  and  $\alpha_E\beta_7$  integrin heterodimer mAb, etrolizumab [62].

In the ulcerative colitis study [62], baseline mean IL-6 and CRP levels were higher than in healthy subjects (Table 3), but lower than has been observed in patients with RA (CRP 40–54 mg/L [48, 64] and IL-6 50–58 pg/mL [48, 64, 65]). For psoriasis, both the tildrakizumab and secukinumab TP-DDI trials showed single-digit baseline levels of CRP (mg/L) and IL-6 (pg/mL) (Table 3).

Taken together, these results suggest that in psoriasis or ulcerative colitis, where the baseline serum pro-inflammatory markers of CRP and IL-6 are lower than in RA, there may not be enough systemic inflammation in the disease state to reduce expression of CYP enzymes. Hence, when cytokine modulatory mAbs were used as treatment for local inflammation, such as in psoriasis, little to no TP-DDI effect was observed on the coadministered substrates of CYP enzymes [54, 56] (Table 2). Several authors have suggested that these pro-inflammatory molecules such as CRP or IL-6 may be potential biomarkers for those at risk for inflammation-related changes in CYP activity [16, 23, 59, 62, 70]; however, currently there are no cutoff concentrations defined, which would suggest a probable risk for TP-DDIs. Literature values for IL-6 in disease populations are known to be variable [71, 72]; therefore, it continues to be important to collect inflammation biomarker data in TP-DDI studies to build relationships between the baseline levels of inflammation and measurable treatment effects on CYP enzymes.

Another consideration in estimating the risk of a TP-DDI is whether the cells in which CYPs are expressed (e.g., hepatocytes) have receptors for the targeted cytokine. If hepatocytes

**TABLE 3** Baseline mean serum CRP and IL-6 concentrations in different disease populations.

Population	CRP (mg/L)	Reference for CRP	IL-6 (pg/mL)	Reference for IL-6
Healthy	<3.1 <sup>1</sup>	1: [56]	0.4–7.3 <sup>1</sup>	1: [62]
Ulcerative colitis	14–18 <sup>2</sup>	2: [63]	8–12 <sup>1</sup>	1: [62]
Psoriasis	4.36 <sup>3</sup> ; 8.56 <sup>4</sup> ; 3.2–5.2 <sup>4</sup>	3: [54], 4: [56]	2.6 <sup>3</sup> ; 2.5–3.3 <sup>4</sup>	3: [54], 4: [56]
Rheumatoid arthritis	40–50 <sup>5</sup> ; 54 <sup>6</sup> ; 25.3 <sup>7</sup>	5: [48], 6: [64], 7: [50]	50 <sup>5</sup> ; 58.4 <sup>6</sup> ; 3.5 <sup>7</sup> ; 52.7 <sup>8</sup>	5: [48], 6: [64], 7: [50], 8: [65]
Crohn's disease	53.9 <sup>9</sup> ; 10 <sup>10</sup>	9: median [66], 10: median [67]	6 <sup>11</sup> ; 7.7 <sup>12</sup>	11: median [68], 12: [69]

or immune cells in the liver (e.g., Kupffer and Stellate cells) do not express a receptor to interact with the targeted cytokine, they are not capable of showing a direct regulation of hepatic CYPs. This is the case for IL-23R [45, 46]. While indirect mechanisms of targeted cytokines affecting CYP gene expression are hypothetically possible, they are less plausible and have not been observed to have an effect for tildrakizumab [54] and guselkumab [60].

### 3.1.2 Immunomodulatory therapeutic proteins

In addition to cytokines which have been administered as therapeutic interventions and mAbs which neutralize cytokines, there are other TPs which modulate the immune system by affecting the regulatory steps involved in the recognition of antigen presenting cells by T cells. As some of these TPs can increase pro-inflammatory cytokine levels, they also have the potential for DDIs with SMDs through downregulation of CYP enzymes [70].

One such example is blinatumomab, which is an antibody fragment lacking an Fc domain and targeting both CD19 on tumor cells and CD3 on T cells. This class of molecules is referred to as bi-specific T-cell engagers (BiTEs). Blinatumomab was approved as a second-line treatment for Philadelphia chromosome-negative relapsed or refractory acute lymphoblastic leukemia. It causes transient increases in liver enzymes and high levels of inflammatory cytokines in the first week of treatment [73]. Blinatumomab step dosing was associated with lower levels of cytokine release and lower mean body temperature. Before blinatumomab infusion, all measured cytokines were below the LOD of 20 pg/mL. Within the first hours after infusion start in cycle 1, levels of IL-2, IL-6, IL-10, TNF- $\alpha$ , and IFN- $\gamma$ , but not IL-4, increased rapidly, reaching peak mean concentrations after 2 h (TNF- $\alpha$ ), 6 h (IL-2), or 24 h (IL-6, IL-10, and IFN- $\gamma$ ) before returning to baseline levels at the end of the first week of treatment. The concentration was at or higher than 1 ng/mL for IL-6, IL-10, and INF $\gamma$  for 3–4 days, which would be sufficient to suppress CYP3A4 activity completely in cultured human hepatocytes [22, 73].

In human hepatocytes, blinatumomab showed no effect on CYP activities, whereas a cytokine cocktail showed in vitro suppression of CYP3A4, CYP1A2, and CYP2C9 activities [74]. A physiologically based pharmacokinetic (PBPK) model was developed to predict the impact on CYPs. The predicted suppression of hepatic CYP activities was <30%, and IL-6-mediated changes in exposure to sensitive substrates of CYP3A4, CYP1A2, and CYP2C9 were less than twofold and lasted <1 week [74]. Although DDIs have not been specifically investigated, the blinatumomab package insert acknowledges the potential for DDIs with SMDs and states: “No formal drug interaction studies have been conducted with BLINCYTO. Initiation of BLINCYTO treatment causes transient release of cytokines that may suppress CYP450 enzymes. The highest drug-drug interaction risk is during the first 9 days of the first cycle and the first 2 days of the second cycle in patients who are receiving concomitant CYP450 substrates, particularly those with a narrow therapeutic index. In these patients, monitor for toxicity (e.g., warfarin) or drug concentrations (e.g., cyclosporine). Adjust the dose of the concomitant drug as needed” [75].

A second example of a TP which modulates the immune system is belatacept, which is designed to block T-cell activation. Belatacept is an immunosuppressive fusion protein containing the extracellular domain of human cytotoxic T lymphocyte antigen 4 (CTLA-4) and the constant-region fragment of IgG1. Belatacept is approved for the prevention of organ rejection in Epstein-Barr virus positive kidney transplant recipients. A probe cocktail TP-DDI study with belatacept showed no major alterations in the levels of several cytokines



(TNF $\alpha$ , IFN- $\gamma$ , IL-2, IL-6, IL-10, and IFN $\alpha$ ), and no clinically relevant PK effects on substrates of CYP1A2, CYP2C9, CYP2C19, CYP2D6, or CYP3A4 [57] (Table 2). Analysis of the effect of belatacept on TNF- $\alpha$ , INF- $\gamma$ , IL-2, IL-6, and IL-10 showed no change from baseline. Mean INF- $\alpha$  levels demonstrated a 15% decrease on day 4 that appeared to be driven by a small number of outlier values.

### 3.2 Immunogenicity-dependent interactions

Immunogenicity often leads to reduced TP exposure; hence, one mechanism by which a SMD can affect TP exposure is by reducing immunogenicity. This immunogenicity-dependent DDI is exemplified in the treatment of RA by anti-TNF $\alpha$  TPs and methotrexate (MTX; an immunosuppressant SMD). MTX is often used in the treatment of RA and several anti-TNF antibodies such as infliximab, adalimumab, and golimumab [76–78] have shown higher exposure in RA patients in the presence of MTX than in its absence (Table 4). The increased exposure of anti-TNF TPs in the presence of MTX has been attributed to immunosuppressing ability of MTX via reduction of ADA to the TPs. A competing hypothesis has been proposed in which MTX lowered the expression of Fc $\gamma$ R, which could potentially affect the PK of mAbs [83]. A recent publication suggests that the TP-DDI with MTX can mostly be attributed to reduced immunogenicity and immunogenicity-mediated clearance [80]. Cynomolgus monkeys were dosed with both golimumab and MTX at higher doses (1.1 mg/kg) than are typically used for autoimmune diseases. The MTX treatment led to a delay in both the incidence and time of onset of ADA to golimumab. There was no observed effect of MTX on golimumab PK prior to the onset of ADA and no effect on Fc $\gamma$ 1R expression. In addition, data from the GO-REVEAL trial in psoriatic arthritis patients [84] were included to show that MTX lowered the incidence of ADA, and subjects who did not receive MTX had on average a ~30% lower trough golimumab concentrations. Importantly, in the ADA

**TABLE 4** Clinical studies in which a therapeutic protein (TP) exposure was monitored for changes when a small molecule drug (SMD) was coadministered.

TP	TP modality	Target	SM	Population	Measure of difference	Reference
Infliximab	mAb	TNF $\alpha$	Methotrexate	Rheumatoid arthritis	30% Decreased clearance of TP in combo	[79]
Adalimumab	mAb	TNF $\alpha$	Methotrexate	Rheumatoid arthritis	1.8 Median trough TP combo/TP mono	[77]
Golimumab	mAb	TNF $\alpha$	Methotrexate	Rheumatoid arthritis	1.4 Trough TP combo/TP mono	[78]
Rituximab	mAb	CD20	Ibrutinib	CLL/SLL	2–3 Mean trough TP combo/TP mono	[81]
Olaratumab	mAb	PDGFR $\alpha$	Doxorubicin paclitaxel/ carboplatin	Soft tissue sarcoma	No difference in model derived CL or V1 between mono or combo therapy	[82]

CLL, chronic lymphocytic leukemia; SLL, small lymphocytic lymphoma; PDGFR $\alpha$ , platelet-derived growth factor receptor- $\alpha$ .

negative subjects, the mean trough concentrations were comparable with and without MTX treatment, suggesting that the presence of ADA resulted in lower trough concentrations and that the observed TP-DDI is primarily modulated through a reduction in immunogenicity.

### 3.3 Target-dependent interactions

The PK of TPs can be affected by high concentrations of their target ligand; hence, drugs which can change the target ligand concentration may also lead to TP-DDIs. One example is that the treatment with statins was associated with a ~20% reduction in the anti-PCSK9 mAb evolocumab  $C_{\max}$  and AUC as compared to without statins [85, 86]. A similar reduction in exposure was observed with another anti-PCSK9 mAb, alirocumab [87, 88]. The observation that this TP-DDI is target related is supported by studies, which have shown that statin treatment upregulates PCSK9 concentrations [89, 90], which then leads to reduction in anti-PCSK9 mAb exposure.

Another example of a target-mediated effect on PK was in a study with an anti-placental growth factor (PlGF) mAb (RO5323441) and an anti-vascular endothelial growth factor (VEGF) mAb bevacizumab in patients with glioblastoma [91]. Both PlGF and VEGF are soluble growth factors, which can bind to VEGF receptors (VEGFR) to stimulate angiogenesis. Monoclonal antibodies which bind these growth factors, therefore, inhibit angiogenesis. In early clinical studies, it was observed that the exposure of RO5323441, when administered in combination with bevacizumab, was ~50% higher relative to monotherapy, while the bevacizumab exposure was not affected (Table 5). The authors attribute this observation to a target-trapping mechanism through VEGFR-1. It is known that VEGF has a higher affinity for VEGFR-1 than does PlGF. In addition, the affinity of PlGF for VEGFR-1 is higher than for the mAb (RO5323441). The hypothesis for the TP-DDI is that in the absence of bevacizumab, endogenous VEGF would occupy VEGFR-1 and PlGF would be bound by RO5323441. In the presence of bevacizumab, VEGF would complex with bevacizumab and, therefore, VEGFR-1 would be available for binding by PlGF. In this situation, PlGF would be bound to the receptor (trapped) resulting in higher concentrations of unbound RO5323441, which would have reduced clearance compared to the PlGF-RO5323441 complex. Supporting this hypothesis is the observation of an inverse relationship of RO5323441 clearance with bevacizumab exposure [91].

**TABLE 5** Clinical studies in which a therapeutic protein (TP-1) was tested for effects on a second therapeutic protein (TP-2).

TP-1	TP-1 target	TP-2	TP-2 target	Population	AUC ratio TP-1 combo/ TP-1 mono (TP-1 dose)	Reference
MINT1526A	Integrin $\alpha 5 \beta 1$	Bevacizumab	VEGF	Solid tumors	1.26 (15 mg/kg)	[92]
RO5323441	PlGF	Bevacizumab	VEGF	Glioblastoma	~1.5 (625, 1250, 2500 mg)	[91]
MEDI3617	Angiopoietin-2	Bevacizumab	VEGF	Solid tumors	0.93 (1500 mg)	[93]

VEGF, vascular endothelial growth factor; PlGF, placental growth factor.

The combination of bendamustine with rituximab (BR) is indicated for lymphoma. In a clinical trial (HELIOS), BR plus ibrutinib, a Bruton's tyrosine kinase inhibitor (BR-I) was compared with BR plus placebo in subjects with previously treated relapsed/refractory chronic lymphocytic leukemia or small lymphocytic lymphoma. Lavezzi et al. (2019) [81] reported that systemic rituximab exposure was higher with BR-I vs BR; mean trough serum concentrations were two to threefold higher in the first three cycles and 1.2- to 1.7-fold higher subsequently (Table 4). The effect of ibrutinib on the PK of rituximab was attributed to the rapid target elimination (CD20 positive B cells), leading to decreased rituximab clearance [81].

Lastly, the Fc domain of mAbs interacts with the neonatal Fc receptor (FcRn). The FcRn is a critical determinant of IgG's homeostasis and FcRn-mediated recycling of IgG ensures a long half-life of IgG [94]. Treatments with mAbs that block the Fc-FcRn interaction are expected to increase the clearance of endogenous IgG and exogenously administered therapeutic antibodies. It was demonstrated that an experimental autoimmune myasthenia gravis model in rats can be effectively treated by FcRn blocking antibodies [95]. Currently, several anti-FcRn mAbs are in clinical development for the treatment of antibody-mediated autoimmune diseases. It has been shown that the reduction of endogenous IgG by FcRn blocking mAbs can be up to 80% of baseline levels [96, 97]. It is conceivable that therapeutic IgG antibodies coadministered with FcRn blocking agents could have greatly reduced half-life and exposure and therefore should be coadministered with caution.

### 3.4 Other interactions

#### 3.4.1 Interactions based on physiology

Several other TP-DDI interactions have been observed that are not easily categorized by the previously discussed mechanisms. One example includes the glucose-dependent insulintropic peptide (GLP-1) receptor antagonists such as exenatide and dulaglutide [98]. In the case of coadministration of exenatide with acetaminophen, the exposure of the latter decreased [58] (Table 2). This was thought to be due to delayed gastric emptying [99], resulting in slower absorption (delayed  $T_{\max}$  and reduced  $C_{\max}$ ).

An additional mechanism of interaction could be through the pharmacodynamic effects of angiogenesis inhibitors. Mouse studies have shown that the angiogenesis inhibitors bevacizumab and soranefib decreased the distribution of an anti-carcino embryonic antigen (CEA) mAb to the tumors of SCID mice bearing CEA-expressing tumors [100, 101]. In the same studies, no changes in the plasma PK of the anti-CEA mAb were noted when co-dosed with the angiogenesis inhibitors. The observation of no alterations in PK has been supported by clinical studies of bevacizumab dosed in combination with other mAbs such as MEDI3617 (an anti-angiopoietin-2 mAb) [93] or MINT1526A (an anti- $\alpha 5\beta 1$  integrin mAb) [92]. In these studies, the plasma PK of MEDI3617 or MINT1526A was not affected by co-treatment with bevacizumab; although, there was no investigation of drug levels in the tumors in humans (Table 5).

#### 3.4.2 Interactions based on binding to proteoglycans

One example of an interaction based on proteoglycan binding is that of palifermin, which is a 140 amino acid recombinant human keratinocyte growth factor. When palifermin was

administered with heparin, the mean AUC of palifermin was ~fivefold higher than without [102]. Several hypotheses for this observation have been described and may contribute. Heparin is known to protect growth factors from proteolysis [103], growth factors complexed with heparin are more slowly cleared than uncomplexed growth factors [104], and heparin can compete with growth factors for binding to cell surface proteoglycans and subsequent uptake and clearance [105].

### 3.4.3 Interactions of antibody-drug conjugates

Special consideration should be applied when studying antibody-drug conjugates (ADCs), as therapeutic modalities consisting of a mAb covalently bound to a SMD (usually a cytotoxic agent) through a chemical linker. ADCs are designed to selectively deliver a potent cytotoxic agent to tumor cells via tumor-specific or over-expressed cell surface antigens. After binding to the cell surface antigen, the ADC is internalized by tumor cells and undergoes lysosomal degradation, leading to the release of the cytotoxic agent. While the mAb exposure is not likely to be affected by coadministered SMDs, the ADC-released cytotoxic agents could be affected. Unconjugated cytotoxic agents formed via proteolytic degradation and/or deconjugation from ADC are expected to behave like SMDs that could be metabolized and excreted by CYPs and transporters. DDIs may still occur through modulation of important elimination pathways. In addition, ADCs are taken up preferentially by the liver, and as a result, interactions with phase 1 and 2 enzymes are possible [106, 107].

One example of an ADC program which investigated possible DDIs is brentuxumab vedotin, which is an ADC in which the antibody targets CD30 and the conjugate is monomethyl auristatin E (MMAE) [108]. For this drug, the ADC was not affected by either a CYP3A4 inhibitor or inducer. The PK of midazolam was also tested but found not to be affected by brentuximab vedotin. However, when the strong CYP3A4 inhibitor ketoconazole was coadministered, the MMAE component showed a 34% increase in AUC. Coadministration of the ADC with rifampin (a potent CYP3A4 inducer) reduced exposure to MMAE by approximately 46% [108]. In patients taking concomitant strong CYP3A4 inhibitors, close monitoring for adverse reactions is recommended due to the increased exposure of MMAE (brentuxumab vedotin label [108a]). These DDI results were also predicted by a PBPK model for brentuximab vedotin [109].

## 4 Potential DDI between emerging modalities

In this section, the major ADME properties of several new modalities and potential DDI with other modalities will be discussed.

### 4.1 Oligonucleotide and mRNA-based drugs

Several oligonucleotide-based drugs have been successfully developed and approved including fomivirsen for the treatment of CMV infections in 1998 (withdrawn in the EU in 2002 and the United States in 2006), pegaptanib for neovascular (wet) age-related macular degeneration in 2004, mipomersen for homozygous familial hypercholesterolemia in 2013,

nusinersen for spinal muscular atrophy in 2016, and eteplirsen for Duchenne muscular dystrophy in 2016. The first investigational mRNA-based therapy that encodes for VEGF-A (AZD8601) has successfully completed a phase I clinical trial [110].

Natural oligonucleotides have poor ADME properties, because they are highly water-soluble polyanionic macromolecules with poor plasma membrane permeability and are readily degraded by nucleases [111]. Following systemic administration, natural oligonucleotides are rapidly cleared from the blood by the kidney and scavenger receptors on the hepatocyte surface. Incorporation of phosphorothioate (PS) into oligonucleotides enhances plasma-protein binding and stability toward nucleases. They also show improved tissue uptake as well as increased affinity to complementary nucleic acids [111, 112]. Oligonucleotides are metabolized by nucleases. Parent drug and nuclease generated smaller oligonucleotide fragments are excreted via the urine.

Clinical studies conducted to investigate potential DDI between 20-ribose-modified PS-ASOs and common co-medications in the target populations have demonstrated no clinically relevant PK interactions [38, 113–118], consistent with the *in vitro* data (Section 2.2).

The innate immune system represents the first line of defense of a host cell to viral infections. It consists of intracellular and cell surface pattern recognition receptors (PRR) such as cytoplasmic retinoic acid-inducible gene I (RIG-I)-like receptors (RLRs) and DNA sensors, and membrane-bound toll-like receptors (TLRs) that recognize pathogen-specific structures called pathogen-associated molecular patterns (PAMPs) [119]. Stimulator of interferon genes (STING) is an important pathway that induces type I interferon production when cells are infected with intracellular pathogens. PAMP recognition by PRRs typically results in rapid induction of type I/III interferons (IFNs) and/or other inflammatory cytokines in the infected cell. Agonists of these PRR pathways are attractive therapeutic modalities to enhance the innate immune response for cancer treatment and are being developed as combination therapy with immune checkpoint inhibitors, which typically enhance the adaptive immune response [120–122]. The cGAS-STING pathway is a component of the innate immune system that functions to detect the presence of cytosolic DNA and, in response, triggers expression of inflammatory genes that can lead to senescence or to the activation of defense mechanisms [122].

The end result of the activation of the innate immune pathway is the release of inflammatory cytokines which, depending on circulating levels, could affect CYP activity. For comparison in RA patients, baseline mean serum CRP levels were in the range of 40–54 mg/L [48, 64] and baseline mean serum IL-6 levels were in the range of 50–58 pg/mL [48, 64, 65]. Although checkpoint inhibitors such as anti-PD1 mAbs have revolutionized the treatment of cancer, only about up to 30% of patients benefit. Expanding the efficacy of checkpoint inhibitors by converting “cold tumors” to “hot tumors” has become vigorously pursued by many pharmaceutical companies [123]. Innate immune modulators are the mainstream approach to perform the task of turning “cold” tumors to “hot” tumors. Because most of these innate modalities are being developed for combination therapies with chemotherapeutic or targeting agents, the potential for DDIs with coadministered drugs cannot be ignored.

The unmethylated CpG oligonucleotides found in bacterial and viral genomic DNAs are potent TLR9 receptor agonists, which activate the innate immune system. CpG oligonucleotides have been optimized as potent adjuvants for vaccine and anticancer therapeutics. HEPLISAV-B is a combination of the TLR9 agonist SD-101 (a CpG oligonucleotide) and hepatitis B surface antigen to elicit an efficient immune response after just two doses [8]. Recently,

SD-101 has been used in combination with a checkpoint inhibitor pembrolizumab to treat advanced solid tumors with a ~78% objective response rate in anti-PD1 naïve patients in a phase 1b trial [124]. SD-101 is a potent TLR agonist that can stimulate a strong IFN- $\alpha$  release from plasmacytoid dendritic cells when administered intratumorally [125, 127]. It is not clear whether the local injection elicits a systemic inflammatory cytokine release, however. Therefore, it is not clear whether TLR9 agonists could affect CYP activity.

## 4.2 Cell-based therapies

Immune cell therapies such as CAR-T cell therapy are emerging as a highly efficacious modality for some liquid tumors [128]. In CAR-T cell therapy, large numbers of T cells targeting tumor surface antigens with immune-stimulating coreceptors are directly infused to the patients, often causing inflammatory cytokine release, also known as cytokine release syndrome (CRS) [126, 128]. CRS is the major side effect of CAR-T therapy and can range in severity from low-grade symptoms to a high-grade syndrome associated with life-threatening multi-organ dysfunction. Patients at high risk of severe CRS include those with comorbidities, a high disease burden, and those who develop early onset CRS within 3 days of cell infusion. High serum levels of IL-6, soluble gp130, IFN $\gamma$ , IL-15, IL-8, and/or IL-10 either before or 1 day after CAR-T-cell infusion are associated with subsequent development of severe CRS [129, 130]. As experience with CAR-T therapy grows, CRS has become a manageable toxicity with the use of steroids and anti-IL-6 mAbs [3, 126, 128, 129, 131]. Tisagenlecleucel (a CAR-T cell therapy for the treatment of B-cell leukemia) induced CRS in 54 (79%) of the 68 pediatric and young adult patients with relapsed/refractory acute lymphocytic leukemia, and 78 (74%) of the 106 adult patients with relapsed/refractory diffuse large B-cell lymphoma receiving tisagenlecleucel [3]. The inflammatory cytokine levels can range from <100 pg/mL in low-grade CRS to over 1000 pg/mL in high-grade CRS [131]. Although the effect of CRS on the PK of SMDs has not been reported, such an effect cannot be excluded. Interestingly, the potential for DDIs related to CRS was not discussed in the label, potentially because the CRS is of short duration.

## 4.3 Oncolytic viruses

Oncolytic viruses (OVs) are replication competent viruses that selectively propagate in tumor cells and/or in the immunosuppressive tumor microenvironment [132, 133]. Introducing an OV causes cellular damage, eventually inducing pro-inflammatory danger-associated molecular pattern and PAMP responses, and promoting phagocytosis of dead or injured virus-infected tumor cells [134]. Thus, a virus infection in a tumor typically ends up breaking tolerance and eliciting innate and adaptive immune responses. Tumor lysis enables reprogramming of the tumor microenvironment during this destructive phase in such a way that it boosts systemic antitumor immunity, thereby providing an ideal accompaniment to immune checkpoint blockade [135, 136]. OV's potential for cancer therapy is exemplified by talimogene laherparepvec (T-VEC), which is a genetically modified herpes simplex virus type 1 designed to selectively replicate in tumors and produce granulocyte-macrophage colony-stimulating factor (GM-CSF) to enhance antigen release, presentation, and systemic



antitumor immune response [137]. The intratumoral injection of T-VEC into melanoma metastases improved the durable response rate compared with subcutaneous GM-CSF in patients with advanced melanoma [138] in phase III trials. The durable and overall response rate for T-VEC was 16% and 26%, respectively, leading to the FDA approval in 2015. When combined with pembrolizumab, the objective response rate and complete response rate increased to 62% and 33%, respectively [139].

OVs can be engineered to further increase their impact on tumor-immune system interactions [140]. For example, the GM-CSF cistron inserted into T-VEC (HSV) and JX594 (vaccinia) OVs drives the release of high concentrations of cytokines at sites of infection, which is considered beneficial for enhancement of dendritic cell recruitment, activation, and function. Since OVs are generally administered locally, the cytokines induced may be limited and, therefore, may not be high enough systemically to affect liver enzymes. However, this may change for OVs that are administered intravenously.

#### 4.4 Immunocytokines

Cytokines are immune regulatory proteins that can be categorized as pro-inflammatory/anti-inflammatory or T helper cell 1 and 2 (Th1/Th2) cytokines. Several cytokines such as IFN- $\alpha$ 2B and IL-2 have been approved for cancer indications. IFN- $\alpha$ 2B has been approved as adjuvant treatment of completely resected high-risk melanoma patients and several refractory malignancies; high-dose interleukin-2 is approved for the treatment of metastatic renal cell carcinoma and melanoma [141]. However, the systemic administration of these agents is often associated with dose-dependent side effects (e.g., hypotension, flu-like symptoms, nausea, and capillary leak), which prevents dose escalation to therapeutically active regimens. To overcome these drawbacks, immunocytokines have been developed which are antibody-cytokine fusion proteins with the potential to preferentially localize on tumor lesions and to activate anticancer immunity at the site of disease [142]. The antibody portion of the fusion protein can anchor cytokines to tumor-associated antigens to alleviate the systemic toxicity effects while enhancing the immune response in the local tumor environment. Several immunocytokines are in clinical development for the treatment of cancer. Two IL-2-based immunocytokines (L19-IL2 and F16-IL2), featuring antibody fragments in non-covalent diabody formats, have been tested in phase I and phase II clinical trials [142]. The L19 antibody is specific to the alternatively spliced extra domain-B of fibronectin, a marker of tumor angiogenesis, while F16 recognizes the A1 domain of tenascin-C. It should be recognized that although these molecules target tumors, they also distribute to the liver [143, 144], raising the possibility of affecting CYP enzyme levels.

## 5 Risk assessment and strategies to evaluate potential TP-DDI

### 5.1 Risk assessment

A risk assessment of the probability and impact of a potential TP-DDI is important to perform in the early stage of drug development, because it provides a framework to create a supportive DDI assessment strategy. Mechanism of action (MOA) and target biology should



be considered, which cytokines may be affected by treatment and what is the expected magnitude of the effect and, if any of the co-dosed drugs could affect the same target. For cytokine effects on CYP downregulation, it is worth establishing whether hepatocytes or Kupffer cells have receptors for the targeted cytokine. The lack of a receptor for the targeted cytokine suggests that changing cytokine levels are less likely to have a direct effect on hepatocytes or Kupffer cells. Interrelated with MOA is the context of the target population and disease severity. For some indications such as psoriasis or RA, there may be existing TP-DDI data for use in estimating the likelihood of an effect in these populations. In estimating the impact of a potential TP-DDI, it is important to consider what medications will be co-dosed in patients. Drugs which have a narrow therapeutic window for safety or efficacy, that also are CYP or transporter substrates, have the highest potential to be impacted from a TP-DDI perspective.

Three drug development scenarios were described in the 2012 FDA draft DDI guidance in which an in vivo assessment of DDI should be performed:

- when an investigational TP is a cytokine or cytokine modulator,
- when a TP will be used in combination with other drug products, and
- when there are known mechanisms or prior experience for a DDI, which are based on mechanisms other than CYP or transporter modulation.

More recently, a regulatory perspective article on TP-DDI was published acknowledging the challenges in this field [145]. The article recommends that during TP-DDI risk assessment, at least the following should be considered and are shown graphically in Fig. 3:

- hypothesized mechanism for the interaction,
- disease type and severity (if mechanism is related to disease condition),
- biologic product type, and
- clearance pathways.

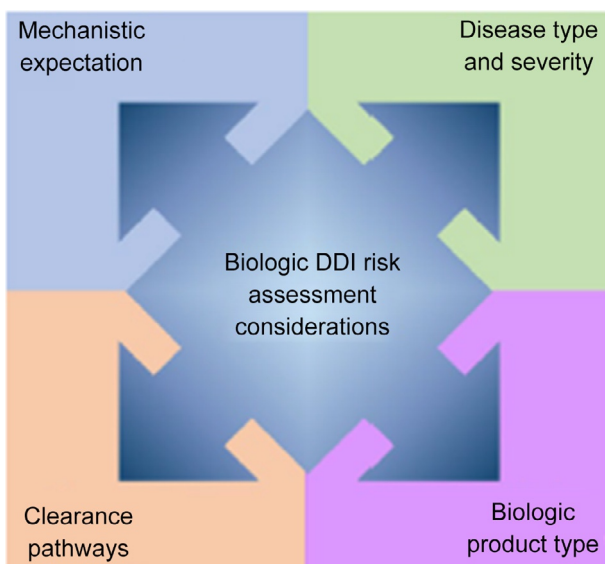


**FIG. 3** Considerations for TP-DDI risk assessment. Drug-drug interaction (DDI) risk assessment considerations for a biologic product. The interplay between the hypothesized mechanism for the interaction, disease and its severity, biologic product type, and clearance pathways, together, inform the potential risk for a DDI with a biologic product. For example, understanding if the biologic is a cytokine or cytokine modulator will inform the mechanism of the potential interaction and may guide which population to consider in an evaluation, if one is needed. Reprinted with permission from S.J. Schrieber, E. Pfuma-Fletcher, X. Wang, Y.C. Wang, S. Sagoo, R. Madabushi, et al., *Considerations for biologic product drug-drug interactions: a regulatory perspective*, *Clin Pharmacol Ther* 105 (2019) 1332–1334.

Thus, the timing and the rigor of a DDI study can be tailored depending on the risk and the development plan. If a risk is identified, it follows that the TP-DDI should be evaluated before the product is administered to patients who are likely to take concomitant medications that could interact with the investigational drug [146].

## 5.2 Exploratory studies to assess TP-DDI risk

Exploratory studies are generally conducted in patients during phase 1 or 2, as an arm of a larger study. In oncology, this has been done as a separate arm in which the objective is to monitor the PK of the TP in combination therapy compared to monotherapy; examples of MEDI3617 or MINT1526A are discussed in Section 3.4.1. If a potentially meaningful change in TP exposure is observed, a more definitive DDI study may be needed to fully characterize the effect. It is also common to use a population PK model in late development, to rule out potential effects of SMDs on TP exposure, an example of which is for an antiplatelet-derived growth factor receptor- $\alpha$  (PDGFR $\alpha$ ) mAb, olaratumab, in an oncology setting in combination with chemotherapy [82].

## 5.3 Dedicated TP-DDI studies

A dedicated study requires robust PK sampling, and patient time in a phase 1 clinic. Studies are designed to be either estimation or hypothesis driven in nature. In an estimation study, the sample size is smaller and depending on intersubject variability, may not be powered to test a hypothesis, yet it still provides a measure of the magnitude of the TP-DDI. Alternatively, a hypothesis-driven study is powered to test a predefined no-effect boundary, such as 80%–125%, based on known intersubject variability. The disadvantage of a hypothesis-driven study is that it may be more challenging to enroll enough patients to be well powered and is less flexible. If the risk is considered high, it makes sense to assess the TP-DDI prior to expanding to a larger population. If the risk is lower, one approach is to use a dedicated study to rule out the possibility of a TP-DDI, for inclusion in the filing package.

## 5.4 Design of studies

If the TP has a long half-life, it is not practical to test for a TP-DDI effect in a crossover manner. Often each side of a potential interaction (effects of TP on SMD vs effects of SMD on TP) is tested separately. Approaches to testing effects of TP on SMDs include individual studies with the TP and the specific SMDs that are commonly used in the target population or with an SMD that is part of a combination therapy, as in oncology. For TPs with long half-lives, single-sequence studies in the same subjects (SMD followed by TP+SMD) or parallel studies (SMD vs SMD+TP) are often performed. When pro-inflammatory cytokine-related downregulation of CYP enzymes is suspected and there is a concern regarding SMD metabolism via the CYP pathways, cocktail studies can be performed to investigate TP effects on SMD probe substrates.

To investigate effects of a SMD on the PK of a TP, a population PK analysis is generally used. The use of population PK modeling as applied to TP-DDIs is discussed in a white paper from the Population PK TP-DDI Working Group [147].

## 5.5 Specific study considerations

DDI studies with TPs are generally performed in patients as opposed to healthy subjects, because many of the effects are related to changes in cytokine levels or target levels, which only occur in patients. Not enough is yet known to extrapolate from studies in healthy subjects to patients. In terms of study specifics, it is sensible to use the same route of administration of that is planned for routine clinical use of the drug. Furthermore, the highest dose expected to be used in clinical practice is generally tested to evaluate the largest possible effects. For TP treatment effects on inflammation, the TP should be dosed to a high enough exposure for a long enough time period such that inflammation (as measured by effect on disease state) is reduced in the patients, prior to dosing the SMD or probe cocktail. The rationale for choosing the time point of maximum inflammation suppression is that cytokine effects on CYP enzyme expression would be minimal and would be expected to show the maximal change compared to the baseline disease state. If the disease affects systemic inflammation, biomarkers such as IL-6 or CRP could be used to choose a treatment time point to assess the SMD exposure. If the disease shows only local inflammation effects, an appropriate measure of efficacy could be used to choose the TP treatment time point to assess SMD exposure. For cocktail studies, genotyping is recommended, particularly for CYPs with high genetic variability. Individuals who have genotypic data that precludes functional CYP enzymatic activity would typically be excluded from the DDI analysis. As the number of patients in a DDI study is generally small, poor metabolizers in a small data set can have large effects on the overall analysis.

## 6 Conclusion and future perspectives

In the past decades, the use of biologics, especially mAbs, has experienced an exponential growth and the combination with small molecules has been on the rise as well. As a result, insights into the potential DDIs between biologics and SMDs have increased. Based on the available data, it can be concluded that the SMD as a victim is generally explained by modulation of CYP enzymes, either by disease states such as infection and inflammation or by drug treatment of the disease state. TP-DDIs with mAbs as victims in several cases are likely caused by increased immunogenicity or mAb target modulation through an SMD or another TP (Fig. 4). In most situations, the resulting DDIs are relatively small and do not require dose adjustment. In support of this statement, several dedicated TP-DDI studies with immunomodulators have been conducted and no clinically meaningful DDIs were identified (Table 2) which required dose adjustment.

Although the mechanistic understanding of DDIs including biologics has increased, prospective quantitative predictions still need experimental investigation and verification. Unlike for SMDs, this is mostly due to the absence of predictive *in vitro* assay systems representative of the disease state, a limited understanding of disease biology or the mechanism of action of the TP. The latter makes the generation and application of PBPK models challenging. In several cases discussed in this chapter, particularly in advanced cancer therapies, modulation of cytokine levels may be only transient or in the local tumor environment. It is unknown whether coadministration of other drugs with these therapies could result in a DDI, and this could benefit from more investigation. In cases where clinical DDI evaluations

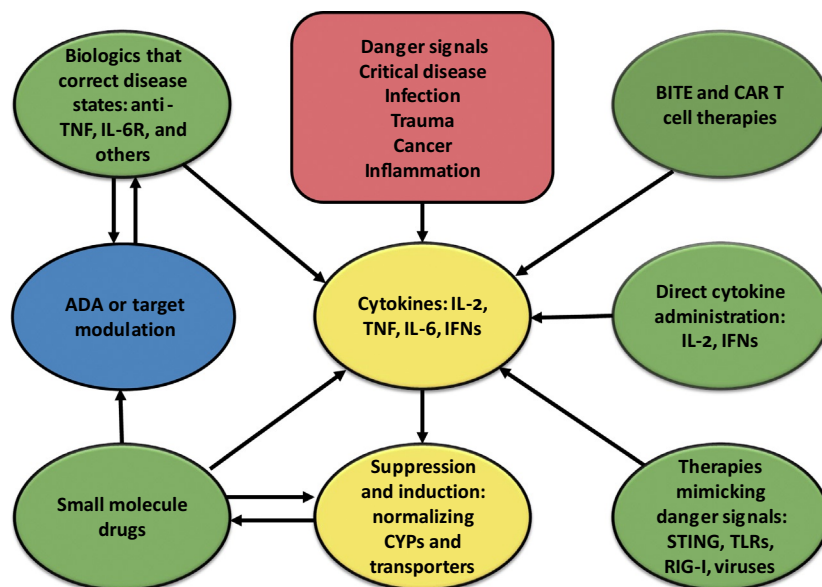


FIG. 4 DDI potential for different therapeutic modalities. DDI potential and pathways of different modalities. Green ovals represent different modalities. For a DDI impact on SMDs, most if not all are mediated by inflammatory cytokines that modulate the activities of CYP enzymes or drug transporters. For a DDI impact on TP, most are through immunogenicity or target modulation.

are needed, the application of drug cocktails particularly at microdose levels may be a practical approach [148].

As more and more emerging therapeutic modalities are used in clinical practice (Fig. 4) especially those that can cause significant release of inflammatory cytokines such as immune-stimulating protein therapeutic and CAR-T cell therapy, it is possible that some may have an impact on the metabolism of SMD and other modalities. Continued efforts are needed to understand to what extent DDIs will be an issue of clinical significance. Because the underlying cause of DDIs in most cases will be related to the disease state, clinical trials to assess DDI risk will need to be conducted in patients. Conduct of such trials in many cases may not be feasible, because of the impact on patients and the long half-life of biologics. Properly designed population PK strategies, therefore, should be leveraged to assess the risk for such interactions [147].

## References

- [1] L. Urquhart, Top drugs and companies by sales in 2018, *Nat. Rev. Drug Discov.* 18 (2019) 245.
- [2] Kite Pharma Inc, YESCARTA™ (Axicabtagene Ciloleucel) Suspension for Intravenous Infusion, <https://www.fda.gov/files/vaccines%2C%20blood%20%26%20biologics/published/Package-Insert—YESCARTA.pdf>, 2017.
- [3] Novartis, KYMRIAH™ (Tisagenlecleucel) Suspension for Intravenous Infusion, 2017.
- [4] Spark Therapeutics Inc, LUXTURN A (Voretigene Neparvovec-Rzyl) Intraocular Suspension for Subretinal Injection, 2017.

- [5] Biogen, SPINRAZA (Nusinersen) Injection, for Intrathecal Use, 2016.
- [6] AveXis Inc, ZOLGENSMA<sup>®</sup> (Onasemnogene Abeparvovec-Xioi) Suspension for Intravenous Infusion, (2019).
- [7] Alnylam Pharmaceuticals Inc, ONPATTRO (Patisiran) Lipid Complex Injection, for Intravenous Use, (2018).
- [8] Dynavax Technologies Corp, HEPLISAV-B [Hepatitis B Vaccine (Recombinant), Adjuvanted] Solution for Intramuscular Injection, 2017.
- [9] BioVex Inc. A Subsidiary of Amgen Inc, IMLYGIC (Talimogene Laherparepvec) Suspension for Intralesional Injection, 2015.
- [10] Moderna, Moderna Announces Dosing of the First Monoclonal Antibody Encoded by mRNA in a Clinical Trial, <https://investors.modernatx.com/news-releases/news-release-details/moderna-announces-dosing-first-monoclonal-antibody-encoded-mrna>, 2019.
- [11] E. Smith, G. Chan, K. Palczewski, K. Lewis, J. Ho, Luxturna: the latest development in gene therapy. Illustrated by L. Nguyen. *Rare Dis. Rev.* (2018), <https://doi.org/10.13140/RG.2.2.32120.49924>.
- [12] K.C. Chang, T.D. Bell, B.A. Lauer, H. Chai, Altered theophylline pharmacokinetics during acute respiratory viral illness, *Lancet* 1 (8074) (1978) 1132–1133.
- [13] M.J. Kraemer, C.T. Furukawa, J.R. Koup, G.G. Shapiro, W.E. Pierson, C.W. Bierman, Altered theophylline clearance during an influenza B outbreak, *Pediatrics* 69 (4) (1982) 476–480.
- [14] S.J. Williams, J.A. Baird-Lambert, G.C. Farrell, Inhibition of theophylline metabolism by interferon, *Lancet* 2 (8565) (1987) 939–941.
- [15] Y.L. Chen, V. Le Vraux, A. Leneuve, F. Dreyfus, A. Stheneur, I. Florentin, M. De Sousa, J.P. Giroud, B. Flouvat, L. Chauvelot-Moachon, Acute-phase response, interleukin-6, and alteration of cyclosporine pharmacokinetics, *Clin. Pharmacol. Ther.* 55 (6) (1994) 649–660.
- [16] J.R. Kenny, M.M. Liu, A.T. Chow, J.C. Earp, R. Evers, J.G. Slatter, D.D. Wang, L. Zhang, H. Zhou, Therapeutic protein drug-drug interactions: navigating the knowledge gaps-highlights from the 2012 AAPS NBC roundtable and IQ consortium/FDA workshop, *AAPS J.* 15 (4) (2013) 933–940.
- [17] A.E. Aitken, T.A. Richardson, E.T. Morgan, Regulation of drug-metabolizing enzymes and transporters in inflammation, *Annu. Rev. Pharmacol. Toxicol.* 46 (2006) 123–149.
- [18] M. Le Vee, V. Lecureur, B. Stieger, O. Fardel, Regulation of drug transporter expression in human hepatocytes exposed to the proinflammatory cytokines tumor necrosis factor-alpha or interleukin-6, *Drug Metab. Dispos.* 37 (3) (2009) 685–693.
- [19] S.M. Huang, H. Zhao, J.I. Lee, K. Reynolds, L. Zhang, R. Temple, L.J. Lesko, Therapeutic protein-drug interactions and implications for drug development, *Clin. Pharmacol. Ther.* 87 (4) (2010) 497–503.
- [20] J.I. Lee, L. Zhang, A.Y. Men, L.A. Kenna, S.M. Huang, CYP-mediated therapeutic protein-drug interactions: clinical findings, proposed mechanisms and regulatory implications, *Clin. Pharmacokinet.* 49 (5) (2010) 295–310.
- [21] L.J. Dickmann, S.K. Patel, L.C. Wienkers, J.G. Slatter, Effects of interleukin 1beta (IL-1beta) and IL-1beta/interleukin 6 (IL-6) combinations on drug metabolizing enzymes in human hepatocyte culture, *Curr. Drug Metab.* 13 (7) (2012) 930–937.
- [22] R. Evers, S. Dallas, L.J. Dickmann, O.A. Fahmi, J.R. Kenny, E. Kravynov, T. Nguyen, A.H. Patel, J.G. Slatter, L. Zhang, Critical review of preclinical approaches to investigate cytochrome p450-mediated therapeutic protein drug-drug interactions and recommendations for best practices: a white paper, *Drug Metab. Dispos.* 41 (9) (2013) 1598–1609.
- [23] J.G. Slatter, L.C. Wienkers, L.J. Dickmann, Drug interactions of cytokines and anticytokine therapeutic proteins, in: H. Zhou, B. Meibohm (Eds.), *Drug-Drug Interactions for Therapeutic Biologics*, John Wiley & Sons, Inc., New Jersey, 2013 (Chapter 13).
- [24] E.T. Morgan, T. Li-Masters, P.Y. Cheng, Mechanisms of cytochrome P450 regulation by inflammatory mediators, *Toxicology* 181-182 (2002) 207–210.
- [25] R. Jover, M. Moya, M.J. Gomez-Lechon, Transcriptional regulation of cytochrome p450 genes by the nuclear receptor hepatocyte nuclear factor 4-alpha, *Curr. Drug Metab.* 10 (5) (2009) 508–519.
- [26] B.N. Zordoky, A.O. El-Kadi, Role of NF-kappaB in the regulation of cytochrome P450 enzymes, *Curr. Drug Metab.* 10 (2) (2009) 164–178.
- [27] T. Nguyen, N. Kishnani, R. Evers, Utility of in vitro methods in drug-drug interaction assessment and prediction for therapeutic biologics, in: H. Zhou, B. Meibohm (Eds.), *Drug Interactions of Therapeutic Proteins*, Wiley, New York, 2013.

- [28] X. Gu, S. Ke, D. Liu, T. Sheng, P.E. Thomas, A.B. Rabson, M.A. Gallo, W. Xie, Y. Tian, Role of NF-kappaB in regulation of PXR-mediated gene expression: a mechanism for the suppression of cytochrome P-450 3A4 by proinflammatory agents, *J. Biol. Chem.* 281 (26) (2006) 17882–17889.
- [29] E. Assenat, S. Gerbal-Chaloin, D. Larrey, J. Saric, J.M. Fabre, P. Maurel, M.J. Vilarem, J.M. Pascussi, Interleukin 1beta inhibits CAR-induced expression of hepatic genes involved in drug and bilirubin clearance, *Hepatology* 40 (4) (2004) 951–960.
- [30] R. Ghose, T.L. Zimmerman, S. Thevananther, S.J. Karpen, Endotoxin leads to rapid subcellular re-localization of hepatic RXRalpha: a novel mechanism for reduced hepatic gene expression in inflammation, *Nucl. Recept.* 2 (1) (2004) 4.
- [31] C.M. Lee, B.S. Lee, S.L. Arnold, N. Isoherranen, E.T. Morgan, Nitric oxide and interleukin-1beta stimulate the proteasome-independent degradation of the retinoic acid hydroxylase CYP2C22 in primary rat hepatocytes, *J. Pharmacol. Exp. Ther.* 348 (1) (2014) 141–152.
- [32] T.J. Carlson, R.E. Billings, Role of nitric oxide in the cytokine-mediated regulation of cytochrome P-450, *Mol. Pharmacol.* 49 (5) (1996) 796–801.
- [33] C.M. Lee, S. Tripathi, E.T. Morgan, Nitric oxide-regulated proteolysis of human CYP2B6 via the ubiquitin-proteasome system, *Free Radic. Biol. Med.* 108 (2017) 478–486.
- [34] A.E. Aitken, E.T. Morgan, Gene-specific effects of inflammatory cytokines on cytochrome P450 2C, 2B6 and 3A4 mRNA levels in human hepatocytes, *Drug Metab. Dispos.* 35 (9) (2007) 1687–1693.
- [35] F. Kazmi, P. Yerino, C. McCoy, A. Parkinson, D.B. Buckley, B.W. Ogilvie, An assessment of the in vitro inhibition of cytochrome P450 enzymes, UDP-glucuronosyltransferases, and transporters by phosphodiester- or phosphorothioate-linked oligonucleotides, *Drug Metab. Dispos.* 46 (8) (2018) 1066–1074.
- [36] D. Buckley, K. Faraz, P. Yerino, B. Ogilvie, A. Parkinson, Inhibition of cytochrome P450 enzymes (CYP), CYP1A2 and CYP2C8, by oligonucleotides in human liver microsomes (HLM): a system-dependent outcome, *Drug Metab. Rev.* 41 (Suppl. 3) (2009) 94–95.
- [37] C.S. Shemesh, R.Z. Yu, M.S. Warren, M. Liu, M. Jahic, B. Nichols, N. Post, S. Lin, D.A. Norris, E. Hurl, J. Huang, T. Watanabe, S.P. Henry, Y. Wang, Assessment of the drug interaction potential of unconjugated and GalNAc3-conjugated 2'-MOE-ASOs, *Mol. Ther.–Nucleic Acids* 9 (2017) 34–47.
- [38] R.Z. Yu, R.S. Geary, J.D. Flaim, G.C. Riley, D.L. Tribble, A.A. van Vliet, M.K. Wedel, Lack of pharmacokinetic interaction of mipomersen sodium (ISIS 301012), a 2'-O-methoxyethyl modified antisense oligonucleotide targeting apolipoprotein B-100 messenger RNA, with simvastatin and ezetimibe, *Clin. Pharmacokinet.* 48 (1) (2009) 39–50.
- [39] P. Sazani, T. Magee, J.S. Charleston, C. Shanks, J. Zhang, M. Carver, J. Saoud, E. Kaye, In vitro pharmacokinetic evaluation of eteplirsen, SRP-4045, and SRP-4053; three phosphorodiamidate morpholino oligomers (PMO) for the treatment of patients with Duchenne muscular dystrophy (DMD) (P5.061), *Neurology* 84 (2015).
- [40] F. Kazmi, C. Sensenhauser, T. Greway, Characterization of the in vitro inhibitory potential of the oligonucleotide Imetelstat on human cytochrome P450 enzymes with predictions of in vivo drug-drug interactions, *Drug Metab. Dispos.* 47 (1) (2019) 9–14.
- [41] B.S. Herbert, G.C. Gellert, A. Hochreiter, K. Pongracz, W.E. Wright, D. Zielinska, A.C. Chin, C.B. Harley, J. W. Shay, S.M. Gryaznov, Lipid modification of GRN163, an N3'→P5' thio-phosphoramidate oligonucleotide, enhances the potency of telomerase inhibition, *Oncogene* 24 (33) (2005) 5262–5268.
- [42] R.Z. Yu, M.S. Warren, T. Watanabe, B. Nichols, M. Jahic, J. Huang, J. Burkey, R.S. Geary, S.P. Henry, Y. Wang, Lack of interactions between an antisense oligonucleotide with 2'-O-(2-methoxyethyl) modifications and major drug transporters, *Nucleic Acid Ther.* 26 (2) (2016) 111–117.
- [43] E.T. Morgan, Impact of infectious and inflammatory disease on cytochrome P450-mediated drug metabolism and pharmacokinetics, *Clin. Pharmacol. Ther.* 85 (4) (2009) 434–438.
- [44] L.J. Dickmann, S.K. Patel, D.A. Rock, L.C. Wienkers, J.G. Slatter, Effects of interleukin-6 (IL-6) and an anti-IL-6 monoclonal antibody on drug-metabolizing enzymes in human hepatocyte culture, *Drug Metab. Dispos.* 39 (8) (2011) 1415–1422.
- [45] S. Dallas, S. Chattopadhyay, C. Sensenhauser, A. Batheja, M. Singer, J. Silva, Interleukins-12 and -23 do not alter expression or activity of multiple cytochrome P450 enzymes in cryopreserved human hepatocytes, *Drug Metab. Dispos.* 41 (4) (2013) 689–693.
- [46] T.V. Nguyen, O. Ukairo, S.R. Khetani, M. McVay, C. Kanchagar, W. Seghezzi, G. Ayanoglu, O. Irrechukwu, R. Evers, Establishment of a hepatocyte-kupffer cell coculture model for assessment of proinflammatory cytokine effects on metabolizing enzymes and drug transporters, *Drug Metab. Dispos.* 43 (5) (2015) 774–785.



- [47] B.J. Brennan, Z.X. Xu, J.F. Grippo, Effect of peginterferon alfa-2a (40KD) on cytochrome P450 isoenzyme activity, *Br. J. Clin. Pharmacol.* 75 (2) (2013) 497–506.
- [48] C. Schmitt, B. Kuhn, X. Zhang, A.J. Kivitz, S. Grange, Disease-drug-drug interaction involving tocilizumab and simvastatin in patients with rheumatoid arthritis, *Clin. Pharmacol. Ther.* 89 (5) (2011) 735–740.
- [49] E.B. Lee, N. Daskalakis, C. Xu, A. Paccaly, B. Miller, R. Fleischmann, I. Bodrug, A. Kivitz, Disease-drug interaction of Sarilumab and Simvastatin in patients with rheumatoid arthritis, *Clin. Pharmacokinet.* 56 (6) (2017) 607–615.
- [50] Y. Zhuang, D.E. de Vries, Z. Xu, S.J. Marciniak Jr., D. Chen, F. Leon, H.M. Davis, H. Zhou, Evaluation of disease-mediated therapeutic protein-drug interactions between an anti-interleukin-6 monoclonal antibody (sirukumab) and cytochrome P450 activities in a phase 1 study in patients with rheumatoid arthritis using a cocktail approach, *J. Clin. Pharmacol.* 55 (12) (2015) 1386–1394.
- [51] G. Jang, A. Kaufman, E. Lee, L. Hamilton, S. Hutton, O. Egbuna, D. Padhi, A clinical therapeutic protein drug-drug interaction study: coadministration of denosumab and midazolam in postmenopausal women with osteoporosis, *Pharmacol. Res. Perspect.* 2 (2) (2014), e00033.
- [52] J.D. Davis, A. Bansal, D. Hassman, B. Akinlade, M. Li, Z. Li, B. Swanson, J.D. Hamilton, A.T. DiCioccio, Evaluation of potential disease-mediated drug-drug interaction in patients with moderate-to-severe atopic dermatitis receiving Dupilumab, *Clin. Pharmacol. Ther.* 104 (6) (2018) 1146–1154.
- [53] J.Q. Tran, A.A. Othman, P. Wolstencroft, J. Elkens, Therapeutic protein-drug interaction assessment for daclizumab high-yield process in patients with multiple sclerosis using a cocktail approach, *Br. J. Clin. Pharmacol.* 82 (1) (2016) 160–167.
- [54] S. Khalilieh, A. Hussain, D. Montgomery, V. Levine, P.M. Shaw, I. Bodrug, L. Mekokishvili, C. Bailey-Smith, X. S. Glasgow, A. Cheng, M. Martinho, M. Iwamoto, Effect of tildrakizumab (MK-3222), a high affinity, selective anti-IL23p19 monoclonal antibody, on cytochrome P450 metabolism in subjects with moderate to severe psoriasis, *Br. J. Clin. Pharmacol.* 84 (10) (2018) 2292–2302.
- [55] A. Khatri, L. Cheng, A. Camez, S. Ignatenko, Y. Pang, A.A. Othman, Lack of effect of 12-week treatment with Risankizumab on the pharmacokinetics of cytochrome P450 probe substrates in patients with moderate to severe chronic plaque psoriasis, *Clin. Pharmacokinet.* 58 (6) (2019) 805–814.
- [56] G. Bruin, A. Hasselberg, I. Koroleva, J. Milojevic, C. Calonder, R. Soon, R. Woessner, D.M. Pariser, B. Boutouyrie-Dumont, Secukinumab treatment does not alter the pharmacokinetics of the CYP3A4 substrate midazolam in patients with moderate to severe psoriasis, *Clin. Pharmacol. Ther.* 106 (6) (2019).
- [57] D. Williams, X. Tao, L. Zhu, M. Stonier, J.D. Lutz, E. Masson, S. Zhang, B. Ganguly, Z. Tzogas, S. Lubin, B. Murthy, Use of a cocktail probe to assess potential drug interactions with cytochrome P450 after administration of belatacept, a costimulatory immunomodulator, *Br. J. Clin. Pharmacol.* 83 (2) (2017) 370–380.
- [58] E. Blase, K. Taylor, H.Y. Gao, M. Wintle, M. Fineman, Pharmacokinetics of an oral drug (acetaminophen) administered at various times in relation to subcutaneous injection of exenatide (exendin-4) in healthy subjects, *J. Clin. Pharmacol.* 45 (5) (2005) 570–577.
- [59] J. Wang, Y.M. Wang, H.Y. Ahn, Biological products for the treatment of psoriasis: therapeutic targets, pharmacodynamics and disease-drug-drug interaction implications, *AAPS J.* 16 (5) (2014) 938–947.
- [60] Janssen Biotech Inc, TREMFYA (guselkumab) Injection, for Subcutaneous Use, 2017.
- [61] Valeant Pharmaceuticals International, SILIQ™ (Brodalumab) Injection, for Subcutaneous Use, 2017.
- [62] X. Wei, J.R. Kenny, L. Dickmann, R. Maciua, C. Looney, M.T. Tang, Assessment of disease-related therapeutic protein drug-drug interaction for Etrolizumab in patients with moderately to severely active ulcerative colitis, *J. Clin. Pharmacol.* 56 (6) (2016) 693–704.
- [63] S. Vermeire, S. O'Byrne, M. Keir, M. Williams, T.T. Lu, J.C. Mansfield, C.A. Lamb, B.G. Feagan, J. Panes, A. Salas, D.C. Baumgart, S. Schreiber, I. Dotan, W.J. Sandborn, G.W. Tew, D. Luca, M.T. Tang, L. Diehl, J. Eastham-Anderson, G. De Hertogh, C. Perrier, J.G. Egen, J.A. Kirby, G. van Assche, P. Rutgeerts, Etrolizumab as induction therapy for ulcerative colitis: a randomised, controlled, phase 2 trial, *Lancet* 384 (9940) (2014) 309–318.
- [64] N. Nishimoto, K. Terao, T. Mima, H. Nakahara, N. Takagi, T. Takeuchi, Mechanisms and pathologic significances in increase in serum interleukin-6 (IL-6) and soluble IL-6 receptor after administration of an anti-IL-6 receptor antibody, tocilizumab, in patients with rheumatoid arthritis and Castleman disease, *Blood* 112 (10) (2008) 3959–3964.
- [65] T. Robak, A. Gladalska, H. Stepień, E. Robak, Serum levels of interleukin-6 type cytokines and soluble interleukin-6 receptor in patients with rheumatoid arthritis, *Mediat. Inflamm.* 7 (5) (1998) 347–353.



- [66] S. Karoui, S. Ouerdiane, M. Serghini, T. Jomni, L. Kallel, M. Fekih, J. Boubaker, A. Filali, Correlation between levels of C-reactive protein and clinical activity in Crohn's disease, *Dig. Liver Dis.* 39 (11) (2007) 1006–1010.
- [67] J. Tibble, K. Teahon, B. Thjodleifsson, A. Roseth, G. Sigthorsson, S. Bridger, R. Foster, R. Sherwood, M. Fagerhol, I. Bjarnason, A simple method for assessing intestinal inflammation in Crohn's disease, *Gut* 47 (4) (2000) 506–513.
- [68] W. Reinisch, C. Gasche, W. Tillinger, J. Wyatt, C. Lichtenberger, M. Willheim, C. Dejaco, T. Waldhor, S. Bakos, H. Vogelsang, A. Gangl, H. Lochs, Clinical relevance of serum interleukin-6 in Crohn's disease: Single point measurements, therapy monitoring, and prediction of clinical relapse, *Am. J. Gastroenterol.* 94 (8) (1999) 2156–2164.
- [69] K. Ogawa, T. Matsumoto, M. Esaki, T. Torisu, M. Iida, Profiles of circulating cytokines in patients with Crohn's disease under maintenance therapy with infliximab, *J. Crohns Colitis* 6 (5) (2012) 529–535.
- [70] R.D. Harvey, E.T. Morgan, Cancer, inflammation, and therapy: effects on cytochrome p450-mediated drug metabolism and implications for novel immunotherapeutic agents, *Clin. Pharmacol. Ther.* 96 (4) (2014) 449–457.
- [71] K.K. Machavaram, L.M. Almond, A. Rostami-Hodjegan, I. Gardner, M. Jamei, S. Tay, S. Wong, A. Joshi, J. R. Kenny, A physiologically based pharmacokinetic modeling approach to predict disease-drug interactions: suppression of CYP3A by IL-6, *Clin. Pharmacol. Ther.* 94 (2) (2013) 260–268.
- [72] E.A. Dowlatshahi, E.A. van der Voort, L.R. Arends, T. Nijsten, Markers of systemic inflammation in psoriasis: a systematic review and meta-analysis, *Br. J. Dermatol.* 169 (2) (2013) 266–282.
- [73] V. Nagele, A. Kratzer, G. Zugmaier, C. Holland, Y. Hijazi, M.S. Topp, N. Gokbuget, P.A. Baeuerle, P. Kufer, A. Wolf, M. Klinger, Changes in clinical laboratory parameters and pharmacodynamic markers in response to blinatumomab treatment of patients with relapsed/refractory ALL, *Exp. Hematol. Oncol.* 6 (2017) 14.
- [74] Y. Xu, Y. Hijazi, A. Wolf, B. Wu, Y.N. Sun, M. Zhu, Physiologically based pharmacokinetic model to assess the influence of Blinatumomab-mediated cytokine elevations on cytochrome P450 enzyme activity, *CPT Pharmacometrics Syst. Pharmacol.* 4 (9) (2015) 507–515.
- [75] Amgen Inc, BLINCYTO® (Blinatumomab) For Injection, for Intravenous Use, 2014.
- [76] R.N. Maini, F.C. Breedveld, J.R. Kalden, J.S. Smolen, D. Davis, J.D. Macfarlane, C. Antoni, B. Leeb, M.J. Elliott, J. N. Woody, T.F. Schaible, M. Feldmann, Therapeutic efficacy of multiple intravenous infusions of anti-tumor necrosis factor alpha monoclonal antibody combined with low-dose weekly methotrexate in rheumatoid arthritis, *Arthritis Rheum.* 41 (9) (1998) 1552–1563.
- [77] M.F. Pouw, C.L. Krieckaert, M.T. Nurmohamed, D. van der Kleij, L. Aarden, T. Rispens, G. Wolbink, Key findings towards optimising adalimumab treatment: the concentration-effect curve, *Ann. Rheum. Dis.* 74 (3) (2015) 513–518.
- [78] Y. Zhuang, Z. Xu, B. Frederick, D.E. de Vries, J.A. Ford, M. Keen, M.K. Doyle, K.J. Petty, H.M. Davis, H. Zhou, Golimumab pharmacokinetics after repeated subcutaneous and intravenous administrations in patients with rheumatoid arthritis and the effect of concomitant methotrexate: An open-label, randomized study, *Clin. Ther.* 34 (1) (2012) 77–90.
- [79] D. Ternant, E. Ducourau, A. Perdriger, A. Corondan, B. Le Goff, V. Devauchelle-Pensec, E. Solau-Gervais, H. Watier, P. Goupille, G. Paintaud, D. Mulleman, Relationship between inflammation and infliximab pharmacokinetics in rheumatoid arthritis, *Br. J. Clin. Pharmacol.* 78 (1) (2014) 118–128.
- [80] W. Wang, J. Leu, R. Watson, Z. Xu, H. Zhou, Investigation of the mechanism of therapeutic protein-drug interaction between methotrexate and Golimumab, an anti-TNFalpha monoclonal antibody, *AAPS J.* 20 (3) (2018) 63.
- [81] S.M. Lavezzi, J. de Jong, M. Neyens, P. Cramer, F. Demirkan, G. Fraser, N. Bartlett, M.S. Dilhuydy, J. Loscertales, A. Avigdor, S. Rule, O. Samoilova, A. Goy, S. Ganguly, M. Salman, A. Howes, M. Mahler, G. De Nicolao, I. Poggesi, Systemic exposure of rituximab increased by Ibrutinib: pharmacokinetic results and Modeling based on the HELIOS trial, *Pharm. Res.* 36 (7) (2019) 93.
- [82] G. Mo, J.R. Baldwin, D. Luffer-Atlas, R.L. Ilaria Jr., I. Conti, M. Heathman, D.M. Cronier, Population pharmacokinetic modeling of olaratumab, an anti-PDGFRalpha human monoclonal antibody, in patients with advanced and/or metastatic cancer, *Clin. Pharmacokinet.* 57 (3) (2018) 355–365.
- [83] S. Wijngaarden, J.A. van Roon, J.W. Bijlsma, J.G. van de Winkel, F.P. Lafeber, Fcgamma receptor expression levels on monocytes are elevated in rheumatoid arthritis patients with high erythrocyte sedimentation rate who do not use anti-rheumatic drugs, *Rheumatology (Oxford)* 42 (5) (2003) 681–688.
- [84] A. Kavanaugh, I.B. McInnes, P.J. Mease, G.G. Krueger, D.D. Gladman, D. van der Heijde, S. Mudivarthi, W. Xu, M. Mack, Z. Xu, A. Beutler, Clinical efficacy, radiographic and safety findings through 2 years of golimumab

- treatment in patients with active psoriatic arthritis: results from a long-term extension of the randomised, placebo-controlled GO-REVEAL study, *Ann. Rheum. Dis.* 72 (11) (2013) 1777–1785.
- [85] S. Kasichayanula, A. Grover, M.G. Emery, M.A. Gibbs, R. Somaratne, S.M. Wasserman, J.P. Gibbs, Clinical pharmacokinetics and pharmacodynamics of Evolocumab, a PCSK9 inhibitor, *Clin. Pharmacokinet.* 57 (7) (2018) 769–779.
- [86] Amgen Inc, REPATHA (Evolocumab) Injection, for Subcutaneous Use, 2015.
- [87] M. Manniello, M. Pisano, Alirocumab (Praluent): first in the new class of PCSK9 inhibitors, *P T* 41 (1) (2016) 28–53.
- [88] Sanofi-aventis U.S. LLC and Regeneron Pharmaceuticals Inc, PRALUENT® (Alirocumab) Injection, for Subcutaneous Use, 2015.
- [89] G. Dubuc, A. Chamberland, H. Wassef, J. Davignon, N.G. Seidah, L. Bernier, A. Prat, Statins upregulate PCSK9, the gene encoding the proprotein convertase neural apoptosis-regulated convertase-1 implicated in familial hypercholesterolemia, *Arterioscler. Thromb. Vasc. Biol.* 24 (8) (2004) 1454–1459.
- [90] J. Mayne, T. Dewpura, A. Raymond, M. Cousins, A. Chaplin, K.A. Lahey, S.A. Lahaye, M. Mbikay, T.C. Ooi, M. Chretien, Plasma PCSK9 levels are significantly modified by statins and fibrates in humans, *Lipids Health Dis.* 7 (2008) 22.
- [91] K. Wang, F.S. Stark, T. Schlothauer, A. Lahr, V. Cosson, J. Zhi, K. Habben, J. Tessier, E. Schick, R.F. Staack, O. Krieter, An apparent clinical pharmacokinetic drug-drug interaction between bevacizumab and the anti-placental growth factor monoclonal antibody RO5323441 via a target-trapping mechanism, *Cancer Chemother. Pharmacol.* 79 (4) (2017) 661–671.
- [92] C.D. Weekes, L.S. Rosen, A. Capasso, K.M. Wong, W. Ye, M. Anderson, B. McCall, J. Fredrickson, E. Wakshull, S. Eppler, Q. Shon-Nguyen, R. Desai, M. Huseni, P.S. Hegde, T. Pourmohamad, I. Rhee, A. Bessudo, Phase I study of the anti- $\alpha$ 5 $\beta$ 1 monoclonal antibody MINT1526A with or without bevacizumab in patients with advanced solid tumors, *Cancer Chemother. Pharmacol.* 82 (2) (2018) 339–351.
- [93] D.M. Hyman, N. Rizvi, R. Natale, D.K. Armstrong, M. Birrer, L. Recht, E. Dotan, V. Makker, T. Kaley, D. Kuruvilla, M. Gribbin, J. McDevitt, D.W. Lai, M. Dar, Phase I study of MEDI3617, a selective angiopoietin-2 inhibitor alone and combined with carboplatin/paclitaxel, paclitaxel, or bevacizumab for advanced solid tumors, *Clin. Cancer Res.* 24 (12) (2018) 2749–2757.
- [94] D.C. Roopenian, S. Akilesh, FcRn: the neonatal Fc receptor comes of age, *Nat. Rev. Immunol.* 7 (9) (2007) 715–725.
- [95] L. Liu, A.M. Garcia, H. Santoro, Y. Zhang, K. McDonnell, J. Dumont, A. Bitonti, Amelioration of experimental autoimmune myasthenia gravis in rats by neonatal FcR blockade, *J. Immunol.* 178 (8) (2007) 5390–5398.
- [96] P. Kiessling, R. Lledo-Garcia, S. Watanabe, G. Langdon, D. Tran, M. Bari, L. Christodoulou, E. Jones, G. Price, B. Smith, F. Brennan, I. White, S. Jolles, The FcRn inhibitor rozanolixizumab reduces human serum IgG concentration: A randomized phase 1 study, *Sci. Transl. Med.* 9 (414) (2017).
- [97] L.E. Ling, J.L. Hillson, R.G. Tiessen, T. Bosje, M.P. van Iersel, D.J. Nix, L. Markowitz, N.A. Cilfone, J. Duffner, J. B. Streisand, A.M. Manning, S. Arroyo, M281, an anti-FcRn antibody: pharmacodynamics, pharmacokinetics, and safety across the full range of IgG reduction in a first-in-human study, *Clin. Pharmacol. Ther.* 105 (4) (2019) 1031–1039.
- [98] K.M. Hurren, N.R. Pinelli, Drug-drug interactions with glucagon-like peptide-1 receptor agonists, *Ann. Pharmacother.* 46 (5) (2012) 710–717.
- [99] C.S. Marathe, C.K. Rayner, K.L. Jones, M. Horowitz, Effects of GLP-1 and incretin-based therapies on gastrointestinal motor function, *Exp. Diabetes Res.* 2011 (2011) 279530.
- [100] L. Abuqayyas, J.P. Balthasar, Pharmacokinetic mAb-mAb interaction: anti-VEGF mAb decreases the distribution of anti-CEA mAb into colorectal tumor xenografts, *AAPS J.* 14 (3) (2012) 445–455.
- [101] V.A. Thomas, J.P. Balthasar, Sorafenib decreases tumor exposure to an anti-carcinoembryonic antigen monoclonal antibody in a mouse model of colorectal cancer, *AAPS J.* 18 (4) (2016) 923–932.
- [102] B.B. Yang, B. Gillespie, B. Smith, W. Smith, A. Lissmats, M. Rudebeck, T. Kullenberg, B. Olsson, Pharmacokinetic and pharmacodynamic interactions between palifermin and heparin, *J. Clin. Pharmacol.* 55 (10) (2015) 1109–1118.
- [103] D.H. Damon, R.R. Lobb, P.A. D'Amore, J.A. Wagner, Heparin potentiates the action of acidic fibroblast growth factor by prolonging its biological half-life, *J. Cell. Physiol.* 138 (2) (1989) 221–226.
- [104] M.A. Bush, E. Samara, M.J. Whitehouse, C. Yoshizawa, D.L. Novicki, M. Pike, R.J. Laham, M. Simons, N. A. Chronos, Pharmacokinetics and pharmacodynamics of recombinant FGF-2 in a phase I trial in coronary artery disease, *J. Clin. Pharmacol.* 41 (4) (2001) 378–385.

- [105] X. Xia, J.P. Babcock, S.I. Blaber, K.M. Harper, M. Blaber, Pharmacokinetic properties of 2nd-generation fibroblast growth factor-1 mutants for therapeutic application, *PLoS One* 7 (11) (2012), e48210.
- [106] S.C. Alley, X. Zhang, N.M. Okeley, M. Anderson, C.L. Law, P.D. Senter, D.R. Benjamin, The pharmacologic basis for antibody-auristatin conjugate activity, *J. Pharmacol. Exp. Ther.* 330 (3) (2009) 932–938.
- [107] C.A. Boswell, E.E. Mundo, C. Zhang, D. Bumbaca, N.R. Valle, K.R. Kozak, A. Fourie, J. Chuh, N. Koppada, O. Saad, H. Gill, B.Q. Shen, B. Rubinfeld, J. Tibbitts, S. Kaur, F.P. Theil, P.J. Fielder, L.A. Khawli, K. Lin, Impact of drug conjugation on pharmacokinetics and tissue distribution of anti-STEAP1 antibody-drug conjugates in rats, *Bioconjug. Chem.* 22 (10) (2011) 1994–2004.
- [108] T.H. Han, A.K. Gopal, R. Ramchandren, A. Goy, R. Chen, J.V. Matous, M. Cooper, L.E. Grove, S.C. Alley, C. M. Lynch, O.A. O'Connor, CYP3A-mediated drug-drug interaction potential and excretion of brentuximab vedotin, an antibody-drug conjugate, in patients with CD30-positive hematologic malignancies, *J. Clin. Pharmacol.* 53 (8) (2013) 866–877.
- [108a] Seattle Genetics, Inc., ADCETRIS® (brentuximab vedotin) for injection, for intravenous use, 2014, [https://www.accessdata.fda.gov/drugsatfda\\_docs/label/2014/125388\\_S056S0781bl.pdf](https://www.accessdata.fda.gov/drugsatfda_docs/label/2014/125388_S056S0781bl.pdf).
- [109] Y. Chen, D. Samineni, S. Mukadam, H. Wong, B.Q. Shen, D. Lu, S. Girish, C. Hop, J.Y. Jin, C. Li, Physiologically based pharmacokinetic modeling as a tool to predict drug interactions for antibody-drug conjugates, *Clin. Pharmacokinet.* 54 (1) (2015) 81–93.
- [110] L.M. Gan, M. Lagerstrom-Fermer, L.G. Carlsson, C. Arfvidsson, A.C. Egnell, A. Rudvik, M. Kjaer, A. Collen, J. D. Thompson, J. Joyal, L. Chialda, T. Koernicke, R. Fuhr, K.R. Chien, R. Fritsche-Danielson, Intradermal delivery of modified mRNA encoding VEGF-A in patients with type 2 diabetes, *Nat. Commun.* 10 (1) (2019) 871.
- [111] S. Andersson, M. Antonsson, M. Elebring, R. Jansson-Lofmark, L. Weidolf, Drug metabolism and pharmacokinetic strategies for oligonucleotide- and mRNA-based drug development, *Drug Discov. Today* 23 (10) (2018) 1733–1745.
- [112] R.S. Geary, E. Wancewicz, J. Matson, M. Pearce, A. Siwkowski, E. Swayze, F. Bennett, Effect of dose and plasma concentration on liver uptake and pharmacologic activity of a 2'-methoxyethyl modified chimeric antisense oligonucleotide targeting PTEN, *Biochem. Pharmacol.* 78 (3) (2009) 284–291.
- [113] Z. Li, M.L. Hard, J.S. Grundy, T. Singh, L.L. von Moltke, I. Boltje, Lack of clinical pharmacodynamic and pharmacokinetic drug-drug interactions between warfarin and the antisense oligonucleotide mipomersen, *J. Cardiovasc. Pharmacol.* 64 (2) (2014) 164–171.
- [114] K.N. Chi, L.L. Siu, H. Hirte, S.J. Hotte, J. Knox, C. Kollmansberger, M. Gleave, E. Guns, J. Powers, W. Walsh, D. Tu, E. Eisenhauer, A phase I study of OGX-011, a 2'-methoxyethyl phosphorothioate antisense to clusterin, in combination with docetaxel in patients with advanced cancer, *Clin. Cancer Res.* 14 (3) (2008) 833–839.
- [115] R.S. Geary, J.D. Bradley, T. Watanabe, Y. Kwon, M. Wedel, J.J. van Lier, A.A. VanVliet, Lack of pharmacokinetic interaction for ISIS 113715, a 2'-O-methoxyethyl modified antisense oligonucleotide targeting protein tyrosine phosphatase 1B messenger RNA, with oral antidiabetic compounds metformin, glipizide or rosiglitazone, *Clin. Pharmacokinet.* 45 (8) (2006) 789–801.
- [116] A.A. Adjei, G.K. Dy, C. Erlichman, J.M. Reid, J.A. Sloan, H.C. Pitot, S.R. Alberts, R.M. Goldberg, L.J. Hanson, P. J. Atherton, T. Watanabe, R.S. Geary, J. Holmlund, F.A. Dorr, A phase I trial of ISIS 2503, an antisense inhibitor of H-ras, in combination with gemcitabine in patients with advanced cancer, *Clin. Cancer Res.* 9 (1) (2003) 115–123.
- [117] S. Mani, C.M. Rudin, K. Kunkel, J.T. Holmlund, R.S. Geary, H.L. Kindler, F.A. Dorr, M.J. Ratain, Phase I clinical and pharmacokinetic study of protein kinase C- $\alpha$  antisense oligonucleotide ISIS 3521 administered in combination with 5-fluorouracil and leucovorin in patients with advanced cancer, *Clin. Cancer Res.* 8 (4) (2002) 1042–1048.
- [118] M.A. Villalona-Calero, P. Ritch, J.A. Figueroa, G.A. Otterson, R. Belt, E. Dow, S. George, J. Leonardo, S. McCachren, G.L. Miller, M. Modiano, M. Valdivieso, R. Geary, J.W. Oliver, J. Holmlund, A phase I/II study of LY900003, an antisense inhibitor of protein kinase C- $\alpha$ , in combination with cisplatin and gemcitabine in patients with advanced non-small cell lung cancer, *Clin. Cancer Res.* 10 (18 Pt 1) (2004) 6086–6093.
- [119] A. Suslov, S. Wieland, S. Menne, Modulators of innate immunity as novel therapeutics for treatment of chronic hepatitis B, *Curr. Opin. Virol.* 30 (2018) 9–17.
- [120] K. Li, S. Qu, X. Chen, Q. Wu, M. Shi, Promising targets for cancer immunotherapy: TLRs, RLRs, and STING-mediated innate immune pathways, *Int. J. Mol. Sci.* 18 (2) (2017).

- [121] J.L. Goldberg, P.M. Sondel, Enhancing cancer immunotherapy via activation of innate immunity, *Semin. Oncol.* 42 (4) (2015) 562–572.
- [122] T. Li, Z.J. Chen, The cGAS-cGAMP-STING pathway connects DNA damage to inflammation, senescence, and cancer, *J. Exp. Med.* 215 (5) (2018) 1287–1299.
- [123] J. Galon, D. Bruni, Approaches to treat immune hot, altered and cold tumours with combination immunotherapies, *Nat. Rev. Drug Discov.* 18 (3) (2019) 197–218.
- [124] A. Ribas, T. Medina, S. Kummar, A. Amin, A. Kalbasi, J.J. Drabick, M. Barve, G.A. Daniels, D.J. Wong, E. V. Schmidt, A.F. Candia, R.L. Coffman, A.C.F. Leung, R.S. Janssen, SD-101 in combination with Pembrolizumab in advanced melanoma: results of a phase Ib, multicenter study, *Cancer Discov.* 8 (10) (2018) 1250–1257.
- [125] M.J. Frank, P.M. Reagan, N.L. Bartlett, L.I. Gordon, J.W. Friedberg, D.K. Czerwinski, S.R. Long, R.T. Hoppe, R. Janssen, A.F. Candia, R.L. Coffman, R. Levy, In situ vaccination with a TLR9 agonist and local low-dose radiation induces systemic responses in untreated indolent lymphoma, *Cancer Discov.* 8 (10) (2018) 1258–1269.
- [126] Z. Wang, W. Han, Biomarkers of cytokine release syndrome and neurotoxicity related to CAR-T cell therapy, *Biomark Res.* 6 (2018) 4.
- [127] S. Wang, J. Campos, M. Gallotta, M. Gong, C. Crain, E. Naik, R.L. Coffman, C. Guiducci, Intratumoral injection of a CpG oligonucleotide reverts resistance to PD-1 blockade by expanding multifunctional CD8+ T cells, *Proc. Natl. Acad. Sci. U. S. A.* 113 (46) (2016) e7240–e7249.
- [128] S.S. Neelapu, S. Tummala, P. Kebriaei, W. Wierda, C. Gutierrez, F.L. Locke, K.V. Komanduri, Y. Lin, N. Jain, N. Daver, J. Westin, A.M. Gulbis, M.E. Loghin, J.F. de Groot, S. Adkins, S.E. Davis, K. Rezvani, P. Hwu, E. J. Shpall, Chimeric antigen receptor T-cell therapy - assessment and management of toxicities, *Nat. Rev. Clin. Oncol.* 15 (1) (2018) 47–62.
- [129] S.L. Maude, N. Frey, P.A. Shaw, R. Aplenc, D.M. Barrett, N.J. Bunin, A. Chew, V.E. Gonzalez, Z. Zheng, S. F. Lacey, Y.D. Mahnke, J.J. Melenhorst, S.R. Rheingold, A. Shen, D.T. Teachey, B.L. Levine, C.H. June, D. L. Porter, S.A. Grupp, Chimeric antigen receptor T cells for sustained remissions in leukemia, *N. Engl. J. Med.* 371 (16) (2014) 1507–1517.
- [130] J.N. Kochenderfer, M.E. Dudley, S.H. Kassim, R.P. Somerville, R.O. Carpenter, M. Stetler-Stevenson, J.C. Yang, G.Q. Phan, M.S. Hughes, R.M. Sherry, M. Raffeld, S. Feldman, L. Lu, Y.F. Li, L.T. Ngo, A. Goy, T. Feldman, D. E. Spaner, M.L. Wang, C.C. Chen, S.M. Kranick, A. Nath, D.A. Nathan, K.E. Morton, M.A. Toomey, S. A. Rosenberg, Chemotherapy-refractory diffuse large B-cell lymphoma and indolent B-cell malignancies can be effectively treated with autologous T cells expressing an anti-CD19 chimeric antigen receptor, *J. Clin. Oncol.* 33 (6) (2015) 540–549.
- [131] D.T. Teachey, S.F. Lacey, P.A. Shaw, J.J. Melenhorst, S.L. Maude, N. Frey, E. Pequignot, V.E. Gonzalez, F. Chen, J. Finklestein, D.M. Barrett, S.L. Weiss, J.C. Fitzgerald, R.A. Berg, R. Aplenc, C. Callahan, S.R. Rheingold, Z. Zheng, S. Rose-John, J.C. White, F. Nazimuddin, G. Wertheim, B.L. Levine, C.H. June, D.L. Porter, S. A. Grupp, Identification of predictive biomarkers for cytokine release syndrome after chimeric antigen receptor T-cell therapy for acute lymphoblastic leukemia, *Cancer Discov.* 6 (6) (2016) 664–679.
- [132] L. Galluzzi, A. Buque, O. Kepp, L. Zitvogel, G. Kroemer, Immunogenic cell death in cancer and infectious disease, *Nat. Rev. Immunol.* 17 (2) (2017) 97–111.
- [133] T. Xia, H. Konno, G.N. Barber, Recurrent loss of STING signaling in melanoma correlates with susceptibility to viral oncolysis, *Cancer Res.* 76 (22) (2016) 6747–6759.
- [134] E.A. Chiocca, S.D. Rabkin, Oncolytic viruses and their application to cancer immunotherapy, *Cancer Immunol. Res.* 2 (4) (2014) 295–300.
- [135] Z.S. Guo, Z. Liu, S. Kowalsky, M. Feist, P. Kalinski, B. Lu, W.J. Storkus, D.L. Bartlett, Oncolytic immunotherapy: conceptual evolution, current strategies, and future perspectives, *Front. Immunol.* 8 (2017) 555.
- [136] B.D. Lichty, C.J. Breitbach, D.F. Stojdl, J.C. Bell, Going viral with cancer immunotherapy, *Nat. Rev. Cancer* 14 (8) (2014) 559–567.
- [137] B.L. Liu, M. Robinson, Z.Q. Han, R.H. Branston, C. English, P. Reay, Y. McGrath, S.K. Thomas, M. Thornton, P. Bullock, C.A. Love, R.S. Coffin, et al., *Gene Ther.* 10 (4) (2003) 292–303.
- [138] R.H. Andtbacka, H.L. Kaufman, F. Collichio, T. Amatruda, N. Senzer, J. Chesney, K.A. Delman, L.E. Spitler, I. Puzanov, S.S. Agarwala, M. Milhem, L. Cranmer, B. Curti, K. Lewis, M. Ross, T. Guthrie, G.P. Linette, G. A. Daniels, K. Harrington, M.R. Middleton, W.H. Miller Jr., J.S. Zager, Y. Ye, B. Yao, A. Li, S. Doleman, A. VanderWalde, J. Gansert, R.S. Coffin, Talimogene Laherparepvec improves durable response rate in patients with advanced melanoma, *J. Clin. Oncol.* 33 (25) (2015) 2780–2788.

- [139] A. Ribas, R. Dummer, I. Puzanov, A. VanderWalde, R.H.I. Andtbacka, O. Michielin, A.J. Olszanski, J. Malvehy, J. Cebon, E. Fernandez, J.M. Kirkwood, T.F. Gajewski, L. Chen, K.S. Gorski, A.A. Anderson, S.J. Diede, M. E. Lassman, J. Gansert, F.S. Hodi, G.V. Long, Oncolytic virotherapy promotes intratumoral T cell infiltration and improves anti-PD-1 immunotherapy, *Cell* 170 (6) (2017) 1109–1119. e10.
- [140] N.B. Elsedawy, S.J. Russell, Oncolytic vaccines, *Expert Rev. Vaccines* 12 (10) (2013) 1155–1172.
- [141] K.C. Conlon, M.D. Miljkovic, T.A. Waldmann, Cytokines in the treatment of cancer, *J. Interf. Cytokine Res.* 39 (1) (2019) 6–21.
- [142] D. Neri, P.M. Sondel, Immunocytokines for cancer treatment: past, present and future, *Curr. Opin. Immunol.* 40 (2016) 96–102.
- [143] C. Klein, I. Waldhauer, V.G. Nicolini, A. Freimoser-Grundschober, T. Nayak, D.J. Vugts, C. Dunn, M. Bolijn, J. Benz, M. Stihle, S. Lang, M. Roemmele, T. Hofer, E. van Puijenbroek, D. Wittig, S. Moser, O. Ast, P. Brunker, I.H. Gorr, S. Neumann, M.C. de Vera Mudry, H. Hinton, F. Cramer, J. Saro, S. Evers, C. Gerdes, M. Bacac, G. van Dongen, E. Moessner, P. Umana, Cergutuzumab amunaleukin (CEA-IL2v), a CEA-targeted IL-2 variant-based immunocytokine for combination cancer immunotherapy: overcoming limitations of aldesleukin and conventional IL-2-based immunocytokines, *Oncoimmunology* 6 (3) (2017) e1277306.
- [144] Y. Liu, W. Zhang, L.H. Cheung, T. Niu, Q. Wu, C. Li, C.S. Van Pelt, M.G. Rosenblum, The antimelanoma immunocytokine scFvMEL/TNF shows reduced toxicity and potent antitumor activity against human tumor xenografts, *Neoplasia* 8 (5) (2006) 384–393.
- [145] S.J. Schrieber, E. Pfuma-Fletcher, X. Wang, Y.C. Wang, S. Sagoo, R. Madabushi, S.M. Huang, I. Zineh, Considerations for biologic product drug-drug interactions: a regulatory perspective, *Clin. Pharmacol. Ther.* 105 (6) (2019) 1332–1334.
- [146] FDA, Guidance for Industry, In Vitro Metabolism- and Transporter- Mediated Drug-Drug Interaction Studies Guidance for Industry, 2017.
- [147] A.T. Chow, J.C. Earp, M. Gupta, W. Hanley, C. Hu, D.D. Wang, S. Zajic, M. Zhu, Utility of population pharmacokinetic modeling in the assessment of therapeutic protein-drug interactions, *J. Clin. Pharmacol.* 54 (2014) 593–601.
- [148] G. Mikus, Probes and cocktails for drug-drug interaction evaluation: the future is microdosing? *Clin. Pharmacol. Ther.* 105 (6) (2019) 1335–1337.



PART III

Strategy related to drug  
metabolism and safety

# Metabolites in safety testing (MIST)

*Simone Schadt, Filipe Lopes, Simon Hauri, Axel Pähler,  
Andreas Brink*

Roche Pharma Research and Early Development, Roche Innovation Center Basel, F. Hoffmann-La Roche Ltd, Basel, Switzerland

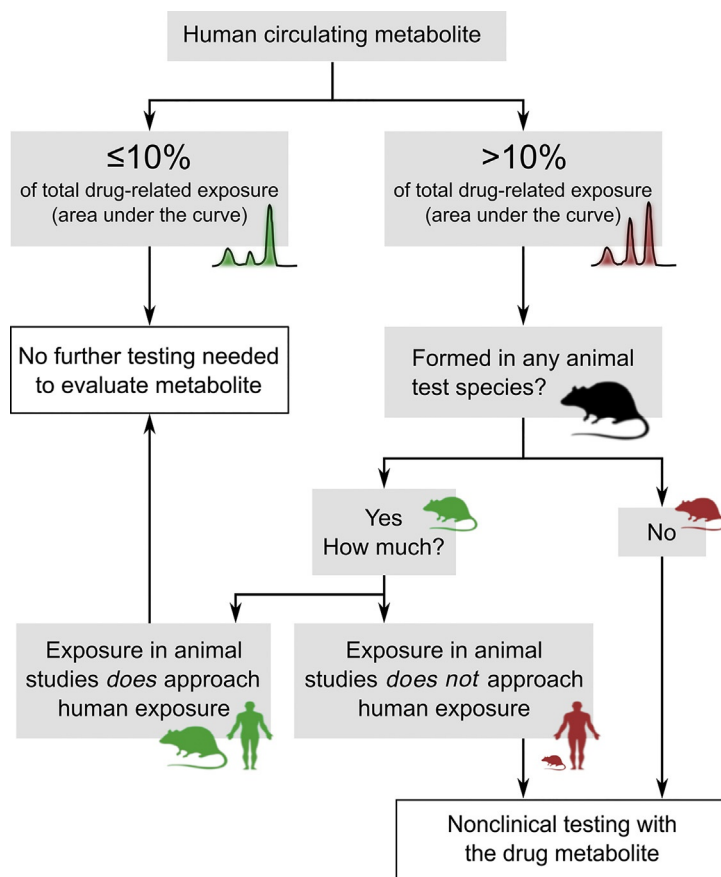
## 1 Introduction

### 1.1 History of guidance on safety testing of drug metabolites

First discussions on metabolites in safety testing (MIST) dated back to the late 1990s and early 2000s, when scientists from the pharmaceutical industry sponsored by the Pharmaceutical Research and Manufacturers of America (PhRMA) exchanged their experience and views on safety assessment of drug metabolites intending to define practical and scientifically based approaches to address contemporary issues in the safety evaluation of metabolites [1]. This committee suggested that metabolites that account for 25% or more of the total drug-related material in human plasma should also be found in toxicology species at an equivalent or greater exposure [1]. Rapidly, a response from scientists of the US Food and Drug Administration (FDA) followed, challenging the 25% threshold [2]. This inspired further discussion of this complex topic, including refined proposals for the safety assessment of metabolites, discussion of examples for drug metabolites causing toxicities [3–8], and a draft guidance document by the FDA in 2005. In 2008, the FDA issued the final guidance document providing recommendations on how to deal with drug metabolites in safety testing for small molecule drugs [9]. This FDA guidance proposed a threshold for safety assessment for metabolites comprising 10% or greater of the parent compound in the systemic circulation at a steady state. For these metabolites, plasma levels should be in the same range in at least one toxicology species. If this is not the case, additional safety studies with the metabolites may be necessary. One year later, in 2009, broader regulatory agreement resulted in a guidance document by the International Conference on Harmonization [ICHM3(R2)] [10] with a different threshold for relevant human metabolites (10% or greater of total drug-related material in circulation) (Fig. 1). Compared to the FDA MIST guidance, which focuses on safety



**FIG. 1** Decision tree for the safety assessment of drug metabolites. Modified from FDA, *Guidance for Industry: Safety Testing of Drug Metabolites*, Food and Drug Administration, US Department of Health and Human Services, Center for Drug Evaluation and Research, Silver Spring, MD, 2016.



testing of metabolites, the ICHM3 guidance on “nonclinical safety studies for the conduct of human clinical trials and marketing authorization for pharmaceuticals” encompasses a far broader scope, and the MIST topic is covered only in a small paragraph, therefore the level of detail is much lower. An ICHM3(R2) Q&A document issued in 2012 provided further important information [11] on concrete requirements for the safety assessment of metabolites, for example, that “characterization of metabolite toxicity would generally be considered adequate when animal exposure is at least 50 percent of the exposure seen in humans” [11]. In 2012, the Chinese Food and Drug Administration (CFDA) issued a guidance document on the safety assessment of metabolites, which is largely in agreement with the FDA guidance [12]. The appearance of these guidance documents was followed by intense discussions between scientist from the pharmaceutical industry about the right strategies for appropriate MIST assessment with regard to type, range, and level of detail of required metabolism studies as well as of their optimum timing during drug discovery and development [13–22]. Finally, in 2016, the FDA issued a revision of the MIST guidance that formally adopted the ICH threshold for relevant human metabolites (Fig. 1).

## 1.2 Summary of the metabolites in safety testing (MIST) guidance

The MIST guidance documents define recommendations on when and how to characterize the safety of human drug metabolites [9–11]. Safety assessment is warranted for major human metabolites that exceed 10% of total drug-related systemic exposure at steady state in humans receiving therapeutic doses of the drug. This is typically based on plasma exposure (AUC of drug concentration in plasma), however,  $C_{\max}$  may be used if more appropriate [9]. Safety coverage should be assured for all major human metabolites in at least one species used in general toxicity, reproductive toxicity, and carcinogenicity studies, respectively. For this, the human exposure at steady state at the to-be-marketed dose (based on the parent drug, time to a steady state of metabolites might be different) is compared with exposure in animals receiving the dose corresponding to the no-observed-adverse-effect level (NOAEL). For disproportionate human metabolites, i.e., metabolites that are not adequately covered in animals, additional safety studies might be necessary, including direct administration of the metabolite in toxicology studies or the use of alternative toxicology species. According to ICHM3 (R2), the characterization of metabolite toxicity would generally be considered adequate when animal exposure at MTD is at least 50% of the exposure seen in humans [11]. However, when a metabolite represents the majority of the total human exposure to drug-related material, the metabolite in animals should exceed that in humans, because this metabolite constitutes the bulk of human exposure [11]. Not all disproportionate human metabolites require safety assessment per se. Most phase II metabolites (conjugates) are pharmacologically inactive and can be considered not to be toxic. The safety assessment of drug metabolites needs to be addressed with the authorities on a case-by-case basis and depends on whether they possess a structural alert (e.g., acyl-glucuronides), are unique to humans or pharmacologically active, circulate at high levels, and/or possess long half-lives [23].

## 2 Technological approaches for MIST assessment

According to the MIST guidance documents, human metabolites exceeding 10% of the total drug-related material in circulation at steady state require evaluation to ensure coverage in safety studies. The question whether a human metabolite is major or not is, therefore, important in drug development projects. It is crucial to address this as early as possible to have sufficient time for structural identification, metabolite synthesis, development of bioanalytical methods to monitor exposure in animal studies, and for adequate safety evaluation. Discovery of a major human metabolite in advanced stages of drug development could result in significant delays of projects. Typically, a methodology based on high-resolution mass spectrometry (HRMS) is used as early as possible in the drug development process (utilizing *in vitro* assays in hepatic microsomes, hepatocytes, and recombinantly expressed drug-metabolizing enzymes). For early metabolite profiling and estimating whether a metabolite might be MIST relevant or not, HRMS plays an important and decisive role and many fit-for-purpose methods have been developed and described in the literature for assessing metabolite level in humans or animals in the absence of reference compounds [17–19, 24–29]. However, it is important to keep in mind that several limitations of HRMS exist mainly due to matrix effects, potential differences in ionization, or extraction efficacies between

(unknown) metabolites and parent drug. Therefore, HRMS data generated without using reference compounds need to be carefully evaluated and interpreted. Recommendations and approaches addressing these factors are, e.g., calibrators or using a mixed plasma approach, which will be discussed later. Mass spectrometry-based methods that are a core part of MIST assessment strategies are complemented by additional technologies [30] such as nuclear magnetic resonance (NMR) spectroscopy, HPLC-radiometric detection, and accelerator mass spectrometry (AMS) [31, 32] (Fig. 2). An emerging technology that sparked interest in the pharmaceutical industry is cavity ring-down spectroscopy (CRDS) [33].

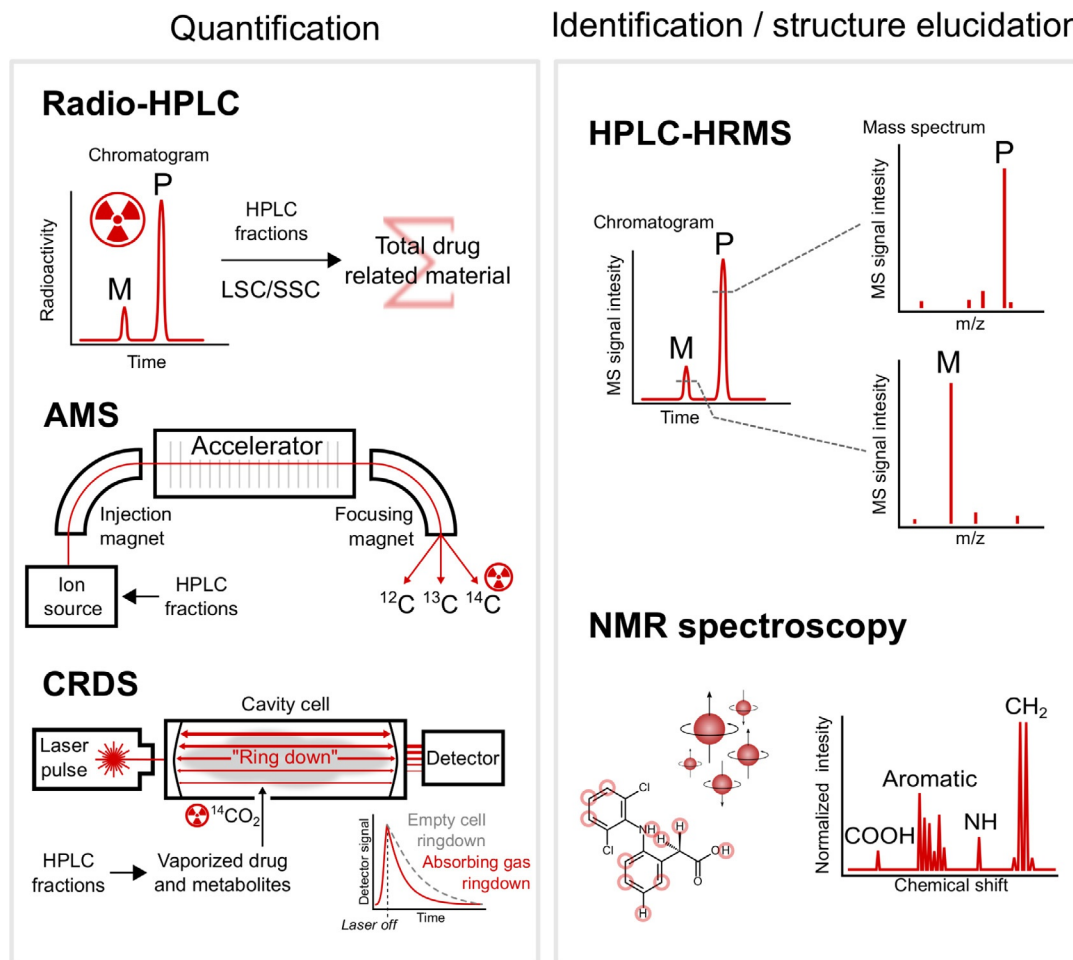


**FIG. 2** Technologies that play important roles for the identification and quantification of MIST relevant metabolites are radio-HPLC and HPLC-HRMS. NMR spectroscopy could be crucial for the definitive structure elucidation of metabolites. Accelerator mass spectrometry (AMS) is a complementary technology to generate radio metabolite profiles at very low levels of circulating radioactivity. Cavity ring-down spectroscopy (CRDS) is a promising quantitative technology currently explored by some pharmaceutical companies.

## 2.1 High-performance liquid chromatography separation and radiometric detection

Historically, HPLC linked to radiometric detection has been used as the method of choice to create drug metabolite (radio) profiles [30]. With the advent of sensitive and sophisticated HRMS instruments, followed by the broad acceptance of approaches using non-labeled compounds, radiometric metabolite profiling became gradually less important. However, radiometric methods still play a role in MIST assessment, because radiochromatograms are used for quantitative determination, and radioactivity enables mass balance in all extraction steps and HPLC column recoveries. Therefore, radiometric detection ensures that all relevant drug-related material is identified.

Radiometric detection can be performed either online by a radio detector connected directly to the HPLC or offline by liquid or solid scintillation counting (LSC/SSC) for the measurement of the collected fraction. Multiwell microtiter plates are especially suited as they can be placed directly into commercially available fraction collectors and SSC plate readers without further sample handling steps [34, 35].

Since retention times are mostly unaffected by the radioactive label, these studies can provide distinct coordinates for further LC-MS and LC-NMR analysis of the unlabeled compound.

## 2.2 High-resolution mass spectrometry

The increasing performance of modern mass spectrometers, especially in terms of resolution, has influenced many scientific research areas including drug metabolism studies [36, 37]. In the recent years, HPLC radio detection has been largely replaced with high-resolution mass spectrometry as the main method of choice for drug metabolite profiling. High-resolution mass spectrometry is able to distinguish mass differences with sub-ppm accuracy enabling the detection and characterization of low abundant analytes in complex biological matrices such as serum, plasma, or tissue homogenates. As a rule of thumb, MS instruments are considered as “high-resolution” instruments when the mass analyzer exceeds  $>10,000$  full-width at half-maximum resolution. The most widely used analyzers are orbitrap [38, 39], FTMS, or time-of-flight mass analyzers [40].

The strategy in early drug metabolite identification by HRMS commonly relies on an online separation by reverse-phase liquid chromatography and electrospray ionization [17]. The applied MS methods at this stage are largely untargeted and may include different precursor ion fragmentation strategies depending on the capabilities of the instrument. The most intense ions are selected for selective fragmentation (DDA, TopN) or the instrument alternates between two different collision energies for an unselective acquisition of full mass range scans in so called all-ion-fragmentation methods (AIF, MS<sup>E</sup>, DIA, SWATH). Post-acquisition software is then required to align the retention time coordinates of the precursor ions and the corresponding fragment ions to extract useful mass spectral information to allow for metabolite identification. The elemental formula and accurate mass of the unchanged (parent) drug is known and serves as a starting point to calculate possible masses of drug metabolites by changing the elemental composition introduced by known biotransformations. Unexpected

metabolites, however, are difficult to account for and might still require radioactive labeling of the drug. Often, this step is undertaken at a later stage in a human ADME study.

HRMS can also be used to compare metabolite profiles from different biological matrices and to assess the qualitative metabolism across species as well as for relative exposure comparisons. These approaches will be explained later.

### 2.3 Nuclear magnetic resonance spectroscopy

NMR spectroscopy is a valuable tool for understanding and characterizing drug metabolism. Its key strength is the capability to elucidate unambiguously the chemical structure of metabolites. The technique is based on measuring local distortions of a magnetic field induced by atomic nuclei possessing a spin, such as  $^1\text{H}$ ,  $^{13}\text{C}$ ,  $^{15}\text{N}$ , or  $^{19}\text{F}$ . This enables the structural elucidation of metabolites based on the molecular formula, which is usually determined by HRMS and quantification of parent and metabolites. The most commonly deployed NMR approaches in drug metabolism studies rely on  $^1\text{H}$  NMR and for fluorinated molecules  $^{19}\text{F}$  NMR [41, 42]. The advantage of  $^{19}\text{F}$  NMR is that spectra of fluorine containing drugs or metabolites could be acquired with almost no interfering background signals in biological matrices, because endogenous fluorinated compounds are virtually absent.

Combining offline HPLC with NMR spectroscopy enables the isolation of major metabolites from *in vitro* experiments for determining the exact site of biotransformation. Structure elucidation by NMR spectroscopy typically requires quantities of the metabolite in the range of 10–100  $\mu\text{g}$ . To achieve this often biosynthesis from the parent drug needs to be scaled up in an accessible and human relevant *in vitro* system. In particular, it is important to ensure that the metabolite elucidated actually corresponds to the metabolite formed in humans *in vivo*. This could be particularly challenging when the *in vivo* metabolite is human specific and if the availability of biocatalysis systems (e.g., recombinant enzymes) is limited [43].

Using cryoprobe technology, which cools down the sample before NMR analysis to  $-253^\circ\text{C}$ , it leads to a significant increase in both sensitivity and throughput. This methodology has been successfully applied to drug metabolites in human plasma. The observed limit of quantification was reported at 10 ng/mL [44]. Those findings demonstrate that the power of NMR is not only limited to the structural characterization of purified metabolites but also readily applicable to early quantitative metabolite analysis [41, 44, 45]. In contrast to mass spectrometry, where the molecular composition influences the detectability (see below), the NMR response of atomic nuclei is directly comparable, even between structurally different molecules [45].

An example of how a drug metabolism study can benefit from NMR is the study of GW766994. The major circulating metabolite in humans, which comprised 74% of drug-related material in plasma after multiple dosing, was only discovered by NMR. It was initially detected by neither LC-MS nor radio-HPLC due to loss of the radiolabel. This example highlights the benefit of using multiple orthogonal analytical technologies [44, 46].

Similar to LC-MS, there are applications of LC-NMR, including an *in-line* chromatographic separation [47]. The advantage is a continuous measurement of multiple analyte without fractionation and injection protocols. The disadvantages are the limitation to analytical scale HPLC and lower injection amounts which correspond to lower sensitivity. While NMR is

a powerful and valuable tool to elucidate the structure of drug metabolites, in order for LC-NMR to become more important in drug metabolism studies, technological improvements in sensitivity need to occur.

## 2.4 Accelerator mass spectrometry and cavity ring-down spectroscopy

Accelerator mass spectrometry allows the very sensitive measurement of  $^{14}\text{C}$  and other radioisotopes in an analytical sample. The technology is based on sample graphitization followed by combustion and detection of the ratio between  $^{14}\text{C}$  and  $^{12}\text{C}$  by accelerating ions to extraordinarily high kinetic energies in a nuclear particle accelerator where they reach several percents of the speed of light. An array of guiding magnets and gaseous ionization detectors (silicon surface-barrier detectors, ionization chambers, and/or time-of-flight telescopes) allow separating the compound of interest from matrix interferences and counting  $^{14}\text{C}$  atoms at femtomolar levels [32]. This incredible sensitivity far exceeds any other radio-analytical method, such as liquid or solid scintillation counting. AMS applies to several elemental isotopes. However, human mass balance studies are almost exclusively carried out with  $^{14}\text{C}$  labeled compounds [48, 49]. In the context of drug metabolism studies AMS is applied in two different ways: first, AMS is used for the direct analysis of total  $^{14}\text{C}$  in a sample (e.g., plasma) and second, for the analysis of specific  $^{14}\text{C}$  containing analytes which are isolated by a separate offline separation method (e.g., HPLC). There have been efforts to propose harmonized guidelines for such quantitative bioanalytical methods combining LC with AMS [49].

An example of how AMS can add unique data to a drug metabolism study is the profiling of dalcetrapib [35]. This prodrug undergoes rapid conversion *in vivo* to its pharmacologically active metabolite M1. However, due to the chemical properties of M1, there are several different variants collectively termed the dalcetrapib active form, all of which undergo further metabolism on their own. In the human mass balance study, radio-HPLC lacked the sensitivity to detect low abundant metabolites. To overcome that limitation, an “LC + AMS” analysis was performed. This led to the identification of over 80 metabolites, however, none of them being major according to the MIST guidelines. Without AMS, it would have not been possible to confirm the absence of a metabolite exceeding 10% of drug-related material in circulation for this highly metabolized drug.

The limiting factors of AMS are the demanding infrastructure for the instrument, the expensive acquisition, and high operating costs. An initiative at the ETH Zürich to reduce the footprint of AMS instruments led to the development of a benchtop AMS instrument, which is commercially available [50]. So far, it was mainly used for radioisotope dating; however, reports are evaluating the application in drug metabolism studies [51].

An alternative technology not yet widely used but of great interest to the drug metabolism community is the quantification of  $^{14}\text{C}$  by cavity ring-down spectroscopy (CRDS) [52–54]. Recent developments in laser and optical detector technology have enabled this spectroscopic method to emerge as an alternative to AMS. CRDS appears to overcome some of the limitations of AMS and might enable sufficiently sensitive  $^{14}\text{C}$  measurements without extensive requirements for laboratory infrastructure as for AMS. The  $^{14}\text{C}$  labeled analyte is vaporized to  $^{14}\text{CO}_2$  and injected into an optical cavity, lined with highly reflective mirrors. The laser light



passes through the cavity and gets gradually absorbed by the gaseous sample. After shutting off the laser, the “ring-down” event manifests as the time it takes for the laser light to decay in the cavity. The composition of the sample influences this decay rate and allows for the quantification of the gas concentration. Recently, a successful application of CRDS has been reported for a drug disposition study [33]. With time and commercialization of the technology, it is expected to encounter CRDS data in MIST assessments as well.

## 2.5 Post-acquisition software tools for metabolite identification

There are several post-acquisition software tools available to facilitate the interrogation of mass spectrometry data and the detection of metabolites in complex matrices, including plasma, urine, feces, and bile. These tools are available within most software packages of high-resolution mass spectrometers. Chapters 2 and 3 provide detailed insights into this topic. We will briefly discuss mass defect filtering (MDF), background subtraction, and the advantages of using MS/MS spectra to identify metabolites.

MDF is an application for discriminating masses of drug-related metabolites (originating from expected and unexpected biotransformations) from potential false-positive analytes in complex biological matrices. It is based on the assumption that most metabolites have delta mass differences within 250 mDa of the parent drug decimals. As a rule of thumb, however, common phase I and phase II metabolites typically fall within the 50 mDa range. Mass spectrometry analysts typically apply multiple MDFs to identify potential various classes of metabolites. For further reading, Zhang and coworkers provided a detailed description of the use of MDF for drug metabolite identification by high-resolution mass spectrometry [55].

Background subtraction is another technique often employed to enable the detection of metabolites in complex matrices [37, 56–59]. In a control sample, the most likely baseline is estimated in a small-time window by defining what is expected to be the highest and lowest intensity values for the background. Then, the estimated and regressed baseline is subtracted from the spectrum of interest containing the analyte and or analyte-related elements. Although this technique is very useful, special care must be taken so that metabolites with relatively low abundances are not discarded [37].

The use of software to facilitate the interpretation of MS/MS spectra is also a widely employed approach. Many software tools allow for the prediction of fragment ions of both parent drug and respective putative metabolites and have algorithms based on chemical fragmentation rules, isotope patterns, and accurate mass of fragment ions, based on molecular formulae, just to name a few. By comparison of MS fragmentation fingerprints of the parent drug and the metabolite, the conservation of characteristic molecular fragments or their shift after metabolic alteration assists the regional identification of drug biotransformations.

The process of metabolite identification has become largely facilitated and partly automated by cheminformatics approaches such as knowledge-based metabolite prediction using, for example, Meteor, MetaDrug, MetaSite, and StarDrop. Software-guided approaches like Mass-MetaSite have been introduced for the automated ranked output of metabolite structures based on the combination of metabolite prediction and interrogation of analytical mass spectrometric data. These approaches are encouraging developments moving away from a sample focused compound-per-compound approach to automated, structure-driven



generic workflows for metabolite identification and structural characterization and are especially valuable for the early phases of drug discovery. Still, unsupervised metabolite identification cannot compete with or replace expert user manual data interpretation [60].

## 2.6 Semiquantitative and quantitative assessment of metabolite coverage

In early development, routine quantification of the metabolite is extremely beneficial for the optimization of a drug. Unfortunately, reference standards and radioisotope labeled compounds are typically not available at such early stages of a project. There is a great need for a semiquantitative approach that provides sufficient quantitative accuracy to allow meaningful decisions during drug development. The routinely applied HRMS method would provide a perfect tool for this challenge. Unfortunately, the mass spectrometric signal response of ionized analytes is not truly quantitative. Several factors can influence the detectability and peak area of a compound by MS [61]. First, the ionization efficiency through electrospray ionization can vary even for structurally similar molecules. Second, the ability to traverse through the ion optics and subsequent effect on the detector may differ. Third, the biological background of co-eluting matrix molecules may influence both ionization and ion transfer. Lastly, the chemical composition of the mobile phase is known to greatly modify all these factors. Empirical findings have shown that the response factor variation of parent and metabolites may range from 0.01 to almost 10-fold [61]. Obviously, this error margin complicates quantitative assessment.

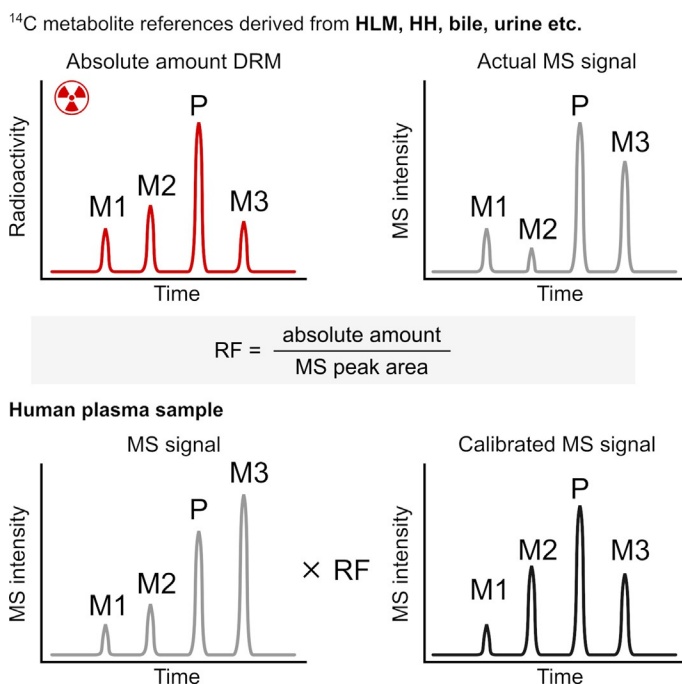
Despite limitations, HRMS has proved to be a valuable tool to assess metabolite coverage *in vitro* and preclinical animal studies in a semiquantitative manner [30]. To do so, the integrated peak area of the metabolite is normalized to the peak area of the parent molecule [61]. This results in a semiquantitative overview of the metabolite profile and can support early decision-making. However, the inherent inaccuracy of this method should be always kept in mind.

## 2.7 Calibrator approaches

Closely related to the comparison of MS responses of metabolite and parent is the use of the UV response signal for the same purpose. Similarly, as described above, the percentage of the metabolite is estimated based on the UV responses of metabolites and parent drug. It relies on the assumption that there is a linear relationship between absorbance and concentration for each analyte of interest. This approach is however compromised by the likely non-equimolar response of drug and metabolites as well as the unknown extraction recovery. Besides, many other non-related components may be present in the complex matrix with a similar retention time and absorbance wavelength which may induce potential estimation errors. Another drawback is the poor sensitivity provided by UV detection. However, in certain cases where certain molecules absorb at a particular frequency which differentiates them from background noise and/or matrix interferences, this can be a very powerful tool to identify drug-related metabolites.

Another method available for the semiquantitative determination of metabolites is by the  $^{14}\text{C}$  calibrator approach [27, 28]. Assuming radioactive standards of parent drug are available, and several metabolites are generated *in vitro* or *in vivo*, the concentration of metabolite(s)

**FIG. 3**  $^{14}\text{C}$ -calibrator approach:  $^{14}\text{C}$ -metabolites are generated in vitro (e.g., by human or animal liver microsomes or hepatocytes) or in vivo (e.g., excreta or plasma from animal ADME studies). A response factor (RF) is derived from the ratio of the MS signal response (metabolite/parent) to the absolute amount determined by the radioactive signal response (metabolite/parent). The MS signal in the human plasma sample is corrected using the response factor to estimate the concentration of metabolite(s).



can be estimated based on the response factor from the ratio of radioactivity response (metabolite/parent) to the corresponding MS response (metabolite/parent) [27] (Fig. 3). This approach improves the accuracy of metabolite estimation compared to the integration of MS peaks. However, for many drug candidates, the generation of all human metabolites in sufficient amounts for such calibration is challenging and in many cases not feasible.

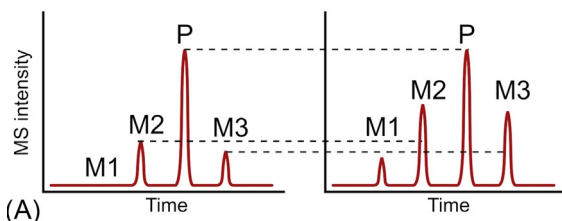
## 2.8 Mixed-matrix approach for direct comparison of metabolite levels in human and animal plasma samples and AUC pooling

The exposure of metabolites in nonradioactive studies can be analyzed by direct comparison of MS responses in animal versus human plasma. For matrix effects to be compensated, human plasma samples can be mixed with blank animal plasma and vice versa [17, 24–26] (Fig. 4A). Besides, for MIST assessment purposes, typically AUC-pooled plasma samples of the human multiple ascending doses (MAD) at the anticipated therapeutic dose cohort are analyzed. MS peak areas are then compared between human AUC-pooled plasma samples [62, 63] and animal AUC-pooled plasma samples from relevant toxicological studies (Fig. 4B). The exposure achieved at the MTD in the animal study could be compared to the maximum exposure in humans at the therapeutic dose. However, depending on the type of toxicity observed at the MTD in animals (case by case, e.g., when considered not monitorable in humans or posing unacceptable risks), comparing exposure at the NOAEL dose might be warranted. This approach enables an overall perspective of the metabolic profile of the cohort being studied and not necessarily individual subjects. The “Hamilton” AUC-pooling

### Cross-species comparison

**Human plasma sample**  
(therapeutic dose)  
+ animal blank plasma

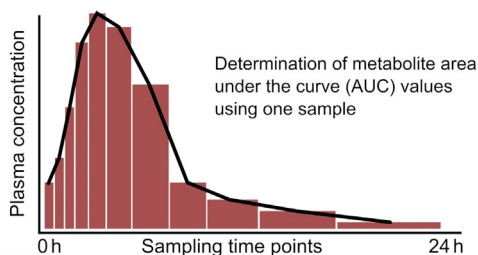
**Animal plasma sample**  
(maximum tolerated dose)  
+ human blank plasma



(A)

**FIG. 4** (A) Cross species comparison by cross spiking of human and animal plasma samples to compensate for matrix effects. Human plasma samples are mixed with blank animal plasma and vice versa. (B) Hamilton AUC-pooling approach: aliquots of plasma samples from different pharmacokinetic time points are pooled in a time-proportionate manner to yield one sample in which the parent drug and metabolite concentrations are proportional to the AUC.

### AUC pooling



(B)

approach is considered robust and reproducible and is often adopted by metabolite profiling scientists carrying out MIST assessments [62, 63] (Fig. 4B).

## 2.9 Bioanalytical methods

Once all metabolites have been cataloged, a rapid, robust, and the highly quantitative method is needed for major human metabolites to efficiently analyze samples from late-stage pharmacokinetic studies. LC-MS is the method of choice, and the availability of reference compounds for both parent and metabolites allows absolute quantification through calibration of the ion response. The instrument of choice is most often a triple-quadrupole MS (QqQ) or quadrupole ion trap (Q-Trap) instrument. They offer adequate specificity and sensitivity and can be operated at higher sampling rates than, e.g., HRMS instruments, and thus acquire more data points per chromatographic peak. [Chapter 1](#) further details the bioanalysis of drugs and metabolites.

## 3 A typical MIST strategy

Supporting drug development programs regarding the MIST guidance, the key challenge for drug metabolism scientists is to find out which metabolites represent greater than 10% of drug-related systemic exposure at steady state as early as feasible to prevent development

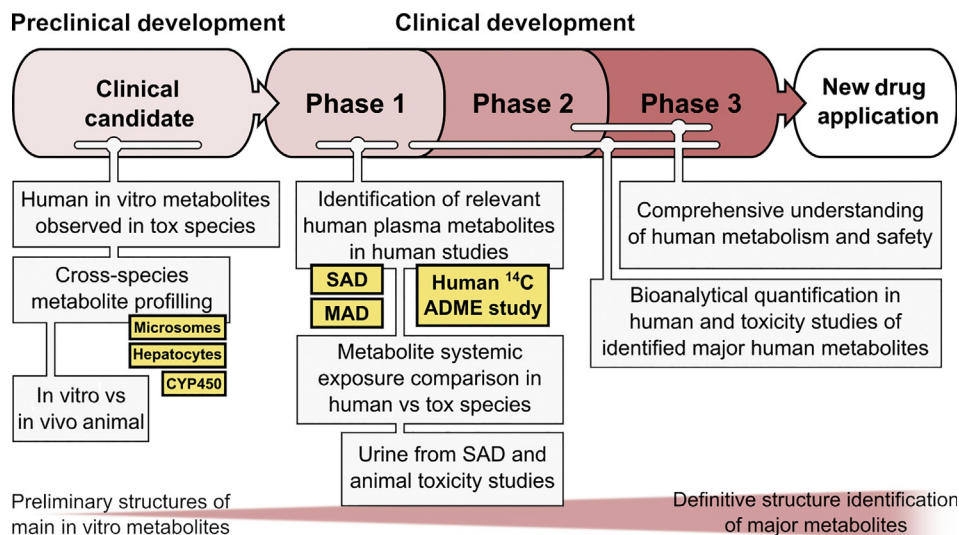


**FIG. 5** Throughout all typical stages of preclinical and clinical development of a small molecule drug candidate, drug metabolism studies are employed with the goal to characterize the relevant human drug metabolites as early as possible. The most important studies informing the MIST assessment are highlighted in bold boxes. The understanding of metabolism as well as the required level of detail, e.g., for metabolite structure identification increases as the drug advances from clinical candidate to medicine.

and marketing delays [9]. For this reason, metabolite safety assessment needs to be considered throughout the different stages of drug discovery and development. Pharmaceutical companies need to develop strategies for how and when to assess metabolite coverage and safety [13, 14, 16–22, 30].

We will describe here a typical MIST assessment strategy in three stages: (1) before entering into human studies, (2) during Phase 1 studies, and (3) before the start of Phase 3 clinical studies (Fig. 5). In addition to these generic considerations, of course, there are project-specific considerations for each development compound depending on characteristics, like potency of the compound, experiences with compounds from similar chemical classes, and the acquired knowledge in preclinical studies about potency and safety. Also, for certain serious therapeutic indications, like life-threatening or serious diseases (e.g., advanced cancer, resistant HIV infection, and congenital enzyme deficiency diseases) without current effective therapy, different strategic considerations may apply and should be evaluated on a case-by-case basis [10, 11, 64, 65].

### 3.1 Stage 1. Before entering human studies

Before a new drug candidate is administered to a human, its metabolism is typically studied in vitro (human and animals) and in vivo (animals) to support the selection of the animal species used in toxicity studies based on the likelihood of coverage of expected human metabolites. A variety of in vitro systems are available, ranging from recombinant enzymes, subcellular fractions like S9 or liver (or less routinely applied, gut, kidney, or

lung) microsomes to hepatocytes [66]. A typical approach would compare the metabolism of a drug candidate in human liver microsomes and cryopreserved hepatocytes with the metabolism observed in animal species which are used for safety testing. Following LC-MS analysis, metabolites are identified and compared across species (Fig. 6). In some cases, already at this stage, full structure elucidation of metabolites by (bio)synthesis and NMR might be warranted. The in vitro metabolite profiles are then further compared to in vivo animal plasma metabolite profiles to establish a qualitative in vitro-in vivo correlation. When translating this information to human, however, one has to keep in mind that differences across species in the plasma metabolite pattern can be due not only to different formation of metabolites (which would be covered by the in vitro experiments) but also to different clearance of the metabolites from circulation, different rate of efflux from liver to blood, and different volume of distribution [67]. Additionally, the metabolite pattern observed in human hepatic preparations might be very valuable to qualify which

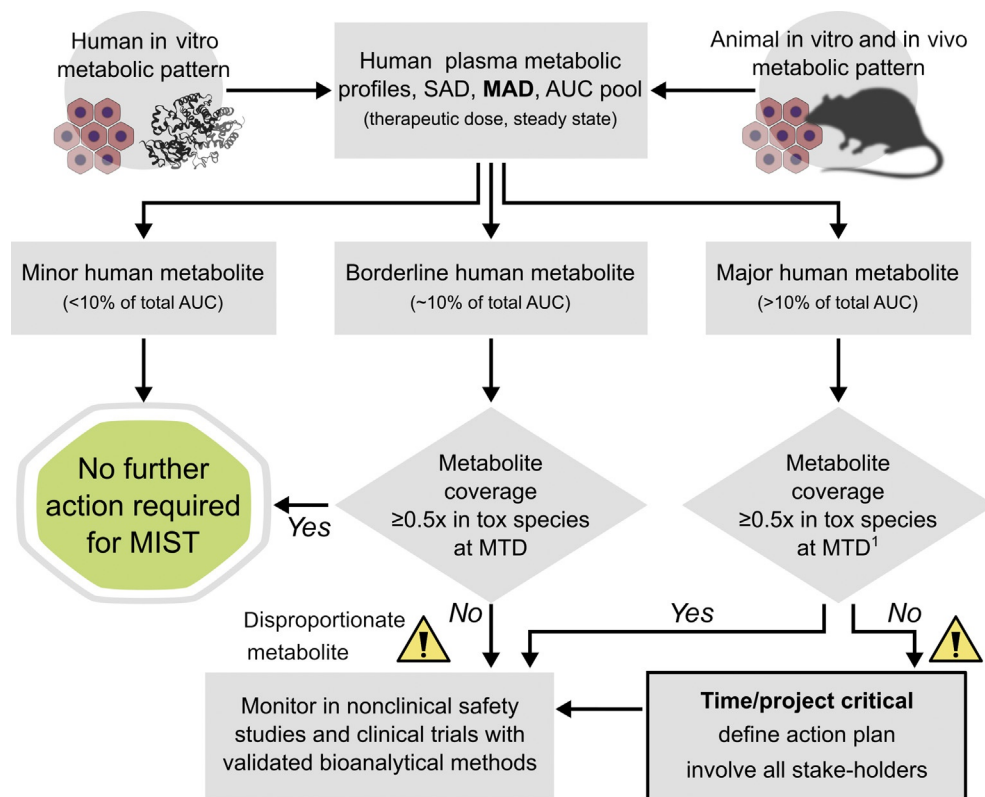


FIG. 6 Typical MIST strategy, starting with in vitro and animal in vivo metabolite assessment. The key stage for MIST assessment of a new drug candidate is in clinical Phase 1 when human plasma samples become available (from first-in-human SAD and MAD studies) for identification and assessment of human circulating metabolites. <sup>1</sup>ICH Q&A: "... when a metabolite composes the majority of the total human exposure, it is appropriate for exposure to the metabolite in animals to exceed that in humans."

metabolites are formed, but the quantitative correlation between *in vitro* and *in vivo* plasma metabolites in humans is often poor. Therefore, a reliable quantitative prediction of MIST-relevant circulating human metabolites from standard *in vitro* and animal *in vivo* data is currently not feasible. Another complicating factor is the increase of low-clearance compounds in pharmaceutical portfolios [68], which makes metabolite identification and evaluation of metabolite relevance more challenging.

Still, the assessment of the *in vitro* drug metabolism early on increases the likelihood of choosing the right species for safety studies that form the metabolites that are relevant to human.

### 3.2 Stage 2. During Phase 1 human clinical studies

Phase 1 human clinical studies are key for MIST assessment of a new drug candidate because plasma samples from Phase 1 clinical studies offer the first opportunity for human circulating metabolites to be identified (Fig. 6). By combining HRMS data-acquisition with post-acquisition software and data-mining technologies, plasma metabolites are identified, typically in single and/or multiple ascending dose studies (SAD and MAD) in human healthy volunteers. Potential human-relevant metabolites are identified, and metabolite exposure at steady state at the anticipated therapeutic dose level is assessed in comparison to metabolite exposure in animals (MTD group). To avoid delays in drug development, key decisions for metabolite safety assessment have to be made at this stage, even though it often remains challenging to determine whether a metabolite exceeds 10% of drug-related material and usually a combination of different methods needs to be applied on a case-by-case basis.

Typically, the first important step is to get an overview of the main drug-related components in circulation in humans from the SAD study. Most useful for HRMS are samples from the highest dose cohort and metabolite identification could be performed on cross-subject plasma pools representative of the study population for individual time points. When later time points are included in the analysis, metabolites with a longer half-life might be observed.

The identification and peak integration of all relevant metabolites by HRMS will then be extended to AUC-pooled plasma samples originating from the human MAD at the anticipated therapeutic dose cohort. Despite the limitations of HRMS described above, this enables the drug metabolism scientist to get an overview of the metabolite profile. Subsequently, the semiquantitative determination of metabolites is refined, for example by the  $^{14}\text{C}$  calibrator approach [27, 28]. This approach improves the accuracy of metabolite estimation compared to the integration of MS peaks. Besides, the exposure of metabolites is analyzed by direct comparison of MS peak areas in animal versus human plasma. For matrix effects to be compensated, human plasma samples can be mixed with blank animal plasma and vice versa [17, 24–26]. Other technologies like NMR might be also considered at this stage [44, 46]. Once all relevant metabolites have been cataloged, absolute quantities of all major human metabolites in circulation are determined by bioanalytical quantitation using authentic reference standards if needed.

In general, total metabolite concentrations are considered for exposure assessment and safety coverage should ultimately be assured for all major human metabolites (>10% of



drug-related systemic exposure) in at least one species used in general toxicity, reproductive toxicity, and carcinogenicity, respectively. For disproportionate human metabolites that are not adequately covered in safety studies carried out in nonclinical species, additional safety studies might be necessary. These can be either safety studies with the drug candidate in additional animal species that form the metabolite at adequate exposure levels, or safety studies where the disproportionate metabolite is synthesized and directly administered to the animals. Alternatively, the parent compound could be fortified with an appropriate amount of the synthesized metabolite to achieve higher systemic exposures of the metabolite in animals. Apart from the regulatory compliant demonstration of adequate metabolite exposure in nonclinical species, appropriate follow-up activities concerning clearance pathways and drug-drug interaction (DDI) potential of metabolites need to be defined upon the availability of human metabolite exposure data. The FDA draft guidance on in vitro DDI studies suggests that circulating metabolites at 25% of parent exposure for metabolites that are less polar than the parent drug and at 100% of parent exposure for metabolites that are more polar than the parent drug should be evaluated for in vitro DDI potential as inhibitor [69].

### 3.3 Stage 3. Before the start of Phase 3 human clinical studies

According to the FDA and ICH guidance, demonstration of adequate metabolite coverage in nonclinical species is required before exposing large numbers of human subjects or long treatment durations (typically before Phase 3). Consequently, by the end of Phase 2, all necessary metabolite assessments should be completed. The human metabolism package is complemented with the human radiolabel ADME study which is typically conducted during Phase 2. The human radiolabel ADME study provides all details on the fate of the total drug-related material. Comprehensive metabolite profiles are obtained in human plasma and excreta, and it is ensured that no metabolites have escaped identification. Even though the human radiolabel ADME study is typically a single-dose study, it can under certain situations still confirm which metabolites exceed 10% of systemic exposure [21]. Besides, the human radiolabel ADME study delivers important and definitive information on the major biotransformation pathways for drug elimination. Together with the knowledge which enzymes are responsible for these major pathway this is critical information to define the required clinical DDI program [69]. Further reading on important key aspects as well as limitations of radiolabel ADME studies in drug development could be found in a review of Penner et al. [70].

## 4 Metabolite safety assessment beyond the MIST guidance documents

The MIST guidance documents provide information on circulating plasma metabolites formed by phase I metabolism. Under the assumption that conjugate-formation is typically enhancing excretion and is not generating pharmacological or toxicological relevant metabolites, only limited regulatory guidance exists for such metabolites. However, also such metabolites may elicit safety concern, and conjugated and excretory metabolites may lead to



kidney or bile duct toxicity and warrant safety assessment [9, 71]. One example is the stable glucuronide metabolite of gemfibrozil which would not per se fall under MIST assessment considerations according to the current regulatory guidance documents. This metabolite, however, was linked to severe safety issues (including fatalities) by inhibiting cerivastatin clearance via CYP2C8 and, to a lesser extent, by inhibiting the organic anion transporter [72, 73], resulting in significant DDI issues.

Reactive metabolites typically are not found in circulation due to their reactivity and consequently short half-lives. In some cases, downstream detoxification products of reactive metabolites like glutathione conjugates and their corresponding cysteinylglycine, cysteine, or *N*-acetylcysteine conjugates may be detected in excreta. Since there is circumstantial evidence that chemically reactive metabolites play a key role for the manifestation of drug-induced idiosyncratic toxicities, such as drug-induced liver injury (DILI), skin rashes, and blood dyscrasias, most pharmaceutical companies use in vitro screens to minimize the risk of chemically reactive metabolite formation of new drug candidates [74–78].

## 5 Conclusion and future outlook

The purpose of any MIST effort must be the evaluation of human circulating metabolites with regard to safety and efficacy. Therefore, a comprehensive understanding of the metabolic fate of new medicines is required to assure appropriate safety profiling before the introduction into a vulnerable patient population. Based on considerations such as dose, duration of treatment, target indication, and clinical benefit, this assessment should be based on individual cases rather than on the technical availability of sophisticated tools or stringent rules. Also, numerous case examples have been shared between pharmaceutical companies, academia, and regulators highlighting the importance of such case-by-case evaluations [9, 23, 30, 79]. Besides, considerations such as contribution to pharmacological activity and potential drug-drug interactions might become drivers for MIST assessment based on absolute rather than relative exposures, for example, a 10% metabolite of a highly potent drug administered at 1 mg daily dose is less likely to elicit off-target DDI compared to a 10% metabolite of a high dose drug administered at 100 mg because in the latter situation it might be more likely that the metabolite reaches concentrations relevant for DDI. Also, consideration such as differences in plasma protein binding between metabolites and species may influence the safety evaluation of human metabolites.

To elicit a pharmacological or toxicological response at a biochemical target, a drug must reach the target tissue first. In the context of MIST, plasma is considered as a surrogate for relevant drug and metabolite concentrations in tissues. However, in some cases the pharmacokinetic behavior of metabolites might differ significantly compared to the parent drug, e.g., metabolite formation might be restricted to certain tissues, metabolites might accumulate in a certain tissue, plasma protein binding, and transporters properties might be different, etc. Over the past years, in situ mass spectrometry-based imaging technologies emerged, which enable discreet localization of drugs and their metabolites in tissue. Mainly MALDI-HRMS imaging proved to be a powerful technology to provide information on drug and metabolite distribution within target and off-target tissues [80, 81]. Related attempts, e.g., based on

DESI-MS or secondary-ion mass spectrometry (SIMS), currently undergo rapid developments and might allow potentially even spatial resolutions down to the single-cell level in the near future [82]. One major limitation of tissue imaging in the context of safety assessment, however, remains the restriction to animal tissue in many cases, and the very limited access to human tissue biopsies.

## References

- [1] T.A. Baillie, et al., Drug metabolites in safety testing, *Toxicol. Appl. Pharmacol.* 182 (3) (2002) 188–196.
- [2] K.L. Hastings, et al., Drug metabolites in safety testing, *Toxicol. Appl. Pharmacol.* 190 (1) (2003) 91–92. author reply 93–4.
- [3] D.A. Smith, R.S. Obach, Seeing through the mist: abundance versus percentage. Commentary on metabolites in safety testing, *Drug Metab. Dispos.* 33 (10) (2005) 1409–1417.
- [4] D.A. Smith, R.S. Obach, Metabolites and safety: what are the concerns, and how should we address them? *Chem. Res. Toxicol.* 19 (12) (2006) 1570–1579.
- [5] K.L. Davis-Bruno, A. Atrakchi, A regulatory perspective on issues and approaches in characterizing human metabolites, *Chem. Res. Toxicol.* 19 (12) (2006) 1561–1563.
- [6] W.G. Humphreys, S.E. Unger, Safety assessment of drug metabolites: characterization of chemically stable metabolites, *Chem. Res. Toxicol.* 19 (12) (2006) 1564–1569.
- [7] T. Prueksaritanont, J.H. Lin, T.A. Baillie, Complicating factors in safety testing of drug metabolites: kinetic differences between generated and preformed metabolites, *Toxicol. Appl. Pharmacol.* 217 (2) (2006) 143–152.
- [8] W.W. Ku, et al., Strategy for genotoxicity testing—metabolic considerations, *Mutat. Res.* 627 (1) (2007) 59–77.
- [9] FDA, Guidance for Industry: Safety Testing of Drug Metabolites, Food and Drug Administration, US Department of Health and Human Services, Center for Drug Evaluation and Research, Silver Spring, MD, 2016.
- [10] ICH, M3(R2) Nonclinical Safety Studies for the Conduct of Human Clinical Trials and Marketing Authorization for Pharmaceuticals, 2010.
- [11] ICH, M3(R2) Nonclinical Safety Studies for the Conduct of Human Clinical Trials and Marketing Authorization for Pharmaceuticals. Questions and Answers(R2), 2013.
- [12] CFDA, Guidance for Industry on Safety Testing of Drug Metabolites, 2012.
- [13] L. Leclercq, et al., Which human metabolites have we MIST? Retrospective analysis, practical aspects, and perspectives for metabolite identification and quantification in pharmaceutical development, *Chem. Res. Toxicol.* 22 (2) (2009) 280–293.
- [14] D. Walker, et al., A holistic strategy for characterizing the safety of metabolites through drug discovery and development, *Chem. Res. Toxicol.* 22 (10) (2009) 1653–1662.
- [15] A.H. Atrakchi, Interpretation and considerations on the safety evaluation of human drug metabolites, *Chem. Res. Toxicol.* 22 (7) (2009) 1217–1220.
- [16] H. Yu, D. Bischoff, D. Tweedie, Challenges and solutions to metabolites in safety testing: impact of the international conference on harmonization M3(R2) guidance, *Expert Opin. Drug Metab. Toxicol.* 6 (12) (2010) 1539–1549.
- [17] S. Ma, et al., Determination of exposure multiples of human metabolites for MIST assessment in preclinical safety species without using reference standards or radiolabeled compounds, *Chem. Res. Toxicol.* 23 (12) (2010) 1871–1873.
- [18] S. Ma, S.K. Chowdhury, Analytical strategies for assessment of human metabolites in preclinical safety testing, *Anal. Chem.* 83 (13) (2011) 5028–5036.
- [19] H. Gao, R.S. Obach, Addressing MIST (metabolites in safety testing): bioanalytical approaches to address metabolite exposures in humans and animals, *Curr. Drug Metab.* 12 (6) (2011) 578–586.
- [20] A.N. Nedderman, et al., From definition to implementation: a cross-industry perspective of past, current and future MIST strategies, *Xenobiotica* 41 (8) (2011) 605–622.
- [21] C. Prakash, et al., Assessment of exposure of metabolites in preclinical species and humans at steady state from the single-dose radiolabeled absorption, distribution, metabolism, and excretion studies: a case study, *Drug Metab. Dispos.* 40 (7) (2012) 1308–1320.

- [22] H. Gao, et al., Meeting report: metabolites in safety testing (MIST) symposium-safety assessment of human metabolites: what's REALLY necessary to ascertain exposure coverage in safety tests? *AAPS J.* 15 (4) (2013) 970–973.
- [23] D. Luffer-Atlas, A. Atrakchi, A decade of drug metabolite safety testing: industry and regulatory shared learning, *Expert Opin. Drug Metab. Toxicol.* 13 (9) (2017) 897–900.
- [24] H. Gao, S. Deng, R.S. Obach, A simple liquid chromatography-tandem mass spectrometry method to determine relative plasma exposures of drug metabolites across species for metabolite safety assessments, *Drug Metab. Dispos.* 38 (12) (2010) 2147–2156.
- [25] Z. Tong, et al., Metabolism of vabicaserin in mice, rats, dogs, monkeys, and humans, *Drug Metab. Dispos.* 38 (12) (2010) 2266–2277.
- [26] R.H. Takahashi, et al., Mixed matrix method provides a reliable metabolite exposure comparison for assessment of metabolites in safety testing (MIST), *Drug Metab. Lett.* 11 (1) (2017) 21–28.
- [27] C. Yu, et al., A rapid method for quantitatively estimating metabolites in human plasma in the absence of synthetic standards using a combination of liquid chromatography/mass spectrometry and radiometric detection, *Rapid Commun. Mass Spectrom.* 21 (4) (2007) 497–502.
- [28] L. Xu, et al., Metabolism and excretion of 6-chloro-9-(4-methoxy-3,5-dimethylpyridin-2-ylmethyl)-9H-purin-2-ylamine, an HSP90 inhibitor, in rats and dogs and assessment of its metabolic profile in plasma of humans, *Drug Metab. Dispos.* 41 (12) (2013) 2133–2147.
- [29] H. Gao, R.S. Obach, Data-driven approach for cross-species comparative metabolite exposure assessment: how to establish fundamental bioanalytical parameters for the peak area ratio method, *Bioanalysis* 6 (5) (2014) 641–650.
- [30] S. Schadt, et al., A decade in the MIST: learnings from investigations of drug metabolites in drug development under the “metabolites in safety testing” regulatory guidance, *Drug Metab. Dispos.* 46 (6) (2018) 865–878.
- [31] P. Swart, et al., The impact of early human data on clinical development: there is time to win, *Drug Discov. Today* 21 (6) (2016) 873–879.
- [32] E. van Duijn, et al., Automated combustion accelerator mass spectrometry for the analysis of biomedical samples in the low attomole range, *Anal. Chem.* 86 (15) (2014) 7635–7641.
- [33] N.A. Kratochwil, et al., Nanotracing and cavity-ring down spectroscopy: a new ultrasensitive approach in large molecule drug disposition studies, *PLoS One* 13 (10) (2018) e0205435.
- [34] G.J. Bruin, et al., A microplate solid scintillation counter as a radioactivity detector for high performance liquid chromatography in drug metabolism: validation and applications, *J. Chromatogr. A* 1133 (1–2) (2006) 184–194.
- [35] C. Husser, et al., Profiling of dalcetrapib metabolites in human plasma by accelerator mass spectrometry and investigation of the free phenothiol by derivatisation with methylacrylate, *J. Pharm. Biomed. Anal.* 152 (2018) 143–154.
- [36] H.K. Lim, et al., Metabolite identification by data-dependent accurate mass spectrometric analysis at resolving power of 60,000 in external calibration mode using an LTQ/Orbitrap, *Rapid Commun. Mass Spectrom.* 21 (12) (2007) 1821–1832.
- [37] M. Zhu, H. Zhang, W.G. Humphreys, Drug metabolite profiling and identification by high-resolution mass spectrometry, *J. Biol. Chem.* 286 (29) (2011) 25419–25425.
- [38] J.L. Bushee, U.A. Argikar, An experimental approach to enhance precursor ion fragmentation for metabolite identification studies: application of dual collision cells in an orbital trap, *Rapid Commun. Mass Spectrom.* 25 (10) (2011) 1356–1362.
- [39] S.J. Perry, S. Nasz, M. Saeed, A high-resolution accurate mass (HR/AM) approach to identification, profiling and characterization of in vitro nefazodone metabolites using a hybrid quadrupole Orbitrap (Q-Exactive), *Rapid Commun. Mass Spectrom.* 29 (17) (2015) 1545–1555.
- [40] M. Wrona, et al., 'All-in-one' analysis for metabolite identification using liquid chromatography/hybrid quadrupole time-of-flight mass spectrometry with collision energy switching, *Rapid Commun. Mass Spectrom.* 19 (18) (2005) 2597–2602.
- [41] A.D. James, et al., Comparison of <sup>19</sup>F NMR and <sup>14</sup>C measurements for the assessment of ADME of BYL719 (Alpelisib) in humans, *Drug Metab. Dispos.* 45 (8) (2017) 900–907.
- [42] J.C. Lindon, I.D. Wilson, <sup>19</sup>F NMR spectroscopy: applications in pharmaceutical studies, *eMagRes* 4 (2) (2015) 189–196.
- [43] G.S. Walker, et al., Biosynthesis of drug metabolites and quantitation using NMR spectroscopy for use in pharmacologic and drug metabolism studies, *Drug Metab. Dispos.* 42 (10) (2014) 1627–1639.

- [44] G.J. Dear, et al., Evaluation of preparative high performance liquid chromatography and cryoprobe-nuclear magnetic resonance spectroscopy for the early quantitative estimation of drug metabolites in human plasma, *J. Chromatogr. B Anal. Technol. Biomed. Life Sci.* 876 (2) (2008) 182–190.
- [45] G.K. Webster, S. Kumar, Expanding the analytical toolbox: pharmaceutical application of quantitative NMR, *Anal. Chem.* 86 (23) (2014) 11474–11480.
- [46] J. Bloomer, C. Beaumont, G.J. Dear, S. North, G. Young, The value of metabolite identification and quantification in clinical studies. Some case studies enabling early assessment of safety in humans: GlaxoSmithKline, in: S.L. Iverson, D.A. Smith (Eds.), *Metabolite Safety in Drug Development*, Wiley, 2016, pp. 275–291.
- [47] G.S. Walker, T.N. O'Connell, Comparison of LC-NMR and conventional NMR for structure elucidation in drug metabolism studies, *Expert Opin. Drug Metab. Toxicol.* 4 (10) (2008) 1295–1305.
- [48] L.T. Vuong, et al., Opportunities in low-level radiocarbon microtracing: applications and new technology, *Future Sci. OA* 2 (1) (2016) FSO74.
- [49] G.C. Young, et al., New frontiers-accelerator mass spectrometry (AMS): recommendation for best practices and harmonization from global bioanalysis consortium harmonization team, *AAPS J.* 16 (2) (2014) 357–359.
- [50] H.A. Synal, M. Stocker, M. Suter, MICADAS: a new compact radiocarbon AMS system, *Nucl. Inst. Methods Phys. Res. B* 259 (1) (2007) 7–13.
- [51] F. Lozac'h, et al., Evaluation of cAMS for (14)C microtracer ADME studies: opportunities to change the current drug development paradigm, *Bioanalysis* 10 (5) (2018) 321–339.
- [52] I. Galli, et al., Spectroscopic detection of radiocarbon dioxide at parts-per-quadrillion sensitivity, *Optica* 3 (4) (2016) 385–388.
- [53] A.D. McCartt, et al., Measurements of carbon-14 with cavity ring-down spectroscopy, *Nucl. Inst. Methods Phys. Res. B* 361 (2015) 277–280.
- [54] A.D. McCartt, et al., Quantifying carbon-14 for biology using cavity ring-down spectroscopy, *Anal. Chem.* 88 (17) (2016) 8714–8719.
- [55] H. Zhang, et al., Mass defect filter technique and its applications to drug metabolite identification by high-resolution mass spectrometry, *J. Mass Spectrom.* 44 (7) (2009) 999–1016.
- [56] H. Zhang, Y. Yang, An algorithm for thorough background subtraction from high-resolution LC/MS data: application for detection of glutathione-trapped reactive metabolites, *J. Mass Spectrom.* 43 (9) (2008) 1181–1190.
- [57] H. Zhang, et al., An algorithm for thorough background subtraction from high-resolution LC/MS data: application to the detection of troglitazone metabolites in rat plasma, bile, and urine, *J. Mass Spectrom.* 43 (9) (2008) 1191–1200.
- [58] P. Zhu, et al., A retention-time-shift-tolerant background subtraction and noise reduction algorithm (BgS-NoRA) for extraction of drug metabolites in liquid chromatography/mass spectrometry data from biological matrices, *Rapid Commun. Mass Spectrom.* 23 (11) (2009) 1563–1572.
- [59] H. Zhang, et al., Algorithm for thorough background subtraction of high-resolution LC/MS data: application to obtain clean product ion spectra from nonselective collision-induced dissociation experiments, *Anal. Chem.* 81 (7) (2009) 2695–2700.
- [60] A. Pahler, A. Brink, Software aided approaches to structure-based metabolite identification in drug discovery and development, *Drug Discov. Today Technol.* 10 (1) (2013) e207–e217.
- [61] P. Hatsis, N.J. Waters, U.A. Argikar, Implications for metabolite quantification by mass spectrometry in the absence of authentic standards, *Drug Metab. Dispos.* 45 (5) (2017) 492–496.
- [62] R.A. Hamilton, W.R. Garnett, B.J. Kline, Determination of mean valproic acid serum level by assay of a single pooled sample, *Clin. Pharmacol. Ther.* 29 (3) (1981) 408–413.
- [63] C.E. Hop, et al., Plasma-pooling methods to increase throughput for in vivo pharmacokinetic screening, *J. Pharm. Sci.* 87 (7) (1998) 901–903.
- [64] ICH, S9 Nonclinical Evaluation For Anticancer Pharmaceuticals, 2009.
- [65] ICH, S9 Nonclinical Evaluation For Anticancer Pharmaceuticals. Questions and Answers, 2018.
- [66] D. Dalvie, et al., Assessment of three human in vitro systems in the generation of major human excretory and circulating metabolites, *Chem. Res. Toxicol.* 22 (2) (2009) 357–368.
- [67] D.A. Smith, D. Dalvie, Why do metabolites circulate? *Xenobiotica* 42 (1) (2012) 107–126.
- [68] L. Di, R.S. Obach, Addressing the challenges of low clearance in drug research, *AAPS J.* 17 (2) (2015) 352–357.

- [69] FDA, Draft Guidance for Industry: In Vitro Metabolism and Transporter-Mediated Drug-Drug Interaction Studies, Food and Drug Administration, US Department of Health and Human Services, Center for Drug Evaluation and Research, Silver Spring, MD, 2017.
- [70] N. Penner, L. Xu, C. Prakash, Radiolabeled absorption, distribution, metabolism, and excretion studies in drug development: why, when, and how? *Chem. Res. Toxicol.* 25 (3) (2012) 513–531.
- [71] B. Lenz, et al., Application of imaging techniques to cases of drug-induced crystal nephropathy in preclinical studies, *Toxicol. Sci.* 163 (2) (2018) 409–419.
- [72] J.A. Staffa, J. Chang, L. Green, Cerivastatin and reports of fatal rhabdomyolysis, *N. Engl. J. Med.* 346 (7) (2002) 539–540.
- [73] Y. Shitara, et al., Gemfibrozil and its glucuronide inhibit the organic anion transporting polypeptide 2 (OATP2/OATP1B1:SLC21A6)-mediated hepatic uptake and CYP2C8-mediated metabolism of cerivastatin: Analysis of the mechanism of the clinically relevant drug-drug interaction between cerivastatin and gemfibrozil, *J. Pharmacol. Exp. Ther.* 311 (1) (2004) 228–236.
- [74] J. Gan, et al., Dansyl glutathione as a trapping agent for the quantitative estimation and identification of reactive metabolites, *Chem. Res. Toxicol.* 18 (5) (2005) 896–903.
- [75] C. Prakash, et al., In vitro screening techniques for reactive metabolites for minimizing bioactivation potential in drug discovery, *Curr. Drug Metab.* 9 (9) (2008) 952–964.
- [76] A. Brink, et al., Minimizing the risk of chemically reactive metabolite formation of new drug candidates: implications for preclinical drug design, *Drug Discov. Today* 22 (5) (2017) 751–756.
- [77] S. Kumar, et al., Approaches for minimizing metabolic activation of new drug candidates in drug discovery, *Handb. Exp. Pharmacol.* 196 (2010) 511–544.
- [78] T.A. Baillie, Approaches to the assessment of stable and chemically reactive drug metabolites in early clinical trials, *Chem. Res. Toxicol.* 22 (2) (2009) 263–266.
- [79] S.L. Iverson, D.A. Smith (Eds.), *Metabolite Safety in Drug Development*, Wiley, 2016.
- [80] J.G. Swales, et al., Mass spectrometry imaging and its application in pharmaceutical research and development: a concise review, *Int. J. Mass Spectrom.* 437 (2019) 99–112.
- [81] S. Schulz, et al., Advanced MALDI mass spectrometry imaging in pharmaceutical research and drug development, *Curr. Opin. Biotechnol.* 55 (2019) 51–59.
- [82] M.K. Passarelli, et al., The 3D OrbiSIMS-label-free metabolic imaging with subcellular lateral resolution and high mass-resolving power, *Nat. Methods* 14 (12) (2017) 1175–1183.

# The use of stable isotopes in drug metabolism studies

Kevin Johnson<sup>a</sup>, Hoa Le<sup>b</sup>, S. Cyrus Khojasteh<sup>a</sup>

<sup>a</sup>Drug Metabolism and Pharmacokinetics, Genentech, South San Francisco, CA, United States

<sup>b</sup>Drug Metabolism, Gilead Sciences, Foster City, CA, United States

## 1 Introduction

Metabolism is one of the major mechanisms of drug elimination from the body [1]. Metabolic pathways are mediated by a large variety of enzymes, albeit P450 and UGT play major roles in the biotransformation of most drugs [2]. The products of drug-metabolizing enzymes (DME), metabolites, in most cases pose little risk due to insignificant pharmacological and toxicological consequences compared to the active drug [3]. At the same time, it is valuable to identify, monitor, quantitate, and elucidate the mechanism of metabolite formation. Traditionally radioisotopes were used for these metabolism studies [4, 5]. While there are certain metabolism experiments still carried out with radiolabel material such as mass balance studies [6], there has been an interest in using stable isotopes for this purpose. Metabolism studies using stable label have been enabled by the technological advances of mass spectrometry [7]. Here, we discuss a strategy for using stable-label isotopes as an approach for assessing metabolite formation. This involves using *in vitro* or *in vivo* approaches depending on the appropriateness of the system and shows case examples to elucidate the mechanism of metabolites formation. In the case of deuterated drugs (Section 3), one of its utility is improving the metabolic clearance [7, 8]. Such efforts have already resulted in the discovery of a new marketed drug called deutetrabenazine (trade name Austedo). These approaches and considerations allow us to expand our understanding of the properties of deuterated drugs and their metabolic fate.

## 2 Use of stable labels for metabolite detection and identification

### 2.1 Stable labels and their application

Stable isotope labeling allows for dissecting many types of metabolism studies. The typical isotopes for this purpose are deuterium ( $^2\text{H}$  or D), carbon-13 ( $^{13}\text{C}$ ), nitrogen-15 ( $^{15}\text{N}$ ), and oxygen-18 ( $^{18}\text{O}$ ). For the most part, these isotopes are considered not to alter the rate and sites of metabolism. This is not entirely true as demonstrated in deuterated drugs (Section 3) and in some special cases carbon-13 (see niacin case study; Fig. 4). The use of a stable label allows for monitoring and quantitating drug material. A seminal article by Baillie described methods and demonstrated its utility [7].

#### 2.1.1 Beyond typical choices of isotopes

Besides the typically enriched stable isotopes mentioned, there are other isotopes that could be considered. For the stable labels discussed thus far, it may require specialized synthetic methods for isotope enrichment in the drug molecules. For the extended list of isotopes included in Table 1, there is no need for extra synthetic steps as these stable isotopes have a large natural abundance. These include boron, chlorine, and bromine atoms. Sulfur-34 could be considered but the limitation is its low natural abundance. With the extended list, the one shortcoming with these isotopes is that they may not be present in every molecule and, therefore, can't be used like the original set described. However, for the molecule that includes them, this could be an impactful tool to consider.

TABLE 1 Stable isotopes that could be used in metabolism studies [9].

Stable isotope	Natural abundance (%)	Isotope mass (Da)	Spin
$^2\text{H}$ (deuterium)	0.0115	2.014102	+1
$^{13}\text{C}$	1.109	13.003355	-1/2
$^{15}\text{N}$	0.4	15.000109	1/2-
$^{18}\text{O}$	0.2	17.999161	0
$^{33}\text{S}$	0.75	32.971459	3/2+
$^{34}\text{S}$	4.25	33.967867	0
$^{10}\text{B}$	19.9	10.012937	3+
$^{11}\text{B}$	80.1	11.009305	3/2-
$^{35}\text{Cl}$	75.76	34.968853	3/2+
$^{37}\text{Cl}$	24.24	36.965903	3/2+
$^{79}\text{Br}$	50.69	78.918338	3/2-
$^{81}\text{Br}$	49.31	80.916290	3/2-

From IUPAC: <https://iupac.org/what-we-do/periodic-table-of-elements/>.



### 2.1.2 Types of studies in drug metabolism

The other consideration is the placement of the label. There are several options based on the type of study. Label could be:

- placed in the compound of interest,
- the incubation media being studied ( $\text{H}_2^{18}\text{O}$ , and  $\text{D}_2\text{O}$ ),
- the soluble gas as in the case of  $^{18}\text{O}_2$ ,
- post-incubation for examining exchangeable hydrogens or hydroxyl moieties with  $\text{D}_2\text{O}$  or  $\text{H}_2^{18}\text{O}$ ,
- in the trapping agents such as GSH and in GST reactions, and
- in the cofactor as in the case of NADPD (compared to NADPH).

Placement of a stable label in the compound of interest has become a commonplace and has shown useful in the detection and identification of metabolites. For example, a stable label was used as a tracer for the antimalarial drug KAF156 for detection and identification of its polar metabolites [10]. Additional case study examples are discussed in the next section.

Tracing the incorporation of hydrogen or oxygen atoms in the molecule following metabolism is an important application in the metabolism studies. For example, both P450 enzymes and aldehyde oxidase (AO) oxidize heteroaromatic rings. The source of the oxygen atom is from air  $\text{O}_2$  molecule in the case of P450 and from the water molecule in the case of AO. Besides the typical inhibitors of such enzymes, labeled  $\text{H}_2^{18}\text{O}$  or  $^{18}\text{O}_2$  could be used for the identification of metabolic pathways and mechanisms. The next section will discuss additional case studies using isotopes for drug metabolism studies.

## 2.2 Cases studies

The following case studies are to demonstrate the utility of stable labels. Here, we will only highlight the relevant aspects in a very succinct manner. For more details, we refer the reader to the original articles.

### 2.2.1 Vismodegib and oxidative pyridine ring cleavage

Vismodegib (GDC-0449; Vismo) is a first in class, orally administered Hedgehog pathway inhibitor that was approved in 2012. It is currently approved for the treatment of advanced basal-cell carcinoma but there are other indications being explored [11, 12]. Vismo has a very slow clearance from the body that allows for prolonged exposure, which is beneficial for sustaining the mechanism of action [13, 14]. Many thoughtful studies were performed to dissect the various ADME properties of these molecules that are beyond the scope of this review [15]. One of the sites of metabolism was involved in ring cleavage of pyridine, and incorporation of stable labels in this ring allowed to better understand this reaction (Fig. 1) [16, 17].

The major metabolites of vismo are formed by aromatic oxidation followed by glucuronidation [16]. In addition, there were three significant metabolites that were formed as a result of pyridine ring cleavage: mainly M9, M13, and M18. These metabolites were formed by the hepatic cytochrome P450 enzymes from various species. A stable-labeled vismo was synthesized to address the mechanism of formation of these metabolites. This compound ( $[^{13}\text{C}_2, ^{15}\text{N}]$ -labeled vismo) had

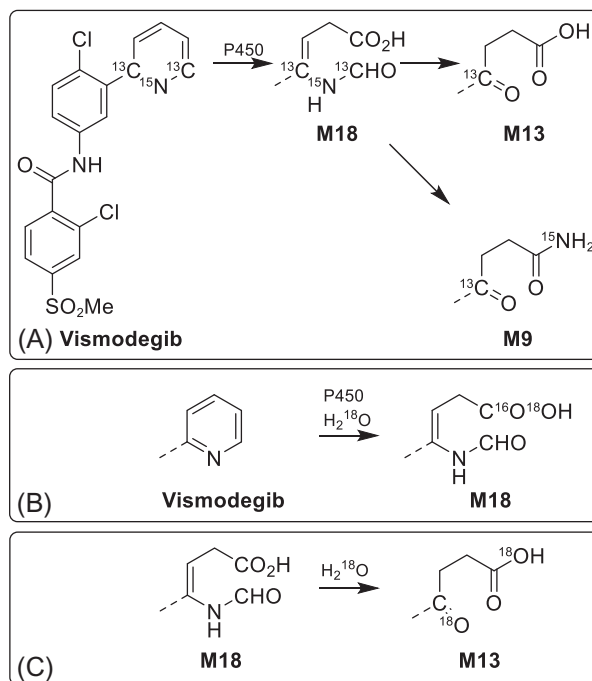


**FIG. 1** (A) Use of stable label in Vismo to determine the source of each stable label and their fate in each metabolite. (B) Vismo metabolism to M18 in the presence of  $\text{H}_2^{18}\text{O}$ . (C) M18 conversion to M13 in the presence of  $\text{H}_2^{18}\text{O}$ .

one  $^{15}\text{N}$  atom at the nitrogen pyridine with its two neighboring carbon atoms being  $^{13}\text{C}$  atoms (C-2 and C-6) (Fig. 2A). In metabolism studies, M18 retained all three labels, M9 retaining two labels, and M13 retained only one label as determined by mass spectrometry. The loss of carbon atoms observed in both M9 and M13 was from the C-6 position of pyridine. Interestingly, the source of the nitrogen atom in the amide of M9 was from the pyridine nitrogen atom. This study allowed us to understand that the scission of the carbon-carbon bond.

Other studies also confirmed the presence of aldehyde intermediates. Evidence for the formation of aldehydes was observed using methoxyamine trapping agent, as well as  $\text{H}_2^{18}\text{O}$ . The incubation with vismo with liver microsomes in the presence of  $\text{H}_2^{18}\text{O}$  incorporated only one oxygen atom from water into M18 (Fig. 1B). This suggests that the other oxygen atoms (mainly two atoms) come from  $\text{O}_2$ , which is consistent with the source of oxygen in the P450 metabolism. The other open question was to address if M18 was the precursor of M13 and M9. This was examined by taking the extracts and drying down and resuspending in  $\text{H}_2^{18}\text{O}$ . In the process, M13 was generated with two  $^{18}\text{O}$  that confirmed but no or little conversion to M9 was observed (Fig. 1C). Here,  $\text{H}_2^{18}\text{O}$  allowed for dissecting the metabolism process by P450 plus the subsequent conversion steps.

### 2.2.2 Using $\text{H}_2^{18}\text{O}$ and $\text{D}_2\text{O}$ to understand tofacitinib metabolism

Tofacitinib is a janus kinase (JAK) inhibitor that is for the treatment of rheumatoid arthritis, psoriatic arthritis, and ulcerative colitis. It is hepatically metabolized, where two of the metabolites are M2 (alcohol) and M4 (acid) (Fig. 2A). They are formed as a result of oxidation and

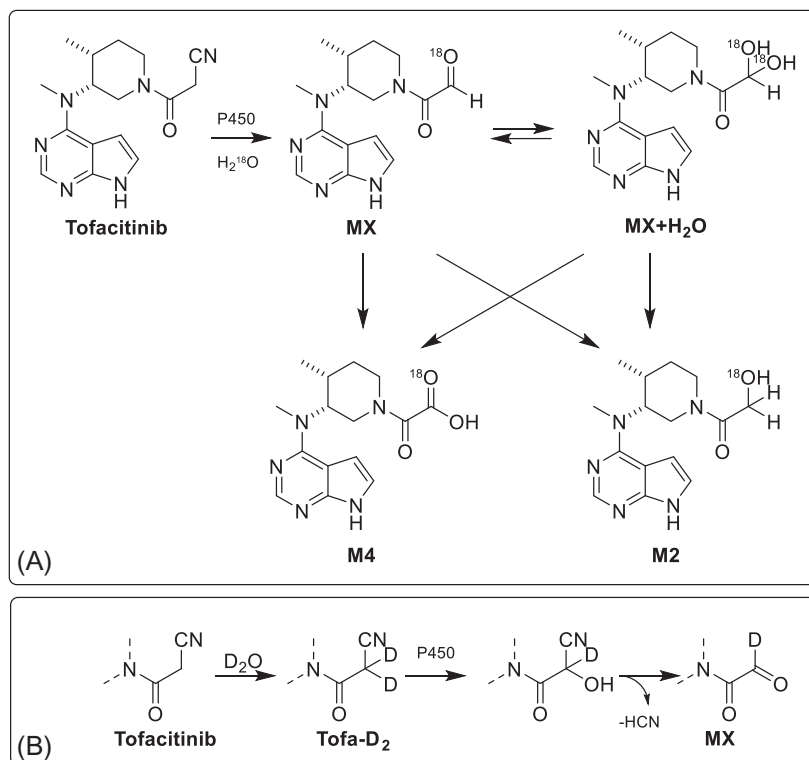


**FIG. 2** (A) Tofacitinib metabolism by P450 in the presence of H<sub>2</sub><sup>18</sup>O to form MX intermediate that is further reduced to M2 or oxidized to M4. (B) Tofacitinib labeling with deuterium oxide (D<sub>2</sub>O) through fast exchange prior to P450 oxidative decyanation to MX.

loss of the nitrile moiety. In vitro studies using human liver microsomes show that a geminal diol intermediate of tofacitinib, MX, by oxidation by P450 at the  $\alpha$ -carbon to the nitrile [18]. MX was further reduced or oxidized to the respectively M2 (alcohol) and M4 (acid). The enzymes involved were characterized to be aldo-keto reductase 1C1, aldehyde oxidase, and possibly CYP3A4. Stable-label studies using H<sub>2</sub><sup>18</sup>O and D<sub>2</sub>O suggested the source of oxygen in MX was from water in the media. But this was due to rapid water exchange with MX in the media prior to reduction to M2. In case of deuterium, one was incorporated in M2 as a result of tofacitinib rapid exchange of two deuterium atoms from D<sub>2</sub>O onto methylene position prior to oxidation and loss of cyanide (Fig. 2B). After the formation of MX, one deuterium was retained and no longer exchanged with water. This deuterium, therefore, was retained in M2 after reduction.

### 2.2.3 Stable-labeled glutathione as a trapping agent for detection of reactive metabolites

The formation of reactive metabolites is considered as one of the contributors to hepatotoxicity [19, 20]. The major class of enzymes involved are typically, but not limited to, cytochrome P450 enzymes. Reactive metabolites are formed as one of the products during metabolism and

are typically electrophilic in nature. For reactive metabolite screening, nucleophile agents such as glutathione are used for trapping the reactive electrophiles. Many factors contribute to the detection of the trapped molecules, which includes the chemical lability of the reactive metabolite, the compatibility of the molecular orbitals (GSH is a soft nucleophile and efficiently reacts with soft electrophiles such as acrylamides or quinone methides), and the stability of the resulting conjugate. The trapped reactive metabolites could be separated and detected using LC-MS/MS [21, 22]. For more specificity, Yan et al. [23] added stable-labeled GSH (called GSX,  $\gamma$ -glutamylcystein-glycin- $^{13}\text{C}_2$ - $^{15}\text{N}$ ) that allowed for ease of identification. GSX included two  $^{13}\text{C}$  and one  $^{15}\text{N}$  on the glycine moiety (Fig. 3). Co-incubation with equal concentrations of both labeled and non-labeled GSH resulted in the formation of two trapped reactive metabolites with a mass difference of 3 Da (Fig. 3). GSX can be used as a marker to minimize artifacts and be assured of the GSH-related conjugates. This was examined in the series of halogenated aniline to examine the mechanism of ipso formation [22]. This method is now further refined to take advantage high-resolution mass spectrometry to provide specificity and sensitivity for identifying and elucidating glutathione conjugates [24].

#### 2.2.4 A disconnect between endogenous and [ $^{13}\text{C}$ ]-labeled niacin

Nicotinic acid (niacin) metabolism in cells is well established [25]. Investigations in niacin metabolism pose complexity due to the presence of endogenous level of niacin and all its metabolites. In order to dissect niacin metabolic pathway, fully [ $^{13}\text{C}$ ]-labeled niacin was studied in human and rat hepatocytes (unpublished report). For the fully labeled niacin, the metabolites observed are nicotinamide and nicotinuric acid (Fig. 4; Table 2). On the other hand, endogenous niacin (unlabeled) is M1, *N*-methyl-2-pyridone-5-carboxamide (2PY), and *N*-methyl-4-pyridone-5-carboxamide (4-PY), which were the result of modification on the pyridine ring. No endogenous niacin itself was detected. Metabolic switching and concentration-dependent metabolism possibly explain the difference observed. Therefore, one has to consider the potential changes in metabolism that could take place once using stable-label tracers.

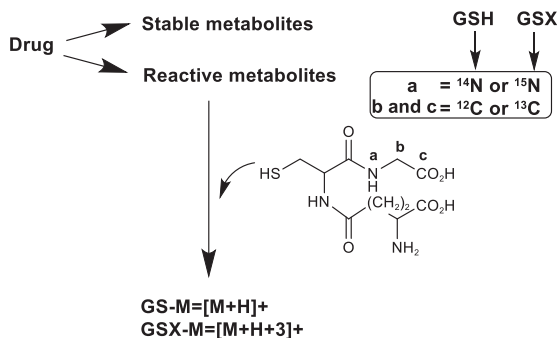
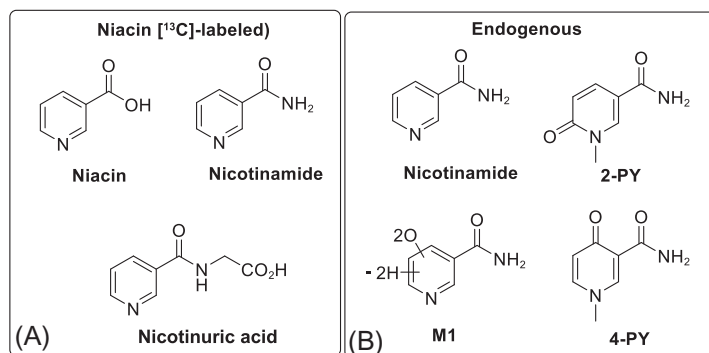


FIG. 3 Formation of reaction metabolites that could react with GSH or GSX. GSH is the natural glutathione (GSH) and GSX is  $\gamma$ -glutamylcystein-glycin- $^{13}\text{C}_2$ - $^{15}\text{N}$  with 3Da higher molecular weight that could aid in glutathione conjugate identification.



**FIG. 4** (A) Niacin metabolites observed from fully <sup>13</sup>C labeled niacin incubated with human and rat hepatocytes after 3 h. For niacin and all the related metabolites, the niacin has <sup>13</sup>C labeled that are not shown. (B) The niacin-related endogenous metabolites and note no niacin was detected.

**TABLE 2** Relative abundance of niacin and its metabolites from rat and human hepatocytes after 3 h of incubation.

Incubation	Labeled niacin			Endogenous (unlabeled)			
	Niacin	Nicotinamide	Nicotinuric acid	Nicotinamide	2-PY	4-PY	M1
Human hepatocytes @3h	43	37	20	89	2	9	<1
Rat hepatocytes @3h	81	11	8	92	4	2	2

### 3 Deuterated drugs

#### 3.1 Deuterium in drug design

The deuterium isotope was discovered back in 1931 by Harold Urey [26], and one of the first forms of bulk production was in the form of deuterium oxide (deuterated water; D<sub>2</sub>O) [27]. For over 60 years, enzymologists/biochemists have been utilizing the heavy isotope to elucidate enzyme reactions mechanisms. One of the earliest uses for incorporation of and utility into small molecules drugs began was in 1961, by deuteration of morphine to monitor biological response [28].

The natural abundance of deuterium is only 0.0115% of the total hydrogen atom (mainly <sup>1</sup>H) [9]. The availability of deuterium-enriched synthetic compounds has exponentially increased over the last several decades, allowing for broad incorporation of deuterium into the ever-expanding chemical space. Readers are directed elsewhere for more in-depth reviews on chemical sources and synthetic techniques [29, 30].

Deuterium has proven utility in elucidating chemical and enzyme reaction mechanisms by slowing rates of carbon-hydrogen (C—H) bond cleavage reactions in organic compounds [31]. The inherent decrease in reactivity stems from the increase in nominal mass of deuterium (compared to <sup>1</sup>H) resulting in a mass increase of ~100%. In comparison, <sup>12</sup>C to <sup>13</sup>C is only ~8% increase in mass. The resulting shorter bond length and lower vibrational frequency (electronic polarizations) leads to a lower zero-point energy and higher activation energy for C—D bond cleavage than the corresponding C—H bond [31, 32]. The effective change

in rates of reaction is termed a primary kinetic (deuterium) isotope effect (KIE or DIE), expressed as the ratio of the rates of non-deuterated to deuterated bond cleavage as described in the following equation.

$$\text{KIE} = k_{\text{H}}/k_{\text{D}} \quad (1)$$

Here,  $k_{\text{H}}$  is the observed rate of reaction of the non-deuterated substrate and  $k_{\text{D}}$  is for the deuterated substrate. The primary KIE for simple C—H vs C—D abstraction reactions has a theoretical limit of  $\sim 9$  at  $37^{\circ}\text{C}$  in the absence of quantum mechanical tunneling [33, 34]. Secondary isotope effects from adjacent atoms can affect the rate of C—D bond cleavage as well, though to a lesser extent. Low atomic purity (isotopic) reagents and low-efficiency labeling reactions can result in suboptimal isotope purity of substrates/products. Significant impurities in deuterium substrate stocks may lead to partially masked isotope effects, particularly with low-turnover compounds. Isotopic purity of the deuterium label should be kept as high as possible, preferably  $>98\%$  to avoid underestimating isotope effects *in vitro* [35]. Most commercial sources provide deuterium purity of 98% or higher, but consideration of the synthetic reactions involved in deuterium incorporation is crucial for high purity substrates.

In general, deuterated drugs have been widely used as internal standards for bioanalytical quantitation by LC-MS. For this purpose, labeling sites of deuterium are chosen for the ease of synthesis, limited chromatographic retention shifts, and optimal mass shift (usually  $>5\text{Da}$  to avoid satellite ion interference). For a metabolism experiment, deuterium must be strategically placed at sites of oxidation. In addition to the modulation of metabolic stability (discussed below), deuterium has utility as a probe to confirm sites of oxidation, in terms of deuterium/hydrogen abstraction (Fig. 5). The loss of a deuterium label is also indicative of site of metabolism.

Toxicity is always a concern when using exogenous substances in biological systems.  $\text{D}_2\text{O}$  in humans has an estimated half-life of  $\sim 10$  days [36] and it is fairly safe in biological systems. It's been reported that *in vitro*, cells can survive in 50% deuterium oxide, and preclinical species (rats) can survive in up to  $\sim 15\%$  total deuterium replacement (fish 30%). This leaves a large *in vivo* safety window for incorporation into drugs that are expected to release very low levels of  $\text{D}_2\text{O}$ .

Using deuterated drugs to study and modulate rates of metabolism has been of great interest to many enzymologists and drug metabolism scientists [28]. Taking advantage of the unique increased bond strength to detect differences in certain reaction rates without changing the substrate/drug structure is the most powerful utility of the stable isotope. This has been an invaluable tool to investigate reaction mechanisms of many classes of enzymes, both for endogenous and exogenous substrates. Incorporation into molecules to assist in describing rate-determining steps of enzymes, change metabolic properties, as well as confirm metabolic structures have been indispensable.

While the utility of deuterium in drug metabolism studies is not a new concept [28], designing drugs with deuterium for discovery and development has only been recently recognized as an important potential strategy to improve the metabolic stability, PK, and safety of drug candidates [37–39]. Incorporation of deuterium into previously approved drugs has been of major scrutiny in terms of acquiring new patent [40, 41]. Under 35 USC §103:

Incubation	Labeled niacin			Endogenous (unlabeled)			
	Niacin	Nicotinamide	Nicotinic acid	Nicotinamide	2-PY	4-PY	M1
Human hepatocytes @3 hr	43	37	20	89	2	9	<1
Rat hepatocytes @3 hr	81	11	8	92	4	2	2

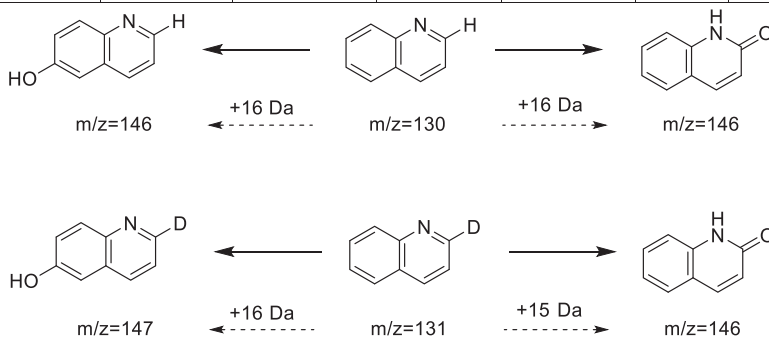


**FIG. 5** Identification of site of oxidative metabolism on quinolone using deuterium. Loss of deuterium after oxidation indicates that is the site of metabolism.

A patent for a claimed invention may not be obtained, notwithstanding that the claimed invention is not identically disclosed as set forth in section 102, if the differences between the claimed invention and the prior art are such that the claimed invention as a whole would have been obvious before the effective filing date of the claimed invention to a person having ordinary skill in the art to which the claimed invention pertains. Patentability shall not be negated by the manner in which the invention was made [42].

The term “obviousness” is used to protect rights on existing patents, where deuterium substitution at metabolic soft spots (sites of oxidation) is not considered “new” technology. Certain companies like Concert Pharmaceuticals whose business model is the development of deuterated versions of drugs face this challenge. Unless there is clear biological benefit when compared to non-deuterated old drugs or specific scientific data to support nonobvious difference presented, companies applying for patents through a “deuterium switch” face major challenges [40, 41].

Despite the legal battles stemmed from “rehashes” of old drugs, the use of deuterium for clinical drug design has been gaining much attention in the past decade. Several companies that presented deuterated drugs as their business model have gained significant attention (Auspex, Concert Pharmaceuticals, Duteria Pharmaceuticals, DeuteRx, Protia, Retrotope) [29]. By 2014, two licensing or acquisitions deals were reported for approximately \$3.5 billion each [43]. Teva acquired Auspex Pharmaceuticals, and Otsuka Pharmaceutical bought Avanir, which was partnered with Concert at the time. It is important to distinguish that novel deuterium containing drugs do not face this challenge, as the chemical matter has no direct comparison. Table 3 summarizes many of the current clinical candidates that contain deuterium, as well as their current status in development. Case studies of deuterated versions of old drugs will be discussed later in this chapter.



**TABLE 3** Deuterated drugs in development.

<b>Compound</b>	<b>Marketed version</b>	<b>Indication</b>	<b>Company</b>	<b>Deuterium substitution</b>	<b>Clinical benefit</b>	<b>Clinical status</b>
Deutetrabenazine (Austedo)	Tetrabenazine	Huntington's disease, tardive dyskinesia	Teva	-OCD <sub>3</sub>	Lower dose/frequency	Approved
CTP-543	Ruxolitinib	Hair loss	Concert	Cydropentane	Improved metabolic stability	Phase II
VX-561 (CTP-656)	Ivacaator (Kaylydeco)	Cystic fibrosis	Vertex	-C(CD <sub>3</sub> ) <sub>3</sub>	Lower dose/frequency	Phase II
AVP-786	Dextromethorphan	Dementia	Avanir/Concert	-OCD <sub>3</sub> , =NCD <sub>3</sub>	Higher bioavailability, lower Quinidine co-dose	Phase II/III
DRX-065	Pioglitazone	NASH	DeuteRx	α-Carbon	Enantiomeric stabilization	Phase I
ALK-001	Retinyl acetate	Stargardt disease, muscular degeneration	Alkeus Pharmaceuticals	Methyl -CD <sub>3</sub>	Reduce toxic metabolite	Phase III
SD-560	Pirfenidone	Idiopathic pulmonary fibrosis	Auspex	Benzyl -CD <sub>3</sub>	Increased plasma half-life	Preclinical
SD-1077	Levodopa	Parkinson's disease	Auspex/Teva	α,β-Carbons	Lower dose/frequency	Preclinical
RT001	Linoleic acid	Freidreich's ataxia	Retrotope	Allylic -CD <sub>2</sub> -	Lower lipid peroxidation	Phase II
BMS-986165	Novel	Psoriasis	BMS	Amide -CD <sub>3</sub>	Slow demethylation	Phase III
CT-730	Apremilast	Inflammation	Celgene/Concert		Improved PK	Phase I
M9831 (VX-984)	Novel	Solid tumors	Merck KGaA/Vertex	Aromatic C-D	Lower aldehyde oxidase metabolism	Phase I
PCS 499 (CTP-499)	Active metabolite of pentoxifylline	Chronic kidney disease	Concert/Processa Pharmaceuticals	Aliphatic -CD <sub>2</sub> and -CD <sub>3</sub>	Metabolically stable active metabolite of pentoxifylline	Phase II

## 3.2 Relevant drug-metabolizing enzymes for utilizing kinetic isotope effects

### 3.2.1 Cytochrome P450 metabolism

One of the most widely studied class of enzymes using deuterium are of the cytochrome P450 superfamily of monooxygenase enzymes, particularly for their broad substrate coverage and importance in drug discovery. As P450s have been responsible for >50% of drug metabolism to date [2, 44], there has been much effort in designing experiments to probe and modulate the general reaction mechanisms of these enzymes. In particular, C—H abstraction reactions are of high interest for deuterium studies involved in determining rate-limiting steps of enzyme catalysis. These reactions are also important and increasingly studied for other enzymes such as aldehyde oxidase and monoamine oxidase, which are discussed later.

Below shows the generally accepted scheme for most P450-catalyzed C—H oxidation reactions involved in various aliphatic and aromatic hydrocarbons (Fig. 6) [35]. For a significant KIE to be observed for a deuterated substrate, the C-H/D abstraction must at least be partially rate limiting. In terms of P450 metabolism, the rate-determining step must be involved in substrate oxidation by the activated complex termed “compound I” (Cpd I) [44]. The hydrogen/deuterium abstraction step occurs through a radical intermediate, which is followed by oxygen rebound (Fig. 7A).

If the rate-determining step is determined by anything other than C-H/D abstraction, such as electron transfer (Fig. 7B) or substrate/product binding (or substrate inhibition [45]), the intrinsic KIE will be reduced or masked completely. In general, the lower contribution of C-H/D abstraction on the rate-determining step, the more an intrinsic deuterium isotope effect will be masked. Medicinal chemistry design and experimental setup are both important factors involved in determining the potential for using a KIE to design novel drugs, or to solve/investigate a metabolism question for drug discovery.

Substituting hydrogen for deuterium on aromatic/allyl systems and on basic alkyl amines most often does not observe any significant KIE. This is because of the single-electron transfer (SET)-type mechanisms that dominate these reactions for P450 oxidation (Fig. 7B). CYP-catalyzed oxidation of aromatic rings involves generation of an arene-epoxide intermediate,

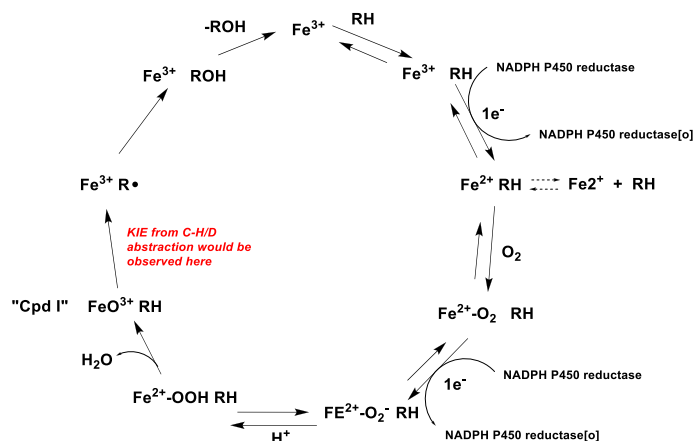


FIG. 6 General CYP P450 catalytic mechanism for substrate (RH) oxidation.

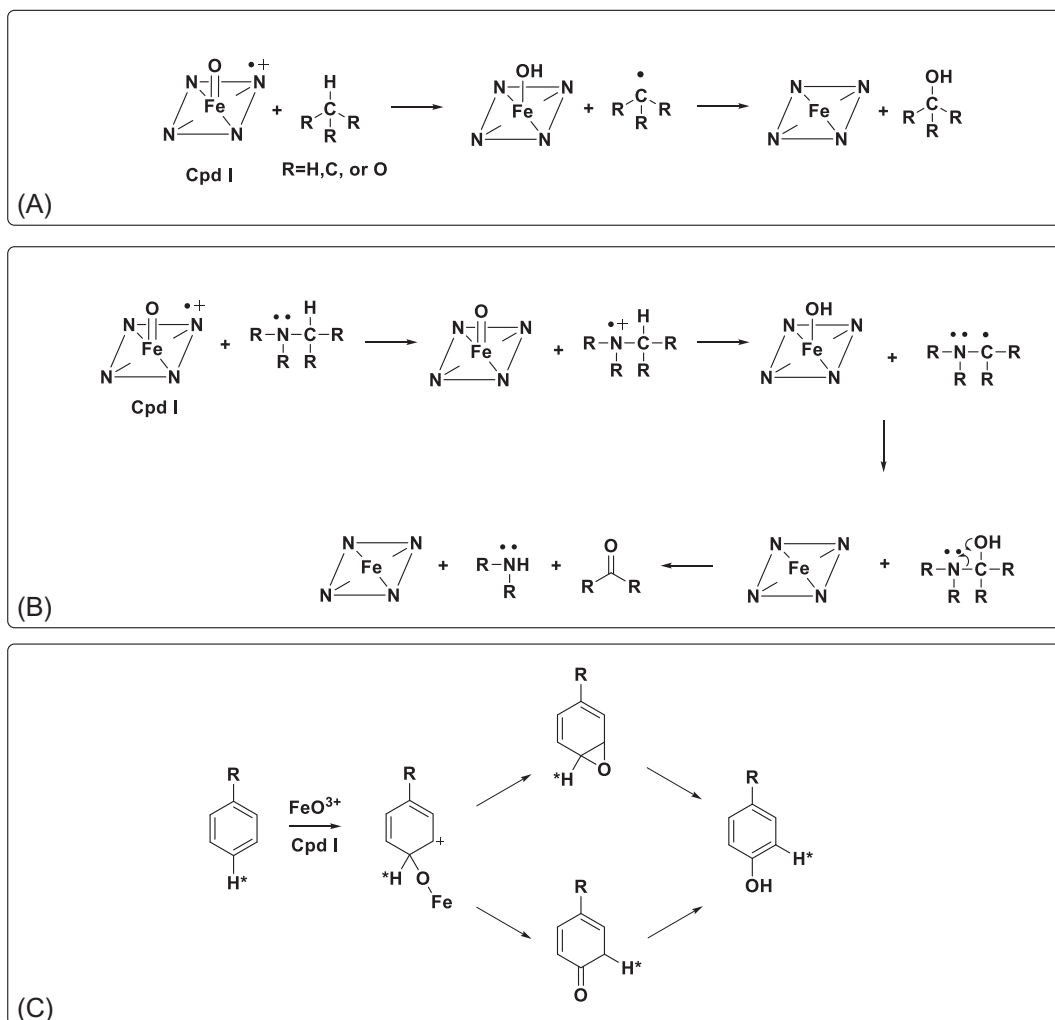


FIG. 7 Representative oxidation reactions catalyzed by P450 enzymes. (A) Hydrogen atom abstraction for carbon oxidation reaction mechanism of aliphatic hydrocarbon. (B) Single-electron transfer initiating *N*-dealkylation reaction mechanism of basic alkyl amines. (C) Aryl hydroxylation reaction mechanism for aromatic rings.

which undergoes intramolecular hydride (deuteride) shift, commonly known as the “NIH shift” [46] (Fig. 7C). The absence of a direct H/D-abstraction step results in little to no change in rate of oxidation (no DIE), and occasionally observe an inverse isotope effect that is instead generally dependent on enzyme [33, 47]. For *N*-dealkylation (by P450) of basic amines, a one-electron abstraction from the nitrogen lone pair is most often rate determining. The loss of hydride (deuteride) via radical shift follows, but the overall KIE again is masked resulting in very minimal observed isotope effect ( $\text{KIE} \leq 2$ ) [48, 49]. Conversely, *N*-dealkylation of amides normally results in a large isotope effect ( $\text{KIE} \geq 7$ ). This is the case for clinical candidate

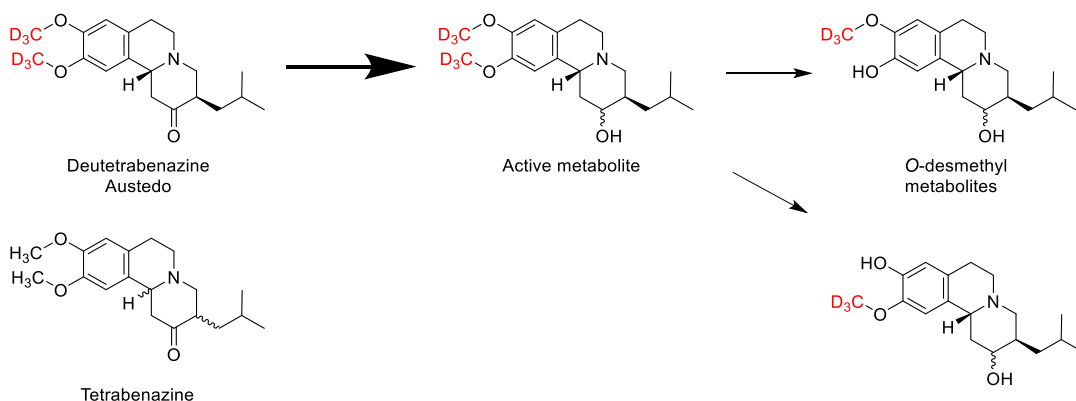


FIG. 8 Metabolism of deuterotetrabenazine.

$d_3$ -Enzalutamide (Fig. 8), and results from the strong delocalization of the nitrogen lone pair (reduced basicity) leading to predominant hydrogen atom transfer (HAT) mechanism in C–H abstraction [50]. More extensive reviews can be found elsewhere [33, 35, 51]. Other non-P450 enzymes investigated with deuterium-labeled drugs include monoamine oxidase, aldehyde oxidase, and dehydrogenases [52, 53]. Each have been shown to have significant observed isotope effects ( $KIE > 5$ ) and are discussed below.

### 3.2.2 Monoamine oxidase metabolism

Mechanistic studies of the two human monoamine oxidase enzymes (MAO-A and MAO-B), which catalyze *N*-dealkylation reactions of endogenous and exogenous alkyl-amine substrates, have shown large KIE depending on the isoform and substrate used ( $KIE = \sim 6$ –12) [54]. Mixed literature reports have reported MAO activity can proceed through a SET or a HAT mechanism, depending on the substrate [55, 56]. But several definitive studies provide strong evidence of hydrogen/deuterium abstraction as rate limiting [54]. *D*-Tyramine (Fig. 9), which is metabolized by MAO, contains two deuterium atoms alpha to the primary amine. This compound has been reported to have increased efficacy presumably due to decreased metabolic clearance by MAO [57].

### 3.2.3 Aldehyde oxidase metabolism

Aldehyde oxidase (AO) metabolism has been of increasing importance for drug discovery efforts. Trends to resolve P450 metabolic liabilities have led to increasing abundance of drugs candidates with heterocyclic aromatic amines, which are common substrates for AO. Deuterium isotope studies with AO substrates have shown observed KIE values of up to  $\sim 5$  for aromatic hydroxylation reactions of heterocyclic amines. Extensive studies with deuterated carbazeran and zoniporide (Fig. 9) are reported in the literature with observed *in vitro* KIE of up to  $\sim 5$  across multiple species [58]. Both compounds have shown little to no change in half-life ( $t_{1/2}$ ) *in vivo*, presumably because of competing elimination pathways. Interestingly, the *D*-carbazeran was reported to have significantly higher  $C_{max}$  in guinea pig leading to higher AUC ( $\sim 22$ -fold increase in both) for oral dose, with very minimal change in the rat ( $DIE < 2$ ).

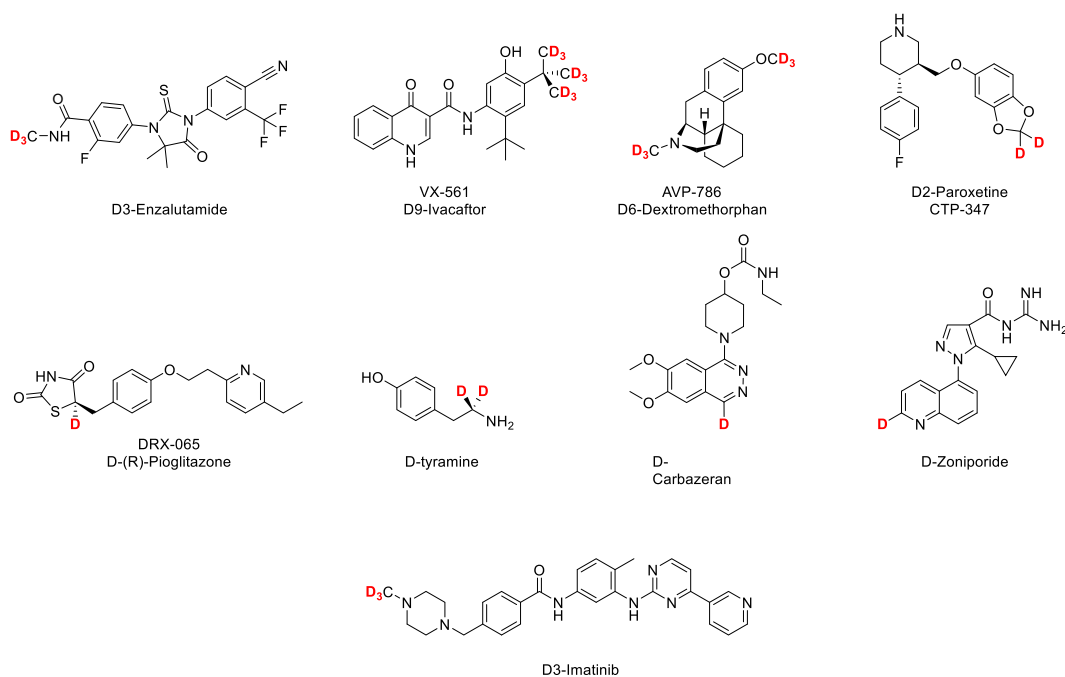


**FIG. 9** Examples of deuterated drugs reported in literature. Deuterium atoms are labeled in *red* to indicate site of metabolism addressed.

The increased exposure was hypothesized to result from decreased first-pass metabolism in the gut. D-Zoniporide showed very minimal isotope effects in vivo ( $KIE < 1.7$ ). This study elegantly shows the importance of understanding major clearance pathways involved in the elimination of potential deuterated drugs for discovery.

### 3.3 Case studies: Deuterated versions of old drugs

Several clinical candidates are currently being investigated as other potential therapies containing deuterium. Table 3 summarizes examples of compounds investigated for PK improvements of previously approved drugs as well as novel drug candidates. Deutetabenazine (Austedo, Fig. 8) was the first deuterated drug to be approved by the FDA. Approved in April 2017 for the treatment of Huntington's chorea and tardive dyskinesia. Tetrabenazine is administered as an isomeric mixture, acting on vesicular monoamine transporter-2 (VMAT-2) protein in the brain [59–61]. Tetrabenazine's efficacy results from rapid first-pass metabolism by carbonyl reductase to the major active circulating metabolites (Fig. 8). These are then further metabolized by P450 2D6 to *O*-desmethyl metabolites. Deutetabenazine was developed to increase stability of the active metabolites by lowering *O*-demethylation by P450 2D6. Initial phase 1 crossover study with deuterated and non-deuterated tetrabenazine showed almost twofold increase in half-life and exposure for the deuterated drug, with only a slight increase in  $C_{max}$  [60, 62], ultimately resulting in a lower and less frequent dosing regimen compared to tetrabenazine.

Here, we present case studies for when the deuterated drug strategy was employed. The examples discussed only include deuterated version of previous drugs, which allow for comparison of PK and metabolism between deuterated and non-deuterated forms. As mentioned earlier, the advantage of using deuterium to solve metabolism issues is that presumably the physical chemical properties are not altered significantly. Meaning only the metabolic properties affected would change, resulting in differences in either metabolic clearance, half-life, bioavailability, exposure, toxicity, DDI potential, or any of the aforementioned ADME-related properties.

### 3.3.1 Lowering clearance

Ivacaftor was the first drug approved for the treatment of cystic fibrosis (CF) with patients with mutations in cystic fibrosis transmembrane conductance regulator (CFTR). Ivacaftor has a human half-life of ~11h and is predominantly oxidized at the *t*-butyl group by P450 3A enzymes into an alcohol and furthermore to a carboxylic acid, which appears in the systemic circulation. A deuterated version (VX-561, previously CTP-656, Fig. 9) was developed to slow metabolic clearance allowing for improved PK and dosing [63]. Substitution of the *t*-butyl group with deuterium resulted in greater than threefold increase in exposure from ivacaftor to VX-561 and an increase in half-life from 11 to 15h, respectively. The phase 1 crossover study showed VX-561 had improved PK compared to ivacaftor, and perhaps could enable once-daily dosing.

### 3.3.2 Improving bioavailability

AVP-786 is an investigational combination drug therapy containing a deuterated dextromethorphan (Fig. 9) and quinidine. Quinidine was originally used as a P450 2D6 inhibitor to improve bioavailability for dextromethorphan (AVP-923). Unfortunately quinidine has been shown to increase the QT interval [64]. In attempts to improve bioavailability of dextromethorphan, and lower the dose of quinidine, selective deuteration of dextromethorphan at the *O*- and *N*-methyl groups was examined. This led to lower clearance and higher bioavailability in comparison with dextromethorphan, allowing the use of significantly lower doses of quinidine that potentially lowers its toxicity.

### 3.3.3 Mitigating reactive metabolite formation/drug-drug interaction

CTP-347 is the deuterated version of paroxetine (Fig. 9). Paroxetine is a selective serotonin reuptake inhibitor for the treatment of major depressive disorder, social anxiety disorder, and premenstrual dysphoric disorder. Paroxetine is metabolized by P450 2D6, but also irreversibly inhibits the enzyme through a mechanism-based inactivation (MBI). Oxidation of the methylene carbon results in the formation of a reactive carbene metabolite that inactivates the enzyme. Therefore, its use is associated with drug-drug interactions with other drugs metabolized by P450 2D6 [65]. Substitution of the methylene hydrogens with deuterium resulted in approximately eightfold decrease in the rate of inactivation of P450 2D6 in vitro, as measured by tamoxifen metabolism [66]. Phase 1 clinical studies with CTP-347 in single and multiple ascending dose were performed with healthy female volunteers [67]. Subjects dosed with CTP-347 retained greater P450 2D6 activity (measured by dextromethorphan metabolism) at similar doses compared to paroxetine. Interestingly, the decrease in MBI resulted in faster clearance of CTP-347 compared to paroxetine, most likely resulting from the retained P450 2D6 activity. This was the first clinical study describing the utility of deuterium substitution to alleviate drug-drug interactions in humans.

### 3.3.4 Slowing chiral inversion

Pioglitazone (Actos) is a marketed drug known for its racemic mixture (1-to-1) of two pharmacologically different enantiomers. The enantiomers are capable of chiral inversion, making isolation and selective administration difficult. The (*R*)-enantiomer shows efficacy for the treatment of nonalcoholic steatohepatitis (NASH), while the (*S*)-enantiomer is associated as a proliferator-activated receptor gamma (PPAR $\gamma$ ) agonist, responsible for side effects including weight gain and edema [68]. Deuteration of the (*R*)-enantiomer slows the chiral inversion, allowing for isolation of a single enantiomer (DRX-065, Fig. 9) for administration of drug devoid of the side effects associated with the (*S*)-enantiomer [69]. This allows for a greater therapeutic window compared to non-deuterated pioglitazone.

## 3.4 How deuterium should be assessed in drug discovery?

The examples thus far described seem to have beneficial improvements upon deuterium substitution. Proper utilization of deuterium to solve PK issues requires prior knowledge of major metabolic clearance pathways in vivo. Without informed chemistry design, a deuterated drug candidate has very low hope of PK improvement, and thus low chance of clinical success. Imatinib is a potent tyrosine kinase inhibitor used for chronic myeloid leukemia, as well as gastrointestinal stromal tumors [70]. Imatinib is extensively metabolized to a less potent *N*-demethylated metabolite by CYP3A and 2C8 enzymes with a <5h half-life in rat [71]. To improve stability and low clearance, a *N*-trideuteromethyl group was incorporated (D3-Imatinib, Fig. 9). In vitro experiment in human and rat liver microsomes (HLM and RLM) resulted in low observed isotope effects ( $k_H/k_D < 1.5$  for intrinsic clearance,  $k_H/k_D = \sim 3$  for *N*-demethylation, estimated from metabolite percent abundance). As discussed earlier, one generally observes low KIE for *N*-dealkylation of basic amines due to high contribution of SET-type reaction mechanisms (Fig. 7) as opposed to HAT [48]. This (along with competing metabolic pathways) resulted in even lower observed KIE for metabolic stability. When studied in vivo, essentially no KIE was observed, and was most likely masked due to non-microsomal or non-hepatic clearance pathways negating the minor KIE expected. This is a good example where informed chemistry design and knowledge of clearance pathways would predict low utility of deuterium for PK improvement.

When in vitro metabolic data are available (specifically type of drug-metabolizing enzymes involved) and metabolic clearance expected to be important, general trends in terms of in vitro KIE to help guide deuterated drug design. As we know certain metabolic reactions will be more sensitive to deuterium incorporation than others, in vitro stability and metabolite identification data are essential for productive placement of deuterium on a molecule. As mentioned above, this depends on both the substrate structure and the enzyme involved in its metabolism. Fig. 10 summarizes the general enzymatic C—H oxidation reactions and expected KIE trends. To summarize, compounds metabolized by alkyl C—H oxidation and *O*-dealkylation reactions make good candidates for KIE studies. Conversely, if oxidation of  $\pi$ -systems (aromatic/desaturated) and/or *N*-dealkylation of basic amines are primary routes of metabolic clearance, these will be poor candidates for deuterium substitution to slow P450 metabolism through a KIE. It is important to remember which enzyme reaction mechanisms involve a rate-determining C—H abstraction (HAT vs SET, Fig. 7) to predict if any significant KIE is to be observed.



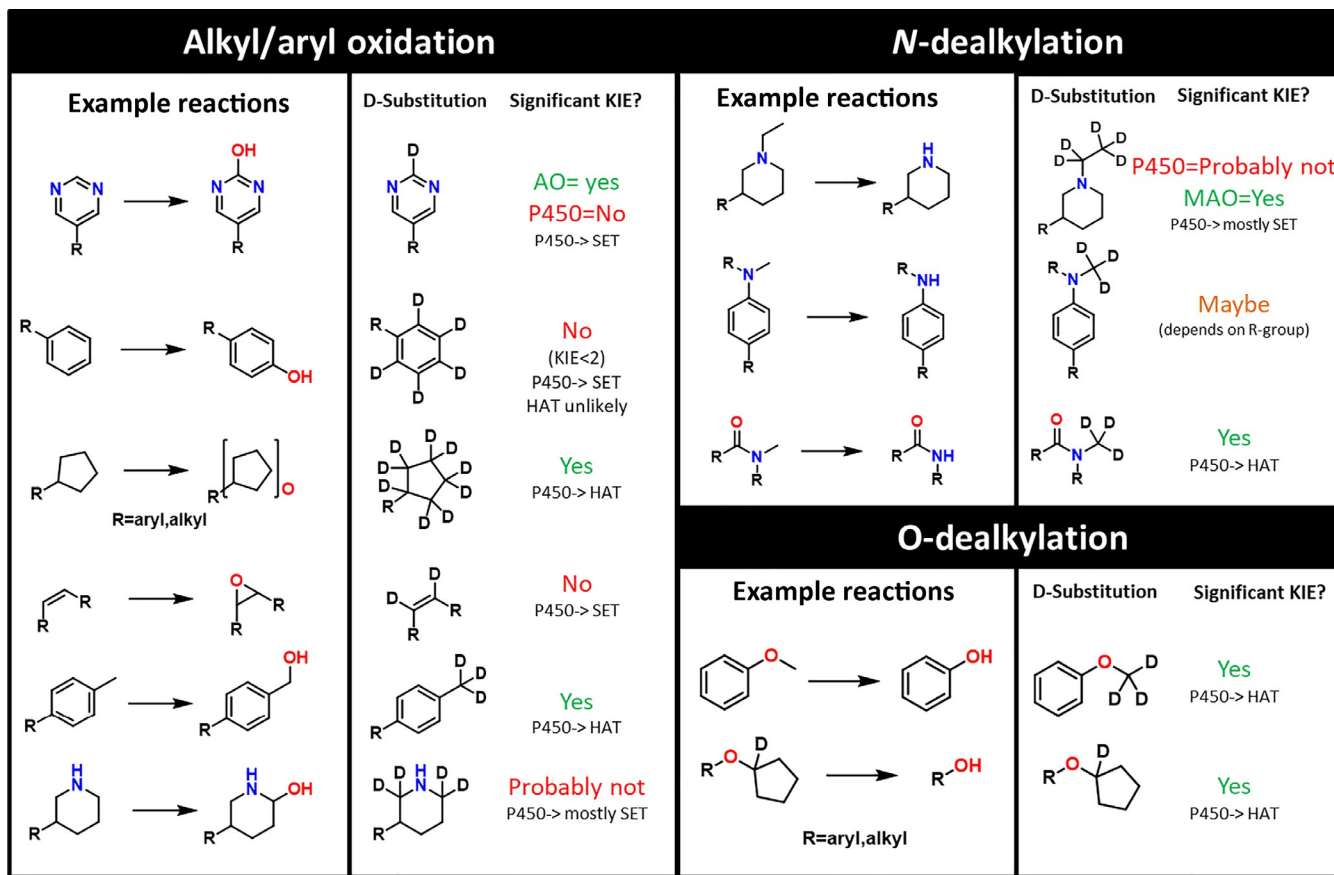
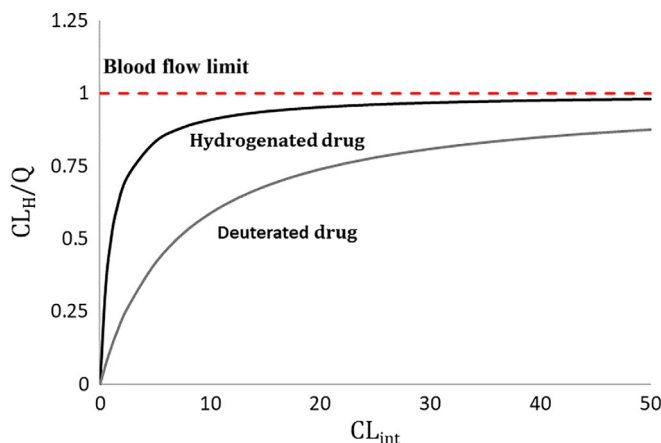


FIG. 10 General trends for in vitro KIE for deuterium replacement at specific sites of metabolism.

Exceptions to these rules do exist, most often for non-P450 oxidation reactions. Monoamine oxidase enzymes will catalyze *N*-dealkylation reactions through a different mechanism than P450. There is evidence supporting MAO oxidation proceeds through a hydride transfer-*type* mechanism, and reported to have high KIE ( $\sim 10$ ) [54, 72]. Aldehyde oxidase has also been shown to be affected by deuterium substitution of aromatic C—H bonds adjacent to heterocyclic aromatic nitrogen atoms (pyridines, etc.). Reported values of  $\text{KIE} = \sim 5$  in vitro are typically reported [58], although there is increasing evidence supporting different kinetic parameters observed for AO metabolism compared to the more well studied drug-metabolizing enzymes like P450 [45].

If one compares the intrinsic clearance ( $\text{CL}_{\text{int}}$ ) and hepatic clearance ( $\text{CL}_{\text{H}}$ ) to hepatic blood flow ( $Q_{\text{H}}$ ) (Eq. 2), a rough prediction of the overall effects of deuterium substitution on in vivo clearance and exposure can be estimated (assuming metabolism is a major route of metabolic clearance) [58]. For orally dosed drugs, if  $\text{CL}_{\text{int}} \gg Q_{\text{H}}$  then a KIE on the  $\text{CL}_{\text{int}}$  may be observed on the hepatic extraction ratio (first pass), which results in an increase in AUC and  $C_{\text{max}}$ , but not in system half-life. Conversely, if  $\text{CL}_{\text{int}} \ll Q_{\text{H}}$  then a KIE on the  $\text{CL}_{\text{int}}$  will be observed as an increase in systemic half-life, AUC, and  $C_{\text{max}}$  (Fig. 11). In addition, as  $\text{CL}_{\text{H}}$  approaches liver blood flow, the kinetic isotope effect on  $\text{CL}_{\text{H}}$  will decrease, meaning larger KIE will be observed on compounds with low/moderate stability. It is important to note that while not all compounds may benefit from a change in clearance or AUC, deuterium can still be useful to direct or alter metabolic pathways while not necessarily having large impacts on overall clearance [39, 58, 66, 73, 74]. This is the case of CTP-347, where a reduction in mechanism-based inactivation was apparent.

$$\text{CL}_{\text{H}} = \frac{Q_{\text{H}} \times \text{CL}_{\text{int}}}{Q_{\text{H}} + \text{CL}_{\text{int}}} \quad (2)$$



**FIG. 11** Theoretical comparison of hydrogenated and deuterated drugs as a function of  $\text{CL}_{\text{int}}$  in reference to blood flow ( $\text{KIE} = 7$ ). At higher  $\text{CL}_{\text{int}}$  values, the observed KIE decreases. *Figure recreated from R. Sharma, et al., Deuterium isotope effects on drug pharmacokinetics. I. System-dependent effects of specific deuteration with aldehyde oxidase cleared drugs, Drug Metab. Dispos. 40 (3) (2012) 625–34.*

## 4 Conclusions and future perspectives

In conclusion, stable isotope-labeled drugs have played an important role as a tool to better understand drug metabolism. Stable isotopes are widely used in academia and industry as markers to identify sites of metabolism and elucidate reaction mechanisms, as well as tracers to monitor and identify administered drug and resulting metabolites *in vivo*. Utilizing stable isotopes to confirm reaction mechanisms facilitate the expansion of drug metabolism sciences. As new modalities and structure designs are routinely used, a thorough understanding of how each new molecule is metabolized is crucial for productive drug design and knowledge of distribution and toxicity for all drug-related material. In the case of deuterated drugs, they are used as internal standards for quantitation, probes to elucidate metabolic reactions, and as substitutes to help optimize pharmacological or toxicological properties of drugs. The latter has already been showcased with the approval of deutetrabenazine, with several more candidates in the clinic to follow. Deuterium substitution of metabolic soft spots has been shown to help with various aspects of drug metabolism. This includes improvement in metabolic stability, as observed in changes in bioavailability,  $C_{\max}$ , AUC, and half-life, as well as mitigation of reactive/toxic metabolites. Each are dependent on the chemical structure, enzymes involved, and routes of elimination to predict the utility of deuterium substitution in drug design. Identification of potential metabolic “soft spot” candidate structures can inform chemists in the discovery phase of a thorough understanding of metabolic clearance mechanisms, and how it relates to total clearance of drug (metabolism and excretion) will ultimately be needed to confidently predict if a new deuterated drug will have any significant benefit when moving a candidate into the clinic. Understanding the utility of these tools will facilitate the design of metabolism studies and solving the challenging problems of the future. This could include but not limited to: elucidation of enzymatic metabolic reactions, preliminary detection of metabolites without radioactive material, studying *in vitro* *in vivo* disconnects and species differences, as well as expand techniques useful for drug design. The ability to change a molecule's nominal mass and/or stability, without significantly altering physical chemical properties is the greatest strength of these techniques, useful to expand our toolbox for ADME sciences and drug design.

## References

- [1] J.A. Williams, et al., Drug-drug interactions for UDP-glucuronosyltransferase substrates: a pharmacokinetic explanation for typically observed low exposure ( $AUC_i/AUC$ ) ratios, *Drug Metab. Dispos.* 32 (11) (2004) 1201–1208.
- [2] M.A. Cerny, Prevalence of non-cytochrome P450-mediated metabolism in Food and Drug Administration-approved oral and intravenous drugs: 2006-2015, *Drug Metab. Dispos.* 44 (8) (2016) 1246–1252.
- [3] D.A. Smith, R.S. Obach, Metabolites in safety testing (MIST): considerations of mechanisms of toxicity with dose, abundance, and duration of treatment, *Chem. Res. Toxicol.* 22 (2) (2009) 267–279.
- [4] P.H. Marathe, W.C. Shyu, W.G. Humphreys, The use of radiolabeled compounds for ADME studies in discovery and exploratory development, *Curr. Pharm. Des.* 10 (24) (2004) 2991–3008.
- [5] E.M. Isin, et al., Use of radiolabeled compounds in drug metabolism and pharmacokinetic studies, *Chem. Res. Toxicol.* 25 (3) (2012) 532–542.
- [6] N. Penner, L. Xu, C. Prakash, Radiolabeled absorption, distribution, metabolism, and excretion studies in drug development: why, when, and how? *Chem. Res. Toxicol.* 25 (3) (2012) 513–531.
- [7] T.A. Baillie, The use of stable isotopes in pharmacological research, *Pharmacol. Rev.* 33 (2) (1981) 81–132.

- [8] F.P. Abramson, et al., Replacing  $^{14}\text{C}$  with stable isotopes in drug metabolism studies, *Drug Metab. Dispos.* 24 (7) (1996) 697–701.
- [9] IUPAC, Periodic Table of Elements, 12-01-2018 04-12-2019; Available from: <https://iupac.org/what-we-do/periodic-table-of-elements/>, 2007.
- [10] S.E. Huskey, et al., Utilization of stable isotope labeling to facilitate the identification of polar metabolites of KAF156, an antimalarial agent, *Drug Metab. Dispos.* 44 (10) (2016) 1697–1708.
- [11] D. Girardi, et al., Targeting the hedgehog pathway in cancer: current evidence and future perspectives, *Cells* 8 (2) (2019) 153.
- [12] J. Bariwal, et al., Design of Hedgehog pathway inhibitors for cancer treatment, *Med. Res. Rev.* 39 (3) (2018) 1137–1204.
- [13] R.A. Graham, et al., A single dose mass balance study of the hedgehog pathway inhibitor vismodegib (GDC-0449) in humans using accelerator mass spectrometry, *Drug Metab. Dispos.* 39 (8) (2011) 1460–1467.
- [14] R.A. Graham, et al., Single and multiple dose intravenous and oral pharmacokinetics of the hedgehog pathway inhibitor vismodegib in healthy female subjects, *Br. J. Clin. Pharmacol.* 74 (5) (2012) 788–796.
- [15] H. Wong, et al., Interplay of dissolution, solubility, and nonsink permeation determines the oral absorption of the hedgehog pathway inhibitor GDC-0449 in dogs: an investigation using preclinical studies and physiologically based pharmacokinetic modeling, *Drug Metab. Dispos.* 38 (7) (2010) 1029–1038.
- [16] Q. Yue, et al., Absorption, distribution, metabolism, and excretion of [(1)(4) $\text{C}$ ]GDC-0449 (vismodegib), an orally active hedgehog pathway inhibitor, in rats and dogs: A unique metabolic pathway via pyridine ring opening, *Drug Metab. Dispos.* 39 (6) (2011) 952–965.
- [17] S.C. Khojasteh, et al., Investigations into the mechanisms of pyridine ring cleavage in Vismodegib, *Drug Metab. Dispos.* 42 (3) (2014) 343–351.
- [18] H. Le, et al., Elucidating the mechanism of Tofacitinib oxidative decyanation, *Drug Metab. Lett.* 10 (2) (2016) 136–143.
- [19] R.A. Thompson, et al., Reactive metabolites: current and emerging risk and hazard assessments, *Chem. Res. Toxicol.* 29 (4) (2016) 505–533.
- [20] T.A. Baillie, A.E. Rettie, Role of biotransformation in drug-induced toxicity: influence of intra- and inter-species differences in drug metabolism, *Drug Metab. Pharmacokinet.* 26 (1) (2011) 15–29.
- [21] L. Jin, et al., Identification of novel glutathione conjugates of disulfiram and diethyldithiocarbamate in rat bile by liquid chromatography-tandem mass spectrometry. Evidence for metabolic activation of disulfiram in vivo, *Chem. Res. Toxicol.* 7 (4) (1994) 526–533.
- [22] C. Zhang, et al., Novel mechanism for dehalogenation and glutathione conjugation of dihalogenated anilines in human liver microsomes: evidence for ipso glutathione addition, *Chem. Res. Toxicol.* 24 (10) (2011) 1668–1677.
- [23] Z. Yan, et al., Rapid detection and characterization of minor reactive metabolites using stable-isotope trapping in combination with tandem mass spectrometry, *Rapid Commun. Mass Spectrom.* 19 (22) (2005) 3322–3330.
- [24] Q. Wang, et al., A high-throughput glutathione trapping assay with combined high sensitivity and specificity in high-resolution mass spectrometry by applying product ion extraction and data-dependent neutral loss, *J. Mass Spectrom.* 54 (2) (2019) 158–166.
- [25] K.L. Bogan, C. Brenner, Nicotinic acid, nicotinamide, and nicotinamide riboside: a molecular evaluation of NAD<sup>+</sup> precursor vitamins in human nutrition, *Annu. Rev. Nutr.* 28 (2008) 115–130.
- [26] H.C. Urey, F.G. Brickwedde, G.M. Murphy, A hydrogen isotope of mass 2, *Phys. Rev.* 39 (1) (1932) 164–165.
- [27] J. Yang, *Deuterium: Discovery and Applications in Organic Chemistry*, Elsevier, 2016, pp. 1–116.
- [28] C. Elison, et al., Effect of deuteration of N–CH<sub>3</sub> group on potency and enzymatic N-demethylation of morphine, *Science* 134 (3485) (1961) 1078–1079.
- [29] T. Pirali, et al., Applications of deuterium in medicinal chemistry, *J. Med. Chem.* 62 (11) 2019, 5276–5297.
- [30] J.F. Liu, et al., A decade of deuteration in medicinal chemistry, in: R.A. Goodnow (Ed.), *Annual Reports in Medicinal Chemistry*, Academic Press, 2017, pp. 519–542 (Chapter 14).
- [31] T.G. Gant, Using deuterium in drug discovery: leaving the label in the drug, *J. Med. Chem.* 57 (9) (2014) 3595–3611.
- [32] K.B. Wiberg, The deuterium isotope effect, *Chem. Rev.* 55 (4) (1955) 713–743.
- [33] S.D. Nelson, W.F. Trager, The use of deuterium isotope effects to probe the active site properties, mechanism of cytochrome P450-catalyzed reactions, and mechanisms of metabolically dependent toxicity, *Drug Metab. Dispos.* 31 (12) (2003) 1481–1498.
- [34] R.P. Bell, Liversidge lecture. Recent advances in the study of kinetic hydrogen isotope effects, *Chem. Soc. Rev.* 3 (4) (1974) 513–544.

- [35] F.P. Guengerich, Kinetic deuterium isotope effects in cytochrome P450 reactions, *Methods Enzymol.* 596 (2017) 217–238.
- [36] R. Tung, The development of deuterium-containing drugs, *Innov. Pharm. Technol.* 32 (2010) 24–28.
- [37] L.E. Dyck, D.A. Burden, A.A. Boulton, Effects of deuterium substitution on the catabolism of  $\beta$ -phenylethylamine: an in vivo study, *J. Neurochem.* 46 (2) (1986) 399–404.
- [38] L.E. Dyck, A.A. Boulton, Effect of deuterium substitution on the disposition of intraperitoneal tryptamine, *Biochem. Pharmacol.* 35 (17) (1986) 2893–2896.
- [39] D.H. Phillips, et al., Reduced genotoxicity of [D5-ethyl]-tamoxifen implicates alpha-hydroxylation of the ethyl group as a major pathway of tamoxifen activation to a liver carcinogen, *Carcinogenesis* 15 (8) (1994) 1487–1492.
- [40] G.S. Timmins, Deuterated drugs; where are we now? *Expert Opin. Ther. Pat.* 24 (10) (2014) 1067–1075.
- [41] G.S. Timmins, Deuterated drugs; updates and obviousness analysis, *Expert Opin. Ther. Pat.* 27 (12) 2017, 1353–1361.
- [42] 35 U.S.C. 103, Conditions for patentability; non-obvious subject matter, [cited 2019 04-10-2019]; Available from: <https://www.bitlaw.com/source/35usc/103.html>.
- [43] B. Halford, Deuterium switcheroo breathes life into old drugs, *Chem. Eng. News* 94 (2016) 32–36.
- [44] L.L. Furge, F.P. Guengerich, Cytochrome P450 enzymes in drug metabolism and chemical toxicology: an introduction, *Biochem. Mol. Biol. Educ.* 34 (2) (2006) 66–74.
- [45] A. Abbasi, et al., The time-course of aldehyde oxidase and the reason why it is nonlinear, *Drug Metab. Dispos.* 47 (5) 2019, 473–483.
- [46] G. Guroff, et al., Hydroxylation-induced migration: the NIH shift. Recent experiments reveal an unexpected and general result of enzymatic hydroxylation of aromatic compounds, *Science* 157 (3796) (1967) 1524–1530.
- [47] K.R. Korzekwa, W.F. Trager, J.R. Gillette, Theory for the observed isotope effects from enzymic systems that form multiple products via branched reaction pathways: cytochrome P-450, *Biochemistry* 28 (23) (1989) 9012–9018.
- [48] O. Okazaki, F.P. Guengerich, Evidence for specific base catalysis in N-dealkylation reactions catalyzed by cytochrome P450 and chloroperoxidase. Differences in rates of deprotonation of aminium radicals as an explanation for high kinetic hydrogen isotope effects observed with peroxidases, *J. Biol. Chem.* 268 (3) (1993) 1546–1552.
- [49] F.P. Guengerich, C.H. Yun, T.L. Macdonald, Evidence for a 1-electron oxidation mechanism in N-dealkylation of N,N-dialkylanilines by cytochrome P450 2B1. Kinetic hydrogen isotope effects, linear free energy relationships, comparisons with horseradish peroxidase, and studies with oxygen surrogates, *J. Biol. Chem.* 271 (44) (1996) 27321–27329.
- [50] J. Jiang, et al., Effect of N-methyl deuteration on metabolism and pharmacokinetics of enzalutamide, *Drug Des. Devel. Ther.* 10 (2016) 2181–2191.
- [51] F.P. Guengerich, Kinetic deuterium isotope effects in cytochrome P450 oxidation reactions, *J. Label. Compd. Radiopharm.* 56 (9–10) (2013) 428–431.
- [52] S. Dragulska, M. Kańska, Enzymatic oxidation of substituted tryptamines catalysed by monoamine oxidase, *Nukleonika* 59 (3) (2014) 91.
- [53] D.C. Pryde, et al., Aldehyde oxidase: an enzyme of emerging importance in drug discovery, *J. Med. Chem.* 53 (24) (2010) 8441–8460.
- [54] J.R. Miller, D.E. Edmondson, Structure – activity relationships in the oxidation of para-substituted benzylamine analogues by recombinant human liver monoamine oxidase A, *Biochemistry* 38 (41) (1999) 13670–13683.
- [55] X. Lu, H. Ji, R. Silverman, *Flavins and Flavoproteins 2002*, Chapman, S, 2002, pp. 817–830.
- [56] S.E. Rigby, et al., A stable tyrosyl radical in monoamine oxidase A, *J. Biol. Chem.* 280 (6) (2005) 4627–4631.
- [57] B. Belleau, et al., Effect of deuterium substitution in sympathomimetic amines on adrenergic responses, *Science* 133 (3446) (1961) 102–104.
- [58] R. Sharma, et al., Deuterium isotope effects on drug pharmacokinetics. I. System-dependent effects of specific deuteration with aldehyde oxidase cleared drugs, *Drug Metab. Dispos.* 40 (3) (2012) 625–634.
- [59] D.M. Paton, Deutetabenazine: treatment of hyperkinetic aspects of Huntington’s disease, tardive dyskinesia and Tourette syndrome, *Drugs Today (Barc.)* 53 (2) (2017) 89–102.
- [60] L. Citrome, Deutetabenazine for tardive dyskinesia: a systematic review of the efficacy and safety profile for this newly approved novel medication—what is the number needed to treat, number needed to harm and likelihood to be helped or harmed? *Int. J. Clin. Pract.* 71 (11) (2017) e13030.

- [61] Z. Yao, et al., Preparation and evaluation of tetrabenazine enantiomers and all eight stereoisomers of dihydro-tetrabenazine as VMAT2 inhibitors, *Eur. J. Med. Chem.* 46 (5) (2011) 1841–1848.
- [62] D. Stamler, M. Bradbury, F. Brown, The pharmacokinetics and safety of deuterated-tetrabenazine (P07.210), *Neurology* 80 (7 Supplement) (2013) P07.210.
- [63] S.L. Harbeson, et al., Altering metabolic profiles of drugs by precision deuteration 2: discovery of a deuterated analog of Ivacaftor with differentiated pharmacokinetics for clinical development, *J. Pharmacol. Exp. Ther.* 362 (2) (2017) 359–367.
- [64] E.M. Russak, E.M. Bednarczyk, Impact of deuterium substitution on the pharmacokinetics of pharmaceuticals, *Ann. Pharmacother.* 53 (2) (2018) 211–216.
- [65] M. Murray, Mechanisms of inhibitory and regulatory effects of methylenedioxyphenyl compounds on cytochrome P450-dependent drug oxidation, *Curr. Drug Metab.* 1 (1) (2000) 67–84.
- [66] V. Uttamsingh, et al., Altering metabolic profiles of drugs by precision deuteration: reducing mechanism-based inhibition of CYP2D6 by paroxetine, *J. Pharmacol. Exp. Ther.* 354 (1) (2015) 43.
- [67] Z. Zhang, W. Tang, Drug metabolism in drug discovery and development, *Acta Pharm. Sin. B* 8 (5) (2018) 721–732.
- [68] S.H. DeWitt, V. Jacques, L.H. Van der Ploeg, DRX-065, the stabilized R-enantiomer of pioglitazone is without PPAR $\gamma$  agonist activity and exhibits the beneficial in vivo pharmacodynamic effects for the treatment of NASH. Parallel 20: Pediatric and Metabolic Liver Diseases: Clinical, Hepatology Abstracts. 66th AASLD Meeting 62 (1) (2015) 281A Abstract 143.
- [69] S.C. Cheetham, et al., Efficacy of DRX-065, the Stabilized R-Enantiomer of Pioglitazone (Pio), in Choline-Deficient (CD) and Methionine/Choline-Deficient (MCD) Diet Mouse Models of Nonalcoholic Steatohepatitis (NASH), Available from: [https://d1io3yog0oux5.cloudfront.net/\\_10707e3f479d410d3a6ee92f5b7d8012/poxelpharma/db/419/3016/file/Poster-AASLD-2016-LB-32-Poster-DeuteRx-Nov-2016.pdf](https://d1io3yog0oux5.cloudfront.net/_10707e3f479d410d3a6ee92f5b7d8012/poxelpharma/db/419/3016/file/Poster-AASLD-2016-LB-32-Poster-DeuteRx-Nov-2016.pdf), 2016.
- [70] S.W. Cowan-Jacob, et al., Imatinib (STI571) resistance in chronic myelogenous leukemia: molecular basis of the underlying mechanisms and potential strategies for treatment, *Mini-Rev. Med. Chem.* 4 (3) (2004) 285–299.
- [71] P.W. Manley, et al., The kinetic deuterium isotope effect as applied to metabolic deactivation of imatinib to the des-methyl metabolite, CGP74588, *Bioorg. Med. Chem.* 21 (11) (2013) 3231–3239.
- [72] H. Gaweska, P.F. Fitzpatrick, Structures and mechanism of the monoamine oxidase family, *Biomol. Concepts* 2 (5) (2011) 365–377.
- [73] A.E. Mutlib, et al., The species-dependent metabolism of Efavirenz produces a nephrotoxic glutathione conjugate in rats, *Toxicol. Appl. Pharmacol.* 169 (1) (2000) 102–113.
- [74] M.D. Threadgill, et al., Metabolism of N-methylformamide in mice: primary kinetic deuterium isotope effect and identification of S-(N-methylcarbamoyl)glutathione as a metabolite, *J. Pharmacol. Exp. Ther.* 242 (1) (1987) 312–319.

# Assessment of stereoselectivity in pharmacology, toxicology, and drug metabolism

*Lushan Yu, Su Zeng*

Institute of Drug Metabolism and Pharmaceutical Analysis, Zhejiang University,  
Hangzhou, People's Republic of China

## 1 Introduction

A chiral compound refers to a molecule having a chiral center or an asymmetric center in the molecular structure, wherein enantiomers are those stereoisomers which are not spatially overlapping and are mirror images of each other. This pair of compounds is like a pair of human left and right hands with chirality, and the source of chiral is Greek *Chiro*. Those stereoisomers which are not enantiomers are referred to diastereomers. In nature, a pair of enantiomers may be present in different amounts, some of which exist only as a single enantiomer. For example, the amino acids constituting the protein are all L-amino acids, and the monosaccharides constituting the polysaccharide and the nucleic acid are D-monosaccharides. Many other natural chiral small molecules also exist primarily as one enantiomer, and this phenomenon is known as chiral preference. Chiral preference makes biological macromolecules or their constituent units such as nucleic acids, proteins, polysaccharides, receptors, and ion channels present asymmetric properties. These asymmetric properties also allow enzymes to catalyze specific chiral substrates, and receptors to bind only to specific chiral ligands. The different pharmacological activities of the enantiomers of a chiral drug can be expressed in different terms: the enantiomer with high affinity ( $aff_{eu}$ ) or high activity with the receptor is called the eutomer; the enantiomer with low affinity ( $aff_{dis}$ ) or low activity with the receptor is called the distomer [1]. The ratio of the affinity or activity of these two enantiomers is named eudisimic ratio,  $ER = aff_{eu}/aff_{dis}$ , which is the magnitude of the systematic



stereoselectivity. In addition, the difference in the value between the logarithm of enantiomer affinities is called superior/inferior index. About 60% commonly used drugs have one or more chiral centers, and many herbal active ingredients have several chiral centers.

## 2 Regulatory considerations on developing chiral drugs

At present, drug regulatory agencies in the United States, Canada, the European Community, Japan, and China have developed technical guidelines for the registration of chiral drugs, which require pharmacology, toxicology, and pharmacokinetics study of each enantiomer when reporting new drugs with chirality. There are many similarities in the requirements of different countries, but they focus on different aspects.

Chiral drugs also need to fit the specific requirements set for single optical enantiomers, and single optical enantiomers which are further developed from the listed racemates except meeting the requirements of general new drugs [2–4]. As for a single optical enantiomer, it is necessary to provide the information of bio-stability *in vivo*. If the optical enantiomer is formed *in vivo*, it is treated as a metabolite and noted in drug development. In preclinical evaluation study, the metabolism and distribution of optical enantiomers should be studied adopting stereoselective detection methods. If the enantiomer is stable in that no racemization or optical configuration conversion occurs, stereoselective detection methods are unnecessary. The stereoselective detection should be utilized in animal experiments for pharmacokinetic studies to demonstrate the acute toxicity and long-term toxicity test results of enantiomeric drugs. As for the doses, routes of administration, and animal species used in the study, they should be the same as those selected in toxicity test. For a single optical enantiomer which is further developed from the listed racemates, if sufficient bridging studies are performed, some experiments do not have to be repeated since the listed racemates already provide a lot of information. However, the important pharmacological activities of enantiomers such as potency, specificity, maximal effect, bioequivalence, etc. should be studied. For racemic compounds, if there is a significant change in the toxicity of the drug, toxicological study should be performed on different enantiomers to determine if only one of the enantiomers is toxic. Toxicological studies of enantiomers usually include long-term toxicity studies with repeated doses (up to 3 months). If there is no difference between the toxicological profiles of the single enantiomer and its racemate, there is no need for further studies. If the single enantiomer is more toxic, further investigations are needed to consider drug effects.

In China, “Provisions for Drug Registration” [5] and the technical guidance [6] have been promulgated to regulate and guide the research and development of chiral drugs. For optical enantiomer R&D, the collected data and related literature comparisons between the racemate and/or single enantiomers should be reported to reflect the rationality of study design. When the safety range of racemate is small and/or the available data may indicate that the unexpected toxicity of a single enantiomer increases significantly, the toxicity of racemate and single enantiomer repeated administration (usually less than 3 months) or other toxicological research data (such as reproductive toxicity) should be provided. The development of chiral drugs should first consider the safety of the drug, and also to develop an enantiomer that is effective with significantly reduced toxicity, enhanced efficacy, improved pharmacokinetics, or any combination above.

### 3 Stereoselectivity in pharmacodynamics

The pharmacological effects of chiral drugs are achieved through strict chiral matching and molecular recognition with macromolecules *in vivo*, presenting differences in mechanism and binding force. When the drug enantiomer binds on different receptors or receptor sub-units, it may produce different pharmacological effects or toxic-side reactions. Although some drugs act on the same receptor, the drug enantiomers may also have different interactions on the receptor, and exert different pharmacological effects. *In vivo*, there are various factors resulting in changes of pharmacodynamic activity between enantiomers. And this diversity in enantiomeric efficacy between chiral drugs is very complex and can be roughly divided into the following cases: case1, selective competitive antagonism; case2, enantiomers have the opposite effects; case3, one enantiomer has side effects; case4, different biological activities; case5, complementarity of enantiomeric effects; case6, the biological activity of a drug is produced by single enantiomer; case7, different action targets present different characteristics; and case8, same biological activity.

#### 3.1 Selective competitive antagonism

*S*-isoprenaline is a  $\beta_1$  receptor agonist, while its *R*-enantiomer acts as a competitive antagonist of *S*-isoprenaline with approximately equivalent affinity. *S*-methadone significantly attenuates the effects of its *R*-enantiomer on contraction and respiration. Benzopyridine analgesic drug, piconadol, *R*-enantiomer of piconadol is an agonist of opioid receptor, having a comparative activity with morphine, while the *S*-enantiomer of piconadol is a blocker of opioid receptors, the activity of which is 1/10 of that of naloxone [7].

#### 3.2 Enantiomers have the opposite effects

Dobutamine is a cardiotoxic drug. Its *S*-enantiomer is a receptor agonist, while *R*-enantiomer is a receptor antagonist. In addition, some enantiomers of dihydropyridine calcium channel blockers have an opposite effect on channel function when used to treat angina and hypertension, such as nivaldipine, amlodipine, and nifedipine. Their *S*-enantiomer is a strong activator for the L-form voltage-dependent calcium channel, while the *R*-enantiomer is a blocker. These drug enantiomers have opposite stereo-configuration requirements for channel binding, thus interacting with different calcium channel states can lead to open (activate) or shut down (inactivate) the calcium channel [8].

#### 3.3 One enantiomer has side effects

Ketamine is a non-barbital central nervous system (CNS) depressant, and the anesthesia or analgesic effects exerted by its *S*-(+)-enantiomer are two to four times stronger than that by its *R*-(-)-enantiomer. What's more, the *R*-(-)-enantiomer of ketamine excites the CNS to produce spirit symptom [9]. The activity of the D-form of ethambutol, an antituberculosis drug, is more than 200 times stronger than that of its L-form, and its toxicity is much lower as well. The levo-enantiomer of the anthelmintic drug tetramisole exerts its anthelmintic effect through inhibition of succinate dehydrogenase in worm muscles, thus causing continuous

contraction leading to paralysis of the parasite. But for the dextro-enantiomer of tetramisole, it causes side effects such as vomiting for the host.

### 3.4 Different biological activities

Dextropropoxyphen is an analgesic, but levopropoxyphen is a cough suppressant. The two enantiomers of timolol have their own therapeutic effects, the *S*-enantiomer of timolol treats cardiovascular disease, while the *R*-enantiomer focuses on treating glaucoma [10]. Spearmint oil and caraway oil are a pair of enantiomers. The former one has antispasmodic, treating colic, and antibacterial effects. The latter one can resist dizziness (vertigo), earache, and strengthen liver function, especially has a prolactin effect on breast-feeding women. And the smell of those two drugs is also different [11].

### 3.5 Complementarity of enantiomeric effects

The  $\beta$ -receptor blockade effect of *S*-(-)-propranolol is about 100 times stronger than that of *R*-(+)-propranolol, but the *R*-form can inhibit the sodium channel, so the antiarrhythmic effect of using racemate is better than that of using only individual enantiomer [12]. The *R*-enantiomer of the antihypertensive drug indacrinone has a diuretic effect, but it has the side effect of increasing uric acid in the blood, while the *S*-enantiomer of indacrinone promotes uric acid excretion and reduces the side effects of the *R*-enantiomer. The combination of these two enantiomers can take advantage of each other and avoid side effects. Further studies have illustrated that the therapeutic effects are best when the ratio of *S*- to *R*-enantiomer is 1:4 or 1:8.

### 3.6 The biological activity of a drug is produced by single enantiomer

Only *S*-enantiomer of  $\alpha$ -methyl dopa has hypotensive effect; (+)-dopa has no physiological effect, while (-)-dopa can treat Parkinson's disease. As for vigabatrin, only the *S*-enantiomer is a GABA transaminase inhibitor. Only *S*-enantiomer of amlodipine has antihypertensive activity, while *R*-enantiomer has no effects [13]. Furthermore, the *S*-enantiomer of amlodipine can increase the therapeutic efficacy by two times with greatly reducing toxic side effects simultaneously. The antihistamine effect of *R*-enantiomer of chlorpheniramine is 100 times stronger than that of the *S*-enantiomer.

### 3.7 Different action targets present different characteristics

The effects of *S*- and *R*-enantiomer of  $\beta$ -receptor partial agonists befunolol and carteolol are the same, both targeted on the guinea pig ciliary body. But in the right aorta and trachea, the effect of the *S*-enantiomer is 10 times stronger than that of the *R*-enantiomer. This result indicates that the  $\beta$ -receptor has no stereoselectivity in the ciliary body and it has stereoselectivity in tissues such as right aorta and trachea [14].

### 3.8 Same biological activity

*S*-(+)- and *R*-(-)-propafenone exert equal effects on the sodium channel-dependent antiarrhythmic class 1 activity [15]. Flecainide is a chiral drug used to treat class I antiarrhythmia. *S*-(+)- and *R*-(-)-flecainide have similar electrophysiologic effects and similar pharmacokinetics [16]. Therefore, flecainide is administered as a racemate.

## 4 Stereoselectivity in pharmacokinetics and ADME properties

Due to the interaction between chiral drugs and biological macromolecules such as drug-metabolizing enzymes, transporters, and proteins, the pharmacokinetic properties of enantiomers, including absorption, distribution, metabolism, and excretion (ADME) can be stereoselective. The concentration of enantiomers in plasma may be significantly different when racemates are administered. Therefore, the stereoselectivity of the chiral drug pharmacokinetics process should be taken into consideration during the evaluation of chiral drug pharmacokinetic parameters or determination of chiral drug plasma concentration-effect relationship [17].

### 4.1 Stereoselectivity of chiral drug absorption and transport

Drugs are absorbed into the body by passive transport or active transport [18]. For the passive transport process, the level and speed of drug absorption depends on the liposolubility of the drug. Because of the small difference in water solubility and fat solubility between the chiral drug enantiomers, solubility generally does not lead to stereoselectivity between the two enantiomers. However, the crystal form of certain drug racemates may differ from their single enantiomer, thus causing a difference in their dissolution rate at the administration site. As for a chiral drug whose absorption process relies on a carrier or undergoes an active process, its absorption exhibits significant stereoselectivity [19]. The important drug transporters include efflux transporters: P-gp, BCRP, MRPs, MATEs and uptake transporters: OATs, OCTs, OATPs, etc. [20].

Transport protein mainly mediates the exchange of chemical materials across lipid membranes, often able to stereoselectively recognize different enantiomeric substrates. An early study found that *L*-dopa is actively absorbed in the intestine mainly through the amino acid transport system, and its absorption rate is much higher than that of *D*-dopa, which is transported by simple diffusion [21]. There are several efflux transporters including P-gp and MRP participating the absorption and efflux of cetirizine, which showed enantioselectivity in the transmembrane process. *R*-cetirizine significantly increased the efflux ratio of rhodamine-123 and doxorubicin in a fashion indicative of the upregulation of P-gp and MRP activities. However, *S*-cetirizine played a role of an inhibitor for P-gp and MRP. Ranitidine modified the absorption of cetirizine enantiomers, suggesting that the potential drug-drug interaction would significantly change the cetirizine pharmacokinetics [22].

Drug-drug interactions can be mediated by drug transporters, and even cause significant changes in drug ADME. Grapefruit juice (GFJ) has been shown to interact with many drugs in a variety of ways, resulting in drug loss of efficacy or toxic side effects. Its mechanism of action

is mainly by inhibiting intestinal CYP3A and P-gp, but also by inhibiting organic anion transport polypeptide (OATPs) to affect the role of other drugs. After a single oral administration of 60-mg fexofenadine tablets in 14 healthy subjects (control group), the plasma concentration of *R*-fexofenadine was always higher than the concentration of the *S*-fexofenadine, and the *R/S* ratio of  $AUC_{0-24h}$  was about 1.58. In the grapefruit juice group (GFJ group), all pharmacokinetic parameters of the two enantiomers changed except  $t_{1/2}$  and  $t_{max}$ . The plasma concentration was significantly decreased and the *R/S* ratio of  $AUC_{0-24h}$  raised to 1.96. This is because fexofenadine is a substrate for the organic anion transporter OATP2B1, which is inhibited by grapefruit juice, therefore, it has an effect on the stereoselective absorption of fexofenadine [23].

Transdermal permeability of L-norgestrel (L-NG) and DL-norgestrel (DL-NG) was investigated by using Valia-Chien double-compartment permeation cells. The results showed that the permeation rates of DL-NG through intact skin were significantly higher than those of L-NG ( $P < 0.01$ ). The permeation rates between L-NG and DL-NG were no significant difference in the skins without stratum corneum [24].

## 4.2 Stereoselectivity of chiral drug distribution

Some chiral drugs have stereoselective plasma protein or tissue binding, which can affect the distribution of their enantiomers in body.

### 4.2.1 Stereoselectivity of interaction between chiral drugs and plasma proteins

The differences in the binding force and affinity of chiral drug enantiomers to the proteins result in a stereoselective effect when they bind to plasma proteins. The binding process of drugs and plasma proteins mainly involves human serum albumin (HSA) and  $\alpha$ 1-acid glycoprotein (AGP). HSA primarily binds acidic drugs, and AGP binds alkaline drugs. But the amount of AGP is only 3% of HSA, and AGP is significantly increased in the disease state. The two enantiomers of the same drug sometimes exhibit different binding properties toward two proteins [25].

The AGP-mexiletine-binding profile exhibited enantioselectivity ( $R > S$ ) to that in human plasma, whereas HSA-mexiletine interaction was selective for the *S*-enantiomer over the *R*-enantiomer at pH7.4. AGP variants and recombinant fragments of HSA have been applied to study enantiomer-binding properties. The study indicated that mexiletine had the highest binding affinity for F1-S, which is a variant of AGP. Based on the computational studies, residues such as Arg90, Leu79, Ser89, and Phe89 showed an energy difference of more than  $-0.35$  kcal/mol between the enantiomers (Fig. 1) [26]. The standard HSA ligands digitoxin, phenylbutazone, and diazepam selectively bind to DOM I, DOM II, and DOM III, respectively. For the chiral drugs, *R*-ketoprofen showed a higher binding affinity toward DOM III than *S*-ketoprofen, whereas *S*-mexiletine bound to DOM II with a greater affinity than *R*-mexiletine [27].

### 4.2.2 Stereoselectivity of interaction between chiral drugs and tissues

Due to the stereoselective environment provided by cell membranes and phospholipids in biological tissues, chiral drugs distribution in different tissues may also have

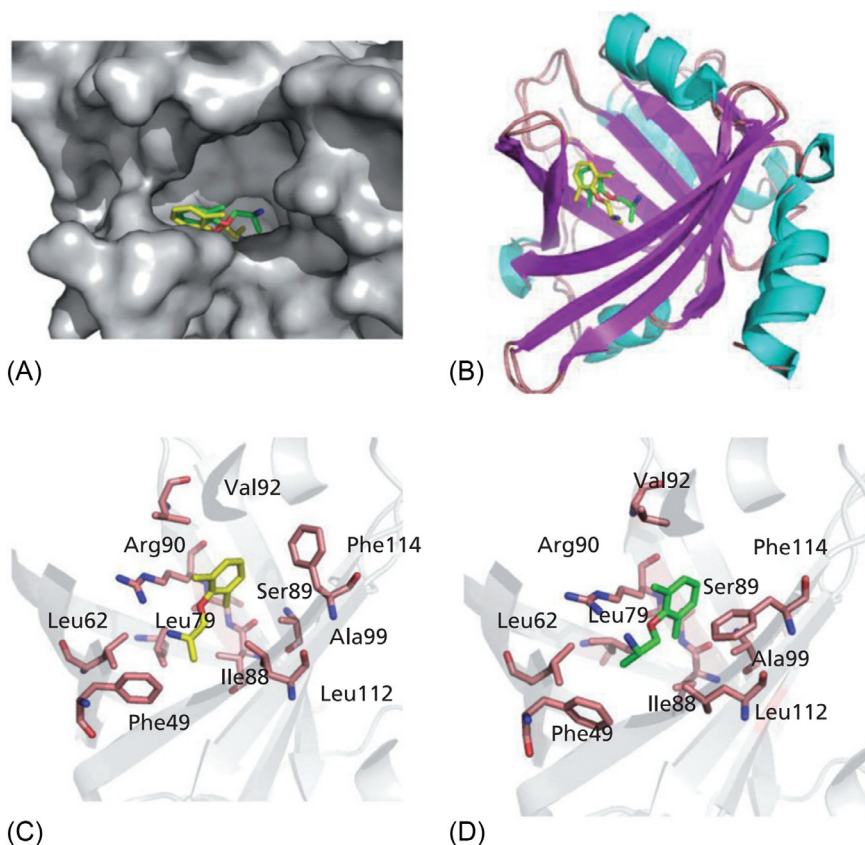


**FIG. 1** The binding modes of *R*-/*S*-mexiletine with AGP. (A) Cavity of hAGP fitted with mexiletine enantiomers; (B) superimposed structures of hAGP binding with mexiletine enantiomers; (C and D) binding pocket residues interact with mexiletine enantiomers. *Yellow*, *R*-mexiletine and *green*, *S*-mexiletine [26].

stereoselectivity. The thiazolidinedione antidiabetic drug pioglitazone has been proved to be a potential drug for the treatment of Alzheimer's disease. When the mouse was administrated racemic pioglitazone, the *R*-enantiomer concentration is 146.6% of *S*-enantiomer concentration in brain tissue, while in plasma the former concentration was 67.7% lower than the latter. Further studies have found that P-gp may act as a stereoselective barrier to block pioglitazone from entering brain tissue, and administration of *R*-enantiomer can increase drug concentration in brain tissue better than administration of racemic, thereby improving the efficacy [28].

There are also existing differences caused by stereoselectivity when chiral drugs passing through the placental barrier. After intravenous injection of 0.25 mg salbutamol, the drug concentration in maternal blood and fetal umbilical cord blood of cesarean section was determined. It was found that the concentration of *R*-enantiomer in the maternal blood was nearly one time lower than that in the fetal umbilical cord blood; while the concentration of *S*-enantiomer concentrations was similar; however, the *R*/*S*-enantiomeric ratio in fetal umbilical cord blood was higher than that in maternal blood [29].



### 4.3 Chirality in drug metabolism

Various subtypes of CYP, including CYP1A2, 2B6, 2C9, 2C19, 2D6, 3A4, etc., have been found to show stereoselective metabolism for various chiral drugs. The metabolic process of chiral drugs is complex. Usually, multiple metabolic pathways metabolize individual enantiomer of drugs with different stereoselective states, and the selective balance of various enzymes involved in metabolic processes leads to differences in the intrinsic clearance rate of drugs. For example, propranolol has a wide range of metabolic pathways, all showing stereoselectivity. The selectivity for N-dehydroxylation and parahydroxylation in human is *R*-enantiomer > *S*-enantiomer, and the selectivity for deamination and glucuronidation is *S*-enantiomer > *R*-enantiomer. Overall, the *S*-enantiomer predominates in plasma. Tetrahydropalmatine (THP) was preferentially metabolized by human liver microsome (HLM). The inhibition of fluvoxamine (inhibitor of CYP1A2) on metabolism of (+)-THP was greater than that of (–)-THP; the metabolic rate of (+)-THP was 5.3-fold of (–)-THP in recombinant human CYP1A2. (–)-THP, but not (+)-THP, significantly inhibited the activity of CYP2D6. (+)-THP was preferentially metabolized by CYP1A2, whereas CYP3A4/5 contributed equally to metabolism of (–)-THP or (+)-THP [30].

Human uridine diphosphate glucuronosyltransferases (UGTs) are a very important enzyme that catalyzes phase II conjugation reaction in human. Stereoselective glucuronidation of propafenone and its  $\beta$ -blocker analogs propranolol, terbutaline, atenolol, esomolol, and sotalol were observed in human recombinant UGT1A9, and *S*-enantiomers of these drugs glucuronidated by human UGT1A9 were much faster than their antipodes [31]. The selective  $\alpha$ 1-adrenergic receptor blocker naftopidil (NAF) racemate has a low oral bioavailability (9% in rats and 18% in humans). The oral bioavailability of *S*-NAF is twice than that of *R*-NAF, probably because the glucuronidation of *S*-NAF is half of that occurred in *R*-NAF [32]. To study the stereoselective glucuronidation, carvedilol (CARV) incubated with three Chinese liver microsomes. The results showed that the values of  $K_m$  and  $V_{max}$  for *S*-CARV and *R*-CARV enantiomers were  $118 \pm 44 \mu\text{mol/L}$ ,  $2500 \pm 833 \text{ pmol}/(\text{min}\cdot\text{mg protein})$  and  $24 \pm 7 \mu\text{mol/L}$ ,  $953 \pm 399 \text{ pmol}/(\text{min}\cdot\text{mg protein})$ , respectively. The results suggested that there was a significant stereoselective glucuronidation of CARV enantiomers, which might partly explain the enantioselective pharmacokinetics of CARV [33].

Metabolic processes tend to be competing. When drugs are involved in multiple metabolic pathways, the two enantiomers may have different preferences for different metabolic pathways. Different metabolic processes may have opposite substrate stereoselectivity, and their differences in metabolic clearance rates are manifested by the selectivity of different metabolic pathways. For example, *S*-warfarin is mainly subjected to 7-hydroxylation metabolism in human, while *R*-warfarin mainly undergoes 6-hydroxylation metabolism and ketone-reductive metabolic reaction. If the drug can be metabolized by more than one pathway, the stereoselectivity of its intrinsic clearance reflects the selectivity balanced results of various enzymes. In addition, if several isozymes are metabolized to produce the same product, each isozyme may also exhibit different stereoselectivity [34]. For example, propranolol undergoes 4-hydroxylation reaction under the action of two different isoenzymes, but only one exhibits stereoselectivity, and for the glucuronidation of flurbiprofen, two isoenzymes showed the opposite stereoselectivity.



Polymorphisms of drug-metabolizing enzymes result in stereoselectivity for metabolism of certain chiral drugs, complicating metabolic drug clearance. CYP2C8.4 and CYP2C9.10 showed significantly lower activity and CYP2C8.3 showed significantly higher activity toward both *R*- and *S*-fluoxetine (FLX) compared with the wild type, while CYP2C9.3, CYP2C9.13, and CYP2C9.16 showed significantly lower activity only toward *R*-FLX (Fig.2). Five CYP2C9 variants and CYP2D6.1 exhibited significantly stereoselective kinetic profiles prior to *R*-FLX, and CYP2C8.3 showed a slight stereoselectivity. Interestingly, obvious substrate inhibition was observed in the CYP2C9 wild type and its three variants only in the case of *R*-FLX (Fig.2). Together, these findings suggest that CYP2C9 and CYP2D6 polymorphism may play an important role in the clearance of FLX and also in the stereoselective kinetic profiles of FLX enantiomers [35]. Flurbiprofen (FPF), available commercially as a racemic mixture, is a propionic acid derivative of nonsteroidal anti-inflammatory drugs (NSAIDs). UGT1A9.2 (C3Y) exhibited a higher  $V_{max}$  (3.2-fold),  $K_m$  (2.1-fold), and intrinsic clearance (1.6-fold) toward *S*-FPF than UGT1A9.1 (wild type) did. UGT1A9.3 (M33T) almost lost the catalytic activity to FPF. A significantly stereoselective difference on the glucuronidation of rac-FPF was seen between the two variants compared with the wild type of UGT1A9 [36].

The metabolism of different subtypes of drug-metabolizing enzymes to chiral drugs presents different degrees of stereoselectivity. And the interaction between different enantiomers of chiral drugs also affects the binding ability between drugs and enzymes. Generally, if the drug metabolism process involves the process of ketone reduction, halogenation, prochiral substituent oxidation, hydrolytic metabolism, etc., this drug may have product stereoselectivity, and its main feature is the appearance of a chiral center during the metabolic

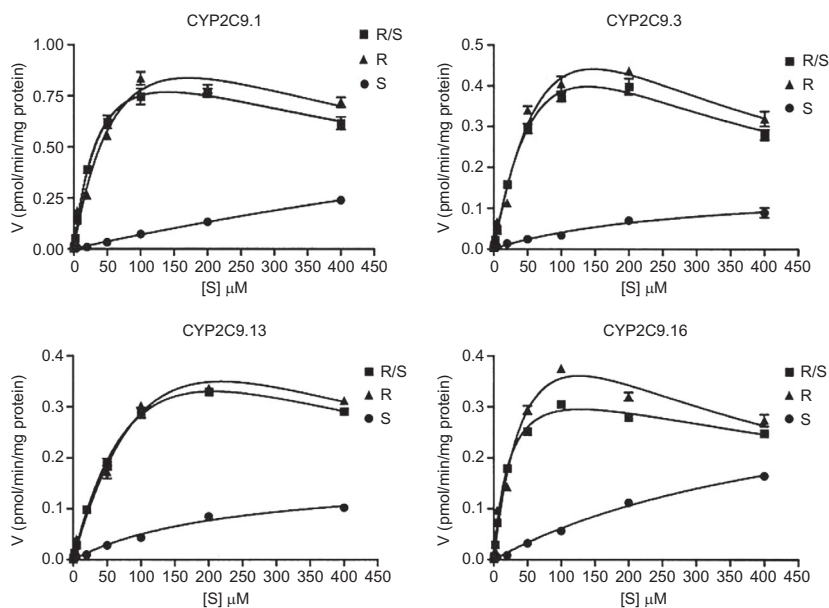


FIG. 2 Kinetics of the *N*-demethylation of *R*-, *S*-, and *R/S*-FLX in recombinant CYP2C9s enzymes [35].

process. Tivantinib is an orally effective targeted antitumor drug, and the metabolism of the drug and its four major metabolites in vitro were studied. It was demonstrated that CYP2C19 can catalyze the formation of M5, the hydroxylated metabolite of tivantinib, but have no catalytic activity for M4, the stereoisomer of M5. CYP3A4/5 has catalytic activity for the formation of both M4 and M5. On the other hand, the alcohol dehydrogenase (ADH) tends to catalyze M4 to become the ketone metabolite M6, rather than M5. Therefore, during the metabolism process of tivantinib, CYP2C19 has stereoselective hydroxylation effect, and the catalytic oxidation of ADH has obvious substrate stereoselectivity [37].

#### 4.4 Stereoselectivity of chiral drug excretion

The kidney is the main organ for drug excretion. Except for glomerular filtration, the active secretion of the renal tubules, the active and passive reabsorption processes all show stereoselectivity, which makes the renal clearance rate of certain drugs present a certain level of stereoselectivity. And there are various reasons accounting for the drug stereoselective excretion.

The formation and elimination of the metabolites of methamphetamine (MA), amphetamine (AMP), and p-hydroxymethyl amphetamine (pOH-MA) showed significant enantioselectivity. The formation of *S*-AMP (7%) was approximately three times larger than that of *R*-AMP (2%), and the excretion of *S*-MA (42%) was lower than that of *R*-MA (52%). The urinary excretion of *S*-pOH-MA was slightly higher than that of *R*-pOH-MA. The drug enzyme CYP2D6, which mediates this transformation, has a better affinity to the *S*-enantiomer of the analog of MA, MDMA. And it can be speculated that this phenomenon may come from the stereoselective characteristic during the process of MA conversion to AMP, causing the lack of *R*-MA converting to *R*-AMP and *R*-pOH-MA. It was reported that the propranolol glucuronidation of the side chain undergoes stereoselective excretion in 16 adult Chinese Han volunteers in urine after an oral administration of 20-mg racemic propranolol. The results showed the elimination rate constant  $k$  of *S*-propranolol glucuronide was less than that of *R*-propranolol glucuronide; and the elimination half-life ( $t_{1/2}$ ),  $T_{max}$  and the cumulative excretion amount ( $X_{u0-24}$ ) of *R*-propranolol glucuronide were significantly less than that of *S*-propranolol glucuronide [38]. The mechanism of enantioselective excretion of propranolol enantiomers is that UGT1A9 prefers catalyzing *S*-enantiomer to form *S*-propranolol glucuronide. The  $CL_{int}$  ratios of *S*-enantiomer to *R*-enantiomer are 3.8 times and 6.5 times for racemic propranolol and individual enantiomers, respectively. Therefore, there are the enantiomer-enantiomer interactions between *S*- and *R*-propranolol in glucuronidation [39].

#### 4.5 Methods for studying chiral drug interactions

In some cases, chiral drugs and other drugs are metabolized by the same drug-metabolizing enzymes or transported by the same transporters. The models of liver microsomes, human recombinant drug-metabolizing enzymes, transgenic cells expressing human drug transporters can be applied to study chiral drug interactions. In vitro studies of the interaction between enantiomers have the following methods:

(1) Individual enantiomer is incubated with enzyme to obtain enzyme kinetic parameters. The Segel's method was used to estimate the overall reaction rate, which was later compared with the actual measured racemic reaction rates. If the measured value is less than the estimated value, showing that there exists inhibition between the enantiomers. Conversely, there may be competitive activation. (2) Isotope-labeled GC/MS combined technique was utilized. When the interaction of amphetamine was studied by deuterium-labeled GC/MS method, it was found that *S*-amphetamine or its metabolite inhibited the metabolism of *R* enantiomer, so the stereoselectivity  $R > S$  of individual incubation changes into  $S > R$  of racemate incubation. (3) The enzymatic kinetic parameters of enantiomers obtained from racemate incubation are determined by chiral chromatography, and later those results are compared with the enzymatic kinetic parameters of the individual enantiomer. Or using a mixture of unequal amounts of enantiomers to measure the concentration of each enantiomer after incubation by chiral chromatography to determine  $IC_{50}$  or plot a Dixon plot to determine  $K_i$ . In the study of metabolic drug interactions in vitro,  $IC_{50}$  and  $K_i$  are two important parameters.  $IC_{50}$  value can be used to evaluate the inhibition ability of the drug. It is generally considered that if  $IC_{50}$  value is  $<1 \mu\text{M}$ , the drug has strong inhibition effect on the enzyme, and if the  $IC_{50}$  value is  $>50 \mu\text{M}$ , the inhibition effect is very weak [40].

In vitro studies can focus on a certain chiral process and, therefore, they are relatively simple. But when applying the data into in vivo study, it should be cautious. Studies in vivo always involve multiple chiral processes, and it is complicated to study the chiral drug interactions occurred at different stages, so combining the results from in vitro studies is necessary. Enantiomeric separation of the parent drugs or metabolites and the acquisition of a single enantiomer are the main constraints for the study of chiral drug interactions. The interaction of chiral drugs is very complicated, and only when the stereochemical factors are measured can they be reasonably explained. For example, the  $\beta$ -receptor blocker carvedilol interacts with digoxin, amiodarone, CsA, nicardipine, nifedipine, fluoxetine, and other drugs, some of which are resulting from inhibiting P-gp-mediated transport, and thus regulating the blood levels of coadministered drugs, and others are resulting from metabolic interactions [41].

## 5 Stereoselectivity in toxicity

The pharmacological activities, metabolic processes, and toxicity are different between enantiomers of chiral drugs in humans. Therefore, the safety of chiral drugs has become a hot spot in new drug research [42].

### 5.1 Toxicity of chiral drugs

The toxicity of a drug involves many factors, such as selectivity to the receptor, ADME of drug, and its metabolites. Thus, between racemate and enantiomer, enantiomer and enantiomer, toxicity can vary widely and often results in the unexpected adverse reactions. Felodipine is a chiral drug, and its adverse reactions are different due to diversity in the pharmacokinetics of *S*- and *R*-enantiomer. The incidence of adverse reactions of *R*-enantiomer, such as headache and facial flushing, is higher than the *S*-enantiomer and the racemate. There are significant differences in the toxicity of different enantiomers in human (Table 1).

**TABLE 1** Examples of toxicity differences between enantiomers in human [43].

Drug	S-enantiomer	R-enantiomer
Tetramisole	Insecticide	Vomiting
Penicillamine	Antiarthritis	Potential carcinogenic toxicity
Ethambutol	Antituberculotic	Blindness
Thalidomide	Sedative	Teratogenic
Fenfluramine	Appetite suppressant	Dizziness and hypnosis

## 5.2 Enantiomeric biotransformation increases toxicity

*R*-(-)-deprenyl is a potent MAO-B inhibitor for anti-Parkinson's disease and antidepressants, while *S*-(+)-deprenyl has only weak activity on MAO-B. *S*-(+)-methyl amphetamine and *S*-(+)-amphetamine which are produced metabolically can cause side effects of central excitability, but the *R*-form of both metabolites has only weak effects on central nervous system. Therefore, *R*-(-)-enantiomer was selected for clinical studies [44]. The local anesthetic effects of two enantiomers of the local anesthetic, prilocaine, are similar. The hydrolysis of *S*-prilocaine is slow, but the *R*-(-)-prilocaine can be rapidly hydrolyzed to produce toluidine, which can cause methemoglobinemia with hematologically toxicity [45].

## 5.3 Chiral inversion increases toxicity

Commonly used nonsteroidal anti-inflammatory drugs (NSAIDs) undergo chiral inversion in vivo. For example, the eutomer of ibuprofen is *S*-(+)-ibuprofen, but *R*-(-)-distomer with low activity can transfer into highly active *S*-(+)-ibuprofen. Due to individual differences and other reasons, it is difficult to control the effective dosage when using the NSAIDs racemate; especially when the renal function is weakened, and the *S*-(+)-eutomer is easily accumulated in the body, causing toxic side effects by inhibiting renal cyclooxygenase and increasing renal ischemia [46].

## 5.4 Toxicity or adverse reactions are inseparable from pharmacological activity

Some side effects of racemic drugs are the extension from pharmacological actions. Development of single active enantiomer with less toxicity by evaluating the toxicity of racemates and optical enantiomers can reduce the side effects of the drug. Phencyclone is an anti-motion sickness drug and has weak central inhibition function. However, during clinical use, adverse reactions such as central inhibition were still found in a few patients. Subsequent research has showed that it is because the *R*-enantiomer of phencyclone is an active enantiomer, which has stronger affinity with M receptor compared with the racemate, while the *S*-enantiomer is an inert enantiomer with no pharmacodynamic activity [47].

## 5.5 Active enantiomers are potentially toxic

In the development of chiral drugs, the routine method is to compare the toxicity between the racemate and its optical enantiomers in order to obtain a single enantiomer with less toxicity. However, it should be noted that even a single enantiomer separated from the racemate may have an unexpected toxic effect. During the development of the blood pressure lowering drug, labetalol, it was found that *RR*-labetalol is the most potent enantiomers of pharmacological activity and does not undergo inversion in vivo. But unfortunately, the liver toxicity of *RR*-labetalol is also increased when the pharmacological activity is enhanced [48]. When the *S*-enantiomer of fenfluramine, a weight-loss drug, was marketed in the United States, it was taken for granted that its clinical toxicity was significantly lower than that of fenfluramine. However, after 1 year, it was also withdrawn due to severe toxic side effects [49].

The thalidomide teratogenic event that shocked the world is a typical example of enantiotoxic toxicity. According to the studies, both *R*- and *S*-enantiomers of thalidomide have sedative effects, and *S*-thalidomide has immunosuppressive effects. The oral experiments in New Zealand white rabbits showed no difference in teratogenic toxicity between the individual enantiomers and their racemates, whereas the mice tests found that the enantiomers were 20 times more toxic than the racemates. It had also been reported that in SWS and Natal rats tests, *S*-thalidomide is teratogenic but the result was not compared to its racemate. There were studies raising objections to the above experiments, and focusing on the purity of used enantiomeric and the interconversion between enantiomers. In addition, studies on the hydrolysis products of thalidomide have shown that its metabolite, phthalimidoglutamic acid, especially its *S*-enantiomer, was associated with the teratogenicity [50].

## 6 Chiral inversion mechanisms

There are mainly two mechanisms causing racemization during the metabolic processes, and they are usually related to epimerization [51]. One mechanism is that the existence of a reversible-binding group causes epimerization of the binding intermediate; the other mechanism is that the opposite reaction results of two metabolic pathways cause epimerization; finally, both of mechanisms leading to one enantiomer transforming into another enantiomer.

### 6.1 Chiral metabolic inversion of nonsteroidal anti-inflammatory drugs

When the metabolism of 2-phenylpropionic acid was studied as early as 1922, it was found that there was metabolic inversion, but the phenomenon was not gotten enough attention. Later, it was observed that even the patient took *R*-(-)-ibuprofen, the ibuprofen in the urine appeared to be right handed. Based on the study of ibuprofen homologs, some scholars have proposed the enantiomeric transformation mechanism of ibuprofen: Coenzyme A synthase stereoselectively converts *R*-(-)-ibuprofen to CoA thioester, forming an intermediate between  $\alpha$  position-acetyl and the highly acidic methine group. At this position, epimerization of deprotonation and reprotonation can occur, followed by hydrolysis to produce *S*-(+)-ibuprofen. *S*-(+)-ibuprofen is excreted as a glycine conjugate, while *R*-(-)-ibuprofen is not a substrate of glycine *N*-acetyltransferase. Inactive *R*-(-)-ibuprofen acts as a prodrug of active *S*-(+)-ibuprofen to exert

effects in racemate [52]. Not all NSAIDs chiral transformation has the same susceptibility as ibuprofen does, and the rate of transformation may vary. When the transformation rate is fast, *R*(-)-ibuprofen acts as a prodrug; when the transformation is slow, the *R*(-)-enantiomer is an unwanted impurity and may cause side effects. Some people have evaluated the bioequivalence of 150 mg *S*(+)-ibuprofen with 200 mg racemate, and clinical trials have shown that taking lower doses of *S*(+)-ibuprofen can reduce the metabolic burden and maintain therapeutic efficacy [53].

In addition, mandelic acid (MA) is generally used as a biological indicator of occupational exposure to styrene, which is classified as a class of hazardous environmental pollutants. It was found to undergo one-directional chiral inversion (*S*-MA to *R*-MA) in Wistar and SD rats in vivo (Fig. 3) [54].

## 6.2 Inversion of the opposite metabolic pathway

Stereochemical inversion was primarily occurred in two opposite metabolic processes: oxidation and reduction mechanisms, such as alcohol-ketone conversion catalyzed by alcohol dehydrogenase. When a chiral secondary alcohol is oxidized to a ketone, usually one enantiomer is preferentially oxidized (substrate stereospecificity); whereas in ketone reduction process, hydrogen is preferentially bound to the carbonyl side (product stereospecificity). These two processes are controlled by different mechanisms, and end in the chiral transformation of alcohol [55].

During the reduction of the ketone by alcohol dehydrogenase, the pre-*R* hydrogen is preferentially converted from the dihydronicotinamide group of the NADH or NADPH coenzyme to form the *S*-alcohol. The ketone undergoes self-rearrangement in the transition state to minimize interaction between the substituent and the enzyme. The ratio of *R*- and *S*-alcohol formation depends on the relative size of the substituents and the presence of other chiral centers in the substrate. The antiepileptic drug, stiripentol, is clinically used as a racemate, and undergoes one-way inversion in the body. After *S*(-)-stilpentyl alcohol was gavage administered to rats, only the *S*(-)-stiripentol enantiomer was found in the blood. The *S*-enantiomer and the *R*-enantiomer can both be found in the blood after gavage administration of the *R*(+)-stiripentol enantiomer. And after the intravenously or intraperitoneally administration of *R*(+)-stiripentol, there is no *S*(-)-stiripentol in blood, indicating that the site of inversion is in the gastrointestinal tract. When the chiral centers are labeled with  $^3\text{H}$

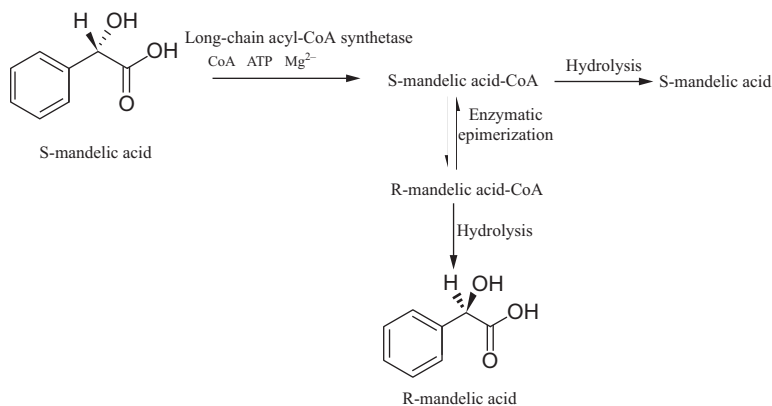


FIG. 3 The probable mechanism of chiral inversion of *S*-MA [54].

and  $^{18}\text{O}$ ,  $^3\text{H}$  remains and the  $^{18}\text{O}$  partial disappears after chiral inversion. So, the gastric acid and gastrointestinal enzyme systems may be involved in this inversion reaction [56].

Chiral sulfoxide compounds such as flosequinan also have stereochemical inversions. These compounds are first reduced by reductase to the corresponding achiral sulfide or amine and then oxidized by a monooxygenase to form an enantiomer. The above chiral inversion phenomenon is more complicated than other conventional metabolic pathways (oxidation, glucuronidation, and deglucuronation) [57]. The dose absorption rate-dependent kinetics and kinetic interactions between the two enantiomers complicate the assessment of the inversion degree. A teratogenic drug like thalidomide, maybe caused by thalidomide itself, has a two-way chiral chemical inversion in vivo. Thus, it is very difficult to assess the differences in toxicity intensity of each enantiome.

## 7 Stereoselective analytical methods

Chiral drug metabolism and pharmacokinetics is very complicated involving chiral inversion and chiral interactions so it is essential to assess enantiomer and/or its metabolites ADME using stereoselective analytical methods. The experimental results from the non-stereoselective analytical methods that cannot separate the enantiomers of chiral drug will be misinterpreted and misleading. There are many stereoselective methods published for bioanalytical assay, such as HPLC, GC, CE, MS, and immunoassay [58]. The most popular technique is chiral chromatography [59].

### 7.1 High-performance liquid chromatography

HPLC is predominant technique for separation and determination of chiral drug enantiomers with indirectly or directly models [60]. The indirect way is achieved by chiral derivatization reagents (CDRs), while the direct way is achieved by chiral mobile phase additives (CMPAs) or chiral stationary phases (CSPs) [61–63]. After the separation, enantiomers are usually detected by ultraviolet (UV), fluorescence (FL), or mass spectrometry (MS) [64–66].

#### 7.1.1 Chiral stationary phases

CSPs have been widely applied to separate and analyze enantiomers of chiral drugs and their metabolites in plasma, urine, and liver microsomes [67]. The numerous CSPs were available commercially including polysaccharide-based and macrocyclic antibiotic CSPs popularly used in HPLC/LC-MS [68–72].

Yu et al. [65] developed a method to separate and quantify the enantiomers of a potent selective 5-HT<sub>1B/1D</sub> receptor partial agonist, *S*-zolmitriptan, and its antipode in rat liver microsomes by using a narrow-bore enantioselective normal-phase Chiralpak AD-H column with hexane-isopropanol-triethylamine as mobile phase (Fig. 4). Hefnawy et al. [73] developed a method to determine the enantiomers of bisoprolol in human plasma using a teicoplanin macrocyclic antibiotic CSP with a polar ionic mobile phase (PIM) consisting of methanol-glacial acetic acid-triethylamine. The human plasma sample was treated by SPE prior to HPLC analysis. Geditz et al. separated (+)- and (–)-mefloquine and their carboxy metabolite in dried blood spots successfully by a quinidine-based zwitterionic chiral stationary phase column, CHIRALPAK ZWIX(–)[74].



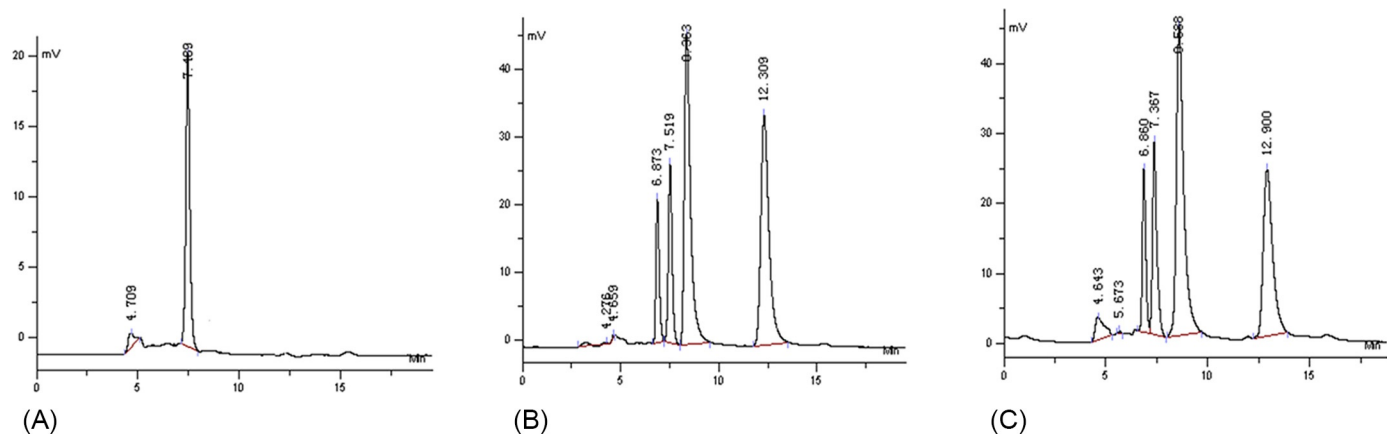


**FIG. 4** Chromatograms of extracted rat hepatic microsomal incubate. (A) Blank sample; (B) blank microsomal incubate with racemic zolmitriptan and diphenytrazol (internal standard); and (C) sample after incubating for 5 min. The peak at 6.8 min is the internal standard, the peak at 9.6 min *R*-zolmitriptan, and the peak at about 12.3 min *S*-zolmitriptan [65].

### 7.1.2 Chiral mobile phase additives

CMPAs can provide a simple and economical method for the chiral separation in some cases. This method employs a conventional achiral column and mobile phase, which has been added a chiral selector. CMPAs method is more versatile, cheaper, and flexible alternative for enantioseparations [62].

CMPAs are classified into the following types: ligand exchangers [75], macrocyclic antibiotics [76], cyclodextrins, etc. [77]. Hatami and Farhadi [78] successfully separated ketoprofen enantiomers in human and rat plasma, using hollow-fiber-based liquid-phase microextraction for sample treatment and vancomycin as a CMPA with an achiral C8 column. Ritter et al. developed a chiral HPLC method for analysis of (+)/(-)-catechin from sulfated and glucuronidated metabolites in human plasma. After plasma was pretreated with solid-phase extraction (SPE), a PM- $\gamma$ -cyclodextrin column was used with HPLC-coulometric electrode-array detection (CEAD) system. The result indicated that (+)-catechin and (-)-catechin showed enantiomeric difference in human plasma after consumption of a cocoa drink [79].

However, the CMPAs can only be used to the enantiomers formed diastereomers, some chiral additives interfere with detection and are difficult to remove from LC system, which may impair chromatographic column.

### 7.1.3 Chiral derivatization reagents

CDRs can react with hydroxyl, amino, carboxyl, and sulfhydryl group of chiral drugs so as to enhance increase the resolution and chromatographic response of enantiomers. There are various kinds of CDRs available commercially, such as acylating reagents, thiocyanic acid, o-phthalaldehyde (OPA), esters reagents, glucuronic acid, etc. [80–83]. Nagao et al. [84] used novel CDRs (PyT-C and PyT-N) for chiral metabolomics identification using high-throughput liquid chromatography and electrospray-ionization mass spectrometry, and the proposed procedure using PyT-C and PyT-N has been applied to human saliva detections. Sun et al. established a RP-HPLC with fluorescence detector for determination of hepatoma-associated DL-amino acids enantiomers in HCC patients' plasma samples using O-phthaldialdehyde (OPA) and N-isobutyryl-L-cysteine (NAC) as CDRs and demonstrated that the concentration of DL-threonine, alanine, tyrosine, valine, and methionine enantiomers has a close relationship with HCC [81]. Yu et al. [85] developed an LC/MS/MS method based on an isotope discrimination mass spectroscopy solution (IDMSS) technique to determine the enantiomers of fluoxetine and norfluoxetine in a CYP2C9 incubation mixture simultaneously. This method has short analysis time, higher resolution, and lower limit of quantification than conventional chiral separation methods.

However, the CDRs, this indirect methods are only suitable to the chiral drugs containing the functional groups to be derivatized. In addition, the derivatization refers to an increase of operation procedures and more errors, and it has to be checked that there is no racemization of enantiomer under the reaction conditions.

## 7.2 Gas chromatography

Chiral gas chromatography is an important technique of chiral chromatography. This analysis method also can be divided into two ways, CDRs and chiral stationary phases (CSPs) [86, 87].

### 7.2.1 Chiral stationary phases

GC CSPs were classified as peptide CSPs, bis-amides CSPs, chiral crown ether CSPs, cyclodextrins CSPs, cellulose CSPs, and chiral-metal CSPs. Among those CSPs, cyclodextrin derivatives CSPs have dominated the field of chiral GC separation [88].

Isoherranen et al. developed a chiral GC/MS method for the analysis of levetiracetam and its enantiomer in dog plasma and urine. This pair of enantiomer was separated on a chiral cyclodextrin capillary column and detected by ion trap mass spectrometry. The method was successfully applied to a pharmacokinetic study of levetiracetam and  $\text{R-}\alpha$ -ethyl-2-oxo-pyrrolidine acetamide in a dog [89].

### 7.2.2 Chiral derivatization reagents

GC CDRs and its derivatization reactions require that the generated corresponding derivatives must be volatile. The commonly used CDRs include carboxylic acid derivatives, amines, alcohols, isothiocyanates, etc. [90]. Tao et al. developed a method for separating chiral phenethylamine agents on an achiral capillary gas chromatography by pre-column chiral derivatization with *S*-(-)-*N*-(fluoroacyl)-prolyl chloride. This method is simple, flexible, and economic for the analysis of chiral amine drug enantiomers in biological fluids and has been used to determine *S*-(+)-methamphetamine in human forensic samples and to analyze enantiomers of amphetamine and fenfluramine in rat liver microsomes [86]. Ding et al. established a GC/MS method for the separation and determination of lactic acid and 2-hydroxyglutaric acid enantiomers by chiral derivatization with *L*-menthol and acetyl chloride. This method was successfully applied to assay of those two pair enantiomers in mouse plasma. The results indicated that *D*-lactic acid concentration in type 2 diabetes mellitus mouse were significantly higher than that in normal mice, suggesting that *D*-lactic acid may serve as an indicator for type 2 diabetes mellitus [91].

## 7.3 Supercritical fluid chromatography

SFC has been used to separate enantiomers of chiral drug in bioanalysis. In comparison to HPLC, chiral SFC separation provides more selective cavity effects of inclusion-type chiral separation phases. Combining SFC with different detectors, especially MS, allows for straightforward use in chiral trace analyses in bioanalysis [92]. The merits of SFC are faster analysis speed, wider polarity compatibility, higher column efficiency, lower cost, and environment-friendly mobile phase. SFC can be used as an alternative to HPLC for many drug substances [93].

An enantioselective SFC-MS/MS assay was validated and applied to separate and simultaneously analyzed oxcarbazepine and its chiral metabolites, *S*- and *R*-licarbazepine, concentrations in beagle dog plasma in a pharmacokinetic study [94]. Coe et al. developed a semiautomated liquid extraction SFC-MS/MS method with high throughput and was applied to *R/S*-warfarin drug-drug interaction study in clinical human plasma with rapid turnaround of sample analysis [95].

## 7.4 Capillary electrophoresis

Capillary electrophoresis (CE) is also used to analyze chiral drugs and their metabolites have shown the advantages of high resolving capability, minimum solvent, and reagent consumption, which are suitable for analysis of biological samples [96].

CE prefers employing CSPs and chiral selectors, such as cyclodextrins, polysaccharides derivatives, macrocyclic antibiotics, proteins, etc. Because the sensitivity of UV detector is low, CE/MS has been regarded as a useful hyphenation technique for analysis of polar ionogenic metabolites in biological samples, such as metabolomics [97]. A method for identifying ecstasy and methadone in plasma was developed using CE-ESI/MS, which was finally successfully applied to quantitation of ecstasy and methadone in real cases obtained from toxicology [98]. Sandbaumhüter et al. studied pharmacokinetics of ketamine and three metabolites in Beagle dogs plasma under sevoflurane vs medetomidine comedication by using enantioselective CE with highly sulfated  $\gamma$ -cyclodextrin as chiral selector. The concentrations of *S*- and *R*-ketamine, *S*- and *R*-norketamine, (2*S*,6*S*)- and (2*R*,6*R*)-hydroxynorketamine, and *S*- and *R*-DHNK were determined. Stereoselectivities were observed for 6-hydroxynorketamine and DHNK, but not for ketamine and norketamine [99]. A CE method for the enantioselective analysis of *cis*- and *trans*-dihydrotrabenazine (diHTBZ) was developed by using tris-phosphate buffer (pH2.5) containing 1% (*w/v*) carboxymethyl- $\beta$ -CD as background electrolyte. The studies of *in vitro* metabolism in human liver microsomes (HLMs) and *in vivo* pharmacokinetics showed a stereoselective metabolism and kinetic profile [100].

## 7.5 Immunoassay

Immunoassay is based on the specific-binding reaction between antigen and antibody (Ab), and is usually used in qualitative and quantitative analysis of biological samples, such as blood, saliva, urine, as well as hormones and cytokines. Due to the specificity and high affinity of the antigen-antibody reaction, immunoassay also has the characteristics of high specificity and high sensitivity. What's more, Abs are chiral molecules and the binding between chiral drugs and Abs may involve stereoselective interactions, so Abs have the potential to recognize drug enantiomers [101]. Stereoselective immunoassay is sensitive, specific, fast, and economical [102]. Due to the high specificity of the antigen-antibody reaction, the enantiomer can be determined without prior separation, and directly gotten from the biological sample complexes, with only dissolution and dilution. However, stereoselective immunoassay is largely neglected in the application of chiral drugs analysis. And because each chiral drug needs a specific antibody, the development of a new immunoassay method becomes more complex [103]. Besides, antibodies may react with compounds whose structure is similar to the target compounds, such as drug metabolites. So immunoassay is expected to be applied for preliminary screening and clinical tests [104].

For rapid and feasible on-site test of *R*- and *S*-ketamine (KT), enantioselective anti-KT antibodies (Ab) were prepared. These antibodies exhibited practical performances in competitive enzyme-linked immunosorbent assay systems. The Ab exhibited the highest enantioselectivity, and cross-reactivity with the *R*- and *S*-enantiomer was 1.3% and 1.7%, respectively [105]. Shen et al. successfully developed polyclonal antibodies to detect *S*- and *R*-styrene oxide protein adducts in WI-38 cells and provided a powerful tool for investigating the biochemical mechanism of cytotoxicity induced by styrene (Fig. 5) [103].

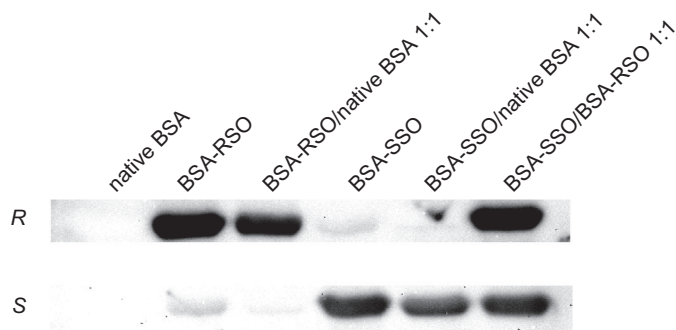


FIG. 5 The enantioselectivity of antisera numbers 1254 and 1257 was assessed by Western blot analysis [103].

## 8 Conclusion

Chiral drugs are widely used, and playing an important role in treating diseases. However, the enantiomers of a chiral drug generally present different pharmacodynamics and pharmacokinetics in biological systems. Especially, for the ADME processes, drug metabolism is the most relevant process with stereoselectivity due to the involvement of the enzymatic system and transporters. Therefore, assessing stereoselectivity in drug metabolism is of great significance whether for chiral pharmaceutical research or for rational use of chiral drug.

Although assessing stereoselectivity in drug metabolism is highly challenging in comparison to typical achiral assays, chiral bioanalytical assays for individual enantiomers and/or their metabolites are necessary. Chiral chromatography is still the most popular method in chiral drug analysis. CSPs are preferred to be used owing to the high speed, reproducibility, and simplicity of the analysis; and CMPAs and CDRs are also used frequently for their low cost. The novel techniques or hyphenation techniques may be helpful for chiral drug study. For example, LC, GC, CE, SFC coupled with tandem mass spectrometry (MS/MS), electrokinetic chromatography [106], two-dimensional (2D) chromatography [107] and isotope discrimination mass spectroscopy [85], etc. have been used for analysis of enantiomers in studying drug metabolism and pharmacokinetics.

## References

- [1] M.E. Bunnage, J.P. Mathias, A. Wood, D. Miller, S.D.A. Street, Highly potent and selective chiral inhibitors of pde5: an illustration of pfeiffer's rule, *Bioorg. Med. Chem. Lett.* 18 (23) (2008) 6033–6036.
- [2] U.S. Food and Drug Administration, FDA's policy statement for the development of new stereoisomeric drugs. U.S. Food and Drug Administration Regulatory Guidelines, 1992.
- [3] European Union, Investigation of chiral active substance. European Union Guideline, 1993.
- [4] The Minister of Health, Guidelines for industry stereochemical issues in chiral drug development. Health Canada Guidelines Document, 2000.
- [5] SFDA of China, Provisions for drug registration, Order 28, 2007.
- [6] SFDA of China, The Technical Guidance for Study on Chiral Drug Quality Control, 2006.
- [7] R.B. Carter, L.A. Dykstra, Effects of piconadol (ly150720) and its stereoisomers on electric shock titration in the squirrel monkey, *J. Pharmacol. Exp. Ther.* 234 (2) (1985) 299–306.
- [8] H. Reuter, H. Porzig, S. Kokubun, B. Prodhom, Calcium channels in the heart - properties and modulation by dihydropyridine enantiomers, *Ann. N. Y. Acad. Sci.* 522 (1988) 16–24.

- [9] K. Zhang, K. Hashimoto, An update on ketamine and its two enantiomers as rapid-acting antidepressants, *Expert. Rev. Neurother.* 19 (1) (2019) 83–92.
- [10] G.C. Chiou, Development of d-timolol for the treatment of glaucoma and ocular hypertension, *J. Ocul. Pharmacol.* 6 (1) (1990) 67–74.
- [11] J. Titus, H.U. Siehl, K.P. Zeller, S. Berger, D. Sicker, The enantiomeric carveone of krause mint and caraway: no disputes about taste, *Chemie. Unserer. Zeit.* 51 (2) (2017) 96–105.
- [12] K. Stoschitzky, W. Lindner, Specific and nonspecific effects of beta receptor blockers: stereoselectively different properties exemplified by (r)- and (s)-propranolol, *Wien. Med. Wochenschr.* 140 (6–7) (1990) 156–162.
- [13] J. Dalal, J.C. Mohan, S.S. Iyengar, J. Hiremath, I. Sathyamurthy, S. Bansal, et al., S-amlodipine: an isomer with difference-time to shift from racemic amlodipine, *Int. J. Hypertens.* 2018 (2018) 8681792.
- [14] K. Koike, T. Horinouchi, I. Takayanagi, Comparison of interactions of r(+)- and s(–)-isomers of beta-adrenergic partial agonists, befunolol and carteolol, with high affinity site of beta-adrenoceptors in the microsomal fractions from guinea-pig ciliary body, right atria and trachea, *Gen. Pharmacol.* 25 (7) (1994) 1477–1481.
- [15] K. Stoschitzky, W. Klein, G. Stark, U. Stark, G. Zernig, I. Graziadei, et al., Different stereoselective effects of (r)- and (s)-propafenone: clinical pharmacologic, electrophysiologic, and radioligand binding studies, *Clin. Pharmacol. Ther.* 47 (6) (1990) 740–746.
- [16] J.K. Smallwood, D.W. Robertson, M.I. Steinberg, Electrophysiological effects of flecainide enantiomers in canine purkinje fibres, *Naunyn Schmiedeberg's Arch. Pharmacol.* 339 (6) (1989) 625–629.
- [17] Q. Zhou, T.W. Yao, S. Zeng, Effects of stereochemical aspects on drug interaction in pharmacokinetics, *Acta Pharmacol. Sin.* 23 (5) (2002) 385–392.
- [18] Y. Wang, J. Cao, X. Wang, S. Zeng, Stereoselective transport and uptake of propranolol across human intestinal caco-2 cell monolayers, *Chirality* 22 (3) (2010) 361–368.
- [19] Q. Zhou, L.S. Yu, S. Zeng, Stereoselectivity of chiral drug transport: a focus on enantiomer-transporter interaction, *Drug Metab. Rev.* 46 (3) (2014) 283–290.
- [20] USFDA, In vitro metabolism- and transporter-mediated drug-drug interaction studies (Guidance Draft), 2017.
- [21] D.N. Wade, P.T. Mearrick, J.L. Morris, Active transport of l-dopa in the intestine, *Nature* 242 (5398) (1973) 463–465.
- [22] Y. He, Y. Liu, S. Zeng, Stereoselective and multiple carrier-mediated transport of cetirizine across caco-2 cell monolayers with potential drug interaction, *Chirality* 22 (7) (2010) 684–692.
- [23] Y. Akamine, M. Miura, H. Komori, I. Tamai, I. Ieiri, N. Yasui-Furukori, et al., The change of pharmacokinetics of fexofenadine enantiomers through the single and simultaneous grapefruit juice ingestion, *Drug Metab. Pharmacokinet.* 30 (5) (2015) 352–357.
- [24] G.S. Chen, S.J. Gong, R.R. Zhou, X.J. Xie, Transdermal permeability of l- and dl-norgestrel through human skin in vitro, *Acta Pharmacol. Sin.* 12 (5) (1991) 437–440.
- [25] Q. Shen, L. Wang, H. Zhou, H.D. Jiang, L.S. Yu, S. Zeng, Stereoselective binding of chiral drugs to plasma proteins, *Acta Pharmacol. Sin.* 34 (8) (2013) 998–1006.
- [26] L. Yu, Y. Hong, L. Li, Y. Jin, M. Zheng, H. Jiang, et al., Enantioselective drug-protein interaction between mexiletine and plasma protein, *J. Pharm. Pharmacol.* 64 (6) (2012) 792–801.
- [27] D. Shi, Y.X. Jin, Y.H. Tang, H.H. Hu, S.Y. Xu, L.S. Yu, et al., Stereoselective binding of mexiletine and ketoprofen enantiomers with human serum albumin domains, *Acta Pharmacol. Sin.* 33 (5) (2012) 710–716.
- [28] K.L. Chang, H.N. Pee, S. Yang, P.C. Ho, Influence of drug transporters and stereoselectivity on the brain penetration of pioglitazone as a potential medicine against Alzheimer's disease, *Sci. Rep.* 5 (2015) 9000.
- [29] D.W. Boulton, J.P. Fawcett, T.M. Fiddes, Transplacental distribution of salbutamol enantiomers at caesarian section, *Br. J. Clin. Pharmacol.* 44 (6) (1997) 587–590.
- [30] S.Y. Sun, Y.Q. Wang, L.P. Li, L. Wang, S. Zeng, H. Zhou, et al., Stereoselective interaction between tetrahydropalmatine enantiomers and cyp enzymes in human liver microsomes, *Chirality* 25 (1) (2013) 43–47.
- [31] S. Xie, S. Zeng, Stereoselective glucuronidation of propafenone and its analogues by human recombinant ugt1a9, *Chem. Pharm. Bull.(Tokyo)* 58 (6) (2010) 879–883.
- [32] X. Liu, L. Zhu, B. Huang, J. Huang, Y. Cai, L. Zhu, et al., Poor and enantioselective bioavailability of naftopidil enantiomers is due to extensive and stereoselective metabolism in rat liver, *J. Pharm. Biomed. Anal.* 132 (2017) 165–172.
- [33] L.Y. You, C.N. Yu, S.G. Xie, S.Q. Chen, S. Zeng, Stereoselective glucuronidation of carvedilol by Chinese liver microsomes, *J Zhejiang Univ Sci B* 8 (10) (2007) 756–764.

- [34] B. Testa, Types of stereoselectivity in drug metabolism: a heuristic approach, *Drug Metab. Rev.* 47 (2) (2015) 239–251.
- [35] Z. Wang, S. Wang, M. Huang, H. Hu, L. Yu, S. Zeng, Characterizing the effect of cytochrome p450 (cyp) 2c8, cyp2c9, and cyp2d6 genetic polymorphisms on stereoselective n-demethylation of fluoxetine, *Chirality* 26 (3) (2014) 166–173.
- [36] H. Wang, L. Yuan, S. Zeng, Characterizing the effect of udp-glucuronosyltransferase (ugt) 2b7 and ugt1a9 genetic polymorphisms on enantioselective glucuronidation of flurbiprofen, *Biochem. Pharmacol.* 82 (11) (2011) 1757–1763.
- [37] Y. Nishiya, D. Nakai, Y. Urasaki, H. Takakusa, S. Ohsuki, Y. Iwano, et al., Stereoselective hydroxylation by cyp2c19 and oxidation by adh4 in the in vitro metabolism of tivantinib, *Xenobiotica* 46 (11) (2016) 967–976.
- [38] L.J. Luan, Q. Shao, J.Y. Ma, S. Zeng, Stereoselective urinary excretion of s(-) and r(+)-propranolol glucuronide following oral administration of rs-propranolol in Chinese han subjects, *World J. Gastroenterol.* 11 (12) (2005) 1822–1824.
- [39] L. Yu, M. Qian, Y. Liu, T. Yao, S. Zeng, Stereoselective metabolism of propranolol glucuronidation by human udp-glucuronosyltransferases 2b7 and 1a9, *Chirality* 22 (4) (2010) 456–461.
- [40] C.L. Crespi, D.M. Stresser, Fluorometric screening for metabolism-based drug-drug interactions, *J. Pharmacol. Toxicol. Methods* 44 (1) (2000) 325–331.
- [41] K. Fukumoto, T. Kobayashi, K. Komamura, S. Kamakura, M. Kitakaze, K. Ueno, Stereoselective effect of amiodarone on the pharmacokinetics of racemic carvedilol, *Drug Metab. Pharmacokinet.* 20 (6) (2005) 423–427.
- [42] S. Mane, Racemic drug resolution: a comprehensive guide, *Anal. Methods (UK)* 8 (42) (2016) 7567–7586.
- [43] S. Zeng, *Chiral Pharmacology and Chiral Pharmaceutical Analysis*, Science Press, 2008.
- [44] K. Magyar, B. Szende, V. Jenei, T. Tabi, M. Palfi, E. Szoko, R-deprenyl: pharmacological spectrum of its activity, *Neurochem. Res.* 35 (12) (2010) 1922–1932.
- [45] A.N. Tran, J.Y. Koo, Risk of systemic toxicity with topical lidocaine/prilocaine: a review, *J. Drugs Dermatol.* 13 (9) (2014) 1118–1122.
- [46] H. Ikuta, A. Kawase, M. Iwaki, Stereoselective pharmacokinetics and chiral inversion of ibuprofen in adjuvant-induced arthritic rats, *Drug Metab. Dispos.* 45 (3) (2017) 316–324.
- [47] L.Y. Wang, Y. Wang, J.Q. Zheng, B.H. Zhong, H. Liu, S.J. Dong, et al., Pharmacological profiles of an anticholinergic agent, phencyclonate hydrochloride, and its optical isomers, *Acta Pharmacol. Sin.* 26 (5) (2005) 527–532.
- [48] E. Riva, T. Mennini, R. Latini, The alpha- and beta-adrenoceptor blocking activities of labelol and its rr-sr (50:50) stereoisomers, *Br. J. Pharmacol.* 104 (4) (1991) 823–828.
- [49] Benfluorex: EU marketing authorisation finally withdrawn, *Prescrire Int.* 19 (109) (2010) 206.
- [50] M. Lukamowicz-Rajska, C. Mittmann, M. Prummer, Q. Zhong, J. Bedke, J. Hennenlotter, et al., Mir-99b-5p expression and response to tyrosine kinase inhibitor treatment in clear cell renal cell carcinoma patients, *Oncotarget* 7 (48) (2016) 78433–78447.
- [51] V. Wsol, L. Skalova, B. Szotakova, Chiral inversion of drugs: coincidence or principle? *Curr. Drug Metab.* 5 (6) (2004) 517–533.
- [52] J.M. Mayer, Stereoselective metabolism of anti-inflammatory 2-arylpropionates, *Acta Pharm. Nord.* 2 (3) (1990) 197–216.
- [53] G. Geisslinger, O. Schuster, K.P. Stock, D. Loew, G.L. Bach, K. Brune, Pharmacokinetics of s(+) and r(-)-ibuprofen in volunteers and first clinical experience of s(+)-ibuprofen in rheumatoid arthritis, *Eur. J. Clin. Pharmacol.* 38 (5) (1990) 493–497.
- [54] L.B. Gao, J.Z. Wang, T.W. Yao, S. Zeng, Study on the metabolic mechanism of chiral inversion of s-mandelic acid in vitro, *Chirality* 24 (1) (2012) 86–95.
- [55] K. Itoh, K. Hoshino, A. Endo, T. Asakawa, K. Yamakami, C. Noji, et al., Chiral inversion of rs-8359: a selective and reversible mao-a inhibitor via oxido-reduction of keto-alcohol, *Chirality* 18 (9) (2006) 698–706.
- [56] C. Tang, K. Zhang, F. Lepage, R.H. Levy, T.A. Baillie, Metabolic chiral inversion of stiripentol in the rat. II. Influence of route of administration, *Drug Metab. Dispos.* 22 (4) (1994) 554–560.
- [57] E. Kashiyama, T. Yokoi, M. Odomi, Y. Funae, K. Inoue, T. Kamataki, Cytochrome p450 responsible for the stereoselective s-oxidation of flosequinan in hepatic microsomes from rats and humans, *Drug Metab. Dispos.* 25 (6) (1997) 716–724.
- [58] Z. Shen, C. Lv, S. Zeng, Significance and challenges of stereoselectivity assessing methods in drug metabolism, *J. Pharm. Anal.* 6 (1) (2016) 1–10.



- [59] M.L. Williams, I.W. Wainer, Role of chiral chromatography in therapeutic drug monitoring and in clinical and forensic toxicology, *Ther. Drug Monit.* 24 (2) (2002) 290–296.
- [60] S. Batra, R. Bhushan, Bioassay, determination and separation of enantiomers of atenolol by direct and indirect approaches using liquid chromatography: a review, *Biomed. Chromatogr.* 32 (1) (2018), <https://doi.org/10.1002/bmc.4090>.
- [61] D. Borg, E. Kolb, C. Lantigua, R. Stripp, Chiral analysis of methamphetamine in oral fluid samples: a method to distinguish licit from illicit drug use, *J. Anal. Toxicol.* 42 (1) (2018) 25–32.
- [62] L. Yu, S. Wang, S. Zeng, Chiral mobile phase additives in hplc enantioseparations, *Methods Mol. Biol.* 970 (2013) 221–231.
- [63] C. Calderon, C. Santi, M. Lammerhofer, Chiral separation of disease biomarkers with 2-hydroxycarboxylic acid structure, *J. Sep. Sci.* 41 (6) (2018) 1224–1231.
- [64] Y. Lushan, Z. Su, Determination of mitiglinide in rat plasma by high-performance liquid chromatography with uv detection, *J. Chromatogr. B Anal. Technol. Biomed. Life Sci.* 834 (1–2) (2006) 204–207.
- [65] L. Yu, T. Yao, S. Ni, S. Zeng, Determination of zolmitriptan enantiomers in rat liver microsomes by chiral high performance liquid chromatography with fluorescence detection, *Biomed. Chromatogr.* 19 (3) (2005) 191–195.
- [66] N. Balaji, B.B. Gabani, U. Todmal, S.P. Sulochana, N.K. Saini, R. Chandran, et al., Enantioselective lc-esi-ms/ms determination of dropropizine enantiomers in rat plasma and application to a pharmacokinetic study, *Biomed. Chromatogr.* 33 (3) (2019) e4434.
- [67] M. Protti, A. Vignali, T. Sanchez Blanco, J. Rudge, F. Bugamelli, A. Ferranti, et al., Enantioseparation and determination of asenapine in biological fluid micromatrices by hplc with diode array detection, *J. Sep. Sci.* 41 (6) (2018) 1257–1265.
- [68] M.C.O. Souza, M.P. Marques, G. Duarte, V.L. Lanchote, Analysis of bupivacaine enantiomers in plasma as total and unbound concentrations using lc-ms/ms: application in a pharmacokinetic study of a parturient with placental transfer, *J. Pharm. Biomed. Anal.* 164 (2019) 268–275.
- [69] L.N. Sun, Y.W. Shen, Y.W. Ying, D. Li, T.F. Li, X.H. Zhang, et al., Stereoselective pharmacokinetics of (R)-(+)- and (S)-(–)-rabeprazole in human using chiral LC-MS/MS after administration of rabeprazole sodium enteric-coated tablet, *Chirality* 30 (12) (2018) 1277–1286.
- [70] L. Luo, X. Wen, Y. Du, Z. Jiang, X. Guo, Enantioselective analysis of lansoprazole in rat plasma by lc-ms/ms: application to a stereoselective pharmacokinetic study, *Biomed. Chromatogr.* 32 (11) (2018) e4345.
- [71] R.S. Arifah, A.E. Ribeiro, A.E. Rodrigues, L.S. Pais, Improving the performance of nadolol stereoisomers' preparative separation using chiralpak ia by smb chromatography, *Chirality* 31 (1) (2019) 62–71.
- [72] M.M. Hefnawy, Y.A. Asiri, N.Z. Al-Zoman, G.A. Mostafa, H.Y. Aboul-Enein, Stereoselective HPLC analysis of tertatolol in rat plasma using macrocyclic antibiotic chiral stationary phase, *Chirality* 23 (4) (2011) 333–338.
- [73] M.M. Hefnawy, M.A. Sultan, M.M. Al-Shehri, Enantioanalysis of bisoprolol in human plasma with a macrocyclic antibiotic hplc chiral column using fluorescence detection and solid phase extraction, *Chem. Pharm. Bull.(Tokyo)* 55 (2) (2007) 227–230.
- [74] M.C. Geditz, W. Lindner, M. Lammerhofer, G. Heinkele, R. Kerb, M. Ramharter, et al., Simultaneous quantification of mefloquine (+)- and (–)-enantiomers and the carboxy metabolite in dried blood spots by liquid chromatography/tandem mass spectrometry, *J. Chromatogr. B Anal. Technol. Biomed. Life Sci.* 968 (2014) 32–39.
- [75] T. Alizadeh, A.N. Shamkhali, Chiral resolution of salbutamol in plasma sample by a new chiral ligand-exchange chromatography method after its extraction with nano-sized imprinted polymer, *J. Chromatogr. B Anal. Technol. Biomed. Life Sci.* 1009–1010 (2016) 96–106.
- [76] L. Ramos, R. Bakhtiar, T. Majumdar, M. Hayes, F. Tse, Liquid chromatography/atmospheric pressure chemical ionization tandem mass spectrometry enantiomeric separation of dl-threo-methylphenidate, (ritalin) using a macrocyclic antibiotic as the chiral selector, *Rapid Commun. Mass Spectrom.* 13 (20) (1999) 2054–2062.
- [77] J. Ye, G. Chen, S. Zeng, Enantiomeric separation of norgestrel by reversed phase high-performance liquid chromatography using eluents containing hydroxypropyl-beta-cyclodextrin in stereoselective skin permeation study, *J. Chromatogr. B* 843 (2) (2006) 289–294.
- [78] M. Hatami, K. Farhadi, Analysis of ketoprofen enantiomers in human and rat plasma by hollow-fiber-based liquid-phase microextraction and chiral mobile-phase additive HPLC, *Can. J. Chem.* 91 (12) (2013) 1252–1257.
- [79] C. Ritter, B.F. Zimmermann, R. Galensa, Chiral separation of (+)/(–)-catechin from sulfated and glucuronidated metabolites in human plasma after cocoa consumption, *Anal. Bioanal. Chem.* 397 (2) (2010) 723–730.

- [80] X.L. Zheng, Q.Q. Yu, Y. Wang, S. Zeng, Stereoselective accumulation of propranolol enantiomers in k562 and k562/adr cells, *Chirality* 25 (6) (2013) 361–364.
- [81] H. Sun, X. Zhou, H. Wu, S. Wu, R. Luo, Determination of hepatoma-associated dl-amino acids enantiomers by rp-hplc with fluorescence detector: application in patients with hepatocellular carcinoma, *Ann. Clin. Lab. Sci.* 48 (4) (2018) 490–495.
- [82] H. Wang, J. Ji, S. Zeng, Biosynthesis and stereoselective analysis of (–)- and (+)-zaltoprofen glucuronide in rat hepatic microsomes and its application to the kinetic analysis, *J. Chromatogr. B* 879 (24) (2011) 2430–2436.
- [83] R.C. Moldovan, E. Bodoki, A.C. Servais, J. Crommen, R. Oprean, M. Fillet, (+) or (–)-1-(9-fluorenyl)ethyl chloroformate as chiral derivatizing agent: a review, *J. Chromatogr. A* 1513 (2017) 1–17.
- [84] R. Nagao, H. Tsutsui, T. Mochizuki, T. Takayama, T. Kuwabara, J.Z. Min, et al., Novel chiral derivatization reagents possessing a pyridylthiourea structure for enantiospecific determination of amines and carboxylic acids in high-throughput liquid chromatography and electrospray-ionization mass spectrometry for chiral metabolomics identification, *J. Chromatogr. A* 1296 (2013) 111–118.
- [85] L. Yu, S. Wang, H. Jiang, H. Zhou, S. Zeng, Simultaneous determination of fluoxetine and norfluoxetine enantiomers using isotope discrimination mass spectroscopy solution method and its application in the CYP2C9-mediated stereoselective interactions, *J. Chromatogr. A* 1236 (2012) 97–104.
- [86] Q.F. Tao, S. Zeng, Analysis of enantiomers of chiral phenethylamine drugs by capillary gas chromatography/mass spectrometry/flame-ionization detection and pre-column chiral derivatization, *J. Biochem. Biophys. Methods* 54 (1–3) (2002) 103–113.
- [87] J. Mifsud, L.J. Sghendo, A novel chiral gc/ms method for the analysis of fluoxetine and norfluoxetine enantiomers in biological fluids, *J. Pharm. Bioallied. Sci.* 4 (3) (2012) 236–245.
- [88] T.J. Ward, K.D. Ward, Chiral separations: a review of current topics and trends, *Anal. Chem.* 84 (2) (2012) 626–635.
- [89] N. Isoherranen, M. Roeder, S. Soback, B. Yagen, V. Schurig, M. Bialer, Enantioselective analysis of levetiracetam and its enantiomer r-alpha-ethyl-2-oxo-pyrrolidine acetamide using gas chromatography and ion trap mass spectrometric detection, *J. Chromatogr. B* 745 (2) (2000) 325–332.
- [90] N.R. Srinivas, W.C. Shyu, R.H. Barbhuiya, Gas chromatographic determination of enantiomers as diastereomers following pre-column derivatization and applications to pharmacokinetic studies: a review, *Biomed. Chromatogr.* 9 (1) (1995) 1–9.
- [91] X. Ding, S. Lin, H. Weng, J. Liang, Separation and determination of the enantiomers of lactic acid and 2-hydroxyglutaric acid by chiral derivatization combined with gas chromatography and mass spectrometry, *J. Sep. Sci.* 41 (12) (2018) 2576–2584.
- [92] L.C. Harps, J.F. Joseph, M.K. Parr, Sfc for chiral separations in bioanalysis, *J. Pharm. Biomed. Anal.* 162 (2019) 47–59.
- [93] R.Q. Wang, T.T. Ong, W.H. Tang, N. Siu-Choon, Recent advances in pharmaceutical separations with supercritical fluid chromatography using chiral stationary phases, *Trends Anal. Chem.* 37 (2012) 83–100.
- [94] Z. Yang, X. Xu, L. Sun, X. Zhao, H. Wang, J.P. Fawcett, et al., Development and validation of an enantioselective sfc-ms/ms method for simultaneous separation and quantification of oxcarbazepine and its chiral metabolites in beagle dog plasma, *J. Chromatogr. B* 1020 (2016) 36–42.
- [95] R.A. Coe, J.O. Rathe, J.W. Lee, Supercritical fluid chromatography-tandem mass spectrometry for fast bioanalysis of r/s-warfarin in human plasma, *J. Pharm. Biomed. Anal.* 42 (5) (2006) 573–580.
- [96] E. Naghdi, A.R. Fakhari, Simultaneous chiral separation of tramadol and methadone in tablets, human urine, and plasma by capillary electrophoresis using maltodextrin as the chiral selector, *Chirality* 30 (10) (2018) 1161–1168.
- [97] R. Ramautar, G.W. Somsen, G.J. de Jong, Ce-ms for metabolomics: Developments and applications in the period 2012–2014, *Electrophoresis* 36 (1) (2015) 212–224.
- [98] J. Schappler, D. Guillaume, J. Prat, J.L. Veuthey, S. Rudaz, Validation of chiral capillary electrophoresis-electrospray ionization-mass spectrometry methods for ecstasy and methadone in plasma, *Electrophoresis* 29 (10) (2008) 2193–2202.
- [99] F.A. Sandbaumhuter, R. Theurillat, R.N. Bektas, A.P.N. Kutter, R. Bettchart-Wolfensberger, W. Thormann, Pharmacokinetics of ketamine and three metabolites in beagle dogs under sevoflurane vs. Medetomidine comedication assessed by enantioselective capillary electrophoresis, *J. Chromatogr. A* 1467 (2016) 436–444.

- [100] M.Z. Bocato, F. de Lima Moreira, N.C.P. de Albuquerque, C.M. de Gaitani, A.R.M. de Oliveira, In vitro enantioselective human liver microsomal metabolism and prediction of in vivo pharmacokinetic parameters of tetrabenazine by dlme-ce, *J. Pharm. Biomed. Anal.* 128 (2016) 528–537.
- [101] P.A. Got, J.M. Scherrmann, Stereoselectivity of antibodies for the bioanalysis of chiral drugs, *Pharm. Res.* 14 (11) (1997) 1516–1523.
- [102] M.M. Cao, M. Li, X. Yan, M.H. Wang, Stereoselectivity of an enzyme-linked, immunosorbent assay for s-bioallethrin, *Anal. Methods* 4 (2) (2012) 534–538.
- [103] S. Shen, F. Zhang, S. Zeng, Y. Tian, X. Chai, S. Gee, et al., Development of enantioselective polyclonal antibodies to detect styrene oxide protein adducts, *Anal. Chem.* 81 (7) (2009) 2668–2677.
- [104] T. Minekawa, A. Kambegawa, K. Shindome, S. Takehara, H. Arakawa, The development of S-Equol diastereoisomer specific ELISA, *Am. J. Anal. Chem.* 3 (2012) 448–454.
- [105] I. Morita, H. Oyama, Y. Kanda, M. Yasuo, A. Ito, M. Toyota, et al., Enantioselective monoclonal antibodies for detecting ketamine to crack down on illicit use, *Biol. Pharm. Bull.* 41 (1) (2018) 123–131.
- [106] Y.Q. Yao, B. Zhang, S. Li, J. Yu, X. Guo, Enantioselective analysis of pheniramine in rat using large volume sample stacking or cation-selective exhaustive injection and sweeping coupled with cyclodextrin modified electrokinetic chromatography, *Talanta* 192 (2019) 226–232.
- [107] C.L. Hsieh, R. Koga, A. Furusho, T. Akita, M. Mita, T. Ide, et al., Enantioselective and simultaneous determination of lactate and 3-hydroxybutyrate in human plasma and urine using a narrow-bore online two-dimensional high-performance liquid chromatography system, *J. Sep. Sci.* 41 (6) (2018) 1298–1306.

# Progress of derisking strategies for drug-induced liver injury (DILI) in the last two decades

---

*Kaushik Mitra*

Department of Drug Metabolism and Pharmacokinetics, Janssen Research and Development, Springhouse, PA, United States

## 1 Introduction

---

Drug-induced liver injury (DILI) remains a major reason for the attrition of new chemical entities during development [1–4]. Additionally, in multiple cases, post-marketing data on approved drugs have unraveled statistically significant information on DILI cases and have led to withdrawal (or restricted prescribing). Current hypotheses include four core, and overlapping, mechanisms: (1) formation of reactive metabolites that can cause chemical and oxidative stress and lead to protein modifications, (2) altered bile acid homeostasis from inhibition of biliary transporters, (3) altered mitochondrial function, and (4) exerting innate and adaptive immune response. Two additional mechanisms that have been considered to play potential roles in DILI are lysosomal impairment via trapping of drug material [5] and endoplasmic reticulum stress perpetuated by the endoplasmic reticulum (ER) unfolded protein response (UPR) mechanism [6] (Fig. 1).

## 2 Challenges in predicting DILI

---

The assessment of DILI risk for new chemical entities continues throughout the process of drug discovery, although the scope may change from hazard assessment to risk prediction in terms of probability of success as the compounds get more mature. At early stages, the core team working on a project may have a few structural scaffolds that they are basing their

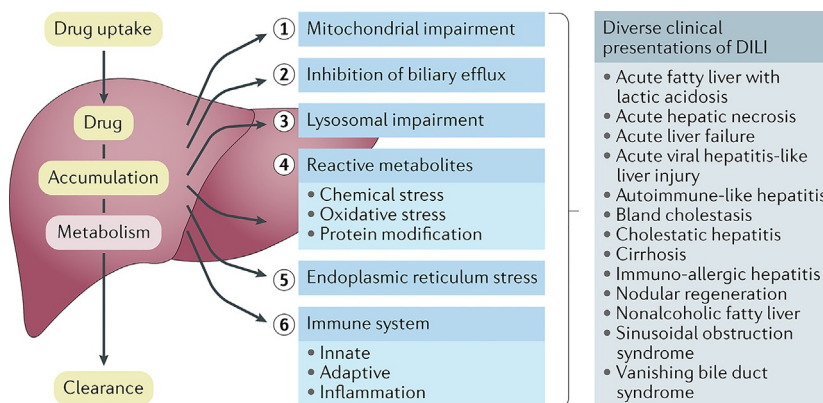


**FIG. 1** Drug-induced liver injury (DILI) can be caused by various chemical insults (steps 1–5) and can present as an array of different pathologies, dependent on the specific function of the liver that is impaired. Furthermore, recruitment of the immune system (step 6) can result in a prolonged or altered pathological phenotype, adding further complexity to the clinical presentation of the condition. *Reprinted with permission from R.J. Weaver, E.A. Blomme, A.E. Chadwick, I.M. Copple, H.H.J. Gerets, C.E. Goldring, A. Guillouzo, P.G. Hewitt, M. Ingelman-Sundberg, K.G. Jensen, S. Juhila, U. Klingmüller, G. Labbe, M.J. Liguori, C.A. Lovatt, P. Morgan, D.J. Naisbitt, R.H.H. Pieters, J. Snoeys, B. van de Water, D.P. Williams, B. Kevin Park, Managing the challenge of drug-induced liver injury: a roadmap for the development and deployment of preclinical predictive models, Nat. Rev. Drug Discov. 19 (2020) 131–148.*

molecules on, and it is important that the fundamental scaffolds are derisked for DILI at this stage before other “druggability” parameters start to get optimized in. Impact at this point may allow the team to deprioritize the more hazardous scaffolds without a significant hit to timelines. Once a scaffold is rendered “safe,” the team then needs to keep monitoring the smaller modifications that are being made during the optimization process to make sure that a DILI liability is not creeping back in. Let’s put this dynamic workflow in perspective of what “derisking” entails; but to get there, we need to first understand the fundamentals of DILI etiology. The causative mechanism of DILI is complex, multifactorial, and not well understood. On a macroscopic level, there appear to be synergistic processes overlapping multiple biological pathways outlined above; additionally, DILI manifestation could be human specific and, thus, often not predicted during the routine assessment of safety in animal models. One could argue that even humans are not predictive of a generic clinical DILI signal as, often enough, such adverse effects are not captured in early and smaller human trials. These macroscopic challenges indicate the difficulty in the tools that can be implemented for the derisking process but, at the least, conclude that one single approach is not going to be sufficient. It thus follows that multiple platforms that look at the various biological processes need to be assessed in parallel. Herein lies the most controversial dogma in DILI-derisking circles: what is the predictability of these tools? If we were to run 50 test molecules, comprising of an equal mix of DILI-positive and DILI-negative clinical compounds through a given assay X, what would a binary outcome look like? As shown in [Table 1](#), Result A is ideal, where the assay X can pick out 88% of the DILI-positive molecules while allowing 92% of the DILI-negative compounds to proceed. Result B indicates that assay X is not so great to pick DILI-positive compounds (with a 52% success rate), but is excellent in keeping the good

**TABLE 1** Three hypothetical outcome scenarios of any assay X, analyzing 50 compounds with an equal mix of DILI-positive and DILI-negative compounds.

DILI	A			B			C			
	+	-		+	-		+	-		
25+	22	3	88%	13	12	52%	22	3	88%	Sensitivity
25-	2	23	92%	2	23	92%	20	5	20%	Specificity

compounds in play (perhaps because the DILI observed in the clinic is not due to the biological mechanism probed by assay X). Result C suggests that assay X can pick out 88% of the DILI-positive compounds but fail miserably in selecting good compounds, allowing only 20% of DILI-negative compounds to proceed.

It could be imagined then, by adding in assays Y and Z if the outcome of each assay looked like Table 1, we would arrive at a multi-factorial assessment where, *cumulatively*, DILI-positive compounds were identified with high success and the clean compounds not unnecessarily terminated. This, of course, is where science is progressing currently. But now, let us take a look at a more microscopic and practical assessment parameter. The above tables were created from algorithmic and empirical assessments of the data generated from assay X with a *binary* readout. Is a binary readout from any of these tools such as a specific protein covalent binding number, a Glu-Gal assay shift value or a transporter inhibition  $IC_{50}$ , appropriate? It makes sense that these values should be considered in light of the load of the drug-related material hypothesized to be causative of the biology that drives assay X [7]. Total plasma  $C_{max}$  of the parent or metabolite (e.g., acyl glucuronide) is often considered as the appropriate correlation parameter; however, one could argue that plasma concentrations might not reflect the causative hepatic amount. Additionally, a school of thought exists in which free drug concentrations, and not the total, is considered as the appropriate driver of toxicity, drawing parallels from the free-drug hypothesis in pharmacology [8].

## 2.1 Bioactivation of drugs to reactive intermediates

Drug metabolism is a way of removing drugs from the body by altering the chemical structure of the molecule. Occasionally, in the process of this conversion, the drug is changed into electrophilic products that can react with endogenous biomolecules such as DNA and proteins. The covalent protein-drug adduct can act as a hapten and trigger immune responses that can elicit adverse effects [9]. The bioactivation and DILI liabilities can be investigated using a multitude of experiments as described below.

### 2.1.1 Metabolite identification via trapping studies

The identification of reactive metabolites is perhaps most conveniently achieved through an *in vitro* trapping study. This experiment involves the incubation of drugs in a metabolically competent system, such as hepatocytes or NADPH-fortified liver microsomes, along with exogenous nucleophiles such as glutathione, cyanide, and semicarbazide. The incubation mixture is subsequently quenched, the protein and cell debris precipitated, and the

supernate analyzed by LC–MS. The presence of adducts of the drugs with the trapping agents suggests that the drug was metabolically converted to an electrophile that was then captured by the nucleophilic head of the trapping agent, thus indicating the drug's propensity to be bioactivated. Besides, the analysis of the products provides valuable data regarding the moiety in the molecule that is being converted into an electrophile; this information can be used to dial out the electrophilic metabolite formation liability in subsequent molecules [10, 11].

### 2.1.2 Covalent binding studies *in vitro* and *in vivo*

Quantitative assessment of *in vitro* and *in vivo* covalent protein binding by reactive metabolites of a new chemical entity provides a measure of its propensity to form electrophilic intermediates. Merck used a target value of 50 pmol-eq of compound covalently bound per milligram of protein, either *in vitro* or *in vivo* in the rat liver under standardized conditions [12]. For compounds that surpassed the target value, metabolite identification studies were typically used to locate the moiety responsible for bioactivation. Once identified, modifications were made to the scaffold to replace the offending moiety, and subsequent metabolism studies and covalent binding analyses were conducted on the newer molecules (Fig. 2) [13]. The compound with the least amount of protein covalent binding, analyzed under identical experimental conditions, was then recommended as the one with the least propensity to cause clinical DILI from a bioactivation mechanism. Used as a tool for a structure–activity relationship, similar to and in conjunction with optimization of other standard drugability parameters for a new chemical entity, this approach provided a theoretical and mechanistic approach to derisking compounds for DILI.

The covalent binding approach suffered from a few challenges, the most practical one being the need for radiolabeled compounds for the assay. In early discovery, where such an analysis had the most impact, synthesis of a radiolabel was largely cost prohibitive. Typical radioisotope used was tritium; unfortunately, there were multiple cases where the tritium label would be removed via metabolism, thus leading to a lower incorrect covalent binding value. In this situation, one could try to understand the mechanism of this tritium loss and, in the case that the tritium loss was associated with a bioactivation mechanism, assume that all the drug material with tritium loss was covalently bound. This would now provide an upper estimate of covalently bound material. The compound could also be radiolabeled with  $^{14}\text{C}$ , a more expensive and time-consuming effort. Another complication in covalent binding studies involves

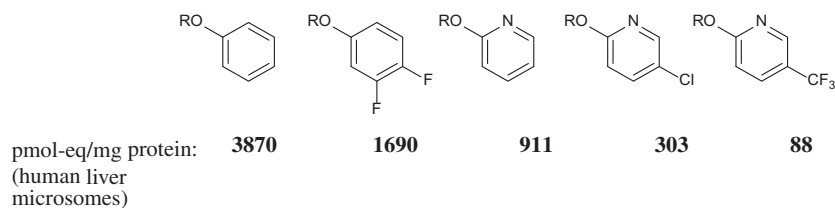


**FIG. 2** Optimization of protein-binding reactivity via SAR studies and subsequent covalent-binding analysis. Metabolite ID studies implicated an epoxidation mechanism at the phenyl ring as the causative step for the high observed covalent binding (3870 pmol-eq/mg protein). Subsequent changes to the molecule, attempting to impact epoxidation through manipulation of the electronics of the ring, showed a steady decrease of covalent binding values. Compound X, with the least amount of covalent binding, would be considered to carry the least hazard from reactive metabolism [13].



situations where the molecules might be split into two parts via metabolism (such as hydrolysis, *N*- or *O*-dealkylation), thus leaving one part of the molecule without a radiolabel. Any protein adduction by that piece would then not be captured in the net covalent binding value. Apart from the cost and time issues with a radiolabel, large-scale synthesis of the material was required for in vivo rat studies that could also be prohibitive early on in discovery. In terms of predictivity of clinical DILI from covalent binding values, one would hypothesize that the clinical dose of the drug and the subsequent deleterious body burden concentration, as well as the pharmacokinetics of the drug or metabolite in question, would be key influencers. Lastly, and perhaps most importantly, bioactivation of the drug and subsequent protein modification is only the first step in the complex cascade that eventually leads to clinical DILI. It is well established that not all drug molecules with high covalent binding cause clinical DILI, so there certainly are biochemical differences in how the cells process this initial event of protein adduction. While the covalent binding approach forwarded by Merck effectively picked out molecules with a propensity to form reactive metabolites and modify proteins, it did not consider dose, drug pharmacokinetics, the body burden of the reactive metabolite and the subsequent biochemical response of the protein-drug adduct in the assessment of risk. Thus, it is not surprising that the correlation of in vitro covalent binding values themselves with clinical DILI events was not strong; but also, as expected, once corrected for clinical dose, an improved relationship was observed [14, 15].

### 2.1.3 Reactive phase II conjugates of carboxylic acid-containing molecules

A specific area of interest in drug bioactivation and its role in adverse effects is for molecules containing carboxylic acids. The  $-\text{COOH}$  group imparts critical pharmacological properties to drug molecules. For pharmacological targets that prefer a carboxylic acid moiety, it is difficult to find isosteres with comparative potency. Carboxylic acid drugs can form acyl glucuronides (AG) or CoA thioesters, both reactive species that have the potential to modify proteins. Acyl glucuronides can undergo direct addition with a protein nucleophile by displacement of the glucuronic acid group (transacylation) or can undergo rearrangement exposing an aldehyde moiety that can subsequently condense with a  $-\text{NH}_2$  residue of a protein (glycation) [16, 17]. There is a fundamental difference between protein adducts formed from transacylation vs glycation. In transacylation, the product is an amide and the glucuronic acid moiety is no longer attached to the drug; in glycation, the adduct is a secondary amine where the ring-opened glucuronic acid moiety forms a distinct bridge (Fig. 3). Note that CoA thioester intermediates may also lead to the same transacylation adducts, hence it is not possible to track down the mechanistic source even if the drug-protein adduct

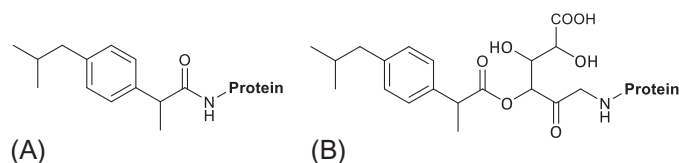


FIG. 3 Protein-trapped products from acyl glucuronide (AG) or CoA intermediates: Product A (amide) can be formed from both AG and CoA (transacylation), while product B (amine) can only be formed from AG via rearrangement (glycation).

is identified. It is also unclear if there are toxicological differences in how transacylated vs glycosylated adducts are processed in the cell, and if one preferentially leads to adverse effects.

Trovafloxacin, an antibiotic that was withdrawn from the market due to hepatotoxicity, is metabolized mainly to its AG. In an UGT1A1-induced Hep G2 cell model where trovafloxacin AG was generated *in situ*, chemokine (C-X-C motif) ligand 2 (CXCL2), a cytokine known to be involved in DILI, was uniquely induced and cell viability was compromised. Additionally, an *in vivo* UGT1 knock-out mouse study showed significantly lower serum levels of alanine aminotransferase than wild type, implicating further the importance of UGT1A1, and hence the AG, in trovafloxacin-induced liver toxicity [18]. Another demonstration of the engagement of an AG in toxicity is for zomepirac; however, interestingly, the toxicity is manifested in the kidney and not in the liver. Zomepirac is cleared primarily through glucuronidation in humans. In a mechanistic mouse model, significant increases in blood urea nitrogen (BUN) and creatinine (CRE) were observed on zomepirac administration. When the zomepirac AG concentrations were artificially elevated by pretreatment with tri-*o*-tolyl phosphate (TOTP, a nonselective esterase inhibitor), proportionally higher values for BUN and CRE were noted, associating AG accumulation in the kidney with *in vivo* toxicological outcome. Histopathological examination revealed vacuolation, infiltration of mononuclear cells, and oxidative stress markers in the kidney of the mouse model [19]. In a similar *in vivo* study with diclofenac (where AG is a known metabolite), it was shown that mice pretreated with the UDP-glucuronosyltransferase inhibitor (–)-borneol exhibited significantly lower levels of alanine aminotransferase levels than in untreated mice. Furthermore, the levels of diclofenac AG in plasma from borneol-treated mice were significantly lower than the untreated ones, establishing a correlation of AG concentrations with hepatic enzyme elevation. Additionally, the mRNA expression of chemokine (C-X-C motif) ligand 1 (CXCL1), CXCL2, and the neutrophil marker CD11b were reduced in the livers of pretreated mice, as were the numbers of infiltrated myeloperoxidase- and lymphocyte antigen 6 complex-positive cells. These results elegantly showed the engagement of innate immunity and neutrophils, initiated by AG, in acute liver injury in mice, and implicated a similar etiology in human DILI [20].

Hazard assessment of AG may be done through covalent binding similar to oxidative/reductive metabolites; however, simpler approaches are available to analyze their reactivity. Irrespective of the nature of the adduct, it is hypothesized that the chemical instability of AG is an apt measure of its protein-modifying ability. Acyl glucuronides of 21 drugs (categorized as “safe,” “warning,” and “withdrawn” in terms of their DILI risk) were analyzed in potassium phosphate buffer (KPB), human serum albumin (HSA) solution, and human plasma. It was found that there was a better correlation of the half-lives of AGs with DILI categorization determined in KPB than those in HSA solution or human plasma. It was determined that a threshold of the half-life of 3.6 h provided a separation between DILI-positive and -negative compounds [21]. It is now a standard procedure in many laboratories in early discovery to assess the reactivity of AG via measurement of half-life in KPB buffer. An alternative approach to quantitative assessment of acyl glucuronide reactivity involves the use of <sup>35</sup>S-labeled cysteine as a trapping agent, selected over glutathione to leverage the free amino group that forms a stable product through intramolecular rearrangement once the initial cysteine sulfur-drug covalent association has been created. In a study of 13 compounds belonging to “safe” and “non-safe” (withdrawn, with a warning) categories, it was found that the [<sup>35</sup>S]Cys assay can accurately bucket the “non-safe” drugs. This relatively easy method

allows the early identification of potentially reactive AG without the need to synthesize the standards [22].

In addition to the reactivity of AG, for a true assessment of risk, one needs to consider if glucuronidation represents a major pathway of elimination of the drug and whether the AG is in circulation such that other organs may be exposed to it as well (as in Zomepirac) [19]. The one glaring blind spot in the assessment of risk from carboxylic acid-containing drugs is the lack of knowledge around the CoA pathway, a product that is significantly more reactive than AGs. Although there are a few examples of detection of CoA intermediates by mass spectrometry, the presence of a CoA pathway for a drug is generally inferred from the presence of downstream products such as taurine conjugates [23]. Note that the labeling of proteins by drug-CoA intermediates has been clearly demonstrated, indicating the potential of this pathway to be a liable factor in potential DILI outcomes [16, 17].

#### **2.1.4 Glaxo Smith Kline multi-assay approach to assess DILI risk from bioactivation**

Glaxo Smith Kline scientists have reported an approach to analyze liabilities in new candidates via the integration of data from multiple bioactivation assays. The assays used are (1) investigation of metabolism-dependent inhibition of CYP isoforms 1A2, 2C9, 2C19, 2D6, and 3A4, (2) GSH adduct formation in human liver microsomes, (3) [<sup>14</sup>C]-radiolabeled drug-protein covalent binding studies in human liver microsomes, and (4) clinical dose. Assessing a learning set of 223 marketed drugs (51% with clinical hepatotoxicity; 49% non-hepatotoxic), it was found that 76% of drugs with a daily dose of <100 mg were non-hepatotoxic; however, drugs with daily dose ≥100 mg or those demonstrating GSH adduction, significant P450 time-dependent inhibition or covalent binding ≥200 pmoleq/mg protein had approximately 65% chance of triggering clinical DILI. Once dose was combined with the readouts from each bioactivation assay, 80%–100% sensitivity was achieved [24].

#### **2.1.5 Transcriptomics approach**

The next milestone in assessing bioactivation-mediated DILI risk would need to go beyond the chemistry of reactive intermediates and visualize downstream cellular responses arising from these initial protein modification events, with the hypotheses that the cellular machinery can select “bad” vs “benign” protein adducts. Research has been directed to assess cellular stress in terms of toxicogenomic, proteomic, and metabolomic approaches, with the expectation that these readouts carry the potential of having insights, as a prelude to DILI, into the perturbation of various biological networks resulting from oxidative stress or electrophile exposure. These endpoints are hypothesized not only to successfully recognize early patterns of change across a broad range of biological networks in response to adverse entities but, guided by potential trigger mechanisms, can also “weed” out the truly deleterious compounds from the benign ones. Along those lines, McMillian et al. have reported an oxidative stress/reactive metabolite (OS/RM) signature to differentiate compounds with DILI liabilities (Fig. 4).

These data were generated from rats administered with a single dose of the drug (2/3 of the reported LD<sub>50</sub> from the Merck Index for most compounds) and necropsied at 24 h. In studying a database of a total of 97 DILI-positive and DILI-negative compounds, sensitivity and specificity were 75% and 98%, respectively. It is to be noted that the statistical outcome relies heavily on the classification of the drugs in the DILI categories, and it is known that there is

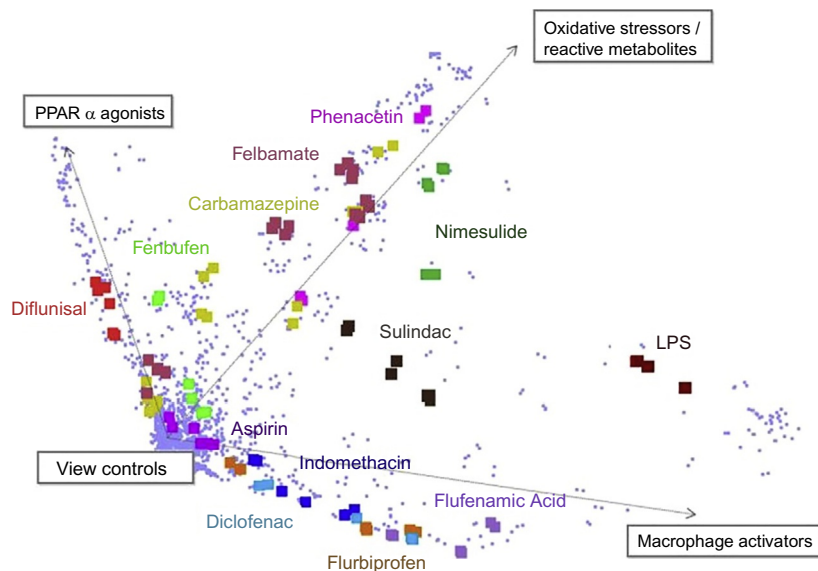


**FIG. 4** PCA-like plot derived with 70 gene responses shows the separation of several idiosyncratic hepatotoxicants with OS/RM responsive genes into three subsets of hepatotoxicity (PPAR $\alpha$ , OS/RM, and MA). Note that most tested drugs fall in either the vehicle or the OS/RM category. Nimesulide and sulindac show OS/RM-like properties with these signature genes, but also are detected by MA signature genes, between OS/RM and MA. Fenbufen and diflunisal resembled PPAR $\alpha$  agonists (possibly due to inhibition of mitochondrial oxidative of endogenous fatty acids with PPAR $\alpha$  agonist activities). Several NSAIDs (indomethacin, flufenamic acid, flurbiprofen, and diclofenac) either directly damage hepatocytes or increase endotoxin entry via damage to the gut and thus produce MA-like effects. Reprinted with permission from A. Leone, A. Nie, J.B. Parker, S. Sawant, L.-A. Piechta, M.F. Kelley, L.M. Kao, S.J. Proctor, G. Verheyen, M.D. Johnson, P.G. Lord, M.K. McMillian, *Oxidative stress/reactive metabolite gene expression signature in rat liver detects idiosyncratic hepatotoxicants*. *Toxicol. Appl. Pharmacol.* 275 (2014) 189–197.

some subjectivity in how these categorizations are made. However, the OS/RM gene expression approach broadly points to high success, indicating that compounds with a positive signature have a high likelihood of an idiosyncratic signal in the clinic, especially if the molecule in question has a clinical daily dose of >50mg. More importantly, a compound clean in this assay has a high probability of not having oxidative stress- or reactive metabolite-centered concern in humans [25–27].

### 2.1.6 Immunomics approach

The pathogenesis of idiosyncratic DILI is often characterized by the indications of immune engagement, such as rash, fever, and eosinophilia. Moreover, the presence of antibodies directed against native or drug-modified proteins, hepatic cytotoxic CD8+ T-cells, and circulating drug specific-cells in patients support immune-based mechanisms for DILI [28]. Electrophilic drugs or metabolites can covalently bind to intracellular proteins, forming haptens that can induce drug-specific antibody or T-cell responses. Thus, the structure of epitopes formed on proteins is key to decipher the drug-immune receptor interaction; this could then lead to better design of molecular scaffolds. Fig. 5 shows a workflow for the identification of reactive metabolites, their protein targets, and potential immunogenic responses. Human serum albumin is

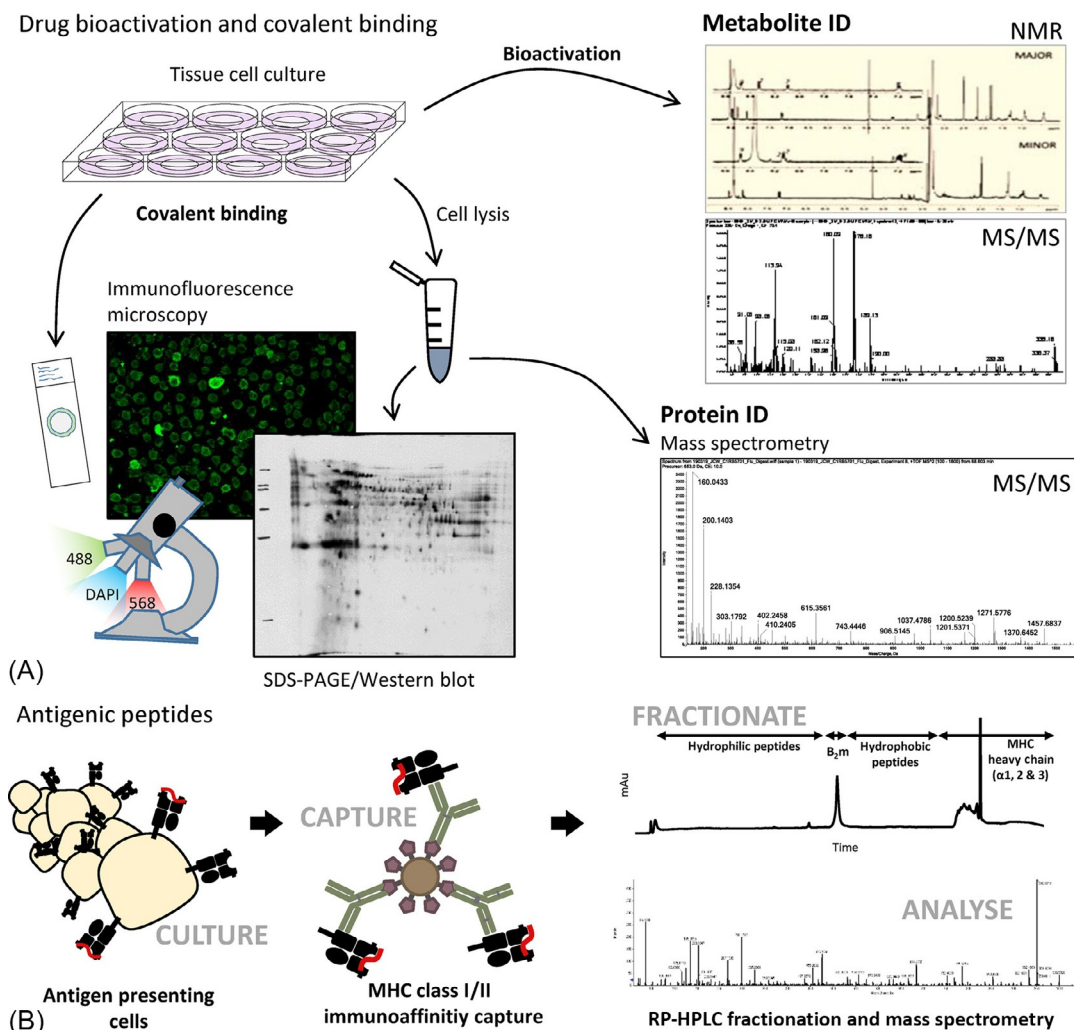


**FIG. 5** Characterization of drug-associated antigens. (A) Drug metabolism in the liver leads to the formation of both stable and reactive metabolites; these metabolites can be characterized by advanced bioanalytical techniques including LC–MS/MS and NMR. Drug protein adducts can be characterized by immunohistochemistry or Western blots using ADAs; the precise structure of epitopes can be determined by LC–MS/MS analysis. (B) Drug associated antigenic peptides presented by specific HLA molecules can be characterized using immunopeptidomic studies; peptides are eluted from antigen-presenting cells using immuno-affinity columns, followed by HPLC purification and LC/MS/MS analysis. *Reprinted with permission from S.-E. Ali, J.C. Waddington, B.K. Park, X. Meng, Definition of the chemical and immunological signals involved in drug-induced liver injury, Chem. Res. Toxicol. 33 (2020) 61–76.*

often modified by reactive small molecules; such adducts are known to activate both anti-drug antibodies and drug-specific T-cells. However, the workflow described above is not conducive to high throughput in early discovery, where a large number of compounds need to be assessed with quick turnaround time; hence, the utility of this approach is more mechanistic at this point. However, it is clear that accuracy in risk prediction will be significantly bolstered if knowledge of the immune responses, resulting from an initial event of protein modification by a drug, can be realized in a time frame that benefits the drug optimization cycle.

### 3 Mitochondrial impairment

Mitochondria play a major role in producing cellular energy through fatty acid oxidation and pyruvate oxidation, and formation of adenosine triphosphate (ATP) via oxidative phosphorylation. While multiple studies have shown that a large number of DILI-positive drugs have mitochondrial perturbation, direct evidence linking such mitochondrial dysfunction to the onset of DILI is limited. This is primarily because of the lack of sensitive and specific translational and mechanistic biomarkers; thus *in vitro* assays currently provide the strongest link to DILI [29, 30].

Two assays, glucose-galactose shift and SeaHorse, have been used to assess the risk of mitochondrial toxicity in new chemical entities. Glucose-galactose shift assay is typically conducted in human hepatocellular carcinoma cells, HepG2. Glucose in the HepG2 culture media is replaced by galactose to force the reliance of ATP generation on mitochondrial oxidative phosphorylation rather than glycolysis, thus making the system more prone to mitochondrial toxicants. Using this system, mitochondrial toxicity is measured as a shift of  $IC_{50}$  values for the reduction of cellular ATP as a function of drug concentration. Modifications to the classical Glu-Gal assay have recently been proposed, where the addition of glutamine has been shown to provide greater predictive ability for mitotoxicants. In the absence of glucose, HepG2 cells were shown to have larger glutamine consumption as a bioenergetics source. Based on this improved understanding of galactose and glutamine metabolism in HepG2 cells, the assay was altered; the modified assay demonstrated 96% sensitivity and 97% specificity in discriminating compounds with known mitochondrial toxicity [31]. The SeaHorse assay is used to measure drug dependent decrease in the rate of oxygen consumption by mitochondria. This assay, typically conducted in Hep G2 or isolated mitochondria, can also provide an understanding of the mechanism of mitochondrial toxicity, such as inhibition of particular complexes in the electron transport chain.

In an analysis of 133 compounds of which 73 were hepatotoxic and 60 did not elicit any organ toxicity, analysis of mitochondrial perturbation with the Glu-Gal assay showed a sensitivity and specificity of 11%–63% and 100%–93%, respectively, under a normalized assay condition of  $1 \times -100 \times$  clinical  $C_{max}$ , with highest sensitivity and specificity achieved at  $100 \times$  clinical  $C_{max}$ . It was also found that  $cLogP$  was the physicochemical parameter most closely associated with mitochondrial toxicity [32]. Another multiparametric assay, designed to assess the global health of mitochondria as a function of drug, investigated mitochondrial membrane permeabilization (swelling), inner membrane permeabilization (transmembrane potential), outer membrane permeabilization (cytochrome *c* release), and alteration of mitochondrial respiration in a dataset of 124 molecules (with 87 DILI-positive compounds and



37 DILI-negative). Using a cutoff of  $C_{20}$  from any assay  $\leq 200 \mu\text{M}$ , the analysis showed a sensitivity and specificity of 94%–92% and 51%–64%, respectively. When the analysis used a cutoff of  $C_{20}$  from any assay  $\leq 100 \times$  clinical  $C_{\text{max}}$ , the 114 compounds (86 DILI positive, 28 DILI negative) remaining in the analysis showed sensitivity and specificity of 94% and 36%, respectively, showing a strong correlation in predicting suboptimal molecules [33]. Analysis of mitochondrial toxicity is routinely used in early drug discovery, either as a stand-alone assay or as a contributor to a hazard matrix as discussed later.

## 4 Transporter inhibition

Transporter proteins in the liver are involved in the transfer of drugs and endogenous molecules across membranes [34, 35] (Fig. 6). Influx of uptake transporters, expressed primarily in the basolateral membrane of hepatocytes, carry molecules from the blood into the hepatic cytosolic compartment. Efflux transporters that are expressed in the basolateral membrane move molecules from the hepatic cytosol to blood, while those expressed at the apical (canalicular) membrane transport molecules from the cytosol to bile. Note that transporters (especially some uptake transporters), depending upon the physiological conditions, may be able to conduct bidirectional transport.

Drugs often interact with and modulate transporter activities, resulting in unexpected outcomes such as in cholestatic DILI. Some drugs act as inhibitors of transporters, thus rendering them inactive for the transfer of their endogenous substrates. Bile salt export protein (BSEP) is engaged in the elimination of bile salts from the liver into the bile; effective drug-mediated inhibition of BSEP would block that elimination pathway and lead to accumulation of bile

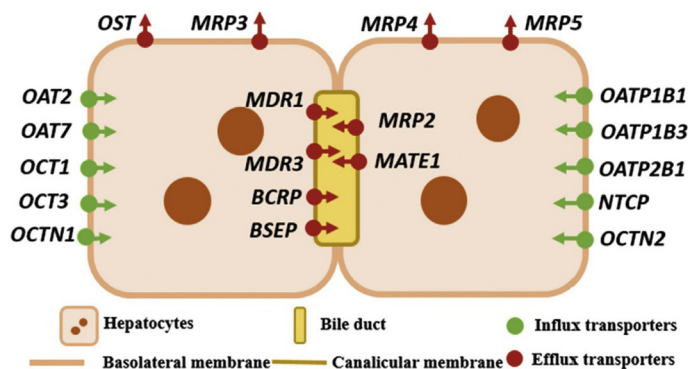


**FIG. 6** Schematic figure of human hepatic and canalicular transport proteins. *BSEP*, bile salt export pump; *MDR*, multidrug resistance; *BCRP*, breast cancer resistance protein; *MRP*, multidrug resistance-associated protein; *NTCP*,  $\text{Na}^+$ -taurocholate cotransporting polypeptide; *OATP*, organic anion-transporting polypeptide; *OST*, organic solute transporter; *OCTN*, organic cation/carnitine transporter; *OCT*, organic cation transporter. Red, ATP-binding cassette (ABC) transporters; green, P-type ATPase. Reprinted with permission from G. Pan, *Roles of hepatic drug transporters in drug disposition and liver toxicity*, in: X. Liu, G. Pan, (Eds) *Drug Transporters in Drug Disposition, Effects and Toxicity. Advances in Experimental Medicine and Biology*, 1141. (2019) Springer, Singapore, legend adjusted for context.



salts in the liver, leading to cholestatic or other hepatocellular injuries. Fasiglifam (TAK-875), a G-protein-coupled receptor 40 (GPR40) agonist indicated for type 2 diabetes, was terminated in phase 3 due to adverse liver effects. In addition to reactive acyl glucuronides that can modify proteins [16], it has been suggested that TAK-875 caused cholestatic liver injury in the clinic by inhibiting hepatobiliary transporters, namely, BSEP, MRP2/3/4, NTCP, and OATP [36, 37]. Other drugs carrying DILI liabilities in the clinical that have been shown to inhibit BSEP are the antidiabetic drug troglitazone and its sulfated metabolite, tolvaptan [35].

Since BSEP inhibition has been implicated to contribute to DILI in multiple cases, it is recommended that new chemical entities are ideally devoid of this liability (Fig. 7).

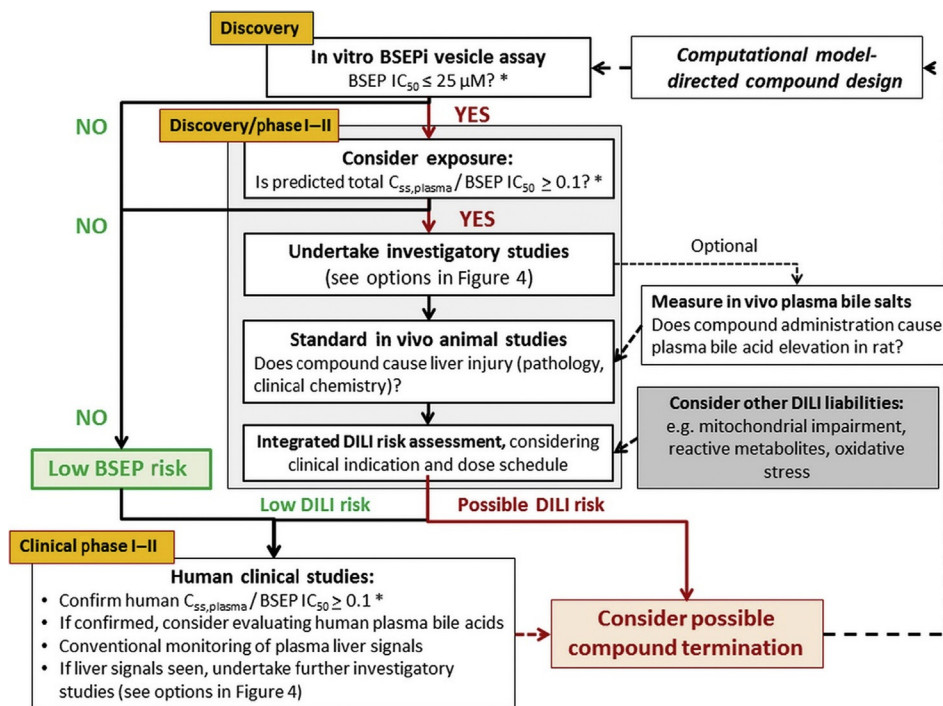


**FIG. 7** DILI potential guided workflow to interpret and mitigate bile salt export pump (BSEP) inhibition in drug discovery and/or early clinical development (phase I/II). The workflow is based on current knowledge and could be considered when making internal decisions on potential BSEP liabilities. The science has not evolved to a point where a standardized decision tree can be constructed and used by regulators due to gaps in our knowledge. (i) \*The suggested cutoff values are based on limited published data and are intended to help focus the additional discussion. Further research/justification is needed to reach the final consensus on the feasibility of the suggested approaches. (ii) In the absence of clinical data, total concentration estimates may be from preclinical efficacy models or from other early predictions of human pharmacokinetics. Total plasma steady-state drug concentrations ( $C_{ss,plasma}$ ) correlation to BSEP concentration of half inhibition ( $IC_{50}$ ) should be revisited when relevant clinical data are available. When total  $C_{ss,plasma}$  is not known, estimated or determined total peak plasma concentration ( $C_{max}$ ) data may be used instead. (iii) A higher likelihood of drug-induced liver injury (DILI) is expected if one or more DILI liabilities are flagged along with BSEP inhibition. Figure reprinted with permission from G. Pan, Roles of hepatic drug transporters in drug disposition and liver toxicity, in: X. Liu, G. Pan (Eds) Drug Transporters in Drug Disposition, Effects and Toxicity. Advances in Experimental Medicine and Biology, 1141. (2019) Springer, Singapore, legend adjusted for context.

The proactive evaluation of BSEP inhibition *in vitro*, in a high-throughput screening manner as described in Fig. 7, during early discovery stages may allow the finding of scaffolds that will not carry the hazard. It is important though that the *in vitro* IC<sub>50</sub>s be considered in the context of *in vivo* exposures. Other transporters such as multidrug resistance-associated protein 2 (MRP2), multidrug resistance protein 3 (MDR3), intestinal apical sodium-bile acid transporter (ASBT), and organic solute transporter (OST) $\alpha/\beta$  are all engaged in the transport of drugs and endogenous molecules and have been implicated as causative mechanisms for DILI. Also, many drugs inhibit multiple transporters, including BSEP, so it becomes difficult to point to a specific transporter as the culprit in the case of these drugs [35–38].

## 5 Overarching derisking approaches independent of mechanism

The identification of compounds that can cause clinical DILI follows a spectrum of analysis that progresses from hazard (or, liability) assessment to the prediction of whether that hazards will translate into clinical risk. Because of the multiple potential contributors to DILI, an assay looking into *one* contributing parameter may successfully identify a hazard, but it will not be able to predict the overall risk. Thus, there need to be multiparametric approaches with multiple assays and analyses that provide a conglomerate of readouts and increases the possibility of success of a risk prediction [39, 40].

### 5.1 Dose, exposure, and physiochemical properties

The dose of a particular drug plays a critical role in DILI due to a higher body burden of the offending entity. It is generally considered that doses >50–100 mg are more prone to DILI [41] if other liability parameters are also applied. Exposure, instead of dose, has also been considered as a measure of the threshold of DILI risk. Using a database of 125 drugs (70 DILI-positive, 55 DILI-negative) from the Food and Drug Administration Liver Toxicity Knowledge Base, it was calculated that human plasma C<sub>max</sub> total  $\geq 1.1 \mu\text{M}$  *alone* was quite successful in differentiating DILI-positive drugs from benign ones, with a sensitivity and specificity of 80% and 73%, respectively [7]. Using a compilation of 1036 FDA-approved drugs [42], drugs classified as “No DILI” ( $n=163$ ) were found to have lower dose and lipophilicity as well as higher Fsp<sup>3</sup> (fraction of carbon atoms that are sp<sup>3</sup> hybridized) than the “Most DILI” ( $n=163$ ) category. In addition, the impact of lipophilicity and Fsp<sup>3</sup> appeared to be greater in the upper 20% spectrum of the dose range [43]. Fsp<sup>3</sup> likely provides an estimate of metabolism that would lead to reactive intermediates: greater sp<sup>3</sup> character signifies benign metabolism. Note that, in early stages of drug discovery when the impact of hazard assessment is most pronounced, a correct clinical dose projection may not be available; thus, discovery teams working on the program may not be able to fall back on the safety net of a low-dose drug if it contains prominent hazards.

The role of dose and physicochemical properties in DILI propensity has been further quantitated in the “rule of two” that states that a high daily dose (>100 mg/day) and lipophilicity (Log  $P > 3$ ) enhance the risk of clinical DILI [44]. Another categorization of compounds

utilizing physicochemical properties of molecules, reflected in their membrane permeability rate and aqueous solubility, is called the biopharmaceutics drug disposition classification system (BDDCS). It was determined that highly permeable compounds were extensively metabolized, while drugs that had poor permeability were primarily eliminated unchanged in the urine or bile [45]. BDDCS features can be used to assign compounds in four categories regarding DILI risk, independent of dose considerations (Table 2). While this approach is not considered to be sufficiently predictive of DILI risk for new drug candidates, it does provide an early readout in terms of hazard assessment given that the input parameters are readily available early on in a discovery program. Interestingly, it is shown that the BDDCS classification of compounds provides a similar benefit of analysis regarding BSEP inhibition as well [45].

## 5.2 Multiparametric approaches

Acknowledging the multifaceted etiology of DILI, several approaches incorporating multiple contributing parameters have been adopted by the pharmaceutical industry to assess DILI risk for their compounds in the discovery pipeline.

### 5.2.1 European Federation of Pharmaceutical Industries and Associations (EFPIA) three-tiered roadmap

A three-tiered roadmap incorporating a myriad of assays, as a holistic strategy to manage human DILI risk, has been recently published by a group of pharmaceutical companies, research enterprises, and academic partners belonging to the European Federation of Pharmaceutical Industries and Associations (EFPIA) [4] (Fig. 8). This strategic vision integrates various test systems, already established or in development, wherein the complexity increases progressively from single-cell two-dimensional platforms to advanced three-dimensional multicellular systems that incorporate tailored factors, such as those that are genetic or disease-related and are known to influence clinical DILI outcomes. In addition to laying out the tiers, the roadmap references the extensive bioanalytical tools that are needed for a thorough analysis, as well as the functional correlation to physiology, pharmacology, and toxicology.

This roadmap serves the purpose of assembling the current thinking around causative factors of DILI using mechanistic models. Tier 1 studies identify hazards of bioactivation, drug or bile acid accumulation due to transporter inhibition, mitochondrial toxicity, and markers of oxidative stress and inflammation. Tier 2 extends these analyses into advanced liver cells that are in more optimal physiological states. Tier 3, where many assays are still in the early stages of development, allows the query of immune engagement as well the effect of specific

TABLE 2 BDDCS classification and DILI risk.

	High solubility ( $\geq 0.3$ mg/mL)	Low solubility ( $< 0.3$ mg/mL)
High permeability, high metabolism	Class 1: Moderate DILI risk	Class 2: High DILI risk
Low permeability, low metabolism	Class 3: Lower DILI risk	Class 4: Data insufficiency

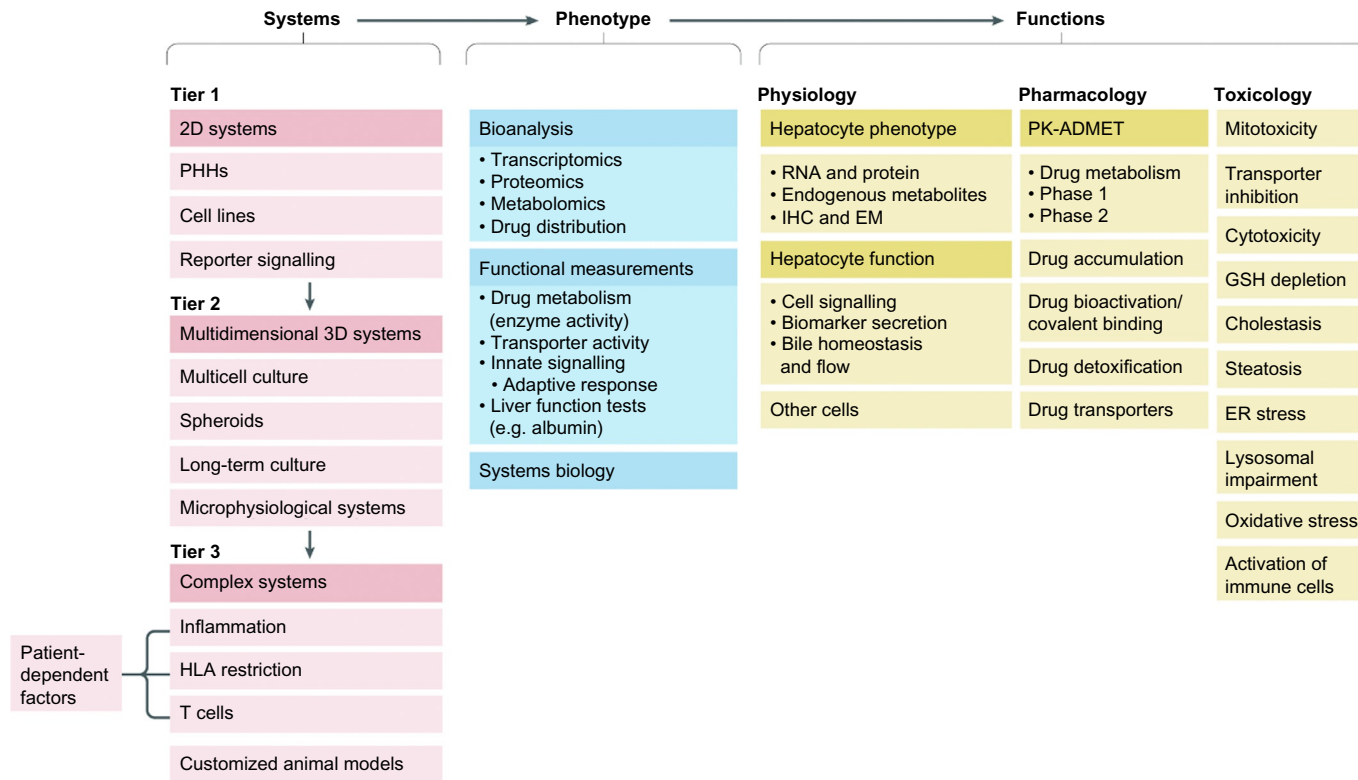


**FIG. 8** Roadmap for the development of “fit-for-purpose” predictive models of human DILI. *ADMET*, absorption, distribution, metabolism, excretion, toxicity; *EM*, electron microscopy; *ER*, endoplasmic reticulum; *GSH*, glutathione; *IHC*, immunohistochemistry; *PHH*, primary human hepatocyte; *PK*, pharmacokinetics. Figure reprinted with permission from R.J. Weaver, E.A. Blomme, A.E. Chadwick, I.M. Copple, H.H.J. Gerets, C.E. Goldring, A. Guillouzo, P.G. Hewitt, M. Ingelman-Sundberg, K.G. Jensen, S. Juhila, U. Klingmüller, G. Labbe, M.J. Liguori, C.A. Lovatt, P. Morgan, D.J. Naisbitt, R.H.H. Pieters, J. Snoeys, B. van de Water, D.P. Williams, B. Kevin Park, *Managing the challenge of drug-induced liver injury: a roadmap for the development and deployment of preclinical predictive models*, *Nat. Rev. Drug Discov.* 19 (2020) 131–148.

biological variables [4]. The need to incorporate bioanalytical techniques such as transcriptomics and metabolomics are becoming more apparent as we seek to look deeper into cellular interpretations of assault [25–27, 46, 47].

### 5.2.2 Roche approach using a combination of assays

Roche has described an approach using a combination of assays covering potential DILI mechanisms: generation of reactive metabolites (via analysis of CYP3A4 time-dependent inhibition and glutathione adduct formation), human BSEP inhibition, mitochondrial toxicity assessments, and cytotoxicity readouts (in fibroblasts and human hepatocytes), calibrated by dose and/or plasma exposure. Using a training set of 81 marketed or withdrawn compounds with different binning categories for DILI (28, 10, 43 with severe, moderate and less concern for DILI, respectively), overall sensitivity of 76%–79% and specificity of 81% was achieved. The assay combination that gave the optimal predictivity in the test set was then applied to an independent test set of 39 compounds (17 and 22 high and low-risk compounds, respectively), providing a sensitivity of 82% and specificity of 76%. Interestingly, the GSH adduct analysis was shown to have the largest impact on the accuracy of prediction [48].

### 5.2.3 Astra Zeneca integrated in vitro hazard matrix and Bayesian machine learning approach

Thompson et al. have reported a process where, prior to the nomination of a compound for development, data from a Hepatic Liability Panel is combined with an estimated RM (Reactive Metabolite) body burden to come up with a Hepatic In Vitro Hazard Matrix. The Hepatic Liability panel is comprised of five quantitative in vitro readouts: (1) toxicity to THLE cells (SV40 T-antigen-immortalized human liver epithelial cells) that do not have metabolic capacity, (2) toxicity to a tailored THLE cell line that selectively expresses the P450 3A4 enzyme, (3) mitochondrial toxicity assessment in HepG2 cells in the glucose-galactose assay, (4) inhibition of human BSEP, and (5) inhibition of rat MRP2 protein (multidrug resistance-associated protein 2). The RM body burden is calculated using the level of in vitro protein covalent binding of a radiolabeled drug in human hepatocytes adjusted for the predicted human dose and the extent of metabolism leading to covalent binding. Using a set of 36 drugs (27 with marked DILI concern and nine with low concerns) through this analysis, discrimination was achieved with high specificity (78%) and sensitivity (100%) [49, 50].

To improve upon these metrics, Williams et al. forwarded a machine learning approach using Bayesian calculations. This approach combines data from in vitro assays such as HepG2/C3A spheroid viability quantitated by the ATP-sensing titer, BSEP inhibition, measurement of mitochondrial toxicity, and bioactivation (as a binary indicator of whether a compound will form a reactive metabolite) with physicochemical assessments such as  $c\text{LogP}$  and total drug  $C_{\text{max}}$ . Using these analytical parameters in a diverse dataset (33 no/low-, 40 medium-, and 23 high-severity DILI compounds), the model demonstrated sensitivity and specificity of 87% and 85%, respectively. By integrating both probability and uncertainty from the data sources and allowing the weighting of the hepatotoxicity assays for DILI severity, the Bayesian model translates hazards into a *quantitative* risk prediction via a user-friendly web interface. The model also provides for the incorporation of newer or improved assays as they become available, thereby enhancing machine learning and narrowing down predictivity [51].

#### 5.2.4 Pfizer hepatic risk matrix (HRM) approach

Pfizer has forwarded an analysis that integrates the biological readouts of new drug candidates into a 4-quadrant DILI hazard prediction matrix [6, 52]. This scoring system integrates the physicochemical properties of a compound using the “Rule of Two Model” [44] (i.e., dose and lipophilicity) or the “Partition Model” (dose, ionization state, lipophilicity, and  $F_{sp^3}$  factor) [43] with biological vectors known to cause DILI (cytotoxicity, mitochondrial dysfunction, and BSEP inhibition) and is based on safety margins in terms of clinical total  $C_{max}$ . The HRM provides a quantitative assessment summing up scores from cytotoxicity readouts, mitochondrial dysfunction, and BSEP inhibition with those from the “Rule of Two” or “Partition Model.” The HRM approach was applied to a 200-drug index from the Liver Toxicity Knowledge Base, annotated as Most-DILI (79), Less-DILI (56), No-DILI (47), and Ambiguous-DILI (18) concerns. Interestingly, it was found that adding other information such as contributions from reactive and cytotoxic metabolites and non-BSEP transporter inhibition to the HRM had minimal impact in DILI prediction. Perhaps the lack of impact on adding the biotransformation component may be explained by the fact the “Partition Model” already incorporates the extent of metabolism via the  $F_{sp^3}$  factor. Both hybrid HRM scoring systems not only successfully identified 70%–80% of the most-DILI-concern drugs but was also able to stratify molecules in terms of incidence and severity of adverse hepatic observations.

---

## 6 Summary

---

Derisking new chemical entities for DILI continues to remain a formidable challenge to the pharmaceutical industry due to its complex etiology and multiple causative mechanisms. The science of risk assessment currently has two broad approaches: dividing up the actionable causative factors (bioactivation, mitochondrial toxicity, and transporter inhibition) and assessing each of these hazards independently; or, looking at overarching parameters that influence each of those mechanisms, often weighted, and providing an overall one-stop analysis (physicochemical properties, dose considerations, and weighted assessment of each biological contribution). In many cases, *in silico* modeling *a priori* is assisting in predicting liabilities such as bioactivation or BSEP inhibition. Assessment is ranging from  $IC_{50}$  determinations of receptor inhibition to multiple-omics approaches (transcriptomics, metabolomics). The sophistication of *in vitro* systems (such as spheroids and advanced liver platforms like HepatoPac) is providing approximations closer to *in vivo* scenarios that are leading to readouts across species, with greater translatability from preclinical data into the clinic. Machine learning approaches incorporating data from various methods are allowing a steady improvement in probability and uncertainty vectors in the assessment. The one underlying variable that needs further incorporation into both of the approaches above is an improved understanding of the dose-toxicity relationship and, by extension, an accurate handle of drug concentrations at the tissue of concern (e.g., liver for DILI) following a clinical dose. Thinking is now also progressing into understanding the next layer of sophistication where the variable of immunomics is brought in to separate “danger” events from “benign” ones at an individual biology level. The field of DILI assessment has seen a



radical growth spurt in the last two decades. More concerted approaches across the industry, academia, and via consortia, might be useful to streamline efforts and push this science around patient safety to even greater success.

## References

- [1] T. Alempijevic, S. Zec, T. Milosavljevic, Drug-induced liver injury: do we know everything? *World J. Hepatol.* 9 (2017) 491–502.
- [2] S. Kumar, K. Mitra, T.A. Baillie, Managing metabolic activation issues in drug discovery, in: P.G. Pearson, L.C. Wienkers (Eds.), *Handbook of Drug Metabolism*, third ed., CRC Press, New York, NY, 2015.
- [3] N. Noureddin, N. Kaplowitz, Overview of mechanisms of drug-induced liver injury (DILI) and key challenges in DILI research, in: M. Chen, Y. Will (Eds.), *Drug-Induced Liver Toxicity. Methods in Pharmacology and Toxicology*, Humana, New York, NY, 2018.
- [4] R.J. Weaver, E.A. Blomme, A.E. Chadwick, I.M. Copple, H.H.J. Gerets, C.E. Goldring, A. Guillouzo, P.G. Hewitt, M. Ingelman-Sundberg, K.G. Jensen, S. Juhila, U. Klingmüller, G. Labbe, M.J. Liguori, C.A. Lovatt, P. Morgan, D.J. Naisbitt, R.H.H. Pieters, J. Snoeys, B. van de Water, D.P. Williams, B. Kevin Park, Managing the challenge of drug-induced liver injury: a roadmap for the development and deployment of preclinical predictive models, *Nat. Rev. Drug Discov.* 19 (2020) 131–148.
- [5] J.A. Shayman, A. Abe, Drug-induced phospholipidosis: an acquired lysosomal storage disorder, *Biochim. Biophys. Acta* 1831 (2013) 602–611.
- [6] R. Kim, M. Emi, K. Tanabe, S. Murakami, Role of the unfolded protein response in cell death, *Apoptosis* 11 (2006) 5–13.
- [7] F. Shah, L. Leung, H.A. Barton, Y. Will, A.D. Rodrigues, N. Greene, M.D. Aleo, Setting clinical exposure levels of concern for drug-induced liver injury (DILI) using mechanistic in vitro assays, *Toxicol. Sci.* 147 (2015) 500–514.
- [8] D. Smith, L. Di, E. Kerns, The effect of plasma protein binding on in vivo efficacy: misconceptions in drug discovery, *Nat. Rev. Drug Discov.* 9 (2010) 929–939.
- [9] D.J. Antoine, D.P. Williams, B.K. Park, Understanding the role of reactive metabolites in drug-induced hepatotoxicity: state of the science, *Expert Opin. Drug Metab. Toxicol.* 4 (2008) 1415–1427.
- [10] M.P. Grillo, Detecting reactive drug metabolites for reducing the potential for drug toxicity, *Expert Opin. Drug Metab. Toxicol.* 11 (2019) 1281–1302.
- [11] F. Li, J. Lu, X. Ma, Profiling the reactive metabolites of xenobiotics using metabolomic technologies, *Chem. Res. Toxicol.* 24 (2011) 744–751.
- [12] D.C. Evans, A.P. Watt, D.A. Nicoll-Griffith, T.A. Baillie, Drug-protein adducts: an industry perspective on minimizing the potential for drug bioactivation in drug discovery and development, *Chem. Res. Toxicol.* 17 (2004) 3–16.
- [13] G.A. Doss, T.A. Baillie, Addressing metabolic activation as an integral component of drug design, *Drug Metab. Rev.* 38 (2006) 641–649.
- [14] R.S. Obach, A.S. Kalgutkar, J.R. Soglia, S.X. Zhao, Can in vitro metabolism-dependent covalent binding data in liver microsomes distinguish hepatotoxic from non-hepatotoxic drugs? An analysis of 18 drugs with consideration of intrinsic clearance and daily dose, *Chem. Res. Toxicol.* 21 (2008) 1814–1822.
- [15] S. Nakayama, R. Atsumi, H. Takakusa, Y. Kobayashi, A. Kurihara, Y. Nagai, D. Nakai, O. Okazaki, A zone classification system for risk assessment of idiosyncratic drug toxicity using daily dose and covalent binding, *Drug Metab. Dispos.* 37 (2009) 1970–1977.
- [16] T. Lassila, J. Hokkanen, S.-M. Aatsinki, S. Mattila, M. Turpeinen, A. Tolonen, Toxicity of carboxylic acid-containing drugs: the role of acyl migration and CoA conjugation investigated, *Chem. Res. Toxicol.* 28 (2015) 2292–2303.
- [17] J. Shang, R. Tschirret-Guth, M. Cancelli, K. Samuel, Q. Chen, H.R. Chobanian, A. Thomas, W. Tong, H. Josien, A.V. Buevich, K. Mitra, Bioactivation of GPR40 agonist MK-8666: formation of protein adducts in vitro from reactive acyl glucuronide and acyl CoA thioester, *Chem. Res. Toxicol.* 33 (2020) 191–201.
- [18] R. Mitsugi, K. Sumida, Y. Fujie, R.H. Tukey, T. Itoh, R. Fujiwara, Acyl glucuronide as a possible cause of trovafloxacin-induced liver toxicity: induction of chemokine (C-X-C motif) ligand 2 by trovafloxacin acyl glucuronide, *Biol. Pharm. Bull.* 39 (2016) 1604–1610.



- [19] A. Iwamura, K. Watanabe, S. Akai, T. Nishinosono, K. Tsuneyama, S. Oda, T. Kume, T. Yokoi, Zomepirac acyl glucuronide is responsible for zomepirac-induced acute kidney injury in mice, *Drug Metab. Dispos.* 44 (2016) 888–896.
- [20] S. Oda, Y. Shirai, S. Akai, A. Nakajima, K. Tsuneyama, T. Yokoi, Toxicological role of an acyl glucuronide metabolite in diclofenac-induced acute liver injury in mice, *J. Appl. Toxicol.* 37 (2017) 545–553.
- [21] R. Sawamura, N. Okudaira, K. Watanabe, T. Murai, Y. Kobayashi, M. Tachibana, T. Ohnuki, K. Masuda, H. Honma, A. Kurihara, O. Okazaki, Predictability of idiosyncratic drug toxicity risk for carboxylic acid-containing drugs based on the chemical stability of acyl glucuronide, *Drug Metab. Dispos.* 38 (2010) 1857–1864.
- [22] H. Harada, Y. Toyoda, Y. Abe, T. Endo, H. Takeda, Quantitative evaluation of reactivity and toxicity of acyl glucuronides by [35S]cysteine trapping, *Chem. Res. Toxicol.* 32 (2019) 1955–1964.
- [23] M.P. Grillo, J.C.M. Wait, M.T. Lohr, S. Khera, L.Z. Benet, Stereoselective flunoxaprofen-S-acyl-glutathione thioester formation mediated by acyl-coA formation in rat hepatocytes, *Drug Metab. Dispos.* 38 (2010) 133–142.
- [24] M.Z. Sakatis, M.J. Reese, A.W. Harrell, M.A. Taylor, I.A. Baines, L. Chen, J.C. Bloomer, E.Y. Yang, H.M. Ellens, J.L. Ambroso, C.A. Lovatt, A.D. Ayrton, S.E. Clarke, Preclinical strategy to reduce clinical hepatotoxicity using in vitro bioactivation data for > 200 compounds, *Chem. Res. Toxicol.* 25 (2012) 2067–2082.
- [25] A. Leone, A. Nie, J.B. Parker, S. Sawant, L.-A. Piechta, M.F. Kelley, L.M. Kao, S.J. Proctor, G. Verheyen, M.D. Johnson, P.G. Lord, M.K. McMillian, Oxidative stress/reactive metabolite gene expression signature in rat liver detects idiosyncratic hepatotoxicants, *Toxicol. Appl. Pharmacol.* 275 (2014) 189–197.
- [26] M. McMillian, A.Y. Nie, J.B. Parker, A. Leone, S. Bryant, M. Kemmerer, J. Herlich, Y. Liu, L. Yieh, A. Bittner, X. Liu, J. Wan, M.D. Johnson, A gene expression signature for oxidant stress/reactive metabolites in rat liver, *Biochem. Pharmacol.* 68 (2004) 2249–2261.
- [27] M. McMillian, A. Nie, J.B. Parker, A. Leone, M. Kemmerer, S. Bryant, J. Herlich, L. Yieh, A. Bittner, X. Liu, J. Wan, M.D. Johnson, P. Lord, Drug-induced oxidative stress in rat liver from a toxicogenomics perspective, *Toxicol. Appl. Pharmacol.* 207 (2005) 171–178.
- [28] S.-E. Ali, J.C. Waddington, B.K. Park, X. Meng, Definition of the chemical and immunological signals involved in drug-induced liver injury, *Chem. Res. Toxicol.* 33 (2020) 61–76.
- [29] D. Pessayre, B. Fromenty, A. Berson, M.-A. Robin, P. Lettéron, R. Moreau, A. Mansouri, Central role of mitochondria in drug-induced liver injury, *Drug Metab. Rev.* 44 (2012) 34–87.
- [30] A. Ramachandran, L. Duan, J.Y. Akakpo, H. Jaeschke, Mitochondrial dysfunction as a mechanism of drug-induced hepatotoxicity: current understanding and future perspectives, *J. Clin. Transl. Res.* 4 (2018) 5–12.
- [31] Q. Xu, L. Liu, H. Vu, M. Kuhls, A.G. Aslamkhan, A. Liaw, Y. Yu, A. Kaczor, M. Ruth, C. Wei, J. Imredy, J. Lebron, K. Pearson, R. Gonzalez, K. Mitra, F.D. Sistare, Can galactose be converted to glucose in HepG2 cells? Improving the in vitro mitochondrial toxicity assay for the assessment of drug-induced liver injury, *Chem. Res. Toxicol.* 32 (2019) 1528–1544.
- [32] P. Rana, M.D. Aleo, M. Gosink, Y. Will, Evaluation of in vitro mitochondrial toxicity assays and physicochemical properties for prediction of organ toxicity using 228 pharmaceutical drugs, *Chem. Res. Toxicol.* 32 (2019) 156–167.
- [33] M. Porceddu, N. Buron, C. Roussel, G. Labbe, B. Fromenty, A. Borgne-Sanchez, Prediction of liver injury induced by chemicals in human with a multiparametric assay on isolated mouse liver mitochondria, *Toxicol. Sci.* 129 (2012) 332–345.
- [34] J.G. Kenna, K.S. Taskar, C. Battista, D.L. Bourdet, K.L.R. Brouwer, K.R. Brouwer, D. Dai, C. Funk, M.J. Hafey, Y. Lai, J. Maher, Y.A. Pak, J.M. Pedersen, J.W. Polli, A.D. Rodrigues, P.B. Watkins, K. Yang, R.W. Yucha, Can bile salt export pump inhibition testing in drug discovery and development reduce liver injury risk? An international transporter consortium perspective, *Clin. Pharmacol. Ther.* 104 (2018) 916–932.
- [35] G. Pan, Roles of hepatic drug transporters in drug disposition and liver toxicity, in: X. Liu, G. Pan (Eds.), *Drug Transporters in Drug Disposition, Effects and Toxicity. Advances in Experimental Medicine and Biology*, 1141, Springer, Singapore, 2019.
- [36] M.A. Otieno, J. Snoeys, W. Lam, A. Ghosh, M.R. Player, A. Poci, R. Salter, D. Simic, H. Skaggs, B. Singh, H.-K. Lim, Fasiglifam (TAK-875): mechanistic investigation and retrospective identification of hazards for drug induced liver injury, *Toxicol. Sci.* 163 (2018) 374–384.
- [37] F.S. Wolenski, A.Z.X. Zhu, M. Johnson, S. Yu, Y. Moriya, T. Ebihara, V. Csizmadia, J. Grieves, M. Paton, M. Liao, C. Gemski, L. Pan, M. Vakilynejad, Y.P. Dragan, S.K. Chowdhury, P.J. Kirby, Fasiglifam (TAK-875) alters bile acid homeostasis in rats and dogs: a potential cause of drug induced liver injury, *Toxicol. Sci.* 157 (2017) 50–61.

- [38] K. Köck, B.C. Ferslew, I. Netterberg, K. Yang, T.J. Urban, P.W. Swaan, P.W. Stewart, K.L. Brouwer, Risk factors for development of cholestatic drug-induced liver injury: inhibition of hepatic basolateral bile acid transporters MRP3 and MRP4, *Drug Metab. Dispos.* 42 (2014) 665–674.
- [39] J. Sanabria-Cabrera, I. Medina-Cáliz, S. Stankevičiūtė, A. Rodríguez-Nicolás, M. Almarza-Torres, M.I. Lucena, R.J. Andrade, Drug-induced liver injury associated with severe cutaneous hypersensitivity reactions: a complex entity in need of a multidisciplinary approach, *Curr. Pharm. Des.* 25 (2019) 3855–3871.
- [40] F.D. Sistare, W.B. Mattes, E.L. LeCluyse, The promise of new technologies to reduce, refine, or replace animal use while reducing risks of drug-induced liver injury in pharmaceutical development, *ILAR J.* 57 (2016) 186–211.
- [41] R. Chan, L.Z. Benet, Evaluation of DILI predictive hypotheses in early drug development, *Chem. Res. Toxicol.* 30 (2017) 1017–1029.
- [42] M. Chen, A. Suzuki, S. Thakkar, K. Yu, C. Hu, W. Tong, DILI rank: the largest reference drug list ranked by the risk for developing drug-induced liver injury in humans, *Drug Discov. Today* 21 (2016) 648–653.
- [43] P.D. Leeson, Impact of physicochemical properties on dose and hepatotoxicity of oral drugs, *Chem. Res. Toxicol.* 31 (2018) 494–505.
- [44] M. Chen, J. Borlak, W. Tong, High lipophilicity and high daily dose of oral medications are associated with significant risk for drug-induced liver injury, *Hepatology* 58 (2013) 388–396.
- [45] R. Chan, L.Z. Benet, Measures of BSEP inhibition in vitro are not useful predictors of DILI, *Toxicol. Sci.* 162 (2018) 499–508.
- [46] A.M. Araújo, M. Carvalho, F. Carvalho, M. de Lourdes Bastos, P. Guedes de Pinho, Metabolomic approaches in the discovery of potential urinary biomarkers of drug-induced liver injury (DILI), *Crit. Rev. Toxicol.* 47 (2017) 638–654.
- [47] J. Jiang, C.D. Pieterman, G. Ertaylan, R.L.M. Peeters, T.M.C.M. de Kok, The application of omics-based human liver platforms for investigating the mechanism of drug-induced hepatotoxicity in vitro, *Arch. Toxicol.* 93 (2019) 3067–3098.
- [48] S. Schadt, S. Simon, S. Kustermann, F. Boess, C. McGinnis, A. Brink, R. Lieven, S. Fowler, K. Youdim, M. Ullah, M. Marschmann, C. Zihlmann, Y.M. Siegrist, A.C. Cascais, E. Di Lenarda, E. Durr, N. Schaub, X. Ang, V. Starke, T. Singer, R. Alvarez-Sanchez, A.B. Roth, F. Schuler, C. Funk, Minimizing DILI risk in drug discovery: a screening tool for drug candidates, *Toxicol. In Vitro* 30 (2015) 429–437.
- [49] R.A. Thompson, E.M. Isin, Y. Li, L. Weidolf, K. Page, I. Wilson, S. Swallow, B. Middleton, S. Stahl, A.J. Foster, H. Dolgos, R. Weaver, J.G. Kenna, In vitro approach to assess the potential for risk of idiosyncratic adverse reactions caused by candidate drugs, *Chem. Res. Toxicol.* 25 (2012) 1616–1632.
- [50] R.A. Thompson, E.M. Isin, Y. Li, R. Weaver, L. Weidolf, I. Wilson, A. Claesson, K. Page, H. Dolgos, J.G. Kenna, Risk assessment and mitigation strategies for reactive metabolites in drug discovery and development, *Chem. Biol. Interact.* 192 (2011) 65–71.
- [51] D.P. Williams, S.E. Lazić, A.J. Foster, E. Semenova, P. Morgan, Predicting drug-induced liver injury with Bayesian Machine Learning, *Chem. Res. Toxicol.* 33 (2020) 239–248.
- [52] M.D. Aleo, F. Shah, S. Allen, H.A. Barton, C. Costales, S. Lazzaro, L. Leung, A. Nilson, R.S. Obach, A.D. Rodrigues, Y. Will, Moving beyond binary predictions of human drug-induced liver injury (DILI) toward contrasting relative risk potential, *Chem. Res. Toxicol.* 33 (2020) 223–238.

# Predictive and translational models for renal drug safety evaluation

Piyush Bajaj<sup>a</sup>, Rosalinde Masereeuw<sup>b</sup>, J. Eric McDuffie<sup>c</sup>,  
Matthew P. Wagoner<sup>a</sup>

<sup>a</sup>Drug Safety Research and Evaluation, Takeda Pharmaceutical International Co., Cambridge, MA, United States <sup>b</sup>Division of Pharmacology, Utrecht Institute for Pharmaceutical Sciences, Utrecht, The Netherlands <sup>c</sup>Investigative & Mechanistic Toxicology, Janssen Research & Development, San Diego, CA, United States

## 1 Background and introduction

The kidneys perform very important functions in the body by removal of waste products and maintenance of blood homeostasis. In healthy human adults, the kidneys receive approximately 25% of the cardiac output to produce 1–2L of urine each day. Being the recipient of a large cardiac output, the kidneys are also an important clearance organ of the body responsible for the elimination of endogenous waste products as well as drugs and their metabolites. In fact, of the top 200 prescribed drugs in the United States in 2010, almost a third of them had renal elimination (drugs are considered as renally eliminated when  $\geq 25\%$  of their absorbed dose is excreted unchanged in urine), with over 90% of them being secreted and less than 10% reabsorbed [1]. This elimination process is a combination of glomerular filtration, active tubular secretion, and passive reabsorption. Considering the central role of renal drug disposition, drug-induced kidney injury (DIKI) accounts for 2%–10% of all safety-related candidate drug attrition, with higher rates observed at clinical stages (Phase 3, approximately 9%) of the drug development process [2–5]. Currently, in the absence of routine histopathology data, drug-induced acute kidney injury (AKI) may be identified by monitoring for clinically relevant elevations in blood urea nitrogen (BUN) and/or Serum Creatinine (SCr). However, the predictivity for AKI using BUN and/or SCr is low for multiple reasons as highlighted by Bonventre et al. [6]. Thus, there has been an urgent need to validate a second generation of translatable and nephron-specific biomarkers to support the early diagnosis of DIKI. Fig. 1A shows the nephron segment-specific biomarkers for AKI [7].

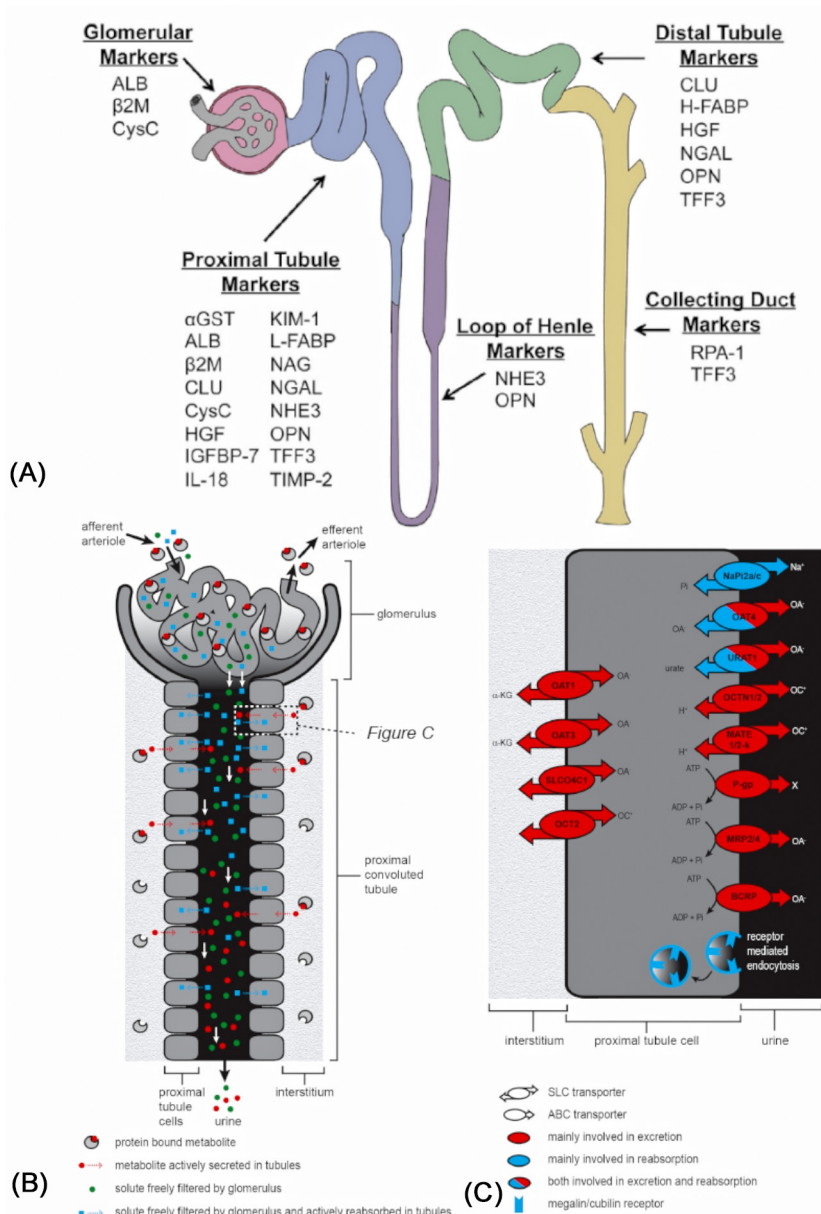


**FIG. 1** (A) Nephron segment-specific biomarkers and (B) solute handling in the glomerulus. Solutes in the serum are freely filtered in the glomerulus (depicted in green and blue), while protein-bound metabolites or drugs (red) are actively secreted via transporter proteins that are expressed in the proximal tubule epithelium. Vital solutes that are filtered by the glomerulus can be reabsorbed by the proximal tubule cells from the luminal site (blue). Only drugs that are filtered and not reabsorbed (green), or drugs that are actively secreted (red), are eliminated via the urine. (C) Transporter mechanisms and location of transporters on the PTECs. Transport mechanisms at the membrane of proximal tubule cells mediate active secretion from the interstitium or reabsorption from the glomerular filtrate at the luminal site. The transport enzymes can be subdivided into SLCs, which are driven by the membrane potential and/or electrochemical gradients, and ABC transporters that hydrolyze ATP to reveal the energy required for their functionality. In addition, megalin and cubilin play an important role in the reabsorption of low molecular weight proteins via receptor-mediated endocytosis. *Figure adapted and reproduced with permission from M. Cárdenas-González, M. Paokovic, and V.S. Vaidya, Biomarkers of acute kidney injury, in Comprehensive Toxicology (third ed.), C.A. McQueen, ed. Elsevier: Oxford (2018) 147–163; M.J. Wilmer, C.P. Ng, H.L. Lanz, P. Vulto, L. Suter-Dick, and R. Masereeuw, Kidney-on-a-chip technology for drug-induced nephrotoxicity screening, Trends Biotechnol. 34 (2) (2016) 156–170 and Copyright Elsevier.*

Among the >20 cell types of nephrons that can be potential targets of xenobiotic toxicity, such as glomerular podocytes, mesangial cells, endothelial cells, the proximal tubule epithelial cells (PTECs) have been most commonly associated with DIKI because of its myriad of transporters and their inherent functions in handling of xenobiotics and endogenous substrates. These transporters work in concert to move endogenous substrates, drugs, and/or their metabolites from the blood side (basolateral) to the urine side (apical) and any imbalance within this carefully orchestrated machinery leads to their accumulation within the cells, which can eventually lead to cell death. These PTEC transporters are part of two superfamilies of carrier proteins, viz., ATP-binding cassette (ABC) and solute carrier (SLC) [1, 9–12]. While every transporter has its own specific importance in the maintenance of homeostasis and drug disposition, the SLC family of transporters responsible for the uptake of organic anions and cations at the basolateral side, namely *SLC22A6* (OAT1), *SLC22A8* (OAT3), *SLC22A2* (OCT2) as well as uptake and efflux transporters present at the apical side, namely *ABCB1* (P-gp), multidrug resistance-associated proteins 2 and 4 (*ABCC2* (MRP2), *ABCC4* (MRP4)), breast cancer resistance protein *ABCG2* (BCRP), and multidrug and toxin extrusion 1 and 2 (*SLC47A1* (MATE1), *SLC47A2* (MATE2K)), play a crucial role in xenobiotic handling as they are known to interact with many renally secreted drugs [1]. Fig. 1B–C shows the process of solute handling in the kidney and the location of renal transporters on the PTECs [8]. Additionally, the apically located peptide transporters, *SLC15A1/2* (PEPT1/PEPT2), that mediate the absorption of drugs that contain certain peptide-like structures, apically located urate transporter, *SLC22A12* (URAT1), involved in the maintenance of uric acid homeostasis, and sodium/glucose cotransporter 2, *SLC5A2* (SGLT2), involved in glucose reabsorption, are important PTEC uptake transporters. Key information related to substrates and inhibitors for PTEC-specific transporters has been widely published previously [1, 13, 14].

The toxicity of many drugs can be ameliorated or exacerbated by selectively blocking the transporters that are responsible for their uptake or efflux in the PTECs. The nephrotoxicity of the chemotherapeutic cisplatin has been associated with renal accumulation determined by its specificity for OCT2 and the MATE family of transporters [15]. Several genetic variants that reduce the functionality of OCT2 can lower its uptake in the PTECs leading to a reduction in cisplatin-induced nephrotoxicity [16]. Additionally, cimetidine, an inhibitor of OCT2, offers significant protection to cisplatin-induced injury without influencing its antitumor activity in pre-clinical models, although this strategy was not amenable in the clinic as very high concentrations of cimetidine were required which cannot be achieved with regular dosing [17, 18]. Tenofovir, a nucleotide antiviral, is taken up from the blood side via OAT1 and effluxed into the urine via MRP4. Ritonavir, an inhibitor of MRPs, increases tenofovir-induced toxicity in patients when taken in combination, compared to patients who were treated with tenofovir alone [19].

While small molecules are eliminated from the kidneys with the help of transporters, the reabsorption of many soluble biomolecules is achieved with the aid of endocytic receptors, megalin and cubilin, in conjunction with amnionless. These endocytic proteins are primarily located at the apical surface of the PTECs and play an extremely important role in the reabsorption and catabolism of biologically important substances like vitamins, hormones, enzymes, etc. However, many aminoglycosides, including gentamicin, tobramycin, and neomycin, cause PTEC toxicity through the megalin-cubilin receptor-dependent uptake leading to their accumulation inside the cells. In fact, it has been shown that mice with genetic or

functional megalin deficiency are protected from aminoglycoside nephrotoxicity [20, 21]. Additionally, drugs from newer modalities such as antisense oligonucleotides, siRNA therapy, and teratogenic antibodies also accumulate in the PTECs via these megalin-cubilin endocytic receptors and can lead to injury if they are present above a critical threshold beyond the adaptation limit of the PTECs [22–26].

In addition to the excretion of xenobiotics, the kidneys can also be involved in metabolism, in turn facilitating their elimination. This has been extensively described previously [27–29] and includes oxidation, reduction, hydrolysis, and conjugation reactions, achieved by a combination of both CYPs and non-CYP enzymes such as uridine-di phosphate-glucuronosyltransferases (UGTs), esterases, glutathione-S-transferases (GSTs), and sulfotransferases (SULTs) [30]. While most of these metabolism reactions lead to detoxification of the xenobiotics, some reactions can lead to the formation of reactive metabolites that can cause injury to the PTECs. For example, glutathione, a strong nucleophile, can get conjugated with soft electrophilic drugs and/or their metabolites in the liver. These glutathione conjugates can then undergo further metabolism in the kidney by the action of ectoproteins such as  $\gamma$ -glutamyltransferase and dipeptidases to form cysteine-S-conjugates which are transported back into the cells to form mercapturic acids, a major detoxification mechanism of many xenobiotics, before finally getting excreted out in the urine. However, sometimes these cysteine-S-conjugates can be catalyzed by  $\beta$ -lyase to form highly reactive thiols that can covalently bind to macromolecules in the cells to produce reactive oxygen species (ROS) and eventually leading to PTEC death [27, 31].

The central role of the kidney in the transport, metabolism, and excretion of drugs and endogenous substrates cannot be overstated. Thus, the mitigation of renal toxicity in the early stages of drug development by screening compounds in physiologically relevant *in vitro* kidney models is an active area of research among several R&D institutions including pharmaceutical companies. This chapter highlights the evolution of these *in vitro* technologies and strategies starting with discussion on simple two-dimensional (2D) *in vitro* platforms, followed by advanced three-dimensional (3D) models such as kidney-on-a-chip, stem cell-derived models, and bioprinted kidney models. Next, we discuss the different translational kidney biomarkers that can be used for developing a bridge between the *in vitro* and *in vivo* studies and allow cross species comparison. Finally, a discussion is presented on *in silico* strategies and the use of machine learning/artificial intelligence (AI) for kidney safety assessment.

## 2 2D *in vitro* models for nephrotoxicity screening

Several studies have established 2D *in vitro* PTEC models to screen compounds that may present nephrotoxic liabilities. Among these, the simplest model includes single transporter transfected cell lines such as human embryonic kidney (HEK)-293. Zhang et al. transfected HEK-293 with OAT1 and OAT3 to investigate the toxicity of nucleotide antivirals such as adefovir, cidofovir, tenofovir, all of which are substrates for OAT1. The researchers showed that HEK-293 OAT1 overexpression cell lines were the most sensitive to these compounds while the wild-type HEK-293 or HEK-293 with other transporters either showed no or significantly less cytotoxicity [32]. They showed that this sensitivity in the HEK-293 OAT1 overexpressing cell line was the result of increased intracellular accumulation of these drugs,



many of which were ~10-fold higher in the cell than the media underscoring the role of OAT1. As antivirals have a very low permeability (low calculated logP values), cell models that lack sufficient transporter expression may present discrepancies in the cytotoxicity of these compounds in an in vitro setting when compared to their in vivo outcome. Thus, HK-2 cells, an immortalized proximal tubule cell line lacking expression of several PTEC-specific transporters, including OAT1/3, do not show toxicity to many compounds with a low permeability and that are substrates for specific transporters [32, 33]. In the same study, it was also interesting to note that even primary human PTECs at passage 3 expressed very low levels of OCT2 compared to the human kidney, while OAT1/3 could not be detected among other transporters via gene expression, suggesting that in conventional 2D static cultures primary PTECs get rapidly dedifferentiated and lose a majority of the important transporters [32]. This emphasizes the need for more advanced models that can be used in vitro to show clinical predictivity.

A study by Huang et al. compared the sensitivity of HK-2 cells, cryopreserved PTECs (commercially available), and freshly isolated PTECs (in-house) across six known nephrotoxicants with both nonspecific endpoints such as enzymatic reduction of 3-[4,5-dimethylthiazole-2-yl]-2,5-diphenyltetrazolium bromide (MTT assay), Alamar Blue (Resazurin) assay as well as kidney injury biomarkers such as kidney injury molecule-1 (KIM-1), neutrophil gelatinase-associated lipocalin (NGAL), and macrophage colony stimulating factor (M-CSF) at the gene and protein level [34]. They concluded that biomarkers (KIM-1, NGAL, M-CSF) provided higher sensitivity compared to nonspecific cytotoxicity endpoints (MTT, Resazurin) and that HK-2 is not a suitable cell model for nephrotoxicity assessment. In contrast, primary PTECs demonstrated a valid dose response for most compounds tested, especially with the biomarkers, KIM-1 and NGAL. Interestingly, freshly isolated PTECs showed an even stronger response to the biomarkers, KIM-1 and NGAL, compared to cryopreserved PTECs. Significantly lower background levels of these injury markers were seen in the freshly isolated PTECs in comparison to cryopreserved PTECs, likely because of the higher passages and repeated freeze–thaw cycles for the commercial cells that might lead to dedifferentiation. These findings suggest that, when possible, freshly isolated PTECs should be chosen over cryopreserved PTECs or HK-2 for better signal resolution of nephrotoxic compounds.

Researchers have also conditionally immortalized PTECs (ciPTECs) by isolating the cells from urine of a healthy volunteer [35] or kidney tissue [36] followed by transfection with the temperature-sensitive SV40-T gene and subcloning. These cells proliferate at the “permissive” temperature (33 °C) and undergo growth arrest after transfer to the “nonpermissive” temperature (at 37 °C), where they differentiate into renal epithelial cells to endogenously express several apical and basolateral transporters, but OAT1/3 and SGLT2 appeared absent. Recently, Nieskens et al. generated ciPTEC-OAT1 and ciPTEC-OAT3 cell lines and demonstrated dose-dependent cytotoxicity to the nucleotide antivirals tenofovir, cidofovir, and adefovir, suggesting that these ciPTEC overexpression cell lines can be promising platforms for nephrotoxicity screening in the early stages of drug development [37]. In addition to the abovementioned cell types, other studies using cell types in 2D platforms have also been used for screening and their advantages/disadvantages have been reviewed extensively previously [8, 30, 38].

One of the main challenges in evaluating the different in vitro PTEC models and comparing them (2D or 3D) is the limited validation. Very few studies include more than 20 compounds for model validation, and hence it becomes extremely hard to draw reasonable statistics or predictive power for the model. Limited reports comparing the nephrotoxic



potential of 40 compounds across HK-2 cells, LLC-PK-1, primary PTECs, and stem cell derived PTECs showed that the primary PTECs that express several transporters had the highest predictivity, while HK-2 cells that lack many transporters showed the lowest predictivity for the compound set investigated. Additionally, gene expression levels of IL-6/IL-8 were more predictive than nonspecific biochemical endpoints such as ATP depletion, GSH depletion, LDH leakage, and cell death [quantified by counting the number of nuclei by high content screening (HCS)] [38–41]. Another report compared the nephrotoxic potential of 39 mechanistically distinct nephrotoxic compounds and concluded that heme oxygenase 1 (HO-1) performed better than traditional endpoints for cell viability [42]. Furthermore, a combination of HO-1 (immunofluorescence stain) with cell count (DAPI nuclear stain) using logistical regression models led to further improvement in the predictivity of the model. Recently Sjögren et al. used the ciPTEC-OAT1 overexpression cell line to screen 62 mechanistically different drugs across a range of human relevant therapeutic exposures ( $C_{max}$ ) using HCS and an applied machine learning algorithm to identify PTEC-positive compounds with very high accuracy [43]. Table 1 summarizes the predictivity metrics and endpoints analyzed across these different studies [39–43].

Nephrotoxicity is not only an issue with small molecules but also biotherapeutics have been reported to cause kidney injury [44]. Among these are antisense oligonucleotides [45], a promising therapeutic platform to treat a variety of genetic diseases, cancer, and viral infections. Most oligonucleotides are excreted primarily via the urine, although slowly due to

**TABLE 1** Predictivity metrics and endpoints analyzed across different validation studies.

Number of compounds tested	Cell type used in the study	Endpoints	Sensitivity (%)	Specificity (%)	Accuracy (%)	AuROC	Reference
Total = 41	Primary PTEC	IL-6/IL-8 expression	91.0	90.0	90.0	0.94	[39–41]
Primary PTEC-toxic: 22	HK-2		50.0	79.0	65.0	0.71	
Secondary PTEC-toxic: 11	LLC-PK1		64.0	74.0	69.0	0.73	
Non-nephrotoxic: 8	Stem cell-derived PTEC		68.0	84.0	76.0	0.80	
	Primary PTEC	ATP depletion	50.0	74.0	62.0	0.65	
	Stem cell-derived PTEC		48.0	79.0	63.0	0.65	
	Primary PTEC	GSH depletion	45.0	74.0	60.0	0.60	
	Primary PTEC	LDH leakage	64.0	58.0	61.0	–	
	Primary PTEC	Cell death	42.0	95.0	69.0	–	
Total = 39	Primary PTEC	Cell number	70.8	100	78.1	0.88	[42]
Primary PTEC-toxic: 24		ATP depletion	54.2	87.5	62.5	0.78	
Secondary PTEC-		Dead cells	70.8	100	64.1	0.86	

TABLE 1 Predictivity metrics and endpoints analyzed across different validation studies—cont'd

Number of compounds tested	Cell type used in the study	Endpoints	Sensitivity (%)	Specificity (%)	Accuracy (%)	AuROC	Reference
toxic: 7 Non-nephrotoxic: 8		HO-1 concentration	75	100	81.3	0.89	
		HO-1 + Cell number	79.2	100	84.4	0.92	
		HO-1 + ATP depletion	67.7	87.5	71.9	0.90	
		HO-1 + Dead cells	79.2	100	84.4	0.90	
Total = 62 Primary PTEC-toxic: 20 Secondary PTEC-toxic: 18 Non-nephrotoxic: 24	ciPTEC-OAT1	Membrane integrity loss	55	87	72.7	–	[43]
		Mitochondrial area above or under nucleus	50	96	75.0		
		Intensity of cellular F-actin staining	45	96	72.7		
		Nuclear size	30	96	65.9		
		Lowest TI from above parameters	75	100	88.6		

Primary PTEC-toxic: compounds that are directly toxic to PTECs. Secondary PTEC-toxic: compounds that are nephrotoxic but not directly PTEC toxic. Non-nephrotoxic: compounds that do not lead to renal toxicity at therapeutic exposures. TI: therapeutic interval, obtained by dividing the 50% activity concentration ( $AC_{50}$ ) by therapeutic  $C_{max}$ ,  $TI = AC_{50}/C_{max}$ .

Adapted and generated from K. Kandasamy, J.K.C. Chuah, R. Su, P. Huang, K.G. Eng, S. Xiong, Y. Li, C.S. Chia, L.-H. Loo, and D. Zink, Prediction of drug-induced nephrotoxicity and injury mechanisms with human induced pluripotent stem cell-derived cells and machine learning methods, *Sci. Rep.* 5 (2015) 12337; Y. Li, K. Kandasamy, J.K. Chuah, Y.N. Lam, W.S. Toh, Z.Y. Oo, and D. Zink, Identification of nephrotoxic compounds with embryonic stem-cell-derived human renal proximal tubular-like cells, *Mol. Pharm.* 11 (7) (2014) 1982–90; Y. Li, Z.Y. Oo, S.Y. Chang, P. Huang, K.G. Eng, J.L. Zeng, A.J. Kaestli, B. Gopalan, K. Kandasamy, F. Tasnim, and D. Zink, An in vitro method for the prediction of renal proximal tubular toxicity in humans, *Toxicol. Res.* 2 (5) (2013) 352–365; M. Adler, S. Ramm, M. Hafner, J.L. Muhlich, E.M. Gottwald, E. Weber, A. Jaklic, A.K. Ajay, D. Svoboda, S. Auerbach, E.J. Kelly, J. Himmelfarb, and V.S. Vaidya, A quantitative approach to screen for nephrotoxic compounds *In Vitro, J. Am. Soc. Nephrol.* 27 (4) (2016) 1015–1028; A.-K. Sjögren, K. Breitholtz, E. Ahlberg, L. Milton, M. Forsgard, M. Persson, S.H. Stahl, M.J. Wilmer, and J.J. Hornberg, A novel multi-parametric high content screening assay in ciPTEC-OAT1 to predict drug-induced nephrotoxicity during drug discovery, *Arch. Toxicol.* 92 (10) (2018) 3175–3190.

high plasma protein binding. Unbound oligonucleotide can be filtered, followed by reabsorption and proximal tubular accumulation, demonstrated by the presence of basophilic granules in the cytoplasm. When exceeding critical threshold levels, oligonucleotide accumulation may become associated with tubular dysfunction [46–49]. Antisense oligonucleotides are suggested to be actively reabsorbed from the ultrafiltrate by receptor-mediated endocytosis, most likely involving megalin-cubilin [50, 51]. Investigations to limit nephrotoxicity include conjugation of oligonucleotides to *N*-acetylgalactosamine (GalNAc), which improves biodistribution toward the liver through asialoglycoprotein receptor (ASGPR) mediated

uptake [52, 53]. However, this does not fully prevent their accumulation in the kidney and nephrotoxicity assessment remains crucial in the preclinical selection of antisense oligonucleotide-based candidate drugs. Using a PTEC-TERT1 cell line and fluorescently labeled antisense oligonucleotides, Sewing et al. investigated the effect of GalNAc conjugation on the accumulation patterns of the compounds [22]. This study and other studies [22, 23] from the same group nicely demonstrated the potential of this in vitro approach revealing the molecular mechanism underlying the nephrotoxicity potency of the class of biotherapeutics and mechanistically studying approaches to improve their safety.

Although a significant portion of kidney damage seems to be associated with PTECs, the glomerular podocytes are also prone to injury because of the large blood flow that is seen by these cells. In vitro studies of kidney glomerular epithelial cells have been documented for several decades [54]. Within 12h of isolation from intact glomeruli, glomerular podocytes exhibit an increase in the number of free surface microprojections, number of cytoplasmic lipid inclusions, and characteristics typical for glomerular epithelial cells, and remain viable for several weeks at 37°C. The glomerular endothelium becomes thickened but also remains viable for several weeks at 37°C. Surface epithelial cells in both cortical and medullary regions become modified into a thin layer of viable cells. The in vitro response of glomerular epithelial cells to xenobiotics may include: an induced loss of cytoplasmic microtubules (e.g., vinblastine, colchicine), loss of podocyte morphology, removal of the glomerular sialic acid surface coat inhibits the formation of free surface microvilli and results in an early loss of podocyte foot processes (e.g., neuraminidase). Loss of podocyte foot processes may be induced by cations and attenuated by cytochalasin B. Interestingly, no effect on viability or morphology of glomerular cells (increased vacuolation) occurs following exposure to puromycin aminonucleoside (PAN), except at very high concentrations of  $\geq 300 \mu\text{g}/\text{mL}$  (hallmark indicator/markers for cultured glomerular epithelial cells). Uniquely so, rat glomerular epithelial cells in culture express characteristics of the parietal, not visceral, epithelium [55]. Similar to the in vivo and in vitro contexts, slices of rat kidney incubated with PAN (100 or 500  $\mu\text{g}/\text{mL}$ ) resulted in significantly decreased numbers of microvilli on podocyte cell bodies on days 1, 2, and 3, increased the number of glomeruli showing a flattening of podocyte cell bodies and major processes on days 2 and 3, and increased the number of glomeruli showing surface membrane blebbing on podocyte foot processes [56].

A conditionally immortalized human podocyte cell line was developed by transfection with the temperature-sensitive SV40-T gene [57]. These cells express phenotypic podocyte markers (e.g., nephrin, podocin, CD2AP, and synaptopodin proteins; slit diaphragm markers: ZO-1, alpha-, beta, and gamma-catenin and P-cadherin; upregulation of cyclin-dependent kinase inhibitors, p27, p57, and cyclin D1 and downregulation of cyclin A). Based on the role of glomeruli, isolated podocytes in culture may support in vitro assessment of glomerular toxicants. Yet in vivo terminally differentiated podocytes are difficult to be maintained in culture in vitro.

### 3 Emerging models for renal safety screening

Characteristics of PTEC and other renal cells, such as cobblestone morphology and expression of unique membrane transporters that support their function, can often be improved when incorporated in an advanced in vitro model. In these advanced kidney models, the

presence of flow and signaling between multiple cells and cell types are crucial. In native kidneys, cells are embedded in an extracellular matrix (ECM) that provides a mechanical support and plays a key role in inter- and intracellular signaling and advances tissue organization and regeneration. The ECM forms a depot for nutrients, gases, and essential molecules like growth factors and cytokines, and consists of a basement membrane (BM) and the stromal matrix (SM). The BM is a sheet-like scaffold residing fibronectin, laminin, proteoglycans and collagens, in particular collagen type IV. The SM is composed of collagen I, proteoglycans, and glycosaminoglycans, which together form fibrous structures providing the major structural support of the ECM. Further, the transmembrane receptor integrins mediate the cell-ECM adhesion and signaling [58, 59].

Recently developed advanced *in vitro* models (including 2.5D) have incorporated these ECM components, thereby providing support in cell adhesion, tissue structure, and function. Moreover, the newly developed kidney models can be divided into four categories: (i) gel-based cultures, allowing cells to grow in 3D structures, but lacking the influence of flow; (ii) hybrid gel-based cultures under shear stress, allowing cells to form 3D structures and exposing them to fluid flow from one side; (iii) membrane-based microfluidics, allowing cells to grow in polarized, 2.5D (demonstrate cuboidal structure on semipermeable Transwell inserts and higher degree of differentiation) [60] structures while being exposed to flow from both sites; and (iv), hollow fiber membranes with flow, allowing cells to form tubule structures that can be perfused, as presented in a simplified scheme (Fig. 2, from [61]).

Gel matrices can provide mechanical support to cells that can then self-organize into 3D structures that have been applied in nephrotoxicity screenings in high-throughput settings, often using renal stress biomarkers (e.g., ROS production) as endpoint indicators. This feature of organizing into 3D structures was first described for Madin-Darby Canine Kidney (MDCK) cells that form so-called spheroids in collagen gels, with a clear basolateral-to-apical orientation [62]. These collagen gels are now often replaced by Matrigel that consists of a mixture of collagens, proteoglycans, and growth factors derived from Engelbreth-Holm-Swarm mouse sarcoma cells [63]. Its application was shown to be useful in studying embryonic stem cell (ESC) and induced pluripotent stem cell (iPSC)-derived renal cell development [64, 65], as well as renal PTEC (RPTEC)/TERT1 cells that self-assemble in this matrix to form polarized 3D tubular structures mimicking the proximal tubule [60]. More recently, it was shown that adult stem cell-derived organoids can develop in tubular structures when grown in Matrigel, comprising all cell types of the tubular segment [66]. While its application was shown to be successful in 3D kidney modeling, the compositions of Matrigel change from batch to batch, resulting in variable outcomes [67]. Attempts to fully replace Matrigel or other biological gels into fully synthetic gels are currently part of ongoing research. Most often, combinations are applied. Using immortalized human renal cortical cells (NKi-2) seeded in a 50:50 gel mixture of Matrigel and rat tail collagen I in semipermeable Transwell plates, formation of 3D branch-like structures was visible within 2 weeks and cultures maintained viability for up to 8 weeks [68]. The 3D cultures expressed several transport proteins, including OAT1, OAT4, MRP2, and MRP4. To validate the model, clinically relevant endpoints of nephrotoxicity were used upon exposures to drugs, including KIM-1 and NGAL, and enhanced sensitivity of this 3D model over 2D cell cultures was demonstrated [68].

Natural polymers, such as alginate, or cell-derived gels, containing hyaluronic acid (HA) and/or collagen mixtures, have been more often successfully used to engineer 3D kidney models [69], some of them applied in drug toxicity screenings. The advantages of hydrogels

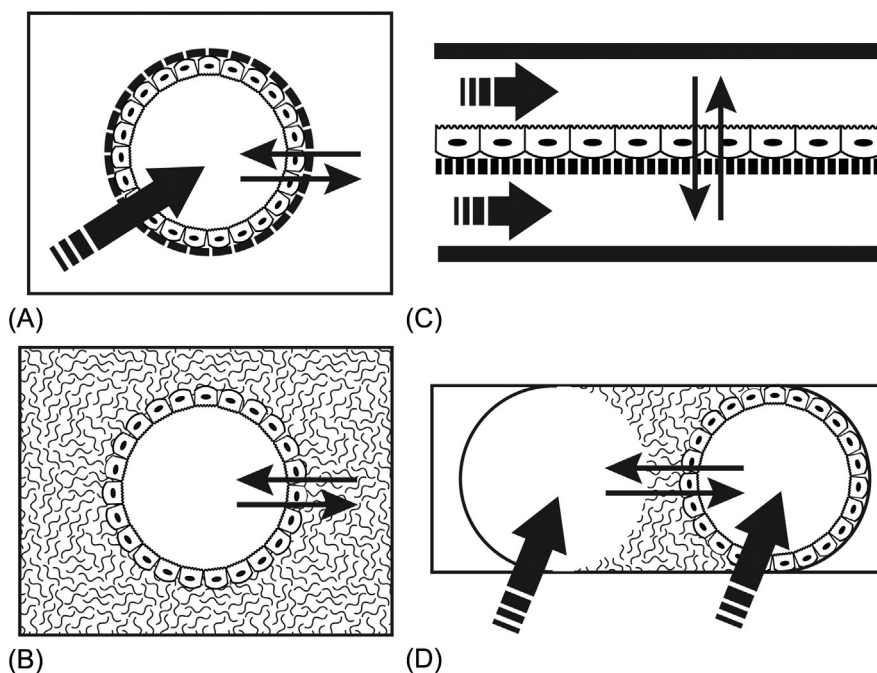


**FIG. 2** Three-dimensional models for studying kidney injury and repair processes. Cells grown on hollow fiber permeable membranes (A) allowing implementation of flow and apical and basolateral compartments. Hollow fiber models allow studying the functional role of PTEC in the clearance of metabolic wastes and are components of bioartificial kidney device developments. Gel-based cultures (B) embedded in ECM-like gel, preserving apical and basolateral phenotype and facilitating diffusion. Gel-based models allow for studying branching and drug toxicity screenings. Microfluidic membrane-based devices (C) consist of multiple channels separated by a permeable membrane seeded with PTEC. Apical and basolateral compartments together with flow are implemented in this model. Transcellular transport is facilitated by PTEC on permeable membranes. Microfluidic models allow to study drug toxicity and kidney diseases. Microfluidic membrane-free devices (D) consist of multiple channels separated by cells seeded on ECM-like structures (e.g., gel supports). Apical and basolateral compartments and flow are incorporated in this model, as well as the ability to study membrane-free transcellular transport. *Reproduced with permission from Ref. R. Masereeuw, J. Vriend, and M.J. Wilmer, Kidney-on-a-chip: technologies for studying pharmacological and therapeutic approaches to kidney repair, in Kidney Transplantation, Bioengineering and Regeneration, G. Orlando, G. Remuzzi, and D.F. Williams, Editors. 2017, Academic Press. 1119–1133 and Copyright Elsevier.*

are that the viability and phenotype of kidney cells can be maintained for a prolonged culture time, allowing also testing of chronic-like exposures to compounds [68, 70–74]. Gel-based systems are also compatible with coculturing for disease modeling, such as cisplatin-induced renal fibrosis [75]. Furthermore, HA appeared to be useful in embedding freshly isolated murine proximal tubules to screen for nephrotoxicity under static culture conditions [70–72]. Tissue preserved well in this gel for up to 6 weeks without any significant phenotypical changes [71]. Exposure to cisplatin or doxorubicin induced cytokines and KIM-1 levels, suggesting tubulotoxicity [71, 72]. The disadvantages of gel-based cultures are the inability to upscale significantly and the formation of hypoxic centers inducing necrosis, especially for spheroid-like methods [76, 77]. The latter may be caused by the lack of flow, providing the tissue with medium components such as nutrients and growth factors. Combining the gel-based systems with flow will overcome these limitations.

The renal epithelial cell experiences shear stress at the luminal side due to glomerular ultrafiltration. The importance of shear stress or flow in cell cultures was underscored by the presence of a primary cilium that functions as a flow sensor of the cells through mechanotransduction [78]. Most microfluidic devices for kidney modeling contain two or more channels separated by permeable membranes or a gel, usually coated with ECM components to advance cell adherence. The first microfluidic 3D kidney models described used MDCK cells [79] or primary rat inner medullary collecting duct (IMCD) cells [80] to demonstrate the advancements. Next, polydimethylsiloxane (PDMS) as a scaffold for a microfluidic system was introduced using soft lithography, in which channels were coated with glass covered fibronectin [81]. Using HK-2 cells, formation of calcium phosphate stones was studied. Applying microfluidics advanced cell viability, expression of membrane transporters and sensitivity to nephrotoxic compounds when compared to static culture conditions [18, 79, 80, 82, 83]. Furthermore, PDMS and glass-based models have been used for optimizing coating [82], membrane design [84], and drug screenings [18, 85, 86].

One of the first advanced biomimetic models of the kidney [organ-on-a-chip or microphysiological systems (MPS)] was developed by the Wyss Institute, consisting of a microfluidic device containing two channels separated by a porous polyester membrane, coated with collagen IV and seeded with primary human PTECs [18]. Applying flow clearly improved cell morphology as cells became more cuboidal and showed increased expression levels of various membrane proteins important in cell polarization. Further, expression of cilia increased when cells were grown under flow as compared to static cultures. As a platform for nephrotoxicity testing, this kidney-on-a-chip model demonstrated susceptibility to OCT2-mediated cisplatin [87]. Cells recovered from cisplatin-induced toxicity when cultured under drug-free conditions for 4 days following a 24h exposure, in line with clinical observations. Still, this model does not fully recapitulate the 3D architecture of a renal tubule.

Weber et al. established a PDMS-based platform by first creating a master mold from machinable wax that was subsequently inverted using cast-molding in polyurethane to generate multiple replica chips that were finally cast with PDMS. Two PDMS halves assembled formed one chip, sandwiched in the center and filled with collagen type I gel from rat tails with microfiber inserts that, after removal, leave a channel to be coated with collagen type IV for primary human PTEC adhesion [88]. Culturing cells in this chip under flow showed tubule structures with improved physiological characteristics, including glucose reabsorption, vitamin D metabolism, and maintained tubular secretion function. After validation, the chip proved to be transferable for drug toxicity screening (Nortis ParVivo microfluidic device, Seattle, WA), but the reproducibility critically depends on the cell sources used [89].

These microfluidic systems have broad perspectives but also face some limitations. The most often applied material for devices, PDMS, is easy to use and cheap, but adhesive to compounds due to its porosity. This was demonstrated, for example, for fluoxetine [90] and tetramethylrhodamine [91]. Coating of the membrane with parylene could partly overcome this problem [92]. Furthermore, flow implemented using pumps and tubings makes chip systems more complicated in tissue cultures and requires additional investments to adjust.

Instead of flow through perfusion, fluidic conditions can also be created by leveling through mechanical forces, a technique applied in OrganoPlates (Mimetas BV, Leiden, The Netherlands), where shear stress is created by leveling on a rocker platform [93]. The plate can consist of two or three channels separated by a phaseguide, which is used to establish a gel support and advances tubule formation. Channels can function both as a gel or medium



perfusion channel. These microtiter plates were shown to be suitable platforms for 3D culturing of renal PTECs and ciPTECs and were compatible with fluorescent assays and biomarker assessments in drug interactions and toxicity testing, opening possibilities to use this platform in high-throughput screening [94–96].

To even closer physiologic mimicry, advanced models can also incorporate two or more cell types to create a coculture in which cross talk can be studied. For example, a coculture of primary human umbilical vascular endothelial cells (HUVEC) and MDCK cells in separated channels, constructed of a hydrogel mixture of collagen type I and alginate, was used to study renal endothelial to epithelial diffusion [74]. Also, this model was used in a similar setup to assess ifosfamide-induced nephrotoxicity [85]. Although treatment had no effect on MDCK cells' viability under static conditions, an inflammatory response was induced upon ifosfamide exposure when biochips were used, again indicating that flow and a 3D environment increase the sensitivity to toxicants. When combined with a 3D liver model using HepG2/C3a and HepaRG cells, MDCK cells responded with an increased sensitivity related to the nephrotoxic metabolites formed by the liver cells [86]. Although the model is an excellent tool to study nephrotoxicity under fluidic conditions, the lack of compartmentalization dividing the apical side from the basal side limits this system to be suitable for transepithelial transport. This was addressed using an integrated liver-kidney model, using HepG2 and rat glomerular endothelial cells in a micromolded liver-kidney chip fabricated by soft lithography [97]. The results demonstrated increased cytotoxicity in cocultures as compared to glomerular cells only. Additionally, using human primary liver cells and PTECs separately cultured in the Nortis ParVivo microfluidic device and linked afterward, hepatocyte-specific bioactivation of aristolochic acid I was demonstrated by an increased cytotoxicity of human PTEC, as assessed by the formation of aristolactam adducts and release of kidney injury biomarkers [98]. An interconnection of four organs-on-a-chip appeared possible, using cell culture inserts as models for human intestine, skin, and kidney, combined with a 3D-based spheroid of liver cells, that maintained functionality for up to 28 days in culture, suitable for ADME studies and repeated dosing [99], although the tissues do not display their physiological geometry. An even longer culture time was achieved using a 3D bio-printed device [100]. In this approach, a convoluted proximal tubule on a chip was created by sacrificial printing, by using a silicone gasket printed on a glass slide forming the outer border of the 3D tissue chip, in which an ECM layer of gelatin-fibrin hydrogel was deposited within the gasket. On the ECM, a fugitive ink of Pluronic F127 was printed onto the ECM layer that ultimately could be liquefied and removed from the final 3D proximal tubule (PT) construct. Directly after fugitive ink printing, metal hollow perfusion pins interfaced through the silicone gasket were brought into contact with the printed ink. After printing, a second ECM layer was deposited as a sandwich over the printed tubule. The metal pins were connected to tubings to allow for cell seeding and perfusion, after removal of the fugitive ink. Human primary and immortalized PTECs were used as cell sources and the chips were cultured for up to 6 days and formed a tissue-like polarized epithelium with a clear renal phenotype and sensitivity toward nephrotoxicants [100]. The researchers took this approach even further by printing a vasculature in close proximity, mimicking the vascularized convoluted tubule that allows studying renal tubular reabsorption [101]. Although very versatile, one of the major limitations of the current 3D bio-printed kidney platforms is their restricted throughput.

Cells cultured within or onto hollow fiber membranes were originally developed for use in renal tubule assist devices (RAD) as bioartificial kidneys [102–106]. These bioengineered



tubules mimic tubular structures and are capable of removing waste products that accumulate in the blood of kidney patients during kidney failure and might function as renal replacement therapy by improving current dialysis treatments [107, 108]. Seeding PTEC in a permeable hollow fiber allows the formation of an apical side facing inward and the basolateral side facing outward or vice versa when cells are cultured on the fibers and increase the membrane surface area and epithelial barrier formation. Increased curvature of hollow fibers might result in more mechanical stress and physiological resemblance, improving the PTEC function [104]. Adding an ECM to synthetic membranes appeared essential for cell adherence and monolayer formation. This was pioneered by Oo *et al.* who used human primary PTEC and hollow polyethersulfone (PES)/polyvinylpyrrolidone (PVP) fiber membranes double-coated with a 3,4-dihydroxy-L-phenylalanine (DOPA) and a collagen IV layer [103]. Cells were cultured in this bioreactor for up to 7 days under perfusion, starting at day three. Upregulated levels of renal-specific markers were shown compared to static conditions [103]. A similar double coating strategy was used with ciPTEC and ciPTEC-OAT1 cultured on hollow PES fibers, and demonstrated active OCT2-mediated transport as well as transepithelial secretion of uremic toxins mediated by OAT1, MRP2/4, and BCRP [106, 107]. Also, a fibrin coating was used with human primary PTECs cultured inside a hollow fiber [102]. Recently, nanofiber scaffolds fabricated by electrospinning poly- $\epsilon$ -caprolactone (PCL) around needle templates were found suitable for ciPTEC-OAT1 and a murine induced renal tubular epithelial cells (iREC) monolayer formation after biofunctionalization with L-DOPA and collagen IV double coating [109]. Biomarker readouts from perfusates of hollow fibers upon exposure to drugs or nephrotoxicants included ROS production, cytokines, and epithelial barrier integrity [110]. The disadvantages of the production of such bioengineered kidney tubules are the time demanding process and that the platform is not highly compatible with large-scale drug screening. The great advantage, though, is the accessibility of both basolateral and apical compartments, allowing for kinetic assessments.

In recent years, there has been a great interest to generate stem cell-derived kidney cells for toxicology applications [39, 111–115]. Several independent labs have generated protocols which tried to mimic *in vivo* nephrogenesis by using a cocktail of small molecules and growth factors to generate kidney organoids which encompass several cells of the nephron, the functional unit of the kidney [112, 114]. A key advantage of these kidney organoids is that these *in vitro* models have the capacity to distinguish different types of nephrotoxins from each other by looking at kidney cell-specific biomarkers, as multiple cell types of the nephron are generated within these organoids. Additionally, by combining iPSCs and progress in genetic engineering, researchers can also make genetic modifications to the cells which can have tremendous applications in understanding the mechanism of toxicity or for discovering new drug targets [116, 117]. Although stem cell models still require some improvements to make them competitive with freshly isolated cells from the kidney, specifically for PTECs in terms of transporter expression and function [115], the attractive features of stem cell-based models such as the ability to incorporate patient/genetic diversity and greater flexibility make them attractive platforms for a number of applications related to drug discovery.

A recently established novel technology to culture human kidney tubular epithelial organoids, or “tubuloids,” from adult stem cells derived from either kidney tissue or urine holds great promise as well [66]. These tubuloids represent proximal as well as distal nephron segments and display active (trans-) epithelial transport function. They have been shown to be very stable during long-term culture. Importantly, these tubuloids can be used for the

modeling of an infectious kidney disease (BK virus), a malignancy (Wilms' tumor), and a hereditary disease (cystic fibrosis) and are therefore suitable to develop personalized disease models for studying pathogenetic mechanisms identifying novel therapeutic targets and monitoring safe and effective treatment(s). Application of tubuloid-derived proximal tubule cells in advanced *in vitro* models in monitoring tubular transport function was demonstrated for both the OrganoPlate as well as hollow fiber membrane platforms [66, 95].

While it is challenging to maintain terminally differentiated podocytes *in vitro*, iPSCs-derived podocytes may provide a robust and reproducible model for investigations [118]. The iPSC-derived podocyte-like cells exhibit typical podocyte-specific morphology and markers (e.g., synaptopodin, podocin, nephrin, and WT-1). Notably, at 48 h posttreatment, matured iPSC-derived podocytes were sensitive to doxorubicin toxicity, characterized by morphological alterations and decreased cell viability. Additional investigations will help to better understand the utilities for this model for detecting changes in soluble DIKI biomarkers.

On-chip models for mimicking the close interactions of the different cell types of the glomerulus have also been developed. This glomerulus-on-a-chip microfluidic device was used to mimic hypertensive nephropathy [119]. The device consists of two channels lined by glomerular endothelial cells and podocytes maintained under fluid flow to emulate the glomerular microenvironment *in vivo*; it was envisaged to support research investigations including but not limited to candidate drug screening. Recently, stem cell-derived kidney cells were directly differentiated into functional podocytes [118] based on modifications of previously described protocols [120, 121]. The monolayers of iPSC-derived human podocytes exhibited morphological, phenotypic, and functional (endocytosis of albumin) characteristics of podocyte foot processes. These cells may serve as a novel tool for *in vitro* glomerular cell (podocyte) toxicity studies and drug safety assessment (e.g., as has been described for doxorubicin that induced morphological changes and cell viability reduction [118]). To date, novel biomarker changes in these iPSC podocytes have not been reported.

#### **4 Translatable kidney safety biomarkers**

As noted in the Introduction, SCr and BUN represent conventional renal biomarkers that are insensitive. Dose stopping criteria based on reference values may be leveraged to contextualize monitorable increases in SCr concentrations. Early detection of DIKI during preclinical studies includes the gold standard diagnostic method—multi-organ histologic examination. Conversely, confirmations of nephrotoxic responses in human clinical studies do not routinely include microscopic evaluation of renal biopsies. Therefore, in the absence of alterations in sCr and/or BUN, next-generation DIKI biomarkers that are more sensitive than SCr or BUN may be leveraged.

Soluble, nonqualified DIKI biomarkers are often simultaneously measured from rodents/nonrodents' biological matrices. Nonclinical studies conducted as part of regulatory packages for candidate drugs are defined within two guidances: International Conference on Harmonization (ICH) M3(R2) [122] and ICH S7A [123]. The latter guidance recommends the inclusion of sCr and BUN among other clinical pathology parameters (Table 2) for Investigational New Drug (IND) Application-enabling GLP (good laboratory practice) 28-day (1-month) nonclinical toxicology studies to eventually support clinical trials. Because nonclinical data

**TABLE 2** Non-qualified and qualified kidney safety biomarker used during in vivo and/or in vitro studies.

<i>DIKI biomarkers routinely used in IND-enabling GLP 28-day nonclinical toxicology studies</i>		
Hematology parameters	Red blood cells, hemoglobin, hematocrit, mean corpuscular volume, mean corpuscular hemoglobin, mean corpuscular hemoglobin concentration, platelets, mean platelet volume, white blood cells, white blood cells differential, reticulocytes	
Serum chemistry parameters	Alanine aminotransferase, aspartate aminotransferase, sodium, potassium, chloride, calcium, magnesium, phosphorus, glucose, cholesterol, triglycerides, gamma glutamyltransferase, albumin, globulin, albumin/globulin ratio, cystatin c, total protein, urea nitrogen, creatinine	
Qualitative urinalysis parameters	Color, clarity, specific gravity, protein, glucose, ketone, bilirubin, urobilinogen, blood, microscopic examination of sediment, pH	
Quantitative urinalysis parameters	Volume, creatinine, protein, gamma glutamyltransferase, <i>N</i> -acetyl glucosaminidase, microalbumin, glucose, osmolality, calcium, chloride, magnesium, phosphorus, potassium, sodium, urea	
<i>Qualified urinary DIKI biomarkers</i>		
Clusterin, cystatin C, kidney injury molecule 1, renal papillary antigen 1, beta 2 microglobulin, trefoil factor 3, albumin, total protein		
<i>Non-qualified urinary DIKI biomarkers</i>		
Alpha 1 microglobulin, neutrophil gelatinase-associated lipocalin, osteopontin, calbindind28k, interleukin 18, alpha-glutathione S-transferase, Mu gamma glutathione S-transferase, retinol-binding protein 4, tamm-horsfall protein (uromodulin), liver-type fatty acid-binding protein		
<i>Nephron region and renal cell specificity for DIKI biomarkers</i>		
<b>Nephron Segment</b>	<b>In Vitro Study</b>	<b>In Vivo Study</b>
Proximal tubule	Transferrin Immunoglobulin G β2-microglobulin α1-microglobulin Clusterin Cystatin C Osteopontin Retinol-binding protein 4 <i>N</i> -Acetyl-D-glucosaminidase Alpha-glutathione S-transferase Gamma-glutamyl transferase Lactate dehydrogenase Interleukin (-8, -18) Neutrophil gelatinase-associated lipocalin monocyte chemoattractant protein-1 Granulocyte-macrophage colony-stimulating factor Platelet-derived growth factor-BB Transforming growth factor-beta 1 Kidney injury molecule 1 Tissue inhibitor of metalloproteinase 2 Insulin-like growth factor binding protein 7 connective tissue growth factor Liver-type fatty acid binding protein	Proteinuria: Total Protein Albumin Transferrin Immunoglobulin G β2-Microglobulin α1-Microglobulin Clusterin Cystatin C Osteopontin Retinol-binding protein 4  Urinary proteins with enzymatic activity: <i>N</i> -Acetyl-D-Glucosaminidase alpha-glutathione S-transferase Gamma-glutamyl transferase Lactate dehydrogenase  Inflammation: Interleukin (-4, -6, -7, -8, -18) Neutrophil Gelatinase-associated Lipocalin Granulocyte-macrophage colony-stimulating factor Platelet-derived growth factor-BB Transforming growth factor-beta 1 Monocyte chemoattractant protein-1 (indicator of lupus nephritis flare)

*Continued*

**TABLE 2** Non-qualified and qualified kidney safety biomarker used during in vivo and/or in vitro studies—cont'd

	( <i>NOT constitutive expressed in mouse</i> ) microRNAs (miR-21, -200c and -423)	Kidney injury molecule 1 (indicator of interstitial nephritis)  Necrosis/degeneration: Kidney injury molecule 1 Tissue inhibitor of metalloproteinase 2 Insulin-like growth factor binding protein 7 Liver-type fatty acid binding protein ( <i>NOT constitutive expressed in mouse</i> ) microRNAs (miR-21, 423, 200c, Let-7d, miR-203, and miR-320)  Regeneration: Connective tissue growth factor, liver-type fatty acid binding protein ( <i>indicator of tubular interstitial fibrosis</i> )
Distal tubule	Clusterin Osteopontin Pi-glutamyl transferase Calbindin-D28K	Proteinuria: Total protein Albumin Clusterin Cystatin C Osteopontin Pi-glutamyl transferase Calbindin-D28K Uromodulin/tamm-horsfall protein
Glomerulus	Kidney injury molecule 1 ( <i>indicator of in vitro cytotoxicity</i> )  Transforming growth factor-beta 1 Platelet-derived growth factor Tumor necrosis factor alpha Type IV collagen Interferon gamma Granulocyte-macrophage colony-stimulating factor Monocyte chemoattractant protein-1	Necrosis: L1 cell adhesion molecule (CD171)  Proteinuria: Transforming growth factor-beta 1 Platelet-derived growth factor Type IV collagen  Type IV Collagen MicroRNAs (miR-10a and miR-30d)  Inflammation: Interleukin (-2, -6, -7, -8, -18) Tumor necrosis factor alpha Type IV collagen Interferon gamma Granulocyte-macrophage colony-stimulating factor Monocyte chemoattractant protein-1 ( <i>indicator of lupus nephritis flare</i> )
Henle's loop	Osteopontin Calbindin-D28K Uromodulin/tamm-horsfall protein	
Collecting/ connect ducts		Calbindin-D28K Uromodulin/tamm-horsfall protein  Inflammation: Interleukin (-2, -6, -7, -8, -18)

are necessary to underpin the clinical data when seeking New Drug Application (NDA) and Biologic License Application (BLA) approvals, morphologic evidence of DIKI incidences and/or severities are expected to correlate with clinically relevant changes in the novel, more sensitive, and often nephron-specific biomarkers [124]. To date, no biomarkers have been qualified for predicting DIKI in animal models, except for rats [125].

Eight urinary proteins were initially qualified for limited context of use when monitoring for DIKI in nonclinical studies in rats [126], representing the first ever formal safety biomarker qualification. The qualified rat urinary (Ur) protein DIKI biomarkers include: kidney injury molecule 1 (Ur KIM-1), urinary clusterin (Ur CLU), urinary albumin (Ur ALB), urinary total protein (Ur TP), urinary  $\beta$ 2 microglobulin (Ur  $\beta$ 2M), urinary cystatin C (Ur CYS C), and urinary trefoil factor-3 (Ur TFF3). The United States Food & Drug Administration (US FDA), the European Medicines Agency (EMA), and the Pharmaceuticals Medical Devices Agency, Japan (PMDA) first acknowledged these parameters as highly sensitive and specific for monitoring DIKI progression in male and female rats [126]. Subsequently, the US FDA and EMA acknowledged urinary renal papillary antigen 1 (Ur RPA-1) as a singly qualified DIKI biomarker in male and female rats as well as the increased level of evidence for the context of use for Ur CLU in male rats [127]. The first and second rat kidney safety biomarker qualification applications were respectively submitted by the Predictive Safety Testing Consortium (PSTC)/Nephrotoxicity Working Group (NWG) within the Critical Path Institute (C-Path) and the Health and Environmental Sciences Institute (HESI)/Committee on Biomarkers of Nephrotoxicity within the International Life Sciences Institute (ILSI). Qualified DIKI biomarkers that may be used by sponsors on a voluntary basis to demonstrate DIKI in GLP rat studies used to support the safe conduct of early-phase clinical trials [126]. Traditional and next-generation biomarkers should be combined with histopathology to enable early identification of DIKI in preclinical studies [2], including but not limited to rats. Recently, the first qualification of human renal safety biomarkers was acknowledged by the US FDA [128]. The first human kidney safety biomarker qualification application was submitted by the Foundation for the National Institutes of Health (FNIH) and PSTC/NWG within C-Path. For quantitative DIKI measurements, urine samples are often collected over short durations (up to 4–16 h) for rats and large animals (e.g., dog, monkeys) and up to a 6-h urine collection period for mice that are housed in metabolism cages without access to food, and as spot (at specified or unspecified time[s]) collections for humans.

The FNIH and Predictive Safety Testing Consortium Nephrotoxicity Working Group within C-Path recently published “The User’s Guide: Kidney Safety Composite Measure Biomarker for Use in Clinical Development” [129]. This guide provides drug development companies with important information about implementing the first ever clinical safety biomarker qualified by the US FDA as a single composite measure of six urine biomarkers, to be used in conjunction with traditional measures of kidney function, a major milestone that will improve the detection of DIKI in Phase 1 clinical trials.

## 5 Context of use of in vitro PTEC models—Mechanistic vs. predictive

Defining the context of use for an in vitro assay is not trivial. All assays have false positives and false negatives, the effect of which must be measured against the predicted benefit of

reduced risk of toxicity brought to the development portfolio. For example, let us look at a portfolio of 1000 compounds for a hypothetical pharmaceutical company. If we assume that up to 50% of a discovery and development portfolio is lost to preclinical and clinical safety [130], we lose about 500 compounds due to safety-related findings. Published data estimate that between 2% and 10% of molecules lost to safety-related attrition are due to nephrotoxicity [2–4]. Thus, 30 compounds would be lost in this portfolio of the hypothetical pharmaceutical company because of nephrotoxicity, assuming an average of 6%. A good *in vitro* nephrotoxicity assay with high performance could be assumed to have both sensitivity and specificity of 90% or above. Thus, the greatest benefit that could be gained with this predictive nephrotoxicity assay would be the removal of 2.7% of the overall portfolio, or 27 compounds, that would later be found to be nephrotoxic. However, this would come at the expense of 10% (100 compounds) of the portfolio as incorrectly flagged (false positive) having a potential nephrotoxic hazard, using 90% specificity of the *in vitro* assay. Thus, this assay would lead to little or no compound enrichment for this hypothetical pharmaceutical company as for every true positive that is identified by this assay there will be roughly about four false positives as well. If assays with similar performance were used as predictive screens for the eight leading causes of safety-related attrition, then over a third of all compounds screened would be predicted to carry at least one false positive, making it difficult to distinguish drug candidates with a genuine risk for safety-related attrition from those that do not. For this reason, predictive screens are most often targeted toward toxicities with high frequency and prevalence, cardiovascular toxicity, and hepatotoxicity [4] using high-confidence endpoints and cutoff values that minimize false positives. Thus, in a drug discovery setting, it is likely that most advanced PTEC models will have their earliest impact on drug candidates only after a potential DIKI hazard has already been identified, especially for small molecules. In this context, PTEC assays can have a profound impact on a drug discovery project, enabling the rapid assessment of DIKI mechanism, screening for cleaner backup chemistries, and assessing the likelihood of clinical translation of preclinical findings.

Recent publications on the concordance between preclinical safety findings and clinical adverse events have shed light on the strengths and weaknesses of the ICH recommended battery of preclinical *in vivo* studies in the detection of DIKI. Monticello et al. [4] examined 182 drug candidates with preclinical and phase I safety data and found that, while rodents and dogs showed high specificity in the detection of renal injury (88% and 91%, respectively), only just half of all drug candidates that caused DIKI in the clinic were detected in preclinical species (43% and 50%, respectively). Clark et al. [131] came to a similar conclusion in their analysis of 3290 approved drugs and formulations where they found that a positive DIKI signal in preclinical species yielded a positive likelihood ratio (“change in clinical risk when the adverse event is observed in an animal study”) of just 3.09, representing a “small, but sometimes important, shift in probability” in the risk of clinical nephrotoxicity. Both studies point to the poor sensitivity of rats and dogs in the standard battery of histopathology and clinical chemistry. The recent acceptance of urinary DIKI biomarkers by regulators may perhaps enhance the predictive power of preclinical species, and it will be important to follow-up on these concordance observations in the years to come to determine if these new methods do indeed improve the sensitivity of DIKI detection and reduce the incidence of late stage DIKI failures [126]. Indeed, it will likely be a combination

of physiochemical properties in *in vitro* and *in vivo* assays with improved DIKI biomarkers that will need to be calibrated for each pharmaceutical company's renal safety strategy.

## 6 Outlook and future perspectives

As highlighted in this chapter, tremendous progress has been made in nephrotoxicity detection in recent years, from a simplistic single transporter expressing cell lines to advanced MPS models capable of recapitulating important aspects of the *in vivo* biology. However, with advancements in *in silico* chemical toxicology analysis and machine learning tools, many researchers are starting to assess the liabilities of compounds in the early stages of discovery by looking at their physiochemical properties along with other inherent determinants of human renal clearance. The first set of models to predict the rate of human renal clearance and perform *in silico* assessment of candidate drugs that are less likely to fail due to renal clearance was described by Paine et al. [132]. Subsequently, Grafström et al. proposed that bioinformatics-driven analyses of data obtained from treated cell models could serve as a Three R's tool and replace some animals in monitoring for inducible toxicity [133]. Select sources of *in vitro*, *in vivo*, and human data that may assist in the development of *in silico* models to aid the understanding of nephrotoxicity mechanisms have been reviewed [134]. Of importance is the usefulness of physiologically based *in silico* pharmacokinetic tools to evaluate kidney transporter engagements. Moreover, GastroPlus software represents a commonly used *in silico* pharmacokinetic model that may be used to incorporate the disposition data across species; it can be leveraged to simulate human PK properties of candidate drugs to aid the prediction of DIKI [135]. Previously, Lee et al. described quantitative structure–activity relationship (QSAR) models for three types of DIKI commonly observed *in vivo*, i.e., tubular necrosis, interstitial nephritis, and tubulo-interstitial nephritis [136]. These models consist of information on the nephrotoxicity of the pharmaceuticals from clinical trial and post-marketing safety databases; they include parent compounds of pharmaceuticals (251 nephrotoxins and 387 non-nephrotoxins) and their major urinary metabolites (307 nephrotoxins and 233 non-nephrotoxins). The predictive accuracies of the best models for each type of kidney injury were >83%. Additionally, the prediction of AKI with a machine learning algorithm using electronic health record data has been reported [137]. Yet the retrospective aspects of this tool deter extrapolating conclusions regarding the impact of the algorithm's predictions on patient outcomes in a clinical setting. These factors speak to the need of *in silico* models with good predictive accuracy.

Interestingly, the prediction of DIKI and related mechanisms using human iPSC-derived PTEC-like cells and machine learning methods appears to enable the development of physiologically relevant *in vitro* models for compound screening and nephrotoxicity prediction [39]. Until now, the PTEC-like cell specific toxicity for 30 compounds was delineated; and PTEC toxicity in humans was predicted with 99.8% training accuracy and 87.0% test accuracy. Renal cell models have been proposed to support screening efforts intended to enable the discovery of therapeutics against kidney diseases, for example, an immortalized mouse podocyte-based HCS phenotypic assay that analyzes thousands



of cells in 96-well plates to quantitatively measure dose-dependent changes in multiple cellular features [138]. The assay has been leveraged to screen >2100 compounds of which 24 small molecules showed protection of podocytes against injury in vitro. Taken together, the murine podocyte model showed utility for identifying novel therapeutics for proteinuric kidney diseases. Lastly, single point HCS assay approaches have evolved to multiplexed assay panels that were initially individually pre-validated. Multiplex cytotoxicity endpoints (LDH, cellular caspase 3/7 activation, resazurin dye reduction, and Hoechst 33342 DNA staining) allow for detection of cellular toxicity following 5- or 24-h incubations with nephrotoxins (e.g., 5-fluorouracil, gentamicin, cisplatin, acetaminophen, para-aminophenol, potassium dichromate, ibuprofen, doxorubicin, cyclosporine, citrinin, and puromycin). As envisaged, this multiplexed platform was more sensitive than single endpoint assays for higher throughput screening in HK-2 cells. Yet soluble PTEC-derived biomarkers have not been coupled to this approach. Similarly, very recently, researchers also combined HCS with Random Forest for 46 diverse kidney toxicants using primary PTECs to generate a multidimensional biomarker panel as molecular signatures for mechanistic derisking of kidney toxicants in vitro [139].

Currently, we believe there is no “ideal/perfect” kidney model for investigating nephrotoxicity and the definition of an “ideal/perfect” model will depend on the question asked from the model and its context of use. If the objective of the in vitro model is to rank order the compounds to minimize renal liabilities in the early stages of drug development, then a model with sustained physiological relevance, especially with respect to transporters such as OAT1/3, OCT2, MRP2/4, P-gp, MATEs, and BCRP and metabolic enzymes such as UGTs, CYPs, and GGTs should be used. This model can be used in conjunction with HCS to look at a variety of different assay parameters [43] that have been optimized to reflect predictivity using a balanced training set of compounds from the perspective of physiochemical properties. Incorporation of therapeutic human exposure ( $C_{\max}$ ) can add further value to the model; however, in the early stages of compound development,  $C_{\max}$  information is seldom available. The ability to measure some of the abovementioned qualified kidney injury biomarkers can be very useful in addition to monitoring imaging-based parameters as it will allow translatability between species as well as in vitro in vivo translation (IVIVT). Combining and comparing the biomarker information obtained from the in vitro kidney models or kidney MPS with physiologically based pharmacokinetic (PBPK) modeling aided quantitative systems pharmacology (QSP) as highlighted in the recent publication, Fig. 3 [140], can also help with IVIVT and identifying favorable dosing regimens for new chemical entities (NCEs). This approach can be beneficial for clinical candidates (Phase 1 and later) as much of the information needed for PBPK/physiologically based toxicokinetic (PBTK) modeling might not be available for NCEs sooner. Thus, a combination of in silico, in vitro, and in vivo information will probably yield the most accurate assessment of nephrotoxicity and understanding renal drug clearance for new entities.

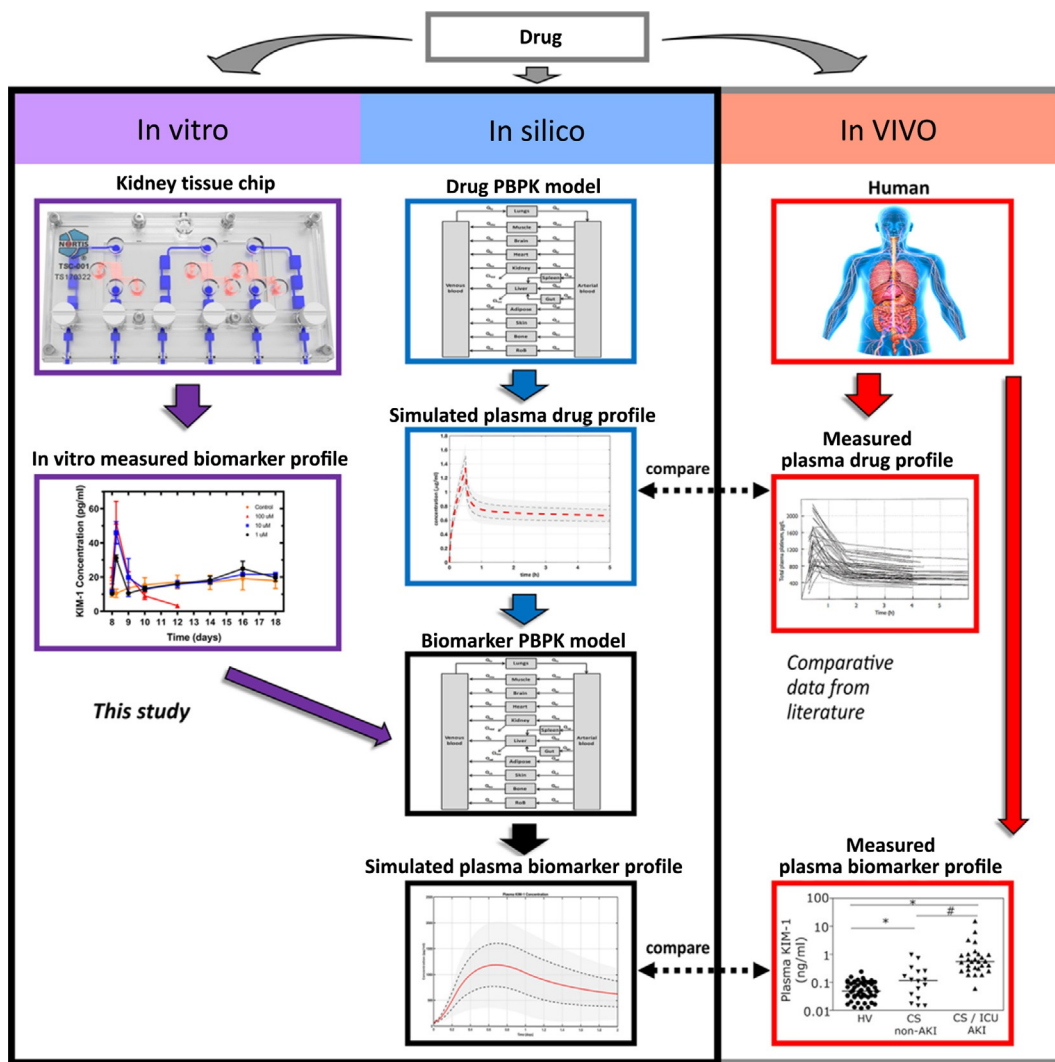


**FIG. 3** Workflow for IVIVT. First, the toxic responses of drugs using clinical biomarkers are evaluated in the kidney MPS (e.g., toxicity, viability; left panel, purple). Computational PBPK models of drugs are simulated to predict drug exposure in human kidneys (middle panel, blue). These simulations are compared with measured drug profiles from patients to assess their validity (right panel, red). Then the QSP models relate the simulated drug human biodistribution profiles to the kidney injury biomarker profile using MPS data (middle panel, black). Finally, the simulations of biomarkers are compared with clinically observed biomarker profiles. *Figure reproduced with permission from C. Maass, N.B. Sorensen, J. Himmelfarb, E.J. Kelly, C.L. Stokes, and M. Cirit, Translational assessment of drug-induced proximal tubule injury using a kidney microphysiological system, CPT Pharmacometrics Syst. Pharmacol. 8 (5) (2019) 316–325. This work is licensed under a Creative Commons Attribution-NonCommercial-NoDerivatives 4.0 International License (<https://creativecommons.org/licenses/by-nc-nd/4.0/>). No changes were made to the original figure.*

## References

- [1] K.M. Morrissey, S.L. Stocker, M.B. Wittwer, L. Xu, K.M. Giacomini, Renal transporters in drug development, *Annu. Rev. Pharmacol.* 53 (2013) 503–529.
- [2] W. Redfern, L. Ewart, T. Hammond, R. Bialecki, L. Kinter, S. Lindgren, Impact and frequency of different toxicities throughout the pharmaceutical life cycle, *The Toxicologist* 114 (2010) 231.
- [3] J.J. Hornberg, M. Laursen, N. Brenden, M. Persson, A.V. Thouggaard, D.B. Toft, T. Mow, Exploratory toxicology as an integrated part of drug discovery. Part I: why and how, *Drug Discov. Today* 19 (8) (2014) 1131–1136.
- [4] T.M. Monticello, T.W. Jones, D.M. Dambach, D.M. Potter, M.W. Bolt, M. Liu, D.A. Keller, T.K. Hart, V. J. Kadambi, Current nonclinical testing paradigm enables safe entry to first-in-human clinical trials: the IQ consortium nonclinical to clinical translational database, *Toxicol. Appl. Pharmacol.* 334 (2017) 100–109.
- [5] S.P. Troth, K. Vlasakova, S. Amur, R.P. Amin, W.E. Glaab, Translational safety biomarkers of kidney injury, *Semin. Nephrol.* 39 (2) (2019) 202–214.
- [6] J.V. Bonventre, V.S. Vaidya, R. Schmodder, P. Feig, F. Dieterle, Next-generation biomarkers for detecting kidney toxicity, *Nat. Biotechnol.* 28 (5) (2010) 436–440.
- [7] M. Cárdenas-González, M. Pavkovic, V.S. Vaidya, Biomarkers of acute kidney injury, in: C.A. McQueen (Ed.), *Comprehensive Toxicology*, third ed., Elsevier, Oxford, 2018, , pp. 147–163.
- [8] M.J. Wilmer, C.P. Ng, H.L. Lanz, P. Vulto, L. Suter-Dick, R. Masereeuw, Kidney-on-a-chip technology for drug-induced nephrotoxicity screening, *Trends Biotechnol.* 34 (2) (2016) 156–170.
- [9] S.K. Nigam, The SLC22 transporter family: a paradigm for the impact of drug transporters on metabolic pathways, signaling, and disease, *Annu. Rev. Pharmacol.* 58 (1) (2018) 663–687.
- [10] S.K. Nigam, W. Wu, K.T. Bush, M.P. Hoenig, R.C. Blantz, V. Bhatnagar, Handling of drugs, metabolites, and uremic toxins by kidney proximal tubule drug transporters, *Clin. J. Am. Soc. Nephrol.* 10 (11) (2015) 2039–2049.
- [11] M.J. Dresser, M.K. Leabman, K.M. Giacomini, Transporters involved in the elimination of drugs in the kidney: organic anion transporters and organic cation transporters, *J. Pharm. Sci.* 90 (4) (2001) 397–421.
- [12] K.M. Giacomini, S.M. Huang, D.J. Tweedie, L.Z. Benet, K.L. Brouwer, X. Chu, A. Dahlin, R. Evers, V. Fischer, K. M. Hillgren, K.A. Hoffmaster, T. Ishikawa, D. Keppler, R.B. Kim, C.A. Lee, M. Niemi, J.W. Polli, Y. Sugiyama, P. W. Swaan, J.A. Ware, S.H. Wright, S.W. Yee, M.J. Zamek-Gliszczynski, L. Zhang, Membrane transporters in drug development, *Nat. Rev. Drug Discov.* 9 (3) (2010) 215–236.
- [13] J.Y.C. Soo, J. Jansen, R. Masereeuw, M.H. Little, Advances in predictive in vitro models of drug-induced nephrotoxicity, *Nat. Rev. Nephrol.* 14 (6) (2018) 378–393.
- [14] P.D. Ward, D. La, J.E. McDuffie, Renal transporters and biomarkers in safety assessment, in: S.J.T. Gowder (Ed.), *New Insights into Toxicity and Drug Testing*, 2013, , pp. 153–174.
- [15] S. Yokoo, A. Yonezawa, S. Masuda, A. Fukatsu, T. Katsura, K.-I. Inui, Differential contribution of organic cation transporters, OCT2 and MATE1, in platinum agent-induced nephrotoxicity, *Biochem. Pharmacol.* 74 (3) (2007) 477–487.
- [16] C. Lanvers-Kaminsky, J.A. Sprowl, I. Malath, D. Deuster, M. Eveslage, E. Schlatter, R.H. Mathijssen, J. Boos, H. Jurgens, A.G. Am Zehnhoff-Dinnesen, A. Sparreboom, G. Ciarimboli, Human OCT2 variant c.808G>T confers protection effect against cisplatin-induced ototoxicity, *Pharmacogenomics* 16 (4) (2015) 323–332.
- [17] H. Katsuda, M. Yamashita, H. Katsura, J. Yu, Y. Waki, N. Nagata, Y. Sai, K. Miyamoto, Protecting cisplatin-induced nephrotoxicity with cimetidine does not affect antitumor activity, *Biol. Pharm. Bull.* 33 (11) (2010) 1867–1871.
- [18] K.J. Jang, A.P. Mehr, G.A. Hamilton, L.A. McPartlin, S. Chung, K.Y. Suh, D.E. Ingber, Human kidney proximal tubule-on-a-chip for drug transport and nephrotoxicity assessment, *Integr. Biol.* 5 (9) (2013) 1119–1129.
- [19] D.M. Moss, M. Neary, A. Owen, The role of drug transporters in the kidney: lessons from tenofovir, *Front. Pharmacol.* 5 (2014) 248.
- [20] R. Nielsen, E.I. Christensen, H. Birn, Megalin and cubilin in proximal tubule protein reabsorption: from experimental models to human disease, *Kidney Int.* 89 (1) (2016) 58–67.
- [21] C. Schmitz, J. Hilpert, C. Jacobsen, C. Boensch, E.I. Christensen, F.C. Luft, T.E. Willnow, Megalin deficiency offers protection from renal aminoglycoside accumulation, *J. Biol. Chem.* 277 (1) (2002) 618–622.
- [22] S. Sewing, M. Gubler, R. Gérard, B. Avignon, Y. Mueller, A. Braendli-Baiocco, M. Odin, A. Moisan, GalNAc conjugation attenuates the cytotoxicity of antisense oligonucleotide drugs in renal tubular cells, *Mol. Ther. Nucleic Acids* 14 (2019) 67–79.
- [23] A. Moisan, M. Gubler, J.D. Zhang, Y. Tessier, K. Dumong Erichsen, S. Sewing, R. Gérard, B. Avignon, S. Huber, F. Benmansour, X. Chen, R. Villaseñor, A. Braendli-Baiocco, M. Festag, A. Maunz, T. Singer, F. Schuler, A. B. Roth, Inhibition of EGF uptake by nephrotoxic antisense drugs In Vitro and implications for preclinical safety profiling, *Mol. Ther. Nucleic Acids* 6 (2017) 89–105.

- [24] N. Lameire, Nephrotoxicity of recent anti-cancer agents, *Clin. Kidney J.* 7 (1) (2014) 11–22.
- [25] R. Nielsen, E.I. Christensen, H. Birn, Megalin and cubilin in proximal tubule protein reabsorption: from experimental models to human disease, *Kidney Int.* 89 (1) (2016) 58–67.
- [26] B. Cen, W. Liao, Z. Wang, L. Gao, Y. Wei, W. Huang, S. He, W. Wang, X. Liu, X. Pan, A. Ji, Gelofusine attenuates tubulointerstitial injury induced by cRGD-conjugated siRNA by regulating the TLR3 signaling pathway, *Mol. Ther. Nucleic Acids* 11 (2018) 300–311.
- [27] L.H. Lash, Role of renal metabolism in risk to toxic chemicals, *Environ. Health Perspect.* 102 (Suppl 11) (1994) 75–79.
- [28] J.O. Miners, X. Yang, K.M. Knights, L. Zhang, The role of the kidney in drug elimination: transport, metabolism, and the impact of kidney disease on drug clearance, *Clin. Pharmacol. Ther.* 102 (3) (2017) 436–449.
- [29] K.M. Knights, A. Rowland, J.O. Miners, Renal drug metabolism in humans: the potential for drug-endobiotic interactions involving cytochrome P450 (CYP) and UDP-glucuronosyltransferase (UGT), *Br. J. Clin. Pharmacol.* 76 (4) (2013) 587–602.
- [30] P. Bajaj, S.K. Chowdhury, R. Yucha, E.J. Kelly, G. Xiao, Emerging kidney models to investigate metabolism, transport, and toxicity of drugs and xenobiotics, *Drug Metab. Dispos.* 46 (11) (2018) 1692–1702.
- [31] C.A. Hinchman, H. Matsumoto, T.W. Simmons, N. Ballatori, Intrahepatic conversion of a glutathione conjugate to its mercapturic acid. Metabolism of 1-chloro-2,4-dinitrobenzene in isolated perfused rat and guinea pig livers, *J. Biol. Chem.* 266 (33) (1991) 22179–22185.
- [32] X. Zhang, R. Wang, M. Piotrowski, H. Zhang, K.L. Leach, Intracellular concentrations determine the cytotoxicity of adefovir, cidofovir and tenofovir, *Toxicol. In Vitro* 29 (1) (2015) 251–258.
- [33] S.E. Jenkinson, G.W. Chung, E. van Loon, N.S. Bakar, A.M. Dalzell, C.D. Brown, The limitations of renal epithelial cell line HK-2 as a model of drug transporter expression and function in the proximal tubule, *Pflugers Arch.* 464 (6) (2012) 601–611.
- [34] J.X. Huang, G. Kaeslin, M.V. Ranall, M.A. Blaskovich, B. Becker, M.S. Butler, M.H. Little, L.H. Lash, M. A. Cooper, Evaluation of biomarkers for in vitro prediction of drug-induced nephrotoxicity: comparison of HK-2, immortalized human proximal tubule epithelial, and primary cultures of human proximal tubular cells, *Pharmacol. Res. Perspect.* 3 (3) (2015), e00148.
- [35] M.J. Wilmer, M.A. Saleem, R. Masereeuw, L. Ni, T.J. van der Velden, F.G. Russel, P.W. Mathieson, L. A. Monnens, L.P. van den Heuvel, E.N. Levtchenko, Novel conditionally immortalized human proximal tubule cell line expressing functional influx and efflux transporters, *Cell Tissue Res.* 339 (2) (2010) 449–457.
- [36] J. Jansen, C.M. Schophuizen, M.J. Wilmer, S.H. Lahham, H.A. Mutsaers, J.F. Wetzels, R.A. Bank, L.P. van den Heuvel, J.G. Hoenderop, R. Masereeuw, A morphological and functional comparison of proximal tubule cell lines established from human urine and kidney tissue, *Exp. Cell Res.* 323 (1) (2014) 87–99.
- [37] T.T. Nieskens, J.G. Peters, M.J. Schreurs, N. Smits, R. Woestenenk, K. Jansen, T.K. van der Made, M. Roring, C. Hilgendorf, M.J. Wilmer, R. Masereeuw, A human renal proximal tubule cell line with stable organic anion transporter 1 and 3 expression predictive for antiviral-induced toxicity, *AAPS J.* 18 (2) (2016) 465–475.
- [38] H.Y. Tiong, P. Huang, S. Xiong, Y. Li, A. Vathsala, D. Zink, Drug-induced nephrotoxicity: clinical impact and preclinical in vitro models, *Mol. Pharm.* 11 (7) (2014) 1933–1948.
- [39] K. Kandasamy, J.K.C. Chuah, R. Su, P. Huang, K.G. Eng, S. Xiong, Y. Li, C.S. Chia, L.-H. Loo, D. Zink, Prediction of drug-induced nephrotoxicity and injury mechanisms with human induced pluripotent stem cell-derived cells and machine learning methods, *Sci. Rep.* 5 (2015) 12337.
- [40] Y. Li, K. Kandasamy, J.K. Chuah, Y.N. Lam, W.S. Toh, Z.Y. Oo, D. Zink, Identification of nephrotoxic compounds with embryonic stem-cell-derived human renal proximal tubular-like cells, *Mol. Pharm.* 11 (7) (2014) 1982–1990.
- [41] Y. Li, Z.Y. Oo, S.Y. Chang, P. Huang, K.G. Eng, J.L. Zeng, A.J. Kaestli, B. Gopalan, K. Kandasamy, F. Tasnim, D. Zink, An in vitro method for the prediction of renal proximal tubular toxicity in humans, *Toxicol. Res.* 2 (5) (2013) 352–365.
- [42] M. Adler, S. Ramm, M. Hafner, J.L. Muhlich, E.M. Gottwald, E. Weber, A. Jaklic, A.K. Ajay, D. Svoboda, S. Auerbach, E.J. Kelly, J. Himmelfarb, V.S. Vaidya, A quantitative approach to screen for nephrotoxic compounds *In Vitro*, *J. Am. Soc. Nephrol.* 27 (4) (2016) 1015–1028.
- [43] A.-K. Sjögren, K. Breitholtz, E. Ahlberg, L. Milton, M. Forsgard, M. Persson, S.H. Stahl, M.J. Wilmer, J. J. Hornberg, A novel multi-parametric high content screening assay in ciPTEC-OAT1 to predict drug-induced nephrotoxicity during drug discovery, *Arch. Toxicol.* 92 (10) (2018) 3175–3190.
- [44] S.P. Troth, F. Simutis, G.S. Friedman, S. Todd, F.D. Sistare, Kidney safety assessment: current practices in drug development, *Semin. Nephrol.* 39 (2) (2019) 120–131.

- [45] J.A. Engelhardt, Comparative renal toxicopathology of antisense oligonucleotides, *Nucleic Acid Ther.* 26 (4) (2016) 199–209.
- [46] W.G. Herrington, D.C. Talbot, M.M. Lahn, J.T. Brandt, S. Callies, R. Nagle, C.G. Winearls, I.S. Roberts, Association of long-term administration of the survivin mRNA-targeted antisense oligonucleotide LY2181308 with reversible kidney injury in a patient with metastatic melanoma, *Am. J. Kidney Dis.* 57 (2) (2011) 300–303.
- [47] R.S. Geary, D. Norris, R. Yu, C.F. Bennett, Pharmacokinetics, biodistribution and cell uptake of antisense oligonucleotides, *Adv. Drug Deliv. Rev.* 87 (2015) 46–51.
- [48] R.L. Juliano, The delivery of therapeutic oligonucleotides, *Nucleic Acids Res.* 44 (14) (2016) 6518–6548.
- [49] S.P. Henry, H. Bolte, C. Auletta, D.J. Kornbrust, Evaluation of the toxicity of ISIS 2302, a phosphorothioate oligonucleotide, in a four-week study in cynomolgus monkeys, *Toxicology* 120 (2) (1997) 145–155.
- [50] F.M. van de Water, O.C. Boerman, A.C. Wouterse, J.G. Peters, F.G. Russel, R. Masereeuw, Intravenously administered short interfering RNA accumulates in the kidney and selectively suppresses gene function in renal proximal tubules, *Drug Metab. Dispos.* 34 (8) (2006) 1393–1397.
- [51] Y. Takakura, Y. Oka, M. Hashida, Cellular uptake properties of oligonucleotides in LLC-PK1 renal epithelial cells, *Antisense Nucleic Acid Drug Dev.* 8 (1) (1998) 67–73.
- [52] Y. Huang, Preclinical and clinical advances of GalNAc-decorated nucleic acid therapeutics, *Mol. Ther. Nucleic Acids* 6 (2017) 116–132.
- [53] M. Tanowitz, L. Hetricks, A. Revenko, G.A. Kinberger, T.P. Prakash, P.P. Seth, Asialoglycoprotein receptor 1 mediates productive uptake of N-acetylgalactosamine-conjugated and unconjugated phosphorothioate antisense oligonucleotides into liver hepatocytes, *Nucleic Acids Res.* 45 (21) (2017) 12388–12400.
- [54] P.M. Andrews, A.K. Coffey, In vitro studies of kidney glomerular epithelial cells, *Scan. Electron Microsc.* 2 (1980) 179–191.
- [55] T. Weinstein, R. Cameron, A. Katz, M. Silverman, Rat glomerular epithelial cells in culture express characteristics of parietal, not visceral, epithelium, *J. Am. Soc. Nephrol.* 3 (6) (1992) 1279–1287.
- [56] J.F. Bertram, A. Messina, G.B. Ryan, In vitro effects of puromycin aminonucleoside on the ultrastructure of rat glomerular podocytes, *Cell Tissue Res.* 260 (3) (1990) 555–563.
- [57] M.A. Saleem, M.J. O'Hare, J. Reiser, R.J. Coward, C.D. Inward, T. Farren, C.Y. Xing, L. Ni, P.W. Mathieson, P. Mundel, A conditionally immortalized human podocyte cell line demonstrating nephrin and podocin expression, *J. Am. Soc. Nephrol.* 13 (3) (2002) 630–638.
- [58] Y.S. Kanwar, J. Wada, S. Lin, F.R. Danesh, S.S. Chugh, Q. Yang, T. Banerjee, J.W. Lomasney, Update of extracellular matrix, its receptors, and cell adhesion molecules in mammalian nephrogenesis, *Am. J. Physiol. Renal Physiol.* 286 (2) (2004) F202–F215.
- [59] A.M. van Genderen, J. Jansen, C. Cheng, T. Vermonden, R. Masereeuw, Renal tubular- and vascular basement membranes and their mimicry in engineering vascularized kidney tubules, *Adv. Healthc. Mater.* 7 (19) (2018) e1800529.
- [60] P.F. Secker, L. Luks, N. Schlichenmaier, D.R. Dietrich, RPTEC/TERT1 cells form highly differentiated tubules when cultured in a 3D matrix, *ALTEX* 35 (2) (2018) 223–234.
- [61] R. Masereeuw, J. Vriend, M.J. Wilmer, Kidney-on-a-chip: technologies for studying pharmacological and therapeutic approaches to kidney repair, in: G. Orlando, G. Remuzzi, D.F. Williams (Eds.), *Kidney Transplantation, Bioengineering and Regeneration*, Academic Press, 2017, , pp. 1119–1133.
- [62] L.E. O'Brien, W. Yu, K. Tang, T.S. Jou, M.M. Zegers, K.E. Mostov, Morphological and biochemical analysis of Rac1 in three-dimensional epithelial cell cultures, *Methods Enzymol.* 406 (2006) 676–691.
- [63] H. Emonard, J.A. Grimaud, B. Nusgens, C.M. Lapiere, J.M. Foidart, Reconstituted basement-membrane matrix modulates fibroblast activities in vitro, *J. Cell. Physiol.* 133 (1) (1987) 95–102.
- [64] R. Morizane, T. Monkawa, S. Fujii, S. Yamaguchi, K. Homma, Y. Matsuzaki, H. Okano, H. Itoh, Kidney specific protein-positive cells derived from embryonic stem cells reproduce tubular structures in vitro and differentiate into renal tubular cells, *PLoS One* 8 (6) (2014) e64843.
- [65] R. Morizane, A.Q. Lam, B.S. Freedman, S. Kishi, M.T. Valerius, J.V. Bonventre, Nephron organoids derived from human pluripotent stem cells model kidney development and injury, *Nat. Biotechnol.* 33 (11) (2015) 1193–1200.
- [66] F. Schutgens, M.B. Rookmaaker, T. Margaritis, A. Rios, C. Ammerlaan, J. Jansen, L. Gijzen, M. Vormann, A. Vonk, M. Viveen, F.Y. Yengej, S. Derakhshan, K.M. Winter-de Groot, B. Artegiani, R. van Boxtel, E. Cuppen, A.P.A. Hendrickx, M.M. van den Heuvel-Eibrink, E. Heitzer, H. Lanz, J. Beekman, J.-L. Murk, R. Masereeuw, F. Holstege, J. Drost, M.C. Verhaar, H. Clevers, Tubuloids derived from human adult kidney and urine for personalized disease modeling, *Nat. Biotechnol.* 37 (3) (2019) 303–313.



- [67] C.S. Hughes, L.M. Postovit, G.A. Lajoie, Matrigel: a complex protein mixture required for optimal growth of cell culture, *Proteomics* 10 (9) (2010) 1886–1890.
- [68] T.M. DesRochers, L. Suter, A. Roth, D.L. Kaplan, Bioengineered 3D human kidney tissue, a platform for the determination of nephrotoxicity, *PLoS One* 8 (3) (2013) e59219.
- [69] K. Jansen, C.C.L. Schuurmans, J. Jansen, R. Masereeuw, T. Vermonden, Hydrogel-based cell therapies for kidney regeneration: current trends in biofabrication and in vivo repair, *Curr. Pharm. Des.* 23 (26) (2017) 3845–3857.
- [70] A.I. Astashkina, C.F. Jones, G. Thiagarajan, K. Kurtzeborn, H. Ghandehari, B.D. Brooks, D.W. Grainger, Nanoparticle toxicity assessment using an in vitro 3-D kidney organoid culture model, *Biomaterials* 35 (24) (2014) 6323–6331.
- [71] A.I. Astashkina, B.K. Mann, G.D. Prestwich, D.W. Grainger, A 3-D organoid kidney culture model engineered for high-throughput nephrotoxicity assays, *Biomaterials* 33 (18) (2012) 4700–4711.
- [72] A.I. Astashkina, B.K. Mann, G.D. Prestwich, D.W. Grainger, Comparing predictive drug nephrotoxicity biomarkers in kidney 3-D primary organoid culture and immortalized cell lines, *Biomaterials* 33 (18) (2012) 4712–4721.
- [73] T.M. DesRochers, E.P. Kimmerling, D.M. Jandhyala, W. El-Jouni, J. Zhou, C.M. Thorpe, J.M. Leong, D. L. Kaplan, Effects of Shiga toxin type 2 on a bioengineered three-dimensional model of human renal tissue, *Infect. Immun.* 83 (1) (2015) 28–38.
- [74] X. Mu, W. Zheng, L. Xiao, W. Zhang, X. Jiang, Engineering a 3D vascular network in hydrogel for mimicking a nephron, *Lab Chip* 13 (8) (2013) 1612–1618.
- [75] S. Moll, M. Ebeling, F. Weibel, A. Farina, A. Araujo Del Rosario, J.C. Hoflack, S. Pomposiello, M. Prunotto, Epithelial cells as active player in fibrosis: findings from an in vitro model, *PLoS One* 8 (2) (2013) e56575.
- [76] C. Godugu, A.R. Patel, U. Desai, T. Andey, A. Sams, M. Singh, AlgiMatrix based 3D cell culture system as an in-vitro tumor model for anticancer studies, *PLoS One* 8 (1) (2013) e53708.
- [77] H. Vorsmann, F. Groeber, H. Walles, S. Busch, S. Beissert, H. Walczak, D. Kulms, Development of a human three-dimensional organotypic skin-melanoma spheroid model for in vitro drug testing, *Cell Death Dis.* 4 (2013) e719.
- [78] S.M. Nauli, F.J. Alenghat, Y. Luo, E. Williams, P. Vassilev, X. Li, A.E. Elia, W. Lu, E.M. Brown, S.J. Quinn, D. E. Ingber, J. Zhou, Polycystins 1 and 2 mediate mechanosensation in the primary cilium of kidney cells, *Nat. Genet.* 33 (2) (2003) 129–137.
- [79] L.C. Snouber, F. Letourneur, P. Chafey, C. Broussard, M. Monge, C. Legallais, E. Leclerc, Analysis of transcriptomic and proteomic profiles demonstrates improved Madin-Darby canine kidney cell function in a renal microfluidic biochip, *Biotechnol. Prog.* 28 (2) (2012) 474–484.
- [80] K.J. Jang, K.Y. Suh, A multi-layer microfluidic device for efficient culture and analysis of renal tubular cells, *Lab Chip* 10 (1) (2010) 36–42.
- [81] Z. Wei, P.K. Amponsah, M. Al-Shatti, Z. Nie, B.C. Bandyopadhyay, Engineering of polarized tubular structures in a microfluidic device to study calcium phosphate stone formation, *Lab Chip* 12 (20) (2012) 4037–4040.
- [82] X. Gao, Y. Tanaka, Y. Sugii, K. Mawatari, T. Kitamori, Basic structure and cell culture condition of a bioartificial renal tubule on chip towards a cell-based separation microdevice, *Anal. Sci.* 27 (9) (2011) 907–912.
- [83] K.J. Jang, H.S. Cho, H.K. Do, W.G. Bae, T.H. Kwon, K.Y. Suh, Fluid-shear-stress-induced translocation of aquaporin-2 and reorganization of actin cytoskeleton in renal tubular epithelial cells, *Integr. Biol.* 3 (2) (2011) 134–141.
- [84] E.M. Frohlich, J.L. Alonso, J.T. Borenstein, X. Zhang, M.A. Arnaout, J.L. Charest, Topographically-patterned porous membranes in a microfluidic device as an in vitro model of renal reabsorptive barriers, *Lab Chip* 13 (12) (2013) 2311–2319.
- [85] L. Choucha Snouber, S. Jacques, M. Monge, C. Legallais, E. Leclerc, Transcriptomic analysis of the effect of ifosfamide on MDCK cells cultivated in microfluidic biochips, *Genomics* 100 (1) (2012) 27–34.
- [86] L. Choucha-Snouber, C. Aninat, L. Grsicom, G. Madalinski, C. Brochot, P.E. Poleni, F. Razan, C.G. Guillouzo, C. Legallais, A. Corlu, E. Leclerc, Investigation of ifosfamide nephrotoxicity induced in a liver-kidney co-culture biochip, *Biotechnol. Bioeng.* 110 (2) (2013) 597–608.
- [87] X. Yao, K. Panichpisal, N. Kurtzman, K. Nugent, Cisplatin nephrotoxicity: a review, *Am. J. Med. Sci.* 334 (2) (2007) 115–124.
- [88] E.J. Weber, A. Chapron, B.D. Chapron, J.L. Voellinger, K.A. Lidberg, C.K. Yeung, Z. Wang, Y. Yamaura, D. W. Hailey, T. Neumann, D.D. Shen, K.E. Thummel, K.A. Muczynski, J. Himmelfarb, E.J. Kelly, Development of a microphysiological model of human kidney proximal tubule function, *Kidney Int.* 90 (3) (2016) 627–637.

- [89] C. Sakolish, E.J. Weber, E.J. Kelly, J. Himmelfarb, R. Mouneimne, F.A. Grimm, J.S. House, T. Wade, A. Han, W. A. Chiu, I. Rusyn, Technology transfer of the microphysiological systems: a case study of the human proximal tubule tissue chip, *Sci. Rep.* 8 (1) (2018) 14882.
- [90] X. Su, E.W. Young, H.A. Underkofler, T.J. Kamp, C.T. January, D.J. Beebe, Microfluidic cell culture and its application in high-throughput drug screening: cardiotoxicity assay for hERG channels, *J. Biomol. Screen.* 16 (1) (2011) 101–111.
- [91] N. Li, M. Schwartz, C. Ionescu-Zanetti, PDMS compound adsorption in context, *J. Biomol. Screen.* 14 (2) (2009) 194–202.
- [92] H. Sasaki, H. Onoe, T. Osaki, R. Kawano, S. Takeuchi, Parylene-coating in PDMS microfluidic channels prevents the absorption of fluorescent dyes, *Sensor Actuat. B-Chem.* 150 (1) (2010) 478–482.
- [93] S.J. Trietsch, G.D. Israels, J. Joore, T. Hankemeier, P. Vulto, Microfluidic titer plate for stratified 3D cell culture, *Lab Chip* 13 (18) (2013) 3548–3554.
- [94] L. Suter-Dick, L. Mauch, D. Ramp, M. Caj, M.K. Vormann, S. Hutter, H.L. Lanz, J. Vriend, R. Masereeuw, M. J. Wilmer, Combining extracellular miRNA determination with microfluidic 3D cell cultures for the assessment of nephrotoxicity: a proof of concept study, *AAPS J.* 20 (5) (2018) 86.
- [95] M.K. Vormann, L. Gijzen, S. Hutter, L. Boot, A. Nicolas, A. van den Heuvel, J. Vriend, C.P. Ng, T.T.G. Nieskens, V. van Duinen, B. de Wagenaar, R. Masereeuw, L. Suter-Dick, S.J. Trietsch, M. Wilmer, J. Joore, P. Vulto, H. L. Lanz, Nephrotoxicity and kidney transport assessment on 3D perfused proximal tubules, *AAPS J.* 20 (5) (2018) 90.
- [96] J. Vriend, T.T.G. Nieskens, M.K. Vormann, B.T. van den Berge, A. van den Heuvel, F.G.M. Russel, L. Suter-Dick, H.L. Lanz, P. Vulto, R. Masereeuw, M.J. Wilmer, Screening of drug-transporter interactions in a 3D microfluidic renal proximal tubule on a chip, *AAPS J.* 20 (5) (2018) 87.
- [97] Z. Li, L. Jiang, Y. Zhu, W. Su, C. Xu, T. Tao, Y. Shi, J. Qin, Assessment of hepatic metabolism-dependent nephrotoxicity on an organs-on-a-chip microdevice, *Toxicol. In Vitro* 46 (2018) 1–8.
- [98] S.Y. Chang, E.J. Weber, V.S. Sidorenko, A. Chapron, C.K. Yeung, C. Gao, Q. Mao, D. Shen, J. Wang, T. A. Rosenquist, K.G. Dickman, T. Neumann, A.P. Grollman, E.J. Kelly, J. Himmelfarb, D.L. Eaton, Human liver-kidney model elucidates the mechanisms of aristolochic acid nephrotoxicity, *JCI Insight* 2 (22) (2017).
- [99] I. Maschmeyer, A.K. Lorenz, K. Schimek, T. Hasenberg, A.P. Ramme, J. Hubner, M. Lindner, C. Drewell, S. Bauer, A. Thomas, N.S. Sambo, F. Sonntag, R. Lauster, U. Marx, A four-organ-chip for interconnected long-term co-culture of human intestine, liver, skin and kidney equivalents, *Lab Chip* 15 (12) (2015) 2688–2699.
- [100] K.A. Homan, D.B. Kolesky, M.A. Skylar-Scott, J. Herrmann, H. Obuobi, A. Moisan, J.A. Lewis, Bioprinting of 3D convoluted renal proximal tubules on perfusable chips, *Sci. Rep.* 6 (2016) 34845.
- [101] N.Y.C. Lin, K.A. Homan, S.S. Robinson, D.B. Kolesky, N. Duarte, A. Moisan, J.A. Lewis, Renal reabsorption in 3D vascularized proximal tubule models, *Proc. Natl. Acad. Sci. U. S. A.* 116 (12) (2019) 5399–5404.
- [102] C.P. Ng, Y. Zhuang, A.W.H. Lin, J.C.M. Teo, A fibrin-based tissue-engineered renal proximal tubule for bioartificial kidney devices: development, characterization and in vitro transport study, *Int. J. Tissue Eng.* 2012 (2013).
- [103] Z.Y. Oo, R. Deng, M. Hu, M. Ni, K. Kandasamy, M.S.B. Ibrahim, J.Y. Ying, D. Zink, The performance of primary human renal cells in hollow fiber bioreactors for bioartificial kidneys, *Biomaterials* 32 (34) (2011) 8806–8815.
- [104] C. Shen, Q. Meng, G. Zhang, Increased curvature of hollow fiber membranes could up-regulate differential functions of renal tubular cell layers, *Biotechnol. Bioeng.* 110 (8) (2013) 2173–2183.
- [105] J. Jansen, M. Fedecostante, M.J. Wilmer, L.P. van den Heuvel, J.G. Hoenderop, R. Masereeuw, Biotechnological challenges of bioartificial kidney engineering, *Biotechnol. Adv.* 32 (7) (2014) 1317–1327.
- [106] J. Jansen, I.E. De Napoli, M. Fedecostante, C.M. Schophuizen, N.V. Chevchik, M.J. Wilmer, A.H. van Asbeck, H.J. Croes, J.C. Pertijs, J.F.M. Wetzels, L.B. Hilbrands, L.P. van den Heuvel, J.G. Hoenderop, D. Stamatialis, R. Masereeuw, Human proximal tubule epithelial cells cultured on hollow fibers: living membranes that actively transport organic cations, *Sci. Rep.* 16 (2015) 16702.
- [107] J. Jansen, M. Fedecostante, M.J. Wilmer, J.G. Peters, U.M. Kreuser, P.H. van den Broek, R.A. Mensink, T.J. Boltje, D. Stamatialis, J.F. Wetzels, L.P. van den Heuvel, J.G. Hoenderop, R. Masereeuw, Bioengineered kidney tubules efficiently excrete uremic toxins, *Sci. Rep.* 6 (2016) 26715.
- [108] C. Legallais, D. Kim, S.M. Mihaila, M. Mihajlovic, M. Figliuzzi, B. Bonandrini, S. Salerno, F.A. Yousef Yengej, M. B. Rookmaaker, N. Sanchez Romero, P. Sainz-Arnal, U. Pereira, M. Pasqua, K.G.F. Gerritsen, M.C. Verhaar, A. Remuzzi, P.M. Baptista, L. De Bartolo, R. Masereeuw, D. Stamatialis, Bioengineering organs for blood detoxification, *Adv. Healthc. Mater.* 7 (21) (2018) e1800430.



- [109] K. Jansen, M. Castilho, S. Aarts, M.M. Kaminski, S.S. Lienkamp, R. Pichler, J. Malda, T. Vermonden, J. Jansen, R. Masereeuw, Fabrication of kidney proximal tubule grafts using biofunctionalized electrospun polymer scaffolds, *macromol, BioScience* (2019)e1800412.
- [110] M. Mihajlovic, M. Fedecostante, M.J. Oost, S.K.P. Steenhuis, E. Lentjes, I. Maitimu-Smeele, M.J. Janssen, L. B. Hilbrands, R. Masereeuw, Role of vitamin D in maintaining renal epithelial barrier function in uremic conditions, *Int. J. Mol. Sci.* 18 (12) (2017) 2531.
- [111] M. Takasato, M.H. Little, A strategy for generating kidney organoids: recapitulating the development in human pluripotent stem cells, *Dev. Biol.* 420 (2) (2016) 210–220.
- [112] M. Takasato, P.X. Er, H.S. Chiu, B. Maier, G.J. Baillie, C. Ferguson, R.G. Parton, E.J. Wolvetang, M.S. Roost, S.M. C. de Sousa Lopes, M.H. Little, Kidney organoids from human iPSCs contain multiple lineages and model human nephrogenesis, *Nature* 526 (2015) 564–568.
- [113] R. Morizane, J.V. Bonventre, Kidney organoids: a translational journey, *Trends Mol. Med.* 23 (3) (2017) 246–263.
- [114] R. Morizane, A.Q. Lam, B.S. Freedman, S. Kishi, M.T. Valerius, J.V. Bonventre, Nephron organoids derived from human pluripotent stem cells model kidney development and injury, *Nat. Biotechnol.* 33 (2015) 1193–1200.
- [115] P. Bajaj, A.D. Rodrigues, C.M. Steppan, S.J. Engle, S. Mathialagan, T. Schroeter, Human pluripotent stem cell-derived kidney model for nephrotoxicity studies, *Drug Metab. Dispos.* 46 (11) (2018) 1703–1711.
- [116] B.S. Freedman, C.R. Brooks, A.Q. Lam, H. Fu, R. Morizane, V. Agrawal, A.F. Saad, M.K. Li, M.R. Hughes, R. V. Werff, D.T. Peters, J. Lu, A. Baccei, A.M. Siedlecki, M.T. Valerius, K. Musunuru, K.M. McNaggy, T. I. Steinman, J. Zhou, P.H. Lerou, J.V. Bonventre, Modelling kidney disease with CRISPR-mutant kidney organoids derived from human pluripotent epiblast spheroids, *Nat. Commun.* 6 (2015) 8715.
- [117] N.M. Cruz, B.S. Freedman, CRISPR gene editing in the kidney, *Am. J. Kidney Dis.* 71 (6) (2018) 874–883.
- [118] C. Rauch, E. Feifel, G. Kern, C. Murphy, F. Meier, W. Parson, M. Beilmann, P. Jennings, G. Gstraunthaler, A. Wilmes, Differentiation of human iPSCs into functional podocytes, *PLoS One* 13 (9) (2018) e0203869.
- [119] M. Zhou, X. Zhang, X. Wen, T. Wu, W. Wang, M. Yang, J. Wang, M. Fang, B. Lin, H. Lin, Development of a functional glomerulus at the organ level on a chip to mimic hypertensive nephropathy, *Sci. Rep.* 6 (2016) 31771.
- [120] O. Ciampi, R. Iacone, L. Longaretti, V. Benedetti, M. Graf, M.C. Magnone, C. Patsch, C. Xinaris, G. Remuzzi, A. Benigni, S. Tomasoni, Generation of functional podocytes from human induced pluripotent stem cells, *Stem Cell Res.* 17 (1) (2016) 130–139.
- [121] B. Song, A.M. Smink, C.V. Jones, J.M. Callaghan, S.D. Firth, C.A. Bernard, A.L. Laslett, P.G. Kerr, S.D. Ricardo, The directed differentiation of human iPSCs into kidney podocytes, *PLoS One* 7 (9) (2012) e46453.
- [122] FDA. M3(R2) Nonclinical Safety Studies for the Conduct of Human Clinical Trials and Marketing Authorization for Pharmaceuticals. 2010. Available from: <https://www.fda.gov/regulatory-information/search-fda-guidance-documents/m3r2-nonclinical-safety-studies-conduct-human-clinical-trials-and-marketing-authorization>. Accessed 2019 April 15.
- [123] FDA. S7A Safety Pharmacology Studies for Human Pharmaceuticals. 2001. Available from: <https://www.fda.gov/regulatory-information/search-fda-guidance-documents/s7a-safety-pharmacology-studies-human-pharmaceuticals>. Accessed 2019 April 15.
- [124] J.-M. Sauer, E.G. Walker, A.C. Porter, The predictive safety testing consortium: Safety biomarkers, collaboration, and qualification, *J. Med. Dev. Sci.* 1 (1) (2015) 34–35.
- [125] J.E. McDuffie, S. Lee, J.Y. Ma, Y. Chen, S. Snook, Acute biomarker panel changes associated with amphotericin B nephrotoxicity in female Sprague-Dawley rats, *J. Toxicol. Sci.* 41 (4) (2016) 459–468.
- [126] F. Dieterle, F. Sistare, F. Goodsaid, M. Papaluca, J.S. Ozer, C.P. Webb, W. Baer, A. Senagore, M.J. Schipper, J. Vonderscher, S. Sultana, D.L. Gerhold, J.A. Phillips, G. Maurer, K. Carl, D. Laurie, E. Harpur, M. Sonee, D. Ennulat, D. Holder, D. Andrews-Cleavenger, Y.Z. Gu, K.L. Thompson, P.L. Goering, J.M. Vidal, E. Abadie, R. Maciulaitis, D. Jacobson-Kram, A.F. Defelice, E.A. Hausner, M. Blank, A. Thompson, P. Harlow, D. Throckmorton, S. Xiao, N. Xu, W. Taylor, S. Vamvakas, B. Flamion, B.S. Lima, P. Kasper, M. Pasanen, K. Prasad, S. Troth, D. Bounous, D. Robinson-Gravatt, G. Betton, M.A. Davis, J. Akunda, J. E. McDuffie, L. Suter, L. Obert, M. Guffroy, M. Pinches, S. Jayadev, E.A. Blomme, S.A. Beushausen, V. G. Barlow, N. Collins, J. Waring, D. Honor, S. Snook, J. Lee, P. Rossi, E. Walker, W. Mattes, Renal biomarker qualification submission: a dialog between the FDA-EMEA and predictive safety testing Consortium, *Nat. Biotechnol.* 28 (5) (2010) 455–462.

- [127] E. Harpur, D. Ennulat, D. Hoffman, G. Betton, J.C. Gautier, B. Riefke, D. Bounous, K. Schuster, S. Beushausen, M. Guffroy, M. Shaw, E. Lock, S. Pettit, Biological qualification of biomarkers of chemical-induced renal toxicity in two strains of male rat, *Toxicol. Sci.* 122 (2) (2011) 235–252.
- [128] FDA. Safety Biomarker paNel to Aid in the Detection of Kidney Tubular Injury in Phase 1 Trials in Healthy Volunteers. 2018. Available from: <https://www.fda.gov/drugs/cder-biomarker-qualification-program/list-qualified-biomarkers>. Accessed 22 April 2019.
- [129] Foundation for the National Institutes of Health Biomarkers Consortium Kidney Safety Biomarker Project Team and Predictive Safety Testing Consortium Nephrotoxicity Working Group. Kidney Safety Composite Measure Biomarker for Use in Clinical Development. 2018. Available from: <https://c-path.org/c-path-fnih-announce-clinical-development-users-guide-for-kidney-safety-biomarkers/>. Accessed 18 March 2019.
- [130] M.J. Waring, J. Arrowsmith, A.R. Leach, P.D. Leeson, S. Mandrell, R.M. Owen, G. Pairaudeau, W.D. Pennie, S.D. Pickett, J. Wang, O. Wallace, A. Weir, An analysis of the attrition of drug candidates from four major pharmaceutical companies, *Nat. Rev. Drug Discov.* 14 (7) (2015) 475–486.
- [131] M. Clark, T. Steger-Hartmann, A big data approach to the concordance of the toxicity of pharmaceuticals in animals and humans, *Regul. Toxicol. Pharmacol.* 96 (2018) 94–105.
- [132] S.W. Paine, P. Barton, J. Bird, R. Denton, K. Menochet, A. Smith, N.P. Tomkinson, K.K. Chohan, A rapid computational filter for predicting the rate of human renal clearance, *J. Mol. Graph. Model.* 29 (4) (2010) 529–537.
- [133] R.C. Grafstrom, P. Nymark, V. Hongisto, O. Spjuth, R. Ceder, E. Willighagen, B. Hardy, S. Kaski, P. Kohonen, Toward the replacement of animal experiments through the bioinformatics-driven analysis of ‘Omics’ data from human cell cultures, *Altern. Lab. Anim.* 43 (5) (2015) 325–332.
- [134] J. Pletz, S.J. Enoch, D.M. Jais, C.L. Mellor, G. Pawar, J.W. Firman, J.C. Madden, S.D. Webb, C.A. Tagliati, M.T. D. Cronin, A critical review of adverse effects to the kidney: mechanisms, data sources, and in silico tools to assist prediction, *Expert Opin. Drug Metab. Toxicol.* 14 (12) (2018) 1225–1253.
- [135] S. Willmann, J. Lippert, W. Schmitt, From physicochemistry to absorption and distribution: predictive mechanistic modelling and computational tools, *Expert Opin. Drug Metab. Toxicol.* 1 (1) (2005) 159–168.
- [136] S. Lee, Y.-M. Kang, H. Park, M.-S. Dong, J.-M. Shin, K.T. No, Human nephrotoxicity prediction models for three types of kidney injury based on data sets of pharmacological compounds and their metabolites, *Chem. Res. Toxicol.* 26 (11) (2013) 1652–1659.
- [137] H. Mohamadlou, A. Lynn-Palevsky, C. Barton, U. Chettipally, L. Shieh, J. Calvert, N.R. Saber, R. Das, Prediction of acute kidney injury with a machine learning algorithm using electronic health record data, *Can. J. Kidney Health Dis.* 5 (2018) 2054358118776326.
- [138] H.W. Lee, S.Q. Khan, M.H. Faridi, C. Wei, N.J. Tardi, M.M. Altintas, H.A. Elshabrawy, S. Mangos, K.L. Quick, S. Sever, J. Reiser, V. Gupta, A podocyte-based automated screening assay identifies protective small molecules, *J. Am. Soc. Nephrol.* 26 (11) (2015) 2741–2752.
- [139] S. Ramm, P. Todorov, V. Chandrasekaran, A. Dohlman, M.B. Monteiro, M. Pavkovic, J. Muhlich, H. Shankaran, W.W. Chen, J.T. Mettetal, V.S. Vaidya, A systems toxicology approach for the prediction of kidney toxicity and its mechanisms in vitro, *Toxicol. Sci.* 169 (1) (2019) 54–69.
- [140] C. Maass, N.B. Sorensen, J. Himmelfarb, E.J. Kelly, C.L. Stokes, M. Cirit, Translational assessment of drug-induced proximal tubule injury using a kidney microphysiological system, *CPT Pharmacometrics Syst. Pharmacol.* 8 (5) (2019) 316–325.

# Immunogenicity: An introduction to its role in the safety and efficacy of biotherapeutics

---

Christopher Gemski, Satyajeet Haridas

Translational Research Bioassay and Immunogenicity Group, Drug Metabolism and Pharmacokinetic Department, Takeda Pharmaceuticals International Co., Cambridge, MA, United States

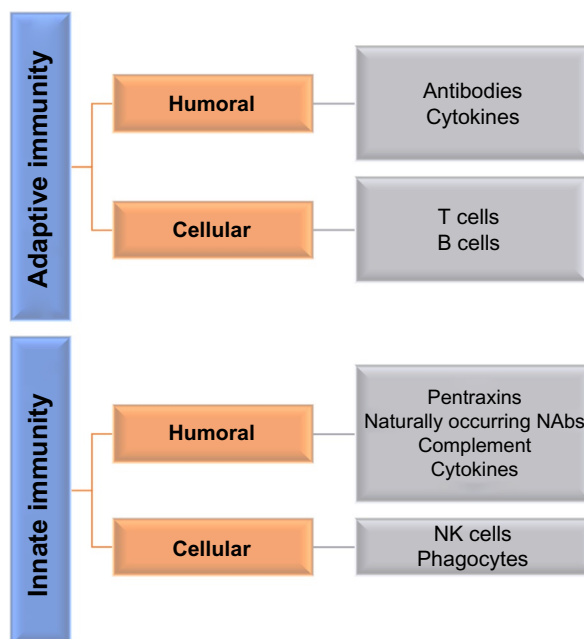
## 1 Introduction

---

Biotherapeutic drug products are usually more complicated than conventional small molecule drugs which lead to new sets of issues, e.g., immunogenicity associated with changes of exposure, efficacy, and adverse side effects. A biological product consists of many components, e.g., carbohydrates, proteins, nucleic acids, or whole cells. Most conventional drugs are pure chemical compounds and are relatively small in comparison to large, more complex, biological drug products. A major challenge of using biological drug products or “biologics” is that they have the potential to be recognized by the immune system and therefore can be immunogenic. This is a potential concern that conventional drugs or “small molecules” typically do not experience.

The recognition of a biologic drug product by the immune system is referred to as *immunogenicity*, defined as the ability of a substance to produce an immune response. This immune response can be divided into two types: innate or adaptive immunity (Fig. 1). Innate immunity is a rapid response by innate cells (dendritic cells, monocytes, macrophages, neutrophils, eosinophils, basophils, and mast cells) which recognize foreign substances via pattern recognition receptors (PRR). Adaptive immunity on the other hand does not occur immediately and produces a more specialized response, which relies on B and T lymphocytes. Both innate and adaptive immunity have cellular and humoral components which will be discussed more in-depth later in this chapter. The scope of this chapter is to present a general overview of how

**FIG. 1** Principle branches of immunity. Adaptive and innate immunity are the principle arms of the immune systems. Each of these branches can be divided into two components: humoral or cellular response.



immunogenicity occurs and to address strategies related to the safety, risk assessment and prediction, and analytical methods useful at various stages of therapeutics development. The goal here is to introduce the basic concepts associated with immunogenicity and the clinical relevance associated with biotherapeutic drug development.

## 2 Overview of immunogenicity

Immunogenicity of a biologic can be influenced by factors associated with its production, route of administration, the molecular feature of the biotherapeutic itself, and even the patient. Other factors that affect the immunogenicity of a biologic drug product are amino acid variations, glycosylation patterns, and chemical modifications such as crosslinking [1]. Clinically it has been observed that switching from an intravenous (i.v.) to subcutaneous (s.c.) route of administration can increase immunogenicity [1]. Although, it should be noted that changing the route of administration does not completely negate immunogenicity as the biologic drug product remains either inherently immunogenic or is not. Immunogenicity caused by impurities and contaminants associated with the production highlights the importance of producing a highly pure drug product. As previously mentioned, the patient can also directly influence immunogenicity. Specifically, the major histocompatibility complex (MHC) classes I and II genetic background of the patient can influence the immune response to a biologic drug product.

When a foreign substance or antigen is recognized by certain cells, it is internalized and cleaved into peptide fragments. Some of these fragments are then presented at the surface

of the cell by the MHC. The MHC is a cell surface protein that forms a complex with T cells via recognition by the T-cell receptor (TCR), thus activating the T cell to respond to the specific peptide fragment presented. MHC molecules can be separated into two classes: MHC I and MHC II, each of which interacts with different types of T cells. In an adaptive cellular response, MHC I presenting cells complex with cytotoxic T cells that express the CD8 cell surface marker and then directly attack any cell that contains the specific antigen fragment that was presented to it. MHC II presenting cells complex with helper T cells that express the CD4 cell surface maker inducing a humoral response resulting in the formation of antidrug antibodies (ADAs) from B cells.

The consequences of ADA formation are important to understand from a clinical perspective. Patients that have tested positive for ADA against a biotherapeutic drug may have the drugs activity neutralized. Neutralizing ADAs (NABs) impair the activity of the biologic by binding to its variable region and prevent targeting, thereby decreasing the drug's efficacy. ADA formation can also alter the pharmacokinetic (PK) profile of a biologic drug. The consequences of these alterations can accelerate the clearance of the biologic drug, thereby reducing the level of drug. Toxicity can also occur following ADA formation. Typically, this can be related to infusion which through multiple complex mechanisms causes the release of cytokines (substances released by certain immune cells that can mediate and regulate immunity), eventually leading to cytokine release syndrome (CRS) and systemic toxicity. Also, making it even more complicated are additional variables that can affect infusion toxicity, e.g., route of administration, number and frequency of doses, and the drug product itself [2].

It has been generally agreed across the industry that the immunogenicity risk profile of a drug in animals does not directly translate to human results because of the species difference of immune systems. Therefore, the effort in the investigation of ADA in animals is mainly for PK profiling, efficacy, and safety data interpretation and not for the prediction of human immunogenicity risk. A useful strategy for prediction of human immunogenicity risk assessment and mitigation includes a combination of *in silico*, *in vitro*, *ex vivo*, and *in vivo* tools. These tools include *in silico* human MHC I- and MHC II-binding prediction algorithms, cell-free MHC binding assays, human peripheral blood mononuclear cell (PBMC) and immune cell-based immunoassays, MHC epitope mapping assays, and *in vivo* studies using humanized mouse models. The utilization of these predictive tools are essential for human immunogenicity prediction and risk assessment and drug candidate screening and prioritization based on the immunogenicity profiles. It is important to note that immunogenicity will likely occur for most biotherapeutics. Therefore, the development of validated assays and a risk assessment plan are necessary when developing a biotherapeutic and submitting results to regulatory authorities.

### 3 Overview of immune response mechanisms

As previously mentioned, immune responses to biotherapeutics have both humoral and cellular components (Fig. 1). The humoral and cellular response mechanisms can also be classified as either innate or adaptive immunity. Since immunogenicity can reduce the efficacy and cause unexpected adverse event, regulatory authorities are highly concerned with

immunogenicity and details of an immunogenicity risk assessment plan are suggested to be part of the application when submitting a new biotherapeutic investigational new drug (IND) application or medicinal product dossier for the first stage of clinical trials. In this chapter, because cellular innate immunity is more difficult to predict, lacking well-validated models at this time, we will focus on discussing in greater detail humoral and cellular adaptive immunity and humoral innate immunity.

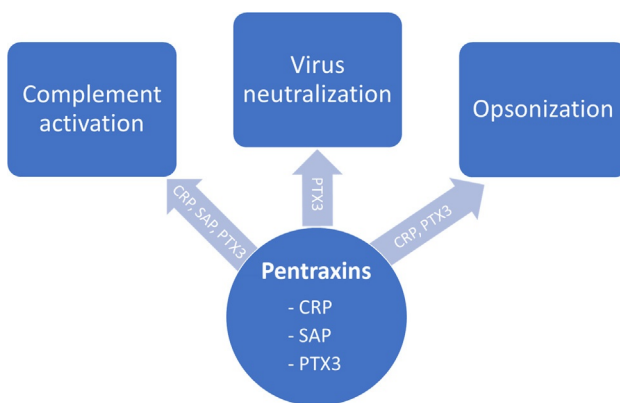
### 3.1 Humoral immunogenicity

Traditionally, the presence of ADA (both neutralizing and non-neutralizing) is what is referred to as humoral “immunogenicity” and represents an adaptive humoral response. Therefore, monitoring the formation of ADA and its impact on PK/PD, safety, and efficacy are important for the approval of a new biologic drug product. While adaptive humoral immunogenicity may be what’s thought of when immunogenicity is spoken of, innate humoral immunogenicity is also important to consider.

Innate humoral immune responses consist of naturally occurring NABs, pentraxins (proteins that act as pattern recognition receptors), and serine protease cascades of the complement pathway [3]. These innate responses occur acutely (minutes to hours) and form the first line of defense against pathogens. This response is important to consider with biotherapeutics such as gene therapies. Gene therapies often use viruses, e.g., retrovirus, adenovirus, and adeno-associated virus to introduce genetic material into cells to repair the cell function. If the virus is recognized by innate immunity, and an inflammatory response is produced, pentraxins will then bind directly to the virus and neutralize it or can mediate other functions such as opsonization by phagocytes and activation of the complement pathways (Fig. 2). Pentraxins are a family of PRR proteins. C-reactive protein (CRP), serum amyloid P (SAP), and pentraxin 3 (PTX3) comprise the short and long pentraxins. The pentraxin family and its multifunctional abilities form a bridge between the cellular and soluble portions of innate immunity.

An adaptive humoral response involves both CD4+ T cells and B cells. CD4+ helper T cells exert their effects indirectly via complex formation of their TCR with MHC II-antigen

**FIG. 2** Pentraxin family protein regulation of innate immunity. CRP, SAP, and PTX3 function by pattern recognition and regulation of virus neutralization, opsonization, and complement activation.



presenting cells (APCs). The key driver for this adaptive response is antigen presentation by MHC II proteins. Once a biotherapeutic is taken up by an APC, it is internalized and degraded into peptides of variable length (9–25 residues). Through cell-to-cell contact, the MHC II-presenting proteins of APCs activate CD4+ helper T cells, which in turn leads to activation of B cells, cytotoxic T cells, and cytokine secretion (Fig. 3) [4]. Activated B cells secrete antibodies that protect the body against foreign antigens. These antibodies, known as antidrug antibodies (ADA) function in several ways to biotherapeutics. ADA formation can affect a biotherapeutics efficacy, PK/PD profile and can induce adverse events (AE) through direct binding leading to neutralization, complement initiation, and in cooperation with the cellular arm for opsonization and antibody-dependent cell-mediated cytotoxicity (ADCC) (Table 1) [5]. Both the B- and T-cell responses here are equally important because they can lead to the formation of memory immune cells, which is a unique feature of adaptive immunity. This is important to consider when developing a biotherapeutic since patients are generally administered repeat doses. The formation of ADA is highly variable depending on the patient. This is because the immunogenicity of the biotherapeutic is not the only factor contributing to the immune response. Other variables like a patient's immune status and genotype influence

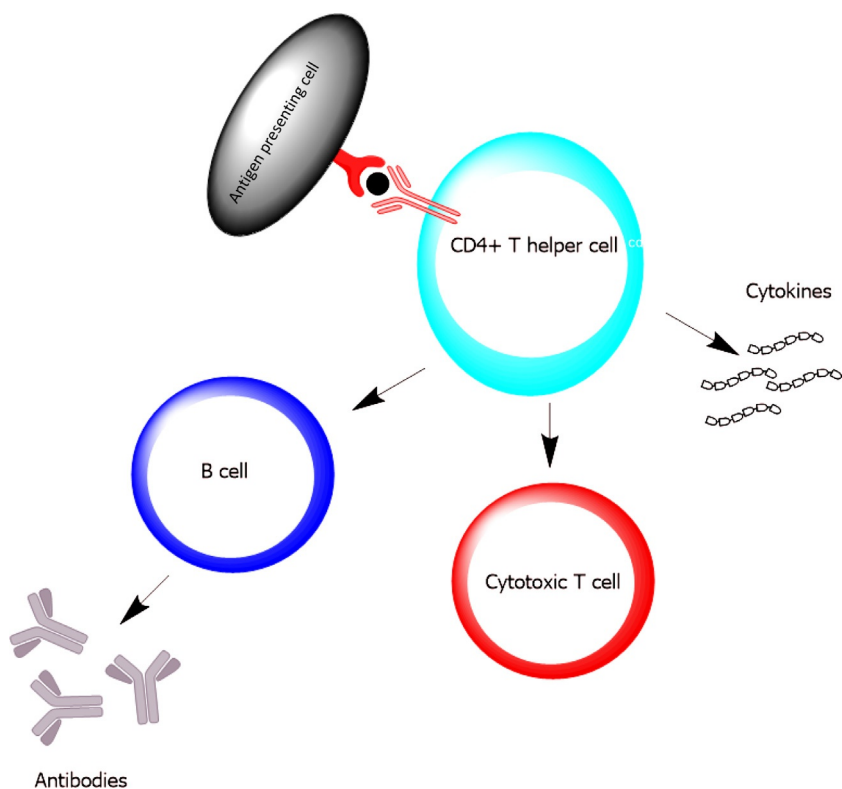


**FIG. 3** Basic schematic representation of helper T-cell activation. APC activation of T-helper cells leading to cytotoxic T-cell and B-cell activation and cytokine secretion.



TABLE 1 Antibody mediated responses.

Adaptive humoral responses			
Neutralization	Complement initiation	Opsonization	ADCC
Direct binding to a foreign antigen leading to inhibition of function, followed by elimination.	Direct binding to a foreign antigen followed by complex formation of soluble serum complement components and initiation of membrane attack complex (MAC).	Direct binding to foreign antigen followed by recruitment of phagocytotic cells via Fc receptor (FcR) binding.	Direct binding to a foreign antigen leading to apoptosis via FcR binding to cytotoxic cells such as, NK cells and granulocytes.

the body's response, and in some cases the dose, route of administration, and impurities in the drug product can all contribute to immunogenicity [6]. Because so many factors can influence immunogenicity, it is important to have a well-defined preclinical strategy when developing a biotherapeutic. Furthermore, at the clinical level, there is no standardization for the detection of ADA. Thus, it is important to have a clear and well-defined method to support the development of a biologic drug product.

### 3.2 Cellular immunogenicity

Adaptive cellular immunogenicity is the cellular immune response by cytotoxic T lymphocytes or CD8+ T cells in response to a foreign or nonself antigen. These nonself antigens can be generated from foreign particles like bacterial/viral DNA, RNA, and protein sequences. These are also produced from misfolding of self-proteins, as well as mutation of DNA leading to the synthesis of a mutated protein. Apart from these, nonhuman antigens can also be present in biotherapeutics such as mAbs, antibody-drug complexes (ADC), cell therapies like CAR-T, iCAR-T, stem cell therapies, and gene therapies. These potentially immunogenic antigens can be present as part of a transgene amino acid sequence in the biotherapeutic or as residues derived from the manufacturing process (host cell proteins and DNA, plasmid DNA from AAV manufacturing for gene therapy [7]).

These potentially immunogenic regions with cellular immune response affect the biotherapeutics efficacy and safety negatively. For example, anti-CAR-T specific CD8+ T cells will limit the peripheral persistence of transferred CAR-T cells [8]. In cases where immune responses were observed, they were associated with a quick reduction in the CAR-T count in vivo and a loss of efficacy [9]. So, how do CD8+ T cells recognize these sequences and illicit a response? The response mechanism can be divided into two steps: (1) presentation via MHC I on the cell surface and (2) activation of CD8+ T cells.

#### 3.2.1 Presentation via MHC I on the cell surface and binding to CD8+ T cells

Nonself amino acid sequences once inside the cell are processed in cytoplasmic organelles and are broken down into smaller 8–11-mer peptides in proteasomes (Fig. 4). Once broken down, they are transported through the transporter associated with antigen processing (TAP) in the endoplasmic reticulum. The immature or partially folded major histocompatibility

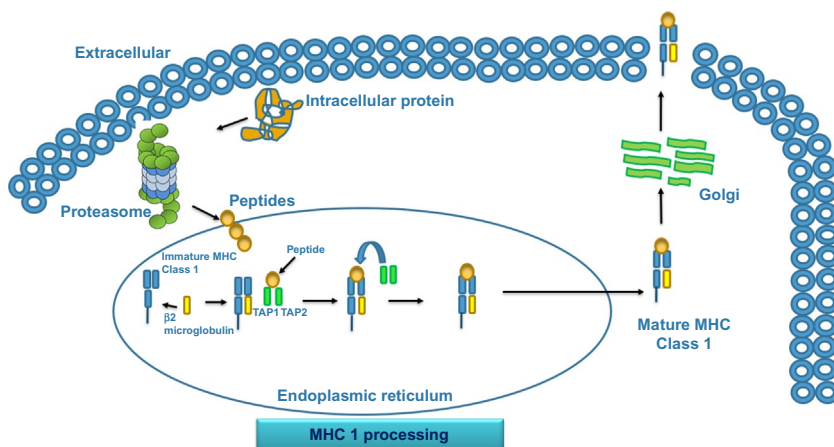


**FIG. 4** Depiction of the MHC class I antigen-processing pathway. The endogenous nonself-peptides are broken down by proteasomes and processed in the endoplasmic reticulum. The mature MHC I peptide complex is transported through the Golgi apparatus to the cell surface.

complex (MHC) class I binds to this TAP. This binds to peptides and is transported to the cell surface through the Golgi apparatus. On the cell surface, peptide MHC I complex (pMHC I) interacts with the TCR on CD8<sup>+</sup> T cells. TCR-mediated recognition of a peptide antigen bound to an MHC-derived molecule represents a central event in the cellular immune response. The TCR contacts the MHC complex through the TCR variable domains [10, 11].

The affinity with which an epitope binds to the MHC I molecule plays an important role in determining its immunogenicity. MHC I, being polygenic and polymorphic, has the capabilities to bind to peptides with different range of specificities. CD8, either as an  $\alpha\alpha$  homodimer or an  $\alpha\beta$  heterodimer, acts as an “assistant” or coreceptor in the function of cytotoxic T lymphocytes. In this ternary complex model, TCR interacts with two  $\alpha$  helices of pMHC and the specific peptide, whereas the coreceptor CD8 acts at a distance from the specific peptide. CD8-pMHC interactions are categorized as rigid body interactions while TCR-pMHC is categorized as induced fit. This implies how TCR shows flexibility to adapt to polymorphic peptide and MHC upon binding [12–15].

### 3.2.2 Activation and cellular response of CD8<sup>+</sup> T cells

After activation, CD8<sup>+</sup> T cells undergo clonal expansion and migration to peripheral regions. They exhibit very high levels of effector functions which can be either cytolytic or non-cytolytic (Fig. 5) [16]. Perforin and granzymes are the most abundant proteins within the lytic lysosomes (granules). Upon binding to target cells and activation of CD8<sup>+</sup> T cells, degranulation aids in the release of these cytolytic proteins into target cells causing lysis. Non-cytolytic mechanism of CD8<sup>+</sup> T cells involves the secretion of various chemokines like IFN- $\gamma$ , TNF- $\alpha$ , and IL-2. These are important for CD8<sup>+</sup> T cell proliferation and persistent activation.

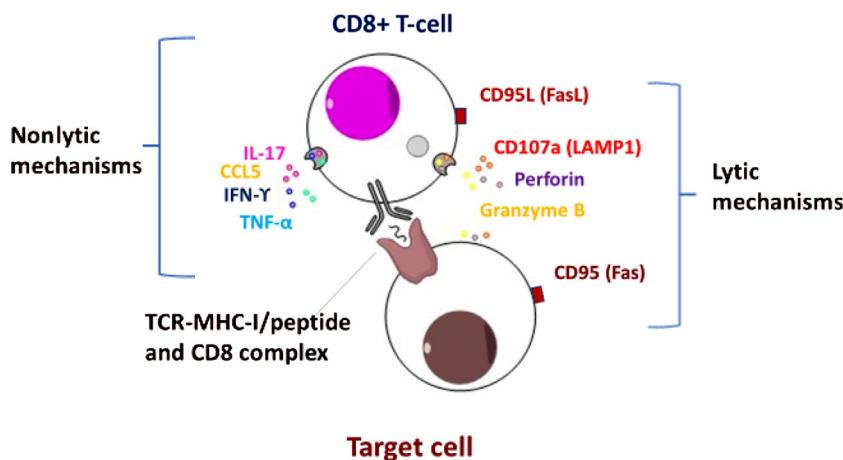


FIG. 5 Depiction of the lytic and non-lytic mechanisms of cellular cytotoxicity by CD8+ T cells. The lytic mechanism involves the release of cytotoxic granules like perforin and granzyme B. The non-lytic mechanism includes the release of cytokines from CD8+ T cells activating other CD8+ T cells to perform the same cytotoxic mechanism.

#### 4 Humoral immunogenicity: Overall risk assessment and mitigation strategies

Currently, it is generally believed that all biotherapeutics are to some degree immunogenic. To try and overcome unwanted immunogenicity associated with a biotherapeutic, drug discovery and development scientists should consider having a preclinical risk assessment strategy and well-defined assays for ADA detection at the clinical level. It should also be noted that not all ADA responses lead to an impact on the safety and efficacy of biotherapeutics. This highlights the importance of understanding how immunogenicity affects a newly developed biologic drug product. The vast majority of ADA responses have very little or no impact on safety and efficacy. However, in some cases, the formation of ADA has a serious effect on a biotherapeutics PK, efficacy, and lead to toxicity-related issues. Regulatory agencies have different opinions and recommended guidelines when it comes to immunogenicity testing. As no standardized testing currently exists, having a well-validated assay is necessary for the application of any new IND filing for a biotherapeutic drug. Here we focused more on the preclinical prediction efforts that currently exist. *In silico*, *in vitro*/*ex vivo*, and *in vivo* models can aid in the development of a biotherapeutic. However, with each models' limitations much more effort is needed to standardize these techniques to develop a candidate with decreased immunogenic outcomes. Using a multitiered approach, in which the previously mentioned tools are combined.

Preclinically, a combination of *in silico*, *in vitro*, and *in vivo* studies can be used to assess immunogenicity risk (Fig. 6). All should be considered since a multitiered approach is suggested by regulatory agencies such as the Food and Drug Administration (FDA) and the European Medical Association (EMA) [17, 18]. Currently, across the industry, ADA formation has been observed to be CD4+ T cell-dependent in most cases. Therefore, a useful starting point for the de-immunization of a biotherapeutic has been *in silico* analysis based on the binding affinity of a drug-derived peptide to T-cell epitopes.

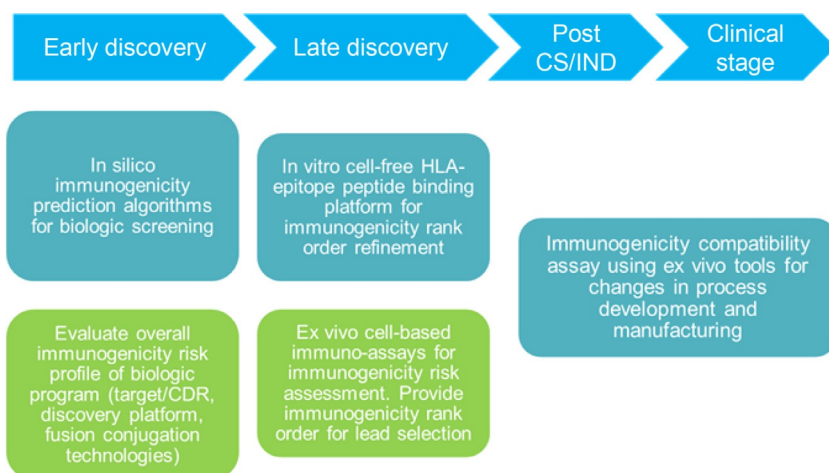


FIG. 6 Proposed immunogenicity risk assessment strategies at various stages of drug development.

Commercially, there are many *in silico* tools available that can predict T-cell epitope binding. These tools function by evaluating a biologic drug's sequence and determining if overlapping peptide fragments can potentially bind to MHC I and II alleles. Tools that predict MHC II allele binding are what is most relevant for the prediction of ADA. The binding affinity of most MHC II alleles has already been determined, which makes these *in silico* tools particularly useful. Many marketed drugs or drugs in development are monoclonal antibodies (mAbs); therefore, mAbs are good examples to look at. However, not all mAbs are engineered the same and differences arise from more than just differences in sequences, but also how each is produced. Orthoclone OKT3 was the first mAb approved by the FDA in 1986. OKT3 was produced by fusing a mouse-derived antibody-producing cell (plasma cell) with immortalized myeloma tumor cells. However, it had limited success because the human immune system recognized the mAb as foreign and neutralized the drug's effectiveness leading to serious side effects. To circumvent this from occurring, next-generation mAbs have since been developed that can be grouped into one of three types (chimeric, human, and humanized). Chimeric antibodies are about 70% human and are generated by grafting mouse variable domains onto human constant domains to retain the specificity but limit potential foreign epitopes. Humanized mAbs are mostly human, except for the murine complementarity-determining regions (CDRs). This has led to a further decrease in unwanted immunogenicity. Finally, "fully human" mAbs have been generated using techniques such as phage display and transgenic mice that express only human antibodies. Regardless of the type of antibody chosen, *in silico* tools allow the optimization of different regions of the mAb, specifically within the CDRs, to avoid T cell epitope binding, and thus reducing the possibility of immunogenicity. Although *in silico* tools are useful, the user should consider other factors that *in silico* tools cannot account for such as route of administration, mechanism of action (MOA), formulation, and contaminants/impurities in the drug product.

Data generated from *in silico* tools bridges nicely with *in vitro/ex vivo* models for immunogenicity risk assessment. Overlapping peptides that have been identified as being potentially immunogenic from *in silico* analysis can be screened in a human immune cell-based system. Examples of this are peripheral blood mononuclear cell (PBMC) assays which consist of both lymphocytes and APCs, or mixed lymphocyte reaction (MLR) assays that can be used to collect cell culture supernatants and analyze the cytokine profile. Also, flow cytometry can be used to analyze T-cell activation markers, which can then be compared to well-defined system controls. PBMCs have also been useful in observing some patient-specific genetic factors, as their phenotype can be determined and screened for specific alleles of interest.

*In vivo* approaches represent the step following *in silico* and *in vitro/ex vivo* assays. Animal models provide an intact immune system for direct measurement of ADA, whereas *in vitro* models rely solely on cytokine measurement and immune cell activation, which are indirect measurements [19–23]. Immune tolerant transgenic mouse models that express specific human proteins represent a useful tool. For instance, the evaluation of ADA response to attributes of human IgG1 has been studied because some of these mouse models are capable of diverse responses to human antibodies [22, 23]. However, transgenic mice like the previously mentioned preclinical methods also have limitations. For example, the mouse strain used is of great importance, since these models cannot evaluate MHC-T cell recognition of peptides and although some transgenic mouse models specific for MHC genes allow for the observation of T-cell responses, they are limited to a single haplotype. Since MHC classes can be quite diverse, this model may not be reflective of a large population. For any of the previously mentioned methods, one should keep in mind that although useful for observing immunogenicity for certain specific factors, there is no fully relevant representation of human MHC and APCs in preclinical models.

## 4.1 Case studies

### 4.1.1 Case study 1: PK assessment in the presence of ADA in animal models

Using a cynomolgus monkey model, Ng et al. developed a PK model to study the impact of ADAs on the PK of adalimumab [24]. As of 2018, adalimumab (sold under the brand name Humira) is the number one top-selling drug globally [25]. Based on the package label insert, the immunogenicity of adalimumab monotherapy was ~13% on average across the different patient populations. Thus, it was important for Ng et al. to develop a prediction tool under these study conditions and in this case, a PK model to estimate the ADA formation rate and drug clearance. This model offered insight on the impact of ADA on PK and ADA formation kinetics by investigating the relationship between neonatal Fc receptor (FcRn)-binding affinity. The authors describe an  $E_{\max}$  model for ADA-mediated clearance, where the  $E_{\max}$  and  $EC_{50}$  were determined to be 1146 pmol/day/kg/log and the ADA titer 7.02 pmol/mL, respectively. The onset of ADA formation was observed to be 8.3 days after dosing and detection of ADA from days 14 to 28 was observed to be associated with decreasing mAb concentrations in serum. This correlated well with observed human data [26]. At the time of publication, this was a novel approach. Although the authors failed to detect the differences of formed ADA

and their effects on PK, it provided a semi-mechanistic model to describe the observed biologic PK in the presence of ADA.

#### **4.1.2 Case study 2: Immune response to AAV vectors in animal models**

Preclinical animal models that predict anti-AAV humoral responses are useful. Literature suggests that 30%–80% of humans have preexisting NABs to AAV; therefore, a relevant model for preclinical prediction is necessary [27]. Fitzpatrick et al. described a strategy for assessing the effect of neutralizing and binding antibodies on AAV transduction both in vitro and in vivo [28]. Using wild-type mice, the authors investigated the role of NABs in AAV clearance from the bloodstream and vector uptake by the liver. Human intravenous immunoglobulin (IVIg) was used as an anti-AAV8 Ab reagent, and the authors passively immunized mice with IVIg or infused them with PBS (control) and 24 h later dosed the animals with an AAV8 vector expressing human factor IX transgene (FIX). Quantification of the subsequent time point samples showed no FIX transgene expression and livers harvested from the mice also showed almost undetectable levels of vector genome after 24 h. The PBS infused mice, which were injected with AAV8-FIX vector had blood samples in which detectable levels of vector were observed for up to 1 week and harvested livers showed detectable levels of FIX expression. These results suggest that NAB formation can significantly impact vector genome transduction in the liver.

To understand how NAB-AAV complexes were cleared, in vitro experiments were set up using a murine hepatocyte cell line. Using flow cytometry, Fitzpatrick et al. showed that the NAB-AAV complexes were still gaining entry into the hepatocytes, however, no transduction was occurring. This meant the AAV capsid could still gain entry through internalization. This strategy helped to elucidate the role of anti-capsid NAB and showed its influence on liver gene transfer.

#### **4.1.3 Case study 3: In silico immunogenicity prediction**

The “deimmunization” of a biotherapeutic should be one of the first steps considered during drug development. Many in silico tool currently exist for various predictions, such platforms include; EpiVax, EpiBase, Biovia, NetMHCIIpan, and immune epitope database (IEDB), to name a few. A in silico tool recently described by Chen et al. utilizes a method of the machine-learning prediction tool for immunogenicity prediction based on MHC II antigen presentation [29]. It is generally agreed upon that current in silico algorithms predicts immunogenicity better for MHC I than for MHC II due to the viable length of the presented peptide. These algorithms generally use in vitro-binding affinity as a surrogate of potential MHC II peptide presentation. MARIA, the tool developed by this team, used peptides presented by APCs and identified using liquid chromatography (LC)-mass spectrometry (MS)/MS as a data training set in addition to predicted binding affinities. The author’s results showed that using the deep neural network trained data sets consistently provided better area-under-curves (AUCs) than did methods such as NetMHCIIpan from the immune epitope database (IEDB). To confirm the validity of the “true ligands,” 10 peptides were synthesized from predicted strong binding epitopes of mantle cell lymphomas (MCL). Using an MCL cell line, 9 of the 10 peptides were identified by MS as strong binders.



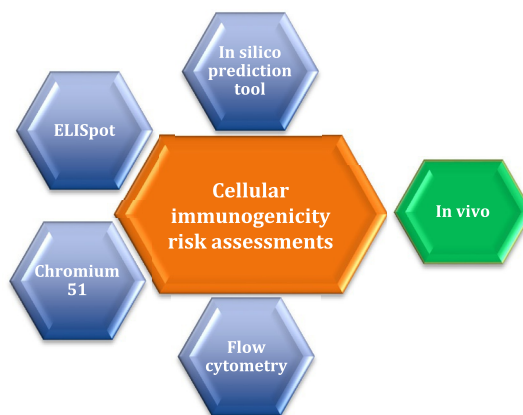
## 5 Cellular immunogenicity risk assessments

Potential cellular immunogenic risk factors include nonhuman/partial human sequences in amino acid structures in biotherapeutics, residual viral proteins from gene transduction process, gene editing associated deletions.

- For CAR (chimeric antigenic receptor) T-cell therapies, CARs are synthetic proteins consisting of various regions including the antigen-binding moiety or single-chain variable fragment (scFv) derived from human/nonhuman mAbs linked by a hinge/spacer and transmembrane sequences of co-stimulatory domains which are an intracellular part of CAR. The CAR structure may also contain unique nonhuman peptide sequences that could potentially be immunogenic. Such epitopes could come from a nonhuman scFv, fusion sites between different human CAR components, viral proteins, and any additional amino acid modifications to CAR [30]. The modification of CAR includes the addition of a safety switch derived from viral proteins, e.g., herpes simplex virus (HSV)-thymidine kinase (TK) [31].
- For gene therapy, the transgene encoding the protein of interest is encapsulated in the adeno-associated virus (AAV) vectors for its transfer into target cells. This viral capsid could be degraded and potentially be presented through MHC I on the cell surface. Capsid-specific CD8+ T cells have been identified as a major hurdle and potential source of immunotoxicity in human recipients of AAV gene transfer. These cytotoxic T lymphocytes (CTLs) can eliminate AAV-transduced cells affecting the efficacy of the gene therapy [32].
- Cell and gene therapy products are generated by the use of DNA editing techniques (CRISPR and TALEN) to modify surface-expressed receptor (CAR-T) or insertion of the transgene (gene therapy) for therapeutic usage. The use of these technologies could potentially leave nonhuman origin proteins (TALEN: construction-related proteins) or create novel immunogenic epitopes (CRISPR: gene editing associate deletions or insertions). These nonself-epitopes could be presented to CD8 T cells and could illicit cellular immunogenic response [9].

There are various ways by which the potential risk of a cellular immunogenic response can be assessed (Fig. 7). This can range from predicting the binding of peptide sequences to MHC I

**FIG. 7** Illustration of the various methods for cellular immunogenicity risk assessments, highlighted in blue or by in vivo analysis highlighted in green.





in silico or to using an artificial neuronal network to analyzing a full-system potential response in humanized mice. There are few in vitro approaches or potential in vivo tools to assess the immunogenic response from CD8 + T cells.

## 5.1 In silico prediction tool

The very first step would be the use of a prediction tool to assess amino acid sequences which can elicit an immune response via a presentation by MHC on the cell surface. MHC class I-binding prediction tools scan a protein's amino acid sequence to determine each sub-sequence's ability to bind a specific MHC class I molecule [16]. This tool will work to predict the IC50 of the binding interaction between the presented peptide/MHC I complex and the TCR on T cells. To characterize the interaction of peptides and various alleles of MHC I, the entire sequence of the biotherapeutic/CAR could be cleaved into identifying overlapping 8–11-mer peptides and running these sequences through one of the immune epitope database analysis methods like the artificial neural network (ANN) method. ANN is a type of machine-learning method which utilizes neuronal brain system inspired method for machine-learning and training. Once trained, they recognize the complicated peptide patterns and can predict the binding prediction for the input of 8–11-mer sequences [16, 33, 34].

This early prediction approach could potentially be used in early-stage discovery to not only assess potential immunogenicity and rank candidate selection but also for designing subsequent research-based biotherapeutic candidates with reduced immunogenic risk.

## 5.2 ELISpot

ELISpot assay is the gold standard to analyze the cytokines like TNF- $\alpha$  and IFN- $\gamma$  secreted by activated CD8+ T cells. ELISpot is a very sensitive assay and can detect a very small number of activated CD8+ T cells. Overlapping 9-mer amino acid sequences are generated from the vector sequences. These are added to PBMC from patient samples and then added to the ELISpot plates for IFN- $\gamma$ . CD8+ T cells specific for these peptides would be activated and secrete IFN- $\gamma$  and will form spots on the ELISpot plates. The output of spot-forming cells forms the basis for cellular immunogenicity assessment in comparison to a positive control, e.g., T cell-specific tetramer [13].

## 5.3 Chromium 51

Another in vitro method is a Chromium 51 ( $^{51}\text{Cr}$ ) release assay [35]. Target cells (CAR-T) could be radiolabeled with  $^{51}\text{Cr}$  and incubated with CD8+ cells. Once CD8+ cells are activated by the presentation of potentially immunogenic regions, their cytotoxic abilities will cause lysis of radiolabeled cells, thereby releasing  $^{51}\text{Cr}$  into the supernatant. This can be collected and analyzed either by gamma counter or mixed with a scintillation cocktail in a microplate (or dried on a LumaPlate) and counted in a liquid scintillation counter [36]. A similar approach could potentially be applied to gene therapy wherein target cells transduced with capsid/transgene, radiolabeled with  $^{51}\text{Cr}$  could be incubated with PMBC.

## 5.4 Flow cytometry

Flow cytometry (FCM) is another potential way to assess cellular immunogenicity. The focus of assessment lies in the measure of activation markers for CD8+ T cells, both on the surface and within the cells. Cell surface activation markers include CD69, CD80, CD25, CD107a, and CD107b. Lysosome-associated marker proteins (LAMP) family are markers of degranulation and migrate onto the surface when perforins are released by activated CD8+ T cells. These can also be measured in the flow assay as well [13].

This method lacks the sensitivity of ELISpot and could need multiple rounds of stimulation from immunogenic regions to amplify activation signals coming from proliferated CD8+ T cells that are quantifiable. Alternatively, cytokines like TNF- $\alpha$ , IFN- $\gamma$ , and interferon  $\beta$  secreted within T cells can be assessed by intracellular staining (ICS) and assessed through FCM.

Another approach within flow cytometry is using MHC I tetramers with fluorophores. These tetramers can be used to detect the activated CD8+ T cells. However, it comes with various limitations like the need for cloned and characterized MHC molecules, very low detection limit (which cannot be improved by simply using more cells), very high variability, etc. It, however, could be used in combination with other methods but does need further optimization [37].

## 5.5 In vivo analysis

There are very little-known information and published literature available for the in vivo analysis of cellular immunogenicity. One of the potential ways could be the use of humanized mice. This could be used as a final frontier in validating the in silico and in vitro immunogenicity risk prediction outcomes.

Humanizing immunodeficient mice by engrafting such mice with human cells or tissues is now a very popular method and has been used in various experimental and clinical studies [38]. Mice engineered in this way can functionally harbor and integrate human hematolymphoid cells and tissues. The idea is to transplant a functional human immune system into mice, which can then be used to evaluate immune responses to infections and vaccines.

The humanized mouse model could be dosed with 9-mer immunogenic peptides which are part of nonself-antigens from CAR constructs/transgene/capsid constructs and blood drawn at 24–48 h timepoints. Isolated PBMCs from blood samples can be analyzed by ELISpot and FCM to look at naïve responses from activated CD8+ T cells against these antigens. The plasma could also be analyzed for cytokines.

These mice can also be restimulated to look at late timepoints and assess adaptive cellular immunogenicity by similar in vitro assays mentioned above. This is a relatively uncharted technique as of now and will further evolve over time.

# 6 Mitigation strategy and case studies for cellular immunogenicity

## 6.1 Modification of AAV

The potential highly immunogenic regions of the AAV can be modified to reduce the cell-mediated immune response. There are several proposed changes to capsid and vector

genomes to improve gene transfer efficacy and possibly evade immunity [7]. To evade immunity, the primary objective would be to engineer these vectors to resist degradation by proteasomes. The resistance to degradation and subsequent conversion to 9-mer peptides would result in less presentation via MHC I and in turn, reduce the cellular immune response.

### **6.1.1 Case study: AAV2 Y—F engineered AAV2 capsid**

One example of a mitigation strategy for gene therapy included the use of an engineered AAV2 capsid (AAV2 Y—F) for transgene delivery. This case study from Martino et al. shows that the use of this engineered AAV vector minimizes in vivo targeting of transduced hepatocytes by capsid-specific T cells in comparison to the unmodified AAV2 vector [32]. Proteasome inhibition has been shown to reduce MHC I presentation of capsid antigen and prevent killing by CTLs and increasing the transduction/transgene expression from AAV vectors. This limited phosphorylation of capsid and vector performance improved likely due to reduced ubiquitination and inhibition of proteasomal degradation. In this case study, in vitro data clearly demonstrated a reduction in MHC I presentation and the killing of hepatocytes. This strategy, however, does not eliminate cellular immunogenicity completely. There is likely capsid degradation by other proteases like cathepsins which will still show an immune response [32].

## **6.2 Humanization of CAR construct**

The potential cellular immunogenicity by CAR-T cells could be minimized by modifying CAR constructs to have fully humanized regions [39]. This includes the scFv, fusion sites between various co-stimulating regions and the potential use of a safety switch. Using the in silico tools, the potentially immunogenic regions can be identified and validated using in vitro and in vivo assessment tools. Once confirmed, these could be eliminated (like safety switch) or modified to have fully human sequences thereby eliminated processing by MHC I and reduced activation of CD8+ T cells.

### **6.2.1 Case study: Reducing the immunogenicity of CAR construct**

Sommermeier et al. showed in a study of how using anti-CD19 fully humanized scFv and modifying fusion sites, a highly functional CAR with less immunogenicity could be generated. They screened highly diverse human VH and VL libraries to isolate human scFvs that recognized the same epitope of CD19 as murine FMC63-derived scFv with a similar affinity.

They also analyzed all 9-mer peptides located in the hinge and transmembrane fusion regions of the CD19-CARs for their potential to bind to human MHC I alleles using the netMHC prediction algorithm. A fusion site between the CD28 transmembrane and the 4-1BB costimulatory domain contained seven 9-mer peptide sequences with an affinity to several MHC class I molecules of <100 nM based on MHC-binding prediction. They modified this region to have only one predicted 9-mer peptide for HLA-A30:01 with an affinity of <100 nM. In vitro and in vivo performance of this modified CAR construct remained highly functional and comparable to the original construct. The authors concluded that CAR-T cells expressing humanized CD19 ScFv were more potent and expressed superior efficacy than T cells expressing the human CD19-CARs in eliminating lymphoma xenografts in NSG mice [30].

### 6.3 Lymphodepletion

This is a widely used strategy wherein chemotherapy drugs like fludarabine and cyclophosphamide are administered before CAR-T therapy. This conditioning and immune suppression are done not only for targeting of cellular immunogenicity but also for the overall management of toxicity and immune response to CAR-T cells. This helps in the initial prevention/reduction of any innate or naïve response to CAR-T cells [9].

## 7 Chapter summary

---

Immunogenicity can be summarized as the immune system reacting to nonself antigens, in this case, biotherapeutics. An immune response against a biotherapeutic can occur either by humoral-mediated or cellular mechanisms. The response can have a major impact on its ADME properties, efficacy, or even cause adverse reactions. A humoral response can lead to the formation of ADA which can be associated with altered clearance and decreased efficacy. A cellular immune response can lead to reduced efficacy, increased side effects, and additional toxicities. The immune response to biotherapeutics not only reduces the efficacy of these therapies but also places a big question mark on safety. As new biotherapeutic modalities evolve, researchers need to come up with new strategies for assessing and reducing immunogenicity earlier in drug development. Regulatory authorities are stressing the utmost importance on immunogenicity assessment and making this an essential part of the approval process.

As we have seen in this chapter, predicting and assessing immunogenicity and including it as a part of drug development is challenging and emergent. As the therapies get more and more personalized, i.e., cell and gene therapies, immunogenicity risk will be a key aspect in the approval process. Not only is it important for achieving success rates in the approval process but also in helping to make the next-generation molecules safer for patients. As researchers focus on these assessments early in the drug development process, this will help in reducing unforeseen delays ultimately benefiting unmet patient needs. Overall strategies have been discussed for preclinical assessment of immunogenicity. Additionally, case examples have been presented showing the uses of these strategies. To lower a biotherapeutic agent's potential immunogenicity risk, it is important to have an early strategy involving a multitiered approach.

### Acknowledgments

Insight and support for this chapter were provided by Cindy Xia, Hyelim Cho, Swapan Chowdhury, and Robert Ogert from the global DMPK and nonclinical regulatory writing and submissions groups at Takeda Pharmaceuticals International Co.

### References

- [1] A. Kuriakose, et al., Immunogenicity of biotherapeutics: causes and association with posttranslational modifications, *J. Immunol. Res.* 2016 (2016) 1298473, <https://doi.org/10.1155/2016/1298473>.

- [2] G. Shankar, et al., Assessment and reporting of the clinical immunogenicity of therapeutic proteins and peptides—harmonized terminology and tactical recommendations, *AAPS J.* 16 (4) (2014) 658–673, <https://doi.org/10.1208/s12248-014-9599-2>.
- [3] S.N. Shishido, et al., Humoral innate immune response and disease, *Clin. Immunol. (Orlando, FL.)* 144 (2012) 142–158, <https://doi.org/10.1016/j.clim.2012.06.002>.
- [4] M. Wieczorek, et al., Major histocompatibility complex (MHC) Class I and MHC class II proteins: conformational plasticity in antigen presentation, *Front. Immunol.* 8 (2017) 292, <https://doi.org/10.3389/fimmu.2017.00292>.
- [5] M. Krishna, S.G. Nadler, Immunogenicity to biotherapeutics—the role of anti-drug immune complexes, *Front. Immunol.* 7 (2016) 21, <https://doi.org/10.3389/fimmu.2016.00021>.
- [6] J. Kuby, *Immunology*, W.H. Freeman and Company, New York, 1998, pp. 357–412.
- [7] P. Colella, G. Ronzitti, F. Mingozzi, Emerging issues in AAV-mediated in vivo gene therapy, *Mol. Ther. Meth. Clin. Dev.* 8 (2018) 87–104 (gene therapy immunogenicity).
- [8] C.H. Lamers, R. Willemsen, P. van Elzakker, S. van Steenbergen-Langeveld, M. Broertjes, J. Oosterwijk-Wakka, et al., Immune responses to transgene and retroviral vector in patients treated with ex vivo-engineered T cells, *Blood* 117 (1) (2011) 72–82 (anti-CAIX).
- [9] B. Gorovits, A. Clements-Egan, M. Birchler, M. Liang, H. Myler, K. Peng, et al., Pre-existing antibody: biotherapeutic modality-based review, *AAPS J.* 18 (2) (2016) 311–320 (Boris CAR-T paper).
- [10] J.W. Yewdell, J.R. Bennink, Immunodominance in major histocompatibility complex class I-restricted T lymphocyte responses, *Annu. Rev. Immunol.* 17 (1) (1999) 51–88 (peptide presentation and activation of CD8 cells).
- [11] M.H. Andersen, D. Schrama, P. Thor Straten, J.C. Becker, Cytotoxic T cells, *J. Invest. Dermatol.* 126 (1) (2006) 32–41 (CD8 activation).
- [12] C.A. Janeway Jr., P. Travers, M. Walport, M.J. Shlomchik, The major histocompatibility complex and its functions, in: *Immunobiology: The Immune System in Health and Disease*, fifth ed., Garland Science, 2001 (MHC allele distribution).
- [13] S. Paul, D. Weiskopf, M.A. Angelo, J. Sidney, B. Peters, A. Sette, HLA class I alleles are associated with peptide-binding repertoires of different size, affinity, and immunogenicity, *J. Immunol.* 191 (12) (2013) 5831–5839 (MHC I binding).
- [14] G.F. Gao, Z. Rao, J.I. Bell, Molecular coordination of  $\alpha\beta$  T-cell receptors and coreceptors CD8 and CD4 in their recognition of peptide-MHC ligands, *Trends Immunol.* 23 (8) (2002) 408–413 (basics of CD8-MHC interactions).
- [15] J. Sun, D.J. Leahy, P.B. Kavathas, Interaction between CD8 and major histocompatibility complex (MHC) class I mediated by multiple contact surfaces that include the alpha 2 and alpha 3 domains of MHC class I, *J. Exp. Med.* 182 (5) (1995) 1275–1280 (CD8-MHC I interactions).
- [16] F. Perdomo-Celis, N.A. TABORDA, M.T. Rugeles, CD8+ T-cell response to HIV infection in the era of antiretroviral therapy, *Front. Immunol.* 10 (2019) 1896 (CD8 HIV, basics of CD8).
- [17] FDA, Immunogenicity Testing of Therapeutic Protein Products—Developing and Validating Assays for Anti-Drug Antibody Detection, FDA, 2019.
- [18] EMA, in: EMA (Ed.), *Guideline on Immunogenicity assessment of therapeutic proteins*, 2017.
- [19] R. Johnson, W. Jiskoot, Models for evaluation of relative immunogenic potential of protein particles in biopharmaceutical protein formulations, *J. Pharm. Sci.* 101 (2012) 3586–3592.
- [20] V. Brinks, D. Weinbuch, M. Baker, Y. Dean, P. Stas, S. Kostense, B. Rup, W. Jiskoot, Preclinical models used for immunogenicity prediction of therapeutic proteins, *Pharm. Res.* 30 (2013) 1719–1728.
- [21] V. Brinks, W. Jiskoot, H. Schellekens, Immunogenicity of therapeutic proteins: the use of animal models, *Pharm. Res.* 28 (2011) 2379–2385.
- [22] V. Bi, V. Jawa, M.K. Joubert, A. Kaliyaperumal, C. Eakin, K. Richmond, O. Pan, J. Sun, M. Hokom, T. J. Goletz, J. Wypych, L. Zhou, K. Ba, L.O. Narhi, T. Arora, Development of a Human Antibody Tolerant Mouse Model to Assess the Immunogenicity Risk Due to Aggregated Biotherapeutics, *J. Pharm. Sci.* 102 (2013) 3545–3555.
- [23] J. Bessa, S. Boeckle, H. Beck, T. Buckel, S. Schlicht, M. Ebeling, A. Kiialainen, A. Koulov, B. Boll, T. Weiser, T. Singer, A.G. Rolink, A. Iglesias, The immunogenicity of antibody aggregates in a novel transgenic mouse model, *Pharm. Res.* 32 (2015) 2344–2359.
- [24] C.M. Ng, K.M. Loyet, S. Iyer, P.J. Fielder, R. Deng, Modeling approach to investigate the effect of neonatal Fc receptor binding affinity and anti-therapeutic antibody on the pharmacokinetic of humanized monoclonal anti-tumor necrosis factor- $\alpha$  IgG antibody in cynomolgus monkey, *Eur. J. Pharm. Sci.* 51 (2014) 51–58.

- [25] Anon. Cancer drugs dominate top 10 best-selling drugs in 2018. <https://www.medscape.com/viewarticle/910600>, 2019. Accessed 10 January 2019.
- [26] G.M. Bartelds, C.L.M. Krieckaert, M.T. Nurmohamed, et al., Development of antidrug antibodies against adalimumab and association with disease activity and treatment failure during long-term follow-up, *JAMA* 305 (14) (2011) 1460–1468, <https://doi.org/10.1001/jama.2011.406>.
- [27] M.E. Nance, D. Duan, Development of next-generation muscle gene therapy AAV vectors, in: *Muscle Gene Therapy*, Springer, Cham, 2019, pp. 193–206.
- [28] Z. Fitzpatrick, C. Leborgne, E. Barbon, E. Masat, G. Ronzitti, L. Van Wittenberghe, F. Jouen, Influence of pre-existing anti-capsid neutralizing and binding antibodies on AAV vector transduction, *Mol.r Ther. Meth. Clin. Dev.* 9 (2018) 119–129.
- [29] B. Chen, M.S. Khodadoust, N. Olsson, et al., Predicting HLA class II antigen presentation through integrated deep learning, *Nat. Biotechnol.* 37 (2019) 1332–1343, <https://doi.org/10.1038/s41587-019-0280>.
- [30] D. Sommermeyer, T. Hill, S.M. Shamah, A.I. Salter, Y. Chen, K.M. Mohler, S.R. Riddell, Fully human CD19-specific chimeric antigen receptors for T-cell therapy, *Leukemia* 31 (10) (2017) 2191 (humanized CAR).
- [31] K. Newick, E. Moon, S.M. Albelda, Chimeric antigen receptor T-cell therapy for solid tumors, *Molecular Therapy-Oncolytics* 3 (2016) 16006 (HSV-TK immunogenicity).
- [32] A.T. Martino, E. Basner-Tschakarjan, D.M. Markusic, J.D. Finn, C. Hinderer, S. Zhou, et al., Engineered AAV vector minimizes in vivo targeting of transduced hepatocytes by capsid-specific CD8+ T cells, *Blood* 121 (12) (2013) 2224–2233 (Engineered AAV and CD8 response).
- [33] M. Andreatta, M. Nielsen, Gapped sequence alignment using artificial neural networks: application to the MHC class I system, *Bioinformatics* 32 (4) (2015) 511–517 (in silico).
- [34] S. Buus, S.L. Lauemøller, P. Worning, C. Kesmir, T. Frimurer, S. Corbet, et al., Sensitive quantitative predictions of peptide-MHC binding by a ‘query by committee’ artificial neural network approach, *Tissue Antigens* 62 (5) (2003) 378–384 (in silico ANN).
- [35] P. Baumgaertner, D.E. Speiser, P. Romero, N. Rufer, M. Hebeisen, Chromium-51 (51Cr) release assay to assess human T cells for functional avidity and tumor cell recognition, *Bio-Protocol* 6 (2016) 16 (CR51).
- [36] Chromium 51 Assay. n.d. <https://www.perkinelmer.com/lab-products-and-services/application-support-knowledgebase/radiometric/chromium-51-release-assay.html>.
- [37] S. Sims, C. Willberg, P. Klenerman, MHC–peptide tetramers for the analysis of antigen-specific T cells, *Expert Rev. Vaccines* 9 (7) (2010) 765–774.
- [38] J. Snyder, O. Duchamp, K. Paz, P. Sathyan, Role of companies and corporations in the development and utilization of PDX models, in: *Patient Derived Tumor Xenograft Models*, Academic Press, 2017, pp. 409–426 (humanized mouse).
- [39] R. Purwar, A. Dwivedi, A. Karulkar, S. Ghosh, A. Rafiq, Lymphocytes in cellular therapy: functional regulation of CAR T cells, *Front. Immunol.* 9 (2018) 3180.



PART IV

# Translational sciences



# Application of genetically modified rodent models in drug discovery and development for translation of clinical ADME properties

Robert S. Jones<sup>a</sup>, Justin Q. Ly<sup>a</sup>, Jae H. Chang<sup>b</sup>

<sup>a</sup>Drug Metabolism and Pharmacokinetics, Genentech, South San Francisco, CA, United States

<sup>b</sup>Preclinical Development, ORIC Pharmaceuticals, South San Francisco, CA, United States

## 1 Introduction

As discussed in many other chapters in this book, the science behind discovering new drugs is continually evolving. What was considered standard practice yesterday may no longer be the most appropriate approach today as newfound knowledge and breakthroughs give rise to paradigm shifts which elevate our ability to tackle challenges associated with drug discovery and development. This pursuit of reinventing our thinking helps mitigate risks in clinical trials which ultimately, brings us closer to discovering drugs that are safer and more effective in patients. However, despite making substantial advancements, many knowledge gaps remain. In particular, one of the major obstacles that impede drug research is how to best utilize preclinical data to maximize the chance of success in the clinic. For example, how appropriate are in vitro subcellular fractions in evaluating potential clinical drug-drug interactions (DDI)? How relevant are in vitro experiments and in vivo pharmacokinetic (PK) studies in preclinical models to estimate human PK parameters? Moreover, how predictive are toxicology experiments in preclinical models to gauge potential safety liabilities in humans? In order to increase the confidence of translating preclinical data to the clinic, the conduct and interpretation of preclinical experiments, as well as their assumptions, are constantly being tested. Concomitantly, new modalities are being explored as additional opportunities arise with technological innovation. In the field of absorption, distribution, metabolism, and excretion (ADME), the fruits of these efforts have been paradigm shifts which have led to the

development of new tools such as physiologically based pharmacokinetic (PBPK) modeling, which incorporate mathematical modeling in the analysis of assorted datasets. Indeed, great strides have been made to bridge these gaps, but scientific progress, almost by definition, creates additional knowledge gaps which require further attention to restore confidence in our ability to discover better drugs. For instance, cytochrome P450s (CYPs) were the focal point of xenobiotic metabolism until metabolizing enzymes such as UDP-glucuronosyltransferases (UGTs) or aldehyde oxidase (AO) began to occupy a larger proportion of drug metabolism. Similarly, assumptions around the mechanism of drug elimination became confounded by drug transporters as experiments showed that drug transporters are not only able to excrete drugs out of the body unchanged, but also to impact the activity of drug-metabolizing enzymes (DMEs) [1]. Consequently, renewed perspectives and tools are constantly needed to enable continued integration to address the evolving science. One of these promising tools are novel animal models which include genetically modified models that express certain human protein(s) or lack expression of certain endogenous protein(s), and models whose organs, such as the liver, have been reconstructed in an attempt to mimic human hepatic function. This chapter will describe the assorted types of novel animal models that are currently available and illustrate how they have been utilized in drug research to address ADME-related questions.

## 1.1 The rise of novel animal models in drug research

In drug research, there is a perpetual struggle around balancing costs/resources and ethics with ensuring smooth and timely progression of a new chemical entity (NCE) through the development life cycle. For example, the fastest way to determine the human PK parameters would be to directly dose the NCE in humans. However, while this approach may satisfy the question around human PK, it is not a reasonable option as it may not only be cost prohibitive, but ethically, NCEs cannot be dosed until their safety has been properly characterized to ensure the wellbeing of healthy volunteers and patients in the clinical trials. A different extreme example is to estimate human PK parameters using only human liver microsomes. While this approach will be exceedingly cost-effective, it is not suitable in adequately characterizing the ADME properties of the NCE to make a thorough assessment of human PK due to the ambiguity in scaling the *in vitro* parameters to humans *in vivo*. Ideally, preclinical *in vivo* models which mirror humans would be a powerful tool to identify and to investigate risks associated with the NCE so that an ideal drug candidate can be found. Unfortunately, the assumption that preclinical animals represent humans is aspirational at best. In fact, *in vivo* preclinical models are not always useful in estimating human PK parameters, in part because there can be striking differences in the expression and activity of DMEs and transporters across species as well as their regulatory pathways. For example, the number of putatively functional full-length CYP genes in human is 57, whereas there are 102 genes in mice and 54 genes in dogs [2]. Accordingly, when compared with humans, the total content determined with spectral analysis of P450 protein was similar in dogs [3], but was higher in mice [4]. When teasing out individual CYP families, there are certain subfamilies such as CYP1A and CYP2E which consist of the same number of isoforms expressed across multiple species (i.e., CYP1A1 and CYP1A2 and CYP2E1); but for other subfamilies such as CYP3A, the number of isoforms expressed varies across species, where there are four isoforms in humans, six

isoforms in mice, five isoforms in rats, two isoforms in dogs, and two isoforms in monkeys [5]. This diversity in expression also likely contributes to differences in the function of CYPs. The metabolism of aminopyrine and benzphetamine in human liver microsomes was approximately two- and five-fold higher than in monkey liver microsomes, respectively, whereas the metabolism of 4-nitroanisole and benzo[a]pyrene was two- to three-fold lower than in monkey liver microsomes, respectively [6]. In the intestine, the metabolism of CYP3A probe substrate testosterone, CYP2D probe substrate bufuralol, and CYP2C probe substrate tolbutamide in human intestinal microsomes was comparable in monkey intestinal microsomes, but was markedly higher in dog intestinal microsomes [7]. Beyond CYPs, species differences in UGT activity have also been demonstrated [8], particularly with N-glucuronidation [9–11]. In addition to DMEs, drug transporters have also demonstrated species dependence on expression and function. One of the most studied drug transporters is P-glycoprotein (Pgp). It is encoded by one ABCB1/Abcb1 gene in humans, monkeys, and dogs, but in rodents, there are two paralogous genes Abcb1a and Abcb1b which exhibit complementary patterns of expression. Protein quantitation determined by LC-MS/MS showed that while the expression of Pgp in the brain was similar between humans [12] and dogs [13], the levels were two- to three-fold higher in the mice [14] and rats [15], respectively. Thus far, the functional differences of Pgp across various species are not extensive as observed with the metabolizing enzymes. However, differences do exist as exemplified by *in vitro* investigations in LLC-PK1 cells transfected with Pgp from various species which reported that human Pgp correlated the best with monkeys, but less with dogs [16]. In fact, in the MDCK cell monolayers which are commonly employed to assess permeability, one group has shown that the active efflux of approximately a third of the molecules in their test set is absolved when endogenously expressing dog Pgp is knocked out [17]. Finally, in addition to metabolizing enzymes and drug transporters, species differences in nuclear hormone receptors which regulate expression of ADME-related genes have been reported. Pregnane X receptor (PXR) is one of the more well-studied nuclear receptors that is important in ADME, as it has been shown to upregulate CYP activity. However, the extent of activity by various PXR ligands varies considerably across multiple species. For example, rifampin is a strong activator of PXR in humans, but not in rodents, whereas dexamethasone is a strong activator of PXR in rodents, but not in humans [18]. Consequently, CYP3A activity in humans is greatly augmented with rifampin compared with dexamethasone, whereas the impact of dexamethasone on Cyp3a activity is much higher in rats than in humans [19]. Therefore, humanized animal models which express human proteins may provide great value in projecting human PK parameters.

In addition to investigating human PK parameters, novel animal models such as knockout (KO) models may be useful in aiding the study of mechanisms associated with drug ADME. For example, in wild-type (WT) animals, Cyp2b10 and Cyp3a11 protein expression increased when treated with phenobarbital. Upregulation with phenobarbital was also observed in the PXR KO animals. However, the inductive effect of phenobarbital was markedly reduced in the constitutive androstane receptor (CAR) KO model, indicating that phenobarbital is a ligand for CAR rather than both CAR and PXR [20]. In another example, the Mdr1a KO mouse model was utilized to demonstrate the role of Pgp in the distribution (particularly into the blood-brain barrier) and elimination resulting in increased neurotoxic sensitivity to ivermectin and vinblastine [21]. In addition to being able to elucidate specific ADME liabilities, understanding the role of ADME-related protein(s) in the disposition of a compound further enables investigation into other scientific questions.

Mice have typically been the species of choice to study mammalian genetics for both practical and scientific reasons. Practically, mice are relatively easy to handle due to their size and domiciliary nature. In addition, the short generation combined with delivery of large litters facilitates the study of multiple generations with the ability to provide an abundant number of animals in a short amount of time. Scientifically, the advantages of working with mice fueled innovative approaches to manipulate the murine genome. Importantly, the breakthrough in DNA sequencing technology paved the path not only to unravel the entire human, but also the murine genome, to reveal that while there are disparities, the murine genome is very similar to the human genome [22]. The objective of this chapter is to provide an overview of various genetically modified animal models mostly in rodents, especially those used in the study of DMEs and transporters.

## 2 Knockout animal models

With the advent of gene-editing technologies such as zinc finger and transcription activator-like effector nucleases (ZFN and TALEN), the ability to generate genetic KO animal models has supported the research and early development of ADME properties of NCEs. These models have not only allowed the investigation of DME and drug transporter contribution to ADME, but also allowed for an understanding of the differences between preclinical species and humans in terms of substrate selectivity, expression, and activity. The models described in this section are intended to serve as case examples of what researchers have used to investigate the contribution of phase I/II DMEs and drug transporters in drug development pertaining to the ADME space. An expanded summary of these rodent models is depicted in Tables 1–3. In using these models, elucidating the impact of enzyme/transporter(s) in the biotransformation, clearance, DDI, and distribution of drugs has not always been successful, and the source of the discrepancy between these preclinical species and humans remains challenging.

Before reviewing the utility of genetically modified rodent models developed for the investigation of drug ADME, it is worthwhile to note that there are rodent models available that exhibit an innate deficiency in well-studied DMEs and transporters. For example, Ugt2b2 activity has been shown to be deficient in Wistar and Fischer 344 (F344) rats, and exhibited reduced glucuronidation activity, specifically for androsterone compared with other strains such as Sprague-Dawley and Long-Evans rats [112–114]. Despite the lower Ugt2b2 activity, Wistar and F344 are not typically regarded as abnormal strains, and have been employed in traditional ADME and toxicology studies. More interesting are rodent strains whose inherent mutations recapitulate some of the phenotypes associated with human disease states. For example, Dubin-Johnson syndrome is a rare condition characterized by jaundice resulting from mutation associated with multidrug resistance associated protein 2 (MRP2). Loss of MRP2 function prevents excretion of conjugated bilirubin into the bile, which instead accumulates in the hepatocytes. Deficiency in Mrp2 has been described in Eisai (EHBR) and transport-deficient mutant (TR-) rat strains, and they have been used as a model for Dubin-Johnson syndrome [115, 116]. These strains are characterized by chronic conjugated hyperbilirubinemia resulting from obstruction of hepatobiliary excretion of conjugated bilirubin and multivalent organic anions. Similarly, a symptom of Crigler-Najjar syndrome is severe hyperbilirubinemia due to the toxic buildup of

**TABLE 1** Phase I/II drug-metabolizing enzyme knockout rodent models.

Enzyme(s)	Species	Purpose	Ref.(s)
Cyp1a1	M	AhR-mediated regulation	[23]
Cyp1a2	M	CYP1A2-mediated metabolism	[24]
Cyp1b1	M	PAH-activation and toxicity	[25]
Cyp1a1/1b1 Cyp1a2/1b1	M	Benzo[a]pyrene detoxification	[26]
Cyp3a1/2	R	CYP3A-mediated elimination	[27]
Cyp3a	M	Midazolam metabolism	[28, 29]
Cyp2c	M	CYP2C9-mediated metabolism	[30]
		Species differences in bile acid metabolism	[31]
Cyp2c/2d/3a	M	Metabolite formation and drug pharmacokinetics	[32]
Cyp2e1	M	Hepatotoxicity of acetaminophen	[33]
Nat1	M	Nat's role in mediating insulin sensitivity	[34]
Nat2	M	Tissue expression and localization of Nat1 and Nat2 in mice	[35, 36]
Nat1/2	M	Characterization of the role of N-acetylation in arylamine-induced toxicity	[37]
Ugt1	M	Development of a mouse model resembling symptoms of hyperbilirubinemia	[38]
Ugt2	M	Glucuronidation of bisphenol A	[39]
Ugt2b2	R	Metabolism of triiodothyronine	[40]
Gstp	M	Hepatotoxicity of acetaminophen	[41]
Sult1e1	M	Estrogen metabolism and regulation	[42, 43]

Abbreviations: M, mouse, R, rat.

**TABLE 2** ABC transporter knockout rodent models.

Name(s)	Gene(s)	Species	Purpose	Ref.(s)
Pgp (Mdr1)	<i>Abcb1a</i>	M	BBB penetration and drug absorption	[21]
	<i>Abcb1a/b</i>	M	Drug interactions with Pgp	[44]
			Activity of the hypothalamic-pituitary-adrenocortical system	[45]
			Pharmacokinetics of fexofenadine	[46]
			Contribution to hepatic steatosis and obesity	[47]
	<i>Abcb1a/b</i>	R	Function of Pgp in vivo in rat	[48]
Mrp1	<i>Abcc1</i>	M	Glutathione efflux in brain astrocytes	[49]
			Endothelial progenitor cell function and survival	[50]

Continued

TABLE 2 ABC transporter knockout rodent models—cont'd

Name(s)	Gene(s)	Species	Purpose	Ref.(s)
Mrp2	<i>Abcc2</i>	M	Biliary excretion of food-derived carcinogens and anticancer drugs	[51]
Mrp3	<i>Abcc3</i>	M	Hepatic efflux of drug sulfate and glucuronide metabolites	[52]
			Protection from diclofenac toxicity	[53]
			Pharmacokinetics of morphine	[54]
Mrp4	<i>Abcc4</i>	M	Hepatic efflux of drug sulfate metabolites	[52]
			Renal efflux of antivirals	[55]
			Efflux of camptothecin analogues in the brain	[56]
Mrp2/3	<i>Abcc2/3</i>	M	Hepatobiliary disposition of fexofenadine	[57]
			Elimination of methotrexate	[58]
Bcrp	<i>Abcg2</i>	M	Sulfasalazine absorption and elimination	[59] [60]
			Disposition of phytoestrogens	[61]
			Pharmacokinetics of various probe substrates	[62]
Mdr1, Mrp1	<i>Abcb1a/b</i> , <i>Abcc1</i>	M	Effect of cigarette smoke on inflammation	[63]
Mdr1, Mrp2/3	<i>Abcb1a/b</i> , <i>Abcc2/3</i>	M	Pharmacokinetics of etoposide	[64]
Bcrp1, Mdr1a/1b	<i>Abcg2</i> , <i>Abcb1a/b</i>	M	Pharmacokinetics of erlotinib	[65]

Abbreviations: M: mouse, R: rat.

Adapted from N. Shin, J.-H. Oh, Y.-J. Lee, Role of drug transporters: an overview based on knockout animal model studies, *J. Pharm. Invest.* 45 (2) (2015) 101–114.

bilirubin. However, unlike Dubin-Johnson syndrome, the root cause of Crigler-Najjar syndrome is a mutation associated with UGT1A1 [117]. As with patients diagnosed with Crigler-Najjar syndrome, the Wistar mutant strain Gunn rats lack Ugt1a activity due to a frame-shift and premature stop codon arising from natural deletion of a single guanosine base resulting in unconjugated hyperbilirubinemia as a consequence of deficiency in bilirubin glucuronidation [118]. Gunn rats have been a valuable model to further probe into the mechanism of Crigler-Najjar syndrome [119]. Both of these models have served as useful tools to study the effect of hyperbilirubinemia on metabolizing enzyme and drug transporter expression, function, and regulation, while also providing insight into the toxicology and disposition of bilirubin. In addition, these models have been used to tease out the contribution of ADME proteins on the disposition of drugs. For example, the biliary excretion of E3040-glucuronide and E3040-sulfate metabolites was significantly decreased using the EHBR model compared to normal rats [120], whereas the interplay of Ugt enzymes and Mrp2 was demonstrated with

**TABLE 3** SLC transporter knockout mouse models.

<b>Name(s)</b>	<b>Gene(s)</b>	<b>Species</b>	<b>Purpose</b>	<b>Ref.(s)</b>
Oct1	<i>Slc22a1</i>	M	Hepatic uptake and intestinal excretion of organic cations	[66]
			Genetic variation in Oct1 and metformin pharmacodynamics	[67]
			Thiamine transport and regulation of hepatic steatosis	[68] [69]
Oct2	<i>Slc22a2</i>	M	Enhancement of antibody-secreting cell differentiation	[70]
			Platinum drug-induced toxicity	[71–73]
Oct1/2	<i>Slc22a1/2</i>	M	Renal secretion of organic cations	[74]
			Metformin pharmacokinetics	[75]
			MPTP-induced dopaminergic toxicity	[76]
Oct3	<i>Slc22a3</i>	M	Decreased anxiety	[77]
			Modulation of histamine and regulatory T cells	[78]
			Pharmacokinetics of metformin	[79]
Octn1	<i>Slc22a4</i>	M	Systemic and intestinal exposure of ergothioneine	[80]
			Gastrointestinal absorption of metformin	[81]
Octn2	<i>Slc22a5</i>	M	Accumulation of carnitine in placenta and fetus	[82]
Oat1	<i>Slc22a6</i>	M	Renal secretion and plasma accumulation of organic anions	[83]
			Modulation of mercury-induced kidney injury	[84]
			Renal toxicity of tenofovir	[85]
Oat3	<i>Slc22a8</i>	M	Organic anion transport in kidney and choroid plexus	[86]
			Pharmacokinetics of penicillin G	[87]
			Clearance of methotrexate	[88]
			Global metabolic and signaling pathways	[89]
Oat1/3	<i>Slc22a6/8</i>	M	Involvement of handling uremic toxins (“chemical” double knockout)	[90]
Pept1	<i>Slc15a1</i>	M	Intestinal permeability of glycylsarcosine	[91]
			Intestinal permeability of valacyclovir	[92]
			Oral absorption of cefadroxil	[93]
Pept2	<i>Slc15a2</i>	M	Disposition of glycosarcosine in kidney and choroid plexus	[94]
			Pharmacokinetics of cefadroxil	[95]
			Endogenous and exogenous carnosine disposition	[96]

*Continued*



TABLE 3 SLC transporter knockout mouse models—cont'd

Name(s)	Gene(s)	Species	Purpose	Ref.(s)
Mate1	<i>Slc47a1</i>	M	Pharmacokinetics and toxicity of metformin	[97] [98]
			Renal pharmacokinetics of cephalexin	[99]
			Lamivudine-indavir DDI	[100]
Oatp1a1	<i>Slco1a1</i>	M	Absorption of deoxycholic acid	[101]
			Alteration of intestinal bacteria and bile acid metabolism	[102]
Oatp1a4	<i>Slco1a4</i>	M	Distribution of drugs across the blood-brain barrier	[103]
			Characterization of null-mice metabolic profile	[104]
Oatp1b2	<i>Slco1b2</i>	M	Pravastatin and rifampin disposition	[105]
			Pharmacokinetics of statins	[106]
			Hepatic uptake of unconjugated bile acids	[107]
Oatp1b	<i>Slco1b</i>	M	Pharmacokinetics of hydroxyurea	[108]
Oatp1a/b	<i>Slco1a/b</i>	M	Hepatic handling of bilirubins, bile acids, and drugs	[109]
			Pharmacokinetics of statins	[110, 111]

Abbreviations: M, mouse.

Adapted from N. Shin, J.-H. Oh, Y.-J. Lee, Role of drug transporters: an overview based on knockout animal model studies, *J. Pharm. Invest.* 45 (2) (2015) 101–114.

mycophenolic acid in the TR-model, a mutant strain of Wistar rats lacking Mrp2 [121]. Besides DMEs and drug transporters, naturally occurring animal models have been employed to study other pharmacokinetic-relevant parameters. For example, while their total protein levels are not altered, Nagase analbuminemic rats (NAR) exhibit deficient levels of albumin in serum and organs [122–124]. The NAR model has been used to demonstrate the free drug hypothesis in that while the total exposure of mycophenolic acid was 29-fold higher in the wild-type animals compared with NAR, the free exposure was comparable [124]. In addition, studies showed the interplay between albumin and organic anion-transporting polypeptides (Oatps), as hepatic uptake of pitavastatin was reduced in NAR animals [125]. While there are several other mutant rodent models available for commercial use, the utility of genetically modified KO animal models has allowed researchers to investigate the overall contribution of particular DMEs or drug transporters to drug ADME. The focus of this section will go beyond the naturally occurring genetic models to highlight instances of how genetically designed animal models have impacted the study of ADME-related properties, as well as outline the advantages and disadvantages of using such models.

*Cyp3a*: There are four isoforms which constitute the CYP3A subfamily. Among them, CYP3A4 is the most prominent isoform involved in the biotransformation of the majority of drugs. To study the impact of CYP3A on ADME properties of drugs, a *Cyp3a* KO mouse model was generated by deleting eight full-length *Cyp3a* genes and three pseudogenes [28].

When compared with the phenotype of the WT animals, the Cyp3a KO animals were viable and fertile without obvious abnormalities. To characterize the effect of deleting Cyp3a on drug ADME properties, the metabolism and disposition of midazolam was compared between WT and Cyp3a KO models in vitro using hepatic and intestinal microsomal preparations, and in vivo following IV administration in intact animals [28, 29]. Midazolam was initially chosen as the model probe substrate because the principal aim of the Cyp3a KO experiments was to mirror the clinical trials as midazolam is one of the preferred probe substrates that is employed in the clinic to assess CYP3A4-related DDIs [126]. Interestingly, in both in vitro and in vivo studies, midazolam metabolism was not meaningfully different between the WT and Cyp3a KO models. Further characterization of the Cyp3a KO model showed that Cyp2c mRNA and protein expression were upregulated [29]. In addition, subsequent studies showed that there is a significant contribution from murine Cyp2c on the metabolism of midazolam [127]. Taken together, these results indicate that midazolam may not be an appropriate substrate to assess human CYP3A4 activity in the Cyp3a KO model. This finding was unfortunate as many clinical drug interaction studies involving CYP3A that are available are conducted with midazolam as the probe substrate. In addition to midazolam, triazolam, which is an analogue of midazolam, is another CYP3A probe substrate highlighted in the FDA guidance. Perloff and colleagues showed that, unlike midazolam, triazolam was more specific for Cyp3a in the mouse [127]. While the database for clinical drug interactions comprising triazolam is smaller than that with midazolam, triazolam offered a reasonable alternative probe substrate for Cyp3a. For instance, triazolam was used as a probe substrate to demonstrate the effect of ketoconazole in the inhibition of Cyp3a and gefitinib in the direct stimulation of Cyp3a with Cyp3a KO and humanized CYP3A transgenic models [128].

One major advantage of the Cyp3a KO model is that it can be used to explore the mechanism of a particular ADME-related phenomenon. For example, atorvastatin is an HMG-CoA reductase inhibitor which is extensively metabolized in the liver by CYP3A. However, its metabolism is gated by hepatic uptake mediated by OATPs. Clinical drug interaction studies showed that inhibition of OATPs by rifampin had a greater impact on atorvastatin plasma concentration than inhibiting CYP3A with itraconazole. Studies conducted with Cyp3a KO and Oatp KO models were valuable not only in recapitulating the clinical DDI profile, but also in providing insight into the differential impact of Cyp3a and Oatps on the plasma and liver concentration of atorvastatin. Specifically, Oatps exhibited a greater impact on the systemic concentration of atorvastatin than Cyp3a, whereas Cyp3a exhibited a greater impact on the liver concentration than Oatps, suggesting that there is a significant drug interaction attributed to both processes, but that DDIs involving Cyp3a may not be apparent due to minimal change associated with the plasma compartment [129].

*Cyp2d*: Besides CYP3A4, CYP2D6 is another important CYP isoform responsible for the metabolism of drugs across many therapeutic areas. One well recognized characteristic of CYP2D6 is that it is associated with genetic polymorphisms exhibiting assorted phenotypes which are categorized as poor, intermediate, extensive, and ultrarapid metabolizers. Accordingly, the disposition of drugs whose elimination is dependent on CYP2D6 can vary significantly, which can compromise the efficacy and/or the toxicity profile of the drug, and may require dose adjustment. An example is with tamoxifen, which has been linked with a higher rate of cancer recurrence for patients who are poor CYP2D6 metabolizers, as the conversion of

tamoxifen to the active metabolite endoxifen is reduced [130, 131]. To better understand how the overall disposition of drugs may be affected by highly variable enzymes such as CYP2D6, a Cyp2d KO mouse model was generated by deleting nine functional murine Cyp2d genes. As observed with Cyp3a KO animals, Cyp2d KO animals were viable and fertile without obvious abnormalities [132]. In addition, Cyp2d KO models showed that the formation of metabolites mediated by CYP2D such as hydroxybufuralol and dextrorphan was greatly reduced. As such, one application of the Cyp2d KO model may be to estimate the impact of polymorphism on exposure variability when investigating drugs that are expected to be extensively metabolized by CYP2D6 in the clinic.

The Cyp2d KO mouse model has also been used to study the factors that drive drug efficacy. For instance, primaquine is an antimalarial agent whose efficacy is dependent on the formation of phenolic metabolites [133]. Experiments conducted with Cyp2d KO mice showed that the clearance of primaquine was reduced by >90% compared to WT animals and, more importantly, the extent of phenolic oxidation was attenuated in the Cyp2d KO model, indicating that the formation of the active phenolic metabolites were catalyzed by CYP2D6 in humans [134]. These data were used to not only elucidate the metabolic profile of primaquine, but also to gain mechanistic insight into the formation of the active phenolic metabolites which can be used to account for a CYP2D6 polymorphism to inform dosing in the clinic.

*Cyp2c*: CYP2C is another important subfamily of enzymes as it is the second most abundant P450 in the liver and is responsible for the metabolism of a large number of drugs. In humans, there are four isoforms and, similar to CYP2D6, CYP2C is polymorphic. Construction of the Cyp2c mouse KO model requires deletion of 15 functional genes, but due to the different localization of Cyp2c44, only 14 genes were removed [30]. Unlike the Cyp3a and Cyp2d KO models, while the Cyp2c KO animals were viable, there were some phenotypic differences when compared to the WT. In particular, Cyp2c KO animals exhibited a decrease in alkaline phosphatase activity, whereas alanine amino transferase and aspartate aminotransferase activities increased, indicative of hepatotoxicity. In addition, reductions in high-density lipoprotein and cholesterol concentrations were observed. With respect to ADME properties, there was downregulation of Ugt expression in the liver. However, as expected, CYP2C-mediated metabolism of tolbutamide in Cyp2c KO was greatly reduced in vitro, resulting in higher exposure in vivo.

One noteworthy application of the Cyp2c KO model has been to assess the potential for a DDI for a CYP3A4 probe substrate: midazolam. As described previously, midazolam is not an ideal probe substrate in any mouse models to study Cyp3a as it is extensively metabolized by murine Cyp2c. Therefore, the Cyp2c KO model was evaluated as a potential alternative tool to study CYP3A-related DDIs in the clinic using midazolam [135]. When compared with WT mice, oral exposure of midazolam was markedly higher in the Cyp2c KO animals, indicating that unlike the Cyp3a KO animals, midazolam disposition was greatly affected in the Cyp2c KO mice. In the presence of an irreversible CYP3A4 inhibitor troleandomycin, the oral exposure of midazolam increased 2.4-fold in the Cyp2c KO animals, without exerting a meaningful effect in the WT animals. While the effect of Cyp3a inhibition on midazolam exposure in the Cyp2c KO animals was an improvement over previous models, the extent of change was still approximately 10-fold lower than what was reported in the clinic, which underscores the limitations of these models in their utility to assess clinical DDIs.

*Cyp1a2*: While the previously discussed KO rodent models are substantially investigated throughout the literature, studies utilizing other phase I/II DMEs have demonstrated their value in understanding the disposition of a variety of drugs. For example, *Cyp1a2* KO mice have been extensively used in the literature to study the metabolism of many xenobiotics, as well as the bioactivation of chemical carcinogens [24]. Unlike previously described Cyps, there is an identical number of analogues between rodents and humans. Besides being widely accepted as the first developed KO Cyp rodent model [136], this model has revealed the importance of CYP1A2 in the metabolism of acetaminophen, caffeine, clozapine, and phenacetin [137]. Beyond metabolic pathway characterization, *Cyp1a2* KO mice have been used to investigate clinically relevant DDIs in several cases. In one such case, a previously reported DDI between the antibiotic, ciprofloxacin, and the cytokine antagonist, pentoxifylline, was demonstrated to be likely mediated by *Cyp1a2*. This hypothesis was supported using the *Cyp1a2* KO model, where Peterson et al. demonstrated that following IV administration of pentoxifylline, there was significantly elevated serum concentrations in the KO compared to the WT mice [138]. In terms of its role in the bioactivation of exogenous chemicals, a well-studied food-based carcinogen, 2-amino-1-methyl-6-phenylimidazo[4,5-b]pyridine (PhIP), was previously believed to be activated to exert its primary carcinogenic effect via CYP1A2 [139]. However, when administered to *Cyp1a2* KO mice, the carcinogenic effect of PhIP was increased compared to WT mice, which suggested that *Cyp1a2* actually may have a protective role in carcinogenesis [140]. This study provided evidence that these KO models may potentially be useful in predicting enzyme-induced toxicity from exogenously administered compounds, which may be useful in relevant patient populations moving forward in drug development.

*Cyp2e1*: Lastly, CYP2E1 is highly conserved across multiple species and there is one isoform in human and across preclinical species. CYP2E1 has been extensively studied due to its impact on the biotransformation of acetaminophen into a reactive metabolite: N-acetyl-p-benzoquinoneimine, which has been shown to cause hepatotoxicity. This role has been supported through the utilization of *Cyp2e1* KO mice, which have demonstrated survival at doses of up to 400 mg/kg, whereas the same doses resulted in >50% lethality in WT mice [33]. Similar to the studies investigating the toxicological effects of acetaminophen, the contribution of *Cyp2e1* was also investigated in the toxicological effects of alcohol in the liver. Kono et al. demonstrated that administration of enteral alcohol to *Cyp2e1* KO and WT mice demonstrated no difference in early alcohol-induced liver injury after measuring serum aspartate aminotransferase levels and comparing liver histology [141]. This research supported the hypothesis that there are other mechanisms, besides *Cyp2e1*-mediated metabolism of alcohol, that potentially contribute to the mechanisms of hepatotoxicity.

*Hepatic CYP reductase null (HRN) model*: Due to the multitude of Cyp isoforms that contribute to drug metabolism, there have been a variety of approaches aimed at simultaneously eliminating multi-Cyp function. While this has been done chemically by administration of a ubiquitous time-dependent inhibitor: 1-aminobenzotriazole, there are still limitations due to the presence of the remaining Cyp activity following administration of this compound [142]. Alternatively, rather than knocking out individual Cyp enzymes or using chemical inhibitors, researchers have developed a conditional hepatic CYP reductase null (HRN) mouse model, which is devoid of CYP reductase that is necessary for electron transfer between NADPH and the heme [143]. Considering that this is a key requirement for the function of

CYP enzymes, the metabolism of compounds is greatly attenuated in the HRN model. For example, CYP probe substrates midazolam, docetaxel, and theophylline all exhibited a pronounced decrease in plasma clearance (~80% for midazolam and theophylline, and ~50% for docetaxel) following intravenous (IV) administration [144]. The authors suggested that this model could potentially be of use in drug discovery for compounds exhibiting high hepatic clearance and low exposure. For instance, much effort and resources can be spent on optimizing preclinical PK properties so that adequate exposures can be achieved to test preclinical proof of concept (POC), especially for novel targets. Unfortunately, due to the uncertain translatability of preclinical models, the worst-case scenario in this endeavor is the lost time and resources if the target does not bear fruit; or, the best-case scenario is the potential delay in being able to test the target in the clinic since preclinical PK may not necessarily mirror human PK. Therefore, being able to assess preclinical POC as quickly as possible to enable decisions on the target is imperative. As such, HRN models can potentially facilitate testing of preclinical POC at an early stage with compounds that are potent but may not exhibit adequate in vivo exposures due to Cyp-mediated clearance. Similarly, HRN models can be used to evaluate other questions around toxicity and test hypotheses in vivo. It is also important to note, however, that an issue moving forward with models such as these is the potential for compensatory changes in other proteins involved in drug ADME. Indeed, genes such as *Cyp2b10*, *Cyp2c29*, and *Cyp7a1* were shown to be significantly augmented in the HRN, whereas genes such as *Cyp7b1* were reduced [145]. Therefore, a comprehensive characterization of the models is necessary prior to making credible comparisons across other KO animal models.

In a more specific manner, Conroy et al. generated a brain neuron-specific Cyp reductase-null mouse model in order to evaluate the contribution of the brain Cyp-mediated metabolism to morphine-related  $\mu$  opioid pharmacodynamics [146]. While the tissue concentrations of morphine were not directly measured in this study, the antinociceptive effect of morphine was significantly attenuated in the KO mice compared to the WT controls. Using this model, results suggested that the pharmacodynamics of morphine-mediated analgesia was in part Cyp-mediated. However, a direct link to morphine concentrations in the brain was not available, and further studies are necessary in order to mechanistically link morphine pharmacokinetics to the pharmacological effect. Nonetheless, this research exemplified how identification of the tissue-specific Cyp-mediated metabolism could be studied using conditional DME KO strains.

*Ugt1*: Beyond phase I DMEs, there has been substantial progress in the utilization of phase II DMEs as they became more visible due to their importance in drug metabolism. Some of the best studied non-CYP enzymes are the UGTs, which are widely accepted as key contributors to the majority phase II metabolism. Out of this family, UGT1A1 has gained much attention due to the clinically relevant mutation *UGT1A1\*28* in Gilbert's syndrome, which results in decreased *UGT1A1* transcription, and ultimately increased serum levels of unconjugated bilirubin. Considering that in humans, UGT1A1 is primarily responsible for bilirubin conjugation in the liver, this disease of hyperbilirubinemia was recapitulated in *Ugt1* KO mice, where serum levels of unconjugated bilirubin were 40–60 times higher than in WT mice [38]. More recently, these mice were used in the development of an AAV-based human UGT1A1 gene therapy strategy to treat Crigler-Najjar syndrome, which exhibits mutations in *UGT1A1* also resulting in increased unconjugated bilirubin [147]. Preclinical results in the *Ugt1* KO mice

showed that total bilirubin concentrations were substantially decreased compared to the untreated mice, which provided evidence for the efficacy of this treatment strategy and supported the clinical translation of this approach.

The combination of KO animal models generated to date has provided additional *in vivo* evidence regarding the mechanism of DME-mediated elimination; however, it is evident that the utility of these models remains limited with regard to elucidating the magnitude of contribution for a particular DME activity. This could be due to a variety of reasons ranging from up/downregulation of other metabolic pathways, as well as the cross talk between proteins involved in hepatic as well as extrahepatic ADME processes.

In addition to phase I/II DMEs, as mentioned previously, there has been increasing evidence that uptake and efflux transporters also play a major role in the disposition of a variety of xenobiotics. Due to this apparent cross talk and interplay between DMEs and transporters, it is necessary to use appropriate preclinical models in order to evaluate the impact on transporter expression and function with regard to drug distribution. The following section below outlines several examples where transporter KO models have been utilized in drug development to provide evidence to support their contribution to clinical ADME.

*P-glycoprotein (Pgp)*: Present throughout all major tissues involved in drug absorption, distribution, and elimination, ATP-binding cassette (ABC) transporter Pgp (ABCB1) has been extensively studied due to its ability to actively efflux drugs from regions such as the blood-brain barrier (BBB), intestine, kidney, and liver. As mentioned in the introduction, because mice express two isoforms of this transporter (Mdr1a/Mdr1b), many studies have been performed in double-KO mice considering there is marked upregulation of Mdr1b in Mdr1a KO mice that likely compensates for the loss in Pgp activity [21]. Using this model, Tahara et al. showed that the intestinal absorption and BBB penetration of fexofenadine, a H1-receptor antagonist, was significantly enhanced while the effects on biliary excretion were limited [46]. This was demonstrated by sixfold higher plasma concentrations after oral administration of fexofenadine and a threefold increase in a steady-state brain-to-plasma concentration ratio compared to WT mice. This study provided evidence that while Pgp plays a major role in the bioavailability and moderating brain concentration of fexofenadine, it does not play a major role in its biliary elimination in mice. While many drugs have the potential to be transported by multiple transporters due to overlapping substrate selectivity, others have investigated rodent models which contain multiple KO mutations with an effort to better understand the combinatorial effect of transporter impact on drug PK. One such example by Marchetti et al. studied the impact of Bcrp1 and Mdr1a/1b on the PK of erlotinib, an inhibitor of epidermal growth factor receptor 1 (EGFR1) [65]. Results demonstrated that Bcrp1/Mdr1a/1b triple KO mice exhibited significantly altered oral bioavailability of erlotinib compared to WT mice (~20% increase), which suggested that attention needs to be given to these specific isoforms when concerning potential DDI with overlapping substrates of Bcrp and Pgp. Similarly, using a Mrp2/Mdr1a/1b triple KO mouse model, Vlaming et al. demonstrated that the biliary excretion of doxorubicin, an anticancer agent, was greatly attenuated (~54-fold decrease) following IV administration, which was much greater than the decrease seen in Mrp2 or Mdr1a/1b KO alone compared to WT mice [51]. These differences supported the dual role of Mdr1a/1b, as well as Mrp2, in the biliary excretion of doxorubicin, which provided characterization of the major transporters involved in its elimination and presented the possibility for optimizing the drug treatment strategy. More recently in 2018, Liang and



colleagues developed and characterized an Mdr1a/1b KO rat model using Sprague-Dawley rats, which may also be used as an additional preclinical model in drug development [48]. Considering there are well-documented cases of species differences in Pgp activity [148, 149], it should be noted that inferences made regarding the preclinical impact of Pgp in rodent KO models on human drug ADME should be made carefully.

*Multidrug resistance protein (MRP2)*: Similar to Pgp, MRP2 has been demonstrated to be heavily involved with the disposition of many compounds in drug development, and it has been extensively studied due to its inherent ability to moderate drug exposure in a number of ADME-related tissues including the intestine, liver, and kidney. Using a Mrp2 KO mouse model, Vlaming et al. provided evidence for the importance of Mrp2 in the exposure of IV administered methotrexate at a high dose of 50 mg/kg; however, this was only a moderate change of ~1.8-fold and may not be a suitable representation of Mrp2's contribution to methotrexate distribution [51]. Also, a twofold increase in Mrp3/4 expression was observed in the livers of these mice, which suggested that these transporters compensated for the inactivation of Mrp2. Like Pgp, while MRP2 exhibits overlapping substrate specificity between rodent and human isoforms, the MRP2-mediated substrate-selective activity has been shown to exhibit differences between mice and humans [150]. It is important that these differences should be taken into account and accurately incorporated when extrapolating from mice to humans to inform clinical ADME predictions.

*Organic cation transporter 1/2 (OCT1/2)*: For drugs that are generally hydrophilic, charged, and cannot permeate the lipid bilayer, solute carrier (SLC) uptake transporters typically play a major role in moderating intracellular drug concentrations. Two of the major transporters demonstrated to be involved in the uptake of commonly administered organic cation drugs are OCT1 and OCT2. Previously using Oct1/2 double KO mice, Higgins et al. revealed that these transporters are significantly involved in the pharmacokinetics of metformin, a treatment for type II diabetes [75]. Specifically, Oct1/2 KO mice exhibited an ~4.5-fold decrease in total plasma clearance and an ~3.5-fold decrease in volume of distribution compared to WT mice after IV administration of metformin. But interestingly, the pharmacodynamics and absolute exposure of metformin to Oct1/2 expressing tissues, such as the kidney and liver, did not differ between the two groups. Using this model, the researchers were able to provide evidence that argued against the concept that pan-OCT inhibition would impact the pharmacology of metformin. Also, the discrepancy highlighted by this study in terms of the disposition and effect of metformin suggests that there are other mechanisms of metformin uptake into the kidney and liver, which emphasizes the need to further characterize these KO animal models in order to better understand the reasons for the PK-PD disconnect.

*Organic anion transporter 1/3 (OAT1/3)*: Due to their role in transporting a variety of commonly administered drugs such as antibiotics, antivirals, diuretics, and NSAIDs, OAT transporters have been on the radar due to their potential roles in DDIs and downstream impact on substrates that are endogenous signaling molecules. Nigam et al. have published a variety of research highlighting OAT function, expression, ligand specificity, and their regulatory roles in the remote sensing and signaling hypothesis [151]. Recently, their lab generated a "chemical double" Oat1/3 KO due to the lethality of genetically knocking out Oat1 and Oat3 simultaneously in mice [90]. This was performed by administering probenecid, an Oat inhibitor, to Oat3 KO mice in order to reach an effective unbound concentration sufficient enough to inhibit Oat1, but not other organic anion transporters. Using this "double" Oat1/3



KO model, a metabolomics analysis was performed and the data suggested that OATs potentially play a major role in the handling of uremic toxins which could impact the toxicology of certain Oat drug substrates. However, considering that probenecid is generally accepted as a nonspecific inhibitor, the results gathered from this study warrant additional validation.

*Organic anion transporting polypeptide 1a/b (Oatp1a/b)*: Unlike the OCTs and OATs, the OATP family is capable of transporting amphiphilic drug molecules and has been studied primarily due to its impact on clinically relevant DDIs and modulation of drug exposure to the liver. Giacomini et al. described the clinical relevance of OATPs in comparison to other transporters, where inhibition of hepatic OATPs generally results in larger increases in systemic exposure in contrast to lower risk transporters [152]. Due to this notion, it is not surprising that researchers are interested in developing preclinical animal models in order to better predict the impact of OATPs on drug ADME. In order to better understand the impact of OATPs on statin PK, Higgins et al. performed a study in Oatp1a/b KO mice which lack three liver Oatp isoforms. Compared to WT mice, the KO mice displayed a significantly increased IV and oral drug systemic exposure due to an increase in oral bioavailability and decreased total clearance and volume of distribution [110]. All three statins tested in this study (pravastatin, atorvastatin, and simvastatin) exhibited varying degrees of change in their PK parameters, and provided useful insight into the potential contribution of hepatic OATP uptake in humans. However, like other preclinical KO models, changes in protein expression, activity, and potential species differences are important to take into consideration in order to accurately predict the impact of a potential DDI or contributions of these transporters.

### 3 Xenobiotic receptor KO models

Considering the species differences in not only the DME or transporter activity and expression, but also regulation, there have been attempts by several researchers to KO xenobiotic receptors which often play a major role in ADME protein transcriptional regulation via endogenous and exogenous signaling pathways. One such attempt at investigating the regulation of these receptors on CYP expression was performed by Xie et al. where a genetically targeted disruption of the promiscuous murine nuclear receptor pregnolone X receptor (PXR) resulted in its deactivation [153]. Due to its ability to induce CYP3A4 gene expression similar to its human homologue: steroid and xenobiotic receptor (SXR), the authors investigated whether these models could be used to study the induction of CYP3A, which could potentially lead to better predictions for a clinically relevant DDI. While the generation of PXR-null mice showed no change in basal murine Cyp3a expression, the induction of Cyp3a via murine-specific inducers (i.e., pregnenolone-16 $\alpha$ -carbonitrile, dexamethasone) was significantly attenuated. In addition, a transgenic PXR-null/SXR-humanized mouse model was generated to verify whether or not the human ligand-specific induction on CYP3A could be evaluated in vivo. Following a single dose of rifampicin (5 mg/kg) via gastric gavage, a large induction of murine Cyp3a11 gene expression was observed in the livers of humanized mice, but not in those of wild-type mice. These authors summarized that these results suggested that the species-specific origin of the receptor largely governed the pattern of

CYP3A induction, which supports the role for unique ligand binding domains for different species.

Soon after, Wei and colleagues generated a CAR KO mouse model to investigate the CAR-mediated ligand-dependent induction of murine Cyp2b10 [154]. Like PXR/SXR, phenobarbital-like compounds have previously demonstrated affinity for CAR [155] which was used in the CAR KO mice to demonstrate the decrease in metabolism of a Cyp2b substrate, the muscle relaxant zoxazolamine. Loss of CAR function was also demonstrated to have a direct impact on the increase in zoxazolamine-mediated paralysis, which the authors claimed was due to decreased zoxazolamine metabolism. While the elimination of zoxazolamine was not monitored, it remains evident that the effect of zoxazolamine sensitivity is CAR-mediated. Subsequently, additional studies performed by the same lab demonstrated that CAR also plays a role in the regulation of Cyp3a11 expression, suggesting a cross talk between PXR and CAR-mediated induction [156]. While chlorpromazine did not induce Cyp3a11 expression in the CAR-deficient mice, the response to other Cyp3a inducers (i.e., clotrimazole and dieldrin) was apparent in the KO mice which supported the notion that Cyp enzymes may be regulated by multiple xenobiotic receptors. This was further demonstrated in a comparative study of CAR-null, Cyp3a-null, and Cyp2b9/10/13-null mice which demonstrated that the compensatory changes in Cyp expression in the CAR-null mice was much greater than those in the Cyp2b and Cyp3a-null mice [157]. This research highlights the usefulness of these models in the elucidation of mechanism of induction for a particular metabolic pathway, which could be used for compound screening in drug development for perpetrators potentially impacting clinical ADME.

While these examples highlight only a few instances on the utilization of KO animal models in drug discovery and development, there are a multitude of other publications that highlight their applications [137, 139, 158]. However, in summary, it is important to clarify the overall advantages and disadvantages of these models in order to understand the underlying capacity for their use in pharmaceutical research.

### 3.1 Advantages

For many reasons, there are advantages to using genetically modified KO animal models for investigating the impact of DMEs and transporters on drug ADME in early development. Firstly, over the past couple of decades, many of these commonly used models have become commercially available through vendors or have been cryopreserved in the event they need to be utilized in a preclinical study. Resources from several vendors offer a wide variety of mice either for purchase or development if it is not already available. Additionally, the NIH Common Fund's Knockout Mouse Phenotyping Program ([www.mousephenotype.org](http://www.mousephenotype.org)) provides phenotyping data of thousands of genetic KO mouse strains which provide researchers with additional information for potentially characterizing DME and transporter function. While there are rarely "close to perfect" preclinical KO models in predicting clinical ADME, the utilization of these models discussed in this chapter offers preliminary insight into the potential implications of DME or transporter contribution to the overall drug ADME in the clinic. It is up to the researcher to investigate and validate whether or not changes encountered in vivo in rodents are necessarily predictive of what is expected or witnessed in humans. This can be

confirmed with a combination of *in silico*, *in vitro*, or additional *in vivo* models using human isoforms to provide support for data validation. Lastly, with the recent development of newer gene editing technologies that have improved cost, efficiency, and specificity compared to conventional methods, it has become more feasible to generate novel KO rodent models in-house.

Aside from practical considerations, scientifically, one of the major advantages of KO animals is that it allows one to investigate the mechanism of a particular ADME phenomenon and to potentially associate it with a particular DME and/or drug transporters as exemplified in some of the aforementioned case studies. Moreover, the ability to collect biological matrices such as tissues or bile from the same animal where PK was determined provides additional insight into the hypothesis being evaluated to strengthen the mechanistic insight which is not possible in the clinic. In addition, the availability of biological matrices to conduct *in vitro* experiments offers a valuable piece of evidence to increase confidence in the assessment of *in vitro* to *in vivo* extrapolation (IVIVE). By deepening our mechanistic understanding, a new hypothesis can be formed to enable a paradigm shift that can aid in our pursuit of developing better drugs.

## 3.2 Disadvantages

Despite the advantages, it is apparent that there are obvious disadvantages to using genetic KO rodent models as highlighted in the literature due to their inherent issues that have made it difficult to extrapolate preclinical ADME studies to humans. One such disadvantage when knocking out transporter or enzyme expression is that the genetic modification may often result in embryonic lethality. This can sometimes be mitigated by the supplementation or treatment of the genetically modified strain with either xenobiotics or nutrients; however, this has the potential to compromise any significant changes witnessed between the KO and WT mice. Another disadvantage is the potential for compensatory changes in gene expression of other DMEs and transporters. For example, Kumar et al. noted evidence of changes in gene, protein expression, as well as activity of a variety of Cyp enzymes in CAR-null, Cyp3a-null, and Cyp2b-null mice [157]. These differences were also observed in this study between male and female rodents, which suggested that these changes in expression and activity may be regulated by gender differences. It has also been demonstrated that Mrp3 protein expression was 299% and 245% upregulated in the liver and kidney, respectively, in EHBR which is genetically deficient in Mrp2 expression versus the Sprague-Dawley rat genetic background [159]. In contrast, others have suggested that a variety of ABC-null rat models only present minor compensatory changes, which do not detract from their ability to study drug transporter-mediated pharmacokinetics [160]. This also applies to several disease models, where fundamental ADME-related proteins may be up/downregulated, which may not be captured to an appropriate extent in a preclinical system. Unfortunately, in some instances, compensatory genetic changes are not fully scrutinized and the laboratories and vendors who make these models available may not have these models adequately characterized. Therefore, it is recommended that the potential for these changes needs to be taken into consideration when assessing the overall enzyme/transporter contribution using these KO animal models. This exemplifies the need for extensive characterization of these models and comprehensive

phenotyping, which will allow researchers to utilize these models appropriately to best predict human drug ADME. Lastly, as mentioned in several of these KO model examples, it is important to understand the apparent species differences between humans and the preclinical genetic strain.

## 4 Humanized transgenic animal models

More recently, several mouse models expressing human orthologs of DMEs and drug transporters have emerged and become available commercially as promising alternatives to bridge the gap between preclinical species and humans. Humanized mouse models in this section, also known as transgenic animal models, refer to the utilization of genetic engineering to inactivate the gene (i.e., KO) encoding for the mouse homologue of a particular transcript followed by inserting the human homologue gene(s) of interest into the mouse genome [knockin (KI) gene]. Originally, the KO/KI technique was developed by Alfred Schinkel at the Netherlands Cancer Institute [28]. To generate a KO mouse model, the *Cyp3a13* gene was disrupted in embryonic stem (ES) cells by replacing the putative promoter region and exons 1 and 2 with the *Pgk*-hygromycin cassette. In addition, eight full-length *Cyp3a* gene clusters and 3 pseudogenes were deleted by inserting *loxP* sites in the *Cyp3a57* gene, and downstream of the *Cyp3a59* gene of ES cells followed by *Pgk*-Cre recombinase transfection. The blastocyst injection of ES cell clones yielded *Cyp3a* cluster and *Cyp3a13*-KO mice, which could be crossed to obtain comprehensive *Cyp3a* family-KO mice. To generate humanized mice with a stable CYP3A4 expression in liver or intestine of *Cyp3a* KO mice, the transgenes (Tg) Tg(APOE-CYP3A4)A1Ahs and Tg(Vil1-CYP3A4)1Ahs were microinjected into murine FVB/N zygotes. The two transgenes were combined into a single strain through crossbreeding, and subsequently the *Cyp3a* KO strain was backcrossed to the Tg(APOE-CYP3A4)A1Ahs Tg(Vil1-CYP3A4)1Ahs line for at least three generations [28].

As discussed in this chapter, multiple genetically engineered mice models ranging from single xenobiotic receptor KOs (Ahr, Car, or Pxr) to multiple receptor KOs (Pxr-Car or Pxr-Car-Ahr) and single *Cyp* KOs (*Cyp1a1/1a2*, *Cyp2c*, or *Cyp3a*) are available. Also, multiple humanized xenobiotic receptors (AHR, CAR, PXR, or PXR-CAR) and humanized CYPs (CYP2C9, CYP2D6, liver and/or gut CYP3A4), including more complex humanized mouse models such as PXR-CAR-CYP3A4/3A7, where both human xenobiotic receptors and CYPs were inserted, are available commercially to bridge the gap between preclinical species and humans. In addition to the humanized CYP models, many humanized transporter models were also generated. These humanized models have been used to understand the disposition of potential drug candidates in humans, as well as the potential for clinically relevant DDIs. A summary of these models and their utilization in ADME studies is depicted in Table 4.

### 4.1 Utility of humanized CYP mouse models to understand human ADME

As discussed throughout this book, understanding drug metabolism in humans is crucial in pharmaceutical development in determining the likelihood of a new drug candidate entering into the market by assessing human PK parameters with high accuracy. As such, empirical and mechanistic approaches are typically employed. In the empirical approach, simple

**TABLE 4** Examples of the utilization of humanized mouse models for in vivo ADME.

<b>Humanized model</b>	<b>Applications</b>	<b>Findings</b>	<b>Ref.(s)</b>
CYP3A4	Comparing the PK of alprazolam, felodipine, midazolam, nifedipine, nitrenipine, and quinidine in humanized CYP3A4 mice to human	Good correlation in hepatic clearance between human and humanized CYP3A4 mice when $f_{m,CYP3A4}$ is applied to $CL_{int,h}$ of humanized mice	[161]
	Understanding the impact of hepatic CYP3A4 on the PK and metabolism of midazolam and cyclosporin A	Midazolam and cyclosporin A, compounds with markedly different in clearance rates and half-lives, demonstrated accelerated kinetics in humanized CYP3A4 mice	[29]
	Comparing the oral disposition of cobimetinib in humanized mice to human and DDI (inhibition) of cobimetinib as a victim drug when coadministered with itraconazole	CYP3A4 intestinal metabolism contributes to the oral distribution of cobimetinib similar to human data. In addition, an eightfold increase in AUC was observed in humanized mice following oral administration of cobimetinib in the interaction study with itraconazole compared to a 6.7-fold of AUC change in human	[162]
CYP3A4/ CYP3A7 or PXR- CAR-CYP3A4/ CYP3A7	DDI (inhibition) of alprazolam, bosutinib, crizotinib, dasatinib, gefitinib, ibrutinib, regorafenib, sorafenib, triazolam, and vandetanib as victim drug when coadministered with itraconazole	With the exception of crizotinib and gefitinib, humanized mice were able to predict the magnitudes of AUC increase of eight compounds, which were within twofold of clinical DDI data	[163]
	DDI (induction) of triazolam as a victim drug when coadministered with different dose levels of rifampicin, sulfapyrazone, and pioglitazone	No change in AUC was observed in the humanized CYP3A7/CYP3A7 mice, however, rifampicin and sulfapyrazone treatment resulted in an AUC decrease of triazolam in a dose-dependent manner in the humanized PXR-CAR-CYP3A4/CYP3A7 mice	[164]
	DDI (induction) of vemurafenib as a victim drug when co-administrated with rifampicin	No change in AUC was observed in the humanized PXR-CAR mice, however, rifampicin caused a decrease in AUC of vemurafenib in the humanized PXR-CAR-CYP3A4/CYP3A7 mice	[165]
PXR-CAR- CYP3A4/ CYP3A7	DDI (induction) of cobimetinib as a victim drug when coadministered with rifampicin	In humanized mice, rifampicin decreased cobimetinib oral exposure by ~80% compared to ~83% of AUC reduction in clinical DDI study	[162]
	DDI (induction) of alprazolam, bosutinib, crizotinib, dasatinib, gefitinib, ibrutinib, regorafenib, sorafenib, triazolam, and vandetanib as victim drug when co-administered with rifampicin	With the exception of ibrutinib and vandetanib, humanized mice were able to predict the magnitudes of AUC decrease of 8 compounds which were within twofold of clinical DDI data	[163]
PXR-CAR- CYP3A4/ CYP3A7- CYP2D6	Investigating the effect of induction mediated by rifampicin on the PK of tamoxifen and its metabolites	In humanized PXR-CAR-CYP3A4/CYP3A7-CYP2D6 mice, rifampicin decreased the AUC of tamoxifen and its metabolites in a similar magnitude as observed in human	[166]

allometry is a widely utilized method for the prediction of human clearance. This method employs *in vivo* data obtained from preclinical species corrected for scaling factor, such as body or brain weight, and typically does not take into consideration the species differences in DMEs and drug transporters [167]. Modifications to the simple method have been proposed such as the rule of exponents to improve its confidence [168]. However, these modifications produce very little improvement in confidence to the method [169]. As for the mechanistic approaches, *in vitro-in vivo* correlation (IVIVC) analyses are commonly used [170]. This method uses the intrinsic hepatic clearance from either liver microsomes or hepatocytes and uses *in vivo* clearance determined from animal PK studies. However, due to variability in activity in the microsomes and hepatocytes, the clearance values obtained from IVIVC also can vary markedly from experimental data [171]. In addition, *in vitro* extrapolation may not always yield what is observed *in vivo* due to the shortcomings of the *in vitro* assays. Reportedly, only 60% of the drugs have a variance in the clearance within twofold between IVIVC and observed values [172], and as reported in the literature [173], *in vitro* assessment of clearance underpredicting *in vivo* clearance has been observed internally. Therefore, some laboratories, including this laboratory, have hypothesized that mice expressing human metabolic enzymes could be useful and may increase the confidence in the prediction of human hepatic clearance.

In one such example demonstrating the utility of the humanized mouse model in bridging the gap between preclinical species and humans, six CYP3A4 substrates (alprazolam, felodipine, midazolam, nifedipine, nitrendipine, and quinidine) were administered to humanized CYP3A4 transgenic animals intravenously and their hepatic intrinsic clearances were determined. A poor correlation ( $R^2 = 0.180$ ) was found when comparing the total CL between human and humanized CYP3A4 mice; however, there was a strong correlation of intrinsic clearance ( $CL_{int}$ ) between the human and humanized CYP3A4 transgenic model ( $R^2 = 0.930$ ) [161]. While this example demonstrates the potential utility of the humanized transgenic animals to predict human CL, it also illustrates the importance of comparing relevant parameters when evaluating novel animal models. That is, since clearance is a function of not only  $CL_{int}$  but also hepatic blood flow and binding parameters which are species-dependent, a comparison of absolute values of total clearance is not appropriate.

To further probe the utility of the humanized CYP model, the contribution of intestinal metabolism to the bioavailability of cobimetinib, an MEK inhibitor, was studied [162]. In the clinic, the observed bioavailability of cobimetinib was 46%, which was lower than expected, and suggested that intestinal first pass metabolism may regulate its bioavailability. When cobimetinib was dosed to control mice and to three different types of transgenic mice with differential expression of human CYP3A4 in the intestine, or in the liver, or in both intestine and liver, the oral exposure of cobimetinib was 80% lower in animals expressing human CYP3A4 in their intestine, compared with animals where human CYP3A4 was only expressed in the liver, suggesting that intestinal CYP3A4 plays a major role in the oral disposition of cobimetinib [162]. Although these humanized mice were able to qualitatively describe the contribution of intestinal first pass metabolism of cobimetinib, they were not able to quantitatively recapitulate clinical observations [174]. Encouraged by these data from the CYP3A4 transgenic model, the authors conducted DDI studies to investigate the effect of CYP inhibition using models expressing human CYP3A4 in their intestine and liver, and CYP induction using a composite humanized PXR-CAR-CYP3A4/CYP3A7 mouse model. The humanized



CYP3A4 liver and intestine mouse showed an eightfold increase in oral exposure of cobimetinib, which is comparable to the ~sevenfold increase in oral cobimetinib exposure in the clinic. Similarly, multiple-day rifampin treatment to induce CYP induction to a composite humanized PXR-CAR-CYP3A4/CYP3A7 led to an ~80% decrease in oral exposure of cobimetinib. While clinical induction data are not available, PBPK modeling predicted an ~83% reduction in oral exposure of cobimetinib from rifampicin-mediated CYP3A4 induction. The data obtained in this study with cobimetinib suggested that humanized transgenic animal models could be used to predict the magnitude of clinical DDI [162, 174].

Since co-pharmacy has been found to be useful in treating multiple different diseases, others also used humanized animals to study the magnitude of DDI of multiple drugs. Humanized CYP3A4 and humanized PXR-CAR-CYP3A4/CYP3A7 were used to study the magnitude of inhibition and induction of alprazolam, bosutinib, crizotinib, dasatinib, gefitinib, ibrutinib, regorafenib, sorafenib, triazolam, and vandetanib as victim drugs following coadministration with itraconazole or rifampicin [163]. With the exception of crizotinib and gefitinib, humanized CYP3A4 mice were able to predict the magnitude of AUC increase in 8 out of 10 compounds following coadministration with itraconazole, and the magnitudes were within twofold of clinical data. As for the induction by rifampicin, humanized PXR-CAR-CYP3A4/CYP3A7 were able to predict the magnitude of AUC decrease in 8 out of 10 compounds with the exception of ibrutinib and vandetanib. Data generated from this study further confirmed that humanized animal models may be used to gain confidence and complement *in vitro* and *in silico* methods for assessing DDI potential/liability of new drugs.

In a similar study looking at multiple gene humanized mice, the PK and metabolism of tamoxifen was characterized in a control mouse, or in a humanized PXR and CAR mouse model, or in a humanized PXR, CAR, CYP3A4/3A7, and CYP2D6 mouse model. In humans, tamoxifen is metabolized primarily by CYP3A4 and CYP2D6, and with multiple doses of rifampicin, the exposure of tamoxifen was reduced by 6.2-fold; additionally, rather than augmenting metabolism, the exposure of its primary metabolites, 4-hydroxytamoxifen, N-desmethyltamoxifen, and endoxifen, was also reduced. Following multiple doses of rifampicin to the humanized animals, rifampicin decreased the exposure of both tamoxifen and its metabolites in humanized PXR-CAR-CYP3A4/3A7-CYP2D6 in a similar magnitude as observed in the clinic [166]. *In vitro* metabolic pathways for tamoxifen and its metabolites were further studied in microsomes prepared from these humanized animals. *In vitro* data from microsomes revealed that the CYP3A4 metabolism was enhanced, whereas no modulation of the CYP2D6 metabolic pathway was observed [166]. These findings supported previous studies indicating that CYP2D6 is not susceptible to induction by rifampicin [175, 176]. Overall, the results gathered from this study showed that human PXR, CYP3A4, and CYP2D6 in these humanized models were functional, and suggested that complex humanized animal models may be suitable to study compounds exhibiting more complicated DDI profiles.

In another instance of utilizing these models, transgenic mice were used to confirm the presence of a circulating human metabolite through metabolite identification. This is considered an important consideration in drug development, considering that most xenobiotic compounds may be susceptible to metabolism and the formation of metabolites is often found to be different between preclinical species and humans. In the humanized CYP3A4 mice study of cobimetinib, the authors investigated whether they could confirm the three circulating



oxidative human metabolites (M12, M18, and M19) of cobimetinib [162]. From the plasma samples of humanized CYP3A4, all three metabolites were observed. Although M12 and M19 were also observed in the plasma of wild-type mice, their presence was not entirely unexpected because mouse Cyp isoforms have the capability to metabolize cobimetinib and produced the same metabolites as in humans. However, it should be noted that the level of M12 was higher in humanized mice expressing intestinal human ortholog of CYP3A4, and M18 was observed only in humanized mice expressing CYP3A4 in their livers. Furthermore, M18 was observed only in humanized mice where human CYP3A4 was expressed. Overall, these data suggested that humanized animal models would be able to have potential utility in metabolite identification comparable to humans.

The current set of data from various humanized mice is encouraging and shows some promise of bridging the gap between preclinical species and humans. However, there are limitations to these humanized animal models. For instance, in the case of investigating DDI potential, these humanized animal models can only be applied to drugs for which CYP phenotyping has been conducted and where  $f_m$  or a single pathway involvement is known and/or confirmed, and with the a priori knowledge that a similar clearance pathway is shared between mice and humans. In the situation where different CYP ortholog(s) in the mouse and human metabolizes a particular drug, aberrant and/or unpredicted observations may be found as seen in the DDI study with midazolam [29]. Despite the limitations, the information obtained from these humanized animal models can be used in conjunction with other data to strengthen our understanding and prediction of clinical ADME properties in the development of new drugs.

## 5 Humanized liver chimeric mouse models

In addition to genetically modified animal models, there have been other attempts to circumvent the translational gap resulting from species differences in the ADME-related proteins. Another innovative approach involves combining genetically modified mice with surgical implantation of human hepatocytes, resulting in a mouse model whose composition of the liver is mainly of human origin. The implementation of this technology often includes using immunocompromised mice (i.e., severe combined immunodeficiency—SCID) and genetically modifying the murine liver to exert a hepatotoxic effect, allowing for the ablation of murine hepatocytes to enable implantation of human hepatocytes. To date, there have been a number of attempts to implement such chimeric liver mouse models for the purpose of understanding the relative contribution of drug receptors, metabolizing enzymes, and transporters to drug ADME. Some attempts at repopulating the liver with human hepatocytes have reported a >95% replacement index (RI) [177]; however, these results are often variable among the different methods and labs that use them to humanize the liver. This section serves as a brief description of three primary humanized liver chimeric mouse models (summarized in Table 5), examples of their application in drug development to inform clinical ADME (summarized in Table 6), and a summary of the advantages and disadvantages in their utility. Other references that are available offer a detailed description of the development of these models as well as other examples of their application in drug metabolism [225, 226].

**TABLE 5** Three major human chimeric mouse models.

	<b>uPA</b>	<b>FRG</b>	<b>TK-NOG</b>
Type	<i>alb-uPA</i> /SCID Albumin promoter- urokinase-type plasminogen activator	<i>Fah</i> <sup>-/-</sup> / <i>Il2rg</i> <sup>-/-</sup> / <i>Rag2</i> <sup>-/-</sup> Triple KO fumarylacetoacetate hydrolase/interleukin 2 receptor subunit gamma/ recombination activating gene 2	<i>alb-HSVtk</i> /SCID/ <i>Il2rg</i> <sup>-/-</sup> Albumin promoter-herpes simplex virus type 1 thymidine kinase/ SCID/ <i>Il2rg</i> knockout
Immunodeficiency	SCID	<i>Il2rg</i> <sup>-/-</sup> / <i>Rag2</i> <sup>-/-</sup>	SCID/ <i>Il2rg</i> <sup>-/-</sup>
Model development	[178–182]	[183, 184]	[185, 186]
Pros	<ul style="list-style-type: none"> <li>• Well-studied ablation of hepatocytes is constitutive</li> </ul>	<ul style="list-style-type: none"> <li>• Controlled hepatocyte ablation (nitisinone; NTBC)</li> <li>• Engraftment of human hepatocytes at any age</li> </ul>	<ul style="list-style-type: none"> <li>• Controlled hepatocyte ablation (ganciclovir)</li> <li>• Engraftment of human hepatocytes at any age</li> </ul>
Cons	<ul style="list-style-type: none"> <li>• Neonatal bleeding [187]</li> <li>• Human hepatocytes replacement is decreased [182]</li> <li>• Kidney disorders are likely [182]</li> <li>• Body size is small [182]</li> <li>• Reproductive organ atrophy [188]</li> <li>• High cost</li> </ul>	<ul style="list-style-type: none"> <li>• Drug administration is necessary with NTBC</li> <li>• Careful maintenance and selection pressure</li> <li>• High cost</li> </ul>	<ul style="list-style-type: none"> <li>• Drug administration is necessary with ganciclovir</li> <li>• Careful maintenance and selection pressure</li> <li>• Male sterility [189]</li> <li>• High cost</li> </ul>

**TABLE 6** Summary of ADME studies performed in human chimeric mouse models.

<b>Background</b>	<b>Purpose</b>	<b>Ref.(s)</b>
uPA/SCID	Comparison of mRNA expression/activity of DME and transporters in <i>Cyp3a</i> KO/chimeric mice with PxB-mice	[190]
	Antiviral treatment of HBV/HCV	[191] [178] [192] [193]
	Metabolite identification of a selective SGLT2 inhibitor (YM543)	[194]
	Metabolite profiling of nefazodone	[195]
	Metabolite identification of a JAK inhibitor (ASP015K)	[196]
	Disposition of four drugs (lamotrigine, diclofenac, MRK-A, and propafenone)	[197]
	Metabolite profiling after oral administration of troglitazone	[198]
	Metabolism of a chymase inhibitor (SUN13834)	[199]

Continued

**TABLE 6** Summary of ADME studies performed in human chimeric mouse models—cont'd

Background	Purpose	Ref.(s)
	Metabolite profiling of clemizole and DDI	[200]
	Metabolism of GW695634, SB-406725, and GW823093	[201]
	Metabolite identification of debrisoquine, warfarin, and in-house compounds	[202]
	Metabolite profiling of 19-norandrost-4-ene-3,17-dione	[203]
	Metabolite profiling of 4-androstene-3,17-dione	[204]
	CYP2C9-mediated metabolism of warfarin	[205]
	OATP-mediated DDI of rosuvastatin and cyclosporine A	[206]
	Pharmacokinetics of Lu AF09535	[207]
	Human clearance and volume of distribution prediction of model compounds	[208] [209]
	Excretion of cefmetazole	[210]
	CYP-induction	[211]
	DDIs via PXR-mediated induction of CYP3A4 and CYP2C	[212]
	Detection of induction of CYP3A4	[213]
	Effect of hepatitis C infection on the pharmacokinetics of antiviral therapeutics	[214]
FRG	Biotransformation and transporter effects of troglitazone	[215]
	Characterization of functional integrity of liver	[216]
	Pharmacokinetics of lumiracoxib	[217]
TK-NOG	Thalidomide/5OH-T metabolism	[218]
	Disposition of melengestrol acetate	[219]
	CYP3A-mediated DDI of thalidomide and midazolam	[220]
	Prediction of cholestatic liver toxicity	[221]
	Pharmacokinetics of bisphenol A	[222]
	Pharmacokinetics and metabolite identification of a partial glucokinase activator	[223]
	Pharmacokinetics of diisononyl phthalate	[224]

*uPA/SCID*: One of the first models for humanized liver chimeric mouse models was developed by expressing the urokinase-type plasminogen activator (uPA) under the albumin (alb) promoter, which results in transgene-induced hepatotoxicity due to the role of uPA in liver remodeling via conversion of plasminogen to the active protease plasmin [178, 191]. Initially, these mice exhibited hemorrhaging and loss of clotting function within a few days following birth, which resulted in a high mortality rate [187]. From these mice, a

specific strain was identified containing a DNA rearrangement of the *uPA*, resulting in its deactivation in hepatocytes [227]. Coupled with SCID, these mice were able to develop human liver chimerism with livers as high as 96% RI [177]. Due to the large body of research surrounding these mice since their development, there are many examples of how these mice have been utilized in the laboratory to study drug ADME-related issues.

After verifying that major human DMEs were expressed in this mouse model, Katoh et al. investigated the utility of this model in studying the human CYP2D6-mediated metabolism of an antihypertensive drug, debrisoquine. The major metabolite of debrisoquine in humans, 4-hydroxydebrisoquine, was shown to be produced substantially following a 2.0 mg/kg oral dose [228]. The presence of a human CYP2D6-mediated metabolism was further supported by in vitro data collected using chimeric liver microsomes, which demonstrated differences in the  $K_m$  and  $V_{max}/K_m$  values for debrisoquine 4'-hydroxylase activity indicating human CYP2D6 activity, which was inhibited by CYP2D6 substrates quinidine and paroxetine. The authors concluded that because of the humanized profile of the debrisoquine metabolism, these mice could potentially be used to investigate the P450-mediated metabolism and DDIs. In the same lab, cefmetazole, a cephalosporin antibiotic, was used as a probe drug to investigate the capabilities of the *uPA*/SCID model to evaluate drug excretion [210]. Seeing that cefmetazole is primarily eliminated in the urine in humans, this was also witnessed in the chimeric mouse model where 81% was eliminated in the urine versus 23.7% in the control mice. The study also demonstrated an increase in mRNA expression of liver human transporters in comparison to homologous murine transporters; however, the gene expression for some human transporters was higher/lower in the chimeric mice compared to the donor hepatocytes, suggesting the occurrence of a potential phenomenon involved in the regulation of these transporters in vivo in the chimeric livers. Nevertheless, the application of this model with regard to its ability to be used as a novel preclinical species to investigate human drug ADME seemed to gain support as additional studies and alternative models were developed.

FRG: Like the *uPA*/SCID humanized liver chimeric mouse model, a similar hepatotoxic effect was witnessed in fumarylacetoacetate hydrolase (*Fah*)-deficient mice, which exhibited an apparent advantage due to the regulation of hepatocyte implantation via nitisinone, an inhibitor of the tyrosine catabolism that promotes selection pressure for FAH-positive transplanted hepatocytes [229]. Subsequently, with some additional genetic modifications, others have demonstrated that fresh and cryopreserved human hepatocytes can be implanted in the triple KO *Fah*/interleukin 2 receptor subunit gamma (*Il2rg*)/recombination activating gene 2 (*Rag2*) with varying levels of success [183, 184]. Upon utilizing a serial transplantation method of human hepatocytes, Azuma et al. reported that the percentage of highly repopulated mice has not only increased in serial transplant recipients but also yielded more consistent results. After additional method development, Bissig et al. reported a higher rate of liver chimerism than was previously reported: up to 95% of human hepatocyte chimerism [230]. Like in the *uPA*/SCID model, FRG mice exhibited mRNA expression of a variety of human CYP enzymes, ABC transporters, and regulatory nuclear receptors; however, there was large variability witnessed in the expression profile for multiple human isoforms across different chimeric mice. While there are not as many studies documenting the usefulness of this model to study drug ADME as in the *uPA*/SCID mice yet as it is still fairly novel technology, there have been increasing instances of using this model to investigate the pharmacokinetics of a variety of drugs.

For example, Samuelsson et al. demonstrated that the FRG mouse model was capable of being used to evaluate the biotransformation and liver transporter effects of troglitazone, an antihyperglycemic agent for the management of type II diabetes [215]. After orally administering 600 mg/kg/day of troglitazone to either the chimeric murinized or humanized FRG mice, metabolite identification revealed both phase I/II metabolic pathways present, and a 15- to 18-fold increase in the formation of troglitazone sulfate in the humanized mice compared to the murinized mice in blood and bile, respectively [215]. Compared to a previous study performed in *uPA/SCID* mice, both models demonstrated human troglitazone sulfate formation; however, the humanized FRG mice also demonstrated production of the glucuronide conjugate nor recapitulate the extent of human metabolism. Additionally, liver humanization decreased after vehicle and troglitazone treatment throughout the study, which may have impacted the magnitude of differences witnessed in these mice. This may present a problem in studies where multiple dosing regimens are necessary and should be taken into consideration where results may potentially be impacted due to an artifact of murine metabolism.

Similar to the troglitazone study, Dickie et al. also investigated the ability of FRG mouse studies to predict the biotransformation and pharmacokinetics of lumiracoxib, a cyclooxygenase II inhibitor [217]. After administration of a single 10 mg/kg oral dose, the distribution and metabolite profile of lumiracoxib showed good correspondence with all major metabolites previously identified in humans, with the exception of the absence of sulfate conjugates, which could potentially be explained via species differences and/or extrahepatic sulfation not accounted for in the model. In order to overcome some of the problems of species differences, a model was developed combining the liver HRN model (*Por*-deficient) with FRG mice (PIRF mice) in order to substantially deplete the remaining murine Cyp activity in combination with a repopulation of human hepatocytes [231]. Using two drugs, gefitinib (anticancer) and atazanavir (antiviral), Barzi and colleagues were able to demonstrate that the PIRF mice showed increased human metabolites present in the serum, urine, feces, and livers, compared to conventional FRG mice. In terms of measuring hepatic drug metabolism, this model serves as an example where the contribution of human metabolism may be studied compared to standard FRG mice where murine Cyp enzymes may still contribute to drug disposition.

TK-NOG: It is one of the more recent attempts at generating humanized liver chimeric mice using albumin promoter-mediated transgenic expression of the herpes simplex virus type 1 thymidine kinase (HSVtk) in an immunocompromised SCID/Il2rg KO mouse strain (TK-NOG) [185]. Upon administration of ganciclovir prior to human hepatocyte transplantation, hepatic HSVtk-mediated phosphorylation of ganciclovir results in cell toxicity and eventually murine hepatocyte ablation, which does not occur in human hepatocytes due to the absence of this enzyme. Using this methodology, Hasegawa et al. demonstrated that the chimeric mouse model could be sustained with functional activity for over 8 months, suggesting its utility as a preclinical model for investigating human drug ADME.

In order to investigate the usefulness of this model at predicting human DDIs, Nishimura et al. used clemizole, a H1 receptor antagonist with potential for HCV treatment, to evaluate human metabolite formation and its ability to exhibit a CYP3A4-mediated DDI [200]. After demonstrating the positive protein expression of human CYP3A4 in the TK-NOG livers, coadministration of clemizole and ritonavir decreased the amount of the human-predominant clemizole metabolites, indicating the potential for a clinically relevant DDI.

Considering that the M1 metabolite of clemizole showed anti-HCV activity, this interaction could potentially have a substantial impact at preventing negative events associated with CYP3A4-mediated elimination of clemizole *in vivo*. Approximately around the same time, Yamazaki et al. supported this notion at using TK-NOG mice for predicting clinical DDI by coadministering thalidomide (oral) and midazolam (intravenous) [220]. From this study, the clearance of midazolam in chimeric mice was enhanced by orally coadministered thalidomide in the chimeric mouse model in contrast to the same coadministration in control NOG mice. Due to the ability of heterotropic activation of CYP3A resulting from thalidomide administration, this study was one of the first to demonstrate the utility of this model in the complexities of CYP3A-mediated DDIs in drug development. More recently in 2017, Kamimura and colleagues evaluated whether the TK-NOG model could be useful in predicting the biotransformation of a partial glucokinase activator, PF-04937319, and its major metabolite (M1), due to the lack of reliability of *in vitro* metabolism studies [223]. Metabolic profiling of this compound in the TK-NOG mice revealed the formation of a carbinolamide metabolite, which was specific to human liver metabolism of this drug. For drugs exhibiting species differences in drug ADME, this study presented the potential utility of the TK-NOG model in capturing human-specific metabolism and PK *in vivo*.

Besides the three more popularized humanized liver chimeric mouse models (i.e., *uPA/SCID*, FRG, and TK-NOG), other humanized liver chimeric mouse strains are continuously being developed to try and circumvent some of the disadvantages of these models. For example, human hepatocytes were co-transplanted with human CD34<sup>+</sup> hematopoietic stem cells to attenuate rejection and to facilitate engraftment of human liver cells [232]. In another example, immature human hepatocytes such as human primary fetal liver cells or human hepatic stem cells were used to repopulate livers of albumin-toxin receptor mediated cell KO SCID mice [233].

In summary, because of the intrinsic limitations of these models, we would like to clarify the general advantages and disadvantages using chimeric mouse models in an effort to avoid incorrect assumptions regarding the utility of these models in predicting human drug ADME (Table 7).

## 5.1 Advantages

Due to the evidence presented in this chapter, as well as other studies, it is evident that humanized liver chimeric mice possess some capabilities at predicting human drug ADME. This notion is supported by the studies investigating human CYP- and/or UGT-mediated metabolism for a wide variety of drugs and their potential to cause clinically relevant DDIs. Another example is around the utility of these models to form disproportionate human metabolites. For drugs that are primarily eliminated via hepatic metabolism, the transplantation of human hepatocytes in mice has been a suitable alternative to using WT rodent models due to the models that have reported extensive humanization via either human albumin concentration or human hepatic gene expression. After several attempts at generating a more suitable model than was previously available, the past couple of decades of research into this technology has allowed for multiple strains to become available that range from their mechanism of hepatotoxicity, immunodeficiency, and maintenance of the model. Due to the

**TABLE 7** Summary of how the various animal models can be utilized to study specific ADME-related properties.

	<b>KO</b>	<b>Humanized transgenic</b>	<b>Chimeric</b>
Human CL prediction	While providing some mechanistic insight into DME involved in the metabolism of drugs, it is not useful to predict human CL	While providing some mechanistic insight into DME involved in the metabolism of drugs, it is not useful to predict human CL	Holds the biggest promise of being able to predict human CL. However, data interpretation is confounded by endogenous mouse proteins
Human metabolite identification	While providing some mechanistic insight into DME involved in the metabolism of drugs, it is not useful for human metabolite assessment	May be used in conjunction with in vitro data (e.g., reaction phenotyping) for targeted human metabolite assessment, but limited utility in the absence of mechanistic knowledge around metabolism profile	Examples demonstrating that it can be a powerful tool to identify human-unique and/or disproportionate metabolite. However, this model is not able to capture the type and extent of metabolites generated by the intestines
DDI evaluation	May be used to confirm a particular DDI involving a specific DME and/or drug transporters	Useful to study compounds if the relationship between DME/drug transporter to the probe substrate has been well characterized	Potentially useful model to study DDI but data may be confounded by endogenous mouse DMEs and drug transporters. More investigations are needed to establish the validity of this model to study DDI
Overall assessment	Benefit of KO model is that it enables the study of the role and contribution of a particular DME or drug transporters. It also can be used to increase exposure to test preclinical efficacy/toxicity hypothesis	Benefit of humanized model is being able to assess the potential DDI liability of a compound	Most promising models that best mirrors human liver ADME proteins. However, data with chimeric animals is confounded by endogenous mouse DMEs and drug transporters. More studies are needed to characterize this model

implantation of whole human hepatocytes compared to the humanization of one, or multiple genes via genetic modifications, chimeric mouse models allow for the presence of the complexities of human hepatic transporter-DME-nuclear receptor cross talk which may not be particularly accounted for in other preclinical models. This allows for researchers to investigate not only drug metabolism, but also enzyme regulation and genetic polymorphisms that are clearly present and may have a significant contribution to drug disposition in vivo. The readily commercially available resources for donor human hepatocytes, both cryopreserved and fresh, allow for the enhanced feasibility at generating these models in-house on different backgrounds. Due to their human origin, it has also been demonstrated that these models can be susceptible to human pathogens which can aid in the study of infectious diseases where other rodent models remain at a disadvantage. Although the application of these models in predicting drug ADME in humans has been demonstrated, the lack of quantitative correlation



or reproducibility of these predictions can be attributed to a series of limitations which restrict their utility to prospectively assess ADME profiles of NCEs.

## 5.2 Disadvantages

The experimental observations witnessed in the examples presented in this chapter offer case examples where humanized liver chimeric mice have successfully been used to predict human drug elimination; however, there are many reasons as to why these models may not be potentially as useful as conventional models. One of the more obvious examples is the feasibility at continuous generation of these models due to their limited life span and lack of recreation capabilities. This, in tandem with their relatively high cost for commercial purchase, complicates studies that require a large sample size to generate meaningful and statistically well powered studies to infer significant results. Also, it is not incorrect to assume that the sample sizes of these studies may need to be larger than what is typically used due to the enhanced variability witnessed in these mice. This can typically not only be variability associated with the degree of liver humanization, but also genetic and interlaboratory differences between mice used for model development. Due to these apparently unavoidable problems, it remains difficult to abrogate the impact of these issues on experimental results, and thus these studies require constant scientific criticism and extensive validation.

Additionally, despite the desire to reach complete humanization of murine liver, the chimeric mouse liver models are not entirely human as their liver still contains endogenous murine hepatocytes. In particular, studies conducted with FRG humanized chimeric models showed higher mRNA expression of murine DMEs and drug transporters such as *Cyp1a1*, sulfotransferases, *Bcrp*, and *Mdr1a*, suggesting the continued presence of remnant mouse genes, along with the loss of metabolic zonation most likely due to the process of repopulating human hepatocytes [216]. Furthermore, the study of ADME is complicated by hepatotoxicity that is associated with FRG chimeric models that arises from dysregulation of hepatocyte proliferation and disruption of bile acid homeostasis [234]. Finally, humanized liver models may not necessarily be a good tool to study oral drug administration in humans due to the lack of extrahepatic humanization in first pass tissues such as the gastrointestinal tract. These tissues, as well as other murine hepatocytes that avoid ablation, contain endogenous Cyps that could confound drug ADME studies, especially when species differences are expected to have a substantial impact on the predictive value of these models. Indeed, these models often fall short in quantitatively mimicking human ADME properties. Attempts to address this limitation have been performed (such as in the *Por*-deficient chimeric mouse model [231]); however, this still does not account for extrahepatic events leading to species differences in human PK. Unfortunately, the localized changes made to chimeric liver models make the drugs that are extrahepatically distributed and metabolized of no apparent advantage compared to WT rodent models. Therefore, it is important to have an initial hypothesis regarding the relative tissue-specific contributions of drug metabolism and disposition when implementing each model. Because these models are relatively new to being implemented in early research and development processes, more comparative analyses using a variety of drugs with different biopharmaceutical classifications are necessary to provide for better inferences into which models provide better preclinical to clinical predictions.

## 6 Conclusions and future perspectives

As discussed in this chapter, the enhanced abilities of genetically modifying preclinical rodent species have allowed for the generation of novel models in an attempt to bridge the gap between rodent and human-specific drug ADME. It is also worth noting that one of the biggest advantages of these models is the ability to extract biological matrices to generate *in vitro* data which can be used to complement *in vivo* data to establish IVIVC. This is a powerful approach which cannot be readily done in the clinic, but, as illustrated in Fig. 1, can enable further study of the mechanism of a particular ADME-related phenomenon in novel animal models to inform clinical prediction. Moreover, mechanistic understanding in the novel animal models provides additional context of how best to utilize human *in vitro* data to translate to the clinic. Advancements pertaining to the efficiency and specificity of genetic engineering technology, such as CRISPR and conditional KO/KI technologies, have, in some cases, increased the complexity of these models to offer better predictive value in drug discovery and early development. The more recent approaches, such as in the *Por*-deficient FRG mice, take a combinatorial approach at improving human PK predictions by utilizing KO and chimeric mouse technology [231]. While this methodology remains much less studied, it has the potential of reducing any experimental artifacts pertaining to endogenous murine metabolism. However, moving forward, better characterization of these models will also be necessary in assessing the validity of some of these IVIVE-related questions. This problem may potentially be alleviated using a multi-‘omics’ approach in assessing ADME-related gene/protein expression, as well as activity, and may help researchers better understand the relative impact of interspecies differences in certain cases. The pros and cons of these models were summarized, and it is important to reiterate that the impact of each of these features on human ADME prediction is a drug-dependent parameter. With this realization, it is necessary to not assume that there is a universal model appropriate for all research questions, but models should follow a “right tool for the right job” paradigm in which they are evaluated on a case-by-case basis. While other fields

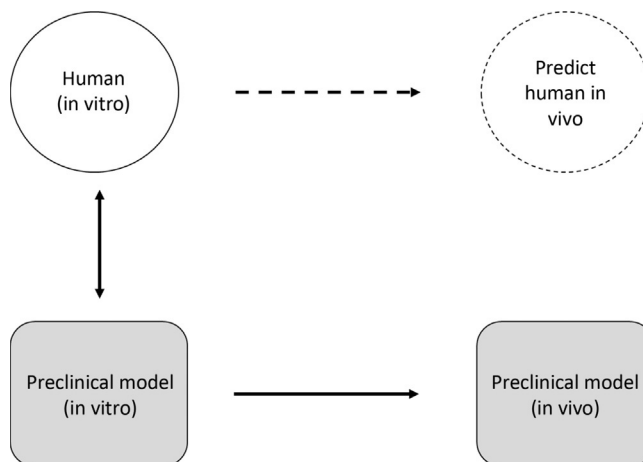


FIG. 1 Unraveling *in vitro* to *in vivo* mechanistic relationship in preclinical models informs clinical predictions.

beyond ADME, such as toxicology and pharmacology, have already been extensively using these novel rodent models for reasons such as generating disease models and studying the impact of exogenously administered biochemical agents, there remains much more evaluation to be done prior to confirming their utility and implementing them in drug development. As such, there are additional works ongoing by various laboratories that are not only devoted to further characterizing these existing models, but also developing new models that address many of the challenges summarized in this chapter.

In summary, there remains much more ground to be covered in terms of utilizing these rodent models for prediction of clinical ADME, and with the increased characterization, realization of the limitations of these approaches, in combination with the continuous effort to generate newer models, there is optimism within the field regarding the improvement and increased implementation of these models in the future.

## References

- [1] J.M. Pascussi, et al., The tangle of nuclear receptors that controls xenobiotic metabolism and transport: Crosstalk and consequences, *Annu. Rev. Pharmacol. Toxicol.* 48 (2008) 1–32.
- [2] D.R. Nelson, et al., Comparison of cytochrome P450 (CYP) genes from the mouse and human genomes, including nomenclature recommendations for genes, pseudogenes and alternative-splice variants, *Pharmacogenetics* 14 (1) (2004) 1–18.
- [3] T. Shimada, et al., Cytochrome P450-dependent drug oxidation activities in liver microsomes of various animal species including rats, guinea pigs, dogs, monkeys, and humans, *Arch. Toxicol.* 71 (6) (1997) 401–408.
- [4] C. Lee, X. Ding, D.S. Riddick, Downregulation of mouse hepatic CYP3A protein by 3-methylcholanthrene does not require cytochrome P450-dependent metabolism, *Drug Metab. Dispos.* 41 (10) (2013) 1782–1786.
- [5] M. Martignoni, G.M. Groothuis, R. de Kanter, Species differences between mouse, rat, dog, monkey and human CYP-mediated drug metabolism, inhibition and induction, *Expert Opin. Drug Metab. Toxicol.* 2 (6) (2006) 875–894.
- [6] H. Souhaili-el Amri, A.M. Batt, G. Siest, Comparison of cytochrome P-450 content and activities in liver microsomes of seven animal species, including man, *Xenobiotica* 16 (4) (1986) 351–358.
- [7] T. Prueksaritanont, et al., Comparative studies of drug-metabolizing enzymes in dog, monkey, and human small intestines, and in Caco-2 cells, *Drug Metab. Dispos.* 24 (6) (1996) 634–642.
- [8] J.A. Boutin, et al., Heterogeneity of hepatic microsomal UDP-glucuronosyltransferase(s) activities: comparison between human and mammalian species activities, *Chem. Biol. Interact.* 52 (2) (1984) 173–184.
- [9] O. Ghosheh, E.M. Hawes, Microsomal N-glucuronidation of nicotine and cotinine: human hepatic interindividual, human intertissue, and interspecies hepatic variation, *Drug Metab. Dispos.* 30 (12) (2002) 1478–1483.
- [10] H. Kaji, T. Kume, Characterization of afloqualone N-glucuronidation: species differences and identification of human UDP-glucuronosyltransferase isoform(s), *Drug Metab. Dispos.* 33 (1) (2005) 60–67.
- [11] M. Lin, et al., Characterizing the in vitro species differences in N-glucuronidation of a potent pan-PIM inhibitor GNE-924 containing a 3,5-substituted 6-azaindazole, *Xenobiotica* 48 (10) (2018) 1021–1027.
- [12] Y. Uchida, et al., Quantitative targeted absolute proteomics of human blood-brain barrier transporters and receptors, *J. Neurochem.* 117 (2) (2011) 333–345.
- [13] C. Braun, et al., Quantification of transporter and receptor proteins in dog brain capillaries and choroid plexus: relevance for the distribution in brain and CSF of selected BCRP and P-gp substrates, *Mol. Pharm.* 14 (10) (2017) 3436–3447.
- [14] J. Kamiie, et al., Quantitative atlas of membrane transporter proteins: development and application of a highly sensitive simultaneous LC/MS/MS method combined with novel in-silico peptide selection criteria, *Pharm. Res.* 25 (6) (2008) 1469–1483.
- [15] Y. Hoshi, et al., Quantitative atlas of blood-brain barrier transporters, receptors, and tight junction proteins in rats and common marmoset, *J. Pharm. Sci.* 102 (9) (2013) 3343–3355.

- [16] T. Takeuchi, et al., Establishment and characterization of the transformants stably-expressing MDR1 derived from various animal species in LLC-PK1, *Pharm. Res.* 23 (7) (2006) 1460–1472.
- [17] E.C. Chen, et al., Evaluating the utility of canine *mdr1* knockout Madin-Darby Canine Kidney I cells in permeability screening and efflux substrate determination, *Mol. Pharm.* 15 (11) (2018) 5103–5113.
- [18] S.A. Jones, et al., The pregnane X receptor: a promiscuous xenobiotic receptor that has diverged during evolution, *Mol. Endocrinol.* 14 (1) (2000) 27–39.
- [19] C. Lu, A.P. Li, Species comparison in P450 induction: effects of dexamethasone, omeprazole, and rifampin on P450 isoforms 1A and 3A in primary cultured hepatocytes from man, Sprague-Dawley rat, minipig, and beagle dog, *Chem. Biol. Interact.* 134 (3) (2001) 271–281.
- [20] Scheer, N., et al., A novel panel of mouse models to evaluate the role of human pregnane X receptor and constitutive androstane receptor in drug response. *J. Clin. Invest.*, 2008. 118(9): p. 3228–3239.
- [21] A.H. Schinkel, et al., Disruption of the mouse *mdr1a* P-glycoprotein gene leads to a deficiency in the blood-brain barrier and to increased sensitivity to drugs, *Cell* 77 (4) (1994) 491–502.
- [22] L.A. Pennacchio, Insights from human/mouse genome comparisons, *Mamm. Genome* 14 (7) (2003) 429–436.
- [23] T.P. Dalton, et al., Targeted knockout of *Cyp1a1* gene does not alter hepatic constitutive expression of other genes in the mouse [Ah] battery, *Biochem. Biophys. Res. Commun.* 267 (1) (2000) 184–189.
- [24] H.C.L. Liang, et al., *Cyp1a2*(–/–) null mutant mice develop normally but show deficient drug metabolism, *Proc. Natl. Acad. Sci. U. S. A.* 93 (4) (1996) 1671–1676.
- [25] J.T.M. Buters, et al., Cytochrome P450 CYP1B1 determines susceptibility to 7,12-dimethylbenz[a]anthracene-induced lymphomas, *Proc. Natl. Acad. Sci. U. S. A.* 96 (5) (1999) 1977–1982.
- [26] S. Uno, et al., Oral benzo[a]pyrene in *Cyp1* knockout mouse lines: CYP1A1 important in detoxication, CYP1B1 metabolism required for immune damage independent of total-body burden and clearance rate, *Mol. Pharmacol.* 69 (4) (2006) 1103–1114.
- [27] J. Lu, et al., CRISPR knockout rat cytochrome P450 3A1/2 model for advancing drug metabolism and pharmacokinetics research, *Sci. Rep.* 7 (2017) 42922.
- [28] A.E. van Herwaarden, et al., Knockout of cytochrome P450 3A yields new mouse models for understanding xenobiotic metabolism, *J. Clin. Invest.* 117 (11) (2007) 3583–3592.
- [29] R.A. van Waterschoot, et al., Midazolam metabolism in cytochrome P450 3A knockout mice can be attributed to up-regulated CYP2C enzymes, *Mol. Pharmacol.* 73 (3) (2008) 1029–1036.
- [30] N. Scheer, et al., Generation and characterization of novel cytochrome P450 *Cyp2c* gene cluster knockout and CYP2C9 humanized mouse lines, *Mol. Pharmacol.* 82 (6) (2012) 1022–1029.
- [31] S. Takahashi, et al., *Cyp2c70* is responsible for the species difference in bile acid metabolism between mice and humans, *J. Lipid Res.* 57 (12) (2016) 2130–2137.
- [32] N. Scheer, et al., Deletion of 30 murine cytochrome p450 genes results in viable mice with compromised drug metabolism, *Drug Metab. Dispos.* 42 (6) (2014) 1022–1030.
- [33] S.S.T. Lee, et al., Role of CYP2E1 in the hepatotoxicity of acetaminophen, *J. Biol. Chem.* 271 (20) (1996) 12063–12067.
- [34] J.W. Knowles, et al., Identification and validation of N-acetyltransferase 2 as an insulin sensitivity gene, *J. Clin. Investig.* 125 (4) (2015) 1739–1751.
- [35] J.A. Loehle, et al., N-acetyltransferase (Nat) 1 and 2 expression in Nat2 knockout mice, *J. Pharmacol. Exp. Ther.* 319 (2) (2006) 724–728.
- [36] V.A. Cornish, et al., Generation and analysis of mice with a targeted disruption of the arylamine N-acetyltransferase type 2 gene, *Pharm. J.* 3 (3) (2003) 169–177.
- [37] K.S. Sugamori, et al., Generation and functional characterization of arylamine N-acetyltransferase Nat1/Nat2 double-knockout mice, *Mol. Pharmacol.* 64 (1) (2003) 170–179.
- [38] N. Nguyen, et al., Disruption of the *Ugt1* locus in mice resembles human Crigler-Najjar type I disease, *J. Biol. Chem.* 283 (12) (2008) 7901–7911.
- [39] M.J. Fay, et al., Xenobiotic metabolism in mice lacking the UDP-glucuronosyltransferase 2 family, *Drug Metab. Dispos.* 43 (12) (2015) 1838–1846.
- [40] T.A. Richardson, C.D. Klaassen, Role of UDP-glucuronosyltransferase (UGT) 2B2 in metabolism of triiodothyronine: effect of microsomal enzyme inducers in Sprague Dawley and UGT2B2-deficient Fischer 344 rats, *Toxicol. Sci.* 116 (2) (2010) 413–421.
- [41] C.J. Henderson, et al., Increased resistance to acetaminophen hepatotoxicity in mice lacking glutathione S-transferase Pi, *Proc. Natl. Acad. Sci. U. S. A.* 97 (23) (2000) 12741–12745.

- [42] M.H. Tong, et al., Spontaneous fetal loss caused by placental thrombosis in estrogen sulfotransferase-deficient mice, *Nat. Med.* 11 (2) (2005) 153–159.
- [43] Y.M. Qian, et al., Targeted disruption of the mouse estrogen sulfotransferase gene reveals a role of estrogen metabolism in intracrine and paracrine estrogen regulation, *Endocrinology* 142 (12) (2001) 5342–5350.
- [44] A.H. Schinkel, et al., Normal viability and altered pharmacokinetics in mice lacking *mdr1*-type (drug-transporting) P-glycoproteins, *Proc. Natl. Acad. Sci. U. S. A.* 94 (8) (1997) 4028–4033.
- [45] M.B. Muller, et al., ABCB1 (MDR1)-type P-glycoproteins at the blood-brain barrier modulate the activity of the hypothalamic-pituitary-adrenocortical system: implications for affective disorder, *Neuropsychopharmacology* 28 (11) (2003) 1991–1999.
- [46] H. Tahara, et al., P-glycoprotein plays a major role in the efflux of fexofenadine in the small intestine and blood-brain barrier, but only a limited role in its biliary excretion (vol 33, pg 963, 2005), *Drug Metab. Dispos.* 34 (6) (2006) 1079.
- [47] M. Foucaud-Vignault, et al., P-glycoprotein dysfunction contributes to hepatic steatosis and obesity in mice, *PLoS One* (2011) 6(9).
- [48] C.M.Z. Liang, et al., Development and Characterization of MDR1 (*Mdr1a/b*) CRISPR/Cas9 Knockout Rat Model, *Drug Metab. Dispos.* 47 (2) (2019) 71–79.
- [49] T. Minich, et al., The multidrug resistance protein 1 (*Mrp1*), but not *Mrp5*, mediates export of glutathione and glutathione disulfide from brain astrocytes, *J. Neurochem.* 97 (2) (2006) 373–384.
- [50] C.F. Mueller, et al., Role of the multidrug resistance protein-1 (MRP1) for endothelial progenitor cell function and survival, *J. Mol. Cell. Cardiol.* 49 (3) (2010) 482–489.
- [51] M.L. Vlaming, et al., Carcinogen and anticancer drug transport by *Mrp2* in vivo: studies using *Mrp2* (*Abcc2*) knockout mice, *J. Pharmacol. Exp. Ther.* 318 (1) (2006) 319–327.
- [52] M.J. Zamek-Gliszczynski, et al., Evaluation of the role of multidrug resistance-associated protein (*Mrp*) 3 and *Mrp4* in hepatic basolateral excretion of sulfate and glucuronide metabolites of acetaminophen, 4-methylumbelliferone, and harmol in *Abcc3*<sup>-/-</sup> and *Abcc4*<sup>-/-</sup> mice, *J. Pharmacol. Exp. Ther.* 319 (3) (2006) 1485–1491.
- [53] R.J. Scialis, et al., Multidrug resistance-associated protein 3 plays an important role in protection against acute toxicity of diclofenac, *Drug Metab. Dispos.* 43 (7) (2015) 944–950.
- [54] N. Zelcer, et al., Mice lacking multidrug resistance protein 3 show altered morphine pharmacokinetics and morphine-6-glucuronide antinociception, *Proc. Natl. Acad. Sci. U. S. A.* 102 (20) (2005) 7274–7279.
- [55] T. Imaoka, et al., Functional involvement of multidrug resistance-associated protein 4 (MRP4/ABCC4) in the renal elimination of the antiviral drugs adefovir and tenofovir, *Mol. Pharmacol.* 71 (2) (2007) 619–627.
- [56] F. Lin, et al., *Abcc4* together with *Abcb1* and *Abcg2* form a robust cooperative drug efflux system that restricts the brain entry of camptothecin analogues, *Clin. Cancer Res.* 19 (8) (2013) 2084–2095.
- [57] X.B. Tian, et al., Impact of basolateral multidrug resistance-associated protein (*Mrp*) 3 and *Mrp4* on the hepatobiliary disposition of fexofenadine in perfused mouse livers, *Drug Metab. Dispos.* 36 (5) (2008) 911–915.
- [58] M.L.H. Vlaming, et al., Impact of *Abcc2* (*Mrp2*) and *Abcc3* (*Mrp3*) on the in vivo elimination of methotrexate and its main toxic metabolite 7-hydroxymethotrexate, *Clin. Cancer Res.* 14 (24) (2008) 8152–8160.
- [59] H. Zaher, et al., Breast cancer resistance protein (*Bcrp/abcg2*) is a major determinant of sulfasalazine absorption and elimination in the mouse, *Mol. Pharm.* 3 (1) (2006) 55–61.
- [60] S. Shukla, et al., Curcumin inhibits the activity of ABCG2/BCRP1, a multidrug resistance-linked ABC drug transporter in mice, *Pharm. Res.* 26 (2) (2009) 480–487.
- [61] J. Enokizono, H. Kusuhara, Y. Sugiyama, Effect of breast cancer resistance protein (*Bcrp/Abcg2*) on the disposition of phytoestrogens, *Mol. Pharmacol.* 72 (4) (2007) 967–975.
- [62] L.Y. Huang, et al., Deletion of *Abcg2* has differential effects on excretion and pharmacokinetics of probe substrates in rats, *J. Pharmacol. Exp. Ther.* 343 (2) (2012) 316–324.
- [63] M. van der Deen, et al., Reduced inflammatory response in cigarette smoke exposed *Mrp1/Mdr1a/1b* deficient mice, *Respir. Res.* 8 (2007) 49.
- [64] J.S. Lagas, et al., P-glycoprotein (*P-gp/Abcb1*), *Abcc2*, and *Abcc3* determine the pharmacokinetics of etoposide, *Clin. Cancer Res.* 16 (1) (2010) 130–140.
- [65] S. Marchetti, et al., Effect of the ATP-binding cassette drug transporters ABCB1, ABCG2, and ABCC2 on erlotinib hydrochloride (Tarceva) disposition in in vitro and in vivo pharmacokinetic studies employing *Bcrp1*<sup>-/-</sup>/*Mdr1a/1b*<sup>-/-</sup> (triple-knockout) and wild-type mice, *Mol. Cancer Ther.* 7 (8) (2008) 2280–2287.

- [66] J.W. Jonker, et al., Reduced hepatic uptake and intestinal excretion of organic cations in mice with a targeted disruption of the organic cation transporter 1 (Oct1 [Slc22a1]) gene, *Mol. Cell. Biol.* 21 (16) (2001) 5471–5477.
- [67] Y. Shu, et al., Effect of genetic variation in the organic cation transporter 1 (OCT1) on metformin action, *J. Clin. Invest.* 117 (5) (2007) 1422–1431.
- [68] L.G. Chen, et al., OCT1 is a high-capacity thiamine transporter that regulates hepatic steatosis and is a target of metformin, *Proc. Natl. Acad. Sci. U. S. A.* 111 (27) (2014) 9983–9988.
- [69] X.M. Liang, et al., Organic cation transporter 1 (OCT1) modulates multiple cardiometabolic traits through effects on hepatic thiamine content, *PLoS Biol.* (2018) 16(4).
- [70] D. Emslie, et al., Oct2 enhances antibody-secreting cell differentiation through regulation of IL-5 receptor alpha chain expression on activated B cells, *J. Exp. Med.* 205 (2) (2008) 409–421.
- [71] G. Ciarimboli, et al., Organic cation transporter 2 mediates cisplatin-induced Oto- and nephrotoxicity and is a target for protective interventions, *Am. J. Pathol.* 176 (3) (2010) 1169–1180.
- [72] J.A. Sprowl, et al., Oxaliplatin-induced neurotoxicity is dependent on the organic cation transporter OCT2, *Proc. Natl. Acad. Sci. U. S. A.* 110 (27) (2013) 11199–11204.
- [73] J.A. Sprowl, et al., Cisplatin-induced renal injury is independently mediated by OCT2 and p53, *Clin. Cancer Res.* 20 (15) (2014) 4026–4035.
- [74] J.W. Jonker, et al., Deficiency in the organic cation transporters 1 and 2 (Oct1/Oct2 [Slc22a1/Slc22a2]) in mice abolishes renal secretion of organic cations, *Mol. Cell. Biol.* 23 (21) (2003) 7902–7908.
- [75] J.W. Higgins, D.W. Bedwell, M.J. Zamek-Gliszczynski, Ablation of both organic cation transporter (Oct)1 and Oct2 alters metformin pharmacokinetics but has no effect on tissue drug exposure and pharmacodynamics, *Drug Metab. Dispos.* 40 (6) (2012) 1170–1177.
- [76] K.C. Wu, et al., Decreased expression of organic cation transporters, Oct1 and Oct2, in brain microvessels and its implication to MPTP-induced dopaminergic toxicity in aged mice, *J. Cereb. Blood Flow Metab.* 35 (1) (2015) 37–47.
- [77] T. Wulsch, et al., Decreased anxiety in mice lacking the organic cation transporter 3, *J. Neural Transm.* 116 (6) (2009) 689–697.
- [78] P.X. Zhu, et al., Targeted disruption of organic cation transporter 3 (Oct3) ameliorates ischemic brain damage through modulating histamine and regulatory T cells, *J. Cereb. Blood Flow Metab.* 32 (10) (2012) 1897–1908.
- [79] Y. Shirasaka, et al., Involvement of organic cation transporter 3 (Oct3/Slc22a3) in the bioavailability and pharmacokinetics of antidiabetic metformin in mice, *Drug Metab. Pharmacokinet.* 31 (5) (2016) 385–388.
- [80] Y. Kato, et al., Gene knockout and metabolome analysis of carnitine/organic cation transporter OCTN1, *Pharm. Res.* 27 (5) (2010) 832–840.
- [81] N. Nakamichi, et al., Involvement of carnitine/organic cation transporter OCTN1/SLC22A4 in gastrointestinal absorption of metformin, *J. Pharm. Sci.* 102 (9) (2013) 3407–3417.
- [82] P.S. Shekhwat, et al., Carnitine content and expression of mitochondrial beta-oxidation enzymes in placentas of wild-type (OCTN2(+/+)) and OCTN2 Null (OCTN2(–/–)) mice, *Pediatr. Res.* 56 (3) (2004) 323–328.
- [83] S.A. Eraly, et al., Decreased renal organic anion secretion and plasma accumulation of endogenous organic anions in OAT1 knock-out mice, *J. Biol. Chem.* 281 (8) (2006) 5072–5083.
- [84] A.M. Torres, et al., Deletion of multispecific organic anion transporter Oat1/Slc22a6 protects against mercury-induced kidney injury, *J. Biol. Chem.* 286 (30) (2011) 26391–26395.
- [85] J.J. Kohler, et al., Tenofovir renal proximal tubular toxicity is regulated By OAT1 and MRP4 transporters, *Lab. Invest.* 91 (6) (2011) 852–858.
- [86] D.H. Sweet, et al., Impaired organic anion transport in kidney and choroid plexus of organic anion transporter 3 (Oat3 [Slc22a8]) knockout mice, *J. Biol. Chem.* 277 (30) (2002) 26934–26943.
- [87] A.L. Vanwert, R.M. Bailey, D.H. Sweet, Organic anion transporter 3 (Oat3/Slc22a8) knockout mice exhibit altered clearance and distribution of penicillin G, *Am. J. Phys. Renal Phys.* 293 (4) (2007) F1332–F1341.
- [88] A.L. VanWert, D.H. Sweet, Impaired clearance of methotrexate in organic anion transporter 3 (Slc22a8) knockout mice: a gender specific impact of reduced folates, *Pharm. Res.* 25 (2) (2008) 453–462.
- [89] W. Wu, et al., Multispecific drug transporter Slc22a8 (Oat3) regulates multiple metabolic and signaling pathways, *Drug Metab. Dispos.* 41 (10) (2013) 1825–1834.
- [90] W. Wu, K.T. Bush, S.K. Nigam, Key role for the organic anion transporters, OAT1 and OAT3, in the in vivo handling of uremic toxins and solutes, *Sci. Rep.* 7 (1) (2017) 4939.



- [91] D. Jappar, et al., Significance and regional dependency of peptide transporter (PEPT) 1 in the intestinal permeability of glycylsarcosine: in situ single-pass perfusion studies in wild-type and Pept1 knockout mice, *Drug Metab. Dispos.* 38 (10) (2010) 1740–1746.
- [92] B. Yang, D.E. Smith, Significance of peptide transporter 1 in the intestinal permeability of valacyclovir in wild-type and Pept1 knockout mice, *Drug Metab. Dispos.* 41 (3) (2013) 608–614.
- [93] M.M. Posada, D.E. Smith, In vivo absorption and disposition of cefadroxil after escalating oral doses in wild-type and Pept1 knockout mice, *Pharm. Res.* 30 (11) (2013) 2931–2939.
- [94] S.M. Ocheltree, et al., Role and relevance of peptide transporter 2 (PEPT2) in the kidney and choroid plexus: in vivo studies with glycylsarcosine in wild-type and PEPT2 knockout mice, *J. Pharmacol. Exp. Ther.* 315 (1) (2005) 240–247.
- [95] H. Shen, et al., Impact of genetic knockout of PEPT2 on cefadroxil pharmacokinetics, renal tubular reabsorption, and brain penetration in mice, *Drug Metab. Dispos.* 35 (7) (2007) 1209–1216.
- [96] M.A. Kamal, et al., Influence of genetic knockout of Pept2 on the in vivo disposition of endogenous and exogenous carnosine in wild-type and Pept2 null mice, *Am. J. Phys. Regul. Integr. Comp. Phys.* 296 (4) (2009) R986–R991.
- [97] M. Tsuda, et al., Targeted disruption of the multidrug and toxin extrusion 1 (mate1) gene in mice reduces renal secretion of metformin, *Mol. Pharmacol.* 75 (6) (2009) 1280–1286.
- [98] K. Toyama, et al., Loss of multidrug and toxin extrusion 1 (MATE1) is associated with metformin-induced lactic acidosis, *Br. J. Pharmacol.* 166 (3) (2012) 1183–1191.
- [99] S. Watanabe, et al., Reduced renal clearance of a zwitterionic substrate cephalexin in MATE1-deficient mice, *J. Pharmacol. Exp. Ther.* 334 (2) (2010) 651–656.
- [100] Q. Li, et al., Indinavir alters the pharmacokinetics of lamivudine partially via inhibition of multidrug and toxin extrusion protein 1 (MATE1), *Pharm. Res.* 35 (1) (2018) 14.
- [101] Y. Zhang, et al., Loss of organic anion transporting polypeptide 1a1 increases deoxycholic acid absorption in mice by increasing intestinal permeability, *Toxicol. Sci.* 124 (2) (2011) 251–260.
- [102] Y. Zhang, et al., Dysfunction of organic anion transporting polypeptide 1a1 alters intestinal bacteria and bile acid metabolism in mice, *PLoS One* 7 (4) (2012) e34522.
- [103] A. Ose, et al., Functional characterization of mouse organic anion transporting peptide 1a4 in the uptake and efflux of drugs across the blood-brain barrier, *Drug Metab. Dispos.* 38 (1) (2010) 168–176.
- [104] L. Gong, et al., Characterization of organic anion-transporting polypeptide (Oatp) 1a1 and 1a4 null mice reveals altered transport function and urinary metabolomic profiles, *Toxicol. Sci.* 122 (2) (2011) 587–597.
- [105] H. Zaher, et al., Targeted disruption of murine organic anion-transporting polypeptide 1b2 (Oatp1b2/Slco1b2) significantly alters disposition of prototypical drug substrates pravastatin and rifampin, *Mol. Pharmacol.* 74 (2) (2008) 320–329.
- [106] M.K. DeGorter, et al., Disposition of atorvastatin, rosuvastatin, and simvastatin in oatp1b2<sup>-/-</sup> mice and intraindividual variability in human subjects, *J. Clin. Pharmacol.* 52 (11) (2012) 1689–1697.
- [107] I.L. Csanaky, et al., Organic anion-transporting polypeptide 1b2 (Oatp1b2) is important for the hepatic uptake of unconjugated bile acids: studies in Oatp1b2-null mice, *Hepatology* 53 (1) (2011) 272–281.
- [108] A.L. Walker, et al., Organic anion transporting polypeptide 1B transporters modulate hydroxyurea pharmacokinetics, *Am. J. Phys. Cell Physiol.* 305 (12) (2013) C1223–C1229.
- [109] E. van de Steeg, et al., Organic anion transporting polypeptide 1a/1b-knockout mice provide insights into hepatic handling of bilirubin, bile acids, and drugs, *J. Clin. Invest.* 120 (8) (2010) 2942–2952.
- [110] J.W. Higgins, et al., Utility of Oatp1a/1b-knockout and OATP1B1/3-humanized mice in the study of OATP-mediated pharmacokinetics and tissue distribution: case studies with pravastatin, atorvastatin, simvastatin, and carboxydichlorofluorescein, *Drug Metab. Dispos.* 42 (1) (2014) 182–192.
- [111] J.H. Chang, et al., Unremarkable impact of Oatp inhibition on the liver concentration of fluvastatin, lovastatin and pitavastatin in wild-type and Oatp1a/1b knockout mouse, *Xenobiotica* 49 (5) (2019) 602–610.
- [112] M. Matsui, M. Hakozaiki, Discontinuous variation in hepatic uridine diphosphate glucuronyltransferase toward androsterone in Wistar rats. A regulatory factor for in vivo metabolism of androsterone, *Biochem. Pharmacol.* 28 (3) (1979) 411–415.
- [113] T.J. Visser, E. Kaptein, E.S. Harpur, Differential expression and ciprofibrate induction of hepatic UDP-glucuronyltransferases for thyroxine and triiodothyronine in Fischer rats, *Biochem. Pharmacol.* 42 (2) (1991) 444–446.



- [114] M. Matsui, F. Nagai, Genetic deficiency of androsterone UDP-glucuronosyltransferase activity in Wistar rats is due to the loss of enzyme protein, *Biochem. J.* 234 (1) (1986) 139–144.
- [115] C.C. Paulusma, et al., Congenital jaundice in rats with a mutation in a multidrug resistance-associated protein gene, *Science* 271 (5252) (1996) 1126–1128.
- [116] P.L. Jansen, W.H. Peters, W.H. Lamers, Hereditary chronic conjugated hyperbilirubinemia in mutant rats caused by defective hepatic anion transport, *Hepatology* 5 (4) (1985) 573–579.
- [117] A. Kadakol, et al., Genetic lesions of bilirubin uridine-diphosphoglucuronate glucuronosyltransferase (UGT1A1) causing Crigler-Najjar and Gilbert syndromes: correlation of genotype to phenotype, *Hum. Mutat.* 16 (4) (2000) 297–306.
- [118] K. Ogawa, et al., Characterization of inducible nature of MRP3 in rat liver, *Am. J. Physiol. Gastrointest. Liver Physiol.* 278 (3) (2000) G438–G446.
- [119] J.R. Chowdhury, R. Kondapalli, N.R. Chowdhury, Gunn rat—a model for inherited deficiency of bilirubin glucuronidation, *Anim. Model Liver Res.* 37 (1993) 149–173.
- [120] O. Takenaka, et al., Different biliary excretion systems for glucuronide and sulfate of a model compound; study using Eisai hyperbilirubinemic rats, *J. Pharmacol. Exp. Ther.* 274 (3) (1995) 1362–1369.
- [121] I.S. Westley, et al., Glucuronidation of mycophenolic acid by Wistar and Mrp2-deficient TR-rat liver microsomes, *Drug Metab. Dispos.* 36 (1) (2008) 46–50.
- [122] S. Nagase, K. Shimamura, S. Shumiya, Albumin-deficient rat mutant, *Science* 205 (4406) (1979) 590–591.
- [123] K. Sugiyama, T. Emori, S. Nagase, Absence of albumin in tissues of analbuminemic rats, *J. Biochem.* 88 (5) (1980) 1413–1417.
- [124] K. Yoshimura, et al., Pharmacokinetics and pharmacodynamics of mycophenolic acid in Nagase analbuminemic rats: evaluation of protein binding effects using the modeling and simulation approach, *Drug Metab. Pharmacokinet.* 30 (6) (2015) 441–448.
- [125] J.H. Chang, et al., Investigating the Impact of Albumin on the Liver Uptake of Pitavastatin and Warfarin in Nagase Analbuminemic Rats, 2019.
- [126] FDA, F.a.D.A., In Vitro Metabolism- and Transporter- Mediated Drug-Drug Interaction Studies: Guidance for Industry (Draft Guidance), C.P. Center for Drug Evaluation and Research, Editor, 2017.
- [127] M.D. Perloff, et al., Midazolam and triazolam biotransformation in mouse and human liver microsomes: relative contribution of CYP3A and CYP2C isoforms, *J. Pharmacol. Exp. Ther.* 292 (2) (2000) 618–628.
- [128] R.A. van Waterschoot, et al., Inhibition and stimulation of intestinal and hepatic CYP3A activity: studies in humanized CYP3A4 transgenic mice using triazolam, *Drug Metab. Dispos.* 37 (12) (2009) 2305–2313.
- [129] J.H. Chang, et al., Differential effects of Rifampin and Ketoconazole on the blood and liver concentration of atorvastatin in wild-type and Cyp3a and Oatp1a/b knockout mice, *Drug Metab. Dispos.* 42 (6) (2014) 1067–1073.
- [130] M.P. Goetz, et al., The impact of cytochrome P450 2D6 metabolism in women receiving adjuvant tamoxifen, *Breast Cancer Res. Treat.* 101 (1) (2007) 113–121.
- [131] K. Kiyotani, et al., Dose-adjustment study of tamoxifen based on CYP2D6 genotypes in Japanese breast cancer patients, *Breast Cancer Res. Treat.* 131 (1) (2012) 137–145.
- [132] N. Scheer, et al., Modeling human cytochrome P450 2D6 metabolism and drug-drug interaction by a novel panel of knockout and humanized mouse lines, *Mol. Pharmacol.* 81 (1) (2012) 63–72.
- [133] B.S. Pybus, et al., The metabolism of primaquine to its active metabolite is dependent on CYP 2D6, *Malar. J.* 12 (2013) 212.
- [134] B.M. Potter, et al., Differential CYP 2D6 metabolism alters primaquine pharmacokinetics, *Antimicrob. Agents Chemother.* 59 (4) (2015) 2380–2387.
- [135] A. Grimsley, et al., Drug-drug interactions and metabolism in cytochrome P450 2C knockout mice: application to toleandomycin and midazolam, *Biochem. Pharmacol.* 86 (4) (2013) 529–538.
- [136] T. Pineau, et al., Neonatal lethality associated with respiratory-distress in mice lacking cytochrome-P450 1a2, *Proc. Natl. Acad. Sci. U. S. A.* 92 (11) (1995) 5134–5138.
- [137] F.J. Gonzalez, S. Kimura, Study of P450 function using gene knockout and transgenic mice, *Arch. Biochem. Biophys.* 409 (1) (2003) 153–158.
- [138] T.C. Peterson, et al., Role of CYP1A2 and CYP2E1 in the pentoxifylline ciprofloxacin drug interaction, *Biochem. Pharmacol.* 68 (2) (2004) 395–402.

- [139] S. Muruganandan, C.J. Sinal, Mice as clinically relevant models for the study of cytochrome P450-dependent metabolism, *Clin. Pharmacol. Therap.* 83 (6) (2008) 818–828.
- [140] S. Kimura, et al., Carcinogenesis of the food mutagen PhIP in mice is independent of CYP1A2, *Carcinogenesis* 24 (3) (2003) 583–587.
- [141] H. Kono, et al., CYP2E1 is not involved in early alcohol-induced liver injury, *Am. J. Phys.* 277 (6) (1999) G1259–G1267.
- [142] K.E. Parrish, et al., In vitro and in vivo characterization of CYP inhibition by 1-aminobenzotriazole in rats, *Biopharm. Drug Dispos.* 37 (4) (2016) 200–211.
- [143] C.J. Henderson, G.J. Pass, C.R. Wolf, The hepatic cytochrome P450 reductase null mouse as a tool to identify a successful candidate entity, *Toxicol. Lett.* 162 (1) (2006) 111–117.
- [144] J.W. Boggs, et al., Assessment of the hepatic CYP reductase null mouse model and its potential application in drug discovery, *Mol. Pharm.* 11 (3) (2014) 1062–1068.
- [145] X.J. Wang, et al., Relationship between hepatic phenotype and changes in gene expression in cytochrome P450 reductase (POR) null mice, *Biochem. J.* 388 (Pt 3) (2005) 857–867.
- [146] J.L. Conroy, et al., Opioids activate brain analgesic circuits through cytochrome P450/epoxygenase signaling, *Nat. Neurosci.* 13 (3) (2010) 284–286.
- [147] F. Collaud, et al., Preclinical development of an AAV8-hUGT1A1 vector for the treatment of Crigler-Najjar syndrome, *Mol. Ther. Methods Clin. Dev.* 12 (2019) 157–174.
- [148] N. Suzuyama, et al., Species differences of inhibitory effects on P-glycoprotein-mediated drug transport, *J. Pharm. Sci.* 96 (6) (2007) 1609–1618.
- [149] S. Baltes, et al., Differences in the transport of the antiepileptic drugs phenytoin, levetiracetam and carbamazepine by human and mouse P-glycoprotein, *Neuropharmacology* 52 (2) (2007) 333–346.
- [150] C. Zimmermann, et al., Species-dependent transport and modulation properties of human and mouse multidrug resistance protein 2 (MRP2/Mrp2, ABCC2/Abcc2), *Drug Metab. Dispos.* 36 (4) (2008) 631–640.
- [151] S.K. Nigam, et al., The organic anion transporter (OAT) family: a systems biology perspective, *Physiol. Rev.* 95 (1) (2015) 83–123.
- [152] International Transporter, C, et al., Membrane transporters in drug development, *Nat. Rev. Drug Discov.* 9 (3) (2010) 215–236.
- [153] W. Xie, et al., Humanized xenobiotic response in mice expressing nuclear receptor SXR, *Nature* 406 (6794) (2000) 435–439.
- [154] P. Wei, et al., The nuclear receptor CAR mediates specific xenobiotic induction of drug metabolism, *Nature* 407 (6806) (2000) 920–923.
- [155] P. Honkakoski, et al., The nuclear orphan receptor CAR-retinoid X receptor heterodimer activates the phenobarbital-responsive enhancer module of the CYP2B gene, *Mol. Cell. Biol.* 18 (10) (1998) 5652–5658.
- [156] P. Wei, et al., Specific and overlapping functions of the nuclear hormone receptors CAR and PXR in xenobiotic response, *Pharm. J.* 2 (2) (2002) 117–126.
- [157] R. Kumar, et al., Compensatory changes in CYP expression in three different toxicology mouse models: CAR-null, Cyp3a-null, and Cyp2b9/10/13-null mice, *PLoS One* (2017) 12(3).
- [158] N. Shin, J.-H. Oh, Y.-J. Lee, Role of drug transporters: an overview based on knockout animal model studies, *J. Pharm. Invest.* 45 (2) (2015) 101–114.
- [159] M. Kuroda, et al., Increased hepatic and renal expressions of multidrug resistance-associated protein 3 in Eisai hyperbilirubinuria rats, *J. Gastroenterol. Hepatol.* 19 (2) (2004) 146–153.
- [160] M.J. Zamek-Gliszczynski, et al., Minor compensatory changes in SAGE Mdr1a (P-gp), Bcrp, and Mrp2 knockout rats do not detract from their utility in the study of transporter-mediated pharmacokinetics, *Drug Metab. Dispos.* 41 (6) (2013) 1174–1178.
- [161] T. Mitsui, et al., A useful model capable of predicting the clearance of cytochrome 3A4 (CYP3A4) substrates in humans: validity of CYP3A4 transgenic mice lacking their own Cyp3a enzymes, *Drug Metab. Dispos.* 42 (9) (2014) 1540–1547.
- [162] E.F. Choo, et al., Use of transgenic mouse models to understand the oral disposition and drug-drug interaction potential of cobimetinib, a MEK inhibitor, *Drug Metab. Dispos.* 43 (6) (2015) 864–869.
- [163] J.Q. Ly, et al., Utility of CYP3A4 and PXR-CAR-CYP3A4/3A7 transgenic mouse models to assess the magnitude of CYP3A4 mediated drug-drug interactions, *Mol. Pharm.* 14 (5) (2017) 1754–1759.
- [164] M. Hasegawa, et al., Quantitative prediction of human pregnane X receptor and cytochrome P450 3A4 mediated drug-drug interaction in a novel multiple humanized mouse line, *Mol. Pharmacol.* 80 (3) (2011) 518–528.

- [165] A.K. MacLeod, et al., Activation status of the pregnane X receptor influences vemurafenib availability in humanized mouse models, *Cancer Res.* 75 (21) (2015) 4573–4581.
- [166] J.H. Chang, et al., Rifampin-mediated induction of tamoxifen metabolism in a humanized PXR-CAR-CYP3A4/3A7-CYP2D6 mouse model, *Drug Metab. Dispos.* 44 (11) (2016) 1736–1741.
- [167] H. Boxenbaum, Interspecies pharmacokinetic scaling and the evolutionary-comparative paradigm, *Drug Metab. Rev.* 15 (5–6) (1984) 1071–1121.
- [168] I. Mahmood, J.D. Balian, Interspecies scaling: predicting clearance of drugs in humans. Three different approaches, *Xenobiotica* 26 (9) (1996) 887–895.
- [169] R. Nagilla, K.W. Ward, A comprehensive analysis of the role of correction factors in the allometric predictivity of clearance from rat, dog, and monkey to humans, *J. Pharm. Sci.* 93 (10) (2004) 2522–2534.
- [170] J.B. Houston, Utility of in vitro drug metabolism data in predicting in vivo metabolic clearance, *Biochem. Pharmacol.* 47 (9) (1994) 1469–1479.
- [171] D. Hallifax, J.B. Houston, Methodological uncertainty in quantitative prediction of human hepatic clearance from in vitro experimental systems, *Curr. Drug Metab.* 10 (3) (2009) 307–321.
- [172] E.M. Howgate, et al., Prediction of in vivo drug clearance from in vitro data. I. Impact of inter-individual variability, *Xenobiotica* 36 (6) (2006) 473–497.
- [173] D. Hallifax, J.A. Foster, J.B. Houston, Prediction of human metabolic clearance from in vitro systems: retrospective analysis and prospective view, *Pharm. Res.* 27 (10) (2010) 2150–2161.
- [174] E.F. Choo, L. Salphati, Leveraging humanized animal models to understand human drug disposition: opportunities, challenges, and future directions, *Clin. Pharmacol. Ther.* 103 (2) (2018) 188–192.
- [175] C. Rodriguez-Antona, et al., Quantitative RT-PCR measurement of human cytochrome P-450s: application to drug induction studies, *Arch. Biochem. Biophys.* 376 (1) (2000) 109–116.
- [176] J.M. Rae, et al., Rifampin is a selective, pleiotropic inducer of drug metabolism genes in human hepatocytes: Studies with cDNA and oligonucleotide expression arrays, *J. Pharmacol. Exp. Ther.* 299 (3) (2001) 849–857.
- [177] C. Tateno, et al., Near completely humanized liver in mice shows human-type metabolic responses to drugs, *Am. J. Pathol.* 165 (3) (2004) 901–912.
- [178] D.F. Mercer, et al., Hepatitis C virus replication in mice with chimeric human livers, *Nat. Med.* 7 (8) (2001) 927–933.
- [179] J.A. Rhim, et al., Replacement of diseased mouse liver by hepatic cell transplantation, *Science* 263 (5150) (1994) 1149–1152.
- [180] M. Dandri, et al., Woodchuck hepatocytes remain permissive for hepadnavirus infection and mouse liver repopulation after cryopreservation, *Hepatology* 34 (4 Pt 1) (2001) 824–833.
- [181] A. Tesfaye, et al., Chimeric mouse model for the infection of hepatitis B and C viruses, *PLoS One* 8 (10) (2013) e77298.
- [182] C. Tateno, et al., Generation of novel chimeric mice with humanized livers by using hemizygous cDNA-uPA/SCID mice, *PLoS One* (2015) 10(11).
- [183] H. Azuma, et al., Robust expansion of human hepatocytes in *Fah(-/-)/Rag2(-/-)/Il2rg(-/-)* mice, *Nat. Biotechnol.* 25 (8) (2007) 903–910.
- [184] K.D. Bissig, et al., Repopulation of adult and neonatal mice with human hepatocytes: a chimeric animal model, *Proc. Natl. Acad. Sci. U. S. A.* 104 (51) (2007) 20507–20511.
- [185] M. Hasegawa, et al., The reconstituted ‘humanized liver’ in TK-NOG mice is mature and functional, *Biochem. Biophys. Res. Commun.* 405 (3) (2011) 405–410.
- [186] H. Suemizu, et al., Establishment of a humanized model of liver using NOD/Shi-scid IL2Rg(null) mice, *Biochem. Biophys. Res. Commun.* 377 (1) (2008) 248–252.
- [187] J.L. Heckel, et al., Neonatal bleeding in transgenic mice expressing urokinase-type plasminogen activator, *Cell* 62 (3) (1990) 447–456.
- [188] N.M. Brezillon, et al., Rescue of fertility in homozygous mice for the urokinase plasminogen activator transgene by the transplantation of mouse hepatocytes, *Cell Transplant.* 17 (7) (2008) 803–812.
- [189] S. Sun, J. Li, Humanized chimeric mouse models of hepatitis B virus infection, *Int. J. Infect. Dis.* 59 (2017) 131–136.
- [190] K. Kato, et al., Development of murine Cyp3a knockout chimeric mice with humanized liver, *Drug Metab. Dispos.* 43 (8) (2015) 1208–1217.
- [191] M. Dandri, et al., Repopulation of mouse liver with human hepatocytes and in vivo infection with hepatitis B virus, *Hepatology* 33 (4) (2001) 981–988.

- [192] A. Kaul, et al., Cell culture adaptation of hepatitis C virus and in vivo viability of an adapted variant, *J. Virol.* 81 (23) (2007) 13168–13179.
- [193] P. Meuleman, G. Leroux-Roels, The human liver-uPA-SCID mouse: a model for the evaluation of antiviral compounds against HBV and HCV, *Antivir. Res.* 80 (3) (2008) 231–238.
- [194] N. Nakada, Evaluation of the utility of chimeric mice with humanized livers for the characterization and profiling of the metabolites of a selective inhibitor (YM543) of the sodium-glucose cotransporter 2, *Pharm. Res.* 34 (4) (2017) 874–886.
- [195] N. Nakada, et al., Murine Cyp3a knockout chimeric mice with humanized liver: prediction of the metabolic profile of nefazodone in humans, *Biopharm. Drug Dispos.* 37 (1) (2016) 3–14.
- [196] N. Nakada, K. Oda, Identification and characterization of metabolites of ASP015K, a novel oral Janus kinase inhibitor, in rats, chimeric mice with humanized liver, and humans, *Xenobiotica* 45 (9) (2015) 757–765.
- [197] T.J. Bateman, et al., Application of chimeric mice with humanized liver for study of human-specific drug metabolism, *Drug Metab. Dispos.* 42 (6) (2014) 1055–1065.
- [198] A.J. Barnes, et al., Endogenous and xenobiotic metabolite profiling of liver extracts from SCID and chimeric humanized mice following repeated oral administration of troglitazone, *Xenobiotica* 44 (2) (2014) 174–185.
- [199] Y. Igawa, et al., In vitro and in vivo metabolism of a novel chymase inhibitor, SUN13834, and the predictability of human metabolism using mice with humanized liver, *Xenobiotica* 44 (2) (2014) 154–163.
- [200] T. Nishimura, et al., Using chimeric mice with humanized livers to predict human drug metabolism and a drug-drug interaction, *J. Pharmacol. Exp. Ther.* 344 (2) (2013) 388–396.
- [201] M. De Serres, et al., Evaluation of a chimeric (uPA+/+)/SCID mouse model with a humanized liver for prediction of human metabolism, *Xenobiotica* 41 (6) (2011) 464–475.
- [202] H. Kamimura, et al., Assessment of chimeric mice with humanized liver as a tool for predicting circulating human metabolites, *Drug Metab. Pharmacokinet.* 25 (3) (2010) 223–235.
- [203] L. Lootens, et al., Steroid metabolism in chimeric mice with humanized liver, *Drug Test. Anal.* 1 (11-12) (2009) 531–537.
- [204] L. Lootens, et al., The uPA(+/-)-SCID mouse with humanized liver as a model for in vivo metabolism of 4-androstene-3,17-dione, *Drug Metab. Dispos.* 37 (12) (2009) 2367–2374.
- [205] T. Inoue, et al., CYP2C9-catalyzed metabolism of S-warfarin to 7-hydroxywarfarin in vivo and in vitro in chimeric mice with humanized liver, *Drug Metab. Dispos.* 36 (12) (2008) 2429–2433.
- [206] M. Uchida, et al., Organic anion-transporting polypeptide (OATP)-mediated drug-drug interaction study between rosuvastatin and cyclosporine A in chimeric mice with humanized liver, *Drug Metab. Dispos.* 46 (1) (2018) 11–19.
- [207] K.G. Jensen, et al., Lack of exposure in a first-in-man study due to aldehyde oxidase metabolism: investigated by use of C-14-microdose, humanized mice, monkey pharmacokinetics, and in vitro methods, *Drug Metab. Dispos.* 45 (1) (2017) 68–75.
- [208] S. Sanoh, et al., Predictability of plasma concentration-time curves in humans using single-species allometric scaling of chimeric mice with humanized liver, *Xenobiotica* 45 (7) (2015) 605–614.
- [209] S. Sanoh, et al., Prediction of in vivo hepatic clearance and half-life of drug candidates in human using chimeric mice with humanized liver, *Drug Metab. Dispos.* 40 (2) (2012) 322–328.
- [210] H. Okumura, et al., Humanization of excretory pathway in chimeric mice with humanized liver, *Toxicol. Sci.* 97 (2) (2007) 533–538.
- [211] M. Kakuni, et al., Chimeric mice with humanized livers: a unique tool for in vivo and in vitro enzyme induction studies, *Int. J. Mol. Sci.* 15 (1) (2013) 58–74.
- [212] M. Hasegawa, et al., Investigation of drug-drug interactions caused by human pregnane X receptor-mediated induction of CYP3A4 and CYP2C subfamilies in chimeric mice with a humanized liver, *Drug Metab. Dispos.* 40 (3) (2012) 474–480.
- [213] C. Emoto, et al., Non-invasive method to detect induction of CYP3A4 in chimeric mice with a humanized liver, *Xenobiotica* 38 (3) (2008) 239–248.
- [214] R. Kikuchi, et al., Effect of hepatitis C virus infection on the mRNA expression of drug transporters and cytochrome p450 enzymes in chimeric mice with humanized liver, *Drug Metab. Dispos.* 38 (11) (2010) 1954–1961.
- [215] K. Samuelsson, et al., Troglitazone metabolism and transporter effects in chimeric mice: a comparison between chimeric humanized and chimeric murinized FRG mice, *Xenobiotica* 44 (2) (2014) 186–195.
- [216] E.C. Chow, et al., Functional integrity of the chimeric (humanized) mouse liver: enzyme zonation, physiologic spaces, and hepatic enzymes and transporters, *Drug Metab. Dispos.* 44 (9) (2016) 1524–1535.

- [217] A.P. Dickie, et al., The pharmacokinetics and metabolism of lumiracoxib in chimeric humanized and murinized FRG mice, *Biochem. Pharmacol.* 135 (2017) 139–150.
- [218] H. Yamazaki, et al., In vivo formation of dihydroxylated and glutathione conjugate metabolites derived from thalidomide and 5-hydroxythalidomide in humanized TK-NOG mice, *Chem. Res. Toxicol.* 25 (2) (2012) 274–276.
- [219] A. Tsukada, et al., Plasma concentrations of melengestrol acetate in humans extrapolated from the pharmacokinetics established in in vivo experiments with rats and chimeric mice with humanized liver and physiologically based pharmacokinetic modeling, *Regul. Toxicol. Pharmacol.* 65 (3) (2013) 316–324.
- [220] H. Yamazaki, et al., In vivo drug interactions of the teratogen thalidomide with midazolam: heterotropic cooperativity of human cytochrome P450 in humanized TK-NOG mice, *Chem. Res. Toxicol.* 26 (3) (2013) 486–489.
- [221] D. Xu, et al., Chimeric TK-NOG mice: a predictive model for cholestatic human liver toxicity, *J. Pharmacol. Exp. Ther.* 352 (2) (2015) 274–280.
- [222] T. Miyaguchi, et al., Human urine and plasma concentrations of bisphenol A extrapolated from pharmacokinetics established in in vivo experiments with chimeric mice with humanized liver and semi-physiological pharmacokinetic modeling, *Regul. Toxicol. Pharmacol.* 72 (1) (2015) 71–76.
- [223] H. Kamimura, et al., Simulation of human plasma concentration-time profiles of the partial glucokinase activator PF-04937319 and its disproportionate N-demethylated metabolite using humanized chimeric mice and semi-physiological pharmacokinetic modeling, *Xenobiotica* 47 (5) (2017) 382–393.
- [224] T. Miura, et al., Human urinary concentrations of monoisononyl phthalate estimated using physiologically based pharmacokinetic modeling and experimental pharmacokinetics in humanized-liver mice orally administered with diisononyl phthalate, *Xenobiotica* 49 (5) (2019) 513–520.
- [225] N. Scheer, I.D. Wilson, A comparison between genetically humanized and chimeric liver humanized mouse models for studies in drug metabolism and toxicity, *Drug Discov. Today* 21 (2) (2016) 250–263.
- [226] K.D. Bissig, et al., P450-humanized and human liver chimeric mouse models for studying xenobiotic metabolism and toxicity, *Drug Metab. Dispos.* 46 (11) (2018) 1734–1744.
- [227] E.P. Sandgren, et al., Complete hepatic regeneration after somatic deletion of an albumin-plasminogen activator transgene, *Cell* 66 (2) (1991) 245–256.
- [228] M. Katoh, et al., In vivo drug metabolism model for human cytochrome P450 enzyme using chimeric mice with humanized liver, *J. Pharm. Sci.* 96 (2) (2007) 428–437.
- [229] K. Overturf, et al., Adenovirus-mediated gene therapy in a mouse model of hereditary tyrosinemia type I, *Hum. Gene Ther.* 8 (5) (1997) 513–521.
- [230] K.D. Bissig, et al., Human liver chimeric mice provide a model for hepatitis B and C virus infection and treatment, *J. Clin. Invest.* 120 (3) (2010) 924–930.
- [231] M. Barzi, et al., A novel humanized mouse lacking murine P450 oxidoreductase for studying human drug metabolism, *Nat. Commun.* 8 (2017).
- [232] M.L. Washburn, et al., A humanized mouse model to study hepatitis C virus infection, immune response, and liver disease, *Gastroenterology* 140 (4) (2011) 1334–1344.
- [233] R.R. Zhang, et al., Human hepatic stem cells transplanted into a fulminant hepatic failure Alb-TRECK/SCID mouse model exhibit liver reconstitution and drug metabolism capabilities, *Stem Cell Res. Ther.* 6 (2015) 49.
- [234] E.C. Chow, et al., Disrupted murine gut-to-human liver signaling alters bile acid homeostasis in humanized mouse liver models, *J. Pharmacol. Exp. Ther.* 360 (1) (2017) 174–191.

# Advances in CRISPR technologies enable novel in vitro tools for ADME studies

*Eugene Chia-Te Chen*

Department of Drug Metabolism and Pharmacokinetics, Genentech, South San Francisco, CA, United States

## 1 Introduction

Class 2 clustered regularly interspaced short palindromic repeat (CRISPR) system was originally discovered as an adaptive immune system in bacteria [1]. The system has since been modified for a plethora of technologies, such as genome editing and was successfully deployed in many cell types and organisms. While several genome editing tools were developed previously, they often rely on protein-DNA recognition mechanisms to disrupt targeted genes. Approaches such as transcription-activator-like effector nucleases (TALENs) and zinc-finger nucleases (ZFNs) require the generation of precisely engineered nucleases for every targeted gene. On the other hand, the CRISPR system only requires the delivery of target-specific single-guide RNAs (sgRNAs) and CRISPR-associated endonuclease (Cas) into target cells. The simplicity of the system not only made it more approachable to researchers, but also enabled continued refinement and modification.

At its inception, CRISPR was developed to disrupt genes by introducing double-strand breaks (DSBs) within the targeted genomic region utilizing Cas endonucleases. Since then, the CRISPR toolbox has expanded far beyond its original utility and now covers applications across the central dogma of molecular biology (Fig. 1). The use of divergent homologs of the Cas proteins made it possible to edit RNA, and the modified catalytically dead Cas9 (dCas9) nuclease enabled the system to repress, activate, or label targeted genes. This transformative technology holds great potential in interrogating drug-metabolizing enzymes and transporters, and further the mechanistic understanding of drug metabolism and disposition.



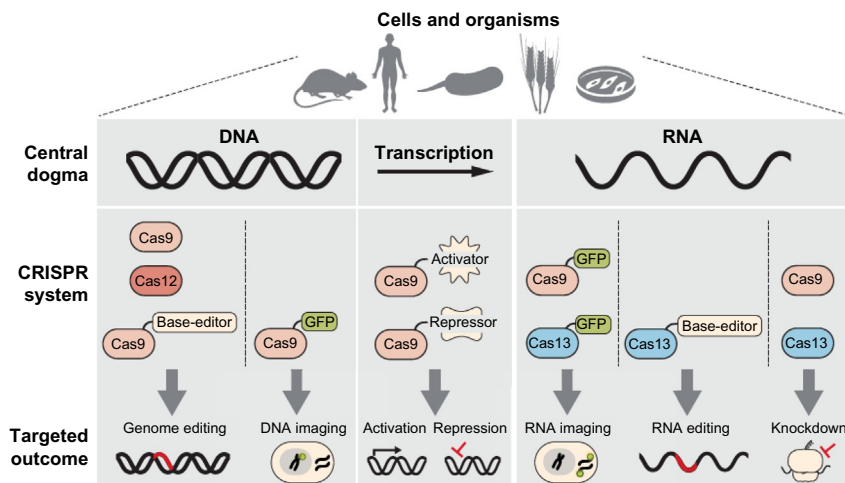


**FIG. 1** CRISPR systems enable genetic manipulation across the central dogma. Using modified and different homologs of Cas proteins, CRISPR has capabilities beyond genome editing. Catalytically deficient Cas proteins (dCas9) fused with fluorescent proteins can be used to image genomic DNA regions. dCas9 proteins fused with transcriptional modifiers can be used to activate or repress transcription. In addition, homologs of Cas proteins (e.g., Cas13) can also be used to expand the applications to RNA as well. *Credit: G.J. Knott, J.A. Doudna, Science 361 (2018) 866–869.*

In this chapter, we focus on in vitro applications of CRISPR relevant to the ADME (absorption, distribution, metabolism, and excretion) field, recent examples utilizing the technology, and opportunities for future ADME studies.

## 2 In vitro applications of CRISPR

### 2.1 Genome editing with CRISPR

In their fight against bacteriophages, bacteria evolved CRISPR as an adaptive immune system consisting of a combination of proteins (Cas proteins) and short RNAs (sgRNAs) [2]. The short sgRNAs are expressed from short protospacers collected from foreign DNA sequences in the bacterial genome and are used to match targeted sequences for cleavage by Cas proteins. Taking advantage of the mechanism, CRISPR was modified to edit the genomic DNA in eukaryotic cells [3]. Using a sgRNA with a 20-bp sequence matching the targeted genetic locus and specific downstream nucleotides [the protospacer-adjacent motif (PAM), a three-nucleotide sequence], Cas protein (specifically, Cas9) forms a complex with the genomic DNA and introduces the DSB [4]. When a DSB is detected, cells will attempt to repair it by nonhomologous end joining (NHEJ) or homology-directed repair (HDR, Fig. 2). NHEJ is an error-prone process and frequently results in random insertions or deletions (indels) at the site of repair. These indels can potentially cause the premature termination of translation or out-of-frame transcription resulting in truncated, nonfunctional versions of proteins, effectively knocking out the targeted gene.



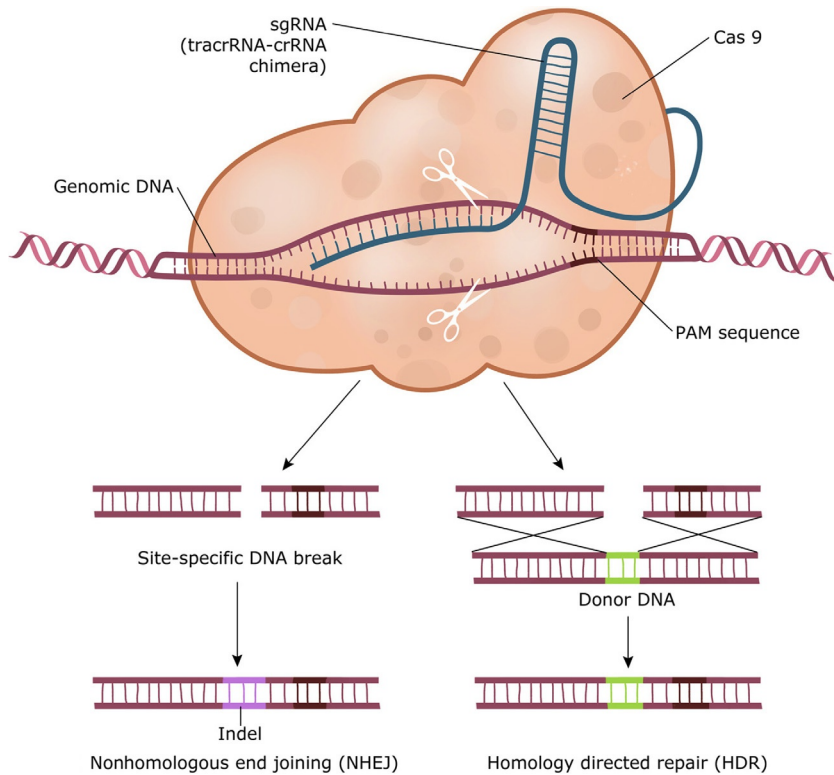


**FIG. 2** DSBs introduced by CRISPR-Cas9 are repaired by NHEJ and HDR. Cas9 protein forms a complex with sgRNA and targeted genomic DNA, and introduced a double break. Cells will attempt to repair the DSBs by either the error-prone nonhomologous end joining (NHEJ) or high-fidelity homology-directed repair (HDR) when a template is available. These repair mechanisms formed the basis of the genome editing utility of CRISPR-Cas9. *Credit: N. Savić, G. Schwank, Advances in therapeutic CRISPR/Cas9 genome editing, Transl. Res. 168 (2016) 15–21.*

In contrast to the high efficiency of NHEJ, HDR occurs at low frequency but with high fidelity when repair templates are available. Exploiting the repair mechanism, the CRISPR system and appropriate repair templates can generate alterations from specific single-nucleotide changes to large insertions such as epitope tags and fluorophores [5]. These repair mechanisms, NHEJ and HDR, formed the basis of the genome editing utility of CRISPR and allowed researchers to manipulate cells and organisms with unprecedented ease. In this section, we will focus on the applications that are more relevant to in vitro ADME studies.

## 2.2 Repression of target genes with CRISPR

An interesting property of the Cas enzyme is the ability to bind to DNA independently of its nuclease activity. Specific point mutations in the nuclease domains of the Cas9 resulted in the loss of the DNA cleavage activity, yet the modified Cas9 retained their ability to bind to DNA sequences targeted by the sgRNAs [3]. In fact, the catalytically deficient Cas (dCas9)

binds so tightly to the targeted DNA sequence; it is able to decrease the expression of targeted genes by blocking the binding of endogenous transcription factors and the activity of RNA polymerase II [6]. This gene repression activity of dCas9 is termed as CRISPR interference (CRISPRi), and further development of the system was made to produce more specific and effective repression of the targeted gene expression. One strategy is to fuse dCas9 with transcriptional repressors, and the fusion of Kruppel-associated box (KRAB) to dCas9 was shown to knockdown the targeted gene successfully [7]. While wild-type Cas9 knocks out the targeted gene by introducing DSB, CRISPRi knocks down the expression at the transcriptional level. In the case of dCas9-KRAB, the system suppresses expression by epigenetic reprogramming through recruiting additional corepressors and epigenetic readers, in addition to the direct interference of transcription machinery. The result is the reversible regulation of gene expression, and the system can be particularly useful for studying essential genes that cause lethality when completely knocked out.

### 2.3 Activation of target genes with CRISPR

Instead of fusion dCas9 with transcriptional repressors, transcriptional activators theoretically can be fused with dCas9 to activate target gene expression. Indeed, initial effort fusing dCas9 with tandem copies of the transactivation domain (VP64) of the Herpes simplex virus was successful in inducing transcription, especially when multiple sgRNAs targeting the same region acted synergistically [8]. The CRISPR-based gene activation system (CRISPRa) was further modified for more robust gene activation. One strategy was to fuse additional transcriptional activators to dCas9 to achieve higher expression. While dCas9 fused with p65, a subunit of NF- $\kappa$ B transcription factor complex, and dCas9 fused with Rta, the Epstein-Barr virus transactivator, produce weaker induction compared to dCas9 fused with V64, the dCas9 fused with the hybrid tripartite V64-p65-Rta (VPR) was able to achieve the highest transcriptional activity [9]. In another strategy, modifications were made to sgRNA in an attempt to boost activation. Crystal structure and functional data revealed portions of sgRNA that do not affect Cas9 activity when modified. Hairpin sequences that selectively bind to MS2 bacteriophage coat proteins were then added to those regions. The modified sgRNA was able to activate transcription through MS2-mediated V64 recruitment and demonstrate higher activity compared to dCas9-V64. Additional optimization of the system resulted in a synergistic activation mediator (SAM) system comprised of dCas9-V64 and MS2 fused with p65 and heat shock factor 1 (HSF1) that offered superior transcriptional activity [10]. Lastly, an antibody-fusion protein was utilized to activate gene expression in the SunTag system. In this system, dCas9 fused with an array of peptide epitopes is co-expressed with the antibody-V64 fusion protein. The peptide array is capable of recruiting up to 24 copies of the antibody-V64 protein resulting in stronger induction compared to the dCas9-V64 approach [11]. While a comparison among various CRISPRa systems demonstrated that all of the modified CRISPRa systems consistently induce stronger gene activation than the original dCas9-V64 system, functional testing and optimization may be required to identify the ideal approach for specific cell types and assays of interest [12].

## 2.4 Genetic screens with CRISPR

Prior to the discovery of RNA interference (RNAi) technology, methods to efficiently and effectively perturb gene expression of in vitro models were lacking. The development of RNAi-based genetic screens offered a useful tool for researchers to generate hypotheses and discover previously unknown genes and pathways involved in specific phenotypes. However, RNAi-based screens suffer from off-target effects, and insufficient knockdown of target genes would potentially lead to false negatives. With the discovery and development of CRISPR, researchers now have an alternative method to knockout, knockdown, or activate genes in genetic screens. Furthermore, the relative ease to synthesize and design sgRNAs and the continued improvement in specificity have made CRISPR an attractive tool for such studies.

Two strategies are available when conducting CRISPR screen: arrayed screens and pooled screens. Both arrayed and pooled libraries come in different sizes ranging from targeting a small subset of genes to targeting the whole genome. Arrayed screens typically come in 96- or 384-well formats where each well contains multiple sgRNAs targeting a single gene. The arrayed library can be delivered to cells in 96- or 384-well formats for positive or negative selection [13]. In contrast, in pooled libraries, sgRNAs targeting individual genes are kept together instead of depositing in separated wells. The sgRNAs are delivered in vectors (usually lentiviral particles) at low efficiency so that each cell only contains a single sgRNA. After positive or negative selection, hits are identified with next-generation sequencing.

While arrayed and pooled libraries targeting the whole genome are commercially available, it might not be the most sensible approach for ADME-related questions. The success of genetic screens relies equally on three components: the perturbation, the model, and the assay. Besides choosing the right model and optimizing the assay, it is as important to select the appropriate library for the screen [14]. For example, it might not be necessary to use a whole-genome library to knockdown 18,000 genes when one is trying to identify the drug-metabolizing enzymes/transporters involved in a particular drug-disposition pathway.

## 3 Examples of CRISPR application in ADME studies in vitro

A recent survey has identified about 50 publications utilizing CRISPR to edit ADME-related genes, including cytochrome P450s (CYPs), solute carriers (SLCs), and ATP-binding cassette (ABC) transporters [15]. Most of these publications used the technology to knockout genes in animal models, such as zebra fish, fruit flies, and rodent species. Of the manuscripts applying CRISPR in vitro, several researchers attempted to reverse drug resistance in cancer-derived cell lines [16–20], and only five manuscripts directly used the technology to address ADME-related questions at the time of publication of this chapter. One manuscript generated an induced pluripotent stem cell line expressing a fluorescence-tagged PXR fusion protein, but no follow-up experiments were reported. In this section, we highlight one publication applying CRISPR to edit a loss-of-function CYP3A5 allele in a liver cell line [21], and three publications knocking out the endogenous P-gp expression in a canine cell line commonly used in permeability determination and efflux transporter assays [22–24].

### 3.1 Genetic modification of *CYP3A5*\*3 in Huh-7 cells

*CYP3A5*\*3 is a loss-of-function allele that is prevalent in Caucasians [25]. Individuals with the loss-of-function allele reported slower metabolism of *CYP3A5* substrates, such as tacrolimus and midazolam [26]. In contrast, individuals with the *CYP3A5*\*1 expresser allele, which is common among African Americans, metabolize these drugs and other *CYP3A5* substrates at a much higher rate compared to those with the *CYP3A5*\*3 allele [27]. The difference in metabolism has clinical implications, and individuals with the functional *CYP3A5* allele often require a higher dose of tacrolimus to reach therapeutic concentration [28]. However, Dorr et al. noted that no cell-based system was available at the time to study the genetic polymorphism in vitro [21].

In order to create such an in vitro model, Dorr et al. identified Huh-7 cell line, a hepatic carcinoma-derived cell line that harbors the *CYP3A5*\*3 loss-of-function allele, for genomic editing. Two strategies were employed to disrupt the exon 3B splice junction to remove exon 3B, and effectively restoring enzyme activity. In one experimental design, the sgRNA targeting the splice junction created a DSB, and the error-prone NHEJ repair mechanism created a 77-bp deletion in the region. In the other, a single-stranded DNA template was

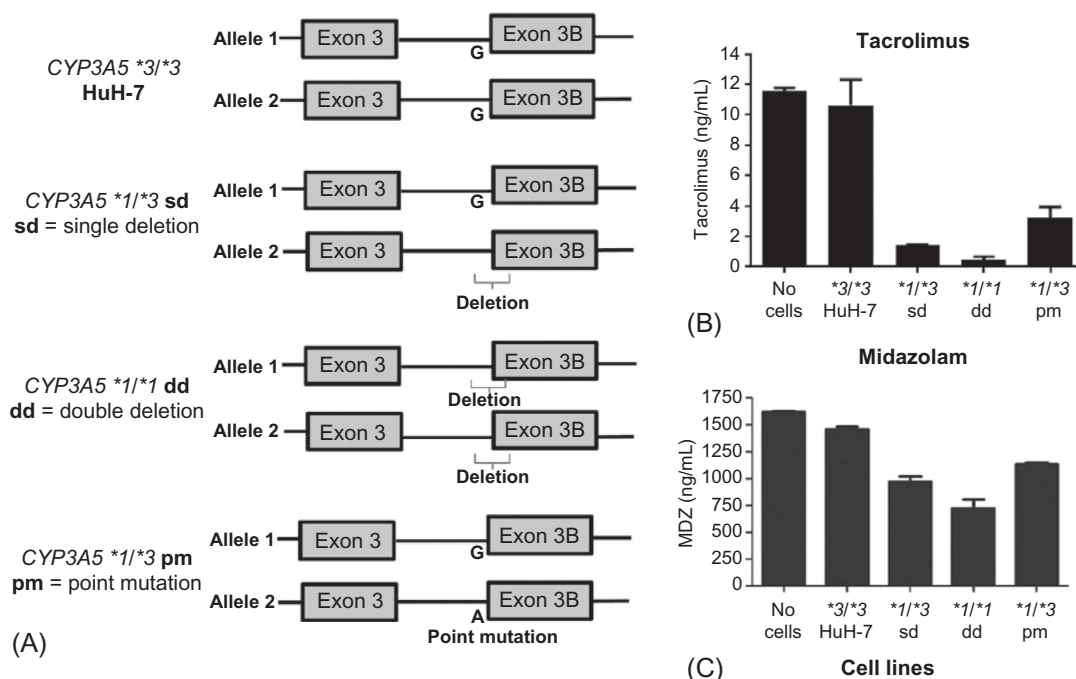


**FIG. 3** Genetic modification of the *CYP3A5*\*3 allele by CRISPR increases tacrolimus and midazolam metabolism. (A) Genetic modifications made to the *CYP3A5*\*3 allele to restore *CYP3A5* expression and activity. The disappearance of tacrolimus (B) and midazolam (C) was used as an indicator of *CYP3A5* activity. Modified Huh-7 harboring one or two copies of functional *CYP3A5*\*1 had higher metabolism activity. The 77-bp deletion of the 3B splice junction from both alleles (\*1/\*1 dd) resulted in the highest enzyme activity. Credit: C.R. Dorr, et al., *Drug Metab. Dispos.* 45 (2017) 957–965.

introduced with the sgRNA, taking advantage of the higher fidelity HDR repair mechanism. The goal was to introduce a single-point mutation within the splice junction. Subsequent single-cell cloning and DNA sequencing identified clones of Huh-7 cells with a variety of indels, and a single clone with the desired point mutation at the splice junction (Fig. 3A). Analysis of mRNA expression levels and metabolism activities demonstrated that CRISPR-mediated gene editing restored *CYP3A5* gene expression and activity in Huh-7 clones with the 77-bp deletion and the point mutation (Fig. 3B and C) [21].

This study elegantly demonstrated the strength of CRISPR and its utility in in vitro ADME studies. The genome editing tool was used to edit the genotype of an endogenous drug-metabolizing enzyme and enabled the study of a clinically significant genetic polymorphism in a hepatocyte cell line. However, the limitation of CRISPR was also exposed. The efficiency of CRISPR in the study was low, and less than 10% of the sorted single-cell clones harbored the desired deletion at the splice junction. The efficiency of HDR-mediated editing was even lower. Out of more than 200 sorted clones, only one clone was successfully edited to carry the heterozygous point mutation. The low gene-editing efficiency and the need to isolate and expand single clones preclude applying CRISPR directly to primary hepatocytes.

### 3.2 Endogenous Canine P-gp knockout in Madin-Darby canine kidney cells

Madin-Darby canine kidney (MDCK) cell line is commonly used in in vitro ADME studies due to its presumed low expression of endogenous metabolizing enzymes and transporters and its ability to become polarized when cultured in the transwell system. Apparent permeability values determined with MDCK cells, the rates of which compounds permeate across an MDCK monolayer, correlated well with absorption in humans [29]. As a result, the MDCK permeability assay is routinely conducted during small-molecule drug discovery. The MDCK cell line is also used in transporter inhibition and substrate studies, where a transporter of interest is overexpressed in MDCK cells, and the inhibition potency or substrate potential of compounds is determined. However, it was discovered that MDCK cells exhibited endogenous efflux activity, and this activity could potentially affect permeability and transporter assay readouts. In order to mitigate the effect, a subpopulation of MDCK cells with low efflux activity was isolated and shown to express a significantly reduced level of canine P-gp (*Mdr1*) mRNA [30]. The observation led to the hypothesis that canine P-gp is responsible for the endogenous efflux activity in the wild-type MDCK cells. The hypothesis was tested when two groups independently knockout canine P-gp in MDCK lines (MDCKI and MDCKII) using CRISPR technology [23, 24].

Both groups used plasmid-based techniques to deliver sgRNA and Cas9 into cells. Using fluorescence-activated cell sorting, single clones of successfully transfected cells were isolated and expanded. The CRISPR-mediated editing of the canine P-gp gene was confirmed by Sanger sequencing and predicted to produce a truncated protein. The canine P-gp knockout was further validated, as the canine P-gp protein was no longer detectable by LC-MS/MS-based proteomics (Fig. 4A). Functional studies showed that while prototypical P-gp substrates showed efflux activity in wild-type cells, no efflux activity was observed in canine P-gp knockout MDCK cells (Fig. 4B). Permeability screens of 135 Genentech compounds in wild-type MDCK cells showed that 38% of the compounds tested exhibited efflux activity. In contrast, none of the 135 compounds showed any efflux activity in the knockout cells,

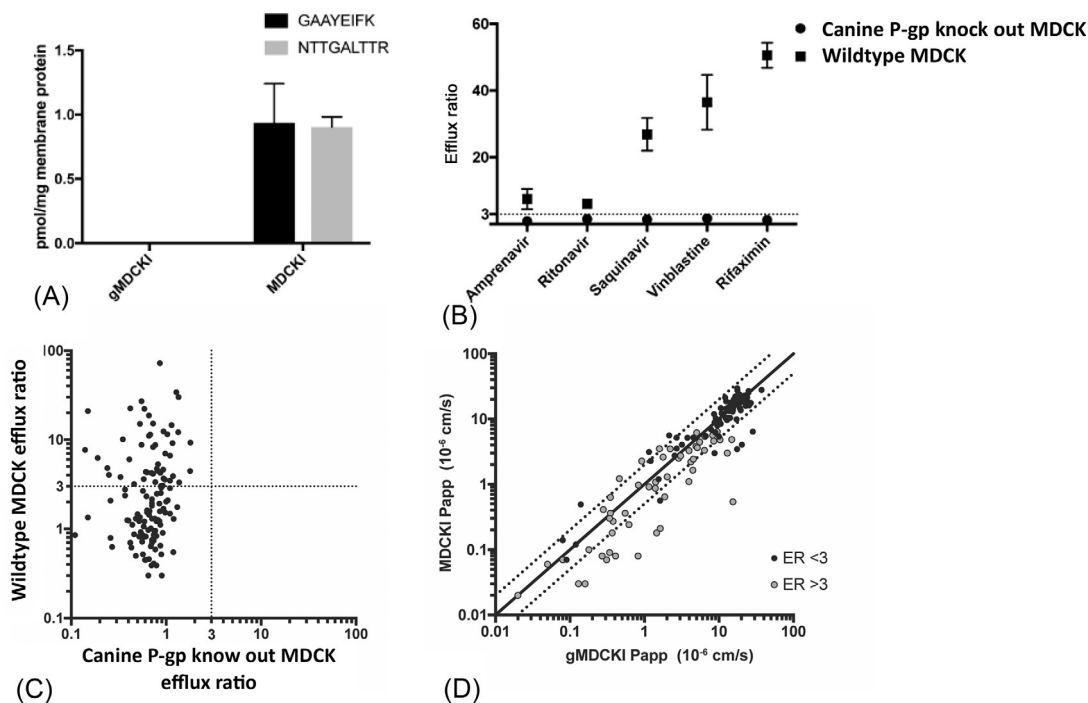


**FIG. 4** CRISPR-mediated canine P-gp knockout eliminated endogenous efflux and improved permeability measurement. (A) Relative quantitation of two peptides mapped to canine P-gp by LC-MS/MS. The monitored peptides were detectable in the wild-type cells but were below the limit of quantitation in the canine P-gp knockout cells. (B) Efflux ratios of prototypical P-gp substrates in wild-type cells were over 3, indicating efflux activity by endogenous transporters. Knocking out canine P-gp reduce the ratios to below 3, suggesting the canine P-gp was responsible for the endogenous efflux activity. (C) Efflux ratios of 135 Genentech compounds determined in wild-type cells and canine P-gp knockout cells. While 35% of compounds had efflux activity in wild-type cells, none showed efflux activity in canine P-gp knockout cells. (D) Apparent permeability of 135 Genentech compounds determined in wild-type cells and canine P-gp knockout cells. About 17% of compounds showed higher permeability in canine P-gp knockout cells. Credit: E.C. Chen, et al., *Mol. Pharm.* 15 (2018) 5103–5113.

suggesting that canine P-gp was largely responsible for the efflux activity observed in wild-type cells (Fig. 4C). About 17% of the compounds tested also showed improved permeability in the canine P-gp knockout cells. Most of these compounds showed efflux activity in the wild-type MDCK cells, which suggests the compounds' intrinsic ability to cross MDCK monolayer were masked by the endogenous efflux activity (Fig. 4D).

Transporter substrate determination is routinely conducted in MDCK cells overexpressing the transporter of interest. However, it is recognized that the transporter-overexpressing model could produce ambiguous results when the compound tested is also an endogenous efflux substrate. In order to mitigate the effect, the US Food and Drug Administration recommended determining net efflux ratios by dividing efflux ratios in transporter-overexpressing cells over wild-type MDCK cells. Nevertheless, calculating the net efflux ratio could potentially result in false negatives and fail to identify transporter substrates correctly. In an effort to improve upon the MDCK model, Karlgren et al. knocked out the canine P-gp in



an MDCK line overexpressing human P-gp with CRISPR and showed that the human P-gp expression and activity was preserved [22]. Separately, Chen et al. achieved the same goal by overexpressing human P-gp in the canine P-gp knockout MDCK cells generated previously. The human P-gp overexpressing MDCK cell lines enabled substrate determination without the contribution of canine P-gp and were able to identify species differences in substrate specificity [24].

In the example above, the authors were able to utilize CRISPR to knockout a specific gene with relative ease compared to other genetic editing tools. The specificity of the technology was also demonstrated when one group was able to design sgRNAs to knockout the canine P-gp exclusively without affecting the overexpressed human P-gp. This example also highlighted the potential of CRISPR to improve routinely used in vitro ADME tools. As a result of the studies, the contribution of endogenous efflux activity is no longer a concern when conducting transporter substrate studies in the canine P-gp knockout MDCK cells, rendering net efflux ratio determination unnecessary.

## 4 Potential opportunities and limitations for CRISPR applications in ADME studies in vitro

---

The discovery of CRISPR transformed molecular biology as it provided researchers with unprecedented power to manipulate genetic information. CRISPR-based technologies are developed at breakneck speed and cover a wide spectrum of applications across the central dogma of molecular biology. Many of these technologies are immediately relevant to in vitro ADME studies and have the potential to enable transformative discoveries. However, CRISPR-based technologies do have technical limitations at the moment, and some of these limitations could pose specific obstacles and challenges to ADME researchers. In this section, we discuss the limitations of CRISPR pertinent to ADME studies and the potential opportunities the technology affords.

### 4.1 Limitations of CRISPR in ADME studies in vitro

One of the major concerns for CRISPR is the off-target effect. In an analysis of the original CRISPR-Cas9 system, it was discovered that off-target effects could occur at sites with up to five mismatches from the targeting region of sgRNAs, and the frequency of mutations at off-target sites can be as high as the intended site [31]. Several approaches were developed to minimize the off-target effect, including engineered Cas enzymes and sgRNA [32, 33]. Many websites also offer algorithms to design sgRNAs and avoid potential off-target sites, though researchers should be mindful whether the website is being updated and maintained [34–37]. If the goal of the experiment is to knockout targeted genes, the CRISPR-STOP approach could be an efficient and precise tool. Instead of the wildtype Cas protein, a mutated nickase Cas9 fused with two additional enzymes is used. The CRISPR-STOP system introduces early stop codon in genes without engaging the error-prone DSB repair mechanism [38]. There are several methods available if it is necessary to identify the off-target sites or



understand the extent of the off-target effects, and there are reviews available for the pros and cons of each method [39, 40].

Delivery and gene-editing efficiency is another challenge. The problem can usually be solved by selecting the appropriate vehicle (e.g., viral transduction, transfection, and electroporation) and optimizing the condition. However, it could be a significant obstacle for ADME researchers since many of the assays are done with primary cells, and many of the options and conditions might not be tolerated. While the low editing efficiency can be overcome by resistance selection or single-cell sorting in immortalized cell lines, these solutions may not be appropriate for many in vitro model systems in ADME research. Most primary cell types are only capable of expansion for a few generations and maintain their phenotypes, and some cell types do not expand in vitro at all. In the example mentioned above, the CYP3A5 editing efficiency was so low that the experiment would not be feasible in primary hepatocytes. However, with the continued improvement in CRISPR efficiency and the development of advanced cell culture systems (e.g., organoids and hepatocyte cocultures), efficient gene editing in primary cell cultures could soon become a reality.

## 4.2 Potential opportunities for CRISPR applications in ADME studies in vitro

The development and improvement of CRISPR-based technologies happen at a rapid pace, and it is not difficult to foresee the community overcoming challenges and opening up new opportunities for the ADME field. Currently, functional studies of drug-metabolizing enzymes and transporters often rely on conducting experiments in primary cells or overexpressing them in immortalized cell lines. However, these approaches are not without disadvantages. A common challenge for studying in primary cells is the lack of specific inhibitors. Inhibitors routinely used in ADME studies often inhibit more than one enzyme or transporter. On the other hand, enzymes and transporters are often overexpressed out of context in cell lines originated from irrelevant tissues. With CRISPR-Cas9 and CRISPRi technologies, researchers can study the function of the enzyme or transporter of interest by precisely knocking it out or knocking it down. The ability to edit multiple genes at once could provide insights into enzyme-transporter interactions or sequential metabolism. Conversely, with the CRISPRa technology, researchers can induce the endogenous expression of drug metabolism enzymes and transporters and study their functions in relevant cell types. Advances in inducible CRISPR systems also have the potential to enable spatial and temporal control of gene expression [41, 42]. Taking advantage of the HDR repair mechanism, researchers can also precisely edit coding and noncoding regions of endogenous genes to study genetic polymorphisms and their effects on gene expression, localization, and function without the need for artificial reporter assay or overexpression system.

Genetic screens with CRISPR-based technology also open up new possibilities for ADME studies. While a pooled whole-genome screen may sound exciting, it is a significant undertaking that requires major resources and multidisciplinary expertise. A focused arrayed CRISPR screen is a practical alternative that should address most ADME-related questions. A loss-of-function CRISPRi or a gain-of-function CRISPRa screen can be utilized to probe beyond the well-studied enzymes and transporters, and identify genes involved in the metabolism and disposition of compounds. As suggested by the literature debate between

Pär Matsson and Douglass Kell over whether multiple transporter-mediated flux is the sole mechanism of cellular drug permeation, a comprehensive CRISPR screen may be needed to truly understand and quantify the impact of transporters on cellular drug permeability [43–45].

Despite the current limitation of CRISPR, it is undeniably a transformative tool for biological sciences. In the short few years since the discovery of CRISPR, it has spurred a plethora of applications and leads to numerous breakthrough discoveries in many fields. The simplicity and adaptability of CRISPR encourage continued development to improve upon the system and expand its capabilities. In the *in vitro* ADME field, CRISPR-based technology has already been applied to create a novel model to study CYP polymorphisms and to improve upon a widely used assay. CRISPR promises a powerful technology that is versatile and accessible. What remains, is for researchers to utilize this toolbox and make great strides in advancing the science of drug absorption, distribution, metabolism, and excretion.

## References

- [1] E.S. Lander, The heroes of CRISPR, *Cell* 164 (2016) 18–28.
- [2] J. van der Oost, M.M. Jore, E.R. Westra, M. Lundgren, S.J.J. Brouns, CRISPR-based adaptive and heritable immunity in prokaryotes, *Trends Biochem. Sci.* 34 (2009) 401–407.
- [3] M. Jinek, K. Chylinski, I. Fonfara, M. Hauer, J.A. Doudna, E. Charpentier, A programmable dual-RNA-guided DNA endonuclease in adaptive bacterial immunity, *Science* (80-) 337 (2012) 816–821.
- [4] S.W. Cho, S. Kim, J.M. Kim, J.S. Kim, Targeted genome engineering in human cells with the Cas9 RNA-guided endonuclease, *Nat. Biotechnol.* 31 (2013) 230–232.
- [5] R.M. Gupta, K. Musunuru, Expanding the genetic editing tool kit: ZFNs, TALENs, and CRISPR-Cas9 the emergence of genome-editing technology, *J. Clin. Invest.* 124 (2014) 4154–4161.
- [6] L.S. Qi, M.H. Larson, L.A. Gilbert, J.A. Doudna, J.S. Weissman, A.P. Arkin, W.A. Lim, Repurposing CRISPR as an RNA-guided platform for sequence-specific control of gene expression, *Cell* 152 (2013) 1173–1183.
- [7] L.A. Gilbert, M.H. Larson, L. Morsut, Z. Liu, G.A. Brar, S.E. Torres, N. Stern-Ginossar, O. Brandman, E.H. Whitehead, J.A. Doudna, W.A. Lim, J.S. Weissman, L.S. Qi, XCRISPR-mediated modular RNA-guided regulation of transcription in eukaryotes, *Cell* 154 (2013) 442.
- [8] P. Mali, J. Aach, P.B. Stranges, K.M. Esvelt, M. Moosburner, S. Kosuri, L. Yang, G.M. Church, CAS9 transcriptional activators for target specificity screening and paired nickases for cooperative genome engineering, *Nat. Biotechnol.* 31 (2013) 833–838.
- [9] A. Chavez, J. Scheiman, S. Vora, B.W. Pruitt, M. Tuttle, E.P.R. Iyer, S. Lin, S. Kiani, C.D. Guzman, D.J. Wiegand, D. Ter-Ovanesyan, J.L. Braff, N. Davidsohn, B.E. Housden, N. Perrimon, R. Weiss, J. Aach, J.J. Collins, G.M. Church, Highly efficient Cas9-mediated transcriptional programming, *Nat. Methods* 12 (2015) 326–328.
- [10] S. Konermann, M.D. Brigham, A.E. Trevino, J. Joung, O.O. Abudayyeh, C. Barcena, P.D. Hsu, N. Habib, J.S. Gootenberg, H. Nishimasu, O. Nureki, F. Zhang, Genome-scale transcriptional activation by an engineered CRISPR-Cas9 complex, *Nature* 517 (2015) 583–588.
- [11] M.E. Tanenbaum, L.A. Gilbert, L.S. Qi, J.S. Weissman, R.D. Vale, A protein-tagging system for signal amplification in gene expression and fluorescence imaging, *Cell* 159 (2014) 635–646.
- [12] A. Chavez, M. Tuttle, B.W. Pruitt, B. Ewen-Campen, R. Chari, D. Ter-Ovanesyan, S.J. Haque, R.J. Cecchi, E.J.K. Kowal, J. Buchthal, B.E. Housden, N. Perrimon, J.J. Collins, G. Church, Comparison of Cas9 activators in multiple species, *Nat. Methods* 13 (2016) 563–567.
- [13] J. Tan, S.E. Martin, Validation of synthetic CRISPR reagents as a tool for arrayed functional genomic screening, *PLoS One* 11 (2016) 1–14.
- [14] J.G. Doench, Am i ready for CRISPR? A user’s guide to genetic screens, *Nat. Rev. Genet.* 19 (2018) 67–80.
- [15] M. Karlgren, I. Simoff, M. Keiser, S. Oswald, P. Artursson, CRISPR-Cas9: a new addition to the drug metabolism and disposition tool box, *Drug Metab. Dispos.* 46 (2018) 1776–1786.

- [16] T. Liu, Z. Li, Q. Zhang, K.D.A. Bernstein, S. Lozano-Calderon, E. Choy, F.J. Hornicek, Z. Duan, Targeting ABCB1 (MDR1) in multi-drug resistant osteosarcoma cells using the CRISPR-Cas9 system to reverse drug resistance, *Oncotarget* 7 (2016) 83502–83513.
- [17] K. Takahashi, T. Inukai, T. Imamura, M. Yano, C. Tomoyasu, D.M. Lucas, A. Nemoto, H. Sato, M. Huang, M. Abe, K. Kagami, T. Shinohara, A. Watanabe, S. Somazu, H. Oshiro, K. Akahane, K. Goi, J. Kikuchi, Y. Furukawa, H. Goto, M. Minegishi, S. Iwamoto, K. Sugita, Anti-leukemic activity of bortezomib and carfilzomib on B-cell precursor ALL cell lines, *PLoS One* 12 (2017) 1–21.
- [18] Y. Yang, J.G. Qiu, Y. Li, J.M. Di, W.J. Zhang, Q.W. Jiang, D.W. Zheng, Y. Chen, M.N. Wei, J.R. Huang, K. Wang, Z. Shi, Targeting ABCB1-mediated tumor multidrug resistance by CRISPR/Cas9-based genome editing, *Am. J. Transl. Res.* 8 (2016) 3986–3994.
- [19] J.S. Ha, J. Byun, D.R. Ahn, Overcoming doxorubicin resistance of cancer cells by Cas9-mediated gene disruption, *Sci. Rep.* 6 (2016) 1–7.
- [20] L. Norouzi-Barough, M. Sarookhani, R. Salehi, M. Sharifi, S. Moghbelinejad, CRISPR/Cas9, a new approach to successful knockdown of ABCB1/P-glycoprotein and reversal of chemosensitivity in human epithelial ovarian cancer cell line, *Iran. J. Basic Med. Sci.* 21 (2018) 181–187.
- [21] C.R. Dorr, R.P. Remmel, A. Muthusamy, J. Fisher, B.S. Moriarity, K. Yasuda, B. Wu, W. Guan, E.G. Schuetz, W.S. Oetting, P.A. Jacobson, A.K. Israni, CRISPR/Cas9 genetic modification of CYP3A5 \*3 in HuH-7 human hepatocyte cell line leads to cell lines with increased midazolam and tacrolimus metabolism, *Drug Metab. Dispos.* 45 (2017) 957–965.
- [22] M. Karlgren, I. Simoff, M. Backlund, C. Wegler, M. Keiser, N. Handin, J. Müller, P. Lundquist, A.C. Jareborg, S. Oswald, P. Artursson, A CRISPR-Cas9 generated Madin-Darby canine kidney expressing human MDR1 without endogenous Canine MDR1 (cABCB1): an improved tool for drug efflux studies, *J. Pharm. Sci.* 1 (2017) 1–5.
- [23] I. Simoff, M. Karlgren, M. Backlund, A.C. Lindström, F.Z. Gaugaz, P. Matsson, P. Artursson, Complete knockout of endogenous Mdr1 (Abcb1) in MDCK cells by CRISPR-Cas9, *J. Pharm. Sci.* 105 (2016) 1017–1021.
- [24] E.C. Chen, F. Broccatelli, E. Plise, B. Chen, L. Liu, J. Cheong, S. Zhang, J. Jorski, K. Gaffney, K.K. Umemoto, L. Salphati, Evaluating the utility of Canine Mdr1 knockout Madin-Darby Canine Kidney I cells in permeability screening and efflux substrate determination, *Mol. Pharm.* 15 (2018) 5103–5113.
- [25] J.-N. Roy, J. Lajoie, L.S. Zijenah, A. Barama, C. Poirier, B.J. Ward, M. Roger, CYP3A5 genetic polymorphisms in different ethnic populations, *Drug Metab. Dispos.* 33 (2005) 884–887.
- [26] H. De Jonge, H. De Loor, K. Verbeke, Y. Vanrenterghem, D.R.J. Kuypers, Impact of CYP3A5 genotype on tacrolimus versus midazolam clearance in renal transplant recipients: New insights in CYP3A5-mediated drug metabolism, *Pharmacogenomics*. (2013).
- [27] R.K. Bains, M. Kovacevic, C.A. Plaster, A. Tarekegn, E. Bekele, N.N. Bradman, M.G. Thomas, Molecular diversity and population structure at the Cytochrome P450 3A5 gene in Africa, *BMC Genet.* 14 (2013) 34.
- [28] P.A. Jacobson, W.S. Oetting, A.M. Brearley, R. Leduc, W. Guan, D. Schladt, A.J. Matas, V. Lamba, B.A. Julian, R.B. Mannon, A. Israni, DeKAF Investigators, Novel polymorphisms associated with tacrolimus trough concentrations: results from a multicenter kidney transplant consortium, *Transplantation*, 91 (2011) 300–308.
- [29] J.D. Irvine, L. Takahashi, K. Lockhart, J. Cheong, J.W. Tolan, H.E. Selick, J.R. Grove, MDCK (Madin-Darby canine kidney) cells: a tool for membrane permeability screening, *J. Pharm. Sci.* 88 (1999) 28–33.
- [30] L. Di, C. Whitney-Pickett, J.P. Umland, H. Zhang, X. Zhang, D.F. Gebhard, Y. Lai, J.J. Federico, R.E. Davidson, R. Smith, E.L. Reyner, C. Lee, B. Feng, C. Rotter, M.V. Varma, S. Kempshall, K. Fenner, A.F. El-Kattan, T.E. Liston, M.D. Troutman, Development of a new permeability assay using low-efflux MDCKII cells, *J. Pharm. Sci.* 100 (2011) 4974–4985.
- [31] Y. Fu, J.A. Foden, C. Khayter, M.L. Maeder, D. Reyon, J.K. Joung, J.D. Sander, High-frequency off-target mutagenesis induced by CRISPR-Cas nucleases in human cells, *Nat. Biotechnol.* 31 (2013) 822–826.
- [32] H. Yin, C.-Q. Song, S. Suresh, S.-Y. Kwan, Q. Wu, S. Walsh, J. Ding, R.L. Bogorad, L.J. Zhu, S.A. Wolfe, V. Koteliansky, W. Xue, R. Langer, D.G. Anderson, Partial DNA-guided Cas9 enables genome editing with reduced off-target activity, *Nat. Chem. Biol.* 14 (2018) 311–316.
- [33] J.H. Hu, S.M. Miller, M.H. Geurts, W. Tang, L. Chen, N. Sun, C.M. Zeina, X. Gao, H.A. Rees, Z. Lin, D.R. Liu, Evolved Cas9 variants with broad PAM compatibility and high DNA specificity, *Nature* 556 (2018) 57–63.
- [34] M. Haeussler, K. Schönig, H. Eckert, A. Eschstruth, J. Mianné, J.-B. Renaud, S. Schneider-Maunoury, A. Shkumatava, L. Teboul, J. Kent, J.-S. Joly, J.-P. Concordet, Evaluation of off-target and on-target scoring algorithms and integration into the guide RNA selection tool CRISPOR, *Genome Biol.* 17 (2016) 148.

- [35] J.G. Doench, N. Fusi, M. Sullender, M. Hegde, E.W. Vaimberg, K.F. Donovan, I. Smith, Z. Tothova, C. Wilen, R. Orchard, H.W. Virgin, J. Listgarten, D.E. Root, Optimized sgRNA design to maximize activity and minimize off-target effects of CRISPR-Cas9, *Nat. Biotechnol.* (2016).
- [36] J.A. Meier, F. Zhang, N.E. Sanjana, GUIDES: sgRNA design for loss-of-function screens, *Nat. Methods* 14 (2017) 831–832.
- [37] S. Bae, J. Park, J.-S. Kim, Cas-OFFinder: a fast and versatile algorithm that searches for potential off-target sites of Cas9 RNA-guided endonucleases, *Bioinformatics* 30 (2014) 1473–1475.
- [38] P. Billon, E.E. Bryant, S.A. Joseph, T.S. Nambiar, S.B. Hayward, R. Rothstein, A. Ciccia, CRISPR-mediated base editing enables efficient disruption of eukaryotic genes through induction of STOP codons, *Mol. Cell.* 67 (2017) 1068–1079.e4.
- [39] X.-H. Zhang, L.Y. Tee, X.-G. Wang, Q.-S. Huang, S.-H. Yang, Off-target effects in CRISPR/Cas9-mediated genome engineering, *Mol. Ther. Nucleic Acids* 4 (2015)e264.
- [40] Y. Cheng, S.Q. Tsai, Illuminating the genome-wide activity of genome editors for safe and effective therapeutics, *Genome Biol.* 19 (2018) 226.
- [41] Y. Nihongaki, S. Yamamoto, F. Kawano, H. Suzuki, M. Sato, CRISPR-Cas9-based photoactivatable transcription system, *Chem. Biol.* 22 (2015) 169–174.
- [42] Y. Gao, X. Xiong, S. Wong, E.J. Charles, W.A. Lim, L.S. Qi, Complex transcriptional modulation with orthogonal and inducible dCas9 regulators, *Nat. Methods* 13 (2016) 1043–1049.
- [43] P. Matsson, C.A.S. Bergström, Computational modeling to predict the functions and impact of drug transporters, *In Silico Pharmacol.* 3 (2015) 8.
- [44] P. Matsson, L.A. Fenu, P. Lundquist, J.R. Winiewski, M. Kansy, P. Artursson, Quantifying the impact of transporters on cellular drug permeability, *Trends Pharmacol. Sci.* 36 (2015) 255–262.
- [45] D.B. Kell, S.G. Oliver, How drugs get into cells: tested and testable predictions to help discriminate between transporter-mediated uptake and lipoidal bilayer diffusion, *Front. Pharmacol.* 5 (2014) 231.

# In vitro-in vivo extrapolation of human hepatic and renal clearance

Ravindra Varma Alluri<sup>a</sup>, Manthena V.S. Varma<sup>b</sup>

<sup>a</sup>Clinical Pharmacology and Safety Sciences, R&D BioPharmaceuticals, AstraZeneca, Cambridge, United Kingdom <sup>b</sup>Medicine Design, Worldwide R&D, Pfizer Inc., Groton, CT, United States

## 1 Introduction

The characterization of drug disposition and prediction of human pharmacokinetics prior to nomination of new drug candidates into drug development has become an expectation in drug discovery. Tools have been developed to assess important dispositional attributes during the drug design phase so that medicinal chemists can simultaneously optimize absorption, distribution, metabolism and elimination (ADME) properties and pharmacological potency. In addition, early studies inform quantitative prediction of several parameters, including clearance, volume of distribution, half-life, oral absorption, oral bioavailability, drug-drug interactions (DDIs), impact of genetic polymorphisms on drug disposition, penetration into target organs and efficacious dose in humans.

Clearance (CL) is an important pharmacokinetic parameter to predict as it determines the systemic/target exposure, half-life, and the DDI potential. The major drug elimination routes in human are metabolism, renal and biliary, primarily occurring in the liver and kidney [1]. It should be emphasized that a drug's predominant elimination process such as metabolism or biliary secretion may not always be its rate-determining step in systemic clearance—the latter being the determinant of systemic drug exposure [2–8]. For any given eliminating organ (i.e., liver and kidney), clearance is determined by the rate at which the drug is delivered to the organ (i.e., blood flow), the extent of drug binding in blood and the intrinsic capability of the organ to clear the drug. Intrinsic clearance is determined by the activities of specific drug-metabolizing enzymes and membrane transporters and can be assessed using in vitro methods based on human-derived reagents.

## 2 ECCS framework to identify rate-determining process for CL

Early identification of clearance mechanism can facilitate adopting the “right” strategy and tools for quantitative pharmacokinetic predictions. A framework called the extended clearance classification system (ECCS) [9] was recently suggested to identify the clearance mechanism (rate-determining step) of new molecular entities (NMEs) using physicochemical properties and in vitro/in silico data readily available in early drug discovery. According to ECCS, NMEs are classified based on permeability, molecular weight (MW) and ionization state, which are previously shown to be strongly associated with major clearance mechanisms—hepatic uptake, metabolism and renal clearance. For example, Benet and coworkers proposed that high-permeable compounds show a high extent of metabolism (>70%) and vice versa [10]. On the other hand, studies demonstrated that high MW ( $\geq 400$  Da) acids/zwitterions undergo hepatic uptake via organic anion transporting polypeptides (OATP) transporters, which is often the rate-determining step in their clearance [11]. In addition, compounds undergoing biliary excretion often involve hepatic uptake as the rate-determining step in their systemic clearance.

A permeability cutoff was suggested in the process of implementing ECCS right from the early stages of drug discovery [12]. Permeability categorization here is based on the low-efflux Madin-Darby canine kidney (MDCK) cell lines [13]. Tools based on artificial membranes (e.g., phospholipid-derived PAMPA membrane) [14] or other cell types (e.g., Caco-2 cells with chemical inhibition of transporters [15]) could be validated to serve this purpose. Since many of the cell types express a wide range of transporters to varying degree, validation should also focus on assessing the risk of misclassification (high vs low permeability) due to active mechanisms. Extensive validation of ECCS resulted in overall good predictive rates [9, 16, 17]. The general characteristics of the six classes with respect to the clearance mechanism are as follows (Fig. 1):

**ECCS Class 1A:** Acids/zwitterions with high permeability and small MW (<400 Da). The clearance of class 1A compounds involves transporter-enzyme interplay, with organic anion transporter (OAT)2-mediated hepatic uptake and subsequent metabolism (extent of metabolism >70%). These compounds tend to be metabolized by UDP-glucuronosyltransferase (UGT)  $\cong$  cytochrome P-450 (CYP)2C enzymes  $\gg$  esterases  $\gg$  CYP3A4 enzymes, e.g., ibuprofen, tolbutamide, warfarin and meloxicam.

**ECCS Class 1B:** Large MW (>400 Da) acids/zwitterions and with high permeability. These compounds often involve hepatic uptake mediated by OATP1B1/1B3 in their systemic clearance. Once in the liver, they are generally metabolized by CYP2C > esterases > UGT > CYP3A enzymes and excreted in bile/urine as metabolites. The extent of metabolism is high (>70%). OATP1B1/1B3 inhibitors such as cyclosporine and rifampicin significantly increase the plasma exposure of these drugs, while CYP inhibitors such as clarithromycin, erythromycin, itraconazole, fluconazole and diclofenac show a limited effect, e.g., cerivastatin, fluvastatin, glyburide and repaglinide.

**ECCS Class 2:** Bases/neutrals with high membrane permeability. Class 2 compounds are cleared by metabolism (extent of metabolism >70%). They are primarily metabolized by enzymes such as CYP3A4  $\gg$  UGT > CYP2D6 > esterases = CYP2C. The high contribution of CYP3A4, CYP2D6 and UGT enzymes is in agreement with the basic nature of many of these drug molecules and their higher lipophilicity ( $\text{Log } D_{\text{pH } 7.4}$ ). Due to the expected rapid



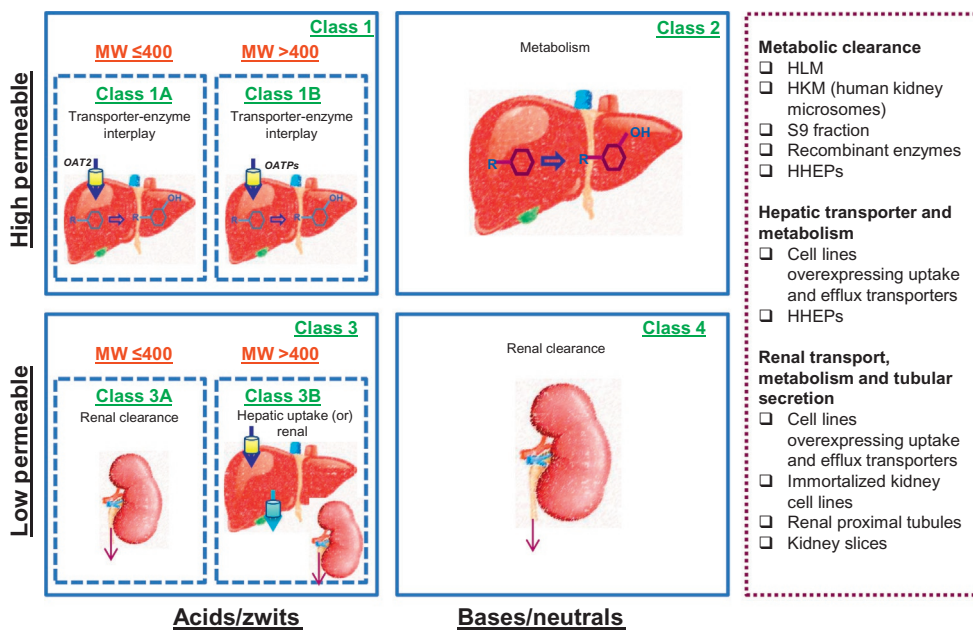


FIG. 1 Extended clearance classification system (ECCS) framework and assay systems used to predict hepatic and renal clearances.

equilibrium between blood and liver compartments, systemic clearance of these drugs can be predicted by human liver microsomes (HLM), human hepatocytes (HHEPs) or other human in vitro systems aligned with the underlying metabolic process, e.g., midazolam, propranolol and dextromethorphan.

ECCS Class 3A: Acids/zwitterions with low permeability and small MW (<400 Da). Class 3A compounds are renally cleared, with OAT1 and OAT3 transporters potentially involved in the active renal secretion. These are also potential substrates for efflux transporters such as breast cancer resistance protein (BCRP), multidrug resistance protein (MRP)2/4 and P-glycoprotein (P-gp), which facilitate active secretion of hydrophilic compounds across the apical membrane of proximal tubule cells, e.g., ciprofloxacin, furosemide and penciclovir.

ECCS Class 3B: Acids/zwitterions with low permeability and large MW (>400 Da). Their mechanism of clearance is either active hepatic uptake and/or renal elimination. The hepatic uptake is typically mediated by OATPs transporters; once in the liver, they tend to be eliminated in bile as unchanged drug. Renal secretion is primarily mediated by OATs, e.g., pravastatin, valsartan and methotrexate.

ECCS Class 4: Bases/neutrals with low permeability. They are primarily eliminated renally with low extent of metabolism <30%. Their renal secretion is likely mediated by OAT1, OAT3 and/or organic cation transporter (OCT)2; and P-gp and multidrug and toxic compound extrusion (MATE)1/2K appear to be the major efflux transporters affecting the renal secretion, e.g., acyclovir, famotidine, metformin and sitagliptin.



### 3 Current IVIVE approaches to predict clearance

#### 3.1 Hepatic clearance

Hepatic disposition more frequently contributes to the overall clearance of small molecule drugs, and thus much emphasis is given to its characterization in pharmacokinetic optimization. Several processes mediate hepatic drug clearance, which include metabolism by enzymes, transporter-mediated uptake and efflux at sinusoidal membrane and efflux at bile canaliculi. Depending on the molecular properties of the compound, one or several of these processes mediate hepatic drug clearance, which can be predicted using ECCS framework. Numerous in vitro assay systems of varying complexity and in vitro-to-in vivo extrapolation (IVIVE) approaches are used during drug discovery and development to predict hepatic clearance via enzymes and/or transporters. Depending on the complexity of the systems used, clearance pathways can be studied in combination or separately and then integrated using mathematical models.

##### **3.1.1 Metabolic clearance and in vitro methodologies**

The major enzymes involved in the metabolism of most marketed drugs are cytochrome P-450 (CYPs) and UDP-glucuronosyltransferases (UGTs), while certain drugs are also metabolized by flavin-containing monooxygenases (FMOs) and aldehyde oxidases (AOs). Several other enzymes like sulfotransferases (SULTs), *N*-acetyl transferases (NATs), xanthine oxidases (XO), monoamine oxidases (MAOs), esterases and amidases also mediate clearance of drug molecules. IVIVE approaches to predict in vivo clearance from in vitro data are well established. These approaches generally work well for CYPs, UGTs, and FMOs enzymes, while for few enzymes (e.g., AOs) in vitro data may not provide quantitative prediction of in vivo clearance [18–25].

Human liver microsomes (HLM) and primary human hepatocytes are the preferred choice of in vitro systems for measuring intrinsic clearance ( $CL_{int}$ ) of test compounds, while cytosolic fractions such as S9 are generally used when non-CYP/UGT enzymes also mediate metabolism [26–28]. HLMs are enriched with CYPs and UGTs and are amendable for high-throughput screens; hence, these are routinely used during early discovery for optimizing unbound  $CL_{int}$  and prediction of hepatic metabolic clearance. Unlike CYPs, microsomal UGT assays require activation using alamethicin or a few bursts of sonication to overcome reaction latency associated with UGTs due to localization of the enzyme active site facing the lumen of the endoplasmic reticulum [29]. Additionally, a few groups have implemented addition of bovine serum albumin (BSA) and essentially fatty acid-free human serum albumin to reduce the inhibitory effect of fatty acids that are released during CYP and UGT microsomal incubations [30–33]. Hepatocytes on the contrary are holistic systems with entire complement of enzymes (CYPs, UGTs, FMOs, AOs, and other cytosolic enzymes) and transporters, and hence are even more favored for scaling overall hepatic clearance.

Recombinantly expressed CYPs and UGTs are most often used for reaction phenotyping, which allows identification of specific isoforms that mediate metabolism. These systems can also be used to assess the relative contribution of individual CYPs/UGTs (i.e., fraction metabolized,  $f_m$ ) to overall metabolism and for predicting hepatic metabolic clearance. However, this would require establishment of intersystem extrapolation factors (ISEF) that account for catalytic activity differences per unit enzyme between recombinant enzymes (e.g., CYPs/UGTs) to that of

native human liver enzyme [34–37]. As the batch-to-batch variability in abundance is high in recombinant systems, along with substantial amounts of inactive protein in the preparations, ISEFs need to be reestablished whenever new batches are used [36, 38].

Unitless ISEF is calculated by measuring  $CL_{int}$  of marker substrates in recombinantly expressed enzymes and in vitro systems (e.g., HLM) (Eq. 1).

$$ISEF - CL_{int} = \frac{CL_{int} \text{ (HLM)}}{CL_{int} \text{ (rhenzyme)} \times \text{enzyme abundance (HLM)}} \quad (1)$$

$CL_{int}$  (HLM) is the intrinsic clearance of marker substrate in HLM,  $CL_{int}$  (rhenzyme) is the intrinsic clearance of marker substrate in recombinant enzyme and enzyme abundance (HLM) is specific enzyme abundance in HLM.

Once ISEFs are established,  $CL_{int}$  from recombinant enzymes can be converted to  $CL_{int}$  in HLM by that enzyme using Eq. (2):

$$CL_{int \text{ enzyme}_j} = CL_{int} \text{ (rhenzyme}_j) \times \text{enzyme}_j \text{ abundance} \times ISEF_{\text{enzyme}_j} \quad (2)$$

where  $\text{enzyme}_j$  is the  $j$ th enzyme isoform tested/analyzed,  $CL_{int \text{ enzyme}_j}$  is intrinsic clearance by  $\text{enzyme}_j$  in HLM (microliters per minute per milligram of protein),  $CL_{int} \text{ (rhenzyme}_j)$  is intrinsic clearance in  $\text{rhenzyme}_j$  (microliters per minute per picomole of enzyme),  $\text{enzyme}_j$  abundance is abundance of  $\text{enzyme}_j$  (picomoles of enzyme per milligram of protein), and  $ISEF_{\text{(enzyme}_j)}$  is ISEF for  $\text{enzyme}_j$ .

$CL_{int}$  in HLM is extrapolated from scaled recombinant data as follows:

$$CL_{int \text{ HLM}} = \sum_{j=1}^n CL_{int \text{ enzyme}_j} \quad (3)$$

where  $CL_{int \text{ enzyme}_j}$  is extrapolated intrinsic clearance by  $\text{enzyme}_j$  in HLM (microliters per minute per milligram of protein).

### 3.1.1.1 IVIVE of metabolic clearance

Experiments to determine  $CL_{int}$  are typically carried out by incubating low concentration ( $\leq 1 \mu\text{M}$ ) of NMEs with HLM (+cofactors), recombinant enzymes (e.g., CYPs and UGTs) or hepatocytes in suspension or grown in sandwich conformation (for low  $CL_{int}$  NMEs) at  $37^\circ\text{C}$  and samples are collected at various time points to measure consumption of the substrate. The natural log of % parent remaining at each time point is plotted against time to calculate the first-order rate constant ( $K_{deg}$ ) and half-life ( $t_{1/2}$ ). In vitro  $CL_{int}$  is calculated from HLM, recombinant enzymes and hepatocytes using Eqs. (4)–(6), respectively.

$$\text{in vitro } CL_{int, \text{HLM}} \text{ (mL/min/mg)} = \frac{0.693}{\text{invitro}_{t_{1/2}}} \times \frac{\text{mL of incubation}}{\text{mg microsomes}} \quad (4)$$

$$\text{in vitro } CL_{int, \text{rhenzyme}_j} \text{ (mL/min/pmol)} = \frac{0.693}{\text{invitro}_{t_{1/2}}} \times \frac{\text{mL of incubation}}{\text{pmol enzyme}_j} \quad (5)$$

$$\text{in vitro } CL_{int, \text{hepatocytes}} \text{ (mL/min/million)} = \frac{0.693}{\text{invitro}_{t_{1/2}}} \times \frac{\text{mL of incubation}}{\text{million hepatocytes}} \quad (6)$$

Scaling in vitro  $CL_{int}$  from HLM and hepatocytes to in vivo  $CL_{int}$  is done by applying physiological scaling factors such as microsomal protein content (40 mg/g liver) and hepatocellularity ( $120 \times 10^6$  hepatocytes/g liver tissue; 21 g of liver/kg body weight), respectively (Eqs. 7, 8) [26, 39]. Hepatic clearance is then calculated by applying one of the liver models, i.e., well-stirred, parallel tube or dispersion models (Eqs. 9–11). All these models assume that there is no permeability limitation within the liver and drug entry into liver is perfusion rate limited. The well-stirred model assumes that drug is well mixed inside the liver. This model is the simplest and most commonly used, which describes hepatic clearance as a function of  $CL_{int}$ , fraction unbound in blood ( $f_{u,B}$ ) and incubation ( $f_{u,inc}$ ) and hepatic blood flow ( $Q_H$ ).

$$\text{in vivo } CL_{int,HLM} \text{ (mL/min/kg)} = \text{invitro } CL_{int} \times \frac{40 \text{ mg microsomes}}{\text{gram of liver}} \times \frac{21 \text{ g liver}}{\text{kg body weight}} \quad (7)$$

$$\text{in vivo } CL_{int,hepatocytes} \text{ (mL/min/kg)} = \text{invitro } CL_{int} \times \frac{120 \times 10^6 \text{ hepatocytes}}{\text{gram of liver}} \times \frac{21 \text{ g liver}}{\text{kg body weight}} \quad (8)$$

$$CL_H \text{ (mL/min/kg)} = \frac{Q_H \times \left( \frac{f_{u,B}}{f_{u,inc}} \right) \times CL_{int}}{Q_H + \left( \frac{f_{u,B}}{f_{u,inc}} \right) \times CL_{int}} \text{ well-stirred model with binding corrections} \quad (9)$$

$$CL_H \text{ (mL/min/kg)} = Q_H \left[ 1 - \exp \left( -\frac{f_{u,B} \times CL_{int}}{Q_H} \right) \right] \text{ Parallel tube model; assumes that drug is mixed only in the infinitely small section along the flow path from input to output of the liver} \quad (10)$$

$$CL_H \text{ (mL/min/kg)} = Q_H \left[ 1 - \frac{4a}{(1+a)^2 \exp \left[ \frac{a-1}{2Dn} \right] - (a-1)^2 \exp \left[ -\frac{(a+1)}{2Dn} \right]} \right] \quad (11)$$

where  $Dn = 0.17$ ,  $a = \sqrt{1 + 4RnDn}$ , and  $Rn = \frac{f_{u,B} \times CL_{int}}{Q_H}$  Dispersion model, based on the flow dynamics in liver (Eq. 11).

### 3.1.1.2 In vitro-to-in vivo correlation (IVIVC) of metabolic clearance

Comparison of predicted vs observed metabolic clearance in humans from different data sets revealed systematic underprediction of hepatic CL from HLM and from hepatocytes, reflecting inadequacies in in vitro material and/or extrapolation approaches [20, 40–44]. Some of the inadequacies in in vitro material and experimental conditions include incomplete recovery of microsomes and hepatocytes from liver tissue, potential loss of enzyme activity during tissue handling and storage, suboptimal experimental conditions such as use of buffers that do not mimic physiological environment, suboptimal substrate concentration (e.g.,  $1 \mu\text{M}$  may not be optimal for compounds, which have a much lower  $K_m$  value), impact of unstirred water layers on the rate of CL and use of microsomes/hepatocytes from a single

donor with poor metabolic activity due to genetic factors. Single donor issues have been addressed by using pooled HLMs and hepatocytes that better represented average enzyme activity in population. Theoretically, other reasons for disconnect include extrahepatic metabolism, uptake and efflux by sinusoidal and canalicular transporters, which are not considered in the abovementioned approaches.

To address underprediction of in vivo CL from in vitro data, empirical approaches that remove the systematic bias via application of an empirical scaling factor (ESF) derived from regression analysis applied to the in vitro and in vivo data have been developed (Eq. 12) [45, 46].

$$\text{ESF} = \frac{\text{Observed CL}_{\text{int}}}{\text{Predicted CL}_{\text{int}}} \quad (12)$$

Similarly, mechanistic approaches incorporating additional processes that better mimic in vivo conditions (e.g., pH differences and binding inside hepatocytes) were introduced into the equation of well-stirred liver model. For instance, Berezhkovskiy hypothesized that for ionizable drugs, the steady-state concentrations are different between extracellular and intracellular water due to pH differences of 7.4 and 7.0, respectively. To account for the differences additional parameter named ionization factor,  $F_I$ , was introduced into the equation for well-stirred model (Eq. 13) [47].

$$\text{CL}_H = \frac{Q_H \times f_{u,B} \times \text{CL}_{\text{int}} \times F_I}{Q_H + f_{u,B} \times \text{CL}_{\text{int}} \times F_I} \quad (13)$$

$F_I$  is the unbound, neutral fraction in plasma divided by the unbound, neutral fraction in intracellular water at equilibrium. For neutral drugs,  $F_I = 1$  and hence Eq. (13) coincides with Eq. (9). For basic drugs with low in vivo extraction, Eq. (13) resulted in higher CL predictions from hepatocyte data [CL underpredicted using Eq. (9)], thereby improving IVIVC. Likewise, CL prediction for acids was lower with Eq. (13) [CL overpredicted using Eq. (9)], thereby improving IVIVC. Similarly, Poulin et al. [48] accounted for drug-binding differences between plasma and liver (i.e., the concentration difference in the major drug-binding protein albumin in plasma vs intracellular liver). This approach involves converting  $f_{u,p}$  in vitro to  $f_{u,\text{liver}}$  in vivo by applying plasma to whole liver concentration ratio (PLR) of human serum albumin (Eq. 14), which was calculated to be 13.3 for humans, rat, and monkey, the value for dog is 8.5. For drugs binding to alpha 1-acid glycoprotein, Eq. (13) is suggested.

$$f_{u,\text{liver}} = \frac{\text{PLR} \times f_{u,p} \times F_I}{1 + (\text{PLR} - 1) \times f_{u,p} \times F_I} \quad (14)$$

For drugs mainly bound to albumin, Eq. (15) corrects for both the specific ( $f_{u,\text{liver}}$ ) and nonspecific ( $f_{u,\text{inc}}$ ) binding that may occur under in vivo and in vitro conditions, respectively.

$$\text{CL} = \frac{Q_H \times R_{\text{BP}} \times \text{CL}_{\text{int,in vivo}} \times \frac{f_{u,\text{liver}}}{f_{u,\text{inc}}}}{Q_H \times R_{\text{BP}} + \text{CL}_{\text{int,in vivo}} \times \frac{f_{u,\text{liver}}}{f_{u,\text{inc}}}} \quad (15)$$

Using Eq. (15), the in vivo CL of 25 drugs that are highly protein bound was predicted well from microsomal data. Subsequent analysis done using a larger data set (139 compounds) showed that CL prediction accuracy improved especially for compounds that are albumin bound, highly bound drugs and drugs with low CL [49]. Subsequent to this, Yamagata et al. using a limited set of compounds ( $n=37$ ) demonstrated that regression approaches showed similar or slightly superior absolute average fold error compared to mechanistic approaches [50]. In the same year, Wood et al. (2017) did a comprehensive examination of predictions from published rat as well as human studies ( $n=128$  and 101, hepatocytes and  $n=71$  and 83 microsomes, respectively), which revealed a trend of increasing underprediction in both systems and species with increasing in vivo intrinsic clearance (Fig. 2). Similar trends have been reported by Ref. [51] with increasing underprediction with increasing in vivo hepatic clearance. Prediction bias was shown to be not associated with compounds that are highly protein bound or substrates for UGTs or nature of the compounds (acid, base or neutral), suggesting inherent limitations with in vitro systems. Despite a decade of research to mechanistically improve IVIVC, underprediction of CL from in vitro data continues to be a common theme. Much research is warranted to mechanistically offset underpredictions and thus empirical scaling factors are suggested as a pragmatic approach for early prediction of CL in humans from in vitro data.

### 3.1.2 Transporter and metabolism interplay

Although metabolism is the major elimination pathway for most drugs, the role of transporters has been increasingly recognized in drug clearance. In the liver, active and/or passive drug transport across the sinusoidal membrane governs the drug availability for subsequent

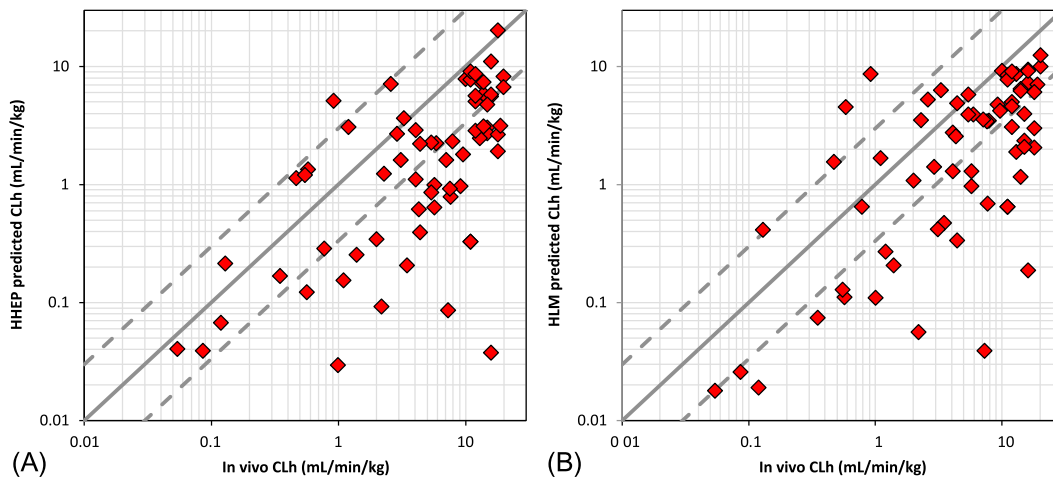


FIG. 2 In vitro-in vivo extrapolation to predict in vivo hepatic clearance from in vitro primary human hepatocytes (A) and human liver microsomes (B). Systematic underprediction of hepatic clearance is noted using the human reagents. Solid and dashed lines represent unity and  $\pm$ threefold error, respectively. Data were extracted from F.L. Wood, J.B. Houston, D. Hallifax, Clearance prediction methodology needs fundamental improvement: trends common to rat and human hepatocytes/microsomes and implications for experimental methodology, *Drug Metab. Dispos.* 45(11) (2017) 1178–1188 and replotted.

biotransformation by the drug-metabolizing enzymes or efflux across the canalicular membrane into bile. Hence, the expression of intrinsic clearance has been further expanded to incorporate distinct processes. In a mathematical sense, the hepatic intrinsic clearance is a function of transporter-enzyme interplay involving several processes such as active uptake clearance ( $PS_{\text{active}}$ ), passive transport clearance ( $PS_{\text{passive}}$ ), active basolateral efflux clearance ( $PS_{\text{efflux}}$ ), intrinsic biliary secretory ( $CL_{\text{bile}}$ ) and metabolic clearance ( $CL_{\text{met}}$ ) Eq. (16) [2, 6–8, 52, 53].

$$Cl_{\text{int,H}} = (PS_{\text{active}} + PS_{\text{passive}}) \times \frac{CL_{\text{met}} + CL_{\text{bile}}}{PS_{\text{passive}} + PS_{\text{efflux}} + CL_{\text{met}} + CL_{\text{bile}}} \quad (16)$$

Eq. (16) indicates that the rate-determining step in the overall elimination changes according to the relative magnitude of individual processes. For instance, when  $PS_{\text{passive}} + PS_{\text{efflux}}$  is smaller than  $CL_{\text{met}} + CL_{\text{bile}}$ , hepatic intrinsic clearance is primarily determined by hepatic uptake ( $PS_{\text{active}} + PS_{\text{passive}}$ ). This means that the value of  $PS_{\text{active}}$  is contributing more to in vivo intrinsic clearance when transporters are more involved in influx process especially for less lipophilic compounds. These compounds (ECCS class 1B and 3B) are likely to show large discrepancies between in vivo (overall) intrinsic clearance and in vitro metabolic clearance. On the other hand, when  $PS_{\text{active}} + PS_{\text{efflux}}$  is appreciable in relation to  $CL_{\text{met}} + CL_{\text{bile}}$ , all the individual processes are required to estimate overall hepatic clearance. Therefore, irrespective of the compound's passive permeability (high or low), uptake transport clearance determines the hepatic clearance of uptake transporter substrates, partially or completely. Although, one must also be aware that the relative magnitude of individual process can change based on the dose (e.g., CL decreases with increased dose due to saturation of metabolism) [20, 54].

Solute carrier family (SLCs) transporters primarily mediate influx or bidirectional transport of substrate drugs, while ATP-binding cassette family (ABCs) transporters efflux drugs out from hepatocytes into blood or bile. Clinical evidence suggests that organic anion transporting polypeptides (OATP)1B1 and OATP1B3 play an important role in hepatic uptake of several drugs, including statins, sartans and certain glinides, while P-glycoprotein (P-gp), breast cancer resistance protein (BCRP) and multidrug resistance protein (MRP) transporters are shown to mediate biliary efflux of statins and several anticancer drugs [55]. Although hepatic uptake could be the rate-determining process in the systemic clearance of several OATP substrates, enzymatic metabolism and/or biliary efflux may also contribute to systemic clearance and elimination from body. For instance, atorvastatin is largely metabolized by CYP3A4 and repaglinide and cerivastatin are metabolized by CYP2C8 and CYP3A4. Recent data suggest that the organic anion transporter (OAT)2 is also expressed in liver and mediate the clearance of high-permeability-low-molecular-weight acid and zwitterion drugs (ECCS class 1A) [56]. Overall, the transporter-enzyme interplay will determine the disposition of dual substrates and these multiple processes should be simultaneously considered using mechanistic models for pharmacokinetic and DDI predictions. To this effect, static mechanistic net-effect models were developed to predict DDIs involving complex transporter-enzyme interplay. Varma et al. showed that net-effect model improved quantitative DDI prediction accuracy (94% within twofold error) of 9 victim drugs (caused by 5 perpetrator drugs involving 62 clinical interaction combinations) that are substrates of OATP1B1 and are metabolized by P450 enzymes or eliminated in bile [57]. Such mechanistic evaluation is important given multiple mechanisms contributing to the DDIs. For example, DDIs with

cyclosporine as perpetrator were evaluated assuming reversible inhibition of OATP1B1, MRP2, BCRP and CYP3A4. Net-effect model predictions are within twofold for 93% (14 of 15) cases, while the *R*-value (which accounts for only uptake clearance) predicted only 46% interactions within twofold. The model performance further improved when in vitro uptake clearance was corrected to recover in vivo clearance.

At early/late stages of drug development whole-body physiologically based pharmacokinetic (PBPK) models with permeability-limited liver models are used to model dynamic changes in the concentration of inhibitor and victim drugs at the sites of interaction [58–61].

### 3.1.2.1 In vitro tools and IVIVE of overall hepatic clearance

Several assay formats have been developed that allows for individual CL processes to be measured separately or in combination (e.g., uptake only, uptake+metabolism or uptake +metabolism+biliary efflux). Assays to determine uptake transporter (e.g., OATPs and OAT)-mediated clearance are performed in vitro using multiple formats. The classical oil spin method measures rate of compound appearance into hepatocytes in suspension, determined after a centrifugation step through a layer of oil to allow the separation of cells and media [62]. The media loss assay allows for rapid determination of uptake by measuring loss of compound from incubation media into hepatocytes [63]. This method is amenable for high-throughput screening and hence can be used during discovery phase. Similarly, hepatocytes grown in two-dimensional (2D) and/or in sandwich formats are also used to determine uptake [64, 65]. These assays, however, require long culturing time (hours or days). Several of these assay formats have been subsequently modified to simultaneously measure uptake and metabolism and mechanistic models were developed to estimate kinetic parameters for sinusoidal uptake, efflux and metabolism [66–71]. Assays to assess overall hepatic clearance (i.e., active uptake+passive diffusion, metabolism and canalicular efflux) are done using sandwich-cultured human hepatocytes (SCHH), which form functional bile canaliculi [72].

Although human hepatocytes are highly valuable tools for predicting in vivo clearance from in vitro data, often the lack of specific inhibitors for transporters (e.g., OATP1B1 and OATP1B3) makes it difficult to pin down the contribution of individual transporters to overall clearance, which are important from a DDI and genetic polymorphism perspective. Hence, mammalian cell lines overexpressing individual transporters (e.g., HEK-OATP1B1) are used to identify specific transporter-mediated uptake and the relative contribution (fraction transported,  $f_t$ ) of the transporter to overall clearance. However, like rhCYPs, relative activity factors (RAFs) need to be established to enable scaling of uptake  $CL_{int}$  data from cell lines to hepatocytes or to the observed in vivo  $CL_{int}$  using semimechanistic or full PBPK models [73].

All the assays described above are typically done by incubating low concentration of NMEs ( $\leq 1 \mu\text{M}$  or at clinically relevant concentrations) with hepatocytes and/or mammalian cells overexpressing individual transporters. To assess active uptake and/or metabolism, assays are typically done in the presence and the absence of inhibitors of uptake transporters (e.g., rifamycin SV for OATPs and OAT2) and or CYP enzymes (e.g., ABT) and samples are collected at predetermined time points. Depending on the assay format, uptake rates are calculated using the following equations:

$$\text{Oil spin method : } CL_{int} = \frac{v}{S} \quad (17)$$



where  $v$  is the initial rate of appearance of drug into hepatocytes and  $S$  is the initial substrate concentration.

$$\text{Media loss : } CL_{\text{int}} = v \times k \quad (18)$$

where  $v$  is the unbound volume of incubation and  $k$  is the elimination rate constant.

Both uptake and metabolism can be simultaneously estimated using compartment mechanistic models to describe drug uptake (active and passive), metabolism and distribution [66–68].

Similarly, in vitro experiments to simultaneously estimate uptake and biliary clearance are carried out using SCHH systems, where the cells are pretreated with  $\text{Ca}^{2+}/\text{Mg}^{2+}$ -containing (to maintain intact bile canaliculi) or  $\text{Ca}^{2+}/\text{Mg}^{2+}$ -free (to destroy bile canaliculi) buffers prior to addition of NMEs. NMEs  $\pm$  uptake transporter inhibitor (e.g., rifamycin SV) are then incubated with SCHH and samples are collected at predetermined time points.  $\text{PS}_{\text{active}}$  and  $\text{PS}_{\text{passive}}$  are calculated by linear regression fitting with initial rate analysis with or without rifamycin [74]. Biliary excretion index (BEI) and in vitro intrinsic biliary clearance are calculated using Eqs. (19), (20), respectively [75–77].

$$\text{BEI (\%)} = \frac{\text{AUC}_{0-15 \text{ m (cell+bile)}} - \text{AUC}_{0-15 \text{ (cell)}}}{\text{AUC}_{0-15 \text{ m (cell+bile)}}} \times 100 \quad (19)$$

$$\text{In vitro } CL_{\text{int,bile}} \text{ (mL/min/mg)} = \frac{\text{Accumulation}_{\text{(cell+bile)}} - \text{Accumulation}_{\text{(cell)}}}{\text{Incubation time} \times \text{concentration in media}} \quad (20)$$

where  $\text{AUC}_{0-15 \text{ m (cell+bile)}}$  and  $\text{AUC}_{0-15 \text{ m (cell)}}$  represent the area under the concentration-time curve of test compounds in SCHH preincubated in standard HBSS and  $\text{Ca}^{2+}/\text{Mg}^{2+}$ -free HBSS, respectively. In vitro hepatobiliary overall intrinsic clearance ( $CL_{\text{int, overall}}$ ) is calculated based on the extended clearance term (Eq. 21)

$$CL_{\text{int, overall}} \text{ (mL/min/mg)} = (\text{SF}_{\text{active}} \times \text{PS}_{\text{active}} + \text{PS}_{\text{passive}}) \times \frac{CL_{\text{int,bile}}}{\text{PS}_{\text{passive}} + CL_{\text{int,bile}}} \quad (21)$$

$\text{PS}_{\text{active}}$  and  $\text{PS}_{\text{passive}}$  represent active uptake intrinsic clearance and passive diffusion, respectively.  $\text{SF}_{\text{active}}$  is scaling factor for active uptake (e.g.,  $\text{SF}_{\text{active}}$  of 10.6 was reported for OATP1B1 substrates) [57]. The in vitro parameters calculated by Eq. (20) or (21) are scaled up to a whole liver to obtain human intrinsic biliary clearance (Eq. 22).

$$\text{Predicted } CL_{\text{int,bile}} \text{ (mL/min/kg)} = \text{in vitro } CL_{\text{int,bile}} \text{ or } CL_{\text{int,total}} \times \text{physiological scalars} \quad (22)$$

Hepatic CL is calculated by applying one of the liver models as detailed in metabolism section. Alternatively, mechanistic approaches were used, wherein the in vitro data (uptake, efflux, metabolism and biliary  $CL_{\text{int}}$ ) have been integrated either into semimechanistic or whole-body PBPK models to simulate in vivo pharmacokinetics.

### 3.1.2.2 IVIVC of overall hepatic clearance

Previous studies demonstrated that for drugs which are OATP substrates (e.g., rosuvastatin), in vitro metabolic clearance alone underpredicts in vivo clearance and IVIVC is improved when hepatic uptake clearance is considered. For instance, Watanabe et al.

showed that the in vitro uptake clearance obtained using human hepatocytes was similar to in vivo hepatic clearance for several statins, suggesting that hepatic uptake is the rate-determining process for the clearance of these drugs [78]. Mao et al. showed that uptake CL data obtained from plated human hepatocytes predicted IV and PO PK profiles of pravastatin without applying SFs [69]. Camenish and Umehara used suspended hepatocytes, liver microsomes, and sandwich-cultured hepatocytes to estimate the intrinsic sinusoidal uptake and efflux, metabolism, and biliary secretory clearances and showed a reasonable in vitro-in vivo extrapolation of human clearance for 13 selected compounds [52]. Although IVIVC improved, several groups have reported underprediction of in vivo CL, indicating that the activity of transporters in cell systems is low compared to in vivo. For instance, Jones et al. reported that active uptake and biliary efflux in SCHH for seven OATP substrates were under- and overpredicted, leading to wide range of empirical scaling factors for uptake (12–161) and biliary efflux (0.024–0.12) with geometric means of 58 and 0.061, respectively [76]. Similar observations were published by several other groups resulting in empirical scaling factors ranging between 10 and 150 [8, 57, 78, 79]. These SFs represent differences in expression/activity levels of transporter proteins in overexpressing cell lines and human hepatocytes grown under different assay formats in a laboratory to that of the in vivo transporter activity and hence can't be readily adopted by other laboratories. Expression levels of transporters in cell lines, isolated hepatocytes and liver tissue are measured using targeted quantitative proteomics LC-MS/MS methods [80, 81]. SFs derived based on the expression differences alone may not always improve IVIVC, as the amount of active vs inactive protein and the activity per pmol of transporter may vary between in vitro systems and in vivo. Hence, middle-out approaches are favored, where in vitro data are incorporated into PBPK models and parameter estimation modules are used to identify SFs that recovers clinical data [61, 69, 82–84]. As the relative contribution of each transporter to overall uptake clearance can change based on the compound, optimizing to identify universal SFs based on uptake into hepatocytes can lead to erroneous predictions of human PK. This can be improved by identifying fractional contribution of each transporter to overall hepatic uptake. Alternatively, identifying selective substrates that have clinical data allows optimizing SFs for that specific transporter using PBPK models. Izumi et al. recently published an approach where uptake clearance of selective OATP1B1 and OATP1B3 substrates were measured in transporter-transfected cell systems and identified scaling factors to extrapolate uptake clearance for the specific transporters in human hepatocytes. This will allow use of transfected cell systems to provide a quantitative index of OATP1B1 and OATP1B3-mediated uptake that helps in optimizing PK properties of OATP1B substrates during nonclinical stages of drug optimization [73].

Recent studies reported that addition of BSA or human serum albumin (HSA) to transport buffer increases hepatic uptake clearance of OATP substrates via albumin-mediated hepatic uptake mechanism, thereby improving IVIVC. To explain enhanced uptake, a mechanistic dissociation model was proposed in which drug-albumin complex interacts with the cell surface, which enhances dissociation of complex and delivers unbound substrates for hepatic uptake [85–87]. Likewise, transported-induced protein binding shift was proposed as a new explanation for protein-facilitated uptake [88]. Similarly, Riccardi et al. [67] using a large set of structurally diverse compounds with different clearance mechanisms and transporter involvement (OATPs, NTCP, OATs) showed that inclusion of 4% BSA showed strong human

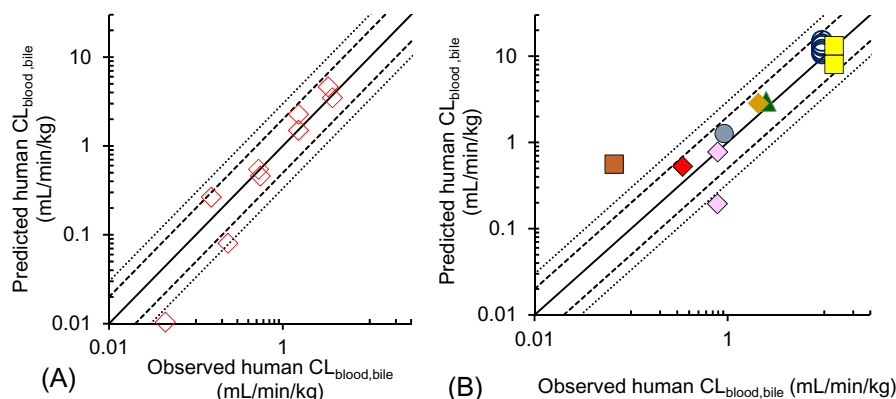


**FIG. 3** In vitro-in vivo extrapolation to predict human hepatobiliary clearance using sandwich-cultured human hepatocytes. Correlation between observed and predicted hepatobiliary blood clearance are depicted following direct scaling of biliary clearance (A), and scaling employing extended clearance term with  $SF_{\text{active}}$  (10.6) for OATP1B-mediated uptake clearance (B). Solid, dashed, and dotted lines represent unity and  $\pm$ two- and  $\pm$ threefold error, respectively. Multiple data points for a given compound represent predictions using different hepatocyte lot. Data reproduced from E. Kimoto, Y.A. Bi, R.E. Kosa, L.M. Tremaine, M.V.S. Varma, *Hepatobiliary clearance prediction: species scaling from monkey, dog, and rat, and in vitro-in vivo extrapolation of sandwich-cultured human hepatocytes using 17 drugs*, *J. Pharm. Sci.* 106(9) (2017) 2795–2804.

IVIVE using a bottom-up approach without any empirical scaling factors. Kimoto et al. showed that for drugs with no significant active uptake in SCHH, the measured intrinsic biliary CL was directly scalable with good predictability (Fig. 3) [75].

Although significant progress has been made in developing new assays and scaling approaches to capture overall hepatic clearance (i.e., uptake, metabolism and biliary efflux), data from in vitro systems by and large continue to underpredict hepatic clearance. Currently, physiologically relevant in vitro models such as organs on chips coupled with flow systems are being developed and investigated with the hope that transporter and enzyme expression and function will be at similar levels to that of the native tissue, thereby enabling better IVIVE [89].

### 3.2 Renal clearance

Renal excretion is a net result of several processes, involving glomerular filtration, active secretion, tubular reabsorption and metabolism. Glomerular filtration is the ultrafiltration of about 10% of total renal blood flow at the glomerulus of the nephron and is defined by the blood flow rate, hematocrit and compound's fraction unbound ( $f_u$ ) in plasma. This is a unidirectional passive process that occurs for most small molecules (mol. wt., 5000 Da) regardless of their ionization state. Renal secretion is a process where transporters actively secrete compounds into the renal tubule, while tubular reabsorption often depends on the passive permeability and degree of ionization of compounds and some contribution from transporters (e.g., peptide transporter (PepT)1/2, OCT1/2, urate transporter (URAT)1). In a recent analysis of 391 compounds with human clearance data, about 31% (123 compounds) showed predominant renal contribution (i.e., renal clearance is >50% of total body clearance).

Furthermore, renal clearance is the primary elimination route for about 60% of antiinfection compounds [90]. Therefore, it is important to predict its clearance to forecast total body clearance and ultimately, the pharmacokinetic profile.

### 3.2.1 Metabolic clearance and IVIVE

Analysis of renal tissue and microsomal samples revealed that the amount/activity of CYP enzymes in kidneys is negligible compared to the liver, while the amount/activity of few UGTs is comparable (e.g., UGT1A6, UGT2B7) or higher (UGT1A9) than that of liver [23, 91–94]. This suggests that metabolism by CYP enzymes is likely to be minimal, while glucuronidation can be significant in kidneys [95, 96]. Like the liver, subcellular fractions such as S9, human kidney microsomes (HKM) and recombinant enzymes are used to determine kidney metabolic clearance. Cytosolic preparations are considered if glutathione-S-transferase (GST) or carboxylesterase (CES)-mediated metabolism in the kidney are of relevance. Consideration of the region used for isolating kidney subcellular fractions is important as most preparations are from kidney cortex, although expression and activity of UGT and GST enzymes have been reported in medulla. Quantitative proteomics data improved our understanding on the regional differences in drug-metabolizing enzymes and differences in enzyme expression between microsomes/cellular systems relative to kidney, which is crucial for prediction of renal clearance from in vitro systems [93, 96]. Human proximal tubular cells are less routinely used for metabolism studies due to high cost, limited constant supply of high-quality preparations and decline in enzyme activity overtime [97].

Although  $CL_{\text{int}}$  measurements can be obtained using in vitro systems discussed above, data on physiological scalars [i.e., microsomal protein per gram of kidney (MPPGK) or cytosolic protein per gram of kidney (CPPGK)] to convert in vitro  $CL_{\text{int}}$  to in vivo  $CL_{\text{int}}$  are sparse compared to liver. Few studies reported scalars based on microsomal protein isolated from mixed tissue or from kidney cortex, with average MPPGK values ranging between 9.3 (mixed tissue) and 26.7 (cortex). Similarly, an average CPPGK value of 53.3 based on isolations from kidney cortex has been reported [96, 98]. More work is needed in this area to confirm physiological scalars, enabling IVIVE of renal metabolic clearance.

### 3.2.2 IVIVE of transporter-mediated CL and tubular reabsorption

Secretory clearance involves vectorial transport of substrates from blood to urine via uptake transporters expressed on the basolateral membrane (blood side) and efflux transporters expressed on apical membrane (urine side) of renal proximal tubule cells. Uptake CL is predominantly mediated by the members of SLC 22A transporter system, which includes organic anion transporters (OATs) and organic cation transporters (OCTs) [98a,b,c], while efflux transporters like Pgp, MRP2/4 and MATE1/2K mediate active secretion into urine.

Renal CL can be mathematically expressed as Eq. (23)

$$CL_R = (CL_{R, \text{fit}} + CL_{R, \text{sec}}) \times (1 - F_{\text{reab}}) \quad (23)$$

Renal filtration clearance can be predicted from GFR and fraction unbound in plasma ( $f_u$ ). In such cases, simple allometry may be used to predict human renal clearance from preclinical data.

For compounds that are actively secreted or reabsorbed, mechanistic in vitro models are required. Several models of varying complexities have been developed to study active transport of drugs in kidney. Cell lines (e.g., MDCK, HEK293, CHO, etc.) transfected with individual transporter are widely used for determination of kinetic parameters. Similarly, both uptake and efflux can be simultaneously studied by overexpressing both the uptake and efflux transporters in a single cell line [99]. Although uptake and efflux  $CL_{int's}$  can be estimated individually and used for IVIVE scaling, it is recommended to generate kinetic data ( $K_m$  and  $J_{max}$ ) to predict saturation of these processes. Unlike uptake transporters, estimation of kinetic parameters for efflux transporters generated in cellular systems requires mechanistic modeling of in vitro data. This is required as the active site for efflux transporters (e.g., P-gp) resides within the cytosol and hence  $K_m$  estimations should be done based on model estimated free cytosolic concentrations [100–102]. As discussed in hepatic section, expression/activity of transporters in cell lines may not be at a similar level to that of in vivo and hence expression vs activity relationships need to be established to enable transporter specific relative expression factors (REFs) to be used with confidence [97]. Such an approach was successfully implemented, and relative activity factors (RAF)s were established using tenofovir (OAT1), acyclovir and ganciclovir (OAT2) and benzylpenicillin and oseltamivir acid (OAT3) as probe substrates. Using in vitro active clearance and estimated RAFs, in vivo renal secretory clearance and total renal clearance of 31 drugs was predicted with average fold errors of 1.89 and 4.4, respectively (Fig. 4) [103].

Although kinetic parameters can be individually measured as detailed above, it is always advantageous to conduct experiments that simultaneously capture active uptake, bidirectional passive transport and metabolic clearance. Primary human renal proximal tubule cells express major enzymes and transporters and hence are holistic systems for studying the

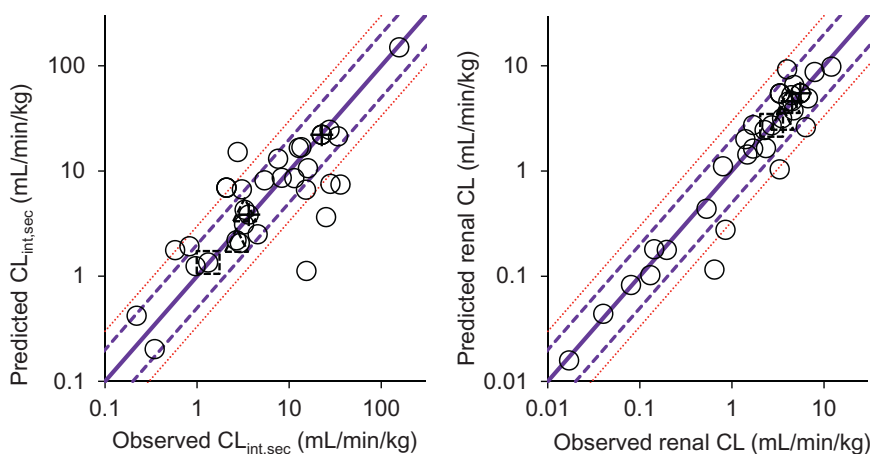


**FIG. 4** In vitro-in vivo extrapolation to predict intrinsic secretory clearance (A) and total plasma renal clearance (B) of 31 drugs. Data points with square, triangle and plus symbols represent OAT1, OAT2, and OAT3 selective substrates, respectively. Diagonal solid, dashed, and dotted lines represent unity, twofold and threefold error, respectively. *Reproduced from S. Mathialagan, M.A. Piotrowski, D.A. Tess, B. Feng, J. Litchfield, M.V. Varma, Quantitative prediction of human renal clearance and drug-drug interactions of organic anion transporter substrates using in vitro transport data: a relative activity factor approach, Drug Metab. Dispos. 45(4) (2017) 409–417.*

interplay between uptake, metabolism and efflux. These cells when maintained in culture for short periods of time retain functional activity, while the activity of some enzymes and transporters goes down up on culturing for longer periods [104–106]. These cells can also be used to study interindividual variability in the expression of enzymes and transporters and the impact on renal clearance. Scaling of kinetic parameters for uptake transporters obtained from this system is performed using proximal tubule cells per gram of kidney (PTCPGK). Similarly, kidney slices can be used to study basolateral uptake of drugs and not tubular secretion. The advantage of this system is the presence of several endogenous transporters that allows for investigating interactions between multiple substrates and inhibitors. The IVIVE of uptake data is performed by kidney weight. The success of these models heavily relies on the quality and continuous supply of the preparations.

Passive renal tubular reabsorption is a contributing process that determines overall renal clearance of drugs. Passive reabsorption of drugs has been correlated with drug lipophilicity and other physicochemical properties. There is currently no consensus on in vitro models to be used to estimate passive reabsorption and several cell lines such as LLC-PK1 and Caco-2 cells have been used to predict passive reabsorption [107, 108]. The renal clearance of 87% of compounds (45 drugs) for which filtration and tubular reabsorption are the major contributors was predicted within threefold using permeability data generated in Caco-2 cells and minimal mechanistic models [108]. Cell lines derived from kidney cells such as LLC-PK1, ci-PTEC, RPTEC/TERT1 have been used to investigate metabolism and tubular secretion. Some of these cell lines have been genetically modified to introduce uptake transporters (e.g., OAT1) that are downregulated in native systems [109, 110].

Recent advances in microengineering enabled growing multiple cell types or renal tubular cells on microchips connected with flow to mimic an in vivo-like environment. Few studies have demonstrated that these systems better mimic kidney toxicity observed in vivo compared to the traditional 2D systems. Similarly, attempts to predict secretory clearance are ongoing. More data are needed in these systems to assess if they offer significant advantages over the existing models [111–114]. Other new technologies on the horizon include bioengineered renal tubules created using renal stem/progenitor cells and bioprinting [115].

Data obtained from all the above systems can be incorporated into commercially available PBPK platforms such as Simcyp and GastroPlus to predict renal clearance using mechanistic kidney models (PBPK-IVIVE) [116, 117]. The predictive ability of these models, however, largely relies on our current understanding of kidney physiology (i.e., tubular flow rates, pH regulation, nephron and proximal tubule number, tubule dimensions and membrane surface area, microsomal and cytosolic protein content of kidney, number of enzymes and transporters) and mechanistic aspects such as electrogenic (e.g., OCT2) and bidirectional (e.g., MATE1/2K) nature of transporters [118]. In addition, the impact of disease state and genetic polymorphism on the expression/activity of enzymes and transporters is being considered [119].

Overall, IVIVE approaches to predict in vivo renal clearance are still emerging. Knowledge gaps in our current understanding of kidney physiology, complex nature of transporters, and requirement of suitable clinical data make prediction of renal clearance from in vitro data currently challenging.



## 4 Conclusions

In conclusion, our understanding of the drug disposition and clearance mechanisms has been steadily growing. We have made significant progress in characterizing these mechanisms and reliable quantitative prediction of clearance in a few cases (e.g., CYP/UGT-mediated clearance). While there are still some gaps, mechanistic prediction of enzyme-based clearance is possible by considering the physiological scalars and account for the expression/activity differences in the in vitro systems such as liver microsomes and human hepatocytes. Such data are routinely generated in the drug design to enable pharmacokinetic optimization and dose predictions. To address gaps leading to underprediction of clearance involving transporter-enzyme interplay new in vitro tools and/or methodologies are needed; however, empirical scalars derived using a sizable drug set may serve the IVIVE purpose in decision-making.

## References

- [1] L. Di, B. Feng, T.C. Goosen, Y. Lai, S.J. Steyn, M.V. Varma, R.S. Obach, A perspective on the prediction of drug pharmacokinetics and disposition in drug research and development, *Drug Metab. Dispos.* 41 (12) (2013) 1975–1993.
- [2] H.A. Barton, Y. Lai, T.C. Goosen, H.M. Jones, A.F. El-Kattan, J.R. Gosset, J. Lin, M.V. Varma, Model-based approaches to predict drug-drug interactions associated with hepatic uptake transporters: preclinical, clinical and beyond, *Expert Opin. Drug Metab. Toxicol.* 9 (4) (2013) 459–472.
- [3] R. Elsby, C. Hilgendorf, K. Fenner, Understanding the critical disposition pathways of statins to assess drug-drug interaction risk during drug development: it's not just about OATP1B1, *Clin. Pharmacol. Ther.* 92 (5) (2012) 584–598.
- [4] Y. Lai, M. Varma, B. Feng, J.C. Stephens, E. Kimoto, A. El-Kattan, K. Ichikawa, H. Kikkawa, C. Ono, A. Suzuki, M. Suzuki, Y. Yamamoto, L. Tremaine, Impact of drug transporter pharmacogenomics on pharmacokinetic and pharmacodynamic variability—considerations for drug development, *Expert Opin. Drug Metab. Toxicol.* 8 (6) (2012) 723–743.
- [5] K.S. Pang, H.J. Maeng, J. Fan, Interplay of transporters and enzymes in drug and metabolite processing, *Mol. Pharm.* 6 (6) (2009) 1734–1755.
- [6] Y. Shitara, T. Horie, Y. Sugiyama, Transporters as a determinant of drug clearance and tissue distribution, *Eur. J. Pharm. Sci.* 27 (5) (2006) 425–446.
- [7] L. Liu, K.S. Pang, The roles of transporters and enzymes in hepatic drug processing, *Drug Metab. Dispos.* 33 (1) (2005) 1–9.
- [8] R. Li, H.A. Barton, M.V. Varma, Prediction of pharmacokinetics and drug-drug interactions when hepatic transporters are involved, *Clin. Pharmacokinet.* 53 (8) (2014) 659–678.
- [9] M.V. Varma, S.J. Steyn, C. Allerton, A.F. El-Kattan, Predicting clearance mechanism in drug discovery: extended clearance classification system (ECCS), *Pharm. Res.* 32 (12) (2015) 3785–3802.
- [10] C.Y. Wu, L.Z. Benet, Predicting drug disposition via application of BCS: transport/absorption/elimination interplay and development of a biopharmaceutics drug disposition classification system, *Pharm. Res.* 22 (1) (2005) 11–23.
- [11] M.V. Varma, G. Chang, Y. Lai, B. Feng, A.F. El-Kattan, J. Litchfield, T.C. Goosen, Physicochemical property space of hepatobiliary transport and computational models for predicting rat biliary excretion, *Drug Metab. Dispos.* 40 (8) (2012) 1527–1537.
- [12] M.V. Varma, I. Gardner, S.J. Steyn, P. Nkansah, C.J. Rotter, C. Whitney-Pickett, H. Zhang, L. Di, M. Cram, K. S. Fenner, A.F. El-Kattan, pH-dependent solubility and permeability criteria for provisional biopharmaceutics classification (BCS and BDDCS) in early drug discovery, *Mol. Pharm.* 9 (5) (2012) 1199–1212.
- [13] L. Di, C. Whitney-Pickett, J.P. Umland, H. Zhang, X. Zhang, D.F. Gebhard, Y. Lai, J.J. Federico, R.E. Davidson, R. Smith, M.V. Varma, Development of a new permeability assay using low-efflux MDCKII cells, *J. Pharm. Sci.* 100 (11) (2011) 4974–4985.



- [14] H. Yu, Q. Wang, Y. Sun, M. Shen, H. Li, Y. Duan, A new PAMPA model proposed on the basis of a synthetic phospholipid membrane, *PLoS One* 10 (2) (2015) e0116502.
- [15] L. Fredlund, S. Winiwarter, C. Hilgendorf, In vitro intrinsic permeability: a transporter-independent measure of Caco-2 cell permeability in drug design and development, *Mol. Pharm.* 14 (5) (2017) 1601–1609.
- [16] A.F. El-Kattan, M.V. Varma, S.J. Steyn, D.O. Scott, T.S. Maurer, A. Bergman, Projecting ADME behavior and drug-drug interactions in early discovery and development: application of the extended clearance classification system, *Pharm. Res.* 33 (12) (2016) 3021–3030.
- [17] M. Varma, A. El-Kattan, B. Feng, S. Steyn, T. Maurer, D. Scott, A. Rodrigues, L. Tremaine, Extended clearance classification system (ECCS) informed approach for evaluating investigational drugs as substrates of drug transporters, *Clin. Pharmacol. Ther.* 102 (2017) 33–36.
- [18] B.C. Jones, A. Srivastava, N. Colclough, J. Wilson, V.P. Reddy, S. Amberntsson, D. Li, An investigation into the prediction of in vivo clearance for a range of flavin-containing monooxygenase substrates, *Drug Metab. Dispos.* 45 (10) (2017) 1060–1067.
- [19] M. Zientek, Y. Jiang, K. Youdim, R.S. Obach, In vitro-in vivo correlation for intrinsic clearance for drugs metabolized by human aldehyde oxidase, *Drug Metab. Dispos.* 38 (8) (2010) 1322–1327.
- [20] M. Chiba, Y. Ishii, Y. Sugiyama, Prediction of hepatic clearance in human from in vitro data for successful drug development, *AAPS J.* 11 (2) (2009) 262–276.
- [21] R.S. Obach, The prediction of human clearance from hepatic microsomal metabolism data, *Curr. Opin. Drug Discov. Devel.* 4 (1) (2001) 36–44.
- [22] J.O. Miners, P.I. Mackenzie, K.M. Knights, The prediction of drug-glucuronidation parameters in humans: UDP-glucuronosyltransferase enzyme-selective substrate and inhibitor probes for reaction phenotyping and in vitro-in vivo extrapolation of drug clearance and drug-drug interaction potential, *Drug Metab. Rev.* 42 (1) (2010) 196–208.
- [23] M.G. Soars, B. Burchell, R.J. Riley, In vitro analysis of human drug glucuronidation and prediction of in vivo metabolic clearance, *J. Pharmacol. Exp. Ther.* 301 (1) (2002) 382–390.
- [24] P.J. Kilford, R. Stringer, B. Sohal, J.B. Houston, A. Galetin, Prediction of drug clearance by glucuronidation from in vitro data: use of combined cytochrome P450 and UDP-glucuronosyltransferase cofactors in alamethicin-activated human liver microsomes, *Drug Metab. Dispos.* 37 (1) (2009) 82–89.
- [25] L. Di, The role of drug metabolizing enzymes in clearance, *Expert Opin. Drug Metab. Toxicol.* 10 (3) (2014) 379–393.
- [26] J.B. Houston, D.J. Carlile, Prediction of hepatic clearance from microsomes, hepatocytes, and liver slices, *Drug Metab. Rev.* 29 (4) (1997) 891–922.
- [27] J.B. Houston, Utility of in vitro drug metabolism data in predicting in vivo metabolic clearance, *Biochem. Pharmacol.* 47 (9) (1994) 1469–1479.
- [28] S.J. Richardson, A. Bai, A.A. Kulkarni, M.F. Moghaddam, Efficiency in drug discovery: liver S9 fraction assay as a screen for metabolic stability, *Drug Metab. Lett.* 10 (2) (2016) 83–90.
- [29] R.L. Walsky, J.N. Bauman, K. Bourcier, G. Giddens, K. Lapham, A. Negahban, T.F. Ryder, R.S. Obach, R. Hyland, T.C. Goosen, Optimized assays for human UDP-glucuronosyltransferase (UGT) activities: altered alamethicin concentration and utility to screen for UGT inhibitors, *Drug Metab. Dispos.* 40 (5) (2012) 1051–1065.
- [30] A. Rowland, K.M. Knights, P.I. Mackenzie, J.O. Miners, The “albumin effect” and drug glucuronidation: bovine serum albumin and fatty acid-free human serum albumin enhance the glucuronidation of UDP-glucuronosyltransferase (UGT) 1A9 substrates but not UGT1A1 and UGT1A6 activities, *Drug Metab. Dispos.* 36 (6) (2008) 1056–1062.
- [31] K.L. Gill, J.B. Houston, A. Galetin, Characterization of in vitro glucuronidation clearance of a range of drugs in human kidney microsomes: comparison with liver and intestinal glucuronidation and impact of albumin, *Drug Metab. Dispos.* 40 (4) (2012) 825–835.
- [32] A. Rowland, D.J. Elliot, K.M. Knights, P.I. Mackenzie, J.O. Miners, The “albumin effect” and in vitro-in vivo extrapolation: sequestration of long-chain unsaturated fatty acids enhances phenytoin hydroxylation by human liver microsomal and recombinant cytochrome P450 2C9, *Drug Metab. Dispos.* 36 (5) (2008) 870–877.
- [33] P. Korprasertthaworn, T.M. Polasek, M.J. Sorich, A.J. McLachlan, J.O. Miners, G.T. Tucker, A. Rowland, In vitro characterization of the human liver microsomal kinetics and reaction phenotyping of olanzapine metabolism, *Drug Metab. Dispos.* 43 (11) (2015) 1806–1814.
- [34] Y. Chen, L. Liu, K. Nguyen, A.J. Fretland, Utility of intersystem extrapolation factors in early reaction phenotyping and the quantitative extrapolation of human liver microsomal intrinsic clearance using recombinant cytochromes P450, *Drug Metab. Dispos.* 39 (3) (2011) 373–382.

- [35] H.K. Crewe, Z.E. Barter, K.R. Yeo, A. Rostami-Hodjegan, Are there differences in the catalytic activity per unit enzyme of recombinantly expressed and human liver microsomal cytochrome P450 2C9? A systematic investigation into inter-system extrapolation factors, *Biopharm. Drug Dispos.* 32 (6) (2011) 303–318.
- [36] R.A. Stringer, C. Strain-Damerell, P. Nicklin, J.B. Houston, Evaluation of recombinant cytochrome P450 enzymes as an in vitro system for metabolic clearance predictions, *Drug Metab. Dispos.* 37 (5) (2009) 1025–1034.
- [37] C.R. Gibson, P. Lu, C. Maciolek, C. Wudarski, Z. Barter, K. Rowland-Yeo, M. Stroh, E. Lai, D.A. Nicoll-Griffith, Using human recombinant UDP-glucuronosyltransferase isoforms and a relative activity factor approach to model total body clearance of laropiprant (MK-0524) in humans, *Xenobiotica* 43 (12) (2013) 1027–1036.
- [38] A.D. Rodrigues, Integrated cytochrome P450 reaction phenotyping: attempting to bridge the gap between cDNA-expressed cytochromes P450 and native human liver microsomes, *Biochem. Pharmacol.* 57 (5) (1999) 465–480.
- [39] N. Hakooz, K. Ito, H. Rawden, H. Gill, L. Lemmers, A.R. Boobis, R.J. Edwards, D.J. Carlile, B.G. Lake, J.B. Houston, Determination of a human hepatic microsomal scaling factor for predicting in vivo drug clearance, *Pharm. Res.* 23 (3) (2006) 533–539.
- [40] K. Ito, J.B. Houston, Prediction of human drug clearance from in vitro and preclinical data using physiologically based and empirical approaches, *Pharm. Res.* 22 (1) (2005) 103–112.
- [41] D.F. McGinnity, M.G. Soars, R.A. Urbanowicz, R.J. Riley, Evaluation of fresh and cryopreserved hepatocytes as in vitro drug metabolism tools for the prediction of metabolic clearance, *Drug Metab. Dispos.* 32 (11) (2004) 1247–1253.
- [42] H.S. Brown, M. Griffin, J.B. Houston, Evaluation of cryopreserved human hepatocytes as an alternative in vitro system to microsomes for the prediction of metabolic clearance, *Drug Metab. Dispos.* 35 (2) (2007) 293–301.
- [43] P. Lancett, B. Williamson, P. Barton, R.J. Riley, Development and characterization of a human hepatocyte low intrinsic clearance assay for use in drug discovery, *Drug Metab. Dispos.* 46 (8) (2018) 1169–1178.
- [44] B. Bonn, P. Svanberg, A. Janefeldt, I. Hultman, K. Grime, Determination of human hepatocyte intrinsic clearance for slowly metabolized compounds: comparison of a primary hepatocyte/stromal cell co-culture with plated primary hepatocytes and HepaRG, *Drug Metab. Dispos.* 44 (4) (2016) 527–533.
- [45] A.K. Sohlenius-Sternbeck, C. Jones, D. Ferguson, B.J. Middleton, D. Projean, E. Floby, J. Bylund, L. Afzelius, Practical use of the regression offset approach for the prediction of in vivo intrinsic clearance from hepatocytes, *Xenobiotica* 42 (9) (2012) 841–853.
- [46] D. Hallifax, J.B. Houston, Evaluation of hepatic clearance prediction using in vitro data: emphasis on fraction unbound in plasma and drug ionisation using a database of 107 drugs, *J. Pharm. Sci.* 101 (8) (2012) 2645–2652.
- [47] L.M. Berezhkovskiy, The corrected traditional equations for calculation of hepatic clearance that account for the difference in drug ionization in extracellular and intracellular tissue water and the corresponding corrected PBPK equation, *J. Pharm. Sci.* 100 (3) (2011) 1167–1183.
- [48] P. Poulin, J.R. Kenny, C.E. Hop, S. Haddad, In vitro-in vivo extrapolation of clearance: modeling hepatic metabolic clearance of highly bound drugs and comparative assessment with existing calculation methods, *J. Pharm. Sci.* 101 (2) (2012) 838–851.
- [49] P. Poulin, C.E. Hop, Q. Ho, J.S. Halladay, S. Haddad, J.R. Kenny, Comparative assessment of in vitro-in vivo extrapolation methods used for predicting hepatic metabolic clearance of drugs, *J. Pharm. Sci.* 101 (11) (2012) 4308–4326.
- [50] T. Yamagata, U. Zanelli, D. Gallemann, D. Perrin, H. Dolgos, C. Petersson, Comparison of methods for the prediction of human clearance from hepatocyte intrinsic clearance for a set of reference compounds and an external evaluation set, *Xenobiotica* 47 (9) (2017) 741–751.
- [51] C.M. Bowman, L.Z. Benet, In vitro-in vivo extrapolation and hepatic clearance-dependent underprediction, *J. Pharm. Sci.* 108 (7) (2019) 2500–2504.
- [52] G. Camenisch, K. Umehara, Predicting human hepatic clearance from in vitro drug metabolism and transport data: a scientific and pharmaceutical perspective for assessing drug-drug interactions, *Biopharm. Drug Dispos.* 33 (4) (2012) 179–194.
- [53] Y. Shitara, Y. Sugiyama, Pharmacokinetic and pharmacodynamic alterations of 3-hydroxy-3-methylglutaryl coenzyme A (HMG-CoA) reductase inhibitors: drug-drug interactions and interindividual differences in transporter and metabolic enzyme functions, *Pharmacol. Ther.* 112 (1) (2006) 71–105.
- [54] M.V. Varma, A.F. El-Kattan, Transporter-enzyme interplay: deconvoluting effects of hepatic transporters and enzymes on drug disposition using static and dynamic mechanistic models, *J. Clin. Pharmacol.* 56 (Suppl. 7) (2016) S99–s109.

- [55] I. Ieiri, S. Higuchi, Y. Sugiyama, Genetic polymorphisms of uptake (OATP1B1, 1B3) and efflux (MRP2, BCRP) transporters: implications for inter-individual differences in the pharmacokinetics and pharmacodynamics of statins and other clinically relevant drugs, *Expert Opin. Drug Metab. Toxicol.* 5 (7) (2009) 703–729.
- [56] E. Kimoto, S. Mathialagan, L. Tylaska, M. Niosi, J. Lin, A.A. Carlo, D.A. Tess, M.V.S. Varma, Organic anion transporter 2-mediated hepatic uptake contributes to the clearance of high-permeability-low-molecular-weight acid and zwitterion drugs: evaluation using 25 drugs, *J. Pharmacol. Exp. Ther.* 367 (2) (2018) 322–334.
- [57] M.V. Varma, Y.A. Bi, E. Kimoto, J. Lin, Quantitative prediction of transporter- and enzyme-mediated clinical drug-drug interactions of organic anion-transporting polypeptide 1B1 substrates using a mechanistic net-effect model, *J. Pharmacol. Exp. Ther.* 351 (1) (2014) 214–223.
- [58] M.V. Varma, Y. Lai, B. Feng, J. Litchfield, T.C. Goosen, A. Bergman, Physiologically based modeling of pravastatin transporter-mediated hepatobiliary disposition and drug-drug interactions, *Pharm. Res.* 29 (10) (2012) 2860–2873.
- [59] M.V. Varma, Y. Lai, E. Kimoto, T.C. Goosen, A.F. El-Kattan, V. Kumar, Mechanistic modeling to predict the transporter- and enzyme-mediated drug-drug interactions of repaglinide, *Pharm. Res.* 30 (4) (2013) 1188–1199.
- [60] M.V. Varma, J. Lin, Y.A. Bi, C.J. Rotter, O.A. Fahmi, J.L. Lam, A.F. El-Kattan, T.C. Goosen, Y. Lai, Quantitative prediction of repaglinide-rifampicin complex drug interactions using dynamic and static mechanistic models: delineating differential CYP3A4 induction and OATP1B1 inhibition potential of rifampicin, *Drug Metab. Dispos.* 41 (5) (2013) 966–974.
- [61] M. Jamei, F. Bajot, S. Neuhoff, Z. Barter, J. Yang, A. Rostami-Hodjegan, K. Rowland-Yeo, A mechanistic framework for in vitro-in vivo extrapolation of liver membrane transporters: prediction of drug-drug interaction between rosuvastatin and cyclosporine, *Clin. Pharmacokinet.* 53 (1) (2014) 73–87.
- [62] S. Miyauchi, Y. Sawada, T. Iga, M. Hanano, Y. Sugiyama, Comparison of the hepatic uptake clearances of fifteen drugs with a wide range of membrane permeabilities in isolated rat hepatocytes and perfused rat livers, *Pharm. Res.* 10 (3) (1993) 434–440.
- [63] M.G. Soars, K. Grime, J.L. Sproston, P.J. Webborn, R.J. Riley, Use of hepatocytes to assess the contribution of hepatic uptake to clearance in vivo, *Drug Metab. Dispos.* 35 (6) (2007) 859–865.
- [64] K.L. Brouwer, D. Keppler, K.A. Hoffmaster, D.A. Bow, Y. Cheng, Y. Lai, J.E. Palm, B. Stieger, R. Evers, In vitro methods to support transporter evaluation in drug discovery and development, *Clin. Pharmacol. Ther.* 94 (1) (2013) 95–112.
- [65] M.J. Zamek-Gliszczynski, et al., ITC recommendations for transporter kinetic parameter estimation and translational modeling of transport-mediated PK and DDIs in humans, *Clin. Pharmacol. Ther.* 94 (1) (2013) 64–79.
- [66] J. Harrison, T. De Bruyn, A.S. Darwich, J.B. Houston, Simultaneous assessment in vitro of transporter and metabolic processes in hepatic drug clearance: use of a media loss approach, *Drug Metab. Dispos.* 46 (4) (2018) 405–414.
- [67] K.A. Riccardi, D.A. Tess, J. Lin, R. Patel, S. Ryu, K. Atkinson, L. Di, R. Li, A novel unified approach to predict human hepatic clearance for both enzyme- and transporter-mediated mechanisms using suspended human hepatocytes, *Drug Metab. Dispos.* 47 (5) (2019) 484–492.
- [68] P. Nordell, S. Winiwarter, C. Hilgendorf, Resolving the distribution-metabolism interplay of eight OATP substrates in the standard clearance assay with suspended human cryopreserved hepatocytes, *Mol. Pharm.* 10 (12) (2013) 4443–4451.
- [69] J. Mao, U. Doshi, M. Wright, C. Hop, A.P. Li, Y. Chen, Prediction of the pharmacokinetics of pravastatin as an OATP substrate using plateable human hepatocytes with human plasma data and PBPK modeling, *CPT Pharmacometrics Syst. Pharmacol.* 7 (4) (2018) 251–258.
- [70] K. Menochet, K.E. Kenworthy, J.B. Houston, A. Galetin, Simultaneous assessment of uptake and metabolism in rat hepatocytes: a comprehensive mechanistic model, *J. Pharmacol. Exp. Ther.* 341 (1) (2012) 2–15.
- [71] T. De Bruyn, A. Ufuk, C. Cantrill, R.E. Kosa, Y.A. Bi, M. Niosi, S. Modi, A.D. Rodrigues, L.M. Tremaine, M.V. S. Varma, A. Galetin, J.B. Houston, Predicting human clearance of organic anion transporting polypeptide substrates using cynomolgus monkey: in vitro-in vivo scaling of hepatic uptake clearance, *Drug Metab. Dispos.* 46 (7) (2018) 989–1000.
- [72] G. Ghibellini, E.M. Leslie, K.L. Brouwer, Methods to evaluate biliary excretion of drugs in humans: an updated review, *Mol. Pharm.* 3 (3) (2006) 198–211.
- [73] S. Izumi, Y. Nozaki, H. Kusuhara, K. Hotta, T. Mochizuki, T. Komori, K. Maeda, Y. Sugiyama, Relative activity factor (RAF)-based scaling of uptake clearance mediated by organic anion transporting polypeptide (OATP) 1B1 and OATP1B3 in human hepatocytes, *Mol. Pharm.* 15 (6) (2018) 2277–2288.

- [74] Y.A. Bi, D. Kazolias, D.B. Duignan, Use of cryopreserved human hepatocytes in sandwich culture to measure hepatobiliary transport, *Drug Metab. Dispos.* 34 (9) (2006) 1658–1665.
- [75] E. Kimoto, Y.A. Bi, R.E. Kosa, L.M. Tremaine, M.V.S. Varma, Hepatobiliary clearance prediction: species scaling from monkey, dog, and rat, and in vitro-in vivo extrapolation of sandwich-cultured human hepatocytes using 17 drugs, *J. Pharm. Sci.* 106 (9) (2017) 2795–2804.
- [76] H.M. Jones, H.A. Barton, Y. Lai, Y.A. Bi, E. Kimoto, S. Kempshall, S.C. Tate, A. El-Kattan, J.B. Houston, A. Galetin, K.S. Fenner, Mechanistic pharmacokinetic modeling for the prediction of transporter-mediated disposition in humans from sandwich culture human hepatocyte data, *Drug Metab. Dispos.* 40 (5) (2012) 1007–1017.
- [77] K. Abe, A.S. Bridges, K.L. Brouwer, Use of sandwich-cultured human hepatocytes to predict biliary clearance of angiotensin II receptor blockers and HMG-CoA reductase inhibitors, *Drug Metab. Dispos.* 37 (3) (2009) 447–452.
- [78] T. Watanabe, H. Kusuhara, K. Maeda, H. Kanamaru, Y. Saito, Z. Hu, Y. Sugiyama, Investigation of the rate-determining process in the hepatic elimination of HMG-CoA reductase inhibitors in rats and humans, *Drug Metab. Dispos.* 38 (2) (2010) 215–222.
- [79] S. Izumi, Y. Nozaki, T. Komori, O. Takenaka, K. Maeda, H. Kusuhara, Y. Sugiyama, Comparison of the predictability of human hepatic clearance for organic anion transporting polypeptide substrate drugs between different in vitro-in vivo extrapolation approaches, *J. Pharm. Sci.* 106 (9) (2017) 2678–2687.
- [80] B. Prasad, R. Evers, A. Gupta, C.E. Hop, L. Salphati, S. Shukla, S.V. Ambudkar, J.D. Unadkat, Interindividual variability in hepatic organic anion-transporting polypeptides and P-glycoprotein (ABCB1) protein expression: quantification by liquid chromatography tandem mass spectroscopy and influence of genotype, age, and sex, *Drug Metab. Dispos.* 42 (1) (2014) 78–88.
- [81] L. Wang, B. Prasad, L. Salphati, X. Chu, A. Gupta, C.E. Hop, R. Evers, J.D. Unadkat, Interspecies variability in expression of hepatobiliary transporters across human, dog, monkey, and rat as determined by quantitative proteomics, *Drug Metab. Dispos.* 43 (3) (2015) 367–374.
- [82] R. Li, H.A. Barton, P.D. Yates, A. Ghosh, A.C. Wolford, K.A. Riccardi, T.S. Maurer, A “middle-out” approach to human pharmacokinetic predictions for OATP substrates using physiologically-based pharmacokinetic modeling, *J. Pharmacokin. Pharmacodyn.* 41 (3) (2014) 197–209.
- [83] Y.A. Bi, J. Lin, S. Mathialagan, L. Tylaska, E. Callegari, A.D. Rodrigues, M.V.S. Varma, Role of hepatic organic anion transporter 2 in the pharmacokinetics of R- and S-warfarin: in vitro studies and mechanistic evaluation, *Mol. Pharm.* 15 (3) (2018) 1284–1295.
- [84] M. Sato, K. Toshimoto, A. Tomaru, T. Yoshikado, Y. Tanaka, A. Hisaka, W. Lee, Y. Sugiyama, Physiologically based pharmacokinetic modeling of bosentan identifies the saturable hepatic uptake as a major contributor to its nonlinear pharmacokinetics, *Drug Metab. Dispos.* 46 (5) (2018) 740–748.
- [85] S. Miyauchi, M. Masuda, S.J. Kim, Y. Tanaka, K.R. Lee, S. Iwakado, M. Nemoto, S. Sasaki, K. Shimono, Y. Tanaka, Y. Sugiyama, The phenomenon of albumin-mediated hepatic uptake of organic anion transport polypeptide substrates: prediction of the in vivo uptake clearance from the in vitro uptake by isolated hepatocytes using a facilitated-dissociation model, *Drug Metab. Dispos.* 46 (3) (2018) 259–267.
- [86] S.J. Kim, K.R. Lee, S. Miyauchi, Y. Sugiyama, Extrapolation of in vivo hepatic clearance from in vitro uptake clearance by suspended human hepatocytes for anionic drugs with high binding to human albumin: improvement of in vitro-to-in vivo extrapolation by considering the “albumin-mediated” hepatic uptake mechanism on the basis of the “facilitated-dissociation model”, *Drug Metab. Dispos.* 47 (2) (2019) 94–103.
- [87] Y. Fukuchi, K. Toshimoto, T. Mori, K. Kakimoto, Y. Tobe, T. Sawada, R. Asaumi, T. Iwata, Y. Hashimoto, K.I. Nunoya, H. Imawaka, S. Miyauchi, Y. Sugiyama, Analysis of nonlinear pharmacokinetics of a highly albumin-bound compound: contribution of albumin-mediated hepatic uptake mechanism, *J. Pharm. Sci.* 106 (9) (2017) 2704–2714.
- [88] C.M. Bowman, H. Okochi, L.Z. Benet, The presence of a transporter-induced protein binding shift: a new explanation for protein-facilitated uptake and improvement for in vitro-in vivo extrapolation, *Drug Metab. Dispos.* 47 (4) (2019) 358–363.
- [89] A.J. Foster, et al., Integrated in vitro models for hepatic safety and metabolism: evaluation of a human Liver-Chip and liver spheroid, *Arch. Toxicol.* 93 (4) (2019) 1021–1037.
- [90] M.V. Varma, B. Feng, R.S. Obach, M.D. Troutman, J. Chupka, H.R. Miller, A. El-Kattan, Physicochemical determinants of human renal clearance, *J. Med. Chem.* 52 (15) (2009) 4844–4852.
- [91] I. de Waziers, P.H. Cugnenc, C.S. Yang, J.P. Leroux, P.H. Beaune, Cytochrome P 450 isoenzymes, epoxide hydrolase and glutathione transferases in rat and human hepatic and extrahepatic tissues, *J. Pharmacol. Exp. Ther.* 253 (1) (1990) 387–394.

- [92] M.G. Soars, R.J. Riley, K.A. Findlay, M.J. Coffey, B. Burchell, Evidence for significant differences in microsomal drug glucuronidation by canine and human liver and kidney, *Drug Metab. Dispos.* 29 (2) (2001) 121–126.
- [93] K. Nakamura, M. Hirayama-Kurogi, S. Ito, T. Kuno, T. Yoneyama, W. Obuchi, T. Terasaki, S. Ohtsuki, Large-scale multiplex absolute protein quantification of drug-metabolizing enzymes and transporters in human intestine, liver, and kidney microsomes by SWATH-MS: comparison with MRM/SRM and HR-MRM/PRM, *Proteomics* 16 (15–16) (2016) 2106–2117.
- [94] D.E. Harbourt, J.K. Fallon, S. Ito, T. Baba, J.K. Ritter, G.L. Glish, P.C. Smith, Quantification of human uridine-diphosphate glucuronosyl transferase 1A isoforms in liver, intestine, and kidney using nanobore liquid chromatography-tandem mass spectrometry, *Anal. Chem.* 84 (1) (2012) 98–105.
- [95] U. Fagerholm, Prediction of human pharmacokinetics—renal metabolic and excretion clearance, *J. Pharm. Pharmacol.* 59 (11) (2007) 1463–1471.
- [96] K.M. Knights, S.M. Spencer, J.K. Fallon, N. Chau, P.C. Smith, J.O. Miners, Scaling factors for the in vitro-in vivo extrapolation (IV-IVE) of renal drug and xenobiotic glucuronidation clearance, *Br. J. Clin. Pharmacol.* 81 (6) (2016) 1153–1164.
- [97] D. Scotcher, C. Jones, M. Posada, A. Rostami-Hodjegan, A. Galetin, Key to opening kidney for in vitro-in vivo extrapolation entrance in health and disease: part i: in vitro systems and physiological data, *AAPS J.* 18 (5) (2016) 1067–1081.
- [98] D. Scotcher, S. Billington, J. Brown, C.R. Jones, C.D.A. Brown, A. Rostami-Hodjegan, A. Galetin, Microsomal and cytosolic scaling factors in dog and human kidney cortex and application for in vitro-in vivo extrapolation of renal metabolic clearance, *Drug Metab. Dispos.* 45 (5) (2017) 556–568; (a) W. Lee, R.B. Kim, Transporters and renal drug elimination, *Annu. Rev. Pharmacol. Toxicol.* 44 (2004) 137–166; (b) B. Feng, J.L. LaPerle, G. Chang, M.V. Varma, Renal clearance in drug discovery and development: molecular descriptors, drug transporters and disease state, *Expert Opin. Drug Metab. Toxicol.* 6 (8) (2010) 939–952; (c) K.M. Morrissey, S.L. Stocker, M.B. Wittwer, L. Xu, K.M. Giacomini, Renal transporters in drug development, *Annu. Rev. Pharmacol. Toxicol.* 53 (2013) 503–529.
- [99] J. Konig, O. Zolk, K. Singer, C. Hoffmann, M.F. Fromm, Double-transfected MDCK cells expressing human OCT1/MATE1 or OCT2/MATE1: determinants of uptake and transcellular translocation of organic cations, *Br. J. Pharmacol.* 163 (3) (2011) 546–555.
- [100] T. Tachibana, S. Kitamura, M. Kato, T. Mitsui, Y. Shirasaka, S. Yamashita, Y. Sugiyama, Model analysis of the concentration-dependent permeability of P-gp substrates, *Pharm. Res.* 27 (3) (2010) 442–446.
- [101] S. Nagar, J. Tucker, E.A. Weiskircher, S. Bhoopathy, I.J. Hidalgo, K. Korzekwa, Compartmental models for apical efflux by P-glycoprotein—part 1: evaluation of model complexity, *Pharm. Res.* 31 (2) (2014) 347–359.
- [102] K. Bittermann, K.U. Goss, Predicting apparent passive permeability of Caco-2 and MDCK cell-monolayers: a mechanistic model, *PLoS One* 12 (12) (2017) e0190319.
- [103] S. Mathialagan, M.A. Piotrowski, D.A. Tess, B. Feng, J. Litchfield, M.V. Varma, Quantitative prediction of human renal clearance and drug-drug interactions of organic anion transporter substrates using in vitro transport data: a relative activity factor approach, *Drug Metab. Dispos.* 45 (4) (2017) 409–417.
- [104] C.D. Brown, R. Sayer, A.S. Windass, I.S. Haslam, M.E. De Broe, P.C. D’Haese, A. Verhulst, Characterisation of human tubular cell monolayers as a model of proximal tubular xenobiotic handling, *Toxicol. Appl. Pharmacol.* 233 (3) (2008) 428–438.
- [105] L.H. Lash, D.A. Putt, H. Cai, Membrane transport function in primary cultures of human proximal tubular cells, *Toxicology* 228 (2–3) (2006) 200–218.
- [106] L.H. Lash, D.A. Putt, H. Cai, Drug metabolism enzyme expression and activity in primary cultures of human proximal tubular cells, *Toxicology* 244 (1) (2008) 56–65.
- [107] A. Kunze, J. Huwyler, B. Poller, H. Gutmann, G. Camenisch, In vitro-in vivo extrapolation method to predict human renal clearance of drugs, *J. Pharm. Sci.* 103 (3) (2014) 994–1001.
- [108] D. Scotcher, C. Jones, A. Rostami-Hodjegan, A. Galetin, Novel minimal physiologically-based model for the prediction of passive tubular reabsorption and renal excretion clearance, *Eur. J. Pharm. Sci.* 94 (2016) 59–71.
- [109] M. Bens, A. Vandewalle, Cell models for studying renal physiology, *Pflugers Arch.* 457 (1) (2008) 1–15.
- [110] L. Aschauer, G. Carta, N. Vogelsang, E. Schlatter, P. Jennings, et al., *Toxicol. In Vitro* 30 (1 Pt A) (2015) 95–105.
- [111] K.J. Jang, A.P. Mehr, G.A. Hamilton, L.A. McPartlin, S. Chung, K.Y. Suh, D.E. Ingber, Human kidney proximal tubule-on-a-chip for drug transport and nephrotoxicity assessment, *Integr. Biol. (Camb.)* 5 (9) (2013) 1119–1129.
- [112] J. Lee, S. Kim, Kidney-on-a-chip: a new technology for predicting drug efficacy, interactions, and drug-induced nephrotoxicity, *Curr. Drug Metab.* 19 (7) (2018) 577–583.

- [113] P. Caetano-Pinto, S.H. Stahl, Perspective on the application of microphysiological systems to drug transporter studies, *Drug Metab. Dispos.* 46 (11) (2018) 1647–1657.
- [114] S.Y. Chang, E.J. Weber, K.V. Ness, D.L. Eaton, E.J. Kelly, Liver and kidney on chips: microphysiological models to understand transporter function, *Clin. Pharmacol. Ther.* 100 (5) (2016) 464–478.
- [115] A.G. Sciancalepore, F. Sallustio, S. Girardo, L. Gioia Passione, A. Camposeo, E. Mele, M. Di Lorenzo, V. Costantino, F.P. Schena, D. Pisignano, A bioartificial renal tubule device embedding human renal stem/progenitor cells, *PLoS One* 9 (1) (2014) e87496.
- [116] S. Neuhoff, L. Gaohua, H. Burt, M. Jamei, L. Li, G.T. Tucker, A. Rostami-Hodjegan, Accounting for transporters in renal clearance: towards a mechanistic kidney model (Mech KiM), in: Y. Sugiyama, B. Steffansen (Eds.), *Transporters in Drug Development: Discovery, Optimization, Clinical Study and Regulation*, Springer New York, New York, NY, 2013, , pp. 155–177.
- [117] W. Huang, N. Isoherranen, Development of a dynamic physiologically based mechanistic kidney model to predict renal clearance, *CPT Pharmacometrics Syst. Pharmacol.* 7 (9) (2018) 593–602.
- [118] H.J. Burt, S. Neuhoff, L. Almond, L. Gaohua, M.D. Harwood, M. Jamei, A. Rostami-Hodjegan, G.T. Tucker, K. Rowland-Yeo, Metformin and cimetidine: physiologically based pharmacokinetic modelling to investigate transporter mediated drug-drug interactions, *Eur. J. Pharm. Sci.* 88 (2016) 70–82.
- [119] D. Scotcher, C. Jones, M. Posada, A. Galetin, A. Rostami-Hodjegan, Key to opening kidney for in vitro-in vivo extrapolation entrance in health and disease: part II: mechanistic models and in vitro-in vivo extrapolation, *AAPS J.* 18 (5) (2016) 1082–1094.



# The role of quantitative modeling and simulation in translational science

Venkatesh Pilla Reddy<sup>a</sup>, Andy Z.X. Zhu<sup>b</sup>

<sup>a</sup>Departments of Modeling and Simulation, Early Oncology Drug Metabolism and Pharmacokinetics, R&D Oncology, AstraZeneca, Cambridge, United Kingdom <sup>b</sup>Department of Drug Metabolism and Pharmacokinetics, Takeda Pharmaceuticals International Co., Cambridge, MA, United States

## List of abbreviations

<b>ADME</b>	absorption, distribution, metabolism, and excretion
<b>CL</b>	clearance
<b>D<sub>2</sub>RO</b>	receptor occupancy of the D <sub>2</sub> receptor
<b>DDIs</b>	drug-drug interactions
<b>Fabs</b>	fraction absorbed
<b>FDA</b>	Food and Drug Administration
<b>Fg</b>	fraction escaping gut metabolism
<b>IV</b>	intravenous
<b>IVIVe</b>	in vitro to in vivo extrapolation
<b>K<sub>a</sub></b>	absorption constant
<b>K<sub>d</sub></b>	is the equilibrium dissociation constant
<b>K<sub>off</sub></b>	dissociation constant
<b>K<sub>on</sub></b>	association constant
<b>mAb</b>	monoclonal antibodies
<b>MID<sup>3</sup></b>	model-informed drug discovery and development
<b>MM</b>	Michaelis-Menten
<b>NCA</b>	noncompartmental analyses
<b>ODE</b>	ordinary differential equations
<b>P-gp</b>	P-glycoprotein
<b>PBPK</b>	physiological-based pharmacokinetic
<b>P<sub>eff</sub></b>	effective permeability
<b>PK</b>	pharmacokinetics
<b>PKPD</b>	pharmacokinetic-pharmacodynamic



PKPD/E	pharmacokinetic-pharmacodynamic efficacy
PXR	pregnane X receptor
QE	quasiequilibrium model
QSP	quantitative system pharmacology
QSS	quasi-steady-state model
RO	receptor occupancy
SC	subcutaneous
TMDD	target-mediated drug disposition
$V_{ss}$	volume of distribution at steady state

## 1 Introduction

---

Over the last 10 years, scientific advances in biomedical research have greatly expanded our knowledge of the mechanistic basis of diseases [1–3]. As a result of those advances, a number of transformative therapies in the field of cancer, rare diseases, and immunology have been developed, which have brought meaningful declines of mortality and morbidity to patients. However, despite the scientific advances in the understanding of disease biology and -omic technologies, the success rate of drug development remains very low [4]. A recent analysis of 7455 clinical drug development programs between 2006 and 2015 showed that the likelihood of regulatory approval for a phase I program is only 9.6% [4]. This is particularly problematic in psychiatry and oncology, where only 5% to 6% of phase I programs and <50% of phase III programs are ultimately approved. One of the reasons behind this low success rate is the lack of a holistic and integrated framework to predict clinical efficacy and toxicity profiles from animal and *in vitro* experiments. A rigorous unifying preclinical to clinical translational framework could facilitate drug discovery and development by identifying the appropriate translational strategies, patient selection criteria, and appropriate biomarkers to guide decision-making.

Mathematical modeling can play an important role in translational science by integrating *in vitro* and *in vivo* data in a quantitative framework to guide data generation across projects, informing design and selection of quality compounds preclinically, and informing clinical decision-making. With the recent advances in computation power and system-level understanding of pharmacology, model-informed drug discovery and development (MID<sup>3</sup>) or model-informed drug development (MIDD) has recently gathered significant attention as a promising enabler of efficient drug discovery and development to inform dose, dosage regimen, and subsequently drug product label [5, 6].

The scientific and regulatory fields have long recognized the utility of a mathematical modeling framework. As early as 2006, the FDA critical path opportunities report advocated the use of modeling and simulation for decision-making in drug development [7]. More recently, the FDA reinforced this idea in their FDA voice blog, which states: “Modeling and simulation play a critical role in organizing diverse data sets and exploring alternate study designs. This enables safe and effective new therapeutics to advance more efficiently through the different stages of clinical trials” [7, 8].

In general, mathematical models can be used in drug development to describe either pharmacokinetic (e.g., time vs concentration) or pharmacodynamic (e.g., time vs. biomarker response) data. Quantitative approaches, including both fit-for-purpose empirical modeling and complex mechanistic quantitative system pharmacology (QSP) modeling can be used to enable accurate decision-making and more efficient drug development [5].

Recent advances in the biological understanding of drug disposition and biomarker response facilitated the construction of physiological or mechanism-based models, which can be used to predict untested scenarios with high degree of confidence. On the pharmacokinetic side, physiological-based pharmacokinetic (PBPK) models started to offer exceptional precision and prediction confidence, which has had a transformative impact on drug development [9]. Many clinical studies are now being replaced by simulations, which dramatically reduced the cost of clinical drug development, time to launch in the market, and reduce burden to patients being enrolled in investigational clinical studies. As an example, antiviral drugs for the treatment of hepatitis C historically needed a lot of drug-drug interaction (DDI) studies due to the complex concurrent medication and hepatic impairments associated with the disease. Telaprevir, which was developed in the 2000s, needed 44 clinical DDI study to understand its pharmacokinetic liabilities. Ten years later, simeprevir which has the same drug target and indication, only conducted 12 clinical DDI studies and used modeling to simulate rest of the scenarios [10]. This represented significant time and cost saving to the drug developer and ultimately the health-care system. A few specific examples of how such modeling work enabled more informed clinical trial design, drive labeling decisions, and provide supportive evidence to eliminate the need for unnecessary clinical studies will be discussed in detail later in this chapter.

In the last 10 years, the compartmental or PBPK modeling framework for small molecules was extended to large molecules in order to account for target-mediated drug disposition (TMDD) to model the pharmacokinetic and target engagement behavior of large molecules such as monoclonal antibodies and bispecific antibodies. In those cases, the TMDD pharmacokinetic modeling process will not only describe the dose to systemic or target tissue exposure relationship, but also the degree of target engagement. A couple of examples how different variations of TMDD models can be used to predict pharmacokinetic and target engagement of large molecules will be discussed.

In addition to pharmacokinetics, mathematical modeling also has broad applications in understanding pharmacodynamic and efficacy data. The results can be used to understand the anticipated exposure-response relationship in humans, while considering the tolerability profile. This information can be used to understand the benefit-risk profile of the investigational drug in different patient populations and maximize the drug's potential in clinical development. Some of the key examples of how modeling and simulation could be used to understand the exposure-response relationship for pharmacodynamic responses will also be discussed.

## 2 Pharmacokinetic modeling

### 2.1 Pharmacokinetic modeling for small molecule drugs

The first step for pharmacokinetic analysis is typically data visualization and noncompartmental analyses (NCA). NCA, including the computation of primary parameters such as area under the concentration curve (AUC), maximum observed concentration ( $C_{\max}$ ), volume of distribution ( $V_{ss}$ ), clearance (CL), bioavailability ( $F\%$ ), half-life ( $t_{1/2}$ ), and absorption rate ( $K_a$ ), is typically the first type of analysis conducted for pharmacokinetic data. NCA analysis provides the most basic information to understand a drug's disposition (i.e.,

the rate and extent of absorption and elimination). NCA is purely observational, and do not have a predictive property for what might happen in the future. However, NCA analyses are helpful in characterizing the absorption, distribution, metabolism, and excretion (ADME) of a drug early-on, while more complex pharmacokinetic-pharmacodynamic (PKPD) or PKPD-efficacy (PKPD/E) models can be applied at the later stages. The principle of NCA has been discussed in detail in the literature [11].

### **2.1.1 Compartmental and population-based PK models**

Compartmental analysis is observational and useful to make predictions of required dose and dosage regimens for a future study. In compartmental-based PK modeling, the body is represented as a system of theoretical compartments arranged in series or parallel to each other. The rate of drug transfer between these compartments and the rate of elimination from these compartments are assumed to follow first-order kinetics. Compartmental models are more often complex than NCA analysis, often require some understanding of biological process (system-specific parameters; e.g., volume of a target compartment) and drug's ADME properties (e.g., permeability, and in vitro intrinsic clearance) to define the initial estimates of the model during model development.

Population-based PK analysis refers to the mathematical/statistical approach that helps to understand a typical or an average response in a given population as well as the variability (both between subject and within subject) [12]. Population-based PK models could answer questions such as “is clearance differ between male and female subjects” or “is the PK different between fasted vs fed condition?” [12]. In addition, population-based models can help to explain the variability in PK data and can identify demographic variables that might influence dose adjustments or different dosage regimen recommendations for a subset of the population. Both compartmental and population-based models are based on the curve fitting of observed data. Often the compartments and parameters (e.g., one- or two-compartment PK models) bear no or little relationship with the physiological functions of the species and thus extensive efforts are required to describe the ADME of a given drug. In contrast, physiologically based modeling allows more mechanistic interpretation of the PK analysis results and is becoming more popular [9, 13].

### **2.1.2 Physiologically-based pharmacokinetic modeling**

PBPK models as shown in Fig. 1 attempt to mathematically portray the mammalian body as a series of compartments that represent tissues and organs connected by the arterial and venous pathways, which are arranged to reflect anatomical layout [9, 14]. These models use actual physiological data such as tissue volumes and blood flow rates, along with compound specific data, to describe the kinetics of the predominant processes that govern the ADME of the compound being investigated. Since PBPK models are mechanistically structured, meaningful predictions can be made, such as extrapolations from high dose to low dose, adult PK to pediatrics, one route of exposure to a different route of exposure, and species to species. Fig. 1 summarizes the elements of a typical PBPK model.

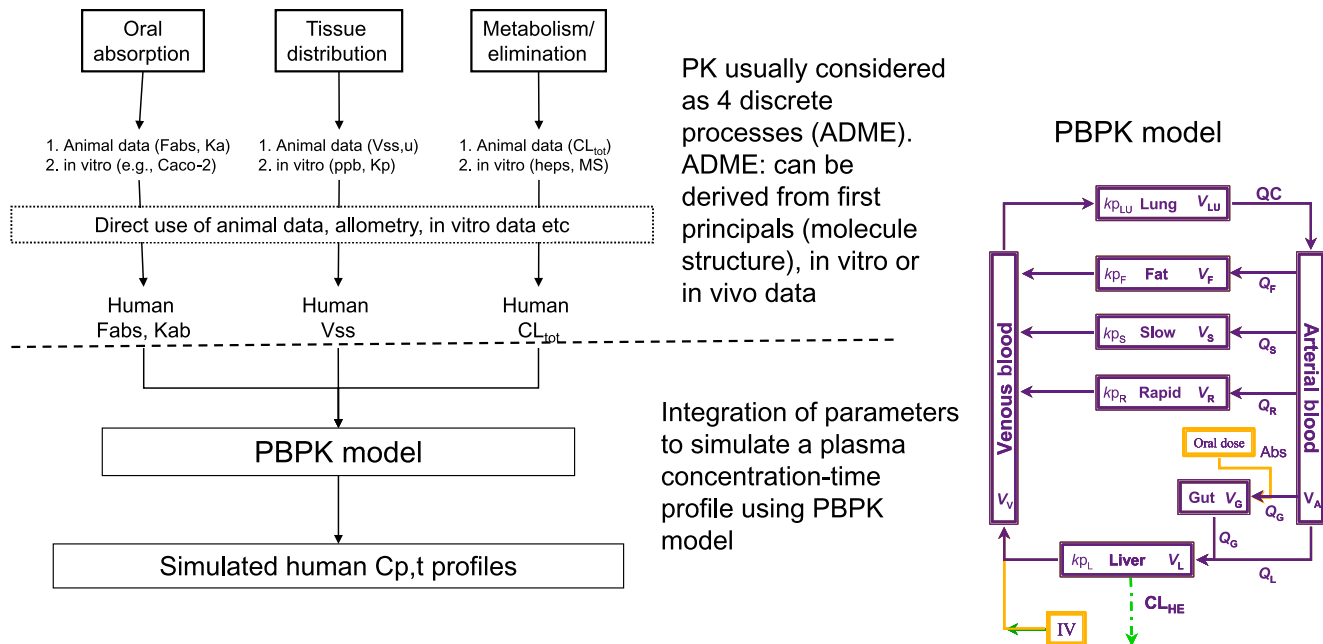


**FIG. 1** Elements of PBPK models. This figure illustrates the process of combining predicted ADME properties into an integrative PBPK model to simulate human PK profile. CL, clearance; fabs, fraction absorbed; hep, hepatocyte; ka, absorption rate; Kp, partition coefficient; mic, microsome; PBPK, physiologically based pharmacokinetics; PPB, plasma protein binding; u, unbound;  $V_{ss}$ , steady-state volume of distribution;  $Q$ , represents blood flow for given organ (e.g.,  $Q_G$ : blood flow to gut;  $Q_R$ , blood flow to rapidly perfusing tissues;  $Q_C$ , blood flow to central and lung tissue;  $Q_F$ , blood flow to fat tissue;  $Q_L$ , blood flow to liver).

### 2.1.2.1 Physiological-based absorption modeling to assess food's and pH's effects on pharmacokinetics

For most drugs, oral delivery is the preferred route of administration. Therefore, a key consideration for many new chemical entities at the preclinical discovery phase of drug development is the rate and extent of intestinal absorption [the uptake of drug molecules from the intestinal lumen (cavity) into the blood]. Gut bioavailability is defined as the net effect of fraction absorbed ( $F_a$ ) and fraction escaping gut metabolism or transporter-mediated intestinal efflux ( $F_g$ ).  $F_g$  can be obtained using in vitro metabolism systems (such as intestinal S9 fractions or recombinant CYP3A) in combination with in vitro obtained permeability clearance ( $CL_{perm}$ ). For compounds that are predominantly metabolized by CYPs,  $F_g$  estimate from in vivo rat is a good model to predict human  $F_g$  [15]. Rat  $F_g$  of a compound can be extracted from its in vivo PK profile by doing PBPK simulation. A lot of uncertainties remain for non-CYP-mediated intestinal loss. The impact of esterases and conjugative enzymes especially UGTs and sulfotransferases on gut metabolism can be high and needs to be better understood in the future. The  $F_a$  of a drug is determined by several factors including the dose, the effective permeability (which covers both passive and active transport components), the available intestinal surface area, and the luminal concentration of drug. Confidence in absorption-related predictions is expected to be high when quantitative assessment of  $F_a$  and absorption rate constant ( $K_a$ ) are reliable [16].  $K_a$  can be derived using the formula  $K_a = 2 * \text{effective permeability} (P_{eff}) / \text{intestinal radius}$  [17].

The absorption of orally administered drugs can be affected if they are taken with food. Therefore, it is usually required to conduct relative food effect bioavailability studies to support new drug applications and drug label recommendations relative to food intake. This recommendation is often informed by both the pharmacokinetic data with food and the therapeutic index of the drug.

The effect of food on drug absorption can be mediated by several mechanisms. Food could delay gastric emptying, could alter intestinal transit time and gut wall metabolism or transport, could physically or chemically interact with dosage formulation or active pharmaceutical ingredient [18]. The pH rises from 1.5 to 5 with food and the recovery of gastric pH to its original fasted condition could take about 2h [19, 20]. Compounds which exhibit a pH-dependent solubility may show significant inter and intraindividual variability in PK in the presence of food [21, 22].

The food effect may be studied at multiple different stages in preclinical and clinical development. Often, a food effect will be conducted early in drug development and may be repeated after formulation change and with the marketed formulation. The effect of different doses, food types (low- and high-fat diet), or times of drug intake in relation to food administration may also need to be characterized.

Various preclinical tools can be used to predict and understand food effects. However, because of the multiple factors involved simple tools are not adequate for reliable predictions. An integrated approach is often required, and physiologically based absorption models have emerged as a vital supportive platform for food effect predictions. The unbound drug fraction is an important component of the modeling of food effects. Under the fed condition, luminal bile salt concentrations are greatly increased on average relative to the fasted state and thus significant proportions of dissolved drug may in fact be

partitioned into the bile micelles. The impact of the partitioning of drug into bile salt micelles results in a complex compound-dependent interplay of solubility, dissolution rate, and effective permeability perhaps best dealt with via an integrated modeling and simulation approach such as PBPK models [23]. Bile micelles can alter the effective permeability ( $P_{\text{eff}}$ ) due to a reduction of the free drug fraction at the epithelial membrane surface and/or a reduction of the diffusion coefficient in the unstirred water layer (UWL), which is adjacent to the epithelial membrane. Further discussion of this interplay in relation to food effects (i.e., due to permeability/solubility limited at epithelial membrane, UWL, or dissolution rate) is given by Sugano and colleagues [24].

These PBPK absorption models, which are used within the industry to predict food effect by integrating drug- and physiology-specific data, have been shown to be promising. However, there are still gaps as highlighted by Oribito consortium, which evaluated the performance of current PBPK absorption models and identified areas that require further improvement in absorption modeling [25]. Li and colleagues showed that among the 48 food effect predictions using PBPK, ~50% of case studies were within 1.25-fold and 75% cases fell within twofold. The best practice for modeling food effects and confidence in the predictions is improving [26].

#### 2.1.2.2 Modeling the interplay between gut transporters and CYP3A

Another important application of absorption PBPK modeling is to understand the interplay of gut efflux transporters and metabolism on drug absorption. This is particularly important to understand the key contributor of nonlinear PK and the impact of metabolic inducers or inhibitors on drug absorption. Transporter such as P-glycoprotein (P-gp) can be induced through pregnane X receptor (PXR)-mediated pathway in a similar manner as the induction of CYP enzymes and gut efflux transporter inhibitor also results in nonlinear PK of PXR substrates. Thus, it is important to account for an interplay between P-gp and CYP3A while modeling the nonlinear absorption or accounting for DDI of P-gp substrates with strong CYP inducers or inhibitors. Observations from clinical CYP3A induction studies can inform P-gp induction studies, as the *in vitro* methods to evaluate the induction of P-gp and other transporters are not well established [27]. Using a top-down PBPK approach, one can account for this interplay if the kinetic parameters are measured for both CYP and transporter of interest. A few examples suggested a scaling factor which simultaneously considering transporter inhibition/induction and CYP3A induction by rifampicin reasonably captured the observed clinical DDI between a test drug and rifampicin [28, 29].

#### 2.1.2.3 Distribution modeling using PBPK

In addition to predicting the impact of various factors on absorption, PBPK models can also be used to predict distribution of drug into tissues (also discussed in [Chapter 11](#)). The steady-state volume of distribution ( $V_{\text{ss}}$ ) is used as a measure of the extent of distribution and binding of a compound in organs and tissues, relative to the concentration in blood. Higher  $V_{\text{ss}}$  would suggest a more extensive distribution into tissues relative to blood.  $V_{\text{ss}}$  does not, however, quantify the rate of drug distribution into tissues. This is not governed solely by differences in binding between tissues and blood and is instead also influenced by physiological properties such as blood flow, capillary permeability, and transport proteins. Drug distribution, therefore, influences the overall kinetics of drug disposition and

is an important property of a compound. In conjunction with clearance,  $V_{ss}$  is a primary determinant of elimination half-life. It largely depends on, and can be predicted with reasonable accuracy from, physicochemical properties such as lipophilicity and acidity/basicity, charge and polarity, supported by plasma protein binding measurements [30, 31]. Because the relative tissue affinity of many compounds is consistent across species (as evidenced by a similar unbound  $V_{ss}$  across species), preclinical *in vivo* data are particularly valuable for predicting human  $V_{ss}$  and good correlation of  $V_{ss,u}$  across the species is shown by Jones et al. [32]. Methods for determining the  $V_{ss}$  are discussed extensively in the literature [32].

The distribution of a compound to target tissues in order to elicit its action is important for the understanding of a drug exposure-response relationship. For example, in CNS drug development, unbound tissue:unbound plasma drug concentration ratios ( $K_{p,uu}$ ) rather than  $K_p$ , which is determined using total tissue to total plasma exposure is preferred [33, 34]. Although PBPK models allow simulation of tissue profiles, direct verification of these predictions is typically not possible due to a lack of quantitative tissue drug concentration data. However, recent work from the authors and Gaohua et al. [35] suggests that having better imaging techniques or robust system parameters may improve the understanding of tissue exposure.

#### 2.1.2.4 Prediction of human clearance (hepatic, renal, and biliary excretion)

Hepatic metabolism is the major clearance route for most drugs, and *in vitro* systems (human liver microsomes and hepatocytes) have proven to be reliable for the prediction of *in vivo* human metabolic clearance [36]. Intrinsic clearance ( $CL_{int}$ ) estimates, corrected for binding to the *in vitro* system and scaled to whole liver, are applied to a well-stirred liver model to obtain hepatic clearance estimates. It is, however, commonly found that direct application of this physiological “scaling” approach results in an underprediction of *in vivo* clearance and consequently a “regression correction” model (based on the correlation between *in vivo* and *in vitro* data for a number of marketed drugs) is applied to improve the accuracy of prediction [37, 38]. There are several choices one could use to predict the human hepatic metabolic CL by either utilizing human liver microsomes or hepatocytes  $CL_{int}$ . Most commonly used IVIVE are liver blood flow (LBF) [39] method with or plasma protein binding correction or  $f_u$  correction intercept method (FCIM) [40].

Allometric scaling approach is an empirically based method, which provides a simple and quick extrapolation of PK parameters based on preclinical species of interest as a function of body size and metabolic rate. Interspecies allometric scaling has been widely used in the prediction of dose and PK parameters of a species of interest, however, the predictive performance could be poor in some cases [41].

Once the above key PK parameters ( $V_d$ ,  $CL$ , and  $K_a$ ) are predicted based on *in vitro* and *in vivo* ADME data, a key performance indicator of the effectiveness of PBPK is the ability to predict human PK, exposure profiles in special populations, DDIs, and human PD/safety profiles. PBPK modeling has now gained reasonable acceptance with the regulatory authorities for the metabolizing enzyme-mediated DDIs. However, the predictive performance of PBPK models for the transporter-mediated DDIs and special population has not been widely recognized [9, 42, 43].



### 2.1.2.5 Gaps and challenges in PBPK modeling

Based on current knowledge, the acceptance rate for PBPK applications is >80% in the regulatory space [9]. However, robust protein abundance data for non-CYP and transporters along with cellular localization of transporters are emerging [44], which could further increase the acceptance rate. Summary of challenges and knowledge gaps for applying PBPK modeling and simulation in drug development for drugs that involves CYPs and transporters are summarized recently by Shebley and Taskar et al. [9, 45].

## 2.2 Pharmacokinetic modeling for biologics

Over the last 20 years, an increasing number of biotherapeutics (including biologics and new modalities such as cell therapy, modified RNA, antisense oligonucleotides, and gene therapies) entered the market. Many of these molecules such as trastuzumab for Her2 positive breast cancers, adalimumab for autoimmune diseases, and rituximab for B-cell malignancies are among the top drugs by sales globally [46]. In fact, six out of the top 10 drugs by sales in 2017 were biologics [46]. This trend is likely to continue since biologics now account for about 30% of the new drugs entering the market [47]. Thus, in-depth understanding of biologics PK/PD is essential for pharmaceutical scientists in the 21st century.

The most common biologic modality in the market today is monoclonal antibodies (mAb). mAbs exhibit many desirable, “drug-like” characteristics. They have good solubility and stability in biological matrix. They are highly selective and specific toward the intended biological targets. They also have low risk of been metabolized into toxic metabolites [48]. However, mAbs have poor to incomplete bioavailability after oral, intramuscular, or subcutaneous administration. They can also exhibit nonlinear distribution and nonlinear clearance depending on target burden and disease status, which complicates dose selection [48]. Therapeutic mAb administration could generate endogenous immune response, which leads to the generation of antidrug antibodies. Those antidrug antibodies may alter the pharmacokinetics and efficacy of the therapeutic antibody [48].

In the section, we will briefly discuss some compartmental and PBPK modeling concepts for absorption and distribution of biologics. Then focus on describing TMDD models and their roles in predicting clearance of mAb. TMDD model is often the most fundamental model structure for biologics PK/PD. Thus, this chapter will explain the different forms in detail.

### 2.2.1 Modeling the absorption and distribution of biologics

Mathematical modeling can be used to understand the absorption of biologic drugs into the central compartment and distribution from the central compartment to tissues. Most of the biologics in the market today are administered either I.V. or S.C. As a result, a common application of absorption modeling for biologics is predicting subcutaneous absorption. Compared to I.V. infusion which is time consuming and requires specific facility and staff, S.-C. injection can be done by the patient or his/her care taker (e.g., insulin). This is very convenient for the patient. PBPK models are often used to predict the bioavailability and rate of absorption for biologics using a combination of previous I.V. PK data in humans and in vitro/animal S.C. PK data [49–52]. This topic is reviewed in detail recently [49]. Some recent research suggested that oral delivery of biologic drugs is possible, but the bioavailability is still

relatively low [53]. Another application of PBPK modeling for large molecules is to predict ocular pharmacokinetics of large molecule after intravitreal injections. This framework has been used to characterize the PK/PD relationship of antivascular endothelial growth factor antibodies in patients with ago-related macular degeneration [54].

An important aspect of biologics PK is tissue distribution. For many biologics, the site of action is in the tissue/tumor rather than in the blood. Thus, it is essential to understand the drug concentration in the tissue/tumors for further PK/PD analysis. PBPK models are generally used to predict the tissue distribution of biologics. In contrast to many small molecule drugs, tissue distribution for biologics is generally permeability limited. Therefore, the two-pore formalism is often used to understand the rate of biologics' diffusion out of the blood vessels into tissues [55, 56]. This model assumes the existence of a high frequency of functional small pores, with limited permeability to large proteins, and an extremely low number of large pores, which more readily permit the passage of biologics from blood to tissue. This model was subsequently applied to many PBPK models of biologics distribution into the tissue/tumor [57–61]. A detail discussion of the mathematical derivation of this hypothesis has been published in the literature [56]. For many biologics which target tumor antigen, the distribution of drug-receptor complex is often limited within the tumor itself resulting in retention of drug in the tumor. Thus, target dynamics is also an important factor to consider when predicting biologics' tissue distribution.

### ***2.2.2 Target-mediated drug disposition models and their role in understanding clearance of biologics***

The clearance of large molecules is generally mediated by both a nonspecific linear process (via endosomal degradation or renal clearance) and a target-specific saturable process. Mathematical modeling can be used to characterize both of the processes. Similar to small molecule drugs, PBPK model is often used to predict the nontarget-mediated clearance of large molecules via endosomal degradation, while TMDD model is often used to predict target-specific clearance processes [62, 63].

TMDD is a phenomenon in which the drug is eliminated due to its high-affinity binding to the pharmacological target (such as a surface receptor or in some cases soluble antigens) [64]. Although TMDD was historically observed with some small molecule drugs (such as warfarin) and peptide hormones, it really started to gain significant attention recently due to the important role it plays in the disposition of biologic drugs. Due to the extraordinary plasma stability of mAbs and their better selectivity and specificity toward their intended biological targets, TMDD is often more readily observed with mAbs compared to small molecules since the nonspecific clearance mechanism for mAbs is much slower than the target-mediated mechanisms. For many biologic molecules, the TMDD model is the theoretical foundation for many PK/PD and QSP predictions.

The principle of mass action is fundamental for modeling TMDD. For most of the small molecule drugs, the receptor-drug interactions can be described using the principle of mass action:

$$C = \frac{R \times D}{K_D + D}$$

where  $C$  is the drug-receptor complex concentration,  $R$  is the receptor concentration/abundance,  $K_D$  is the equilibrium dissociation constant, and  $D$  is the free drug concentration. The key assumption of this model is that the concentration of drug is much greater than concentration of receptors, so the formation of complex does not affect the concentration of drug (i.e., target binding does not affect drug pharmacokinetics). The key advantage of this model is its simplicity. It requires very small amount of data/parameter measurements. Due to its convenience of calculation and deterministic nature, this model is routinely used to calculate receptor occupancy in a regulatory setting to determine the first starting dose in humans for many mAb therapies [65]. However, although the model assumption is generally true with small molecules, it is often not the case for antibodies. For drugs with higher affinity, the concentration of unbound drug is affected by its binding to the receptor and the binding model can be described by

$$C = \frac{1}{2} \times \left[ K_D + D + R - \sqrt{(K_D + D + R)^2 - 4 \times D \times R} \right]$$

Although this equation can be often used to describe receptor-drug interactions in vitro, it is still limited in term of describing the impact of target binding on in vivo PK behavior since it assumes steady-state conditions, where the total amount of receptor and drug remain constant. Of note,  $D$  in this equation is initial total drug concentration.

### 2.2.3 General dynamic of TMDD model

Recognizing the limitations of previous static binding models, Levy et al., building on previous work by others, introduced the modern concept of TMDD using warfarin as an example [64, 66]. The general properties of the ordinary differential equations (ODE) system were subsequently investigated by Mager and Jusko in 2001 [67]. The general TMDD model is an ODE system describing the second-order binding ( $K_{on}$ ) and first-order dissociation ( $K_{off}$ ) of drug ( $D$ ) to receptor ( $R$ ) to produce a complex ( $C$ ) (Fig. 2). It is flexible enough to include receptor turnover rates ( $K_{syn}$  and  $K_{deg}$ ) as well the receptor-mediated endocytosis of complex (Fig. 2). As illustrated in Fig. 3, the plasma concentration vs time profiles are poly-exponential with steeper distribution phase at lower doses. Using noncompartmental analysis, the apparent volume of distribution and clearance (when binding process is not saturated) decreases as

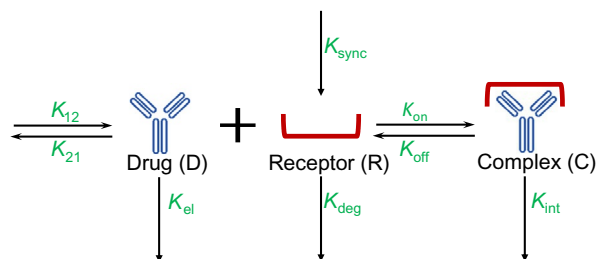


**FIG. 2** General TMDD model structure. This diagram summarizes the model structure of the general TMDD model with a central and peripheral compartment. The drug administration, distribution, and elimination happen in the central compartment. The drug can bind to the receptor and form complex in the central compartment as well.  $K_{12}$ : transport rate constant from compartment 1 to compartment 2.  $K_{21}$ : transport rate constant from compartment 2 to compartment 1.  $K_{el}$  is the elimination rate constant of the drug.

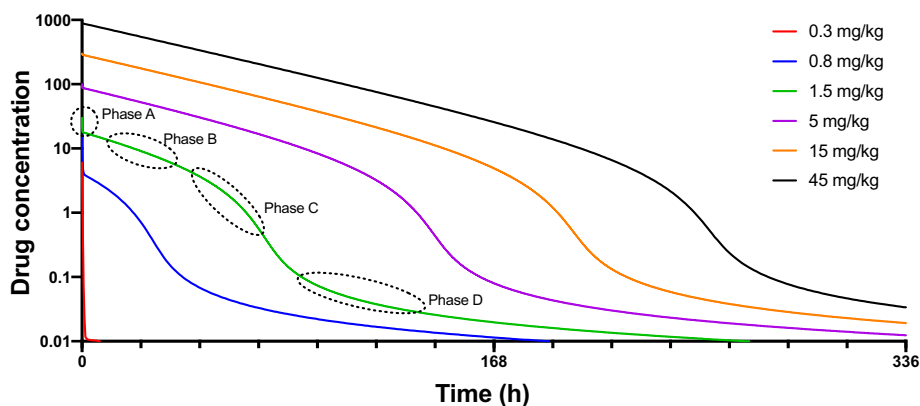


**FIG. 3** Different phases of drug elimination for a typical monoclonal antibody with target-mediated disposition. Pharmacokinetic profile under different doses to illustrate the different phases of drug elimination for a typical monoclonal antibody. Phase A is the initial rapid decrease in drug concentration, typically reflecting the rapid binding of the ligand to the receptor. The slope of this phase is highly dependent on  $K_{on}$ . Phase B is a linear elimination phase, where all the receptors have drug bound. The drug elimination in this phase is typically determined by the nonspecific clearance rate. Thus, the slope of this phase is highly dependent on  $K_{el}$ . Phase C is a mixture phase, where not all the receptors are fully saturated and both receptor-mediated and nonspecific clearance play a role in drug's elimination. The slope of this phase is influenced by parameters related to receptor dynamics ( $K_{syn}$  and  $K_{int}$ ) and drug-receptor interaction ( $K_{on}$  and  $K_{off}$ ). Phase D is the terminal phase, where elimination of the drug is predominately mediated via complex interactions. Thus, the slope of this phase is highly dependent on  $K_{int}$  and  $K_{off}$ .

dose increases [67]. This model was used to describe the pharmacokinetics of imirestat, bosentan, and recombinant human interferon- $\beta$  [67, 68]. The model assumes that the binding of the ligand to the target is simple and noncooperative. The internalized ligand-receptor complexes are not recycled. The drug-receptor binding occurs only in the central compartment, receptor and complex do not diffuse to peripheral compartments.

$$\frac{dD_{tissue}}{dt} = k_{12} * D - k_{21} * D_{tissue}$$

$$\frac{dD}{dt} = -k_{el} * D - k_{on} * D * R + k_{off} * C - k_{12} * D + k_{21} * D_{tissue}$$

$$\frac{dR}{dt} = k_{sync} - k_{deg} * R - k_{on} * D * R + k_{off} * C$$

$$\frac{dC}{dt} = k_{on} * D * R - k_{off} * C - k_{int} * C$$

$$R_0 = \frac{k_{sync}}{k_{deg}}$$

As illustrated in Fig. 3, there are typically four distinct phases in the concentration vs time curve for a drug exhibiting TMDD behavior [69, 70]. Phase A is the initial rapid decrease in drug concentration, typically reflecting the rapid binding of the ligand to the receptor. The slope of

this phase is highly dependent on  $K_{on}$ . Phase B is a linear elimination phase, where all the receptors have drug bound. The drug elimination in this phase is typically determined by the nonspecific clearance rate. Thus, the slope of this phase is highly dependent on  $K_{el}$ . Phase C is a mixture phase, where not all the receptors are fully saturated and both receptor-mediated and nonspecific clearance play a role in drug's elimination. The slope of this phase is influenced by parameters related to receptor dynamics ( $K_{syn}$  and  $K_{int}$ ) and drug-receptor interaction ( $K_{on}$  and  $K_{off}$ ). Phase D is the terminal phase, where elimination of the drug is predominately mediated via complex interactions. Thus, the slope of this phase is highly dependent on  $K_{int}$  and  $K_{off}$ .

The major limitation of the general TMDD model is that the parameters associated with binding (especially  $K_{on}$  in phase A) may not be identifiable using in vivo PK data. The initial drop in concentration is typically too rapid to be captured in PK time course in vivo. To improve parameter identifiability, a number of approximations were made to the general TMDD model in order to enable better fitting of experimental data.

#### 2.2.4 Constant receptor amount ( $R_{total}$ ) model

A common simplification of the general TMDD model is to assume there is a constant amount of receptor in the system at all time ( $R_{total} = R_0 = K_{syn}/K_{deg}$ ). This model assumes degradation rates of the receptor ( $K_{deg}$ ) and the complex ( $K_{int}$ ) are similar since it may not be possible to identify both parameters experimentally. Thus, the binding of drug to receptor does not modify the receptor internalization rate. Under this assumption, the ODE system for the general TMDD model can be reduced [69].

Upon a single-dose administration, the constant receptor model can still capture the four phases dynamics of the general TMDD model. However, since  $K_{deg}$  is assumed to be the same as  $K_{int}$ , now  $K_{deg}$  will determine both the onset of phase C and the height/slope of phase D. The limitation of this model is that there is limited flexibility to independently determine the slope of phase D. Also, under multiple dosing scenarios, this model will not be able to capture any time-dependent change in receptor levels. For some oncology drugs, since the drug is killing target-expressing cells, the total amount of receptors can decrease overtime resulting in lower target-mediated clearance and longer drug PK [71–73]. The constant receptor amount model will not be able to capture this aspect.

#### 2.2.5 Quasi-equilibrium model (QE)

Another commonly used assumption to simplify the general TMDD model is to assume drug-receptor binding occurs much faster than target dynamics and drug elimination. This is the basic assumption for the quasi-equilibrium (QE) model (also known as the rapid-binding model) and the quasi-steady-state (QSS) model.

The quasi-equilibrium (QE) model was originally developed by Mager and Krzyzanski in 2005 [74]. It assumes that the two binding parameters ( $K_{on}$  and  $K_{off}$ ) are a lot faster compared to other parameters in the model for biologic-receptor interactions. Thus, the ODE system can be simplified to

$$\frac{dD_{tissue}}{dt} = k_{12} * D - k_{21} * D_{tissue}$$

$$\begin{aligned} \frac{dD_{\text{tot}}}{dt} &= -k_{\text{el}} * D - k_{12} * D - \frac{R_{\text{tot}} * k_{\text{int}} * D}{K_D + D} + k_{21} * D_{\text{tissue}} \\ \frac{dR_{\text{tot}}}{dt} &= k_{\text{sync}} - k_{\text{deg}} * R_{\text{tot}} - (k_{\text{int}} - k_{\text{out}}) * \frac{R_{\text{tot}} * D}{K_D + D} \\ D &= 0.5 * \left[ (D_{\text{tot}} - R_{\text{tot}} - K_D) + \sqrt{(D_{\text{tot}} - R_{\text{tot}} - K_D)^2 + 4 * K_D * D_{\text{tot}}} \right] \\ R_0 &= \frac{k_{\text{sync}}}{k_{\text{deg}}} \end{aligned}$$

The advantage of this model is that the number of parameters in the model has been reduced by one thus improving the ability of the model to fit to experimental data. Due to the assumption of rapid binding, the initial rapid decline of drug concentration (phase A of Fig. 3) is generally not captured by the QE model. Therefore, the model is not suitable to fit short time interval experiments. In addition, it also has limited flexibility for changing the slope of phase C and should not be used if the elimination of the complex ( $K_{\text{int}}$ ) is faster than  $K_{\text{off}}$  [75]. Despite those trade-offs, the QE model is very useful for predicting the terminal half-life of the drug and can be used to predict the dose-dependent clearance of drug at high dose [70, 76]. This model sometimes can overpredict the concentration of free receptors [77]. This framework can be also applied to the modeling of bispecific antibodies PK [78].

### 2.2.6 Quasi-steady-state model

Another commonly used rapid-binding model is the quasi-steady-state (QSS) approximation [75]. The QSS model assumes the associations of drug to target, complex dissociation and internalization are all fast (i.e.,  $K_{\text{on}} \times D \times R = (K_{\text{off}} + K_{\text{int}}) \times C$ ), which give an equilibrium constant of  $K_{\text{SS}} = \frac{K_{\text{off}} + K_{\text{int}}}{K_{\text{on}}}$ . The general behavior of QSS model is similar to the general TMDD model if binding, dissociation, and elimination of the complex are fast. Compared to the QE model, the QSS model is more accurate when  $K_{\text{int}}$  is faster than  $K_{\text{off}}$  and generally predict the concentration of free receptor more accurately especially when the amount of free receptors is low [77]. Thus, QSS model will provide a better fit and good approximation for very potent drugs, where most of the receptor will be occupied compared to other TMDD approximations. However, the limitation of QSS model is that it is not good for calculating terminal half-life of drugs compared to QE model.

### 2.2.7 Michaelis-Menten model

Michaelis-Menten (MM) model is a further simplification of the rapid-binding models by (1) introducing a new parameter  $V_{\text{max}}$  which is equal to  $K_{\text{int}} * R_0$ , (2) assume that  $\frac{R_0 \times K_D}{(K_D + D_0)}$  is smaller than 1, and (3) assuming total receptor concentration is low compared to the unbound drug concentration. In this model, the target is assumed to be fully saturated, thus it would be a good approximation to the full model when there is a large initial concentration of the drug (i.e., when a high dose is given). It has fewer parameters so model fitting is easier. The MM model is also accurate at predicting the phase when the amount of unbound receptor is approximately zero and the next phase where it increases before the terminal phase is reached

[75]. However, for the MM model to be accurate for all doses, the rate of elimination of the complex needs to be high [75]. If this rate is low, then only concentrations for high-dose levels can be predicted using this model. This approximation eliminates phase A and phase D.

Another notable property of MM model is the requirement for dose correction. In all the above models, even though the equations have been simplified and equilibriums have assumed to have been reached, the initial conditions of the models remain the same as they were for the full TMDD model. However, Yan et al. showed that this may not be the case for MM model [79]. In the time taken for the system to reach equilibrium, some of the injected drug would bind to the target and should be considered. A corrected initial condition for the MM model has been proposed in the literature [75].

### 3 Modeling pharmacodynamic response

#### 3.1 Pharmacodynamic modeling for small molecule drugs

MID<sup>3</sup> or MIDD is an emerging science that quantifies drug effects using pharmacokinetic-pharmacodynamic models, taking into account of disease progression and trial information (e.g., baseline, covariates, dropout rate), to accelerate drug development and to give scientific support to regulatory and therapeutic decisions (Fig. 4) [5]. PKPD models represent the mathematical and statistical relationships between dose, plasma drug concentration, disease biomarker levels, and drug effect. PKPD models combined with efficacy data can help with providing evidence of efficacy when properly verified, thereby saving time and cost. Moreover, MID<sup>3</sup> helps to reduce the number of clinical trials and regulatory review cycles to improve the benefit of the drug at a lower risk. The key concepts for the quantitative analysis of PKPD data and their application to “what if scenarios,” were

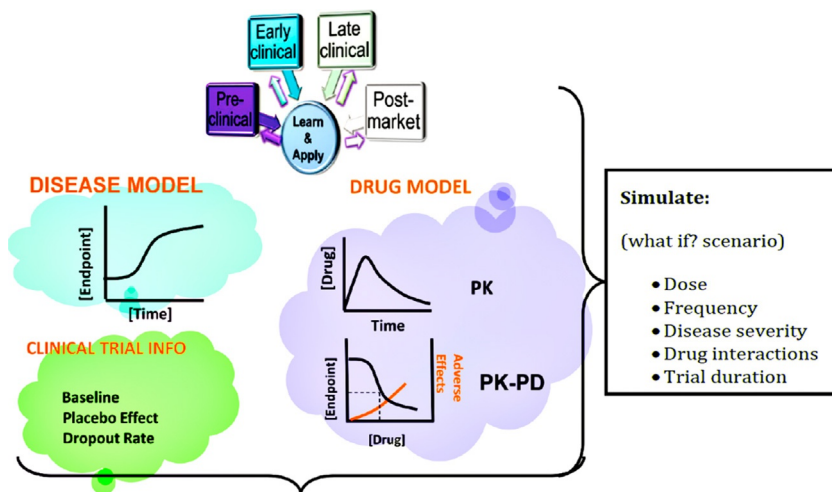


FIG. 4 Learn and apply paradigm for PKPD modeling. Steps of model-based drug development under clinical settings. Adapted from Powell and Gobburu 2007 PMID: 17538553.



built upon the “learn and apply” paradigm proposed by Lewis B. Sheiner [80] (Fig. 4). This learn and apply paradigm is also reflected in the FDA Guidance for Industry [81]. The benefits of translational PKPD are:

*Improved drug efficacy:* Mechanistic PKPD modeling in translational drug research will lead to a better understanding of drug efficacy and safety, thereby reducing attrition in drug discovery and improving the efficiency of the drug development process. PKPD modeling allows researchers to examine all the data collected, including in vitro, in vivo, and clinical, for a given drug (pooled analysis), thus increasing the ability to understand the drug’s efficacy, its therapeutic window, and its side effects using the totality of data. There is a constant struggle to determine the proper dosage for a drug to provide therapeutic relief while simultaneously minimizing side effects. Frequently, in an attempt to decrease the side effects, a lower dosage is administered, leading to a less-than-desired efficacy. With the help of exposure or biomarker-response analyses, one could optimize the exposure to the required level in order to achieve balanced clinical effects.

*Enhanced decision-making:* Translational PKPD modeling and simulation approach helps to make data-driven decisions. Since the flow of information is bidirectional (modeling simulations) in this PKPD modeling approach, one can use the adapt, learn, and apply paradigm during various stages of drug development to make go/no-go decisions based on the available data at the time.

*Enabling earlier decision-making:* By using features like clinical utility index (a criterion that describes the usefulness of a drug therapy derived using the efficacy and adverse events data) and interim analysis (analysis of data that is conducted before data collection has been completed), PKPD modeling allows to make go/no-go decisions earlier in the drug development cycle and thereby helps with reducing the research and development costs.

Following section summarizes a few PKPD modeling examples ranging from early discovery projects to development projects covering CNS and oncology therapeutic areas to illustrate the benefits of PKPD modeling.

### **3.1.1 PKPD modeling to predict efficacy of D<sub>2</sub> receptor antagonists for the treatment of schizophrenia**

Schizophrenia is a debilitating disease impacting about 1% of the population. Dopamine D<sub>2</sub> receptor antagonists are commonly used to treat schizophrenia. It is often not clear that how receptor occupancy of the D<sub>2</sub> receptor (D<sub>2</sub>RO) observed in animals translates to human receptor occupancy, efficacy, and safety. An extensive translational PKPD modeling analysis was carried out for schizophrenia, which integrates receptor-binding data across species and clinical data (both efficacy and safety) across seven compounds. In this example, Pilla Reddy and coworkers predicted the D<sub>2</sub>RO of antipsychotics while considering the interplay between other receptor such as 5-hydroxytryptamine 2 (5-HT<sub>2</sub>) receptors using the workflow as shown in Fig. 5. The model was scaled to the human situation using minimal in vitro and preclinical data, which would be available at the discovery stage [82, 83]. The key findings of this work were that D<sub>2</sub>RO in preclinical species and in human can be predicted with in vitro data such as  $K_{on}$ ,  $K_{off}$ , physiochemical properties of the drug, basic in vivo PK profiles, in vitro permeability, and efflux transporter data.

This work demonstrates how one can leverage the available PKPD data and modeling and simulation approaches before embarking on in vivo screening and optimization of chemistry

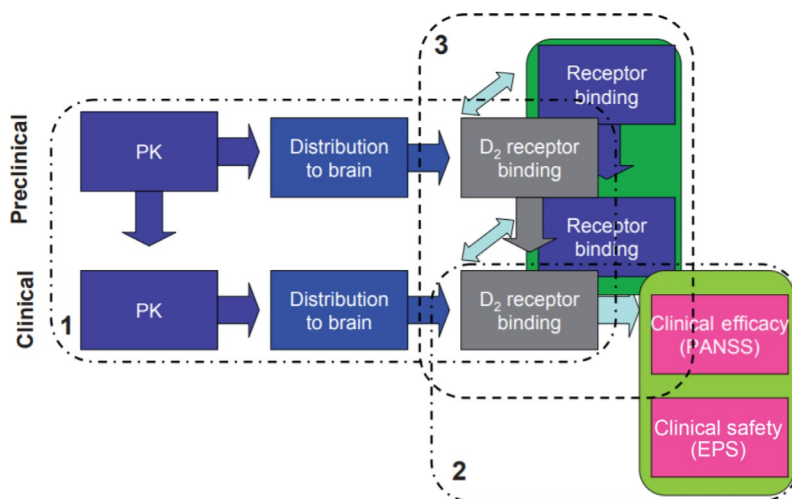


**FIG. 5** Schematic of PKPD/E workflow for large datasets of antipsychotic drugs. Schematic of PKPD/E workflow for large datasets of antipsychotic drugs. The components modeling framework that scales in vitro and preclinical in vivo information to the human situation included (1) predicting receptor occupancy in human using in vitro binding data and preclinical information; (2) linking level and duration of D<sub>2</sub> receptor occupancy of antipsychotics to efficacy and safety; and (3) extrapolation of translation concepts from D<sub>2</sub> receptors to other receptor subtypes such as 5-hydroxytryptamine-2 receptors.

for a compound with right binding kinetics. This platform model structure could be used to optimize drug development strategies for future compounds for the treatment of schizophrenia.

### 3.1.2 Using translational PKPD modeling to accelerate EGFR inhibitor development for the treatment of lung cancer

A subset of nonsmall-cell lung cancer (NSCLC) is caused by mutations in epidermal growth factor receptor (EGFR). Tyrosine kinase inhibitors targeting sensitizing EGFR mutations are the standard of care for this subset of lung cancer patients. Early and detailed mechanistic PKPD modeling work to understand the inhibition of EGFR by osimertinib contributed to one of the fastest drug development and approval in the industry [84, 85]. Fig. 6 illustrates the PKPD model, which was used to quantify the level and duration of EGFR inhibition required to drive efficacy preclinically. The model structure contains a semiphysiological PK model to describe the absorption and metabolism of osimertinib and an indirect response PD model (type 2 indirect response model) to describe pEGFR inhibition [86]. The profile of drug-induced inhibition of phosphorylated EGFR was linked to tumor growth inhibition in preclinical models. The N-demethylated metabolite was known to have less selectivity for T790M-EGFR vs wild-type EGFR. Thus, the relative concentrations of osimertinib vs this metabolite in humans were important to establish the therapeutic index.

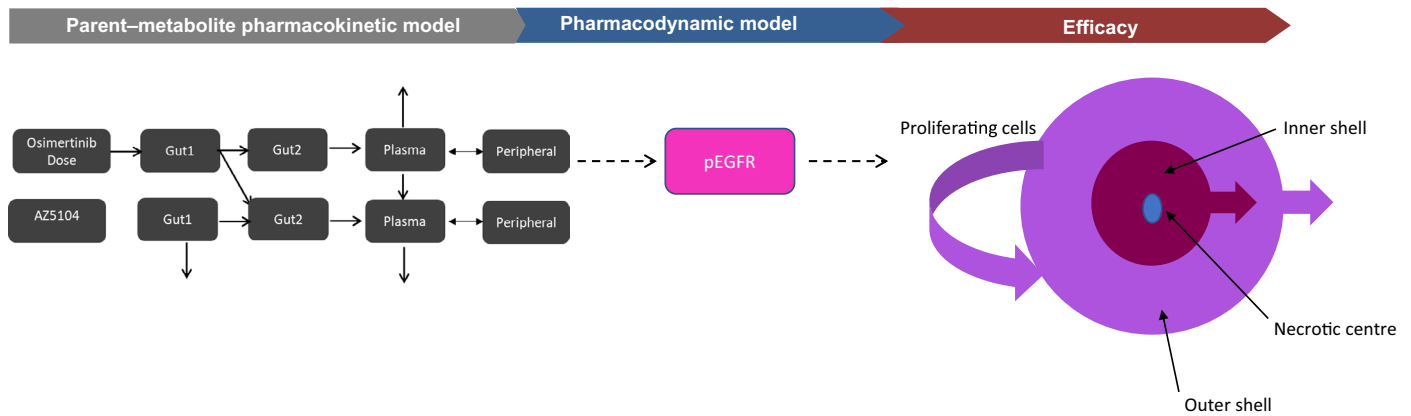


**FIG. 6** Schematics of PK/PD efficacy model. Parent-metabolite pharmacokinetics model was linked to irreversible binder pharmacodynamic model using pEGFR biomarker and dynamics of pEGFR was used to describe the efficacy data observed in tumor xenografts.

This PKPD model illustrates the importance of considering of both the parent drug and pharmacologically active metabolite in PKPD modeling to establish therapeutic index.

### 3.2 Special considerations for biologic pharmacodynamic modeling

Many PD models are modality independent and can be shared between small molecules and large molecules if the PK is properly described. However, an important aspect of PD modeling for biologics is to understand the dynamics of receptor occupancy (RO) or drug-receptor complex. A unique aspect of TMDD model is that it can also be used to generate the dynamic of RO and drug-receptor complex. Aston et al. conducted a mathematical analysis of the general TMDD model to determine the relationship between the target affinity of a mAb and its in vivo potency (defined by maximum receptor binding) [87]. The analysis suggested that higher binding affinity generally is associated with better in vivo potency. However, the potency achieved by increasing the association constant  $K_{on}$  is different from the potency achieved by decreasing the dissociation constant  $K_{off}$ .  $K_{off}$ 's effect on maximum receptor binding often saturates, whereas increasing  $K_{on}$  does not. Thus, increasing  $K_{on}$  was more effective than decreasing  $K_{off}$ . For certain targets, the duration of receptor bindings is less dependent on the binding rates and improving the bindings affinity above certain value will not result in longer pharmacological action [88]. It is important to keep this property in mind in designing biologic drugs.

---

## 4 Conclusions

---

We are in the midst of a paradigm shift for drug development. The growing knowledge of basic molecular and cellular mechanisms underlying diseases as well as the availability of large amount of data will allow mathematical models to adequately describe the processes involved and make quantitative predictions. The goal of modeling and simulation scientists in the pharmaceutical industry is to build a comprehensive translational understanding of drug pharmacology to increase the success rate and efficiency of drug development. The ultimate vision is for modeling to predict drug pharmacology from bench to bedside. The concept of using simulation to guide physical experiments is used in many other industries. Today, it is difficult to imagine one would build a bridge or airplane without significant amount of in silico simulations first. With the advances in PKPD modeling, a similar approach could be applied to drug development to improve the success rate and efficiency. To achieve this goal, large collaborative efforts utilizing high throughput “-omic” data are needed to map out large biological networks in order to build comprehensive PKPD models. Those models should be validated using large amount of preclinical and clinical data (i.e., with pharmacological perturbations). Once validated, those models can then be used to make future predictions with confidence and reduce the amount of experimentation.

In summary, this chapter provided a brief overview of commonly used pharmacokinetic and pharmacodynamic modeling concepts used in drug development. Despite many practical challenges, significant advances have been made to establish a mathematical modeling framework to facilitate the PKPD/E prediction and translation in many therapeutic areas.

Application of big data and machine learning techniques could drive the future advances in this field [89]. The growing acceptance of mathematical modeling in drug development will provide a unifying framework for evaluating the potential of an investigational drug product. Lessons learnt from the models could help to determine the best clinical development strategy and the kinds of patients who would benefit the most from the new drug. Together, a model-based development paradigm will result in a rational and more efficient drug development process.

## References

- [1] D.S. Chen, I. Mellman, Oncology meets immunology: the cancer-immunity cycle, *Immunity* 39 (1) (2013) 1–10.
- [2] D. Hanahan, R.A. Weinberg, The hallmarks of cancer, *Cell* 100 (1) (2000) 57–70.
- [3] D. Hanahan, R.A. Weinberg, Hallmarks of cancer: the next generation, *Cell* 144 (5) (2011) 646–674.
- [4] A. Mullard, Parsing clinical success rates, *Nat. Rev. Drug Discov.* 15 (7) (2016) 447.
- [5] E.M. Workgroup, et al., Good practices in model-informed drug discovery and development: practice, application, and documentation, *CPT Pharmacometrics Syst. Pharmacol.* 5 (3) (2016) 93–122.
- [6] R. Madabushi, Y. Wang, I. Zineh, A holistic and integrative approach for advancing model-informed drug development, *CPT Pharmacometrics Syst. Pharmacol.* 8 (1) (2019) 9–11.
- [7] U.S. Department of Health and Human Services, F.a.D.A., Critical Path Opportunities Report, 2006.
- [8] S. Gottlieb, How FDA Plans to Help Consumer Capitalize on Advances in Science, Available from: <https://blogs.fda.gov/fdavoices/index.php/tag/in-silico-tools/>, 2017.
- [9] M. Shebley, et al., Physiologically based pharmacokinetic model qualification and reporting procedures for regulatory submissions: a consortium perspective, *Clin. Pharmacol. Ther.* 104 (1) (2018) 88–110.
- [10] J. Snoeys, et al., Mechanistic understanding of the nonlinear pharmacokinetics and intersubject variability of simeprevir: a PBPK-guided drug development approach, *Clin. Pharmacol. Ther.* 99 (2) (2016) 224–234.
- [11] J. Gabrielsson, D. Weiner, Non-compartmental analysis, *Methods Mol. Biol.* 929 (2012) 377–389.
- [12] D.R. Mould, R.N. Upton, Basic concepts in population modeling, simulation, and model-based drug development, *CPT Pharmacometrics Syst. Pharmacol.* 1 (2012). e6.
- [13] V. Pilla Reddy, et al., Physiologically based pharmacokinetic modeling for olaparib dosing recommendations: bridging formulations, drug interactions, and patient populations, *Clin. Pharmacol. Ther.* 105 (1) (2019) 229–241.
- [14] H.M. Jones, et al., Physiologically based pharmacokinetic modeling in drug discovery and development: a pharmaceutical industry perspective, *Clin. Pharmacol. Ther.* 97 (3) (2015) 247–262.
- [15] C.R. Jones, et al., Gut wall metabolism. application of pre-clinical models for the prediction of human drug absorption and first-pass elimination, *AAPS J.* 18 (3) (2016) 589–604.
- [16] A.S. Darwich, et al., IMI - Oral biopharmaceutics tools project—evaluation of bottom-up PBPK prediction success part 3: identifying gaps in system parameters by analysing in silico performance across different compound classes, *Eur. J. Pharm. Sci.* 96 (2017) 626–642.
- [17] H. Lennernas, Regional intestinal drug permeation: biopharmaceutics and drug development, *Eur. J. Pharm. Sci.* 57 (2014) 333–341.
- [18] S.A. Johansson, et al., Effect of food intake on the pharmacodynamics of tenapanor: a phase 1 study, *Clin. Pharmacol. Drug Dev.* 6 (5) (2017) 457–465.
- [19] A.S. Taha, et al., Gastric and duodenal mucosal blood flow in patients receiving non-steroidal anti-inflammatory drugs—influence of age, smoking, ulceration and *Helicobacter pylori*, *Aliment. Pharmacol. Ther.* 7 (1) (1993) 41–45.
- [20] T.L. Russell, et al., Upper gastrointestinal pH in seventy-nine healthy, elderly, North American men and women, *Pharm. Res.* 10 (2) (1993) 187–196.
- [21] K.N. Chi, et al., Food effects on abiraterone pharmacokinetics in healthy subjects and patients with metastatic castration-resistant prostate cancer, *J. Clin. Pharmacol.* 55 (12) (2015) 1406–1414.
- [22] D.M. Brainard, et al., Effect of low-, moderate-, and high-fat meals on raltegravir pharmacokinetics, *J. Clin. Pharmacol.* 51 (3) (2011) 422–427.

- [23] J.M. Miller, et al., The solubility-permeability interplay: mechanistic modeling and predictive application of the impact of micellar solubilization on intestinal permeation, *Mol. Pharm.* 8 (5) (2011) 1848–1856.
- [24] K. Sugano, et al., Prediction of food effect by bile micelles on oral drug absorption considering free fraction in intestinal fluid, *Eur. J. Pharm. Sci.* 40 (2) (2010) 118–124.
- [25] A. Margolskee, et al., IMI—oral biopharmaceutics tools project—evaluation of bottom-up PBPK prediction success. Part 2. An introduction to the simulation exercise and overview of results, *Eur. J. Pharm. Sci.* 96 (2017) 610–625.
- [26] M. Li, et al., Predictive performance of physiologically based pharmacokinetic models for the effect of food on oral drug absorption: current status, *CPT Pharmacometrics Syst. Pharmacol.* 7 (2) (2018) 82–89.
- [27] FDA, In Vitro Metabolism- and Transporter-Mediated Drug-Drug Interaction Studies Guidance for Industry, Available from: <https://www.fda.gov/regulatory-information/search-fda-guidance-documents/vitro-metabolism-and-transporter-mediated-drug-drug-interaction-studies-guidance-industry>, 2017.
- [28] C. Wagner, et al., Predicting the effect of CYP3A inducers on the pharmacokinetics of substrate drugs using physiologically based pharmacokinetic (PBPK) modeling: an analysis of PBPK submissions to the US FDA, *Clin. Pharmacokinet.* 55 (4) (2016) 475–483.
- [29] S. Yamazaki, et al., Application of physiologically based pharmacokinetic modeling in understanding bosutinib drug-drug interactions: importance of intestinal P-glycoprotein, *Drug Metab. Dispos.* 46 (8) (2018) 1200–1211.
- [30] P. Poulin, F.P. Theil, Development of a novel method for predicting human volume of distribution at steady-state of basic drugs and comparative assessment with existing methods, *J. Pharm. Sci.* 98 (12) (2009) 4941–4961.
- [31] T. Rodgers, M. Rowland, Mechanistic approaches to volume of distribution predictions: understanding the processes, *Pharm. Res.* 24 (5) (2007) 918–933.
- [32] R.D. Jones, et al., PhRMA CPCDC initiative on predictive models of human pharmacokinetics. Part 2. Comparative assessment of prediction methods of human volume of distribution, *J. Pharm. Sci.* 100 (10) (2011) 4074–4089.
- [33] N. Colclough, et al., Building on the success of osimertinib: achieving CNS exposure in oncology drug discovery, *Drug Discov. Today* (2019).
- [34] D.A. Smith, M. Rowland, Intracellular and intra-organ concentrations of small molecule drugs: theory, practice, and promise, *Drug Metab. Dispos.* (2019).
- [35] Y. Guo, et al., Advancing predictions of tissue and intracellular drug concentrations using in vitro, imaging and physiologically based pharmacokinetic modeling approaches, *Clin. Pharmacol. Ther.* 104 (5) (2018) 865–889.
- [36] R.S. Obach, Prediction of human clearance of twenty-nine drugs from hepatic microsomal intrinsic clearance data: an examination of in vitro half-life approach and nonspecific binding to microsomes, *Drug Metab. Dispos.* 27 (11) (1999) 1350–1359.
- [37] R.J. Riley, D.F. McGinnity, R.P. Austin, A unified model for predicting human hepatic, metabolic clearance from in vitro intrinsic clearance data in hepatocytes and microsomes, *Drug Metab. Dispos.* 33 (9) (2005) 1304–1311.
- [38] A.K. Sohlenius-Sternbeck, et al., Practical use of the regression offset approach for the prediction of in vivo intrinsic clearance from hepatocytes, *Xenobiotica* 42 (9) (2012) 841–853.
- [39] H. Tang, et al., Interspecies prediction of human drug clearance based on scaling data from one or two animal species, *Drug Metab. Dispos.* 35 (10) (2007) 1886–1893.
- [40] B.J. Ring, et al., PhRMA CPCDC initiative on predictive models of human pharmacokinetics. Part 3. Comparative assessment of prediction methods of human clearance, *J. Pharm. Sci.* 100 (10) (2011) 4090–4110.
- [41] Q. Huang, J.E. Riviere, The application of allometric scaling principles to predict pharmacokinetic parameters across species, *Expert Opin. Drug Metab. Toxicol.* 10 (9) (2014) 1241–1253.
- [42] European Medicines Agency, Guideline on the Reporting of Physiologically Based Pharmacokinetic (PBPK) Modelling and Simulation, Available from: [https://www.ema.europa.eu/en/documents/scientific-guideline/guideline-reporting-physiologically-based-pharmacokinetic-pbpbk-modelling-simulation\\_en.pdf](https://www.ema.europa.eu/en/documents/scientific-guideline/guideline-reporting-physiologically-based-pharmacokinetic-pbpbk-modelling-simulation_en.pdf), 2018.
- [43] FDA, Physiologically Based Pharmacokinetic Analyses—Format and Content Guidance for Industry, (2018).
- [44] S. Billington, et al., Interindividual and regional variability in drug transporter abundance at the human blood-brain barrier measured by quantitative targeted proteomics, *Clin. Pharmacol. Ther.* (2019).
- [45] K. Taskar, et al., PBPK models for evaluating membrane transporter mediated DDIs: current capabilities, case studies, future opportunities and recommendations, *Clin. Pharmacol. Ther.* (2019).
- [46] L. Urquhart, Market watch: top drugs and companies by sales in 2017, *Nat. Rev. Drug Discov.* 17 (4) (2018) 232.
- [47] A. Mullard, 2018 FDA drug approvals, *Nat. Rev. Drug Discov.* 18 (2) (2019) 85–89.

- [48] W. Wang, E.Q. Wang, J.P. Balthasar, Monoclonal antibody pharmacokinetics and pharmacodynamics, *Clin. Pharmacol. Ther.* 84 (5) (2008) 548–558.
- [49] L. Kagan, Pharmacokinetic modeling of the subcutaneous absorption of therapeutic proteins, *Drug Metab. Dispos.* 42 (11) (2014) 1890–1905.
- [50] M. Viola, et al., Subcutaneous delivery of monoclonal antibodies: how do we get there? *J. Control. Release* 286 (2018) 301–314.
- [51] L. Zhao, et al., The antibody drug absorption following subcutaneous or intramuscular administration and its mathematical description by coupling physiologically based absorption process with the conventional compartment pharmacokinetic model, *J. Clin. Pharmacol.* 53 (3) (2013) 314–325.
- [52] N. Varkhede, M.L. Forrest, Understanding the monoclonal antibody disposition after subcutaneous administration using a minimal physiologically based pharmacokinetic model, *J. Pharm. Pharm. Sci.* 21 (1s) (2018) 130s–148s.
- [53] D. Vllasaliu, et al., Recent advances in oral delivery of biologics: nanomedicine and physical modes of delivery, *Expert Opin. Drug Deliv.* 15 (8) (2018) 759–770.
- [54] L.A. Hutton-Smith, et al., A mechanistic model of the intravitreal pharmacokinetics of large molecules and the pharmacodynamic suppression of ocular vascular endothelial growth factor levels by ranibizumab in patients with neovascular age-related macular degeneration, *Mol. Pharm.* 13 (9) (2016) 2941–2950.
- [55] B. Rippe, B. Haraldsson, Fluid and protein fluxes across small and large pores in the microvasculature. Application of two-pore equations, *Acta Physiol. Scand.* 131 (3) (1987) 411–428.
- [56] B. Rippe, B. Haraldsson, Transport of macromolecules across microvascular walls: the two-pore theory, *Physiol. Rev.* 74 (1) (1994) 163–219.
- [57] L.T. Baxter, et al., Biodistribution of monoclonal antibodies: scale-up from mouse to human using a physiologically based pharmacokinetic model, *Cancer Res.* 55 (20) (1995) 4611–4622.
- [58] L.T. Baxter, et al., Physiologically based pharmacokinetic model for specific and nonspecific monoclonal antibodies and fragments in normal tissues and human tumor xenografts in nude mice, *Cancer Res.* 54 (6) (1994) 1517–1528.
- [59] G.Z. Ferl, A.M. Wu, J.J. DiStefano 3rd, A predictive model of therapeutic monoclonal antibody dynamics and regulation by the neonatal Fc receptor (FcRn), *Ann. Biomed. Eng.* 33 (11) (2005) 1640–1652.
- [60] K.L. Gill, et al., A bottom-up whole-body physiologically based pharmacokinetic model to mechanistically predict tissue distribution and the rate of subcutaneous absorption of therapeutic proteins, *AAPS J.* 18 (1) (2016) 156–170.
- [61] D. Hardiansyah, C.M. Ng, Two-pore minimum physiologically-based pharmacokinetic model to describe the disposition of therapeutic monoclonal IgG antibody in humans, *Pharm. Res.* 35 (3) (2018) 47.
- [62] H.M. Jones, et al., A physiologically-based pharmacokinetic model for the prediction of monoclonal antibody pharmacokinetics from in vitro data, *CPT Pharmacometrics Syst. Pharmacol.* (2019).
- [63] H.M. Abdallah, A.Z.X. Zhu, A minimal physiologically-based pharmacokinetic model demonstrates role of the neonatal Fc receptor (FcRn) competition in drug-disease interactions with antibody therapy, *Clin. Pharmacol. Ther.* (2019).
- [64] G. Levy, Pharmacologic target-mediated drug disposition, *Clin. Pharmacol. Ther.* 56 (3) (1994) 248–252.
- [65] H. Saber, et al., An FDA oncology analysis of immune activating products and first-in-human dose selection, *Regul. Toxicol. Pharmacol.* 81 (2016) 448–456.
- [66] Y. Sugiyama, M. Hanano, Receptor-mediated transport of peptide hormones and its importance in the overall hormone disposition in the body, *Pharm. Res.* 6 (3) (1989) 192–202.
- [67] D.E. Mager, W.J. Jusko, General pharmacokinetic model for drugs exhibiting target-mediated drug disposition, *J. Pharmacokinet. Pharmacodyn.* 28 (6) (2001) 507–532.
- [68] A.K. Volz, et al., Target-mediated drug disposition pharmacokinetic-pharmacodynamic model of bosentan and endothelin-1, *Clin. Pharmacokinet.* 56 (12) (2017) 1499–1511.
- [69] L.A. Peletier, J. Gabrielsson, Dynamics of target-mediated drug disposition, *Eur. J. Pharm. Sci.* 38 (5) (2009) 445–464.
- [70] L.A. Peletier, J. Gabrielsson, Dynamics of target-mediated drug disposition: characteristic profiles and parameter identification, *J. Pharmacokinet. Pharmacodyn.* 39 (5) (2012) 429–451.



- [71] S.C. Chen, et al., Population pharmacokinetics and exposure-response of trastuzumab emtansine in advanced breast cancer previously treated with  $\geq 2$  HER2-targeted regimens, *Br. J. Clin. Pharmacol.* 83 (12) (2017) 2767–2777.
- [72] X.S. Xu, et al., Clinical implications of complex pharmacokinetics for daratumumab dose regimen in patients with relapsed/refractory multiple myeloma, *Clin. Pharmacol. Ther.* 101 (6) (2017) 721–724.
- [73] D.R. Mould, The pharmacokinetics of biologics: a primer, *Dig. Dis.* 33 (Suppl 1) (2015) 61–69.
- [74] D.E. Mager, W. Krzyzanski, Quasi-equilibrium pharmacokinetic model for drugs exhibiting target-mediated drug disposition, *Pharm. Res.* 22 (10) (2005) 1589–1596.
- [75] L. Gibiansky, et al., Approximations of the target-mediated drug disposition model and identifiability of model parameters, *J. Pharmacokinet. Pharmacodyn.* 35 (5) (2008) 573–591.
- [76] A. Marathe, W. Krzyzanski, D.E. Mager, Numerical validation and properties of a rapid binding approximation of a target-mediated drug disposition pharmacokinetic model, *J. Pharmacokinet. Pharmacodyn.* 36 (3) (2009) 199–219.
- [77] J.P. Davda, R.J. Hansen, Properties of a general PK/PD model of antibody-ligand interactions for therapeutic antibodies that bind to soluble endogenous targets, *MAbs* 2 (5) (2010) 576–588.
- [78] J. Schropp, et al., Target-mediated drug disposition model for bispecific antibodies: properties, approximation, and optimal dosing strategy, *CPT Pharmacometrics Syst. Pharmacol.* 8 (3) (2019) 177–187.
- [79] X. Yan, W. Krzyzanski, Dose correction for the Michaelis-Menten approximation of the target-mediated drug disposition model, *J. Pharmacokinet. Pharmacodyn.* 39 (2) (2012) 141–146.
- [80] L.B. Sheiner, Learning versus confirming in clinical drug development, *Clin. Pharmacol. Ther.* 61 (3) (1997) 275–291.
- [81] FDA, Exposure-Response Relationships—Study Design, Data Analysis, and Regulatory Applications, Available from: <https://www.fda.gov/regulatory-information/search-fda-guidance-documents/exposure-response-relationships-study-design-data-analysis-and-regulatory-applications>, 2003.
- [82] V. Pilla Reddy, et al., Pharmacokinetic-pharmacodynamic modeling of severity levels of extrapyramidal side effects with markov elements, *CPT Pharmacometrics Syst. Pharmacol.* 1 (2012). e1.
- [83] M. Johnson, et al., Translational modeling in schizophrenia: predicting human dopamine D2 receptor occupancy, *Pharm. Res.* 33 (4) (2016) 1003–1017.
- [84] P. Morgan, et al., Impact of a five-dimensional framework on R&D productivity at AstraZeneca, *Nat. Rev. Drug Discov.* 17 (3) (2018) 167–181.
- [85] J.W. Yates, et al., Irreversible inhibition of EGFR: modeling the combined pharmacokinetic-pharmacodynamic relationship of osimertinib and its active metabolite AZ5104, *Mol. Cancer Ther.* 15 (10) (2016) 2378–2387.
- [86] N.L. Dayneka, V. Garg, W.J. Jusko, Comparison of four basic models of indirect pharmacodynamic responses, *J. Pharmacokinet. Biopharm.* 21 (4) (1993) 457–478.
- [87] P.J. Aston, et al., Mathematical analysis of the pharmacokinetic-pharmacodynamic (PKPD) behaviour of monoclonal antibodies: predicting in vivo potency, *J. Theor. Biol.* 281 (1) (2011) 113–121.
- [88] A.P. Chimalakonda, R. Yadav, P. Marathe, Factors influencing magnitude and duration of target inhibition following antibody therapy: implications in drug discovery and development, *AAPS J.* 15 (3) (2013) 717–727.
- [89] J. Vamathevan, et al., Applications of machine learning in drug discovery and development, *Nat. Rev. Drug Discov.* (2019).

# PK/PD-driven starting and effective human dose determination for immuno-oncology drugs

*Dhaval K. Shah, Farah Al Qaraghuli, Wanying Zhang*

Department of Pharmaceutical Sciences, School of Pharmacy and Pharmaceutical Sciences,  
The State University of New York at Buffalo, Buffalo, NY, United States

## 1 Introduction

Immuno-oncology (I-O) is the study and development of novel treatments that take advantage of the body's own immune system to fight cancer. In the recent years, the discovery and development of I-O therapies has changed the landscape of cancer therapy [1]. Clinical and commercial success of these therapies represent a significant milestone for the treatment of cancer. These therapies include immune checkpoint inhibitors (ICIs) such as ipilimumab and pembrolizumab, which work by blocking the interaction of checkpoint proteins on the cancer cells with the binding partners on T-cells, to promote the recognition and elimination of cancer cells by body's immune system (Fig. 1) [2]. I-O therapies also include agonistic antibodies (e.g., anti-OX40 and anti-CD28), which target and activate co-stimulatory molecules on the T-cells to promote the recognition and destruction of cancer cells (Fig. 1) [3]. T-cell engaging bispecific molecules, such as blinatumomab, are another class of I-O agents that are capable to simultaneously binding a receptor on the T-cell (e.g., CD3) and an antigen on the cancer cell (e.g., CD19) to facilitate retargeting of the T-cells to kill the cancer cells (Fig. 1) [4]. Other emerging class of I-O therapies include engineered immune cells like chimeric antigen receptor (CAR) or T-cell receptor (TCR) expressing T-cells (e.g., axicabtagene ciloleucel), which are designed to recognize an antigen on targeted tumor cells to facilitate their targeted killing (Fig. 1) [5]. Oncolytic viruses (OVs) like T-VEC also represent an upcoming class of I-O agents, which are engineered to selectively infect the tumor cells and promote their destruction via the help of stimulated immune responses [6].

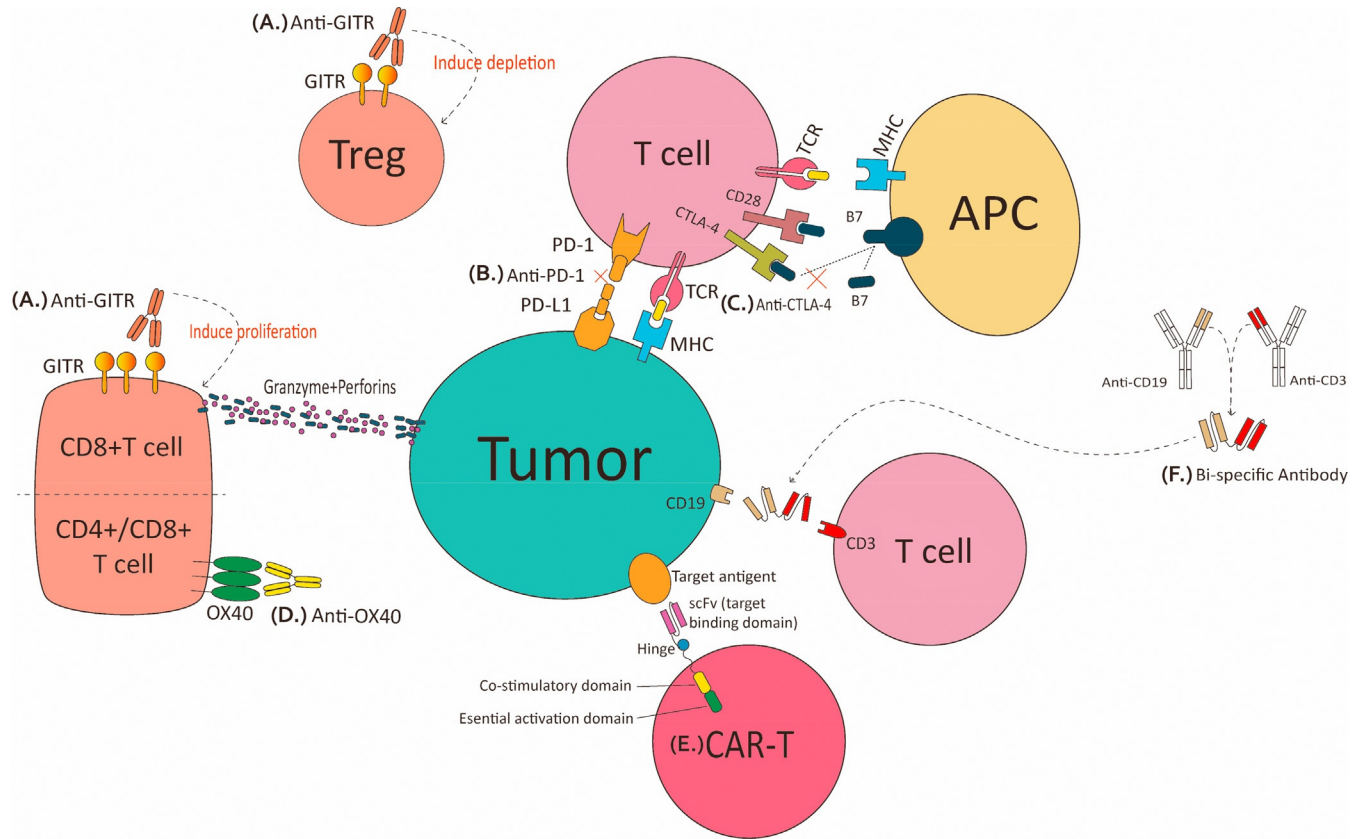


**FIG. 1** Mechanisms-of-actions for several immuno-oncology agents. (A) *Anti-GITR*. GITR receptors are mostly expressed on CD8+ and regulatory T-cells. Anti-GITR antibody binds to both cell type, which induces proliferation of CD8+ cells and depletion of regulatory cells. (B) *Anti-PD1*. Tumor cells express PD-L1 receptors that bind to PD-1 receptors on T-cells. Anti-PD1 antibody (and anti-PDL1 antibody) can prevent this interaction. (C) *Anti-CTLA-4*. T-cells express CTLA-4 that can bind to B7 on antigen presenting cells. Anti-CTLA-4 antibody binds to CTLA-4 on T-cells and prevents B7 interaction. (D) *Anti-OX40*. OX40 receptors are present on T-cells. Anti-OX40 antibody binds to these receptors and induces expansion and survival of T-cells. (E) *CAR-T*. The binding region on CAR-T cells can be varied depending on the desired target antigen. These engineered cells can directly kill antigen expressing cancer cells. (F) *Bispecific antibody (BsAb)*. BsAb can bind to two receptors/targets together. As shown in the figure, binding to both CD3 receptor on T-cells and CD19 receptors on tumor cells can lead to the killing of CD19 expressing cancer cells by the T-cells.

While I-O therapies can manifest durable clinical responses in many cancer patients, these therapies come with their own set of problems. It is well-known that I-O therapies only work in certain population of the patients, and there are no universal biomarkers that can help differentiate responders from nonresponding patient populations. Since the immune system between preclinical animal models and human patients is very different, it also becomes challenging to a priori identify an optimal dosing regimen and clinically viable biomarker for a successful preclinical-to-clinical translation of I-O therapies. In addition, since most of the I-O therapies are designed to activate the immune system, they can unleash a cascade of unpredictable and unintended autoimmune reactions. These reactions can lead to increased frequency of toxicities known as immune-related adverse events (irAEs), which can be life threatening or even fatal. These toxicities are difficult to recognize, may manifest in any organ, and may vary in onset, frequency, or severity [7]. In fact, I-O therapy may also cause cancers to grow quickly after the beginning of the treatment via an unusual phenomenon known as hyperprogressive disease (HPD), which has been described across different tumor types for ICIs like anti-PD-1 and anti-PD-L1 antibodies [8].

Given that I-O therapies can eradicate the cancer, and at the same time could lead to fatal toxicities, it becomes very important to choose the right dosing regimen for clinical evaluation of these agents. Accurately predicting the first-in-human (FIH) starting dose and efficacious human dose (EHD) using the preclinical data is very important, as these doses determine the safety and clinical viability of these molecules. It is equally important to choose the correct recommended phase-II dose (RP2D) and recommended human dose (RHD), as simply relying on maximum tolerated dose (MTD)-based approaches to determine the clinical dose may not be ideal for I-O agents [9]. There are several ways to determine these doses. One of them is to use *in vitro* and *ex vivo* approaches to determine minimally anticipated biological effect levels (MABEL) that provide desired target occupancy or cytokine release profiles, which can be used to determine the FIH dose. Another approach involves the use of preclinical safety data from immunologically compatible species to determine no-observed adverse effect level (NOAEL) or highest nonseverely toxic dose (HNSTD), which can be used to determine the FIH dose. One can also use efficacious exposure levels from preclinical animal models to project the EHD levels. However, a more quantitative and integrated approach is to establish exposure-response (E-R) relationships based on preclinical data, and develop mechanism-based and translationally relevant pharmacokinetics-pharmacodynamics (PK/PD) models, which can then be utilized to predict FIH and EHD dose levels [10]. Moreover, these PK/PD models can also be used to establish more robust E-R relationships for I-O therapies in the clinic, which can be used to finalize the optimal dosing regimen in the clinic. In this chapter, we have provided selected case studies to demonstrate the usage of PK/PD-based approaches for dose selection of I-O agents.

## 2 Dose selection for immune-activating agents

When it comes to the selection of FIH dose for immune-activating agents, Saber et al. have provided a well-explained overview of approaches used by the drug developers for submission to the FDA [11]. It is important to note that the main objective of FIH dose selection for

oncology patients is to identify a safe dose that is sufficiently high to minimize exposure of patient to subtherapeutic doses, and allow rapid attainment of RP2D dose. Saber et al. have used more than 25 immune-activating molecules in their analysis, which included ICIs, agonistic antibodies, and Fc-modified antibodies targeting PD1, PD-L1, CD40, GITR, OX40, OX40L, CD33, CD38, CD19, CD137, c-fms, B7 family member antigen, and CTLA-4. It was found that most sponsors used a variety of MABEL approaches to set FIH doses. One of the approaches included *in vitro* activity data from experiments that measure cytokine release, T-cell proliferation, T-cell activation, target cell lysis, and/or ADCC/CDC activity, to determine a concentration/dose that would lead to ~20% of the maximum pharmacological activity (EC<sub>20</sub>, 20% PA). Another approach included *in vitro* binding data to estimate the plasma concentration of the drug that would provide ~20% of target receptor occupancy (20% RO). In addition, mouse xenograft data were also used to determine the lowest dose that results in antitumor activity, and other methods that integrate target expression in humans and PK modeling were also utilized. However, the authors found that MABEL-based approaches in general resulted in lower starting doses, and evaluated few other methods for computing the FIH dose. One of the methods was based on a dose that achieves 20%–80% PA, and the other method was based on a dose that achieves 20%–80% RO. In addition, 1/6th of the HNSTD or 1/10th of the NOAEL dose were also evaluated. The authors concluded that selection of the FIH dose based on animal toxicology studies (i.e., 1/6th HNSTD or 1/10th NOAEL dose) resulted in human doses that were unsafe for several molecules examined, and MABEL-based approaches resulted in very low FIH doses that required many dose escalation steps to reach an optimal biological dose (OBD), MTD, or a clinically recommended dose. It was suggested that there is a need to optimize FIH dose selection/optimization method for immune-activating agents to minimize the number of patients exposed to subtherapeutic doses. Furthermore, novel approaches like 20%–80% RO approach may provide a FIH dose that is close to the final clinical dose and demonstrate acceptable levels of toxicities.

When it comes to *a priori* predicting the clinically efficacious dose of immune-activating agents, PK/PD M&S-based approaches can be used to translate preclinical efficacy data to the clinic. Lindauer et al. [12] have presented an example of the usage of mechanistic PK/PD model (Fig. 2) to translate preclinical efficacy data of pembrolizumab to the clinic for predicting the lowest effective dose in the patients. The authors used PK and efficacy data of surrogate anti-PD-1 antibody (DX400) in colon adenocarcinoma-bearing mice, and the occupancy of the PD-1 receptor in mouse blood and tumor, to develop a mechanism-based preclinical PK/PD model. The final model consisted of a two-compartment model to characterize plasma PK of anti-PD-1 antibody, a physiologically based PK (PBPK) component to characterize tumor exposure of the antibody, a receptor-binding model with a feedback that increased the expression of PD-1 upon upregulation of the T-cells, and a tumor growth and PD-1 receptor occupancy-driven tumor kill model to characterize *in vivo* efficacy of the antibody. The preclinical model was able to characterize plasma PK of the antibody, PD-1 receptor occupancy in the tumor, and tumor growth inhibition data very well [12]. The preclinical PK/PD model was subsequently translated to the clinic by allometrically scaling the parameters related to the degradation of pembrolizumab-PD-1 complex from mouse to human, changing tumor exposure parameters from mouse to human, changing the PD-1 binding parameters from the surrogate to pembrolizumab values, and changing the

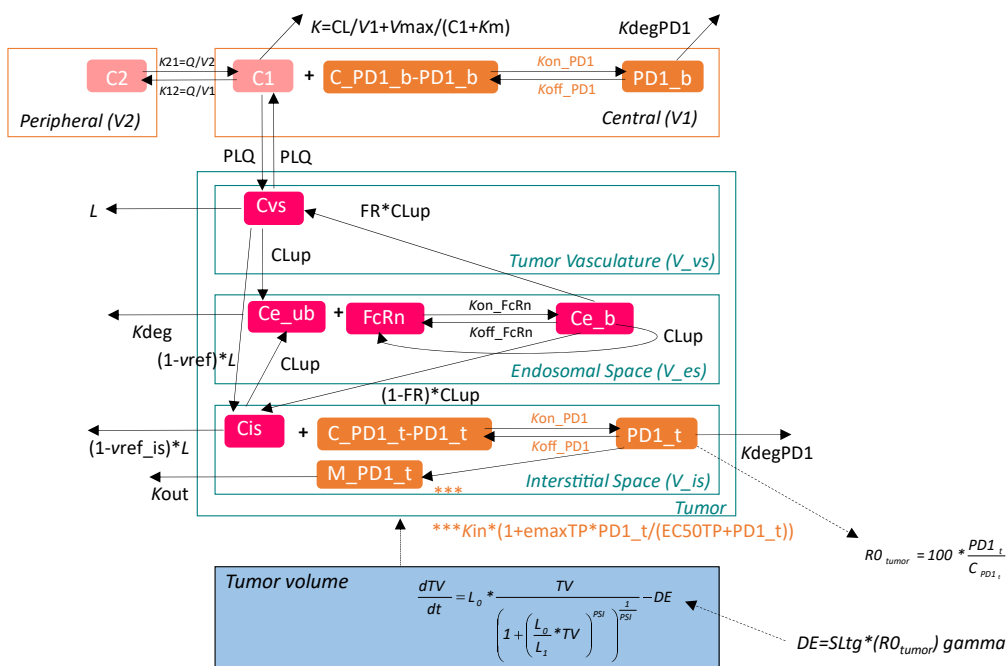


**FIG. 2** The mechanism-based PK/PD model developed by Lindauer et al. for predicting the effective dosing regimen of pembrolizumab (Keytruda) in the clinic using preclinical efficacy data generated with anti-PD-1 surrogate molecules in mouse tumor models. The model structure consists of: (i) a 2-compartment PK model to characterize plasma PK of anti-PD-1 antibody; (ii) a component of the antibody physiologically based PK (PBPK) model to characterize tumor PK of the antibody; (iii) a receptor-binding model with a feedback mechanism that increased the expression of PD-1 upon upregulation of T-cell, to account for drug binding to the target antigen; and (iv) a tumor growth and PD-1 receptor occupancy-driven tumor kill model to characterize the in vivo efficacy of the anti-PD-1 antibody. Key: C1 = pembrolizumab concentration in the central compartment; C2 = pembrolizumab concentration in the peripheral compartment; PD-1<sub>b</sub> = pembrolizumab and PD-1 complex; C<sub>PD-1\_b</sub> = total PD-1 receptor concentration in blood; C<sub>vs</sub> = pembrolizumab concentration in the vasculature; C<sub>e\_ub</sub> = concentration of unbound pembrolizumab in the endosomal space; FcRn = Fc receptor levels; C<sub>e\_b</sub> = pembrolizumab and PD-1 complex in the endosomal space; C<sub>is</sub> = pembrolizumab concentrations in the interstitial space; C<sub>PD-1\_t</sub> = total PD-1 concentration in the tumor; C<sub>PD-1\_b</sub> = total PD-1 concentration in blood; PD-1<sub>t</sub> = pembrolizumab and PD-1 complex in the tumor; PD-1<sub>b</sub> = pembrolizumab and PD-1 complex in blood; M<sub>PD-1\_t</sub> = amount of PD-1 receptors in the tumor; V<sub>max</sub> = maximum elimination rate of the saturable pathway; V<sub>1</sub> = volume of distribution in the central compartment; V<sub>2</sub> = volume of distribution in the peripheral compartment; K<sub>m</sub> = Michaelis-Menten constant; V<sub>es</sub> = endosomal space of the vascular endothelial cells.

parameters for tumor size and tumor growth rate to clinically relevant values. The translated human PK/PD model was used to simulate the efficacy of pembrolizumab in melanoma patients using various dosing scenarios. The model revealed that the lowest clinical dose that would result in a high probability of reducing the tumor size by >30% (i.e., attainment of partial response) was 2 mg/kg pembrolizumab given every 3 weeks (Q3W). In addition, the model also revealed that reducing the dosing interval to every 2 weeks (Q2W) or increasing the dose to 10 mg/kg would show a minimal improvement in the efficacy. As such, the translated PK/PD model confirmed 2 mg/kg given Q3W as the optimal clinical dosing regimen for



pembrolizumab. This analysis by Lindauer et al. highlights the use of PK/PD M&S for establishing a preclinical E-R relationship for immune-activating agents, with the potential for translating the relationship into the clinic [12].

Finalization of the correct clinical dose for the target population is also an extremely important step during the clinical development of immune-activating agents. This process typically requires early and precise characterization of drug disposition in patients, along with the development of quantitative relationships between drug exposure and clinical risks/benefits. Clinical development of anti-PD1 antibody nivolumab provides a nice example of how modeling and simulation can be used to support the clinical dose selection of immune-activating agents [13, 14]. Nivolumab monotherapy was tested in diverse tumor types (e.g., melanoma, renal cancer, nonsmall cell lung cancer, etc.), and dose-exposure, exposure-response (i.e., clinical efficacy), PD-1 receptor occupancy, as well as clinical safety data from dose-ranging studies in all the tumor types were used simultaneously to facilitate the selection of a uniform dose of nivolumab in all tumor types. The E-R relationship developed based on melanoma and renal cancer trials revealed that the objective response rate did not show any further improvement beyond 1 mg/kg dose, and nonsmall cell lung cancer trials revealed that there was no improvement in the response beyond 3 mg/kg dose. After integrating all this clinical information, an optimal monotherapy dose of 3 mg/kg given Q2W was selected as the optimal dose for the clinical evaluation of nivolumab across different tumor types during the confirmatory phase-3 studies. Interestingly, the E-R relationship developed based on the observed objective response rates at each dose level of nivolumab was not monotonous, and nivolumab clearance appeared as the most important parameter that determined the probability of nivolumab response. This unexpected effect of clearance on the efficacy of nivolumab was further confirmed while developing the quantitative relationship between overall survival (OS) and exposure of nivolumab using the semiparametric Cox proportional-hazards model [14]. As such, mathematical modeling revealed that a patient's ability to clear nivolumab may be used as a surrogate biomarker for long-term survival benefits obtained after the treatment with the immune-activating agent. Of note, an E-R relationship between nivolumab dose and irAEs-associated discontinuation or death (AE-DC/D) was also established in the clinic [13]. However, this relationship was not helpful in deciding the clinical dose because the E-R relationship appeared to be flat and the risk of AE-DC/D was similar across multiple dose levels (1–10 mg/kg) and tumor types.

### 3 Dose selection for T-cell engaging bispecific molecules

T-cell engaging bispecific molecules represent a class of very complex I-O agents, whose mechanism-of-action involves multiple molecular species and nonlinear relationships. Therefore, predicting the pharmacology of these agents is extremely challenging. Saber et al. have presented an FDA analysis for FIH dose selection for these molecules [15]. They examined 17 CD3 (a receptor on T-cells) engaging bispecific molecules, which differed in their molecular structure (50–190 kDa, full-length IgG, or antibody fragments), valency (divalent, trivalent, or tetravalent), the presence of effector function (via modified Fc domain or different IgG subtypes), and binding to the second antigen (CD19, CD20, CD123, CD33, CEA, P-cadherin,



PSMA, HER2, GPA33, B7H3, and EPCAM). It was found that different MABEL-based approaches were used by the sponsors for FIH dose selection of T-cell engaging bispecific molecules. Dose selection based on 20% PA in the most sensitive assay was the most common approach used, followed by dose selection based on 10% activity, which was measured as target cell cytotoxicity, T-cell proliferation, T-cell activation, or cytokine release. Percentage RO measurements/calculations and the results from toxicological studies were also used to support the selected FIH doses by demonstrating that the doses would result in <10%–20% RO and the doses were below the tolerated doses in the animals. In some cases, the FIH dose was selected based on 50% PA in the most sensitive *in vitro* assay. HNSTD and NOAEL data observed from preclinical safety studies were also used to support the FIH doses. However, it was found that approaches based on RO, HNSTD, or NOAEL were not acceptable for selecting the FIH dose of T-cell engaging bispecific molecules, as they resulted in doses close to or above the MTDs, highest human doses (HHDs), or the RHD. Instead, the authors proposed that a FIH dose that corresponds to 10%–30% PA would be a better approach. A FIH dose corresponding to 50% PA was also found to be an acceptable approach for many T-cell engaging bispecific molecules. The authors also highlighted that the most common toxicities were related to cytokine release, and that FIH doses of T-cell engaging bispecific molecules can be increased following intra-patient dose escalations strategy.

Considering the complexity of the mechanism involved in the pharmacology of T-cell engaging bispecific molecules, use of a PK/PD M&S-based approach is essential for *a priori* predicting clinically efficacious dose of these molecules. This approach accounts for the differences in the effector-to-target cell ratios (E:T), antigen expression levels, drug-binding parameters, and drug exposure between different systems (e.g., *in vitro* vs. *in vivo*, different tumor types, etc.) to provide an accurate prediction of drug pharmacology in a given scenario. Betts *et al.* have presented a great example of how a mechanistic PK/PD model can be developed and used to predict clinically efficacious dose of a CD3 engaging bispecific molecule [16]. First, the authors used preclinical data generated using the CD3XP-cadherin bispecific molecule in mice xenograft to develop the PK/PD model. The model described the disposition of the bispecific molecule and T-cells in the central and tumor compartment of the model, included dose-dependent proliferation and contraction of T-cells within the tumor, accounted for the binding of the bispecific molecule to the tumor cells and T-cells in the tumor microenvironment to form the trimers, and used the trimer concentrations in the tumor to drive the killing of the tumor cells. The model was also used to derive tumor static concentrations (TSC) of the trimer, which represent the minimal efficacious concentration at which tumor growth and death rates are equal. This “threshold” concentration combines tumor growth and drug effect parameters, and can be used as a translational factor for extrapolating xenograft data to the clinic. The mouse PK/PD model for CD3XP-cadherin bispecific molecule was subsequently translated to human. The human PK parameters for the drug were obtained by allometric scaling of cynomolgus monkey PK parameters. System parameters like T-cell concentration in the circulation and tumors, tumor cell concentrations, and typical tumor volumes were changed to clinically relevant values. In addition, the human PK/PD model accounted for the binding of the drug to circulating target (i.e., soluble P-cadherin) in the central compartment, and assumed that the T-cells in the human tumor are at a steady state (i.e., T-cell proliferation/contraction kinetics were not included). The translated human PK/PD model revealed that ~0.1–1 mcg/kg doses would yield efficacious tumor trimer concentrations.

Jiang et al. [17] have performed a retrospective analysis to show that similar PK/PD model could also be developed for preclinical-to-clinical translation of clinically approved T-cell engaging bispecific molecule blinatumomab. Their PK/PD model revealed that following either the priming dose of 9 mcg/day or the full dose of 28 mcg/day, blinatumomab is expected to cause near-complete or complete depletion of B-cell in the blood. However, blinatumomab would induce incomplete depletion of B-cells in the bone marrow following 9 mcg/day priming dose, and the full dose of 28 mcg/day would be required to attain near-complete depletion of B-cells in the bone marrow. The results of their PK/PD model simulations were consistent with the observed blinatumomab clinical data [18].

While the late-stage clinical experience with T-cell engaging bispecific molecules has been limited, clinical development of blinatumomab provides an insight into finalization of the clinical dose for these molecules. The totality of PK, PD, safety, and efficacy data were used to support the final dose and schedule of blinatumomab administration in the patients [19]. While blinatumomab was effective after short intravenous infusions in preclinical species, this approach was abandoned after unsuccessful clinical trials in patients. As such, blinatumomab and similar bispecific T-cell engager (BiTE) constructs are now administered via continuous IV infusion in the patients due to their short plasma half-life. During the clinical evaluation, it was found that increasing the concentrations of blinatumomab led to increased redistribution of T-cells, increased depletion of B-cells, and increased cytokine levels. Also, doses beyond 28 mcg/d did lead to improvement in the efficacy for nonresponders. In addition, it was observed that the average steady-state concentration of blinatumomab ranged from 500 to 700 pg/mL after 28 mcg/d administration, which was above the *in vitro* IC<sub>50</sub> value observed with human leukemia cell line after incubation with T-cells from the least-sensitive patients. It was also observed that stepwise increase in the dosing led to better tolerability profile (i.e., dampened cytokine peak levels), and 2-week drug-free period between the cycle was able to maintain continuous suppression of B-cell, while providing favorable tolerability profile for the molecule. As such, a 4-week on and 2-week off dosing schedule, with 9 mcg/d dose for the 1st week and 28 mcg/d dose for the remaining 3 weeks, was finalized for blinatumomab administration. Since the PK of blinatumomab was not affected by demographic characteristics such as body weight, body surface area, gender, age, disease type, or baseline disease characteristics, a fixed dosing was finalized for blinatumomab administration in the adult patients.

#### 4 Dose selection for emerging class of I-O therapies

Adoptive cell therapies like the CAR-T therapy have been gaining popularity as anticancer agents. In the last couple of years, the FDA has approved the first two CAR-T therapies, which include axicabtagene ciloleucel (Yescarta) for the treatment of diffuse large B-cell lymphoma and tisagenlecleucel (Kymriah) for the treatment of non-Hodgkin lymphoma. The PK/PD behavior of these molecules is not always predictable, and till now the dose selection process for these molecules remains empirical. In fact, clinically approved doses of the FDA-approved CAR-T therapies were not chosen based on any preclinical investigations, but were empirically derived based on clinical observations. Yescarta is administered as a single 30-min IV

infusion to attain the dose of 2 million CAR-positive T-cells per kg of patient body weight, with the maximum dose of 200 million cells per patient. In addition, administration of Yescarta is preceded by fludarabine and cyclophosphamide conditioning chemotherapy to enhance the efficiency of CAR-T therapy. Kymriah is administered as a single infusion of 0.2–5 million transduced viable T-cells per kg of patient's body weight if the patient weighs  $\leq 50$  kg, and total dose of 10–250 million transduced viable T-cells per patient if the patient weighs  $> 50$  kg. As such, while a formal clinical pharmacology analysis of CAR-T cells has not been included in the BLA applications, patient's body weight has been assumed as a significant covariate for the dosing purpose. It is also important to note that the dosing of CAR-T therapy is often limited by the CRS and other toxicities, and tocilizumab as well as corticosteroids are often coadministered to increase the tolerability of these molecules.

Oncolytic viruses are another type of I-O agents that are gaining popularity. Talimogene laherparepvec (T-VEC, Imlygic), which is used for the treatment of melanoma, is the only FDA-approved oncolytic virus. It is essentially a modified herpes simplex virus (HSV) that is administered locally in tumor lesions to infect the tumor cells and promote their destruction. Since the route of administration and mechanism-of-action for oncolytic viruses is very different, the dosing of these agents is also atypical. To the best of our knowledge, detailed clinical pharmacology and PK/PD analysis of talimogene laherparepvec has not been performed to support FIH or final clinical dosing of these agents [20]. In the clinic, the dose of talimogene laherparepvec depends on the size of the lesion, with increasing volume of virus suspension given for increasing maximal diameter of the lesion. For bigger lesions with the longest diameter  $> 5$  cm, up to 4 mL of virus suspension is administered per lesion; and for smaller lesions with  $< 0.5$  cm diameter, up to 0.1 mL virus suspension is administered per lesion. For the first dose, up to 4 mL of talimogene laherparepvec is administered at a concentration of 1 million plaque forming units (PFU) per mL. Three weeks after the initial treatment, up to 4 mL of viruses at a concentration of 100 million PFU per mL are administered as a second dose. All subsequent doses are administered 2 weeks apart at up to 4 mL of viruses at a concentration of 100 million PFU per mL. As the field of oncolytic virus is getting matured, more detailed dose-finding and PK/PD studies are conducted with the viruses, as published for oncolytic adenovirus enadenotucirev by Machiels et al. [21].

---

## 5 Future directions

---

It is increasingly becoming clear that the traditional MTD-based approach developed for chemotherapy may not be ideal for I-O agents. Since the toxicities of I-O therapies may be delayed and more variable, using MTD as the RP2D may lead to therapeutic failure of I-O agents, due to toxicity-related discontinuations or large number of dose reductions in late-stage clinical trials [9]. As such, finding the right dosing schedule that balances the risks and benefits of I-O therapies is essential for their clinical success. This can be accomplished with the help of a multidisciplinary team, which can integrate novel experimental and quantitative approaches within a translational and precision medicine paradigm. The two biggest areas of innovation that can revolutionize the current practice of dose determination for I-O agents are novel clinical trial design and integrated systems pharmacology models of the

immune system. Some innovations in clinical trial design include thinking beyond the “3+3” design to develop more adaptive dose-finding trials, investigation of a range of phase-2 doses rather than studying a single phase-2 dose, and development of early approaches to establish E-R relationships for the safety and efficacy of I-O agents rather than just performing ad hoc E-R analyses. Innovations in the PK/PD M&S space include development of molecule or disease-specific systems-based models. These models can be used as a platform for linking preclinical and early clinical end points with the late efficacy end points (e.g., OS), to comprehensively understand the E-R relationships and optimize the dosing regimen for I-O therapies as early as possible. These models can also provide an opportunity to a priori identify the optimal dosing schedules of I-O therapies while transitioning to different patient populations or drug combinations [22].

## References

- [1] J. Tang, A. Shalabi, V.M. Hubbard-Lucey, Comprehensive analysis of the clinical immuno-oncology landscape, *Ann. Oncol.* 29 (1) (2018) 84–91.
- [2] P. Darvin, S.M. Toor, V. Sasidharan Nair, E. Elkord, Immune checkpoint inhibitors: recent progress and potential biomarkers, *Exp. Mol. Med.* 50 (12) (2018) 165.
- [3] W.C.M. Dempke, K. Fenchel, P. Uciechowski, S.P. Dale, Second- and third-generation drugs for immuno-oncology treatment—the more the better? *Eur. J. Cancer* 74 (2017) 55–72.
- [4] E. Dahlen, N. Veitonmaki, P. Norlen, Bispecific antibodies in cancer immunotherapy, *Ther. Adv. Vaccines Immunother.* 6 (1) (2018) 3–17.
- [5] L. Zhao, Y.J. Cao, Engineered T cell therapy for cancer in the clinic, *Front. Immunol.* 10 (2019) 2250.
- [6] J. Raja, J.M. Ludwig, S.N. Gettinger, K.A. Schalper, H.S. Kim, Oncolytic virus immunotherapy: future prospects for oncology, *J. Immunother. Cancer* 6 (1) (2018) 140.
- [7] T. Kadono, Immune-related adverse events by immune checkpoint inhibitors, *Nihon Rinsho Meneki Gakkai Kaishi* 40 (2) (2017) 83–89.
- [8] S. Champiat, R. Ferrara, C. Massard, B. Besse, A. Marabelle, J.C. Soria, et al., Hyperprogressive disease: recognizing a novel pattern to improve patient management, *Nat. Rev. Clin. Oncol.* 15 (12) (2018) 748–762.
- [9] Y. Ji, J.Y. Jin, D.M. Hyman, G. Kim, A. Suri, Challenges and opportunities in dose finding in oncology and immuno-oncology, *Clin. Transl. Sci.* 11 (4) (2018) 345–351.
- [10] X. Zhao, X. Wang, Y. Feng, S. Agrawal, D.K. Shah, in: M.A. Tabrizi, G.G. Bornstein, S.L. Klakamp (Eds.), *Application of PK-PD Modeling and Simulation Approaches for Immuno-Oncology Drugs*, in *Development of Antibody-Based Therapeutics: Translational Considerations & Challenges*, Springer Singapore, Singapore, 2018, pp. 207–222.
- [11] H. Saber, R. Gudi, M. Manning, E. Wearne, J.K. Leighton, An FDA oncology analysis of immune activating products and first-in-human dose selection, *Regul. Toxicol. Pharmacol.* 81 (2016) 448–456.
- [12] A. Lindauer, C.R. Valiathan, K. Mehta, V. Sriram, R. de Greef, J. Ellassaiss-Schaap, et al., Translational pharmacokinetic/pharmacodynamic modeling of tumor growth inhibition supports dose-range selection of the anti-PD-1 antibody pembrolizumab, *CPT Pharmacometrics Syst. Pharmacol.* 6 (1) (2017) 11–20.
- [13] S. Agrawal, Y. Feng, A. Roy, G. Kollia, B. Lestini, Nivolumab dose selection: challenges, opportunities, and lessons learned for cancer immunotherapy, *J. Immunother. Cancer* 4 (2016) 72.
- [14] X. Wang, Y. Feng, G. Bajaj, M. Gupta, S. Agrawal, A. Yang, et al., Quantitative characterization of the exposure-response relationship for cancer immunotherapy: a case study of nivolumab in patients with advanced melanoma, *CPT Pharmacometrics Syst. Pharmacol.* 6 (1) (2017) 40–48.
- [15] H. Saber, P. Del Valle, T.K. Ricks, J.K. Leighton, An FDA oncology analysis of CD3 bispecific constructs and first-in-human dose selection, *Regul. Toxicol. Pharmacol.* 90 (2017) 144–152.
- [16] A. Betts, N. Haddish-Berhane, D.K. Shah, P.H. van der Graaf, F. Barletta, L. King, et al., A translational quantitative systems pharmacology model for CD3 bispecific molecules: application to quantify T cell-mediated tumor cell killing by P-cadherin LP DART((R)), *AAPS J.* 21 (4) (2019) 66.

- [17] X. Jiang, X. Chen, T.J. Carpenter, J. Wang, R. Zhou, H.M. Davis, et al., Development of a Target cell-biologics-effector cell (TBE) complex-based cell killing model to characterize target cell depletion by T cell redirecting bispecific agents, *MAbs* 10 (6) (2018) 876–889.
- [18] M. Zhu, A. Kratzer, J. Johnson, C. Holland, C. Brandl, I. Singh, et al., Pharmacokinetics/pharmacodynamics (PKPD) of blinatumomab in patients with relapsed/refractory B-precursor acute lymphoblastic leukemia (r/r ALL), *J. Clin. Oncol.* 33 (15\_suppl) (2015) 2561.
- [19] T. Yuraszek, S. Kasichayanula, J.E. Benjamin, Translation and clinical development of bispecific T-cell engaging antibodies for cancer treatment, *Clin. Pharmacol. Ther.* 101 (5) (2017) 634–645.
- [20] E.E. Burke, J.S. Zager, Pharmacokinetic drug evaluation of talimogene laherparepvec for the treatment of advanced melanoma, *Expert Opin. Drug Metab. Toxicol.* 14 (4) (2018) 469–473.
- [21] J.P. Machiels, R. Salazar, S. Rottey, I. Duran, L. Dirix, K. Geboes, et al., A phase 1 dose escalation study of the oncolytic adenovirus enadenotucirev, administered intravenously to patients with epithelial solid tumors (EVOLVE), *J. Immunother. Cancer* 7 (1) (2019) 20.
- [22] O. Milberg, C. Gong, M. Jafarnejad, I.H. Bartelink, B. Wang, P. Vicini, et al., A QSP model for predicting clinical responses to monotherapy, combination and sequential therapy following CTLA-4, PD-1, and PD-L1 checkpoint blockade, *Sci. Rep.* 9 (1) (2019) 11286.

# Index

---

Note: Page numbers followed by *f* indicate figures and *t* indicate tables.

## A

- AAV. *See* Adeno-associated virus (AAV)
- Absolute bioavailability, 200–202
- Absorption, distribution, metabolism, and excretion (ADME), 40–41, 311–312, 555–558, 562–563
- Absorption, distribution, metabolism, excretion, and toxicity (ADMET), 359
- Accelerator mass spectrometry (AMS), 421–422, 425–426
- concomitant microtracer, 201*f*
- absolute bioavailability, 200–202
- kinetic isotope effect (KIE), 199
- human ADME study, 195–196
- hybrid studies (macrotracer), 193, 194*t*, 196–198
- microdose, 193
- Accurate radioisotope counting, 44
- Acetaminophen, 565
- Acetyl-gestagens, 163
- $\alpha$ 1-Acid glycoprotein (AGP), 466
- Active pharmaceutical ingredient (API), 158, 165–166*t*, 167
- Acute kidney injury (AKI), 507, 525
- Acylcarnitine metabolites, 91–93, 92*f*
- Acyl glucuronides (AG), 11, 491–492
- Adalimumab, 544–545
- Adaptive immunity, 535–536, 536*f*
- ADAs. *See* Antidrug antibodies (ADAs)
- ADCC. *See* Antibody-dependent cell-mediated cytotoxicity (ADCC)
- ADCs. *See* Antibody-drug conjugates (ADCs)
- Adeno-associated virus (AAV), 546, 548–549
- Adenosine triphosphate (ATP), 312–315, 496
- ADH. *See* Alcohol dehydrogenase (ADH)
- ADMET. *See* Absorption, distribution, metabolism, excretion, and toxicity (ADMET)
- AKI. *See* Acute kidney injury (AKI)
- AKRs. *See* Aldo-keto reductases (AKRs)
- Albumin, 373, 558–562, 615
- Alcohol dehydrogenase (ADH), 469–470
- Aldehyde oxidases, 130, 134–135, 146, 223–227, 224–225*t*, 441, 456, 555–556, 612
- challenges, 253
- clinical significance and DDI, 253
- drugs, 264, 265–266*t*
- in vitro-in vivo correlation (IVIVC), 251
- metabolism, 451–452
- molybdenum and flavin-dependent enzymes, 251
- reaction phenotyping of, 252–253
- substrates and metabolites, 252–253, 252*f*
- Aldo-keto reductases (AKRs)
- challenge, 264
- clinical significance, 264
- drugs, 264, 265–266*t*
- human-animal comparison, 263
- substrates, 262–263, 263*f*
- substrate specificity, 261–262
- All ion fragmentation (AIF), 87
- Allometric scaling approach, 640
- Alzheimer's disease, 251
- AMG 221, metabolites of, 122, 123–124*f*
- Amino acids, 169–172, 170–171*t*, 461–462
- 1-Aminobenzotriazole, 565–566
- Amiodarone, 125
- Amodiaquine, 127, 128*f*
- Amphetamine (AMP), 160–162, 470–471, 478
- AMS. *See* Accelerator mass spectrometry (AMS)
- Analog-to-digital converter (ADC), 51
- Anandamide, 25
- Androsterone, 558–562
- Angiogenesis inhibitors, 400
- Antalarmin, 125, 126*f*
- Antiadsorptive agents, 9–10
- Antibody-dependent cell-mediated cytotoxicity (ADCC), 538–540
- Antibody-drug conjugates (ADCs), 5, 17, 401
- Antibody-fusion protein, 598
- Antibody, HLM-based P450 reaction phenotyping, 219
- Antibody mediated responses, 538–540, 540*t*
- Antidrug antibodies (ADAs), 5, 536–540, 544–545
- Antisense oligonucleotides, 512–514
- AOs. *See* Aldehyde oxidases
- AOXs. *See* Aldehyde oxidases
- APCI. *See* Atmospheric pressure chemical ionization (APCI)
- API. *See* Active pharmaceutical ingredient (API)

- Arachidonic acid metabolites, 170–171*t*, 174  
Area under the curve (AUC), 393, 545  
Artemether, 165–166*t*, 168  
Artificial neural network (ANN), 547  
Aryl hydrocarbon receptor (AhR), 291  
Asialoglycoprotein receptor (ASGPR), 512–514  
Astemizole, 217  
Atmospheric pressure chemical ionization (APCI), 14  
  bioanalytical SFC applications, 158–159  
  drug metabolite identification, 45–46  
Atmospheric pressure ionization (API)  
  bioanalytical SFC applications, 157–158  
  drug metabolite identification, 45–47  
Atmospheric pressure laser ionization (APLI), 158–159  
Atmospheric pressure photoionization (APPI), 14, 46–47, 158–159  
Atorvastatin, 351–352, 562–563, 617–618  
ATP. *See* Adenosine triphosphate (ATP)  
ATP-binding cassette (ABC) transporters, 509, 599, 617–618  
  BCRP, 314–315  
  bile salt export protein (BSEP/ABCB11), 315  
  genomic mutations (polymorphisms), 312  
  knockout rodent models, 559–560*t*  
  multidrug resistance proteins (MRPs/ABCCs), 315  
  P-glycoprotein (P-gp), 314  
Authentic matrix and authentic analyte approach, 24  
AVP-786, 453  
Axicabtagene ciloleucel (Yescarta), 664–665
- B**  
*Bacillus megaterium*, 132  
Background-exclusion data-dependent acquisition (BE-DDA), 83–84, 85*f*  
Background subtraction (BS)  
  metabolite identification, 89*f*, 90–91, 100–102, 102*f*  
  TCM components, detection and characterization of, 104–107, 106*f*  
Basement membrane (BM), 514–515  
Bayesian machine learning approach, 502  
BBB. *See* Blood-brain barrier (BBB)  
BDDCS. *See* Biopharmaceutics drug disposition classification system (BDDCS)  
Bendamustine with rituximab (BR), 400  
Benign recurrent intrahepatic cholestasis (BRIC), 315  
Benzopyridine, 463  
Bevacizumab, 399–400, 399*t*  
4 $\beta$ -hydroxylcholesterol, 24–25  
Bile salt export protein (BSEP), 497–499, 498*f*  
Biliary excretion index (BEI), 323–324  
Bioactivation, 489–496  
  carboxylic acid-containing molecules, 491–493  
  covalent binding, 490–491  
  Glaxo Smith Kline multi-assay approach, 493  
  immunomics approach, 494–496  
  metabolite identification, 489–490  
  transcriptomics approach, 493–494  
Bioanalysis (BA), 3, 429  
  acyl glucuronide metabolite, 11  
  contemporary bioanalysis, 3–6  
  discovery, nonclinical development, and clinical support, 3, 4*f*, 6  
  full, partial, and cross validations, 6–7, 7*t*  
  LC-MS bioanalysis, 11–12, 14, 32–33  
  biomarker quantitation, 14–15, 23–26  
  of large molecules (*see* Large molecules, LC-MS bioanalysis)  
  metabolites and MIST, 14–15, 27–32  
  microsampling technology, 14–15, 20–23  
  sample extraction method, 12  
  tissue bioanalysis, 4–5, 10–11  
  sample collection, considerations for, 7–8  
  materials and labeling, 8  
  SFC applications (*see* Supercritical fluid chromatography (SFC))  
  SOPs and regulatory guidelines, 6–7  
  urine bioanalysis, 4–5, 9–10  
Bioequivalence (BE), 5, 168–169, 473–474  
Biomarkers, 170–171*t*, 173–174  
  fatty acid amide hydrolase (FAAH) biomarkers, 25–26  
  LC-MS analysis, 14–15  
  assay selectivity, 23–24  
  4 $\beta$ -hydroxylcholesterol, 24–25  
  challenges, 23–24  
  fatty acid amide hydrolase biomarkers, 25–26  
  7 $\alpha$ -hydroxy-4-cholesten-3-one (C4), 25, 26*f*  
  leukotriene B<sub>4</sub> (LTB<sub>4</sub>), 24  
  nonqualified DIKI biomarkers, 520–523, 521–522*t*  
  qualified DIKI biomarkers, 520–523, 521–522*t*  
  translatable kidney safety biomarkers, 520–523  
Biomimetic catalysts, 120*f*, 125–126  
Biopharmaceutics Classification System (BCS), 204  
Biopharmaceutics drug disposition classification system (BDDCS), 499–500, 500*t*  
Biotherapeutic drugs, 535  
Biotransformation, 73–74  
  of amodiaquine to metabolites, 127, 128*f*  
  enantiomeric biotransformation, 472  
  whole-cell microbial biotransformation (*see* Microbial biotransformation)  
Blinatumomab, 397, 657, 664  
Blood-brain barrier (BBB), 314, 567–568  
Blood microsampling, LC-MS bioanalysis  
  method development, 22–23  
  sample collection techniques, 20–21, 21*f*  
Blood urea nitrogen (BUN), 492, 507, 520



- Bosentan, 139–141, 139–140*f*  
Bovine serum albumin (BSA), 373, 612, 620–621  
Breast cancer resistance protein (BCRP), 349–350, 617–618  
BSEP. *See* Bile salt export protein (BSEP)
- C**
- Calibration curve, 373  
Calibrator approach, 427–428, 428*f*  
Cannabinoids, 160–162, 161*t*  
Capillary electrophoresis (CE), 478–479  
Capillary microsampling sampling (CMS), 20–23, 21*f*  
Carbon carrier, 188–192, 188*f*  
Carboxylesterase (CES), 622  
  challenges, 261  
  chemical inhibitors, 258–260  
  clopidogrel, 258, 259*f*  
  2-cyclohexyl-2-phenylglycolic acid (CPGA), 258  
  drug-drug interactions, 261  
  drugs, 264, 265–266*t*  
  ester drugs, hydrolysis of, 258, 259*f*  
  experimental design, for CES reaction phenotyping, 256–261  
  human carboxylesterases, CES1 1 (hCE-1), 256, 257*t*  
  human carboxylesterases, CES1 2 (hCE-2), 256, 258*t*  
  human liver S9 (HLS9), 258  
  hybridization analyses, 256  
  intrinsic clearances, calculation of, 260  
  irinotecan (CPT-11), 258–260, 259*f*  
  nordihydroguaiaretic acid (NDGA), 258  
Carcinoembryonic antigen (CEA), 400  
Carotinoids, 170–171*t*, 173–174  
Cas proteins, 595–596, 597*f*  
Cavity ring-down spectroscopy (CRDS), 205, 421–422, 425–426  
CDRs. *See* Chiral derivatization reagents (CDRs); Complementarity-determining regions (CDRs)  
CE. *See* Capillary electrophoresis (CE)  
Cefmetazole, 579  
Cell lysis technique, 363–364  
Cell surface activation markers, 548  
Cellular immune response, 540–541, 550  
Cellular immunogenicity, 540–541  
  CD8+ T cells  
    activation and cellular response of, 541, 542*f*  
    MHC I on cell surface and binding to, 540–541, 541*f*  
  mitigation strategy and case studies  
    AAV, modification of, 548–549  
    humanization of CAR construct, 549  
    lymphodepletion, 550  
  risk assessments, 546–548, 546*f*  
  Chromium 51, 547  
  ELISpot, 547  
    flow cytometry, 548  
    in vivo analysis, 548  
    in silico prediction tool, 547  
Centyrin, 17–18, 18*f*  
Cerivastatin, 213–214, 617–618  
CFDA. *See* Chinese Food and Drug Administration (CFDA)  
Chemical derivatization  
  derivatization reagents, for functional groups, 57, 58*t*  
  isomeric metabolite characterization, 60, 61*f*  
  polar metabolites, 57–58, 59*f*  
  site of glucuronidation, 61–62  
  unstable metabolites, 60, 60*f*  
  unusual metabolite characterization, 58–59, 59*f*  
Chemical inhibitors, HLM-based P450 reaction phenotyping, 219–220, 220*t*  
Chemical synthesis, 120–121, 120*f*  
  AMG 221, metabolites of, 122, 123–124*f*  
  clopidogrel, active metabolites of, 123, 123–124*f*  
  phase II (conjugate) metabolites, 123–125  
  phase I oxidized metabolites, 121–123  
Chemotherapeutic drugs, SFC-MS/MS method, 165–166*t*, 167  
Chimeric antibodies, 543  
Chimeric antigen T cells (CAR-T) cell therapies, 387–388, 403, 408, 546, 657, 664–665  
Chinese Food and Drug Administration (CFDA), 419–420  
Chinese hamster ovary (CHO) cells, 321  
Chiral chromatography, 480  
Chiral compounds  
  definition, 461–462  
  LC-MS bioanalysis, 30–31  
  supercritical fluid chromatography (SFC), 45  
Chiral derivatization reagents (CDRs), 475, 477–478, 480  
Chiral drugs, 462, 480  
  absorption and transport, 465–466  
  distribution in different tissues, 466–467  
  excretion, 470  
  interactions, 470–471  
  metabolic process of, 468  
  metabolism, 468–470, 475  
  pharmacological effects of, 463  
  toxicity of, 471  
Chiral gas chromatography, 477–478  
  chiral derivatization reagents, 478  
  chiral stationary phases, 478  
Chiral inversion  
  of JNJ-A, 30–31

- Chiral inversion (*Continued*)  
mechanisms, 473–475  
nonsteroidal anti-inflammatory drugs, 473–474  
opposite metabolic pathway, 474–475  
toxicity, 472
- Chiral LC-MS bioanalysis, 30–31
- Chiral mobile phase additives (CMPAs), 477, 480
- Chiral preference, 461–462
- Chiral secondary alcohol, 474
- Chiral stationary phases (CSPs), 154, 475–476, 480
- Chiral sulfoxide compounds, 475
- 2-Chloro-1-methylpyridinium iodide (CMPI), 57
- Chromium 51 (<sup>51</sup>Cr), 547
- Cimetidine, 320, 509
- Cisplatin, 509, 515–516
- Citalopram enantiomers, 164–166, 165–166*t*
- Clemazole, 580–581
- Clenbuterol enantiomers, SFC-MS/MS method, 161*t*, 163
- Clopidogrel, metabolites of, 123, 123–124*f*
- Clustered regularly interspaced short palindromic repeat (CRISPR), 595, 596*f*  
ADME studies in vitro, 599–603  
CYP3A5\*3, genetic modification of, 600–601, 600*f*  
limitations in, 603–604  
MDCK cells, endogenous canine P-gp knockout in, 601–603  
potential opportunities, 604–605
- CRISPR-Cas9, 266, 597*f*, 603–604  
activation of target genes, 598  
genetic screens, 599  
genome editing, 596–597  
in vitro applications, 596–599  
repression of target genes, 597–598
- CMPAs. *See* Chiral mobile phase additives (CMPAs)
- CMS. *See* Capillary microsampling (CMS)
- CNV. *See* Copy number variation (CNV)
- Cobicistat (COBI), 314
- Coculture systems, 392–393
- Codeine, 214, 245
- Coenzyme Q10, SFC-MS/MS method, 165–166*t*, 168
- Collisional induced dissociation (CID), 47–48
- Compartmental-based PK modeling, 636
- Complementarity-determining regions (CDRs), 543
- Concomitant microtracer approach, 201*f*  
absolute bioavailability, 200–202  
advantages, 199–200  
criteria, 199  
definition, 193  
design features, outputs, and literature examples, 194*f*  
extravascular and intravenous doses, 199  
isotope mixing, principles of, 199, 200*f*  
kinetic isotope effect (KIE), 199
- Conditionally immortalized PTECs (ciPTECs), 511
- Constant receptor amount ( $R_{total}$ ) model, 645
- Constitutive androstane receptor (CAR), 291, 391
- Copy number variation (CNV), 360–361
- Correlated spectroscopy (COSY), 138–139
- Correlation analysis, 222–223, 223*t*
- Covalent binding, 490–491
- Cox proportional-hazards model, 662
- CpG oligonucleotides, 402–403
- CRDS. *See* Cavity ring-down spectroscopy (CRDS)
- C-reactive protein (CRP), 393, 538, 538*f*
- Creatinine (CRE), 492
- Crigler-Najjar syndrome, 244, 558–562, 566–567
- CRISPR. *See* Clustered regularly interspaced short palindromic repeat (CRISPR)
- CRISPR-based gene activation system (CRISPRa), 598
- CRISPR interference (CRISPRi), 597–598
- CRISPR-STOP approach, 603–604
- Critical quality attributes (CQA), 16–17
- Cross-section measurements (CCS), 53–54
- Cross species comparison, of human and animal plasma samples, 428–429, 429*f*
- CRP. *See* C-reactive protein (CRP)
- CRS. *See* Cytokine release syndrome (CRS)
- Cryoprobe technology, 119–120, 128, 424
- CSPs. *See* Chiral stationary phases (CSPs)
- CTLs. *See* Cytotoxic T lymphocytes (CTLs)
- Cyclosporin A (CsA), 141, 141–142*f*, 314
- Cystic fibrosis (CF), 453
- Cytochromes P450 (CYPs), 232, 311–312, 390, 392, 396, 407, 555–556, 565–566, 599, 612, 622  
CYP1A1 and CYP1B1-mediated amodiaquine, 127, 128*f*  
CYP2C9, 215  
CYP2C19, 214–215  
CYP2D6, 214  
fmCYP3A, determination of, 227–229  
*vs.* FMO/AO metabolism, 223–227  
HLM-based P450 reaction phenotyping, 217–219  
antibodies, 219  
chemical inhibitors, 219–220, 220*t*  
correlation analysis, 222–223, 223*t*  
Silensomes, 221–222, 221*f*
- HRMS application, in reaction phenotyping, 97, 98*f*  
metabolism, 449–451, 449*f*  
recombinant P450 assays (*see* Recombinant P450 (rP450) enzymes)  
regulatory guidance/risk assessment/examples, 229–231  
victim DDI, 213–214

- Cytokine-dependent interactions  
  cytokines and therapeutic proteins targeting  
    cytokines, 393–397  
    immunomodulatory therapeutic proteins, 397–398  
Cytokine release syndrome (CRS), 403, 537  
Cytosolic protein per gram of kidney (CPPGK), 622  
Cytotoxic T lymphocytes (CTLs), 546
- D**
- Dabigatran etexilate (DE), 318–319  
Daidzein, 165–166*t*, 167  
Dansyl aziridine, 60, 60*f*  
Dapagliflozin, 245  
Data-dependent acquisitions (DDA), 51, 52*f*  
  MS/MS acquisition, metabolite identification, 74–76, 75*f*, 101–102  
  accurate mass inclusion list-dependent acquisition, 77–82  
  background exclusion DDA, 83–84, 85*f*  
  ion intensity-dependent acquisition, 77  
  isotope pattern-dependent acquisition, 83, 84*f*  
  mass defect-dependent acquisition, 82–83, 82*f*  
  pseudo-neutral loss, 83  
  TCM components, detection and characterization of, 103  
Data-independent acquisitions (DIA), 51, 74–76, 84–86, 101–102  
  all ion fragmentation (AIF), 87  
  MS<sup>E</sup> approach, 51–52, 52*f*, 86  
  SONAR acquisition, 52–53, 54*f*, 65  
  SWATH acquisition, 52, 53*f*, 65, 86, 87*f*  
  TCM components, detection and characterization of, 103  
DDIs. *See* Drug-drug interactions (DDIs)  
Dead Cas9 (dCas9), 595–596, 598  
Debrisoquine, 579  
Denatured proteins, 364  
De novo synthesis, 288–289  
Desalting, 364–365  
Design of experiments (DoE) approach, 154  
Deuterated drugs, 446, 452*f*, 457  
  deuterium in drug design, 445–448  
  drug-metabolizing enzymes  
    aldehyde oxidase metabolism, 451–452  
    cytochrome P450 metabolism, 449–451  
    monoamine oxidase metabolism, 451  
  old drugs, versions of, 452–454  
    improving bioavailability, 453  
    lowering clearance, 453  
    reactive metabolite formation/drug-drug interaction, 453  
    slowing chiral inversion, 454  
Deuterated tetrabenazine, metabolism of, 451*f*, 452  
Deuterium, 457  
  atoms, 451, 452*f*  
  in drug design, 445–448  
  labeling sites of, 446  
  natural abundance, 445  
Deuterium oxide (D<sub>2</sub>O), 442–443  
Deutetrabenazine, 439, 452, 457  
Dexamethasone, 556–557  
Dextropropoxyphen, 464  
DIA. *See* Data-independent acquisitions (DIA)  
Diclofenac metabolites, 82–83, 82*f*  
Differential mobility separation (DMS), 54  
Dihydroartemisinin, 165–166*t*, 168  
Dihydro-ziprasidone, H/D exchange scheme of, 56, 56*f*  
2,3-Diketopiperazine metabolites, 122  
DIKI. *See* Drug-induced kidney injury (DIKI)  
DILI. *See* Drug-induced liver injury (DILI)  
Dilute and shoot (DS), 159–162  
1,2-Dimethylimidazole-4-sulfonyl chloride (DMISC), 57–58, 61  
Distomer, 461–462  
Distribution modeling, PBPK, 639–640  
DMEs. *See* Drug-metabolizing enzymes (DMEs)  
DMPK. *See* Drug metabolism and pharmacokinetics (DMPK)  
2D NMR spectroscopy, 138–139, 141–144, 141–145*f*  
D<sub>2</sub>O. *See* Deuterium oxide (D<sub>2</sub>O)  
Dobutamine, 463  
Doping control, bioanalytical SFC applications, 161*t*, 162–163  
Double-strand breaks (DSBs), 595–596, 597*f*  
Doxorubicin, 515–516, 567–568  
D<sub>2</sub> receptor antagonists, 648, 649*f*  
Drug antibody ratio (DAR), 17  
Drug-associated antigens, 494–496, 495*f*  
Drug-drug interactions (DDIs), 120–121, 204, 213–214, 388–389, 407, 465–466, 617–618, 635, 640  
  absorption-based DDIs, 354–356  
  aldehyde oxidases (AOXs), 253  
  aldo-keto reductases (AKRs), 264  
  carboxylesterase (CES), 261  
  clinical drug interaction assessment, 300  
  cultured cell systems, 278  
  cytochrome P450 (CYP450), 24  
  for different therapeutic modalities, 407, 408*f*  
  drug metabolizing enzymes, 274, 276–277*t*  
  EMA guidance, 229, 230*t*  
  between emerging modalities  
    cell-based therapies, 403  
    immunocytokines, 404  
    oligonucleotide and mRNA-based drugs, 401–403  
    oncolytic viruses, 403–404  
  enzyme-mediated DDIs, NMEs

- Drug-drug interactions (DDIs) (*Continued*)  
  as inducers, 345–346*t*, 348–349  
  as inhibitors, 342–343*t*, 346–347  
  as substrates, 349–351  
  FDA and PMDA guidances, 229, 230*t*  
  flavin-monooxygenase (FMO), 247–248  
  hepatic and intestinal cytochrome P450 (CYP)  
    expression, 274, 275–276*t*  
  hepatocytes, 278  
  metabolism-based drug interaction potential, in vitro  
    assessment of  
      enzyme induction, 290–292  
      inhibitor, characterization of, 283–290  
      substrates, characterization of, 279–283  
  monoamine oxidase (MAO), 251  
  olaparib, risk assessment for, 229, 231*t*  
  PBPK modeling and simulations, 352–353  
  physiological detoxification process, 274  
  polypharmacy, 273–274  
  potential, 377  
  quantitative in vitro to in vivo predictions  
    drug metabolizing enzyme induction, prediction of,  
      297  
    first-pass intestinal metabolism and integration,  
      multiple DDI mechanisms, 298–299  
    irreversible inhibition prediction, 296–297  
    reversible inhibition predictions, basic principles of,  
      292–294  
    selection of inhibitor concentration, [I], 294–296  
  recombinant enzyme system, 274–278  
  toxic metabolites, 274  
  transporter-mediated DDIs, NMEs  
    as inhibitors, 348*t*, 351–352, 351*f*  
    as substrates, 349–351, 350*f*  
  UDP-glucuronosyltransferases (UGTs), 244–245, 274,  
    275–276*t*
- Drug-induced kidney injury (DIKI), 507, 524–525
- Drug-induced liver injury (DILI), 315, 487, 488*f*, 499–503  
  bioactivation of drugs to reactive intermediates,  
    489–496  
  dose, exposure, and physiochemical properties,  
    499–500  
  multiparametric approaches, 500–503  
    Bayesian machine learning approach, 502  
    hepatic risk matrix (HRM) approach, 503  
    in vitro hazard matrix, 502  
    Roche approach using combination of assays, 502  
    three-tiered roadmap, 500–502, 501*f*  
  prediction, challenges in, 487–496
- Drug metabolism and pharmacokinetics (DMPK), 374
- Drug/metabolite-protein interactions, 377
- Drug-metabolizing enzymes (DMEs), 439, 555–558, 579,  
  595–596, 599, 604  
  aldehyde oxidase metabolism, 451–452  
  cytochrome P450 metabolism, 449–451, 449*f*  
  monoamine oxidase metabolism, 451
- Drug metabolizing enzymes and transporters (DMET)  
  quantitative proteomics, 359, 360*f*, 361–371, 372*f*,  
  377  
  applications of, 374–377, 374*t*  
    differential tissue and regional protein distribution,  
      376  
    drug-drug interaction potential, 377  
    drug/metabolite-protein interactions, 377  
    interindividual variability and precision medicine,  
      376–377  
    interspecies differences, in protein expression, 375  
    in vitro and in vivo models, characterization of, 375  
    in vitro to in vivo extrapolation, 375  
    subcellular localization of proteins, 376  
  basic workflow of, 361–369  
    liquid chromatography, peptide separation using,  
      365  
    mass spectrometry analysis, 366  
    post-digestion processing, 364–365  
    procurement, homogenization, and protein  
      extraction, 362–364  
    protein extraction and digestion methods, 364  
    protein quantification approaches, 366–369  
    proteotypic peptides, selection of, 361–362  
    untargeted MS acquisition approaches, 366–369
- Drug transporters, 595–596, 599, 604
- Dry blood spot (DBS), 20–22, 21*f*
- DSBs. *See* Double-strand breaks (DSBs)
- Dubin-Johnson syndrome, 315, 558–562
- Dulaglutide, 19–20, 20*f*
- E**
- ECCS. *See* Extended clearance classification system (ECCS)
- ECM. *See* Extracellular matrix (ECM)
- Efficacious human dose (EHD), 659
- EFPIA. *See* European Federation of Pharmaceutical Industries and Associations (EFPIA)
- EGFR. *See* Epidermal growth factor receptor (EGFR)
- Electrochemistry (EC), 120*f*, 126–127
- Electrospray ionization (ESI), 14, 62  
  bioanalytical SFC applications, 156, 158–159  
  drug metabolite identification, 46
- ELISA. *See* Enzyme-linked immunosorbent assay (ELISA)
- ELISpot assay, 547
- EMA. *See* European Medicines Agency (EMA)
- Embryonic stem cell (ESC), 515
- Empirical scaling factor (ESF), 615
- Enantiomeric biotransformation, 472

- Endoxifen, 563–564  
Enhanced-fluidity liquid chromatography (EFCL), 156  
Enzyme-linked immunosorbent assay (ELISA), 360–361  
Epacadostat (EPA), 131, 131f  
Epidermal growth factor receptor (EGFR), 649–651, 650f  
19-Epischolarisine, 165–166t, 168  
Epstein-Barr virus transactivator, 598  
ESC. *See* Embryonic stem cell (ESC)  
*Escherichia coli*, 132–134  
Estriol-3-glucuronide (E3G), 61–62  
Estriol-16-glucuronide (E16G), 61–62  
Estriol-17-glucuronide (E17G), 61–62  
1-Ethyl-3-(3-dimethylaminopropyl)-carbodiimide (EDC), 57  
Ethylenediaminetetraacetic acid (EDTA), 252–253  
2-Ethylpyridine (2-EP) bonded silica phase, in SFC, 154  
European Bioanalytical Forum (EBF), 4–5  
European Federation of Pharmaceutical Industries and Associations (EFPIA), 500  
European Medicines Agency (EMA), 6–7, 229, 230t, 274, 523  
Eutomer, 461–462, 472  
Exposure-response (E-R) relationships, 659–662, 665–666  
Extended clearance classification system (ECCS), 610–611, 611f  
Extensive metabolizers (EMs), 214–215  
Extracellular matrix (ECM), 514–515, 518  
Extracted ion chromatography (EIC), 15–16  
    in vivo TCM components, detection and identification of, 103–104  
    metabolite identification, 88  
Ezetimibe, 165–166t, 168–169  
Ezlopitant, 58, 59f
- F**  
Factor IX transgene (FIX), 545  
Fasiglifam, 497–498  
Fat-soluble vitamins, 170–171t, 173–174  
Fatty acid amide hydrolase (FAAH) biomarkers, 25–26  
FCM. *See* Flow cytometry (FCM)  
Fexofenadine, 567–568  
First-in-human (FIH)  
    bioanalytical method, 6  
    dose selection for, 659  
    immune-activating agents, 659–660  
    T-cell engaging bispecific molecules, 662–663  
First time in human (FTIH) study, 202–203  
Fish odor syndrome. *See* Trimethylaminuria disorder  
FIX. *See* Factor IX transgene (FIX)  
Flavin adenine dinucleotide (FAD)-binding domain, 224–225  
Flavin-containing monooxygenases (FMOs), 134, 223–227, 224–225t, 612  
    catalytic cycle, 246  
    challenges, 247  
    clinical significance and DDI, 247–248  
    *vs.* CYP, in vitro relative contribution, 246  
    drugs, 264, 265–266t  
    genetic polymorphism, 245  
    *N*-oxidation, 245  
    phenotype, experimental design for, 247  
    *S*-oxidation, 245  
    xenobiotics, 245  
Flosequinan, 475  
Flow cytometry (FCM), 548  
Flow scintillation analyzer (FSA), 242–243  
<sup>19</sup>Fluorine-nuclear molecular resonance spectroscopy (<sup>19</sup>F NMR) approach, 198  
FMOs. *See* Flavin-containing monooxygenases (FMOs)  
Food and Drug Administration (FDA), 6–7, 229–231, 230–231t, 273–274, 311–312, 326–328, 340, 419–420, 523  
Fraction metabolized (*f<sub>m</sub>*), 280–283, 282f  
Fraction metabolized AO (fmAO), 226  
Fraction metabolized FMO (fmFMO), 226  
Fragment ion search (FISH), 95–96  
Furafylline, 280–283, 281t  
Fusion proteins, 397–398, 404
- G**  
Ganciclovir, 580  
Gas chromatography chiral derivatization reagents (GC CDRs), 478  
Gas chromatography chiral stationary phases (GC CSPs), 478  
GastroPlus software, 525  
Gel-based cultures, 515–516, 516f  
Gel matrices, 515  
Gemfibrozil, 213–214  
General dynamic TMDD model, 643–645, 643f  
Gene therapy, 387–388, 538, 546  
Genetically modified rodent models, in drug discovery and development  
    humanized liver chimeric mouse models, 576–583  
        advantages, 581–583  
        disadvantages, 583  
    humanized transgenic animal models, 572–576  
    knockout animal models, 558–569  
    novel animal models in drug research, 556–558  
    xenobiotic receptor KO models, 569–572  
        advantages, 570–571  
        disadvantages, 571–572  
Genetic screens, CRISPR, 599, 604–605  
Genome editing, CRISPR, 596–597  
Gilbert's syndrome, 244  
Ginkgolides, 165–166t, 168

- Glaxo Smith Kline multi-assay approach, 493  
Glomerular filtration, 507, 621–622  
Glucose-galactose shift assay, 496  
Glucuronide metabolites, chemical synthesis of, 123–124  
Glutathione (GSH), 60, 83, 84*f*, 97–100, 99*f*, 125, 443–444  
Glutathione-S-transferase (GST), 622  
Granulocyte-macrophage colony-stimulating factor (GM-CSF), 403–404  
Granzymes, 541  
Grapefruit juice (GFJ), 465–466  
Graphitization process, AMS, 188–189, 188*f*  
GSK1278863 metabolites, 164–166, 165–166*t*  
GST. *See* Glutathione-S-transferase (GST)  
GSX, 443–444, 444*f*  
Gut bioavailability, 638
- H**
- Hamilton AUC-pooling approach, 428–429, 429*f*  
Hanks balanced salt solution (HBSS), 323–324  
HCS. *See* High content screening (HCS)  
HDR. *See* Homology-directed repair (HDR)  
Heat shock factor 1 (HSF1), 598  
Helper T-cell activation, 538–540, 539*f*  
HepaRG cells, 291–292  
Hepatic clearance, 612–621  
    metabolic clearance and in vitro methodologies, 612–616  
    transporter and metabolism interplay, 616–621  
Hepatic CYP reductase null (HRN) model, 565–566  
Hepatic metabolism, 225, 346–347, 640  
Hepatic risk matrix (HRM) approach, 503  
Herpes simplex virus (HSV), 598  
Herpes simplex virus type 1 thymidine kinase (HSVtk), 580  
Heteronuclear multiple bond correlation (HMBC), 138–139, 141–144, 143*f*  
Heteronuclear single-quantum correlation (HSQC), 138–141, 139–142*f*  
Hexadecanedioic acid (HDA), 316–317  
Hexafluoroacetylacetone (HFAA), 58–59, 59*f*  
High content screening (HCS), 511–512, 525–526  
High-energy collision dissociation (HCD), 87  
Highest human doses (HHDs), 662–663  
Highest nonseverely toxic dose (HNSTD), 659  
    immune-activating agents, 659–660  
    T-cell engaging bispecific molecules, 662–663  
High-performance liquid chromatography (HPLC), 151, 475–477  
    chiral derivatization reagents, 477  
    chiral mobile phase additives, 477  
    chiral stationary phases, 475–476  
    HPLC-radiometric detection, 421–422  
High-resolution mass spectrometry (HRMS), 65, 74, 109–111, 421–424, 432  
    bioanalysis, 14, 31–32  
    bioanalytical SFC applications  
        detection in, 158*f*, 159  
        modified nucleosides, 169–172  
        nonsteroidal SARMS, 163  
    data-dependent MS/MS acquisition, for metabolite identification, 74–76, 75*f*  
        accurate mass inclusion list-dependent acquisition, 77–82  
        background exclusion DDA, 83–84, 85*f*  
        ion intensity-dependent acquisition, 77  
        isotope pattern-dependent acquisition, 83, 84*f*  
        mass defect-dependent acquisition, 82–83, 82*f*  
        pseudo-neutral loss, 83  
    data-independent acquisition, for metabolite identification, 74–76, 84–86  
    all ion fragmentation (AIF), 87  
    MS<sup>E</sup> approach, 86  
    SWATH acquisition, 86, 87*f*  
    in vivo metabolite profiling and identification, 100–102, 101–102*f*  
    metabolic soft-spot analysis, 96–97, 98*f*  
    nontargeted data-processing methods  
        background subtraction (BS), 89*f*, 90–91  
        metabolomics approach, 91–93, 91*f*  
        reactive metabolite screening, 96–100, 99*f*  
        software-assisted metabolite prediction and identification, 93, 93–94*t*  
        metabolite structural identification, 94–96  
        site of metabolism prediction, software for, 93–94  
    targeted data-mining, for metabolite identification, 74–76, 75*f*  
        extracted ion chromatography (EIC), 88  
        isotope pattern filter (IPF), 88–89  
        mass defect filter (MDF), 88, 89*f*  
        neutral loss filter (NLF), 89–90  
        product ion filter (PIF), 89–90  
    TCM components, detection and structural characterization of (*see* Traditional Chinese medicine (TCM), HRMS technology)  
HIV protease inhibitors, 165–166*t*, 166–167  
HMBC. *See* Heteronuclear multiple bond correlation (HMBC)  
HNSTD. *See* Highest nonseverely toxic dose (HNSTD)  
Homology-directed repair (HDR), 597, 597*f*  
HPLC. *See* High-performance liquid chromatography (HPLC)  
HRM approach. *See* Hepatic risk matrix (HRM) approach  
HRMS. *See* High-resolution mass spectrometry (HRMS)  
HSA. *See* Human serum albumin (HSA)

- HSQC. *See* Heteronuclear single-quantum correlation (HSQC)
- Human chimeric mouse models, 576, 577–578*t*
- Human clearance, prediction of, 640
- Human embryonic kidney (HEK)-293, 510–511
- Human intestinal microsomes (HIMs), 280–283
- Humanization, of CAR construct, 549
- Humanized CYP mouse models, 572–576
- Humanized liver chimeric mouse models, 576–583
- advantages, 581–583
  - disadvantages, 583
  - FRG, 579
  - TK-NOG, 580
  - uPA/SCID, 578–579
- Humanized transgenic animal models, 572–576
- Human liver cytosol (HLC), 252–253
- Human liver microsomes (HLMs), 241–242, 280–283, 612–613
- P450 reaction phenotyping, 217–219
  - antibodies, 219
  - chemical inhibitors, 219–220, 220*t*
  - correlation analysis, 222–223, 223*t*
  - Silensomes, 221–222, 221*f*
  - ramelteon, *in vitro* metabolism of, 280–283
- Human serum albumin (HSA), 466, 492–496, 620–621
- Humoral immunogenicity, 538–540
- case studies
  - immune response to AAV vectors in animal models, 545
  - PK assessment in presence of ADA in animal models, 544–545
  - in silico* immunogenicity prediction, 545
  - risk assessment and mitigation strategies, 542–545, 543*f*
- Hydralazine, 252–253
- Hydrogen/deuterium (H/D) exchange, 56
- Hydrophilic interaction chromatography in conjunction with tandem mass spectrometry (HILIC-MS/MS), 28–29, 30*f*
- 7 $\alpha$ -Hydroxy-4-cholesten-3-one, 25, 26*f*
- 4-Hydroxyatorvastatin (4-OH-ATV), 86, 87*f*
- 4-Hydroxydebrisoquine, 579
- Hydroxylated polybrominated diphenyl ethers (OH-BDEs), 163–164
- Hyperbilirubinemia, 558–562, 566–567
- Hyperprogressive disease (HPD), 659
- I**
- Ibrutinib, 31, 341–344, 400
- Ibuprofen, 472–474
- IC<sub>50</sub>-shift approach, 289, 290*f*
- IEDB. *See* Immune epitope database (IEDB)
- Imatinib, 56, 57*f*, 454
- Imipramine, 99–100, 99*f*
- Immobilized ion affinity chromatography (IMAC), 17–18
- Immune cell-based immunoassays, 537
- Immune checkpoint inhibitors (ICIs), 657
- Immune epitope database (IEDB), 545
- Immune-related adverse events (irAEs), 659
- Immune response, 487, 489, 494–496, 535–541
- to AAV vectors in animal models, 545
  - to biotherapeutics, 550
  - cellular immunogenicity, 540–541
  - humoral immunogenicity, 538–540
- Immune tolerant transgenic mouse models, 544
- Immunoassay, 479
- Immunocytokines, 404
- Immunogenicity, 535–538, 550
- Immunomics, 494–496
- Immunomodulatory therapeutic proteins, 397–398
- Immuno-oncology (I-O) therapies, 665–666
- dose selection for, 659
  - CAR-T therapy, 664–665
  - immune-activating agents, 659–662
  - oncolytic viruses (OVs), 657, 665
  - T-cell engaging bispecific molecules, 662–664
- hyperprogressive disease (HPD), 659
- immune-related adverse events (irAEs), 659
  - mechanisms-of-actions, 657, 658*f*
- Incurred sample reanalysis (ISR), 6–7
- Induced pluripotent stem cell (iPSC), 515, 519–520, 525–526
- Induced renal tubular epithelial cells (iREC), 518–519
- Inductively coupled mass spectrometry (ICP-MS), 55–56
- Innate immune modulators, 402
- Innate immune system, 402, 535–536, 536*f*
- In silico* immunogenicity prediction, 545
- In silico* prediction tool, 547
- Intact protein bioanalysis, 16–17
- Intermediate metabolizers (IMs), 214–215
- International Transporter Consortium (ITC), 326–328
- Interspecies differences, in protein expression, 375
- Intersystem extrapolation factors (ISEF), 218, 612–613
- Intravenous immunoglobulin (IVIg), 545
- Intrinsic clearance (Cl<sub>int</sub>), 609, 640
- Investigational new drug (IND), 537–538
- In vitro-in vivo* correlation (IVIVC), 574, 614–616, 616*f*, 619–621, 621*f*
- In vitro in vivo* translation (IVIVT), 526, 527*f*
- In vitro* PTEC models, 523–525
- In vitro* to *in vivo* extrapolation (IVIVE), 18–19, 359, 375, 613–614, 618–619
- hepatic clearance, 612–621
  - quantitative prediction, 274–278, 292–299
  - renal clearance, 621–624
- Ionization techniques, 45–47



- Ion mobility mass spectrometry, 53  
Ipilimumab, 657  
iPSC. *See* Induced pluripotent stem cell (iPSC)  
Irinotecan, 245, 258–261, 259f  
Iron porphyrin catalyst, 125  
ISEF. *See* Intersystem extrapolation factors (ISEF)  
Isobaric sulfate metabolite, 31–32  
Isomeric metabolite characterization, 60, 61f  
Isopropanol, 155–156  
IsoScore, 95  
Isotope discrimination mass spectroscopy solution (IDMSS), 477  
Isotope pattern filter (IPF), 88–89, 99–100, 99f  
Isotopic dilutor, 188–189  
Itraconazole, 279, 279f  
Ivacaftor, 349, 453
- J**  
Janus kinase (JAK) inhibitor, 442–443
- K**  
Ketamine, 164–166, 165–166t, 463–464  
Ketoconazole, 219–220, 228, 244–245  
Kidney injury molecule-1 (KIM-1), 511, 523  
Kinetic isotope effect (KIE), 199, 449–452  
Knockout (KO) animal model, 557–569  
    constitutive androstane receptor (CAR) KO model, 557, 570  
    Cyp1a2 KO model, 565  
    Cyp3a KO mouse model, 562–563  
    Cyp2c mouse KO model, 564  
    Cyp2d KO mouse model, 563–564  
    Cyp2e1 KO model, 565  
    Mdr1a KO mouse model, 557  
    Mrp2 KO mouse model, 568  
    Ugt1 KO model, 566–567  
KPB. *See* Potassium phosphate buffer (KPB)  
Krebs-Henseleit buffer (KHB), 323  
Kruppel-associated box (KRAB), 597–598  
Kupffer cells, 404–405  
Kynuramine, 249–251, 249f
- L**  
LAMP. *See* Lysosome-associated marker proteins (LAMP)  
Large molecules, LC-MS bioanalysis, 5–6, 14–15  
    advantages, 15  
    antibody drug conjugate (ADC), 5, 17  
    bottom-up approach, 12–13, 15–16  
    drug metabolizing enzymes and transporters, 18–19  
    half-life extended biotherapeutics, 19–20  
    LBA, 15  
    monoclonal antibodies (mAb), 15–17  
    protein biomarkers, 18  
    protein-drug conjugates (PDC), 17–18, 18f  
    sample preparation, challenges for, 12–13  
    top-down approach, 12–13, 15–16  
Leukotriene B<sub>4</sub> (LTB<sub>4</sub>), 24  
Limit of detection (LOD), 160–162  
Limit of quantification (LOQ), 160–162  
Lipidomics analysis, bioanalytical SFC applications, 170–171t, 174–175  
Liposomes, 5  
Liquid chromatography-mass spectrometry (LC-MS), 5–6, 74  
    bioanalysis, 6, 10–12, 14–15, 20–33  
    polar metabolites, LC retention and sensitivity in, 57–58, 59f  
Liquid-liquid extraction (LLE), 12, 25  
    bioanalytical SFC applications, 156–157, 159  
    natural and synthetic cannabinoids, analysis of, 160–162  
    drug metabolite identification, 43  
Liquid scintillation counting (LSC), 185–187  
Lobaplatine, 165–166t, 167  
Lower limit of quantitation (LLOQ), 6–7, 18, 25, 186–187, 189, 373  
Lumefantrine, 165–166t, 168  
Lumiracoxib, 580  
Lymphodepletion, 550  
Lysosome-associated marker proteins (LAMP), 548
- M**  
MABEL. *See* Minimally anticipated biological effect levels (MABEL)  
Macrophage colony stimulating factor (M-CSF), 511  
MAD. *See* Multiple ascending doses (MAD)  
Madin-Darby canine kidney (MDCK) cells, 321, 515, 518, 601–603  
Major histocompatibility complex (MHC), 536–537, 547  
    MHC I-antigen, 536–537, 540–541, 541f  
    MHC II-antigen, 536–540, 545  
Mandelic acid (MA), 474  
Mantle cell lymphomas (MCL), 545  
MAO. *See* Monoamine oxidase (MAO)  
Mass analyzers, metabolite identification  
    hybrid quadrupole orthogonal time of flight (QTOF) (see Quadrupole orthogonal time of flight (QTOF))  
    orbitrap mass spectrometers, 54  
    triple quadrupoles and scan functions (see Triple stage quadrupoles (TSQ) mass spectrometers)  
Mass defect filter (MDF), 426  
    in vivo TCM components, detection and identification of, 103–104, 105f  
    metabolite identification, 82–83, 82f, 88, 89f, 99–100, 99f  
MassFragment, 95

- Mass Frontier, 95–96  
Mass-MetaSite, 95  
Mass spectral trees similarity filter (MSTF), 107, 108f  
Mass spectrometry (MS)  
  liquid chromatography-mass spectrometry (LC-MS)  
    (see Liquid chromatography-mass spectrometry (LC-MS))  
  peptide signal, analysis of, 366, 367f  
  quantitative proteomics, 360–361  
Mass-to-charge ratio detection, 50–51  
Mathematical modeling  
  absorption and distribution of biologics, 641–642  
  constant receptor amount ( $R_{\text{total}}$ ) model, 645  
  general dynamic TMDD model, 643–645, 643f  
  Michaelis-Menten model, 646  
  quasi-equilibrium model, 645–646  
  quasi-steady-state model, 646  
  target-mediated drug disposition, 642–643  
  in translational science, 634  
Matrix effects (ME), 157  
Maximum tolerated dose (MTD), 659  
  immune-activating agents, 659–660  
  T-cell engaging bispecific molecules, 662–663  
MCL. *See* Mantle cell lymphomas (MCL)  
M-CSF. *See* Macrophage colony stimulating factor (M-CSF)  
Mechanism-based inhibitors (MBI), 220, 288–290  
Mechanism of action (MOA), 404–405  
Mefenamic acid, 245  
Melatonin, 169–172, 170–171f  
Membrane transporters, 313f  
  ATP-binding cassette (ABC) proteins  
    BCRP, 314–315  
    bile salt export protein (BSEP/ABCB11), 315  
    genomic mutations (polymorphisms), 312  
    multidrug resistance proteins (MRPs/ABCCs), 315  
  P-glycoprotein (P-gp), 314  
  solute carrier (SLC) proteins  
    multidrug and toxin extrusion (MATE)  
      transporters, 318  
    organic anion transporters, 317  
    organic anion transporting polypeptides (OATP),  
      316–317  
    organic cation transporters, 317  
Metabolic clearance and in vitro methodologies, 612–616  
  in vitro-to-in vivo correlation, 614–616, 616f  
  in vitro to in vivo extrapolation (IVIVE), 613–614, 622  
Metabolic soft-spot analysis, HRMS application in,  
  96–97, 98f  
Metabolite bioanalysis, LC-MS, 14–15, 27  
  chiral compounds, 30–31  
  polar metabolites, 28–29, 30f  
  quantitation strategy, 27–28, 29f  
  sample analysis, unexpected assay challenge during,  
    31–32  
Metabolite identification (MetID)  
  accurate radioisotope counting, 44  
  detector, selection of, 41  
  HRMS-based data acquisition and processing  
    methods (see High-resolution mass spectrometry (HRMS))  
  inductively coupled mass spectrometry (ICP-MS),  
    55–56  
  ionization techniques, 45–47  
  mass analyzers  
    hybrid quadrupole orthogonal time of flight (QTOF)  
      (see Quadrupole orthogonal time of flight (QTOF))  
    Orbitrap mass spectrometers, 54  
    triple quadrupoles and scan functions (see Triple  
      stage quadrupoles (TSQ) mass spectrometers)  
  microscintillation counter, 44  
  sample preparation  
    goal of, 41–42  
    liquid-liquid extraction (LLE), 43  
    protein precipitation (PPT), 43–44  
    solid-phase extraction (SPE), 42  
    supported phase liquid extraction (SLE), 43  
  supercritical fluid chromatography (SFC), 45  
  trapping studies, 489–490  
  ultra-performance liquid chromatography (UPLC),  
    44–45  
  ultraviolet (UV) detection, 44  
  wet chemistry techniques combined with MS  
    chemical derivatization (see Chemical  
      derivatization)  
    hydrogen/deuterium (H/D) exchange, 56  
    NMR spectroscopy, 41, 62–64, 63f  
Metabolite production scale-up, 120–121  
  biomimetic catalysts, 120f, 125–126  
  chemical synthesis, 120–121, 120f  
    AMG 221, metabolites of, 122, 123–124f  
    clopidogrel, active metabolites of, 123, 123–124f  
    phase II (conjugate) metabolites, 123–125  
    phase I oxidized metabolites, 121–123  
  combined synthetic and biosynthetic approach,  
    135–136, 136f  
  electrochemistry (EC), 120f, 126–127  
  mammalian tissue fractions, 128–129  
  recombinant enzymes, 120f  
    cytochrome P450 enzymes, 132–134, 133f  
    non-CYP phase I enzymes, 134  
    oxidizing enzyme systems, 134–135  
    recombinant UGTs, 135  
  whole-cell microbial biotransformation, 120f, 129–131  
    accessing disproportionate human metabolites, for  
      toxicology studies, 130–131

- Metabolite production scale-up (*Continued*)  
    accessing multipathway-derived metabolites, 131, 131f  
    advantage of, 129  
    immobilized microbial systems, 130
- Metabolite purification, 120f, 136–138
- Metabolite safety assessment, 433–434
- Metabolites in safety testing (MIST), 14–15, 27–32, 96, 419–420  
    assessment strategy, 429–433  
    decision tree for, 420f  
    guidance documents, 421, 433–434  
    high-performance liquid chromatography, 423  
    history of guidance on, 419–420  
    radiometric detection, 423  
    technological approaches, 421–429, 422f
- Metabolomics  
    drug metabolite identification, 91–93, 91f  
    TCM components, detection and characterization of, 104
- Metalloporphyrins, 125
- MetaSense, 96
- MetaSite, 93–94, 93–94f
- Metformin, 568
- Methamphetamine (MA), 470
- Methotrexate (MTX), 398–399, 568
- 1-Methyl-4-phenylpyridinium (MPP), 317
- 4-Methyl-1-phthalazinone, 252–253, 252f
- MHC. *See* Major histocompatibility complex (MHC)
- Michaelis-Menten kinetics, 241–244, 283–285, 321, 359–360, 646
- Microbial biotransformation, 120f, 129–131  
    accessing disproportionate human metabolites, for toxicology studies, 130–131  
    accessing multipathway-derived metabolites, 131, 131f  
    advantage of, 129  
    immobilized microbial systems, 130
- Microchannel plate (MCP) detector system, 51
- Microfluidic systems, 517
- Microphysiological systems (MPS), 517, 525–526, 527f
- Microplate scintillation counter, 44
- Microplate scintillation counting (MSC), 185–186
- Microsampling, LC-MS bioanalysis, 14–15  
    blood and plasma  
        bioanalytical method development, 22–23  
        sample collection techniques, 20–22, 21f  
    sample collection, 20
- Microsomal protein per gram of kidney (MPPGK), 622
- Midazolam, 562–564, 580–581
- MIDD. *See* Model-informed drug development (MIDD)
- Minimally anticipated biological effect levels (MABEL), 659  
    immune-activating agents, 659–660  
    T-cell engaging bispecific molecules, 662–663
- MIST. *See* Metabolites in safety testing (MIST)
- Mitochondrial impairment, 496–497
- Mitochondrial toxicity, 496, 500–502
- Mixed-matrix approach, 428–429
- MK-7246, 245
- Moclobemide, 251
- Model-informed drug development (MIDD), 634, 647–648
- Model-informed drug discovery and development (MID<sup>3</sup>), 634, 647–648
- Modified sgRNA, 598
- Molybdenum cofactor (MoCo), 225
- Monoamine oxidase (MAO), 456  
    catalytic cycle of, 248–249, 249f  
    challenges, 250–251  
    clinical significance, 251  
    drugs, 264, 265–266t  
    experimental designs, for MAO phenotyping  
        fluorometric assay, 249–250  
        HPLC analysis, 250  
        LC-MS analysis, 250  
    FAD-binding domain, 248–249  
    membrane-binding domain, 248–249  
    metabolism, 451  
    substrate-binding domain, 248–249  
    substrates of, 249–250, 250t
- Monoclonal antibodies (mAbs), 15–17, 399, 543, 641
- Morphine, 214, 245
- Morphine-3-glucuronide (M3G), 61
- Morphine-6-glucuronide (M6G), 61
- MPPGK. *See* Microsomal protein per gram of kidney (MPPGK)
- MPS. *See* Microphysiological systems (MPS)
- MS<sup>E</sup> approach, 51–52, 52f  
    metabolite identification, 86, 101–102  
    TCM components, profiling and characterization of, 103
- MTD. *See* Maximum tolerated dose (MTD)
- Multidrug resistance associated protein 2 (MRP2), 558–562, 568
- Multidrug resistance proteins (MRPs), 617–618
- Multiple ascending doses (MAD), 428–429, 432
- Multiple reaction monitoring (MRM), 15–16, 49–50, 49f, 366
- Multivariate data analysis (MDA), 91–93, 91f
- Multiwell microtiter plates, 423
- Mxed lymphocyte reaction (MLR) assays, 544
- N**
- Nagase analbuminemic rats (NAR) model, 558–562
- Natural polymers, 515–516
- N-butyl-4-(4-hydroxyphenyl)-1,8-naphthalimide (NHPN), 244

- N-(3-carboxypropyl)-4-hydroxy-1,8-naphthalimide (NCHN), 244
- N-demethylated metabolite, 649–651
- Nephrotoxicity, 512–514, 523–524  
of chemotherapeutic cisplatin, 509  
screening, 2D in vitro models for, 510–514
- Neutralizing ADAs (NAbs), 537–538
- Neutral loss filter (NLF), 89–90, 99–100
- Neutral loss (NL) scan, 49, 49f
- Neutrophil gelatinase-associated lipocalin (NGAL), 511
- New chemical entity (NCE), 229, 241, 526, 556–557
- New drug application (NDA), 340
- New drug candidates, metabolites of, 40
- New molecular entities (NMEs), 340, 610, 619  
enzyme-mediated DDIs  
as inducers, 345–346f, 348–349  
as inhibitors, 342–343t, 346–347  
as substrates, 349–351  
transporter-mediated DDIs  
as inhibitors, 348t, 351–352, 351f  
as substrates, 349–351, 350f
- New psychoactive substances (NPS), 160–162, 161t
- Niacin, 444, 445f, 445t
- Nilotinib, 244–245
- N-isobutyryl-L-cysteine, 477
- Nitric oxide (NO), 391
- Nitrotryptophan, 377
- Nivolumab monotherapy, 662
- NMEs. *See* New molecular entities (NMEs)
- Noncompartmental analyses (NCA), 635–636
- Non-cytochrome P450 (CYP) enzymes (Non-CYP enzymes)  
aldo-keto reductases (*see* Aldo-keto reductases (AKRs))  
biotransformation, 237–238  
carboxylesterases (*see* Carboxylesterase (CES))  
flavin-monooxygenase (*see* Flavin-containing monooxygenases (FMOs))  
monoamine oxidase (*see* Monoamine oxidase (MAO))  
UDP-glucuronosyltransferase (UGT)  
allelic diversity, 238  
challenges, 243–244  
chemical inhibitors, inhibition study with, 243  
clinical relevance and drug-drug interactions (DDI), 244–245  
glucuronidation, 238  
human UGT genes, 238  
reaction phenotyping of, 241–242  
recombinant human UGT enzymes, incubation with, 242–243  
transferases, 238  
UGT1A isoforms, 238, 239–240t  
UGT2B isoforms, 238, 240–241t  
uridine 5'-diphosphate glucuronic acid (UDPGA), 238  
xanthine oxidase enzyme (*see* Xanthine oxidase (XO))
- Nonhomologous end joining (NHEJ), 596–597, 597f
- Nonlinear chromatography, 42
- Nonsmall-cell lung cancer (NSCLC), 649–651
- Nonsteroidal anti-inflammatory drugs (NSAIDs), 472–474
- Nonsteroidal selective androgen receptor modulators (nonsteroidal SARMs), 163
- Non-synonymous single nucleotide polymorphisms (nsSNPs), 264
- Nontargeted data-processing methods, HRMS  
background subtraction (BS)  
metabolite identification, 89f, 90–91  
TCM components, detection and characterization of, 104–107, 106f  
metabolomic approach  
metabolite identification, 91–93, 91f  
TCM components, detection and characterization of, 104
- No-observed adverse effect level (NOAEL), 659  
immune-activating agents, 659–660  
T-cell engaging bispecific molecules, 662–663
- Normal-phase chromatography (NPLC), 28–29
- NSAIDs. *See* Nonsteroidal anti-inflammatory drugs (NSAIDs)
- Nuclear magnetic resonance (NMR) spectroscopy, 119–120, 421–422, 424–425  
metabolites, structural characterization of, 41, 62–64, 63t  
metabolite structure elucidation, 138  
1D and 2D NMR experiments, 138–139  
stepwise determination of metabolite structures, 139–144
- Nuclear Overhauser spectroscopy (NOESY), 138–139, 144, 144–145f
- Nucleic acid, 461–462
- Nucleotide-binding domains (NBD), 314–315
- O**
- Oil spin method, 618
- Olaparib, 229, 231t
- Oleoyl ethanolamide (OEA), 25
- Oligonucleotides (ON), 392  
antisense oligonucleotides, 509–510, 512–514, 641  
CpG oligonucleotides, 402–403  
mRNA-based drugs, 401–403  
natural oligonucleotides, 402
- Omeprazole, 214–215, 291, 355
- Oncolytic viruses (OVs), 388–389, 403–404, 657, 665
- O-phthalaldehyde (OPA), 477
- Optical detectors, 44

- Optical enantiomers, 462
- Optimal biological dose (OBD), 659–660
- Optimized quantitative analysis approaches  
 calibration curve, surrogate matrix, and LLOQ, 373  
 inclusion of positive control sample, 371–372  
 multiple peptides, use of, 371  
 multiple product ions, use of, 371  
 optimized practices, 373  
 SIL peptide and exogenous protein internal standards, 373
- Orbitrap mass spectrometers, 54
- Ordinary differential equations (ODE) system, 643–644
- Organic anion transporter 1/3 (OAT1/3), 568–569
- Organic anion transporting polypeptide 2 (OATP2), 120–121
- Organic anion transporting polypeptide 1a/b (Oatp1a/b), 569
- Organic anion transporting polypeptides (OATPs), 558–562, 569, 617–618
- Organic cation transporter 1/2 (OCT1/2), 568
- Organ-on-a-chip, 517
- Orthoclone OKT3, 543
- Osimertinib, 649–651
- Oxcarbazepine, 165–166*t*, 169
- Oxylipins, 170–171*t*, 174–175
- P**
- PAHs. *See* Polycyclic aromatic hydrocarbons (PAHs)
- Palifermin, 400–401
- Palmitoyl ethanolamide (PEA), 25
- PAM. *See* Protospacer-adjacent motif (PAM)
- Parallel reaction monitoring (PRM), 15–16
- Parkinson's disease, 251
- Paroxetine, 453
- Pathogen-associated molecular patterns (PAMPs), 402
- Pattern recognition receptors (PRR), 402, 535–536
- Pazopanib, 245
- PBMC. *See* Peripheral blood mononuclear cell (PBMC)
- PCA. *See* Principal component analysis (PCA)
- Pembrolizumab, 657, 660–662, 661*f*
- Pentoxifylline, 565
- Pentraxin 3 (PTX3), 538, 538*f*
- Pentraxins, 538
- Peptide labeling and quantification/calibration, 369*t*
- Perforin, 541, 542*f*, 548
- Peripheral blood mononuclear cell (PBMC), 537, 544
- Permeability categorization, 610–612
- Peroxygenases, 134–135
- P-glycoprotein (P-gp), 314, 318–319, 556–557, 567–568, 617–618, 639
- Pharmaceutical Research and Manufacturers of America (PhRMA), 419–420
- Pharmaceuticals and clinical analysis, SFC applications, 165–166*t*  
 active pharmaceutical ingredient (API), 167  
 ketamine enantiomers and metabolites, SFC-MS, 164–166  
 SFC-MS/MS method  
 citalopram enantiomers, 164–166  
 coenzyme Q10, 168  
 daidzein, 167  
 ezetimibe, 168–169  
 ginkgolides, 168  
 GSK1278863 metabolites, 164–166  
 HIV protease inhibitors, 166–167  
 lobaplatine, 167  
 lumefantrine, artemether, dihydroartemisinin, 168  
 model compounds, 168  
 n-butylphtalimid, 168–169  
 oxcarbazepine and chiral licarbazepine, 169  
 piroxicam, 168–169  
 probucol, 168–169  
 rabeprazole, 169  
 racemic cetirizine, 164–166  
 risperidone and chiral metabolite, 167  
 scholarisine, 19-episolarisine, vallesamine, and picrinine, 168  
 taxane drugs, 167  
 sulfonamide antibiotics and metabolites, SFC-UV method, 164
- Pharmaceuticals and Medical Devices Agency (PMDA), 229, 230*t*, 523
- Pharmacodynamic (PD) modeling  
 for biologics, 651  
 for small molecule drugs, 647–651
- Pharmacogenetics (PGx) Database, 353–354
- Pharmacokinetic (PK) modeling, 475, 609, 625  
 for biologics, 641–647  
 for small molecule drugs, 635–641  
 compartmental and population-based PK models, 636  
 physiologically-based pharmacokinetic modeling, 636–641, 637*f*
- Pharmacokinetics-pharmacodynamics (PK/PD) models, 647–648, 647*f*, 659  
 dosing regimen  
 blinatumomab, 664  
 CD3XP-cadherin bispecific molecule, 663  
 oncolytic virus, 665  
 pembrolizumab, 660–662, 661*f*  
 schizophrenia, D<sub>2</sub> receptor antagonists for, 648–649, 649*f*
- Phencyonate, 472
- Phenol metabolites, 122
- Phosphate ester prodrug, LC-MS/MS bioanalysis, 31–32

- Phosphatidylethanol, 161*t*, 162
- Phosphorothioate (PS), 402
- Phosphorothioates antisense oligonucleotides (PS-ASOs), 392
- p-hydroxymethyl amphetamine (pOH-MA), 470
- Physiological-based absorption modeling, 638–639
- Physiologically based pharmacokinetic and pharmacodynamic (PBPK/PD) modeling, 376–377
- Physiologically based pharmacokinetic (PBPK) modeling, 202–204, 229, 326, 397, 526, 618–620, 635–641, 637*f*
- distribution modeling, 639–640
- EMA guidance, 229
- FDA and PMDA guidances, 229
- food's and pH's effects on pharmacokinetics, 638–639
- gaps and challenges in, 641
- gut transporters and CYP3A, 639
- human clearance, prediction of, 640
- modeling and simulations, 352–353
- olaparib, DDI risk assessment for, 229, 231*t*
- Picrinine, 165–166*t*, 168
- Pioglitazone, 454, 466–467
- Piroxicam, SFC-MS/MS method, 165–166*t*, 168–169
- Pitavastatin, 320, 558–562
- Placental growth factor (PGF), 399
- Plaque forming units (PFU), 665
- Plasma microsampling, LC-MS bioanalysis, 14–15
- method development, 22–23
- sample collection techniques, 21–22, 21*f*
- POC. *See* Proof of concept (POC)
- Polar analytes, 161*t*, 163
- Polar ionic mobile phase (PIM), 475
- Polar metabolites, 169–172, 170–171*t*
- of ezlopitant, dansyl chloride derivatization, 58, 59*f*
- LC-MS bioanalysis of, 28–29, 30*f*
- Polycyclic aromatic hydrocarbons (PAHs), 158–159, 163–164
- Polydimethylsiloxane (PDMS), 517
- Polysaccharides, 461–462
- Poor metabolizers (PMs), 214–215
- Population-based PK models, 636
- Porcine kidney epithelial (PK1) cells, 321
- Posaconazole, UGT
- chemical inhibitors, inhibition study with, 243
- chemical structure of, 242, 242*f*
- pooled HLM, incubation with, 242
- recombinant human UGT enzymes, incubation with, 242–243
- Post-acquisition software tools, for metabolite identification, 426–427
- Post-digestion processing, 364–365
- Posttranslational modification (PTM), 12–13, 359–360, 362
- Potassium phosphate buffer (KPB), 492–493
- Precision medicine, 376–377
- Precursor ion (PI) scan, TSQ mass spectrometer, 48, 48*f*, 50
- Pregnane X receptor (PXR), 291–292, 391, 556–557, 569–570, 639
- Primaquine, 563–564
- Principal component analysis (PCA), 91–93, 91*f*, 373
- Probenecid, 320
- Probucol, SFC-MS/MS method, 165–166*t*, 168–169
- Procurement, homogenization, and protein extraction, 362–364
- Product ion filter (PIF), 89–90
- Progress curve approach, 289–290
- Pro-inflammatory cytokines, 389
- Proof of concept (POC), 565–566
- Propafenone, 129, 468
- Propranolol, 134–135, 468
- Protease inhibitors, 12–13, 166–167, 244–245, 349–350
- Protein
- ATP-binding cassette (ABC) proteins
- BCRP, 314–315
- bile salt export protein (BSEP/ABCB11), 315
- genomic mutations (polymorphisms), 312
- multidrug resistance proteins (MRPs/ABCCs), 315
- P-glycoprotein (P-gp), 314
- biomarkers, LC-MS bioanalysis, 18
- extraction and digestion methods, 364
- labeling approaches, 369, 370*f*
- quantification, 366–369, 367–368*f*
- solubilization and denaturation, 364
- solute carrier (SLC) proteins
- multidrug and toxin extrusion (MATE) transporters, 318
- organic anion transporters, 317
- organic anion transporting polypeptides (OATP), 316–317
- organic cation transporters, 317
- subcellular localization of, 376
- Protein-drug conjugates (PDC), 17–18, 18*f*
- Protein precipitation (PPT), 12, 43–44, 159
- Protein standards for absolute quantification (PSAQ), 368
- Proteoglycans, 400–401
- Proteomics, 377
- DMET quantitative proteomics (*see* Drug metabolizing enzymes and transporters (DMET) quantitative proteomics)
- targeted proteomics, 361
- untargeted/global proteomics, 361
- Proteomics-based Research Initiative for Non-CYP Enzymes (PRINCE) program, 266–267
- Proteotypic peptides, 361–362
- Protospacer-adjacent motif (PAM), 596

- Proximal tubule cells per gram of kidney (PTCPGK), 623–624
- Proximal tubule epithelial cells (PTECs), 509, 511, 518–519, 525–526
- PRR. *See* Pattern recognition receptors (PRR)
- PSAQ. *See* Protein standards for absolute quantification (PSAQ)
- Pseudo-neutral loss-dependent acquisition, 83
- PTCPGK. *See* Proximal tubule cells per gram of kidney (PTCPGK)
- PTECs. *See* Proximal tubule epithelial cells (PTECs)
- Puerarin, 104, 105f
- PXR. *See* Pregnane X receptor (PXR)
- Q**
- Quadrupole orthogonal time of flight (QTOF), 50–51
- data-dependent acquisitions (DDA), 51, 52f
  - data-independent acquisitions (DIA), 51
  - MS<sup>E</sup> concept, 51–52, 52f
  - SONAR acquisition, 52–53, 54f, 65
  - SWATH acquisition, 52, 53f, 65
  - ion mobility mass spectrometry, 53
- Quality control (QC), 371
- Quantitative concatemer (QconCAT), 243–244, 368
- Quantitative NMR (qNMR), 138–141
- Quantitative proteomics, 359–361, 377
- Quantitative systems pharmacology (QSP), 526, 634
- Quasi-equilibrium (QE) model, 645–646
- Quasi-steady-state (QSS) model, 646
- 4-Quinazolinone, 134
- Quinidine, 453
- R**
- Rabeprazole, 165–166t, 169
- Racemic cetirizine, 164–166, 165–166t
- Radiodetection methods, 185–186, 186f
- Radiometric detection, 423
- RAFs. *See* Relative activity factors (RAFs)
- Raloxifene, 252–253, 375
- Ramelteon, 280–283, 281t, 282f
- Ranitidine metabolites, 100–102, 102f
- Reactive metabolites, 434, 489–491, 502
- formation of, 443–444, 444f
  - screening, HRMS application in, 96–100, 99f
- Reactive nitrogen species (RNS), 377
- Receptor occupancy (RO), 651
- Recombinant enzymes, 120f
- cytochrome P450 enzymes, 132–134, 133f
  - non-CYP phase I enzymes, 134
  - oxidizing enzyme systems, 134–135
  - recombinant UGTs, 135
- Recombinant P450 (rP450) enzymes, 132–134, 133f, 215, 218
- advantages of, 217
  - AZD6738, 217
  - CYP3A, 216–217
  - CYP2J2, 217
  - human hepatocytes and HLM, 217
  - intersystem extrapolation factors (ISEF), 218
  - in vitro experiments, 216
  - P450/POR ratio, 215–217
  - P450s and accessory proteins, interactions of, 215–216, 216f
  - relative activity factors (RAF), 218
  - substrate and enzyme concentration, selection of, 218
- Recommended human dose (RHD), 659
- Recommended phase-II dose (RP2D), 659
- REFs. *See* Relative expression factors (REFs)
- Regioselective biotransformations, 129
- Relative activity factors (RAFs), 218, 243–244, 260–261, 618, 623
- Relative expression factors (REFs), 623
- Renal cell models, 525–526
- Renal clearance, 621–624
- metabolic clearance and IVIVE, 622
  - transporter-mediated CL and tubular reabsorption, 622–624
- Renal drug safety evaluation
- in vitro PTEC models, 523–525
  - nephrotoxicity screening, 2D in vitro models for, 510–514
  - renal safety screening, emerging models for, 514–520
  - translatable kidney safety biomarkers, 520–523
- Renal epithelial cell, 517
- Renal excretion, 621–622
- Renal safety screening, 514–520
- Renal secretion, 621–622
- Renal toxicity, 510
- Renal tubule assist devices (RAD), 518–519
- Repaglinide, 352, 617–618
- Retinoic X receptor (RXR), 391
- Reversed-phase HPLC methods, 137–138
- Reversible inhibitors, 286–288
- Rifampin, 245, 291
- Risperidone and chiral metabolite, 165–166t, 167
- Ritonavir, 509, 580–581
- RNA interference (RNAi) technology, 599
- Rotating frame Overhauser spectroscopy (ROESY), 138–139
- R/S-amphetamine, SFC-MS/MS method, 160–162, 161t
- S**
- Sandwich-cultured hepatocyte (SCH) system, 323–324
- Sandwich-cultured human hepatocytes (SCHH), 618–619
- SAP. *See* Serum amyloid P (SAP)
- Saichinone, 245



- Scaled-up production, of drug metabolites.  
*See* Metabolite production scale-up
- SCHH. *See* Sandwich-cultured human hepatocytes (SCHH)
- Schisandrol B, 104, 105*f*
- Schizophrenia, 648–649, 649*f*
- Scholarisine, 165–166*t*, 168
- SeaHorse assay, 496
- Secondary emission multiplier (SEM), 51
- Segel's method, 471
- Selected ion monitoring (SIM) mode, 158
- Selective androgen receptor modulators (SARMs), 163
- Semiquantitative and quantitative assessment, of metabolite coverage, 427
- Sequential windowed acquisition of all theoretical fragment ions (SWATH), 52, 53*f*, 65, 86, 87*f*, 101–102
- Serum amyloid P (SAP), 538, 538*f*
- Serum creatinine (SCr), 507, 520
- Severe combined immunodeficiency (SCID), 579
- SFC. *See* Supercritical fluid chromatography (SFC)
- Short RNAs (sgRNAs), 596, 598
- SILAC. *See* Stable isotope labeling with amino acids in cell culture (SILAC)
- Silensomes, 221–222, 221*f*
- Simeprevir, 635
- Single ion reaction (SIR) monitoring, 49
- Single nucleotide polymorphisms (SNP), 360–361
- SLC transporter knockout mouse models, 561–562*t*
- SM. *See* Stromal matrix (SM)
- Small molecule drugs (SMDs), 387–388, 393–396, 406
- Software-assisted metabolite prediction and identification, 93, 93–94*t*  
metabolite structural identification, 94–96  
site of metabolism prediction, software for, 93–94
- Solid-phase extraction (SPE), 12  
bioanalytical SFC applications, 156–157, 159  
drug metabolite identification, 42
- Solute carriers (SLCs), 509, 599, 617–618  
multidrug and toxin extrusion (MATE) transporters, 318  
organic anion transporters, 317  
organic anion transporting polypeptides (OATP), 316–317  
organic cation transporters, 317
- SONAR data-independent acquisition, 52–53, 54*f*, 65
- Soranefib, 400
- Stable isotope labeled metabolite (M STIL), 28, 29*f*
- Stable isotope labeled parent drug (P STIL), 28, 29*f*
- Stable isotope-labeled (SIL) peptides, 243–244, 364–366, 373
- Stable isotope labeling with amino acids in cell culture (SILAC), 369
- Stable label, for metabolite detection and identification, 440, 440*t*, 457  
cases studies, 441–444  
disconnect between endogenous and [<sup>13</sup>C]-labeled niacin, 444  
H<sub>2</sub><sup>18</sup>O and D<sub>2</sub>O, facitinib metabolism, 442–443  
stable-labeled glutathione, 443–444  
vismodegib and oxidative pyridine ring cleavage, 441–442  
stable labels and their application, 440–441  
drug metabolism, types of studies in, 441  
isotopes, choices of, 440
- Standard operation procedures (SOPs), 6–7
- Steady-state volume of distribution (*V*<sub>ss</sub>), 639–640
- Stereochemical inversion, 474
- Stereoenantiomers, 461–462
- Stereoselective analytical methods, 475–479  
capillary electrophoresis, 478–479  
gas chromatography, 477–478  
chiral derivatization reagents, 478  
chiral stationary phases, 478  
high-performance liquid chromatography, 475–477  
chiral derivatization reagents, 477  
chiral mobile phase additives, 477  
chiral stationary phases, 475–476  
immunoassay, 479  
supercritical fluid chromatography, 478
- Stereoselective immunoassay, 479
- Stereoselectivity  
chiral drugs  
absorption and transport, 465–466  
distribution, 466–467  
excretion, 470  
in pharmacodynamics, 463–465  
biological activity of drugs, 464  
complementarity of enantiomeric effects, 464  
different action targets, 464  
different biological activities, 464  
enantiomer side effects, 463–464  
opposite effects of enantiomers, 463  
same biological activity, 465  
selective competitive antagonism, 463  
in toxicity, 471–473  
active enantiomers, 473  
chiral drugs, 471  
chiral inversion, 472  
enantiomeric biotransformation, 472  
pharmacological activity, 472
- Steroid analysis, SFC-MS/MS method, 170–171*t*, 172–173, 173*f*
- Steroid and xenobiotic receptor (SXR), 569
- Stimulator of interferon genes (STING), 402
- Stromal matrix (SM), 514–515

- Sulfonamide antibiotics and metabolites, 164, 165–166*t*
- Supercritical fluid chromatography (SFC), 45, 478
- detection
    - high-resolution accurate mass spectrometry (HRMS), 158*f*, 159
    - MS/MS detection, 158–159, 158*f*
    - SFC-MS hyphenation, 158–159, 158*f*
    - ultraviolet (UV) detection, 157–158, 158*f*
  - drugs of abuse, doping control and toxicological analysis, 161*t*
    - acetyl-gestagens, 163
    - cannabinoids, 160–162
    - clenbuterol enantiomers, 163
    - doping substances, 162–163
    - new psychoactive substances (NPS), 160–162
    - PHDPE, 163–164
    - phosphatidylethanol, 162
    - polar analytes, 163
    - polyaromatic hydrocarbon (PAH) pyrene, 163–164
    - R/S-amphetamine, 160–162
    - SARMs, 163
    - synthetic cannabinoids, 160–162
  - endogenous metabolites, metabolomics, and lipidomics, bioanalysis of, 170–171*t*
    - amino acids, 169–172
    - arachidonic acid metabolites, 174
    - disease biomarkers profiling, 173–174
    - fat-soluble vitamins and carotenoids, 173–174
    - lipids, 174–175
    - melatonin and *n*-acetyl-serotonin, 169–172
    - modified nucleosides, 169–172
    - oxylipins, 174–175
    - plant metabolic profiling, 169
    - polar metabolites, 169–172
    - steroid analysis, 172–173, 173*f*
    - tocopherols and tocotrienols, 173–174
    - triacylglycerols, 174–175
    - vitamin D metabolites, 173–174
  - method development, for bioanalysis, 157
    - achiral and chiral columns, particle size of, 154, 155*f*
    - additives, 156
    - chiral stationary phase (CSP) screening, 154
    - column selection, 154
    - cosolvent/modifier, 154–156, 155*f*
    - 2-ethylpyridine (2-EP) bonded silica phase, 154
    - injection solvent, nature of, 156–157
    - makeup solvent, 156
    - mobile-phase composition, 156
    - stationary-phase screening, 154
    - validation, 157
  - pharmaceuticals and clinical analysis
    - (*see* Pharmaceuticals and clinical analysis, SFC applications)
    - preparative separation, 151
    - sample preparation, 159
    - stereoisomers, purification of, 151
    - supercritical fluid
      - carbon dioxide (CO<sub>2sc</sub>), 152–153
      - characteristics of, 152–153
      - solvents, 151, 152*t*
- Supercritical fluid extraction (SFE), 159
- Superficially porous particles (SPP), 154
- Supported phase liquid extraction (SLE), 43
- Surrogate matrix, 373
- SWATH. *See* Sequential windowed acquisition of all theoretical fragment ions (SWATH)
- SXR. *See* Steroid and xenobiotic receptor (SXR)
- Synergistic activation mediator (SAM) system, 598
- Synthetic cannabinoids, 160–162, 161*t*
- ## T
- Talidomide, 473
- Talimogene laherparepvec (T-VEC), 387–388, 657, 664–665
- Tamoxifen, 122, 229, 563–564, 575
- TAP. *See* Transporter associated with antigen processing (TAP)
- Target-dependent interactions, 399–400
- Targeted data-mining, HRMS
  - in vivo TCM components, detection and identification of, 103–104, 105*f*
  - metabolite identification, 74–76, 75*f*
    - extracted ion chromatography (EIC), 88
    - isotope pattern filter (IPF), 88–89
    - mass defect filter (MDF), 88, 89*f*
    - neutral loss filter (NLF), 89–90
    - product ion filter (PIF), 89–90
- Targeted proteomics, 361, 366
- Target-mediated drug disposition (TMDD), 635, 642–643, 651
- Taxane drugs, SFC-MS/MS method, 165–166*t*, 167
- T-cell engaging bispecific molecules, 657, 662–664
- T-cell receptor (TCR), 536–537
- Telaprevir, 635
- Tenofovir, 509
- Terfenadine, 213–214
- Tetrabenazine, 452
- Tetradecanedioic acid (TDA), 316–317
- Tetraethylammonium (TEA), 317
- Thalidomide, 475, 580–581
- Therapeutic protein (TP), 393, 394–395*t*, 398*t*
- Therapeutic protein–drug–drug interactions (TP-DDI), 389*f*
  - of antibody–drug conjugates, 401
  - based on binding to proteoglycans, 400–401
  - based on physiology, 400

- CYP enzymes and transporters, *in vitro* effects on, 391–393
- cytokine-dependent interactions
- cytokines and therapeutic proteins targeting cytokines, 393–397
  - immunomodulatory therapeutic proteins, 397–398
- immunogenicity, 391
- immunogenicity-dependent interactions, 398–399
- major mechanisms of, 389–391
- risk assessment, 404–406
- specific study considerations, 407
- target-dependent interactions, 399–400
- therapeutic targets, 390
- Thiamine transporter 2 (ThTR2), 326–328
- Three-dimensional models, for kidney injury and repair, 515, 516*f*
- 3D-quantitative structure-activity relationship (3D-QSAR) modeling, 325–326
- Time-dependent inhibitors, 288–290
- Time-to-digital converter (TDC), 51
- Tisagenlecleucel (Kymriah), 664–665
- Tissue bioanalysis, 4–5, 10–11
- Tissue homogenization, 363–364
- Tivantinib, 469–470
- TMDD. *See* Target-mediated drug disposition (TMDD)
- Tocopherols and tocotrienols, 170–171*t*, 173–174
- Tofacitinib, 64, 64*f*, 442–443, 443*f*
- Tofoglifozin, 202
- Toll-like receptors (TLRs), 402
- Total correlated spectroscopy (TOCSY), 138–139
- Toxicity, stereoselectivity in, 471–473
- active enantiomers, 473
  - chiral drugs, 471
  - chiral inversion, 472
  - differences between enantiomers in human, 471, 472*t*
  - enantiomeric biotransformation, 472
  - pharmacological activity, 472
- Toxicological analysis, bioanalytical SFC applications, 161*t*, 163–164
- Tozadenant, 196
- Traditional Chinese medicine (TCM), HRMS technology, 102–103
- data-dependent acquisitions (DDA), 103
  - data-independent acquisitions (DIA), 103
  - individual TCM components, metabolic pathway determination, 107, 108*f*
  - LC-HRMS analytical strategy, 107–109, 109*f*
  - targeted data-mining techniques, 103–104, 105*f*
  - untargeted data-mining techniques, 104–107, 106*f*
- Transcription-activator-like effector nucleases (TALENs), 558, 595
- Transcriptomics approach, 493–494
- Transepithelial electrical resistance (TEER), 322
- Transient familial neonatal hyperbilirubinemia, 244
- Translational PKPD models
- EGFR inhibitor development for treatment of lung cancer, 649–651, 650*f*
  - enabling earlier decision-making, 648
  - enhanced decision-making, 648
  - improved drug efficacy, 648
- Transmembrane domains (TMD), 314–315
- Transporter associated with antigen processing (TAP), 540–541
- Transporter inhibition, 497–499
- Transporter-mediated CL and tubular reabsorption, 622–624
- Transporter-mediated drug interactions
- challenges, 329–330
  - drug disposition, clinical significance of, 318–320, 319*t*
  - evaluation, regulatory landscape of, 326–329
    - inhibitor of transporters, investigational drug, 328–329
    - ITC white paper, 326–328
    - substrate of transporters, investigational drug, 328  - membrane transporters (*see* Membrane transporters)
  - perspectives, 329–330
  - transporter liabilities, in drug discovery and development
    - animal models, use of, 324–325
    - biomarkers for *in vivo* assessment, application of, 326, 327*t*
    - membrane vesicle-based assay, 321–322
    - polarized cell-based systems and bidirectional transporter assays, 322
    - primary cell-based assays, 323–324
    - recombinant transfected cell-based systems, 321
    - in silico* modeling, transporter proteins, 325–326
- Transporter proteins, 497
- Triacylglycerols, 170–171*t*, 174–175
- Triazolam, 562–563
- Trifluoperazine, 134
- Trimethylamine (TMA), 247–248
- Trimethylamine oxide (TMAO), 247–248
- Trimethylaminuria disorder, 247–248
- Triple stage quadrupoles (TSQ) mass spectrometers, 47
- full MS scan mode, 47, 48*f*, 50
  - multiple reaction-monitoring mode (MRM), 49–50, 49*f*
  - neutral loss mode (NL), 49, 49*f*
  - precursor ion scan mode, 48, 48*f*, 50
  - product ion scan mode, 48, 48*f*
  - single ion reaction (SIR) monitoring, 49
- Troglitazone, 580
- Troleandomycin, 219, 288–289, 564
- Trovafloxacin, 492

- Tubuloids, 519–520  
Tumor static concentrations (TSC), 663  
Tyrosine kinase inhibitors (TKIs), 244–245, 649–651
- U**
- UDP-glucuronosyltransferases (UGTs), 274, 275–276*t*  
  allelic diversity, 238  
  challenges, 243–244  
  chemical inhibitors, inhibition study with, 243  
  clinical relevance and drug-drug interactions (DDI), 244–245  
  glucuronidation, 238  
  human UGT genes, 238  
  posaconazole (*see* Posaconazole, UGT)  
  reaction phenotyping of, 241–242  
  recombinant human UGT enzymes, incubation with, 242–243  
  transferases, 238  
  UGT1A isoforms, 238, 239–240*t*  
  UGT2B isoforms, 238, 240–241*t*  
  uridine 5'-diphosphate glucuronic acid (UDPGA), 238
- Ultra-performance liquid chromatography (UPLC), 44–45
- Ultrarapid metabolizers (UMs), 214–215
- Ultraviolet (UV) detection  
  bioanalytical SFC applications, 157–158, 158*f*  
  cannabinoids, 160–162, 161*t*  
  sulfonamide antibiotics and metabolites, 164, 165–166*t*  
  drug metabolite identification, 44
- Unstirred water layer (UWL), 638–639
- Untargeted MS acquisition approaches, 366
- Upper limit of quantitation (ULOQ), 6–7
- Uridine 5'-diphospho-glucuronosyltransferase (UGT), 135, 204, 311–312, 468, 555–556, 566–567, 612
- Urinary albumin (Ur ALB), 523
- Urinary  $\beta$ 2 microglobulin (Ur  $\beta$ 2M), 523
- Urinary clusterin (Ur CLU), 523
- Urinary cystatin C (Ur CYS C), 523
- Urinary total protein (Ur TP), 523
- Urinary trefoil factor-3 (Ur TFF3), 523
- Urine bioanalysis, 4–5, 9–10
- Urokinase-type plasminogen activator (uPA), 578–579
- UWL. *See* Unstirred water layer (UWL)
- V**
- Vallesamine, 165–166*t*, 168
- Vascular endothelial growth factor (VEGF), 399
- Vismodegib, 441–442, 442*f*
- Vitamin D, 158–159, 170–171*t*, 173–174
- Volumetric adsorptive microsampling (VAMS), 20–22, 21*f*
- Voriconazole, 223
- V64-p65-Rta (VPR), 598
- W**
- Warfarin, 215
- Western blotting, 360–361
- Wet chemistry techniques combined with MS  
  chemical derivatization (*see* Chemical derivatization)  
  hydrogen/deuterium (H/D) exchange, 56  
  NMR spectroscopy, 41, 62–64, 63*t*
- Whole-cell microbial biotransformation. *See* Microbial biotransformation
- Whole-cell photosensitizer approach, 132–134
- X**
- Xanthine oxidase (XO), 134  
  challenges, 255  
  clinical significance and DDI, 255  
  drugs, 264, 265–266*t*  
  experimental designs, for XO phenotyping  
    colorimetric assay, 255  
    fluorimetric assay, 254–255  
    spectrophotometric assay, 254  
  hydrogen peroxide (H<sub>2</sub>O<sub>2</sub>), 253–254  
  mammalian tissues, 253–254  
  uric acid, 253–254, 254*f*
- Xanthinuria, 255
- Xenobiotic receptor KO models, 569–572  
  advantages, 570–571  
  disadvantages, 571–572
- Z**
- Zidovudine, 245
- Zinc finger nucleases (ZFNs), 558, 595
- Ziprasidone metabolite, 60, 60*f*
- Zoxazolamine, 570

# IDENTIFICATION AND QUANTIFICATION OF DRUGS, METABOLITES, DRUG METABOLIZING ENZYMES, AND TRANSPORTERS

## Concepts, Methods, and Translational Sciences

A critical review of advances in analytical technologies for the detection and quantification of drugs, metabolites, biomarkers, enzymes, and transporters.

*Identification and Quantification of Drugs, Metabolites, Drug Metabolizing Enzymes, and Transporters, second edition* is completely updated to provide an overview of the last decade's numerous advances in analytical technologies for the detection and quantification of drugs, metabolites, and biomarkers. This new edition goes beyond LC-MS and features all-new chapters on how to evaluate drug absorption, distribution, metabolism, and excretion, potential for hepatic and renal toxicity, immunogenicity of biotherapeutics and translational tools for predicting human dosage, safety, and efficacy of small molecules and biologics. This book will be an important handbook and desk reference for pharmacologists, toxicologists, clinical scientists, and students interested in the fields of pharmacology, biochemistry, and drug metabolism.

### Key Features

- Four sections in the book with 24 chapters give readers an overview of state-of-the-art techniques for identifying and quantifying drugs, metabolites, and biomarkers, including a chapter on new approaches for quantification of enzymes and transporters in different tissues.
- Focuses on the role of drug metabolism enzymes, transporters in disposition, and drug-drug interactions, as well as strategies for evaluating drug metabolism and safety using advanced liver and kidney models. Discussions on immunogenicity risks of biologics and their evaluation methods have been included.
- Includes several chapters on advanced translational sciences to predict human dosage, pharmacokinetics, and efficacy for small molecules and biotherapeutics.
- All chapters are written by experts with a wide range of practical experience from the industry and academia.

Edited by

### Shuguang Ma

Principal Scientist, Department of Drug Metabolism and Pharmacokinetics, Genentech Inc., South San Francisco, CA, United States

### Swapan K. Chowdhury

Director of DMPK, Takeda Pharmaceutical International Co., Cambridge, MA, United States



ELSEVIER

[elsevier.com/books-and-journals](http://elsevier.com/books-and-journals)

ISBN 978-0-12-820018-6



9 780128 200186